Lecture Notes in Civil Engineering

Boeing Laishram
Abhay Tawalare *Editors*

Recent Advancements in Civil Engineering

Select Proceedings of ACE 2020

Springer

Lecture Notes in Civil Engineering

Volume 172

Lecture Notes in Civil Engineering (LNCE) publishes the latest developments in Civil Engineering—quickly, informally and in top quality. Though original research reported in proceedings and post-proceedings represents the core of LNCE, edited volumes of exceptionally high quality and interest may also be considered for publication. Volumes published in LNCE embrace all aspects and subfields of, as well as new challenges in, Civil Engineering. Topics in the series include:

- Construction and Structural Mechanics
- Building Materials
- Concrete, Steel and Timber Structures
- Geotechnical Engineering
- Earthquake Engineering
- Coastal Engineering
- Ocean and Offshore Engineering; Ships and Floating Structures
- Hydraulics, Hydrology and Water Resources Engineering
- Environmental Engineering and Sustainability
- Structural Health and Monitoring
- Surveying and Geographical Information Systems
- Indoor Environments
- Transportation and Traffic
- Risk Analysis
- Safety and Security

To submit a proposal or request further information, please contact the appropriate Springer Editor:

– Pierpaolo Riva at pierpaolo.riva@springer.com (Europe and Americas);
– Swati Meherishi at swati.meherishi@springer.com (Asia - except China, and Australia, New Zealand);
– Wayne Hu at wayne.hu@springer.com (China).

All books in the series now indexed by Scopus and EI Compendex database!

More information about this series at https://link.springer.com/bookseries/15087

Boeing Laishram · Abhay Tawalare
Editors

Recent Advancements in Civil Engineering

Select Proceedings of ACE 2020

Springer

Editors
Boeing Laishram
Department of Civil Engineering
Indian Institute of Technology Guwahati
Guwahati, Assam, India

Abhay Tawalare
Department of Civil Engineering
Visvesvaraya National Institute
of Technology
Nagpur, Maharashtra, India

ISSN 2366-2557 ISSN 2366-2565 (electronic)
Lecture Notes in Civil Engineering
ISBN 978-981-16-4395-8 ISBN 978-981-16-4396-5 (eBook)
https://doi.org/10.1007/978-981-16-4396-5

This Springer imprint is published by the registered company Springer Nature Singapore Pte Ltd.
The registered company address is: 152 Beach Road, #21-01/04 Gateway East, Singapore 189721, Singapore

Preface

Economic growth of a country is strongly related with the extent of infrastructure development being experienced by the country. It is a well-established fact that construction industry has both strong backward and forward linkages with infrastructure development. In fact, the most commonly adopted strategy to revive the economy is to make investment in infrastructure development and reap the benefits of the multiplier effects of the investment. The different streams of civil engineering, thus, have strong relationships with the various aspects of infrastructure development, and the fruitful exchanges of ideas and knowledge will help in solving real challenges in implementation of infrastructure projects.

The International Conference on Advances in Civil Engineering 2020 (ACE 2020) is being organised by the Department of Civil Engineering in association with Department of Applied Mechanics, Visvesvaraya National Institute of Technology, Nagpur (VNIT Nagpur). ACE 2020 provides an opportunity for researchers from academia and practitioners interested in the field of construction management and materials, environmental management, transportation engineering, water resources engineering and structural engineering to gather virtually and exchange latest know-how on implementation of different types of infrastructure projects.

ACE 2020 also marks the Diamond Jubilee Celebration of VNIT Nagpur. The Institute has grown from being an institute sponsored by Government of India and Government of Maharashtra in 1960 to an Institute of National Importance declared vide the National Institutes of Technology Act, 2007 (29 of 2007). The themes selected for the conference highlight the various streams in which the associated departments have grown over the years during the journey from being a regional engineering college to an Institute of National Importance.

ACE 2020 covers the areas where progress has been made in the various fields of civil engineering in recent times. Papers submitted for ACE 2020 have been organised into seven generic themes—construction management, construction materials, environmental engineering, geotechnical engineering, transportation engineering, water resource engineering and structural engineering. The number of papers selected by double blind peer review process under the above-mentioned

themes is 90. The themes such as construction materials, transportation engineering, construction management and water resources engineering have attracted major share of the papers from both India and abroad.

Construction Management is one of the fields of civil engineering which is emerging to be an important catalyst for ensuring creation of quality infrastructure projects within the stipulated time, cost and scope. The papers submitted under this theme established the current trend of the construction industry wherein majority of the papers are relating to adoption of building information modelling for either safety planning, reducing errors or to explore the adoption of BIM and smart cities concepts. Another area which has attracted the attention is relating to the factors affecting the success of projects. Implication of the pandemic on the construction industry in the form of claims and dispute management is another interesting area which is expected to attract the attention of the researchers under this theme.

Construction Materials is an area which has attracted the attention of the researchers on account of the renewed focus on the search of sustainable materials to fulfil the sustainable development goals. A significant number of papers have been submitted under this theme relating to the studies undertaken in search of sustainable materials. Some of the notable studies on sustainable materials are relating to use of sugarcane biomass ash, lime sludge, waste paper sludge, fly ash, bamboo reinforced concrete and stabilised mud blocks enriched with steel slag. A significant number of papers have also concentrated on evaluation of the physical properties of concrete and its derivatives when blended with different materials such as recycled glass, red ash, biocementation and basalt fibre. Finally, besides experimental studies, mathematical models to predict performance of concrete have also been the focus of research in some of the papers submitted under this theme.

Environmental Engineering deals with the assessment, monitoring, and treatment of different forms of contamination in wetland and groundwater. Papers under this theme have also focussed on assessment of impact of lockdown due to COVID-19 pandemic on the ambient air quality and the role of natural ventilation in addressing the indoor air pollution. Finally, the application of soft computing techniques in environmental engineering has also been included under this theme wherein fuzzy sets have been used for optimization of water distribution network.

Geotechnical Engineering problems addressed by the papers submitted under this theme focus on numerical formulations of geotechnical problems through investigation on behaviour of open-ended driven piles, failures of gabion wall and dynamic behaviour of fly ash stabilised expansive soil. The focus of some the papers has also been on devising new ground improvement techniques such as exploring the effectiveness of plastic coated natural fibre reinforcement and EPS-based lightweight geomaterial for geotechnical applications.

Transportation Engineering theme has been successful in inviting papers under two broad categories of transportation pavement materials and transportation planning. Papers relating to pavement materials have tried to address the goal of sustainable development through exploration of incorporating waste materials in pavement construction such as shredded waste plastic on warm stone mastic asphalt, crushed concrete in granular sub-base and utilization of industrial waste.

Most of the papers relating to transportation planning are with respect to transportation modelling and optimisation using techniques such as macroscopic analysis and fuzzy sets to predict traffic flow pattern and driver behaviour under naturalistic driving environment. In addition to these papers, few papers have focussed on developing a framework for dynamic toll pricing, devising economic strategies to alleviate traffic congestion.

Water Resources Engineering is amongst one of the themes which have attracted significant number of papers. The paper under this theme cover topics such as GIS and remote sensing applications in water resources such as 3D geomodelling for dam site characterization, hydrodynamic simulation, reduction in reservoir storage capacity using satellite imageries and feasibility assessment using geospatial approach. This theme also include papers on flood and watershed management strategies and rainfall trend anomalies analysis.

The final section of the proceedings contains papers relating to **Structural Engineering**, and papers submitted under this theme are relating to application of soft computing techniques such as finite element method for analysis of punching shear in RC column to footing connection and application of multifractal cross-correlation analysis for structural health monitoring. In addition to this, papers dealing with structural analysis and design for blast and impact resistance are also included under this theme.

The programme for ACE 2020 comprises of seven plenary sessions and three parallel tracks. The plenary sessions comprise of keynote lectures and panel discussions on papers presented by authors.

ACE 2020 would not have been possible without the support of many people and organisations. The support of Prof. P. M. Padole, the *patron*, has made it possible for the team to organise ACE 2020 successfully. We would also like to thank Prof. Rajesh Gupta, *principal convenor*, and Prof. Yashwant Katpatal, *convener organising committee*, for taking the initiatives of organising various teams for this event, contacting faculties at international level for arranging the keynote speakers and guiding the organising team time to time with their valuable suggestions. We are also thankful to the members of the organising committee for their support and efforts put forward by them to make the conference a big success. We, therefore, would like to thank specifically session coordinators: Dr. Avinash Vasudeo, Dr. Manmohan Goel, Dr. Ashwini Mirajkar, Dr. Mangesh Madurwar, Dr. Swapnil Wanjari, Dr. Shilpa Dongre, Dr. Shrabony Adhikari, Dr. Amit Padade, Dr. B. Karthik, Dr. V. Srinivasan, Dr. Udit Jain, Dr. Sitarami Reddy and Dr. Ashish Khatri.

We are also thankful to the following individuals for providing the necessary assistance in the publication of the proceedings. The effort of Dr. Swati Bhave, Dr. Arpita Saha, Dr. Vaidehi Dakwale, Dr. Sonal Dhanvijay and Priya Vyas and Deena Maria Bonaparte from Springer was very crucial in bringing out of this publication. We would like to thank all of them for their valuable inputs.

We hope that this publication will be of assistance and use to the new generation of researchers to pursue research along the new dimensions and problems identified from ACE 2020. Finally, on behalf of my co-editors, I would like to express our sincere appreciation to all the authors and reviewers for their significant contributions to the success of the conference.

Guwahati, India — Prof. Boeing Laishram
Nagpur, India — Dr. Abhay Tawalare

Contents

About the Editors

Dr. Boeing Laishram is currently Professor of Civil Engineering at Indian Institute of Technology, Guwahati, India. He has 5 years of industrial experience and 15 years of teaching experience. He did his Ph.D. from Indian Institute of Technology, Madras. His area of research interest includes public private partnerships in infrastructure development, financing the infrastructure projects, risk management, sustainable procurement process and labour productivity. He has published 21 research articles in reputed international journals. He is reviewers for many journals. He has received best paper awards three times and PMI India Young Research Award 2012. He is also engaged in providing consultancy services to many government organisations.

Dr. Abhay Tawalare is currently Assistant Professor of Civil Engineering at Visvesvaraya National Institute of Technology, Nagpur, India. He has 8 years of industrial experience and 11 years of teaching experience. He did his Ph.D. from Indian Institute of Technology, Guwahati. His area of research interest includes relational contracting, management of public sector construction projects, stakeholder management in mega construction projects and evaluation of public private partnership in infrastructure services by municipality. He has published 10 research articles in reputed international journals. He is well known consultant in central India and providing advisory services to many construction organisations.

Utilising BIM in Construction Safety Planning: A Systematic Review

Priyanka Prashar and J. Uma Maheswari

Abstract The construction industry is always associated with hazards. According to the Health and Safety Executive (HSE), the construction sector accounts for the most considerable amount of fatal injuries. Technology can overcome such issues by enhancing safety at construction sites. Building information modelling (BIM) is an upcoming concept and is gaining popularity in the construction industry. Attempts have been made to summarise the application of BIM in safety, but studies have not summarised it systematically. Therefore, the purpose of this study is to review the existing knowledge of BIM in construction safety and identify the gaps in existing studies. A systematic review was conducted on the articles published from 2009 to 2020. For the study, three topics were selected, including BIM for construction safety, prevention through design (PtD), and automated rule-based checking. The findings observe that BIM allows to identify the hazards and mitigate them before the construction commences. Additionally, a significant number of accidents are linked with the design and safety issues can be assessed automatically using BIM in the design phase. Therefore, the use of BIM can improve the safety performance of the construction industry.

Keywords Building information modelling · Construction safety planning · Prevention through design · Automated rule-based checking

1 Introduction

The construction industry in India constitutes around 8.2% of India's Gross Domestic Product (GDP) and employs nearly 57.5 million people [1]. Besides, the construction industry is linked to a significant number of work-related accidents.

P. Prashar (✉) · J. U. Maheswari
Department of Civil Engineering, Indian Institute of Technology, New Delhi 110016, India
e-mail: Priyanka.Prashar@civil.iitd.ac.in

J. U. Maheswari
e-mail: J.Uma.Maheswari@civil.iitd.ac.in

B. Laishram and A. Tawalare (eds.), *Recent Advancements in Civil Engineering*, Lecture Notes in Civil Engineering 172,
https://doi.org/10.1007/978-981-16-4396-5_1

Annually, around 60,000 fatal accidents occur in construction sites across the world, which estimates one fatal accident every ten minutes [2]. More than 48,000 workers die annually from occupational accidents in India, and there are nearly 37 million occupational accidents which cause absence from work of at least four days [3]. Construction workers in developed countries around the world are 3–4 times more likely to meet with fatal accidents at work than other industries such as the manufacturing industry and agriculture industry. In developing countries, this number estimates to be 3–6 times higher compared to the developed countries [4]. These statistics indicate that the construction industry is hazardous; therefore, there is a dire need to improve safety in the construction industry.

The construction safety, besides time, cost, and quality, is a success factor of a project [5]. Planning is a significant step in safety management that incorporates the identification of all possible hazards, hazardous operations, and safety measures [6]. Research shows that one of the best ways to prevent occupational injuries and fatalities is to eliminate hazards and minimise risks early in the design phase or redesign process and incorporate safe design methods into all phases of hazard and risk mitigation [7, 8]. This concept is known as prevention through design (PtD). According to this method, design professionals (specifically architects and engineers) consider construction worker safety when designing a facility [9]. The construction design must be evaluated to verify the quality and performance of the design and identify issues before construction takes place [10]. Traditionally, such evaluation is done manually, which is labour-intensive, time-consuming, and inefficient [11]. The process to automatically review the design is known as automated rule-based checking.

Building information modelling (BIM) is becoming increasingly popular in the architectural engineering construction (AEC) industry and is changing the approach to safety [12]. This study aimed to explore the research addressing BIM for improving construction safety. Limited studies have been carried out to date. Researchers have attempted to summarise the application of BIM in safety in the past decade, but studies have not summarised it systematically. More safety investigations could have been done to date as the global construction industry has not accomplished the mission on "zero accident sites". This study has discussed the existing knowledge on construction safety, BIM for construction safety, safety through design, and automated rule-based checking associated with BIM.

2 Research Methodology

The study aimed to gain knowledge regarding the studies of the integration of BIM with construction safety and point out the gaps. A systematic review of the existing literature was carried out. This systematic review is carried out according to Preferred Reporting Items for Systematic Reviews and Meta-Analyses (PRISMA) [13]. The databases used for the study were Science Direct, Emerald Insight, and ASCE library. Publications from the government agencies responsible for

regulating workplace safety and industry reports were also used. Articles published from 2009 to 2020 were selected for the study. The research conducted on buildings were only selected for this study. In the initial search, 142 papers were found, out of which 123 were articles, and 19 were other documents such as reports, publications, and articles found on individual searches. The information of all the documents was reviewed. Out of which 16 documents were duplicates, so were removed, and on further screening, 84 documents were excluded as they were not relevant to our study. Finally, 42 documents were selected for the study, which is illustrated in Fig. 1 in a PRISMA flow diagram.

3 Results and Discussion

The final articles included in the study are distributed in Table 1, depending upon their resources. Figure 2 shows the distributions of the studies according to the regions. According to Table 1, the majority of papers in the area of construction safety associated with BIM were published in automation in construction journal. Figure 2 shows that the United States has conducted most research in this area, and the Indian construction industry lags far behind in the research. India should carry out research to exploit the benefits of using BIM in construction safety.

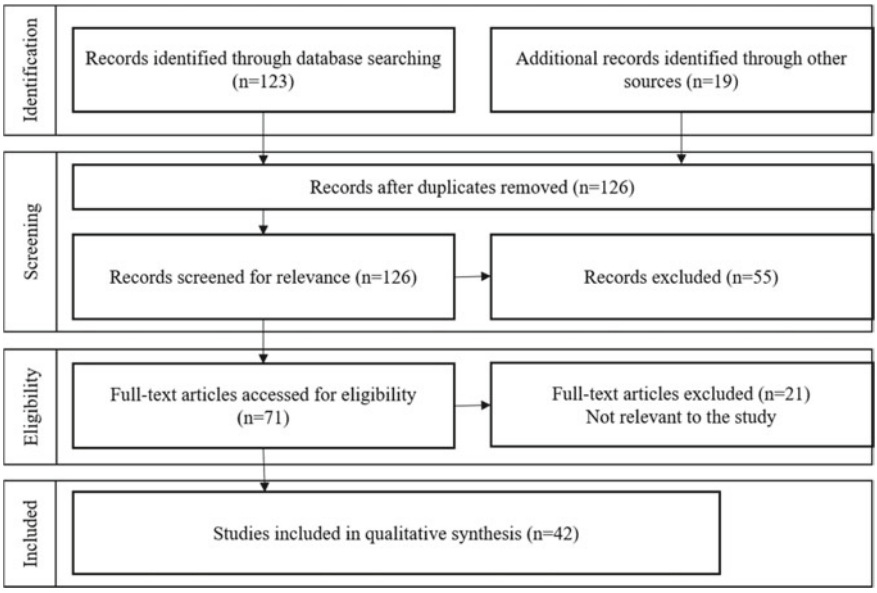

Fig. 1 PRISMA flow diagram

Table 1 Distribution of the articles according to their sources

Source	No. of articles
Automation in construction	6
Procedia engineering	3
Safety science	2
Journal of safety research	2
Journal of construction engineering and management	2
Journal of computing in civil engineering	2
Engineering, construction and architectural management	1
Construction innovation	1
International journal of project management	1
Practice periodical on structural design and construction	1
Journal of engineering, design and technology	1
International journal of architectural research	1
Conference proceedings	10
Others	9

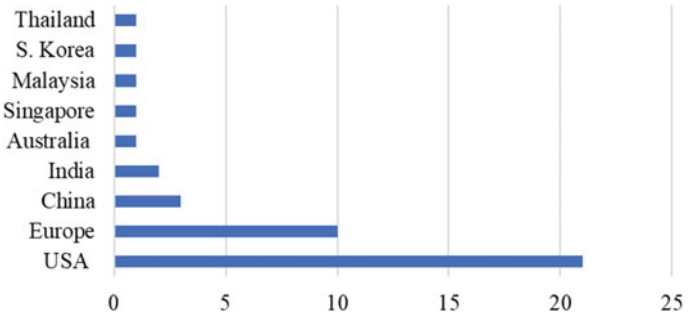

Fig. 2 Distribution of articles according to the regions

3.1 Safety Planning

The construction industry is associated with hazardous work due to which construction workers are exposed to hazards. Adequate project planning and hazard recognition must be carried out collaboratively and throughout the project lifecycle to promote safety in construction projects [14]. Safety planning, traditionally, is carried out separately from the design and planning phase of the project [15]. It also is carried out through manual observations that result to be labour-intensive, error-prone, and often highly inefficient [16]; it relies on 2D drawings that cause difficulties in using and analysing safety plans [6]. Such problems can be resolved with the help of building information modelling (BIM).

The research found that 46% of respondents believed that BIM could improve the safety of construction workers [17]. BIM 3D modelling can assist teams in identifying and correcting errors and omissions that may lead to safety hazards earlier in the design process. BIM enables better communication and understanding among various stakeholders [18]. 4D-BIM is a vital technology for construction-site safety-related planning activities, connecting the safety viewpoint more closely to construction planning, enabling visualisation of safety arrangements in construction projects at different times, and providing more illustrative communication-site plans [19]. In a survey, it was found that 53% of respondents believed that BIM has a significant effect on improving construction safety in comparison with the other current tools such as risk assessment and review tools [20].

3.2 Highlights of the BIM-Based Safety Studies

The studies have shown that prevention through design (PtD) is a useful tool to improve safety [9, 21]. Decisions taken during the design process affects means and methods of construction, thus affecting construction safety [22]. The incorporation of safety while designing plays an essential role in eliminating/reducing the hazards. The implementation of DfS within the construction industry is affected by-designer attitude, designer awareness/knowledge and education, DfS tools, clients' influence/motivation, and legislation [23]. A study showed that given a high awareness and a positive attitude towards the DfS concept, the level of involvement in DfS practices among design professionals is shallow [24]. Therefore, designers should be motivated and made aware of getting involved in DfS. Training should be provided to the designers so that they engage in the DfS concept and exploit the benefits out of it. Researchers concluded that BIM has the potential to achieve DfS [25, 26]. In 2010, Kamardeen [27] proposed a PtD tool that can be integrated with a BIM model. Eastman et al. [28] introduced the process of rule checking in BIM. Researchers from the Georgia Institute of Technology introduced the first preliminary results of an automated safety rule checker for BIM [29]. Later, researchers carried out studies to develop BIM-based tools/ methodologies to enhance safety, as shown in Table 2. On the other hand, Fig. 3 shows the types of hazards adopted in the studies conducted so far, which shows that most of the studies focused on falling prevention. This demonstrates the need to address other types of hazards.

Table 2 BIM-based tools

Year	Tools/ methodologies	Description	Hazards	BIM dimension	Citation
2010	4D BIM for safety planning, management, and communications	Visualisation of BIM-based 4D safety railings for fall/ edge protection	Falls	4D	[30]
2011	BIM-based design for a construction worker safety tool	Designing for safety suggestions available to designers and constructors	Falls	3D	[31]
2011	Automated safety code checking tool	Safety planning can be considered in the design stage for early detection and application of protective safety system	Falls	4D	[29]
2013	Automated rule-checking framework	Automatically identifies the potential safety hazards and apply corresponding prevention methods	Falls	4D	[12]
2014	PtD tool	PTD suggestions available to designers and constructors	Falls	3D	[32]
2014	Automated safety planning plug-in	Automate safety planning and enhance the safety knowledge of construction practitioners to reduce accidents in the site	Falls, struck by objects	4D	[33]
2015	Automated rule-checking framework	Detect and visualise the potential fall hazards effectively during the safety design and planning stages	Falls	4D	[15]
2015	A BIM-based quality checking process	Communication and collaboration among the project party concerned for improving safety management	Falls, fire, collision	4D	[34]
2016	DfS approach	Automatically identify potential safety problems resulted from the design by integrating BIM with design safety rules	Falls	3D	[35]
2016	Database for near miss information in BIM	Allows construction-site workers to report near misses and visualise within an BIM	Near miss	3D	[36]

(continued)

Table 2 (continued)

Year	Tools/ methodologies	Description	Hazards	BIM dimension	Citation
2016	Automated safety planning platform	Automatic identification of safety hazards related to activities working on scaffolding and preventive measures can be prepared before construction	Falls	4D	[37]
2017	Testing of visualisation technologies (BIM, 4D simulations) in real-life projects	The technology identifies hazards and communicates safety plans to workers	Fatal four	4D	[38]
2018	BIM-integrated risk review system	Help designers identify risk related to their design element	Falls, fire escape	3D	[39]
2019	BIM-integrated PtD knowledge-based plug-in	assess safety risks during the design phase automatically	Falls, collapse, struck by object, electrocution	3D	[40]
2019	PtD tool addressing top levels of the hierarchy of control	Eliminate or mitigate risks before construction	–	4D	[41]
2020	Integration of H&S risk management into the design phase	Allows collaboration among technicians involved in the design process, which can reduce the number of accidents originating in the design phase	Falls	3D	[42]

4 Conclusion

The construction industry is becoming as complex as the technology is developing. With the increase in construction work, the risk associated with it also increases. Therefore, safety is an essential part of a project. Safety not only depends on the performance of a contractor, but it also depends on the performance of other key participants such as designer and owner. Technology such as BIM can also enhance safety performance. The study presented the papers in construction safety associated with BIM from 2009 to 2020. The study established a relationship between safety management and BIM. It was observed that (a) tools such as PtD and automated rule checking have the ability to augment the capabilities of BIM to

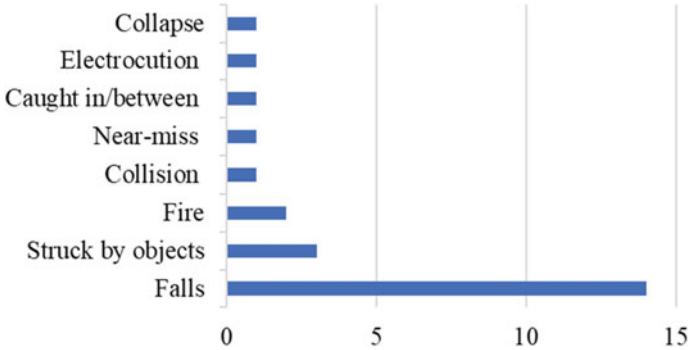

Fig. 3 Types of hazards addressed in this study

foster safety; (b) a significant number of accidents are linked with the design; (c) safety issues can be automatically assessed using BIM in the pre-construction phase of a project.

Findings show that there is a need to provide PtD training to make the designers aware of the benefits of its use. The research showed that the risk leading to the incident could be reduced or eliminated if the design is considered for safety. Also, it was observed that the majority of the research is theoretical, and real-world implementation is required. The majority of the studies focused on the lower levels (engineering and administrative controls) of the hierarchy of controls; therefore, future studies should focus on the higher levels (elimination and substitution). Also, most studies have focused on fall hazard prevention; other hazards such as struck by objects, electrocution, and caught-in/between. should also be explored. There is limited research on near misses, which can be explored in the future. Although research in improving safety using BIM is carried out, problems still exist in the construction sites. Therefore, there is a need to develop robust tools to enhance safety at sites.

References

1. KPMG (2020) COVID-19: assessment of economic impact on construction sector in India. KPMG, India
2. International Labour Organization (ILO) (2005) Facts on safety at work. ILO, Geneva
3. Hämäläinen P (2010) Global estimates of occupational accidents and fatal work-related diseases. Tampere University of Technology, Finland
4. International Labour Organization (ILO) (2014) Safety and health in the construction sector—overcoming the challenges. ILO, Geneva
5. Bansal VK (2011) Application of geographic information systems in construction safety planning. Int J Project Manage 29:66–77
6. Chantawit D, Hadikusumo BH, Charoenngam C, Rowlinson S (2005) 4DCAD-Safety: visualising project scheduling and safety planning. Constr Innov 5:99–114

7. Department of Health and Human Services (2010) Prevention through design plan for the national initiative. Department of Health and Human Services, USA
8. Gambatese JA, Gibb AG, Brace C, Tymvios N (2017) Motivation for prevention through design: experiential perspectives and practice. Pract Period Struct Des Constr 22:04017017
9. Toole TM, Gambatese J (2008) The trajectories of prevention through design in construction. J Saf Res 39:225–230
10. Nawari NO (2019) A generalised adaptive framework (GAF) for automating code compliance checking. Buildings 9:86
11. Sacks R, Eastman C, Lee G, Teicholz P (2018) BIM handbook: A guide to building information modeling for owners, designers, engineers, contractors, and facility managers. John Wiley & Sons, USA
12. Zhang S, Teizer J, Lee JK, Eastman CM, Venugopal M (2013) Building information modeling (BIM) and safety: automatic safety checking of construction models and schedules. Autom Constr 29:183–195
13. Moher D, Liberati A, Tetzlaff J, Altman DG, The PRISMA Group (2009) Preferred reporting items for systematic reviews and meta-analyses: the PRISMA statement
14. Webb TA, Langar S (2019) Utilising BIM as a tool for managing construction site safety: a review of literature. In: 55th ASC annual international conference proceedings, Associated Schools of Construction, USA, pp 339–347
15. Zhang S, Sulankivi K, Kiviniemi M, Romo I, Eastman CM, Teizer J (2015) BIM-based fall hazard identification and prevention in construction safety planning. Saf Sci 72:31–45
16. Getuli V, Ventura SM, Capone P, Ciribini AL (2017) BIM-based code checking for construction health and safety. Procedia Eng 196:454–461
17. Suermann PC, Issa RRA (2007) Evaluating the impact of building information modeling on construction. In: Proceedings of the 7th international conference on construction applications of virtual reality, USA, pp 206–215
18. Del-Puerto CL, Clevenger CM (2010) Enhancing safety throughout construction using BIM/VDC. In: Proceedings of the BIM-related academic workshop, USA, pp 1–7
19. Kiviniemi M, Sulankivi K, Kähkönen K, Mäkelä T, Merivirta ML (2011) BIM-based safety management and communication for building construction. VTT, Finland
20. Kasirossafar M, Shahbodaghlou F (2013) Building information modeling for construction safety planning. In: ICSDEC 2012: developing the frontier of sustainable design, engineering, and construction. American Society of Civil Engineers, USA, pp 1017–1024
21. Gangolells M, Casals M, Forcada N, Roca X, Fuertes A (2010) Mitigating construction safety risks using prevention through design. J Safety Res 41:107–122
22. Tymvios N, Gambatese JA (2016) Perceptions about design for construction worker safety: viewpoints from contractors, designers, and university facility owners. J Constr Eng Manag 142:04015078
23. Poghosyan A, Manu P, Mahdjoubi L, Gibb AG, Behm M, Mahamadu AM (2018) Design for safety implementation factors: A literature review. J Eng Des Technol 16:783–797
24. Abueisheh Q, Manu P, Mahamadu AM, Cheung C (2020) Design for safety implementation among design professionals in construction: the context of Palestine. Safety Sci 128:104742
25. Ku K, Mills T (2010) Research needs for building information modeling for construction safety. In: International proceedings of associated schools of construction 45nd annual conference. Associated Schools of Construction, USA
26. Xiaer X, Dib H, Yuan J, Tang Y, Li Q (2017) Design for safety (DFS) and building information modeling (BIM): a review. In: ICCREM 2016: BIM application and off-site construction. American Society of Civil Engineers, China, pp 69–80
27. Kamardeen I (2010) 8D BIM modelling tool for accident prevention through design. In: 26th annual ARCOM conference 1. ARCOM, Australia, pp 281–289
28. Eastman C, Lee JM, Jeong YS, Lee JK (2009) Automatic rule-based checking of building designs. Autom Constr 18:1011–1033

29. Zhang S, Lee JK, Venugopal M, Teizer J, Eastman C (2011) Integrating BIM and safety: An automated rule-based checking system for safety planning and simulation. In: Proceedings of CIB W099 99, pp 24–26
30. Sulankivi K, Kähkönen K, Mäkelä T, Kiviniemi M (2010) 4D-BIM for construction safety planning. In: Proceedings of W099-special track 18th CIB world building congress 2020, pp 117–128
31. Qi J, Issa RRA, Hinze J, Olbina S (2011) Integration of safety in design through the use of building information modelling. In: Computing in civil engineering, pp 698–705
32. Qi J, Issa RR, Olbina S, Hinze J (2014) Use of building information modeling in design to prevent construction worker falls. J Comput Civ Eng 28:A4014008
33. Irizarry J, Zolfagharian S, Ressang A, Nourbakhsh M, Gheisari M (2014) An automated safety planning approach for residential construction sites in Malaysia. Int J Constr Manage 14(3):134–147
34. Park S, Kim I (2015) BIM-based quality control for safety issues in the design and construction phases. Int J Arch Res 9:111–129
35. Hongling G, Yantao Y, Weisheng Z, Yan L (2016) BIM and safety rules based automated identification of unsafe design factors in construction. Procedia Eng 164:467–472
36. Shen X, Marks E (2016) Near-miss information visualisation tool in BIM for construction safety. J Constr Eng Manag 142:04015100
37. Kim K, Cho Y, Zhang S (2016) Integrating work sequences and temporary structures into safety planning: automated scaffolding-related safety hazard identification and prevention in BIM. Autom Constr 70:128–142
38. Azhar S (2017) Role of visualisation technologies in safety planning and management at construction jobsites. Procedia Eng 171:215–226
39. Hossain MA, Abbott EL, Chua DK, Nguyen TQ, Goh YM (2018) Design for safety knowledge library for BIM-integrated safety risk reviews. Autom Constr 94:290–302
40. Yuan J, Li X, Xiahou X, Tymvios N, Zhou Z, Li Q (2019) Accident prevention through design (PtD): integration of building information modeling and PtD knowledge base. Autom Constr 102:86–104
41. Jin Z, Gambatese J, Liu D, Dharmapalan V (2019) Using 4D BIM to assess construction risks during the design phase. Eng Constr Arch Manage
42. Cortés-Pérez JP, Cortés-Pérez A, Prieto-Muriel P (2020) BIM-integrated management of occupational hazards in building construction and maintenance. Autom Constr 113:103115

Exploring Regulation of Entry in the Construction Sector in South Africa

Salome Chiloane-Nwabueze, Tiku Tanyimboh, and Alistair Glendinning

Abstract Construction sector plays a key role in the economic development of a country. The management of this sector is thus crucial to maximise the performance of the sector and of the economy. This paper explores entry requirements that could be considered in the South African construction sector for contractor grading, to help improve the sector's performance. One way of achieving this goal is through entry regulation. Organisations and some countries worldwide have some form of entry regulation to manage the construction sector. To minimise business failure and poor performance, new entrants need to have at least a recognised qualification in the aspiring field of works. This will contribute to ensure that new entrants have the relevant knowledge of the field which they aspire to enter. Moreover, sectors have been subcategorized based on different areas of speciality to ensure that contractors operate within the area of their speciality. This is to enable proper management of entrants and enhance construction sector performance. The requirements that may be considered for contractor progression are also indicated.

Keywords Contractor grading and progression · Industry sector entry requirements · Construction industry and sector · Civil engineering · Infrastructure

S. Chiloane-Nwabueze (✉) · T. Tanyimboh · A. Glendinning
School of the Civil and Environmental Engineering, University of Witwatersrand, Private Bag 3, Johannesburg 2050 Wits, South Africa
e-mail: 0511487h@students.wits.ac.za

T. Tanyimboh
e-mail: tiku.tanyimboh@wits.ac.za

A. Glendinning
e-mail: alistair.glendinning@wits.ac.za

B. Laishram and A. Tawalare (eds.), *Recent Advancements in Civil Engineering*, Lecture Notes in Civil Engineering 172,
https://doi.org/10.1007/978-981-16-4396-5_2

1 Introduction

Economic development can be measured by the physical development of infrastructures such as bridges, roads and buildings, and job creation [1] which are mainly offered by the civil engineering and general building construction sectors. The aim of all parties (i.e. client, contractor, consultants, suppliers and end-users) involved in a construction project in either the public or private sector is to successfully complete the project on schedule, within planned budget, with the highest quality and in the safest manner [2]. This is, however, not always the case as at times contracts are awarded to contractors who are unable to deliver the project outputs. For the economy to grow rapidly, the project performance of contractors who are undertaking infrastructure projects should be high especially in the public sector as the infrastructure is constructed for public use.

The Construction Industry Development Board [3] indicates that the failure rate of infrastructure projects in South Africa (SA) has greatly increased. Factors such as time, cost, quality, and client satisfaction are some of the indicators that are used to measure performance in a project environment [4]. Unfortunately, many contractors in government infrastructure projects fall short when assessed against these indicators [5]. In a survey undertaken by Construction Industry Development Board [3], around 12% of the South African infrastructure projects surveyed had levels of defects that were regarded as inappropriate. It is estimated that this translates into a cost of around US $250 million per year [3].

The Construction Industry Development Board (CIDB) was established by an act of parliament of the Republic of South Africa (RSA). This is the Construction Industry Development Board Act No. 38 of 2000 [6] which founded the regulatory body (CIDB) for the construction industry of South Africa. According to the Act, the objectives of the CIDB are not only to grow the South African economy through the construction industry but also to develop improved industry performance and best practice.

One way of improving the industry performance and best practice in the construction sector is to ensure that the process for grading contractors is efficient, effective and is benchmarked with international practices and norms. Presently, the CIDB grade contractors based on financial capability and projects implemented. There are no requirements which are considered for new entrants in the construction sector. This paper introduces a possible framework that could be considered by the South African Construction Industry Development Board for registration of new entrants and for contractor progression through the grades.

This framework was proposed due to the need to introduce entry-level requirements in the construction sector in South Africa by the CIDB National Stakeholder Forum as one way of improving the South African construction sector [7]. International comparisons were carried out for benchmarking purposes, to help achieve this goal. The framework is yet to be considered by the CIDB, and workshops for the relevant industry stakeholders are envisaged.

2 Literature Review

As indicated, the CIDB not only seeks to grow the South African economy through the construction industry but also seeks to develop improved industry performance and best practice [6]. Presently, the CIDB does not have minimum requirements for entry in the construction sector. A study conducted by the CIDB has shown that entry requirements would likely increase the success rate of Grade 1 contractors and would also make it easier for companies seeking to develop enterprises to select entities with potential [8]. Many countries require those wishing to establish a limited liability company to undertake additional steps, including the deposit of a minimum amount of paid-up capital. A certain amount of regulation may be justified based on public interest, particularly where there is risk of market failure [9].

Currently, the South African construction and the civil engineering sector does not have a minimum requirement for contractors who wish to enter the construction industry. The CIDB requires the following documents for registration: application form, proof of company registration, identity documents, tax clearance certificate, electrical certificate for electrical and related types of works (EB) works, financial statement for the two years immediately preceding the application (for contractor progression) and track record documents (project appointment or award letter, completion certificate, and payment certificate) [10]. Project completion certificate and payment certificate are required for contractors who are applying for grade progression.

It is interesting to note that only electrical and related types of works (EB) require some form of certification, which is not the case with civil engineering (CE) and general building (GB) works. It is observed from the requirements that for contractors to progress from one grade to the next, not much emphasis is placed on the contractor's technical knowledge and expertise. It is assumed implicitly that when contractors have implemented projects and are financially within the required specifications, they are then competent to move to the next grade.

The CIDB has set up guidelines for reporting contractor performance [5]. The contractor performance report should include records of contractors' breach of contract resulting in either termination and/or cancellation of contract [11]. These efforts by the CIDB indicate that importance is placed on client satisfaction, which is a measure of project performance. Client satisfaction can also be used to indicate the performance of the contractor in relation to time, cost and quality.

The grading system of the CIDB needs to be robust as contractors are awarded projects based on the grade which contractors hold. The CIDB Act No. 38 of 2000 established the CIDB in order to implement an integrated strategy for the reconstruction, growth and development of the construction industry. The CIDB Regulations, adopted in 2004, provide a framework for grading contractors in terms of their capabilities and the volume/nature of the projects they can undertake.

Initially, the grade of a contractor was based on two methods, one based on the track record and the other on the available capital. The latter method meant that a contractor could achieve a high grading provided it had available capital, regardless

of its track record. This led to the amendment of the CIDB regulations in 2013 to provide for a ranking framework based on both the track record and available capital. The two criteria, however, seem to be inadequate as the sectors performance is not generally good, as indicated in the CIDB report [3]. The increase in the failure rate of South African infrastructure projects indicates that improved contractor and project management frameworks are needed to support decision makers.

3 Regulation of Entry in Construction Sector

The importance of having robust grading systems and entry requirements in the construction sector to improve the performance of the sector cannot be emphasised enough. It is posited herein that the development of minimum entry requirements for registering a construction firm can assist in improving the construction sector in South Africa. This section considers possible requirements for regulation of new entrants into the construction sector and minimum requirements for progressing to the next grade. The focus of the study is to develop requirements for the Civil Engineering (CE) category. The Construction Industry Development Board (CIDB) has various disciplines under the Civil Engineering category.

Civil Engineering is defined by the CIDB as the construction works primarily concerned with materials such as steel, concrete, earth and rock and their application in the development, extension, installation, maintenance, removal, renovation, alteration, or dismantling of building and engineering infrastructure [12]. It includes water, sewerage, roads, railways, harbours, transport, urban development and municipal services [12].

From the definition, it is evident that civil engineering is very broad. So, it will be practical and safer to adopt subcategories. A contractor who intends to register as a Grade 1 (new entrant) cannot be eligible to do all works of civil engineering. Organisations such as the World Bank and some other countries including Malaysia and Mauritius have also adopted subcategories. This enables contractors to be awarded work which they are capable or rather qualified to execute. The proposed minimum entry requirements for Construction (Roads, Infrastructure and Airfields: Subcategory 01) is as shown in Table 1.

Table 1 indicates the minimum entry requirements of Grade 1 for construction works (Roads, Infrastructure and Airfields: Subcategory 01). Grade 1 is the entry level with the tender value less than or equals to R500 000 (South African Rands). Plant and Equipment are not a requirement for Grade 1 contractors but are, however, a requirement for contractor progression through the grades. Academic qualifications are also considered, and they should be approved by the South African Qualifications Authority (SAQA). Experience of key staff or number of successfully completed projects by the company/key staff is not considered for Grade 1. Table 1 is a typical example of the minimum requirements for entry for civil engineering subcategories/specialisations.

Table 1 Grade 1 entry requirements for construction works (adapted from [13])

Civil engineering works—subcategory 01: construction (roads, infrastructure and airfields)								
Grade	Tender value not exceeding	Plant and equipment		Financial status	Qualifications of key staff			Experience of the company or key staff
		Equipment type	Minimum quantity		Academic qualifications	No of key staff	Relevant experience of key staff	Number of projects successfully completed by the company or key staff
1	R500 000	None	None	Bank account	Certificate in highway engineering or roads technician certificate	1	None	None

All subcategories/specialisations have similar minimum entry requirements. The difference in the Grade 1 requirements is in the academic qualifications which are indicated in Table 2 for all subcategories. Contractors who wish to work in the civil engineering industry must have a certificate in a specific area as depicted in Table 2.

The certificate should be equivalent to National Qualification Framework (NQF) Level 4 and the qualification should be approved by the South African Qualifications Authority. This will ensure that contractors who wish to enter the construction sector have adequate knowledge of the sector which they wish to enter. It is expected that the introduction of this measure will also assist in minimising business failure rate of Grade 1 contractors as indicated by CIDB [8].

For progression through the grades, minimum entry requirements will be considered which includes technical capacity, experience, plant and equipment, financial status and past performance. Over and above the stipulated minimum requirements contractors would be encouraged to acquire training to attain Contractor Continuous Development (CCD) Points. Table 2 depicts the minimum entry requirements for contractor registration.

The suggested Contractor Continuous Development Points for different grades and renewal periods are shown in Table 3. The CCD points would be required for approval of an application to renew the registration certificate. Only CCD points obtained by the company owner, director or full-time employees or certificates held by the company may be considered. Contractors would be encouraged to stay abreast of development in the construction and the business sectors.

Table 2 Sub-categories and academic qualifications for civil engineering (adapted from [13])

Subcategories	Academic qualifications
Construction (roads, infrastructure and airfields: subcategory 01)	Certificate in highway engineering or roads technician certificate
Railways—subcategory 02	Certificate in highway engineering or roads technician certificate and certificate in civil/water engineering
Dams—subcategory 03	Certificate in civil/water engineering
Road surfacing—subcategory 04	Certificate in highway or roads technician certificate
Bridges—subcategory 05	Certificate in civil engineering
Water supplies, sanitation, reticulation and irrigation works—subcategory 06	Certificate in civil/water engineering
Water and sewerage treatment plant works—subcategory 07	Certificate in civil/water engineering and certificate in mechanical engineering
Water engineering works—subcategory 08	Certificate in mechanical engineering and certificate in water/structural/civil engineering
Specialised construction work—subcategory 09	Diploma in civil/structural engineering
Drilling works—subcategory 10	Any trade across all built environment disciplines
Roads ancillary works—subcategory 11	Certificate in civil engineering

Table 3 Required contractors' continuous development points for the renewal of registration (adapted from [14])

Grades	Minimum points for renewal periods indicated		
	1 year	2 years	3 years
1–3	10	20	30
4–6	20	40	60
7–8	30	60	90
9	40	80	120

Table 4 Contractor grading and registration requirements

Criteria	Requirements
Grade	Each contractor is registered within a grade according to the contractor's capability to fulfil the criteria for such. The grade limits the contractor to participate in tenders or to carry out work for certain values
Category	A contractor can be registered in the civil engineering, construction of buildings (i.e. general buildings), mechanical engineering and electrical engineering categories
Specialisation	Each specialisation is registered under a category and grade in the contractor registration certificate. For civil engineering, the specialisation falls within one of the subcategories indicated above
Classification level	For contractor status, applicants must attach information on the projects they have carried out with a valid certificate in the latest three (3) year period. The status should indicate whether contractors are active/dormant within the last three-year period or if they are new contractors. Moreover, the Broad-Based Black Economic Empowerment (BBBEE) level should also be indicated

It is thus important for contractors to be registered in line with the requirements which are depicted in Table 4.

Presently, the CIDB does not distinguish between local and international contractors. An international contractor is a local contractor registered with CIDB and will carry out or has carried out construction work abroad. Applicants must be registered with CIDB for at least 3 years, have active status and comply with Broad-Based Black Economic Empowerment Act 53 of 2003 [15]. International/foreign qualifications will need to be SAQA approved.

4 Discussion

As indicated, presently, the construction sector in South Africa does not have a minimal requirement for contractors who wish to enter the construction industry. Anyone with or without technical knowledge can register a construction firm. It is posited herein that the development of a minimal entry requirement for registering a construction firm can assist in improving the status quo of the construction sector in

South Africa. The aim of developing the minimum requirement is not to restrict entry into the construction sector but to rather manage the sectors entrants to ensure that people with the relevant skills and knowledge with a minimal probability of failing enter the sector.

Having such requirements would likely increase the success rate of Grade 1 contractors and would also make it easier for companies seeking to develop enterprises to select entities with potential [8]. Any minimum criteria for the registration would, however, need to consider the currently registered Grade 1 contractors. The high representation of historically disadvantaged individuals, women and youth amongst Grade 1 contractors highlights the importance of this category as a route in transformation of the construction industry [8].

The manner in which contractors enters the construction sector in South Africa needs to be regulated to enhance the sectors performance at the same time not hamper new entrants. This should be done in line with what literature suggests that regulation of entry can be good, but it needs to be well managed to enable new entrants in the sector [16, 17]. In South Africa, the Construction Industry and Development Board (CIDB) stipulates that all contractors who intend to bid for or participate in tenders in the South African public sector need to be registered with the CIDB [10]. There are no technical requirements that new business entrants need to adhere to in order to be registered with the CIDB. Whilst progression through the grades only requires contractors to be financially viable and proof of completed projects. The lack of the sectors adequate regulation is quite alarming as regulation can assist to improve the sectors performance and possibly save lives since majority of the construction works is utilised by the public. The proposed framework will assist in improving the sectors performance.

5 Conclusions

This paper investigated minimum entry requirements that could be adopted by the South African construction sector. This was done by looking at how countries worldwide regulate new entrants into the construction sector. The aim is to manage the influx of construction sector new entrants in order to ensure that only those with the relevant skills and experience enter the sector. These entry requirements may assist in improving the South African construction sector performance. The management of the sector should, however, not prohibit new entrants unduly. The requirements for the new entrants consider the contractors' technical qualification in the registered speciality/subcategory. Other requirements such as experience, relevant plant and equipment and completed projects are self-evidently not emphasised or prioritised as new entrants would likely have less experience and capital.

Another key factor that is considered is the contractor continuous development points. This is critical for consideration of contractors' progression as contractors need to stay abreast with development in their field and expand business knowledge

to decrease failure rates of the business. The requirements of entry for international firms have also been touched on. The requirements for international firms are currently not considered explicitly by the South African CIDB.

References

1. Alzahrani JI, Emsley MW (2013) The impact of contractors' attributes on construction project success: a post construction evaluation. Int J Project Manage 31(2):313–322
2. Abiodun OE, Segbenu NS, Oluseye O (2017) Factors affecting contractors performance in construction project delivery in Akure, Ondo State, Nigeria. J Knowl Manage 6(4):1–23
3. Construction Industry Development Board (2011) Construction quality in SA: a client perspective. Construction Industry Development Board, Pretoria, South Africa
4. Cheung SO, Suen HCH, Cheung KKW (2004) PPMS: a web-based construction project performance monitoring system. Autom Constr 13(3):361–376
5. Mohlala FT (2015) The relationship between project performance of emerging contractors in government infrastructure projects and their experience and technical qualifications: an analysis of 30 projects conducted in the Mpumalanga Province over the 2011–2013 period. Masters dissertation, University of Witwatersrand, Johannesburg
6. Republic of South Africa (2000) Construction Industry Development Board Act No 38 of 2000
7. Construction Industry Development Board (2016) National stakeholder forum report. http://www.cidb.org.za/Events/Documents/cidb%20NSF%20Report%20%20%2029%20March%202016.pdf. Accessed 05 July 2019
8. Construction Industry Development Board (2016) Study of grade 1 contractors. http://www.cidb.org.za/publications/Documents/Study%20of%20Grade%201%20Contractors%20Report.pdf. Accessed 10 Oct 2019
9. Forth J (2019) The impact of entry regulations on business growth. City Research Online, City University, London. http://openaccess.city.ac.uk/22413/. Accessed 01 Feb 2020
10. Construction Industry Development Board (CIDB) (2011) Guidelines for contractor registration. http://www.cidb.org.za/documents/kc/cidb_publications/brochures/brochure_contractor_registration_guidelines.pdf. Accessed 30 Sept 2018
11. Construction Industry Development Board (CIDB) (2013) 2012/2013 Annual report. Construction Industry Development Bank, Pretoria, South Africa
12. Construction Industry Development Board (2017) Comprehensive guide to contractor registration: version 6. http://www.cidb.org.za/publications/Documents/Comprehensive%20Guide%20to%20Contractor%20Registration.pdf. Accessed 22 Jan 2020
13. World Bank (2018) The minimum requirements for registration of works contractors. http://www.ppadb.co.bw/Manuals%20%20Acts/Minimum%20Requirements%20for%20registration%20of%20Works%20Contractors%20Rev%2002.pdf. Accessed 04 Feb 2020
14. Construction Industry Development Board Malaysia (2016) Contractor registration requirements and procedures handbook: requirements and procedures for contractor registration with the construction industry development board. http://www.cidb.gov.my/images/content/pdf/Kontraktor/CRLTRANSLATION14112016FINAL.pdf. Accessed 04 Feb 2020
15. Republic of South Africa (2003) Broad-Base Black Economic Empowerment Act No 53 of 2003
16. Djankov S, La Porta R, Lopez-de-Silanes F, Shleifer A (2000) The regulation of entry. Q J Econ 117(1):1–37
17. Klapper LF, Laeven L, Rajan RG (2004) Business environment and firm entry: evidence from international data. The World Bank

Benefits of BIM in Reducing Errors in Indian Construction Projects

Divyesh Patel and V. P. S. Nihar Nanyam

Abstract Efficient project delivery is essential in the Indian construction industry. This efficiency can be achieved by reducing errors in construction projects to minimize cost and time. The chances of errors in the designing stage are high, which can lead to construction delays and other claims. BIM (Building Information Modeling) is a technology that can reduce not only human efforts but also the likelihood of errors. BIM is emerging rapidly and transforming the Indian real estate and construction sectors. This study verifies the BIM functionalities that help reduce the design and human errors that occur at various intervals of the project. This study also helps BIM users identify possible errors and their perceived severity, which can occur while working in a construction environment and avoiding these errors by applying BIM functionalities to achieve optimum time and cost. The quantitative technique was difficult to carry out for evaluation. Hence, the qualitative approach for research is carried out based on the perception shared by construction professionals working on the BIM platform. Ineffective design coordination between the design and planning teams, detailing errors, clashing of elements, and lags in most up-to-date information were found to be the most severe errors that affect the project. The analysis explains the seven functionalities that were beneficial in reducing errors. Functionalities with similar natures of reducing errors were clubbed into compound clusters. Although quantity take-off was not very beneficial, it formed a greater number of clusters with other functionalities. Among several functionalities, the natures of the coordination model and work-sharing with a central cloud database were more similar in avoiding chances of errors. More attention is needed on technologies and software that will help reduce such errors. Training on BIM-based software is essential for the Indian construction industry to utilize effective project management systems and reduce claims.

Keywords BIM functionalities · Effective management · Collaboration · Reducing errors

D. Patel (✉) · V. P. S. N. Nanyam
RICS School of Built Environment, Amity University, Noida, India
e-mail: nnanyam@ricssbe.edu.in

B. Laishram and A. Tawalare (eds.), *Recent Advancements in Civil Engineering*, Lecture Notes in Civil Engineering 172,
https://doi.org/10.1007/978-981-16-4396-5_3

1 Introduction

In the present-day construction industry, delays are very common and lead to increases in time and cost. These delays are generally caused due to various kinds of errors such as human errors, design errors, technology errors, communication errors, and social errors, all of which occur during different phases of the construction projects. BIM (Building Information Modeling) is a platform that reduces not only our efforts but also the likelihood of errors. It provides us with a prototype that connects technology with the people and the process to efficiently deliver the project within the built environment [1]. Most of the research conducted is on the errors that occur in a construction project, how they arise, and the time and cost factors associated with them. Most of the research highlights the benefits of BIM in different phases of construction, along with the barriers in adopting BIM. The commonly used technology interfaces on-site are design software, structural software, spreadsheets such as MS Excel and project management software such as MS Project. These interfaces regulate and monitor daily activities which still lead to delays and errors. The authors tried to analyze using regression analysis the BIM functionalities which are beneficial in reducing errors in a construction project. The research will put forward the benefits of BIM in reducing the errors in the Indian construction sector. The sub-objectives of the study are as follows: To identify the most obvious errors that occur in a project and their possibilities of occurrence, to identify the BIM functionalities that help reduce the errors, to determine their severity index, to check the hypothesis and cluster similar functionality and arrive at compound clusters.

2 Errors in a Construction Project

If we take any project from the past, we will find that errors can occur at any stage of the construction lifecycle. Reducing the occurrence of these errors is the major issue faced by construction professionals in India. McDonald defines an error as an accidental deviation from correct practices which can lead to an increase in budgeted cost and schedule overruns, which are both inconvenient and preventable [2]. According to Ganesh, defects and rework are major contributors to decreasing the quality of a project [3]. This can be avoided with BIM technology where rework is minimized at the design stage itself. Poor management and supervision also lead to construction and management errors which ultimately lead to cost overrun. The cost overrun has greater risk which may lead to liquidation from both the contractor and client. The goals of construction projects like budget, quality, performance, and completion of projects on time are exaggerated by success factors [4]. The errors can lead to cost overrun and rework, so, understanding the benefits of BIM at various levels of the project lifecycle remains a top priority. But no researcher has brought together the ways of reducing errors with the help of BIM in the

Table 1 List of identified errors

Errors	References
Wrong estimates of quantities	[5]
Faults due to incorrect/incomplete information and omission in design (element in design is missing)	[5]
Complexity of drawing leading to errors	[5]
Clashing of elements/variation in alignment between two elements	[6]
Ineffective design coordination between design and planning team	[7]
Interoperability issues leading to errors	[8]
Errors due to lack of visualization feature at different condition	[9]
Changes in drawing leading to reworks	[5]
Detailing errors in fabrication	[9]
Lag in most up-to-date information/loss of data lead to errors	[5]

construction lifecycle. Table 1 shows the list of identified errors with their references (Refer with: Table 1).

3 Benefits of BIM in the Indian Context

Error prevention is not solely focused on the aspect of design but also the aspects of audits, error management, training and review, and verification. The major difficulties are different ideologies on BIM platform, interoperability issues, lack of demand, and lack of knowledge of BIM or training for BIM users, but the organizations in general have shifted focus to sharing and providing the BIM knowledge among stakeholders [10]. The coordination model through BIM curtails the risks and errors arising during the construction lifecycle of the project [11]. BIM could help reduce the construction time and even the spending on operations as well as the overhead cost of the entire project [12]. Wong et al. conducted a survey that helped them collect quantitative data for statistical analysis, in which they identified 7 important factors that can influence design error and formed a conceptual framework for design error reduction (DER) model via BIM. Further, they conducted a VIF test for multicollinearity among independent variables, tested for reliability using Cronbach's coefficient alpha, and finally analyzed data with multiple regression analysis to form a regression equation. The study helped find the most beneficial BIM factor to reduce design error [13]. Human error can be reduced with the help of a system that focuses on perceived behavior and working during the overall project life cycle [14]. The development of strategic planning for the implementation of BIM depends on the characteristics and peculiarities of each industry, company, and project [15]. BIM significantly improves the performance of projects by using innovation in tools and strategic processes of information and detailing [14]. If the BIM experts and design team work with standard formats such

as RICS NRM cost plan, RIBA stages, and ICMS standards, confusion can be avoided for further processing of post-construction stages. Reducing change orders versions of the supervising engineer consultant, especially those undocumented by the entrepreneurs of the administration, leads to financial and extension of time claims from the contractor [16]. The project team can utilize BIM technology which helps reduce cost, increase profitability, improvise execution process, and enhance client/customer relationships [17]. The project manager should identify and analyze all types of risks and try to develop a system of control and monitor design change, scope change, and design errors by stakeholders in order to reduce rework [2]. When all users work as a team, they look for and find faults in each other's contributions [17]. BIM can contribute to substantial savings by enhancing the quality of the project environment and allowing the organization to make expected outcomes that lead to the growth of the company [1]. Project strategy and organization strategy should align together to reduce the chances of accidents, errors, and negligence during construction [14]. Teams implementing BIM should be very careful about the legal consequences such as data protection and associated propriety issues and risk sharing [17]. Table 2 shows the list of BIM functionalities identified from different sources (Refer with: Table 2).

4 Methodology

The research was carried out in two phases. The first phase involves a literature review of various journal and conference articles. In the second phase, a questionnaire was developed using the various problems identified. The questionnaire was divided into three parts. The first part collected the ground information about the respondents, the second part contained questions about the probability of errors, and the last part was on the benefits of BIM in reducing errors. The responses for the questionnaire were collected using email invitations, online surveys, LinkedIn invitations, and during personal visits. A total of 60 responses were received from

Table 2 List of BIM functionalities

BIM functionalities	References
Coordination model for clash detection and interference check	[18]
Fabrication modeling and documentation	[6]
3D parametric modeling (structural, architectural, MEP and construction)	[19]
Interoperability and IFC (industry foundation class)	[20]
Detailed documentation	[21]
3D design visualization and simulation	[22]
Quantity take off (QTO)	[22]
4D scheduling	[23]
Work-sharing with central cloud project database	[22]

experienced and inexperienced BIM users, out of which 49 were considered valid owing to complete *i*. Among these 49 respondents, 23 had less than 5 years of experience, 17 had more than 5 years but less than 10 years of experience, and 9 had more than 10 years of experience. The market survey for identifying the most probable errors was conducted to help the authors meet the objective of making a severity index of errors which was referred from method given by Farrokh Almei, a Ph.D. scholar [24]. The respondents could mark the probability of error on a scale of 1–5, with 1 being the least probable and 5 with the highest probability. The BIM functionality was identified from the Autodesk website which helped complete the analysis of data using a chi-square test for hypothesis testing and cluster analysis to identify homogeneous groups of functionalities that reduce errors. The respondents were allowed to grade the benefits of reducing errors by individual benefit on a scale of 1–5, where 1 meant the least effective and 5 meant the most effective. The third objective was achieved by conducting a regression analysis of the responses floated through the questionnaire survey and utilizing the regression coefficient for further analysis of the severity of errors. The fourth objective was achieved by performing a chi-square test to arrive at the beneficial functionalities that can reduce errors. The chi-square goodness-for-fit test is a hypothesis test for checking whether a variable behaves in a certain manner or not. The fifth objective of gauging similarity in the nature of the functionalities that can reduce errors was done using cluster analysis. This also helped identify compound clusters formed within the mentioned functionalities.

5 Data Analysis

The data collected from the survey provides the probabilities of occurrences of such errors which was used as input for regression analysis using SPSS software. The responses for the question "Have you worked on the BIM platform?" were selected as the independent factor (*Y*), while all the responses for the probability of occurrence of individual errors (10 errors in total) were taken as the dependent variables (*X*). Multiple regression analysis was performed under IBM SPSS statistics which generate regression coefficients. Now, using the regression coefficients of individual errors, the severity of each respective error was calculated.

5.1 Severity Index of Errors

Considering the highest value of the regression coefficient *r* to be 1 and the lowest value to be 0, the severity of each error was calculated using the following formula. For example, *r* for the error of clashing of elements is 0.0943, and severity was calculated as $(0.0943 - (-0.0792))/(0.1095 - (-0.0792))$ which is equal to 0.919

(Refer with: Eq. 1). Similarly, all severity is calculated and the ranking function was used in excel to find the ranking order.

$$\text{Severity} = (\text{Coefficient} - \text{Min. of range})/(\text{Max. of range} - \text{Min. of range}). \quad (1)$$

The severity index (Refer with: Table 3) shows that there are five severe errors, namely, ineffective design coordination between the design and planning teams, clashing of elements/variation in alignment between two elements, lags in most up-to-date information/loss of data leading to errors, detailing errors in fabrication drawings and improper management of documents which affect the project highly. The rest of the five errors are less severe and have fewer chances of bringing about variations in cost.

5.2 Chi-Square Goodness-for-Fit Test

A chi-square test is a statistical-hypothetical test where the distribution of the test statistic is a chi-square distribution when the null hypothesis is true [25]. Friedrich Robert Helmert first introduced the chi-square statistical test. "The chi-square test is a useful test for goodness of fit of an observed distribution with the theoretical

Table 3 Severity index table (Author's compilation)

S. No.	List of errors	*R* coefficients	Severity	Rank	
1	Wrong estimates of quantities	−0.0791	0	1	
2	Complexity of drawing leading to errors	−0.0013	0.4125	4	
3	Clashing of elements/variation in alignment between two elements	0.0942	0.9193	9	High
4	Detailing errors in fabrication drawings	0.0671	0.7757	7	High
5	Ineffective design coordination between design and planning team	0.1094	1	10	High
6	Errors due to lack of 3D visualization feature	−0.0348	0.2349	3	
7	Faults due to incorrect/incomplete information and omission in design (element in design is missing)	−0.0784	0.0039	2	
8	Lag in most up-to-date information/loss of data lead to errors	0.0787	0.8371	8	High
9	Interoperability issues leading to design errors	−0.0010	0.4141	5	
10	Improper management of documents	0.0344	0.6024	6	High

distribution, and in qualitative data to test the 'independence' of two criteria of classification" [25].

The following are the null hypothesis (H_0) and the alternative hypothesis (H_a) that were considered: H_0 = BIM functionality is helpful in reducing the errors; H_a = BIM functionality is not helpful in reducing the errors. Table 4 presents information on the null hypothesis and the alternative hypothesis for the identified BIM functionality (Refer with: Table 4). All nine benefits were taken as input data for analysis with considering expected values for very high, high, medium, low, very low choice as 20%, 60%, 10%, 5%, and 5% respectively. After analyzing the data in IBM, SPSS analysis software, test statistics Table 5 was generated.

Table 4 BIM functionality with null hypothesis and alternative hypothesis

BIM benefits	Identification	H_0	H_a
Coordination model for clash detection and interference check	F1	If F1 is beneficial to reduce errors	If F1 is not beneficial to reduce errors
Fabrication modeling and documentation	F2	If F2 is beneficial to reduce errors	If F2 is not beneficial to reduce errors
3D parametric modeling	F3	If F3 is beneficial to reduce errors	If F3 is not beneficial to reduce errors
Interoperability and IFC	F4	If F4 is beneficial to reduce errors	If F4 is not beneficial to reduce errors
Detailed documentation	F5	If F5 is beneficial to reduce errors	If F5 is not beneficial to reduce errors
3D design visualization and simulation	F6	If F6 is beneficial to reduce errors	If F6 is not beneficial to reduce errors
Quantity take off (QTO)	F7	If F7 is beneficial to reduce errors	If F7 is not beneficial to reduce errors
4D scheduling	F8	If F8 is beneficial to reduce errors	If F8 is not beneficial to reduce errors
Work-sharing with central cloud project database	F9	If F9 is beneficial to reduce errors	If F9 is not beneficial to reduce errors

Table 5 Chi-square test output on SPSS

Test statistics									
Identification	F7	F3	F6	F9	F1	F8	F4	F2	F5
Chi-Square	8.041[a]	9.503[a]	13.597[b]	4.367[a]	44.095[a]	10.626[a]	12.837[a]	6.510[a]	14.708[b]
Df	4	4	4	4	4	4	4	4	4
Asymp. Sig. (*p* value)	0.090	0.050	0.009	0.359	0.000	0.031	0.012	0.164	0.005

[a]3 cells (60.0%) have expected frequencies less than 5. The minimum expected cell frequency is 2.5
[b]3 cells (60.0%) have expected frequencies less than 5. The minimum expected cell frequency is 2.4

5.3 *Cluster Analysis*

Cluster analysis is dividing the data into groups which are useful or meaningful or both, based on their characteristics [26]. The most common method is hierarchical clustering. It generates a series of cluster groups with cluster solutions from 1 to *n*. The software generated coefficients show the distance in similarity as coefficients (Refer with: Table 6). The dendrogram so formed graphically shows the clusters merged and helps identify the number of clusters that have a similarity. The authors used the single linkage method for forming the dendrogram.

The first cluster was formed between work-sharing with a central cloud project database and coordination model for clash detection and interference check, as they have a similarity in reducing errors (Refer with: Fig. 1). The second cluster was formed between fabrication modeling and documentation and work-sharing with the central cloud project database. The third cluster was formed between 3D parametric modeling structure and 3D visualization and simulation. The fourth cluster was formed between 3D visualization and simulation and work-sharing with the central cloud project database. The fifth cluster was formed between QTO and 4D scheduling. The sixth cluster was formed between 4D scheduling and 3D

Table 6 Agglomeration table with coefficients using SPSS software

Agglomeration schedule						
Stage	Cluster combined		Coefficients	Stage cluster first appears		Next stage
	Cluster 1	Cluster 2		Cluster 1	Cluster 2	
1	4	5	0.071	0	0	2
2	4	8	0.088	1	0	4
3	2	3	0.097	0	0	4
4	2	4	0.097	3	2	6
5	1	6	0.105	0	0	6
6	1	2	0.108	5	4	7
7	1	7	0.108	6	0	8
8	1	9	0.110	7	0	0

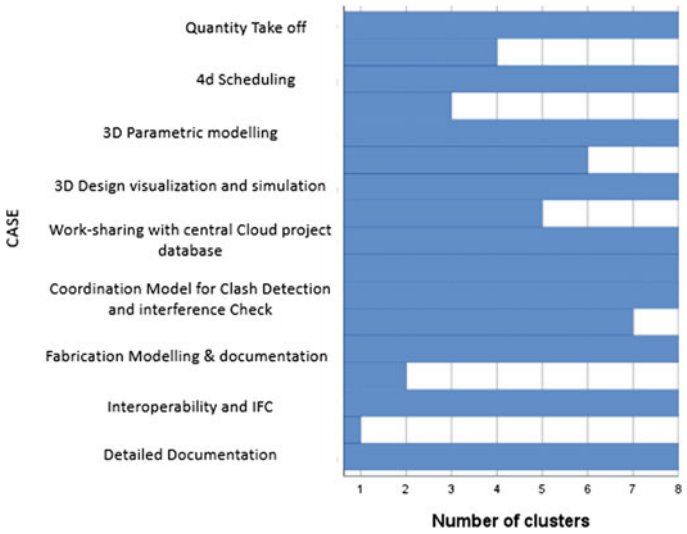

Fig. 1 Number of clusters versus functionality graph (generated from SPSS)

parametric modeling structure. The seventh cluster was formed between fabrication modeling and structure and Interoperability and IFC (Industry Foundation Class). The eighth cluster was formed between detailed documentation and fabrication modeling and documentation.

According to Marielle Caccam and Jewel Refran, "The single linkage method defines the similarity between clusters as the shortest distance from any object in one cluster to any object in the other." It is also known as group linkage.

The first stage shows (Refer with: Table 6) cluster formation between coordination model for clash detection and interference check (4) and work-sharing with central cloud project database (5) as they are more similar in nature. The cluster created (Refer with: Fig. 2) by joining these two appears in the next stage. The second stage shows cluster formation between work-sharing with central cloud project database (5) and Fabrication modeling and documentation (8). The cluster created joining these two appears in stage 4. The third stage shows cluster formation between 3D parametric model structure (2) and 3D visualization and simulation (3). This cluster has a nature similar to the stage 2 cluster which forms a compound cluster. These two, on joining further, appear in stage 4. The fourth stage is the cluster formation of stage 2 and stage 3 clusters which are work-sharing with central cloud project database and Fabrication modeling and documentation along with 3D parametric model structure and 3D visualization and simulation respectively. This further contributes to stage 6. The fifth stage is the cluster formed between quantity take-off (1) and 4D scheduling (6). The sixth stage is cluster formation between stage 1 and stage 2 clusters which possess attributes such are coordination model for clash detection and interference check, work-sharing with central cloud project

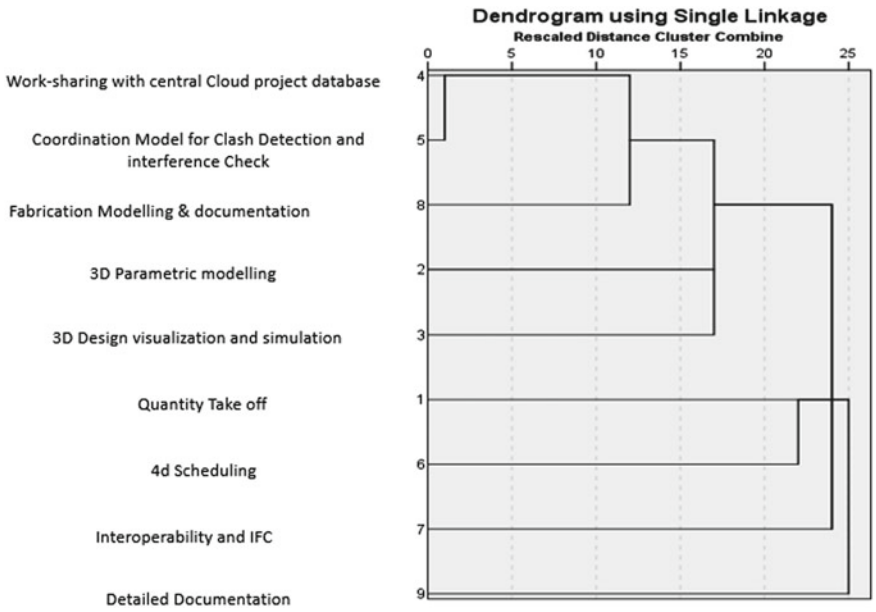

Fig. 2 Dendrogram of functionality (generated from SPSS)

database, work-sharing with central cloud project database, and fabrication modeling and documentation.

This further contributes to the cluster formation of stage 5. The seventh stage is cluster formation of interoperability and IFC (7) and quantity take off (QTO) (1). The eighth stage is cluster formation between QTO (1) and detailed documentation (9).

6 Conclusion

The research concludes that out of ten identified errors, there are five severe errors, i.e., ineffective design coordination between the design and planning teams, clashing of elements/variation in the alignment of two elements, lags in most up-to-date information/loss of data leading to errors, detailing errors in fabrication drawings and improper management of documents which affect the project highly. Other errors were less severe and least affected the project. BIM is the technology that helps project participants reduce their efforts for any project. The chi-square test concludes that null hypothesis of the BIM functionalities like coordination model for clash detection and interference check, 3D parametric modeling (structural, architectural, Mechanical, Electrical, and Plumbing MEP and constructional), interoperability and IFC, detailed documentation, 3D visualization and simulation, and 4D scheduling are accepted i.e., beneficial in reducing the errors in a

construction project in the Indian Construction sector. QTO, fabrication modeling and documentation, and work sharing with the central cloud database are not beneficial in reducing errors as their null hypothesis was rejected. The cluster analysis through the dendrogram concludes that there was a total of 8 cluster formations and several compound-cluster formations. The functionality QTO forms the highest number of clusters i.e., 4 with 4D scheduling, interoperability and IFC, detailed documentation, and 3D parametric modeling structure. The first stage cluster formation explains that work-sharing and the coordination model share strong similar nature in reducing errors than others. The eighth stage formation of the cluster shows that QTO and detailed documentation have weak nature of similarity and are farthest in sharing similar bonds or reducing errors. The first compound cluster formed between the first stage cluster and fabrication modeling and documentation. This research is just the perceptions of people who responded to the survey and is restricted to the Indian construction sector. The output may vary from project to project and people to people as the mindsets regarding BIM and other software of different types of project participants will be different. Further correlation analysis between errors and benefits can be performed to identify which BIM functionality is more effective in reducing errors. More focus is needed on technology and software that will help reduce such risks and errors. Training and education on BIM-based software are essential for the Indian construction industry to entertain effective project management systems and reduce claims.

References

1. Sawhney A, Kapoor S, Kamthan N, Agarwal PB, Jain S (2014) BIM adoption and outlook in India. Amity University, Noida, India, RICS School of Built Environment
2. McDonald R (2013) Root causes & consequential cost of rework. North America Construction, xlcatlin, New York
3. Ganesh MS (2016) Technology poor quality in building projects. Int J Eng Sci Res Technol 5(7)
4. Shibani A, Arumugam K (2015) Avoiding cost overruns in construction projects in India. Manage Stud 3(7–8):192–202. https://doi.org/10.17265/2328-2185/2015.0708.003
5. Cindrela Devi A, Ananthanarayanan K (2017) Factors influencing cost over-run in Indian construction projects. MATEC Web Conf 120:02023. https://doi.org/10.1051/matecconf/201712002023
6. Tommelein I, Gholami S (2012) Root causes of clashes in building information models. In: 20th conference of the international group for lean construction
7. Riley D, Horman M (2001) The effects of design coordination on project uncertainty. Computer Science
8. Pniewski V (2011) Building information modeling (BIM) interoperability issues in light of interdisciplinary collaboration. Collaborative Modeling Ltd., London, United Kingdom
9. Dai F, Feng Y, Hough R (2014) Photogrammetric error sources and impacts on modeling and surveying in construction engineering applications. Vis Eng 2:2. https://doi.org/10.1186/2213-7459-2-2
10. Evuri GS, Amiri-Arshad N. A study on risks and benefits of building information modeling (BIM) in a construction organization. Bachelor of Science Thesis in 'Software Engineering and Management', 15

11. Doumbouya L, Gao G, Guan C (2016) Adoption of the building information modeling (BIM) for construction project effectiveness: the review of BIM benefits. Am J Civil Eng Arch 4(3):74–79
12. Yan H, Damian P (2008) Benefits and barriers of building information modelling. In 12th International conference on computing in civil and building engineering, vol 161
13. Wong JKW, Zhou JX, Chan APC (2018) Exploring the linkages between the adoption of BIM and design error reduction. Int J Sustain Dev Plan 13(1):108–120. https://doi.org/10.2495/SDP-V13-N1-108-120
14. Love PED, Edwards DJ, Han S et al (2011) Design error reduction: toward the effective utilization of building information modelling. Res Eng Des 22:173–187. https://doi.org/10.1007/s00163-011-0105-x
15. Neto JP (2016) Approach for BIM implementation: a vision for the building industry. In: 24th Annual conference of the international group for lean construction, no 1, pp 143–152
16. Abdulnabi ERHR, Agarwal VC (2016) Claims in construction projects design errors and change orders. Int J Civil Eng Technol 7(6):123–130. http://www.iaeme.com/IJCIET/issues.asp?JType=IJCIET&VType=7&IType=6
17. Azhar S, Hein MF, Sketo BS (2008) Building information modelling (BIM): benefits, risks and challenges. McWhorter School of Building Science, pp 1–10
18. Autodesk Help (2014) About coordination model. https://knowledge.autodesk.com/support/revit-products/learn-explore/caas/CloudHelp/cloudhelp/2018/ENU/Revit-Collaborate/files/GUID-A5B877B0-F587-43F1-94C8-550CBBCB8A90-htm.html
19. Autodesk Help (2017) About parametric modeling relationships. https://knowledge.autodesk.com/support/revit-products/getting-started/caas/CloudHelp/cloudhelp/2018/ENU/Revit-GetStarted/files/GUID-71F2C8EE-2A90-4076-A6C7-702082566DDF-htm.html
20. Autodesk Help (2017) About IFC. https://knowledge.autodesk.com/support/revit-products/learn-explore/caas/CloudHelp/cloudhelp/2018/ENU/Revit-DocumentPresent/files/GUID-0D546BEA-6F88-4D4E-BDC1-26274C4E98AC-htm.html
21. Majenta Solutions (2018) BIM documentation. https://bim.majentasolutions.com/bim-services/bim-documentation/
22. Autodesk, Revit (2018) Whats new on Revit. https://www.autodesk.com/campaigns/whats-new
23. Autodesk, Revit (2017) https://www.autodesk.in/products/revit-family/overview?referrer=%2Fproducts%2Frevit-family%2Foverview
24. Development of Severity Index (2009) [Film] Directed by Farrokh Alemi. s.l.: Youtube
25. Research Optimus (2016) What is chi-square test? https://www.researchoptimus.com/article/what-is-chi-square.php
26. Statistics Solutions (2018) Conduct and interpret a cluster analysis. http://www.statisticssolutions.com/cluster-analysis-2/

Stakeholder Management in Public–Private–Partnership Projects: A Review

Rakhee Das, L. Boeing Singh, and Mohammad Jawed

Abstract Involvement of stakeholders in various infrastructure projects is encouraged by governments all over the globe. It tends to bring in openness, transparency, and accountability in a project to attain its continuing goals for benefit of the community. The Indian Government in its 12th Five Year Plan has introduced the concept of public–private–people partnership (PPPP) in order to involve people in different stages of an infrastructure project. In current PPP model, the interaction and engagement is among the public and private agency, and this model fails to involve people within the governance structure of the project (people here refers to the public who are not generally involved in the project, whereas stakeholders refer to the group of people who are involved in the actual construction project). The current PPP procurement process clearly identifies how public agency will interact and engage private sector in various phases of PPP projects but fail to involve people in it. In order to successfully adopt PPPPs, the procurement process needs to be clear on how to engage the public in various phases of the project lifecycle. One of the mechanisms to streamline the public participation in PPP projects would be to adopt strategies to encourage public participation placed on the principles of stakeholder management. Stakeholder management is about managing the relationships between the organization and its stakeholders. Involvement of public in PPP projects will require integration of stakeholder management process in individual phase of the project lifecycle such as in project identification, design and tendering, construction, and project implementation stage by adopting various means of tools and techniques.

R. Das (✉)
Department of Civil Engineering, National Institute of Technology, Rourkela, India
e-mail: dasr@nitrkl.ac.in

L. B. Singh · M. Jawed
Department of Civil Engineering, Indian Institute of Technology Guwahati, Guwahati, India
e-mail: boeing@iitg.ac.in

M. Jawed
e-mail: jawed@iitg.ac.in

B. Laishram and A. Tawalare (eds.), *Recent Advancements in Civil Engineering*, Lecture Notes in Civil Engineering 172,
https://doi.org/10.1007/978-981-16-4396-5_4

Keywords PPP · PPPP · Stakeholder · Stakeholder management · Project lifecycle

1 Introduction

Rapidly growing urban population has directed to the problem of insufficiency of basic urban services. Insufficiency of these services had led to decline in quality of life of people in the urban areas. This is mainly affected due to non-availability of infrastructure services and also the growing rate of current infrastructure facilities are not enough to cope with growing urbanization [29, 43]. The government is, thus, facing pressure to expand and improve public facilities. Hence, they came up with public–private partnership (PPP) as a solution to tackle its shortcomings. PPP is a contractual agreement between a government organization and a private party for arranging a service, where the management and risk part of the responsibility is borne by the private party [50, 59]. Private sectors were invited to enter into contractual agreements with the government for construction or management, operation and management, and providing facilities or services. PPPs have become a regular practice of government services since 1980s in managing these facilities all over the world across various infrastructure facilities including road construction, telecommunication, hospitals, schools, and universities [12, 21, 35, 63]. This transfer of ownership has offered solution for the failures of public ownership and brought improved outcomes on management and performance of infrastructure service facilities [54]. International lending agencies are constantly urging the developing countries to incorporate private sector in water reforms. Although widespread of private sector participation (PSP) is much supported in Latin America, it is still rare in India [33, 34]. However, the National Water Policy, 2002, of the Government of India has encouraged PSP in water resources [41, 60]. The private sector involvement was aimed to bring about financial assistance to support projects, efficiency in service delivery, connecting poor households, better management, and advanced technology [1, 20, 42, 58].

On the contrary, it has been argued that the introduction of PPP in infrastructure projects in many countries has led to increase in price of services and decrease in consumer participation. Many literatures reveal that private sector in order to maximize profit neglect the poor/LIG section of society in providing services [1, 15, 19, 27, 37, 55–57, 64]. PPP basically in water sector in many countries has led to increase in price of services and decrease in consumer participation. Privatization has not improved access in water sector and its equitable distribution of resources [36]. In Cochabamba, Bolivia, a private entity was awarded 40-year concession, but five months later, the population agitated against the increase in water tariff and the contract has to be annulled [10, 40, 45]. Many countries like Ecuador, Paraguay, Rio de Janeiro, and Lima have recently experienced anti-privatization protests against privatization of infrastructure facilities. These anti-privatization demonstrations and street protests by public have led to cancelation of water privatization

projects in these countries [40]. In Nicaragua, the Government passed a law restricting against privatization of any sort of provisions of water services [40, 52]. India attempted for delivering full privatized water supply in build-own-operate-transfer (BOOT) contract was initiated by the New Tirupur Area Development Corporation Limited. Tirupur project has not met with too much opposition against its installation, but now after installation, anti-privatization activists are showing their agitation when the textile producers tried to control the community's water supply [41].

Franceys and Gerlach [17], Jingling et al. [30], and Li et al. [38] have found that effective public participation (PP) is one of the key factors to improve the efficiency of an infrastructure project and to succeed in its comprehensive management. Many developed countries like the U.S.A and the U.K have identified various public participation practices and formulated various methods to achieve them [9]. However, the Indian Government has also taken the initiative to encourage involvement of people in development of infrastructure through PPP projects. In the 12th Five Year Plan of India, the Indian Government has introduced the concept of PPPP to involve people in PPP infrastructure projects. But the five-year plan failed to mention who, where, and when in a PPP project people should be involved. In order to successfully adopt PPPPs, the procurement process is needed to be clear on how to engage the public in various phases of the project lifecycle. This paper discusses on how to involve people and make them play a key role in the implementation of PPPP projects.

2 Typical PPP Procurement Process

The private sector is accountable for carrying out construction, operation, and substantial management of project by bearing certain risks. During the operation phase, the public sector monitors the conduct of the private sector and impose the contract terms. The costs for service is recovered from charges on services used and sometimes recovered from public sector in terms of payments [14]. PPPs help the public sector in achieving the infrastructural service targets in potential cost, quality, and scale. Moreover, PPPs differ from the traditional public sector route and these differences or change requires adjustments in approach and competences of the public sector. The advantages of a typical PPP process are outlined [14] as (i) access finance (ii) attain efficiency using private sector skills (iii) increased transparency (iv) create assets, maintenance throughout operating lifetime, and delivery of a service.

The typical PPP procurement process basically comprises four phases. The phases include project identification, development, procurement, and management [14]. ***Phase 1: Project identification***—In this phase, a PPP project is identified according to the need for infrastructure services and options for achieving those services. This phase ensures that the quality of PPP is increased by identifying and checking the projects. The sponsoring agencies at the conclusion of this phase

identify a project that is suitable for development as a PPP. Further, in Phase 2 the project undergoes more detailed study and preparation. ***Phase 2: PPP decision, project appraisal and clearance***—This phase evaluates the suitability for development of PPPs. After being considered as suitable, the projects are studied in detail and an application is forwarded for clearance to continue procurement [14]. ***Phase 3: Final approval and procurement***—In this phase, the process for procurement begins and the final approval is made. Applications were made for final approval and negotiations with the preferred bidder were carried out and finally technical and financial closure is attained. This phase ensures that the best private sector is selected and given contract to [14]. ***Phase 4: Implementation and monitoring***—This is the longest phase of the PPP life cycle. After selection and contracting with the suitable private sector, the project goes through the construction and operation phases. The private sector constructs and operate the facility, whereas the public sector monitors the functioning of the sector in the contractual period and ensures that the service is delivered to the required agreed standards [14]. Table 1 shows the different phases of typical PPP procurement processes with its respective tools and techniques used with the respective responsibility bearers of the process.

Table 1 PPP process phases with its major functions and responsibility [14]

Phases of PPP process	Functioning of the stages	Tools and techniques to be adopted	Responsibility
Project identification	In accordance with the need for infrastructure services, PPP projects are identified	• PPP financial viability indicator model • PPP family indicator tool • PPP mode validation tool • PPP suitability filter • Readiness filter	Central ministry, urban local body, public sector corporate, PPP cell, project development
PPP decision, project appraisal	Detailed study of suitable PPPs and their application for clearance and procurement	• PPP financial viability indicator model • VFM indicator tool • Readiness filter	Sponsoring authority, PPP agencies, such as a PPP cell or project development agency
Final approval	Negotiations with preferred bidder and the project accepted to technical and financial closure	• PPP financial viability indicator model • Readiness filter • VFM indicator tool	Sponsoring authority, project development agency and external advisors
Implementation and monitoring	Undergoes construction and operation phases. The public sector monitors the functioning of PPP	Readiness check to be sure that the Sponsor is well enough prepared for the contract management role	Contract management team within the sponsor

Further, it has been observed that the involvement of people in the design, implementation, and management of PPP projects is not clearly defined in the current procurement process. The public is being marginalized and they began feeling like they are strangers during the PPP processes, and they are only considered as customers liable for paying tariffs for getting the finished products [16, 23]. Moreover, failing to participate formally in a project, many local people try alternate means of involvement like social mobilization, legal petition, public protest, and agitation [13]. Hence, it is a need for specific legal framework specifying the authority needed to be involved in different phases of a PPP procurement process [49].

3 Stakeholder Management

One of the mechanisms to streamline public participation in PPP projects would be to adopt strategies to encourage public participation based on the principles of stakeholder management. As per the principles of stakeholder management, stakeholders are the groups/individuals that are afflicted or can affect the progress of the project [16, 18]. An organization can be influenced in different ways by the stakeholders having interest in different stakes that may be a cause of major conflict. Therefore, organizations should consider the needs and expectations of stakeholders [8]. Stakeholder management is about managing the relationships between the organization and its stakeholders. It is, therefore, important to maintain support of the groups involved in the project by considering and balancing their related interests [8].

Stakeholder management is normally implemented through the following sequential steps: (i) identification, (ii) analysis, (iii) issues, and (iv) engagement [16]. In stakeholder identification process, the role leaders of government or agency project manager includes stakeholders that have information that cannot be gained otherwise and participants who are important for successful implementation of the project. The process of stakeholder identification is carried out among the participant stakeholders by adopting certain tools/techniques. To successfully employ approaches for handling stakeholders, primary stakeholders (stakeholders without whom a project cannot sustain) are needed to be fully involved in the governance and execution of the project, while the secondary stakeholders (can influence or are influenced by the project) are needed to be actively managed in the project. The prime priority for management focus is given to stakeholders with high impact and importance and the stakeholders with low impact and importance need the least management effort. The tools like power/interest and influence/interest matrix are used to identify the influential stakeholders. After identifying the potential influential stakeholders, the role leaders of the government or project manager identifies the various important issues of the stakeholders. The role leaders of the government/project manager confirm the level of engagement of the stakeholders in different stages of the project along with the preferred form of engagement and

Table 2 Stakeholder management strategies

Stakeholder management strategies	Definition	Tools and techniques to be adopted	References
Stakeholder identification	Identify all stakeholders involved or influenced by the water project	Brainstorming/brain writing/ crawford slip method	[4, 8]
Stakeholder analysis	Identify the most influential stakeholders and their potential threats and cooperation to the project	Brainstorming/brain writing/ crawford slip method to achieve Stakeholder power/ interest and influence/ interest matrix	[8, 51]
Stakeholder issues	Identify the potential interest and concerns of the stakeholders	• Position statements by stakeholders • Press releases, public statement • Survey of stakeholders around typical major issue areas • Stakeholder interview • Single or multi-stakeholder workshop • On-line forums • Moderated blogs	[48]
Stakeholder engagement	Adopt suitable tools for communication with the stakeholders and engagement of stakeholders in different stages of the project	• Meetings • Workshops • Press releases • Multimedia • Customer care center • Website • Notifications	[16, 23]

associated frequency in which the stakeholders are needed to be engaged. Table 2 shows the typical stakeholder management strategies with their tools and techniques to be adopted for implementation purposes.

4 Stakeholder Engagement Strategies for PPP Projects

Involvement of people in PPP projects will require integration of stakeholder management process in each phase of the project lifecycle. Table 3 shows the stakeholder engagement techniques in different PPP procurement phases. In the project identification stage, as part of the project identification and need analysis study, the public authority should try to identify all the stakeholders that will be either influenced by the project or can influence the project. After this, attempt should be made to identify the most influential stakeholders from the list of

Table 3 Stakeholder engagement in different PPP procurement phases

PPP stages	Tools	References
Project identification and conception stage	• Meetings, focus group discussions, problem trees and preference ranking, public hearings, written responses, roving exhibitions, surveys, press, conference, publication, face to face interview • DSS (Decision support system) with 3D animation • Internet-based hall for workshop of meta-synthesis for public participation • Neighborhood transopoly with public participation geographic information systems (PPGIS) • Strategic option development and analysis (SODA) • Web-based public participation geographical information system • Public participation geographic information systems (PPGIS) • GIS-based spatial decision support system (SDSS) on the Internet • Playful public participation	[2, 3, 5–7, 11, 22, 24–26, 31, 32, 38, 39, 44, 46, 47, 61, 62]
Design and tendering stage	• DSS (Decision support system) with 3D animation • Neighborhood transopoly with public participation geographic information systems (PPGIS) • Strategic option development and analysis (SODA)	[7, 38, 39, 44, 53, 61]
Construction stage	• Engage public on issues emerged during the construction which go against social expectation • Public participation geographical systems (PPGIS) and modeling of a project delivery timeline	[31, 47]
Implementation stage	• Capacity-building and training programs to enable stakeholders to acquire the technical skills necessary to participate in effective monitoring	[28, 44]

identified stakeholders and evaluate the threats. The stakeholders are needed to be engaged to share their views to set priorities, objectives, and purpose of the project. Hence, all the information is needed to be disclosed to the stakeholders so that the output could be reviewed and verified. Moreover, for setting project scope, draft development on the project proper notification to the public regarding the project is to be made along with conducting public consultation on the respective matter. This consultation would help in identification of visions and desires for the development of the project as a whole. In this stage of project identification and conception,

stakeholder could be involved through traditional tools like meetings, focus group discussions, problem trees and preference ranking, public hearings, written responses, roving exhibitions, surveys, press, conference, publication, face to face interview. Further some advanced techniques could also be used like (i) DSS (Decision Support System) with 3D animation [26, 39]. This participation technique helps in making own design and insert various parameters in the form of a game. However, a polling system was also developed to get better view of the people at specific issues and sharing the results finally to the people graphically. (ii) Another form of tool for public participation is the Internet-based Hall for Workshop of Meta-synthesis. It combines scientific theory, knowledge and data with specialist's judgment [5, 62] (iii) Neighborhood Transopoly with Public Participation Geographic Information Systems (PPGIS): It is a tool for interactive planning for laymen to understand and participate in community planning in to promoting the integration and unity in communities [7] (iv) 3D visualization framework: Through it, the people can handily obtain both the macro-vision of a project on the global scale and the micro-details on the street scale [61] (v) (Environmental Decision Support Systems (EDSS) with application of Bayesian networks (Bns) [24]: A Bayesian network (Bn), also called a Bayesian belief network, is a type of decision support system based on probability theory. It map out cause-and-effect relationships amid variables and program them to find variables that is likely affecting another (vi) Strategic option development and analysis (SODA): Interview and reason plotting are used to identify individual views on an issue [25] (vii) Web-based public participation geographical information systems [22, 32]: Online participatory systems inform and engage the public and bring them public nearer to a participatory planning system (viii) 4D PPGIS based on Google Earth and Facebook [31]: Aims at visualizing geo-referenced urban activities and support public discussions concerning planning proposals (ix) GIS-based Spatial Decision Support System (SDSS) on the Internet [2, 6]: It allows to access users background information relevant to the problem, access GIS datasets and information about data. This can be identified by the people and help in finding suitable sites. The people can here choose site constraints and weight each of the given factor maps (x) Playful public participation in urban planning [47]: It includes playful features of narrative, walking and moving, sketching, drawing, and games.

In the design and tendering stage, the public should be made aware of the private sector involved and their past project records and operations. Further, public are needed to be made aware on the factors that may have an impact on the design consideration of the project infrastructure. Further, feasible design layout and its alternatives are to be made available to the interested groups or public for discussion against the design criteria. A final public involvement meeting is to be held for discussion and modification for maximum esthetic appeal or convenience [38, 44, 53]. The traditional tools adopted are as brainstorming session, direct discussion, public hearings, district forums, and written responses roving exhibitions and surveys. Besides, these some advanced techniques used in project identification and conception stage could also be used for designing of a project like (i) DSS (Decision Support System) with 3D animation used to make own design feature in the game

system by allowing users to insert various parameters in the design and then saving the design [26, 39] (iii) Neighborhood Transopoly with Public Participation Geographic Information Systems (PPGIS) [7] (iv) 3D visualization framework: Through it the macro and micro vision of project could be obtained on globe and street scale. Public can select available urban planning solution for visual investigation and comparison in a virtual globe-based 3D visualization environment [61].

In the construction phase, engage public on issues emerged during the construction which go against social expectation by briefing about the time and cost of construction by updating developing visualize geo-referenced tool for past, current and future urban activities and support public discussions regarding planning proposals and construction process [31, 47].

Lastly, in the implementation and monitoring stage, there is a need for public participatory monitoring process, and the monitoring reports are to be disclosed publicly. Capacity-building and training programs to enable participatory stakeholders to acquire the technical skills necessary to participate in effective monitoring are to be given prime importance [28, 44].

5 Conclusions

Public opposition has been one of the main reasons for failure of infrastructure projects in several instances due to various factors. The public is being marginalized to be the end-users liable for paying tariffs [16, 23]. Public involvement is being ruled out completely in traditional PPP projects, but the new concept of PPPP has encouraged the involvement of people in these PPP infrastructure projects. Hence, understanding the concepts of stakeholder management and involvement in infrastructure projects is an essential step toward success of a project. This would create a strong feeling of involvement and participation among people. Stakeholder engagement approaches are important factors for involving people in a project. This paper presents a comprehensive way to engage the most critical effort of stakeholder management in a typical PPP procurement process. It uses the typical PPP procurement process and typical stakeholder management strategies to propose and develop the stakeholder engagement approaches. This strategy is particularly useful for water infrastructure with people as deeply influential stakeholders. The presented stakeholder engagement strategy framework brings the public to the center of PPP procurement process to have a stake of their own. By exercising this relatively new approach, there would be a shift in the decision-making power from the policy makers to the people/community. Stakeholder engagement strategy approach can therefore be valuable for public and private sector providers in implementing PPP projects successfully. As it attempts to move more toward people-oriented and supported service production. Further research is to be conducted to establish whether the tools and techniques are appropriate and adequate. However, there is a need to develop a framework for people with differing education level and technical knowledge.

References

1. Bakker K (2007) Trickle down? private sector participation and the pro-poor water supply debate in Jakarta, Indonesia. Geoforum 38(5):855–868
2. Barton J, Plume J, Parolin B (2005) Public participation in a spatial decision support system for public housing. Comput Environ Urban Syst 29(6):630–652
3. Brody SD, Godschalk DR, Burby RJ (2003) Mandating citizen participation in plan making: six strategic planning choices. J Am Plan Assoc 69(3):245–264
4. Bryson JM (2004) What to do when stakeholders matter: stakeholder identification and analysis techniques. Public Manag Rev 6(1):21–53
5. Cao LB, Dai RW (2003) Agent-oriented metasynthetic engineering for decision making. Int J Inf Technol Decis Mak 02(02):197–215
6. Carver S, Evans A, Kingston R, Turton I (2000) Accessing geographical information systems over the world wide web: improving public participation in environmental decision-making. Inf Infrastruct Policy 6(3):157–170
7. Chen R (2011) The applications of neighborhood transopoly in public participation decision making. In: IEEE 19th international conference on geoinformatics, pp 1–5
8. Chinyio E, Olomolaiye P (2009) Construction stakeholder management. Wiley
9. Das R, Jawed M, Laishram B (2018) Development of framework for public consultation in a water supply project. In: Urbanization challenges in emerging economies: energy and water infrastructure; transportation infrastructure; and planning and financing. American Society of Civil Engineers, Reston, VA, pp 90–101
10. Davis J (2005) Private-sector participation in the water and sanitation sector. Annu Rev Environ Resour 30(1):145–183
11. De Oliveira S, Vivacqua AS, Borges M (2012) Scenario-based collaboration: an approach to refinement of plans through public engagement. In: IEEE 16th International conference on computer supported cooperative work in design (CSCWD), pp 135–142. IEEE
12. Devkar GA, Mahalingam A, Kalidindi SN (2013) Competencies and urban public private partnership projects in India: a case study analysis. Policy Soc 32(2):125–142
13. Diduck AP, Pratap D, Sinclair AJ, Deane S (2013) Perceptions of impacts, public participation, and learning in the planning, assessment and mitigation of two hydroelectric projects in Uttarakhand, India. Land Use Policy 33:170–182
14. DoEF (2010) PPP toolkit for improving PPP decision-making processes. Department of Economic Affairs, Ministry of Finance, Government of India. http://toolkit.pppinindia.com/urban-transport/module1-oopi-india-lffpii.php?links=oindia1b
15. Dore MHI, Kushner J, Zumer K (2004) Privatization of water in the UK and France—what can we learn? Utilities Policy 12(1):41–50
16. El-Gohary NM, Osman H, El-Diraby TE (2006) Stakeholder management for public private partnerships. Int J Project Manage 24(7):595–604
17. Franceys RWA, Gerlach E (2011) Consumer involvement in water services regulation. Utilities Policy 19(2):61–70
18. Freeman RE (2010) Strategic management: a stakeholder approach. Cambridge University Press
19. García-Valiñas MÁ, González-Gómez F, Picazo-Tadeo AJ (2013) Is the price of water for residential use related to provider ownership? Emprical evidence from Spain. Utilities Policy 24:59–69
20. Graham A (2011) The objectives and outcomes of airport privatisation. Res Transp Bus Manag 1(1):3–14
21. Grimsey D, Lewis MK (2002) Evaluating the risks of public private partnerships for infrastructure projects. Int J Project Manage 20(2):107–118
22. Hanzl M (2007) Information technology as a tool for public participation in urban planning: a review of experiments and potentials. Des Stud 28(3):289–307

23. Henjewele C, Fewings P, Rwelamila PD (2013) De-marginalising the public in PPP projects through multi-stakeholders management. J Fin Manag Prop Constr 18(3):210–231
24. Henriksen HJ, Rasmussen P, Brandt G, Von Bülow D, Jensen FV (2007) Public participation modelling using Bayesian networks in management of groundwater contamination. Environ Model Softw 22(8):1101–1113
25. Hjortsø CN (2004) Enhancing public participation in natural resource management using Soft OR—an application of strategic option development and analysis in tactical forest planning. Eur J Oper Res 152(3):667–683
26. Hongzhi W, Yan W (2011) Game analysis of public participation in environmental protection. In: 2011 International conference on management and service science (MASS), 12–14 Aug 2011, pp 1–4
27. Hwang BG, Zhao X, Gay MS (2013) Public private partnership projects in Singapore: factors, critical risks and preferred risk allocation from the perspective of contractors. Int J Project Manage 31(3):424–433
28. IFC (2007) Stakeholder engagement: a good practice handbook for companies doing business in emerging markets. International Finance Corporation, World Bank Group, Pennsylvania Avenue, Washington, U.S.A
29. Jenerette G, Larsen L (2006) A global perspective on changing sustainable urban water supplies. Global Planet Change 50(3–4):202–211
30. Jingling L, Yun L, Liya S, Zhiguo C, Baoqiang Z (2010) Public participation in water resources management of Haihe river basin, China: the analysis and evaluation of status quo. Procedia Environ Sci 2:1750–1758
31. Kandil A, Hastak M, Dunston PS (2014) Development of 4D public participation GIS to improve communication of city transformation processes. Bridges https://doi.org/10.1061/9780784412329.125
32. Kingston R, Carver S, Evans A, Turton I (2000) Web-based public participation geographical information systems: an aid to local environmental decision-making. Comput Environ Urban Syst 24(2):109–125
33. Kuczynski PP (1999) Privatization and the private sector. World Dev 27(1):215–224
34. Lakshmanan L (2008) Public–private partnership in Indian infrastructure development: issues and options. Reserve Bank of India Occasional Papers 29(1)
35. Larner W, Laurie N (2010) Travelling technocrats, embodied knowledges: Globalising privatisation in telecoms and water. Geoforum 41(2):218–226
36. Lee C (2011) Privatization, water access and affordability: evidence from Malaysian household expenditure data. Econ Model 28(5):2121–2128
37. Lee S (2010) Development of public private partnership (PPP) projects in the Chinese water sector. Water Resour Manage 24(9):1925–1945
38. Li THY, Thomas Ng S, Skitmore M (2012) Public participation in infrastructure and construction projects in China: from an EIA-based to a whole-cycle process. Habitat Int 36 (1):47–56
39. Mahmoud H, Arima T (2011) A web-based public participation system that supports decision making. J Asian Arch Build Eng 10(1):77–84
40. McKenzie D, Mookherjee D (2003) The distributive impact of privatization in Latin America: evidence from four countries. Institute for Economic Development, Boston University
41. McKenzie D, Ray I (2009) Urban water supply in India: status, reform options and possible lessons. Water Policy 11(4):442–460
42. Megginson WL, Netter JM (2001) From state to market: a survey of empirical studies on privatization. J Econ Lit 39(2):321–389
43. MoUD (2009) Urban infrastructure development scheme for small and medium towns (UIDSSMT)—overview and salient features. Ministry of Urban Development, Government of India
44. Ng ST, Wong JM, Wong KK (2013) A public private people partnerships (P4) process framework for infrastructure development in Hong Kong. Cities 31:370–381

45. Nickson A, Vargas C (2002) The limitations of water regulation: the failure of the Cochabamba concession in Bolivia. Bull Lat Am Res 21(1):99–120
46. Pomeroy R, Douvere F (2008) The engagement of stakeholders in the marine spatial planning process. Mar Policy 32(5):816–822
47. Poplin A (2012) Playful public participation in urban planning: a case study for online serious games. Comput Environ Urban Syst 36(3):195–206
48. Prieto B (2011) Stakeholder management in large engineering and construction program. PM World Today 13 (2011)
49. Prokopy LS (2005) The relationship between participation and project outcomes: evidence from rural water supply projects in India. World Dev 33(11):1801–1819
50. Roehrich JK, Lewis MA, George G (2014) Are public–private partnerships a healthy option? a systematic literature review. Soc Sci Med 113:110–119
51. Savage G, Nix TW, Carlton JW, Blair JD (1991) Strategies for assessing and managing organizational stakeholders. Executive 5(2):61–75
52. Semple K (2002) Turmoil in Latin America threatens decades of reform: economic woes, political unrest raise anxieties. The Boston Globe, Boston, MA
53. Sherman MD (2001) Effective use of public involvement to achieve aesthetic quality in bridge design. Transp Res Record: J Transp Res Board 1770(1):181–187
54. Shirley M, Walsh P (ed) (2001) Public versus private ownership: the current state of the debate. World Bank, Washington DC
55. Silvestre HC (2012) Public–private partnership and corporate public sector organizations: alternative ways to increase social performance in the Portuguese water sector? Utilities Policy 22:41–49
56. Wang H, Xie J, Li H (2010) Water pricing with household surveys: a study of acceptability and willingness to pay in Chongqing, China. China Econ Rev 21(1):136–149
57. Wibowo A, Mohamed S (2010) Risk criticality and allocation in privatised water supply projects in Indonesia. Int J Project Manage 28(5):504–513
58. Wilder M, Lankao PR (2006) Paradoxes of decentralization: water reform and social implications in Mexico. World Dev 34(11):1977–1995
59. World Bank Institute (2012) Public–Private–Partnerships—reference guide version 1.0. International Bank for Reconstruction and Development/International Development Association or The World Bank, Washington, D.C., USA
60. WSP (2011) Trends in private sector participation in the Indian water sector: a critical review, based on a study undertaken by the Water and Sanitation Program Program, World Bank. New Delhi, India
61. Wu H, He Z, Gong J (2010) A virtual globe-based 3D visualization and interactive framework for public participation in urban planning processes. Comput Environ Urban Syst 34(4):291–298
62. Xie A, Liu Y (2010) Study on public participation in public project decision under e-government environment. In: 2010 International conference on IEEE e-business and e-government (ICEE), pp 4609–4611
63. Yarrow G (1999) A theory of privatization, or why bureaucrats are still in business. World Dev 27(1):157–168
64. Zhong L, Mol A (2008) Participatory environmental governance in China: public hearings on urban water tariff setting. J Environ Manage 88(4):899–913

The Role of a Quantity Surveyor Throughout the Lifecycle of a Construction Project

Basavaraj Chandrashekar Reddy, V. P. S. Nihar Nanyam, and Mithil Haldankar

Abstract The QS is a major key player in a construction project. The involvement of QS in different phases of a project is obligatory in order to meet the project requirement. QS acts as a 'Financial police' for a project. The role of a QS is different when working for different organizations such as consultant and main contractor. In order to know the involvement of QS in each project phase when working as a consultant QS and main contractor QS, this study is carried out through data collection by means of a survey done with the QS professionals working currently in the industry. The findings from the survey revealed that the role of the QS working in a consultant and main contractor organization is much different w.r.t to requirement, work and project. The required competencies, skills and experience will also matter when working in the industry as professional QS. Various software tools used by the QS were also found out during this study. Knowledge of the role of a QS in an entire project lifecycle when working for different organizations like consultant and main contractor will help in understanding the things in better way w.r.t to services to be provided, activities, objectives and scope stated for the project which in turn will reflect the professional way of approaching and working in the industry. The study will also be useful to civil engineering graduates who are willing to opt for the quantity surveying profession, industry quantity surveying professionals, educational institutions, service providers and other stakeholders in the construction industry.

Keywords Quantity surveyor · Construction · Consultant · Main contractor · Civil engineering · Stakeholders · Competencies

B. C. Reddy (✉) · V. P. S. N. Nanyam
RICS School of Built Environment, Amity University, Noida, India
e-mail: basavarajr.mq19n@ricssbe.edu.in

V. P. S. N. Nanyam
e-mail: nnanyam@ricssbe.edu.in

M. Haldankar
Shapoorji Pallonji Mideast LLC, Abu Dhabi, Dubai, United Arab Emirates

B. Laishram and A. Tawalare (eds.), *Recent Advancements in Civil Engineering*, Lecture Notes in Civil Engineering 172,
https://doi.org/10.1007/978-981-16-4396-5_5

1 Introduction

The construction industry is one of the largest sectors that contributes to the respective country's GDP and globally. It covers most of the markets from real estate to infrastructures. Construction professionals are the key to run the project effectively and efficiently [1]. A lot of changes have happened to the construction industry from past decades and till now which comprised of challenges the construction practice, standards, ethics, technology, approach, etc.

Client, consultant, main contractor are the major stakeholders for the project execution. In a construction project, involvement of professionals such as project manager, quantity surveyor, architects, structural engineer, etc. are really required to finish the project completely. Each one of the construction professionals required competencies in order to provide the best services and to deliver the project in better possible way w.r.t to sustainability, cost, quality and time. Each one of the construction professionals working for a project has their own roles and responsibilities in providing the best possible services throughout the lifecycle of a project. Considering the project's cost, the QS comes into the picture. QS is the person who looks after the cost of an entire project lifecycle. In order to handle this, there need to be a professional body for the quantity surveyors which builds the required competencies up to date. The title QS was not much used and aware in past decades, which on passing many generations, the QS title came into the picture. The modern quantity surveyors have come up with competencies that provide better services to the project and adds value to it. QS roles are different w.r.t to the stakeholder that the person is working for, i.e. client-side QS/consultant-side QS, main contractor-side QS, in each of them, the QS roles differs in the perspective of stakeholder's requirement. Modern QS also works and provides various optimum services to different kinds of industry such as automobile, mining, agriculture, telecom, manufacturing and petrochemical. So, the QS professionals in the built environment is most demanded and required for a construction project. No literatures are available in Indian context for QS, so this is why we are resorting for this paper. The paper tries to understand the importance of QS in a construction project, to identify changes in the roles of QS in different stages of a construction project, to identify the activities/services by QS to a construction project in the perspective of client/consultant and main contractor.

2 Structure of the Paper

The structure of the paper is as follows: Sect. 1 introduction: background, motivation and objectives, Sect. 3 literature review, Sect. 4 methodology, Sect. 5 data collection, Sect. 6 results and discussion, Sect. 7 concluding the paper.

3 Literature Review

Nnadi and Abel [2] described QS is a profession that acts an important role in the construction markets and they even referred as an accountant, construction economist. QS is in charge of the cost of planning of a project. They described that construction cost in Nigeria is almost higher in number, so they found that effective role of QS in the project execution in Nigeria. They conducted an oral interview, literature review and investigation of data collected. They found that there are quite more in the number of QS professionals, but their competences are not utilised much, issues found with them such as no record of documents, corruption and in-accuracy in quantities. They described a sample project data, like the cost of a project with and without the involvement of QS, and found that QS role is more important to bring up more profit and feasible cost estimates of a project and even the duration of the project found variance. Even from the data collected, they found that there was no involvement of QS in the pre-contract stage [2]. So, they concluded that a bill should be passed by the government of the south region, Nigeria, for utilization of QS in a construction project.

Olanrewajua and Anahveb [3] described QS is a role to provide services for the construction project/industry. QS is involved in various stages of the project and its components. QS competences and services are much required for the project to achieve the stakeholder's objectives. They described this study to examine the QS services for the building services work in a project and their involvement. They collected data through questionnaire survey and found that detailed and analytical cost technique is most adopted for building service estimates, cost advice and also found that the services by QS for the building services package are down streamed in the supply chain [3]. They concluded that QS is actively involved in this procurement of building services engineering.

Shayan et al. [4] described that in the construction industry of the generations upcoming, the QS professionals demands them to update their competences for the changes happening. QS is the profession to provide services to manage the construction project efficiency and cost w.r.t to changes in the trends. They conducted questionnaires and interviews and found challenges and roles for the QS such as BIM, sustainability and its bits of advice to the project [4]. The research also advised QS professionals to update their competences in accordance with the trends in the industry.

Osubor [5] described that in any construction project the value for money is most looked in aspect. The QS profession for the construction project and industry is invaluable. But they found that in Nigeria for the heavy construction works like bridges, roads, oil and gas projects where QS services for these works are hard to find. They found that QS profession is most found more in building and housing projects. They conducted a study on QS professionals and experienced, to work in all aspects of construction projects and technologies to satisfy clients and to deliver the project in the best possible value for money. They collected ten substructure projects data's and used for this study. They found that QS person was not involved in heavy construction projects where the developers and clients could not obtain

value for money. They conducted a Questionnaire survey to the stakeholders of the construction industry and data was tabulated and calculated using Z-score tool at 5% significance and found that QS services are more important for heavy construction projects and they stated that the duties of QS are lacking because of threats, unawareness of global practices, less use of QS for the project [5].

Agboola and Salawu [6] described that architects and QS are the professional roles in which their progress in the construction industry as partners are most found in the south-west, Nigeria. The two professional roles are key for a project in clients' perspective in terms of cost. The research work was mainly focused on the roles of QS and architect in a project and their coordination for achieving the common objectives. The methodology of data collection adopted was thorough questionnaire and the data are tabulated and calculated using relative important method. They identified that these two roles have impact on cost-effectiveness for a project w.r.t to the objectives stated. The client compromise on the construction cost estimated depends on unless and until the client is satisfied and justified from the QS and architect professional roles for a project [6].

From the literature review, the research gap findings are: not much study has happened in the Indian context or QS or roles defined for client/consultant, contractor so that is the reason behind the objectives stated.

4 Methodology

The work is carried out by conducting online questionnaire survey (questions were open-ended) to the industry QS professionals as a case study so as to identify the roles of a QS in the construction project and their competencies, tools, and team information. In the responses received, a few are identified as from professional construction bodies including RICS, AIQS, NZIQS, CIQS etc. were part of this questionnaire survey. The methodology carried out (refer with: Fig. 1) is as follows.

5 Data Collection

The questionnaire survey for data collection is categorised into: respondent's info, team info, professional info and tool's info. The data collection was done through Google form consisting of questionnaires and the form was circulated through the

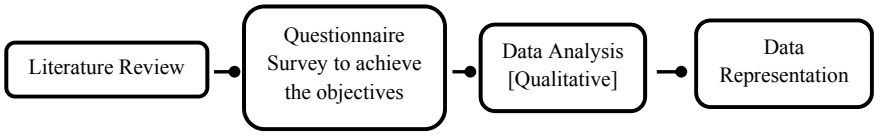

Fig. 1 Flow chart of methodology

Table 1 Respondents profile details

Experience level	Senior level 22%, Junior level 28%, Mid-level 50%
Type of organization	Client 14%, Consultant 51%, Contractor 35%
Years of experience	21–30 years: 4%, 11 to 20 years: 12%, 0.5 to 10 years: 84%

LinkedIn platform to the industry QS professionals profiles and few samples through phone calls. Total responses received = 52, but 49 are valid for data analysis; therefore, 49 is the total number of responses were considered. Though the response rate is small, for the study we have administrated the questionnaire form over ally to 512 industry QS but only 52 (10%) number of responses was returned. From this, it can be said that remaining 90% might have less in understanding the QS discipline/awareness of QS part. The collection of data was done during the period from April to May 2020. The following data (refer with: Table 1) represent the respondent's profile.

6 Results and Discussion

All the details mentioned below are from the qualitative data analysis in which the Google Form was extracted into the excel format and using pivot table method the data was segregated, identified and compiled to the required data from each response. Each finding in the paper will help the readers/students/candidates to clear all the disturbances in understanding the role and functions of QS.

6.1 Competencies

The competencies which are stated by the industry QS professionals from the data collected is as follows; These competencies are found to be important in order to meet the requirements, to understand and for career growth in the QS profession.

(1) *Knowledge Areas*: Quantification and costing, contract management, basic mathematics, commercial management, accounting principles and procedures, market management, conduct rules, ethics and professional practices, business planning, valuation, conflict avoidance, data management, negotiation, construction method, materials and technology, sustainability and environmental practice, construction law, project evaluation, health and safety, value engineering, procurement and tendering, building economics, construction information technology, building information and modelling, project management. The few knowledge areas which are mentioned is from the industry QS professionals that are found to be mandatory in order to understand the subject in a better way and build professionalism in the QS career.

(2) *Skills Sets*: Communication (Written and Oral), Team work, presentation skills, reporting skills, arithmetic skills, business acumen, forecasting skills, analytical skills, time management, computer skills, visualising skills, technical skills, flexible to adapt and work under pressure, problem solving, attention to details, strong numeracy, negotiation skills, quantitative and aptitude skills, ability to motivate, client care, software skills, correlation skills. The few skills which are mentioned is from the industry QS professionals which are found to be important in order to work smart and deal with real-time works in a better possible way.

6.2 Team Info

The team info details will give an idea to the readers in a general way that how the QS teams are created and assigned works for a project in an organization. QS team in an organization is made based on: Type of organization and Project scale. Works are assigned in a team based on: experienced person's in a team and work package.

6.3 QS Professional Info

(1) Who is a Quantity Surveyor?
QS are the backbone of any construction project. They help management to maintain budget and cash flow of any project. QS is the one who controls the project commercially as well as technically. Striving to complete a job within budget without diminishing the quality. They are the cost engineers and the "financial police" on any project ensuring all avenues are explored for cost-saving and profit maximization. Role of QS plays a vital role that is interconnected to other departments.

(2) The Roles assigned for Quantity Surveyor in different phases of a construction project is as follows;

   (a) The roles of a *Consultant QS* working for a *Client*
   Pre-contract Stage: Coordination with client, vendors, team members, reviewing drawings received at all stages of project life cycle, coordinating with designers and other consultants for clarification needed in drawings reviewed, finalising makes, advising on procurement route and contract type, preparation of BOQ, quantity take off, rate analysis, receiving quotes for preparing cost estimate, preparing cost plan, preparing RFQ, releasing tender, bid comparison and evaluation and thereby advising on competitive bidder to client, preparing RFP, reading between lines of a tender received to fulfil client's requirement.

Post-contract Stage: Project monitoring and preparing financial report, inspecting compliances during project execution, vetting RA bills received, preparing estimate to complete, preparing schedule of activities, documentation, evaluating variations and claims submitted by contractor, preparing monthly cost report.
Hand-over Stage: Preparation of handover report, compiling hand over documents, final bill documents.
The above roles mentioned will help the reader to clear all the disturbances in understanding the role of consultant QS.

(b) The roles of a *Main Contractor QS* working for a *Client*
Pre-contract Stage: Quantity take-off, rate analysis, studying tender drawings, sending tender queries to client/consultant, attending negotiation meetings, studying of tender documents, attending value engineering workshops.
Post-contract Stage: Award of contract, selecting and awarding sub-contractors, evaluating the sub-contractor bid, preparing budget, coordinated with consultant, client and sub-contractors, estimating additional scope if added to the project and making substantial documents to claim from the client, attending meeting with the concern parties in order to finalise and get approval of the variation orders and claims, submission of interim payment application and final valuation for client approvals, evaluation and finalization of variation for the sub-contractor works, quantities take off as per the site requirements and physical measurement, preparation of bill, preparation of monthly financial reports/cost report, evaluating and certifying sub-contractor's payment, evaluating estimated cost to complete at each stage of the project, maintaining risk registers.
Hand-over Stage: Preparation of Handover report, compiling hand over documents, final bill documents.
The above roles mentioned will help the reader to clear all the disturbances in understanding the role of main contractor QS.

(3) Difference between the Consultant QS and Main Contractor QS
The basic difference in the role of QS when working in consultant and main contractor firm is as follows (refer with: Table 2); the listed differences will give an insight knowledge about the activities of a QS.

(4) Factors influencing QS to change roles in a construction project lifecycle is as follows;
The factors mentioned will give an idea to the readers in a general way that the QS role changes while performing the activities when these factors pops up, i.e. Depends on Client's requirement, Situations and Cost are the three basic points that can influence the QS to change roles during the project execution.

Table 2 Difference between the consultant QS and contractor QS

Consultant QS	Main contractor QS
Here the QS is called as PQS	Here the QS is called as Main Contractor QS (CQS)
Control's cost	Executes the work as per the budget
Performs as per the client needs	Performs as per the contract
Provides services to clients such as; Cost Planning and estimation, Feasibility studies, Lifecycle costing, Cost–benefit analysis, Valuation, Value engineering	Provides services as per the agreed contract such as; Forecasting cost and cash flow, Sub-contracting works, Project values, Profit generation
Provides the best advice and opinion on the project to the client	Provides project to complete on budget
Evaluates and certifies; variation and claims submitted by Contractor QS	Prepares and submits variation and claims to Consultant QS
Evaluates and approves the payment application submitted by Contractor QS	Prepares and submits payment application to Consultant QS

6.4 Tools Info

Various software tools (refer with: Table 3) used by the QS professionals in the current market situation is as follows;

The readers/students/candidates who are looking at QS profession can actually understand that these are the tools used for QS and they can enhance their skills. The software tools will help the readers to understand the list of software's available in this arena and that can also help the readers enhancing the technological capability. This could contribute to the creation of awareness in QS tools. The above listed various software tools are found to be useful to deal with large scale projects and to perform the works in the limited time frame. Having awareness of these tools will help QS professionals when working for overseas companies/project so as to understand and build coordination.

Table 3 Tools info

Costing, take-off and construction management tools	CostX,, CCS Candy, Build Smart, Planswift, PDF Editor, Cubit, Build soft: Cubit, Coins, True Viewer, PDF X Change Viewer, DimX, WinQS, ProEst, Glodon's Cubicost, CATO, Cost OS, Sigma estimates, OST, CampEx, Vico Office
Office tools	Microsoft Excel, PowerPoint, Word, Outlook, SharePoint
CAD modelling tools	AutoCAD, Autodesk design review, Revit
Project management tools	MS Project, Oracle-Primavera
ERP tools	SAP, Oracle-ERP
Accounting tools	Sage, Eque 2

7 Conclusion

The professionalism in the construction industry is important for each and every roles that the person handles to deliver the project without any consequences and satisfying the client needs, in the same way we found out from the qualitative analysis that the QS working for a different organization such as consultant QS, contractor QS have different roles and responsibilities to reach the organization needs respectively. The roles of QS which entitle to be known in order to handle the sequence flow of work and to avoid overlapping. Work done by the QS in each of the project phases acts as an input to the other subsequent work. From the data collected, it can be stated that the requirement of professional QS w.r.t to competencies, awareness of concepts and tools utilization for the project and the roles of QS to be known when working in a consultant/contractor organization will help the readers/students/candidates in a QS career. Getting a professional degree in QS from the universities and standard bodies (RICS, etc.) might help in his/her QS profession because it meets all possible requirement that the QS should have. There is a need for improvement in the QS role while working for a project, i.e. w.r.t sustainability practices, BIM utilization; because the construction industry is moving towards the digital technology/advanced technology. The research work can be further carried out regarding; the importance and difference between professional QS and non-professional QS on a construction project, Career path for QS in future w.r.t to the software's/technology present in the current market situation. The data presented is limited to the responses if the responses are increasing the aspect of clarity can be enhanced. The face to face interview with the industry QS professionals will give in-depth knowledge and can have a real-time experience. The civil engineering graduates who are willing to opt the QS as their profession this paper will help them to have an oversight before taking the decision.

References

1. Cartlidge D (2009) Quantity surveyor's pocket book, 1st edn. Elsevier Ltd
2. Nnadi E, Abel UA (2016) Utilization of quantity surveyors' skills in construction industry in south eastern Nigeria. Int J Latest Res Eng Technol (IJLRET) 2(2):42–51
3. Olanrewajua A, Anahveb PJ (2015) Duties and responsibilities of quantity surveyors in the procurement of building services engineering. Elsevier 123:352–360
4. Shayan S et al (2019) Emerging challenges and roles for quantity surveyors in the construction industry. Int J 14(1):82–96
5. Osubor O (2017) Where there is no quantity surveyor: the dilemma of civil/heavy engineering construction project delivery. IOSR J Eng (IOSRJEN) 07(03):88–95
6. Agboola OP, Salawu RA (2015) Examining the roles of architects vis-à-vis quantity: surveyors in the building industry at south west, Nigeria. Int J Res Soc Sci 4(09):79–89

Smart Cities in the Development of Sustainable Infrastructure—Systematic Literature Review of Two Decades Research

Tharun Dolla, Reena Bisht, and Boeing Laishram

Abstract Smart cities occupied important focus of governments across the countries in the modern world. However, there is a need to take stock of the research carried so far to enable and direct the trajectory of future research. To this end, this study has undertaken a systematic literature review of studies published on the topic of smart cities in Scopus database in the past two decades. The findings indicated that the focus of smart cities in construction management research as has been poor. The study found that the top three journals that have published research on smart cities are Cities, Journal of Cleaner Production, and the Journal Sustainable Cities and Society. Furthermore, though Indian government is embarking with an ambitious plan of developing hundred smart cities, the current research trend to support this program has been minuscule due to dearth of studies carried in India. Thus, future research needs to focus on smart cities research with much theoretical depth and empirical adequacy concerning research gaps of smart city research globally and in India, conception of smart city concept, and smart cities for disaster/pandemic management. Many studies exist concerning systematic literature review on smart cities research, but this study is still insightful and shows knowledge gaps concerning the status quo of research.

Keywords Smart cities · Systematic literature review · Sustainable infrastructure · Infrastructure development

T. Dolla (✉) · R. Bisht · B. Laishram
Infrastructure Engineering and Management, Civil Engineering, IIT Guwahati, Guwahati, India
e-mail: tharun@iitg.ac.in

R. Bisht
e-mail: b.reena@iitg.ac.in

B. Laishram
e-mail: boeing@iitg.ac.in

B. Laishram and A. Tawalare (eds.), *Recent Advancements in Civil Engineering*, Lecture Notes in Civil Engineering 172,
https://doi.org/10.1007/978-981-16-4396-5_6

1 Introduction

The mention of *Smart Cities* can be found way back in the literature in 90s. The definition and function of the term itself changes with different school of thought and field of study, and various approaches have been made so far to define this term. It has also been interpreted by different stakeholders such as researchers, practitioners, businessmen and policymakers, who have considered smart city from different perspectives, generally based on subjects of urban economy, quality of life, governance, living and natural environment, people participation and mobility [1]. Though a certain agreement does stand across all the interpretations that *Smart City* does not define a particular attribute/s of a city, varied attributes are working towards addressing the problems of the city and improving the quality of life of its inhabitant. The attributes can be as diverse as tools that meet the local needs through virtual guides, digital portals and knowledge bases and at the same time global environments, sustainable infrastructure, and ICT infrastructure for ecological use. So in essence, Smart City can be described as an urban development model that utilizes and harmonizes the different aspects of human and technological capital for the sustainable development of urban cluster and enhancement of the quality and prosperity of life [2].

In the same line of thought, it can be inferred that smart city development poses a challenge for the project managers working in traditional infrastructure and/or construction management field due to the added complexity arising from integration of smart technologies; such as ICT, environment sustainability, with the traditional infrastructure development, where all systems are integrated as part of a larger city level infrastructure (both soft and hard) accessible to all the users both physically and technologically [3]. This paper intends to provide an overview of the published papers in academia.

2 Research Methodology

Although there were three choices given for selecting the academic databases available for this study, i.e. Web of Science, Scopus or the top journals as listed, the database that has been chosen for this particular exercise is Scopus digital database. Scopus has been adopted not only due its ease of accessibility but the availability of comprehensive and reliable database. For the study, the last inquiry was made on Scopus on Jan 30, 2020, and the search criteria sought the following combinations of these keywords: “smart AND cities”, “project AND management” OR “construction AND management” OR “infrastructure”. These were limited to subject areas of Business, Management and Accounting, and Engineering. These keywords were identified to confine the search space: “Smart City”, “Smart Cities”, “Urban Growth”, “Urban Planning”, “Sustainability”, “Urban Development”, “Infrastructure”, “Transportation System”, “Housing”, “Construction Industry”,

"Renewable Energies", "Smart Infrastructures", "Waste Management", and, "Smart Mobility". Also, "Computer Science" was excluded from the criteria of search. Only paper published in English language were considered with publication status as "Final". As a result, 692 article results were generated. To parse the data, further constraint was put by including only journals articles, resulting in finally 306 articles. Out of these further filtering was done by title and abstract analysis for the relevant field. The search parameters were limited to publications from 1999 to 2020 (Fig. 1).

3 Findings

The systematic literature analysis gave insights to the analysis of the following parameters: the publication numbers through the years, journals (distribution among journals and the main publishing journals), research areas, geographic scope (data or case study relating to geographic provenience, location, or both), project sector, research topics, and a list of most cited papers.

3.1 Publication Numbers Through the years

The graph in Fig. 2 shows that the publication progress had been slow from the year 1999 to 2014, years such as 2002, 2004–2006 being zero. Since 2014, there is an exponential growth in the publication numbers and this trend may continue over the next years as more interest in the field and related projects are being developed around the world.

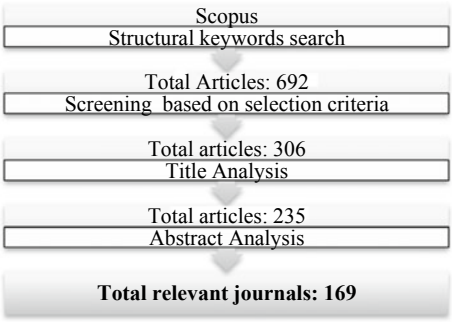

Fig. 1 Flowchart of the research methodology

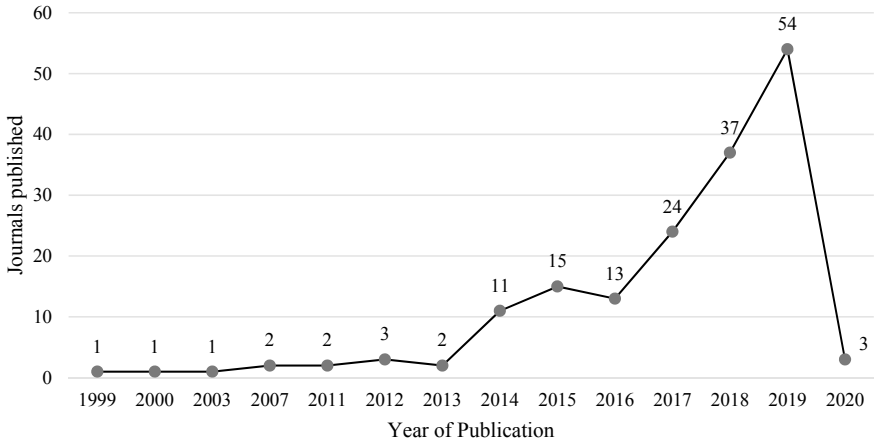

Fig. 2 Growth of publication numbers through the years

3.2 Journals

The 169 papers were distributed across 86 different journals. The top journals with most number of publication are tied between *Cities* and *Journal of Cleaner Production* with 17, and *Sustainable Cities and Society* with 17 publications at second (refer Fig. 3). Although the first position based on the number of citations for a journal is held by *Journal of Cleaner Production* (17), while second is held by *Cities* (16) (refer Fig. 4).

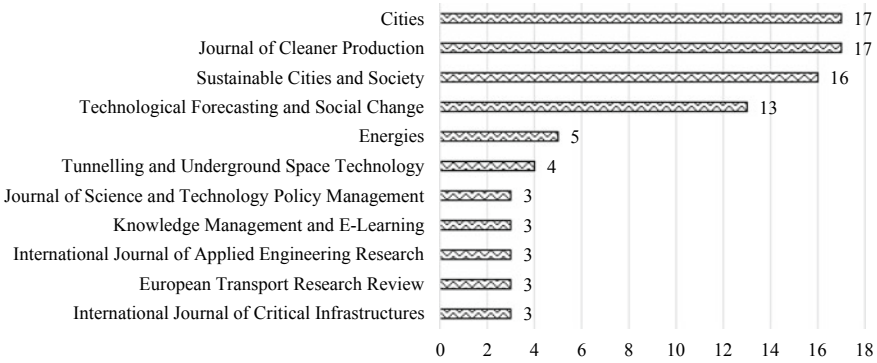

Fig. 3 Top journals and number of publication

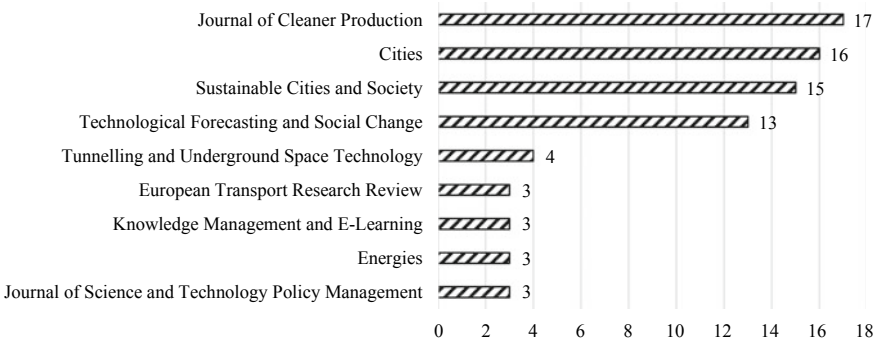

Fig. 4 Top journals based on citations

3.3 Research Areas

For the purpose of this study, the search area had already been restricted to Business, Management and Accounting, and Engineering. From the database thus gathered and depicted in Fig. 5, it is inferred that the maximum amount of publications is done in the area of Engineering (104), followed by Business, Management and Accounting (86) and Social Science (62). The research areas also include, in no particular order, Energy (45), Environmental science (32), Arts and Humanities (3), Decision Sciences (11) and Psychology (13). This makes the multidisciplinary nature of the concept Smart Cities evident, even when involving typically technical contents (engineering, management and infrastructure). It is possible that the results will fluctuate outside the search parameters as set for this study, still the multi-disciplinary nature will still hold true for Smart Cities, as a concept.

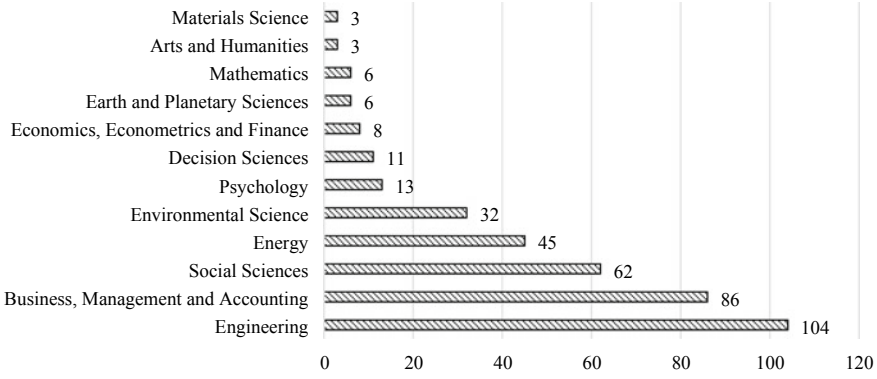

Fig. 5 Number of documents based on top ten research areas

3.4 Research Origins

The documents are spread over 48 countries based on their origin. Among the research, the USA holds the largest number of publication numbers with 27 papers, followed by Italy with 24 papers. India (15) also shows a good standing at fourth. Australia is in the fourth place, with 34 papers published, followed by Portugal, Germany, Switzerland, Italy, Spain, India, Brazil, Netherlands, Taiwan, and Belgium, publishing between 10 and 15 papers each (Fig. 6). In the top ten countries, India, China and Portugal are the only developing countries, contributing 21% to the 169 documents. Meanwhile, the top three countries, namely US, UK and Italy, contribute 43%.

3.5 List of Most Cited Papers

Out of 169 papers, based on how often they have been cited, the most relevant paper is *"Smart city policies: A spatial approach"* written by Angelidou [4], which reviews the factors which differentiate policies for the development of smart cities and is cited in 233 papers. The maximum it has been cited for areas related to social science (25.9%), computer science (14%), business, management and accounts (13%), and engineering (12.8%) (refer Fig. 7). This can be seen as an example of the multi-disciplinary nature of the smart cities concept. The top 10 papers are depicted in Table 1.

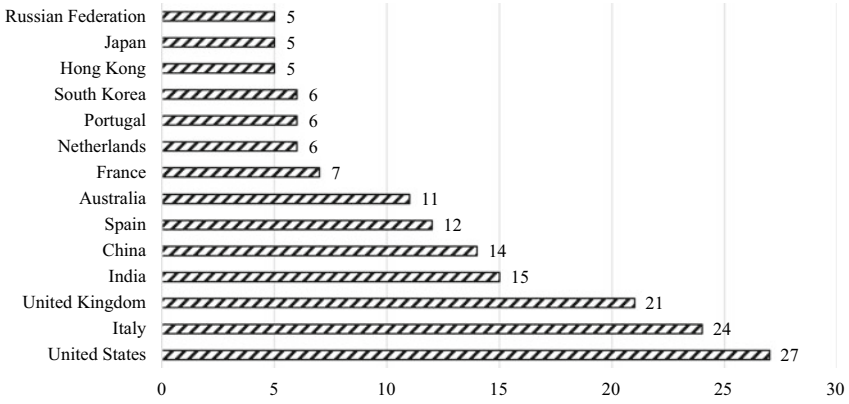

Fig. 6 Distribution of documents over top ten country of origin

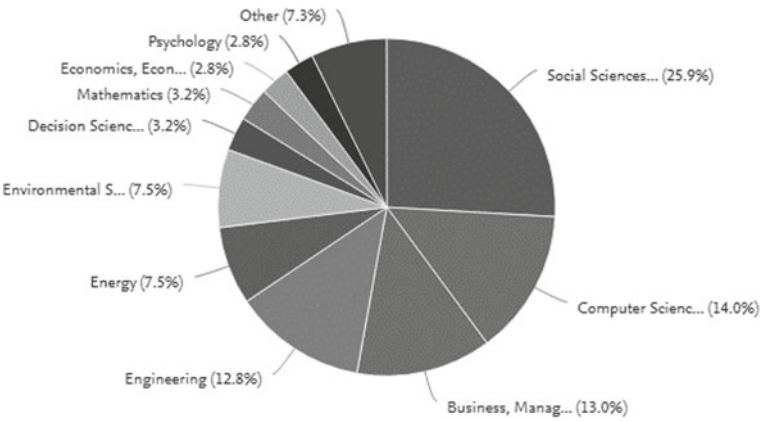

Fig. 7 Documents cited by subject area for Angelidou [4]

Table 1 Top ten papers based on citations

Paper ranks	Cited by
1. Angelidou [4]	233
2. De Jong et al. [5]	228
3. Lee et al. [6]	167
4. Djahel et al. [7]	148
5. Mahizhnan [8]	132
6. Yigitcanlar and Lee [9]	103
7. Talari et al. [10]	97
8. Gharaibeh et al. [11]	94
9. Mattoni et al. [12]	77
10. Petrolo et al. [13]	71

4 Discussion of Trends and Major Findings

The themes of this discussion are as follows.

1. Research trend of smart city research carried globally and in India
2. Conception of smart city concept
3. Smart cities for disaster/pandemic management.

The conceptions of ethics, data privacy were the main concerns of the social scientist. Data security and vulnerability protection were the key directions of computer scientists. The business, management and accounts research has largely of focused on developing the frameworks necessary to support the incorporation of smart city agenda by focusing on the planning and development phases. Engineering division focused on providing technological solutions to the make the city ‘smart’. However, the research done by construction management field is scant.

There is little effort carried so far to carryout international case studies and comparing them across the institutional and country-level frameworks. Moreover, smart city research can take advantage of the priority areas laid over by the CIB commission [14]. They include—energy, building, land use, infrastructure and asset management, transport and mobility, community and users. A mapping of extant literature within these themes can lay out expose the research gaps. Morphological exercise is a suitable research tool in this. Developing similar themes for India may be highly profitable and can support the implementation through the smart city mission. Particular attention can be paid to inquire the extent of sustainability principles in the smart cities by developing suitable metrics.

The review enforced that not every conception of smart city across the research is the same. One strand focuses on the high-frequency models where digitization is sought to have fully generated data and analytics of various assets and services by using sensors. This is propelled the generate of huge data sets. Given that data is useless unless it is used to generated meaning to it, big data analytical techniques have emerged from this high-frequency cities. It can be observed that high-frequency cities are predominant in smart city projects of developed countries and are dependent on the real times streamed data. The present development of developing countries including India can be understood as low frequency cities. Low-frequency cities can be understood as the provision of assets and services that can improve the livelihood of citizens [15, 16]. India is slowly progressing towards the goal of being a high-frequency city. For instance, the establishment of integrated command and control centers in more than 15 cities of Indian are an example. Apart from these understanding, there is a dire need to focus on sense making of the development of these ubiquitous smart cities. It is often called as the utopia of smart cities.

There is little focus on the Indian smart cities particularly that are stemming from Indian research institutions. In particular, though there are about 15 papers published with the context of India, those studies are far from being critical and useful to support the smart city paradigm of India. For instance, these studies on focused on sectors such as energy and related policies, readiness of the using internet of things in India, structured changes that are need to map assets and utilities of facilities management, procurement integration issues, financing issues in Indian urban infrastructure, implications and motivations of ranking systems adopted in India. There are no empirical case studies and the existing studies fail to offer practical implications for practitioners. Moreover, the studies did not engage any theoretical framework. On the other hand, international research on the smart cities have advanced with a stage where a digital twin has been constructed for major cities. Though Indian cities are among top megacities in terms of populations, not a single study has been reported on these megacities, let alone other cities of India. There is a tremendous research gap in the Indian context.

The amalgamation of infrastructure with ICT can help in providing optimized solutions in real-time for housing, transport, energy and other infrastructure needs which are sustainable for the future [3]. This concept of smart cities can also rise as a key strategy in combating poverty, inequality, unemployment, energy

management and environment protection. For project managers involved in traditional infrastructure development, this poses as a new challenge since integrating the ICT solution with infrastructure is a major component of this smart cities concept. This integration increases the complexity of project planning as the life cycle of physical infrastructure is way different that its ICT counterpart. Furthermore, the number of smart cities projects throughout the world is increasing with access to private expertise needed to modernize the infrastructure systems of urban areas. There is little research carried particularly in the influence of smart city developments on the disaster management of a city [17, 18]. This influence can be analyzed in the future research. Particular attention can be paid to the role of integrated command and control centres which are perceived as the heart of the city infrastructure in the agenda of being 'smart.'

5 Conclusion

The objective of this paper was to undertake bibliometric analysis of smart cities in context of management related to infrastructure, project, construction and engineering and understanding the concept of smart cities. The analysis was carried on database of Scopus for about two decades of research. Since 2012, the number of publications has shown an upward growth. This growth is expected to increase only since as the density, expansion and demand of better quality of living of urban areas are increasing throughout the world, the policymakers, researchers, practitioners and industry are looking towards solutions for fulfilling these demands of population. The study has offered critical insights on themes namely the conception of smart city concept, research trend of smart city research carried globally and in India, and smart cities for disaster/pandemic management. This study is not immune to criticism and contains certain limitations, regarding search tool Scopus and selection of limiting parameters for research on search tool. Although Scopus is considered one of the world's leading and comprehensive citation database, other citation platforms have not been explored which might contain different search results. The search criteria adopted in this study's bibliometric analysis also identified a number of false positives which required manual analysis and some papers' exclusion. The search parameters were also based on field preference and his understanding of the concept, and not tested scientifically.

References

1. Rodríguez-Bolívar MP (2015) Transforming city governments for successful smart cities, vol 8. Springer International Publishing, Cham
2. Albino V, Berardi U, Dangelico RM (2015) Smart cities: Definitions dimensions performance and initiatives. J Urban Technol 22(1):3–21. https://doi.org/10.1080/10630732.2014.942092

3. Dolla T, Laishram B (2018) Procurement of low carbon municipal solid waste infrastructure in India through public-private partnerships. Built Environ Proj Asset Manage 8(5):449–460. https://doi.org/10.1108/BEPAM-10-2017-0087
4. Angelidou M (2014) Smart city policies: a spatial approach. Cities 41:S3–S11. https://doi.org/10.1016/j.cities.2014.06.007
5. de Jong M, Joss S, Schraven D, Zhan C, Weijnen M (2015) Sustainable–smart–resilient–low carbon–eco–knowledge cities; making sense of a multitude of concepts promoting sustainable urbanization. J Cleaner Prod 109:25–38. https://doi.org/10.1016/j.jclepro.2015.02.004
6. Lee JH, Phaal R, Lee S-H (2013) An integrated service-device-technology roadmap for smart city development. Technol Forecast Soc Change 80(2):286–306. https://doi.org/10.1016/j.techfore.2012.09.020
7. Djahel S, Doolan R, Muntean G-M, Murphy J (2015) A communications-oriented perspective on traffic management systems for smart cities: challenges and innovative approaches. IEEE Commun Surv Tutorials 17:125–151. https://doi.org/10.1109/COMST.2014.2339817
8. Mahizhnan A (1999) Smart cities: The Singapore case. Cities 16(1):13–18. https://doi.org/10.1016/S0264-2751(98)00050-X
9. Yigitcanlar T, Lee SH (2014) Korean ubiquitous-eco-city: a smart-sustainable urban form or a branding hoax? Technol Forecast Soc Change 89:100–114. https://doi.org/10.1016/j.techfore.2013.08.034
10. Talari S, Shafie-khah M, Siano P, Loia V, Tommasetti A, Catalão J (2017) A review of smart cities based on the internet of things concept. Energies 10(4):421. https://doi.org/10.3390/en10040421
11. Gharaibeh A, Salahuddin MA, Hussini SJ et al (2017) Smart cities: a survey on data management, security, and enabling technologies. IEEE Commun Surv Tutorials 19:2456–2501
12. Mattoni B, Gugliermetti F, Bisegna F (2015) A multilevel method to assess and design the renovation and integration of smart cities. Sustain Cities Soc 15:105–119. https://doi.org/10.1016/j.scs.2014.12.002
13. Petrolo R, Loscrì V, Mitton N (2017) Towards a smart city based on cloud of things a survey on the smart city vision and paradigms. Trans Emerg Telecommun Technol 28(1):e2931. https://doi.org/10.1002/ett.2931
14. Miimu A, Janne P (2016) Research roadmap report smart city vision. CIB General Secretariat, Delft
15. Dolla T, Laishram B (2020) Governance issues in PPP procurement options analysis of social infrastructure: case of Indian waste management sector. J Infrastruct Syst 26(4)4020040. https://doi.org/10.1061/(ASCE)IS.1943-555X.0000578
16. SCM (2020) City wise projects under smart cities mission. Smart Cities Mission 2020. http://smartcities.gov.in/content/innerpage/city-wise-projects-under-smart-cities-mission.php
17. Ford DN, Wolf CM (2020) Wolf smart cities with digital twin systems for disaster management. J Manag Eng 36(4):1–10. https://doi.org/10.1061/(ASCE)ME.1943-5479.0000779
18. Rosen J et al (2002) The future of command and control for disaster response. IEEE Eng Med Biol Mag 21(5):56–68. https://doi.org/10.1109/MEMB.2002.1044166

Assessing the Effect of Audit Compliance, Conflict Management and Bureaucratic Attitude on the Success of Public Projects

Arava Sai Sreekar, Sulakshya Gaur, and Abhay Tawalare

Abstract The public sector projects and programs are an important driving tool for the country's economy. However, in the recent past the Indian construction sector that boasts of several big projects has been marred by various issues. In view of this, this study aims at exploring factors that can lead to the success of public projects in stipulated time, budget and set quality. To address these challenges, 25 factors under three constructs, audit compliance, conflict management and bureaucratic attitude were identified through exhaustive literature study. On the basis of responses collected by 222 respondents, conflict management and bureaucratic attitude are the two important constructs that associated with the success of project. The findings of this study would be helpful to the decision makers and other stakeholders by providing them better insights of the factors affecting the success of project.

Keywords Public construction project · Project success factors · Conflict management · Audit compliance · Bureaucratic attitude

1 Introduction

The public sector projects in India are always facing the challenge of time and cost overruns regularly. According to the flash report by MoSPI [1] for January, there are 1692 central sector infrastructure projects amounting to 150 crores and above. Out of these, 552 projects are delayed as per their original schedule. Also, 101 projects have suffered additional delays as per their date of completion in the previous month. Apart from this, these projects are anticipated to have a cost overrun of 19.41% from their initially determined costs. Some of the important reasons for these delays account to land acquisition, tie-up of project financing, law

A. S. Sreekar · S. Gaur · A. Tawalare (✉)
Department of Civil Engineering, Visvesvaraya National Institute of Technology, Nagpur, Maharashtra, India
e-mail: abhaytawalare@civ.vnit.ac.in

B. Laishram and A. Tawalare (eds.), *Recent Advancements in Civil Engineering*, Lecture Notes in Civil Engineering 172,
https://doi.org/10.1007/978-981-16-4396-5_7

and order problem, lack of infrastructure support, etc. [1]. The credibility of project success can be expanded if the innate qualities of the project can be altogether comprehended, proper contractual plans are adopted, a competent management team is assigned, and a sound monitoring and control framework is established. Chan et al. [2] found out project team commitment and client's and contractor's competencies as important factors for successful project outcomes. Already many studies have been conducted by researchers on identifying such common success factors. Apart from such common success factors, public sector projects face challenges such as they need to satisfy various political interests and need to follow bureaucratic procedures, rules and regulations [3]. The public projects are also exposed to financial audit and an investigation by external organizations [4]. Chua et al. [5] inferred that project success is not resolved only by monitoring and controlling efforts but need to handle the conflicts arising during monitoring and controlling activities. Therefore, this study focuses on three different constructs that are audit compliance, conflict management and bureaucratic attitude of public employees in project success. Thus, the objective of this study is to assess the effect of audit compliance, conflict management and bureaucratic attitude on the success of public projects in India.

2 Literature Review

The literature review was done to understand the concept of constructs such as audit compliance, conflict management and bureaucratic attitude and to identify factors related to each construct suitable in Indian context. Audit compliance is a mechanism for recognizing shortcomings and deviations from laws and guidelines and by evaluating appropriateness where there are insufficient or deficient. It promotes transparency and responsibility, by detailing deviations from and violations of authorities, so remedial moves might be made and those responsible might be considered answerable for their activities. Conflict is an expressed struggle among the parties involved in the project who see contradictory objectives and scarce rewards and obstruction from the other party in achieving project goals. Conflict management is the way toward removing negative aspect of conflict and brings positivity by appropriate time bound dispute resolution mechanism [6]. Bureaucracy system is characterized by its clear hierarchy of authority, unbending division work, composed and rigid guidelines, regulations and methods. Bureaucratic attitude is the attitude possessed by the bureaucrats who operate on written policies, rules and regulations keeping aside logical, emotional and sentimental issues [7]. The factors identified through literature review for audit compliance, conflict management and bureaucratic attitude are summarized in Table 1.

Table 1 Factors contributing to audit compliance, conflict management and bureaucratic attitude

	Factors	Source(s)
Audit compliance (AC)	External monitoring and control (AC1)	[8–11]
	Awareness of and compliance with rules and regulation (AC2)	[8, 10]
	Contractual compliance (AC3)	[2, 12]
	Procedural compliance (AC4)	[4]
	Auditors competency (AC5)	[13, 14]
	Independence of internal auditor (AC6)	[9, 10]
	Management policies and encouragement (AC7)	[9, 13, 15]
	Completeness of operating and information system (AC8)	[10]
	Adequate documentation and reporting (AC9)	[9, 16]
	Use of lessons learned from previous projects (AC10)	[12, 16]
Conflict management (CM)	Adequate communication among all project participants (CM1)	[2, 8, 11, 16]
	Act positively and cooperate (CM2)	[4, 11]
	Slow payment for completed work (CM3)	[15, 17]
	Dispute resolution mechanism (CM4)	[2, 8]
	Common objective (CM5)	[2, 8]
	Adequate source of information (CM6)	[11, 16]
Bureaucratic attitude (BA)	Corruption free environment provided (BA1)	[8, 9, 12]
	Fear of punishment (BA2)	[2, 11, 15]
	Rigid approach in decision making (BA3)	[11, 18]
	Arbitrariness in decision making (BA4)	[9, 18]
	Group decision making (BA5)	[16, 18]
	Slow decision making (BA6)	[14, 18]
	Multi-level hierarchy (BA7)	[16]
	Transfer of risk to lower person (BA8)	[4, 16]
	Non-flexibility nature (BA9)	[4, 14, 16, 18]
Public project success	Time (T)	[11, 12]
	Cost (C)	[11, 12]
	Quality (Q)	[11, 12]

3 Research Methodology

This study used a combination of literature study and questionnaire survey method to fulfill all the defined objectives. Literature study was used in determining the important component to the identified three constructs that were associated with the project success. Questionnaire survey was in turn used to determine the degree of association of individual components toward public project success. A theoretical model of the study is presented in Fig. 1.

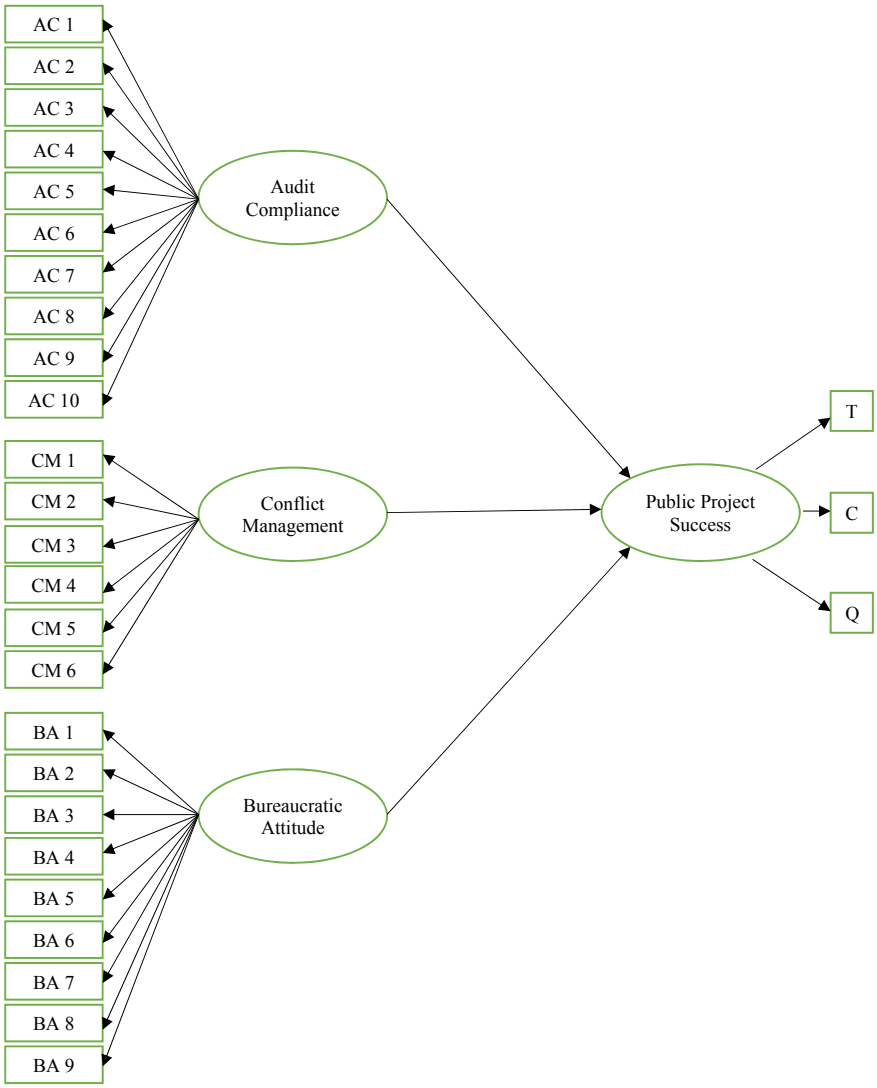

Fig. 1 Theoretical model

A five-point Likert scale was used for collecting the response where '1' represented no association and '5' represented very high association of factors to project success. Pilot study with 25 respondents was conducted before sending the questionnaire for responses. Few corrections with the identified factors were made to make it more understandable to the respondents. The respondents who participated in the pilot study were not included in the final survey. A total of 520 questionnaires were sent to engineers working in public projects for response, and 222 responses

were obtained back. This reflects a response rate of 42.69%, which can be considered good as compared to "20–30% response rate in construction industry" [19].

All the respondents had either a diploma or a degree in their respective fields of education. (Forty-five percentage of respondents had a graduate degree and 50% respondents had a PG as their qualification.) They were equally experienced and belonged to various profiles of their job. The respondents comprised of engineers (32%), project manager (27%), consultant (14%), contractor (12%), clients (8%) and auditors (7%).

4 Data Analysis

Prior to factor analysis, the reliability of the five-point scale used in survey was determined by obtaining the Cronbach's alpha coefficient. The Cronbach's alpha values were above 0.6 and within acceptable limit. One-sample *t*-test was done against the test value of 3 (since a five-point scale was used, average of which stands out at 3) at a significance level of 0.05. The factors that had factor loading less than 0.05 were accepted and considered for further analysis. Factor analysis was used to further reduce the identified factors to a small number of critical factors. After the complete exploratory analysis, six factors from audit compliance construct, three from conflict management and six from bureaucratic attitude construct were determined. The factor loadings with Cronbach's alpha value, KMO value and the percentage variance explained from these factors are presented in Table 2.

The measurement model was then subjected to 'confirmatory factor analysis (CFA)', to check for convergent and divergent validity of the model [20]. Measurement model was then checked for goodness of fit. The model's GOF was measured using the following indices: (a) χ^2/DF (degree of freedom), (b) normal fit index (NFI), (c) Tucker–Lewis index (TLI), (d) comparative fit index (CFI), (e) incremental fit index (IFI), and (f) root-mean-squared error of approximation (RMSEA). The factors having the value of factor loadings as 0.5 and above [20] were considered, and the remaining were dropped off from their respective constructs. The final SEM model was then prepared and was underwent through similar checks of CFA and tests for GOF. The final SEM model is presented in Fig. 2.

Goodness-of-fit (GOF) values for the models, i.e., measurement model, conceptual model and final SEM, are presented in Table 3. The χ^2/DF value increased from 1.942 to 2.963 and that of RMSEA increased from 0.065 to 0.091. However, other index values showed some changes but lie within the acceptable limits of the indices as shown in Table 3.

Table 2 Exploratory factor analysis results

	Factors	Factor loadings	Cronbach alpha	KMO value	Explained variance (%)
Audit compliance (AC)	AC2	0.776	0.623	0.713	62.80
	AC3	0.804			
	AC4	0.777			
	AC6	0.863			
	AC7	0.84			
	AC9	0.63			
Conflict management (CM)	CM1	0.807	0.629	0.652	60.50
	CM2	0.793			
	CM6	0.731			
Bureaucratic attitude (BA)	BA3	0.712	0.692	0.742	59.80
	BA4	0.724			
	BA6	0.617			
	BA7	0.55			
	BA8	0.552			
	BA9	0.599			
Public project success	T	0.945	0.788	0.638	70
	C	0.849			
	Q	0.707			

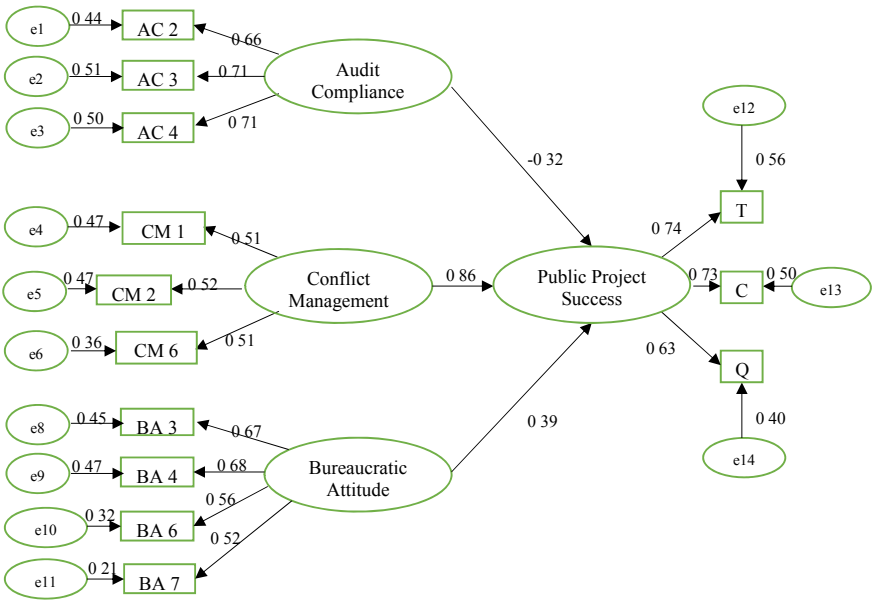

Fig. 2 Final model

Table 3 Goodness-of-fit values

Fit index	Cutoff value	Measurement model	Conceptual model	Final SEM
χ^2/degree of freedom	1–3	1.942	2.963	2.896
Normal fit index (NFI)	0 (no fit)—1 (perfect fit)	0.79	0.552	0.591
Tucker–Lewis index (TLI)	0 (no fit)—1 (perfect fit)	0.857	0.601	0.615
Comparative fit index (CFI)	0 (no fit)—1 (perfect fit)	0.883	0.641	0.678
Incremental fit index (IFI)	0 (no fit)—1 (perfect fit)	0.886	0.65	0.688
Root-mean-square error of approximation (RMSEA)	<0.05 (very good) —0.1 (threshold)	0.065	0.091	0.092

5 Discussions

The findings of this study that have an implication on the success of public project are conflict management and bureaucratic attitude. Audit compliance was found to be an insignificant construct in the study showing negative factor loading. The factors under the above-mentioned constructs need to be considered while managing the public projects. These two constructs are mentioned in detail below.

5.1 Conflict Management

The factor of act positively and cooperate was found to be correlated highest with CM. It had a loading of 0.52, which is a bit more than the other two factors, i.e., adequate communication between all project participants and adequate source of information with a factor loading of 0.51 each. These findings in turn lay emphasis to the importance of proper communication channel [11] between the involved stakeholders and the importance of a sense of positive workplace culture that motivates the project participants to work cordially and in a swift manner [21]. Also, the adequate relay of information between the participants needs to be addressed properly as it serves as an important cornerstone for resolution of conflicts quickly and efficiently [22].

5.2 Bureaucratic Attitude

Bureaucratic attitude came out as the second important construct that can affect the success of project. The factor arbitrariness in decision making was found to be

correlated with BA with a factor loading of 0.68. This factor represents a positive aspect of decision-making ability of the personnel involved. They make their decision taking into account the existing rules and norms [16], and their plans do not have any bias and are not influenced by any outside influence. The factors such as rigid approach in decision making (0.67), non-flexibility (0.56) and slow decision making (0.52) are the other factors in the BA construct that showcases some drawbacks in the decision-making ability of the bureaucrats that can hamper the success of project. In Indian context, decision-making process is very slow as there is no mechanism in place which compels the authority for time-bound decisions. Absence of time-bound decision-making approach directly affects the progress of the projects as contractors have to wait for the final decision at each level of organizational hierarchy.

5.3 Insignificant Construct

Audit compliance was found to be an insignificant construct in this study. However, regular audit of the work is an important measure undertaken to keep the project on track, but in this study, it was found to be an insignificant one. The reason could be that the procurement process and auditing process are well defined by state and central government in India. Complying with the audit rules is a mandatory procedure in all public projects, and everyone is following it. Therefore, respondents have not given much importance to factors contributing toward this construct, and responses were found to be outlier in comparison with other factors.

6 Conclusion

This study aimed to determine the critical success factors associated with success of public projects. To determine the success of public project on the basis of time, cost and quality, the identified success factors were classified under three constructs of audit compliance, conflict management and bureaucratic attitude. It was found that the constructs of conflict management and bureaucratic attitude are significantly correlated with the success of public project. This result demonstrated that the projects need to have a very swift method of dispute resolution and efficient communication along with the apt decision-making ability of decision makers to ensure the success of projects. There needs to be good relationship between the stakeholders of the project for quick decision making that remains free of any future conflict and are according to the stipulated rules and regulations. The findings of this study will be helpful to all the concerned stakeholders of the project, as it provides some essential parameters on which the success of project can depend.

However, further study needs to be conducted to have a deeper analysis of the construct of audit compliance, which is found insignificant in this study.

The construct of audit compliance is an essential tool to control and eradicate corruption, and hence, a deeper analysis of this construct seems to be necessary for future studies.

References

1. IPMD, Flash report on central sector projects. 2020, Ministry of Statistics and Programme Implementation: New Delhi.
2. Chan AP, Ho DC, Tam C (2001) Design and build project success factors: multivariate analysis. J Constr Eng Manag 127(2):93–100
3. Amoatey C, Hayibor MVK (2017) Critical success factors for local government project stakeholder management. Built Environ Project Asset Manage 7(2):143–156
4. Tabish SZS, Jha KN (2012) The impact of anti-corruption strategies on corruption free performance in public construction projects. Constr Manag Econ 30(1):21–35
5. Chua DKH, Kog YC, Loh PK (1999) Critical success factors for different project objectives. J Constr Eng Manag 125(3):142–150
6. Grisham T (2013) Conflict: Philosophy and Culture. J Leg Aff Disput Resolut Eng Constr 5(1):13–21
7. Faria JHD, Meneghetti FK (2011) Bureaucracy as organization, power and control. Revista de Administração de Empresas 51(5):424–439
8. Tabish SZS, Jha KN (2011) Identification and evaluation of success factors for public construction projects. Constr Manag Econ 29(8):809–823
9. Kling R (2008) Taxpayers are fighting back: transparency and accountability does not mean inefficiency. In: 3rd international public procurement conference pp 1205–1210
10. Chaiwong D, Factors affecting efficiency in internal auditing performance and operational outcome of the large THAI listed companies. Int J Arts & Sci 5(1):311
11. Jha K, Iyer K (2007) Commitment, coordination, competence and the iron triangle. Int J Project Manage 25:527–540
12. Hatush Z, Skitmore M (1997) Criteria for contractor selection. Constr Manag Econ 15(1):19–38
13. Baharud-din Z, Shokiyah A, Ibrahim MS (2014) Factors that contribute to the effectiveness of internal audit in public sector. Int Proc Econom Dev Res 70:126
14. Zimmerer TW, Yasin MM (1998) A leadership profile of American project managers. Project Manage J 29(1):31–38
15. De Lara PZM (2006) Fear in organizations: does intimidation by formal punishment mediate the relationship between interactional justice and workplace internet deviance? J Manager Psychol 21(6):580–592
16. Hussein B (2018) Catagorization of project success factors according to project characteristics insights from 21 project cases from Norway
17. Rijckeghem CV, Weder di Mauro B (1997) Corruption and the rate of temptation: do low wages in the civil service cause corruption? In: IMF Working Paper.1997, International Monetary Fund
18. Muspratt MA (1984) Construction research and education. J Prof Issues Eng 110(1):7–18
19. Akintoye A (2000) Analysis of factors influencing project cost estimating practice. Constr Manage Econom 18(1):77–89
20. Hair JF et al (2019) Multivariate data analysis, 8th edn. Cengage Learning, EMEA, Hampshire, United Kingdom
21. Tawalare A, Laishram B, Thottathil F (2020) Relational partnership in public construction organizations: front-Line employee perspective. J Constr Eng Manag 146(1):1–17
22. Tawalare A, Laishram B (2019) Factors hindering effective partnering in Indian public sector construction organizations. J Fin Manag Prop Constr 25(1):83–105

The Rhetoric of Smart City—A Conceptual Critique of Indian and the US Developments

Tharun Dolla and Jason von Meding

Abstract Smart city concept has attracted a lot of attention from urban development and planning researchers. This paper critically analyzes the rhetoric of the smart city agenda. The context of the Indian and the US smart city programs are compared and contrasted. In doing this, the study proffered theoretical and empirical directions for future research by identifying research gaps and a research question. The findings indicate that Indian and US smart city developments are quite distinct though both are democratic countries. More comparative case studies across the geographies are needed to unveil the practice of smart city development to anchor the praxis to the theory development.

Keywords Smart city · Critical theory · India · USA · A conceptual critique

1 Introduction

Cities have been the focal points of human movement and development. These were viewed as the epicenters of wealth and infrastructure [1]. With rapid urbanization, the influx of rural population toward the city has brought various challenges concerning the infrastructure provision. This challenge is coupled with cities being built over short periods or for a purpose as opposed to that evolved over the years. Eventually, most of the world population would be living in a city in some sense. Also, there is a shift of urbanization from the west to the global south. The world has 33 cities that have 10 million inhabitants or more. These are called megacities. Of these, 27 cities are in regions that are less developed. India has five of these megacities [2].

T. Dolla (✉)
Infrastructure Engineering and Management, Civil Engineering, IIT Guwahati, Guwahati, India
e-mail: tharun@iitg.ac.in

J. von Meding
Florida Institute for Built Environment Resilience, University of Florida, Gainesville, USA
e-mail: jason.vonmeding@ufl.edu

B. Laishram and A. Tawalare (eds.), *Recent Advancements in Civil Engineering*, Lecture Notes in Civil Engineering 172,
https://doi.org/10.1007/978-981-16-4396-5_8

Interestingly, among the cities that are expected to become a megacity by 2039, nine of 10 cities are in developing countries. Though its size popularly characterizes the city, urban researchers also argued that city is characterized not merely by size but the interactions [1] and is also viewed as a network [3].

Connected with the scale at which the cities are growing is the challenge of smart city development. To the prevailing conditions, the expectations of livable and efficient cities have stimulated the thinking of smart cities. This agenda of developing smart cities is often termed as utopia or everyone's dreamland [4]. Though smart cities have been in the points of interest in the 90s [5], in 2007, the European Union has initiated a project to rank its cities according to its smartness. Since then, their dimensions of measurement namely: smart economy, smart people, smart governance, smart mobility, smart environment, and smart living have become a tacit benchmark [6]. Since then, many governments are aspiring to develop smart cities, and this sector has become a point of interest to corporates as well. For instance, South Korea and Japan have been developing a series of ubiquitous and eco-cities since the early 2000s; the Amsterdam smart city initiative began in 2009; Singapore launched its Smart Nation initiative in 2014; India launched its mission of building 100 smart cities in 2015; and China has recently been receiving attention for eagerly adopting the latest smart technology for urban management since 2013, to promote further and regulate the development of smart city initiatives. India and China lead the smart city projects where around 300 smart city pilot projects are in progress [7]. A previous estimate posits that by 2020, at least 40 cities globally would have become smart cities. Many big corporate companies are bullying to sell the idea of a smart city. For instance, IBM has formally trademarked the ownership of 'smarter cities' out of their corporate vision and marketing strategy in 2011, where the previous recorded a decline in their business. Not only so, but there is a tremendous rise in the smart city market as well. The global smart cities market is expected to surge to US $2.57 trillion by 2025 from its share of US $737 billion in 2018. This is a whopping 3.5 times increase.

There is extreme criticism, however, on the smart city development. Technology-based interventions tend to be the core of smart city development that can improve the monitoring and management capabilities. These ambiguities deal with the understanding of what encompasses a smart city and how to achieve them. At the outset, smart city development is plagued by concept ambiguity and process ambiguity [8]. In a deeper sense, it is often regarded as the rhetoric of the corporates and neoliberal agendas [9, 10]. The smart city development that is criticized as corporate storytelling and is also attacked is that this storytelling does not mention the possible alternative development but only intends to sell the ICT-based technologies [5]. Thus, they bear the impression that they are reproducing 'power dynamics and priorities' of the colonial era [4]. They are argued to aggravate the social divide while the information technology professionals are to capture the new space created, and corporate executives and other elites would reap the fruit of smart city developments. Also, it is argued that there would be an extreme disparity between the 'core' and the periphery of the smart city [4]. It was criticized that the typical natural evolution toward the communities becoming smart is jeopardized,

and communication aspects of the communities are crippled [11] while citizens are compelled to be technologically literate [5]. This is causing a threat to privacy and democracy [12]. On the other hand, citizen satisfaction and well-being are often ignored in the global ranking systems [13], Interoperability between various technologies is an issue that can cause conflicts that collaboration and thus effect smart city developments [14]. Moreover, the smart city is developed often myopic view. In other words, most of their road maps are silent on what to achieve in the next ten years and beyond, thus posing a threat of non-reusable sunk investments, if planned inappropriately [14].

Smart cities are still unavoidable because rapid urbanization trend is inevitable, however. It is projected that by 2030, at least 60.4% of the world's population is expected to live in urban areas or cities [2]. Considering this growth, there is increased advocacy in the perception of various stakeholders to use information and communication technologies (ICT) in shaping the cities to be smart. Also, smart cities are regarded particularly effective during the times of pandemics and disasters (either human-made or natural) [15, 16]. This is because the erstwhile non-informational infrastructure assets are equipped with sensors that generate huge data, and when put to proper use, various governance activities can be benefited. Thus, instead of throwing the baby and the bathtub due to the criticism of smart cities, the development can be and needs to be pursued with rigor. The development needs to be grounded on the principles that can safeguard ethics, politics, and democracy. Furthermore, urban planning is expected to handle new concerns such as resilience, disaster reduction, and the 2030 UN Agenda Sustainable Development Goal (SDG) 11 that aims to 'make cities and human settlements inclusive, safe, resilient and sustainable' [17].

Smart cities have become one of the most sought-after topics of interest among researchers of disciplines such as urban policy, construction management, and public administration. This is because they are regarded as the solution to many urbanization problems across the globe and as pathways to sustainable development. Though profit motivations are quite a norm of the private sector's functioning, public sector agencies need guidance to develop the competency related to decision-making and negotiation so that the public and their interests are protected. This requires a thorough understanding of the motivations, urgency, policy framework, implementation mechanism, and processes that are followed. These issues are not addressed so far in the extant literature. In this vein, a study addressing the development of smart cities aimed to resolve the tension is essentially the need of the hour.

2 Research Methodology

The present study has set a conceptual critique as a research objective. Usually conceptual papers have twofold agenda [18, 19]. First to review the extant literature conceptually to understand the field and identify the research gaps and possibly a

research question. Second, to set out a discussion of theoretical and empirical issues to aid future research. In the first step, qualitative literature review is undertaken by using manual coding procedures [20]. Besides, review is carried out to identify a suitable theoretical framework to carry out the intended research inquiry. This paper presents these two aspects.

3 Findings of Indian and the US Agenda of Smart Cities

3.1 India

India sees a higher magnitude of challenges due to the size and scale of proposed smart cities. On the one hand, the government of India has sought to transform its existing cities into smart cities. India through its Swach Bharat Mission (SBM) has initiated to develop 100 smart cities. Among the 100 cities and towns that are expected advance into smart cities, 25 are capital cities, 24 are a commercial hubs, 16 are culture and tourism hubs, five are harbor cities, three are union territories, and three are healthcare and education centers [21]. The mission funds the projects. SBM has also set of much broader objectives to rank cities than just develop the cities. Furthermore, in 2018, the Ministry of Housing and Urban Affairs, the Government of India has launched to come up with a city livability index on the smart city projects. This is because Indian cities did not fare well in terms of livability index. According to a recent report, New Delhi, the capital of India, occupied 180th on how positively the residents evaluate their present lives. This place is among the bottom ten of all the city rankings. Furthermore, New Delhi also saw an adverse change in people's perception in recent times [22]. Indian stakeholder relate to the smart city developments to as providing sustainable and eco-friendly solutions rather a technologically loaded concept such as the ubiquitous city and digital city [23]. Moreover, organizationally, the developments are perceived to be seen in two major fronts. One is upgrading the existing assets and services where in the interventions of incorporating smart solutions to water distribution and its grid, disaster management enhancements to name a few. The other is more of a horizontal capability enhancing with the help of integrated command and control centers (ICCC) which aid to manage the whole city. Smart City project of MOHUA has developed a maturity assessment framework for guidance if one wants to develop a ICCC facility for their city. Now, there are many ICCC facilities developed and many are in pipeline. The interest toward ICCC has been increasing due to the versatile level of services these centers have offered in handling the Covid-19 pandemic. While these 100 smart cities projects are also criticized as being utopia of development, India has been pushing its mission ‘Digital India’. The budgetary allocation to this mission for 2020–21 has been increased by 23% to INR 3958 crore rupees to cater to the need of the projected 153 crore population by 2025. Some of the notable smart city projects in the green field category are Naya

Raipur in Chhattisgarh) and Dholera in Gujarat of India, and most of the other smart city projects are brownfield.

3.2 USA

For various reasons, smart city development in the USA has seen a decline, particularly in its deployments. There is a significant reduction or perhaps fewer allocations of budget to the smart city development in the USA. According to one heuristic estimate, The USA is working 40 smart cities. This is only around 4% of projects globally [24]. Smart city projects in the USA are marked with projects concerning energy efficiency through smart grids, bike, pedestrian-friendly interventions, smart parking systems, smart lanes, adaptive intelligent transportation systems, free internet access, and e-vehicle smart grids. These are more steered and governed by the local counties, and funds are raised locally, except that concerned departments such as the department of transportation are involving in granting the projects. Some aspects, such as technology-driven sensors, are used. The developments are raising data security and privacy concerns in the USA. There is no federal policy or mission to strategize and develop smart cities across the USA. Thus, it is apparently discreet and city-level interventions that are driving the smart city market in the USA. Nevertheless, the USA is still one of the top markets for smart city projects in 2020, according to IDC [25]. In addition, US $1 billion smart city grants are proposed by the contenders of the presidential election with much focus on green infrastructure. Such a consensus and focus were not observed in 2016, and this grant is at a much higher level when looked at from the investments in the past decade. The USA does have but localized and discreet smart city ranking also. For example, the Smart City Challenge launched by the US Department of Transportation in 2015 is concerned with transportation projects only [26].

Based on the above conceptual review, a comparison of smart city developments between India and the USA is conceptualized, as shown in Table 1. This review

Table 1 Smart city development comparison between India and the USA

India	USA
Service led or utility-driven	Technology driven
Less amount of user data	More amount of user data
Ethical vulnerability is low	Ethical vulnerability is high
Social inclusion is the main issue	Social inclusion and data security are the main issues
Politically and centrally motivated	Decentralized and locally motivated
Top-down approach	Bottom-up approach
Presence of centralized ranking system	Absence of centralized ranking system
Common and themed interventions	Discreet and city-level interventions

clearly points out that there is considerable variation in smart city developments across the two nations. This observation ties with the underlying logic of policies and project implementations that emerges from culture, governance, and the economy.

By grounding on the above conceptual analysis, further research can be anchored on the following research question:

How does the current development paradigm shift from conventional city development, and What tensions or risks emerge in the development of smart cities?

4 Way Forward

Addressing the set-out research question could help in theoretical development necessary for practical application and policy praxis for policymakers and urban planners. At one level, India and the USA have contrasting models of smart city developments at present. This does not mean that they never intersect. In this context, this study could unveil the risks that are encountered in the current development paradigm in both countries. This could lead to more grounded theory. On another level, the influence and involvement of power dynamics in the smart city development could be revealed. This could enhance the strategies and policies that are needed to wield the development of smart cities in a citizen-centric and democratic manner. Though both India and the USA are democratic, the political scenario is expected to bring differential results. Concerning the USA, from the New Urbanism movement in the USA of the 1980s that has laid the path to the present smart city growth and the resultant notion of the technology-based intelligent city to the most recent advances [5], a critical evaluation could assimilate the results on aspects necessarily begging immediate interventions.

4.1 Empirical Directions

The proposed objective is to examine the smart city development in the context of India and the USA. This would be done by using various data collection methods such as narrative inquiry, questionnaire surveys, and expert interviews to support the inquiry. Moreover, the case study is a method that can generate meaningful theories. This needs a theoretical lens to support the inquiry. Theoretical developments often need to have a grounding in historical contexts, normative, and methodological reflection [27]. Moreover, a theory is argued to make empirical data meaningful to support practice. Critical theory is suggested to have a powerful interpretive strength and methodological soundness and is quite suitable for this inquire [28].

4.2 Theoretical Directions

Critical theory was developed by the Frankfurt school of Germany during and post-World War I and gained importance after the notable contributions of Henri Lefebvre (1901–1991). Critical theory has the potential to expose or illuminate why various situations exist. 'Critical' in this context meant an evaluation of the reality, with the power to expose the positives and possibilities of change, particularly by revealing the loopholes and inadequacies in the policy praxis [28]. Such theoretical developments are often called as the conscious and articulated aspects of practice, of action. Neil Brenner notes that critical urban theory "…*insists that another, more democratic, socially just, and sustainable form of urbanization is possible* [29]". Critical theory is a powerful framework due to its natures such as the theoretical, reflective, critical, and power to expose the disconnection of possible and actual [27, 29]. For instance, the city's rights can be thoughts pertaining to the information, the use of multiple services and activities surrounding the urban areas. This is because critical theorists often associate profit motive as a euphemism to greed in a capitalistic society. In the context of urban development, critical theory is said to be effective in answering questions such as the inclusive growth within the cities, effective identification of the stakeholders, and the actors that can play a critical role in the change-making process or otherwise.

Concerning cities and the analysis within and among cities, critical theory encompasses the essential elements such as in relation to power, inequality, injustice, and exploitation [30]. More distinctively, critical theory can help is its understanding of the complexity of covert domination and thus leading to power as an important context for theoretical inquiry. It also concretely engages the analysis of the structure and dependent social action [27]. Critical theory has found applications in many fields, including legal studies, organizational studies, public administration planning, and policy research [27]. For instance, critical theory was used to understand the political and theoretical aspects related to climate change. However, applying to infrastructure management research related to smart city development has not been attempted so far. According to Marcuse et al. [31], exposing, proposing, and politicizing the key issues is the end objective of the inquiry using critical theory. Thus, critical theory is a suitable theoretical lens for the present objective.

In this context, the inquiry of social divides or social structures of inequality can be examining the role of power structures [32]. Philosopher Michel Foucault introduced governmentality to describe the dispersed forms of power that allow states to govern a population. Thus, the theory of power can lend support to the theoretical and empirical studies. The competing preferences of different stakeholders lead to power becoming important, and thus inquiry would require the usage of theory of power. Given that India's development agenda is a top-down approach through SBM, power structures are important. Moreover, it is argued that urbanization is a confluence of multiple social power strategies by the authorities" [10].

Also, the competing preferences bring social dilemmas to the stakeholders. Social dilemmas represent a conflict when groups work with a common goal, but reaching the goals requires both parties. In such a case, when the groups have conflicting interests, joint action becomes dejected. Nevertheless, if the goal is achieved, all the groups receive the benefit, even to those who did not cooperate. This is particularly important given the tension of corporate business strategies, and the needs and the interests of the public might have conflicting interests. These dilemmas include a value that is referred to as value dilemma comprising of traditional democratic values and efficiency-related values [33]. McCarter and Kamal [34] argued that trust, efficacy, and social responsibility are the three cooperation mechanisms that are identified by social dilemma theory. All of these are particularly relevant in the smart city context. They also pointed out that social dilemmas are inherent in partnerships between the public sector and the private sector. Thus, engaging the social dilemmas from the lens of critical theory would be quite useful in the present discourse.

4.3 Theoretical and Practical Contributions

This research can contribute to at least three theoretical developments. It could expand the body of knowledge in the context of governance, particularly that bearing with power and politics. It could demonstrate the application of critical theory to urban problems of infrastructure development. It could advance the strategies available in the contexts involving dilemmas of social nature.

Concerning practical implications, given the intense focus of smart cities in the current urban infrastructure program of India, the present study is an early step to map the necessary developments and the research/practice trajectory. Besides, in the context of 'corporate storytelling' criticism, government agencies need to understand and extract the projects in a democratic and socially justifiable manner. For instance, it is very well understood that sanctions are to be imposed by the government. The private sector could not volunteer to disclose the points of necessary monitoring [35]. Thus, the outcome of such a study could enhance the implementation of smart city projects and can be of great help to policymakers, implementation agencies, and nodal agencies.

5 Conclusions

Smart agenda is propelled by the many governments across the world. Considerable amount of literature advocates that smart cities are the only way forward to handle the rapidly increasing population while criticism exists that this smart city agenda is a 'neoliberal' agenda that feeds the capitalist. In this context, a study to understand the developments in smart city projects is a quite useful endeavor. With this

objective, this study aimed to understand the rhetoric of smart city agenda, compare and contrast the Indian and the US development agenda, and development a research trajectory for further inquiry. The findings indicate that Indian and US smart city developments are quite distinct though both are democratic countries. More comparative case studies across the geographies are needed to unveil the practice of smart city development so as to anchor the praxis to the theory development.

References

1. Batty M, Ferguson P (2011) Defining city size. Environ Plann B Plann Des 38(5):753–756
2. UN (2018) The world 's cities in 2018, The world's cities in 2018—data booklet (ST/ESA/SER.A/417). United Nations, Department of Economic and Social Affairs, Population Division, New York
3. Brenner N, Schmid C (2015) Towards a new epistemology of the urban? City 19(2–3): 151–182
4. Moser S (2015) New cities: old wine in new bottles? Dialogues Hum Geogr 5(1):31–35
5. Söderström O, Paasche T, Klauser F (2014) Smart cities as corporate storytelling. City 18 (3):307–320
6. Giffinger R, Fertner C, Kramar H, Kalasek R, Pichler-Milanović N, Meijers E (2007) Smart cities ranking of European medium-sized cities. Vienna University of Technology, Centre of Regional Science, Vienna
7. Sarkar A (2017) Smart cities: a futuristic vision. Smart City J 1–20.
8. Wang D (2017) Foucault and the smart city. Des J 20(sup1):S4378–S4386
9. Joo Y-M, Tan T-B (2020) Smart cities in Asia: an introduction. In: Smart cities in Asia, pp 1–17
10. Whitehead M (2013) Neoliberal urban environmentalism and the adaptive city: towards a critical urban theory and climate change. Urban Stud 50(7):1348–1367
11. Maček A, Ovin R, Starc-Peceny U (2020) Smart cities marketing and its conceptual grounds. Naše gospodarstvo/Our Econ 65(4):110–116
12. Poole S (2014) The truth about smart cities: 'In the end, they will destroy democracy'. The Guardian, 17 December
13. Heaton J, Parlikad AK (2020) A conceptual framework for the alignment of infrastructure assets to citizen requirements in smart cities. In: Value based and intelligent asset management, vol 90. Springer International Publishing, Cham, pp 39–63
14. SCW (2020) Open and interoperable smart cities : closing the gap. Smart Cities World, London
15. Ford DN, Wolf CM (2020) Smart cities with digital twin systems for disaster management. J Manag Eng 36(4):1–10
16. Rosen J, Grigg E, Lanier J, McGrath S, Lillibridge S, Sargent D, Koop CE (2002) The future of command and control for disaster response. IEEE Eng Med Biol Mag 21(5):56–68
17. Panagiotopoulou M, Stratigea A, Leka A (2020) Gathering global intelligence for assessing performance of smart, sustainable, resilient, and inclusive cities (S2RIC), pp 305–345
18. Dolla T, Laishram B (2019) Bundling in public–private partnership projects—a conceptual framework. Int J Product Perform Manag 69(6):1177–1203
19. Jabareen Y (2009) Building a conceptual framework: philosophy, definitions, and procedure. Int J Qual Methods 8:49–62
20. Saldaña J (2009) The coding manual for qualitative researchers, 1st edn. SAGE Publications Inc., Thousand Oaks

21. SCM (2020) City wise projects under smart cities mission. Smart Cities Mission. Available http://smartcities.gov.in/content/innerpage/city-wise-projects-under-smart-cities-mission.php. Accessed 25 July 2020
22. De Neve J-E, Krekel C (2020) Cities and happiness: a global ranking and analysis. In: The World Happiness Report
23. Praharaj S, Han JH, Hawken S (2017) (2018), "Urban innovation through policy integration: critical perspectives from 100 smart cities mission in India." City, Cult Soc 12(June):35–43
24. Bane P (2020) 2021 looks good for smart cities in the US. Smart Cities Council North America, Reston
25. IDC (2019) IDC's worldwide smart cities spending guide. IDC Corporate USA, Framingham
26. DoT US (2016) Smart city challenge: lessons for building cities of the future. US Department of Transportation, Washington, DC
27. Morrow RA, Brown DD (1994) Critical theory and methodology. SAGE Publications, Inc
28. Marcuse P (2009) From critical urban theory to the right to the city. City 13(2–3):185–197
29. Brenner N (2009) What is critical urban theory? City 13(2–3):198–207
30. Kuecker GD, Hartley K (2020) How smart cities became the urban norm: power and knowledge in New Songdo city. Ann Am Assoc Geogr 110(2):516–524
31. Marcuse P, Imbroscio D, Parker S, Davies JS, Magnusson W (2014) Critical urban theory versus critical urban studies: a review debate. Int J Urban Reg Res 38(5):1904–1917
32. White SK (2004) The very idea of a critical social science: a pragmatist turn. In: The Cambridge companion to: critical theory, pp 310–335
33. Grotenbreg S, Altamirano M (2019) Government facilitation of external initiatives: how Dutch water authorities cope with value dilemmas. Int J Water Resour Dev 35(3):465–490
34. McCarter MW, Kamal DF (2013) Recognizing and resolving social dilemmas in supply chain public-private partnerships. J Bus Logist 34(4):360–372
35. Koppenjan JFM, Enserink B (2009) Public-private partnerships in urban infrastructures: reconciling private sector participation and sustainability. Public Adm Rev 69(2):284–296

COVID-19: Claims and Dispute Management in Construction

N. K. R. Akshayah and V. P. S. Nihar Nanyam

Abstract The COVID-19 pandemic has affected many commercial activities around the globe, and the construction industry is unquestionably on the wrong end of the curve. Many construction projects are delayed and are already in a huge loss. The stakeholders of construction projects are left clueless, wondering about the new normal. During this uncertain situation, the construction industry is facing a sudden surge in the number of claims being submitted. This research is intended to understand the claims and dispute management aspects of construction, to find the frequent type of claim due to the pandemic and to address the procedure and provisions to claim under FIDIC contracts and Indian Contract Act. From the questionnaire survey, Extension of Time claim turned out to be the most frequent claim, and the procedure adopted for successful claiming of EOT has been explained with a sample project case.

Keywords COVID-19 · Claims management · Dispute resolution

1 Introduction

Claims and dispute management plays a crucial part in delivery of construction projects. However, in reality identifying and reporting these claims are mostly given less importance. Claims are in fact affecting the projects life cycle by instilling disputes and conflicts along with it. The claims should be sensibly solved in time for successful completion of the projects. Conflicts and disputes arise due to unsettled claims; hence, the involved parties should be aware of the claim's management procedure, the type of construction claims and their causes. Claims can be defined as "*demand or assertion by one of the parties seeking, as a matter of right,*

N. K. R. Akshayah (✉) · V. P. S. N. Nanyam
RICS SBE, Amity University, Noida, Uttar Pradesh, India
e-mail: akshayahr.mc19n@ricssbe.edu.in

V. P. S. N. Nanyam
e-mail: nnanyam@ricssbe.edu.in

B. Laishram and A. Tawalare (eds.), *Recent Advancements in Civil Engineering*, Lecture Notes in Civil Engineering 172,
https://doi.org/10.1007/978-981-16-4396-5_9

adjustment or interpretation of contract terms, payment of money, extension of time or other relief with respect to the terms of the contract" [1]. According to FIDIC "*claim is a request/ assertion by one party to other party for relief/entitlement under any clause of these conditions or otherwise in connection with, or arising out of, the contract or the execution of the work*". In general claim is an assertion of rights [2].

2 Literature Study

The literature study is conducted to find out the types of claims, classifications of claims with respect to many factors and to understand the dispute avoidance and resolution methods. A survey conducted by Moura and Teixeira [3] showed that the frequent type of claims made by the contractors was change claims, and the delay claims invoked were very less. This shows that the contractors were able to complete the project without any delay caused by the employer. The delay in construction is inevitable due to the pandemic. Delay may occur due to the employer as well as the contractor and may or may not affect the completion time. Hence, it is not necessary that extension of time claim should include the additional cost for loses [4]. The possible source of delay may be due to deviation in resource deployed from the planned, productivity of deployed resources, deviation from baseline and due to any unforeseen factors. These causes may result in alteration of CPM, project duration, milestone activities and can be identified and analyzed through various delay analysis techniques [5]. The report released by Turner and Townsend [6] states that in Middle East construction industry, COVID-19 may cause serious disruption and suspension of works due to labor and material shortages. The Delay analysis has to be done in order to claim Extension of Time. There are many types of delay analysis technique, but the Time Impact analysis is accepted widely. Other techniques like as planned or as built are far more expensive, time consuming and require the records from the site [7].

2.1 Research Gap

The literature study gave an insight to the current situation, and the claims arising due to unprecedented situations like pandemic. But the exact figures of the occurrence of these claims due to COVID-19 and the impact it had on the project time and cost cannot be found out just by literature study. These are all considered as research gap and necessitated the need for conducting a survey.

3 Claims Due to COVID-19

The contractual implications due to COVID-19 have caused increase in number of claims and disputes in the industry. The contractual claims that occur due to the site closure, supply chain shutdown and other government restrictions are as follows:

3.1 Delay and Disruption

Delay claims are common type of contractual claims in construction. The delay may occur due to various reasons pertaining to Contractor or Owner. The unprecedented event like COVID-19 has evidently caused delay to many projects in recent times. Before making a delay claim, the contractor must check the root cause of the delay. Employer's delays are usually excusable delays for which the contractor can claim for EOT or additional cost. The delay may be critical (that is affecting the project completion date) or uncritical [4]. There is a slight difference between delay and disruption. Disruption refers to hindrances to the progress of works whereas delay refers to the lateness. In case of disruptions, the contractor must prove that the progress has been disrupted due to pandemic. The additional cost claimed for critical delay refers to prolongation cost whereas the additional cost occurred due to disruptions but didn't affect the completion date is referred as disruption cost. In both the cases, the contractor can claim for additional cost and time or both.

3.2 Suspension

Due to COVID-19, the projects were shut down for few weeks to few months. The employer can instruct the contractor for temporary suspension of whole or part of work [8]. Sometimes, the contractor may also suspend the work due to payment issues with the owner, provided if there is a clause mentioned in the contract otherwise it will be treated as a breach of contract only. Clause 8.8 and 8.9 in FIDIC (Red book) 1999 provides the base for suspension related claims to recover the loss or EOT for suspension of works.

3.3 Termination

The parties can choose to terminate the contract due to Force majeure event if it becomes impossible to proceed the work. In such a case, both parties are freed from any further obligations under the contract. As for any losses already incurred, these will be allocated between the parties [8].

4 Data Collection and Analysis

The questionnaire form was designed with the aim to answer the objectives of the research. The questions were designed in such a way that it was answerable by both the employers/clients and the contractors. The form was circulated to construction professionals all around the world. The form received a total of 53 responses and were taken for analysis. The questionnaire contains the parameters like rate, rank, severity and frequency. A descriptive analysis is done using Tableau software. The *Cronbach Alpha test* was performed to find out the internal consistency of the responses. The alpha value is 0.99**.** This shows that the survey results are highly reliable.

52% of respondents had more than 10 years of experience in the industry. This shows that the respondents are competent, and the collected data are valid. The survey conducted had predominantly around 63% of contractors and the remaining were Clients and Consultants. Around 36% of the respondents worked in Residential building projects, 30% in commercial, 17% in infrastructure projects and the remaining in Industrial and institutional projects. 79% of the contractors were prevented from fulfilling their contractual obligations due to COVID-19. The pandemic has caused a huge impact on the project cost and time. Both the cost and schedule impact lie in the very high range as shown in Fig. 1.

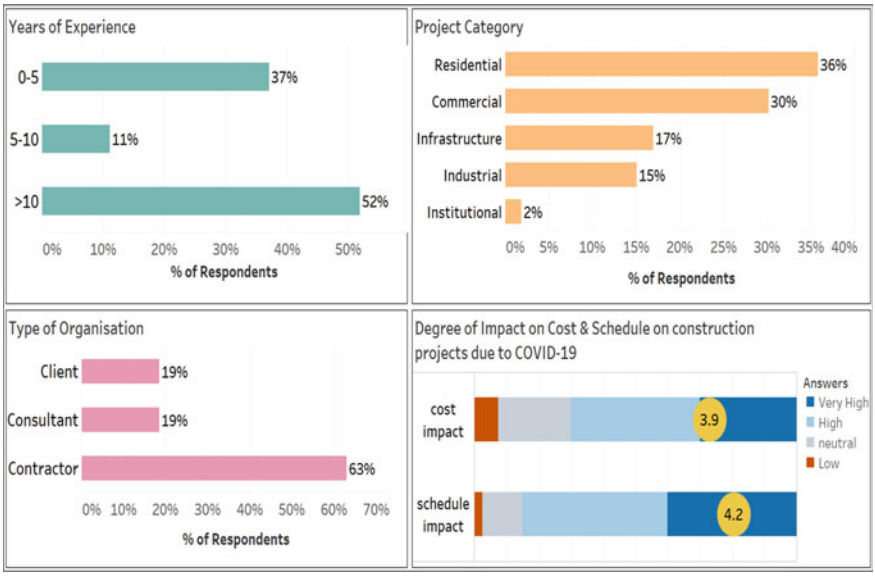

Fig. 1 Demographics of respondents and impact of COVID-19 on project cost and schedule

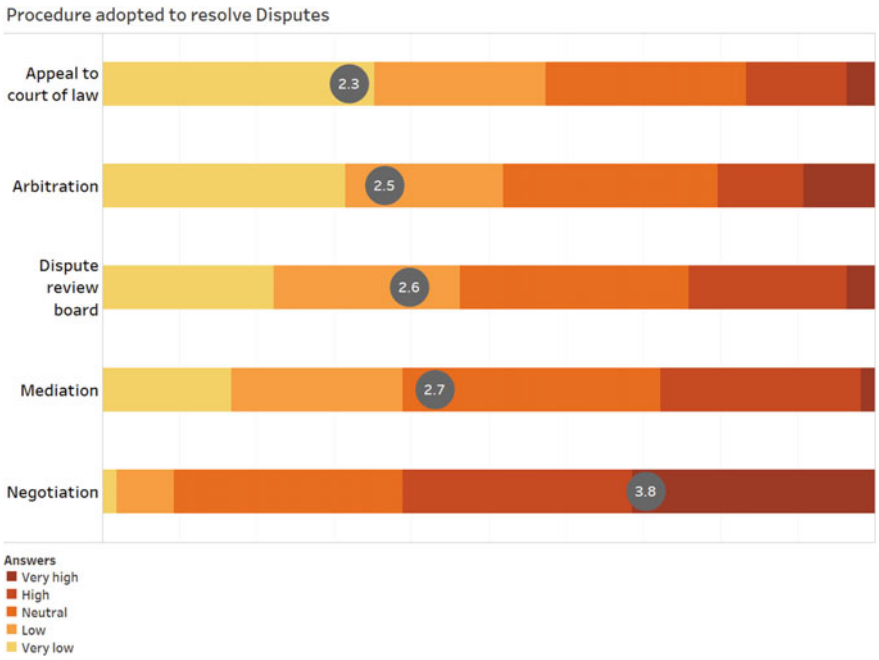

Fig. 2 Dispute resolution

The survey shows that Negotiation is the highest adopted method of resolving the disputes, see Fig. 2. The other methods are below average showing that they are least or rarely adopted methods. The advantage of negotiation is:

- Aid in maintaining a good relationship between the parties involved.
- Speedy resolution.
- No distractions in Cash flow.
- Has high success rate if a principle approach followed.
- Inexpensive and no third party involved.

The main object of the survey is to find out claims that are made frequently due to the impact of COVID-19 pandemic. From Fig. 3, it is evident that the Extension of Time (EOT) is having the highest frequency of 80% followed by the Additional Cost claim and suspension of work.

5 Procedure and Provisions to Claim EOT

In, India the lockdown has caused the site shut down for around 2 months. This has in fact delayed the projects and the standard form of contracts like FIDIC, NEC or JCT are not followed. Only big infrastructure project or projects funded by

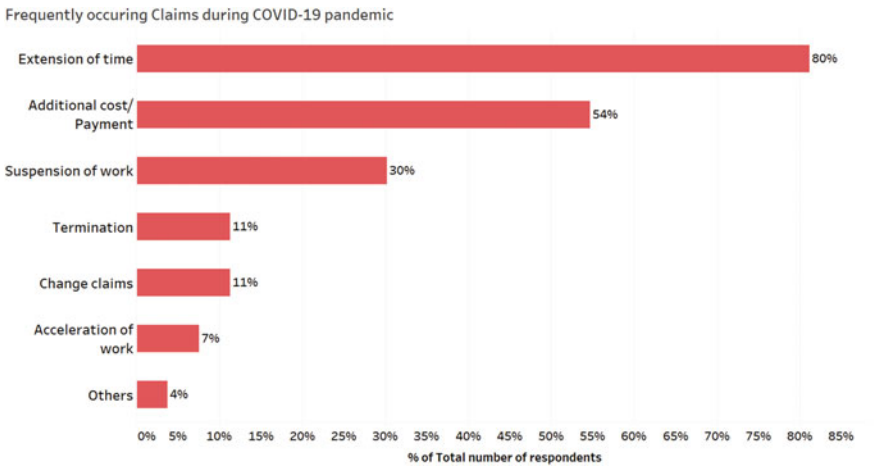

Fig. 3 Frequent type of claim due to COVID-19

international agencies follow FIDIC contracts in India. Hence to claim for Extension of time this general procedure can be followed.

5.1 Identify the Cause of Delay

Usually the delay occurs either due to client or contractor. Based on the source of delay, it can be classified as excusable and un-excusable delay. The cause of delay may be due to Government restriction, suspension of works, Loss in productivity, Labor shortage, Health and safety issues. They must be first identified and recorded. Some common causes of delay due to COVID-19 are: Site shut down from 22 March 2020 to 19th May 2020 in INDIA, Labor shortage, Migrant labor not returning to work, Transport restrictions and other government restrictions, Procurement delay, cash flow issues and Health and safety issues.

5.2 Delay Notice

A delay notice should be submitted to the client in written format. The notice should be submitted within 28 days from identifying the delay occurred in the project. This step is to alert the engineer about the situation of delay so that he can assess it. This step also aids in timely EOT and maintain the Cashflow.

5.3 Delay Analysis

There are various delay analysis technique that can be carried out to calculate the time needed for completion of the project. The delay analysis may be prospective or retrospective in nature. The selection of delay analysis method depends on terms of the contract, type of works, nature of the delay, information available and timing of the analysis [9]. Some of the delay analysis methods are discussed in Table 1.

5.4 Presentation of Claim

The EOT claims must be presented with all the evidence of the delay identified. It should contain the description of type and cause delay, contractual provisions, period of delay, date of notice issued, delay analysis methodology, proof documents for delay and its effects and finally, a statement of request for Extension of time. The following are the records to be kept as proof:

1. Approved and updated program schedule
2. Delay analysis calculations and methods used
3. Actual versus Planned progress schedule and resource schedule
4. Labor Productivity details
5. Cash flow records and forecast, profit and loss account (In case of EOT along with compensation)
6. Minutes of the meetings and correspondence letters.

Table 1 Delay analysis techniques

1. As planned versus as built	It is a simplest method of delay analysis, comparing the as built vs planned schedule. But it cannot calculate concurrent delays, and the as build data are difficult to get
2. Impacted as planned	It is another simple forensic technique, adding the delay event into the planned schedule can calculate the delay. The weakness of this method is that it rely only on as planned schedule and cannot be used for complex projects
3. Collapsed as built	This method can be performed by removing the delay event from the schedule to show the impact it has caused to the completion of the project
4. Time impact analysis	It is the most widely used prospective delay analysis technique. The fragnet schedule of concurrent delay events is inserted into the updated schedule to identify the delay that has occurred or will occur in future

5.5 Client/Consultant

The Engineer or consultant will be at the receiving the claim notice from the contractor. He may reject the claim or respond with a request for additional documents, if sufficient information is not available to assess the delay or may accept the claim. After receiving a claim notice, the client/consultant can consult the engineers or legal party to verify the facts and legal terms adopted. The reason for delay and the method used to quantify the delay can be cross-checked. The client should send a determination report stating the reasons for his decision.

5.6 Time Impact Analysis for a Sample Project

The Time Impact Analysis (TIA) is the widely accepted delay analysis method around the world. Time Impact Analysis is usually performed on an on-going project and hence considered as prospective analysis [7]. A sample project is taken to perform delay analysis. The Time Impact Analysis is worked out and explained in a Step by step process below:

5.6.1 Step 1: Develop a Schedule Delay Fragnet

To calculate the extension of time required, the delay event should be identified. The sample project is in India, and the delay duration is from 23.03.2020 to 19.05.2020, the site was closed due to lockdown for a period of 51 days. The labors reverse-migrated to their natives and returned to site after 18 days. There was a procurement delay for 7 days, and the fragnet is shown in Fig. 4

5.6.2 Step 2: Most Recently Updated Schedule

The schedule should be updated prior to the delay event and should be approved by the client. It is done in order to understand the status of the project before delay. The project start is at 12.09.2019, and the project end date is at 14.07.2020.

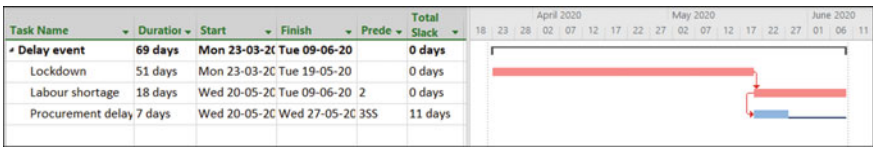

Fig. 4 Delay fragnet

5.6.3 Step 3: Insert Fragnet into the Updated Schedule

The fragnet of delay event should be merged into the updated schedule. Set the durations of delay activities as zero and recalculate CPM. At this point, the dates should match with the updated schedule. Otherwise, correct the fragnet insertion. The delay event is merged into the updated project schedule. The project start and end date should be the same, since the delay duration is not updated yet.

5.6.4 Step 4: Insert Durations of Delay

After getting approval from the client for the duration of delay, insert duration and recompute CPM. Now, the project duration has changed to 279 days, and the end date is shifted to 1.10.2020.

5.6.5 Step 5: Identify the Activities Causing Delay

Identify the critical activity altering the project completion date. If the delay fragnet is not critical, then it means that the project is disrupted not delayed. But here, the delay activity is altering the completion date of the project.

5.6.6 Step 6: Determine the Time Impact of Delay Event

Identify the period of delay in the activity. In this project, brickwork is delayed for a period of 9 days before the delay event has occurred. Hence, this is an un-excusable delay.

5.6.7 Step 7: Identify the Actual Dates of Delay

The delay has occurred from 23 March 2020 to 25 June 2020. The difference between the durations minus the un-excusable delay gives the EOT period. In the sample project considered, the contractor needs an extra 48 days to complete the project.

5.7 The Advantage of Time Impact Analysis Method

The Time Impact analysis is the recommended analysis method for delay calculation. The advantages of this method are as follows:

- It is a prospective analysis method- “forward looking”.
- The actual progress of the project is taken into consideration.

- An accurate method for delay calculations for projects in construction stage.
- The delay activities are segregated in a fragnets for the ease of analysis.

5.8 Disadvantages of TIA

- It requires Accurate progress information of the project, otherwise the results will be wrong.
- Needs expertise in handling this method.

5.9 Provisions for Claiming Under FIDIC and Indian Contract Act

On 11th March 2020, World Health Organization announced that COVID-19 as a pandemic. Though the word pandemic is not listed under the Force majeure events, the pandemic can still be taken as the Force majeure because it says, "but is not limited to" the specified events. On May 14th the finance ministry of India ordered to treat COVID-19 as a Force Majeure event. "All the projects registered under RERA, having completion date on or after March 25th can be given extension of completion date." The following are the provisions to claim under FIDIC and Indian Contract Act. The FIDIC red book, 1999 contains clauses 19.1 to 19.6 specially framed to claim for Force Majeure. Under "Sec 32: Enforcement of contract contingent on an event happening" and "Sec 56: Doctrine of Frustration of Contract" in the Indian Contract Act, 1872 can be used to claim for disruption due to unforeseen circumstances.

6 Conclusion

This research was conducted to identify the recurring claim in the construction Industry due to the COVID-19 and to provide the process to be followed and provisions for claiming under FIDIC and Indian Contract Act. Through literature study the types and source of claims occurring due to pandemic was identified. A questionnaire survey was conducted to extent of impact on the project due to COVID-19 and the frequently occurring claims due to it. The data analysis was done using Tableau Desktop software, and the results have been discussed. It was found that Extension Of Time was claimed frequently due to COVID-19 impact on the project schedule. The step by step process to be followed for claiming EOT is explained from a contractor and client's perspective. The delay analysis techniques

were studied, and the Time Impact Analysis was performed on a sample project, and the step by step methodology to conduct TIA is provided. The survey also identified the most common dispute resolution method as negotiation, and the advantages of negotiation were discussed.

6.1 Limitations

The research gave solution only for Extension Of time claim, since it was frequent claim due to COVID-19. The EOT can also be claimed along with additional costs for the losses incurred. The procedure for additional cost claim is not discussed in this research. The Delay analysis considered only one window of delay-due to pandemic. The concurrent delay cases were not taken for study. The provisions are given for claiming under FIDIC and Indian Contract Act alone.

6.2 Future Scope of Research

The procedure to claim for additional cost or prolongation cost can be a future scope of the project. The delay analysis for concurrent delays can be conducted on a case project. The delay and losses occurring due to inefficient claims management can be conducted as a case study.

References

1. Levin P (1998) Construction contract claims, changes, and dispute resolution. American Society of Civil Engineers
2. Contract FIDIC (1999) Federation Internationale des Ingenieurs Conseils
3. Moura HMP, Teixeira JMC (2007) Types of construction claims: a Portuguese survey
4. Designing Buildings Wiki, "Employer delay" (2019). https://www.designingbuildings.co.uk/wiki/Employer_delay
5. BIS (2013) Construction project management—guidelines
6. Turner, Townsend (2020) Middle east client guidance: coronavirus (COVID-19)
7. AACE International Recommended Practice No. 52R-06 (2006) Time impact analysis—as applied in construction
8. Murdoch J, Hughes W (2015) Construction contracts: law & management. Routledge
9. RICS (2014) Extension of time. RICS guidance note, no. 1

Factors Affecting Delays in Infrastructure Construction Projects

Arun Kumar Ahuja and Awanish Gaurav

Abstract Construction delays have always been a major cause of concern for construction industry and attained focus from many researchers. Projects having long life cycle, particularly infrastructure projects, are highly uncertain in delivering projects within contractual time frame. Infrastructure projects in developing nation have seen various factors impacting the project delivery which in turn measured as overall time, cost and quality of projects. An attempt is made in this paper to understand and to identify various factors contributing to delays based on claim settlement and to see the pattern followed by these factors. In this study secondary data have been collected from reliable sources which translate verdicts of arbitration cases arise in construction industry. The collected data have been analyzed to identify the factors affecting construction project delays and reflecting in decisions of verdict. The study reveals that the factor "delay in taking approval and availing permits to the contractor from statutory authorities and handover" plays predominant role and generally resulted in monetary compensation and time extension, factor titled "delay due to change orders/change in scope of work and work stoppage" generally resulted in time extension and "delay due to late handing over of site and late delivery drawings and documents" has resulted in monetary compensation. Findings of this study enable us to exercise suitable strategy during project execution as a part of decision making.

Keywords Construction delays · Developing economy · Strategic management

A. K. Ahuja (✉) · A. Gaurav
RICS School of Built Environment, Amity University, Noida, Uttar Pradesh 201313, India
e-mail: aaahuja@ricssbe.edu.in

A. Gaurav
e-mail: awanishg.mc18n@ricssbe.edu.in

B. Laishram and A. Tawalare (eds.), *Recent Advancements in Civil Engineering*, Lecture Notes in Civil Engineering 172,
https://doi.org/10.1007/978-981-16-4396-5_10

1 Introduction

Construction sector employs more than 100 million people throughout the world and contributes for 6% of world GDP, according to the world economic forum. In fact, it accounts for roughly 5% of overall GDP in advanced nations and 8% of GDP in emerging economies [1]. The construction sector has substantial linkages with other industries, which means its effect on GDP, and economic growth stretches much further than the direct contribution of construction practices. Projects completion improves GDP.

Indian construction industry being the second largest industry in India after agriculture occupies key position in development. Construction of infrastructure projects involves lots of time and cost, and most certainly in India these projects encounter various problems. Infrastructure project delay leads to time and cost overruns due to varying factors affecting the project completion. Any time delay or cost overruns during execution of project, generic type of claims is delay claims, which settles either by time extension, monetary compensation or combination of both monetary and time extension. There can be multiple factors in a project that lead to delay in the project; based on the severity of those factors, it is assessed whether the delay claims will be approved in favor of the contractor or it will be counted as a liquidated damage. Also, if the claim is in favor of contractor, it is needed to be assessed whether it is monetary in nature or extension of time (EOT) or both.

All these decisions are taken in the stage of dispute resolution where in a third party is involved to make the decision, in India which is usually judges or arbitrator. Indian construction industry involving huge capital and time is most prone to conflicts which results into disputes. These disputed projects are presented to the judiciary system of India, who further settles the claims.

In this paper we tried to find the most popular or common factors which cause the delays of an infrastructure project along with and its pattern that shows how these cases were resolved in the Indian judiciary system under litigation or arbitration cases. Case laws were collected from online platforms in data collection.

2 Indian Scenario in Construction Delays

A standard and well-drafted document having clear scope and requirement can avoid many clashes; however, many claims and disputes are raised by the parties due to improper contract management and some other unforeseen events. Delay is one of the main sources of claim and often experienced issues in the construction industry where its characteristics are well understood, but basic causes and resulting impacts are not recognized by experts. Therefore, a lot of projects are suffering from project delay globally.

As far as delay in Indian construction scenarios is concerned, Indian government's Ministry of Statistics and Program Implementation (MOSPI) [2] has revealed those out of the 782 construction projects it monitors in India, a total of 215 projects are delayed with the overrun time varying from 1 to 261 months. The main causes listed are delays in the purchase of land, securing forest/environment clearances, completion of project funding, finalization of comprehensive engineering, tendering, ordering and supply of equipment, lack of infrastructure support and links, changes in scale, delays in tendering, ordering and supply of equipment, law and order issues.

Moreover, in the infrastructure sector of India delays and cost overruns have become a trademark, whereas only a few of the Indian infrastructure projects complete without any of the time or cost overruns. Delays and cost overruns have important economic as well as political consequences. Due to problems in executing projects people must wait longer for the commissioning of public projects. Benefits offered by infrastructure projects act as supply to other sectors. To look at it another way, delays and cost overruns decrease the productivity of the existing economic resources.

3 Literature Review

There has been a lot of research around the globe in order to study and analyze the delays impacting a project. Most of them are based upon the RII methods to rationalize the various factors responsible for causing delays in a project.

Iyer et al. [3] in his two research journals emphasized upon the various factors causing the delay-related disputes in any construction contracts. His findings have been cited in many journals and research works. In his paper he explains about the major factors impacting the project schedule and causing delays among which late handing over of site, irregular changes in scope, change orders, inadequate site conditions, poor performance and supervision are few major factors leading to the delay in a construction project.

Another very eminent work by Patil et al. [4] in his research paper about the delays in construction work of infrastructure projects has mentioned that there are 5 most important factors responsible for any construction delay and those are land acquisition, environmental impacts, financial closure, change orders and poor site management and supervision.

Some of the other major contributors in the field of delay analysis have all mentioned various factors that are responsible for delay in a project. Out of which if we try to summarize the factors causing delays in a project from the contractors' perspective, then these are delay in attaining approvals and permits from various statutory authorities, delay in delivering designs/drawings, etc., inefficient feasibility studies, underestimation of project completion date and budget, decision making, approvals are another very popular reason of causing delays in a project [5, 6].

Apart from Indian scenarios [7] has done a very conclusive research in studying the general causes of delays in a construction project globally. His research on 28 developing countries includes UAE, INDIA, CHINA, South Africa, Libya, Pakistan, etc. In study he has mentioned factors like delay in decision making, improper design management, inadequate feasibility study and poor contract management and ill-communication that are the prominent causes of delays in a project.

While reviewing literature, it has been observed that most of the research and findings are conducted in the horizon of delay analysis, whereas only a few of the research papers, journals are available to understand the claims management and claim settlement in the construction project. With any delay in the construction project, responsibility of stakeholder is identified and delay is registered as claim, which sometimes becomes disputed because of scope clarity or the impact of factor causing delay on various subsequent decision and actions by stakeholders, so when the delay claims are filed, then it is important to know the various factors based on which the claims in any project are awarded or rejected. Hence the factors considered in claim settlement and the patterns for these factors can help in strategy making and drafting contractual document.

Zoran Stojadinovic is a Serbian researcher who has explained about the claim quantification claims management and various types of claims and its possible compensations [8]; in his research, it is seen that claims are broadly of seven types, viz., delay and schedule extension claim, acceleration, compression, impact and ripple claims, inefficiency and disruption claims, formal and constructive change order claims, quantum merit claims, wrongful termination claims, breach of contract claims. Out of these seven claims we limited our scope to delay claims which further has three classifications based on the verdict of arbitration court, i.e., (1) extension of time, (2) monetary compensation, (3) combination of time and monetary companion, and (4) claim is rejected in some cases. Now this occurrence of delays can be direct, concurrent and serial delays. Also, delay claims can also be subdivided based on the monetary compensation available for it. Therefore, from the perspective of a contractor claims are compensable, non-compensable and inexcusable [5]. Mitigation strategies were developed for delay claims and how the situations of dispute can be avoided. It has a very interesting diagram which helps in understanding the responsibility of stakeholders in a construction project for claim prevention. It explains how each stakeholder is responsible for leading to claims and how these parties can help in resisting the scenarios of filing of claims.

Other than these studies, some other research studies have been referred to for the data [9–12].

4 Methodology

In this research the approach is to gather data from various disputed random claims, which were resolved by arbitration court of law either settlement awarded or rejected, identifying the factors responsible for delays and assessing the pattern of

factors impacting decision of arbitration court. This study will be important to understand the factors causing delay in project completion and help in establishing a pattern to the decision making in claims settlement in the delay claims and support in business strategy.

This research is performed based upon the secondary data extracted from reliable online sources which transcript the verdict of arbitration cases as repository of primary data and with utmost logical database available across India in context with the built environment sector. The data are processed on MS excel to provide with some figures to subjectify the expected outcomes and pattern followed in dispute resolution. To understand the modern construction scenarios, we have weighted this research upon the case studies having timeline of 2010 to present, wherein the cases are strictly subjected to delayed projects and claim-related cases.

All the cases selected in the study, from the online platform, are classified under these heads to simplify the understandings of the cases and to make it more selective in order to support our research work. The data which have been drafted are limited by certain conditions that are:

- Cases selected for study are in between the year of application of 2010 and 2019.
- Union of India or any subsidiary authority under Indian Government is considering as at least one of the two parties (Plaintiff or Defendant).
- Only the verdict relating to the delay claims and settlements is considered in this study.

Once we set up an opinion on the factor causing the delays in the project and the type of claims, the effort is stressed upon attempt to again rank the factors based upon the frequencies and responses in the court on the various different cases in terms of claims settlement. The whole idea behind is to lessen the load of the Indian judiciary system and helping the clients and contractors to find a pattern that causes delays and accordingly to draft a better contract document to mitigate the chances of dispute such that predetermining the compensations corresponding to the delay claims having certain factors of delay in it.

5 Data Collection

In this research there are two types of data collected, one is factors causing delays in the project from literature and another is factors causing delays from settlement of arbitration case laws.

For the first database, referred as (data set #1), i.e., factors causing the delays in project, we have relied upon prominent researchers in the area of delay analysis & claims management with perspectives of contractor's viewpoint. We concentrated on built environment sector rather than sectorial project in this study. Hence related research papers were taken into consideration while identifying factors causing the delays in a construction project.

Table 1 Factors responsible for delays as per journals and researches

S. No	Factors responsible for delay	Cited by
1	Change order by client during project/rework, additional work orders	[4–7, 9–12]
2	Delay due to subsurface conditions	[4, 9]
3	Delay due to late handing over of site	[4, 9, 10]
4	Under estimation of cost and duration of project	[9, 10, 12]
5	Delay in attaining approvals from authorities	[4, 9, 10]
6	Delay due to late supply of drawings, materials, facilities	[4, 6, 7, 9, 10, 12]
7	Insufficient feasibility studies and surveying	[4, 7, 9, 10]
8	Environmental impacts on project	[3, 4, 10]
9	Delay due to finances, late release of payments	[4–6, 10–12]
10	Delay in decision making, stage passing	[5, 7, 10]

The credibility of our findings will be justified by the background research work done by these researchers as well as the literature review done by us to support the understanding of us in this research, shown in Table 1.

For the second database, referred as (data set #2, shown in Tables 2 and 3), i.e., factors of delay identified from claims settlement by court of law, we have utilized the records available of the case laws registered under the Indian judiciary system, these are basically the cases which have been trialed inside courts of India, and these have been recorded by some 'go to platforms' who have stored cases appeared in the court and their judgments as repository. In one of such platforms we have used the advanced search method to find out the court cases which concerns us. We have invested our time in studying these cases and formulating a worksheet to uphold the secondary data using which we can identify factors based on decision and establish a pattern, and these cases are specifically centered on the built environment sector and involve parties that have disputes because of delays in the project or sometimes due to disagreement toward delay claims. In each of the cases the scenarios differ, and the conditions of the project are also different. We study these cases and summarize the judgment and identify the type of compensation awarded to the contractor identifying factors responsible for the delays in that project.

Out of many such platforms we have visited "*LegitQuest*" as our source of transcripted database as it provides a good interface to ease the filtering and searching and understanding the judgments by simplifying the jargons of law in their own words. In this website using advanced search option we were able to find out 210 cases related to the built environment, taking 210 cases as the population of the subject in which we are conducting research. Since 210 cases are a very huge number for sampling, thus using the concepts of sampling and making a sample of 10% of the population, i.e., 21 cases to be precise, these 21 cases are top cases listed below according to year of application as per their relevance to the area we are researching (Tables 2 and 3). These cases involve disputed cases of construction

Table 2 List of cases between 2010 and 2015

Date of application	Court type	Case name	Claimant	Respondent (defendant)
25-02-2010	High Court of Delhi	All India Radio V. M/s. Unibros & Another	All India Radio	M/s. Unibros & Another
27-04-2010	High Court of Andhra Pradesh	M/s. Tarapore & Company V. M/s. Hindustan Steel Works Construction Ltd	M/s. Tarapore & Company	M/s. Hindustan Steel Works Construction Ltd
26-08-2010	High Court of Andhra Pradesh	V. Thyagarajan and Bros., Engineers & Contractors V. Union of India & Another	V. Thyagarajan and Bros	Union of India
13-12-2010	High Court of Delhi	Kalyan Chandra Goyal V. Executive Engineer, Southern Western Division-8, Delhi Development Authority	Kalyan Chandra Goyal	Delhi Development Authority
10-02-2011	High Court of Judicature at Calcutta	Union of India (UOI) V. Cementone	Union of India	Cementone
20-12-2011	High Court of Delhi	Rama Construction Company V. Municipal Corporation of Delhi	RAMA Construction Company	MCD, New Delhi
08-02-2012	High Court of Delhi	Delhi Development Authority V. M/s. Associates Builders	Delhi Development Authority	M/s. Associates Builders
16-05-2012	High Court of Delhi	Gas Authority of India Ltd. (Gail) V. M/s. Bhageertha Engineering Ltd	Gas Authority of India Ltd. (Gail)	M/S. Bhageertha Engineering Ltd
17-09-2012	High Court of Judicature at Bombay	Union of India V. M/s. Suraj Infrastructures Pvt. Ltd. Having its office at 101/102	Union of India	M/s. Suraj Infrastructures Pvt. Ltd
27-09-2012	High Court of Delhi	Unitech Limited V. Housing & Urban Development Corporation	Unitech Limited	Housing & Urban Development Corporation

(continued)

Table 2 (continued)

Date of application	Court type	Case name	Claimant	Respondent (defendant)
10-12-2013	High Court of Judicature at Bombay	Board of Trustees for Jawaharlal Nehru Port V. Gateway Terminals India Pvt. Ltd	Board of Trustees for Jawaharlal Nehru Port	Gateway Terminals India Pvt. Ltd
11-08-2014	High Court of Judicature at Bombay	M/s. Mascon Multiservices & Consultants Pvt. Ltd. V. Bharat Oman Refineries Ltd	M/s. Mascon Multiservices & Consultants Pvt. Ltd	Bharat Oman Refineries Ltd
06-05-2015	High Court of Judicature at Bombay	Union of India, Through Dy. Chief Engineer (Con)/ Works V. M/s. Vinay Agarwal	Union of India	M/s. Vinay Agarwal
02-11-2015	High Court of Delhi	Union of India V. M/s. Ktech Engineers Builders Co Pvt Ltd. & Another	Union of India	M/s. Ktech Engineers Builders Co Pvt Ltd

Table 3 List of cases between 2016 and 2018 considered in study are tabled below

Date of application	Court type	Case name	Claimant	Respondent (defendant)
22-09-2016	High Court of Judicature at Madras	Union of India, Rep. by the Executive Engineer, Chennai V. M/s. Consolidated Constructions Consortium Ltd., Chennai & Another	M/s. Consolidated Construction Consortium Ltd	Union of India represented by Ex. Engg, Chennai
10-10-2017	In The High Court of Judicature at Hyderabad	M/s. Jaiprakash-Gayatri Joint Venture, Rep. by its Authorised Signatory V. State of Andhra Pradesh, Rep. by its Principal Secretary, Irrigation and Command Area Development Department	M/s. Jaiprakash-Gayatri Joint Venture	State of Andhra Pradesh
25-05-2018	High Court of Delhi	National Highway Authority of India V. Gayatri Jhansi Roadways Limited	National Highway Authority of India	Gayatri Jhansi Roadways Limited (GJRL)
09-07-2018	The Madurai Bench of Madras High Court	The Superintending Engineer, WRO/PWD, Tirunelveli V. S. Karuppaiah, Contractor, Madurai & Another	The Superintending Engineer, WRO/ PWD, Tirunelveli	S. Karuppaiah, Contractor, Madurai
09-07-2018	Before the Madurai Bench of Madras High Court	The Superintending Engineer, WRO/PWD, Tirunelveli V. S. Karuppaiah, Contractor, Madurai & Another	WRO/PWD, Tirunelveli	S. Karuppaiah, Contractor, Madurai
01-11-2018	High Court of Delhi	M/s. Harcharan Dass Gupta Construction Pvt. Ltd. V. MCD & ANR	M/s. Harcharan Dass Gupta Construction Pvt. Ltd	Municipal Corporation of Delhi
14-11-2018	High Court of Delhi	M/s. Satya Parkash & Bros (P) Ltd. V. Government of NCT of Delhi & ANR	M/s. Satya Parkash & Bros (P) Ltd	Government of NCT of Delhi & ANR

works where at least one party has filed for delay claims based on certain factors of delay which then is countered by the other party and eventually the judge offers the judgment which is usually the claim rewarded or rejected. So, in our research we are trying to trace a pattern of this judgment where we can figure out the response of the judgments for any delay claims applied by a contractor depending upon the factors accountable for delay.

6 Classification of Sample Data

The case laws listed above were studied, and information related to factors and verdict was extracted from the database. It was done in a much-organized manner by segregating the information under various heads such as date of application, court type, case name, claimant, respondent, delay duration (days), brief of case, reasons for delay, verdict and type of claim approved with citations.

After the preparation of the sheet with all the above-mentioned headings we have tried to analyze the nature of the data by counting the varying cases using functions of MS excel. It basically gives a better picture of analytics of the data. So, to understand the nature of data we have calculated the number of cases of similar compensation. So, the classification of cases was done in between—

- Monetary compensation—claimant was awarded monetary compensation.
- Extension of time—claimant was awarded extension of time.
- No claims approved—claimant's claim was rejected.
- Both time and monetary compensation—claimant was awarded both monetary compensation and extension of time.

So out of the sample of 21 cases we acknowledged that 38% of cases were having the claim settlement of extension of time, 24% of cases had claim settlement of both time and monetary compensation, whereas cases of judgment stating no claim approval and only monetary compensation were just 19% each (Fig. 1; Table 4).

So, from this representation we have acquired an idea of the nature of the sample collected. We can state that majority of cases that goes under trial under delay claims results in an outcome jury awarding the claims with extension of time as compensation. Also, we can say that approximately 50% cases that go under trial

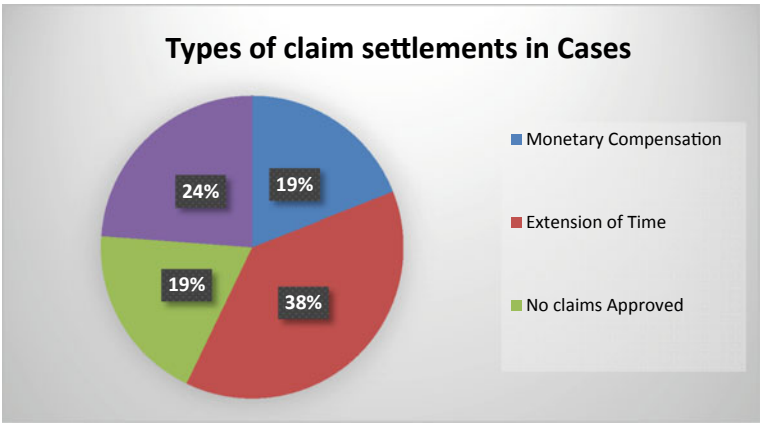

Fig. 1 Piechart representation of sample

Table 4 Classification of sample

Types of compensation	No. of cases
Monetary compensation	4
Extension of time	8
No claims approved	4
Both time and monetary compensation	5

result into awarding some or the other type of compensation to the contractor. It is important to note that the values of percentage may differ as the sample size is increased.

7 Data Analysis

To establish a relationship among the two separate databases, i.e., factors causing delay in project and types of claim settlements it is important to identify a link between these two data sets. So, we determined the link from the cases (Data Set #2) in which every case has few factors that cause delay in the project and we utilized those factors or reasons that lead to delay as our link to establish a relationship among these two data sets.

We have segregated the factors of delay under the groups of claims types, such that every factor will lie under the group of either monetary compensation, extension of time or both time and monetary compensation. Through this it will give an idea of the recurrence of the factors of delay under each claim type. Eventually, using those recurrences of the factor we will be able to rank those factors based on frequency form random selection of project cases of all types of settlement.

So, the idea behind linking these data sets is to establish a new ranking of factors of delay in a construction project based upon the claim types, justified by the primary data sets. Through this ranking we will be able to comment on the claim settlements or type of compensation prevalent in the Indian judicial system when the delay claim is filed in the court in the case of a dispute. Therefore, the group listing of the factors is shown in Fig. 2.

So, we have created three groups for the type of claims awarded in the cases of the sample data and inside those groups we have enlisted the factors that were mentioned in the cases. Among those enlisted factors of delay, we have counted the recurrence of the factors in the individual cases and based on that we have plotted pattern for this in Fig. 3.

It is important to understand that cases where no claims were approved cannot be classified as a group because if no compensation is provided, then it signifies that no delay claims were approved and similarly no delay was there in the project as per the context of the Indian judicial system. No injuries mean no reward.

For the monetary compensation & extension of time	For the compensation of extension of time	For the monetary compensations
•Delay in Taking approval & Availing permits to the contractor from statutory authorities •Delay due to late Handing over of site •Delay due to stopping of work by client due to their reasons •Delay due to late decision making and approval by engineer and designers in charge •Delay due to external factors	•Delay due to change orders/ change in scope of work •Delay due to unavailability of resources/manpower •Delay due to late releasing of funds/mobilisation advance •Delay due to Force Majeure/ Notified Suspension of Work •Miscellaneous	•Delay due to late Handing over of site. •Delay due to extra contractual works/ Reworks •Delay in Issuing Working drawings/Omission & obstructions •Delay in Conveyance of Material/ other facilities •Delay in Clearing payments

Fig. 2 Group listing of the factors

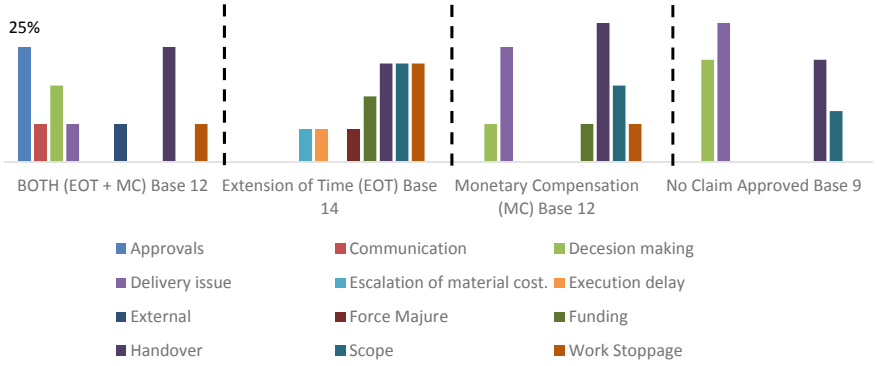

Fig. 3 Mapping of factors in decision making based on frequency

8 Conclusions and Discussion

From this study, we can identify various factors involved in decision making and were able to make a pattern of such factors on claims settlement and shortlisting some most critical factors that are responsible for a delay in any construction project and also what sort of compensation should be best suited for such cases.

For example, if the client is unable to attain approvals and permissions from the statutory authorities leading to the delay in the project. So, when a contractor files a delay claim stating the reason of delay being delay in approvals, then the client is

liable to compensate the contractor with both time and monetary compensation considering all remaining actions done and informed well in time.

So, as evident in the cases taken, due to this grouping of factors it became very easy to determine the compensation or the outcome of the delay claims whether to be approved or discarded.

From the data analysis of the sample data we can comment that in the case of both time and monetary compensation critical factors are delay in providing approvals to the contractor, delay in handing over of site, delay due to unnotified stopping of work by client, etc, whereas in the case of extension of time as compensation delays due to change in scope of work, delay due to unavailability of resources such as machinery, manpower and material (if obligated to client), delay in releasing of finances such as advances, running account bills are the most critical factors that impact on deciding the claim settlement type. Finally, in the case of monetary compensation, it is very similar to the case of both time and monetary compensation because in most of the construction scenarios the major fight is attaining the monetary compensations which is why the factors on which the monetary claims are approved are more or less similar to the case of both time and monetary compensation. So, in the monetary compensation, factors impacting the decision are delay in handing over of site as the most critical, delay due to extra contractual work, delay because of client's obstruction and approvals.

In the current times of fast redressal system, it is very important to understand the significance of time and money and in the current built environment sector there are numerous examples of delayed resolution of claims filed by the contractor. During the research, it has been observed that a lot of cases which has been trialed into courts are some or the other disputed cases wherein the parties are not satisfied with the judgments and hence they reach out to the highest order of court to review their cases. In order to make satisfactory and quick decisions courts usually refer to the cases from the past and justify their judgment. So, as to end this tedious process of judgment we conducted a research with anyway a very small sample size just to figure out a way through which the claims settlement process can be reduced, and the claims can be rewarded easily.

References

1. Renz A, Solas MZ (2016) Shaping the future of construction a breakthrough in mindset and technology. World Economic Forum, Switzerland
2. MOSPI (2016) Ministry of statistics and programme implementation annual report 2015–16. New Delhi, pp 103
3. Iyer KC, Chaphalkar NB, Joshi GA (2008) Understanding time delay disputes in construction contracts. Int J Project Manage 26(2):174–184
4. Patil SK, Gupta AK, Desai DB, Sajane AS (2013) Causes of delay in Indian transportation infrastructure projects. Int J Res Eng Technol 2(11):71–80
5. Salunkhe AA, Patil RS (2014) Effect of construction delays on project time overrun: Indian scenario. Int J Res Eng Technol 3(1):543–547

6. Chaphalkar N, Iyer KC (2014) Understanding time delay disputes in construction contracts. Australas J Constr Econ Build 14(1):32–44
7. Islam MS, Trigunarsyah B (2017) Construction delays in developing countries: a review. J Constr Eng Project Manage 7(1):1–12
8. Stojadinovic Z (2018) Claims on construction projects-quantification and prevention. In: Contemporary construction practice. Serbia, pp 83–112
9. Shahsavand P, Marefat A, Parchamijalal M (2018) Causes of delays in construction industry and comparative delay analysis techniques with SCL protocol. Eng Constr Archit Manag 25(4):497–533
10. Doloi H, Sawhney A, Iyer KC, Rentala S (2012) Analysing factors affecting delays in Indian construction projects. Int J Project Manage 30(4):479–489
11. Shanmugapriya S, Subramanian K (2013) Investigation of significant factors influencing time and cost overruns in indian construction projects. Int J Emerg Technol Adv Eng 3(10): 734–740
12. Singh R (2010) Delays and cost overruns in infrastructure projects: extent causes and remedies. Econ Pol Wkly 45(21):43–54

Model to Predict Additional Usable Carpet Area in Building Redevelopment Projects of Housing Societies in Mumbai City

Vinod Vanvari and Sumedh Mhaske

Abstract Mumbai city is witnessing redevelopment of old buildings since decade and half due to space scarcity, particular geometry, geography and ever persisting demand of housing. Redevelopment is happening for public buildings, private buildings and also for buildings under housing societies. There are various constraints and considerations, multiple stake holders, changing polices, challenges at site. Hence, there are many determinants which directly or indirectly affect process of building redevelopment projects of housing societies. However, the additional usable carpet area which tenants are going to get when their building is undergoing redevelopment, is the key determinant governing not only the process, but also decision making done by the stake holders. This additional carpet area is function of financial feasibility of project, which in turn is dependent on many factors like plot size, its geometry and location, market value prevailing in locality, Floor space Index (FSI) consumed and balance. Research study is carried out by interacting stake holders through semi-structured interviews and analysing valid responses of structured questionnaire using SPSS. Many determinants are found including additional usable carpet area to the tenants. Further using this key determinant, based on financial feasibility, mathematical model of area factor is developed. This model facilitates prediction of additional usable carpet area which tenants can get once their society building undergoes entire process of redevelopment. The model is also tested by adopting sensitivity analysis. This paper attempts to illustrate need and use of this model along with its limitations.

Keywords Building redevelopment projects · Housing societies · Process · Area factor · Additional usable carpet area

V. Vanvari (✉) · S. Mhaske
Department of Civil and Environmental Engineering, Veermata Jijabhai Technological Institute (VJTI), Matunga, Mumbai 400019, India
e-mail: vbvanvari_p13@ci.vjti.ac.in

S. Mhaske
e-mail: symhaske@ci.vjti.ac.in

B. Laishram and A. Tawalare (eds.), *Recent Advancements in Civil Engineering*, Lecture Notes in Civil Engineering 172,
https://doi.org/10.1007/978-981-16-4396-5_11

1 Introduction

Decent housing and the supporting urban infrastructure are fundamental drivers of improving quality of life. India has a more ambitious target in mind, the government recently announced *Housing for All* policy which aims to provide every citizen access to adequate housing by 2022. Here the government has articulated the policy of incentivizing the private sector to participate in effective redevelopment of entire slum community [1]. However, there is segment above slum but below affluent class, i.e. redevelopment of buildings belonging to housing societies.

2 Literature Review

Urban development department of State government and Municipal Corporation of city through development control regulations and reforms, govern the redevelopment of buildings in the segment of housing societies from time to time [2, 3]. This segment does not catch attention of national policy makers. Activity of building redevelopment of housing societies in spite of many risks and challenges is taking place steadily and saliently since last decade and half or more. Obvious reason, land available is scarce [4]. The redevelopment process has its specific pattern for delivery and business dynamics [5, 6].

2.1 Review of Literature Studied

After studying the relevant literature, the following area was called for further study relevant to the area concerned.

2.1.1 Feasibility of Building Redevelopment Projects

Before any project is proposed and promoted, it is imperative to have feasibility studies related to the same, so as to ascertain its successful accomplishment. For building redevelopment projects, it is necessary to have complete feasibility study because of the following reasons.

First, in Mumbai city, the space for developing a new green field project is scarce and the old buildings are to be redeveloped into new tall buildings with prevailing development control regulations to accommodate both, the tenants and potential flat purchasers in near future. It is a complex process involving multiple stake holders with varied interests. Secondly, for redeveloping a building, there needs to be a redeveloping agency or some proper team for self-redevelopment.

Lastly, project must comply to all kind of norms and regulations such as social, legal, statutory besides financial feasibility. Hence, study of all types of feasibility as below is a must.

- Environmental feasibility
- Physical feasibility
- Socio-economic feasibility
- Financial feasibility.

Figure 1 depicts four parameters of feasibility.

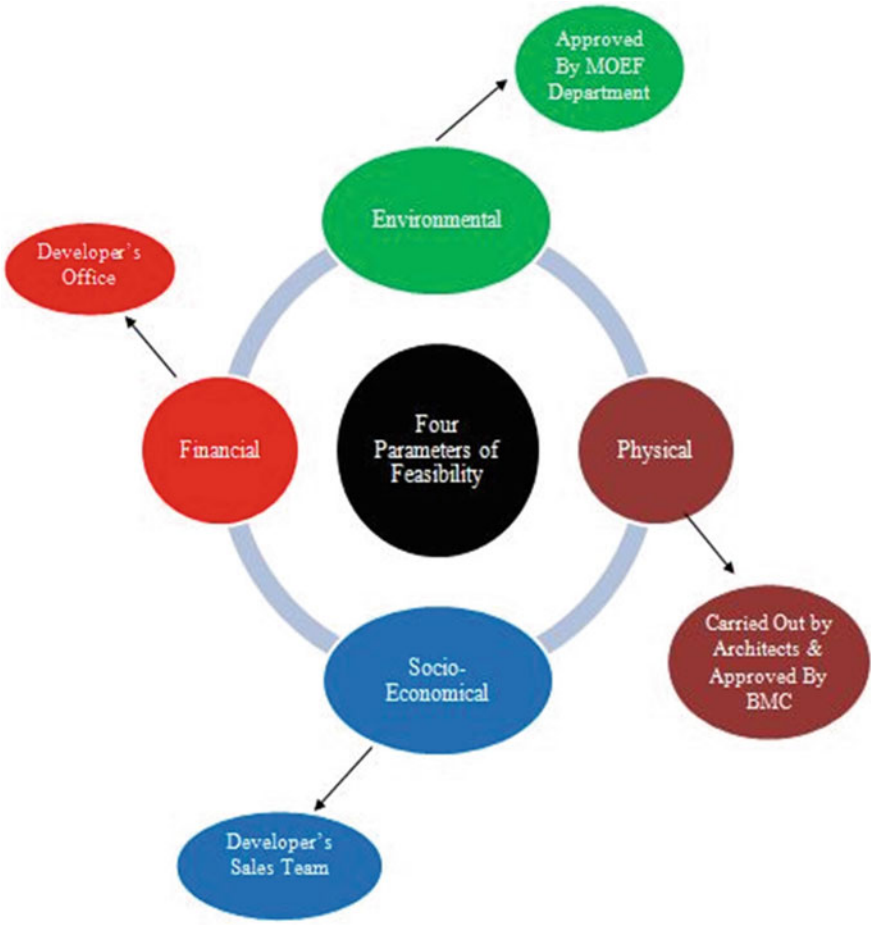

Fig. 1 Parameters of feasibility of building redevelopment projects

2.1.2 Financial Feasibility of Building Redevelopment Projects

Financial feasibility study is an assessment of the financial aspect of the project. For instance, the cost of expanding production will entail five crores, whereas revenue is expected to increase by eight crores. Thus, the project is feasible as its revenue is more than its costs.

All the types and parameters of feasibility are important. However, financial feasibility is one of the main parameter, as it is an assessment of the financial aspect of the project. As long as project is financially feasible, all the stake holders are interested in the same. Financial feasibility of building redevelopment projects of housing societies is closely related to additional usable carpet area, which members expect in new housing units after redevelopment process. Hence, financial feasibility is studied in this context.

Financial feasibility depends on the following:

- Ready Reckoner Rate.
- Market Rate.
- Construction cost.
- Miscellaneous cost.
- Corpus Fund.
- Months of Rent.
- Rent.
- Profit margin.

Ready Reckoner Rate (R_r): These rates are the prices of the residential property, land or commercial property for a given location and are published periodically and regulated by the respective state governments. A homeowner or a buyer would be required to pay the stamp duty and registration amount on higher of the reckoner rate and the actual price of the property.

For this research work, Ready Reckoner Rates of previous years were taken for analysis purpose in which financial feasibility was carried out.

Market Rate (R_m): Market price is the value of such an asset for a transaction between a seller and buyer; it is done at an arm's length principle with the price determined by the market forces of supply and demand. They are determined by the seller's expectation of price and the buyer's inclination to pay. Market rate is a price range arrived at by looking at actual transaction prices in a location and is a better indicator of what seller's demand and what buyers are willing to pay.

Construction Cost (R_c): Expense incurred by a contractor for labour, material, equipment, financing, services, utilities, etc., plus overheads and contractor's profit. Costs such as that of land, architectural design, consultant and engineer's fee are not *construction* costs.

Miscellaneous Cost (R_d): These include shifting charges, out of pocket expenses, processing fees and stamp duty.

Corpus Fund (R_b): Although, the builder pays rent to the members, he also pays them the charges required to shift the furniture and other important valuables while

vacating the old building. These charges paid by the builder to the members are known as Corpus fund.
Months for Rent (T): These are the months in number for which builder will provide rent to the members to get shifted to alternative accommodation till the process.
Rent (R_a): In a redevelopment building, the builder has to pay a rent to all the members who were previously living in the building during the time of construction, depending upon the old area of the flat of the members. The rent to be given to the members varies from ward to ward, area to area.
Profit Margin (R_p): This is mark up as percentage on gross income which builder expects for his efforts, expertise and investments.

The following are the important terms that require understanding financial feasibility for project:

Net Income: Net Income is the developer's total profit which is obtained by subtracting all the costs incurred in the project (Outgoings). For the purpose of the feasibility check of the redevelopment buildings the net income is assumed to be 20% of the Gross Income.
Gross Income: Gross Income is defined as the total revenue obtained from the project without taking into account all the cost incurred in the project. It is obtained from the summation of the Net Income and the Outgoings.
Outgoings: Outgoing is defined as the cost incurred in developing the project. It includes the following: Construction Cost, Miscellaneous Cost, Corpus Fund, Rent cost, F.S.I Expenses, Corporate Expenses. Sum of all these costs should be less than the gross income which the developer will get after selling the flats.
Hence if Gross Income of Project > Outgoings of the project, then the project would be feasible.
Proposed Area Factor: Area Factor is defined as the ratio of the new carpet area which can be feasibly provided in place of the old carpet area of the building. It should always be greater than one (1) for the project to be deemed as feasible. It can be mathematically represented as:

$$\text{Proposed Area Factor}(A_f) = \text{New Carpet Area}(A_{new})/\text{Old Carpet Area}(A_{old})$$

3 Methodology Adopted

This research paper is outcome of specific methodology adopted. Interaction with all the stake holders of building redevelopment projects such as tenants, builders/developers, experts and officials of regulatory authorities is carried out to search the determinants of process of these projects.

After relevant literature review, actual data related to these projects were collected through field visits, pre-designed questionnaire (253 valid responses) besides inputs through 41 semi-structured interviews. "Additional usable carpet area"

which is particular for each building redevelopment project, is a buzz word. To predict additional usable carpet area, model is evolved to calculate area factor for a particular project. The same is tested through sensitivity analysis using actual data of seventeen building redevelopment projects of housing societies in Mumbai city.

4 Data Collection and Analysis

Actual data of two projects of redevelopment of buildings of housing societies are collected and analysed in the context of financial feasibility as below.

4.1 Financial Feasibility of Two Building Redevelopment Projects

The classification of project with respect feasibility category based on mathematical model of area factor (Refer Table 1) for predicting additional carpet area which members will get, is developed by carrying out financial feasibility of two ongoing building redevelopment projects. Once area factor is determined, additional usable carpet area can be arrived at. Additional useful carpet area is the main concern to both, i.e. members and builder in building redevelopment projects of housing societies. The data such as number of flats, old area, new expected area, market rate, TDR (Transfer of development Rights) rate, construction cost, miscellaneous cost, etc., are collected for two projects to carry out financial feasibility, and hence, mathematical model is evolved for area factor which helps in predicting additional carpet area.

4.2 Case Study 1

Financial Feasibility of the Project l in S-Ward, Borivali (west) (during 2011–2017)

The plot is of a redevelopment building with 32 existing members having carpet area 500 sq. of each flat. If the builder plans to have 24 sale flats with a profit margin of 20%, then the additional area the builder can provide considering the

Table 1 Area factor value and its interpretation

$A_f > 1$	Project is feasible
$A_f = 1–1.25$	Project is scarcely feasible
$A_f = 1.25–1.5$	Project is moderately feasible
$A_f > 1.5$	Project is absolutely feasible

Table 2 Project 1 data

Name of project	Sahajeevan co-operative housing society ltd
Location ward and duration	Borivali (2011–2017)
Old members number (N_{old})	32
New members [sale flat numbers] (N_{new})	24
Total flats (N)	56
Old area (A_{old})	500 sq. ft
Construction cost/sq. ft. (R_c)	Rs. 1800
Misc cost/sq. ft. (R_d)	Rs. 2300
Corpus/sq. ft. (R_b)	Rs. 2000
Rent/sq. ft. (R_a)	Rs. 40
Total number of months for which rent is proposed to be paid (T)	37
Ready Reckoned Rate (R_r)	Rs. 3577
TDR purchased if any (R_t)	Rs. 2267
Profit margin in % (R_p)	20%
Market rate for sale flats in Rs./sq. ft. for carpet (R_m)	Rs. 21,450/sq. ft
Area provided, i.e. area of new flats in sq. ft. (A_{new})	690

feasibility of the project is determined. This is arrived at considering the following data (Refer Table 2).

Analysis

Construction cost	$= (A_{old} \times N \times A_f \times R_c) + ((A_o \times N_o) \times 0.7\ R_c)$ 0.7 is for fungible FSI
	$= (500 \times 56 \times A_f \times 1800) + (500 \times 32 \times 0.7 \times 1800)$
	$= 50,400,000A_f + 20,160,000$
Misc cost	$= R_d \times A_{old} \times N \times A_f = 64,400,000A_f$
Corpus fund	$= R_b \times A_{old} \times N_{old} = 32,000,000$
Rent cost	$= R_a \times A_{old} \times N_{old} \times T = 2,368,000$
Profit	$= R_m \times A_{old} \times A_f \times N_{new} \times R_p = 51,480,000A_f$
FSI expenses	$= 0.67 \times R_t \times A_{old} \times A_f \times N_{new} = 18,226,680A_f$
TDR expenses	$= 0.68 \times A_{old} \times A_f \times N_{new} \times 0.66R_r = 19,264,291A_f$
Gross income	$= R_m \times A_{old} \times A_f \times N_{new} = 257,400,000A_f$
Profits + outgoings	$= 203,770,971A_f + 75,840,000$
Gross income	$=$ Profits + outgoings
257,400,000 A_f	$= 203,770,971\ A_f + 75,840,000$
Area factor A_f	$= 1.41415949$
Area calculate A_c	$= A_{old} \times A_f$
	$= 500 \times 1.41415949$
% Deviation	$= (A_c - A_{new})/A_{new}$
	$= (707.0797 - 690) \times 100/690$
	$= 2.475325$

Area Factor Formula

$$A_{\mathrm{f}} = \frac{N_{\mathrm{old}}(R_a \times T + R_b + 0.7R_{\mathrm{c}})}{\left(R_{\mathrm{m}} \times N_{\mathrm{new}}(1 - R_p) - N(R_{\mathrm{c}} - R_d) - N_{\mathrm{new}}(0.67R_t + 0.4488R_{\mathrm{r}})\right)}$$

$$A_{\mathrm{f}} = 1.41415949$$

where

A_{f}	Area factor
N_{old}	Old number of members
N_{new}	New number of members
R_{r}	Ready Reckoner Rate
R_{m}	Market Rate
R_a	Rent per sq. ft.
R_b	Corpus fund per sq. ft
R_{c}	Construction rate
R_d	Miscellaneous costs rate
R_{p}	Profit margin
N	Total number of flats in the new building

As per information gathered during interviews, the range of area factor is decided on basis of which the projects are classified as below:

A_{f} = 1.414. Therefore, the project is moderately feasible.

4.3 Case Study-2

Financial Feasibility of Lalit Kutir Housing Society, Juhu, (K-West Ward) (2017–2022)

This is small housing society with 20 members in JVPD scheme in western suburbs of Mumbai. It is ready for undergoing redevelopment (Table 3).

Table 3 Project 2 data

Name of project	Lalit Kutir co-op housing society ltd
Location ward and duration	JVPD (2017–2022)
Old members number (N_{old})	20
New members [sale flat members] (N_{new})	12
Total flats (N)	32
Old area (A_{old})	470.82 sq. ft
Construction cost/sq. ft. (R_c)	Rs. 3500
Misc cost/sq. ft. (R_d)	Rs. 2635
Corpus/sq. ft. (R_b)	Rs. 4460
Rent/sq. ft. (R_a)	Rs. 130
Total number of months for which rent is proposed to be paid (T)	40
Ready Reckoned Rate (R_r)	Rs. 8000
TDR purchased if any (R_t)	Rs. 2800
Profit margin in % (R_p)	20%
Market rate for sale flats in Rs./sq. ft. for carpet (R_m)	Rs. 40,000
Area provided, i.e. area of new flats in sq. ft. (A_{new})	925

Calculation

Construction cost	$= (A_{old} \times N \times A_f \times R_c) + ((A_o \times N_o) \times 0.7\ R_c)$ 0.7 is for fungible FSI
	$= (470.82 \times 32 \times A_f \times 3500) + (470.82 \times 20 \times 0.70 \times 3500)$
	$= 52,731,840A_f + 23,070,180$
Misc cost	$= R_d \times A_{old} \times N \times A_f = 39,699,542.4A_f$
Corpus fund	$= R_b \times A_{old} \times N_{old} = 41997144$
Rent cost	$= R_a \times A_{old} \times N_{old} \times T = 48,965,280$
Profit	$= R_m \times A_{old} \times A_f \times N_{new} \times R_p = 45,198,720\ A_f$
FSI expenses	$= 0.67 \times R_t \times A_{old} \times A_f \times N_{new} = 10,599,100A_f$
TDR expenses	$= 0.68 \times A_{old} \times A_f \times N_{new} \times 0.66R_r = 20,285,186A_f$
Gross income	$= R_m \times A_{old} \times A_f \times N_{new} = 225,993,600A_f$
Profits + Outgoings	$= 168,514,388A_f + 114,032,604$
Gross income	$=$ Profits + outgoings
225,993,600 A_f	$= 168,514,388A_f + 114,032,604$
Area factor A_f	$= 1.983892952$
Area calculate A_c	$= A_{old} \times A_f$
	$= 470.82 \times 1.983892952$
	$= 934.0565$
% Deviation	$= (A_c - A_{new})/A_{new}$
	$= (934.0565 - 925) \times 100/925$
	$= 0.9790789$

Area Factor Formula

$$A_{\mathrm{f}} = \frac{N_{\mathrm{old}}(R_a \times T + R_b + 0.7R_{\mathrm{c}})}{\left(R_{\mathrm{m}} \times N_{\mathrm{new}}(1 - R_{\mathrm{p}}) - N(R_{\mathrm{c}} - R_d) - N_{\mathrm{new}}(0.67R_t + 0.4488R_{\mathrm{r}})\right)}$$

$$A_{\mathrm{f}} = 1.983892952$$

where

A_{f} Area factor
N_{old} Old number of members
N_{new} New number of members
R_{r} Ready Reckoner Rate
R_{m} Market rate
R_a Rent per sq. ft.
R_b Corpus fund per sq. ft
R_{c} Construction rate
R_d Miscellaneous costs rate
R_{p} Profit margin
N Total number of flats in the new building.

As per information gathered during interviews, the range of area factor is decided on basis of which the projects are classified as below:

A_{f} = 1.983. Therefore, the project is absolutely feasible.

Thus, this is mathematical model to predict area factor as well, to assess financial.

4.4 Proposed Mathematical Model of Area Factor to Predict Additional Carpet Area

Therefore the value of the new area factor obtained for two projects is as follows:

A_{f} = 1.414 for Borivali Project.

A_{f} = 1.91 for Juhu Project.

Thus the mathematical model for predicting area factor is as follows:

$$A_{\mathrm{f}} = \frac{N_{\mathrm{old}}(R_a \times T + R_b + 0.7R_{\mathrm{c}})}{\left(R_{\mathrm{m}} \times N_{\mathrm{new}}(1 - R_p) - N(R_{\mathrm{c}} - R_d) - N_{\mathrm{new}}(0.67R_t + 0.4488R_{\mathrm{r}})\right)}$$

where

A_{f} Area factor
N_{old} Old number of members
N_{new} New number of members

R_r Ready Reckoner Rate
R_m Market rate
R_a Rent per sq. ft.
R_b Corpus fund per sq.ft
R_c Construction rate
R_d Miscellaneous rate
R_p Profit margin
R_u Corporate expenses
N Total number of flats in the new building.

4.5 Sensitivity Analysis and Limitations of Mathematical Model

The sensitivity analysis studies the output of a mathematical model influenced by different sources of uncertainty in its inputs. In this research study, a mathematical model is developed for area factor, which facilitates prediction of additional usable carpet area for tenants in redevelopment projects of housing societies. This area factor depends on several components such as location of ward, duration, total flats, area, construction cost, corpus, rent, miscellaneous expenses. The sensitivity analysis is carried out to check whether the mathematical model is able to predict area factor reasonably close to actual value by sampling 17 projects. The projects are chosen from all over Mumbai; locations are Bandra, Ghatkopar, JVPD, Borivali. The number of flats in these projects is ranging from 20 to 60 with an exception of 258. The area of a flat ranges from 450 to 800 sq. ft.

Actual data of building redevelopment projects were collected, and the area factor is determined using mathematical model developed for sampled projects, where the components affecting area factor are varied for all components. This worked out area is compared with actual area provided to the members. It was found that the model is predicting the area factor fairly correct under various conditions. The highest deviation of the area from its actual value is 5%. It is observed that there is small deviation which is not exceeding 5%. Thus, this mathematical model to predict additional usable carpet area stands tested to sensitivity analysis.

However, there are few limitations to this mathematical model. This model is suitable only for situations when all the flats in housing society undergoing redevelopment are of same area and all are residential units.

4.6 Application of Mathematical Model to Arrive at Additional Carpet Area

The additional carpet area to tenants is important. The tenants are non-technical lot; if expert works out correct additional area for them and conveys to them with proper explanation of components, they gets satisfied. The mathematical model so developed can be used with excel sheets for working out new area feasible for redevelopment projects in all the wards. This will be handy to stakeholders of all such building redevelopment projects in entire Mumbai city.

5 The Most Important Finding and Summary of Findings

This research study has brought the following most important finding.

The additional usable area, which tenants get while agreeing to undergo for process of redevelopment of their buildings, is the key determinant of this process. Results have revealed that while analysing data of responses of questionnaire posed to the tenants, 71% expressed that, other reasons for getting them into redevelopment process is, gaining more usable carpet area (refer Table 4 and Fig. 2). Hence, **predicting near accurate carpet area is of very much relevance**.

The research study has also brought out the other relevant findings as below.

- 14.6% buildings going for redevelopment being unsafe and dilapidated.
- 34% buildings are put for redevelopment because they are uneconomic to repair.
- Majority of societies (about 80%) adopt builder/developer model to get their buildings redeveloped. **Hence, predicting additional carpet area is of high relevance**.

Table 4 Redevelopment is required because

	Number	Per cent
Yes more floor area, funds and facilities	58	70.7
No	15	18.3
Total	73	89.0
NA	9	11.0
Grand Total	82	100.0

Source Authors

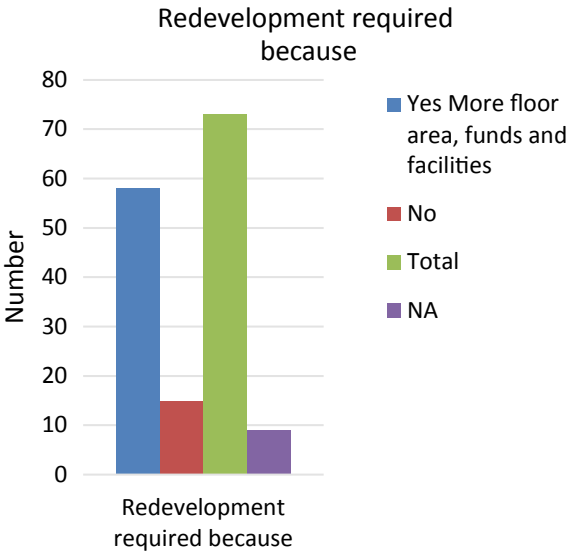

Fig. 2 Other reasons for getting into redevelopment

6 Conclusions

Redevelopment of buildings in Mumbai city is FSI driven. In spite of various inconveniences and risks, members of housing societies would like to go for redevelopment process, as it leads to many advantages in situations with limited options of repairing old buildings with no modern amenities. Developers would like to venture into these projects because of scarcity of land in city and suburbs supplemented by decent housing prices. Land and/or FSI is basic raw material for business activity. Land is scare; however, redevelopment activity facilitates availability of FSI. Experts and regulatory authorities play their role in the process which has a set pattern. It is imperative to get complete feasibility of building redevelopment projects during initiation phase. This includes physical feasibility, socio-economic feasibility, environmental feasibility and financial feasibility.

Additional usable carpet area expected by tenants is identified as the key determinant of the process of building redevelopment projects. However, this additional usable carpet area which can be comfortably given to the tenants by the developer is depending on financial feasibility of these projects. This study has given mathematical model of area factor predicting fair accurately additional usable carpet area which can be given to the tenants in the context of financial feasibility of the project. This can be handy to stake holders of building redevelopment projects of housing societies in Mumbai city.

References

1. Hindman M et al (2015) Addressing slum redevelopment issues in India. Dow sustainability fellowship
2. MCGM 1991 Development control regulations
3. MCGM 2014–34 Development control regulations
4. Nallathing R (2014) Land based Instruments for Urban Infrastructure development: The experience of TDR in Mumbai. NICMAR J Constr Manag XXIX(1, Jan–Mar Sp Issue):51–65
5. PEATA (1998) D.C regulations hand book 1991
6. http://www.redevelopmumbai.com/redevelopment-rules-regulations-html

An Exploratory Study on Mental Well-Being of Employees in Construction Organisations

V. Paul C. Charlesraj and Moksshitha Shri

Abstract Well-being is about the psychological capital linked to happiness and life satisfaction. The concept of well-being in construction is poorly defined and predominantly focuses on stress. Human resources management (HRM) practices in an organisation influence the physical and mental wellbeing of the employees and promote high performance behaviours. In the human intrinsic construction industry, major problems are related to the lack of skilled labour, stress, working hours, workload, inefficient leadership, mismatch of job and employee, delays in project and cost over runs. Understanding and facilitating physical and mental well-being of employees through various HRM interventions can result in improved organisations' performance. It has been attempted to study the factors influencing the mental well-being of employees in a large construction organization in India using mixed methods research. Semi-structured interviews and questionnaire survey were used for data collection. *Supervisor attitude* and *training* showed significant contribution to the employee well-being. It has been observed that there is a positive relationship between employee well-being and employee performance. All the factors are positively correlated with employee well-being; specifically, *training*, *job stress* and *equality* have shown a strong correlation. *Training* has a moderate positive correlation with performance, while *motivation* exhibited a weak negative correlation with performance. These results would greatly help the construction organisations to formulate HRM strategies for improved performance and well-being of employees.

Keywords Construction organisation · Employee performance · Human resource management · Mental well-being

V. P. C. Charlesraj (✉) · M. Shri
RICS School of Built Environment, Delhi NCR 201313, India
e-mail: vpcharlesraj@ricssbe.edu.in

M. Shri
e-mail: moksshithas.mc18n@ricssbe.edu.in

B. Laishram and A. Tawalare (eds.), *Recent Advancements in Civil Engineering*, Lecture Notes in Civil Engineering 172,
https://doi.org/10.1007/978-981-16-4396-5_12

1 Introduction

Performance management process ensures that the goals of an organisation are being met effectively and efficiently. Workforce or the human capital is the most valuable asset for any organisation, especially in construction industry, which comprises of medium sized enterprises. Construction industry is a labour intensive industry often handling complexities regarding skilled labours, delays, schedules and finances. The solutions to these problems are identified as labour management, standardisation, motivation, modernisation, modularisation, training and development.

Human resource management (HRM) practices include policies and processes to improve the effectiveness of the organisation to meet the intended goals. HRM aspects include planning, compensating, staffing, training, developing, labour management and appraisals. Training and development, incentive compensation, internal promotions and participation have positive impact on an organisation's performance. Strategic HRM influences the organisational choice like internal recruitment or outsourcing, control or flexibility, narrow or broad job class, heavy or loose work plans. Appropriate HRM practices result in increasing (i) employee commitment, (ii) satisfaction and motivation, (iii) productivity and performance, (iv) development and coordination and (v) employee potential and well-being.

Employee well-being or ill-being is about physical, emotional and mental state of individual. Well-being is not just about illness or the absence of disease; it is about the psychological capital linked to happiness and life satisfaction. Employee well-being will include cognitive and emotional components both; further, emotional is divided into positive and negative dimensions, influencing the organisational performance. Also, positive and negative experience contributes equally to job satisfaction [1]. There are issues with managing mental health in construction due to the inherent nature of the industry [2]. It has been attempted to study the factors influencing the mental well-being of employees in a large construction organisation using mixed methods research. Preliminary findings of the study are presented in this article.

2 Literature Review

HRM practices in an organisation greatly contribute to the well-being of employees and in turn to the performance. A review of literature on the impact of HRM practices on organisational performance and the role of mental well-being of employees on performance have been presented in this section.

2.1 Impact of HRM Practices on Performance

HRM practices have a positive relationship with organisational performance [3]. Some of the key HRM practices that can be followed for continuous and significant competitive advantage are: employee security ensuring long standing commitment with the organisation; selectivity in recruiting right people in a right way; high wages attract people and help recruiting outstanding people and increase profits; incentive pay, more than money recognition, fair treatment and benefits pay off; employee ownership aligns the interests of employee with shareholders by make them the shareholders; information sharing; participation and empowerment to encourage decentralization; self-managed teams reduce the levels in management and enable coordination and peer monitoring; training and skill development always contribute to positive enhanced returns without affecting the structure of work by upgrading skills; cross utilization and cross training as it gives variety and change in pace and activities; symbolic egalitarianism signalling both insiders and outsiders equally; wage compression reduces the competition within and increases mutual coordination; and internal promotion ensures management knowledge about its employees and business [4].

High performance work practices include comprehensive talent acquisition, selection procedures, training, incentives, management systems and employee involvement, which can improve the skills, knowledge, motivation and the quality of work [5]. Managers can foster the performance of the organisation by using HRM practices to increase the employee motivation, strengthening the bond between performance and awaiting opportunity to align organisational goals to individual efforts. Compensation based on excellence systems increases the performance of the individuals and the productivity of the organisation as it attracts the best candidates [6]. Training and development not only improve the employee abilities and skill, but also improve the candidate's satisfaction. Mobility either horizontal or vertical decreases the recruitment and selection costs enabling motivation regarding internal promotions.

2.2 Role of Mental Well-being of Employees on Performance

The concept of well-being has multiple disciplines which include physical well-being, social well-being and psychological well-being [7]. Well-being can be associated to work or outside work. The well-being associated to work is the overall happiness and mental, physical health of the work force. If there is imbalance, it may result in absenteeism, retention, depression, reduced productivity of the individuals. Presenteeism can be related to sickness, or family stress or the job-related stress referred as job stress-related presenteeism [8]. Supervisors attitude plays an important role in the mental well-being of the employees working under him/her.

Favourable attitude of supervisor includes managing workload, problem solving, handling stress, considering employees and taking responsibility. Supervisors behaviour has contribution to psychiatric distribution in affecting employee well-being and also both source and moderator of stress [9]. An individual's positive state of mind for the development, i.e. confidence, ability, success, perseverance, hope and optimistic attitude to bounce back even at problems, is known as the psychological capital, which results in superior performance at workplace. Psychological capital is necessary for the human capital development and performance management [10].

Construction industry is primarily a male dominated industry with long working hours, insufficient time with family, high work-loads, resulting in poor well-being [11]. Well-being phenomena include job satisfaction, stress, depression, happiness, burnout, mental health, emotional health, etc., influencing psychological climate. It has been reported that working under stress results in low productivity and this has implications on health like the increased hormone production leading to absenteeism and health and safety. Job dissatisfaction, poor well-being, smoking, and drinking are the responses to stress causing health issues may lead to cardiac problems or heart attack and early retirement of the employee which in-turn is a waste of all the training and development activities given to the candidate along with the loss of experienced employee. This results in replacement of employee and until then it is loss of manpower [12].

Feedback process, offering guidance, flexible hours, reducing working hours and workload, mentoring on well-being, employee assistance programmes and stress audit help in studying the stress profile to design action plan to counter the impacts of stress [13, 14]. A study on the causal relationship between stressors and stresses reported four main categories of stressors, namely task stressors, organisational stressors, personal stressors and physical stressors that were found to have significant impact on both the subjective and the objective stresses of construction project managers [15]. Further, it has been established that job stress is the antecedent of burnout and negatively impacts the performance of construction project managers [16]. In addition, intercultural coping can also have a significant impact on mental health of construction workers [17].

2.3 Summary of Literature Review

The key variables (12) that contribute to the mental well-being of employees in an organisation have been identified from the literature reported above and are presented in Table 1.

The primary objective of this study was to explore the relative significance of the above factors in their contribution to the mental well-being of employees. Also, it has been attempted to establish the relationship among these factors, mental well-being and the performance.

Table 1 Factors influencing the well-being of employees

Sl.#	Variables	Description	Source(s)
1	Supervisor attitude	The way supervisor mentors the subordinates, supports them, and effective leadership	[8, 9, 18]
2	Employee participation	Involving employees in policy making, decision making and making them feel a valuable part of the organisation	[8, 9, 18, 19]
3	Work-life balance	Amount of work to be done by an employee or time to complete the task given	[8, 9, 18]
4	Job stress	Includes the pressure of work and job security issues	[1, 2, 8, 9, 12, 15–17, 20]
5	Health problems	Stress and long work hours can cause anxiety, burnout, heart problems or clinical depression	[1, 9, 12]
6	Presenteeism	Present in office more than required hours due to job insecurity like working while sick or exhaustion	[8, 9]
7	Flexibility	Opportunity to accomplish the work in the way employee wishes to fulfil the targets assigned	[8]
8	Training	Learning and Development process of one's capability, knowledge and skills	[2, 5, 21, 22]
9	Motivation	Influence of organisation culture and climate to set targets and achieve them	[5, 23]
10	Job satisfaction	Contentment of employees with the job and the organisation	[7, 18]
11	Employee commitment	Attachment of employee with the organisation and respect for the psychological contract between employee and organisation	[18, 24]
12	Equality	Treating all the employees fair, no one is superior to other with respect to caste, creed, colour, or race	[18]

3 Problem Description

The premise for this study is HRM practices in an organisation have a direct impact on the variables influencing the mental well-being of the employees and in turn on the performance as shown in Fig. 1. The HRM strategy of an organisation is operationalised through various HRM practices. These practices have direct influence on the enablers/inhibitors of well-being of employees in addition to the personal characteristics, supervisor attitude and work experience. The well-being is having a positive impact on the performance of the employees and in turn performance of the organisation.

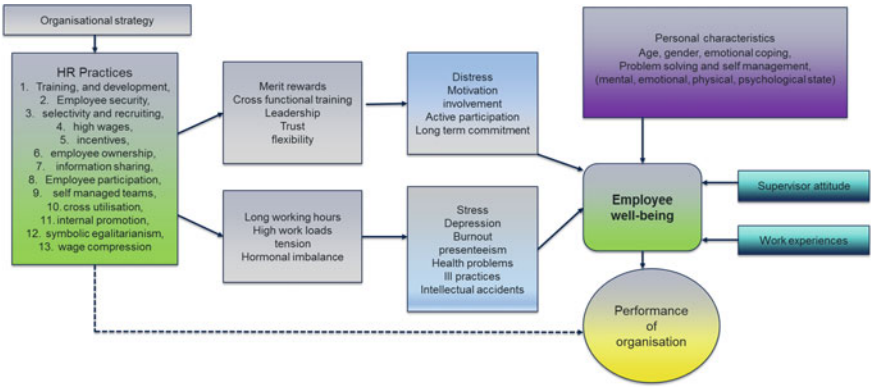

Fig. 1 Relationship between HRM practices and employee well-being

4 Research Methodology

Literature review and case study analysis were used as the primary research methods. Semi-structured interview with expert and questionnaire survey among employees were used for data collection. Summary measures were used to understand the relative significance of factors impacting mental well-being of employees, and correlation analysis was used to establish relationships. The process is shown in Fig. 2. The variables (and their indicators) influencing the employee mental well-being were identified using literature review and verified by the expert having more than 10 years of experience in HRM in construction sector. The variables and indicators used in this study are presented in Table 2. A questionnaire survey instrument has been designed to collect the opinion on the chosen indicators and performance on a five-point Likert scale. The anchors of summated scaled contained the following range of options: strongly agree, agree, neutral, disagree, and strongly disagree. Purposive sampling method is used in the survey. This research study has been approved by the ethics committee of the university.

Fig. 2 Research methodology

Table 2 Indicators of well-being and associated variables

ID	Indicators	Variables
I1	Supervisor is supportive	Supervisor attitude
I2	Supervisor balances between productivity and well-being	
I3	Supervisor provides appreciation and encourages employees	
I4	Employees feel a significant part of organisation	Employee participation
I5	Employees are involved in decision making	
I6	Employees experience a huge pile of work most of the days	Work-life balance
I7	Employee works extra hours to complete tasks	
I8	Employees are subjected to very long working hours	
I9	Employees feel the job is stressful	Job stress
I10	Employees experiences stress causing health problems	Health problems
I11	Work stress distracts attention of employee	Presenteeism
I12	Proportion of employee's workday goes in coping up with stress	
I13	Employees are provided flexibility to accomplish work	Flexibility
I14	Training programmes are aligned to employees' requirements	Training
I15	Employees are provided rewards and appreciation	Motivation
I16	Employee satisfaction and happiness	Job satisfaction
I17	I am likely a long-lasting employee for the organisation	Employee commitment
I18	All employees are treated fairly	Equality

5 Data Collection, Analysis and Results

5.1 Data Collection

A leading large construction organisation, functional for the past 8 decades was selected for the study. For the research, a mixed approach was employed to study on the objectives with help of expert interview and questionnaire.

HR manager of the organisation was interviewed to understand the organisation culture and the HRM practices within the organisation. The questions included about the HR functions/processes such as onboarding, recruitment and selection, training, employee participation and flexibility to employees, career development opportunities provided to employees.

Purposive, non-probability sampling is employed for the survey on employee well-being. The participants were selected based on their availability in the office hours and willingness to take part in the survey as it was circulated in the office. This sampling technique helps in obtaining useful results as people who volunteer choose for themselves and isn't representative of other characteristics like the age, gender, marital status, experience but questions on the identified employee mental well-being indicators which includes supervisor behaviour, flexibility, workload and stress, motivation trainings and participation. There were 32 valid responses (100% response

rate) from the cross section of employees of project management and construction management roles, and this data were subsequently used for analysis.

5.2 Data Analysis and Results

The responses received through five-point Likert scale were codified for analysis; highest favourableness was awarded 5 and one with lowest was awarded 1.

Cronbach's alpha was calculated to test the internal consistency of the instrument used and reliability of data collected. The calculated alpha value was found to be 0.84, which is greater than 0.7 (minimum required for social research), and this validated the instrument used for data collection and reliability of data collected. Descriptive data analysis is conducted on the data collected. Arithmetic mean is used as a summary measure of an indicator. Sum of responses for the 18 questions on the indicators by a respondent is used as the measure of well-being (out of 90).

The relationship between the employee mental well-being score and the self-rated performance is presented in Fig. 3. It can be noted that there is a positive relationship between them.

The mean scores of the mental well-being indicators are shown in Fig. 4 in order to understand their relative significance on the contribution to the well-being of employees. The top-rated indicators of well-being are:

- Supervisor is supportive (I1)
- Training programmes are aligned to employees' requirements (I14)
- Supervisor provides appreciation and encourages employees (I3).

The least-rated indicators are:

- Employees are subjected to very long working hours (I8)
- Employees experiences stress causing health problems (I10)
- Employees feel the job is stressful (I9).

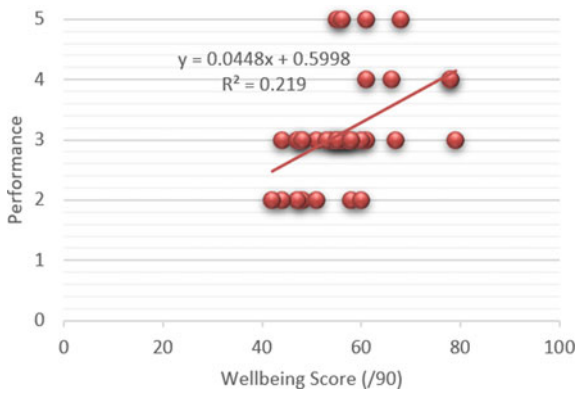

Fig. 3 Employee mental well-being score versus performance

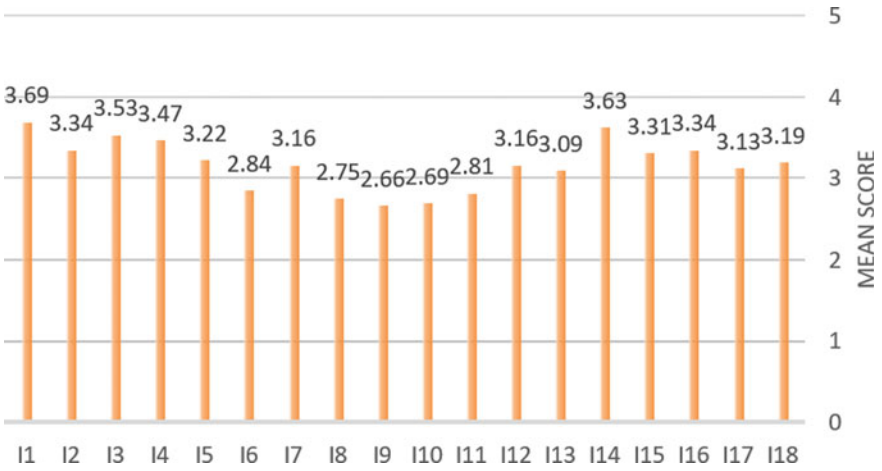

Fig. 4 Mean scores of indicators

Similarly, the mean mental well-being scores of variables were calculated and presented in Fig. 5. It can be noted that *supervisor attitude* and *training* significantly contribute to the employee well-being followed by *job satisfaction* and *employee participation*. *Health problems* and *job stress* seems to be least significant. It implies that the mental well-being is more influenced by the supporting positive environment rather than the negative factors such as stress and long work hours.

Fig. 5 Mean scores of variables

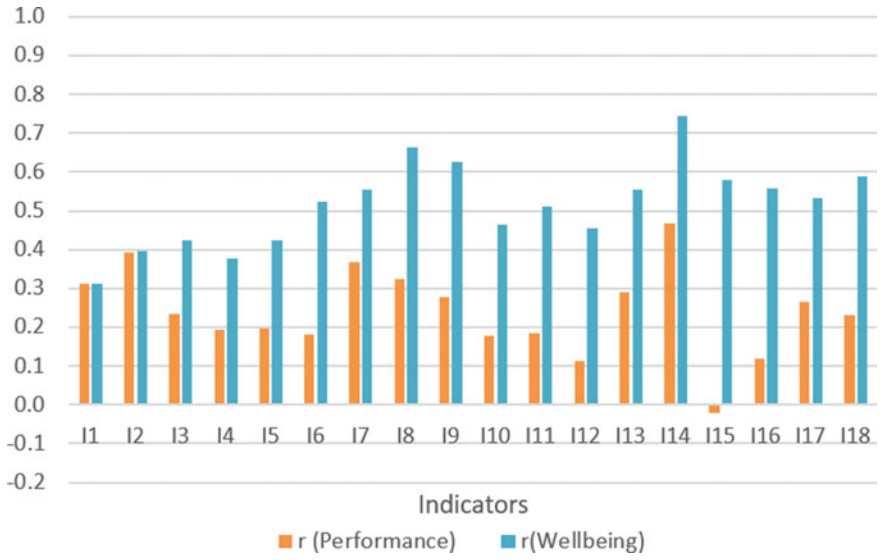

Fig. 6 *r*-values of indicators

Correlation Analysis

Correlation analysis using Pearson's correlation coefficient has been conducted to establish the relationships among the indicators and variables and performance and mental well-being. The *r*-values corresponding to indicators are presented in Fig. 6. In general, all the indicators are positively correlated with the performance as well as mental well-being (with varying strength) except *employees are provided rewards and appreciation (I15)*, which is negatively correlated with performance, but the strength is low. The variable level analysis revealed similar results that all of them are positively correlated with employee mental well-being (Fig. 7); specifically, *training*, *job stress* and *equality* have shown a strong positive correlation and others showing moderate strength. *Training* has a moderate positive correlation with performance, while *motivation* exhibited a weak negative correlation with performance.

6 Discussions

This study reinforced the fact that the mental well-being of employees has a positive relationship with the performance, which justifies the attention to the well-being.

Further, HRM practices may consider promoting the best practices of *supervisor attitude*, *training*, *job satisfaction* and *employee participation* aspects as they were reported as key enablers of mental well-being. Specifically, able support by

Fig. 7 *r*-values of variables

supervisors, training programmes that are tailored to the needs of the employees and rewards and recognition positively motivate the employees. Similarly, minimal attention may be paid to *health problems* and *job stress*-related aspects *since* they are reported as the least influential on the mental well-being. Specifically, long work hours and stress-related problems seem to be less consequential as far as mental well-being is concerned.

A general positive correlation analysis results are encouraging, and special attention is required with respect to rewards and recognition, which was negatively correlated; but this can be still be in line with the notion that the employees are biased in their opinion when it comes to rewards and recognition. Specific HRM interventions in *training*, *job stress* and *equality* may be required to identify and promote the best practices. Similarly, special attention is required to ensure that employees are remain motivated for enhanced performance.

7 Summary and Conclusions

The present study explored the association between employee mental well-being and their performance. Specifically, the relationships among the factors and indicators of employee well-being and performance in the context of a major construction organisation. The mixed methods research results revealed that there is in general a positive correlation between the factors influencing the mental well-being and performance, which justifies that need for focussing on promoting the HRM practices that fosters mental well-being of employees. It gains much more importance during the crisis due to a pandemic such as one created by COVID-19. HRM

strategies may pay special attention to *supervisor attitude*, *training*, *job satisfaction*, *employee participation, health problems*, *job stress, training and equality,* as they emerged as the critical factors that influence the mental well-being and performance of employees. Some of the possible interventions could be but not limited to: development of screening methods to detect sign of job stress; time keeping programmes and trainings; and teams to identify mental ill-health problems and improve health of employees. The findings of this study are based on a single case organisation that shall limit the application to only such large construction organisations in India. An extended study among wider cross section of organisations in construction industry may reveal deeper insights. It would be interesting to compare the similar studies conducted among organisations in other sectors for cross-sector learning and adopt the best practices. There is scope for studying the connection between the mental and emotional well-being of employees.

References

1. Anderson N (2001) Handbook of industrial work, and organisational psychology, vol 2
2. Clarke N, Bradley JG, Spillane JP (2020) Mental health and well-being in micro enterprises in the construction industry: an Irish perspective. In: Proceedings of the 36th annual ARCOM conference, 7–8 Sept 2020. UK Association of Researchers in Construction Management, pp 746–754
3. Ping CH, Arokiasamy L, Kassim KAA (2019) Influence of human resource management practices on Malaysian construction organisational performance. Glob Bus Manage Res: An Int J 11(1):367
4. Pfeffer J (1995) Producing sustainable competitive advantage through the effective management of people. Acad Manage Perspec 9(1):55–69
5. Delaney JT, Huselid MA (1996) The impact of human resource management practices on perceptions of organisational performance. Acad Manage J 39(4):949–969
6. Harel GH, Tzafrir SS (1999) The effect of human resource management practices on the perceptions of organisational and market performance of the firm. Hum Resour Manage 38(3):185–199
7. Brunetto Y, Teo STT, Shacklock K, Farr-Wharton R (2012) Emotional intelligence, job satisfaction, well-being and engagement: explaining organisational commitment and turnover intentions in policing. Hum Resour Manage J 22(4):428–441
8. Gilbreath B, Karimi L (2012) Supervisor behavior and employee presenteeism. Int J Leadersh Stud 7(1):114–131
9. Gilbreath B, Benson PG (2004) The contribution of supervisor behaviour to employee psychological well-being. Work Stress 18(3):255–266
10. Peterson SJ, Luthans F, Avolio BJ, Walumbwa FO, Zhang Z (2011) Psychological capital and employee performance: a latent growth modeling approach. Pers Psychol 64(2):427–450
11. Sang KJC, Dainty ARJ, Ison SG (2004) The impact of the structure and culture of well-being: directions for future research. In: Proceedings of the 20th annual ARCOM conference, pp 495–503
12. Davidson MJ, Sutherland VJ (1992) Stress and construction site managers: issues for Europe 1992. Employee Relations MCB UP Ltd 14(2):25–38
13. Huhtala H, Parzefall MR (2007) A review of employee well-being and innovativeness: an opportunity for a mutual benefit. Creativity Inno Manage 16(3):299–306

14. Bell N, Powell C, Sykes P (2015) Securing the well-being and engagement of construction workers: an initial appraisal of the evidence. In: Proceedings of the 31st annual association of researchers in construction management conference ARCOM 2015, pp 489–498
15. Leung M, Chan YS, Yu J (2009) Integrated model for the stressors and stresses of construction project managers in Hong Kong. J Constr Eng Manage ASCE 135(2):126–134
16. Leung M, Chan YSI, Dongyu C (2011) Structural linear relationships between job stress, burnout, physiological stress, and performance of construction project managers. Eng Constr Architec Manage 18(3):312–328
17. Liu Q, Feng Y, London K (2020) Conceptual model for managing mental health in the culturally diverse construction workforce. In: Proceedings of the 36th annual ARCOM conference, 7–8 Sept 2020. UK Association of Researchers in Construction Management, pp 595–604
18. Baptiste NR (2008) Tightening the link between employee wellbeing at work and performance: a new dimension for HRM. Manag Decis 46(2):284–309
19. Wagner JA (1994) Participation's effects on performance and satisfaction: a reconsideration of research evidence. Acad Manage Rev 19(2):312–330
20. WHO (2002) Nations for mental health, Chapter 2
21. Huang T-C (2000) Are the human resource practices of effective firms distinctly different from those of poorly performing ones? Evidence from Taiwanese enterprises. Int J Hum Resour Manage 11(2):436–451
22. Guest DE (2011) Human resource management and performance: a review and research agenda. Int J Hum Resour Manag 8(3):263–276
23. Huselid MA (1995) The impact of human resource management practices on turnover productivity, and corporate financial performance. Acad Manage J 38(3):635–672
24. Alfes K, Shantz A, Truss C (2012) The link between perceived HRM practices, performance and well-being: the moderating effect of trust in the employer. Hum Resour Manage J 22(4): 409–427

Evaluation of Bid in Construction Industry Based on Multi-criteria Approach Using TOPSIS

Saurabh Gupta and Syam Nair

Abstract In the construction industry, the bidding pattern is now a multivariable based. There are many variables such as management capability, technical capability, financial capability, social influence, contribution to the project, organizational management, and health and safety records, which impact the successful competition of construction projects. Incorporating and scoring all these variables is a time-consuming and complicated process of decision-makers. In this paper, the literature survey is conducted to find the various key parameters that impact the bid evaluation. The concept of multi-criteria decision making (MCDM) is used for three different hypothetical cases. The MCDM-based technique for order of preference by similarity to ideal solution (TOPSIS) algorithm is used with the help of a computer program to rank the bid. The study conducted shows that the variation of closeness coefficient varies with the weight assigned to each criterion.

Keywords Contract evaluation · Bid evaluation · TOPSIS · Bidding strategy · Construction industry

1 Introduction

For the construction industry, the process of tendering and evaluation of bid is a complex task. An awarded contract with no-proper evaluation may affect the performance of the project in the long run. As infrastructure development has been rapid since the last decade, that requires public organizations to outsource the construction work through public tender [1] The management part for the public organization involves not only timely completion of the project but also maintain the required quality of the project. The traditional approach for the selection of best

S. Gupta (✉) · S. Nair
Department of Civil Engineering, Indian Institute of Technology Kanpur, Kanpur, India
e-mail: saurabg@iitk.ac.in

S. Nair
e-mail: syamnair@iitk.ac.in

B. Laishram and A. Tawalare (eds.), *Recent Advancements in Civil Engineering*, Lecture Notes in Civil Engineering 172,
https://doi.org/10.1007/978-981-16-4396-5_13

bid is based on the quoted lowest price. The contract awarded to the lowest bid has faced several project delivery problems and quality issues [2]. The present scenario not only involves cost, time, and quality as a factor for bid selection but also involves technical, financial, and management capability of the bidder [3]. To overcome these issues, the bid must be evaluated under various parameters but not limited to cost [4].

The competitive parameters between the contractors, which was traditionally the lowest bid, results in poor output, such as quality issues and delays in project completion [3]. The current approach for awarding the contract is now changed and involves several competitive parameters. Many research approaches have been attempted to address the issue by incorporating various parameters for evaluating the bid. In this paper, the focus is made on the evaluation of bid based on various key parameters. The first portion of this paper discusses various key competitive parameters for the bid selection from the available literature and the second portion demonstrate three model generation using those parameters and using the MCDM tool Technique for Order Preference by Similarity to the Ideal Solution (TOPSIS) for the selecting the best bid. Figure 1 shows the workflow of the research work that involves a literature survey for the key parameters and the selection of key parameters and assigning weights.

2 Literature Review

The literature on bidding, contract disputes, project delays in construction projects has been very extensive, and several articles have been published. The strategy behind this literature review search is to avoid the bivariate approach model and emphasis more on multivariate approach to use all available data. The literature survey on multi-attributes approaches for bid selection indicated that several techniques of MCDM are considered for bid evaluation such as Analytic hierarchy process (AHP) [5, 6], Fuzzy TOPSIS [7, 8], TOPSIS [5, 9, 10], Fuzzy AHP [7].

Past studies have also considered maximum likelihood estimators for validating a model for no-loss, optimal, and breakeven for selecting bid with the inclusion of multi-decision variables and described with the actual case study data by Skitmore and Pemberton [11]. While Cheng et al. [12] considered critical management skills and contextual characteristics for partnering success that includes predefined compatible goals, effective communication, mutual trust, etc. The key parameters of the bid were divided into six categories by Hatush and Skitmore [3] namely, bid amount, financial capacity, technical ability, managerial capability, health and safety, and reputation. These six subheads were further divided into subcategories, which are indicated in Table 1, and unidimensional utility theory is used to score bid based on assign weight for each category and further weight distribution for category [3]. Shen et al. [13] classified the key parameters similar fashion but used MCDM tool TOPSIS for finding ranking of bidders with a case study for China. Zavadskas and Vilutiene [14] used a utility function for selecting the contractor for

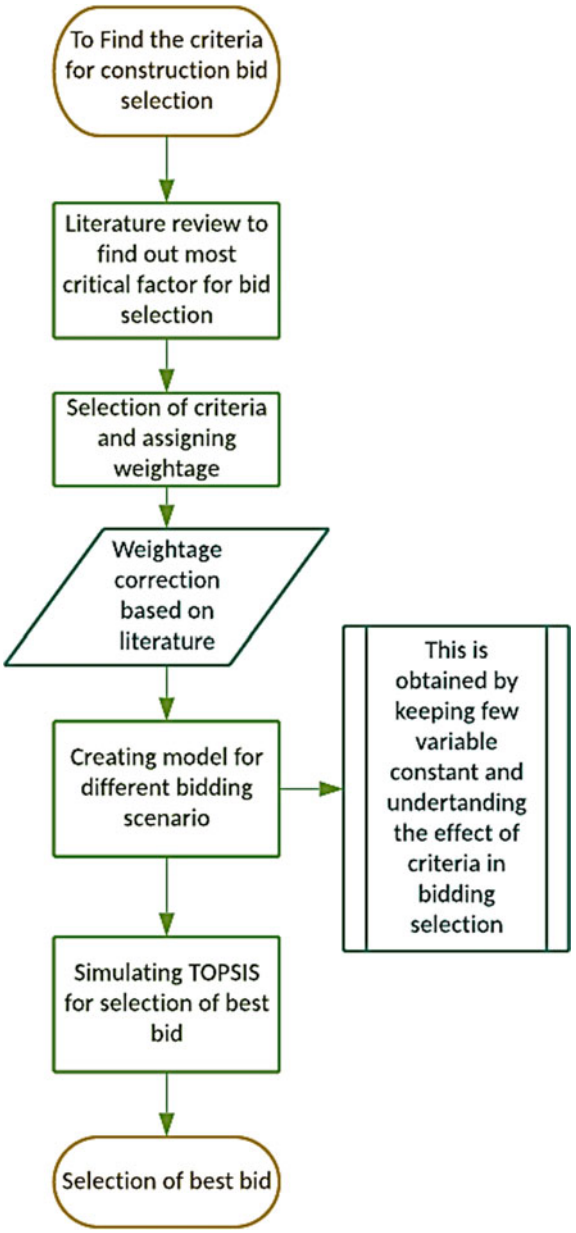

Fig. 1 Flowchart showing steps involved in bid evaluation

multi-block apartment maintenance. Zavadskas et al. [15] further implemented Hodges-Lehmann rule for determining parameters including different levels and creating a model based on metric score. Similarly, Huang et al. [16] considered the duration, total cost, quality, and resource levelling coefficient as a parameter and

Table 1 Key parameters and their subcategories for Bid evaluation

S. No.	Parameter	Subcategory
1	Bid amount [3]	Advance payment for the project
		Capital bid
		Routine maintenance
		Major/Minor repairs
2	Management capability	Quality [13], Past performance and quality [3]
		Time [13]
		Risk [13]
		Contract [13]
		Safety [13]
		Environmental [13]
		Project management organization [3]
3	Technical capability	Technology, plant and equipment [3]
		R&D cell [13]
		Innovative history [13]
		Experience [3]
4	Financial capability	Creditability [13], credit rating [3]
		Financial status [3, 13]
		Financial stability [3]
		Capital
		Procuring ability
5	Social influence	Image and reputation [13]
		Past failures [3]
		Business and coverage
		Past client/contractor relationship [3]
6	Marketing ability	Public relation
		Bidding and pricing
		Market info and coverage
7	Contribution to project	Quality
		Price
		Time
		Safety
		Environmental
8	Organizational management	Human resource management
		Training programs
		Operation
9	Health and safety records [3]	Occupancy safety OSHA/PHE
		Management safety accountability
		Experience modification rate

optimized the model using TOPSIS. Fuzzy is a tool for converting linguistic term to a numerical value Jaskowski, Biruk, and Bucon [17] uses Fuzzy-AHP for the assigning weight for the parameters based on group discussion between the experts. In a study for the Indian context, which emphasizes on time, post-construction warranty period, and past performance as the key parameters for the selection of bid [18]. Sipahi and Esen [19] uses AHP for bid evaluation for a case study of Istanbul. Again TOPSIS is used by Ewa [10] with fuzzy for crisp and interval data. In another study Cheaitou et al. [20], along with the key parameter, contractor risk is also included with fuzzy logics, and Bi-model optimization was used to select the best bid. In recent studies, fuzzy TOPSIS was used several times for determining the priority of dam selection [8].

From the literature, many researchers use various key parameters along with time and cost for bid evaluation. In Table 1, column two shows the various parameter can be used for bid evaluation, and column describes the subcategory under which a key parameter can be further bifurcate. The novelty of this research is to combine all available key parameters to include, which directly and indirectly affect the bid evaluation.

3 Research Methodology

Multiple-criteria decision analysis (MCDA) or multiple criteria decision making (MCDM) is a sub-discipline of operation research that principally evaluates multiple conflicting criteria in the decision-making process. The process involves designing computational and mathematical tools to support the subjective evaluation of a finite number of decision alternatives under a finite number of performance criteria and sub-criteria [5]. In our studies, TOPSIS is used for analyzing multi-attribute objectives. The bid evaluation framework has four stages with the specific procedure for each stage, as discussed next.

3.1 Stage I Selection of Key Parameters

The stage aims to select the parameters discussed in the literature review presented in Sect. 2. The values from Table 1 are used and reorganized. The parameters are (i) Bid amount, (ii) Management Capability, (iii) Technical Capability, (iv) Financial Capability, (v) Social Influence, (vi) Contribution to project, (vii) Organizational management, (viii) Health and safety records.

3.2 Stage II Assigning Weight to Key Parameters

This stage aims to assign the weights for parameters based on the literature available. There are mainly three types of decision-makers: risk-averse, risk-neutral, and risk-prone [3]. Thus, the weights for all parameters are different for different from the decision-maker. Hatush and Skitmore [3] had allotted 55% for the bid amount, 15% for financial soundness, 10% to technical ability and management capability each, and 5% to health and safety and reputation each. In another study, Daghouri et al. [5] allotted 42% weight for the bid amount and 18% for quality. Zavadskas et al. [15] have presented a different approach for considering 18% weight for the bid amount and distributed weights more uniformly between the quality of the project, experience of the firm, duration of the project, communication (12–14%). Shen et al. [13] have allotted 65% of weight to bid amount, 20% for the construction plan, and 10% for reputation and track record. Thus based on the literature, three models are developed and examined. The first case gives priority to the bidding price; the second case considered a balance between the bid amount, and other parameters allotted 50% weights to cost and rest divided equally to other parameters. In the third, the weights are divided equally to all parameters, all three cases are shown in Table 2. An attempt has been made to simulate all three possible behaviors of decision makers.

3.3 Stage III Bid Data Creation

Bidding data is created for the research purpose and is tabulated in Table 3. The pattern followed in data creation is observed from literature to simulate it as a real case study [3, 13]. For column, the Bid amount is in a million INR (Indian currency), and the rest of the parameter is in range of 1–10 where 10 represents the highest and 1 represents the lowest.

Table 2 Weights for parameters for three cases

S. No.	Parameters	Abv	Case 1	Case 2	Case 3
1	Bid amount	P_1	0.8	0.5	0.125
2	Management capability	P_2	0.1	0.05	0.125
3	Technical capability	P_3	0.1	0.05	0.125
4	Financial capability	P_4	0	0.05	0.125
5	Social influence	P_5	0	0.05	0.125
6	Contribution to project	P_6	0	0.2	0.125
7	Organizational management	P_7	0	0.05	0.125
8	Health and safety records	P_8	0	0.05	0.125

Table 3 Radom Bid value for the model

	P_1 (in Mn INR)	P_2	P_3	P_4	P_5	P_6	P_7	P_8
Bid 1	10.5	9	10	9	8	8	10	7
Bid 2	9.8	10	8	9	7	8	7	6
Bid 3	11	10	9	8	9	9	7	7
Bid 4	11.2	10	10	9	8	9	7	7

3.4 Stage IV Matrix Creation and Evaluation Using TOPSIS

The implementation of TOPSIS tool includes the following procedure steps:

Step 1: The first step is to construct the decision matrix: where row represents the alternatives available, and column represents the evaluation criteria.

$$A_{mn:}\{a_{ij}/i \in (1,2,\ldots,m), j \in (1,2,\ldots,n)\} \tag{1}$$

Step 2: In the second step, the normalized decision matrix is calculated using the decision matrix from Step 1 by using the following equation:

$$r_{ij} = \frac{x_{ij}}{\sqrt{\sum_{j=1}^{j} x_{ij}^2}}, \quad j = 1,2,3,\ldots,j \text{ and } i = 1,2,3,\ldots,n \tag{2}$$

where x_{ij} = original weight score of decision matric and r_{ij} = normalized weight score of decision matric.

Step 3: In the third step, the weighted normalized decision matrix is obtained using the following equation:

$$v_{ij} = w_i * r_{ij}, \quad j = 1,2,3,\ldots,j \text{ and } i = 1,2,3,\ldots n \tag{3}$$

where w_i = weight of evaluation criteria and r_{ij} = normalized decision matrix.

Step 4: It is important to understand the best the positive ideal solution (PIS) and negative ideal solution (NIS) for the bids thus determined with the below equation:

$$A* = \{v_1^*, v_1^*, \ldots, v_n^*\} \text{ maximum values} \tag{4}$$

where $v_i^* = \{\max(v_{ij}) \quad \text{if } j \in J;\ \min(v_{ij}) \quad \text{if } j \in J^-\}$.

$$A^- = \{v_1^-, v_1^-, \ldots, v_n^-\} \text{ min values} \tag{5}$$

where $v_i^- = \{\min(v_{ij}) \quad \text{if } j \in J;\ \max(v_{ij}) \quad \text{if } j \in J^-\}$.

Step 5: Next step is to calculate the separation measures of each alternative from PIS and NIS

$$d_i^* = \sqrt{\sum_{j=1}^{n} \left(v_{ij} - v_j^*\right)^2}, \quad j = 1, 2, 3, \ldots, J \tag{6}$$

$$d_i^- = \sqrt{\sum_{j=1}^{n} \left(v_{ij} - v_j^-\right)^2}, \quad j = 1, 2, 3, \ldots, J \tag{7}$$

Step 6: Final steps involves the calculation of the relative closeness coefficient of the ideal solution of each bid using Eq. 8.

$$\mathrm{CC}_i = \frac{d_i^-}{d_i^* + d_i^-} \quad i = 1, 2, 3, \ldots, J \tag{8}$$

Step 7: The highest closeness coefficient CC_i represents the best bid. Thus for ranking of the bids, the CC_i is used. The highest is most valuable, and the lowest in the least A MATLAB code is developed and used for performing the steps mentioned in Stage IV.

4 Result and Discussion

The application of the methodology discussed in the previous section (Sect. 2) is illustrated through an example, as shown in Table 3. Three different cases are prepared by scoring different parameters. Bid 1 has an average bid amount with a good rating for other parameters, while Bid 2 has less value of Bid amount but with less competitive rating for the rest of the parameters. Bid 3 and Bid 4 have an approximate equal bid amount and a similar rating for the rest of the parameters.

The first step involved in the TOPSIS algorithm is to create a decision matrix, and scores are indicated as the decision point in the rows, and the first column contains the evaluation criteria, as shown in Table 4, which is calculated based on Eq. 2. The next step is to obtain the weighted normalized decision matrix using weight from Table 2 multiplied to the corresponding decision point from Table 4, and the result is shown in Table 5. The fourth step in the algorithm is to calculate the $A*$ and A^-. Equations 4 and 5. are used for calculating $A*$ and A^-.

In the fifth step, the Euclidean distance is calculated from the $A*$ and A^-. To calculate d_i^* and d_i^-, Equations 6 and 7 are used, and finally, CC_i of every alternative is calculated from Eq. 8. The highest value of the CC_i denotes the 1st rank, and subsequent value denotes the respective rank, which is shown for Case 1, Case 2, and Case 3 in Table 7. The result obtained has to be examined in two ways (1) comparison within themselves, to understand the impact of incorporating

Table 4 Normalized decision matrix for bid evaluation for Case 1

Alternatives	Price/cost	Management capability	Technical capability	Financial capability	Social influence	Contribution to the project	Organizational management	Health and safety records
Bid 1	0.4934801	0.46108397	0.5383819	0.513657	0.4981	0.4697762	0.63628476	0.51745
Bid 2	0.4605814	0.51231552	0.4307055	0.513657	0.4358	0.4697762	0.44539933	0.44353
Bid 3	0.5169792	0.51231552	0.4845437	0.456584	0.5603	0.5284982	0.44539933	0.51745
Bid 4	0.5263788	0.51231552	0.5383819	0.513657	0.4981	0.5284982	0.44539933	0.51745

Table 5 Weighted normalized decision matrix for Case 1

Alternatives	Price/cost	Management capability	Technical capability	Financial capability	Social influence	Contribution to the project	Organizational management	Health and safety records
Bid 1	0.3947841	0.0461084	0.0538382	0	0	0	0	0
Bid 2	0.3684652	0.05123155	0.0430706	0	0	0	0	0
Bid 3	0.4135833	0.05123155	0.0484544	0	0	0	0	0
Bid 4	0.421103	0.05123155	0.0538382	0	0	0	0	0

Table 6 Calculation of ideal best and ideal worst solution for Case 1

$A*$	0.3684652	0.05123155	0.0538382	0	0	0	0	0
A^-	0.421103	0.0461084	0.0430706	0	0	0	0	0

multi-criteria in the evaluation. (2) comparison of result based on available literature.

The calculations for Case 1 are shown in Tables 4, 5, 6. Similarly, the calculation is done for Case 2 and Case 3, and the closeness coefficient for all three cases are shown in Table 7, along with the rank of bids. CC_i is a distance that shows the best payoff from the best solution and worst solution available. From the result of different cases, the effect of weights can be clearly seen.

- For Case 1, the closeness coefficient for Bid 2 is highest as weight for the bid amount is 80%, along with technical capability and management capability of 10% each.
- In Case 2, the rank comes out to be the same as Case 1, but the closeness coefficient is different; this is due to the different weightage of the bid amount that changes from 80 to 50%. This is due to the marginal difference in the bid amount quoted.
- When all the parameters weighted 12.5% each, the ranking changed, and Bid 1 proven to be the best alternative among all bids.
- The variation in the result is due to the incorporation of weights of factors such as social influence, management capability, technical capability, financial capability, contribution to project, organizational management, health and safety records. That shows the overall chances of project success will be high when the bidder is evaluated from all angles, which affects a project directly or indirectly.

When we compare the result to the previous study, only a few researchers had considered these many parameters. For a fair comparison, only the study corresponds to the scope of this researches is considered. Shen et al. [13] considered the similar parameter and further subdivided them, the result obtained is based on AHP algorithm, that shows lowest bid is not the only solution when included construction master plan and organization structure in the evaluation. Similarly, when compared to another study based on similar multi-variate evaluation using utility theory, the result shows the role of decision-maker will not vary much when

Table 7 Closeness coefficient and rank obtained for Case 1, 2, and 3

Alternatives	Case 1		Case 2		Case 3	
	CC_i	Rank	CC_i	Rank	CC_i	Rank
Bid 1	0.5146922	2	0.499229685	2	0.7028424	1
Bid 2	0.8308418	1	0.652761463	1	0.2729537	4
Bid 3	0.1887586	3	0.333743557	3	0.4474973	2
Bid 4	0.1846947	4	0.16119226	4	0.3848712	3

multiple criteria are incorporated in the evaluation. This study also shows a similar result which shows the applicability of TOPSIS in the multi-criteria-based bid evaluation.

The models illustrated in this section show a typical method for awarding tender considering multi-criteria. Different type of construction project requires different weights for various parameter thus bid based on just cost and time is not effective. The result shows the different result for the same bid when the weights of parameters involved in the bid evaluation gets changed.

5 Conclusions

There is a need for a bid selection technique that can incorporate multiple variables. The inclusion of multiple variables in the bid evaluation process helps managers and decision-makers to take leverage of all the available information. Incorporating several criteria, and sub-criteria make assessment more complex and time-consuming. MCDM techniques permit both quantitative criteria and qualitative criteria (using fuzzy logic) can be included in decision making. As demonstrated in this paper, TOPSIS is selected for its simplicity, practicality, and suitability in highly competitive situations. Three hypothetical case studies is illustrating the method and in which have been analyzed. The assessment of the relative weights was based on literature. The algorithm is performed with the help of developed computer programming that appears to be eminently suited to construction bid evaluation. From the results, the variation can be observed when the respective weight is changed. This study helps in understanding the importance of different parameters affecting the bid selection process, which is useful, considering different projects have different risks involved. In the future, actual bids can be used as input to check the robustness of the algorithm.

References

1. Ashraf J, Uddin S (2016) New public management, cost savings and regressive effects: a case from a less developed country. Crit Perspect Account 41:18–33. https://doi.org/10.1016/j.cpa.2015.07.002
2. Russell JS, Skibniewski MJ (1988) Decision criteria in contractor prequalification. J Manag Eng 4(2):148–164. https://doi.org/10.1061/(ASCE)9742-597X(1988)4:2(148)
3. Hatush Z, Skitmore M (1998) Contractor selection using multicriteria utility theory: an additive model. Build Environ 33(2–3):105–115. https://doi.org/10.1016/S0360-1323(97)00016-4
4. Mbachu J (2008) Conceptual framework for the assessment of subcontractors' eligibility and performance in the construction industry. Constr Manag Econ 26(5):471–484. https://doi.org/10.1080/01446190801918730

5. Daghouri A, Mansouri K, Qbadou M (2018) Information system performance evaluation and optimization using AHP and TOPSIS: Construction industry case. In Proceedings of 2018 international conference on optimization and applications ICOA 2018, no Mcdm, pp 1–8. https://doi.org/10.1109/ICOA.2018.8370589
6. Mafakheri F, Dai L, Slezak D, Nasiri F (2007) Project delivery system selection under uncertainty: multicriteria multilevel decision aid model. J Manag Eng 23(4):200–206. https://doi.org/10.1061/(ASCE)0742-597X(2007)23:4(200)
7. Lima Junior FR, Osiro L, Carpinetti LCR (2014) A comparison between fuzzy AHP and fuzzy TOPSIS methods to supplier selection. Appl Soft Comput J 21:194–209. https://doi.org/10.1016/j.asoc.2014.03.014
8. Ulfiana D, Suharyanto S (2019) Analysis of fuzzy TOPSIS method in determining priority of small dams construction. J Tek Sipil dan Perenc 21(2):46–53. https://doi.org/10.15294/jtsp.v21i2.19957
9. Li Y, Liang X (2016) In-depth study on the evaluation of green construction based on TOPSIS. In: ICCREM 2016 BIM application and off-site construction—Proceedings 2016 international conference on construction and real estate management, pp 593–599. https://doi.org/10.1061/9780784480274.070
10. Ewa R (2011) Multi-criteria decision making models by applying the topsis method to crisp and interval data. Mult Criteria Decis Making/University Econ Katowice 6(Mcdm):200–230
11. Skitmore M, Pemberton J (1994) A multivariate approach to construction contract bidding mark-up strategies. J Oper Res Soc 45(11):1263–1272. https://doi.org/10.1057/jors.1994.199
12. Cheng EWL, Li H, Love PED (2000) Establishment of critical success factors for construction partnering. J Manag Eng 16(2):84–92. https://doi.org/10.1061/(ASCE)0742-597X(2000)16:2(84)
13. Shen LY, Li QM, Drew D, Shen QP (2004) Awarding construction contracts on multicriteria basis in China. J Constr Eng Manag 130(3):385–393. https://doi.org/10.1061/(ASCE)0733-9364(2004)130:3(385)
14. Zavadskas EK, Vilutiene T (2006) A multiple criteria evaluation of multi-family apartment block's maintenance contractors: I—Model for maintenance contractor evaluation and the determination of its selection criteria. Build Environ 41(5):621–632. https://doi.org/10.1016/j.buildenv.2005.02.019
15. Zavadskas EK, Turskis Z, Tamošaitiene J (2008) Contractor selection of construction in a competitive environment. J Bus Econ Manag 9(3):181–187. https://doi.org/10.3846/1611-1699.2008.9.181-187
16. Huang JW, Wang XX, Zhou YH (2009) Multi-objective decision optimization of construction schedule based on improved TOPSIS. In: Proceedings of international conference on management and service science MASS 2009, pp 1–4.https://doi.org/10.1109/ICMSS.2009.5303790
17. Jaskowski P, Biruk S, Bucon R (2010) Assessing contractor selection criteria weights with fuzzy AHP method application in group decision environment. Autom Constr 19(2):120–126. https://doi.org/10.1016/j.autcon.2009.12.014
18. Padhi SS, Mohapatra PKJ (2010) Centralized bid evaluation for awarding of construction projects—a case of India government. Int J Proj Manag 28(3):275–284. https://doi.org/10.1016/j.ijproman.2009.06.001
19. Sipahi S, Esen O (2010) Multi-criteria model for bidding evaluation: an alternative selection of the best firms for the presentation of Istanbul 2010. Manag Decis 48(2):296–313. https://doi.org/10.1108/00251741011022635
20. Cheaitou A, Larbi R, Al Housani B (2019) Decision making framework for tender evaluation and contractor selection in public organizations with risk considerations. Socio-econ Plann Sci 68(Jan 2017):100620. https://doi.org/10.1016/j.seps.2018.02.007

Assessing the Critical Success Factors for PWD Projects in Rural Area

Ajinkya Umberje, Sulakshya Gaur, and Abhay Tawalare

Abstract Public sector construction projects are always criticized for issues of time and cost overrun. Many researchers have worked on this problem and came out with a success list of factors for the successful completion of public projects. Public Works Department (PWD) Maharashtra is facing the same challenge, but the organization is executing more projects in the rural area. Therefore, it is necessary to identify success factors for this organization with the context of working in a rural area. To address this, 25 factors were identified, and their degree of importance was determined through a questionnaire survey. Considering 122 valid responses, factors were ranked based on their means and were further checked for the difference of opinion by one way ANOVA, and thereafter, the factor analysis was done. Through factor analysis, all the factors were extracted into 7 components to decide the new factors to lead projects toward success. The critical success factors emerge, which are the client's preparedness, employee training, project manager's competency, contractor's efficiency, project management, external environment, and transparent procurement. The findings of this study will help the practicing managers as well as all the other stakeholders associated with the project. The identified CSF's will provide them a clear insight as to which components they need to address to make a project a successful one.

Keywords PWD · Public construction projects · Project success factors · Public Works Department · Factor analysis

1 Introduction

Public Works Department (PWD) is one of the oldest government organizations in Maharashtra. With a history of over 150 years, PWD has served its roles in serving the needs of people by the construction of roads, bridges, and buildings. It has

A. Umberje · S. Gaur · A. Tawalare (✉)
Department of Civil Engineering, Visvesvaraya National Institute of Technology, Nagpur, Maharashtra, India
e-mail: abhaytawalare@civ.vnit.ac.in

B. Laishram and A. Tawalare (eds.), *Recent Advancements in Civil Engineering*, Lecture Notes in Civil Engineering 172,
https://doi.org/10.1007/978-981-16-4396-5_14

numerous functions that include the construction of roads and bridges; construction of government buildings; carrying out resettlement work in the case of any natural calamity; design, construction, and maintenance of runways, etc. [1]. However, the projects are faced with the continuous issue of time and cost overrun. This issue is witnessed due to improper distribution of risks; lack of trust/limited trust; and not defining the goals and objectives of the project properly beforehand among the contracting parties [2].

Numerous studies have been conducted in the past that focused on determining various success factors for construction projects and the construction industry at large. Some of the factors associated with the success of the project relate to the competency level of the top management along with their experience and performance, being identified by Tripathi and Jha [3]. Similarly, Alias et al. [4] identified management and coordination; quality issues and errors; administration and bureaucracy; decision issues, and waiting as important factors associated with the delay in the projects. But these success factors can't be directly adopted for PWD projects as PWD executes more projects in the rural area of the state. Also, PWD projects need to satisfy various political interests, need to follow various bureaucratic procedures, rules, and laws, and exist in the midst of a public audit.

In this context, it is necessary to identify the critical success factors associated with the projects undertaken by PWD so that these factors will help the PWD engineers to focus on few critical issues for improvement of the project performance. Therefore, this study aimed to identify critical success factors for PWD projects in Maharashtra.

2 Literature Review

Various factors play a pivotal role in the success of any project; however, some specific factors come out to be more important than others. These key factors are termed as critical success factors. The success of any project is defined when it achieves all the set goals and objectives [5]. The expression critical success factor (CSF) was first coined in the construction field by Sanvido et al. [6]. They used CSF's as an element that could help in anticipating project success. Since then, numerous studies have been done that focused on determining various important factors that can lead to the success of projects.

De Silva et al. [7] identified 46 problems encountered by the construction industry in Sri Lanka. They grouped these identified factors into 10 categories, i.e., financial; government policies/practices; technology; management and coordination; research and development; resource; safety; training and development; social and skill. Similarly, in a study conducted by Kazaz et al. [8] to investigate the causes of time overrun in construction projects in Turkey, 34 factors were determined. These factors were categorized into environmental; financial; labor-based; managerial; owner-based; project-based and resource-based factors.

The importance of CSF's for the project success was agreed upon by the project managers and contractors in a study conducted by Garbharran et al. [9] in the South African construction industry. Through their study, they identified 18 CSF's and grouped them under 4 COM's, i.e., comfort, competence, communication, and commitment.

Taking into account the previous literature, a list of 25 CSF's important for the success of PWD projects was prepared. The list of identified CSF's is presented in Table 1.

3 Research Methodology

This study used a quantitative research methodology to achieve the specified objective. An exhaustive literature review was done to determine the critical success factors for PWD projects. The degree of importance of the identified factors was determined by the help of a questionnaire survey. The questionnaire survey used a five-point 'Likert Scale' to obtain the response from the respondents, where '5' represents a strong agreement with the factor and '1' represented the least agreement with the factor. A pilot study was conducted to determine the adequacy of the prepared questionnaire, and necessary changes were made as per the recommendations of the respondents in the pilot study. Two Deputy Engineers and 3 contractors participated in the pilot study. The survey was conducted during April & May 2019. A total number of 255 questionnaires were sent by email for obtaining the responses across the state. Out of that 122 valid responses were obtained back. It represents a response rate of 48% which is considered adequate [19].

The valid responses comprised of 72 responses (59%) from the PWD Engineers and 50 responses (41%) belonged to private contractors who were associated with the PWD projects. The respondents were also categorized based on their experience. Four categories were determined, experience between 0–5 years had 17 responses; 6–10 years had 27; 11–20 years had 42; and more than 20 years' experience accounted for 36 responses. Classification of respondents based on their experience presents the credibility of obtained responses.

4 Analysis and Results

The responses were analyzed using SPSS software. Before factor analysis, the reliability of the five-point scale was determined using Cronbach alpha value. The Cronbach alpha value came out to be 0.877 and was well within the acceptable limits. The means of the factors were determined to rank them based on the obtained responses. Since the responses were obtained by two groups, i.e., the employees of PWD and private contractors working on PWD projects, it became essential to determine the consistency among the two groups of respondents. To

Table 1 Identified critical success factors for project success

S. No.	Factors	Abraham [10]	Kuwaiti et al. [11]	Arslan and Kivrak [12]	Tan and Ghazali [13]	Tabish and Jha [14]	Tripathi and Jha [3]	Yong and Mustaffa [15]	Chen et al. [16]	Chan et al. [17]	Inayat et al. [18]
1	Nature of the client			✓	✓		✓		✓	✓	✓
2	Contractor's reputation			✓	✓	✓	✓		✓		
3	Selection of project					✓					
4	Competent bidding process					✓		✓			
5	Government policies		✓								✓
6	Stable economy			✓			✓	✓		✓	✓
7	Financial capability		✓						✓		✓
8	Political interference	✓	✓			✓		✓	✓	✓	✓
9	Goal setting	✓			✓			✓			
10	Top management support		✓	✓	✓	✓					
11	Transparent procurement process		✓				✓		✓		
12	Project management	✓	✓	✓	✓					✓	
13	Communication and information sharing		✓			✓		✓	✓	✓	✓
14	Commitment within all parties		✓			✓		✓			
15	Effective decision making	✓			✓						
16	Competent project manager				✓	✓		✓			

(continued)

Table 1 (continued)

S. No.	Factors	Abraham [10]	Kuwaiti et al. [11]	Arslan and Kivrak [12]	Tan and Ghazali [13]	Tabish and Jha [14]	Tripathi and Jha [3]	Yong and Mustaffa [15]	Chen et al. [16]	Chan et al. [17]	Inayat et al. [18]
17	Competent project team								✓	✓	
18	Training and education	✓		✓							✓
19	Adoption of latest technology	✓	✓	✓	✓				✓	✓	✓
20	Resource management		✓			✓	✓				
21	Quality and safety programs		✓	✓	✓				✓		
22	Employee enhancement	✓	✓			✓					
23	Monitoring and feedback				✓		✓	✓		✓	
24	Demand and variations					✓		✓			
25	Corruptions					✓					✓

carry out this, 'Analysis of Variance', i.e., one-way ANOVA test was done for each factor, taking into account both respondent groups. Two hypotheses were generated for the ANOVA test.

Null Hypothesis (H_o): There is a significant difference in opinion among engineers working in PWD and engineers working in contractor organizations regarding critical success factors of PWD projects.

Alternate Hypothesis (H_a): There is no significant difference in opinion among engineers working in PWD and engineers working in contractor organizations regarding critical success factors of PWD projects.

The significance level was set at 0.05 to check the obtained data for agreement between the respondents. 17 factors out of the identified 25 factors had a significance of above 0.05, and hence, these factors failed to reject the null hypothesis. Table 2 presents the ranking of factors along with the results of the ANOVA test.

From the above results, it can be seen that the respondents from PWD and contractor organizations disagreed on 17 factors out of a total of 25 factors, thus, showing a significant difference of opinion.

With the help of factor analysis, the identified CSF's were grouped into different components. Factor analysis used principal component analysis as it explains maximum variance by the minimum number of underlying factors [20]. Only the factors with a mean value above 4 were considered in factor analysis as it represents that the respondents emphatically concur with its significance for executing PWD projects. These 7 components accounted to explain 66.37% of the total variance. Table 3 presents the factors under their respective components with their factor loadings.

5 Discussion

The identified success factors were extracted into 7 components that present an important tool for the success of PWD projects. Client-related factors were the most important component as it explained 11.85% of the total variance. It was followed by training-related factors (11.057%); project manager-related factors accounting for 10.46% of the variance; contractor-related factors (10.04%); project-related factors (9.62%); external environmental factors (7.08%); and procurement-related factors (6.27%). The seven identified critical success factors are discussed below.

5.1 Client's Preparedness

Monitoring and feedback were the highest-ranked factor in this component. It was followed by the nature of the client; employee's enhancement; demands and variations and stable economy. The factors in this component emphasized the role

Table 2 Ranking of factors and ANOVA test significance values

S. No.	Factors	Mean	Rank	ANOVA significance
1	Nature of the client	4.69	8	0.466
2	Contractor's reputation	4.13	24	0.017
3	Selection of project	4.64	10	0.714
4	Competent bidding process	4.6	14	0.213
5	Government policies	3.5	25	0.03
6	Stable economy	4.22	22	0.763
7	Financial capability	4.7	7	0.369
8	Political interference	4.8	4	0.023
9	Goal setting	4.53	15	0.182
10	Top management support	4.35	20	0.031
11	Transparent procurement process	4.14	23	0.023
12	Project management	4.61	13	0.515
13	Communication and information sharing	4.86	3	0.109
14	Commitment within all parties	4.62	12	0.867
15	Effective decision making	4.87	2	0.436
16	Competent project manager	4.92	1	0.205
17	Competent project team	4.71	6	0.792
18	Training and education	4.42	19	0.321
19	Adoption of latest technology	4.32	21	0.028
20	Resource management	4.68	9	0.007
21	Quality and safety programs	4.46	17	0.334
22	Employee enhancement	4.63	11	0.872
23	Monitoring and feedback	4.73	5	0.83
24	Demand and variations	4.45	18	0.388
25	Corruption	4.48	16	0

of the client in managing a project and in turn leading it to be a successful one. The client should be proactive in planning as the work needs to avoid too many variations. In PWD projects, local political leaders interfere mostly during the execution of the work which leads to a change of scope of work and invites variations. These are unavoidable situations and cannot be overlooked as powers of development have been precipitated to the village level through Panchayat Raj System in India [21]. Monitoring is an important factor in maintaining the quality of work. But, due to a lack of Junior Engineers in PWD Maharashtra, a single junior engineer has to look after many sites simultaneously. In this situation, he has to depend on the contractor's engineer for maintaining the quality of work. Another important factor is the stable economy of the country. After demonetization and implementation of new Goods and Service Tax (GST) rules, the economy has been shattered due to which contractors faced financial problems.

Table 3 Components of CSF's for the success of PWD projects

S. No.	Component name	Factors	1	2	3	4	5	6	7
1	Client's preparedness	Nature of the client	0.556						
		Stable economy	0.644						
		Monitoring and feedback	0.722						
		Employees enhancement	0.48						
		Demand and variations	0.61						
2	Employee training	Training and education		0.818					
		Quality and safety programs		0.773					
		Adoption of the latest technology		0.837					
3	Project manager's competency	Communication and information sharing			0.804				
		Effective decision making			0.838				
		Competent project manager			0.8				
4	Contractor's efficiency	Competent bidding process				0.543			
		Contractors reputation				0.823			
		Project management				0.579			
		Commitment within all parties				0.473			
		Competent project team				0.587			
5	Project management	Selection of project					0.668		
		Financial capability					0.661		
		Goal setting					0.426		
		Top management support					0.509		
6	External environment	Political interference						0.503	
		Resource management						0.587	
		Corruption						0.83	
7	Transparent procurement	Transparent procurement process							0.852

5.2 Employee Training

Training and education were ranked as the most important factor in this component. The two other factors are quality and safety programs and the adoption of the latest technologies. Proper training of the project participants will make them aware of new technologies, lead them in developing safe working conditions on-site and make them aware of the importance of maintaining the overall quality of construction work by designing a quality assurance program. Though PWD arranges many training programs for its engineers, contractors are always reluctant to spend money on training. PWD Maharashtra should take lead in arranging combined training programs for own engineers and contractors' engineers to develop a highly skilled workforce. This will also help them to develop co-operative relationships and motivate them toward developing problem-solving skills by themselves [22]. Also, on rural projects, many unskilled laborers work on-site who are not aware of quality and safety procedures related to construction. The culture of training needs to be developed so that unskilled laborers also learn the standardized procedures in construction.

5.3 Project Manager's Competency

Communication and information sharing were the most important factor under this group followed by effective decision making and competency of project manager for the success of the project. These factors emphasize the importance of communication and the effective decision-making process for the swift resolution of conflicts and disputes [22]. Deputy Engineer acts as a project manager in PWD projects. The project manager's competency in handling the human resources on site is very important as qualified engineers are reluctant to stay at the site in the rural area. The project manager should motivate these engineers to work on sites in the rural area. Arranging the material on time is a major task in rural areas due to the long travel time. The project manager should plan material procurement so that the scarcity of material may not arise. Project managers need to maintain cordial relations with village people so that they can cooperate during project execution. He must communicate effectively with higher authorities from time to time as well as local political leaders to acquaint them about the project progress and difficulties.

5.4 Contractor's Efficiency

The competent bidding process was the highest-ranked factor among this group. It was followed by the reputation of the contractor, project management, commitment between all parties, and a competent project team. PWD has established an

electronic tendering system to ensure a transparent contractor selection process. But the real problem starts with tremendous competition among the local contractors to win a bid. The local contractors quote bid prices too low, many times less than 20% below than tendered cost. Due to this, reputed contractors hesitate to take part in the bidding process in PWD projects in the rural area. If work is allotted to the reputed contractor, then PWD engineers need not worry more about quality of work as they are always committed to good project management practices to deliver quality projects so that their reputation in the market does not hamper [23].

5.5 Project Management

The factor associated with the selection of projects was ranked the highest under this group. This was followed by financial capability, goal setting, and support from top management for the success of the project. If a reputed contractor is working on the project, then he works in good coordination with client engineers to meet the time-bound goals of the project. Also, his financial capacity is more to maintain the progress of the work. But most of the time, local contractors win the bids of PWD projects in rural areas who do not have a proper project management system and always depend on payment from clients to maintain the progress of work. Many times funds may not available from the government for timely payment and the common public criticizes PWD engineers.

5.6 External Environment

These factors may not come as direct influencing factors but play an important role in the success of projects. Political interference was ranked as the most important followed by resource management and corruption that may result in the failure of the project. Many times the local politicians or politically motivated people try disturbing the project implementation by raising new demands related project's scope that results in the delay of projects. This also sometimes results in the violation of rules and law for the sake of personal gains and may lead to cost overrun in the projects. PWD engineers need to tackle such situations very carefully so that projects can be completed within cost and time.

5.7 Transparent Procurement

The last component is associated with the procurement-related factor and has only one-factor transparent procurement process under it. An effective and transparent procurement process needs to be established to allow proper competition among the

participants so that the quality of material along with the completed work is at the top quality and in optimized cost. As mentioned earlier, PWD has established an electronic tendering system to ensure a transparent contractor selection process. This has prevented cartel formation by contractors which was a major problem faced by PWD engineers prior to the implementation of E-Tendering.

6 Conclusion

This study aimed to determine various critical success factors associated with the PWD project in Maharashtra. The identified factors are categorized into seven components, i.e., client's preparedness, employee training, project manager's competency, contractor's efficiency, project management, external environment, and transparent procurement. These factors emphasize the communication between the associated project stakeholders and the competency of the project manager. These are deemed as important because, in any event of a dispute, it will help in its swift resolution if there exists a proper and efficient decision-making mechanism. The findings of this work also stressed on the eradication of corruption and extensive political interference from the work to make it a successful one. These critical success factors are discussed with problems faced by PWD which will be helpful for this organization to design specific organizational strategies to overcome their problems. However, the study is based on a small sample size that is also one geographic area Maharashtra which may result in the generalization of results over a vast geographic area of the country. Still, within the limitations, this study provides general guidelines for project success in rural areas.

References

1. PWD Maharashtra. About us: Public Works Department, Government of Maharashtra, India [cited 2020 7/16/2020]. Available https://pwd.maharashtra.gov.in/about-us
2. Chan DWM et al (2010) Identifying the critical success factors for target cost contracts in the construction industry. J Facil Manag 8(3):179–201
3. Tripathi KK, Jha KN (2018) Determining success factors for a construction organization: a structural equation modeling approach. J Manag Eng 34(1):04017050
4. Alias Z et al (2014) Determining critical success factors of project management practice: a conceptual framework. Procedia Soc Behav Sci 153:61–69
5. Parfitt MK, Sanvido VE (1993) Checklist of critical success factors for building projects. J Manag Eng 9(3):243–249
6. Sanvido V et al (1992) Critical success factors for construction projects. J Constr Eng Manag 118(1):94–111
7. De Silva N, Rajakaruna R, Bandara K (2008) Challenges faced by the construction industry in Sri Lanka: perspective of clients and contractors. Build Resil 158
8. Kazaz A, Ulubeyli S, Tuncbilekli NA (2012) Causes of delays in construction projects in Turkey. J Civ Eng Manag 18(3):426–435

9. Garbharran H, Govender J, Msani T (2012) Critical success factors influencing project success in the construction industry. Acta structilia 19(2):90–108
10. Abraham GL (2003) Critical success factors for the construction industry. In: Construction Research Congress: Wind of Change: Integration and Innovation, pp 1–9
11. Kuwaiti EA, Ajmal MM, Hussain M (2017) Determining success factors in Abu Dhabi health care construction projects: customer and contractor perspectives. Int J Constr Manag 18 (5):430–445
12. Arslan G, Kivrak S (2008) Critical factors to company success in the construction industry. Proc World Acad Sci Eng Technol 45:404–407
13. Derrick J-ZT, Mohamed GFE (2011) Critical success factors for Malaysian contractors in International Construction Projects using Analytical Hierarchy Processin EPPM, Singapore. Singapore
14. Tabish S, Jha K (2011) Important factors for success of public construction projects. In: 2nd International Conference on Construction and Project Management IPEDR.Singapore, IACSIT Press
15. Yong YC, Mustaffa NE (2013) Critical success factors for Malaysian construction projects: an empirical assessment. Constr Manag Econ 31(9):959–978
16. Chen YQ et al (2012) Interrelationships among critical success factors of construction projects based on the structural equation model. J Manag Eng 28(3):243–251
17. Chan AP, Scott D, Chan AP (2004) Factors affecting the success of a construction project. J Constr Eng Manag 130(1):153–155
18. Inayat A, Melhem H, Esmaeily A (2015) Critical success factors in an agency construction management environment. J Constr Eng Manag 141(1):06014010
19. Akintoye A (2000) Analysis of factors influencing project cost estimating practice. Constr Manag Econ 18(1):77–89
20. Hair JF et al. (2019) Multivariate data analysis, 8 ed., Hampshire, United Kingdom, Cengage Learning, EMEA
21. Tawalare A (2019) Identification of risks for Indian highway construction. In: IOP Conference Series: Materials Science and Engineering, IOP Publishing
22. Tawalare A, Laishram B (2019) Factors hindering effective partnering in Indian public sector construction organizations. J Fin Manag Prop Constr 25(1):83–105
23. Tawalare A, Laishram B (2019) Relational contracting in public sector construction organisations: evidence from India. Int J Public Sector Perform Manage 5:206

Compressive Strength of Concrete Using Recycled Glass and Red Ash as a Partial Replacement of Fine Aggregate (Experimental Investigation)

Muluken Gebre Worku, Pandurang B. Khawal, and Shashi Shekhar Singh

Abstract This research presents the study on the effect of recycled waste glass and red ash as a partial replacement of fine aggregate on compressive strength of concrete and workability. The mechanical properties by applying slump value and compressive strength were investigated. Experimental study carried out by conducting laboratory tests for concrete making materials (coarse aggregate, fine aggregate recycled crushed glass, red ash). The fine aggregate in each grade of concrete was replaced by recycled crushed glass and red ash 25 and 50% by volume. The control mix without incorporation of recycled crushed glass and red ash was prepared which was used as a reference for comparison of test results with those specimens produced by partial replacement. Generally, five concrete mixes were prepared including the control mix for C-25. Slump test was conducted for each concrete mix of fresh concrete. The properties of hardened concrete were studied by conducting compressive strength. The compressive strength test was carried out on the 7th, 14th and 28th days. The test results obtained by partial replacement were compared with the result of the control mix. In line with it the results, the one obtained by partial replacement of recycled waste glass in concrete specimens was slightly greater than that of the control mix by its compressive strength and higher workability. The compressive strength values of concrete with partially replaced red ash are close to the same as the normal concrete mix design with lower workability. Generally, the result reveals that recycled crushed glass and red ash can be used for structural concrete.

Keywords Concrete mix · Recycled crushed glass · Red ash · Compressive strength · Workability · Mechanical properties

M. G. Worku (✉)
Ethiotelecom, Addis Ababa, Ethiopia

P. B. Khawal
Dr. Babasaheb Ambedkar Marathwada University, Aurangabad, India

S. S. Singh
Department of Civil Engineering, Maddawalabu University, Bale Robe, Ethiopia

B. Laishram and A. Tawalare (eds.), *Recent Advancements in Civil Engineering*, Lecture Notes in Civil Engineering 172,
https://doi.org/10.1007/978-981-16-4396-5_15

1 Introduction

1.1 Back Ground of the Study

The innovation of advanced technology in construction materials is increasing very rapidly. In past few decades, various research was carried out on concrete to maximize the qualities in both the aspect, i.e., strength and durability qualities. Now concrete is not only a construction material that only consisting cement, aggregates and water only, but has become an innovative engineering material that mixes with other new materials and makes quality superior in every aspect of the requirement for construction. Generally, crushed stones of rocks are used as conventional coarse aggregates whereas Natural River sand is used as fine aggregate, both are available naturally [1]. As concrete is the 2nd most usable material behind water by humans so due to their higher quantity usage leading to depletion of this naturally available material at faster rate results in increased cost of construction. Because of the quick development of construction exercises, ordinary aggregate sources are draining quickly prompting a noteworthy increment in the cost of construction. For sustainable development, these materials need to be utilized carefully and option materials should be looked at to supplant ordinary aggregate [2]. In the meantime because of fast industrialization, creation of the waste material is expanding step by step. Its disposal has turned into a genuine issue. The answer for this issue is to arrange disposal on landfill sites or utilize this waste for some positive movement. In the perspective of this, the choice is—it is possible that we ought to limit the waste at the creation level or use it.

Traditionally, locally available materials like red ash are in use as a fine aggregate in concrete production without checking its property, it might deliver concrete financially economical [3]. In our research we had delivered the issue identified with the deficiency of ordinary materials and an issue of disposal of waste material, using locally available material like red ash and utilization of waste glass for creation of concrete. This is achieved by checking the fresh concrete for its workability and preparing the cube for compressive tests for different types of material proportions at different time intervals.

1.2 Statement of the Problem

- Natural sand is the only source of fine aggregate in our country; hence another additional source should be arranged.
- Post-consumer glass represents a major component of solid waste and difficulty in locating convenient markets that will accept glass collected for recycling.
- Red ash (locally available material) procured from Bale Zone was used as a partial replacement for river sand without checking its properties.

1.3 Objective of the Study

1. To Study the influence of recycled glass and red ash on the compressive properties of concrete.
2. To identify the effects of adding waste glass and red ash on the fresh properties of concrete (i.e., workability).

2 Materials

a. Cement: The type of cement used for the study is MUGER PPC 32.5 R.
b. Fine Aggregate: The fine aggregate (natural sand) was purchased from the nearby market around the robe. It was thoroughly washed with tap water so as to remove the silt and debris on it. The conducted laboratory physical tests were sieve analysis (gradation), fineness modulus, unit weight and silt content. Sieve analysis is used to determine the particle size distribution of the aggregate (Table 1).

The test results of physical properties for fine aggregate are summarized in Table 6. As can be seen in the table the silt content of the sample is 3%, which is lower than the allowable limit of 5% so it complies with the standard.

Silt Content

Silt content is a fine material that is less than 150 µm. It is unstable in the presence of water if we use silty sand for bonding, it will reduce bonding and strength. Excessive quantity of silt not only reduces bonding of cement and fine aggregate but also affects the strength and durability of work [4].

Table 1 Sieve analysis test result of fine aggregate

Sieve size (mm)	Wt. of sieve (g)	Wt. of sieve and retained (g)	Wt. of retained (g)	%ge retained (%)	Cumul. coarser (%)	Cumul. passing (%)	Standard limit (%)
9.5							100
4.75	427	433	6	1.20	1.20	98.80	95–100
2.36	387	402	15	3.00	4.20	95.80	85–100
1.18	374	446	72	14.40	18.60	81.40	50–85
600 µm	326	532	206	41.20	59.80	40.20	25–60
300 µm	302	452	150	30.00	89.80	10.20	10–30
150 µm	269	310	41	8.20	98.00	2.00	2–10
Pan	254	264	10	2.00			
Total			500		271.60		

Fineness Modulus FM = Cumulative Coarser %/100 FM = 271.6/100 = 2.7

$$\text{Silt content} = (v1/v2) * 100$$

The permissible content in sand percentage should be less than 5%.

According to our investigation in silt content determination of fine aggregate (river sand).in the first test the silt content is 9%. This value indicates remedial action should be taken to minimize the amount of silt content in sand [5]. Hence the sand is washed thoroughly by using tap water and the silt content is reduced to 3% (Table 2).

c. Coarse Aggregate

The coarse aggregate used for the study was purchased from a crusher plant found around the robe. The maximum size of aggregate used for the study was 12.5 mm.

The types of laboratory tests conducted for coarse aggregate was sieve analysis (gradation) (Table 3).

d. Recycled Crushed Glass

The recycled crushed glass used for the study was collected from robe town waste dumping area around kebele chaka place known as koshe. The collected bottles and glazes were thoroughly washed with tap water to remove the debris and dirt. The maximum aggregate size of recycled crushed glass was 4.75 mm which is the same as that of coarse aggregate (Table 4).

e. Red Ash: Red ash (locally available material) is widely available and highly effective for usage in concrete as a partial replacement of fine aggregate and depending upon the variety of mix proportions [6]. In this study we use 1:2:3 mix proportion (C-25) it enhances the performance of the red ash cement concrete, Factorial experiments were done with 0%, 25%, 50%, sand replacement by volume of sand (Table 5).

Table 2 Laboratory test result of fine aggregate

Description	Test result
Silt content (%)	3
Fineness modulus	2.71

Table 3 Sieve analysis test result of coarse aggregate

Sieve size (mm)	Wt. of sieve (g)	Wt. of sieve and retained (g)	Wt. of retained (g)	%ge retained (%)	Cumul. coarser (%)	Cumul. passing (%)	Standard limit (%)
19				0	0	100	100
12.5	1158	1220	62	3.11	3.11	96.89	90–100
9.5	1160	1220	294	14.73	17.4	82.16	40–85
4.5	1265	2905	1640	82.16	100	0	0–10
			1996				

Table 4 Sieve analysis test result of crushed glass

Sieve size (mm)	Wt. of sieve (g)	Wt. of sieve and retained (g)	Wt. of retained (g)	%ge retained (%)	Cumul. coarser (%)	Cumul. passing (%)	Standard limit (%)
9.5							100
4.75	427	433	20	1.33	1.33	98.67	95–100
2.36	387	402	48	1.87	3.20	96.80	85–100
1.18	374	446	240	16.67	19.87	80.13	50–85
600 µm	326	532	600	40.00	59.87	40.13	25–60
300 µm	302	452	444	29.60	89.47	10.53	10–30
150 µm	269	310	122	8.13	97.60	2.40	2–10
Pan	254	264	26	2.40	100.00		
Total			1500				

Table 5 Sieve analysis test result of red ash

Sieve size (mm)	Wt. of sieve (g)	Wt. of sieve and retained (g)	Wt. of retained (g)	%ge retained (%)	Cumul. coarser (%)	Cumul. passing (%)	Standard limit (%)
9.5							100
4.75	427	433	27	1.35	1.35	98.65	95–100
2.36	387	402	64	3.20	4.55	95.45	85–100
1.18	374	446	300	15.00	19.55	80.45	50–85
600 µm	326	532	800	40.00	59.55	40.45	25–60
300 µm	302	452	592	29.60	89.15	10.85	10–30
150 µm	269	310	167	8.35	97.50	2.50	2–10
Pan	254	264	50	2.50	100.00		
Total			2000				

3 Testing Arrangement

In this study, a total of 5 types of concrete mixes comprised of a grade of concrete (C 25) were produced. Fine aggregate was partially replaced with recycled crushed glass and red ash aggregate at 25 and 50% by volume. In addition, a control mix was produced for the purpose of comparing the test results with samples produced by partial replacement of recycled crushed glass and red ash separately [7].

The mix proportion of the basic ingredients that is cement, fine aggregate and water were the same for the control mix and for concrete produced by partially replacing the recycled crushed glass and red ash, except replacing the fine aggregate with an equal volume of recycled crushed glass and red ash. C25 grade of concrete was prepared in the study; the reason for selecting this grade is that it is the most common grade of concrete widely used in the construction industry of our country [8].

In general 30 concrete test cubes for compressive strength test of concrete were used in the study for C25 grade of concrete. The following tests were conducted on each concrete mix:

1. Slump test
2. Compressive strength test at the 7th, 14th and 28th days

3.1 Batching of Materials

See Table 6.

3.2 Test for Workability of Concrete

The following procedure was followed to conduct a slump test of concrete. The slump cone was cleaned with water. It was firmly held with feet on the steps and it was filled one third with concrete and it was compacted 25 times with a tapping rod. Two further layers were added to a height of 100 mm and each was compacted 25 times. The surplus concrete was struck off using steel float. The cone was carefully lifted vertically upwards and then it was turned over and placed near the mold concrete. The tamping rod was placed over the empty cone and it reached over the slumped concrete. Measurement was taken from the underside of the rod to the surface of the concrete [9].

3.3 Test for Compressive Strength of Concrete

Concrete mix was prepared with the calculated amount according to the mix design. Cubical molds were prepared and oiled properly in order to easily remove the

Table 6 Mix proportioning

Mix	Concrete grade	W/C ratio	Cement (kg)	Water (kg)	Fine agg. (kg)	Coarse agg. (kg)	Crushed glass (kg)	Red ash (kg)
A	C-25	0.64	12.5	8	11.89	16.84	10.64	–
B	C-25	0.64	12.5	8	17.83	16.84	5.32	–
C	C-25	0.64	12.5	8	11.89	16.84	–	9.89
D	C-25	0.64	12.5	8	17.83	16.84	–	4.94
E	C-25	0.64	12.5	8	23.78	16.84	–	–

concrete cubes from the mold. Concrete was filled in the cubical molds and each was compacted 25 times. The surface was smoothed and excess concrete was removed using a spatula and the casting date was written on it. The mold was removed after 24 h and it was placed in water for curing [10].

The concrete specimens were crushed on the 7th, 14th and 28th days. The concrete specimens were loaded to failure using concrete compressive strength testing machine and the failure load was recorded [11]. The stress was calculated by dividing the load at failure by the contact area of the specimen (the testing machine displayed the failure load and it also calculated the stress [12]).

4 Test Results and Discussions

4.1 General

This section discusses the laboratory results of the tests carried out to investigate the hardened and fresh properties of the concrete prepared by partially replacing fine aggregate with recycled crushed glass and red ash and to compare the result with the control mix. In this part of the study, the results of the slump and compressive strength test for the C25 grade of concrete are presented. Furthermore, analysis and discussion are also made based on the obtained test results.

4.2 Test Results of Concrete

4.2.1 Properties of Fresh Concrete

Since the long-term properties of hardened concrete; strength, volume stability and durability are seriously affected by its degree of compaction. It is vital that the consistency or workability of fresh concrete be such that the concrete can be properly compacted and also that it can be transported, placed and vibrated sufficiently easily without segregation, which would be detrimental to such compaction.

Workability is the amount of useful internal work necessary to produce full compaction. The useful internal work is a physical property of concrete alone and is the work or energy required to overcome the internal friction between the individual particles in the concrete.

Workability

The slump test was adopted as the primary measure of concrete workability in this study and was undertaken in accordance with EBCS (Ethiopian Building Code of Standard) (Table 7).

Table 7 Workability test results

Type of mix	W/C ratio	Slump measured	Difference from the nominal	Percentage difference
C-25	0.64	65 mm	–	–
50% glass	0.64	75 mm	10 mm	15% increase
25% glass	0.64	68 mm	3 mm	4.6% increase
25% red ash	0.64	60 mm	5 mm	7.7% decrease
50% red ash	0.64	42 mm	21 mm	32.3% decrease

An initial slump of 65 mm was obtained for the plain concrete mix, with mixes containing waste glass exhibiting slumps ranging from 15 to 30% higher than that of the control. Regardless of these discrepancies, it can be seen that the slump demonstrates an increasing trend in response to the addition of waste glass. Similar observations have been recorded in previous research, concluding that this may be attributed to a combination of poor glass geometry and reduction in fineness modulus. It is therefore suggested that the reduction in the slump is solely due to the angular geometry of glass particles, which reduces the availability of cement paste and hence the fluidity of the mix. Despite the reduction in slump values, all concrete mixes were considered workable and were within tolerance levels of 25 mm. No excessive bleeding or segregation of concrete specimens was encountered during preparation, supporting earlier research that indicated fine aggregate replacements less than 50% had minimal negative effects on properties of fresh concrete. Also with mixes containing red ash exhibiting slumps ranging from 7.7 to 32.3% lower than that of the control. Regardless of these discrepancies, it can be seen that the slump demonstrates a decreasing trend in response to the addition of red ash as a partial replacement of fine aggregate.

4.2.2 Properties of Hardened Concrete

To investigate the hardened properties of concrete compressive strength test is conducted.

Compressive Strength Test

An increasing trend can be witnessed along with the addition of glass aggregate until the maximum compressive strength (16.9 MPa) was developed at a replacement level of 25%. All mixture proportions containing waste glass to this point exceeded the strength developed by the control, with the 25% glass mix recording a compressive strength 1% higher. These findings support earlier research conducted by Tuncan et al., where the compressive strength of concrete after 7 days of curing was found to increase with the addition of glass, albeit at lower levels of replacement. Addition of waste glass beyond the optimum level resulted in a

significant reduction to the level of compressive strength developed. At a glass replacement level of 50%, the compressive strength achieved (15.2 MPa) was 5.8% below the control and 6.8% below the maximum recorded value.

The results closely mirror that of the seven-day test, with the compressive strength following an increasing trend with the addition of waste glass up until an optimum percentage of 25%. At this point, the maximum compressive strength developed was 25.45 MPa, 2.2% higher than that achieved by the control (24.9 MPa). The increase in strength above that of the control may be attributed to the angular nature of the glass aggregate, which has a greater surface area than the naturally rounded sand particles. This increased surface area allows for greater bonding with the cement paste, resulting in a stronger concrete matrix.

The specimen containing 50% waste glass was found to have achieved a compressive strength of 21.25 MPa, 14.7% lower than that achieved by the control. This concurs with the results obtained from the 7-day test and it can therefore be concluded that levels of glass replacement in excess of 25% adversely affect the development of compressive strength. Similar findings were obtained by Malik et al. [7], who found that compressive strength reduced by 8% at a glass replacement percentage of 50% when adopting a similar glass particle distribution as to that adopted in this study. While previous studies have implied that this tendency is a result of reduced adhesion between the glass particles and cement paste.

Similarly with the compressive strength following an increasing trend with the addition of red ash up until an optimum percentage of 25%. At this point, the maximum compressive strength developed was 25.1 MPa 0.8% higher than that achieved by the control (24.9 MPa). The increase in strength above that of the control may be attributed to the angular nature of the red ash, which has a greater surface area than the naturally rounded sand particles and the roughness of the particles. This increased surface area allows for greater bonding with the cement paste, resulting in a stronger concrete matrix.

The specimen containing 50% red ash was found to have achieved a compressive strength of 22.1 MPa, 11.2% lower than that achieved by the control. This concurs with the results obtained from the 7-day test and it can therefore be concluded that levels of red ash replacement in excess of 25% adversely affect the development of compressive strength.

The results from this study suggest that the angular nature of the glass particles and red ash may further contribute to the witnessed reduction in strength. It is suggested that where glass aggregate and red ash are present in higher proportions, there is insufficient cement paste available within the mix to facilitate bonding with all particles, resulting in the formation of microscopic voids which adversely affect concrete strength (Fig. 1).

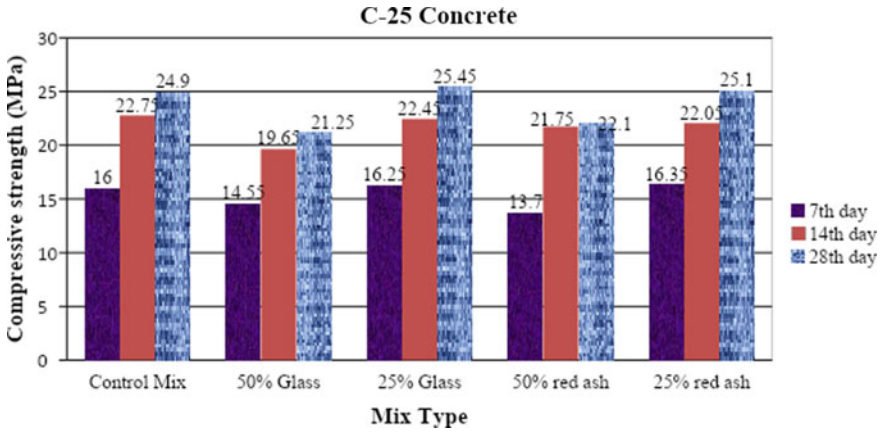

Fig. 1 Graphical representation of compressive strength test results

5 Conclusion

The replacement of fine aggregate with recycled crushed glass increased the compressive strength test result of the concrete mix when compared with the control mix At this point, the maximum compressive strength developed was 25.45 MPa, 2.2% higher than that achieved by the control (24.9 MPa). There is a decrease in compressive strength with an increase in the percentage of the waste glass. The specimen containing 50% waste glass was found to have a strength of 21.25 MPa, 14.7% lower than that achieved by the control. There is a marginal increase in compressive strength of concrete at 25% replacement and Mixes containing waste glass exhibiting slumps ranging from 15 to 30% higher than that of the control. Generally, the partial replacement of recycled waste glass in concrete specimens was slightly greater than that of the control mix by its compressive strength and higher workability.

Similarly with the compressive strength following an increasing trend with the addition of red ash up until an optimum percentage of 25%. At this point, the maximum compressive strength developed was 25.1 MPa 0.8% higher than that achieved by the control (24.9 MPa) Also with mixes containing red ash exhibiting slumps ranging from 7.7 to 32.3% lower than that of the control. The compressive strength value of concrete with partially replaced red ash is close to the same as the normal concrete mix design with lower workability. Locally available materials like red ash can be used as a fine aggregate in concrete.

References

1. Sukesh C, Katakam BK, Saha P, Shyam Chamberlin K (2012) A study of sustainable industrial waste materials as partial replacement of cement, vol 28. IPCSIT © (2012). IACSIT Press, Singapore
2. Sai Kumar AVS, Rao K (2014) Study on strength of concrete with partial replacement of cement with quarry dust and Metakaolin. Int J Innovative Res Sci Eng Technol 3(3)
3. Kothai1 PS, Malathy R (2014) Utilization of steel slag in concrete as a partial replacement material for fine aggregates. Int J Innovative Res Sci Eng Technol 3(4)
4. Yerramala A (2014) Properties of concrete with eggshell powder as cement replacement. Indian Concr J 88(10)
5. Kamala R, Krishna Rao B (2012) Reuse of solid waste from building demolition for the replacement of natural aggregates. Int J Eng Adv Technol (IJEAT) 2(1). ISSN: 2249-8958
6. Mustafa Al Bakri AM, Norazian MN, Kamarudin H, Mohd Salleh MAA, Alida A (2013) Strength of concrete based cement using recycle ceramic waste as aggregate. Adv Mater Res 740:734–738
7. Iqbal Malik M, Bashir M, Ahmad S, Tariq T, Chowdhary U (2013) Study of concrete involving use of waste glass as partial replacement of fine aggregates. IOSR J Eng (IOSRJEN) 3(7):08–13. e-ISSN: 2250-3021, p-ISSN: 2278-8719 (‖V6‖)
8. Raval AD, Patel IN, Pitroda J (2013) Bio-efficient concretes: use of ceramic powder as a partial replacement of cement. IJITEE 3(2). ISSN: 2278-3075
9. Lakshmi NS (2010) Studies on concrete containing E plastic waste. Int J Environ Sci 1(3)
10. Freeda Christy C, Tensing D (2010) Effect of class-F fly ash as partial replacement with cement and fine aggregate in mortar. Ind J Eng Mater Sci 17:140–144
11. Vijayakumar G, Vishaliny H, Govindarajulu D (2013) Studies on glass powder as partial replacement of cement in concrete production. ISO 9001:2008 Certified J 3(2). ISSN 2250–2459
12. Muthusamy K, Sabri NA (2012) Cockle shell: a potential partial coarse aggregate replacement in concrete. Int J Sci Environ Technol 1(4):260–267

Flow and Strength Characteristics of CLSM Using Gypsum Dry Wall

Minakshi Uchibagle and B. Ram Rathan Lal

Abstract This paper deals with an experimental result that is carried out on new controlled low strength material (CLSM) prepared by blending pond ash, with gypsum drywall from a demolished structure. The use of gypsum drywall is according to the proportion of 0, 10, 15 and 25% by weight of the total of pond ash, cement and water. As a binding 53 grade of ordinary Portland cement was used, the percentage of cement was used 20 and 10%. Potable water was used to mix the materials. A 75-mm-diameter and 150-mm-height cylindrical specimen was used to measure the compressive strength for 7-, 14- and 28-day curing period. The effect of the curing period, different percentages of gypsum drywall and mix ratio on the compressive strength, flowability, initial setting time and density of CLSM were studied according to ACI 229 R, and experimental results are presented in this paper. Test results specify that the flowability decreases with increasing mix ratio and gypsum drywall, percentages, and compressive strength increases with increasing curing period. For each curing period, the compressive strength increased up to 10% and then decreased with increasing value of mix ratio. For entire mix ratios, the maximum compressive strength of 9.9 MPa was noticed for mix ratio 0.1. As an increase in the percentage of gypsum drywall, there is a gradual decrease in flowability. The utilisation of Pond ash and blast furnane slag can solve its disposal problem in an environment-friendly manner leading toward sustainable development. Studies show that pond ash and gypsum drywall have potential to use in CLSM to solve the disposal problem for an eco-friendly environment.

Keywords Gypsum drywall · Controlled low strength material (CLSM) · Pond ash (PA)

M. Uchibagle (✉) · B. Ram Rathan Lal
KITS, Ramtek, India

B. Laishram and A. Tawalare (eds.), *Recent Advancements in Civil Engineering*, Lecture Notes in Civil Engineering 172,
https://doi.org/10.1007/978-981-16-4396-5_16

1 Introduction

Controlled low-strength material (CLSM) is one of the self-levelling and self-compacting cementitious materials for backfill used in place of compacted conventional fill [1]. CLSM is also called as flowable fill, self-compacted backfill material, soil cement, slurry, flowable mortar, etc. [2, 3]. The application of CLSM has a broad range such as structural fill conduit bedding, pavement base, trench backfilling, conduit bedding and void filling [4]. Generally, the cost of CLSM is more than conventional granular backfill or compacted soil, but CLSM has many advantages including less equipment requirement (flowable) and less on-site labour and speedy construction, the ability for use in the tight or confined access area. Generally, CLSM has sufficient strength and acts as a substantial structural fill and backfill material. Harden time depends on water content used in CLSM mixture; usually, CLSM mixture contains more water and requires more time to harden (in some cases 8–24 h). Ramme et al. [5] recommended that scratching can be minimising that the use of more volumes of fine grade material in CLSM. Gypsum dry wall and pond ash are fine material use in the proposed CLSM. Gypsum contains high contents of $CaSO_4$, which is used as a binder [6]. Gypsum dry wall board is used in many innovative and architectural construction activities. Dry wall resulting due to new or demolish old building are dumped nearby roadside and then landfilling. Reference [7] is reported that these dry walls release harmful H2S gas into the atmosphere. The problem of disposal of these dry walls become serious for the upcoming future. Therefore, this study overall focused on the use of gypsum dry wall in CLSM. Waste generated from the thermal power plant is fly ash, bottom ash and pond ash. The bottom ash is mixed with fly ash, and this slurry is disposed in pond dykes near thermal power plant. This huge pond ash creates posing threat to the area near the power plant. Wet disposal method is the best method and mostly used in industries. Pond dykes required more land to store huge pond. In India where the ratio of land to population is small, this disposal of pond ash is not easy and suitable need for some other disposal methods. This is the need of present study.

Many studies were carried out on CLSM in many countries like Canada, United State of America, Australia, Japan, Korea and very few researches were done in Asian countries such as India. Industrial waste and local waste are mostly used in the construction of CLSM signifying from most studies. Studies show that local waste and the industrial by-product are used in CLSM, which is an effective way to solve the disposal problem of waste. Powdered gypsum, quarry dust, rise husk, pond ash, fly ash, blast furnane slag, bagasse ash are mostly utilised in CLSM in India. For example, Siddique studied spent foundry sand and industrial by-product in CLSM [8, 9], Chittoori utilised native high plasticity clay in construction of CLSM [10], Raghavendra used bagasse ash and also gypsum wall board and blast furnane slag in CLSM [11–14]. Ram Rathan Lal and Marjive examined the behaviour of EPS beats and stone dust in the CLSM [15].

The objective of this paper is to develop sustainable CLSM by using Industrial by-product, which can solve the problem of disposal of such industrial by-product like pond ash and use demolish gypsum dry wall, which can solve the disposal of demolishing structure by environment-friendly manner. In conventional CLSM, natural resources like sand are used, which create the scarcity of sand in the proposed CLSM; no natural resources are used, which is environment-friendly CLSM.

2 Material and Methods

Pond ash was obtained from an NTPC power plant, Mouda, Nagpur. Table 1 shows the properties of pond ash. Gypsum dry wall is collected from local demolish building. Ordinary Portland cement of grade 53 was used in the present work. CLSM required more water to become flowable, so good quality simple tap water was used.

3 Mix Proportions

The ACI Committee 229 was framed up in 1985 to establish a report that includes applications, handling, performance, proportioning and placement of CLSM mixture for different applications. As there is no other than this code available for CLSM since 1999, it is used in the present paper. Generally, for establishing the mix design of CLSM, trial and error or past experience was used. In the present paper, mix ratio is defined as ratio of the weight of gypsum dry wall to the weight of pond ash. The mix proportion of various CLSM mixture is shown in Table 2.

3.1 Compressive Strength

The compressive strength of CLSM is a very important property, and it is correlated to mix the component of material as mainly CLSM is used as structural fill or backfill. In the present study, a cylinder of size 75 mm × 150 mm was used for testing compressive strength as per ASTM D4832 and ACI229R. The material is flowable so cylindrical mould was covered by plastic and no vibration and rodding

Table 1 Physical property of pond ash

Properties	Pond ash
Specific gravity (G)	2.0
Optimum moisture content (OMC)	16%
Maximum dry unit weight ($\Upsilon_{d\ max}$)	1.3 g/cc

Table 2 Mix proportion of different CLSM mixtures

Sr. No.	GW/PA	C/PA	V_w/V
1	0	0.2	45
2	0.1	0.2	45
3	0.15	0.2	45
4	0.25	0.2	45
5	0	0.1	45
6	0.1	0.1	45
7	0.15	0.1	45
8	0.25	0.1	45

required. For each mix total, 12 cylinders were casted for compressive strength test. The curing was done for 7, 14 and 28 days. The water content was maintained at 0.45 for all concrete mixtures. The moisture pond ash was kept in the oven for 30 min. The mixture cement by pond ash 0.2 and gypsum dry wall to pond ash ratio consider 0, 0.1, 0.15, and 0.25. The proportions of the CLSM mixtures employed are shown in Table 2.

Figure 1 shows the relationship between mix ratio and compressive strength for a various curing period of C/PA = 0.2. The specimen was tested for 7 days, 14 days, and 28 days. The result indicates that the pond ash and gypsum dry wall used in CLSM mix affect the compressive strength from graph. It can be noticed that the strength the of CLSM mix increases as curing period increases. The same graph was observed for all mixes. For 0 to 10% replacement of gypsum dry wall in CLSM, the compressive strength increases, and when gypsum dry wall content in CLSM increases more than 10 to 25%, the compressive strength was observed to decrease and the maximum compressive strength of 9.9 MPa was observed for mix ratio of 0.1 (Gw/PA).

Figure 2 shows the relationship between mix ratio and compressive strength for a various curing period of C/PA = 0.1. The specimen was tested for 7 days, 14 days, and 28 days. The result specifies that compressive strength observed is

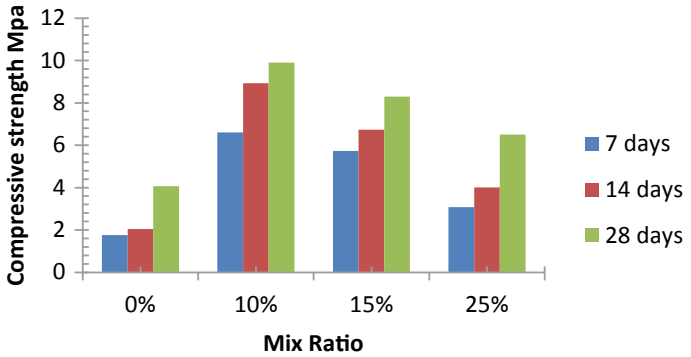

Fig. 1 Compressive strength C/PA = 0.2

less as compared to C/PA = 0.2. It was due to less content of cement. The graph shows that CLSM strength increases as curing period increases. As the percentage of gypsum drywall increases, compressive strength increases up to mix ratio 0.1 (GW/PA) and then it gradually decreases, and for C/Pa = 0.1 the maximum compressive strength of 6.9 MPa was observed for a mix ratio of 0.1 (Gw/PA).

3.2 *Flowability*

According to ASTM D610, the test of flowability was conducted by using an open-ended cylinder 75 mm × 150 mm. Figure 4 shows that when mix ratio increases the flowability decreases for both cases, i.e. for C/Pa = 0.1 and C/PA = 0.2. From Fig. 4, it was observed that when the gypsum dry wall content increases from 0, 10, 15 and 25%, the flowability decreases. Gypsum that adds in CLSM flowability was drastically reduced; it is possible because of the substantial increase in the gypsum content at normal room temperature when gypsum is mixed with the water fast to react chemically to bring dihydrate form ($CaSO_4$, $1/2H_20 + 1/2H_20 = CaSO_4.2H_20$). High-gypsum CLSM required more water to become flowable fill (Fig. 3).

3.3 *Density*

Dry density was measured after attending 7-, 14- and 28-day curing at the time of testing. Density was calculated by taking an average of densities of three cylinder. First weight of cylinder was calculated accurately as well as volume of cylinder was determined, and densities of the mixtures were calculated in kg/m^3. Figure 5 shows that the density of CLSM mix decreases as increasing mix ratio.

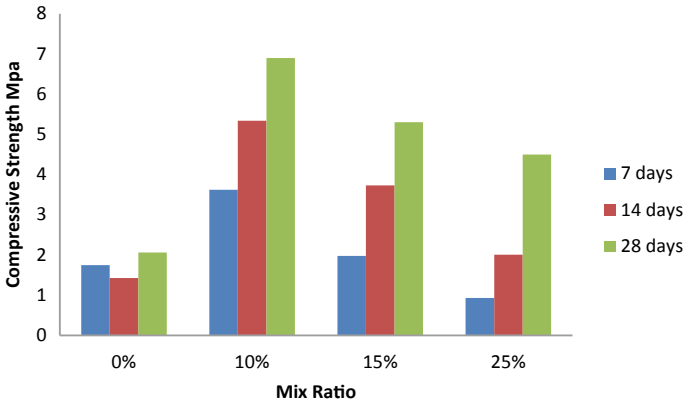

Fig. 2 Compressive strength C/PA = 0.1

Fig. 3 Flowability

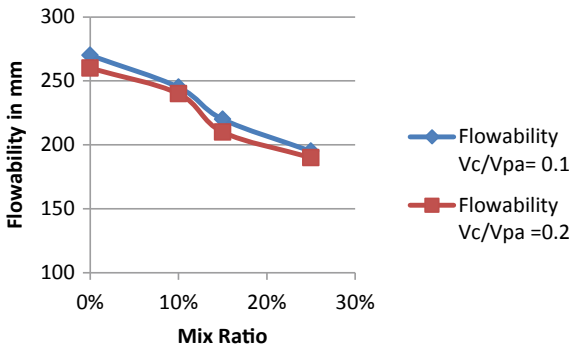

Fig. 4 Flowability for various mixes

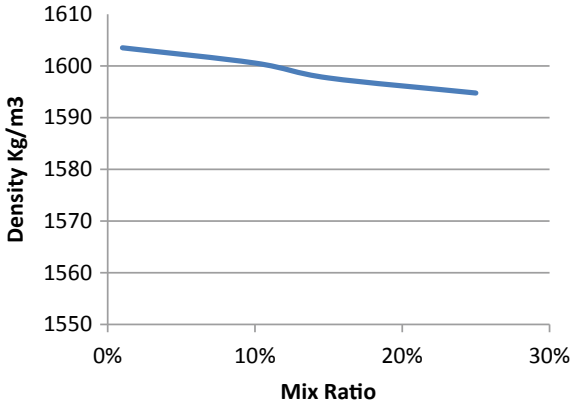

Fig. 5 Density of material

3.4 Initial Setting Time

The initial and the final setting times of the mixtures were determined according to ASTM. Initial setting time for all CLSM mix ranges from 24 to 30 h.

4 Conclusions

Present studies show properties of newly developed CLSM. Based on the experimental study, the following conclusions are drawn as follows:

1. When gypsum added in CLSM mixture, it improves the stability (bleeding) of the mixture and therefore gypsum is efficiently used in CLSM.
2. For 0 to 10% replacement of gypsum dry wall in CLSM, the compressive strength increases, and when gypsum dry wall content in CLSM increases more than 10 to 25%, the compressive strength is observed to decrease.
3. For all mix ratios, the maximum compressive strength of 9.9 MPa was observed for mix ratio of 0.1 (Gw/PA).
4. As an increase in the percentage of gypsum drywall, there is a gradual decrease in flowability.
5. Pond ash and gypsum drywall have the potential to use in CLSM to solve the disposal problem for an eco-friendly environment.

References

1. ACI 229R-94 (2005) Controlled low-strength materials. CLSM recommendations by ACI Committee 229, pp 1–15
2. Hitch JL (1998) Test methods for controlled low-strength material CLSM past present and future. In: Howard Hitch AK (ed) The design and application of controlled low-strength materials. ASTM STP 1331, American Society for Testing and Materials, pp 3–10
3. Tikalsky P, Gaffney M, Regan R (2000) Properties of controlled low strength material containing foundry sand. ACI Mater J 97(6):698–702
4. ASTM D6103-04 (2004) Test method for flow consistency of controlled low strength material. ASTM Int 4:1–3
5. Ramme BW, Naik TR, Kolbec HJ (1995) Construction experience with CLSM fly ash slurry for underground facilities. In: Fly ash slag silica fume and other natural pozzolans-proceedings fifth international conference. American Concrete Institute, Farmington Hill Mich, pp 403–441
6. Singh M, Garg M (1999) Cementitious binder from flyash and other industrial wastes. Cem Concr Res 29(3):309–314
7. Blanco A, Pujadas P, Cavalaro S, Aguado A (2014) Methodology for the design of controlled low strength material application to the backfill of narrow trenches. Constr Build Mater 23–30
8. Siddique R (2009) Utilization of waste materials and by-products in producing controlled low-strength materials. Resour Conserv Recy 54:1–8

9. Siddique R, Noumowe A (2016) Utilization of spent foundry sand in controlled low strength materials and concrete. Resour Conserv Recy 53:27–35
10. Chittoori B, Puppal AJ, Raavi A (2014) Strength and stiffness characterization of controlled low-strength material using native high-plasticity clay. Mater Civil Eng 6
11. Raghavendra T, Sunil M, Udayashankar BC (2016) Controlled low-strength materials using bagasse ash and fly ash. ACI Mater J 113(4):447–457
12. Raghavendra T, Udayashankar BC (2014) Flow and strength characteristics of CLSM using ground granulated blast furnace slag. J Mater Civ Eng 26:9
13. Raghavendra T, Siddanagouda Y, Jawad F, Adarsha C, Udayashankar BC (2016) Performance of ternary binder blend containing cement, waste gypsum wall boards and blast furnace slag in CLSM. In: International conference on sustainable design, engineering and construction, Procedia Eng, pp 104–111
14. Raghavendra T, Udayashankar BC (2015) Engineering properties of controlled low strength materials using flyash and waste gypsum wall boards. Constr Build Mater 101:548–557
15. Marjive V, Badwaik V, Ram Rathan Lal B (2016) Experimental studies on controlled low strength material using stone dust and EPS beads. Int J Eng Technol 8:265–268

Experimental Investigations on Stabilized Mud Blocks Enriched with Steel Slag for Sustainable Construction

Vibha N. Dalawai, Lakshmi Srikanth, and Ishwarya Srikanth

Abstract Stabilized mud block (SMB) is one of the most plausible options to bring down the greenhouse gas emission in the construction industry. With well-defined stabilization techniques, the mud block can attain the same strength as that of burnt brick blocks as specified in Bureau of Indian Standards (BIS). This research study presents the experimental investigations on adobe blocks made from selected locally available soil having 54% sand, 14% silt, and 32% clay, stabilized with cement and fly ash along with lime, to obtain an alternate material to burnt bricks that can attain a minimum 28-day compressive strength minimum of 3.5 MPa as per BIS. In the present study, steel slag has been incorporated in place of river sand, to minimize the clay content, thus conserving natural resources. Size of the adobe block selected for the study is 100 mm × 150 mm × 250 mm. The compressive strength of the block is tested for 7, 14, and 28 days by maintaining the soil content at 70%, steel slag at 20% and varying the percentage of cement from 10 to 4% by partially replacing with fly ash. From the experimental findings, it is confirmed that 28-day compressive strength of block having 10% cement is 3.97 MPa, and on replacement of 2% of cement with fly ash as stabilizer, the compressive strength increased to 4.58 MPa. This study also demonstrates the effective utilization of steel slag in soil with low sand content. This study concludes that adobe block containing 70% soil, 20% steel slag, along with 2% fly ash and 8% cement as stabilizers, achieves the maximum compressive strength. The embodied energy consumed during the manufacturing of materials that are used in making adobe blocks is 55% lesser than that of burnt brick. In addition, the cost per block is around 50% lesser when compared to burnt brick.

V. N. Dalawai (✉) · L. Srikanth
CMR Institute of Technology (VTU), Bengaluru, India
e-mail: vibha.d@cmrit.ac.in

L. Srikanth
e-mail: lakshmi.s@cmrit.ac.in

I. Srikanth
Florida Atlantic University, Boca Raton, USA
e-mail: isrikanth2016@fau.edu

B. Laishram and A. Tawalare (eds.), *Recent Advancements in Civil Engineering*, Lecture Notes in Civil Engineering 172,
https://doi.org/10.1007/978-981-16-4396-5_17

Keywords Adobe mud block · Compressive strength · Steel slag · Fly ash · Embodied energy · Manufacturing cost

1 Introduction

The growing demand for materials in the construction industry has led to exploitation of natural resources, resulting in steep hike in the prices of construction materials [1]. Sustainability in building construction includes both conservation of natural resources and reduction in the generation of carbon footprint. Hence, there is a need to produce sustainable materials with low energy consumption and minimal environmental impact during both manufacturing and operational stages [2]. Many researchers have proposed alterative building materials to concrete block such as stabilized mud block and compressed earth block that are environment friendly and economically viable with adequate compressive strength [3, 4]. Several studies have revealed that production of unfired bricks, also commonly known as stabilized mud blocks, consumes less energy and releases 80% less carbon-di-oxide into the atmosphere. Hence, they are the viable and reliable alternatives to conventional fired bricks [5, 6]. Reddy et al. [7] studied the assorted characteristics of soil cement blocks containing highly sandy soil by altering cement content. When the cement content was increased from 6 to 8%, it was observed that the compressive strength and modulus of elasticity of the block were raised to 2.5 times.

Kabiraj et al. [8] arrived at an appropriate mix proportion by combining locally available building materials such as soil, sand, clay, grits, and jute for making cost-effective, environment friendly compacted earth blocks. They concluded that blocks having 7.5% cement content satisfied strength and water absorption criteria and were cheaper than the burnt clay bricks by 36.66%. James et al. [9] studied the performance of adobe type of stabilized mud blocks by replacing ordinary Portland cement (OPC) with sugarcane bagasse ash (SBA) as stabilizer. Their study revealed that utilization of 4% cement with 8% SBA in soil blocks met the compressive strength and water absorption requirements as per BIS specifications. Malkanthi et al. [10] performed a study on compressed stabilized earthen blocks to investigate the usefulness of lime and lime–cement combination as stabilizers with low content of clay and silt. Currently, there exist only limited published literature on the use of steel slag as a complete replacement for sand in making adobe block. In this study, steel slag has been incorporated in place of river sand, thus conserving natural resources. The objectives of the present study are:

- To determine the required optimum percentage of stabilizers for adobe blocks to achieve a compressive strength that meets BIS norms.
- To carry out X-ray diffraction analysis in order to match the properties of fly ash to cement and steel slag to sand.

- To minimize the usage of the sand and utilize industrial waste to maintain the required compressive strength of the adobe bock, for sustainable building infrastructure.
- To compute embodied energy of each unit to demonstrate that the use of industrial waste can bring down the amount of energy during production of blocks.
- To carry out cost analysis to demonstrate that utilization of industrial waste can bring down the manufacturing cost of adobe blocks significantly.

2 Material Properties and Methodology

2.1 Material Properties

In the present study, ordinary Portland cement (OPC) of grade 53, class C fly ash, steel slag, lime were used with soil to make mud blocks. The chemical composition of fly ash and cement is listed in Table 1. Fly ash contains nearly about 15–25% cementitious material and more than 20% lime. Cement and fly ash were tested for different physical and chemical properties to ascertain their basic properties conforming to Bureau of Indian Standards (BIS) [11]. In the present study, soil was collected from Doddaballapur Taluk, Bangalore Rural District, Karnataka. The results from the gradation of soil revealed that clay content present in the soil was more than required. Steel slag was added to soil as sand replacement to bring down the effect of clay.

2.1.1 Characteristics of Cement and Fly Ash

Walker [3] suggested that SMB should have a minimum cement content of 5 to 10% to attain a characteristic compressive strength of 1–2 MPa when plasticity index is 15–20. It is important to derive the chemical composition of cement and fly ash as they are made of complex and heterogeneous minerals. X-ray powder diffraction (XRD) analysis was used to study their chemical composition. Figures 1 and 2 illustrate the results obtained from XRD test. The chemical composition of

Table 1 Experimental results on chemical properties of cement and fly ash

Properties	Chemical composition in %						Fineness of cement (%)	Normal consistency (% at 7 mm penetration)	Specific gravity
	SiO_2	Al_2O_3	Fe_2O_3	CaO	MgO	SO_3			
Cement	27.9	1.6	4.2	66.4	5.4	0.2	10	28	3.15
Fly ash	53.6	13	2.5	13.4	10	7.4	8.2	34	2.6

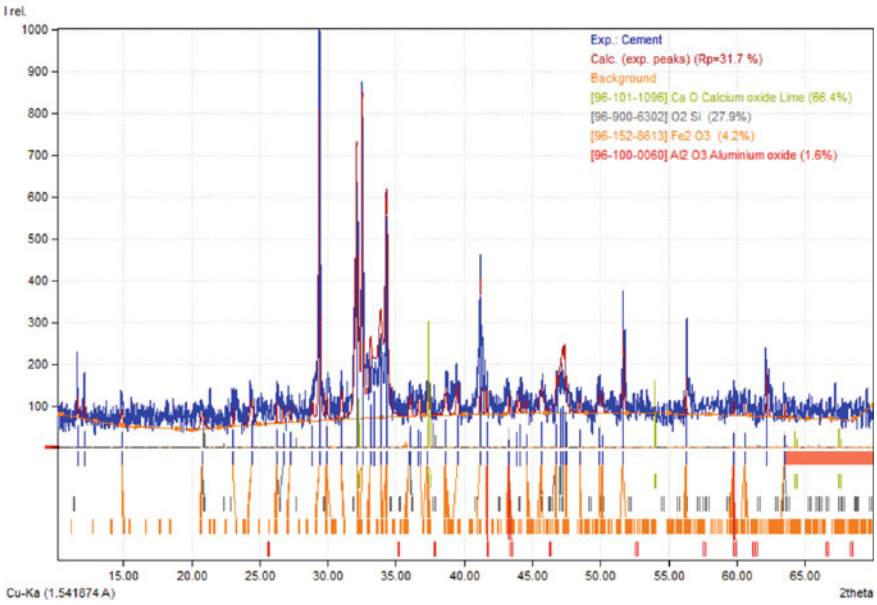

Fig. 1 XRD analysis of cement

Fig. 2 XRD analysis of fly ash

Table 2 Characteristics of soil

Characteristics	Specific gravity	Water content (%)	Liquid limit (%)	Plastic limit (%)	Shrinkage limit (%)	Maximum dry density (gm/cc)	Optimum moisture content (%)
Result	2.6	2.45	31.62	14.28	7.41	2.1	15

cement and fly ash is listed in Table 1 and it is well in agreement with the experimental analysis conducted by Zhuang et al. [12], conforming to American Society for Testing and Materials (ASTM C-168) standards. The percentage of CaO, which imparts strength to concrete, is more in cement compared to fly ash. This deficiency is compensated by the dominant presence of SiO_2 in fly ash-based concrete. Cement and fly ash are also studied for their physical properties in accordance with BIS norms [13, 14] and the test [15] results are shown in Table 1.

2.1.2 Soil Characteristics

The preliminary studies on soil are performed in accordance with BIS [16–18] norms and listed in Table 2. It is observed that the plasticity index of soil (i.e., liquid limit–plastic limit) is 17.34, which is well in agreement with Walker [3].

2.1.3 Characteristics of Steel Slag and River Sand

Basic oxygen furnace (BOF) slag, commonly known as steel slag, is a waste material from steel industry. Steel slag in the granulated form was procured from Jindal Southwest (JSW) Steel Limited in Bellary, Karnataka. The chemical properties of steel slag used in the study were obtained by XRD analysis as explained in the previous subsection. Figures 3 and 4 show the graphical pattern of the chemical composition of river sand and steel slag. The physical properties of steel slag and the results from XRD analysis are shown in Table 3. The sieve analysis is carried out to obtain the grain size distribution and to investigate the possibility of introducing steel slag as river sand replacement. Figure 5 illustrates the comparison of the grain size distribution of river sand, steel slag, and soil.

2.2 Methodology

2.2.1 Mix Design of Adobe Blocks

Tests are conducted on trial and error basis to arrive at an appropriate percentage of stabilizer and mix design of SMB. To achieve the required compressive strength of

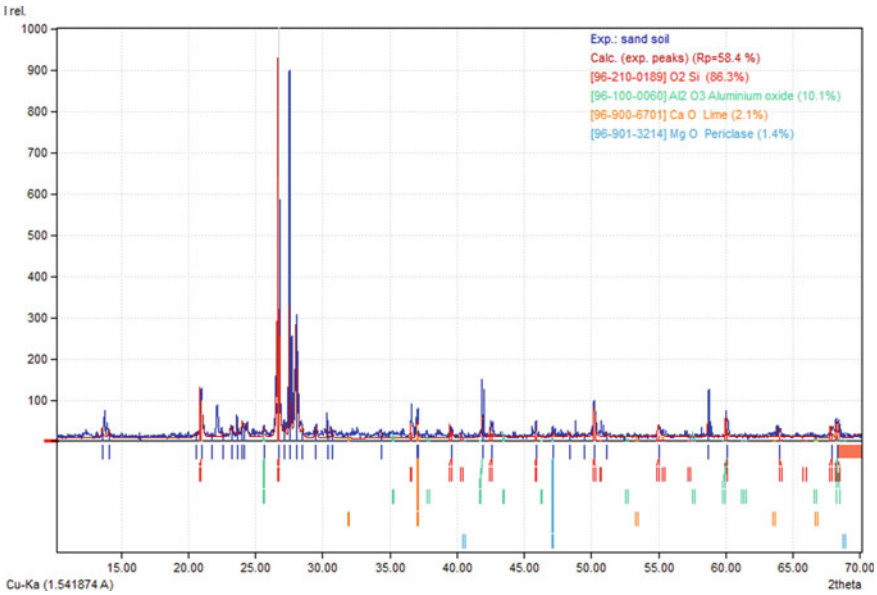

Fig. 3 XRD analysis of steel slag

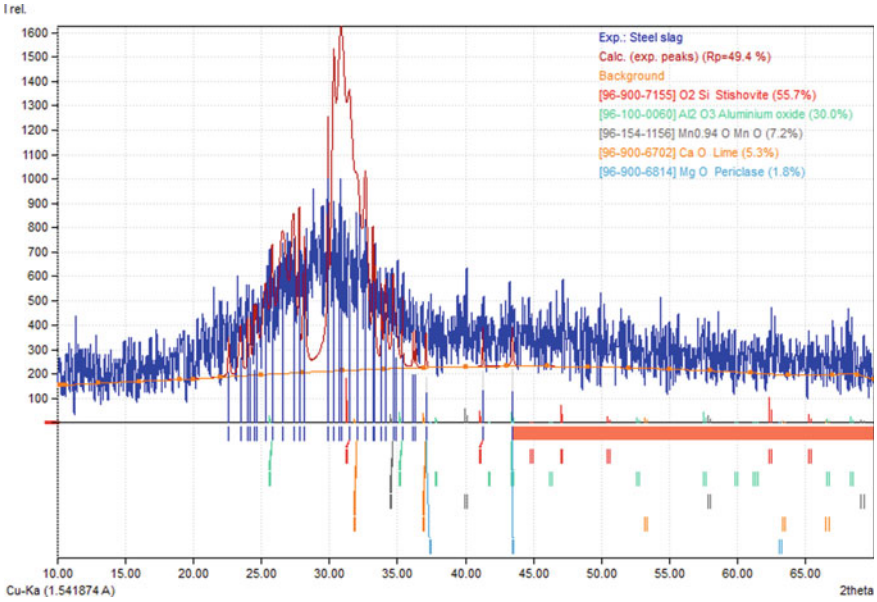

Fig. 4 XRD analysis of river sand

Table 3 Experimental results on chemical and physical properties of steel slag and river sand

	Chemical composition in %							
	SiO	Al_2O_3	CaO	MgO	MnO	Specific gravity	Density (gm/cc)	Water absorption (%)
Steel slag	55.7	14.0	5.3	1.8	7.2	2.45	1.28	4.34
River sand	85.7	10.1	2.1	1.4	0.8	2.70	1.42	0.2

Fig. 5 Molding and casting of adobe blocks

3.5 MPa in accordance with BIS specifications, the proportion adopted is 90% soil, 8% cement, and 2% fly ash (viz., 10% stabilizer). A water content of 18% is chosen based on the investigation carried out by James et al. [9].

2.2.2 Proportioning

The soil consists of 54% sand, 14% silt, and 32% clay. Jagadish [19] recommended that the range of sand and clay content in any soil should be of 65–75% and 5–15%, respectively, with stabilizing agent of up to 6%. Hence, to bring down the clay content in the present soil sample, it is proposed to add 20% of steel slag in lieu of river sand. This study investigates five different mix proportions and in the fifth proportion, 2% of lime is introduced to investigate its effect on the compressive strength. Table 4 illustrates the different proportions of materials considered in this study.

Table 4 Proportions of the materials per block

Proportion	Soil		Steel slag		Fly ash		Cement		Lime	
	(kg)	%	(kg)	%	(kg)	%	(kg)	%	(kg)	%
1	2.62	70	0.75	20	Nil	Nil	0.375	10	Nil	
2	2.62	70	0.75	20	0.075	2%	0.3	8	Nil	Nil
3	2.62	70	0.75	20	0.15	4%	0.225	6	Nil	Nil
4	2.62	70	0.75	20	0.225	6%	0.15	4	Nil	Nil
5	2.62	70	0.75	20	0.15	4%	0.15	4	0.075	2%

2.2.3 Casting and Curing

Adobe method is adopted to prepare blocks as per BIS norms [20], with wooden molds of size 100 mm × 150 mm × 250 mm. The mixture is compacted well by making smooth balls and dropping them from a height of 0.5 m. Special attention is paid to the corners and edges to avoid honeycombing. Blocks are first cured by sprinkling water by hand twice a day for initial 3 days. Then, wet curing is employed by placing dampened gunny bags over the mud blocks for a period of 3 weeks. Figure 5 shows the casting process.

2.2.4 Experimental Investigation

The compressive strength of the stabilized mud blocks was determined in accordance with BIS criterion [21]. The compressive strength depends on the soil type and amount of stabilizer used and the maximum strength is arrived by altering the proportions of stabilizer. Heath et al. [5] stated that the durability of the stabilized blocks increases with increase in its strength.

3 Results

3.1 Compression Test

Compression tests on the adobe blocks are performed as per the procedure prescribed in BIS [21] which stipulates that the minimum compressive strength of burnt brick should not be less than of average compressive strength as given in Indian Standard Common Burnt Clay Building Bricks—Specification IS 1077 (1992). Three specimens of each proportion are tested for compressive strengths at 7, 14, and 28 days of curing. Table 5 summarizes the average compressive strength of three specimens in each proportion.

Table 5 Compression strength of blocks of different proportions

Proportion	Compressive strength (MPa) in day		
	7 days	14 days	28 days
1st proportion	2.13	2.40	3.97
2nd proportion	2.27	3.07	4.58
3rd proportion	2.23	2.53	4.2
4th proportion	1.47	2.07	3.11
5th proportion	1.95	2.37	3.31

3.2 *Embodied Energy*

The embodied energy is defined as the sum total of energy necessary for the entire product lifecycle. In the context of building materials, this includes the energy consumed in manufacturing, transportation, and delivery/assemblage of building materials at the site. In the present study, embodied energy consumed during the manufacturing of materials used in making adobe blocks is computed. The energy consumption of each block is calculated by considering the energy per kg of each material (refer with Table 6). These energy values are obtained from India Construction (IFC) Materials Database Methodology Report [22] and a study done on embodied energy carried out by Reddy et al. [23]. The calculations indicate a 50% reduction in the energy consumption during the manufacturing of adobe block in comparison with burnt bricks. Table 6 shows the cost analysis performed on adobe blocks of different proportions. Production of adobe blocks is 50% cheaper than burnt bricks, considering at the current market rate of Rs. 5.5/piece of burnt brick.

From Table 5, it is observed that the strength of adobe block varies with different proportions of stabilizing agent. There is a gain in the compressive strength as the number of day of curing increases. It is also observed that when 2% of fly ash is added with 8% of cement, there is an increase in compressive strength in 7, 14, and 28 days. However, there is a reduction in strength when the fly ash percentage shoots above 2%. A maximum compressive strength of 4.58 MPa in 28 days is achieved at 2% fly ash and 8% cement as stabilizer. By adding 2% lime in the last trial, it is found that there is an increase in 28-day compressive strength when compared to the third and fourth proportions (refer with Fig. 6). Figure 6 also shows the variation in the cost and the manufacturing embodied energy of different building materials used in each proportion. As the proportion of cement is replaced by fly ash, the embodied energy drops to an extent of more than 50% when compared with burnt brick. This value is also well within the range of manufacturing embodied energy of materials used in soil cement blocks [23]. The cost of burnt brick in the market is 5.5 Rs./piece whereas the cost of adobe block ranges between 2 and 2.5 Rs./piece without compromising on the compressive strength.

4 Conclusions and Recommendations for the Future Work

This study presents experimental investigation on adobe blocks made from selected locally available soil having 54% sand, 14% silt, and 32% clay, stabilized with cement and fly ash along with lime, to obtain an alternate material to burnt bricks that can attain a minimum 28-day compressive strength of 3.5 MPa as per BIS. In this study, steel slag has been incorporated in place of river sand, thus conserving natural resources.

Table 6 Embodied energy in manufacturing the materials per block and cost per block of different proportions

Proportion	Evaluation criteria	Cement (kg/block)	BF slag (kg/block)	Lime (kg/block)	Fly ash (kg/block)	Soil (kg/block)	Total
1st proportion	Weight (kg/block)	0.37	0.75	0	0	2.62	3.74 (kg/block)
	Embodied energy (MJ)	2.4	0.48	0	0	0	2.88 (MJ/block)
	Cost (Rs.)	2.1	0.34	0	0	0	2.44 (Rs./block)
2nd proportion	Weight (kg/block)	0.3	0.75	0	0.07	2.62	3.74 (kg/block)
	Embodied energy (MJ)	1.26	0.34	0	0.14	0	1.74 (MJ/block)
	Cost (Rs.)	1.92	0.48	0	0	0	2.40 (Rs./block)
3rd proportion	Weight (kg/block)	0.22	0.75	0	0.15	2.62	3.74 (kg/block)
	Embodied energy (MJ)	1.26	0.34	0	0.29	0	1.89 (MJ/block)
	Cost (Rs.)	1.44	0.48	0	0	0	1.92 (Rs./block)
4th proportion	Weight (kg/block)	0.15	0.75	0	0.22	2.62	3.74 (kg/block)
	Embodied energy (MJ)	0.84	0.34	0	0.42	0	1.60 (MJ/block)
	Cost (Rs.)	0.96	0.48	0	0	0	1.44 (Rs./block)
5th proportion	Weight (kg/block)	0.15	0.75	0.07	0.15	2.62	3.74 (kg/block)
	Embodied energy (MJ)	0.84	0.34	1.28	0.29	0	2.75 (MJ/block)
	Cost (Rs.)	0.96	0.48	0.34	0	0	1.78 (Rs./block)

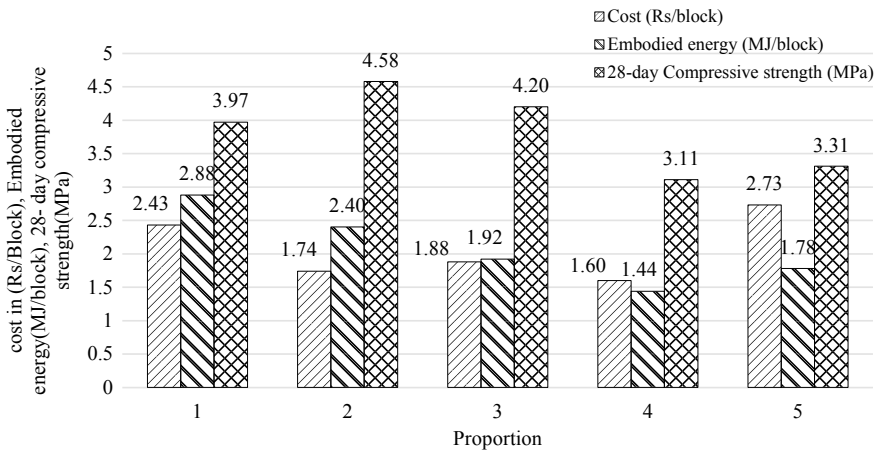

Fig. 6 Graphical representation of cost per block, embodied energy per block, and average compressive strength at 28 days

- The compressive strength of the block is tested for 7, 14, and 28 days by maintaining the soil content at 70%, steel slag at 20%, and varying the percentage of cement from 10 to 4% by partially replacing with fly ash.
- A 28-day compressive strength of 3.97 MPa is achieved with 10% cement in the adobe block, which is more than the minimum strength requirement (3.5 MPa) as per BIS specifications.
- Replacement of 2% of cement with fly ash as stabilizer to the selected soil is effective in increasing the 28-day compressive strength to 4.58 MPa.
- With increase in fly ash content as replacement to cement, the compressive strength of adobe block decreased.
- It is noted that the compressive strength of the block with 4% fly ash, 4% cement, and 2% lime is higher than that of 4% of fly ash, 6% of cement. This increase could be attributed to the calcium content present in lime.
- It is concluded that the mix proportion 2 which comprises of 70% soil, 20% steel slag, along with 2% fly ash and 8% cement as stabilizers gives the maximum compressive strength, resulting in 55% less embodied energy when compared to the burnt brick and this value is well within the range of soil cement blocks.
- Since adobe blocks cost only 50% of that of brick blocks, they are economical and can provide considerable cost savings when employed in building construction without compromising on the strength of the masonry.
- Further research can be carried out on the adobe blocks with varying proportions of lime content and steel slag for the selected soil type. The scope could also be extended by introducing different types of industrial waste to the SMB. Determination of compressive strength and durability of interlocking mud masonry system can be another extension to the present study. Furthermore, different types of joint system and interlocking system can also be explored.

References

1. Kariyawasam KKGKD, Jayasinghe C (2016) Cement stabilized rammed earth as a sustainable construction material. Constr Build Mater 105:519–527
2. Arooz FR, Halwatura RU (2018) Mud-concrete block (MCB): mix design & durability characteristics. Case Stud Constr Mater 8:39–50
3. Walker PJ (1995) Strength, durability and shrinkage characteristics of cement stabilised soil blocks. Cem Concr Compos 17(4):301–310
4. Venkatarama Reddy BV, Gupta A (2006) Tensile bond strength of soil-cement block masonry couplets using cement-soil mortars. J Mater Civil Eng 18(1):36–45
5. Heath A, Walker P, Fourie C, Lawrence M (2009) Compressive strength of extruded unfired clay masonry units. Proc Inst Civil Eng Constr Mater 162(3):105–112
6. Oti JE, Kinuthia JM, Bai J (2009) Engineering properties of unfired clay masonry bricks. Eng Geol 107(3–4):130–139
7. Reddy BV, Gupta A (2005) Characteristics of soil-cement blocks using highly sandy soils. Mater Struct 38(6):651–658
8. Kabiraj K, Mandal UK (2012) Experimental investigation and feasibility study on stabilized compacted earth block using local resources. Int J Civil Struct Eng 2(3):838–850
9. James J, Pandian PK, Deepika K, Manikanda Venkatesh J, Manikandan V, Manikumaran P (2016) Cement stabilized soil blocks admixed with sugarcane bagasse ash. J Eng (Article ID 7940239) 1–9
10. Malkanthi SN, Balthazaar N, Perera AADAJ (2020) Lime stabilization for compressed stabilized earth blocks with reduced clay and silt. Case Stud Constr Mater 12:e00326
11. BIS 40312 (1999) Methods of physical tests for hydraulic cement
12. BIS 3812 (2003) Specification for fly ash for use as pozzolana and admixture
13. BIS 12269 (1987) Specifications for 53 grade ordinary Portland cement
14. Zhuang XY, Chen L, Komarneni S, Zhou CH, Tong DS, Yang HM, Yu WH, Wang H (2016) Fly ash-based geopolymer: clean production, properties and applications. J Cleaner Prod 125:253–267
15. BIS 4031 (1988) Method of physical tests for hydraulic cement. Bureau of Indian Standards
16. BIS 2720 (1983) Methods of test for soils: part 1-preparation of dry soil sample for various tests. Bureau of Indian Standards, New Delhi, India, pp 1–10
17. BIS: 2720 (1985) Part 4, methods of test for soils–grain size analysis
18. BIS 2720 (1985) Methods of test for soils: part 5 determination of liquid and plastic limit. Bureau of Indian Standards, New Delhi, India, pp 1–16
19. Jagadish KS (2008) Alternative building materials technology. New Age International
20. BIS 5454 (1978) Methods for sampling of clay building bricks. Bureau of Indian Standards, New Delhi
21. BIS 3495 (1976) Part 1 to 4, methods of tests of burnt clay building bricks, New Delhi
22. IFC India Construction Materials Database Methodology Report 2017
23. Reddy BV, Jagadish KS (2003) Embodied energy of common and alternative building materials and technologies. Energy Build 35(2):129–137

Sustainable Construction Using Steel FRP Composites

Snehal Abhyankar

Abstract Sustainable construction using composites is used all over the world in respect of its strength, durability, high mouldability, stability and relative low cost. Repair, rehabilitation and retrofitting projects involve use of fibres in concrete. A combination of steel and polypropylene fibres is termed as steel–polypropylene fibre-reinforced concrete (SPFRC). The composites consist of steel fibre that provides the structural improvement, whereas polypropylene fibre enhances the resistance to plastic shrinkage cracking. To enhance strengths, fibres are added in concrete. Sustainable solutions demand different ways to minimize the failure of the concrete structures.

Keywords Sustainable · Composites · SPFRC · Cracks · Flexural strength · Compressive strength

1 Introduction

The concrete roads are applied to axle load repetitions during its design period losing its serviceability due to rapid deterioration in the form of micro- and macro-cracks. Shrinkage in the concrete may also result in the formation of cracks. Concrete without any fibres may develop cracks due to plastic shrinkage, drying shrinkage and other reasons of changes in volume of concrete, and development of these micro-cracks causes elastic deformation of concrete. Deterioration of concrete structures due to steel corrosion is a matter of considerable concern since the repairing of these structures proved to be a costly process. The addition of fibres in the plain concrete will control the cracking due shrinkage, reduce the bleeding of water, meet the required values of flexural strength and enhance the strain capacity of the plain concrete [1]. In FRC (fibre-reinforced concrete) thousands of small fibres are dispersed and distributed randomly in the concrete during mixing and thus improve concrete properties in all directions (Krishna and Rao 2014). Chang

S. Abhyankar (✉)
Department of Civil Engineering, VNIT, Nagpur, India

B. Laishram and A. Tawalare (eds.), *Recent Advancements in Civil Engineering*, Lecture Notes in Civil Engineering 172,
https://doi.org/10.1007/978-981-16-4396-5_18

et al. (1995) studied the behaviour of fibres-reinforced concrete. When steel and polypropylene fibres are mixed in the concrete, it is known as steel–polypropylene fibre-reinforced concrete (SPFRC). Reinforcing the concrete structures with fibres such as polypropylene is one of the possible ways to provide all the criteria of the durable repair material.

The experimental investigation involves testing properties of constituents of SPFRC like aggregate, sand and cement [2]. The investigation for variation of percentage of fibres in SPFRC mixes was done. The amounts of fibres in the SPFRC mixes are varied from 0.5 to 1% of the total volume of concrete [3]. Both steel and polypropylene fibres vary in proportion. For these purposes, two types of steel fibres, namely crimped steel fibre and hooked end steel fibre, are used separately with polypropylene fibres. Steel fibres vary from 0.25 to 0.85%. Polypropylene fibres vary from 0.15 to 0.25% [4]. All the strength tests were carried out on the SPFRC samples. Now after comparing the test results, type of steel fibres to be preferred with optimum content of fibre mix is proposed [5].

2 Experimental Program

2.1 Experimental Program for SPFRC

Sample mixes are prepared by using IS 10262-2009. The combinations of varying percentage of steel and polypropylene fibres with various SPFRC mixes [6], i.e. SPFRC-A, SPFRC-B, SPFRC-C and SPFRC-D with hooked end fibre and crimped steel fibres, were prepared. Tests on cement, sand and aggregates were performed. Similarly, the properties of the aggregate are required to be evaluated [7]. In Fig. 1 schematic representation of usage of steel and polypropylene fibres is given.

2.2 Materials and Tests

Workability of SPFRC Mixes

Figure 2 represents the workability test results of SPFRC mixes. The results show initially slump is less after crimped and hooked fibres added in concrete [8]. Steel fibres considerably affect the workability behaviour [9]. As the steel fibre content increases, the workability decreases. In SPFRC-C mix when hooked end steel fibres were used, the reduction was about 44% [10].

On the one hand, when SPFRC-C comprises the hooked end steel fibres, the compressive strength at 7 days increased by 21.42% than the normal concrete, whereas for 28 days this value increased by 26% than normal concrete [11].

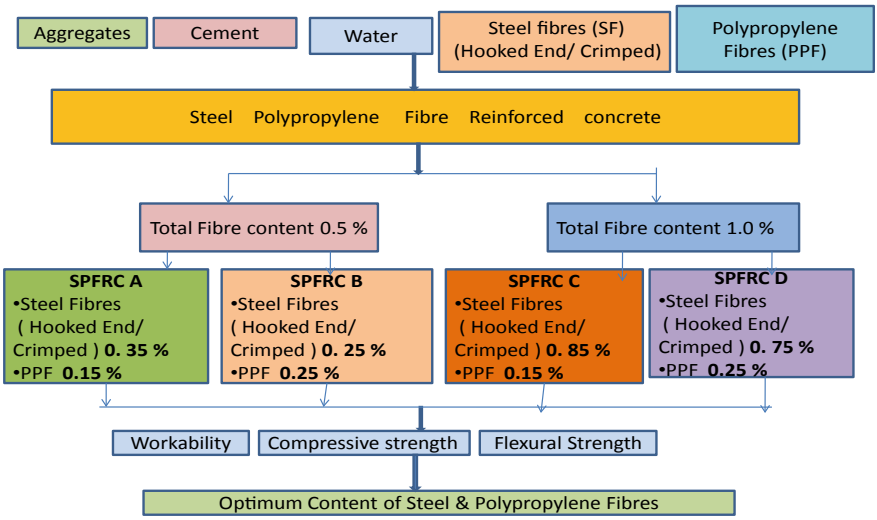

Fig. 1 Methodology for usage of steel and polypropylene fibres in concrete mixes

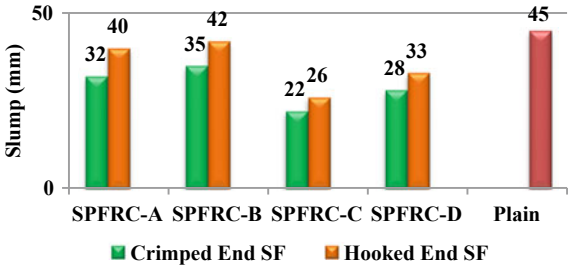

Fig. 2 The slump of SPFRC mixes

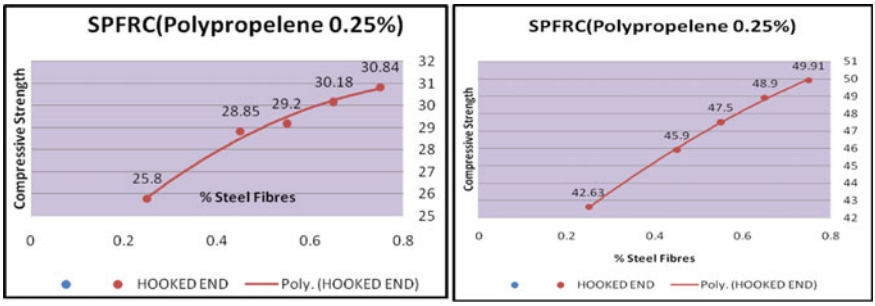

Fig. 3 7-day and 28-day compressive 0.25% hooked end steel fibres with % var. PP fibres

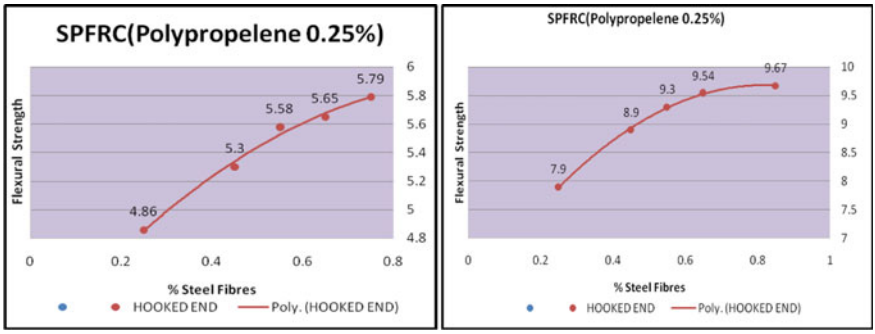

Fig. 4 7-day and 28-day flexural 0.25% hooked end steel fibres with % var. PP fibres

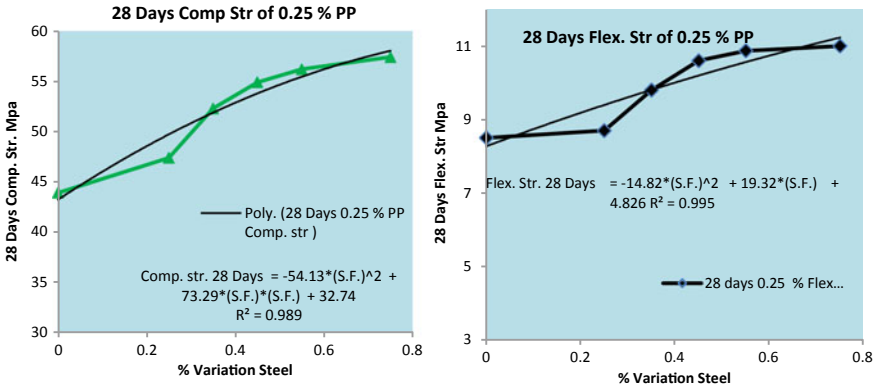

Fig. 5 28-day compressive and flexural strength 0.25% PP fibres with % var. hooked end steel fibres

Figure 3 represents variation of compressive strength of 0.25% hooked end steel and PP fibres.

On other hand, when SPFRC-C comprises the hooked end steel fibres, the flexure strength at 7 days increased by 21.42% than the normal concrete [12]. Figure 4 represents a variation of flexural strength of 0.25% hooked end steel fibres with PP fibres [13].

For 28 days this value increased by 92% than normal concrete. Figure 5 represents a variation of 28-day compressive and flexural strength.

Flexure strength is also considerably influenced by steel fibre and increases by increasing the quantity of steel fibre [14]. Table 1 represents correlation between 28-day compressive str and flexural str of 0.25% hooked end steel and PP fibres.

Table 2 represents formula for the prediction of flexural strength at 28 days for 0.25% hooked end steel fibres with varying PP fibres.

Table 1 Correlation between 28-day comp. str and flex. str. for 0.25% PP fibres with % var. hooked end steel fibres

Sr. No.	% PP fibres	Predicted comp. str. with fibres in MPa	Sqrt (f_{ck})	Predicted flex. str F_{flex} in MPa	F_{flex}/ sqrt (f_{ck})
1	0.25	47.68	6.9050	8.72	1.2634
2	0.35	51.76	7.1945	9.77	1.3575
3	0.45	54.76	7.3999	10.51	1.4207
4	0.55	56.68	7.5283	10.96	1.4562
5	0.75	57.26	7.5670	10.97	1.4502
					1.3896

Table 2 Formula for prediction of flexural strength

Formula for the prediction of flexural strength at 28 days for 0.25% PP fibres with varying steel %	
F_{flex} = −14.82 * (%sf) * (%sf) + 19.32 * (%sf) + 4.826	R^2 = 0.995
F_{flex} = 1.38968 * sqrt (Fc)	
Fc = −54.13 * (%sf) * (%sf) + 73.29 * (%sf) + 32.74	R^2 = 0.989

3 Conclusions

- Strength characteristics are also influenced by the type of fibres and their dosage. The experimental investigation revealed that hooked end steel fibres are more effective.
- It is possible to produce fibre concrete composites using polypropylene fibres in combination with steel fibres, and the performance of such concrete will be better than plain concrete.
- The addition of steel fibres aids in converting the properties of brittle concrete to ductile material, but the addition of steel fibres with polypropylene fibres makes the results better than that and generally it improves the compressive strength and flexural strength of plain cement concrete, but the improvement in strength does not always increase with a larger dosage of fibres.

References

1. Ravikumar C, Ramasamy V, Thandavamoorthy T, (2015) Effect of fibers in concrete composites. Int J Appl Eng Res. 10. 419–430
2. Kumar M, Khadwal A (2014) Strength evaluation of steel-nylon hybrid fibre reinforced concrete. Int J Eng Res Appl 4(7)(Version 6):32–36. ISSN: 2248-9622

3. Zhang XX, Abd Elazim AM, Ruiz G, Yu RC (2008) Fracture behavior of steel fibre reinforced concrete at a wide range, Benjamin, J. R., Tsunamis of the Arabian Peninsula a guide of historic events. Sci Tsunami Hazards 27(1):37
4. Buendia AML, Sanchez MDR, Climent V, Guillem C (2013) Surface treated polypropylene fibres for the reinforced concrete. Cem Concr Res 54:29–35
5. Girish MG, Chandrashekhar A, Ravi Shankar AU (2012) Flexural fatigue analysis of steel fibre reinforced concrete. Int J Earth Sci Eng 05(01):1352–1357. ISSN 0974-5904
6. Buratti N, Mazzotti C, Savoia M (2011) Post cracking behavior of steel and micro synthetic fibre reinforced concretes. Constr Build Mater 25:2713–2722
7. Parveen AS (2013) Structural behaviour of fibrous concrete using polypropylene fibres. Int J Mod Eng Res 3(3):1279–1282. ISSN: 2249-6645
8. Soutos MN, Le TT, Lampropoulos AP (2012) Flexural performance of fibre reinforced concrete made with steel and synthetic fibres. Constr Build Mater 36:704–710
9. Kang ST, Lee BY, Kim J-K, Kim YY (2011) The effect of fibre distribution characteristics on the flexural strength of steel fibres reinforced ultra high strength concrete. Constr Build Mater 25:2450–2457
10. Yap SP, Alengaram UJ, Jumaat MD (2013) Enhancement of mechanical properties in polypropylene and nylonefibre reinforced oil palm shell concrete. Mater Des 49:1034–1041
11. Kaikea A, Achoura D, Duplan F, Rizzuti L (2014) Effect of mineral admixtures and steel fiber volume contents on the behavior of high performance fiber reinforced concrete. Mater Des 63:493–499
12. Brown R, Shukla A, Natarajan KR (2002) Fiber reinforcement of concrete structures. Report No. URITC FY 99-02, University of Rhode Island
13. Joshi SV, Waghe UP (2017) Effect of mixing fiber cocktail on flexural strength of concrete. Int J Civil Eng Technol 8(9):983–992. ISSN Print: 0976-6308 and ISSN Online: 0976-6316
14. Kang ST, Lee YB, Kim JK, Kim YY (2011) The effect of fibre distribution characteristics on the flexural strength of steel fibre-reinforced ultra high strength concrete. Constr Build Mater 25:2450–2457

Development of Mix Design and Correlation Studies Between Mechanical Properties of Ternary Blended High-Strength Concrete

Venkateswara Rao Jampani and Gopishankar Kaduluri

Abstract This experimental investigation presents the results of the mechanical properties of high-strength concrete, whose 28 days compressive strength is higher than 70 MPa. Mix design particulars of M-70 grade high-strength concrete were obtained according to IS 10262:2009 guidelines. To achieve the economy and to improve mechanical properties of control mix, supplementary cementitious materials, namely slag, fly ash, silica fume, and quartz powder, were incorporated in the mix as partial replacement of cement. The water-to-binder ratio for all mixtures was kept as 0.25. Total replacement of cement by cementitious materials was kept constant for all mixes, as 20% by weight of cement. Of all the combinations of cementitious materials, slag and silica fume as 20% replacement of cement performed well with respect to the workability and mechanical properties. Correlation equations were also developed between compressive strength and other mechanical properties and compared with the established equations by the previous researchers.

Keywords Silica fume · Slag · Fly ash · Compressive strength · Split tensile strength · Flexural strength

1 Introduction

High-strength concrete as per ACI 363 [1] was defined as concrete having its 28-day cylinder compressive strength greater than 41 MPa. Use of superplasticizers and strengthening blenders like silica fume and other pozzolonic materials such as fly ash or ground granulated blast furnace slag was proving to be the most efficient and economical way of preparing high-strength concrete [2–4]. Shannag [5]

V. R. Jampani (✉)
Civil Engineering Department, Lakireddy Bali Reddy College of Engineering, Mylavaram, Andra Pradesh 521230, India

G. Kaduluri
Department of Civil Engineering, Godavari Institute of Engineering and Technology, Rajahmundry, Andra Pradesh, India

B. Laishram and A. Tawalare (eds.), *Recent Advancements in Civil Engineering*, Lecture Notes in Civil Engineering 172,
https://doi.org/10.1007/978-981-16-4396-5_19

reported that with the use of natural pozzolan and silica fume combinations it is possible to produce high-strength mortars and concretes of compressive strength in the range of 69–110 MPa. Jianyong and Pei [6] investigated the effect of 25% replacement of cement by weight with combination of slag and silica fume, and the results indicated that there was a significant improvement in the mechanical properties of concrete when compared to control mix. Sayed and Mohamed [7] studied the effect of partial replacement of cement in high-strength concrete by silica fume and the mechanical properties of high-strength concrete were evaluated over a period of 1 year. The percentage of replacement of silica fume was in the range of 5–25% by weight of cement. Results of this investigation showed that optimum percentage of replacement of silica fume from the aspect of compressive strength development was found to be 15%, and beyond this, a decline noticed in the strength values was noticed. Mazloom et al. [8] observed improved performance in the short-term mechanical properties and reduction in creep characteristics of high-strength concrete after replacing 15% by weight of the cement with silicafume.

Haque and Kayali [9] reported that 10% replacement of cement in high-strength concrete mixes by class F fly ash enhanced the compressive, tensile properties, and the elastic modulus when compared to the conventional mixes. The water penetrability of the concrete with fly ash replacement also significantly improved. Elshekh et al. [10] replaced cement by fly ash in the range of 10–30% in high-strength concrete mixes and found that it results in significant improvement in workability, compressive strength, and its brittleness properties. Feng et al. [11] investigated the effect of two different replacements of cement 20 and 35% by weight with ultra-fine fly ash. Results indicated that there was a decrease in adiabatic temperature with an increase in percentage replacement by ultra-fine fly ash. At the same time, there is a decrement in early compressive strength and enhancement in the permeability of concrete compared to the control concrete.

Alani et al. [12] examined on the engineering and transport properties of green high-strength concrete by partially replacing the cement with ternary blended binders namely ordinary Portland cement, densified silica fume, and ultrafine palm oil fuel ash. From the results, it was concluded that up to 65% replacement of cement with combination of ultrafine palm oil fuel ash and densified silica fume leads to production of high-strength concrete with superior engineering and transport properties. Annadurai et al. [13] developed M-60 grade concrete by following ACI 211.4R-93 guidelines. High range water reducers and silica fume were used in this investigation. High-strength concrete with 28 days compressive strength of 60 MPa was developed by Raj et al. [14] by adopting the guidelines of both BIS and ACI code methods of mix design. Ternary blending binders were employed in the production of this mix, namely red-mud and metakaolin along with cement. Sinha and Verma [15] investigated the effect of ternary blenders namely cement, fly ash, and alccofine on M60 garde concrete along with 1% steel fibers. The results indicated that concrete made with cement, fly ash, and alccofine has superior fresh and hardened properties compared to conventional mix as well as mix with fly ash and cement.

Mohammed et al. [16] developed statistical regression analysis equations for calculating split tensile and flexural strengths from the known compressive strength values of high-strength concrete made from the combination of cement and silica fume in which the ratio of silica fume to cement was varied between 6 and 15% by weight. Suitability of the proposed equations in line with the previous recommendations provided by the researchers was discussed. Gajendran et al. [17] examined the influence of ternary blenders namely metakaolin, silica fume, and cement on the compressive and tensile strength properties of M60 grade high-performance concrete. It was found that replacement of cement by metakaolin and silica fume in ratio of 15% and 5%, respectively, results in better compressive and tensile properties. Relationship between the compressive strength was also studied and found that the 0.5 power relationship as per IS 456-2000 was not accurate according to the results obtained in the investigation. Kim et al. [18] investigated on the mechanical properties of high-performance concrete by incorporating the fly ash and slag in the range of 10–30% and 10–70%, respectively. Test results indicated that with increase in fly ash and slag the compressive and tensile strength properties were improved. An empirical relation between the tensile and compressive strength values and compared with those equations given by ACI, EC, JSCE, and KCI codes. Juki et al. [19] studied the effect of waste PET bottles used as artificial fine aggregate, on the compressive, splitting tensile, and flexural strength at the age of 28 days. A relationship for the prediction of splitting tensile and flexural strength was also derived from the compressive strength of concrete and was compared with the previous correlation equations developed by Neville and ACI building code.

The present investigation is targeted toward the development of the mix design of M-70 grade high-strength concrete as per IS 10262:2009 [20] guidelines without and with the use of supplementary cementitious materials, namely slag, fly ash, silica fume, and quartz powder. Correlation was also developed between compressive strength and other mechanical properties and were compared with the established equations as provided in the previous literatures such as by IS 456-2000 [21], ACI363-1997 [22], ACI31-1999 [23], Neville [24], Carrasquilo [25], Nogouchi and Tomosawa [26], and Rashid et al. [27].

2 Materials and Mix Proportions

2.1 Cement and Supplementary Cementitious Materials

Ordinary Portland cement (OPC) used in this study was produced by Ultra-Tech in compliance with IS 12269-1987. The cementitious materials used in this study were 53 grade ordinary Portland cement, fly ash, ground-granulated blast furnace slag, silica fume, and quartz powder, respectively, and their physical properties are given in Table 1. Chemical composition of cementitious materials is provided in Table. 2. Fly ash (FA) sample was obtained from NTPC Visakhapatnam, Andhra Pradesh, India.

Table 1 Physical properties of cementitious materials

Physical property	Cement	Fly ash	GGBS	Silica fume	Quartz powder
Specific gravity	3.12	2.21	2.79	2.3	2.5
Specific surface (m^2/kg)	320	320	375	–	–
Initial setting time (min)	109	–	210		

Table 2 Chemical compositions of cementitious materials

Oxides	Mass (%)				
	Cement	Fly ash	GGBS	Silica fume	Quartz powder
CaO	60.45	1.41	34.61	1.65	–
SiO_2	21.74	58.13	34.4	91.7	97
Mgo	3.38	0.71	8.83	1.78	–
Al_2O_3	6.61	32.55	16.3	1.1	0.4
Fe_2O_3	3.71	4.044	0.68	0.92	0.07
Na_2O	0.15	0.17	0.22	–	0.15
K_2O	0.2	0.96	0.63	–	0.1
SO_3	0.5	0.12	1.44	0.86	

Ground-granulated blast furnace slag, silica fume, and quartz powder are collected from locally available sources. The particle size of silica fume and quartz powder ranges between 90 μm to 150 μm and 75 μm to 90 μm, respectively. Particle size in the case of fly ash and slag the lies in the range of 37 μm to 45 μm and 53 μm to 75 μm, respectively. The physical appearance of the cementitious materials used in this investigation is shown in Fig. 1.

2.2 Aggregates

The coarse aggregate used was crushed gravel with maximum particle size of 10 mm and having a specific gravity of 2.68. Locally available natural river sand was used as fine aggregate having a specific gravity of 2.65, with a fineness modulus of 2.39.

2.3 Superplasticizer

Chemical admixture CONPLAST WL, with a specific gravity of 1.2, was used for improving the workability of concrete. The dosage of super-plastcizer was about 1% of the combined weight of the cementitious materials for all the mixes.

(a) GGBS (b) Silica fume (c) Quartz powder (d) Fly ash

Fig. 1 Physical appearance of supplementary cementitious materials

2.4 Mix Proportions

The mixture proportions used in the present study are selected based on the trial tests conducted as per IS 10262:2009 method of mix design with desirable compressive strength and workability. The control mix was prepared using OPC alone, and for the other mixes, part of cement is replaced with combinations of fly ash, slag, silica fume, and quartzite powder. The water/binder ratio and the slump of control mix were kept as 0.25 and 25 mm, respectively. Details of mix proportions for all the mixtures prepared are given in Table 3.

The control mix did not contain fly ash/slag and silica fume/quartz powder and was marked as OPC. The combined weight of supplementary cementitious materials was kept at 20% by replacing the same amount of cement in order to keep the weight of binding materials in concrete remains unaltered. Replacement of cement by fly ash/slag and silica fume was 16 and 4%, respectively. Mixes wherein fly ash (FA), silica fume (SF) and slag (S), SF combinations used were labeled as C + FA + SF and C + S + SF respectively. Mix with combination of slag, silica fume (3%), and quartz powder (1%) is labeled as C + S + SF + QP. The slump of concrete is reduced after the addition of cementitious materials indicating that further replacement of cement leads to stiffer mixes. The reason in the reduction of the slump may be attributed to the reduced particle size and hence part of superplasticizer adsorbed on the surface of finer particles.

3 Mixing Procedure and Specimen Preparation

For each of the mix mentioned in Table 3, measured quantities of cementitious materials namely cement, fly ash, ground blast furnace slag, silica fume (or) quartzite powder were taken in to the drum type mixer. These materials were mixed until uniform color was achieved. Later, fine and coarse aggregates were added and mixed again for a period of two to three minutes. Tap water along with the super-plasticizer is added at this stage and mixing continued for two more minutes. Fresh concrete obtained was casted into cubes of 150 mm and 150 × 300 mm cylindrical molds in three layers using a tamping rod by giving 25

Table 3 Mix proportions (kg/m^3) of concrete

Mix identification	Cement	Fly ash	Slag	Silica fume	Quartz powder	Coarse agg.	Fine agg.	Water	Slump (mm)
OPC	600					1020	714	150	30
OPC + FA + SF	480	96		24		1020	714	150	25
OPC + S + SF	480		96	24		1020	714	150	27
OPC + S + QP + SF	480		96	18	6	1020	714	150	23

strokes. After casting the molds, to reduce the entrapped air bubbles, further compaction is allowed on vibration table for about 30–45 s. After thorough compaction, specimens were kept undisturbed for a period of 24 h at room temperature. Prismatic molds of size 100 × 100 × 500 mm were also casted in the similar manner. The concrete specimens were removed from the molds and immersed in water till the date of testing.

4 Testing Procedures

Compressive strength of the concrete specimens was performed on 150 mm cubes at 3, 7, 14, and 28 days of curing period according to the procedure stipulated in IS 516-1959 [28]. The flexural strength and split tensile tests were performed in order to evaluate strength development of concrete specimens at above mentioned curing periods in accordance with IS 516-1959 and IS 5816-1999 [29] respectively. The arrangement of the samples in the respective testing machine is shown in Fig. 2.

5 Test Results and Discussions

5.1 Compressive Strength

Compressive strength of concrete mixes was determined at the age of 3, 7, 14 and 28 days. Figure 3 shows the compressive strength development of four concrete mixes. For the control mix the compressive strength development at the age of 3, 7,

(a) Compressive strength test (b) Flexural strength test (c) Split tensile strength test

Fig. 2 Concrete samples arrangement for testing

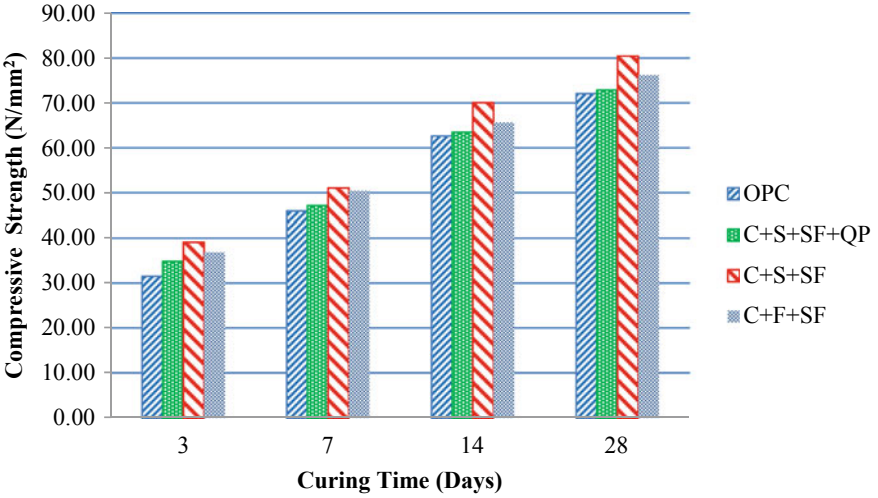

Fig. 3 Compressive strength development of mixes with curing period

and 14 days is about 44, 64, and 87% of its 28 days compressive strength. This indicates that strength development in high-strength concrete follows a similar trend as that of normal concrete. When 20% of cement was replaced with fly ash and silica fume, the rate of increments in the strength at 3, 7, 14 and 28 days were 17, 10, 5 and 6% respectively compared to control concrete. When the slag and silica fume combination was used for 20% replacement of cement the rate of increments in the compressive strength of concrete were 24, 11, 12, and 12%, respectively, at the age of 3, 7, 14, and 28 days of curing period respectively.

But slag, silica fume, and the quartz powder combination were used as a replacement only marginal increment in the compressive strength was noticed when compared to the strengths of control mix with 100% OPC.

5.2 Tensile Strength

Figure 4 shows split tensile strength of high-strength concrete at 3, 7, 14 and 28 days of curing period. The rates of increments in the split tensile strength of concrete when combinations of slag and silica fume were used for 20% replacement of cement in the control mix were 25, 15, 10, and 7%, respectively.

The enhancement in the split tensile strength of concrete when 20% of cement in the control mix was replaced with fly ash and silica fume was found to be 18, 12, 5 and 3% at the age of 3, 7, 14, 28 days, respectively. Use of slag, silica fume, and quartz powder combination as a replacement does not significantly improve the tensile strengths except at the very early curing periods.

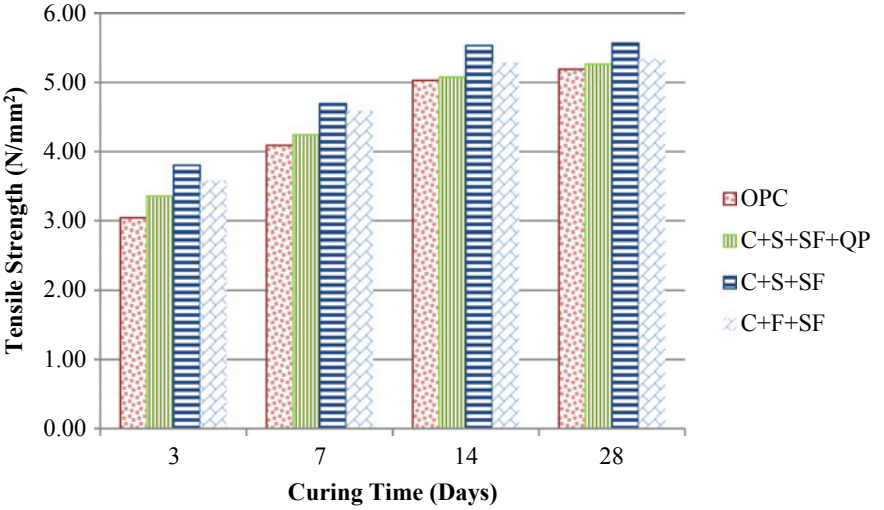

Fig. 4 Tensile strength development of mixes with curing period

Figure 5 shows a comparison between the calculated split tensile strength based on 28 days compressive strength of concrete using empirical formula as provided in the literature such as ACI 318-99, Neville [24], Rashid et al. [27] with the experimentally tested data. It was observed that the experimentally obtained values of tensile strengths were slightly higher than the values obtained by using ACI 318-99 and Neville [24]. By performing statistical regression analysis on the test data, the splitting tensile strength can be calculated from the following power equation $f_{st} = 0.40 f_c^{0.598}$. The test results of obtained split tensile strengths were in good agreement with the values calculated from compressive strength values using Rashid et al. [27].

5.3 *Flexural Strength*

The flexural strength development of four concrete mixes at 3, 7, 14 and 28 days of curing period is shown in Fig. 6. By replacing 20% of cement in the control mix with a combination of slag and silica fume, there was an increment in the flexural strengths by 23, 12, 9 and 11% respectively at the age of 3, 7, 14 and 28 days respectively. When a combination of mineral admixtures slag, silica fume and quartz powder are used there was not much improvement in the flexural strength particularly at later ages of curing periods. The rate of increments in the flexural strength was 22, 10, 4 and 7%, when fly ash and silica fume combination was replaced with 20% of cement in the control mix.

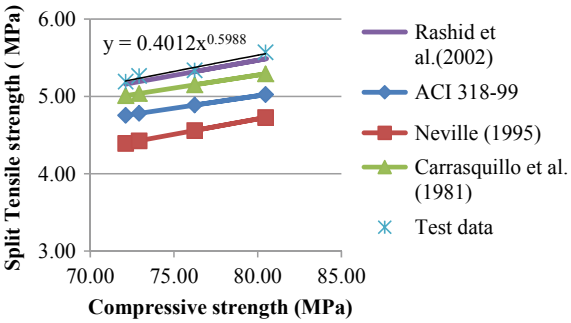

Fig. 5 Correlation between experimentally evaluated split tensile strengths and empirically verified values

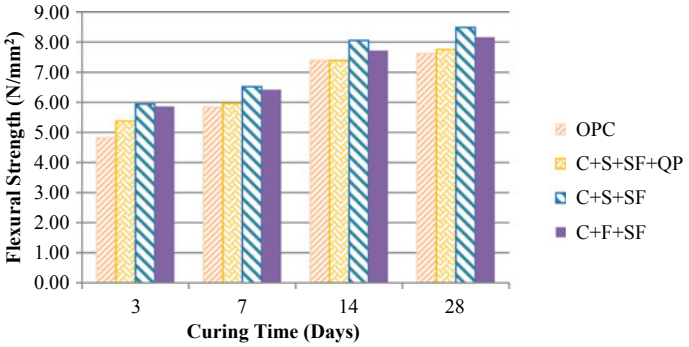

Fig. 6 Flexural strength development of mixes with curing period

Figure 7 shows a contrast between the experimentally determined flexural strength of concrete mixes with those calculated values of flexural strengths based on 28 days compressive strength of concrete using empirical formula as provided in the literature such as Noguchi and Tomosawa [26], IS 456-2000, ACI 363 [22], Rashid et al. [27], etc. with the experimentally tested data. It was observed that the experimentally obtained values of flexural strengths were slightly higher than the values obtained by using IS 456:2000. By performing statistical regression analysis on the test data, the flexural strength can be calculated from the following power equation $f_f = 0.1186(f_c)^{0.974}$. The test results of obtained split tensile strengths were in good agreement with the values calculated from compressive strength values using Rashid et al. [27] and ACI 363 [22]. Tested values of flexural strengths are marginally lower than those values calculated using Noguchi and Tomosawa (1995) equations.

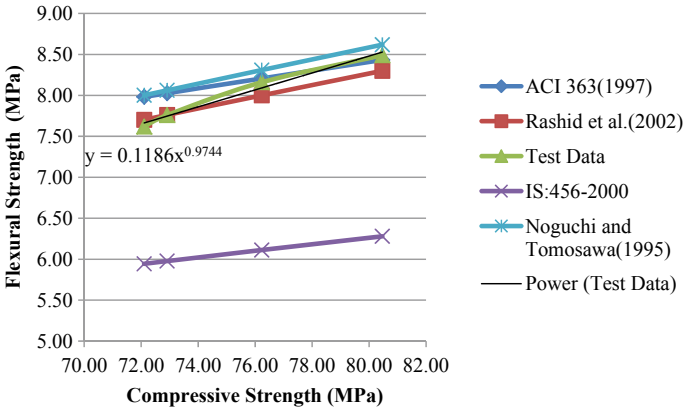

Fig. 7 Correlation between experimentally evaluated flexural strengths and empirically verified values

6 Conclusions and Recommendations

Based on the results obtained from the experimental investigations, the following conclusions were drawn.

(1) The mix proportion details provided in this experimental study corresponds to the characteristic strength of 70 Mpa. Hence it is possible to attain high compressive strengths up to 70 Mpa using the guidelines of IS 10262:2007. It was found that for low workability mixes up to 25–30 mm slump, use of mineral admixtures like fly ash, slag and silica fume combinations with 1% of super-plasticizer by weight of binder results in further enhancement of mechanical properties.

(2) Use of mineral admixtures like slag, fly ash and silica fume combinations significantly enhances early strength development than even strengths at later ages of curing periods, which may be assisting in early removal of form works and consequently faster construction practices can be made possible. Replacement of 20% of cement in the conventional mix with a combination of slag and silica fume led to better compressive, split tensile, and flexural strengths compared to combination of fly ash, silica fume. Use of quartz powder does not show any significant improvement in mechanical properties.

(3) Split tensile strengths of high-strength concrete at the age of 28 days within the range of compressive strengths from 72 to 80 Mpa were well correlated with the empirical equations provided by Rashid et al. [27] and Carrasquilo et al. (1995) compared to those suggested by Neville [24] and ACI 318-11.

(4) Flexural strength of high-strength concrete at the age of 28 days for the given range compressive strengths in this study were well correlated with the empirical approach provided by Rashid et al. [27], ACI 363 (1996) and

Noguchi and Tomosawa (1995). For the given range of compressive strengths considered in this study, experimentally obtained flexural strength values were on the lower side compared to those values calculated according to IS 456-2000 based on compressive strength values.

The scope of the present investigation was considered up to 20% replacement of cement with mineral admixtures; however, studies on the influence of chemical admixtures and other combinations of percentage replacement of mineral admixtures for enhancing the workability and strength of high-strength concrete mixes are recommended.

References

1. ACI Committee 363R-92 (1997) Report on high-strength concrete. American Concrete Institute, Farmington Hills, MI
2. Gupta S (2014) Development of ultra-high performance concrete incorporating blend of slag and silica fume as cement replacement. Int J Civ Struct Eng Res 2:35–51
3. Naik TR, Singh SS, Hossain MM (1996) Enhancement in mechanical properties of concrete due to blended ash. Cem Concr Res Sci Direct 49–54
4. Naiqian F (1992) Technology of High Strength Concrete China. Publishing House, Beijing, Building Materials Industry
5. Shannag MJ (2000) High strength concrete containing natural pozzolan and silica fume. Cem Concr Compos Sci Direct 399–406
6. Jianyong L, Pei T (1997) Effect of slag and silica fume on mechanical properties of high strength concrete. Cem Concr Res Sci Direct 833–837
7. Sayed AE, Mohamed RAS (2009) Investigations on the mechanical properties of high strength silica-fume concrete (HSSC) mixes at different ages. J Eng Sci 37:581–592
8. Mazloom M, Ramezanianpour AA, Brooks JJ (2004) Effect of silica fume on mechanical properties of high-strength concrete. Cem Concr Compos Sci Direct 347–357
9. Haque MN, Kayali O (1998) Properties of high-strength concrete using a fine fly ash. Cem Concr Res Sci Direct 1445–1452
10. Elshekh AEA, Shafiq N, Nuruddin MF, Fathi A (2013) Mechanical properties of high strength concrete using fly ash. IEEE Bus Eng Ind Appl Colloquium (BEIAC) 306–310
11. Feng J, Liu S, Wang Z (2015) Effects of ultrafine fly ash on the properties of high-strength concrete. J Therm Anal Calorim 12:1213–1223
12. Alani AH, Johari MAM, Aldahdooh MAA, Muhamad Bunnori N (2019) Development of engineering and transport properties of green high strength concrete utilizing ternary blended binders. Eur J Environ Civ Eng 1–17
13. Annadurai A, Ravichandran A (2014) Development of mix design for high strength concrete with admixtures. IOSR J Mech Civ Eng 10:22–27
14. Raj RR, Pillai EP, Santhakumar AR (2013) Evaluation and mix design for ternary blended high strength concrete. Procedia Eng 51:65–74
15. Sinha DA, Verma AK (2017) An Experimental Investigation on the effect of addition of ternary blend on the mix design characteristics of high strength concrete using steel fibre. MS & E 225:012163
16. Mohammed AA, Assi DK, Abdulrahman AS (2015) Tests on tensile and compressive strengths of high strength concrete containing silica fume. Proc SELTH 301–308

17. Gajendran KA, Anuradha R, Venkatasubramani G (2015) Studies on relationship between compressive and splitting tensile strength of high performance concrete. ARPN J Eng Appl Sci 10:6151–6156
18. Kim JE, Park WS, Yun SH, Jang YI, Yun HD, Kim SW, Kim DG (2015) The relationship of compressive strength and tensile strength of high-performance concrete key engineering materials, vol 627. Trans Tech Publications Ltd., pp 385–388
19. Juki MI, Awang M, Annas MMK, Boon KH, Othman N, Roslan MA, Khalid FS (2013) Relationship between compressive splitting tensile and flexural strength of concrete containing granulated waste polyethylene terephthalate (PET) bottles as fine aggregate. Adv Mater Res 79:356–359
20. Indian Standard IS 10262 (2009) Recommended guidelines for concrete mix design
21. Indian Standard IS 456 (2000) Plain and reinforced concrete code of practice (4th revision)
22. ACI Committee 363 (1997) State-of-the-art report on high strength concrete, pp 1–37
23. American Concrete Institute (1999) Building code requirements for reinforced concrete (ACI 318-1999) and Commentary—ACI 318R-1999. American Concrete Institute, Detroit
24. Neville AM (1995) Properties of concrete, vol 4. Longman, London
25. Carrasquillo RL, Nilson AH, Slate FO (1981) Microcracking and behavior of high strength concrete subject to short-term loading. J Proc 78:179–186
26. Noguchi T, Tomosawa F (1995) Relationship between compressive strength and various mechanical properties of high strength concrete. J Struct Constr Eng 472:11–16
27. Rashid MA, Mansur MA, Paramasivam P (2002) Correlations between mechanical properties of high-strength concrete. J Mater Civ Eng 14:230–238
28. Indian Standard IS 2002 516 (1959) Methods of tests for strength of concrete. Bureau of Indian Standards
29. BIS 5816-1999 (1999) Method of test for splitting tensile strength of concrete

Effect of Aggregate Gradation on Mechanical Properties of Pervious Concrete

Mycherla Chaitanya and G. Ramakrishna

Abstract Pervious concrete is widely regarded as permeable concrete and has a significant impact on the environment. The strength of pervious concrete largely depends on coarse aggregate due to the absence of adequate fine aggregate. This paper delineates the impact of coarse aggregate gradation on the mechanical properties of pervious concrete. Four different coarse aggregate gradations of 10–4.75, 12.5–10, 12.5–4.75 and 12.5–2.36 mm were used to prepare the pervious concrete mixes. In addition, the amount of fine aggregate is also varied for the above gradations to suggest the optimum mix. The prepared mixtures were tested for compressive strength, flexural strength and permeability. The permeability of the specimens was evaluated as per the procedure described in IRC: 44. The comparative analysis between the above mentioned gradations regarding the mechanical properties is also discussed.

Keywords Pervious concrete · Coarse aggregate gradation · Fine aggregate · Mechanical properties · Permeability

1 Introduction

The rapid growth of urbanization has lead to massive constructions across the globe. The increased number of structures and paved surfaces has a bleak impact on the environment which leads to the use of environment friendly materials and infrastructures. The urge of transforming impermeable paved surfaces to permeable paved surfaces is imperative. Pervious concrete is one such paved material which allows water to pass through it and there by recharging the ground water table. Pervious concrete has been identified as a *Best management Practice* (BMP) for

M. Chaitanya (✉) · G. Ramakrishna
Pondicherry Engineering College, Pillaichavadi, Puducherry, India
e-mail: mycherlac@pec.edu

G. Ramakrishna
e-mail: grkv10@pec.edu

B. Laishram and A. Tawalare (eds.), *Recent Advancements in Civil Engineering*, Lecture Notes in Civil Engineering 172,
https://doi.org/10.1007/978-981-16-4396-5_20

storm water management [1]. Pervious concrete can be typically defined as a paved permeable surface that can allow storm water to percolate through it.

Pervious concrete is composed of coarse aggregate, cement, water and without or with little amount of fine aggregate to facilitate the permeability. Coarse aggregate, being the major load bearing component in the pervious concrete, has to be selected with utmost care. Various types of coarse aggregates can be used in preparing the pervious concrete mixes, and out of all pervious concrete made of river gravel was found to have higher compressive strength. Aggregate gradation is also one of the key factors to be considered in designing a pervious concrete mix. Pervious concrete made of single sized aggregates was found to have high permeability but low strength. Many researchers have worked on different coarse aggregates and their effects on properties of pervious concrete. Pervious concrete as a pavement material has many applications but restricted to lower vehicular loads because of its low strength. The absence of fine aggregate in pervious concrete facilitates the permeability of water whereas the large number of voids leads to the hindrance of strength. Various studies have been carried out to increase the strength of pervious concrete and to make it viable for higher vehicular loads. The aggregate size, shape and type have a significant effect on the mechanical properties of pervious concrete. Pervious concrete made of river gravel was found to produce higher compressive strength than other aggregates [2]. Volcanic Pumice aggregate was found to produce high porosity pervious concrete samples with slight decrease in strength. Fibers are found to be effective in improving the durability characteristics and no significant effect on the mechanical properties of pervious concrete. High strength pervious concrete can be developed using silica fumes and super plasticizers [3–5].

In the present study, different *coarse aggregate gradations* composed of varying percentage of coarse aggregate sizes were used to prepare the pervious concrete mixes. In addition, the effect of fine aggregate on pervious concrete composed of different gradations is also studied, and a comparative analysis is made between the different mixes used in the study. A brief emphasis is also made on the experimental procedure for conducting permeability test as per IRC 44.

2 Experimental Program

2.1 Materials and Properties

The conventional pervious concrete is composed of coarse aggregate, cement, water and fine aggregate. The preliminary tests on all the materials were done prior to their use in mix design. OPC of 53 grade and potable water is used for the mix design.

2.1.1 Coarse Aggregate

Gravel is used in the present study as coarse aggregate, and Table 1 details the test results conducted in accordance with IS 2386 and ASTM C 29. The coarse aggregate gradations used in the study vary from 12.5 to 2.36 mm size. Mixes were prepared using single sized aggregates of (12.5–10) and (10–4.75) mm and a combination of both comprising 50% each and then a well graded mixture of aggregates comprising 50% of (12.5–10), 40% of (10–4.75) and 10% of (4.75–2.36) mm. The designation of these gradations is shown in Table 2.

2.1.2 Fine Aggregate

M-sand is used as a fine aggregate material in the present study, and the properties are shown in Table 3.

2.2 Mix Design and Test Methods

The pervious concrete was batched, mixed and cured according to ACI 522R. The target void content was 20%, and the water-cement ratio was varied from 0.28 to

Table 1 Preliminary test results of coarse aggregate

Sl. No.	Property	Test result
1.	Specific gravity	2.80
2.	Density (kg/m^3)	1590
3.	Water absorption (%)	0.8
4.	Impact value (%)	23
5.	Crushing value (%)	26
6.	Abrasion resistance (%)	29
7.	Angularity	8

Table 2 Gradation of coarse aggregate

Sl. No.	Gradation (mm)	Designation
1.	12.5–10 and 10–4.75	M_1
2.	12.5–10	M_2
3.	10–4.75	M_3
4.	12.5–2.36	M_4

Table 3 Properties of M-sand

Sl. No.	Property	Test result
1.	Specific gravity	2.30
2.	Water absorption	3%

0.36. The paste volume was reduced by 1% for every 10% addition of fine aggregate. The compression and flexural strength tests are conducted according to IS: 516. Cylindrical specimens of 100 × 200 (mm) for compressive strength and prisms of 100 × 100 × 500 (mm) for flexural test were used.

2.2.1 Permeability Test

The permeability of pervious concrete can be determined either by *constant head* method or *falling head* method. Various researchers have adopted different methods to determine the permeability of pervious concrete but in this study, the method described in IRC 44 was used [6]. The principle involved in this method is to measure the time taken by 1000 ml of water to infiltrate through the specimen. Cylindrical specimens of 100 × 200 (mm) were used for the test. The specimen has to be wrapped around the circumference to prevent the horizontal flow of water prior to pre-wetting. Water should be poured into the specimen at a rate sufficient to maintain the head between the two lines marked at a distance of 15 and 25 mm from the top of the sample [6]. The time required for measured volume of water to infiltrate through the cross sectional area of the specimen has to be noted down. The test setup adopted in this study is shown in Fig. 1.

Fig. 1 Permeability test setup

3 Results and Discussion

3.1 Compressive Strength

The compressive strength test results of the four gradations of coarse aggregates used are shown in Fig. 2. The results indicated that pervious concrete made of M_4 *gradation* has more compressive strength than the other gradations which is attributed to the decrease in voids for a well graded aggregate mix. As the M_4 gradation has more variety of sizes and also the presence of smaller sized aggregates enhanced the compressive strength [7]. The 7-days compressive strength of all the mixes is around 75–80% of the 28-days compressive strength which is in conjunction with the previous studies [8].

M-sand was added in proportions as 0, 10 and 20% of coarse aggregate to all the gradations to observe the effect of fine aggregate on strength of pervious concrete. Trends indicated that the strength is high for 10% fine aggregate addition which is in accordance with the literature [9] and decreased for 20% fine aggregate for all gradations due to the reduction in cement paste resulted in poor bonding between the aggregates [10]. The strength results of four gradations with varying percentage of fine aggregate are shown in Fig. 3.

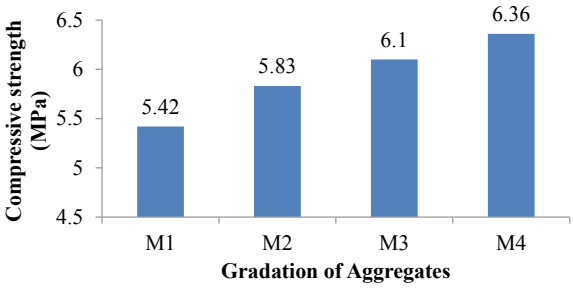

Fig. 2 Compressive strength of pervious concrete for different gradations

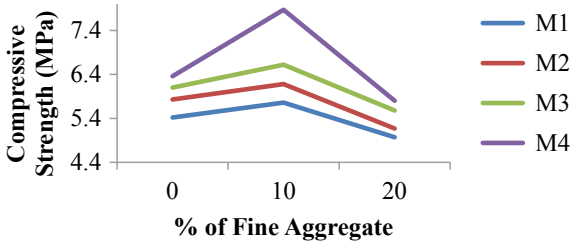

Fig. 3 Comparison of four gradations with fine aggregate

Table 4 Flexural strength test results

Sl. No.	Gradation	0% FA (MPa)	10% FA (MPa)	20% FA (MPa)
1.	M_1	1.70	1.84	1.49
2.	M_2	2.01	2.12	1.50
3.	M_3	2.30	2.67	1.82
4.	M_4	2.60	2.74	2.28

3.2 *Flexural Strength*

The 28-day's flexural strength test results of all the four gradations for varying proportion of fine aggregate are presented in Table 4. Trends indicated that the flexural test results are in line with the compressive strength results, maximum being for the 10% fine aggregate addition. The maximum flexural strength is achieved for M_4gradation with 10% fine aggregate.

3.3 *Comparison Between Compressive Strength and Permeability*

The permeability of all the mixes was determined according to the procedure mentioned in IRC44.

Three specimens were tested for each mix design, and the average value is considered. Permeability is found to be high for 0% fine aggregate addition for all the gradations. The high permeability of mixes prepared without fine aggregate is attributed to the large void spaces. The key observation inferred from the study is permeability that was found to be least for all the mixes prepared with 20% fine aggregate, even though the strength of mixes prepared with 20% are less compared to other mixes. The reason for low permeability of these mixes is attributed to fewer voids due to the increased amount of fine aggregate and also the less cement paste volume as mentioned in ACI 522 R [10]. A comparative graph shown in Fig. 4 was

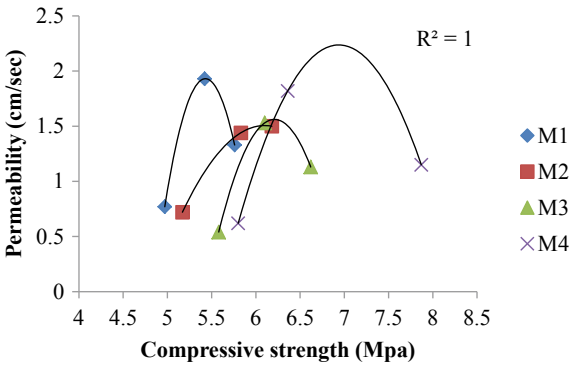

Fig. 4 Compressive strength versus permeability

made between the compressive strength and permeability for all the gradations to observe the distribution, and it was found to be a *polynomial distribution* for all the gradations with $R^2 = 1$.

4 Conclusions

Based on the work carried out, the following conclusions are drawn:

- Aggregate size has a profound effect on strength and permeability properties of pervious concrete. The pervious concrete mix prepared using well graded aggregate of 12.5–2.36 mm size has high strength which is 19–28% higher than the single sized aggregates.
- The compressive and flexural strength are found to be maximum for an addition of 10% fine aggregate which is 20% higher than the mix without fine aggregate.
- Flexural strength being the key parameter in the design of pavements was improved by 50% with aggregate gradation. However, no much significance effect of fine aggregate on flexural strength was observed.
- Permeability is reduced by 40% approximately with fine aggregate addition for all the gradations. However, all the permeability values are within the acceptable limits according to ACI522R.
- The comparative analysis between compressive strength and permeability revealed a polynomial distribution with an accuracy of $R^2 = 1$.

Acknowledgements The authors gratefully acknowledge the AICTE for financial support vide Research Promotion Scheme (RPS-NDF) research project grant number: 8-17/RIFD/RPS-NDF/Policy-1/2018-19 dated 13th March 2019.

References

1. Uma Maguuesvari M, Narasimha VL (2013) Studies on characterization of pervious concrete for pavement applications. Procedia—Social and Behavioral Sciences
2. Kevern JT, Wang K, Schaefer VR (2010) Effect of coarse aggregate on freeze-thaw durability of pervious concrete. J Mater Civil Eng 22:469–475
3. Hariyadi and Tamai H (2015) Enhancing the performance of porous concrete by utilizing the pumice aggregate. Procedia Eng (Elsevier) 732–738
4. Kevern JT, Biddle D, Cao Q (2014) Effects of macrosynthetic fibers on pervious concrete properties. J Mater Civil Eng
5. Chen Y, Wang K, Wang X, Zhou W (2013) Strength, fracture and fatigue of pervious concrete. Constr Build Mater 97–104
6. IRC (2017) Guidelines for cement concrete mix design for pavements. Indian Roads Congress, IRC 44:2017
7. Yang J, Jiang G (2003) Experimental study on properties of pervious concrete pavement materials. Cem Concr Res 33:381–386

8. Chandrappa AK, Biligiri KP (2016) Pervious concrete as a sustainable pavement material—research findings and future prospects: a state-of-the-art review. Constr Build Mater 111: 262–274
9. Bonicelli A, Arguelles GM, Pumarejo LGF (2016) Improving pervious concrete pavements for achieving more sustainable urban roads. Procedia Eng (Elsevier) 1568–1573
10. American Concrete Institute (2010) Report on pervious concrete ACI 522R-10

Artificial Neural Network (ANN) Models for Prediction of Steel Fibre-Reinforced Concrete Strength

A. M. Shende, K. P. Yadav, and A. M. Pande

Abstract The objective of the present research paper is to develop artificial neural network simulation and analyse the most important π-term from five independent pi terms (aspect ratio, aggregate–cement ratio, water–cement ratio, percentage of fibre and control strength) for prediction of SFRC strength. The output of this network can be evaluated by comparing it with experimental strength and the predicted ANN simulation strength. The study becomes more fruitful when the most influencing π-term is calculated for the prediction of SFRC strength.

Keywords ANN model · 5 independent π terms · Predicted SFRC strength

1 Introduction

To arrive at mathematical model, the process started with the development of some preliminary mathematical relations and then arriving at some single generalized equations. Mathematical models are developed to predict the strength of SFRC for different grade of concrete, for different aspect ratio and different percentage of steel [1–8, 13].

Shende et al. [3–6] studied the investigation for (1) Grade of concrete M20, M30 and M40 (2) Aspect Ratio 50, 60 and 67 (3) Percentage of steel fibres 0, 1, 2 and 3%. The mathematical modelling to calculate predicted compressive strength, flexural strength and split tensile strength of SFRC are studied by shende [9] in 2013. In this paper, an attempt is made to extend the work by developing artificial neural network model by using five independent π terms that is control strength,

A. M. Shende (✉)
Priyadarshini J.L. College of Engineering, Nagpur, Maharastra, India

K. P. Yadav
Sangam University, Bhilwara, Rajasthan, India

A. M. Pande
Y.C.C.E. Nagpur, Nagpur, India

B. Laishram and A. Tawalare (eds.), *Recent Advancements in Civil Engineering*, Lecture Notes in Civil Engineering 172,
https://doi.org/10.1007/978-981-16-4396-5_21

percentage of steel fibre, aspect ratio, water–cement ratio and aggregate–cement ratio for the prediction of steel fibre-reinforced concrete compressive strength, flexural and split tensile strength.

1.1 Artificial Neural Network Simulation

Artificial neural network simulation is developed to predict strength of SFRC by using control strength, percentage of fibres, aspect ratio, water–cement ratio and aggregate–cement ratio. The experimental data-based modelling has been achieved through mathematical models for the five independent pi terms. In such complex phenomenon involving nonlinear systems, it is also planned to develop artificial neural network (ANN). The output of this network can be evaluated by comparing it with observed data. For the development of ANN, the designer has to recognize the inherent pie terms that are predicted SFRC strength. Same ANN Simulation model can predict compressive strength, flexural strength and split tensile strength.

1.2 Artificial Neural Network Simulation [10]

An artificial neural network (ANN) consists of three layers, i.e. the input layer, the hidden layer and the output layer. Its nodes represent neurons of the brain. The specific mapping performed depends upon the architecture and synaptic weight values between the neurons of ANN network. An artificial neural network is highly distributed representation and transformation that works in parallel. It is utmost important to compare the data generated through experimentally observed data and ANN data to validate the phenomenon.

2 Procedure for Artificial Neural Network Phenomenon

The observed data from the experimentation are separated into two parts viz. input data or the data of independent pi terms and the output data or the data of dependent pi terms. The input data and output data are imported to the programme, respectively. Through principle component analysis, the normalized data are uncorrelated. This is achieved by using “prestd” function. The input and output data are then categorized into three categories viz. testing, validation and training. The common practice is to select initial 75% training, last 75% data for validation and middle overlapping 50% data for testing. This is achieved by developing a proper code.

1. The data are then stored in structures for training, testing and validation.
2. Looking at the pattern of the data, feed forward backpropagation type neural network is chosen.
3. This network is then trained using the training data. The computational errors in the actual and target data are computed, and then, the network is simulated.
4. The uncorrelated output data are again transformed onto the original form by using "poststd" function.
5. After simulating the ANN, it is found that experimentally observed values are very close and in good agreement with the ANN predicted values.

Figure 1 shows simple multilayer feed forward network for ANN, and Fig. 2 shows the flow diagram of ANN simulation.

Table 1 shows comparison of the values of dependent pi terms computed by experimentation, and ANN and the values of *R* squared error in ANN, number of iterations, values of the regression coefficients for dependent pi terms and the plots of the actual data and target data for the dependent pi terms are shown in Figures for all response/dependent variables (Figs. 3, 4, and 5).

It can be seen that the highest change takes place in strength, because of the π term π_5 (control strength) whereas the least change takes place due to π_4 (Aspect Ratio). Thus, π_5 related to control strength variables is the most important π term.

3 Conclusions

ANN Simulation model developed for prediction of SFRC strength, using strength of controlled concrete, percentage of fibres, aspect ratio, aggregate–cement ratio and water–cement ratio, can very well be used in prediction of compressive strength, flexural strength and split tensile strength of SFRC using the five parameters listed above.

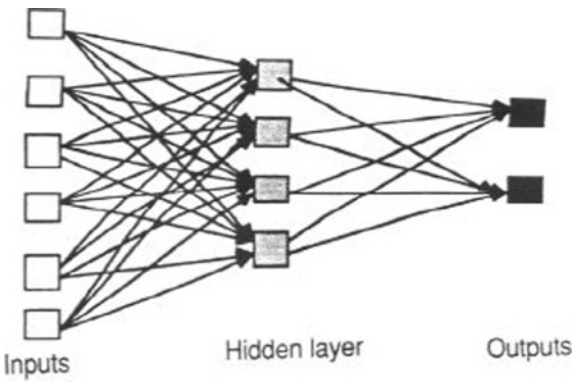

Fig. 1 Simple multilayer feed forward network (ANN) [11]

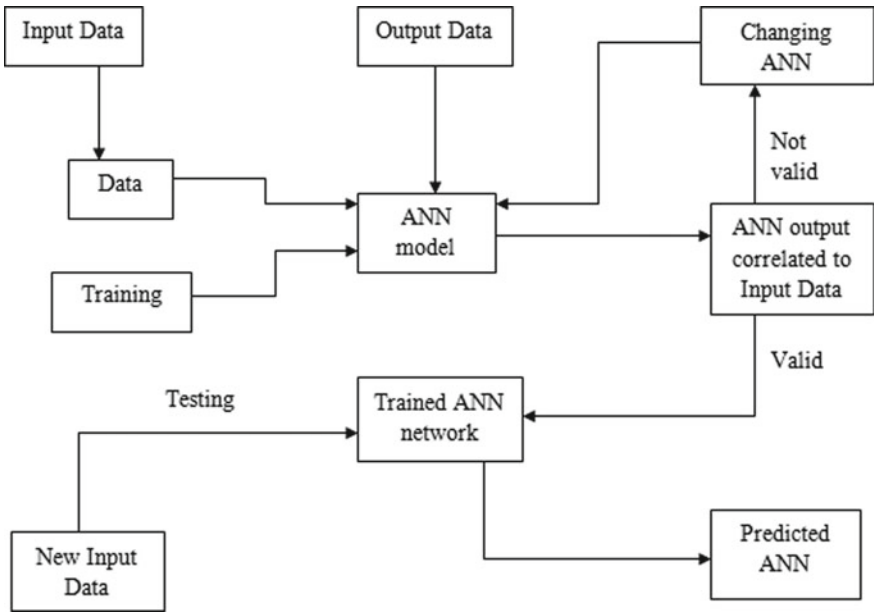

Fig. 2 ANN simulation flow diagram [11]

Table 1 Performance analysis of ANN and comparison of experimental and predicted strength (out of 511 reading first 30 are reported here) [9]

Sr. No.	Expem	ANN	% Error	Sr. No.	Expem	ANN	% Error
1	35.9	38.5987	7.52	16	50.64	43.2541	14.59
2	39.06	39.2254	0.42	17	50.3	34.9614	30.49
3	39.74	39.1644	1.45	18	50.99	38.7512	24.00
4	39.6	37.3213	5.75	19	51.74	43.2541	16.40
5	35.3	34.3013	2.83	20	42.07	25.3025	39.86
6	42	38.9383	7.29	21	42.81	25.3025	40.90
7	36.83	37.3213	1.33	22	40.88	25.3025	38.11
8	42.74	39.2254	8.22	23	42.22	25.3025	40.07
9	37.21	38.5987	3.73	24	41.73	25.3025	39.37
10	34.9	34.3013	1.72	25	43.11	25.3025	41.31
11	38.43	27.745	27.80	26	44.44	25.3025	43.06
12	37.4	28.8231	22.93	27	40.58	25.3025	37.65
13	37.5	30.2178	19.42	28	43.11	25.3025	41.31
14	45.47	34.9614	23.11	29	42	21.6538	48.44
15	47.54	38.7512	18.49	30	45	29.5809	34.26

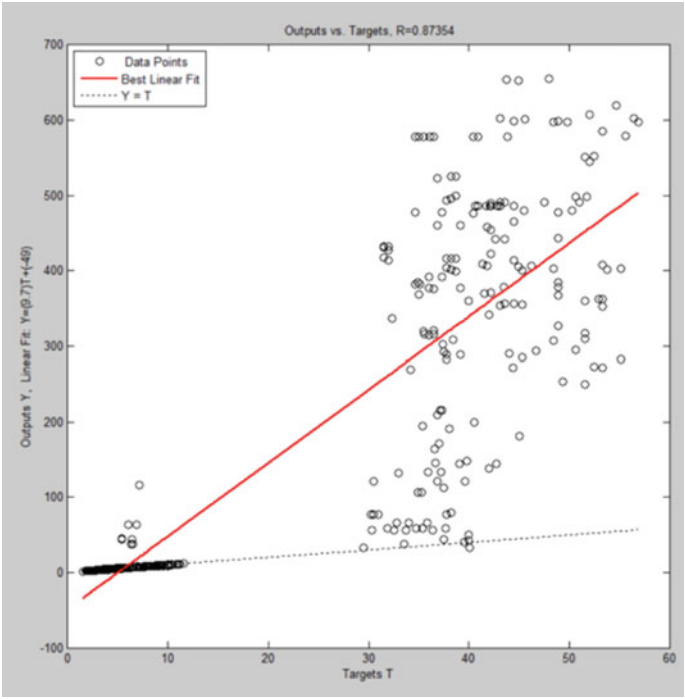

Fig. 3 Target versus output graph (R^2 = 0.7569)

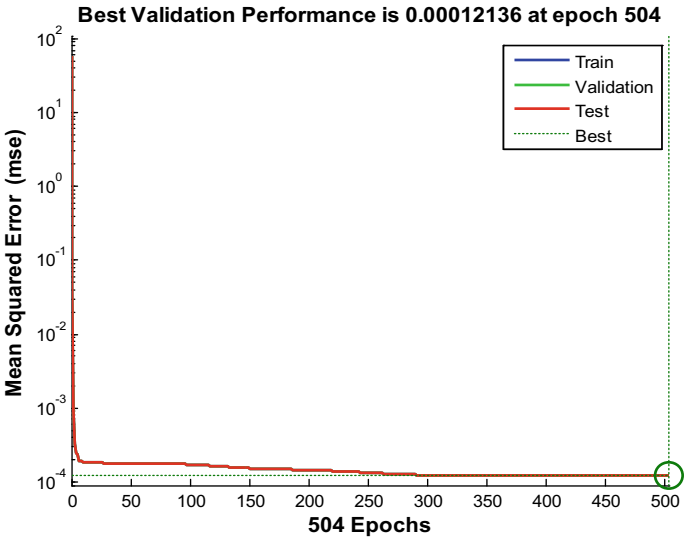

Fig. 4 Shows best validation performance

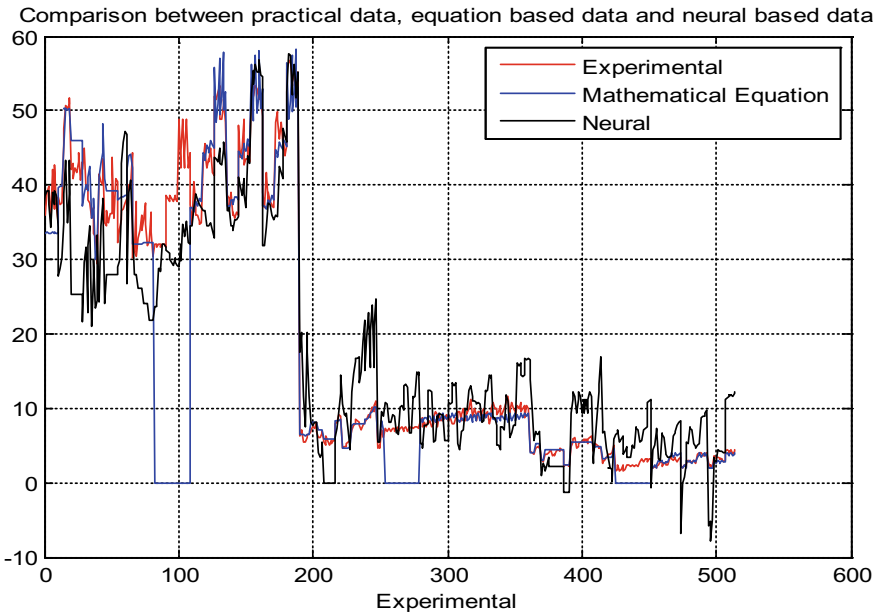

Fig. 5 Comparisons between experimental data and ANN predicted strength

Table 2 Performance analysis of ANN and comparison of experimental and predicted strength (out of 511 reading last 30 are reported here) [9]

Sr. No.	Expem	ANN	% Error	Sr. No.	Expem	ANN	% Error
480	2.94	7.5136	155.56	496	2.48	−7.951	420.63
481	2.87	7.3098	154.70	497	2.15	−5.080	336.30
482	2.77	7.0995	156.30	498	3.68	3.3104	10.04
483	3.04	5.1728	70.16	499	3.11	3.0076	3.29
484	2.69	4.8827	81.51	500	3.33	2.7036	18.81
485	2.55	4.5849	79.80	501	3.4	4.4983	32.30
486	3.82	5.1421	34.61	502	2.97	4.3142	45.26
487	3.82	5.3294	39.51	503	3.14	4.1259	31.40
488	4.1	5.4323	32.50	504	3.18	4.2223	32.78
489	3.96	8.6742	119.05	505	2.83	4.0866	44.40
490	3.54	8.874	150.68	506	3.04	3.9522	30.01
491	3.54	8.9836	153.77	507	4.25	11.1336	161.97
492	3.54	9.3628	164.49	508	4.39	11.2961	157.31
493	3.96	9.6801	144.45	509	4.25	11.5593	171.98
494	2.55	−5.885	330.81	510	4.1	11.7152	185.74
495	2.26	−5.163	328.48	511	4.39	11.8019	168.84

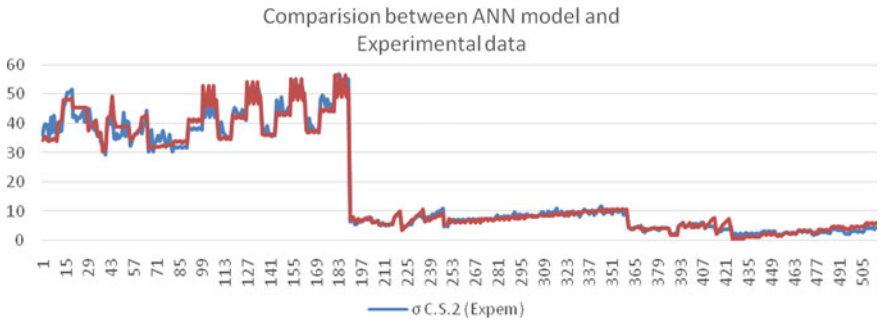

Fig. 6 Graphical comparison between ANN model and experimental data-based model for prediction of SFRC strength

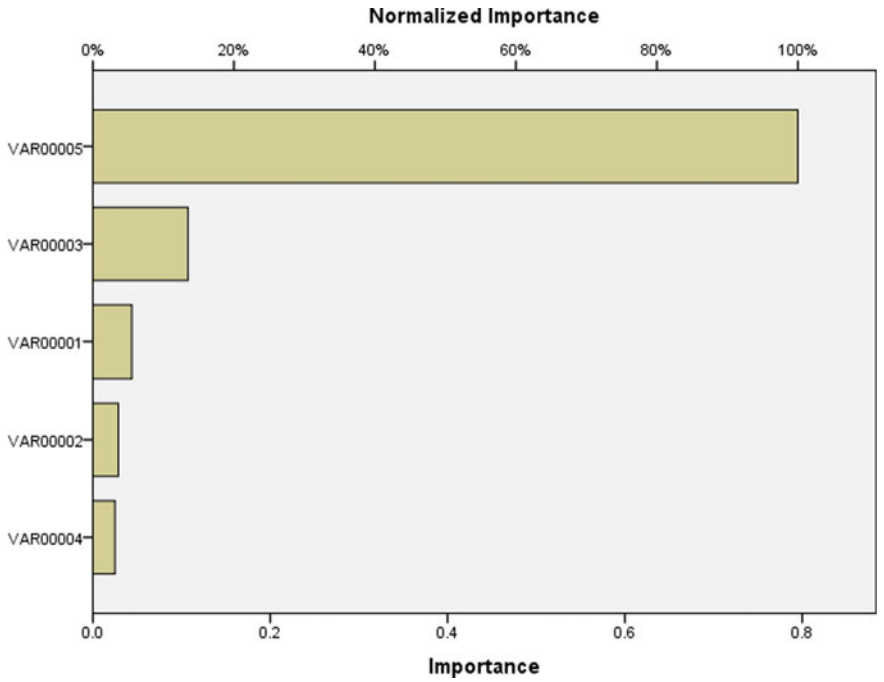

Fig. 7 Shows the importance of π terms in ascending order

The significance of this model can very well be seen from the data presented in column experimental strength and the predicted ANN simulation strength in Tables 1 and 2.

From Fig. 6, it is clear that ANN simulation model developed for prediction of compressive strength, flexural strength and split tensile strength when compared

with experimental strength it is observed that predicted strengths and observed experimental strength are close to each other.

Figure 7 shows the importance of independent π terms. Control strength π5 is the most influencing terms in this model.

References

1. MacDonald CN, Trangsrud J (2004) Steel fibre reinforced concrete pre-cast pipe. Proc ICFRC I:19–28
2. Coutts RSP (2005) A review of Australian research into natural fibre cement composites. Cem Concr Compos 27:518–526
3. Shende AM, Pande AM (2011) Experimental study and prediction of tensile strength for steel fiber reinforced concrete. Int J Civil Struct Eng 1(4):910–917
4. Haroon SA, Yazdani N, Tawfiq K (2004) Properties of fibre reinforced concrete for florida applications. Proc ICFRC I:135–144
5. Jagannathan (2010) Flexural strength characteristics of hybrid fibre reinforced cementitious matrix. Proc Int Conf Innovation I:347–353
6. Shende AM, Pande AM (2011) Mathematical model to calculate predicted compressive strength and its comparison with observed strength. Int J Multi Res Adv Eng (IJMRAE) Appl 3(IV):145–156
7. Sashidhar C, Rao HS, Ramana NV (2004) Strength characteristics of fiber-reinforced concrete with Metakaolin. Proc ICFRC I:247–256
8. Shende AM, Pande AM (2011) Comparative study on steel fibre reinforced cum control concrete under flexural and deflection. Int J Appl Eng Res 1(4):942–950
9. Shende AM. The investigation and comparative study on properties of steel fibre reinforced concrete members. Thesis
10. Modak P, Moghe SD (1998) Design & development of a human powered machine for the manufacture of lime-fly-ash-sand-bricks. J Int Hum Powered Veh Assoc U.S.A. (Hum Power) 13:3–8
11. Moghe SD, Modak JP (1998) Design and development of a human powered machine for the manufacture of lime-fly-ash-sand bricks. Hum Power 13:3–8

Recycling Potential of Sugarcane Biomass Ash as an Improved Pozzolanic Binder and Sustainable Masonry Product

Vasudha D. Katare and Mangesh V. Madurwar

Abstract The population growth, increased demand of construction materials, and its higher costs have caused the need to investigate sustainable and cost-effective construction materials. Around the world, cement is an important construction ingredient. Cement production plays a significant role in global CO_2 emissions. Investigating an alternative supplementary cementitious/pozzolanic material could effectively minimize the CO_2 emissions. The sugarcane biomass ash (SCBA) is an agro-industrial solid waste. The reviewed literature reports the wide usage of SCBA as a pozzolanic material. The pozzolanic behavior mainly depends upon the factors, namely particle fineness and the loss on ignition value. The pozzolanic characterization of SCBA was quantified by various methods, namely pozzolanic activity index, electrical conductivity, and the Chapelle activity. The study revealed that the as-received/raw SCBA has low pozzolanicity. Its application as a raw material in manufacturing bricks was studied. The present chapter also investigates the methodology for improving the pozzolanic characterization of raw SCBA. The devised mechanical and thermal treatment significantly enhanced the pozzolanicity of raw SCBA. Its application in the blended cementitious mortar was investigated. The research study serves the purpose of effective solid waste management and the development of innovative sustainable construction materials.

Keywords Sugarcane biomass ash · Solid waste management · Pozzolanicity · Treatment · Bricks

V. D. Katare (✉)
Department of Civil Engineering, College of Engineering Pune, Pune, India

M. V. Madurwar
Department of Civil Engineering, Visvesvaraya National Institute of Technology, Nagpur, India

B. Laishram and A. Tawalare (eds.), *Recent Advancements in Civil Engineering*, Lecture Notes in Civil Engineering 172,
https://doi.org/10.1007/978-981-16-4396-5_22

1 Introduction

The solid wastes management is one of the burning issues in India. The accumulated solid waste is a burden to the environment. Reusing such solid wastes in the manufacturing of building materials is a sustainable solution to the environmental pollution, higher costs of building materials, and the land disposal problems. After Brazil, India is the second largest producer of sugarcane crop. The sugar industry generates the major by-product called as 'Bagasse,' i.e., sugarcane biomass. This by-product is further utilized for the generation of electricity, leaving behind its ash as a waste product, i.e., sugarcane biomass ash (SCBA) [1]. The SCBA has pozzolanic properties. In recent years, it has been widely utilized as a mineral admixture. The sugar industrial processing has a major impact on the pozzolanicity of SCBA [2]. There are many parameters on which the pozzolanic characterization of SCBA depends, namely the crop origin, soil conditions, industrial combustion process (temperature and duration), and cooling duration [3]. The particle size and its loss on ignition value are the two major factors. The ultra-ground SCBA accelerates the pozzolanic reaction rate. The micro-sized particles improve the packing density of the cement mixes [4, 5]. The densification can protect the reinforcement steel from corrosion action by restricting the entry of water from the pore spaces. So it indirectly helps to make the structure more durable [6–9]. The industrial processing of sugarcane biomass results into its improper combustion. The black color of SCBA reflects the unburnt or partially burnt carbonaceous matter. The presence such organic matter hampers the pozzolanic reaction. If such SCBA is thermally treated, the black color SCBA turns into whitish gray color. Such a pure form of SCBA is suitable for the pozzolanic activity [10].

Brick is one of the most important units of a building. Many attempts were made to incorporate the industrial wastes (sewage sludge, fly ash, ground granulated blast furnace slag, steel industry dust, and red mud) in the manufacturing of the bricks [11–14]. A significant amount of energy is spent in the making of building materials by the conventional way [15]. The bricks can be made energy efficient and affordable by incorporating the SCBA in it [16]. The method is need to be devised to get the ultra-ground and thermally treated SCBA to improve the pozzolanicity.

The present chapter focuses on the characterization of the SCBA. It investigated the methodology for the mechanical and thermal treatment of SCBA. Further, the pozzolanic properties were evaluated by various methods, namely pozzolanic activity index, reactive silica, electrical conductivity, and Chapelle activity. Further, the relation between pozzolanic properties with respect to its grinding duration was evaluated using ANOVA technique. The bricks were designed and developed using this combination of as-received SCBA, crusher dust, and lime. The optimum combination of brick was determined. The physico-mechanical properties were tested on the developed bricks.

2 Methodology Adopted

2.1 Characterization of Raw Material

The collection of sugarcane biomass ash (SCBA) was made from M/s Manas Agro-industries and Infrastructure Limited, Nagpur (MS), India. The collected SCBA was blackish gray in color. The characterization methods of SCBA are tabulated in Table 1.

53 grade OPC (confirming to IS 12269: 2013), natural river sand, calcium hydroxide (saturated solution), phenolphthalein indicator, and hydrochloric acid were used in the analysis of pozzolanicity [17].

In the manufacturing of bricks, the blend of SCBA and lime (confirming to IS 712: 1984) was used as a binder. Crusher dust was used as a replacement to the natural river sand (size 6 mm down). Both the materials, lime and crusher dust, were collected from the local supplier of Nagpur (MS), India [18].

2.2 Development of an Improved Pozzolanic Binder

An improved pozzolanic binder was developed from raw SCBA by considering the two factors, namely (1) particle size and (2) loss on ignition value.

The developed pozzolanic binder will act as a partial substitute of cement. The particle size of substitute material and the parent material should be nearly same for better results. So, for reducing the particle size of SCBA, the vibrating cup mill machine was used. The machine is based on the frictional force. As the ash is soft-natured material, frictional force plays a substantial role in breaking the particles of SCBA. As this is a laboratory-based study, vibrating cup mill was used. For large-scale study, high energy ball mills can be used for reducing the particle size. The samples were denoted as "SCBA: M<grinding duration in min>," where M stands for the mechanical treatment.

The raw SCBA has many impurities such as unburnt or partially burnt organic matter, and carbonaceous matter. The black color of SCBA reflected the presence of carbon in it. Such impurities are the main reason for hampering the strength of

Table 1 Characterization methods of SCBA

Property	Method
Granulometric analysis	Saturn digitizer model 5205-laser particle size analyzer
Microstructure	Scanning electron microscope
Chemical composition	PANalytical PW2403 MagiX
XRD analysis	PANalytical X'Pert Pro X-ray diffraction
Physical properties	IS 1727: 1967 (reaffirmed 2004)
Thermal analysis	TG analysis

cement when partially replaced by the same. The loss on ignition value can be improved by the thermal treatment. The thermal treatment makes the SCBA thermally stable by combusting all the impurities. After thermal treatment, the SCBA turns into its pure form having a chemical composition dominated by silicon dioxide percentage with the reduced value of loss on ignition. The samples after thermal treatment were denoted as "SCBA: T." The samples after both the treatments (i.e., mechanical as well as thermal) were named as "SCBA: M<grinding duration in min>: T, where T stands for thermal treatment.

2.2.1 Pozzolanicity Methods

The pozzolanicity of SCBA was quantified by four methods, namely electrical conductivity, Chapelle activity, reactive silica, and strength activity index.

Electrical conductivity gives the measure of pozzolanicity of the sample. The drop in electrical conductivity of the saturated suspension of $Ca(OH)_2$ (200 ml) after adding 5 gm of SCBA in it is nothing but its pozzolanicity. Luxan et al. (1989) has given the experimental procedure [19].

Chapelle activity is a titration-based method. This method allows the pozzolanic reaction between silica and calcium hydroxide. It gives an amount of fixed calcium oxide by deducting an amount calcium oxide obtained after the titration from its initial amount [20].

The amount of non-reactive silica was washed off by acid-washing treatment. So, the reactive silica is calculated by deducting the non-reactive part of silica from the total silica amount. The followed procedure is specified in Indian Bureau of Mines Manual Report 2012 [21].

The strength activity index was carried out as specified in ABNT NBR 5752: 1992 [22]. The mortar blocks were prepared by the procedure as specified in IS 2250: 2000 [23]. 35% part of OPC was replaced by SCBA in blended mortar blocks, whereas the control mortar blocks were prepared by incorporating 100% OPC. The percentage ratio of 28 days compressive strength of sample mortar block to the control mortar block is known as strength activity index.

2.3 Development of Composite Bricks

Different mix compositions of as-received SCBA, lime, and crusher dust were prepared in making composite bricks. Lime proportion was kept constant throughout the mix design trials as 20% by weight. The percentage weight proportion of crusher dust and SCBA was varied from 0–30% to 80–50%, respectively. The water-to-mix ratio was kept in the range of 0.25–0.32. The homogeneous mix was obtained in the mixture by mixing the ingredients for about 4–5 min. The freshly prepared mix was filled in the brick molds of size 230 mm × 110 mm

Table 2 Details of the brick composition

Sample No.	SCBA: crusher dust: lime
1	0.80: 0.00: 0.20
2	0.75: 0.05: 0.20
3	0.70: 0.10: 0.20
4	0.65: 0.15: 0.20
5	0.60: 0.20: 0.20
6	0.55: 0.25: 0.20
7	0.50: 0.30: 0.20

× 80 mm. The mix was pressed in molds with the help of pressure gauge having the pressure of about 20 MPa. After this, the sample bricks were taken out of the molds and kept for curing. The brick samples were named as detailed in Table 2.

2.3.1 Experimentation Methods of Developed Bricks

Water absorption [IS 3495 (Part-II): 1992] [24], dry density [IS 2185 (Part-I): 1979] [25], efflorescence [IS 3495 (Part-III): 1992] [24], and compressive strength [IS 3495 (Part-I): 1992] [24] experiments were carried out on the designed bricks.

3 Results and Discussion

3.1 Physico-chemical Characterization of Raw Material

Figure 1 shows the granulometric distribution of the SCBA particles. Due to the sliding and vibratory action in vibratory cup mill, faster breakage of particles was observed. The particle size reduced significantly only after the grinding duration of 30 s. For the further grinding durations, distinct particle size distribution curves were not observed. But an increased grinding duration reduced the particle size. The D50 (average particle size) of as-received SCBA was reduced from 55.009 to 3.521 µm after the grinding for 15-min duration.

Figure 2 shows the microstructure of the as-received SCBA and SCBA: M15 particles. Irregularly shaped particles were observed in as-received SCBA, but most of the particles were either cellular or prismatic. Figure 2b shows the microscopic view of milled SCBA: M15 particles. The observed microstructure was porous.

The maximum component of oxides composition present in SCBA: T was silica (SiO_2) (79.50%). The loss on ignition percentage (LOI) value was less than 12%. The MgO and SO_3 percentage was observed to be less than 5% and 3%, respectively (Table 3). The percentage of $SiO_2 + Al_2O_3 + Fe_2O_3$ was 81.65%. The SCBA: T satisfy all the allowable limits of oxides composition as given in IS 3812: 1981 [26].

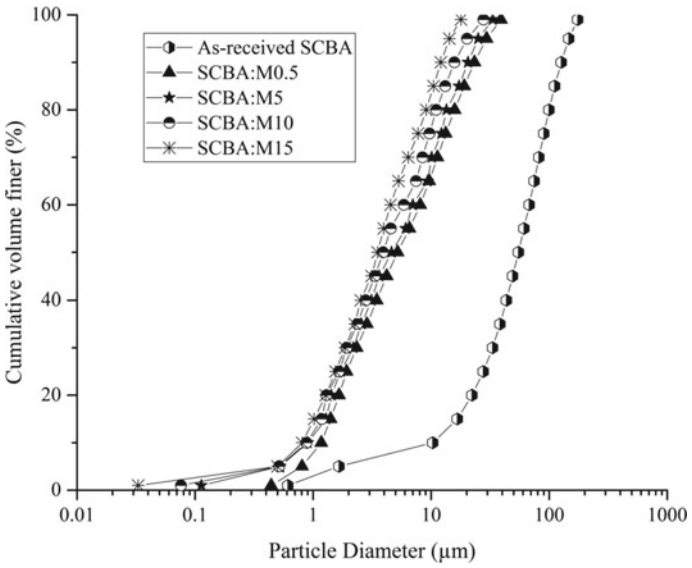

Fig. 1 Particle size distribution of SCBA

The X-ray diffractograms of as-received SCBA and SCBA: M15: T are shown in Fig. 3. The phases observed in as-received SCBA were quartz, cristobalite, and calcite. A large number of high-intensity peaks indicated the crystalline nature of the particles, while the X-ray diffractogram of SCBA: T was scattered in wide angular range with low intensity and a single peak. Purely amorphous phase was seen in SCBA: T.

The physical properties are tabulated in Table 4. The lightweight carbonaceous matter and fibrous particles present in SCBA decreased the specific gravity and bulk density of the particles. But due to such particles, the water requirement of SCBA has increased to achieve the required consistency. The setting time of SCBA was also observed to be higher as compared to the cement because of the same reason. The drying shrinkage and lime reactivity were observed to be 0.132% and 2.6 N/mm^2, respectively. The lime reactivity depends upon the presence of amorphous silica in the sample. But the crystalline phases were observed in as-received SCBA so that the lime reactivity was observed to be lesser (2.6 N/mm^2) than the permissible limit (4.5 N/mm^2). A very lesser expansion of 0.082% was observed in the autoclave soundness test.

Figure 4 shows the thermal stability of the SCBA sample. The increased temperature shows different zones of the mass change. Mass loss up to 500–600 °C temperature was due to the evaporation of water molecules present in microstructural pores. Further zone of mass change was occurred due to the thermal degradation of the organic matter (carbonaceous and fibrous matter). At last, an increase in the mass was seen due to the thermal sintering action.

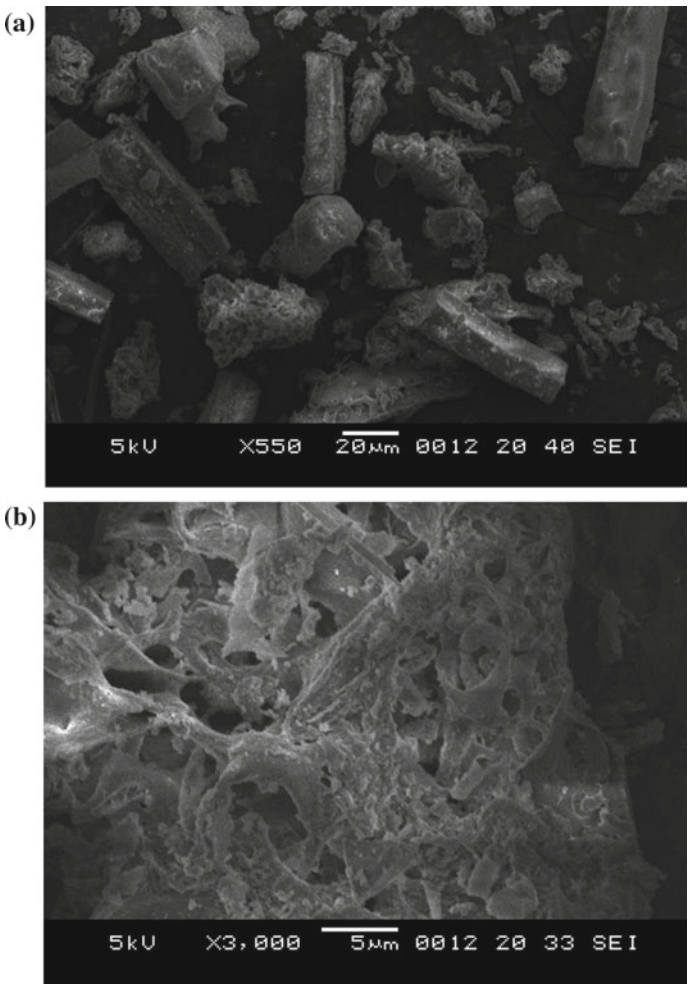

Fig. 2 Scanning electron microscope analysis of **a** as-received SCBA, **b** mechanically treated SCBA

Table 3 Chemical composition of SCBA: T

Oxides (%)	SiO_2	LOI	P_2O_5	CaO	MgO	Fe_2O_3	Al_2O_3	MnO_2	Na_2O
SCBA: T	79.50	4.95	3.20	3.14	2.07	1.12	1.03	0.13	0.12

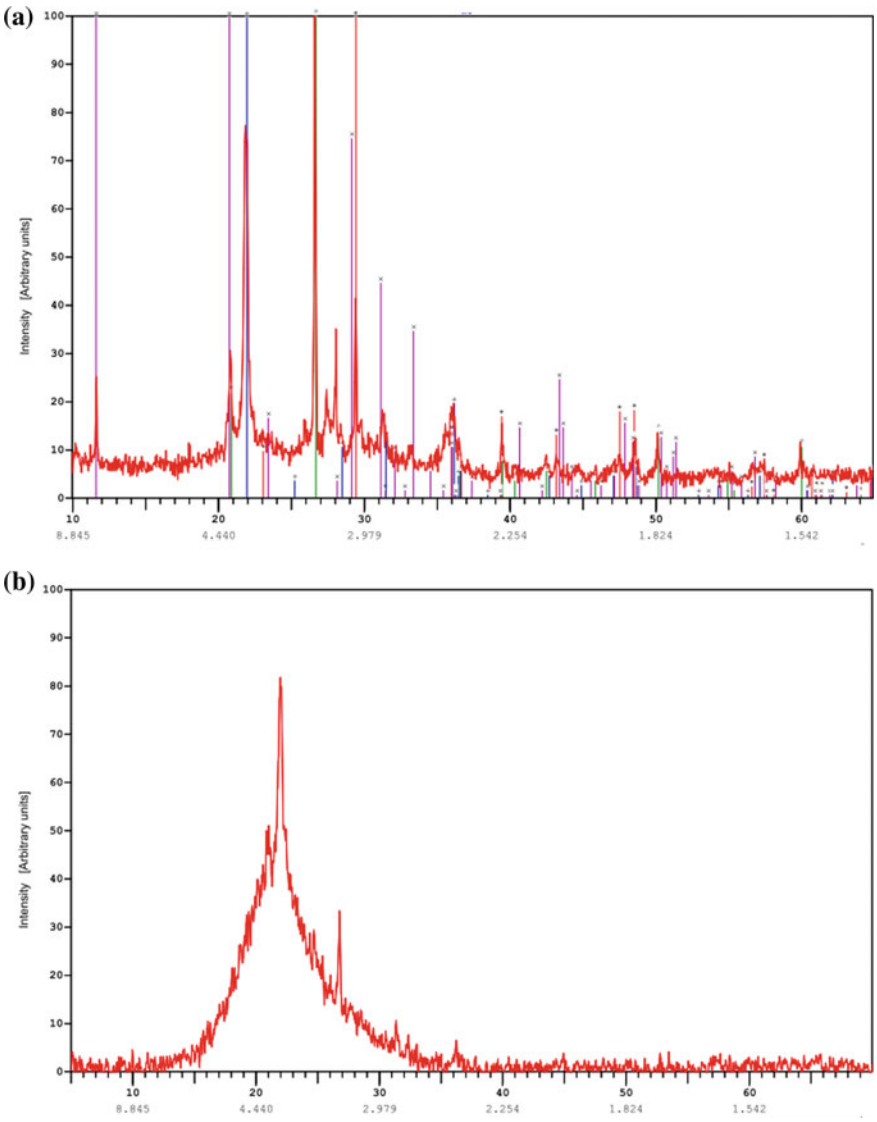

Fig. 3 X-ray diffraction phases of **a** as-received SCBA, **b** SCBA: M15: T

3.2 Pozzolanicity Characterization

Figure 5 gives the relation of pozzolanic activity index and reactive silica with respect to the grinding duration. The relation was established using ANOVA technique. The statistical analysis gives a reliable and significant regression model. Both the properties were improved with respect to the grinding duration. Nonlinear

Table 4 Physical properties of as-received SCBA

Sr. No.	Physical properties	Results	Permissible limit (BIS 3812 (Part 1): 2013)
1.	Specific gravity	1.95	–
2.	Bulk density (kg/l)	0.302	–
3.	Setting time (min)		
	Initial Final	190 275	–
4.	Consistency (%)	36.5	–
5.	Drying shrinkage (%)	0.132	–
6.	Lime reactivity (N/mm^2)	2.6	Min 4.5
7.	Soundness by autoclave (%)	0.082	–

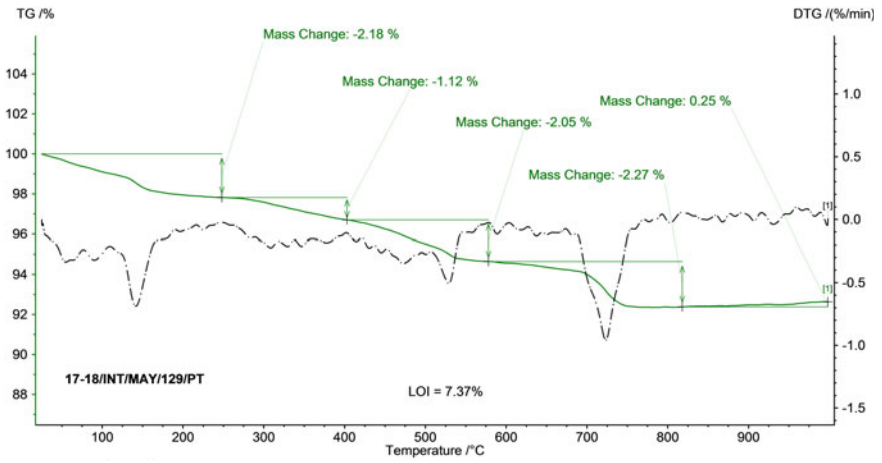

Fig. 4 Thermo-gravimetric analysis of SCBA

logarithmic fitting curve pattern was observed. The respective equations are shown in Fig. 5. The range of R2 value for pozzolanic activity index and reactive silica was found to be 0.95–0.96 and 090–0.96, respectively. The pozzolanic behavior of SCBA was significantly improved by reduced particle size. Further improvement in the pozzolanicity was observed due to the thermal treatment.

Figure 6 gives the relation of electrical conductivity and Chapelle activity with respect to the grinding duration. The drop in electrical conductivity of calcium hydroxide suspension was observed due to the calcium hydroxide [$Ca(OH)_2$] fixation on the surface area of reactive SCBA. The greater the drop in electrical conductivity of $Ca(OH)_2$ suspension, the more is the pozzolanic activity. The as-received and thermally treated particles of SCBA followed the nonlinear logarithmic curve pattern for the electrical conductivity drop property. The R2 value of

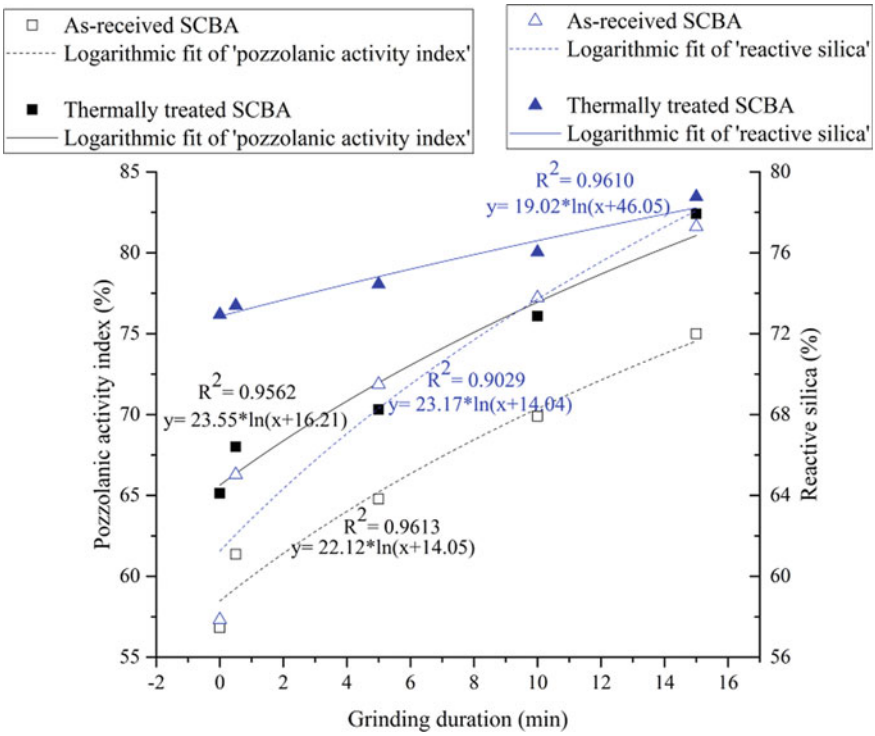

Fig. 5 Relation of pozzolanic activity index and reactive silica with respect to grinding duration

electrical conductivity property for the as-received SCBA and thermally treated SCBA was observed to be 0.87–0.93. The similar logarithmic pattern was observed for Chapelle activity. As the grinding duration increased, the Chapelle activity was also found to be increased for both the particles (as received and thermally treated). The R2 value of as-received and thermally treated particles for Chapelle activity was 0.95 and 0.93, respectively.

3.3 Bricks Characterization

3.3.1 Physico-mechanical Properties

The physico-mechanical properties such as compressive strength, density, water absorption, and efflorescence were found out. Figure 7 shows the compressive strength and density of the brick samples. It shows that as the SCBA content in brick composition increased, the density was found to be decreased. Increase in SCBA proportion from 50 to 80% decreased the density by 25%. The maximum

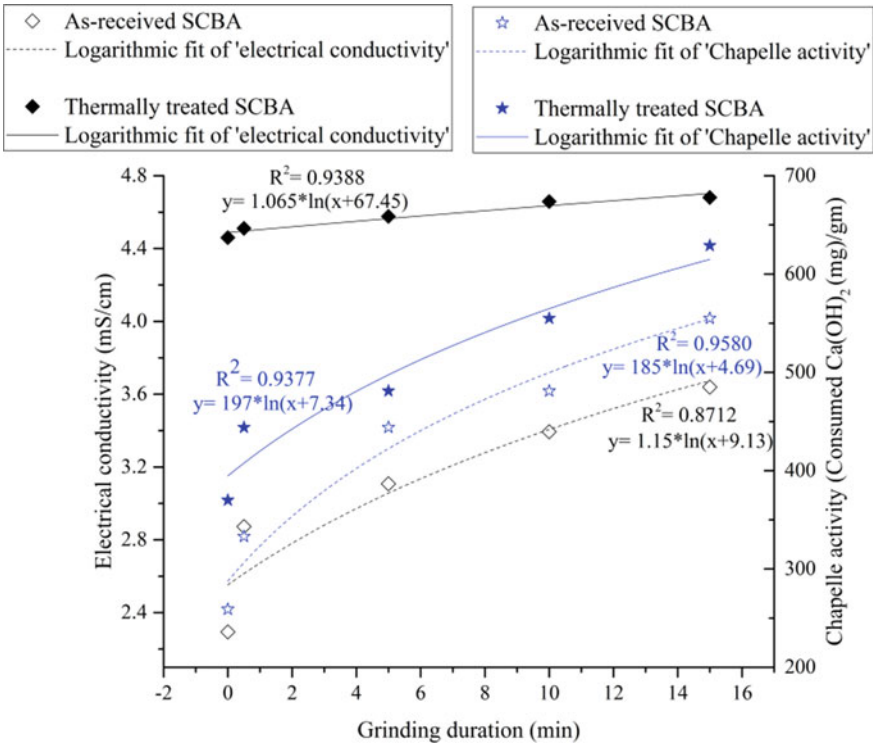

Fig. 6 Relation of electrical conductivity and Chapelle activity with respect to grinding duration

density was obtained for mix sample 7, which was 33% lesser than that of commercial clay and fly ash bricks. The minimum density was obtained for the mix sample 1, which was found to be 42% lesser than that of commercial clay and fly ash bricks. All the mix composition samples meet the criterion of Class 3.5 of burnt clay brick of IS 1077: 1992 [27]. The increased SCBA content (from 50 to 80%) resulted in the reduction in compressive strength by 50%. The mix 7 has the maximum compressive strength among all other developed samples. The obtained compressive strength was found to be 188% higher as compared to the commercially available clay bricks and comparable to the commercial fly ash brick.

Not much variation in water absorption values of all the brick samples was observed. All the water absorption values were approximately 20% (Fig. 8). The water absorption was higher because of the water holding property of SCBA. No efflorescence was seen on the surface area of brick when soaked in water for 24 h.

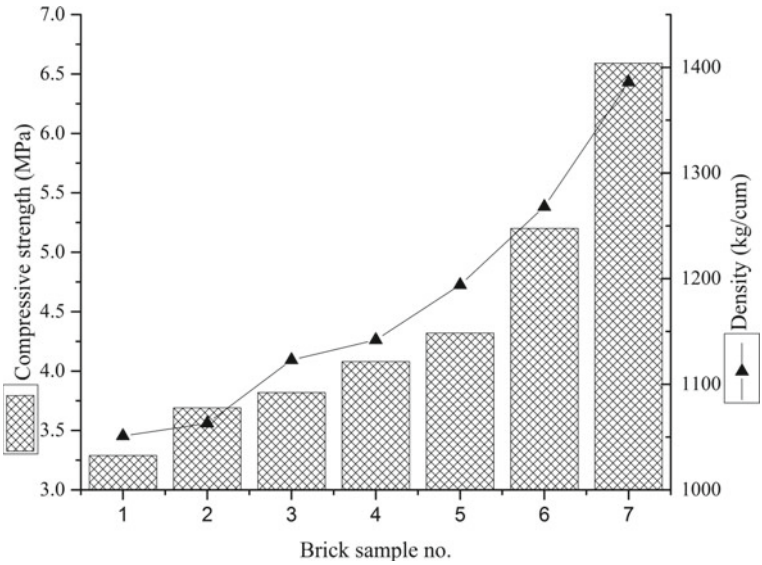

Fig. 7 Compressive strength (MPa) and density (kg/cum) of the developed bricks

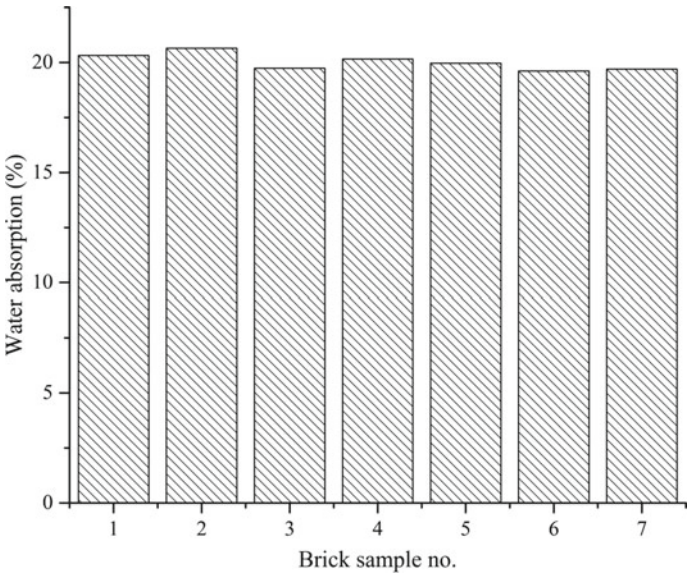

Fig. 8 Water absorption (%) of the developed bricks

4 Conclusions

In this research study, an attempt is made to develop the high performance pozzolanic material and the sustainable, light weight masonry product, i.e., bricks using the SCBA. The performance was compared with the respective control/ conventional product.

The suitability of the SCBA as a pozzolana or supplementary cementitious material was proved in its physico-chemical characterization. The mechanical and thermal treatments were investigated to improve the pozzolanic behavior of SCBA. The combination of both the treatments gives the further improved results of pozzolanic properties. All the pozzolanic properties (pozzolanic activity index, reactive silica, electrical conductivity, and Chapelle activity) established a nonlinear logarithmic curve pattern against the grinding duration.

The mix composition of SCBA, crusher dust, and lime resulted in an innovative sustainable and lightweight brick. The mix composition having SCBA (50%), crusher dust (30%), and lime (20%) has resulted in the compressive strength of 6.59 MPa. The developed brick satisfied the requirement given in IS 2185 (Part-I): 1979 [25] and SP 21: 1983 [28] for a building material. Various applications of SCBA in the manufacturing of building materials automatically solve its disposal problems. The recycling of solid wastes in the making of building materials could solve the environmental problems and conserve the natural resources for future generations.

Acknowledgements The authors would like to thank Visvesvaraya National Institute of Technology (VNIT), M/s Manas Group of Industries, Jawaharlal Nehru Aluminium Research Development and Design Centre (JNARDDC), Indian Bureau of Mines (IBM), M/s Maharashtra Enviro Power Limited (MEPL), M/s Heat Treat Well, M/s Geotech services, National Environmental Engineering Research Institute (NEERI), Nagpur, for the technical and other support.

References

1. Madurwar MV, Mandavgane SA, Ralegaonkar RV (2014) Use of sugarcane bagasse ash as brick material. Curr Sci 107(6):1044–1051
2. Cordeiro GC (2016) Use of sugar cane bagasse ash and rice husk ashes as a mineral admixture in concrete. DSc thesis, Univ Fed do Rio Janeiro, Brazil
3. Katare VD, Madurwar MV (2017) Experimental characterization of sugarcane biomass ash—a review. Constr Build Mater 152:1–15. https://doi.org/10.1016/j.conbuildmat.2017.06.142
4. Goldman A, Bentur A (1993) The influence of microfillers on enhancement of concrete strength. Cem Concr Res 23(2):962–972
5. Katare VD, Madurwar MV (2020) Pozzolanic performance resemblance of milled sugarcane biomass ash using different pozzolanicity test methods. Adv Cem Res 32(5):205–215
6. Neville AM, Brooks JJ (1987) Concrete technology. Prentice Hall, United Kingdom, pp 242–246

7. Madani H, Bagheri A, Parhizkar T, Raisghasemi A (2014) Chloride penetration and electrical resistivity of concretes containing nanosilica hydrosols with different specific surface areas. Cem Concr Compos 53:18–24
8. Nili M, Ehsani A (2015) Investigating the effect of the cement paste and transition zone on strength development of concrete containing nanosilica and silica fume. J Mater Des 75: 174–183
9. Mehta PK, Monteiro PJM (2017) Concrete: microstructure, properties and materials. McGraw Hill, New York
10. Brindley G, Nakahira M (1958) A new concept of the transformation sequence of kaolinite to mullite. Nature 181:1333–1334
11. Amritphale SS, Patel M (1987) Utilization of red mud, fly ash for manufacturing bricks with pyrophyllite. Silic Indus 52(3–4):31–35
12. Malhotra SK, Tehri SP (1995) Building materials from granulated blast furnace slag—some new prospects. Indian J Eng Mater Sci 2(2):80–82
13. Domlnguez EA, Ullmann R (1996) Ecological bricks' made with clays and steel dust pollutants. Appl Clay Sci 11(2–4):237–249
14. Tay BJ (1987) Bricks manufactured from sludge. J Environ Eng 113(2):278–284
15. Buchanan AH, Honey BG (1994) Energy and carbon dioxide implications of building construction. Energy Build 20(3):205–217
16. Madurwar MV, Mandavgane SA, Ralegaonkar RV (2015) Development and feasibility analysis of bagasse ash bricks. J Energy Eng 141(3):04014022
17. Bureau of Indian Standards (BIS) (2013) Ordinary Portland cement-specifications. IS: 12269, New Delhi, India
18. Bureau of Indian Standards (BIS) (1984) Spcification for building lime. IS: 712, New Delhi, India
19. Luxán MD, Madruga F, Saavedra J (1989) Rapid evaluation of pozzolanic activity of natural products by conductivity measurement. Cem Concr Res 19(1):63–68
20. Raverdy M, Brivot F, Paillere A, Bron R (1980) Appreciation de l'activite pouzzolanique de constitutes secondaires. In: Proceedings of 7th Congres International de la Chimie des Ciments, Paris, France, pp 3–6
21. Indian Bureau of Mines (IBM) (2012) Manual of procedure for chemical and instrumental analysis of ores, minerals, ore dressing products and environmental samples, Nagpur
22. Brazilian Association of Technical Standards (1992) Pozzolans–pozzolanic activity—determination of pozzolanic activity index with Portland cement. ABNT NBR 5752, Rio de Janeiro, Brazil
23. Bureau of Indian Standards (BIS) (2000) Code of practice for preparation and use of masonry mortar. IS: 2250, New Delhi, India
24. Bureau of Indian Standards (BIS) (1992) Methods of tests of burnt clay building bricks, part 1 determination of compressive strength, part 2 determination of water absorption, part 3 determination of efflorescence, Part 4: determination of warpage. IS: 3495, New Delhi, India
25. Bureau of Indian Standards (BIS) (2005) Concrete masonry units, Part 1: hollow and solid concrete blocks. IS: 2185, New Delhi, India
26. Bureau of Indian Standards (BIS) (2013) Pulverized fuel ash- specification: for use as pozzolana in cement, cement mortar and concrete. IS 3812 (Part 1), New Delhi, India
27. Bureau of Indian Standards (BIS) (1992) Common Burnt clay building bricks -specification. IS: 1077, New Delhi, India
28. Bureau of Indian Standards (BIS) (1983) Summaries of Indian standards for building materials (first revision). SP: 21, New Delhi, India

Application of Biocementation for Augmentation of Mechanical Properties of Fly Ash Concrete

Snigdha P. Bhutange and M. V. Latkar

Abstract The poignant carbon footprint contributed by construction industry is one of the most concerned areas for researchers. Concrete is the material that is used worldwide for construction purposes on a large scale. Search for a novel substitution of cement in concrete has become the most emphasized practice in past decades. Fly ash is one of the partial cement replacement materials in concrete which is considered to be a sustainable practice as it helps to curtail environmental harms. However, partially replacing cement with fly ash compromises the strength of concrete significantly. Biocementation is a recently emerged green technique that improves the properties of a wide range of construction materials by calcium carbonate precipitations produced by microbial activities. The current investigation focuses on application of biocementation in fly ash amended concrete. Results showed substantial improvement in characteristics of Fly Ash Concrete (FAC).

Keywords Concrete · Fly ash · Calcium carbonate · Biocementation

1 Introduction

Fine powder that is generated as a by-product of burning pulverized coal in power plants is known as fly ash. Fly ashes are seen to bear pozzolanic and/or cementitious properties which is why they can be amended with concrete [1]. Incorporation of fly ash in cement concrete has been proved to be a sustainable solution as it is known to have many environmental and health hazards if released in an open environment [1, 2]. Even though the utilization of fly ash in concrete is a sustainable practice, incorporation of high percentages of fly ash in concrete by replacing cement results in concrete having comparatively lower strength [3, 4]. Biocementation has the potential to compensate for the compromised strength resulted from the replacement of cement with fly ash [4, 5].

S. P. Bhutange (✉) · M. V. Latkar
Civil Engineering Department, Visvesvaraya National Institute of Technology (VNIT), Nagpur, Maharashtra 440010, India

B. Laishram and A. Tawalare (eds.), *Recent Advancements in Civil Engineering*, Lecture Notes in Civil Engineering 172,
https://doi.org/10.1007/978-981-16-4396-5_23

Microbially induced calcium carbonate precipitation (MICCP) is a process that occurs in nature and has molded the entire globe [6–8]. To count a few magnificent examples of calcification existing in nature, we have ant hills and coral reefs in terrestrial and aquatic ecosystems, respectively. Taking note of nature, many researchers have tried to utilize this naturally occurring phenomenon for the betterment of construction materials. Among many sustainable technologies, microbially induced calcification has proven to improve the properties of construction materials significantly [9]. Urea hydrolysis is the most eminent pathway among the several pathways of microbial calcification due to its easily controllable $CaCO_3$ producing mechanism [10].

Carbonate ions (CO_3^{2-}) are produced as a part of the metabolism of bacterial mass and their conversion to $CaCO_3$ when provided with Ca^{2+} is the principle involved in MICCP. The following flow chart (Fig. 1) explains the sequence of processes occurring in MICCP [11, 12].

Incorporation of bacterial mass into the matrix of construction materials is found to enhance their mechanical strength and durability. This happens due to coverage of microvoids within the matrix by $CaCO_3$ precipitations formed due to bacterial activity [13, 14].

In their metabolic reactions, few bacterial species secrete urease enzymes. This enzyme essentially initiates the urea hydrolysis reaction. Many researchers employ this bacterial behavior for the betterment of construction materials.

Achal et al. (2010) incorporated *Bacillus* sp. CT-5 in cement mortar specimens resulting in about 33% increment in compressive strength and 17% diminution in water absorption after four weeks of curing as compared to plain mortar specimens devoid of bacteria [15]. Achal et al. (2011) encouraged the utilization of industrial waste, corn steep liquor (CSL) to grow ureolytic bacteria by superseding the conventional expensive growth media for producing calcium carbonate. Water absorption of bacterially treated specimens was found to be reduced by five times than control specimens [16]. Achal et al. (2011) extended the application of biocementation for the improvement of fly ash amended cement mortar. Study on mortars with 10, 20 and 40% concentrations of fly ash was undertaken. Bacterial

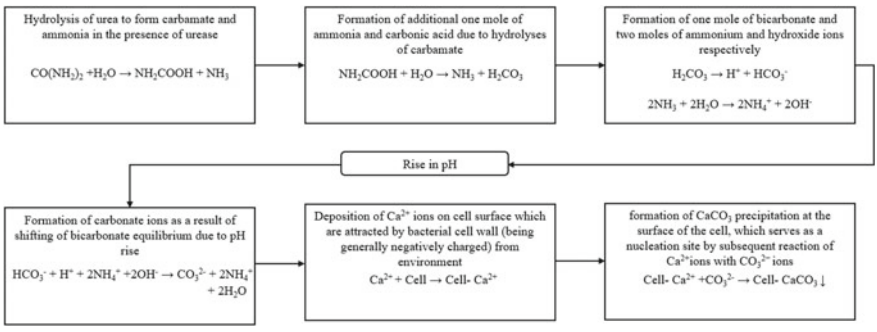

Fig. 1 Sequence of processes occurring in MICCP

activity resulted in an enhancement of 19, 14 and 10% of compressive strength for 10, 20 and 40% of fly ash concentration of mortar respectively as compared to control specimens. Control mortar specimen showed three times more water absorption than specimens treated with bacteria [17]. Chahal et al. (2012) added *Sporosarcina pasteurii* in FAC mix and observed an increment of 22% in compressive strength (28 days). Water absorption of bacterial fly ash concrete (FAC) specimen was four times less than control specimen [18].

The aim of the current study is to improve characteristics of fly ash infused concrete by using rhizospheric soil rich in mixed bacterial populations. This study promotes the use of low cost bacterial growth nutrients. Grinded lentil seeds were used to grow bacterial culture instead of commercially available peptone which is expensive. D-glucose as a source of carbon was replaced by sugar. Lentil seeds contain 25 g proteins/100 g dry weight [19].

2 Materials Used and Methodology

2.1 Cement, Aggregates, Water and Fly Ash

In the current study ordinary Portland cement of grade 53 and locally available natural river sand (fine aggregate) confirming to IS 383: 1970 of zone II having a specific gravity of 2.60 were used [20]. Coarse aggregates having a maximum size of 20 mm and below as per IS 383: 1970 were used in this study [20]. Locally available tap water confirming to IS 456: 2000 was used throughout the study [21]. Class F fly ash obtained from Koradi thermal power plant, Maharashtra, India was used [22]. Figure 2 shows the chemical components of cement, sand and fly ash in %.

2.2 Bacterial Source, Bacterial Solution and Control 1 Solution

For the present study, rhizospheric soil collected from the garden was used as a mixed bacterial source. Bacterial solution was prepared using tap water. An attempt was made to use low cost ingredients to provide nutrients to grow bacteria. Table 1 shows the composition of the growth medium used to grow a mixed culture of bacteria.

All the ingredients shown in Table 1 were added in water. The prepared solution was then kept in an incubator at 37 °C for 24 h. To confirm the presence of cell biomass in the resulting solution, optical density (OD) was measured in a spectrophotometer at 600 nm after incubation [23]. The optical density was 0.860, thus indicating sufficient bacterial growth. The supernatant of the soil-bacterial mix solution was then decanted from the soil to get a bacterial solution devoid of soil.

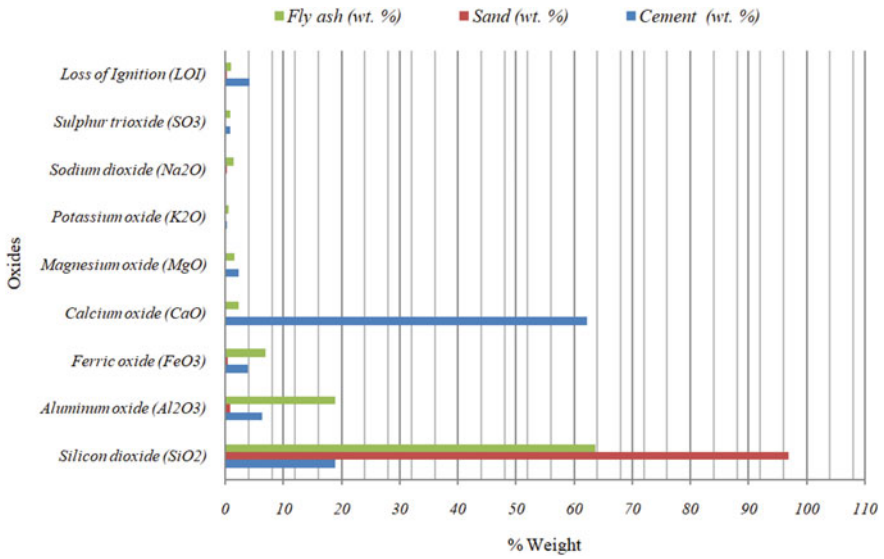

Fig. 2 Chemical component of cement, sand and fly ash in %

Table 1 Composition of bacterial solution

Sr. No.	Nutrient source	Ingredient
1	Bacterial source	Rhizospheric soil
2	Protein source	Lentil seed (*Lens culinaris*) powder
3	Vitamin source	Meat extract
4	Calcium source	Sugar

Addition of urea as a substrate and calcium hydroxide as a calcium source was done. 5 g/l of urea was added. Around 1.2 times of urea (which was calculated stoichiometrically), i.e., 6 g/l calcium hydroxide was added. Also, the pH value of the solution at every stage was measured as it indicates the various stages of ureolysis reaction. Figure 3 shows the pH of the bacterial solution at different stages.

For the preparation of control 1 solution, all ingredients were added in a similar manner except bacterial source (soil). Control 1 solution was prepared with an intention to monitor whether there are any effects of added ingredients on the performance of FAC. Table 2 shows the constituents of control, control 1 and bacterial solution.

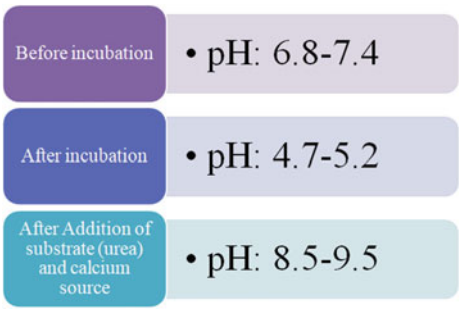

Fig. 3 pH of the bacterial solution at different stages

Table 2 Constituents of control, control 1 and bacterial solution

Sr. No.	Constituent (g/l of water)	Control solution	Control 1 solution	Bacterial solution
1	Soil	0	0	200
2	Lentil seed powder	0	10	10
3	Meat extract	0	3	3
4	Sugar	0	0.5	0.5
5	Urea	0	5	5
6	Calcium hydroxide	0	6	6

2.3 Specimen Preparation

The mix design was done as per IS 10262: 2009 to develop 28 days compressive strength of 30 MPa and slump of 70–100 mm [24]. Tap water, control 1 solution and bacterial solution were used to cast control specimens, control 1 specimens and bacterial FAC specimens respectively. Figure 4 shows details of specimens with dimensions required for different tests as per standards. Proportions for the concrete mix are given in Table 3. All specimens were cast using a fresh mix, compacted well and vibrated using a mechanical vibrator. Standard procedures were followed for demolding and curing of the specimen. Specimens were prepared and tested for compressive strength and water absorption in triplicates for 3, 7, 14, 28 and 90 days considering three trials for each specimen case. Similarly, split tensile strength, flexural strength test and UPV test were performed for 28 and 90 days respectively. In other words, an average total of nine cubes was taken for all strength tests. For all durability tests, average values obtained for three specimens were taken.

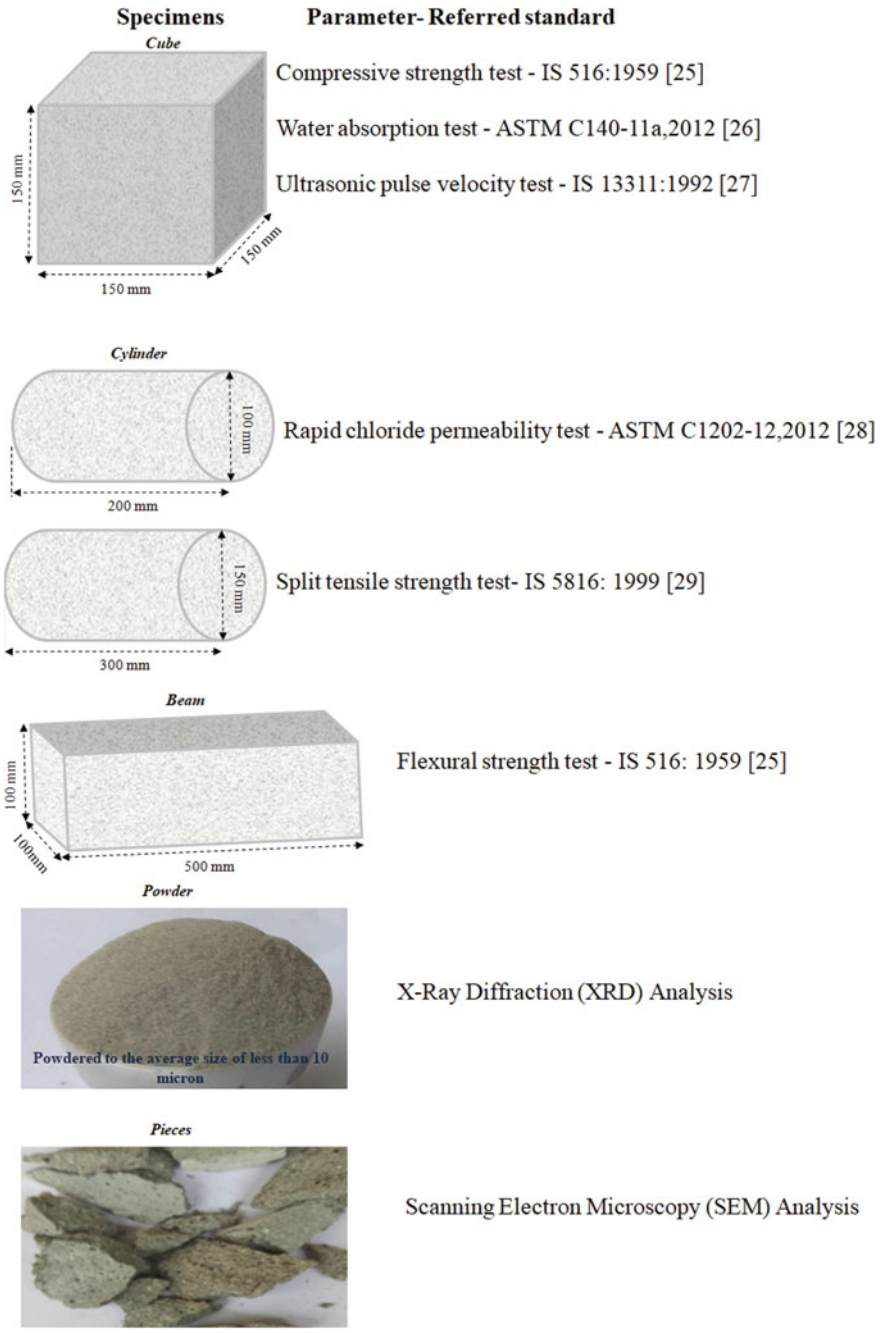

Fig. 4 Details of specimens

Table 3 Mix proportion of concrete for 1 m^3

Ingredients	Quantity in kg/m^3
Cement	280
Fly ash	70
Total water	188
Sand	843
Coarse aggregate	1165

3 Results and Discussion

3.1 Compressive Strength

Compressive strength test of control, control 1 and bacterial FAC specimens were done by the standard procedure given in IS 516: 1959 [25]. Figure 5 shows the average compressive strengths of control, control 1 and bacterial FAC specimens for all the adapted curing periods. Results show that the compressive strength of bacterial FAC specimens was around 7, 11, 13, 15 and 16% more than control specimens for 3, 7, 14, 28 and 90 days respectively. However, compressive strength values of control and control 1 specimens showed no significant difference. Thus, this is clear that the added ingredients do not have any prominent effect on the performance of specimens and only the bacterial $CaCO_3$ precipitation is responsible for increment in strength.

3.2 Water Absorption

Standard method mentioned in ASTM C140-11a, 2012 [26] was followed for testing the water absorption of the specimens. The water absorptions of the specimens were calculated by deducting the dry weights from saturated weights.

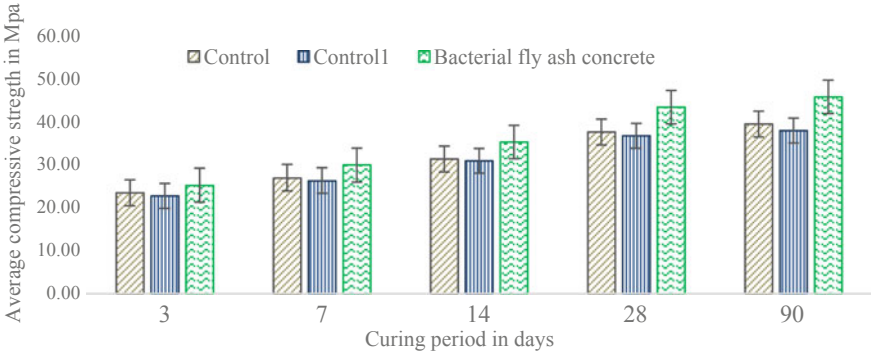

Fig. 5 Average compressive strength versus curing period in days

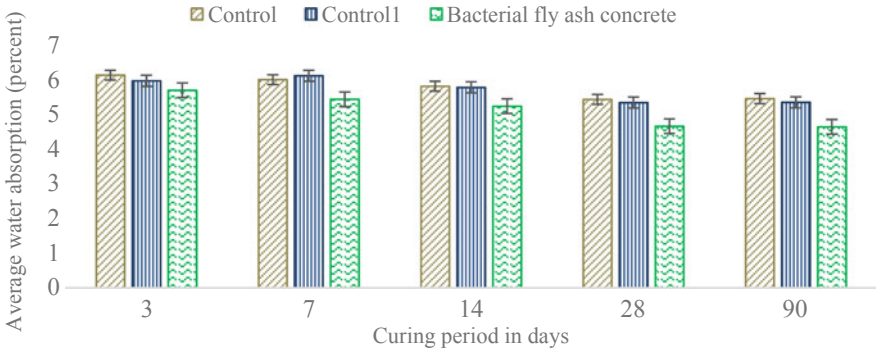

Fig. 6 Average water absorption (percent) versus curing period in days

Figure 6 shows a graph of average water absorption (percent) versus curing period in days. No significant difference was found in average water absorptions (percent) of control 1 and control specimens. Average percent water absorption values of bacterial FAC specimens were around 7, 9, 10, 14 and 15% less than control specimens for 3, 7, 14, 28 and 90 curing days respectively.

3.3 Split Tensile Strength Test and Flexural Strength Test

28th and 90th day's control, control 1 and bacterial FAC specimens were used for split tensile strength test and flexural strength test as per IS 5816: 1999 [27] and IS 516: 1959 [25] respectively. Figure 7 shows split tensile strength and flexural strength values of control, control 1 and bacterial FAC specimens. Average split

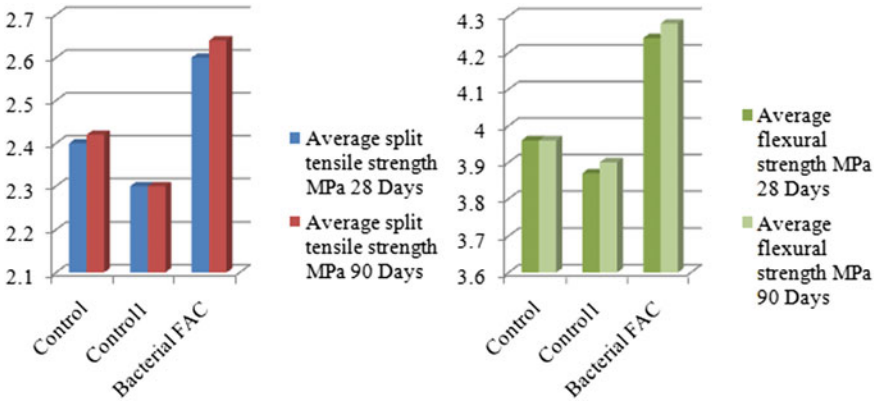

Fig. 7 Average split tensile strength and average flexural strength values of control, control 1 and bacterial FAC specimens for 28 and 90 days

tensile strength of bacterial FAC specimens was found to be increased by 8.33 and 9.09% than control specimens for 28 and 90 days respectively. Also, the average flexural strength of bacterial FAC specimens with respect to control specimens for 28 and 90 days of curing was augmented by 7.07% and 7.82% respectively.

3.4 Ultrasonic Pulse Velocity (UPV) Test

Grade of concrete pertaining to homogeneousness and extent of other imperfections such as voids, cracks, etc. is determined by a non-destructive test known as ultrasonic pulse velocity (UPV) test. The UPV of specimens for 28 and 90 days of curing were measured as per IS 13311: 1992 [28] the average values of which are depicted in Table 4. Higher pulse velocity values are indicative of the better quality of concrete with regard to density, homogeneity and uniformity. The pulse velocity values of all the specimens are given in Table 4. Results indicated that all specimens come under the good quality grading of concrete as per IS 13311: 1992 [28].

3.5 Statistical Analysis

Statistical accuracy of the data of the aforementioned tests was analyzed by Analysis of Variance (ANOVA). The *p*-values of all the data were found to be smaller than 0.05 that depicts significant difference among the data. Thus, it can be implicated that the bacterial activities indeed are responsible for the improvement in bacterial FAC specimens.

3.6 Durability Tests

Chloride, Sulfate and Carbonation Tests: It is clear from the strength test results that control and control 1 specimens show similar behaviors and ingredients of

Table 4 Average UPV values of control, control 1 and bacterial FAC specimens for 28 and 90 days

Specimens	Pulse velocity in km/s		Concrete quality grading as per IS 13311: 1992
	28 days	90 days	
Control specimen	3.70	3.75	Good
Control 1 specimen	3.55	3.67	Good
Bacterial FAC specimen	4.25	4.25	Good

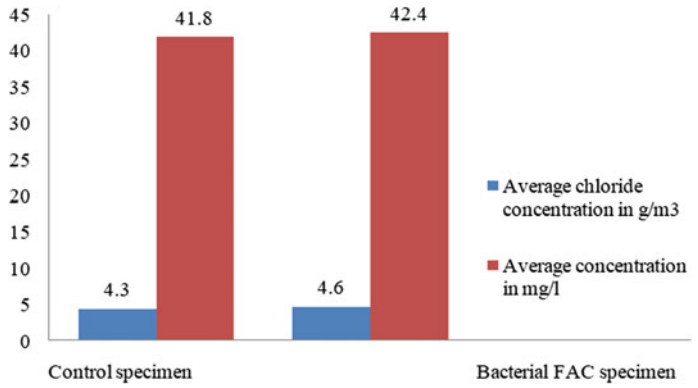

Fig. 8 Average concentrations of chlorides and sulfates of control and bacterial FAC specimens

control 1 do not show any positive or negative impact. Thus, it is proved that the sole reason for the improvement in the performance of FAC is bacterial activity. Therefore, only control and bacterial FAC specimens were subjected to all the durability tests and control 1 specimens were not included. Acceptable chloride and sulfate concentrations for cement concrete with embedded metal are 0.4 kg/m^{3}and 400 mg/l respectively, as per IS 456: 2000 [21]. Argentometric method was used for analyzing the chloride concentrations of extracted samples bacterial FAC and control specimens [29]. As per IS 3025: 1986, sulfate concentrations in the extracted samples were determined by the turbidimetric method [30]. Figure 8 shows the average soluble chloride and sulfate concentrations of control and experimental samples. For the carbonation test, phenolphthalein solution was sprayed on freshly exposed surfaces of control and bacterial FAC specimens [31]. A pink color was obtained in control as well as bacterial FAC specimens indicating that sufficient $Ca(OH)_2$ is present (Fig. 9). This indicates that both the specimens were not much carbonated. The results of these tests indicate the good durability and resistance to weathering of bacterial FAC.

Fig. 9 Carbonation test

Rapid Chloride Permeability Test (RCPT): To monitor the resistance of experimental specimens to the penetration of chloride ions, RCPT was performed as per the guidelines mentioned in ASTM C1202-12, 2012 [32]. The average values of charge passed for control and Bacterial FAC specimens were found to be in the range 850 C-992 C and 770 C-828 C, respectively. The permeability class for both control specimens and bacterial FAC specimens was 'very low' as per ASTM C1202-12, 2012. Obtained values of chloride ion permeability of both the specimens indicate good quality of the concrete in a durability point of view.

3.7 Scanning Electron Microscopy (SEM) Analysis

Scanning electron microscopy was performed to study the microstructures of control and bacterial FAC specimens. 28th day's specimens of both control and bacterial FAC were subjected to this analysis by scanning electron microscope (JSM-6380A). Figure 10 shows the Scanning electron micrographs of both specimens. The $CaCO_3$ precipitations are clearly visible in the scanning electron micrograph of bacterial FAC specimen, thus, proving the better performance of bacterial FAC specimens due to bacterial activity.

3.8 Energy Dispersive X-Ray (EDX) Analysis

EDX analysis was performed to prove the existence of calcium carbonate mineral in the matrix of bacterial FAC specimens as shown in Fig. 11a, b. Calcium is visibly more in bacterial FAC specimen than in control specimen which may be because of calcium carbonate depositions induced by bacterial activities in the former.

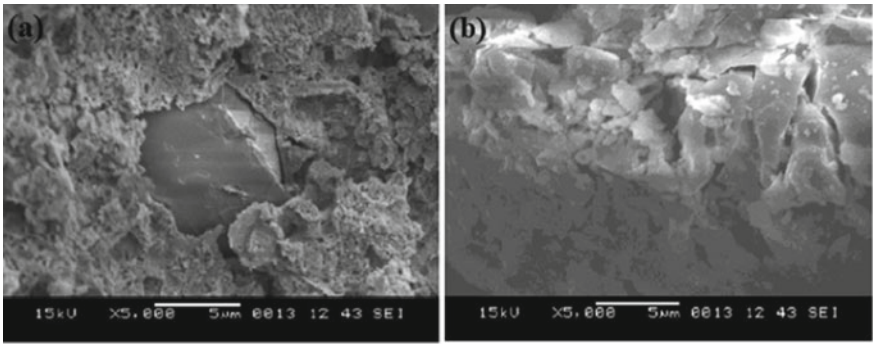

Fig. 10 SEM images of **a** control specimen and **b** bacterial FAC specimen

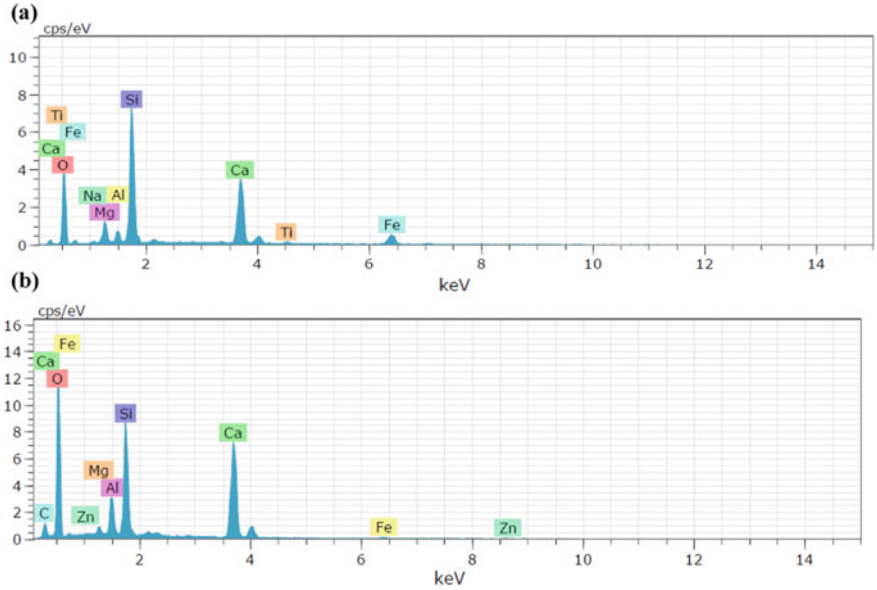

Fig. 11 EDX analysis of **a** control specimen and **b** bacterial FAC specimen

3.9 X-Ray Diffraction (XRD) Analysis

XRD analysis was done in order to investigate the presence of types of crystalline forms of calcium carbonate viz. vaterite, aragonite and calcite. The control and bacterial FAC specimens were analyzed by using an XPERT-PRO diffractometer system. Pulverized specimens having an average particle size of less than 10 microns were used for the XRD analysis. 2θ values of 10–99 degrees were used to scan the specimens. The resultant XRD patterns of both the specimens are shown in Figs. 12a and 7b. Evidently more peaks of vaterite, aragonite and calcite crystals were found in bacterial FAC specimen than control specimen. The reason behind this might be the occurrence of $CaCO_3$ precipitated by ureolytic bacteria in bacterial FAC specimen.

4 Discussion

Earlier many researchers have successfully used biocementation to improve a wide range of construction materials. Present study aimed at knowing the effect of biocementation on the properties of FAC. Considerable improvement in compressive strength, water absorption, split tensile strength and flexural strength of bacterial FAC was observed. Also, biocemented FAC qualified for all durability tests.

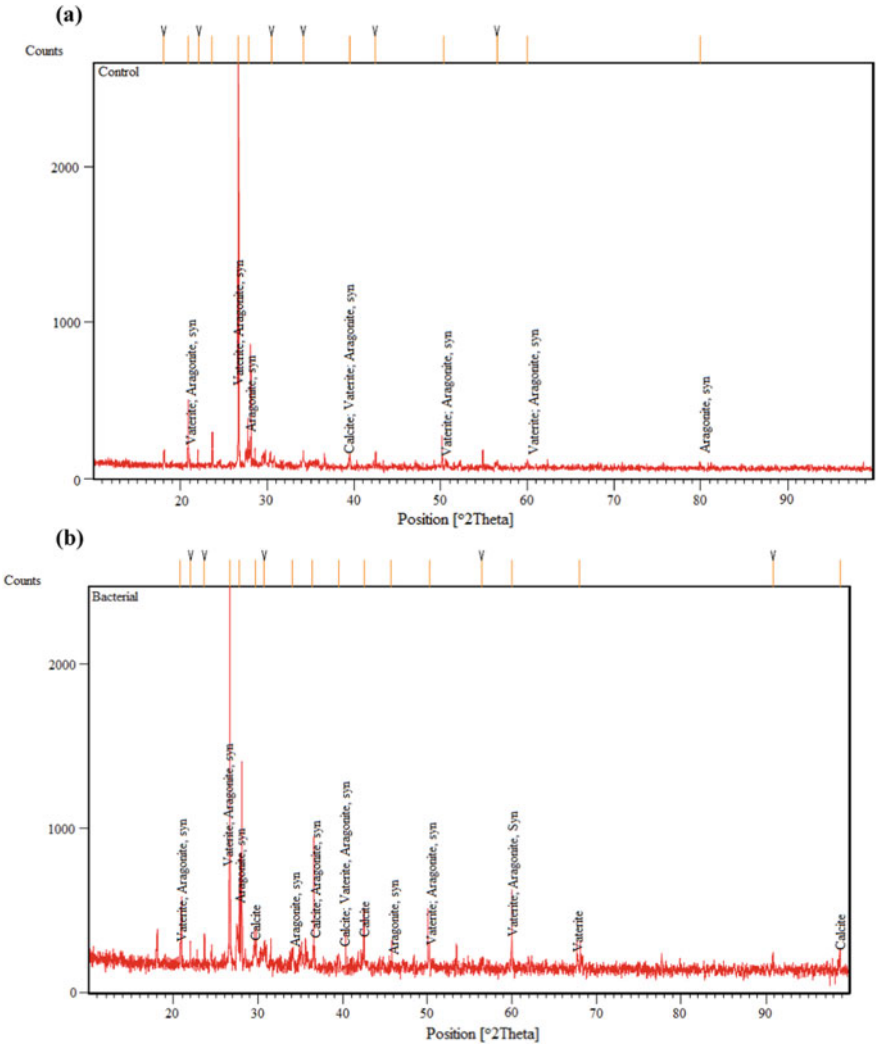

Fig. 12 XRD analysis of **a** control specimen and **b** bacterial FAC specimen

SEM results clearly showed very less void spaces in bacterial FAC as compared to control due to the presence of calcium carbonate precipitation in the bacterial FAC. EDX graphs indicated the presence of more calcium and XRD graphs showed more peaks of crystals of calcium carbonate in bacterial FAC specimens than control specimen. All the above results seem to be the direct consequence of the deposition of bacterially induced calcium carbonate within the matrix of FAC.

5 Conclusions

Biocementation has the potential to improve the strength and durability aspects of FAC. Application of biocementation to FAC involves the utilization of waste (fly ash) to strengthen and increase the life of huge structures by means of environmentally friendly techniques. In this study, ureolytic bacteria were incorporated in FAC. Strength and durability attributes of the bacterially treated FAC were tested and compared with the control FAC (without any bacteria). Following conclusions can be drawn from the current study.

- Biocementation has a potential to overcome the drawbacks of FAC.
- The strength and durability aspects of FAC were significantly improved with the incorporation of bacteria.
- Rhizospheric soil has a great potential to serve as a source of ureolytic bacteria for the biocementation process.
- Also, low cost ingredients such as lentil seeds as a source of proteins and sugar as a carbon source for bacterial growth resulted in double fold advantage by reducing the cost.
- Execution of this technique may prove to be a strong step towards economy and sustainability. More work on this track may help to reach complete goals of sustainable development in the construction field.

References

1. Fraay AL, Bijen JM, De Haan YM (1989) The reaction of fly ash in concrete a critical examination. Cem Concr Res 19(2):235–246
2. Katare VD, Madurwar MV (2017) Application of solid wastes for the production of sustainable concrete. International sustainable buildings symposium. Springer, Cham, pp 108–121
3. Berryman C, Zhu J, Jensen W, Tadros M (2005) High-percentage replacement of cement with fly ash for reinforced concrete pipe. Cem Concr Res 35(6):1088–1091
4. Bhutange SP, Latkar MV (2020) Microbially Induced calcium carbonate precipitation in construction materials. J Mater Civ Eng 32(5):03120001
5. Charpe AU, Latkar MV (2020) Effect of biocementation using soil bacteria to augment the mechanical properties of cementitious materials. Mater Today Proc 21:1218–1222
6. Charpe AU, Latkar MV, Chakrabarti T (2018) Biocementation: an eco-friendly approach to strengthen concrete. In: Proceedings of the institution of civil engineers-engineering sustainability, vol 172, no 8. Thomas Telford Ltd., pp 438–449
7. Bhutange SP, Latkar MV, Chakrabarti T (2019) Role of biocementation to improve mechanical properties of mortar. Sādhanā 44(2):50
8. Pei R, Liu J, Wang S, Yang M (2013) Use of bacterial cell walls to improve the mechanical performance of concrete. Cem Concr Compos 39:122–130
9. Tarczewski R (2015) Formation of sustainable infrastructure using microbial methods and humanization of man-made environment. Procedia Manuf 3:1704–1711
10. Whiffin VS. Microbial CaCO3 precipitation for the production of biocement. Doctoral dissertation, Murdoch University

11. Talaiekhozan A, Keyvanfar A, Shafaghat A, Andalib R, Majid MA, Fulazzaky MA, Zin RM, Lee CT, Hussin MW, Hamzah N, Marwar NF (2014) A review of self-healing concrete research development. J Environ Treat Tech 2(1):1–11
12. Charpe AU, Latkar MV, Chakrabarti T (2017) Microbially assisted cementation—a biotechnological approach to improve mechanical properties of cement. Constr Build Mater 135:472–476
13. Bang SS, Galinat JK, Ramakrishnan (2001) Calcite precipitation induced by polyurethane-immobilized *Bacillus pasteurii*. Enzyme Microb Technol 28(4–5):404–9
14. Achal V, Pan X (2014) Influence of calcium sources on microbially induced calcium carbonate precipitation by *Bacillus* sp. CR2. Appl Biochem Biotechnol 173(1):307–17
15. Achal V, Mukherjee A, Reddy MS (2010) Biocalcification by Sporosarcina pasteurii using corn steep liquor as the nutrient source. Ind Biotechnol 6(3):170–174
16. Achal V, Mukherjee A, Reddy MS (2011) Effect of calcifying bacteria on permeation properties of concrete structures. J Ind Microbiol Biotechnol 38(9):1229–1234
17. Achal V, Pan X, Özyurt N (2011) Improved strength and durability of fly ash-amended concrete by microbial calcite precipitation. Ecol Eng 37(4):554–559
18. Chahal N, Siddique R, Rajor A (2012) Influence of bacteria on the compressive strength, water absorption and rapid chloride permeability of concrete incorporating silica fume. Constr Build Mater 37:645–651
19. Bhatty RS, Slinkard AE, Sosulski FW (1976) Chemical composition and protein characteristics of lentils. Can J Plant Sci 56(4):787–794
20. BIS (Bureau of Indian Standard) (1970) IS 383: specification for coarse and fine aggregate from natural sources for concrete (Second revision), New Delhi, India
21. BIS (Bureau of Indian Standard) (2000) IS 456: plain and reinforced concrete-code of practice, New Delhi, India
22. ASTMC618-03 (2002) Standard specification for coal fly ash and raw or calcined natural pozzolan for use, pp 1–3
23. Pelczar MJ, Chan EC, Krieg NR, Edwards DD, Pelczar MF (1993) Microbiology: concepts and applications. McGraw-Hill, New York
24. BIS (Bureau of Indian Standard) (2009) IS 10262: Indian concrete mix design guide lines, New Delhi, India
25. BIS (Bureau of Indian Standard) (1959) IS 516: methods of tests for strength of concrete, New Delhi, India
26. ASTMC140-11a (2012) Standard test methods for sampling and testing concrete masonry units and related units, pp 1–17. https://doi.org/10.1520/C0140-11A
27. BIS (Bureau of Indian Standard) (1999) IS 5816: splitting tensile strength of concrete-method of test, New Delhi, India
28. BIS (Bureau of Indian Standard) (1992) IS 13311: non-destructive testing of concrete methods of test (ultrasonic pulse velocity), New Delhi, India
29. American Public Health Association (APHA), American Water Works Association (AWWA), Water Environment Federation (WEF) (2017) Standard methods for the examination of water and wastewater. American Public Health Association, Washington DC. https://doi.org/10.1007/s10295-008-0514-7
30. BIS (Bureau of Indian Standard) (1986) IS 3025: methods of sampling and test (physical and chemical) for water and wastewater (reaffirmed 2003) part 24 sulphates, New Delhi, India
31. RILEM, CPC-18 (1988) Measurement of hardened concrete carbonation depth. Mater Struct 21:453–455. https://doi.org/10.1007/BF02472327
32. ASTMC1202-12 (2012) Standard test method for electrical indication of concrete's ability to resist chloride, pp 1–8. https://doi.org/10.1520/C1202-12.2

Mechanical Properties of Polypropylene Fiber-Reinforced Geopolymer Composites: A Review

Amardeep Meena, Navdeep Singh, and S. P. Singh

Abstract The inclusion of fibers enhances the ductile nature, reduced the brittle behavior and reinforced the concrete composites. Recently, geopolymer composites (GPCs) have attracted researches due to their low CO_2 footprint and low consumption of energy. Besides, such composites are good in compressive behavior, while the same performs poorly in tensile and flexural behavior. To avoid such concerns, fibers give a fair and gentle solution to the brittle nature of GPCs. Hence, the combination of these two attracts to study the nature of improved behavior of composites, i.e., fiber-reinforced geopolymer composites (FRGCs). The present paper gives an overview of the mechanical properties of GPCs with polypropylene fibers. In addition to this, the paper also elaborates on the mechanical properties based on different kinds of GPCs (aluminosilicate materials based) with polypropylene (PP) fibers. This study confirmed that using different kinds of GPCs as single or blended with PP fibers improved the mechanical characteristics of the composites with enhanced bond strength.

Keywords Geopolymer composites · Polypropylene fibers · Mechanical properties

1 Introduction

The emission of greenhouse gases and continuing dumping of industrial by-products has raised environmental concerns dramatically. The cement manufacturing companies contributed up to 7% of total carbon dioxide (CO_2) emission, estimated to be about 23 billion tons (BT) of CO_2 release globally [1–3].

A. Meena (✉) · N. Singh · S. P. Singh
Department of Civil Engineering, Dr. B.R. Ambedkar National Institute of Technology Jalandhar, Jalandhar, India
e-mail: navdeeps@nitj.ac.in

S. P. Singh
e-mail: spsingh@nitj.ac.in

B. Laishram and A. Tawalare (eds.), *Recent Advancements in Civil Engineering*, Lecture Notes in Civil Engineering 172,
https://doi.org/10.1007/978-981-16-4396-5_24

The cement consumes a huge amount of raw materials and energy during the manufacturing process which is non-renewable in nature and is not feasible in the current scenario of sustainability. Utilization and management of industrial waste and by-products can reduce energy consumption and can be an alternate material in the field of construction industry [4]. For nearly the past two decades, several investigations have been carried out to reduce cement consumption in the concrete by substituting with cementing materials such as slag (ground-granulated blast furnace slag, GGBS), fly ash (FA), silica fume (SF), metakaolin (MK), rice husk ash (RHA).

Geopolymer concrete is also known as the third-generation concrete and is recently in current trend because of the full replacement of cement. The introduction of a geopolymer with 100% replacement of ordinary Portland cement (OPC) by different aluminosilicate materials mainly FA can reduce about 80% CO_2 emission in comparison to cement production [5]. The GPC has shown significantly similar mechanical properties of conventional hardened concrete which shows excellent compressive strength but correspondingly weak in brittle behavior [6]. Generally, fibers are incorporated in normal concrete to enhance its ductility by reinforcing the concrete. Similarly, the fibers were used to improve the brittleness in GPC. There are many studies, during the last decades which have successfully evaluated the mechanical behavior of reinforced GPC with many types of fibers including metallic, synthetic or natural. Fibers like polypropylene, carbon, polyvinyl alcohol, steel fibers, natural fibers, basalt, asbestos and glass fibers were used to investigate the mechanical behavior of GPC by various researchers. It has been observed that in GPC, under the effect of loading, the initiated cracks propagate hurriedly resulting in rapid loss of load-carrying capacity. However, in FRGC, the addition of the fibers in the concrete gives the bridging effect at the crack initiating interface after cracking of the hardened concrete which improves its residual mechanical properties [7–9].

The overview of this study is to understand the impact on the mechanical properties of GPC made with FA, GGBS, MK, etc., as the replacement of cement incorporating PP fibers. Based on the strength or the stiffness fibers are classified as low and high modulus fibers. Polypropylene fibers are low modulus fibers which are generally used to replace asbestos fibers for health and safety concerns. PP fibers are thermoplastic polymer with a wider range of practical applications in various fields. The main properties of PP fibers are shown in Table 1 [7, 10–20]. Among the aforementioned aluminosilicate materials, the FRGC made with GGBS has been proven to be better compressive strength in comparison to the FRGC made with other aluminosilicate materials. Many studies have reported that GPC made with GGBS in addition to metallic fibers has enhanced the impact, bond, toughness, flexural, fracture properties, tensile and compressive strength. Similarly, the incorporation of non-metallic fibers in GPC has improved mechanical behavior [10, 21–24]. Furthermore, the inclusion of natural fibers like cotton, jute, sisal and coir fibers has shown the better mechanical performance of FRGC in comparison to the conventional GPC [25]. However, limited information is available on fracture

Table 1 Properties of PP fibers

Reference	Fiber		Density (g/cm^3)	Tensile strength (MPa)	Young's modulus (GPa)
	Length (mm)	Diameter (μm)			
Ranjbar et al. [7]	12.19	~40	NA	310–414	0.345
Akturk et al. [10]	12	30–40	NA	570–660	NA
Bhutta et al. [11]	50	880	0.91	700	NA
Chindaprasirt and Rattanasak [12]	3	15	NA	557	4.16
Al-mashhadani et al. [13]	12	7.5	NA	750	NA
Farooq et al. [14]	12	50	0.91	500–700	3–3.5
Wang et al. [15]	3–19	17	0.91	461	4.987
Guo et al. [16]	6	130–150	0.91	>358	>3.5
Moradikhou et al. [17]	6–12	NA	0.91	310	3.5
Abdollahnejad et al. [18]	10	12	0.91	910	9.6
Ranjbar et al. [19]	12	40	NA	310	3.5
Zhang et al. [20]	3	10	1.36–1.4	550	13.5

behavior, fiber pull-out performance, impact strength and punching shear of such composites. Correspondingly, to the best of the authors, no experimental work has been reported on the fatigue and shear behavior of PP-FRGC.

2 Compressive Strength

Compressive strength is the most important property of the concrete. Generally, the overall quality of concrete is defined by its compressive strength as it directly or indirectly correlated with the mechanical and durability characteristics of the concrete. Bhutta et al. [11] studied on the mechanical performance of GPC incorporating 0.5% PP fibers, by volume (50 mm × 88 μm ϕ) in FA-geopolymer mortar activated with sodium-based alkali activator. The results confirmed that the 28 days compressive strength improved up to 23.2%. Another study was carried out in addition to 0.5 and 1% PP fibers of 12 mm × 18 μm ϕ and the result confirmed that the increased fiber content enhanced the early age compressive strength up to 40%. Though the 28 days compressive strength was reported to reduce by 31.73% [26]. Similar conclusions were reported that with 0.5% content of PP fibers (length 12 mm and diameter 36 μm) improves the compressive strength by 5.3–18.92% [12, 27, 28]. On the contrary, Al-mashhadani et al. [13] reported that with an increasing percentage of PP fibers from 0.4 to 1.2%, the compressive strength decreases. Similar assumptions were made with 0.5, 1, 1.5, 2 and 3% PP fiber

percentage content that the compressive strength decreases by 20.63–44.32% [14, 15, 29, 30]. Ranjbar et al. [7] also confirmed that increasing PP fiber content up to 5% in GPC has an adverse effect on the compressive strength due to the weak interface of the matrices. Recent studies on slag based GPC have revealed that addition of 0.5 and 1% PP fibers improved the compressive strength [26, 31]. Another investigation on MK-based GPC with 2% PP fiber inclusion has reportedly improved the compressive strength up to 65.44% [16]. However, other studies suggested that 0.2% fiber addition has shown higher compressive strength in comparison to the GPC mixes with 0.15 and 0.25% PP fiber content [17]. Similarly, studies on GPCs based with FA-slag, FA-SF (Silica Fume), slag-ceramic, slag-ladle slag, etc., have concluded that compressive strength increases with 0.2–1.4% PP fiber content by 9.5–40% [8, 18, 26, 32–35]. On the other hands, addition of PP fibers by 1 and 1.5% in FA-slag based GPC has reported to have adverse effect on the compressive strength [36]. Noushini et al. [37] incorporated 0.5% volume fractions of monofilament PP fibers (length 18 mm and diameter 22 μm) and fibrillated PP fibers of varying dimensions in 65% FA, 20% ultra-fine FA and 15% slag-based GPC. The FRGC-containing PP fibers have shown an average decrease in compressive strength. This may be due to the small number of air pockets in GPC around the fibers and the low elastic modulus of the PP fibers. However, other studies on blended GPC-like natural zeolite, multifilament-PP (PP-MF) and split-film-PP (PP-SF) based with ladle slag-gypsum GPC with 0.5–1% fiber incorporation concluded that compressive strength was enhanced by 23.76–75.47% [9, 10, 38, 39].

3 Flexural Strength

The flexural test assesses the tensile strength indirectly. Flexural strength signifies the maximum stress (highest tensile value) induced within the unreinforced concrete to withstand failure in bending. Al-mashhadani et al. [13] investigated on mechanical properties of PP fiber-reinforced GPC (12 mm × 0.75 μm ϕ) varying from 0.4 to 1.2% by volume in FA -based geopolymer mortars stimulated with sodium hydroxide, NaOH (12 M) solution and sodium silicate (Na_2SiO_3). The results concluded that with increasing PP fiber content improved the flexural up to 14.66%. Similar study with 0.5% incorporation of PP fiber has been reported to improve the flexural by 23.2% [11]. Bagheri et al. [29] found the comparable flexural strength of Class F FA-based geopolymer mortars containing 0.5% PP fibers (length 19 mm and diameter 40 μm) to those containing 1% fibers. Another study was carried out in addition to 0.5 and 1% PP fibers of 12 mm × 18 μm ϕ and the result confirmed that the increased fiber content enhanced the early age flexural up to 25.64%. Though the 28 days flexural strength was reported to reduce by 19.12% [26]. Previous investigations have confirmed that increasing content of PP fibers up to 5% in GPC enhanced flexural strength [7, 19]. Korniejenko et al. [40] investigated the mechanical properties of FA-based geopolymer paste in addition to

5% to 20% PP fibers. The outcome of the study confirmed that GPC incorporating 10, 15 and 20% exhibited the higher flexural strength. Puertas et al. [26] concluded that inclusion of 0.5 and 1% PP fibers of 12 mm × 18 μm ϕ in alkali-activated slag mortar reduces the early age flexural strength up to 11.11 and 14.1% at later age. Further, similar conclusions with 0.15, 0.25 and 2% inclusion of PP fibers in GPC based on FA to concluded that with increasing the percentage of fibers, flexural strength increases up to 40%, and thereby, the addition of fibers improves the ductility of the GPC [10, 16, 17, 28, 30, 31]. Mohseni [41] incorporated 0.3–1% PP fibers by weight with different monomer ratios 2, 2.5 and 3 in GPC. The results indicated that the mechanical properties enhanced by 10% with percentage increment of fibers content and monomer ratio to 2 and 3 which may be attributed to the nepheline crystalline formation. The addition of 1% fibers with monomer ratios of 2, 2.5 and 3 enhanced the 28 days flexural strength by 28%, 25% and 28%, respectively, as compared to the addition of 0.3% fibers. Thus, confirming that PP fibers control cracks thereby reducing the crack width and eventually strengthening the flexural strength. Uysal et al. [42] added 0.8% PP fibers of 12 mm × 0.075 μm ϕ in geopolymer mortar based with MK. SF and colemanite were used to partially substitute MK ranging from 10 to 40% in GPC. The outcome concluded that GPC mixes with partial replacement with SF incorporation 0.8% fibers have higher flexural strength compared to control mix and mixes with colemanite replacement.

Shaikh et al. [36] designed FA-/slag-based GPC incorporating 1 and 1.5% PP fibers of 12–19 mm × 2.2 μm ϕ containing 80% FA and 20% slag geopolymer mortar. It has been concluded that with the percentage increment of PP fiber, the flexural strength exhibited no significant improvement. Similar conclusions were drawn from another study on GPC based with 50% slag-50% FA in addition to 0.5 and 1% PP fibers of 12 mm × 18 μm ϕ that with increasing PP fiber content from 0.5 to 1%, the flexural strength decreases [26]. Abdollahnejad et al. [43] confirmed that 1.5% PP fibers addition in 50% FA, 40% slag and 10% Na_2SiO_3-based GPC improved flexural strength at 28 days curing age, though, the flexural decreases with advancing curing period which may be due to the weaker interfacial bond of the matrices. But with prolonged curing, the flexural and tensile strength improved due to filling up of gaps between the interfacial transition zone by the chemical products formed, thus improving the bond behavior [8, 32, 34, 37, 44]. Hence, confirming that the amalgamation and content of fibers have more impact on the flexural strength rather than the curing days. GPC based with blended SCMs such as slag/ceramic, slag/ladle slag, natural zeolite with 0.5 to 1% PP fibers inclusion was reported to have improved the flexural strength by 40.9–173%; however, with increasing PP fiber to 1.5%, the flexural reduces [18, 35, 38]. This may be due to the weak bond at the interface matrix between the smooth PP fiber surface and GPC [45]. Nguyen et al. [9] incorporated 2% volume fractions of multifilament-PP (PP-MF) fibers and split-film-PP (PP-SF) fibers to alkali-activated ladle slag-based geopolymer mortars. The result concluded that the flexural strength was improved by 309%. Similar conclusions were drawn from another investigation that ladle slag-gypsum-based GPC in addition with 2% PP-MF and PP-SF improved in flexural strength was up to 65.68% [39].

4 Tensile Strength

As the tensile strength of the concrete is low, fibers play an important role to increase the tensile strength of the concrete and reduce its brittleness. So it is important to evaluate this property for FRGC. Bagheri et al. [29] found that the comparable tensile strength of Class F FA-based geopolymer mortars containing 0.5% PP fibers to those containing 1% fibers. Another study on FA-based GPC mixes in addition of 0.5 and 1% PP fibers confirmed that the increased fiber content enhanced the early age tensile strength up to 15.6%. Though the 28 days tensile strength was reported to reduce by 12.5% [26]. Similar study with 0.5% incorporation of PP fiber has been reported to improve the tensile strength up to 23% [11]. Farooq et al. [14] incorporated 2 and 3% PP fibers of 12 mm × 50 μm ϕ in geopolymer mortars with varying sand content, based on Class-F FA activated using different molarities of NaOH (8 M and 12 M) and Na_2SiO_3. The result concluded that the FRGC 8 M with higher sand content incorporating PP fibers has shown higher tensile strength in comparison to the FRGC 12 M with lower sand content and the control mix. This may be attributed to the large elongation of the fibers prior to fracture. Further, similar conclusions were made with 0.15, 0.25 and 2% inclusion of PP fibers in GPC based on FA that with increasing the percentage of fibers, tensile strength increases up to 24%, and thereby, the addition of fibers improves the ductility of the GPC [17, 28, 31]. Abdollahnejad et al. [43] confirmed that 1.5% PP fibers addition in 50% FA, 40% slag and 10% Na_2SiO_3-based GPC with prolonged curing tensile strength improved due to filling up of gaps between the interfacial transition zone by the chemical products formed, thus improving the bond behavior [8, 32, 34, 37, 44]. Similar assumptions were made from the study with 2% volume fractions inclusion of multifilament-PP (PP-MF) fibers and split-film-PP (PP-SF) fibers to alkali-activated ladle slag-based geopolymer mortars concluded that tensile strength were improved by 103% [9].

5 Elastic Modulus

The modulus of elasticity is the mechanical properties that assess stiffness of a material. Bagheri et al. [29] confirmed that the incorporation of 1% fibers increased the elastic modulus compared to those GPC mixes containing 0.5% fibers. Similar studies have reported that the inclusion of 0.1–20% PP fibers has improved modulus of elasticity [10, 31, 40, 47]. However, another study concluded that addition to 0.5 and 1% PP fibers in alkali-activated slag mortar reduced the 28 days elastic modulus by 17.59% [26]. Other studies also suggested that the modulus of elasticity decreases with increasing fiber content [18, 26, 33].

6 Fracture Properties: Ultimate Load Capacity, Ductility

Fracture properties are fundamental mechanical properties of concrete attributed to its substantial role in the advancement of the crack generated between the binder and aggregates, significantly controlling the fracture mechanics of the concrete structures. Subsequently, other fundamental mechanical characteristics of concrete play important role in fiber-reinforced GPC. Al-mashhadani et al. [13] reported that increasing PP fiber content improved the toughness, ultimate load capacity and mid-span deflection up to 215.51%, 14.66% and 103.57%, respectively. Bagheri et al. [29] confirmed that the incorporation of 1% fibers increased the toughness compared to those containing 0.5% fibers. However, recent studies on slag-based GPC with 0.1–2% PP fiber addition have reportedly enhanced the fracture toughness, fracture energy, fracture energy, ductility and reduced brittleness index of the GPC [10, 31, 41]. Other studies suggested that the rupture modulus decreases, and however, mid-span deflection and Poisson's ratio improved with increasing fiber content [26, 33]. Studies on MK-based and ladle slag-gypsum-based GPC have reported that add up to 1% PP fibers increases the toughness by 56.2 times in comparison to control mix and fracture toughness by 149% to 666% for the GPC with 2% PP-MF and PP-SF, respectively [9, 34, 39]. Akturk et al. [10] incorporated 2% PP fibers in 97% NCAS and 3% calcium hydroxide (CH)-based geopolymer mortars. The result confirmed that the fracture toughness of CH-modified reinforced mixes was increased by 92% with 100% CH and with 40% NH-substitution, and the fracture toughness of CH-modified reinforced mixes was increased by 40.28% as compared to plain mixes. Table 2 represents the impact of PP fibers on the mechanical properties of GPC based on aluminosilicate materials. It can be noted that most of the studies on PP fibers reinforced GPC for the past years are mainly focused on FA, slag and blended-based. Although very few studies on mechanical properties have been reported on PP fibers in MK-based GPC indicating more research on MK and slag-based GPC incorporating PP fibers is required.

7 Conclusions

Based on the available literature reviewed, the following conclusions have been drawn for mechanical properties of PP-FRGC.

- The improvement in compressive strength is possible with low loading of PP fibers content of about 0.2–1% by 19–40% for FA-based GPC. However, the bond strength between the matrix and fibers improvement is conceivable with surface texture and varying geometric characterization.
- Higher content of PP fibers in FA-GGBS based reduces mid-span deflection and improves ductility, flexural, tensile, elastic modulus and fracture properties such as fracture toughness, fracture energy. Though the increasing fiber content may have adverse effect on the compressive strength.

Table 2 Impact of PP fibers on the mechanical properties of GPC based on aluminosilicate materials

GP-matrix	Fiber			Impact	Source
	Length (mm)	Diameter (μm)	Content (%)		
FA-mortar	12	0.75	0.4–1.2	Increased ultimate load, flexural strength mid-span deflection, flexural toughness, and abrasion resistance, reduced compressive strength	Al-mashhadani et al. [13]
FA-mortar	50	88	0.5	Increased mechanical strength and toughness Reduced compressive and tensile strength	Bhutta et al. [11]
FA-mortar	50	88	0.5 and 1	Increased mechanical strength and toughness Reduced compressive and tensile strengths	Bhutta et al. [46]
FA-mortar	19	40	0.5 and 1	Increased toughness and elastic modulus comparable flexural strength	Bagheri et al. [29]
FA-mortar	12	18	0.5 and 1	Flexural and compressive strengths increased after 2 days and also decreased after 28 days	Puertas et al. [26]
FA-mortar	12	36	0.5–1.5	Compressive and splitting strengths increased after 7–28 days with 0.5% fibers, while decreased with 1 and 1.5% fibers	Sabna et al. [47]
FA-mortar	12	50	2 and 3	Addition of 2 and 3% fibers increased the compressive strength with 8 M NaOH and decreased with 12 M NaOH observed post-crack bridging tensile strength very low and tensile strain capacity high	Farooq et al. [14]
FA-paste	3	15	0.5	Compressive and tensile strengths increased after 1-month	Chindaprasirt and Rattanasak [12]
FA-paste	12	40	0.5–4	Compressive and flexural strengths increased after 7 days, while decreased after 56 days	Ranjbar et al. [7]

(continued)

Table 2 (continued)

GP-matrix	Fiber			Impact	Source
	Length (mm)	Diameter (μm)	Content (%)		
FA-paste	12.19	~40	0.5–5	Enhanced flexural strength after 3–14 days with 1–3% fibers Enhanced flexural strength after 3–56 days with 4–5% fibers reduced compressive strength	Ranjbar et al. [19]
FA/ slag-mortar	–	2.2	1 and 1.5	Compressive strength increased after 28 days with 1% fibers	Shaikh et al. [36]
FA/ slag-mortar	12	18	0.5 and 1	Compressive strength increased after 2 and 28 days Flexural strength decreased after 2 days, while increased after 28 days	Puertas et al. [26]
FA/ slag-concrete	6	–	0.2–1.4	Compressive strength decreased with 0.2 and 1.4% fibers, while increased with 0.6 and 1% fibers flexural strength decreased with 0.2 and 1% fibers, while increased with 0.6 and 1.4% fibers	Abdollahnejad et al. [32]
FA/ slag-concrete	20	–	0.2–1.4	Compressive and flexural strengths increased with 1.4% fibers	Abdollahnejad et al. [32]
FA/ slag-concrete	18, 19, 51	22	0.5	Compressive strength, modulus of elasticity and modulus of rupture decreased after 28 days indirect tensile strength and Poisson's ratio increased after 28 days	Noushini et al. [37]
FA/ slag-concrete	12	–	0.5 and 1	Compressive strength increased with 0.5% fibers after 7 and 28 days, while decreased with 1% fibers	Rahul et al. [33]

(continued)

Table 2 (continued)

GP-matrix	Fiber			Impact	Source
	Length (mm)	Diameter (μm)	Content (%)		
MK/ FA-paste	3	10	0.25–0.75	Flexural strength and impact energy increased after 1 and 3 days with 0.25–0.75% fibers Compressive strength increased after 1 and 3 days with 0.25–0.5% fibers, while decreased with 0.75% fibers after 3 days	Zhang et al. [20]
FA/steel slag-mortar	12	18–30	0.1–0.4	Slightly decreased 3 days compressive strength, but increased flexural strength Increased 7 days compressive and flexural strengths Increased 28 days compressive strength. 0.1–0.3% fibers increased 28 days flexural strength Increased the maximum displacement and the maximum load	Guo and Pan [44]

- The MK-based GPC composites and their limited studies surely attract attention as the percentage inclusion of fiber improved the flexural strength, and the MK incorporation has enhanced the compressive strength.
- As a concrete reinforcement, high-strength PP fibers exhibit higher performance. But its (low modulus fibers) application is still rising due to the remarkably enhanced ductility of the GPC when mixed with higher modulus fibers like steel fibers.

References

1. Lakshmi K, Rao MSN (2019) Experimental study on geopolymer concrete by using glass fibres. Int Res J Eng Technol 06:1693–1698. https://doi.org/10.15623/ijret.2015.0404019
2. Part WK, Ramli M, Cheah CB (2015) An overview on the influence of various factors on the properties of geopolymer concrete derived from industrial by-products. Constr Build Mater 77:370–395. https://doi.org/10.1016/j.conbuildmat.2014.12.065
3. Ozbakkaloglu T, Xie T (2016) Geopolymer concrete-filled FRP tubes: behavior of circular and square columns under axial compression. Compos Part B Eng 96:215–230. https://doi.org/10.1016/j.compositesb.2016.04.013

4. Lloyd NA, Rangan BV (2010) Geopolymer concrete with fly ash. In: 2nd international conference on sustainable construction materials and technologies, Ancona, Italy, pp 1493–1504
5. Davidovits J (1989) Geopolymers and geopolymeric new materials. J Therm Anal 35: 429–441
6. Tempest B, Sanusi O, Gergely J, Ogunro V, Weggel D (2009) Compressive strength and embodied energy optimization of fly ash based geopolymer concrete. In: World coal ash, WOCA conference—proceeding, Lexington, KY, USA, pp 1–17
7. Ranjbar N, Talebian S, Mehrali M, Kuenzel C, Metselaar HSC, Jumaat MZ (2016) Mechanisms of interfacial bond in steel and polypropylene fiber reinforced geopolymer composites. Compos Sci Technol 122:73–81. https://doi.org/10.1016/j.compscitech.2015.11.009
8. Su Z, Guo L, Zhang Z, Duan P (2019) Influence of different fibers on properties of thermal insulation composites based on geopolymer blended with glazed hollow bead. Constr Build Mater 203:525–540. https://doi.org/10.1016/j.conbuildmat.2019.01.121
9. Nguyen H, Carvelli V, Adesanya E, Kinnunen P, Illikainen M (2018) High performance cementitious composite from alkali-activated ladle slag reinforced with polypropylene fibers. Cem Concr Compos 90:150–160. https://doi.org/10.1016/j.cemconcomp.2018.03.024
10. Akturk B, Akca AH, Kizilkanat AB (2020) Fracture response of fiber-reinforced sodium carbonate activated slag mortars. Constr Build Mater 241:1–13. https://doi.org/10.1016/j.conbuildmat.2020.118128
11. Bhutta A, Borges PHR, Zanotti C, Farooq M, Banthia N (2017) Flexural behavior of geopolymer composites reinforced with steel and polypropylene macro fibers. Cem Concr Compos 80:31–40. https://doi.org/10.1016/j.cemconcomp.2016.11.014
12. Chindaprasirt P, Rattanasak U (2017) Synthesis of polypropylene fiber/high-calcium fly ash geopolymer with outdoor heat exposure. Clean Technol Environ Policy 19:1985–1992. https://doi.org/10.1007/s10098-017-1380-7
13. Al-mashhadani MM, Canpolat O, Aygörmez Y, Uysal M, Erdem S (2018) Mechanical and microstructural characterization of fiber reinforced fly ash based geopolymer composites. Constr Build Mater 167:505–513. https://doi.org/10.1016/j.conbuildmat.2018.02.061
14. Farooq M, Bhutta A, Banthia N (2019) Tensile performance of eco-friendly ductile geopolymer composites (EDGC) incorporating different micro-fibers. Cem Concr Compos 103:183–192. https://doi.org/10.1016/j.cemconcomp.2019.05.004
15. Wang Y, Zheng T, Zheng X, Liu Y, Darkwa J, Zhou G (2020) Thermo-mechanical and moisture absorption properties of fly ash-based lightweight geopolymer concrete reinforced by polypropylene fibers. Constr Build Mater 251:118960. https://doi.org/10.1016/j.conbuildmat.2020.118960
16. Guo L, Wu Y, Xu F, Song X, Ye J, Duan P, Zhang Z (2020) Sulfate resistance of hybrid fiber reinforced metakaolin geopolymer composites. Compos Part B 183:1–10. https://doi.org/10.1016/j.compositesb.2019.107689
17. Moradikhou AB, Esparham A (2020) Physical & mechanical properties of fiber reinforced metakaolin-based geopolymer concrete. Constr Build Mater 251:1–12. https://doi.org/10.1016/j.conbuildmat.2020.118965
18. Abdollahnejad Z, Mastali M, Luukkonen T, Kinnunen P, Illikainen M (2018) Fiber-reinforced one-part alkali-activated slag/ceramic binders. Ceram Int 44:8963–8976. https://doi.org/10.1016/j.ceramint.2018.02.097
19. Ranjbar N, Mehrali M, Behnia A, Pordsari AJ (2016) A comprehensive study of the polypropylene fiber reinforced fly ash based geopolymer. PLoS ONE 11:1–20. https://doi.org/10.1371/journal.pone.0147546
20. Zhang ZH, Yao Z, Zhu HJ (2009) Preparation and mechanical properties of polypropylene fiber reinforced calcined kaolin-fly ash based geopolymer. J Cent South Univ Technol 16: 49–52

21. Novais RM, Carvalheiras J, Seabra MP, Pullar RC, Labrincha JA (2017) Effective mechanical reinforcement of inorganic polymers using glass fibre waste. J Clean Prod 166:343–349. https://doi.org/10.1016/j.jclepro.2017.07.242
22. Balamurugan R, Balachandran R (2017) Experimental investigation of glass fibre reinforced geo polymer concrete. Eng Sci Technol 7:15–19
23. Vilaplana JL, Baeza FJ, Galao O, Alcocel EG, Zornoza E, Garcés P (2016) Mechanical properties of alkali activated blast furnace slag pastes reinforced with carbon fibers. Constr Build Mater 116:63–71. https://doi.org/10.1016/j.conbuildmat.2016.04.066
24. Shaikh F, Haque S (2018) Behaviour of carbon and basalt fibres reinforced fly ash geopolymer at elevated temperatures. Int J Concr Struct Mater 12(1):1–12. https://doi.org/10.1186/s40069-018-0267-2
25. Mohammed L, Ansari MNM, Pua G, Jawaid M, Islam MS (2015) A review on natural fiber reinforced polymer composite and its applications. Int J Pol Sci 1–15
26. Puertas F, Amat T, Fernández-Jiménez A, Vázquez T (2003) Mechanical and durable behaviour of alkaline cement mortars reinforced with polypropylene fibres. Cem Concr Res 33:2031–2036. https://doi.org/10.1016/S0008-8846(03)00222-9
27. Thampi T, Sreevidya V (2014) Influence of fibers in strength characteristics of ferro-geopolymer mortar. Int J Adv Struct Geotech Eng 03:23–27. http://basharesearch.com/IJASGE/1030105.pdf
28. Patil SS, Patil AA (2015) Properties of polypropylene fiber reinforced geopolymer concrete. Int J Curr Eng Technol 5:2909–2912
29. Bagheri A, Nazari A (2018) Fibre-reinforced boroaluminosilicate geopolymer: a comparative study. Ceram Int Press 44(14):16599–16605
30. Reed M, Lokuge W, Karunasena W (2014) Fibre-reinforced geopolymer concrete with ambient curing for in situ applications. J Mater Sci 49:4297–4304. https://doi.org/10.1007/s10853-014-8125-3
31. Zhu J, Zheng WZ, Qin CZ, Xu Z, Wu YQ (2018) Effect of different fibers on mechanical properties and ductility of alkali-activated slag cementitious material. In: 2nd international conference new material and chemical industry (NMC12017), pp 1–7. https://doi.org/10.1088/1757-899X/292/1/012060
32. Abdollahnejad Z, Zhang Z, Wang H, Mastali M (2018) Comparative study on the drying shrinkage and mechanical properties of geopolymer foam concrete incorporating different dosages of fiber, sand and foam agents. Springer International Publication, pp 42–48. https://doi.org/10.1007/978-3-319-59471-2
33. Rahul S, Mithanthaya IR, Marathe S (2017) Study of strength characteristics of geopolymer concrete using ceramic aggregate as coarse aggregates with addition of polypropylene fibers. Int J Curr Eng Sci Res 4:42–46
34. Sukontasukkul P, Pongsopha P, Chindaprasirt P, Songpiriyakij S (2018) Flexural performance and toughness of hybrid steel and polypropylene fibre reinforced geopolymer. Constr Build Mater 161:37–44. https://doi.org/10.1016/j.conbuildmat.2017.11.122
35. Mastali M, Alzaza A, Shaad KM, Kiinnunen P, Abdollahnejad Z, Woof B, Illikainen M (2019) Using carbonated BOF slag aggregates in alkali-activated concretes. Materials 12:1–27. https://doi.org/10.3390/ma12081288
36. Uddin F, Shaikh A (2020) Tensile and flexural behaviour of recycled polyethylene terephthalate (PET) fibre reinforced geopolymer composites. Constr Build Mater 245:1–10. https://doi.org/10.1016/j.conbuildmat.2020.118438
37. Noushini A, Hastings M, Castel A, Aslani F (2018) Mechanical and flexural performance of synthetic fibre reinforced geopolymer concrete. Constr Build Mater 18:454–475. https://doi.org/10.1016/j.conbuildmat.2018.07.110
38. Baykara H, Cornejo MH, Espinoza A, García E, Ulloa N (2020) Preparation, characterization, and evaluation of compressive strength of polypropylene fiber reinforced geopolymer mortars. Heliyon 6:1–10. https://doi.org/10.1016/j.heliyon.2020.e03755

39. Nguyen H, Staudacher M, Kinnunen P, Carvelli V, Illikainen M (2019) Multi-fiber reinforced ettringite-based composites from industrial side streams. J Clean Prod 211:1065–1077. https://doi.org/10.1016/j.jclepro.2018.11.241
40. Korniejenko K, Mikula J, Łach M (2015) Fly ashbased fiber-reinforced geopolymer composites as the environmental friendly alternative to cementitious materials. In: International conference on bio-medical engineering and environmental technology (BMEET 2015), London, pp 164–171
41. Mohseni E (2018) Assessment of Na_2SiO_3 to NaOH ratio impact on the performance of polypropylene fiber-reinforced geopolymer composites. Constr Build Mater 186:904–911. https://doi.org/10.1016/j.conbuildmat.2018.08.032
42. Uysal M, Al-mashhadani MM, Aygörmez Y, Canpolat O (2018) Effect of using colemanite waste and silica fume as partial replacement on the performance of metakaolin-based geopolymer mortars. Constr Build Mater 176:271–282. https://doi.org/10.1016/j.conbuildmat.2018.05.034
43. Abdollahnejad Z, Mastali M, Woof B, Illikainen M (2020) High strength fiber reinforced one-part alkali activated slag/fly ash binders with ceramic aggregates: microscopic analysis, mechanical properties, drying shrinkage, and freeze-thaw resistance. Constr Build Mater 241:1–16. https://doi.org/10.1016/j.conbuildmat.2020.118129
44. Guo X, Pan X (2018) Mechanical properties and mechanisms of fiber reinforced fly ash–steel slag based geopolymer mortar. Constr Build Mater 179:633–641. https://doi.org/10.1016/j.conbuildmat.2018.05.198
45. Vaidya S, Allouche EN (2011) Strain sensing of carbon fiber reinforced geopolymer concrete. Mater Struct 44:1467–1475. https://doi.org/10.1617/s11527-011-9711-3
46. Bhutta A, Farooq M, Banthia N (2019) Performance characteristics of micro fiber-reinforced geopolymer mortars for repair. Constr Build Mater 215:605–612. https://doi.org/10.1016/j.conbuildmat.2019.04.210
47. Sabna J, Sreevidya V, Venkatasubramani R (2014) Mechanical properties of fibrous geopolymer mortar in relation with curing conditions. Int J Civil Struct Eng 4(3):365–371. https://doi.org/10.6088/ijcser.201304010035

Study on Energy Requirements of Building Envelope Developed from Glass Powder Foamed Geopolymer Blocks

Khan Asudullah Khan, Ashwin Raut, C. Rama Chandrudu, and C. Sashidhar

Abstract This work aimed at providing a sustainable material for the building envelope to reduce the dependency on the mechanical cooling. The goal was to develop a material which is eco-friendly in nature and has low thermal transmittance (U-value). The development of foamed geopolymer consisting of glass powder as an alumina silicate source material has been done. Further, the developed material was compared with the conventional building materials. For validation of the glass powder foamed geopolymer (GPFG) blocks, they were tested for physical, mechanical and thermal performance. Also, the energy profile of building envelope comprising GPFG blocks was investigated and compared with conventional wall material. The eQuest simulation system was used as a tool to generate the energy profile model of building envelope. The experimental results of the GPFG blocks showed better thermal performance than conventional wall material. Also, the energy profile of the building envelope developed using GPFG clocks suggests annual energy consumption to be approximately 7.8% lower than that of conventional wall material.

Keywords Glass powder · Energy analysis · Geopolymer · Thermal transmittance

K. A. Khan · C. Sashidhar
Department of Civil Engineering, Jawaharlal Nehru Technological University, Anantapur, India

A. Raut (✉)
Department of Civil Engineering, Koneru Lakshmaiah Education Foundation, Vaddeswaram, Guntur (Dt.), AP 522502, India

C. Rama Chandrudu
Department of Civil Engineering, Chiranjeevi Reddy Institute of Engineering and Technology, Anantapur, India

B. Laishram and A. Tawalare (eds.), *Recent Advancements in Civil Engineering*, Lecture Notes in Civil Engineering 172,
https://doi.org/10.1007/978-981-16-4396-5_25

1 Introduction

Currently, building sectors is striving to be more and more sustainable in its approach. In order to achieve sustainability, the focus is to incorporate sustainable construction materials having certain features such as lightweight, thermally insulated, low-carbon footprints and better durability performances. Geopolymer is termed as a sustainable material which is currently being a major step towards suppressing the consumption of cementitious products. In the past decades, there have been a lot of advancements in terms of ways of development of geopolymer and its performance as well [1].

Foamed concrete is one of the recent advances in sustainable energy-efficient products. Due to its porous nature, it has several benefits such as easy handling and transportation, easy installation, being energy efficient and providing thermal and acoustic insulation. Foamed concrete is generally used for non-structural applications such as cast in situ and precast non-load bearing wall systems, facades, sandwich panels and insulation screeds [2]. The preparation of foamed concrete can be done by using two methods, i.e. chemical foaming and mechanical foaming. Chemical foaming can be done by generating voids in the mix by endogenous gas formation with the introduction of alumina powder or hydrogen peroxide (H_2O_2) or zinc powder in the mix, whereas in mechanical foaming method, bubbles are generated by mixing surfactants in the mix or premade foam is added to the mix [3].

Since geopolymer has been seen as one of the sustainable alternatives to the energy consumptive cementitious binder, researchers are trying to incorporate foaming concepts in geopolymer as well. Apart from a sustainability aspect, certain challenges in development of foamed geopolymer have to be tackled during its preparation. Emphasis should be given to control the nature, distribution and size of voids during the development of foamed geopolymer [4]. Also, the challenge is to achieve required strength for the indented applications while balancing it with foamed geopolymer's porous nature.

In this research, the focus is to develop the foamed geopolymer for reducing the energy usage of the building. Also, this research intends to use glass powder as a primary alkali silicate source material for the development of foamed geopolymer. In this research, a detailed energy analysis using eQuest simulation tool was conducted for building developed from waste glass powder-incorporated foamed geopolymer.

2 Materials and Methods

The raw materials utilized to produce the glass powder foamed geopolymer blocks are glass powder, fly ash, sodium silicate, sodium hydroxide and alumina powder. Initially, a copper slag geopolymer block (CSGB) consisting of copper slag as a

source material was developed. The raw materials required to develop the CSGB were divided into three parts;

(i) Solids—consisting of copper slag (CS), fly ash (class F) (FA) and crusher dust (CD),
(ii) Liquids—sodium silicate (Na_2SiO_3) and sodium hydroxide (NaOH),
(iii) Foaming agent—alumina powder (2% of solids).

The physical properties of copper slag and fly ash are listed in Table 1. The chemical composition of fly ash and copper slag is mentioned in Table 2, which provides an insight into the oxide ratio for understanding the reactivity of the materials during the process.

The process for foamed geopolymer starts with the preparation of an alkali solution one day prior to the casting of the blocks. The liquid ingredients (i.e. sodium hydroxide and sodium silicate) are intermixed to form an alkaline solution having the ratio of NA_2SiO_3/NaOH = 2.4. The solution consists of sodium hydroxide having a molarity of 14 M. The next day, the solid ingredients were mixed as per the proportion of fly ash/copper slag/crusher dust as 0.4:0.3:0.3. Once the all solids were batched and mixed together for 5–10 min, the prepared alkaline solution was poured in the dry mix and mixed to form a homogenous geopolymer mixture. During the wet mixing, a chemical foaming agent, i.e. alumina powder, was added to generate the voids. The mixture was transferred to the moulds, and moulds were completely filled without any compaction. The foamed geopolymer was transferred for oven curing at 60 °C until the geopolymer gets hardened. The physical (ASTM C20—2015 [8]), mechanical (ASTM C67—2014 [9]) and thermal (using Hot Disk TPS 2500S [10]) testing was conducted taking the average of three samples for each test to analyse the performance of foamed geopolymer.

Table 1 Physical properties of raw materials

Sr. No.	Name of test		Test method	FA	GP	Specification as per IS 3821 [5]
1	Grain size analysis	Gravels	IS 2720: 1985 [6]	0	2.1	–
		Sand		23.1	61.2	
		Silt and clay		76.9	36.6	
2	Consistency (%)		IS 1727 [7]	29.5	32	–
3	Specific gravity (g/cc)		IS 1727 [7]	1.995	2.67	–
4	Drying shrinkage (%)		IS 1727 [7]	0.025	1.805	–
5	Initial setting time (min)		IS 1727 [7]	120	144	Min 30 min
6	Final setting time (min)		IS 1727 [7]	230	268	Max 600 min
7	Compressive strength (MPa)		IS 1727 [7]	–	29.04	Min 80% of plain cement mortar cube
8	Soundness by autoclave (%)		IS 1727 [7]	–	0.05	0.8 max

Table 2 Chemical composition of raw materials

Sample	Fly ash	Glass powder
SiO_2	50.47	68.89
TiO_2	9.6	0.064
Al_2O_3	28.76	4.147
MnO	0.04	NA
Fe_2O_3	4.3	0.52
CaO	0.81	9.904
MgO	0.39	2.717
Na_2O	0.09	12.938
K_2O	0.77	0.568
P_2O_5	0.31	0
SO_3	4.3	0.198
BaO	ND	NA

After the comparative performance assessment of GPFG blocks, the energy simulation was conducted by using eQuest software to understand the impact of the materials on the energy requirements of the buildings. A standard residential building model as shown in Fig. 1 having a floor area of 3,000 sq. ft. was used for simulation purpose. The weather condition for modelled building was considered for Hyderabad region (latitude: 17.387140; longitude: 78.491684) having hot and dry climate. For the comparative analysis, similar model was developed having same features except the wall properties having red clay bricks as a base material provided as an input parameter.

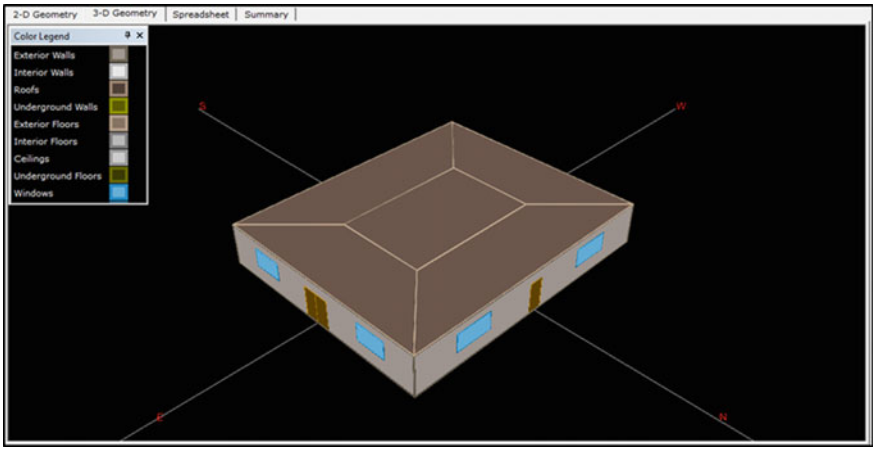

Fig. 1 eQuest model of building for energy analysis

3 Results and Discussion

Table 3 shows the comparative physical performance of glass powder incorporated with foamed geopolymer (GPFG) blocks and red clay bricks. From the results of physical performance, it is observed that the developed GPFG blocks are much lighter in density than the traditional red clay bricks which make transportation and handling of the material comparatively much easier. However, due to the porous nature of GPFG blocks the water absorption rate is much higher, but it complies with the standard criteria laid out by IS 3495 (Part 2): 1992 [11].

The mechanical performance is one of the crucial criteria for any building material. It is observed from Table 4 that the GPFG blocks have slightly lower compressive strength than that of traditional red clay blocks. But it meets the standard requirements of acceptability of 3.5 MPa as per IS 3495 (Part I): 1992 [11]. The main purpose of developing the GPFG blocks is to provide a sustainable alternative over red clay bricks having sustainability aspect as its primary feature. It is important that sustainable materials should provide benefits for the users during their operational stage. Thus, focusing on minimizing operational energy of buildings and to achieve this objective, the product should have an insulation property as a key feature.

Hence, thermal performance becomes one of the crucial features of the building materials; the thermal performance of GPFG blocks is shown in Table 5. The thermal conductivity is related to density and porosity of material. Thus, due to the porous nature of the GPFG blocks this restricts the particle-to-particle heat transfer

Table 3 Physical performance of developed materials

Physical performance	Red clay bricks	GPFG blocks
Avg. bulk density (kg/m^3)	1925	541.3
Avg. water absorption (%)	5.0 ± 0.25	13.89 ± 0.69

Table 4 Mechanical performance of developed materials

Mechanical performance	Red clay bricks	GPFG blocks
Avg. compressive strength (MPa)	4.61 ± 0.23	3.66 ± 0.18

Table 5 Thermal performance of developed materials

Thermal performance	Red clay bricks	GPFG blocks
Avg. thermal conductivity (W/m K)	0.72	0.167
Avg. specific heat capacity (J/kg K)	840	891
R-value (m^2 k/W)	0.138	0.598
Thermal diffusivity (m^2/s)	3.462×10^{-7}	3.462×10^{-7}
Thermal effusivity (Wk^{-1} m^{-2} s$^{1/2}$)	1078.9	283.8

causing low thermal conductivity values in GPFG blocks as compared to those in red clay blocks. Also, the heat capacity of material plays a crucial role in affecting thermal mass of the material. Non-steady heat transfer of the material is one of the factors affecting the indoor temperature due to the hourly variation of outdoor ambient temperature. Thus, to understand the speed of propagation of heat by conduction, the thermal diffusivity is computed. It is evident from the table that the thermal diffusivity is lower in case of GSFG blocks than red clay bricks, indicating better thermal performance against non-steady heat transfer. The thermal effusivity is related to the ability of material to absorb heat. The data presented in the table point out that GPFG blocks have lower thermal diffusivity than that of red clay bricks. Thus, all the data regarding thermal performance of materials strongly suggest that GPFG block proves to be a better thermal insulator than red clay brick.

The insulation performance of the building materials has a direct correlation with the energy requirements of the buildings. The insulation properties of building envelope bring down the load on the heating and cooling requirements affecting the overall energy demand of requirement for the building. The results of the simulation study performed using eQuest simulation tool are shown in Fig. 2. The results clearly show the percentage reduction in the energy needs for space cooling. The reduction of total annual energy contribution of 3% and peak load demand of 5% was observed if the building envelope is having GPFG blocks instead of traditional clay blocks. The total annual energy requirement for traditional clay bricks was observed to be 210.82×10^3 kWh, whereas the total annual energy requirement for GPFG blocks was 173.92×10^3 kWh, having total savings of 36.9×10^3 kWh.

Table 6 shows the monthly total energy consumption for both traditional red clay bricks and GPFG blocks. Table 6 shows the peak values during the months of April

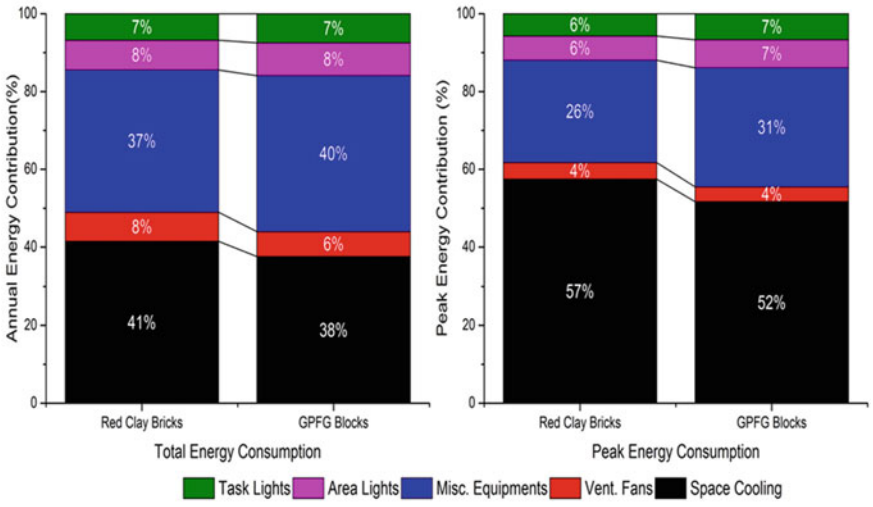

Fig. 2 Total energy and peak energy consumption for the modelled building

Table 6 Space cooling and total energy requirements for building

Months	Red clay bricks		GPFG blocks	
	Space cooling requirement ($\times 10^3$ kWh)	Total energy requirement ($\times 10^3$ kWh)	Space cooling requirement ($\times 10^3$ kWh)	Total energy requirement ($\times 10^3$ kWh)
January	11.1	36.02	9.96	34.18
February	12.67	35.37	10.11	32.16
March	20.65	46.04	16.2	40.83
April	24.85	50.4	19.32	44.15
May	26.65	51.86	20.42	44.9
June	21.24	46.08	17.34	41.44
July	18.96	44.68	16.17	41.15
August	17.76	43.1	15.25	39.85
September	17.78	42.55	15.23	39.28
October	17.73	43.46	15	40
November	11.4	34.1	9.89	31.9
December	10.05	35.82	9.05	34.07

and May due to the peak summer climatic conditions. It can be observed that the total energy requirement during the summer season is approximately 40% of total energy requirements of building envelope. The monthly energy consumption data show peak during the month of May contributing to 44,900 kWh energy demand for building envelope having GPFG blocks as a wall material. The space cooling requirements are reduced to a value of 20,420 kWh for GPFG blocks in the month of May, which is approximately 45.5% compared with traditional burnt red clay bricks. The energy requirement values for space cooling are low for building envelope having GPFG blocks due to the low heat transfer rate of the material which prevents the transfer of heat through the wall system. The insulated GPFG blocks do not allow the building envelope to raise its temperature, thus reducing the dependency on the cooling system.

The energy savings have an impact on the overall cost savings, which is analysed by using the monthly electricity costing represented in Fig. 3. The monthly electricity bills reached its peak during the month of May due to the energy consumption caused by the climatic conditions. The electricity bill was 26,000 $ for the month of May for building envelope having traditional red clay bricks, whereas the electricity bill was 22,600 $ for the month of May for building envelope having FCSG blocks. The total electricity bills savings were found to be 13.07% for the month of May having peak energy consumption. The annual electricity bills generated for the building envelope having GPFG blocks as a wall insulation were 225,992 $, whereas the annual electricity bills were higher in case of traditional red clay bricks. The annual saving on electricity bills shows approximately 9.9%

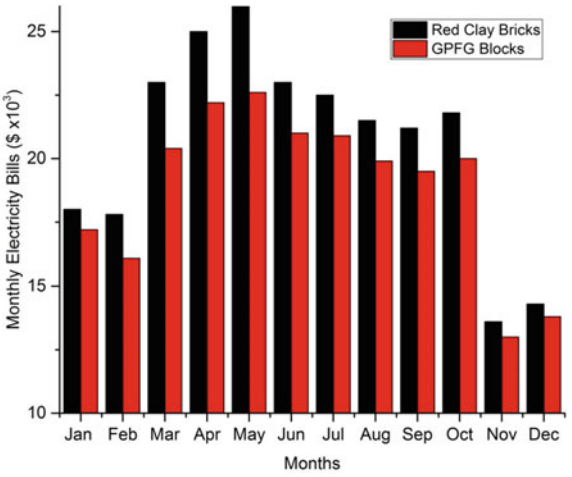

Fig. 3 Monthly energy costing of the modelled building

reduction with the usage of FCSG blocks instead of traditional red clay bricks. Thus, it is clearly evident that in terms of economic aspects, GPFG blocks prove to be more economical than the currently used red clay bricks.

References

1. Davidovits J (2008) Geopolymer chemistry and applications. Geopolymer Institute
2. Amran M, Farzadnia N, Ali AA (2015) Properties and applications of foamed concrete; a review. Constr Build Mater 101:990–1005
3. Hajimohammadi A, Ngo T, Mendis P (2017) How does aluminum foaming agent impact the geopolymer formation mechanism? Cem Concr Compos 80:277–286
4. Zhang Z, Provis JL, Reid A, Wang H (2014) Geopolymer foam concrete: an emerging material for sustainable construction. Constr Build Mater 56:113–127
5. Indian Standard IS 3821 (1975) Methods of mass of aluminum coating on hot-dip aluminized iron or steel articles
6. Indian Standard IS 2720-4 (1985) Methods of test for soils—part 4: grain size analysis
7. Indian Standard IS 1727 (1967) Methods of test for pozzolanic materials
8. American Standards ASTM C20-00 (2015) Standard test methods for apparent porosity, water absorption, apparent specific gravity, and bulk density of burned refractory brick and shapes by boiling water. ASTM International, West Conshohocken. www.astm.org
9. American Standards ASTM C67-12 (2014) Standard test methods for sampling and testing brick and structural clay tile
10. American Standards ASTM C1044-16 (2016) Standard practice for using a guarded-hot-plate apparatus or thin-heater apparatus in the single-sided mode. ASTM International, West Conshohocken. www.astm.org
11. Indian Standard IS 3495 Part I (1992) Methods of tests of burnt clay building bricks part 1 determination of compressive strength

Pozzolanic Rendering of Lime Sludge and Sandstone Reject Blend

Sandeep P. Tembhurkar, Akshaykumar Raut, and Mangesh V. Madurwar

Abstract The author has investigated the pozzolanic property of blended industrial rejects collected in sludge form from the textile industry and sandstone quarry. The pozzolanic potential of a blend of rejects was examined at 10, 20, 25, 30 and 35% replacing the primary binder, i.e. cement. The percentage replacement of each material was examined after mechanical treatment, i.e. grinding for 30 min duration. Percentage replacement was carried out based on quantitative presence of SiO_2, Al_2O_3 and Fe_2O_3 in industrial rejects to meet the requirement of IS 3812: (Part 1) 2013. The Pozzolana Activity Index, Chapelle Activity, and Electrical Conductivity tests were used to verify the pozzolanic ability of the blend. The Lime Sludge Reject (LSR) and Sandstone Sludge Reject (SSR) were characterized physically, chemically and mineralogically. The Ordinary Portland Cement (OPC) control mix will be used to compare the performance of blended concrete. The 28 days characteristic compressive strength (CCS) and durability properties were investigated. The identified industrial reject blend shows the improved pozzolanic efficiency when analysed statistically for optimum replacement of cement to make the cement industry more sustainable.

Keywords Pozzolanicity · Supplementary cementitious material · Industry rejects · Lime sludge · Sandstone sludge

1 Introduction

The solid wastes are being generated all around the world from the agriculture, industries and mines. Asia alone generates 4.4 billion tons of solid wastes in a year [1]. In India, it was 960 million tons annually noted in the last decades [2]. The generated material has been used in the landfilling and remaining material has been dumped on the open land. The dumped waste gets decomposed by environmental

S. P. Tembhurkar · A. Raut · M. V. Madurwar (✉)
Department of Civil Engineering, Visvesvaraya National Institute of Technology, Nagpur, Maharashtra, India

B. Laishram and A. Tawalare (eds.), *Recent Advancements in Civil Engineering*, Lecture Notes in Civil Engineering 172,
https://doi.org/10.1007/978-981-16-4396-5_26

gases, moisture and temperature. The society needs an alternative to the disposal of the wastes that comes from these industries. On the other hand, huge natural resources are getting used/exploited in manufacturing of the cement which is a primary binder material for the construction industry [3], which makes the cement industry as one of the largest CO_2 contributing industries [4, 5].

During the ancient civilization, the lime was used as a binder in many constructions [6]. Several materials are being used as pozzolana and supplementary binder with the cement [5]. Pozzolana plays an important role in the hydration process. The chemical compositions and morphological characterization are responsible for the proper pozzolanic reactions. Silica and alumina are the main oxides which react with water and for the formation of C–S–H gel in concrete [7]. CaO is the agent which participates mainly in binding. Many industrial rejects have been used in the concrete after proper treatment like Rice Husk Ash (RHA) [8], Granulated Blast Furnace Slag (GGBS) [9], Sugarcane Bagasse Ash (SCBA) [10] and Red Mud (RM) [11], etc.

In the present work, the pozzolanicity and compressive strength of paper mill waste and sandstone quarry sludge are studied. The Pozzolana activity index, Chapelle activity and Electrical conductivity methods were used to confirm the pozzolanic characteristic of the material. Chemical composition was carried out using X-ray Fluorescence and material phases were studied using X-ray Diffraction plots. Compressive strength at 28 days was experimentally determined to study the suitability for raw material blends in concrete.

2 Material and Methodology

2.1 Materials

In this experimental work the industrial rejects were used, which are available near to study area, i.e. Nagpur city, Maharashtra, India. Lime Sludge Reject (LSR), the by-product of paper mill industry and Sandstone Reject (SSR), a by-product of the stone quarry was collected. The Ordinary Portland Cement (OPC-53 grade) meeting the requirement as per IS 12269: 2013 [12] was used as a primary binder. The coarse aggregate of 20 mm, 10 mm and fine aggregate (Natural sand) was collected from the local market as per the IS 383-2016 [13]. The filler material was characterized as per IS 2386 (P1)-1963 [14].

2.2 Methodology

The collected material was ground in a high energized planetary ball mill to reduce the size of the raw material. Materials were milled for 30 min. duration. The milled

Table 1 Physical properties of lime sludge and sandstone sludge

Properties	LSR		SSR		OPC
Milling duration	0 min	30 min	0 min	30 min	–
Specific gravity	2.17		2.38		3.14
Density (g/cm^2)	0.36	0.48	0.63	0.67	1.25
Setting time—initial (min)	35	34	63	54	125
Final (min)	410	380	515	490	210
pH	8.35	9.22	9.04	8.89	6.8
Consistency (%)	–	39	–	33.44	28.5
Soundness (%)	0.021	0.01	−0.049	−0.051	1

samples are kept in airtight bags to maintain the humidity of materials [4, 15]. The granulometric distribution (particle size analysis) of samples was performed using the Saturm Digitizer model 5205. The characterization of the material was carried out using X-ray Fluorescence (XRF) and X-ray Diffraction (XRD). Physical properties such as Specific gravity, bulk density, Soundness, Initial and Final setting time, etc., were tested [16]. The pozzolanic properties of the milled sample were tested by Pozzolanic Activity Index as per specified in ABNT NBR 5752 [ABNT, 1992], Chapelle Activity [17] and Electrical conductivity [18]. The Pozzolanic Index test was carried out on the exposed mortar cubes by replacing the cement with 35%. The cubes were tested for the compressive strength after the 28 days water bath. The chemical titration method was performed to check the pozzolanicity of the material by Chapelle test. The quantity of $Ca(OH)_2$ was determined in this method. Electrical conductivity test was used to find the reactive drop of $Ca(OH)_2$ and Silica present in samples. At the temperature of 40 ± 1 °C, 5 gm sample and the $Ca(OH)_2$ dissolved liquid was stirred for 2 min duration. The difference between initial and final reading will indicate pozzolanicity of sample for the electrical conductivity test.

The concrete mix trial was designed for the M30 grade of the concrete (Standard Concrete as per IS 456: 2000). Table 1 shows the mix design for individual replacement and a blend of LSR and SSR. The LSR and SSR blend was used by replacing the cement at 10, 20, 25, 30 and 35%. The individual replacement of cement by 30% LLR and 30% SSR was also attempted. Three samples of 150 mm × 150 mm × 150 mm of each concrete trial were tested for characteristics compressive strength, after 28 days of continuous curing as per IS 2185 (P-1) 2005 [19]. The durability properties (viz. chloride content and sulphate content) of blended concrete were also tested to check its suitability for extreme environmental conditions [16].

3 Results and Discussion

3.1 Particle Size Distribution

The collected raw materials were ground in high energized planetary ball mill for 30 min. Figure 1 shows the granulometric distribution of as-received and milled LSR and SSR. The particle size of as-received LSR was noted at D50 = 349.68 nm and after milling for 30 min it becomes D50 = 306.5 nm. The average particle size of the as-received SSR was D50 = 310.56 nm and after milling for 30 min it becomes D50 = 280.12 nm, respectively. According to the particle size distribution curve, the particle size of the as-received sample was finer than that of a milled sample of LSR. It may be due to the agglomeration of material particles by the excess heat generated during the milling process.

3.2 Physical Properties

Table 2 shows the results of the physical properties of milled and as-received material. Specific gravity remains unchanged after milled for 30 min duration. The Specific gravity of as-received and a milled sample of LSR and SSR was 2.17 and 2.38, respectively. Grinding process has increased the density of LSR and SSR by 33% and 6%, respectively. It indicates that the particle surface area was increased and voids percentage reduced in material volume, which might help in improving the concrete strength. Initial and final setting time of ground material was higher than the OPC by 80% and 133% for LSR and SSR, respectively. The milled

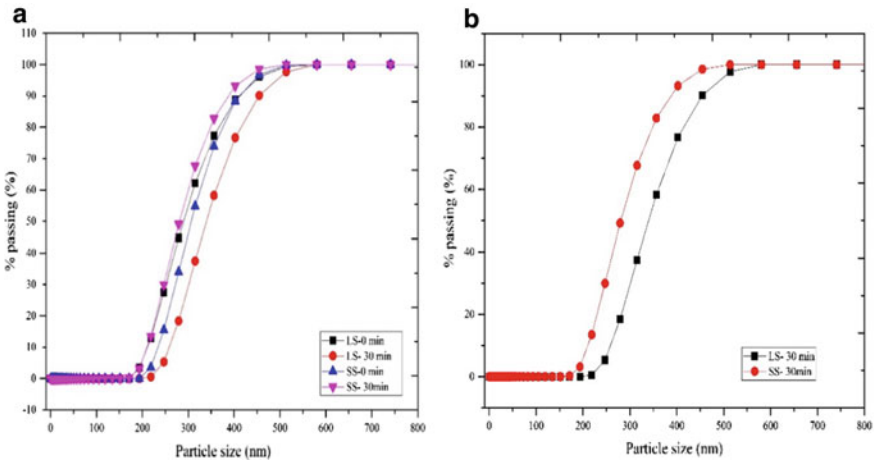

Fig. 1 Granulometric distribution curve of LSR and SSR

Table 2 Design mix proportions for M30 grade of concrete

Trials	OPC %	Lime sludge %	Sandstone sludge %	Natural sand %	Water cement ratio	Coarse aggregate %	
						20 mm (60%)	10 mm (40%)
LSR + SSR-1	90	5	5	100	0.42	60	40
LSR + SSR-2	85	7.5	7.5				
LSR + SSR-3	80	10	10				
LSR + SSR-4	75	12.5	12.5				
LSR + SSR-5	70	15	15				
LSR	70	30	0				
SSR	70	0	30				
Control concrete	100	0	0				

materials required more time to complete the hydration process. From the pH test, it was observed that all rejects were more alkaline than the OPC. The consistency of grind LSR and SSR was noted higher than that of OPC by 36% and 17%, respectively, which means that LSR and SSR required more water binder ratio than the OPC to achieve standard consistency. The soundness test measures the volumetric change in the paste of the material due to the presence of the excess Lime and Magnesia. The percentage of lime and magnesia presenting LSR and SSR were comparatively less than the OPC, signifying lesser volume changing in soundness [IS1489 (Part 1): 1991] [20].

The X-ray Diffraction of the as-received and milled materials is shown in Fig. 2. As-received LSR was reflecting a crystalline phase. After ultrafine grinding, the scattered lines between 20º and 30º at 2θ position show the presence of amorphous silica. As-received crystalline LSR converted to the amorphous phase due to mechanical milling that helps significantly to improve the pozzolanic property of the material. The morphology of the SSR was not changed even after the milling. Only the particle size of the material gets changed. The XRD plot shows the crystalline phase before and after milling.

The chemical composition of as-received and milled material is compared in Table 3. The comparative data indicate that silica present in the SSR (0–30 min) is 28 times higher than the LSR (0–30 min). SiO_2, Al_2O_3 and Fe_2O_3 are not adequate to use as a supplementary cementitious material as per IS 3812: 2013 [21].

3.3 Pozzolanic Activity

The pozzolanicity results of the materials are mentioned in Table 4. Pozzolana activity index (PAI), Chapelle activity test (CA), and Electrical conductivity (EC) were performed for checking the potential pozzolanic ability of the samples.

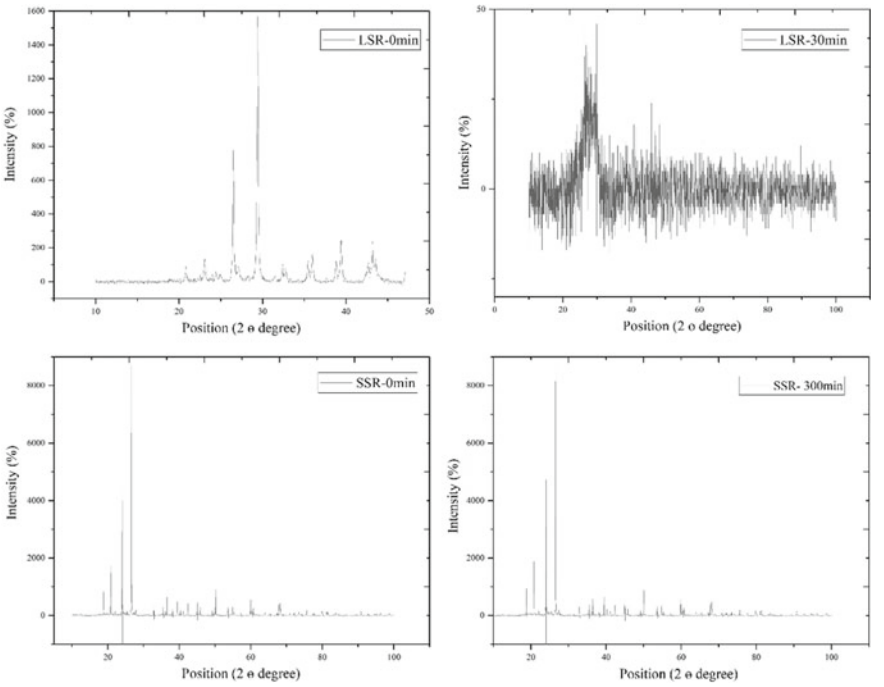

Fig. 2 X-ray diffraction of lime sludge reject and sandstone sludge reject

Table 3 Chemical composition of LSR and SSR in percentage

Sample ID	SiO_2	Al_2O_3	CaO	MgO	Fe_2O_3	LOI	Al + Si + Fe
LSR—0 min	3.13	0.88	62.46	0.12	0.23	31.31	4.24
LSR—30 min	3.37	1.09	58.87	0.14	0.35	33.89	4.81
SSR—0 min	85.32	6.18	0.39	0.79	2.68	1.94	94.18
SSR—30 min	85.47	5.81	0.96	0.82	2.37	2.02	93.65

Table 4 Pozzolanicity of LSR and SSR in percentage

Sample ID	Milling duration (min)	PAI (N/mm^2)	CA (mg $Ca(OH)_2$/g sample)	EC (μS/cm)
LSR	WM	7	184.39	4.12
	30 min	9	491.69	5.01
SSR	WM	13	184.39	4.04
	30 min	18	614.62	4.10

In PAI test 35% of cement was replaced to cast the mortar blocks at 1:3 proportion. In PAI test SSR and LSR achieved the compressive strength as per IS 2250: 1981. The LSR PAI was improved after ultrafine milling but was less than the SSR-milled sample. It was caused because of the insufficient availability of compound silicon dioxide to form the C–S–H gel. The available silicon dioxide was not sufficient for hydration reaction and comparatively an amount of CaO was excess which forms undesirable $Ca(OH)_2$. LOI content was excess in LSR sample, and hence it may require the suitable thermo-mechanical/thermo-chemical or calcination treatment to reduce it. The Chapelle activity test was performed to find the suitability of pozzolana chemically in the laboratory of Civil Engineering Department, VNIT, Nagpur. The trend shows that the milling process enhanced the pozzolanic property in Chapelle activity. In this method, the amount of $Ca(OH)_2$ was determined, which participated in silica and alumina gel formation. The $Ca(OH)_2$ mg/g of SSR was 1.26 times higher than the LSR after milling the materials. The Electrical conductivity test was also used to find the reactive drop of $Ca(OH)_2$ and Silica present in samples. The difference between initial and final reading on electrical conductivity meter is shown in Table 4. The electrical conductivity drop of all the samples before and after milling clearly shows that samples were the good pozzolanic material potential.

3.4 Compressive Strength of Concrete

The compressive strength of LSR and SSR blended concrete is shown in Fig. 3. The compressive strength was compared for 28 days of curing duration. The strength of blended concrete was checked at 10, 20, 25, 30 and 35% cement replacement. The increase in percentage replacement of blend of LSR and SSR reduced the strength of concrete; it decreased by 68% at 35% cement replacement. The compressive strength was gradually increased up to the 30% cement replacement by around 20% at individual percentage replacement. From the obtained compressive strength results, it is clear that the LSR cannot be used as a supplementary cementitious material due to non-availability of sufficient amount silicon dioxide as per IS 3812: P-1-2013 though the material showed the improvement in pozzolanic properties after mechanical milling which may be due to the increase in surface area, reaction rate, increase in compaction factor, etc. Similarly the SSR samples have shown the significant presence of silica in its chemical analysis but the X-ray diffractometer plot clearly shows the crystalline nature of silicon dioxide which will not take part in contributing the secondary C–S–H gel, and hence SSR material also cannot be used as supplementary cementitious materials. This entire experimentation shows the importance of concrete trials in the construction industry as all the available pozzolanicity test shows the positive results but the material characterization and concrete trials rule out the possibility of utilization of LSR and SSR as supplementary cementitious material. The carried out study shows that the material samples are alkaline, having all the oxides which are generally present in

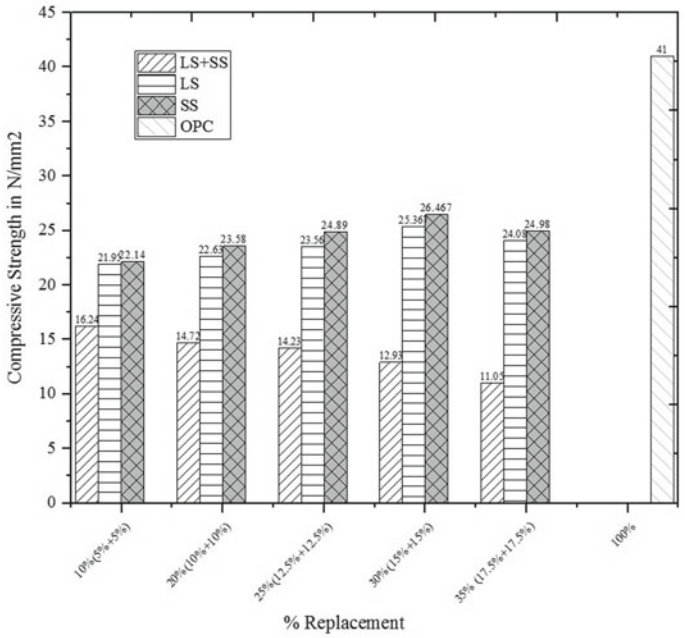

Fig. 3 Compressive strength of LSR and SSR at different % replacement

OPC and due to crystalline phase the material will not take part in hydration process and becomes inert, and hence the identified material directly can be used as filler material without any thermo-mechanical treatment for low-grade concrete or filler material for masonry building brick/block, etc., so that the identified problem of waste disposal also gets addressed along with the sustainability aspect of building construction industry.

4 Conclusion

From the results described in this work the following conclusion can be drawn:

- The material shows the agglomeration due to increasing the duration and energy of the milling, which was affected by the gradation of material. Therefore, the suitable grinding method can be used.
- The Pozzolanic performance was improved by milling process which was confirmed by the results of Pozzolana Activity Index, Chapelle Activity test and Electrical Conductivity.
- The morphological results discovered that the as-received LSR sample was crystalline and after milling for 30 min duration it converted to an amorphous

phase. There was no significant change observed in the XRD pattern of as-received and a milled sample of SSR, and hence it is predicted that SSR was fully crystalline material and will not take part in the hydration process.

- The results of the XRF revealed that the LSR required the other mechanical treatment to nullify the LOI presence. Due to the unavailability of sufficient SiO_2, the LSR could not participate in secondary C–S–H gel formation of hydration reaction. Similarly, the SSR contained 82% of crystalline SiO_2 (from the crystalline phase XRD Plot) shows the unsuitability of SSR to become supplementary Cementitious Material/Pozzolana which proved from the XRD.
- The increase in replacement percentage decreased the compressive strength of blended concrete. From all the tests and experimentation, it was proved that the LSR and SSR were pozzolanic, but cannot be used as a supplementary cementitious material in concrete.

As the materials are crystalline and having other chemical compounds similar to that of cement the same can be used as a filler material for low-grade concrete, for making the concrete for a temporary structure. It also can be used by the local building brick/block manufacturing industry as a replacement to natural sand. This will also help to achieve sustainability in building construction industry by addressing the issue of waste disposal.

References

1. Madurwar MV, Ralegaonkar RV, Mandavgane SA (2013) Application of agro-waste for sustainable construction materials : a review. Constr Build Mater 38:872–878. https://doi.org/10.1016/j.conbuildmat.2012.09.011
2. Katare VD, Madurwar MV (2017) Experimental characterization of sugarcane biomass ash—a review. Constr Build Mater 152:1–15. https://doi.org/10.1016/j.conbuildmat.2017.06.142
3. Ganesan K, Rajagopal K, Thangavel K (2007) Evaluation of bagasse ash as supplementary cementitious material. Cem Concr Compos 29(6):515–524. https://doi.org/10.1016/j.cemconcomp.2007.03.001
4. Katare VD, Madurwar MV (2018) Pozzolanic performance resemblance of milled sugarcane biomass ash using different pozzolanicity test methods. Adv Cem Res 1–11. https://doi.org/10.1680/jadcr.18.00061
5. Cordeiro GC, Toledo Filho RD, Tavares LM, Fairbairn EMR (2009) Effect of calciantion temperature on the pozzolanic activity of sugarcane bagasse ash. Constr Build Mater
6. Walker RO, Spavia SA (2011) Physical properties and reactivity of pozzolans and their influence on theproperties of lime pozzolan pates. Mater Struct 44
7. Zain MFM, Islam MN, Mahmud F, Jamil M (2011) Production of rice husk ash for use in concrete as a supplementary cementitious material. Constr Build Mater 25(2):798–805. https://doi.org/10.1016/j.conbuildmat.2010.07.003
8. Sensale D (2006) Strength development of concrete with rice-husk ash. Cem Concr Compos 28:158–160. https://doi.org/10.1016/j.cemconcomp.2005.09.005
9. Singh M, Garg M (1999) Cementitious binder from fly ash and other industrial wastes. Cem Concr Res 29:309–314
10. Madurwar MV, Mandavgane SA, Ralegaonkar RV (2014) Use of sugarcane bagasse ash as brick material. Curr Sci 107(6):1044–1051. https://doi.org/10.1046/j.1365-2222.2000.00820.x

11. Tsakiridis PE, Oustadakis P (2004) Red mud addition in the raw meal for the production of Portland cement clinker. 116:103–110. https://doi.org/10.1016/j.jhazmat.2004.08.002
12. Bureau of Indian Standards (BIS) (2013) No title 'ordinary Portland cement-specifications'. IS 12269, New Delhi, India
13. IS383 (2016) Coarse and fine aggregate for concrete (third edn). Indian Standard Code, pp 1–17
14. Bureau of Indian Standards, IS 2386-3 (1963) Methods of test for aggregates for concrete, part 3: specific gravity, density, voids, absorption and bulking
15. Cordeiro GC, Toledo Filho RD, Tavares LM (2008) Pozzolanic activity and filler effect of sugar cane bagasse ash in Portland cement and lime mortars. Cem Concr Compos 30:410–418. https://doi.org/10.1016/j.cemconcomp.2008.01.001
16. Bureau of Indian Standard. Indian Standerd 456:2000
17. Raverdy M et al (1980) Appreciation de l'activite pouzzolanique de constitutes secondaires. In: Proceedings of 7e congr int la Chim. des Ciments, Paris, Fr
18. Luxan MM (1989) Rapid evaluation of Pozzolanic activity of natural products by conductivitiy measurement. Cem Concr res 19
19. BIS: 2185 (2005) Indian standard concrete masonry units, part 1: hollow and solid concrete blocks. Bureau of Indian Standard, New Delhi, p 17
20. Bureau of Indian Standard (BIS) (1991) Portland pozzolana cement-specification. IS 1489 (part 1, third rev), New Delhi, India
21. IS: 3812 (Part-1) (2013) Pulverised fuel ash—specification, vol 3812. Bureau of Indian Satandard, pp 1–12

Use of Fly Ash and Bottom Ash in Lieu of Natural River Sand in Pavement Quality Concrete Dosed with a New Generation Superplasticizer (Master FlyAsh)

Abhyuday Titiksh, Swapnil P. Wanjari, Ashim Kumar Goswami, V. Debnath, and Chandrasekar Somu

Abstract This study was aimed at exploring the possibility of utilizing fly ash (FA) and bottom ash (BA) as fine aggregates in pavement quality concrete (PQC), in the presence of a fast-acting new generation superplasticizer (NG-SP) procured from Aaradhya Chemicals, Nagpur. Multiple mix designs were carried out but only three trial mixes containing varying proportions of FA and/or BA are presented here for the sake of brevity. Upon obtaining the desired flowability, the physio-mechanical characteristics of the batches were evaluated in terms of compressive strength, flexural strength, split tensile strength, water absorption and abrasion resistance. Durability studies were also conducted to assess the long-term behavior of the pavement. The samples containing 100% FA as exhibited superior performance as compared to the other mixes. Overall, both Trial 1 (100% FA) and Trial 2 (50% FA + 50% BA) exhibited acceptable strength properties as per the codal requirements of IRC 15: 2011 for PQC, with a 28-day compressive strength of 50.92 N/mm^2 and 49.76 N/mm^2 respectively. The samples of Trial 3 (100% BA), however, failed to meet the necessary codal requirements for PQC, enabling us to conclude that complete replacement of river sand in concrete pavements with either 100% FA or a combination of FA and BA in equal proportion is an eco-friendly and cost-effective alternative to the traditional mix design approach. Post lab evaluation, a 50 m^3 site trial was undertaken at NTPC Khargone and was found to be satisfactory.

Keywords Fly ash · Bottom ash · New generation SP · Sand replacement · HVA concrete

A. Titiksh (✉) · S. P. Wanjari
Department of Civil Engineering, Visvesvaraya National Institute of Technology, Nagpur, India

A. K. Goswami · V. Debnath · C. Somu
National Thermal Power Corporation, Khargone, India
e-mail: vdebnath@ntpc.co.in

B. Laishram and A. Tawalare (eds.), *Recent Advancements in Civil Engineering*, Lecture Notes in Civil Engineering 172,
https://doi.org/10.1007/978-981-16-4396-5_27

1 Introduction

Natural river sand is used as a fine aggregate in concrete. However, the non-availability of required graded sand in and around the construction sites and in all seasons possesses problems and sometimes adversely affects the progress of the work. Albeit having alternatives such as manufactured sand and crushed stones, a permanent solution to the river sand shortage has yet to be presented [1–5]. Furthermore, bottom ash utilization is the bare minimum in plant area [6, 7]. In this paper, we would like to elaborate how a new liquid superplasticizer (Master FlyAsh Superplasticizer, Aaradhya Chemicals, Nagpur) specially designed for the utilization of fly ash/bottom ash as a complete replacement to river sand/crushed sand was used in concrete in NTPC, Khargone as recommended by VNIT, Nagpur (NTPC Approved Third Party Lab). This admixture is an innovative product (under the Make in India initiative) which complies with IS 9103: 1999 (Concrete admixture —Specification) to be used in concrete as per the requirement of IS 456: 2000 (Plain and reinforced concrete—Code of practice). M/s Aaradhya Chemicals, Nagpur had applied for BIS certification for the Master FlyAsh new generation superplasticizer (NG-SP) and the license for the same has been granted.

Replacement of sand was carried out at varying percentages, however, only the results of the three adopted trial mixes are presented here for the sake of brevity. The performance of the trial batches were compared in terms of compressive strength, split tensile strength, flexural strength, water absorption and abrasion resistance. Durability studies was also carried out and the concrete was evaluated in terms of the results of rapid chloride permeability test (RCPT) and accelerated carbonation test. The adopted NG-SP was also cross-checked in accordance with the stipulations laid down in IS 9103: 1999 and was found to be satisfactory.

2 Materials and Mix Design

Ordinary Portland Cement 43 grade (OPC 43) conforming to IS 8112: 2013 manufactured by UltraTech Cement (procured locally) was used in this study. Table 1 presents the physical and chemical properties of the cement. Crushed stone aggregate quarried from Pachgaon, Maharashtra (with maximum size 20 mm) was procured from local vendors and used in accordance with the stipulations laid down in IS 383: 2016. The results of aggregate testing are presented in Table 2. FA and BA used in this study were procured from Selda Thermal Power Plant, National Thermal Power Corporation, Khargone, India (NTPC Khargone). They are a by-product and hence their physical, mineralogical and chemical characteristics are highly dependent on multiple variables including coal form and mineralogical structure, furnace processing situations, etc. The chemical analysis of FA was carried and it was characterized as a low-calcium Class-F FA. The same for BA was not carried out as BA is characterized simply by size. The BA used in this study was slightly coarser in nature.

Table 1 Physio-chemical properties of cement and FA used in this study

Chemical properties	OPC 43 cement		Class-F FA	
	Observed	Requirement as per IS 8112: 2013	Observed	Requirement as per ASTM C618
Calcium oxide (CaO) (%)	58.7	–	5.33	–
Silica content (SiO_2) (%)	19.6	–	52.32	–
Ferric oxide (Fe_2O_3) (%)	6.32	–	5.16	–
Aluminum oxide (Al_2O_3)	8.48	–	27.13	–
SiO_2 + Fe_2O_3 + Al_2O_3 (%)	34.4	–	84.61	>70%
$\frac{CaO-0.7SO_3}{2.8SiO_2+1.2Al_2O_3+0.65Fe_2O_3}$	0.835	0.66–1.02	0.028	–
Ratio of Al_2O_3 to Fe_2O_3	1.341	>0.66		
Sulphate (SO_3) (%)	1.3	<3.5%	0.15	<5%
Magnesia (MgO) (%)	0.76	<6%	1.57	<5%
Soda + Potash (Na_2O + K_2O) (%)	0.49	<0.6%	0.044	<1.5%
Loss on ignition (%)	3.1	<5%	4.48	<6%
Fineness by blains (m^2/kg)	293	>225 m^2/kg	329	–
Soundness (mm)	2	<10 mm	0.08	–
Specific gravity	3.14	–	2.23	–
Normal consistency (%)	31.5	–	–	–
Vicat time of setting (min)				
Initial	140	30 minimum	–	–
Final	455	600 maximum	–	–

Table 2 Physical properties of coarse aggregates used in this study

Properties	10 mm coarse aggregates	20 mm coarse aggregates	Requirement as per IS 383: 2016
Bulk loss density (kg/m^3)	2350	2325	–
Bulk compacted density (kg/m^3)	2581	2564	–
Organic impurities	Nil	Nil	<1%
Material fines than 75 μ (%)	–	–	<15%
Silt/clay content (%)	–	–	<1%
Soundness (Na_2SO_4) (%)	8.7	8.9	<12%
Alkali aggregate reaction (%)	0.04	0.05	<0.1%

As declared earlier, multiple mix designs were carried out, however, only three mix designs corresponding to a 28-day compressive strength of 40 MPa (M40), typically used for PQC, are shown here for conciseness. They are designated as follows:

Table 3 Concrete mix design adopted for this study

Properties	Trial 1 (control)	Trial 2	Trial 3	Trial 4
Grade of concrete	M40	M40	M40	M40
Cement (kg/m^3)	450	400	400	400
FA (kg/m^3)	–	512	185	–
BA (kg/m^3)	–	–	165	509
Free water (kg/m^3)	140	160	160	165
Total water (kg/m^3)	184	214	219	234
River sand (kg/m^3)	860	–	–	–
10 mm aggregate (kg/m^3)	420	473	545	478
20 mm aggregate (kg/m^3)	640	945	1025	966
SP (kg/m^3)	4.5	3.2	3.4	3.6
SP details	*Auramix 300*	NG-SP (*Master FlyAsh*)		
Slump				
Initial	Collapse	Collapse	Collapse	Collapse
After 1 h (mm)	55	60	55	50
Air content (%)	2	1.5	1.7	1.9
Density (kg/m^3)	2555	2568	2557	2563

- 'Trial 1' (100% FA),
- 'Trial 2' (50% FA + 50% BA), and
- 'Trial 3' (100% BA)

The mix design was done in accordance with IS 10262: 2019 and IRC 15: 2011 and the concrete mix proportions are presented in Table 3. The trial mixes were dosed with a commercially available new generation poly-carboxylate (PC) based SP procured from *Aaradhya Chemicals* (*Trade name-Master FlyAsh*). The same was cross-checked according to the codal provisions of IS 9103: 1999 [8] and was found to be satisfactory as shown in Table 4. The mix design was carried out for moderate exposure conditions with a target slump and retention time of 25–40 mm and 60 min respectively.

3 Experimental Investigation

The concrete mixes were prepared by 15 min mixing in a power driver concrete pan mixer and properties of fresh concrete were evaluated in terms of slump and unit weight in accordance with IS 1199 (Part 7): 2018. The freshly mixed concrete was allowed to rest in the mixing pan for an hour and then placed in the respective molds for testing as per IS 516: 1959. The molds, after filling the concrete (Fig. 1), were compacted on a power-driven vibrating table and left to set. They were kept in a cool place at an ambient temperature of 27 ± 2 °C and covered with a damp jute

Table 4 Chemical properties of the NG-SP '*Master FlyAsh*' used in this study

Properties	Observed values	Values declared by the manufacturer	Requirement as per IS 9103: 1999
Relative density	1.09	1.1	Within 0.02 of the value stated by the manufacturer
pH	6.4	6.5	6.0 minimum
Dry material content (%)	27.9 (=DMC)	27 (=T_1)	$0.95T_1 < DMC < 1.05T_1$
Chloride content (%)	0.0021	0.2 maximum	Within 10% of the value or within 0.2% whichever is greater as stated by the manufacturer
Ash content (%)	3.41 (=AC)	3.5 (=T_2)	$0.95T_2 < AC < 1.05T_2$

Fig. 1 Cube specimens of 100% FA before demoulding and marking

mat. The blocks were demoulded after 24 h, marked (Fig. 2) and placed inside a water curing tank (Fig. 3). They appeared to be free from surface defects and/or cracks and had a smooth finish. The cubes containing 100% FA appeared to be grayish in color while the ones containing 100% BA appeared to be dark gray in shade.

4 Results and Discussions

The results of the compression test are shown in Fig. 4. It can be clearly seen that all the trials except Trial 4 have successfully achieved the desired target mean strength within 28 days. This means the pavement can easily take up the design load. The point of interest was Trial 2, i.e., 100% FA samples achieving a slightly

Fig. 2 Marking on cube samples

Fig. 3 Water curing of samples

higher strength in comparison to the other trials. This can be attributed to the large quantity of FA which is known to hydrate at a later age and contribute mainly to the 28 days strength of the concrete. However contrary to the observed results, prior studies have shown the 28 days strength of HVFA for higher dosages of FA to be very low. A possible explanation for this scenario is the presence of NG-SP which may have chemically activated the excess FA in the mix, thereby making it contribute to the strength gain fairly quicker. These findings are in stark contrast to the ones reported by [6, 7, 9–20], also suggesting the involvement of the NG-SP in the chemical reactions. The 3-day, 7-day and 28-day compressive strength of Trial 2 (100% FA) were observed to be 21.31 N/mm^2, 36.28 N/mm^2, and 50.92 N/mm^2 respectively while the same for Trial 3 (50% FA + 50% BA) were observed to be 20.35 N/mm^2, 33.68 N/mm^2, and 49.76 N/mm^2 respectively. These values easily surpassed the minimum strength requirements as per Indian codal provisions

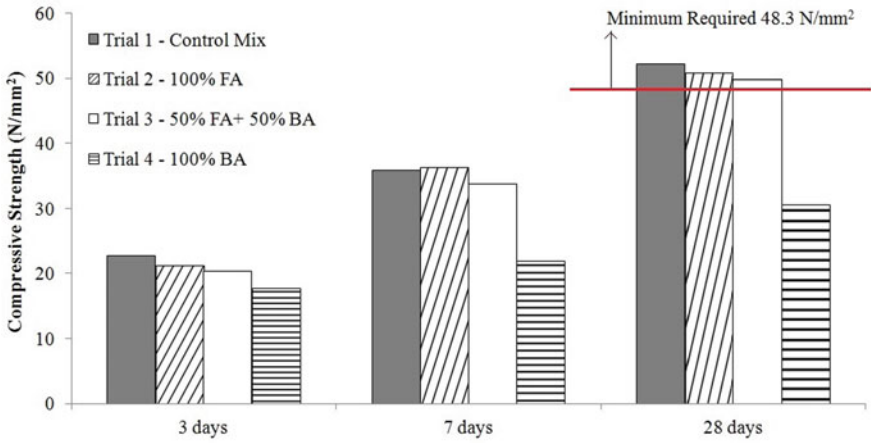

Fig. 4 Results of compressive strength test

indicating that the design mix adopted was optimal. This can result in a substantial saving in terms of cement used as the trials used 50 kg/m^3 lesser cement as compared to conventional PQC mixes.

On the other hand, the results of Trial 3 failed to meet the minimum requirements of codal provisions. There was a dramatic decrease of 16.37%, 39.58% and 39.81% in the 3-day, 7-day and 28-day compressive strength of Trial 3 (100% BA) samples respectively as compared to Trial 1. The comparatively coarser BA particles failed to provide the necessary bonding to the concrete and this suggests that complete replacement of natural river sand with BA is not a feasible alternative for concrete pavement works. It might be possible to obtain the necessary strength characteristics by varying the types and dosages of admixtures used in the concrete.

The tests for flexural strength and split tensile strength were carried out as explained earlier and the average results of three samples for each trial are presented in Figs. 5 and 6 respectively. Samples of 100% FA (Trial 1) exhibited a 28-day flexural strength of 5.83 N/mm^2 and a split tensile strength of 3.78 N/mm^2 which met the minimum requirements as per the Indian codal provisions. These higher values can possibly be attributed to two reasons-chemical activations of FA in presence of NG-SP which led to the early strength gain of concrete; and the presence of more fines in the form of FA which led to a dense more solid microstructure of the concrete.

Samples of 50% FA + 50% BA (Trial 2) exhibited a slight decrease of 4.8% while samples of 100% BA (Trial 3) exhibited a staggering 48.19% decrease in the 28-day flexural strength. This indicated that although incorporating either FA or a combination of FA and BA in equal proportions in PQC exhibited acceptable strength characteristics, incorporating 100% BA in the mix in place of fine aggregates tends to reduce the strength drastically. The inter-particle bonding seems to be weak when BA is introduced in the mix in the case of Trial 3 and the same is

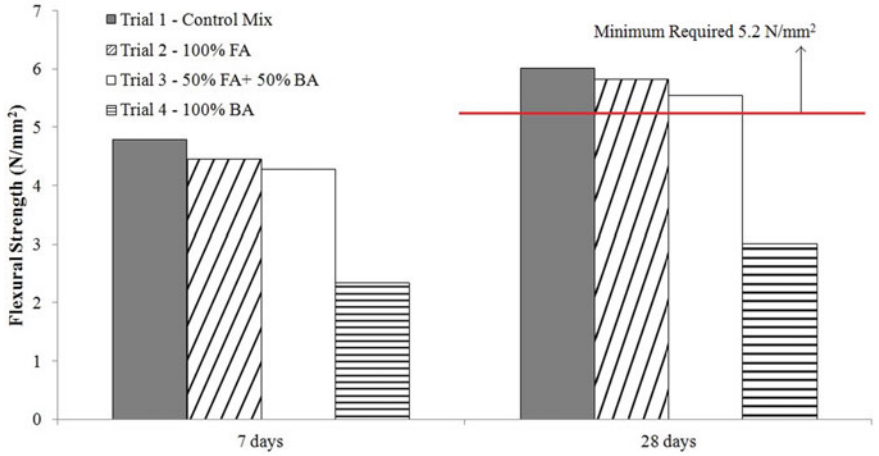

Fig. 5 Results of flexural strength test

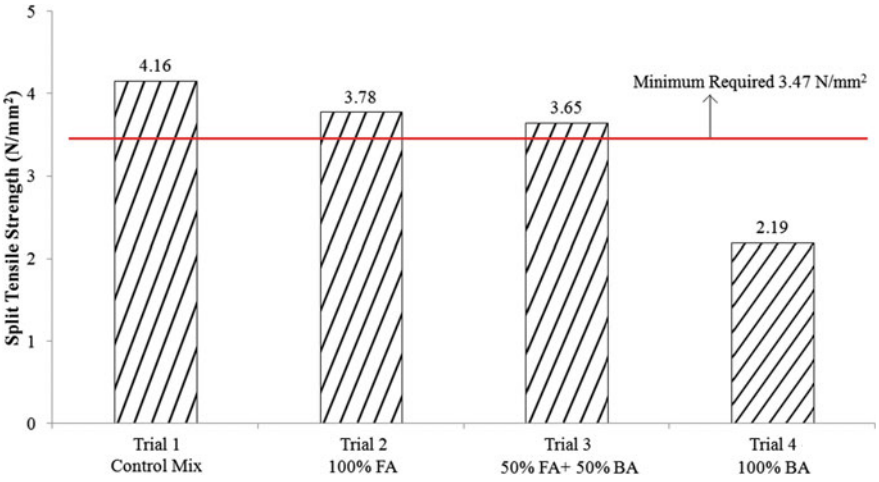

Fig. 6 Results of split tensile strength test

also evident by the results of Trial 2 wherein the flexural strength is slightly reduced in contrast to Trial 1. Similarly, the split tensile strength of Trial 2 and Trial 3 also exhibited a decrease of 3.43% and 42.63% respectively. These observations clearly indicated that both Trials 1 and 2 easily met the strength requirements of PQC.

The results of water absorption test and abrasion resistance test are presented in Figs. 7 and 8 respectively. All the trial samples exhibited water absorption less than 6% which is in compliance with the codal requirements, except Trial 3 whose water absorption was 9.53%. The samples of Trial 1 exhibited water absorption of only

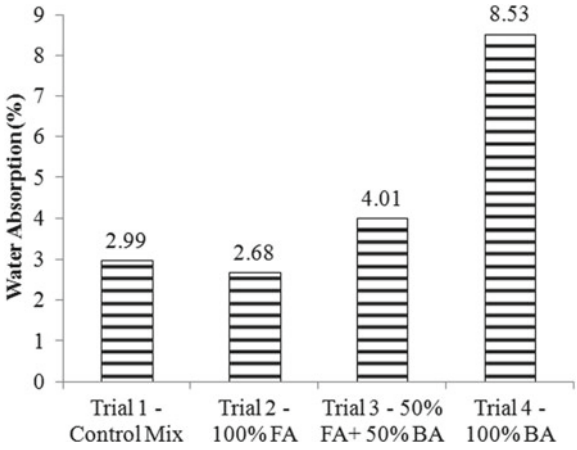

Fig. 7 Results of water absorption test

2.68% while samples of trial 2 exhibited a water absorption of 4.01%. This can be attributed to the denser packing of the materials in Trial 1 due to the presence of finer FA particles, which makes it more impermeable. With the introduction of BA, the inter-particle spacing increased which led to slightly higher water absorption in Trial 2. The water absorption of Trial 3 samples was observed to be 8.53% which is 47.83% higher in comparison to Trial 1.

The volumetric loss was roughly the same for all the trial samples indicating an almost similar resistance to abrasion. However, Trial 1 samples exhibited the highest abrasion resistance with the least volumetric loss of 2214 mm^3/5000 mm^2. A well-graded aggregate sample properly bonded with cement and ash is crucial to providing resistance against abrasive forces which are a combination of normal loads and shear loads from the traffic. The trial samples exhibited roughly the same abrasion depth of 0.4–0.6 mm which is within the acceptable limit of 2 mm. These abrasion resistance values are likely to further improve with the age of concrete.

The results of durability studies in terms of RCPT and carbonation depth are presented in Figs. 9 and 10 respectively. As per ASTM C1202, samples of Trials 1, 2 and 3 exhibited excellent resistance to chloride migration while Trial 4 exhibited acceptable results. A total of 3 samples were tested for each trial mix. The obtained value of charge passed for all the samples lies in the ranges of either 100–1000 Coulombs or 1000–2000 Coulombs corresponding to Very Low and Moderate permeability classes respectively. Hence, durability as per RCPT is found to be satisfactory for all the trials. The mean carbonation depth for 3 samples when tested after 28 days was also found to be almost similar with Trial 2 samples exhibiting the least carbonation depth of 8.1 mm.

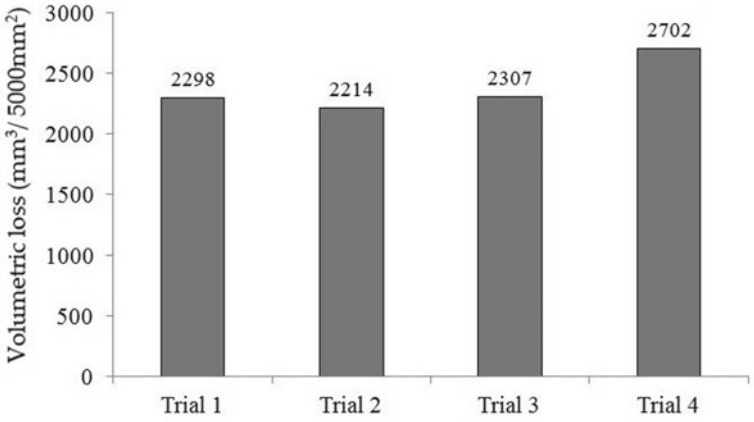

Fig. 8 Results of abrasion resistance test

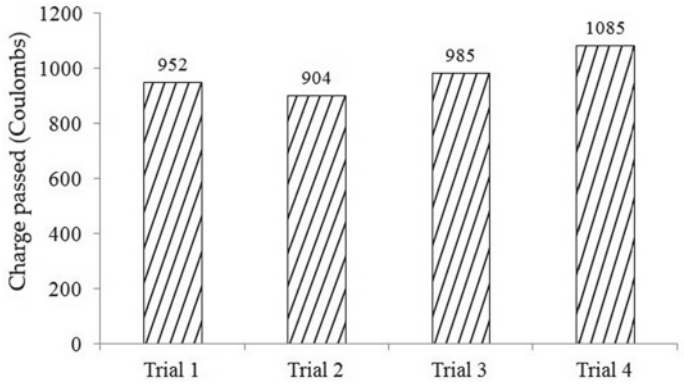

Fig. 9 Results of RCPT

5 Case Study at NTPC Khargone

After obtaining satisfactory laboratory results, a case study was carried out at NTPC, Khargone with the consultation of VNIT, Nagpur. The physical and chemical properties of FA and BA were evaluated at VNIT, Nagpur (samples of 200 kg of each BA and FA were sent to VNIT by NTPC Khargone). Based on the suitability of FA and BA and the recommendations of VNIT, various trail mixes at the site lab were conducted at Khargone. Inputs from the site about concrete mix were taken and subsequently, a suitable mix design was provided by VNIT, Nagpur after carrying out the durability studies (Table 5).

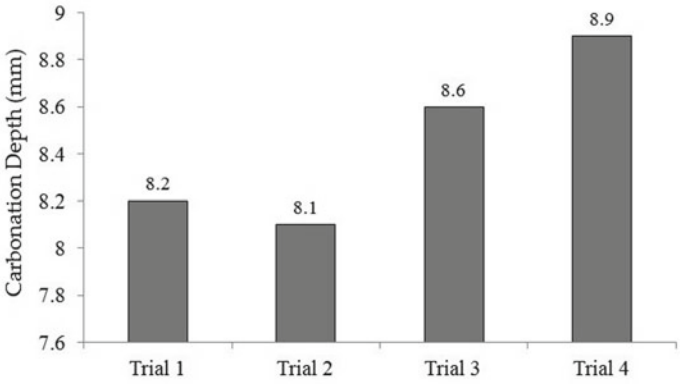

Fig. 10 Results of accelerated carbonation test

Table 5 Work description at NTPC Khargone

S. No.	Grade of concrete	Description
1	M 25	100% replacement of natural sand with 50% fly ash + 50% bottom ash using Admixture—Master FlyAsh Superplasticizer
2	M40—pavement quality concrete	
3	M 10—dry lean concrete (DLC)	

5.1 Works Carried Out at NTPC Khargone

Completed

1. M25—150 m stretch of walkway from Aux. Boiler to Compressor house
2. M25—Paving concrete—Safety Park

In-Pipeline

1. M25—300 m Stretch walk walkway from Compressor house to FOPH
2. DLC M10 and M40—5 km single-lane railway siding road (Fig. 11)

Tangible Benefits

Grade	Rate as per DSR 2016 per cum (INR)	Rate as per VNIT design mix per cum (INR)	Cost benefit per cum (INR) (*Approx*)
M25	6351/–	5506/–	*845/–*
M40 (PQC)	6615/–	5995/–	*620/–*
M10 (DLC)	4854/–	4425/–	*429/–*

Fig. 11 Road segment cast at NTPC Khargone

Intangible Benefits
FA and BA utilization especially in concrete have significant environmental benefits such as conservation of other natural resources (river sand). Furthermore, the technique provides a sustainable method for the safe disposal of FA and BA which otherwise would have been either dumped in landfills, causing leaching problems, or utilized in a very small proportion in the construction industry.

Future Plans

- 100% replacement of sand by 100% bottom ash
- M20—trail mix in site lab is in progress with the consultation of VNIT, Nagpur
- M25 and M35—Research and study is in progress with the consultation of VNIT, Nagpur

6 Summary and Conclusions

This work was aimed at exploring the possibility of incorporating FA and/or BA as a substitute to natural river sand in PQC works. Three trial mix designs were presented in this paper. All the trials were dosed with a new generation PC based superplasticizer (Trade name: *Aaradhya Master FlyAsh*). Trial 1 contained 100% FA, Trial 2 used a combination of 50% FAF + 50% BA and Trial 3 contained 100% BA as fine aggregates respectively. Based on this study, the following conclusions can be drawn:

- Addition of NG-SP greatly improves the performance of concrete containing 100% FA and 50% FA + 50% BA as fine aggregates. This is evident both from laboratory evaluation and case studies undertaken at the site.

- The 28 days compressive strength of batches containing 100% FA and 50% FA + 50% BA was observed to be 53.99 MPa and 51.72 MPa respectively. Hence these are suitable for PQC works.
- Samples of Trial 2 (50% FA + 50% BA) exhibited the satisfactory performance in terms of strength and durability characteristics with the least variation from design requirements. Owing to the fact that BA utilization in today's market is very low, it is safe to conclude that the replacement of river sand in the concrete pavement with a combination of 50% FA and 50% BA is a practically feasible alternative.
- The above trials also required 50 kg/m^3 lesser cement in comparison to traditional PQC design mixes, suggesting that acceptable strength for pavement concrete can be obtained with 9–10% lower cement dosage provided a compatible NG-SP is used.
- The compressive, flexural and split tensile strength of samples from Trial 1 (100% FA) exhibited far superior performance in comparison to the other mixes. Their physio-mechanical characteristics were even better than that of Trial 2 (50% FA + 50% BA). This could be attributed to the dense packing and higher bonding provided by the FA in the mix.
- The carbonation depth and chloride migration were nominal in the case of Trials 1 and 2 suggesting that complete replacement of fine aggregates with FA or a combination of FA and BA in equal proportions is not detrimental to concrete pavement's durability.
- Looking at the results of this study, it is, therefore, safe to conclude that incorporation of NG-SP in concrete pavements is a potentially attractive solution to tackle the issue of effective FA and/or BA utilization for PQC and DLC in the country.

References

1. Yoshitake I, Ueno S, Ushio Y, Arano H, Fukumoto S (2016) Abrasion and skid resistance of recyclable fly ash concrete pavement made with limestone aggregate. Constr Build Mater 112:440–446
2. Chi M, Huang R (2013) Binding mechanism and properties of alkali-activated fly ash/slag mortars. Constr Build Mater 40:291–298
3. Uygunoglu T, Topcu IB, Gencel O, Brostow W (2012) The effect of fly ash content and types of aggregates on the properties of pre-fabricated concrete interlocking blocks (PCIBs). Constr Build Mater 30:180–187
4. Kumar A, Kumar S (2013) Development of paving blocks from synergistic use of red mud and fly ash using geopolymerization. Constr Build Mater 38:865–871
5. Gencel O, Koksal F, Ozel C, Brostow W (2012) Combined effects of fly ash and waste ferrochromium on properties of concrete. Constr Build Mater 29:633–640
6. Kumar B, Tike GK, Nanda PK (2007) Evaluation of properties of high-volume fly-ash concrete. J Mater Civ Eng 19(10):906–911
7. Agrawal US, Wanjari SP, Naresh DN (2019) Impact of replacement of natural river sand with geopolymer fly ash sand on hardened properties of concrete. Constr Build Mater 209:499–507

8. IS 9103: 1999 (1999) Indian standard concrete admixtures—specification. Bureau of Indian Standards, New Delhi, India
9. Li G, Zhao X (2003) Properties of concrete incorporating fly ash and ground granulated blast-furnace slag. Cem Concr Compos 25:293–299
10. Jones MR, Halliday JE, Csetenyi LJ, Zheng L, Strompinis N (2015) Utilising stockpiled fly ash to manufacture sand for mortar. In: 2015 world of coal ash (WOCA) conference—May 5–7, 2015
11. Banupriya C, John S, Suresh R, Divya E, Vinitha D (2017) Experimental investigations on geopolymer bricks/paver blocks. Indian J Sci Technol 9
12. Narayanan N, Ramamurthy K (2000) Microstructural investigations on aerated concrete. Cem Concr Res 30(3):457–464
13. Siddique R (2003) Effect of fine aggregate replacement with Class F fly ash on the abrasion resistance of concrete. Cem Concr Res 33:1877–1881
14. Bilir T, Gencel O, Bekir I (2015) Properties of mortars with fly ash as fine aggregate. Constr Build Mater 93:782–789
15. Guneyisi E, Gesoglu M, Altan I, Oz HO (2015) Utilization of cold bonded fly ash lightweight fine aggregates as a partial substitution of natural fine aggregate in self-compacting mortars. Constr Build Mater 74:9–16
16. Agrawal US, Wanjari SP, Naresh DN (2017) Characteristic study of geopolymer fly ash sand as a replacement to natural river sand. Constr Build Mater 150:681–688
17. Singh M, Siddique R (2014) Strength properties and micro-structural properties of concrete containing coal bottom ash as partial replacement of fine aggregate. Constr Build Mater 50:246–256
18. Gesoglu M, Güneyisi E, Özturan T, Oz HÖ, Asaad DS (2014) Self-consolidating characteristics of concrete composites including rounded fine and coarse fly ash lightweight aggregates. Compos Part B 60:757–763
19. Salami BA, Johari MAM, Ahmad ZA, Maslehuddin M (2016) Impact of added water and superplasticizer on early compressive strength of selected mixtures of palm oil fuel ash-based engineered geopolymer composites. Constr Build Mater 109:198–206
20. Akhlaghi O et al (2017) Modified poly(carboxylate ether)-based superplasticizer for enhanced flowability of calcined clay-limestone-gypsum blended Portland cement. Cem Concr Res 101:114–122

Effect of Biocementation on Concrete using Different Calcium Sources

Anuja U. Charpe and M. V. Latkar

Abstract Nowadays, in the various engineering applications, a new technology known as microbially induced calcium carbonate precipitation (MICCP) or biocementation is used widely. A large number of soil microorganisms exhibit urease producing ability. Urease (enzyme) catalyses hydrolysis of urea to produce ammonia (NH_3) and carbon dioxide (CO_2). This reaction can be used to generate calcium carbonate ($CaCO_3$) in the existence of calcium ions. The $CaCO_3$ gets precipitated and can be used to enhance the mechanical strength of construction materials. In the present research study, influence of biocementation on concrete was studied using bacterial solution. An attempt has been made to investigate the influence of different types of calcium sources like calcium chloride ($CaCl_2$) and calcium sulphate ($CaSO_4$) on biocementation. The bacterial concrete specimens were subjected to biocementation using these two calcium sources and it was found that among the calcium sources, calcium sulphate showed more promising results exhibiting considerable enhancement in compressive strength and decrement in water absorption capacity.

Keywords Compressive strength · Bacterial solution · Calcium chloride · Calcium sulphate

1 Introduction

Concrete is a widely used man-made construction material in the modern era. It is preferred widely due to the ease of availability of its components. It is a strong and comparatively inexpensive construction material. Due to its massive production,

A. U. Charpe (✉)
Department of Civil Engineering, Velagapudi Ramakrishna Siddhartha Engineering College, Vijayawada, India

M. V. Latkar
Department of Civil Engineering, Visvesvaraya National Institute of Technology, Nagpur, India

B. Laishram and A. Tawalare (eds.), *Recent Advancements in Civil Engineering*, Lecture Notes in Civil Engineering 172,
https://doi.org/10.1007/978-981-16-4396-5_28

there are adverse effects on the environment [1]. Cementitious materials get deteriorated due to the constant exposure to hard weathering. This makes the materials more porous, thus making them permeable to the penetration of aggressive and damaging substances. Also, these materials are prone to form cracks. These problems often lead to corrosion of cementitious materials due to either penetration or ingression of moisture and other deteriorating substances (such as sulphates, chlorides, acids), thus causing reduction in durability [2].

Specific microorganisms have the capability to generate $CaCO_3$ as a part of their metabolism; this phenomenon is generally known as biocementation or microbially/microbiologically induced calcium carbonate precipitation (MICCP) [3, 4]. A large number of soil microorganisms exhibit urease producing ability. A novel application of microbially induced mineral deposition caused due to the metabolic activities of specific bacteria in construction materials to ameliorate the overall properties has become a potential research area. Common soil bacterial species like *Bacillus* can deposit $CaCO_3$ under suitable conditions [5].

Bacterial species *Bacillus subtilis* when added in concrete increased the compressive strength by about 15% and also reduced porosity at curing period of 28 days [6].

Biomineralization is the leading ecofriendly technique used to protect concrete structures by dealing with the problem of cracks. Self-healing of concrete by using biological approach has potential to address all drawbacks of matrix of concrete. Genetically modified form of *Bacillus subtilis* which is known as "*Bacilla Filla*" has an outstanding ability to reach deep inside the cracks in order to heal it [7].

A study was executed on cracks in mortar where various types of media like urea corn steep liquor (UCSL) and urea yeast extract (UYE) for the growth of *Sporosarcina pasteurii* were used. Crystals of biogenic calcium carbonate were detected inside the cracks. It was concluded that UCSL as an industrial waste could be used as a source of carbon for *S. pasteurii* cells and has the ability to form $CaCO_3$ in cement-based mortar [8].

Dhone et al. used a cost-effective alternative in which soil bacterial solution was prepared using two different protein sources viz. peptone and lentil seeds in order to observe the increment in compressive strength of cementitious materials. Around 15.26 and 15.73%, increment in the compressive strength of bio-OPC specimens was found as compared to conventional control specimens having 0.35 as W/C ratio with peptone and lentil seeds, respectively [9]. On the similar lines, different studies were carried out on OPC cement, mortar and concrete where lentil seeds powder, table sugar, meat extract were used as nutrient medium for the growth of soil bacteria along with urea as a substrate and gypsum as a calcium source. It was found that there was a considerable increment in compressive strength and decrement in water absorption capacity of cementitious materials [10–14]. When extract of rhizospheric soil was used as nutrient medium for *Bacillus cereus* and *Enterobacter cloaca*, it was found that the soil extract supports the growth of ureolytic bacteria [15].

$$CO(NH_2)_2 + H_2O \rightarrow NH_2COOH + NH_3 \quad (1)$$

$$NH_2COOH + H_2O \rightarrow NH_3 + H_2CO_3 \quad (2)$$

$$H_2CO_3 \rightarrow H^+ + HCO_3^- \quad (3)$$

$$2NH_3 + 2H_2O \rightarrow 2NH_4^+ + 2OH^- \quad (4)$$

$$HCO_3^- + H^+ + 2NH_4^+ + 2OH^- \rightarrow CO_3^{2-} + 2NH_4^+ + 2H_2O \quad (5)$$

$$Ca^{2+} + \text{Cell} \rightarrow \text{Cell-}Ca^{2+} \quad (6)$$

$$\text{Cell-}Ca^{2+} + CO_3^{2-} \rightarrow \text{Cell-}CaCO_3 \downarrow \quad (7)$$

In MICP technique, bacteria assist the hydrolysis of urea. Urease (enzyme) is produced by some bacteria as part of their metabolic activity. Urea hydrolysis is carried out in the presence of urease enzyme, and carbamate and ammonia are produced. This chemical reaction leads to high pH. Due to further hydrolysis, ammonia and carbonic acid are formed, these products subsequently produce carbonate, ammonium and hydroxide ions. The reactions give rise to a high pH, where carbonate ions are formed due to shifting of bicarbonate equilibrium. Further bacteria draw Ca^{2+} ions from the surroundings which get deposited on the cell wall which is negatively charged. Subsequently, Ca^{2+} reacts with CO_3^{2-} ions which forms $CaCO_3$ [16].

In the present study, influence of biocementation on concrete was studied using bacterial solution with two different calcium sources. An attempt has been made to investigate the influence of two different calcium sources like calcium chloride and calcium sulphate on biocementation.

2 Methodology

2.1 Preparation of Bacterial Solution

Soil (200 g/l) as a source of bacteria was used in tap water to prepare bacterial solution. For the growth of bacteria nutrients like powder of lentil seed (20 g/l), table sugar (0.5 g/l) and meat extract (3 g/l) were added as a source of protein, carbon and vitamins. After mixing all these ingredients, this mixture was incubated at 37 °C for 24 h. Later, on the supernatant, i.e. uppermost part of the solution was separated from bottom part, i.e. soil and optical density of the bacterial solution was measured in a spectrophotometer at wavelength of 600 nm and was observed to be 0.88, indicating good bacterial growth. Urea (5 g/l) as substrate was added in the solution. Two different types of calcium sources viz. calcium chloride (8 g/l) and

calcium sulphate (10 g/l) were added in the solution. The concentrations of urea and calcium sources were calculated as per stoichiometry.

2.2 Control I Solution Preparation

Control I solution was prepared using exactly same ingredients as bacterial solution excluding bacterial source (soil). This was done in order to study the influence of the ingredients and chemicals present in bacterial solution, other than soil, on concrete.

2.3 Raw Materials and Concrete Mix Design

In this research study, ordinary Portland cement (OPC) 53 grade conforming to IS 12269 [17] and locally existing natural river sand as per IS 383 [18] of zone II were used. Coarse aggregates of two sizes, i.e. 10 and 20 mm were used. Normal tap water confirming to IS 456 was used for making control specimens [19]. Concrete mix was designed for 25 MPa target strength at 28 days of curing period as per BIS 10262 with the water-to-cement ratio (W/C) of 0.5 [20].

2.4 Specimen Preparation

Standard size concrete cubes of 150 mm were prepared. Five different types of specimens were prepared in the study. The composition of the specimens is mentioned in Table 1.

Table 1 Types and composition of specimens

Types of specimen	Composition
Control specimens	Tap water + OPC cement + natural river sand + aggregates
Control ($CaCl_2$) specimens	Control I solution + urea + $CaCl_2$ + OPC cement + natural river sand + aggregates
Control ($CaSO_4$) specimens	Control I solution + urea + $CaSO_4$ + OPC cement + natural river sand + aggregates
Bioconcrete ($CaCl_2$) specimens	Bacterial solution + urea + $CaCl_2$ + OPC cement + natural river sand + aggregates
Bioconcrete ($CaSO_4$) specimens	Bacterial solution + urea + $CaSO_4$ + OPC cement + natural river sand + aggregates

2.5 Curing Conditions

All the specimens were prepared and well compacted using vibration machine and de-moulding was done after 24 h. Curing for 3, 7 and 28 days was adopted in the study for all specimens. Room temperature (27 ± 2 °C) was maintained for the curing. Normal tap water was used to cure all specimens. An effect of MICCP on the parameters like compressive strength and water absorption of concrete were monitored. Entire experiments were executed in triplicate.

3 Results

3.1 Compressive Strength Test

Compressive strength test was executed as per IS 4031 (part 6) at the curing of 3, 7 and 28 days for all the types of specimens [21]. In case of specimens prepared using calcium chloride as a calcium source, on an average, the compressive strength of bioconcrete specimens increased by 10.01%, 12.80% and 17.34% as against the control specimens, for curing period of 3, 7 and 28 days, respectively, as shown in Fig. 1. Whereas, the specimens prepared using calcium sulphate as a calcium source, showed an average increase of 14.53%, 17.92% and 22.83% as against the control specimens for 3, 7 and 28 days of curing period as shown in Fig. 2.

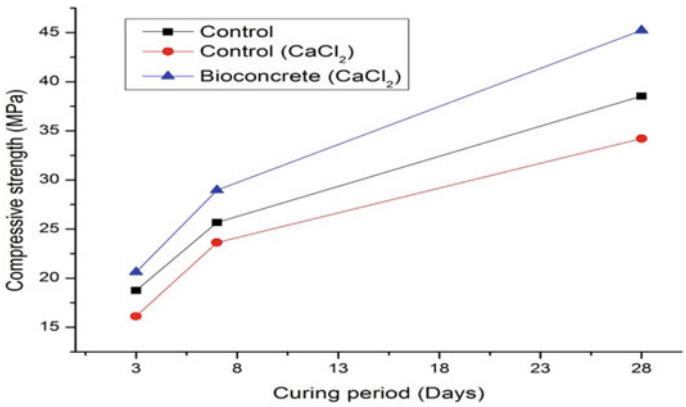

Fig. 1 Average compressive strength of control, control ($CaCl_2$) and bioconcrete ($CaCl_2$) specimens at 3, 7 and 28 days of curing period

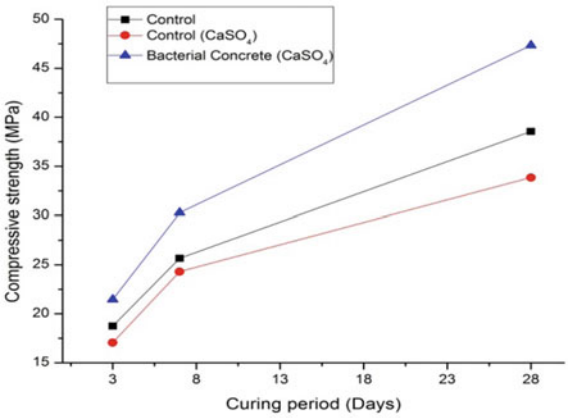

Fig. 2 Average compressive strength of control, control ($CaSO_4$) and bioconcrete ($CaSO_4$) specimens at 3, 7 and 28 days of curing period

3.2 Water Absorption Capacity

Water absorption capacity test was performed on all types of specimens as per ASTM C140-11 [22]. All specimens were immersed in water for 24 h, after which the specimens were taken out, dabbed with dry cloth and their saturated weights were taken. The specimens were then kept in oven maintained at a temperature of 110 ± 5 °C for 24 h. After 24 h of ovendrying, the weights of specimens were noted. Figure 3 shows the values of water absorption of control, control ($CaCl_2$) and bioconcrete ($CaCl_2$) specimens at a curing age of 3, 7 and 28 days. Water absorption values of bioconcrete ($CaCl_2$) specimens were found to be approximately reduced by 4.8, 7.2 and 11.0% for 3, 7 and 28 days of curing, respectively, when compared to control specimens. For specimens prepared using calcium sulphate as a calcium source, the reduction in water absorption capacity of bioconcrete ($CaSO_4$) specimens was observed to be approximately 6.8, 10.5 and 14% for 3, 7 and 28 days of curing period, respectively. The results are depicted in Fig. 4.

3.3 Scanning Electron Microscopy Analysis

The effect of biocementation using calcium chloride and calcium sulphate on concrete matrices was also observed using SEM. Control sample and the samples of bioconcrete ($CaCl_2$) and bioconcrete ($CaSO_4$) of 28 days curing were scanned under SEM. As clear from the SEM results, both the bioconcrete specimens have less void spaces as comparing to control specimen. This is due to deposition of $CaCO_3$ in the void spaces of the bioconcrete due to biocementation which is

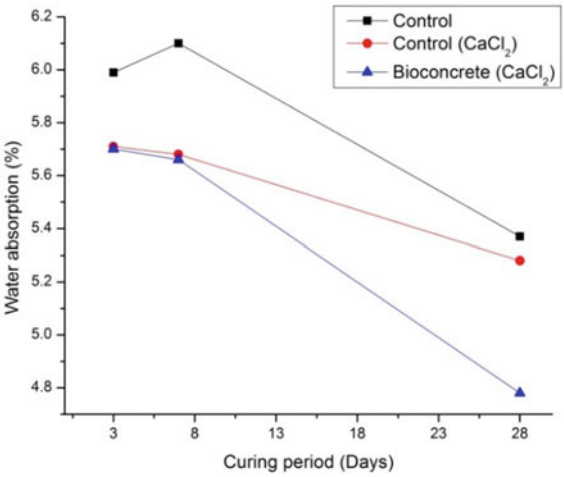

Fig. 3 Average water absorption of control, control ($CaCl_2$) and bioconcrete ($CaCl_2$) specimens at 3, 7 and 28 days of curing period

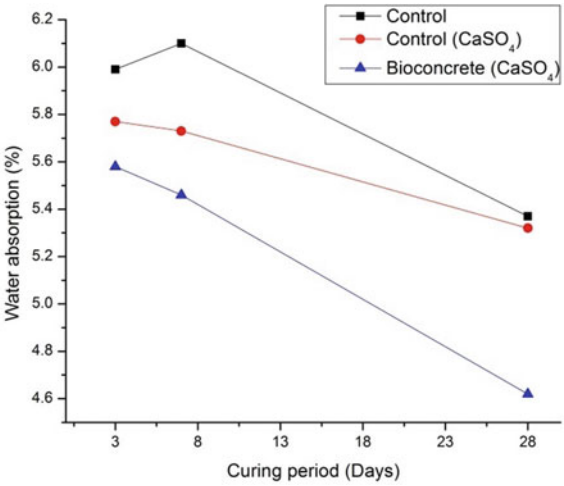

Fig. 4 Average water absorption of control, control ($CaSO_4$) and bioconcrete ($CaSO_4$) specimens at 3, 7 and 28 days of curing period

enhancing the mechanical properties. When micrographs of both bioconcrete specimens were compared, it was found that the void spaces in bioconcrete ($CaCl_2$) were more as compared to void spaces in bioconcrete ($CaSO_4$) sample. The scanning electron micrographs of control, bioconcrete ($CaCl_2$) and bioconcrete ($CaSO_4$) specimens are shown in Fig. 5.

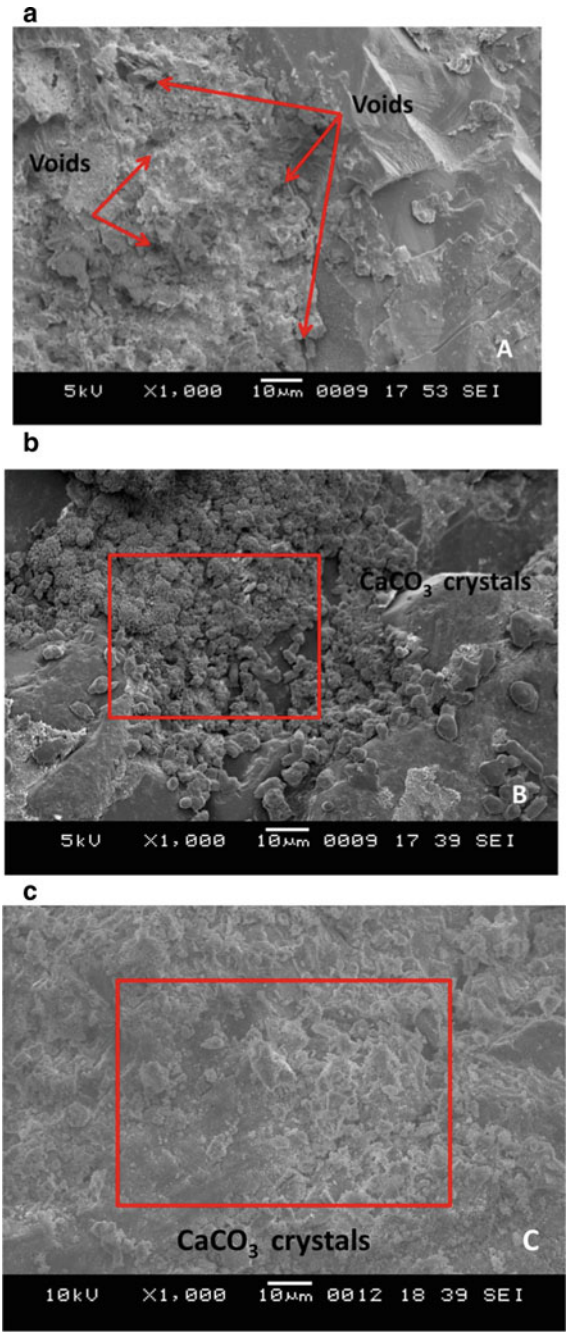

Fig. 5 SEM micrographs for **a** control **b** bioconcrete ($CaCl_2$) and **c** bioconcrete ($CaSO_4$) specimens

4 Discussion

The aim of this research was to observe the effect of MICCP using different calcium sources on concrete. It was observed that calcium sulphate showed better results as compared to calcium chloride. Conventionally in biocementation technique, calcium chloride is commonly used as a calcium source. But use of calcium chloride in higher amount may cause corrosive problems in concrete, so to avoid these problems, calcium sulphate as a calcium source for bacteria can be effectively used. Calcium sulphate specimens have showed encouraging results of 22.83% increase in compressive strength and 14% reduction in water absorption capacity for 28 days of curing period. This increment in compressive strength and reduction in water absorption capacity is caused because of the deposition of $CaCO_3$ in the concrete matrices. Higher amount of $CaCO_3$ crystals deposition was observed in bioconcrete ($CaSO_4$) specimens as when compared to bioconcrete ($CaCl_2$) specimens in SEM analysis.

5 Conclusion

Use of calcium sulphate as a calcium source is proved to be an effective source for the bacteria to deposit $CaCO_3$ in concrete matrix. MICCP or biocementation has evidenced to be the most promising, sustainable and ecofriendly technology in construction industry. More research in the field of biocementation would help to ameliorate properties of cementitious materials and increase durability of structures too.

References

1. Jonkers HM, Thijssen A, Muyzer G, Opuroglu SE (2010) Application of bacteria as self-healing agent for the development of sustainable concrete. Ecol Eng 36:230–235
2. Samudre MP, Mangulkar MN, Saptarshi SD (2014) A review of emerging way to enhance the durability and strength of concrete structures: microbial concrete. Int J Innovative Res Sci Eng Technol 3:9311–9316
3. Stocks-fischer S, Galinat JK, Bang SS (1999) Microbiological precipitation of $CaCO_3$. Soil Biol Biochem 31:1563–1571
4. Achal V, Mukherjee A, Basu PC, Reddy MS (2009) Strain improvement of Sporosarcina pasteurii for enhanced urease and calcite production. J Ind Microbiol Biotechnol 36:981–988. https://doi.org/10.1007/s10295-009-0578-z
5. Verma RK, Chaurasia L, Bisht V, Thakur M (2015) Bio-mineralization and bacterial carbonate precipitation in mortar and concrete. Biosci Bioeng 1:5–11
6. Pei R, Liu J, Wang S, Yang M (2013) Use of bacterial cell walls to improve the mechanical performance of concrete. Cem Concr Compos 39:122–130

7. Gupta SG, Rathi C, Kapur S (2013) Biologically induced self healing concrete: a futuristic solution for crack repair. Int J Appl Sci Biotechnol 1:85–89. https://doi.org/10.3126/ijasbt.v1i3.8582
8. Amiri A, Bundur ZB (2018) Use of corn-steep liquor as an alternative carbon source for biomineralization in cement-based materials and its impact on performance. Constr Build Mater 165:655–662. https://doi.org/10.1016/j.conbuildmat.2018.01.070
9. Dhone RS, Latkar MV, Charkraborty T, Ralegaonkar RV (2015) Application of soil bacteria to improve compressive strength of portland cement. In: Proceedings of the first international conference on bio-based building materials, pp 331–333
10. Charpe UA, Latkar VM, Chakrabarti T (2017) Microbially assisted cementation a biotechnological approach to improve mechanical properties of cement. Constr Build Mater 135:472–476. https://doi.org/10.1016/j.conbuildmat.2017.01.017
11. Charpe AU, Latkar MV, Chakrabarti T (2018) Biocementation: an eco-friendly approach to strengthening concrete. In: Proceedings of the institution of civil engineers-engineering sustainability, pp 1–13
12. Charpe AU, Latkar MV (2020) Effect of biocementation using soil bacteria to augment the mechanical properties of cementitious materials. Mater Today Proc 21:1218–1222. https://doi.org/10.1016/j.matpr.2020.01.072
13. Bhutange SP, Latkar MV, Chakrabarti T (2019) Role of biocementation to improve mechanical properties of mortar. Sadhana 44:1–8. https://doi.org/10.1007/s12046-018-1023-7
14. Bhutange SP, Latkar MV (2020) Microbially induced calcium carbonate precipitation in construction materials. J Mater Civ Eng 32(5):544–549. https://doi.org/10.1061/(ASCE)MT.1943-5533.0003141
15. Bhutange SP, Latkar MV, Chakrabarti T (2020) Studies on efficacy of biocementation of cement mortar using soil extract. J Cleaner Prod 274:122687
16. Talaiekhozan A, Keyvanfar A, Shafaghat A, Andalib R, Majid MZA, Fulazzaky MA (2014) A review of self-healing concrete research development. J Environ Treat Tech 2(1):1–11
17. Bureau of Indian Standard (BIS) (2013) Ordinary Portland cement 53 grade—specifications. IS 12269
18. Bureau of Indian Standard (BIS) (1970) Specification for coarse and fine aggregate from natural sources for concrete. IS 383
19. Bureau of Indian Standard (BIS) (2000) Plain and reinforced concrete-code of practice. IS 456
20. Bureau of Indian Standard (BIS) (2009) Concrete mix proportioning—guidelines. IS 10262
21. Bureau of Indian Standard (BIS) (1988) Methods of physical tests for hydraulic cement—determination of compressive strength of hydraulic cement other than masonry cement. IS 4031, part 6
22. American Society for Testing and Materials (ASTM) (2012) Standard test methods for sampling and testing concrete masonary units and related units. ASTM C140–11:1–17. https://doi.org/10.1520/C0140-11

Bamboo-Reinforced Concrete Lintel—A Sustainable Approach

Vijay R. Wairagade and Ishwar P. Sonar

Abstract The performance of the bamboo as reinforcement in concrete structural elements can be successful if matured, straight, seasoned, and treated bamboo harvested in winter is used. As a part of PhD research work, the author has investigated mechanical properties of locally available bamboo culms. In this research, the feasibility of bamboo strips application as a flexure reinforcement in concrete lintel beams is evaluated. Detailed experimental analysis of 12 simply supported bamboo-reinforced concrete lintel beams subjected to a two-point load test was carried out up to collapse to study their behaviour under bending. All the tests carried out on locally available treated bamboo strips suggest the potential to replace steel as reinforcement in lintel beams, as a sustainable approach for low-cost housing. There is a need to adopt such technology on a trial project basis to utilize the satisfactory performance of such bamboo-reinforced concrete (BRC) members.

Keywords Bamboo · Concrete · Reinforcement · Lintel

1 Introduction

Bamboo is one of the fastest growing grass plants and has got a great economic potential. Bamboo has been used in constructions of bridges and houses for thousands of years in Asia. Bamboo takes less energy to harvest and transport. Therefore, bamboo has low manufacturing costs compared with steel, and bamboo is widely expected to be possible even in countries and regions that have no advanced manufacturing technology and construction techniques. The use of renewable resources by the construction industry will help to achieve a more sustainable pattern of consumption of building materials.

The research and investigations reported in International Network for Bamboo and Rattan (INBAR 2002) [1] had revealed bamboo's advantages as a construction

V. R. Wairagade (✉) · I. P. Sonar
COEP, Pune, India
e-mail: ips.civil@coep.ac.in

B. Laishram and A. Tawalare (eds.), *Recent Advancements in Civil Engineering*, Lecture Notes in Civil Engineering 172,
https://doi.org/10.1007/978-981-16-4396-5_29

material. The advantages of bamboo are ecological value, competitive mechanical properties, social and economic value, and low energy consumption. Studies show that steel requires 50 times more energy than bamboo to produce a material equivalent of 1 m^3 per unit stress. The tensile strength of bamboo is relatively high and can reach up to 370 MPa. This makes bamboo an attractive alternative to steel in tensile loading applications. The ratio of tensile strength to specific weight of bamboo is six times greater than that of steel [2]. Attempts made in the past have established and substantially confirmed that bamboo could be a possible sustainable alternative of various conventional materials for housing and building construction segment.

Khare [3] performed tensile tests on three types of bamboo (Moso, Solid, and Tonkin) to obtain their constitutive relation. Tests results indicated that bamboo reinforcement enhanced the load carrying capacity by about 250% as compared to the initial crack load in the concrete beam. Brink and Paul [4] reported a study at U. S. Naval Civil Engineering Laboratory, Port Hueneme, California. This report provides a set of instructions on the selection and preparation of bamboo for reinforcing. Construction principles for bamboo-reinforced concrete are discussed. It was found that the concrete mix designs may be the same as that used with steel, with a slump as low as workability will allow. High early-strength cement is preferred to minimize cracks caused by swelling of bamboo. It was recommended that the amount of bamboo reinforcement in concrete be 3–4% of the concrete's cross-sectional area as the optimum amount.

Lima et al. [5] had studied the durability aspect of bamboo to be used as reinforcement in cement concrete mixtures and analysed that while working as reinforcement in concrete, bamboo splints have larger dimensions than any other types of fibres, which implies that the majority of bamboo fibres are completely enclosed in the parenchyma and they are not in direct contact with the alkalinity of the cement matrix; therefore, the higher number of the fibre end points is less vulnerable to deterioration. The durability performance of the bamboo was discussed on the basis of results of tensile test obtained before and after being exposed to 6 months of ageing.

Ghavami [6] studied bonding on two types of bamboo, treated and untreated. In this test, the treated bamboo, 0.97 N/mm^2, was more effective than the untreated bamboo, 0.52 N/mm^2, with up to 90% improved bond stress. Agarwal and Maity from IIT, Kharagpur [7], studied axial compression and bending test performed on plain, steel, and bamboo-reinforced concrete members. The load deformation curves displayed significant nonlinearity, indicating that bamboo has the capacity to absorb energy. Plain concrete and untreated bamboo-reinforced column showed a brittle behaviour, whereas in steel- and bamboo-reinforced columns more ductile behaviour was observed. Furthermore, the results exhibited that the maximum load carrying capacity of treated bamboo-reinforced column was nearly equivalent to that of steel-reinforced column.

Nayak et al. [8] have reported that by opting advanced bamboo-reinforced technique instead of conventional steel reinforcement technique, one can make a structure very economical without compromising the strength criteria. In their project, the team had designed a single-story structure, opting advanced

bamboo-reinforced technique in place of conventional steel reinforcement. Wakchaure et al. [9] presented a case study of a two-story residential building at Ahmednagar, at UKIERI Concrete Congress. All the structural elements were designed with concrete grade M20 and bamboo reinforcement of Dendrocalamus strictus purchased from local market. They revealed that there is a 68% of saving in the reinforcement cost. The authors emphasized a need to continue with more focus and detailed research on bamboo-reinforced concrete with bamboo species available in Indian continent.

Ferreira et al. [10] studied six bamboo-reinforced beams tested for ultimate load and compared to the ultimate load predicted according to ACI 318. He revealed that the loss of bond between bamboo strips and concrete can be compensated with increasing the utilization of steel stirrups. Further, it is concluded that structural design of bamboo-reinforced concrete beams is similar to that of the steel-reinforced concrete beams as long as steel stirrups are employed. The cracking of the bamboo-reinforced beams occurred due to bending. Despite the limited number of test on bamboo-reinforced concrete beams, bamboo as a sustainable material can potentially be employed as a substitute of the steel reinforcement.

2 Experimental Program

2.1 Selection of Bamboo Culms and Preparation of Bamboo-Reinforced Concrete Lintels

The Dendrocalamus strictus bamboo culms were procured from the easily available local open market of Pune city and nearby Talegaon. The samples selected are of minimum 4 years age, 40–50 mm in diameter, and collected in winter so that they will contain minimum starch and are brownish in appearance. For air-drying, samples are left open for 4–6 weeks. The guidelines provided in IS codes 15,912–2012, 9096–2006, 6874–2008, 8242–1978, National Building Code of India SP-7:2005 (Part 6, Section 3B), FSI, Dehradun, Technical Literature by the International Network for Bamboo and Rattan (INBAR) and ISO 22,156:2004–Bamboo Structural Design are considered for the selection and determination of physical and mechanical properties of bamboo.

Table 1 shows the important physical and mechanical properties of bamboo tested in this work.

Table 1 Physical and mechanical properties of bamboo

Sr. no.	Test	Results
1	Compressive strength (Avg.)	59 MPa
2	Modulus of rupture (Avg.)	107 Mpa
3	Tensile strength (Avg.)	117 MPa
4	Modulus of electricity (Avg.)	18 GPA

Fig. 1 Bamboo specimens for various tests

To check the feasibility and reliability as a reinforcing material and to select an appropriate kind of bamboo specimen (Fig. 1), a series of tests are conducted on the selected bamboo samples to find out physical and mechanical properties [11].

To study the structural behaviour (flexural strength, deflection, and failure pattern) of bamboo-reinforced concrete lintel beams, a two-point loading test was conducted. In total, 12 beams of dimensions 200 mm × 250 mm × 1200 mm were casted which includes a variation in percentage of bamboo reinforcement (Figs. 2 and 3). This includes three RCC beams for comparison. Design mix concrete of M25 grade was used for casting of all 12 lintel beams. Concrete mix was designed as per IS 10262:2009. The IS 456:2000 specifies the characteristic compressive strength of M25. A working stress method was used for the design of bamboo-reinforced lintel beam, as it is approved by the researchers. The percentage of bamboo reinforcement provided as reinforcement in the bamboo-reinforced beams is in the range from 1.96 to 3.91. The percentage of steel reinforcement is 0.48. The casted reinforced beams were covered with gunny bags and cured for

Fig. 2 Treated bamboo cages ready for casting

Fig. 3 BRC lintels ready for testing

28 days before conducting the test. These beams were tested in UTM of capacity 400 kN at a loading rate of 0.5 mm/s. The loading, deflection, and crack pattern were constantly monitored during the test until the failure of the beam.

2.2 Method of Test—Bamboo Specimens and Bamboo-Reinforced Concrete Lintels

For compression test, undamaged specimens were taken. The samples were tested in CTM of capacity 2000 kN (Figs. 4 and 5) as per the guidelines provided in AC162-2000, IS: 6874–2008, and ISO 3787–1976. The specimen was placed so that the centre of the movable head is vertically above the centre of the cross section of the specimen, and a small load of not more than 1 kN was initially applied to set the specimen. The load was applied continuously during the test to cause the movable head of the testing machine to travel at a constant rate of 0.01 mm per second. The final reading of the maximum load, at which the specimen fails, was recorded.

One of the most important mechanical properties of the bamboo required to check the feasibility and reliability as a reinforcing material is its tensile strength. The test was conducted on the samples collected from the selected culms, and accordingly, test specimens were prepared to an accuracy of 0.1 mm as per the guidelines mentioned in IS 6874:2008. The prepared specimens (Fig. 6) were tested in UTM of capacity 400 kN and at a constant rate of loading 0.01 mm/s. Modulus of elasticity was also evaluated by using the tensile test results.

To study the structural behaviour (flexural strength, deflection, and failure pattern) of bamboo-reinforced concrete lintel beams, a two-point loading test (Fig. 7) was conducted. A total of 12 lintel beams of dimensions 200 mm × 250 mm 1200 mm were casted. A clear cover of 25 mm to bamboo strips was provided.

Fig. 4 Bamboo samples for compression test

Fig. 5 Compression testing of bamboo sample

Bamboo strips were treated by using oil paint and silica powder. This coating provides very good bond stress as compared to other materials [11]. At 28-day curing period, lintel beams were tested in UTM of 400 kN capacity by applying a two-point load arrangement, at a loading rate of 0.5 mm/s. Figure 8 shows test set-up describing arrangement of loading and deflection at centre was measured using a dial gauge of least count 0.001. During test, flexural failure was observed from the crack pattern. Figure 9 shows mode of failure and crack pattern.

Fig. 6 Tensile testing of bamboo sample

Fig. 7 Two-point load set-up for BRC lintel

3 Results and Discussion

Compression Strength Test: The average compressive strength of the bamboo specimens at three different levels of bamboo culm is found to be 59 MPa.

Tensile Strength test: The average tensile strength of the bamboo specimen is found to be 117 N/mm^2. The modulus of elasticity is calculated as 17 GPa. The variation of load and displacement is shown in Fig. 10.

Two-point Load Test on BRC Lintel Beams: Details of test results of bamboo-reinforced beam specimens and conventional steel-reinforced beam specimens are shown in Table 2. For all the lintel beams (RC and BRC), the ultimate

Fig. 8 Flexure failure of BRC lintel beam

Fig. 9 Two-point load set-up for BRC lintel

experimental load is more than the calculated load. Also, except 1.96% BRC lintel beams, all beams show better load carrying capacity at allowable deflection of 3 mm (span/350). Results of bamboo-reinforced lintel beams with 2.93% and 3.91 % of bamboo splints as reinforcement are found suitable compared to 0.48% RC lintel beams. The results of 3.91% of bamboo-reinforced lintel beams are higher than the results of 0.48% RC lintel beams.

From the load deflection curves as shown in Fig. 11, it is observed that the behaviour of BRC members with 2.93% and 3.91% reinforcement is very much like RC members with 0.48% reinforcement. Test results indicate that the load carrying capacities of lintels are more than the expected load. The average FOS observed is 1.99. Since flexural stiffness of bamboo is less, bamboo-reinforced lintel beams may show higher deflection, showing flexural cracks; hence, flexural capacity of bamboo-reinforced beams corresponding to allowable deflections may be considered instead of ultimate capacity.

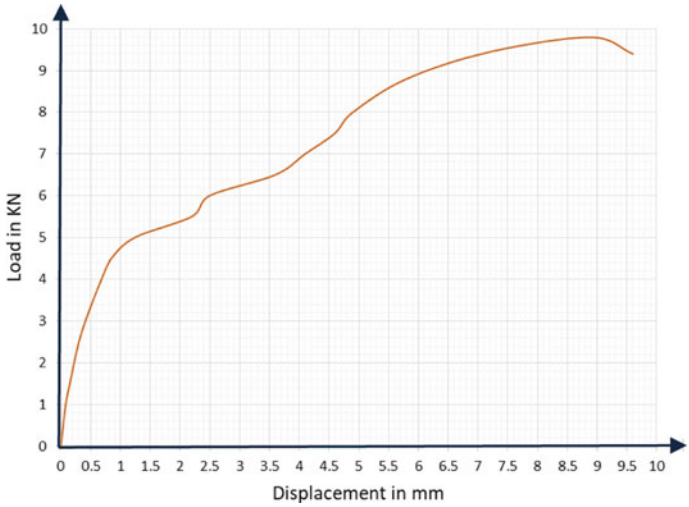

Fig. 10 Load–displacement curve for bamboo specimen

Results clearly indicate reserve strength after post-cracking (plastic stage) and more load absorption capacity without fail. There is no sudden failure of the lintels.

4 Conclusion

In this study, the feasibility of the usage of bamboo as reinforcement in concrete lintels has been evaluated through a series of experimental investigations by conducting test on bamboo-reinforced beams of size 200 mm × 250 mm × 1200 mm using M25 grade concrete. The physical and mechanical properties of bamboo show its potential to be considered as reinforcement in place of steel. From the test results of the flexural test conducted on bamboo-reinforced lintel beams, it is observed that performance of BRC beam is like conventional RCC beam, giving an average factor of safety as 1.50. The suggested percentage of treated bamboo as reinforcement is equal to 3.91%.

Considering the satisfactorily results after a series of tests conducted on bamboo specimens and later performance of the BRC lintels, there is a scope to utilize bamboo for the development of eco-friendly construction products like BRC lintels for the sustainable development. In view of the tremendous development in the construction sector in rural areas and the need of the sustainability consideration, BRC lintels are going to prove their significance.

The novelty of this research includes the use of fully treated half bamboo specimens as reinforcement in BRC lintels. Splitting of bamboo culms into two pieces can be done by using simple basic cutting tools, and the treatment of oil paint

Table 2 Summary of experimental results from experimental work on BRC lintel beams and conventional RCC beam

Sr. no.	Type	Reinforcement (%)	Load at first crack (kN)	Load at perm. defl. (kN)	Ultimate load (kN)	Design BM (WSM) kN-m	BM at perm. deflection (experimental) kN-m	Ultimate BM (experimental) kN-m	FOS
1	Steel set-1 (Avg.)	0.48	50.8	46.04	81.52	7.23	8.05	14.26	1.77
2	Steel set-2 (Avg.)	1.96	30.56	17.68	39.56	4.05	3.09	6.92	2.24
3	Steel set-3 (Avg.)	2.93	51.84	39.56	89.88	5.99	6.92	15.73	2.27
4	Steel set-4 (Avg.)	3.91	36.36	56.64	81.92	7.90	9.91	14.34	1.45

(WSM—working stress method, FOS—factor of safety)

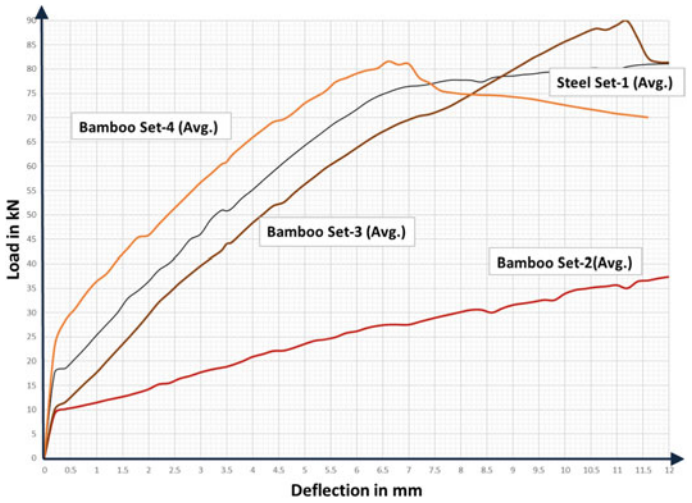

Fig. 11 Results from flexural test conducted on BRC lintel beams

is also easy to apply and economical too. Patent of pull-out test attachment for specifically half bamboo specimens which were used in this research work has been already filed.

Acknowledgements Board of College and University Development, Savitribai Phule Pune University, Pune, has funded for this project under the research proposal scheme.

References

1. International Network for Bamboo and Rattan (INBAR 2002) A Project on Bamboo Structures at the Technical University of Eindhoven
2. Maity D, Behera S, Mishra M, Majumdar S (2009) Bamboo reinforced concrete wall as a replacement to brick and mud wall. J Inst Eng Archit Eng Div 90:5–10
3. Khare L (2005) Performance evaluation of bamboo reinforced concrete beams. The University of Texas at Arlington
4. Brink FE, Paul JR (1966) Bamboo reinforced concrete construction. US Naval Civil Engineering Laboratory, Port Hueneme, California
5. Lima HC, Willrich FL, Barbosa NP, Rosa MA, Cunha BS (2008) Durability analysis of bamboo as reinforcement. Mater Struct 41(5):981–989
6. Ghavami K (2005) Bamboo as reinforcement in structural concrete elements. Cement Concr Compos 27:637-649
7. Agarwal A, Maity D (2011) Experimental investigation on behaviour of bamboo Reinforced concrete members. In: Proceedings of 16th international conference on composite structures (ICCS 16) Porto
8. Nayak A, Bajaj AS, Jain A, Khandelwal A, Tiwari H (2013) Replacement of steel by bamboo reinforcement. IOSR J Mech Civil Eng 8(1):50–61

9. Wakchaure MR, Kute SY, Mehetre PR (2016) Bamboo Reinforced Concrete For Sustainable Development. UKIERI concrete congress—concrete research driving profit and sustainability, pp 1576–158
10. Ferreira GC, Beraldo AL, Moreno Jr AL, Silva AOBD (2016) Flexural and shear behaviour of concrete beams reinforced with Bamboo. Int J Sustain Materi Structu Syst 2:335–347
11. Wairagade VR, Sonar IP (2019) Bamboo concrete bond strength. Int J Eng Adv Technol (IJEAT) 9(1):747–752

Experimental Investigation on Mechanical and Durability Properties of Basalt Fibre-Reinforced Concrete

Panugalla Rama Rao and Mycherla Chaitanya

Abstract This study investigates the mechanical and durability properties of basalt fibre-reinforced concrete (BFRC). For this purpose, the compressive strength, flexural strength, split tensile strength and bond strength test were conducted on BFRC with 0, 1, 2, and 3% of fibre by weight of cement. In addition, the performance of BFRC was evaluated through the durability studies, namely Abrasion, Rapid Chloride Permeability test and Acid resistance test. The results showed that there is a significant effect of basalt fibre on flexure, split tensile and bond strength. The durability studies revealed that the performance of BFRC was improved significantly than the conventional concrete.

Keywords Basalt fibre · Mechanical properties · Durability properties · Fibre-reinforced concrete · Performance

1 Introduction

The conventional concrete mix is composed of coarse aggregate, fine aggregate, cement and water. This plain concrete has two major deficiencies: a low tensile strength and low strain at fracture [1–3]. These deficiencies have led to developing considerable new approaches to modify the brittle properties of concrete. One such approach is addition of fibre to the concrete mix. The primary role of fibre is to modify the cracking mechanism which reduces the macrocracks in the concrete to microcracks.

The addition of fibre to the plain concrete is found to improve the concrete mechanical and durability properties [4]. The properties of fibre-reinforced concrete depend highly on the type of fibre used and their orientation and size [5]. Various fibre used in concrete applications are glass fibre, carbon, steel and polyester fibre. In recent decades, there is an increased research in the usage of basalt fibre.

P. Rama Rao (✉) · M. Chaitanya
Pondicherry Engineering College, Puducherry, India

B. Laishram and A. Tawalare (eds.), *Recent Advancements in Civil Engineering*, Lecture Notes in Civil Engineering 172,
https://doi.org/10.1007/978-981-16-4396-5_30

Basalt fibre is an inorganic fibre which can counteract the deficiencies in plain concrete because of its high strength and improved strain to failure. In addition, the basalt fibre have enormous benefits in concrete applications as they possess high temperature resistance, good stability, chemical resistance, non-toxic, natural and economical [6]. Many researchers have worked on basalt fibre-reinforced concrete (BFRC) and made some valuable contributions in the concrete applications. The flexural strength and tensile strength are enhanced significantly, whereas there is no significant effect of fibre on the compressive strength of concrete. In the present study, the mechanical and durability properties of basalt fibre-reinforced concrete are investigated.

2 Research Significance

This article presents the experimental results of basalt fibre-reinforced concrete made of M50 grade concrete. Various studies have been carried out on BFRC on different grades of concrete but no study has been done on M50 grade basalt fibre-reinforced concrete. The durability properties of BFRC were tested through abrasion, RCPT and acid resistance test. This study helps in understanding the effect of basalt fibre on higher grades of concrete.

3 Experimental Work

3.1 Materials and Properties

The materials used in the present study include cement, coarse aggregate, fine aggregate, basalt fibre, admixtures and water. Super plasticizer of Conplast SP430 and potable water was used in the present study. The properties of all the materials are described in detail below.

3.1.1 Cement

Ordinary Portland Cement of 53 grade was used in the present study, and testing was done according to IS: 4031 [7]. The properties of the cement used are presented in Table 1.

Table 1 Physical properties of cement

Sl. No	Property	Result
1	Fineness	98%
2	Specific gravity	3.12
3	Standard consistency	33%
4	Initial setting time	36 min
5	Final setting time	112 min
6	Compressive strength	55.3 (N/mm^2)

3.1.2 Aggregates

The coarse aggregate and fine aggregate used in the present study are tested according to IS 2386 [8] and their properties are shown in Table 2.

3.1.3 Basalt Fibre

The basalt fibre used in the present study are 12 mm in length and 1 micron size as shown in Fig. 1.

Table 2 Properties of aggregates

Sl. No	Property	Coarse aggregate	Fine aggregate
1	Specific gravity	2.7	2.62
2	Fineness modulus	6.9	3.3
3	Water absorption	0.1%	0.52%

Fig. 1 Chopped basalt fibre

3.2 Mixing, Placing and Compaction

Mix design was done considering the moderate exposure condition according to the procedure mentioned in IS 10262 [9]. The mixing of all the ingredients was done for a period of 5 min using a pan mixer as shown in Fig. 2. The placing of concrete in the moulds and manual compaction was done.

3.3 Methods and Testing

The prepared specimens were cured for a period of 28 days in the curing tank. The specimens were then tested for compressive strength, flexural strength, tensile strength and bond strength. The durability of mix is also analysed through abrasion, Rapid Chloride Permeability test (RCPT) and acid resistance test. The workability of the concrete mix for different percentages of basalt fibre was determined by the slump cone test. Four mixes were prepared for different percentages of basalt fibre by weight of cement. The mix designation and quantities of various ingredients are shown in Table 3.

Fig. 2 Concrete mixing

Table 3 Quantities of various ingredients

Sl. No	Mix designation	Cement (kg/m^3)	FA (kg/m^3)	CA (kg/m^3)	W/C Ratio	SP (kg/m^3)	BF (kg/m^3)
1	M_0	394.32	710.26	1194.23	0.4	4.14	0
2	M_1	394.32	710.26	1194.23	0.4	4.14	3.94
3	M_2	394.32	710.26	1194.23	0.4	4.14	7.89
4	M_3	394.32	710.26	1194.23	0.4	4.14	11.83

4 Results and Discussion

4.1 Mechanical Properties

4.1.1 Workability

The results indicate that the workability of concrete decreased with the addition of fibre as shown in Table 4. Hence, there is an inverse relation existed between the workability and the fibre content. The decrease in workability of concrete is due to the stiffness of the fibre. Even chopped basalt fibre are flexible but there is some stiffness associated with fibre because of shorter length. This stiffness of the fibre will obstruct the flow of the mix. In order to avoid this, it requires more water for better workability.

4.1.2 Compressive Strength

The compressive strength of basalt fibre-reinforced concrete mix is found to be lower than the plain concrete mix. Further, with the increase in fibre content the compressive strength was found to decrease as shown in Fig. 3. The decrease in the compressive strength ranges from 0.36% to 11.38%. The increase in the variation of

Table 4 Workability of mixes

Sl. No	Mix	Slump (mm)
1	M_0	80
2	M_1	60
3	M_2	33
4	M_3	10

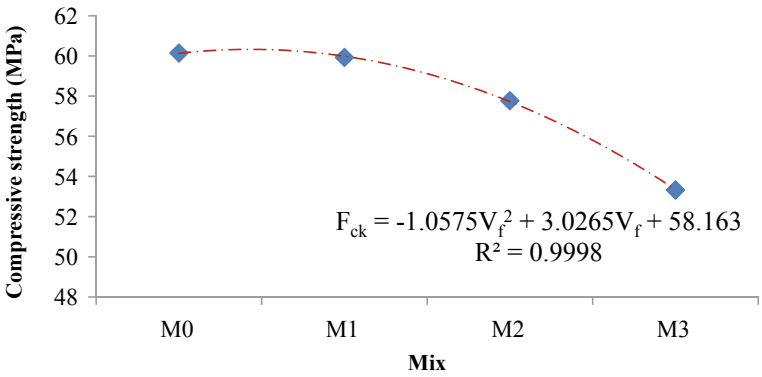

Fig. 3 Compressive strength of mixes

strength is directly proportional to the fibre content. The maximum percentage of loss after the addition of fibre was found to be 11.38%. The loss of compressive strength is due to porosity caused by the inclusion of fibre. The variation of compressive strength with fibre content is a perfect second-order polynomial which indicates parabolic variation. After the analysis of experimental data, a graph is plotted between the compressive strength and fibre content and also mathematical equation as shown.

$$F_{ck} = -1.0575\ V_f^2 + 3.0265\ V_f + 58.163 \quad (1)$$

where F_{ck} is Compressive strength and V_f is volume of fibre content.

4.1.3 Flexure and Split Tensile Strength

The flexural strength test conducted on the specimens indicated that the strength increases with the addition of fibre. So the flexural strength is directly proportional to the fibre content. The increase in the flexural strength is about 5.05%, 28.57% and 28.92% for 1%, 2% and 3% fibre content compared to control mix. The increment in the flexural strength is due to the bridging action of fibre. During the transverse bending, the fibre act like a bridge in the surrounded matrix. There is not much strength variation between 2 and 3% fibre content. It may be due to the improper bond between the matrix and the fibre in the case of higher fibre content. The variation of strength after the addition of fibre is shown in Fig. 4. The Spline variation is observed for flexural strength. The following third-order polynomial is obtained from the graph.

$$F_s = -0.3983\ V_f^3 + 2.92\ V_f^2 - 5.6817\ V_f + 8.9 \quad (2)$$

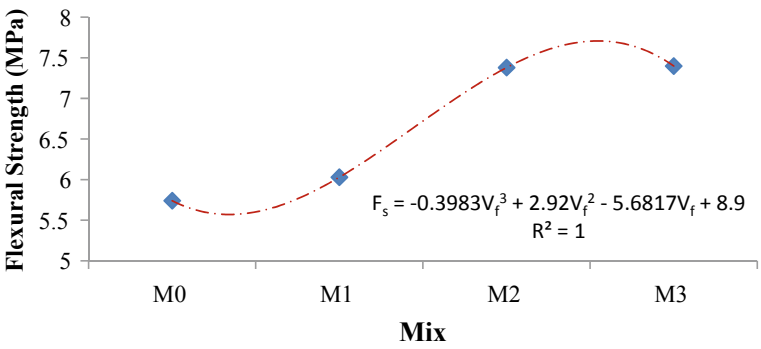

Fig. 4 Flexural strength of mixes

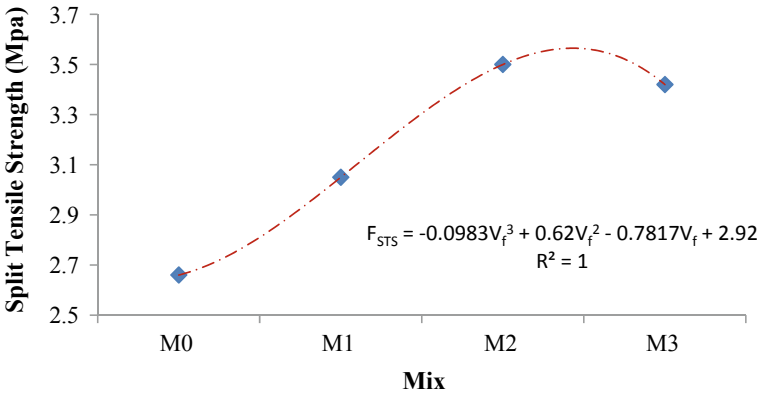

Fig. 5 Split tensile strength of mixes

where F_s is Flexural strength and V_f is volume of fibre content.

The split tensile strength results indicated that the tensile strength gain was increased up to 2% addition of fibre and then the strength decreased slightly as shown in Fig. 5. The tensile strength has improved about 14.62%, 31.58% and 28.57% for 1%, 2% and 3%. For 3% fibre content a slight decrement in tensile strength is observed. This negative effect may be due to the weaker adhesion between fibre and matrix. From the graph it is known that a perfect cubic polynomial relation is existed between the tensile strength and the fibre content. From the graph the following equation is obtained.

$$F_{STS} = -0.0983\ V_f^3 + 0.62\ V_f^2 - 0.7817\ V_f + 2.92 \tag{3}$$

where F_{STS} is Split Tensile Strength and V_f is volume of fibre content.

4.1.4 Bond Strength

The bond strength of the concrete was determined by pull out test and the results indicated that the bond strength of the concrete improved significantly with the addition of fibre as shown in Fig. 6. From the test results it is proved that there is a good interlocking existed between the fibre and the inserted reinforcement bar. The bond strength increased about 13.88–34.38 compared to control mix. The linear increment in the bond strength was observed from the graph. The following relation is found from the graph.

$$F_{bs} = 1.04V_f + 8.275 \tag{4}$$

Here F_{bs} is Bond Strength and V_f is volume of fibre content.

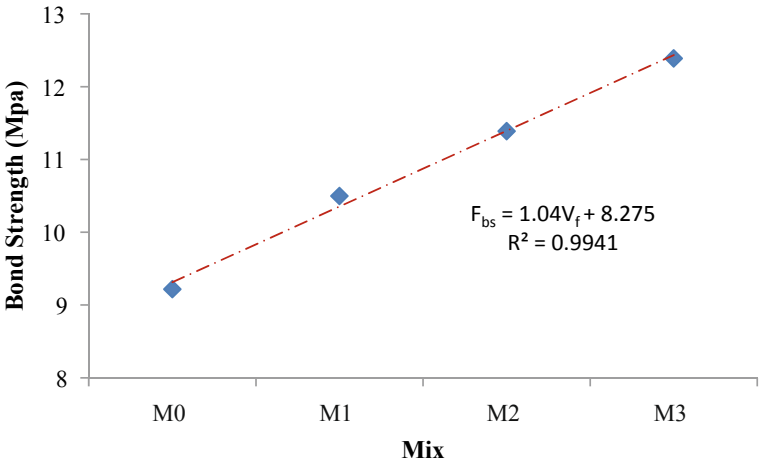

Fig. 6 Bond strength of mixes

4.2 Durability Properties

4.2.1 Rapid Chloride Permeability Test

The test was conducted on 12 RCPT cell specimens and the results indicated that the chlorine permeability of concrete was decreased with increase in fibre content as shown in Table 5. The possible reason for decrement in the flow of electrons is either by reduction in porosity due to filling of micropores of concrete with or by the accumulation of charged electrons on the surface of the fibre. For the better understanding of this effect, microstructural analysis is needed.

4.2.2 Abrasion Resistance of Concrete

The abrasion resistance of concrete was tested by underwater method as per ASTM C 1138 [10]. The test was conducted for a period of 72 h and the results are

Table 5 RCPT results

Sl. No	Mix	Current passed	Remarks
1	M_0	1010	Low
2	M_1	820	Very low
3	M_2	750	Very low
4	M_3	600	Very low

Table 6 Average depth of abrasion

Sl. No	Mix	Depth of abrasion (mm)
1	M_0	3.38
2	M_1	2.22
3	M_2	2.0
4	M_3	1.9

presented in Table 6. The test results revealed that the increase in the fibre content results in a decrease in the abrasion of concrete. These positive results are due to the better bonding between the fibre and the cement paste. The fibre are holding the matrix strongly against the continuous agitation of metal balls.

4.2.3 Acid Resistance

The acid resistance of the concrete was found out by immersing the specimens in both acids such as HCL and H_2SO_4 for a period of 28 days. The acid resistance of the concrete was estimated by measuring the compressive strength. The results indicated that the cubes immersed in Sulphuric acid degraded more than the specimen immersed in hydrochloric acid for both plain and fibre-reinforced concrete. The loss of strength ranges from 9.71% to 19.68% in the case of hydrochloric acid and 10%–25.18% in the case of Sulphuric acid as shown in Fig. 7. The high loss of strength in Sulphuric acid is because the leaching of concrete is more in this solution. However, the addition of fibre decreased the degradation effectively as shown in Table 7.

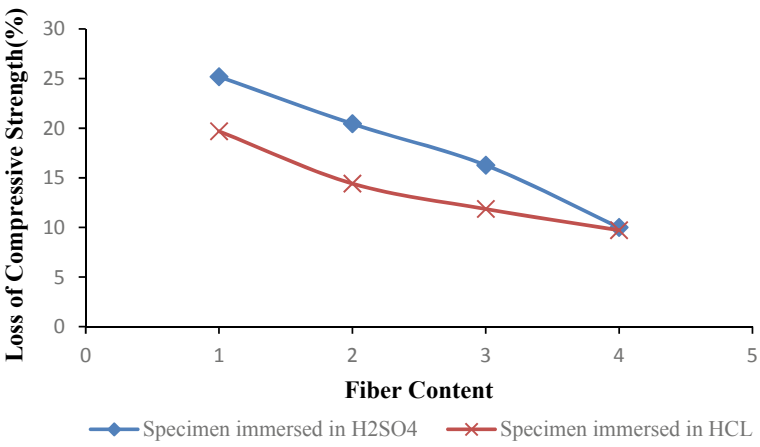

Fig. 7 Loss of compressive strength after exposed to acidic medium

Table 7 Compressive strength of cubes immersed in HCL and H_2SO_4 solution

Sl. No	Type of mix	Average compressive strength (MPa)		
		Before immersion in acids	After immersion in HCL for 28 days	After immersion in H_2SO_4 for 28 days
1	M_0	60.15	48.31	45
2	M_1	59.93	51.29	47.68
3	M_2	57.78	50.93	48.38
4	M_3	53.33	48.15	48

5 Conclusions

- The compressive strength was reduced from 60.15 to 53.33 MPa with the addition of basalt fibre, and the maximum percentage loss of strength was 11.38%.
- The flexural strength was found to increase with the addition of fibre, and the maximum strength gain was 30%.
- The split tensile strength was found to be high for 2% basalt fibre addition, and the maximum strength gain was 30%.
- The percentage increase in bond strength was 13.88% for M_1, 23.56% for M_2 and 34.38% for M_3.
- The chlorine permeability of concrete was found to decrease with the addition of basalt fibre.
- The abrasion resistance of fibre-reinforced concrete is more compared to plain concrete, and it is found to be increasing with increase in fibre content.

References

1. Arslan ME (2016) Effects of basalt and glass chopped fibres addition on fracture energy and mechanical properties of ordinary concrete: CMOD measurement. Constr Build Mater 114:383–391
2. Jiang C, Fan K, Wu F, Chen D (2014) Experimental study on the mechanical properties and microstructure of chopped basalt fibre reinforced concrete. Mater 58:187–193
3. Branston J, Das S, Kenno SY, Taylor C. Mechanical behaviour of basalt fibre reinforced concrete. Constr Build Mater 124:878–886
4. Mindness S. Proceedings of the international conference sustainable construction materials and technologies. Thirty years of fibre reinforced concrete research at the University of British Columbia, pp 259–268
5. Kumbhar PV (2014) An overview: basalt rock fibres-new construction material. Acta Eng Int 2(1):11–18
6. Dhand V, Mittal G, Rhee KY, Park S-J, Hui D (2015) A short review on basalt fiber reinforced polymer composites. Composites: Part B 73:166–180

7. IS 4031-1988. Method of physical tests for hydraulic cement
8. IS 2386-1962. Methods of test for aggregates for concrete
9. IS10262-2009. Indian standard concrete mix proportioning—guidelines
10. ASTM C1138. Standard test method for abrasion resistance of concrete. Under Water Method

Using Isothermal Calorimetry to Predict Setting Time of Cement-Based Materials (CBMs)

Arvind Vishavkarma
and Kizhakkumodom Venkatanarayanan Harish

Abstract In this study, the rate of heat evolution curve obtained from isothermal calorimetry is used for predicting the setting time. A derivative curve plot from the rate of heat evolution was used to determine the initial setting time (IST) and final setting time (FST) of cement paste and mortar containing different w/c ratio. Also, conventional methods such as IS 4031(part-5) and ASTM C403 were taken to determine the setting times. The correlation was developed between setting time obtained from the derivative plot and IS 4031 for cement paste sample, and derivative plot and ASTM C403 for mortar samples. The study indicates that the isothermal calorimetry techniques can be used to determine the setting time with ± 0.37–4.48 h deviation for cement paste and ± 0.43–3.78 h for the mortar, regardless of IST and FST. Further, a very high coefficient of correlation with 0.95 for IST and 0.99 for FST was obtained. Besides, longer setting times were obtained from the calorimetry method as to IS and ASTM setting time method.

Keywords Isothermal calorimetry · Setting time · Rate of heat evolution · Derivative curve · Coefficient of correlation

1 Introduction

The major clinker phases in OPC are C_3S (alite), C_2S (belite), C_3A (aluminate), C_4AF (ferrite) and gypsum and form the hydration products at different stages of hydration. Each phase can dissolve and precipitate as new strength forming products at a different time period. The silicate phases can dissolve and precipitate in the form of C–S–H, which provides the strength in the CBMs. However, aluminate phases can form other compounds like ettringite and monosulfoaluminate at the early stage of hydration [1]. The formation of these chemical compounds is

A. Vishavkarma (✉) · K. V. Harish
Department of Civil Engineering, Indian Institute of Technology Kanpur, Uttar Pradesh, 334 Faculty Building, Kanpur 208016, India
e-mail: kvharish@iitk.ac.in

B. Laishram and A. Tawalare (eds.), *Recent Advancements in Civil Engineering*, Lecture Notes in Civil Engineering 172,
https://doi.org/10.1007/978-981-16-4396-5_31

exothermic and complex and plays a critical role in the early and later stage properties of CBMs. The hydration of CBMs is significantly influenced by the hydration reaction and affects the early age properties, such as setting time, workability, strength grain and thermal shrinkage behaviour [2]. The various parameters, such as chemical and mineral admixtures, concrete mix constituents, construction procedures and environmental conditions, influence the rate of heat evolution of cementitious materials [3, 4]. "The Modern CBMs have much complex chemical system" due to the addition of chemical and minerals admixtures and various types of sources of ingredients incorporated in the production of CBMs. Hence, compatibility issue is increasing attention. The abnormal behaviour of certain materials results in a flash and false sets, which can affect the placement and strength development of CBMs [5]. Some of the construction procedures and environmental conditions influenced the problems in placing of CBMs. However, the existing guidelines for the construction have lack of information, specification and proper test method to assess the properties at an early age.

The CBMs set time has been determined by the IS 4031 and ASTM C403. These methods are arbitrary in terms of nature, time and labour consuming for those materials having a long setting time. The accuracy of this method is also affected by the skill of the operator. Many researches have used the rate of heat evolution curve based on the first and second derivatives of CBMs to determine the initial and final setting time [5, 6]. Sandberg and Liberman [7] evaluated the setting time using both derivative and fraction method based on concrete temperature development under a semi-adiabatic condition. The setting time of CBMs has been controlled by three-dimensional microstructure development that involves new phase growth, nucleation and formation of cement hydration products [1]. These processes depend on the cement hydration, which can be understood and characterized by the heat evolution from the cementitious materials [8]. Therefore, it is rational to determine the setting time from the Isothermal calorimetry curve. In the present paper, Vicats test, penetration and isothermal calorimetry test were used to determine the initial and final setting time. Further, setting time from isothermal calorimetry is correlated with the setting time determined from the IS 4031 (part 5) and ASTM C403 test methods.

2 Experimental Investigation

2.1 Research Programme

Ordinary Portland Cement (OPC) confirming to the IS: 8112 was used. Their oxide compounds found using the XRF, CaO, SiO_2, Fe_2O_3, Al_2O_3, MgO and loss of ignition of cement were determined to be 58.15, 19.90, 3.67, 4.57 and 3.37, respectively. River sand obtained locally was used as fine aggregates in mortar mixtures, and the physical properties of sand such as its water absorption and

specific gravity were determined to be 1.04% and 2.60%, respectively. The sieve analysis data indicated that the sand belonged to Zone II category as per IS 383 specifications [9]. No chemical admixtures were used in the mixture. Two samples were prepared for each w/c ratio for the all test method used in this study. The IDs are represented in the generalized form as M–x% where M—indicates mortar mixtures having a w/c ratio of 'x' % by weight of cement. The typical water-to-cement ratio (w/c) and sand-to-cement ratio (s/c) are used as the 0.35, 0.45 and 0.55 and 2.5, respectively. Isothermal calorimetry, Vicats test and penetration resistance test were used to determine the IST and FST of cement paste and mortar.

2.2 Test Method

The details of test methods used in this paper such as Vicats test, penetration test and isothermal calorimetry are provided in Table 1. Isothermal calorimetry has been

Table 1 Details of the test methods and silent features

Tests	Test Method	Salient features
Vicats test	IS: 4031 (Part 5) [7]	• Environmental condition: temperature of 27 ± 2 °C and 65 ± 5% of relative humidity • IST: Needle failed to penetrate 5 ± 2 mm from the bottom of the mould • FST: Annual attachment needle gently applied to the surface of the test block such that the needle was not able to make an impression on the surface test block
Penetration resistance	ASTM C403 [12]	• Mortar prepared and filled in 150 × 150 × 150 mm cubes in the three equal layers, and each layer was tempered 25 times by tempering rod • Penetration needles: 645, 323, 161, 65, 32, 16 mm^2 bearing area (maximum to the lower bearing area) • Depth of penetration on mortar: 25 ± 2 mm in the 10 ± 2 s • Distance between two penetration needles: Not more than 50 mm • IST and FST: Stress equals 3.5 MPa and 27.6 MPa, respectively
Isothermal calorimetry	ASTM C1702 [10, 11]	• I-Cal 4000 HPC unit and the schematic figure is shown in Fig. 1 • Reference cells to be used in the holder depend on the amount of sample taken • The heat produced by the test specimen flows through the heat sensor and into the heat sink • "Stabilization" has to be performed to prevent the temperature difference between specimen and reference cell • Specimen was prepared based on the standard procedure, and 150 g (∼100–200 g reference cell) of the sample was taken • After placing the specimen, the unit was closed, and several parameters such as mix time, specimen mass, cement mass and water mass were entered in the I-Cal Commander software

(a) Inside view of the unit showing four channels

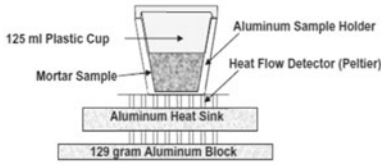

(b) Schematic showing different parts inside a single channel of the isothermal calorimetry unit

Fig. 1 Isothermal calorimetry unit, **a** inside view of the unit showing four channels, **b** schematic showing different parts inside a single channel of the isothermal calorimetry unit

used extensively in recent years as a specialized technique for evaluating the heat of hydration of CBMs system [10, 11]. A schematic of the single-channel calorimetry unit is shown in Fig. 1.

2.2.1 Setting Time from Rate of Heat Evolution Curve

The calorimetry test method is used to determine the set time of CBMs shows in Fig. 2, similar to the technique used for the AdiaCal calorimeter data analysis [7].

In this method, the first derivative of the rate of heat evolution (q) curve with respect to the time (t), d(q)/d(t), is derived from the original heat evolution data.

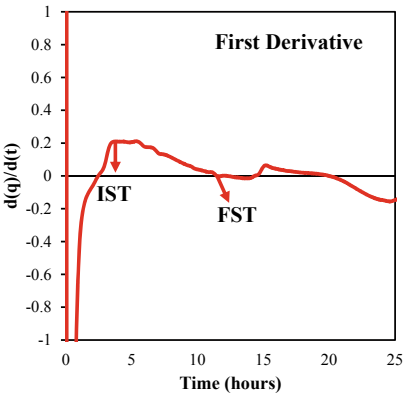

(a) Cement based materials

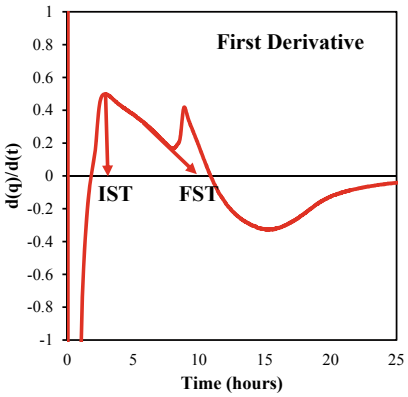

(b) Different w/c ratio

Fig. 2 Prediction of setting time using the rate of heat evolution curve, **a** cement-based materials, **b** different w/c ratio

When the first derivative curve comes to its peak value, the increase in the rate of heat evolution is the highest. The point is around the starting time of the second hydration peak and should be correlated to the initial setting time and shown in Fig. 2a. Hence, this point is called the initial setting time of the materials. After this point, a reduction in first derivative value is observed. When the first derivative close to zero shows the rate of heat evolution, the materials start to slow down, and the time of this point is called the final setting time of CBMs.

The initial setting time from the heat evolution curve of cement paste and mortar is defined as the time when the first derivative of the rate of heat evolution curve reaches its peak value. For the cement paste and mortar having different w/c ratio, the first derivative of the rate of heat evolution of cement paste and mortar started increasing again before reaching zero. To determine the final setting time, line A in Fig. 2b is extended and pass through the time axis, and the intersecting point on time axis is called as the final setting time of the cement paste and mortar.

3 Results and Discussion

3.1 Effect of w/c Ratio on Setting Time

IST and FST for cement paste and mortar are shown in Fig. 3a. From the figure, both initial and final setting time of cement paste and mortar increase with an increase in w/c ratio, that indicates the slower rate of microstructural built-up in CBMs. This phenomenon may be due to an increase in the w/c ratio which causes a reduction in cement content and increase in water content thereby causing a significant deacceleration in the cement hydration because of the dilution effect [13]. The other possible reason is that hydration kinetics are significantly influenced by the water-filled porosity according to Powers model [14]. Hence, the increases in w/c ratio increase the water-filled porosity and responsible for the deacceleration [15]. The IST and FST obtained from the isothermal calorimetry based on the rate of heat evolution curve form the cementitious materials and supported by the total heat evolution curve. However, more explanation for the results from Vicats test is difficult due to the arbitrary nature of the test. In Fig. 3b, normalized initial setting time (IST) of cement paste for M-0.45 and M-0.55 is ∼35% and ∼75% higher than M-0.35 respectively, and for mortar they are ∼47% and ∼80% higher than the M-0.35 respectively. Similarly, the final setting time of cement paste for M-0.45 and M-0.55 is ∼17% and ∼29% higher, and for mortar they are ∼71% and 96% higher than the M-0.35 respectively. This result is consistent with other research [6].

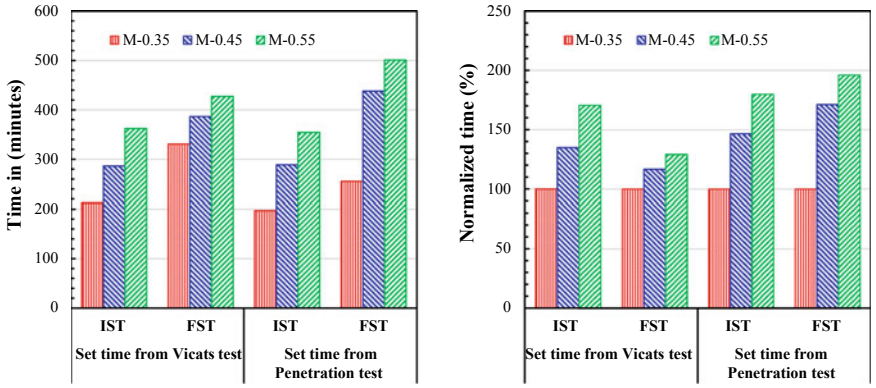

(a) Setting time from different methods (b) Normalized setting time from different methods

Fig. 3 Effect of w/c ratio on setting time, **a** setting time from different methods, **b** normalized setting time from different methods

3.2 Relationship Between Setting Time

Table 2 shows the initial and final setting time determined for the cement paste and mortar using Vicats test, penetration resistance and isothermal calorimetry test. The efforts were made to establish the relationship between setting time regardless of the difference in test principle and procedure. Three different w/c ratios were chosen and found the IST and FST of cement paste which is reported in Table 2. From the table, IST determined from Vicats test is higher than isothermal calorimetry. However, reverse trends are obtained for the FST. Similar trends were obtained for the IST and FST for the mortar specimens. The reason behind these trends explained in Sect. 3.1.

Figure 4a shows that the setting time determined from the isothermal calorimetry has a good linear relationship with the setting time determined from IS 4031 (part-5). The strong coefficient of determination (R^2) for IST and FST is ∼0.97 and ∼0.99, respectively, for the different w/c ratio. The initial setting times determined from the calorimetry method almost similar to IS 4031 because of all

Table 2 Initial and final setting time of cement paste and Mortar

Mixture ID	Cement paste				Mortar			
	IST (hours)		FST (hours)		IST (hours)		FST (hours)	
	VT	IC	VC	IC	PR	IC	PR	IC
M-0.35	3.35	2.98	5.52	10.00	3.28	2.85	4.27	8.05
M-0.45	4.78	5.25	6.45	10.80	4.81	2.95	7.30	9.10
M-0.55	6.08	6.35	7.13	11.40	6.08	3.10	8.35	9.98

Note VT—Vicats test, IC—Isothermal calorimetry and PR—Penetration resistance

point lies at equality line. However, for FST, they lies above the equality line which indicate that the final setting times determined by calorimetry method is longer than IS 4031. The difference between both methods is due to their different mechanisms for determining the setting times. As in IS 4031 method, penetration of a needle on a cement specimen is a physical process, and its release from the hook of Vicat frame is through gravity. It may not necessarily generate the same concentrated stress on the specimen every time. The calorimetry method measures heat from the specimen at a constant environment/temperature. At the same time, Vicats test was performed on the laboratory environment, which can increase a certain degree of hydration due to higher degree of chemical reactions.

The relationship between ASTM C403 and calorimetry is shown in Fig. 4b. For the initial setting time, all points lie below the equity line, which indicates that the calorimetry setting time is significantly lower than ASTM results. For the final setting time, all points above the equity line show the calorimetry final setting times are higher than the ASTM method. However, there was a significant linear relationship with R^2 value of ~0.97 and ~0.95 for IST and FST. The difference between the two results is due to two methods which have a very different definition for setting time. The ASTM C403 method is based on the penetration force, while the calorimetry method is based on the rate of the chemical reaction. The other possible reason is both methods provide a test sample with different environmental/temperature conditions. The ASTM C403 test sample performed at room temperature conditions is due to the semi-adiabatic effect, i.e. the temperature of the sample increased increases with time. However, during the calorimetry test, the sample was in a controlled-environment condition. The temperature of the sample was kept constant [5, 16].

The IST and FST determined from Vicats and penetration resistance method are arbitrary in nature and not supported by any scientific explanation regarding the

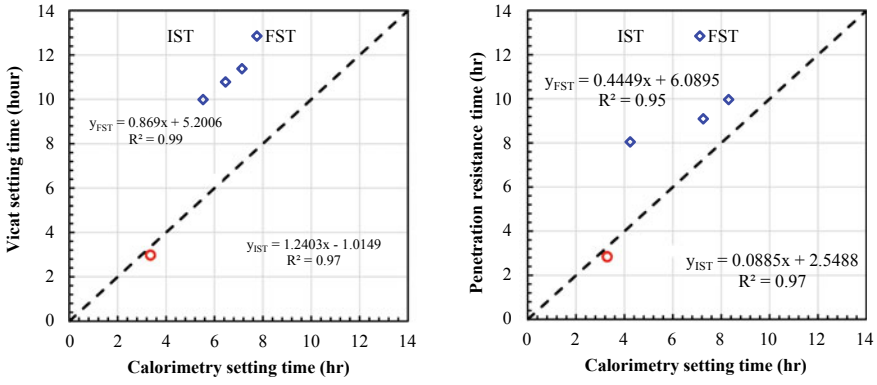

(a) Vicat test vs Isothermal calorimetry

(b) Penetration resistance vs Isothermal calorimetry

Fig. 4 Correlation between different test methods, **a** Vicat test versus isothermal calorimetry, **b** penetration resistance versus isothermal calorimetry

selection of IST and FST. However, in the isothermal calorimetry method, IST and FST are considered when the nucleation and acceleration stages end. These stages are correlated with the rate of heat evolution and total heat evolution of CBMs. In the past, many researchers established the relationship between hydration reactions and the rate of heat evolution and total heat evolution curve [4, 17]. Therefore, the rate of heat evolution curve from the isothermal calorimetry test could be used to determine the setting time of cement paste and mortar setting time.

4 Conclusions

The following finding and conclusions can be drawn from the present study:

1. With increases in w/c ratio, IST and FST of cement paste and mortar increase regardless of two different test procedures.
2. The setting time of cement paste and mortar can be well predicted from the derivative of the rate of heat evolution curve calculated from the isothermal calorimetry. The predicated results showed a good linear relationship with those from the IS 4031(part-5) for cement paste and ASTM C431 for the mortar.
3. Among all methods, isothermal calorimetry method provides the logical explanation for selection for the IST and FST setting time; hence, it can be used to calculate the IST and FST of CBMs.

Acknowledgements The authors thank Aamna Sarfaraz for providing a quick check with the English language that was used in the paper. I also thank the technical staff from the Structural Engineering Laboratory, IIT Kanpur.

References

1. Mehta PK, Monteiro PJM (2006) Concrete microstructure, properties, and materials. McGraw-Hill
2. Neville AM, Brooks JJ (1987) Concrete technology. Longman Scientific & Technical, England
3. Frølich L, Wadsö L, Sandberg P (2016) Cement and concrete research using isothermal calorimetry to predict one day mortar strengths. Cem Concr Res 88:108–113. https://doi.org/10.1016/j.cemconres.2016.06.009
4. Suraneni P, Weiss J (2017) Examining the pozzolanicity of supplementary cementitious materials using isothermal calorimetry and thermogravimetric analysis. Cement Concr Compos 83:273–278. https://doi.org/10.1016/j.cemconcomp.2017.07.009
5. Ge Z, Wang K, Sandberg PJ, Ruiz JM (2009) Characterization and performance prediction of cement-based materials using a simple isothermal calorimeter. J Adv Concr Technol 7 (3):355–366
6. Hu J, Ge Z, Wang K (2014) Influence of cement fineness and water-to-cement ratio on mortar early-age heat of hydration and set times. Constr Build Mater 50:657–663. https://doi.org/10.1016/j.conbuildmat.2013.10.011

7. Sandberg JP, Liberman S (2007) Monitoring and evaluation of cement hydration by semi-adiabatic filed calorimetry. In: Wang K, Schindler AK (eds) Concrete heat development: monitoring, Prediction, and Management Georgia NY: Curran Associates, IN, pp 13–24
8. Pang X, Bentz DP, Meyer C, Funkhouser GP, Darbe R (2013) Cement and concrete composites a comparison study of Portland cement hydration kinetics as measured by chemical shrinkage and isothermal calorimetry. Cement Concr Compos 39:23–32. https://doi.org/10.1016/j.cemconcomp.2013.03.007
9. IS 383 (2016) Coarse and fine aggregate for concrete- specification
10. ASTM C1702 (2013) Standard test method for measurement of heat of hydration of hydraulic cementitious materials using isothermal conduction. West Conshohocken, PA. https://doi.org/10.1520/C1702-13
11. ASTM C1679 (2014) Standard practice for measuring hydration kinetics of hydraulic cementitious mixtures using isothermal calorimetry. ASTM International, West Conshohocken, PA. https://doi.org/10.1520/C1679-14
12. ASTM C403, "ASTM C 403 (2005) Standard test method for time of setting of concrete mixtures by penetration resistance. ASTM C 403–95, Annual Book of ASTM Standards, American Society for Testing and Materials, Pennsylvania, 1998. ASTM, pp 1–7. https://doi.org/10.1520/C0403
13. Arora A, Sant G, Neithalath N (2016) Ternary blends containing slag and interground/blended limestone: hydration, strength, and pore structure. Constr Building Mater 102:113–124. https://doi.org/10.1016/j.conbuildmat.2015.10.179
14. Bentz DP (2006) Influence of water-to-cement ratio on hydration kinetics: simple models based on spatial considerations. Cem Concr Res 36(2):238–244. https://doi.org/10.1016/j.cemconres.2005.04.014
15. Langan BW, Weng K, Ward MA (2002) Effect of silica fume and fly ash on heat of hydration of Portland cement. Cem Concr Res 32(7):1045–1051. https://doi.org/10.1016/S0008-8846(02)00742-1
16. Bentz DP, Barrett T, De I, Weiss WJ (2012) Relating compressive strength to heat release in Mortars. Adv Civil Eng Mater 1(1):1–14. https://doi.org/10.1520/ACEM20120002
17. Frølich L, Wadsö L, Sandberg P (2016) Using isothermal calorimetry to predict one day mortar strengths. Cement Concr Res 88:108–113. https://doi.org/10.1016/j.cemconres.2016.06.009

State of the Art: Ultra-High-Performance Concrete: From Fundamental to Applications

Snehal Abhyankar and R. V. Ralegaokar

Abstract This is the paper which studies recent developments in the region of UHPC and UHPFRC characteristics, the methodology of design. UHPFRC is recognized as innovative new material, with distinct characteristics (high strength, very good ductility, less permeable, great capacity in compression and good toughness) as compared to conventional concrete. It really matters how the material behaves and exhibits for structural applications. But currently, the available codes are not suited with this new material and should be reviewed before its application. Both material properties and mechanical properties of materials are evolved. It includes knowledge regarding hydration; test on permeability; effect of fibres; methods mix design; bonding of fibre matrix. Concepts of mechanical properties with some design recommendations studied. Different applications of UHPFRC constructed were mentioned.

Keywords Ultra-high-performance fibre-reinforced concrete (UHPFRC) · UHPC · Material properties · Design procedures · Mechanical behaviour · Sustainable material

1 Introduction

UHPC is an innovative material with very high strength and at par durability. It possesses the potential to offer sustainable and approachable solution to enhance life of buildings and other infrastructure components [1]. UHPC applications from parts of building, features of architecture features, bridges, repair, rehabilitation, towers, gas and oil towers and industrial applications in off-shore [2]. Construction of roads and bridges is most desirable in UHPC application [3]. The usage of UHPC for bridges and bridge components can be seen in various countries including many countries like Australia, China, Czech Republic, Canada, Austria, Japan, Switzerland, Italy, Netherlands, New Zealand, Slovenia, Germany, Malaysia

S. Abhyankar (✉) · R. V. Ralegaokar
Department of Civil Engineering, VNIT, Nagpur, India

B. Laishram and A. Tawalare (eds.), *Recent Advancements in Civil Engineering*, Lecture Notes in Civil Engineering 172,
https://doi.org/10.1007/978-981-16-4396-5_32

and the United States (USA) [2]. Initially, most of the projects in these countries were supported by different government agencies to develop as demo projects for future implementation [4]. Actually, it did not apply as slow follow-up progress [5]. The reasons for non-implementation may be less knowledge of design codes as well as less information about both the material and methodology of production. Factor of high cost also limits the implementation [2]. Now, more governmental and private organizations are taking more interest in utilizing this new, innovative and promising material.

2 Definition and Development of UHPC

Ultra-high-performance concrete (UHPC) is defined as 'concrete that has minimum specified compressive strength of 150 MPa with specified durability, tensile ductility and toughness requirements; fibres are generally included to achieve specified requirements' by ACI Committee 239 [6]. UHPC class materials as specified as 'cementitious-based composite materials with discontinuous fibre reinforcement that exhibit compressive strength above 150 MPa, pre- and post-cracking tensile strength above 5 MPa and enhanced durability via a discontinuous pore structure' by Federal Highway Administration (FHWA) of USA [7].

Fibre-reinforced concrete (FRC) was introduced before more than 55 years in modern times [8]. Almost before one thousand years ago, materials were strengthened by using fibres like straws and horsehairs [9]. Construction industry nowadays uses various fibre-reinforced concrete (FRC) for multiple applications [10]. The term coined UHPFRC stands for fibre-reinforced UHPC. Concrete is the most required construction material in the industry all over the world. It is estimated that the world concrete production is about six billion cubic metres per year [11]. The estimates indicate that China consumes 40% of the world's concrete production [12, 13]. Qualities of concrete as strength and durability, ability for it to be placed in many forms and its low price have made it most popular and important in construction industry [14]. The best advantage of concrete is its strong compressive strength [15]. Research and development in the field of concrete has vast changes in technology. In 1930s, effort began to enhance compressive strength of concrete, from last 45 years, significant achievement [16].

Cementitious matrix has brittleness; to overcome, fibres are added. To control fracture process, cracking behaviour is controlled by fibres. Though cracks get developed, fibres provide post-cracking strength and toughness [8]. The classification of fibres is done on materials used, like steel, synthetic, mineral and aspect ratio [10]. A large variety of shapes, sizes and lengths of fibres are available. It includes simple hooked end, twisted and corrugated fibres [17]. Amount of fibres is expressed in either volume fraction or percentage. For the same amount of volume fraction, smaller size fibres will be more as compared to larger fibres. Controlling micro-cracking is done efficiently with use of large numbers of dense smaller fibres [18]. Micro-cracks may lead to macro-cracks which can be better monitored and

controlled by longer fibres [9]. As per technical papers review, volume fraction for fibre-reinforced concrete may range from 0.25% to 2% by volume of matrix [19]. The papers reviews claim that available commercial UHPC mixes possess fibres in ratio 2%–6% of volume fraction [20].

Actually, UHPC starts developing more after year 2000. Learning and discussions by expertise, technical people lead to acknowledgement that new or advanced concrete should possess not only high strength but also excellent characteristics ultimately leading to UHPC and UHPFRC [21]. Advanced concrete manufacturing techniques open more opportunities for wide range of applications. According to the study done currently, technicians and researchers prefer only sustainable UHPC varieties having lower initial cost and lower materialistic cost [5, 22–29]. In order to reduce consumption of cement in manufacturing concrete, other materials like fly ash, ground-granulated blast furnace slag and rice-husk ash can be used to produce UHPC which may be sustainable. UHPC-specific structural design rules are not available, so wide-scale application has been restricted [6, 30]. For ASTM and ACI, the main task is to frame design rules and testing standards [6]. For design of UHPC structures, task group 8.6 of FIP is having responsibility of recommendations. From Australia, Japan Society of Civil Engineers and SETRA-AFGC in France, some guidelines recommendations are available [7].

Literature reviews add reports that UHPC manufacturing requires normal temperature [31]. A new, innovative, environmental friendly and sustainable material UHPC is gaining more popularity as it has low cost as compared to other materials [32]. Many countries started implementation and application of UHPC from year 2000. In France, structures like bridges, facades and slabs have been built with UHPC [33]. In US highway infrastructures, UHPC plays very important role in maintenance and development [15]. Many more construction activities in bridge structures were carried in Australia [34]. Structures requirement in situ reinforcement were made using UHPC in Switzerland [35]. Netherlands and Spain did construction of bridges using UHPC [22, 23 and 36]. Construction industry demands sustainable solutions; so as initiative in Malaysia, UHPC was used for constructing bridges. Since 2010, totally 113 UHPC bridges were constructed in Malaysia [37].

3 Fundamentals of UHPC

It took about almost 15 years for researchers, technicians and industrialist to develop [38, 39] UHPC to make it ready for applications. The highest compressive strength of UHPC could be 200 MPa. In 1980s, a concept was coined to prepare concrete with very high strength [40]. Study done on design mixes in such way that ultrafine particles should be densely packed. For getting this result, minimum W/B ratio is chosen [41]. Ductile behaviour of UHPC may be enhanced by addition of small steel fibres [42]. UHPC has extraordinary excellent performance in the application of infrastructures, buildings and more increasing applications in new

areas [43]. Grand View Research done market survey on global market size valued at USD$ 892 million in 2016. As per extended prediction, expected growth will be 8.6% to USD$ 1867.3 million in 2025 [3].

4 UHPC Mixtures

For ultrafine material selection of size of grain with accurate physical and chemical characteristics is required [38, 39]. Commercially available UHPC occurs with costly initial manufacturing cost than conventional concrete. Larrad and Sedran [41] presented linear packing density model for design of UHPC. This model fails in explaining the relationship existing between materials ratios as well as packing density because of linear nature of mode [44]. Later on, this was improved by using virtual density theory defined as solid suspension model (SSM) [45]. Fluid mortar is manufactured with 0.14 W/B ratio, and compressive strength 236 MPa, and 4 days curing are needed with 90° [46]. This research took next level by De Larrad teammates by improvising current model based on the concept of compaction index and virtual packing density. Compressible packing model is developed for next-generation packing [42, 45, 46]. Richard and Cheyrezy [9] have successfully developed two UHPC products, namely RPC 200 and RPC 800, by optimizing the granular mixture using CPM. Using particle size, density and shapes, Geisenhansluke and Schmidt [41] designed a locally produced UHPC mixture. Table 1 shows mixture proportions and strength results [47–50].

The proportions of SP differ between 1.4 and 7.5% by mass of cement or binder [22, 30].

Table 2 shows proportions of two mixtures with different fibre dosage and their spread values (Máca et al., 2013) [47, 50]. An ecological UHPC mixture was developed by Fennis et al. based on particle packing technology. In this new approach, cement content consumption is reduced to more than 50%. A theory known as SP water demand, an innovative way, was developed by Lohas and Ramge [50] to achieve good workable concrete by using water-to-powder ratio. UHPC having compressive strength 180 MPa was manufactured by Park et al. by acknowledging effect of W/B and effect of replacement proportion of fillers.

Figure 1 shows compressive and flexural strength of two different mixtures at different fibre contents (Máca et al., 2013) [47–50]. Wille et al. [52] developed UHPC using local materials without any special type of mixer and heat treatment with a compressive strength exceeding 200 MPa. Workability test from mini slump measurement is done based upon that spread flow properties design made. There is variation in air content by using results of spreadsheet. So to regularize and give accurate prediction of compressive strength of UHPC, a statistical relation was proposed by considering the combined effect of air voids and W/C.

Table 1 Mixture proportions and strength results (Wille et al., 2012)

Sr. No	TYPE	UHPC				UHPFRC				SifCon
		A[a]	B[a]	C	D	A[a]	B[a]	C	D	
1	Cement	1.00	1.00	1.00	1.00	1.00	1.00	1.00	1.00	1.00
2	Silica fume	0.25	0.25	0.25	0.25	0.25	0.25	0.25	0.25	0.25
3	Glass powder	0.25	0.25	0.25	0.25	0.25	0.25	0.25	0.25	0.25
4	Water	0.220	0.195	0.190	0.180	0.212	0.200	0.185–0.195	0.18–0.20	0.207
5	Super-plasticizer [b]	0.0054	0.0108	0.0108	0.0114	0.0054	0.0108	0.0108	0.0108	0.0108
6	Sand A[c]	0.28	0.30	0.31	1.05	0.27	0.28	0.29	0.92	0.76
7	Sand B [d]	1.10	0.71	0.72	0.00	1.05	0.64	0.67	0.00	0.00
8	Ratio of sand A/B	20/80	30/70	30/70	100/0	20/80	30/70	30/70	100/0	100/0
9	Fibre	0.00	0.00	0.00	0.00	0.15/0.25	0.22	0.18–0.27	0.22–0.31	0.71
10	Fibre in vol %	0	0	0	0	1.5/2.5	2.5	2.0–3.0	2.5–3.5	5[e]/8[f]
11	f_c [cube, 28d] MPa	194	207	220–240	232–246	207/213	219	227–261	251–291	270[e]/292[f]
12	f_t [tension] MPa	6.1–7.4 [g]	6.9–7.8 g	7.4–8.5 g	8.2–9.0 g	8.2/14.2	15	16–20	20–30	37[e]

[a]non-vibrated, non-surface cut
[b]Solid content
[c]Max. grain size 0.2 mm (1/128 in.)
[d]Max. grain size 0.8 mm (1/32 in.)
[e]Twisted (T) fibre
[f]Straight (S) fibre
[g]At first cracking, followed by immediate failure

Table 2 Proportions of two mixtures with different fibre dosage and their spread values (Máca et al., 2013)

Sr. No	Type of component	UHPFRC 2–2	UHPFRC 2–3	UHPFRC 3–2	UHPFRC 3–3
		Proportions by weight			
1	Cement CEM I 52, 5R	1	1	1	1
2	Silica fume	0.25	0.25	0.25	0.25
3	Glass powder	0.25	0.25	0.25	0.25
4	Water	0.22	0.22	0.22	0.22
5	HRWR: Sika SVC 20 Gold			0.031	0.031
6	HRWR:Sika ViscoCrete 20He			0.019	0.019
7	HRWR:Sika ViscoCrete 30He	0.025	0.025		
8	HRWR: Sika ViscoCreate 1035	0.025	0.025		
9	Fine sand 0.1/0.6 mm	0.42	0.42	0.42	0.42
10	Fine sand 0.3/0.8 mm	0.8	0.7	0.8	0.7
11	Fibres	0.2	0.3	0.2	0.3
12	Spread [mm]	153	140	240	160

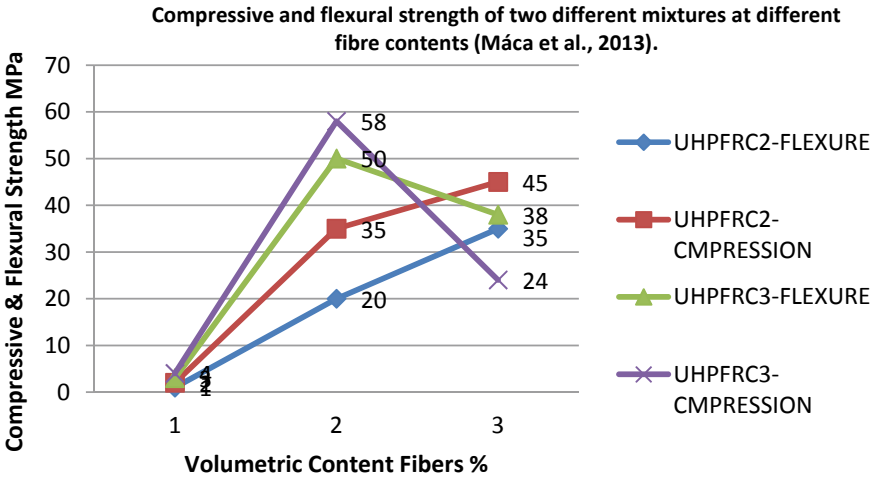

Fig. 1 Compressive and flexural strength of two different mixtures at different fibre contents (Máca et al., 2013)

5 Applications of UHPC

5.1 Infrastructures

UHPC area started exposure in application in year 1985, so more experimentation and research works have been done [1]. For a novel approach towards designing, architecture and construction techniques for particular requirements of client, various combinations of UHPCs were created. First of its kind, civil engineering structure, prestressed hybrid pedestrian bridge over the Magog River in Sherbrooke, Canada, using UHPC application was built in 1997 [15]. In the corrosive, aggressive environment of Cattenom and Civaux nuclear cooling towers in France, the corroded steel beams were replaced [21, 53]. In 2001, new bridge named Bourg-les-Valence was constructed in France for cars and trucks [26]. A detailed study was done to modify conventional design components of bridges by using UHPC with more durable and high-strength material properties. Optimisation of design was done by using UHPC. A lot of research and development in the field of construction all over the world lead to the construction of many such bridges. Using UHPC, the Seonyu footbridge with a main span of 120 m in South Korea was started in 2002 and was completed in 2004 [26]. The interesting fact of Seonyu Bridge is, it was constructed with less almost half of the material as required in conventional design and great equivalent strength [54]. In 2003, the 50 m-span Sakata-Mirai footbridge was completed in Japan [55]. New invention of using perforated web in UHPC leads to overall reduction in weight of structure as well as it looks beautiful aesthetically [39]. In North America (USA and Canada), Asia and Australia and Europe, UHPC bridges for pedestrian traffic have been constructed after the successful completion [28]. Research on high- and ultra-high-performance fibre-reinforced concretes was developed by IITs and SERC, Chennai [56]. The 28-day compressive strength of the composites ranged from 81 MPa high-performance concrete (HPC) to 188 MPa reactive powder concrete (RPC) by SERC investigations. Academic institutions experiment on different types of fibres—both steel and polymer—like PVA or PP, gets result on strain-hardening behaviour. SERC, Chennai, used UHPC overlay for repairing damaged RCC beams [57, 58].

5.2 Construction of Building Components

Different parts of buildings like sunshades, cladding and roof components are manufactured by UHPC in the last decades [59]. To find innovative material, UHPC has to create light, slender and aesthetic durable structures. A project 2014 is highlighted for its high geometric complicated designs made with UHPC. Uniquely designed prefabricated UHPC panels filled through vacuum is used [60]. Museum of European and Mediterranean Civilizations [9] located at the port area of Marseille in France is exemplary example. Extensive use of UHPC is done in this

building. In roofs and canopies of Shawnessy LRT station in Canada, new innovative material UHPC was used. So many applications and constructed structures like precast thin curve shells in wastewater treatment plant were constructed in France [46].

5.3 Non-structural Elements

Preference by choice is given to UHPC by its excellent characteristics to repair and retrofit existing structures [46, 50]. A bridge over the La Morge River in Switzerland [29], the first application on UHPC overlay, was reported on. Bridge deck curbs were repaired and replaced by UHPC. Inspection done after 1 year observed no cracks in this prefabricated UHPC slab. At the Hosokawa river tunnel in Japan [19], hydraulic construction repair and rehabilitation using UHPC was done. At Caderousse and Beaucaire Dams in France [34], high flexural strength and densely packed microstructure made UHPC an extra potential state-of-the-art material [61]. In China, repair work of high-speed railway cover plates was done by using UHPC [9, 40].In France, nuclear reactor containment walls were repaired using UHPC [39]. Marine areas deal with aggressive agents, so UHPC usage acts as wonderful durable material. Recent literature reviews by researchers in successful designs of windmills were done [38, 39, 53, 54]. Maritime signalization structures with UHPC were rejuvenated excellently [54]. In Japan, UHPC slab was constructed at the Haneda Airport over the sea [62].

6 Future Challenges and Gaps Identified

A lot of research have to be done to reduce quantity of local raw materials, waste products and content of Portland cement to prepare good mixtures [42]. Since few years, empirical skills with knowledge on the design and construction of UHPC structures have been gained, but for some reasons, they may not be easily shared [63]. No guidelines for design and construction of UHPC structures are available. In different countries, variety of UHPCs have different experience, so it is difficult to arrive at conclusion at international level [63]. Countries like France, Japan, China, German and Switzerland have made standardization efforts as demand for UHPC growing [64]. Limitation for number of skilled architects, engineers and experts in the UHPC design and construction is another concern [65]. A large demand and popularity of UHPC expect more skilled workforce, specialized teams [63]. Five major competitors for global UHPC market could be identified, with products mainly distributed in Europe and North America [66]. Currently, research with nanotechnology and experimental investigations by using nanoparticles is applied to enhance its properties. Research has started to study the behaviour of hydration products in UHPC at nano-scale level [67]. To solve problems of

shrinkage related with UHPC, nanotechnology may provide solutions. To enhance applications for wider scope, UHPC should be made cost-effective [68]. One area of research is to replace steel fibres by polyethylene fibres so to cut cost [67]. New mineral admixtures to produce sustainable UHPC need to be explored. The use of internal water curing is a very important method to enhance the properties of concrete, especially at low w/b ratio mixes [69]. It is necessity to study durability of UHPC [63]. Focus should be given on serviceability limit and fatigue problems. The experimental validation and implementation of the proposed prefabricated elements should also be carried out. Applications of UHPC in marine structures have been reported with promising results [38, 50, 70]. This gives the possibilities of UHPC to be applied in more severe environmental conditions. UHPC blocks with different shapes could be precast and assembled into a structure, just like a jigsaw puzzle. Much time and labour can be saved to build this kind of UHPC structure. Japan has started the fundamental studies on this concept in the effort to revolutionizing the construction industry [33].

7 Conclusions

Some advanced properties of UHPC like high strength and excellent durability were developed due to homogeneity and making structure densely packed. In 1990s, a large collection of data of information of the material and its design were collected. Construction started with various countries to introduce it to building and bridge applications of UHPC structures. More technical reviews papers were published in France, Japan, Germany and Switzerland. In 2016, two French national standards were published for UHPC for changes in the technical guidelines and recommendations which are used in designing UHPC. The international Technical Level accepted UHPC further because of these clear and codified specifications. In North America, Asia and Europe, many applications of UHPC mainly concentrate on the sustainability and lifetime services. During journey of UHPC constructions for the past 10 years, more than 90 bridges have been constructed in Malaysia and another 20 bridges at various stages of construction. Applications of UHPC are being great success throughout the world. There are few limitations in using UHPC when acting as barriers for implementation. High initial cost, limited codes, design difficulties and complex fabrication technique together with the limited available resources severely hampered its commercial development and application in modern construction industry, especially in the developing countries. To make UHPC commercially successful, the industry should cooperate in a much better way with academic institutions, governmental bodies, owners and end-users. A sharing of knowledge between end-users and developers is needed. We need to pay more attention to local recommendations and standard designs for handling UHPC. A research in developing more sustainable model along with economic and cost-reducing UHPC is expected. In order to expand acceptance of UHPC, more works have to be done to replace expensive components. To minimize

environmental impact, more innovative approaches are expected. Designers, architects and engineers should be more open to this new material and technology. All these collaborative efforts may lead to enhancing importance of UHPC as new advanced construction material in present as well as in the future endeavours for more sustainable construction.

References

1. Schmidt M, Fehling E (2005) Ultra-high performance concrete: research development and application in Europe. In: The 7th international symposium on the utilization of high-strength/high-performance concrete, pp 51–78
2. Voo YL, Foster S, Pek LG (2017) Ultra-high performance concrete—technology for present and future. In: ACI Singapore, building construction authority joint seminar on concrete for sustainability, productivity and the future
3. Grand View Research (GVR) (2017) Ultra-high performance concrete (UHPC) market analysis by product, by application, and segment forecasts, pp 2014–2025
4. Schmidt M (2012) Sustainable building with ultra-high performance concrete (UHPC)—coordinated research program in Germany. In: Proceedings of Hipemat, 3rd international symposium on UHPC and nanotechnology for high performance construction materials, pp 143–25
5. Azmee NM, Shafiq N (2018) Case study ultra-high performance concrete: from fundamental to applications. Case Stud Constr Mater
6. Ahlborn, Theresa M (2015) Advancing UHPC in the United States concrete construction market. In: 4th Asian conference on 'ecstasy in concrete', ACECON 2015, Indian Concrete Institute, Kolkata, October, 2015, pp 1–8
7. Federal Highway Administration, U.S. Department of Transportation, Ultra—High Performance Concrete: A State-of-the-Art Report for the Bridge Community, Publication no. FHWA–HRT–13–060, June 2013, p 171
8. Zollo RF (1997) Fiber-reinforced concrete: an overview after 30 years of development. Cem Concr Compos 19(2):107–142
9. Richard P, Cheyrezy M (1995) Composition of reactive powder concretes. Cem Concr Res 25 (43):1501–1511
10. Soufeiani L, Raman SN, Jumaat MZB, Alengaram UJ, Ghadyani G, Mendis P (2016) Influences of the volume fraction and shape of steel fibers on fiber-reinforced concrete subjected to dynamic loading—a review. Eng Struct 124:405–417
11. Brandt AM (2008) Fibre reinforced cement-based (FRC) composites after over 40 years of development in building and civil engineering. Compos Struct 86(1):3–9
12. Voo YL, Nematollahi B, Said ABM, Gopal BA, Yee TS (2012) Application of ultra-High performance fiber reinforced concrete—the Malaysia perspective. Int J Sustain Constr Eng Technol 3(1):26–44
13. Uche OAU (2008) Influence of recycled concrete aggregate (RCA) on compressive strength of Plain concrete. Cont J Eng Sci 30–36
14. Zdeb T (2013) UHPC—properties and technology. Bull Polish Acad Sci Tech Sci 54(1):183–193
15. O'Neil EF, Neeley BD, Cargile JD (2001) Tensile properties of very high strength concrete for penetration-resistant structures. US Army Engineers Research and Development Center
16. Spasojevic A (2008) Structual implications of ultra-high performance fiber-reinforced concrete in bridge design. PhD Thesis Lausanne, Switzerland

17. Hassan AMT, Jones SW, Mahmud GH (2012) Experimental test methods to determine the uniaxial tensile and compressive behaviour of ultra high performance fibre reinforced concrete (UHPFRC). Constr Build Mater 47:874–882
18. Park SH, Kim DJ, Ryu GS, Koh KT (2012) Tensile behaviour of ultra-high performance hybrid fibre reinforced concrete. Cem Concr Compos 46:172–184
19. Malesev M, Radonjanin V, Marinkovic S (2010) Recycled concrete as aggregate for structural concrete production. Sustain J 1204–1225
20. Larsen IL, Thorstensen RT (2020) Review article, the influence of steel fibres on compressive and tensile strength of ultra high performance concrete: a review. Constr Build Mater 254:119459
21. Acker P, Behloul M (2004) Ductal1 technology: a large spectrum of properties, ultra-High performance concrete, Kassel, Germany, pp 11–48
22. Tirimanna D, Falbr J (2013) FDN modular UHPFRC Bridges. In: Proceedings of international symposium on ultra-high performance fiber-reinforced concrete, pp 395–0404
23. Naaman AE, Wille K (2012) The path to ultra-high performance fiber reinforced concrete (UHP-FRC): five decade of progress. In: Proceedings of 3rd international symposium on UHPC and nanotechnology for high performance construction materials, pp 3–13
24. Blais PY, Couture M (1999) Precast, prestressed pedestrian bridge—world's first reactive powder concrete structure. PCI J 44(5):55–61
25. Acker P, Behloul M (2004) Ductal1 technology: a large spectrum of properties, ultra-high performance concrete. Kassel, Germany, pp 11–48
26. Hajar Z, Simon A, Lecointre D, Petitjean J (2004) Design and construction of the world first ultra-high performance road bridges. In: Proceedings of the international symposium on ultra-high performance concrete, pp 39–48
27. Behloul M, Lee KC (2003) Ductal! Seonyu footbridge. Struct Concr 4(4):195–201
28. Tanaka Y, Meakawa K, Kameyama Y et al (2011) The innovation and application of UHPFRC bridges in Japan. In: Designing and building with UHPFRC—state of the art and development, ISTE Ltd, London, pp 148–187
29. Toutlemonde F, Resplendino J (2011) Designing and building with UHPFRC: state of the art and development, ISTE, London
30. Perry VH. Case studies on innovative applications and challenges of introducing breakthrough technologies (UHPC) in the construction industry, in: Ref.10, pp 33–41
31. Rossi P (2013) Influence of fibre geometry and matrix maturity on the mechanical performance of ultra-high-performance cement based composites. Cem Concr Compos 47:246–248
32. Wang W, Liu J, Agostini F, Davy CA, Skoczylas F, Corvez D (2014) Durability of an ultra high performance fibre reinforced concrete (UHPFRC) under progressive aging. Cem Concr Res 55:1–13
33. Abbas S, Soliman AM, Nehdi ML (2015) Exploring mechanical and durability properties of ultra-high performance concrete incorporating various steel fiber lengths and dosages. Constr Build Mater 435:429–441
34. Tuan NV, Ye G, Breugel KV et al (2011) The study of using rice husk ash to produce ultra-high performance concrete. Constr Build Mater 25(4):2030–2045
35. Bruhwiler E, Denarie E (2008) Rehabilitation of concrete structures using ultra-high performance fiber reinforced concrete. Proceedings of 2nd international symposium on ultra-high performance fiber-reinforced concrete, pp 895–902
36. Grunewald S, Kohne H, Nio M et al (2013) Optimization of a slender bridge in UHPFRC. In: Proceedings of international symposium on ultra-high performance fiber-reinforced concrete, pp 339–388
37. Maher KT, Voo YL (2016) Taking ultra-high performance concrete to new height—the Malaysian experience. Aspire Concr Bridge Magaz, Summer 2016:36–38
38. Hassan AMT, Jones SW, Mahmud GH (2012) Experimental test methods to determine the uniaxial tensile and compressive behaviour of ultra high performance fibre reinforced concrete (UHPFRC). Constr Build Mater 47:8434–8882

39. Rossi P (2013) Influence of fibre geometry and matrix maturity on the mechanical performance of ultra-high-performance cement-based composites. Cem Concr Compos 47:246–248
40. Bache HH (1981) Densified cement ultrafine particle-base materials. In: 2nd International conference on superplasticizers in concrete, pp 185–443
41. Larrard F, Sedran T (1994) Optimization of ultra-high performance concrete by the use of a packing model. Cem Concr Res 24:9943–1009
42. Larrard FD, Sedran T (2002) Mixture-proportioning of high-performance concrete. Cem Concr Res 32(11):1699–1704
43. Yu R, Spiesz P, Brouwers HJH (2014) Mix design and properties assessment of ultra-high performance fibre reinforced concrete (UHPFRC). Cem Concr Res 54:29–39
44. Yu R, Spiesz P, Brouwers HJH (2015) Development of an eco-friendly ultra-high performance concrete (UHPC) with efficient cement and mineral admixtures uses. Cem Concr Compos 55:383–394
45. Geisenhanslüke C, Schmidt M (2004) Methods for modelling and calculation of high density packing for cement and fillers in UHPC. In: Proceedings of the international symposium on ultra-high performance concrete
46. Hajar Z, Novarin M, Servant C, Genereux G, Przybyla D, Bitar D (2013) Innovative solution for strengthening orthotropic decks using UHPFRC: the illzach Bridge. In: Proceedings of international symposium on ultra-high performance fiber-reinforced concrete, pp 117–126
47. Wille K, Naaman AE, El-Tawil S et al (2012) Ultra-high performance concrete and fiber reinforced concrete: achieving strength and ductility without heat curing. Mater Struct 45:309–324
48. Wille Kay, Montesinos P, Gustavo J (2012) Effect of beam size, casting method, and support conditions on flexural behavior of ultra high-performance fiber-reinforced concrete. ACI Mater J Farmington Hills 109(3): 379–388
49. Cho C, Kim Y, Feo L, Hui D (2012) Cyclic responses of reinforced concrete composite columns strengthened in the plastic hinge region by HPFRC mortar. Compos Struct 94 (7):2246–2253
50. Kim BS, Kim S, Kim YJ, Park SY, Koh KT, Joh C (2012) R&D activities and application of ultra high performance concrete to cable stayed bridges
51. Moreillon L, Menetrey P (2013) Rehabilitation and strengthening of existing RC structures with UHPFRC: various applications. In: Proceedings of international symposium on ultra-high performance fiber-reinforced concrete, pp 127–136
52. Wille K, Naaman A, Montesinos G (2011) Ultra-high performance concrete with compressive strength exceeding 150 MPa (42 ksi): a simpler way. ACI Mater J 108(1):46–54
53. Tayeh BA, Bakar BHA, Johari MAM, Voo YL (2013) Utilization of ultra-high performance fibre concrete (UHPFC) for rehabilitation—a review. In: 2nd International conference on rehabilitation and maintenance in civil engineering, pp 525–538
54. Ma J, Schneider H (2002) Properties of ultra-high-performance concrete. Leipzig Annu Civil Eng Rep (LACER) 25–32
55. Resplendino J, Toutlemonde F, France M (2013) The UHPFRC revolution in structural design and construction. In: Proceedings of international symposium on ultra-high performance fiber-reinforced concrete, pp 791–804
56. The Federal Highway Administration (FHWA) (2013) Ultra-High performance concrete: a state-of-the-art report for the Bridge Community Publication No. FHWA-HRT-13-055, McLean, VA, pp 2201–2296
57. Mullick AK (2014) Durability advantage of concrete with ternary cement blends and applications in India. In: Proceedings of 2nd international conference on 'advances in chemically—activated materials' (CAM 2014), Changsha, China, RILEM Proceedings PRO 92, pp 320–335
58. Proceedings of the 1st international symposium of Asian concrete federation on ultra high performance concrete, (ACF 2015), October 2015, Kolkata, Indian Concrete Institute, p 107

59. Cavill B, Chirgwin G (2004) The world's first RPC road bridge spepherds gually creek bridge, NSW. In: Cavill B, Chirgwin G (eds) Proceedings of 5th austroads bridge conference
60. Spasojevic A (2008) Implications of ultra-high performance fiber-reinforced concrete in bridge design, PhD Thesis Lausanne, Switzerland
61. Shi C, Wu Z, Xiao J, Wang D, Huang Z, Fang Z (2015) A review on ultra-high performance concrete: part I. Raw materials and mixture design. Constr Build Mater 4341–4351
62. Vernet CP (2004) Ultra durable concrete: structure at the micro and nanoscale, MRS Bulletin Retrived from
63. Weina M (2017) Design and performance of cost-effective ultra-high performance concrete for prefabricated elements. Doctoral Dissertations, p 2582
64. Tayeh BA, Bakar BHA, Johari MAM, Voo YL (2012) Mechanical and permeability properties of the interface between normal concrete substrate and ultra-high performance fiber concrete overlay. Constr Build Mater 36:538–548
65. SAMARIS Management Group, Full Scale Application of UHPFRC for the Rehabilitation
66. Yang SL, Millard SG, Soutsos MN, Barnett SJ, Le TT (2009) Influence of aggregate and curing regime on the mechanical properties of ultra-high performance fibre reinforced concrete (UHPFRC). Constr Build Mater 48(6):4291–4298
67. Liu RG, Han FH, Yan PY (2013) Characteristics of two types of CSH gel in hardened complex binder pastes blended with slag. Sci China Technol Sci 54(797–805):1395–1402
68. Racky P (2004) Cost effectiveness and sustainability of UHPC. In: Proceedings of the international symposium on ultra-high performance concrete
69. Stengel T, Schießl P (2008) Sustainable concrete with UHPC—from life cycle inventory data collection to environmental impact assessment. In: Proceedings of the 2nd international symposium on ultra-high performance concrete, pp 454–468
70. Shah S, Weiss W (1998) Ultra high strength concrete: looking toward the future. ACI Special Proceedings

The Potential Use of Waste Paper Sludge for Sustainable Production of Concrete—A Review

Rajwinder Singh, Mahesh Patel, and Karanvir Singh Sohal

Abstract Every year, each developing and non-developing country is facing problems in managing the generated enormous amount of solid wastes. Waste paper sludge (WPS) is also one of the wastes which are produced during the manufacturing of paper. This waste led to cause the major health, environmental and economic issues for the society as it possesses heavy metals and high disposal costs. Thus, in order to provide an appropriate solution to the problems, various researchers have made attempts to use this waste by converting it into a useful form in the construction applications. Studies have found that WPS can be used as alternative building material when added to the mix up to a certain limit. This paper reviews the effect of the incorporation of WPS on the durability and mechanical properties of concrete. The physical and chemical properties of WPS are also enlisted with appropriate discussion.

Keywords Waste paper sludge · Sustainable concrete · Waste management · Safe disposal

1 Introduction

Worldwide, numerous types of solid wastes materials are generated every day through industrial, agricultural and domestic activities. The amount of solid wastes produced in the year 2002 was around 12 billion tons, and it is estimated that this quantity could grow up to 19 billion tons by the year 2025 [1, 2]. The higher production rate, improper handling and disposal of wastes have led to cause a major hazard to human health and the environment [3]. The researchers of various fields are working on the utilization of generated solid wastes as a sustainable material for

R. Singh (✉) · M. Patel
Dr BR Ambedkar National Institute of Technology, Jalandhar, Punjab, India
e-mail: patelm@nitj.ac.in

K. S. Sohal
Guru Nanak Dev Engineering College, Ludhiana, Punjab, India

B. Laishram and A. Tawalare (eds.), *Recent Advancements in Civil Engineering*, Lecture Notes in Civil Engineering 172,
https://doi.org/10.1007/978-981-16-4396-5_33

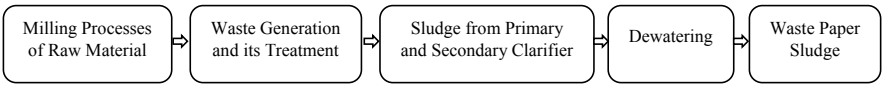

Flowchart. 1 Different steps involved in the production of waste paper sludge

other possible applications through the recycling and reusing techniques. Over the years, different types of industrial and agricultural wastes have been utilized in construction activities as pozzolan or cementitious by-products for the formation of blended cement-based mixes. The inclusion of industrial wastes such as fly ash [4], silica fume [5] and copper slag [6], whereas agricultural wastes such as sugarcane bagasse ash [7], rice husk [8] and sawdust ash [9] as a supplementary cementitious material have resulted in causing a significant impact on the properties of concrete when added up to a certain limit. The waste paper sludge is a by-product of the paper and pulp industry, which is formed during the dewatering process of the waste sludge. The WPS consists of high content of organic matter along with some part of inorganic compounds like $CaCO_3$ and clays. These inorganic compounds usually originate during the de-inking and whitening processes [10]. Approximately, 204 million tons of paper is manufactured each year in the paper and pulp industry. It has been reported that in the year 2005, Europe has generated 99.3 million tons of paper out of which 11 million tons of by-products was generated [11]. Each unit of the manufactured paper produces around 24% of paper sludge waste, i.e. ¼ of the total production of paper is WPS [12], whereas the total of 69% of produced WPS is directly disposed of in the landfills [13]. The amount and characteristics of the WPS depend upon the raw material and the processes used for the manufacture of paper [10]. The calcination of the WPS at a controlled environment can lead to the alteration of the properties of the sludge. It has been reported that if the temperature ranges from 700 to 750 °C, the clayey compound present in the WPS, i.e. kaolinite, will be altered into a highly active metakaolinite [14], which suggests that it will act as a pozzolan [15]. Besides, the utilization of WPS in the above-mentioned applications, the use of WPS by converting it into ash in the blended cement has also been checked by researchers [16, 17]. The various processes involved in the generation of waste paper sludge are illustrated in Flowchart 1:

This paper reviews the information of the previous studies conducted on the feasibility of the incorporation of waste paper sludge by converting it into ash as a substitution material for the cement for the sustainable formation of cement-based mortar and concrete matrix.

2 Physical Properties of WPSA

The physical properties of the waste paper sludge used in the previous studies were observed in detail. The WPSA is generally generated during the calcination process of the waste paper sludge generated from paper and pulp industries. Before

incineration of the waste paper sludge, it consists of small fibres, organic and inorganic compounds, and possesses rough texture. The properties such as specific gravity, bulk density, water absorption and fineness modulus were commonly examined in the previous literature. The specific gravity of the WPSA has been reported to be around 2.40–2.99 [17, 18], whereas bulk density ranges between 1295 and 1435 kg/m^3 [18]. Its pH ranges from 7 to 12 which can vary according to its particle packaging density and composition. [19]. The water absorption capacity of the ash has been found to be around 25% [20]. The fineness modulus of the obtained ash has been found to be 3.82 [21].

3 Environmental Significance

The hazardous impacts caused by the waste paper sludge have led to act as a hazard to the environment and human health. The land which is subjected to the direct disposal of waste paper sludge has caused to increase in the pH and the organic content in the soil [22]. When the effluent generated during the processing of the paper, discharged into the marine streams, it causes an adverse effect on the liver of the fishes, ultimately affecting the population and reproduction process in the fishes [23].

4 Chemical Composition

The chemical compositions of WPSA used by the various researchers in the previous studies are given in Table 1.

Table 1 suggests that WPSA consists of a major share of CaO and SiO_2, which are the two main ingredients of cement. The presence of these compounds indicates that the utilization of WPSA may cause a certain change in the performance of the blended cement matrix.

5 Results and Discussions

5.1 Influence of WPSA on the Properties of Blended Cement Paste and Concrete

5.1.1 Consistency

The normal consistency of the cement paste lies in between 26% and 33% [16], whereas it has been noticed that the cement pastes containing the different dosages of the WPSA exhibited the normal consistency which has reported to be much

Table 1 Elemental composition of WPSA used in the available literature

References	SiO_2	Al_2O_3	Fe_2O_3	TiO_2	MgO	CaO	Na_2O	K_2O	P_2O_5	L.O.I
[24]	13.9	8.3	0.5	0.25	1.6	47.1	0.23	0.3	0.2	26.7
[25]	29.7 + - 0.2	12.9 + -0.2	10.1 + -0.1		2.73 + -0.08	22.7 + -0.2		1.83 + -0.06	12.4 + -0.2	
[26]	18.01	10.14	0.55	0.26	2.58	19.82	0.25	0.21	0.1	47.62
[27]	20.46	12.1	0.82	0.32	3.38	54.2	0.21	0.42	0.28	
[28]	29.2	2.65	1.74	< 0	0.86	50.88	0.30	< 0.01	0.67	12.52
[29]	25.7	18.88	0.87	0.68	5.15	43.51	1.58	1.31	0.52	
[30]	0.7	1	0.1		0.8	95.1				50
[31]	7.96	6.08	0.17	0.15	0.62	32.3		0.05		52.6

higher than the reference paste [28], that signifies that the WPSA particles absorb more amount of water which lead to providing the stiffer structure to the paste at the normal addition of water.

5.1.2 Initial and Final Setting Times

When the waste paper sludge has been used to substitute the cement content, the variation in the setting times of the blended cement has been observed. It has been noticed that less time has been taken by the blended cement paste to show the initial setting as compared to the control cement mix [32, 33], the reason behind could be linked with the excessive lime content present in the sludge, which helps the cement to set quickly [34].

5.1.3 Workability

In previous studies, when the WPSA has been used as an alternative material for substitution of the content of cement, the variation in the slump values has been observed as the content of ash is increased [16, 27]. It has been noticed that there is a strong connection between the amount of waste paper sludge and slump which shows that as the quantity of WPSA increases, the cement and concrete mix becomes even stiffer [35]. It has been found that when the content of waste sludge ash in the cement matrix was increased, a significant reduction in the slump was noticed [21, 28]. The large volume of superplasticizer is needed for the higher replacement of WPSA in the mix to make the concrete extra workable. The presence of major content of CaO causes the fast setting and early hydration, and it has been suggested that it is better to mix the superplasticizer with water beforehand its direct addition to the concrete during mixing [36]. The addition of 5% WPSA has caused an improvement in the workability of blended cement mixes [16]. The addition of another mineral admixture with WPSA has also caused some improvement in the workability, but still, the manufactured concrete was not reported in the pumpable form [37]. The reason behind this could be due to the higher absorption of water by the particles of WPSA than the cement particles, proportion and physical properties of WPS and carbon content, which causes a drop in the workability of the blended cement mix. Another reason may be attributed to the low density of WPSA, which increases the porosity and causes higher water demand [16, 38].

5.1.4 Compressive Strength

The compressive strength of the concrete samples manufactured by the addition of WPSA showed that the maximum strength of concrete has been observed at 5% substitution of cement with WPSA after 28 days of water curing, whereas further

increment in the content of the WPSA in concrete has caused the noticeable reduction in the strength. [28, 39]. The decrease in the strength has been caused by the decrease in the suitable quantity of cement required in the hydration process and the more amount of water used to mix the ingredients properly [40]. Similarly, in case of mortar, the maximum compressive strength has been achieved at 5% addition of WPSA to the cement at 28 days of curing, whereas the noticeable decrease in the strength has been observed as the higher content of WPSA has been introduced to the cement [20, 41], which is because of the lower pozzolanic activity of the WPSA which affects the compressive strength of the manufactured mortar [42]. Some of the studies have suggested that the trend of increase in the compressive strength has been noticed by up to 10 per cent replacement of the cement with WPSA [43, 44]. A few researchers have suggested that a significant drop in the compressive strength has been observed at 10 percentage addition of WPSA [45, 46]

5.1.5 Split Tensile Strength

The split tensile strength of the mixes manufactured with the addition of WPSA showed an improvement in the performance of manufactured concrete [16]. The results of the earlier conducted studies describe that when the addition of the WPSA was ensured up to 5%, the notable increase in the split tensile strength has been observed when compared to the reference concrete mix when tested after 28 days. Beyond 5% addition, the reduction in the split tensile has been observed which may be caused by the increase in the water–cement ratio and weak bonding between the blended cement paste and concrete ingredients [39]. It has also been reported in the previous literature that the mineral admixtures possess a tendency to improve the transition zone of the microstructure of the mix [47].

5.1.6 Flexural Strength

The flexural values of the mortar and the concrete samples consisting of the varying dosages of the WPSA have been studied in the previously conducted studies. The positive influence of the integration of the WPSA on the performance of the concrete has been observed [43]. It has been seen that after 28 days at the replacement percentage of 5% of the cement with WPSA give rise to the maximum increase in the flexural strength of the concrete mix in comparison with the reference mix or mix containing other replacement percentages [41]. Another study on the formation of the geopolymer cement blended with the WPSA along with the blast furnace slag (BFS) revealed that the incorporation of the WPSA can influence the flexural strength when tested after 50 days of curing. This could be due to the used activator (NaOH) which successfully led to an increase in the pH of the mix and cause the discharge of Ca compound gets which ultimately gives rise to the dissolution of the silicate part of the BFS for the formation of the C–A–S–H product. As the duration

Table 2 Summarized effect of the addition of waste paper sludge ash in the concrete

Fresh and hardened properties	Influence on the blended cement and concrete paste	
	Positive	Negative
Consistency		•
Setting times	•	
Workability		•
Compressive strength	•	
Split tensile strength	•	
Flexural strength	•	
Water absorption		•

of the curing period has been extended, the C–A–S–H originates to impart the increase in the strength of the mix [30].

5.1.7 Water Absorption

The amount of water absorption of the specimens provides an indirect measure of the durability of the mix. The lesser the water absorption, the better will be the performance of the concrete in the aggressive environments. It has been observed that when the amount of introduction of WPSA increased, the concrete showed high absorption of water [17, 39]. A similar pattern has been observed, when recycled aggregates along with waste paper sludge have been used for the production of concrete [48, 49]. The reason behind the more water absorption values in case of recycled aggregates and WPSA may be due to the adhered cement paste on the aggregates, the cracks on its surface and the low SiO_2 of WPSA, which reduces the amount of the pozzolanic reaction as compared to the other mineral admixtures [50]. A study suggested that the minimum reduction in the water absorption of the mix has been observed at 5% of the substitution of cement with WPSA [17].

The overall effect of the usage of waste paper sludge ash as a replacement material of cement on the properties of blended cement and concrete paste is illustrated in Table 2.

6 Economic Feasibility

The cost analysis done by the researchers has suggested that the usage of the WPSA as a substitution material for the cement has caused in the production of the low-cost concrete which may further be helpful to reduce the overall expenditure of the constructional activity [21, 51].

7 Conclusions

This review research paper has made an effort to collect all appropriate data on the use of the WPSA in cement for the sustainable manufacturing of blended cement paste and concrete. The physical and chemical properties of WPSA used in earlier studies by the researchers have also been examined thoroughly. Based on the reviewed available data, the following conclusions have been drawn:

- The usage of waste paper sludge ash in the concrete mix has represented the better results when the replacement up to 5% of cement is done; beyond that limit, a noteworthy decrease in the mechanical and durability properties has been observed.
- The idea of integration of WPSA for the production of geopolymer and recycled aggregate concrete has led to show better performance in comparison with the only use of waste paper sludge ash for concrete production.
- As the incorporation of WPSA has reduced the cost of concrete production, a huge amount of money can be saved during the purposes of temporary or low-load bearing constructions.
- The utilization of WPSA in the cement-based materials can ensure to reduce the problems associated with its disposal and safe stabilization.

Readers are suggested to explore the scope of utilization of WPSA along with a varying dosage of different mineral and chemical admixtures to check their effect on the mechanical and durability properties of concrete for longer curing periods. The feasibility of the integration of WPSA with self-healing microbes can also be evaluated.

References

1. Moura WA, Gonçalves JP, Lima MBL (2007) Copper slag waste as a supplementary cementing material to concrete. J Mater Sci 42(7):2226–2230
2. Naidu T, Govinda Rajulu B, Ramlal S (2017) A study on the properties of concrete on partial replacement of cement and sand with copper slag. Int J Recent Trends Eng Res 3(12):40–50
3. Patil MV (2015) A study on properties and effects of copper slag in concrete. In: Proceedings of 18th IRF international conference, pp 24–29. ISBN: 978-93-84209-82-7
4. Thomas MDA, Shehata MH, Shashiprakash SG (1999) The use of fly ash in concrete: classification by composition. Cement, Concr Aggregates 21(2):105–110
5. Siddique R (2011) Utilization of silica fume in concrete: review of hardened properties. Resour Conserv Recycl 55(11):923–932
6. Shi C, Meyer C, Behnood A (2008) Utilization of copper slag in cement and concrete. Resour Conserv Recycl 52(10):1115–1120
7. Cordeiro GC, Toledo Filho RD, Tavares LM, Fairbairn EMR (2008) Pozzolanic activity and filler effect of sugar cane bagasse ash in Portland cement and lime mortars. Cement Concr Compos 30:410–418
8. Al-Khalaf MN, Yousif HA (1984) Use of rice husk ash in concrete. Int J Cem Compos Lightweight Concr 6(4):241–248

9. Obilade IO (2014) Use of saw dust ash as partial replacement for cement in concrete. Int J Eng Sci Invention 3(8):36–40
10. Likon M, Trebše P (2012) Recent advances in paper mill sludge management. Industrial waste, pp 73–90
11. Monte MC, Fuente E, Blanco A, Negro C (2009) Waste management from pulp and paper production in the European Union. Waste Manage 29:293–308
12. Miner R (1991) Environmental considerations and information needs associated with an increased reliance on recycled fiber. In: Focus 95+ proceedings, TAPPI PRESS, Atlatnta, pp 343–362. Mill waste materials. Journal of analytical and applied pyrolysis, vol 86, pp 66–73
13. Progress in Paper Recycling Staff (1993) Utilisation of mill residue (Sludge). Mill Survey: Progress in Paper Recycling 3(1):64–70
14. Pera J, Amrouz A (1988) Development of highly reactive metakaolin from paper sludge. Adv Cem Based Mater 7:49–56
15. Frías M, García R, Vigil R, Ferreiro S (2008) Calcination of art paper sludge waste for the use as a supplementary cementing material. Appl Clay Sci 42(1–2):189–193. https://doi.org/10.1016/j.clay.2008.01.013
16. Sumit AB, Raut SP (2013) Utilization of waste paper pulp by partial replacement of cement in concrete. Int J Eng Res Appl (IJERA) 1:300–309
17. Ahmad S, Malik MI, Wani MB, Ahmad R (2013) Study of concrete involving use of waste paper sludge ash as partial replacement of cement. IOSR J Eng (IOSRJEN) 3(11):6–15
18. Tay JH (1987) Sludge ash as filler for Portland cement concrete. J Environ Eng 113(2): 345–351
19. Mochizuki Y, Yoshino H, Saito E, Ogata T (2003) Effects of soil improvement due to mixing with paper sludge ash. Fujita Tech Res Rep 39:99–109
20. Fava G, Ruello ML, Corinaldesi V (2011) Paper mill sludge ash as supplementary cementitious material. J Mater Civ Eng 23(6):772–776
21. Alam M, Berera V (2015) An experimental study on use of hypo sludge in cement concrete. Int J Progr In Civil Eng 2(1):1–23
22. Honeycutt CW, Clapham WM, Zibilske LM (1988) Heat units for describing carbon mineralization and predicting net nitrogen mineralization. Soil Sci Soc Am J 52(5):1346–1350
23. Oikari AOJ, Nakari T (1982) Kraft pulp mill effluent components cause liver dysfunction in trout. Bull Environ Contam Toxicol 28(3):266–270
24. Goñi S, Frías M, de la Villa RV, Vegas I (2013) Decalcification of activated paper sludge–fly ash-Portland cement blended pastes in pure water. Cement Concr Compos 40:1–6. https://doi.org/10.1016/j.cemconcomp.2013.04.002
25. Yagüe A, Valls S, Vázquez E, Albareda F (2005) Durability of concrete with addition of dry sludge from waste water treatment plants. Cem Concr Res 35(6):1064–1073. https://doi.org/10.1016/j.cemconres.2004.07.043
26. García R, Vigil de la Villa R, Vegas I, Frías M, Sánchez de Rojas MI (2008) The pozzolanic properties of paper sludge waste. Constr Build Mater 22(7):1484–90. https://doi.org/10.1016/j.conbuildmat.2007.03.033
27. Ferrándiz-Mas V, Bond T, García-Alcocel E, Cheeseman CR (2014) Lightweight mortars containing expanded polystyrene and paper sludge ash. Constr Build Mater 61:285–292. https://doi.org/10.1016/j.conbuildmat.2014.03.028
28. Kejela BM (2020) Waste paper ash as partial replacement of cement in concrete. Am J Constr Build Mater 4(1):8–13
29. Mavroulidou M, Boulouki G, Unsworth C (2013) Incorporating waste paper sludge ash as partial cement replacement in concrete. In: Proceeding of the 13th international conference of environment science and technology, pp 5–7
30. Adesanya E, Ohenoja K, Luukkonen T, Kinnunen P, Illikainen M (2018) One-part geopolymer cement from slag and pretreated paper sludge. J Clean Prod 185:168–175. https://doi.org/10.1016/j.jclepro.2018.03.007

31. Santa RAAB, Bernardin AM, Riella HG, Kuhnen NC (2013) Geopolymer synthetized from bottom coal ash and calcined paper sludge. J Clean Prod 57:302–307. https://doi.org/10.1016/j.jclepro.2013.05.017
32. Vegas I, Frías M, Urreta J. San José JT (2006) Obtaining a pozzolanic addition from the controlled calcination of paper mill sludge. Performance in cement matrices. Materiales de Construccion 56(283):49–60
33. Frías M, Vegas I, de la Villa RV, Giménez RG (2011) Recycling of waste paper sludge in cements: characterization and behavior of new eco-efficient matrices. Integr Waste Manage 2:11301
34. Dunster AM (2007) Paper sludge and paper sludge ash in Portland cement manufacture. BREWRT 177/WR0115
35. Wong HS, Barakat R, Alhilali A, Saleh M, Cheeseman CR (2015) Hydrophobic concrete using waste paper sludge ash. Cem Concr Res 70:9–20. https://doi.org/10.1016/j.cemconres.2015.01.005
36. Gailius A, Laurikietytė Ž (2003) Waste paper sludge ash and ground granulated blast furnace slag as binder in concrete. J Civ Eng Manag 9(3):198–202
37. Neville AM (1995) Properties of concrete, 4th edn. Longman, Harlow
38. Banfill P, Frias M (2007) Rheology and conduction calorimetry of cement modified with calcined paper sludge. Cem Concr Res 37(2):184–190
39. Ahmadi B, Al-Khaja W (2001) Utilization of paper waste sludge in the building construction industry. Resour Conserv Recycl 32(2):105–113
40. Shabbir F, Ejaz N, Khan D, Ahmad N, Hussain J, Tahir MF (2015) Investigation of using paper industry waste (hypo sludge) in concrete mix. J Eng Appl Sci 34(2):7–12
41. Mozaffari E, O'Farrell M, Kinuthia JM, Wild S (2006) Improving strength development of wastepaper sludge ash by wet-milling. Cem Concr Compos 28(2):144–152
42. Bin Mohd Sani MSH, bt Muftah F, Ab Rahman M (2011) Properties of waste paper sludge ash (WPSA) as cement replacement in mortar to support green technology material. In: 2011 3rd International symposium and exhibition in sustainable energy and environment (ISESEE), pp 94–99. IEEE
43. Kadu A, Gajghate VK (2016) Optimization of hypo sludge ash in design mix concrete: a review. Int J Sci Technol Eng (IJSTE) 2(7):133–135
44. Abishek GL (2017) Experimental study on behaviour of paper sludge concrete. IIOAB J 8 (3):73–78
45. Maheswaran S, Ramesh Kumar V, Bhuvaneshwari B, Palani GS, Iyer NR (2011) Studies on lime sludge for partial replacement of cement. In: Applied mechanics and materials, vol 71, pp 1015–1019. Trans Tech Publications Ltd
46. Pitroda J, Zala LB, Umrigar FS (2013) Innovative use of paper industry waste (hypo sludge) in design mix concrete. Int J Adv Eng Technol 4(1):31–35
47. Chindaprasirt P, Jaturapitakkul C, Rattanasak U, Chalee W (2009) Comparative study on the characteristics of fly ash and bottom ash geopolymers. Waste Manage 29:539e543
48. Bui NK, Satomi T, Takahashi H (2019) Influence of industrial by-products and waste paper sludge ash on properties of recycled aggregate concrete. J Clean Prod 214:403–418. https://doi.org/10.1016/j.jclepro.2018.12.325
49. Fauzi MA, Sulaiman H, Ridzuan ARM, Azmi AN (2016) The effect of recycled aggregate concrete incorporating waste paper sludge ash as partial replacement of cement. In: AIP conference proceedings, vol 1774, No 1, p 030007. AIP Publishing LLC
50. Mozaffari E, Kinuthia JM, Bai J, Wild S (2009) An investigation into the strength development of wastepaper sludge ash blended with ground granulated blastfurnace slag. Cem Concr Res 39(10):942–949. https://doi.org/10.1016/j.cemconres.2009.07.001
51. Srinivasan R, Sathiya K, Palanisamy M (2010) Experimental investigation in developing low cost concrete from paper industry waste. The bulletin of the polytechnic institute of jassy, construction. architecture section (Romania), pp 43–56

Monitoring Heavy Metals Concentrations in a Natural Wetland and Aquatic Plant *Eichhornia Crassipes* for Assessment of Its Biomonitoring Potential

Siddhant Dash and Ajay S. Kalamdhad

Abstract In the present study, seven heavy metals, i.e., Cr, Cd, Fe, Mn, Cu, Pb and Mg were used for estimation of heavy metal pollution and the bioconcentration and translocation factors corresponding to the plant *Eichhornia crassipes* in Deepor Beel, Assam, India. Sediment and water hyacinth (*Eichhornia crassipes*) samples were collected from three different zones of the wetland; zone I is proximate to the Boragaon landfill region, zone II is the central portion of the wetland and zone III constitutes the site in the industrial zone. It was observed that the heavy metal concentrations in the sediment column of the wetland are significantly higher compared to the water hyacinths. Furthermore, in the water hyacinth samples collected from the three zones, it was observed that the heavy metal concentrations were significantly higher in the roots as compared to the shoots. This indicated an insignificant translocation of heavy metals from the roots to the shoots, as a result of which, all the heavy metals are concentrated in the roots. This was verified by the translocation factor, whose values were found to be minimal and inconsequential. Also, the bioconcentration factor of the water hyacinth samples was estimated and found to be higher in the central and industrial region, which suggests that the metal availability was very low in the landfill region, despite having considerably higher concentrations of heavy metals in the sediments. The findings of the study would prove to be consequential in determining the adverse effects of eutrophication and heavy metal contamination in the wetland, which would thereby aid in undertaking necessary steps in curbing the pollution levels.

Keywords Heavy metal pollution · Sediment contamination · Bioconcentration factor · Translocation factor · *Eichhornia crassipes*

S. Dash (✉) · A. S. Kalamdhad
Department of Civil Engineering, Indian Institute of Technology Guwahati, Guwahati, Assam 781039, India

B. Laishram and A. Tawalare (eds.), *Recent Advancements in Civil Engineering*, Lecture Notes in Civil Engineering 172,
https://doi.org/10.1007/978-981-16-4396-5_34

1 Introduction

Trace heavy metals form an essential component of human metabolism in the form of micro-nutrients to perform several biochemical functions within the body [1]. Such essential micro-nutrients include Cr, Co, Cu, Mn, Mo, Fe, Se and Zn. On the contrary, there also exist some non-essential components which play a significant role in imparting high toxicity levels among the living entities of the natural ecosystem. These include trace metals such as As (as a metalloid), Cd, Hg and Pb, which exhibit their toxicity levels through competition with the essential components [2]. Although, the vital components possess positive traits in the living entities, however, when present in amounts exceeding the desired limits, these heavy metals also start exhibiting highly toxic characteristics [3]. The primary reason for toxicity remains in the heavy metals' inability to decompose/degrade with time and their ability to accumulate in the natural ecosystem (in all four spheres of water, sediments, flora and fauna) [4]. Various natural (such as volcanic eruption and weathering of rocks and ores) and anthropogenic (such as urban sprawl, metal industry including processes like mining, extraction and processing and electricity generation) constituents aid in the release of heavy metals to the natural environment [5–10].

Wetlands play an essential role in balancing the natural ecosystem through various functionalities such as flood control, water quality enhancement edaphic characteristics, dominant vegetation and climatic features [11]. However, the pollution of the wetlands due to several anthropogenic factors has led to a steep rise in heavy metal and organic deposition [12]. However, the heavy metals, unlike organic pollutants, cannot be removed through natural processes [13]. Their discharge into the water column of an aquatic ecosystem renders them to deposit in the sediment column through precipitation. Once precipitated and deposited in significant amounts, these heavy metals tend to move up and bioaccumulate in higher trophic levels, thus aiding in the biomagnification process [14, 15]. Plants have a high ability of metal absorption essential for their growth and development [16]. Rooted macrophytes or plants are exposed to heavy metal contamination due to their stagnant nature [17]. They have tremendous potential for heavy metal bioaccumulation due to their root exposure to the sediments and the shoots to the water column, thereby extracting a significant amount of heavy metals through both columns [18, 19]. Thus, necessary monitoring programs should be carried out for heavy metal contamination among the plant samples and the sediment and water columns, thereby establishing a definite relationship. The present study's principal objective was to analyze the levels of Cd, Cr, Cu, Fe, Mn, Ni and Pb in sediments of Deepor Beel and the primary macrophyte growing in the wetland *Eichhornia crassipes*, commonly called water hyacinth and assess its biomonitoring potential.

2 Materials and Methods

2.1 Study Area

Deepor Beel (Fig. 1) is one of the largest freshwater lakes of the Brahmaputra Valley, located in Guwahati [20]. It can be considered the lungs of the bustling city, assimilating a large amount of municipal and industrial wastewater and agricultural runoff daily [21, 22]. The dilution and dispersion of pollutants in the Deepor Beel reduces the pollutants' concentration in the waters whose ultimate fate lies in the mighty Brahmaputra river. The word 'Deepor' is derived from the Sanskrit word 'dipa' which means elephant and 'Beel' is an Assamese word denoting lake. When translated together, the term 'Deepor Beel' means the Lake of Elephants, which sounds apt given the lake's role in maintaining the ecology of the area. However, the lake is not only a habitat for elephants but also a wide variety of other mammals, birds, reptiles, amphibians and birds. Deepor Beel is famous for being the home to several migratory birds such as spot-billed pelican (*Pelicanus philipensis*), lesser and greater adjutant stork (*Leptoptilos javanicus* and *L. dubius*) and baer's pochard (*Aythya baeri*) which visit the lake during the winter season. The floral diversity of the lake is equally immense like the faunal diversity. It was owing to its ecological significance, especially as the habitat of waterfowls, that it was declared a Ramsar site in 2002 [23]. However, in recent decades, the wetland is undergoing substantial deterioration, resulting from various anthropogenic activities, such as encroachment and the setting up of many small-and-large-scale industries in the western part as well as a landfill in the eastern part, which assimilates the entire city's municipal solid wastes. The primary pollutants resulting from these industries and landfill

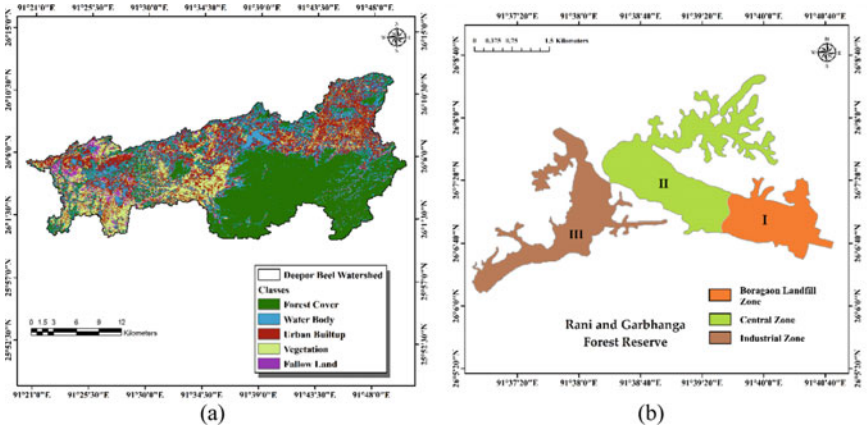

Fig. 1 Study area (Deepor Beel) with **a** LULC map and **b** sampling zones

remains trace heavy metals [24]. It has, therefore, become highly essential for restoration of the wetland to its original state, which is possible through continuous monitoring.

2.2 Sampling and Laboratory Analyzes

Sediment and water hyacinth samples were collected for March 2018 (pre-monsoon season) and June 2018 (monsoon season) from three zones, as depicted in Fig. 1. The environmental conditions were found to be stable during the sampling period. The plant samples collected were first washed with distilled water and then oven-dried until no further weight loss was observed. The plant samples were then cut into two parts, roots and shoots and were ground to finer particles such that they can pass through 75 μ IS sieve. Similarly, the sediment samples were first crushed and passed through 2 mm IS sieve to avoid any debris. The passed particles were then ground and subjected to fine sieving through a 75 μ IS sieve for obtaining the final powdered samples for the digestion process.

The powdered plant and sediment specimens were then digested in an acid solution (H_2O_2/HNO_3, 2:3 ratio). After digestion, they were diluted using Milli-Q water to a sample volume of 25 mL. The samples were finally analyzed for six different heavy metals (Cr, Cd, Fe, Mn, Cu and Pb) in the atomic absorption spectrophotometer (AAS) (Varian-Spectra 55B) in triplicates. Deionized water was used for solutions and analyses unless otherwise specified and all the sampling and analysis procedures adhered to APHA [25].

2.3 Statistical Processing

Post laboratory analyzes, the values were used for determining the bioconcentration and translocation factors for assessing the mobility of each element in the species. Equations 1–2 were used for determining both factors:

$$\text{Bioconcentration Factor (BCF)} = \frac{C_{\text{root}}}{C_{\text{sediment}}} \tag{1}$$

$$\text{Translocation Factor} = \frac{C_{\text{shoot}}}{C_{\text{root}}} \tag{2}$$

where C_{element} signifies the concentrations of heavy metals in that particular element (in this case root, sediment and shoot).

Greater BCF values infer a larger bioaccumulation capability [26]. TF reveals the flux of a given component inside the plants. Higher TF values mean a more excellent translocation capability [27].

3 Results and Discussion

3.1 Heavy Metals in Sediments and Plant Samples

Tables 1 and 2 depict the mean concentrations of heavy metals in both pre-monsoon and monsoon periods for sediments and plants respectively. It can be clearly observed that for both plant and sediment samples, the Boragaon landfill plays a crucial role in heavy metal pollution. It can be primarily attributed to the leaching effect from the landfill. Furthermore, the roots of the plants are observed to have significantly higher concentrations as compared to that of the shoots. This shows that the water hyacinths have poor translocation capacity and hence, the metals are accumulated on the roots. The statistical correlation between the heavy metals accumulated in the shoots and roots of the water hyacinths and the sediment column of the wetland, as well as the three zones from which samples were collected, is represented through Figs. 2, 3 and 4.

3.2 Bioconcentration and Translocation Factors

Tables 3 and 4 indicate the uptake of heavy metals from sediments to plants (BCF) and translocation within plants (TF), respectively. It was observed that the metal uptake from sediments were considerably higher for plants found in the industrial and central region, for most heavy metals, while least BCF was found for

Table 1 Heavy metal concentrations in sediment samples (mg/kg) collected from different zones of Deepor Beel (data expressed as mean value ± standard deviation)

Area (Zone)	Cr	Cd	Fe	Mn	Cu	Pb	Mg
Central	153.253 ± 2.759	39.025 ± 5.565	7713.148 ± 35.113	338.431 ± 7.210	20.385 ± 3.261	156.477 ± 0.728	7519.015 ± 512.830
Boragaon	215.699 ± 13.360	54.489 ± 26.944	8532.086 ± 170.021	409.245 ± 34.913	29.549 ± 15.791	181.362 ± 3.525	9513.126 ± 2483.176
Industrial	172.928 ± 6.099	43.897 ± 12.300	7971.170 ± 77.618	360.742 ± 15.939	23.272 ± 7.209	164.317 ± 1.609	8147.297 ± 1133.624

Table 2 Heavy metal concentrations in roots and shoots of plant samples (mg/kg) collected from different zones of Deepor Beel (data expressed as mean value ± standard deviation)

Area (Zone)	Cr		Cd		Fe		Mn		Cu		Pb		Mg	
	R	S	R	S	R	S	R	S	R	S	R	S	R	S
Central	1.02 ± 0.08	0.08 ± 0.02	0.05975 ± 0.0002	0.0592 ± 0.005	31.45 ± 2.9557	20.12 ± 0.8132	10.85 ± 0.0707	3.34 ± 0.2263	0.685 ± 0.0071	0.665 ± 0.0212	0.1534 ± 0.0120	0.1415 ± 0.0044	30.55 ± 0.5657	28.825 ± 0.9546
Boragaon	2.30 ± 0.08	0.13 ± 0.01	0.0648 ± 0.006	0.06245 ± 0.0001	51.40 ± 0.3290	24.91 ± 1.9021	11.85 ± 0.0707	3.85 ± 0.3536	0.72 ± 0.0141	0.705 ± 0.0212	0.1966 ± 0.0066	0.1818 ± 0.0021	36.91 ± 0.1131	35.94 ± 0.6647
Industrial	1.80 ± 0.08	0.1 ± 0.01	0.0626 ± 0.002	0.0594 ± 0.0017	43.82 ± 1.2938	27.09 ± 1.0270	11.25 ± 0.0707	3.38 ± 0.1061	0.70 ± 0.0141	0.695 ± 0.0071	0.1816 ± 0.0147	0.1469 ± 0.0571	36.62 ± 0.6223	31.01 ± 0.4243

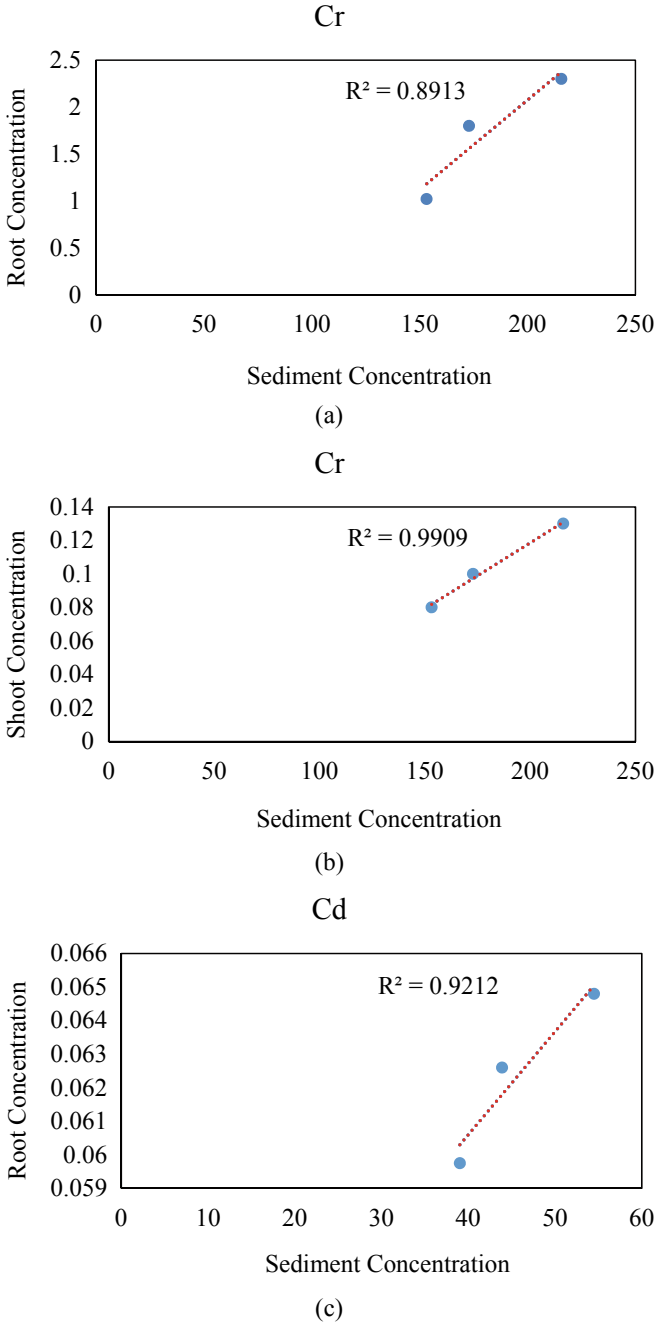

Fig. 2 Correlation between heavy metal concentrations found in sediment samples and shoots and roots of Eichhornia crassipes

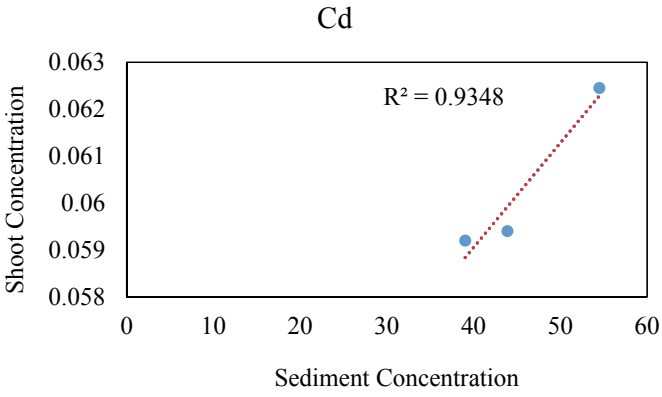

(d)

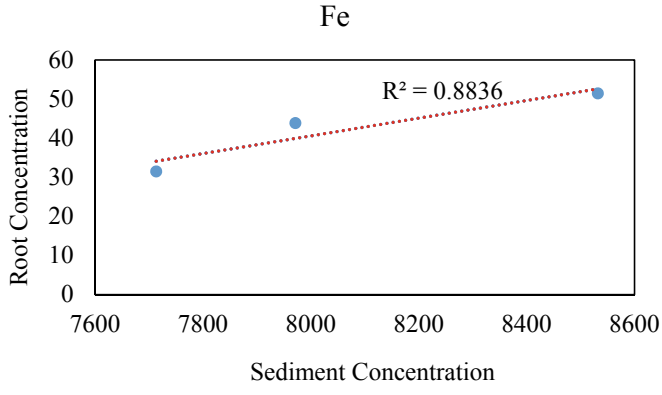

(e)

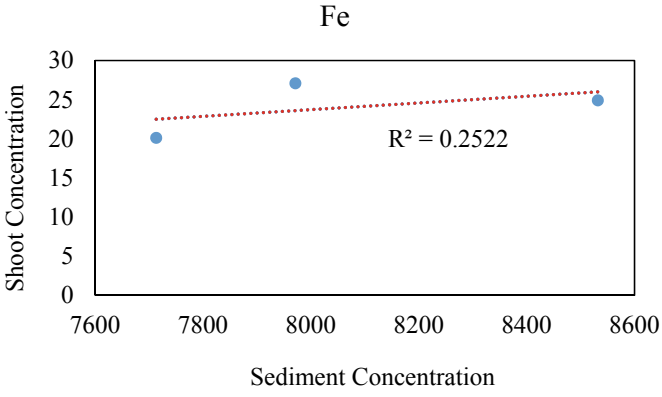

(f)

Fig. 2 (continued)

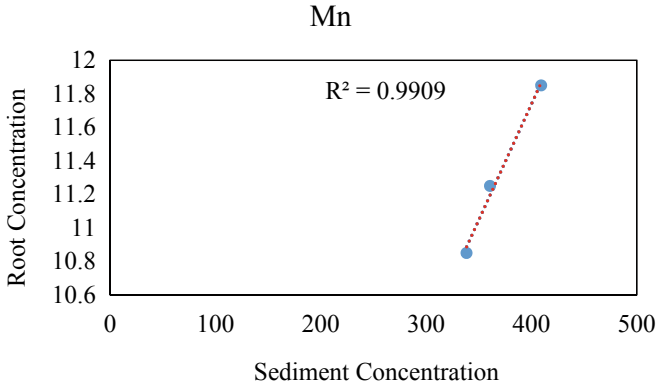

(g)

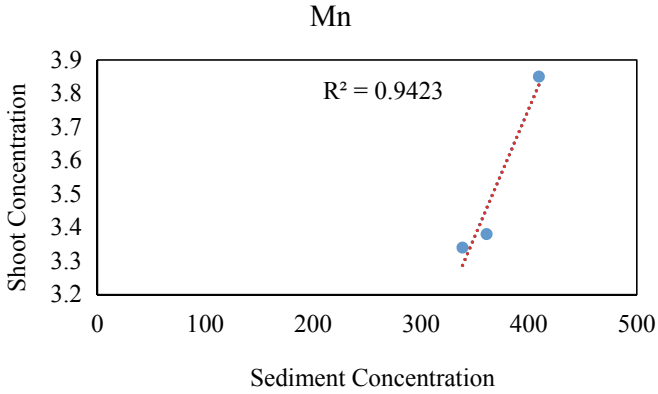

(h)

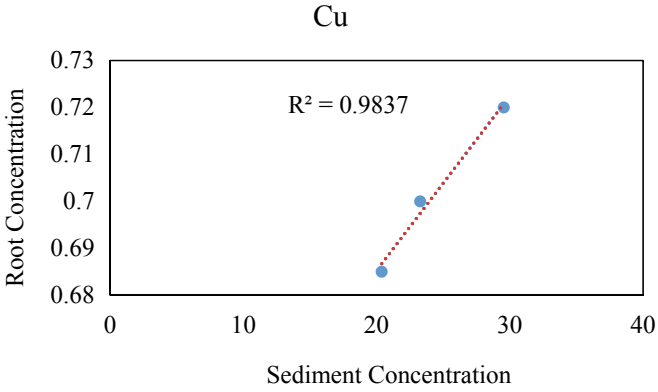

(i)

Fig. 2 (continued)

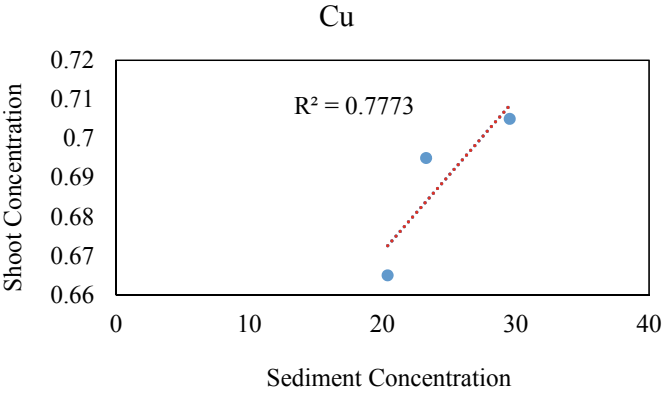

(j)

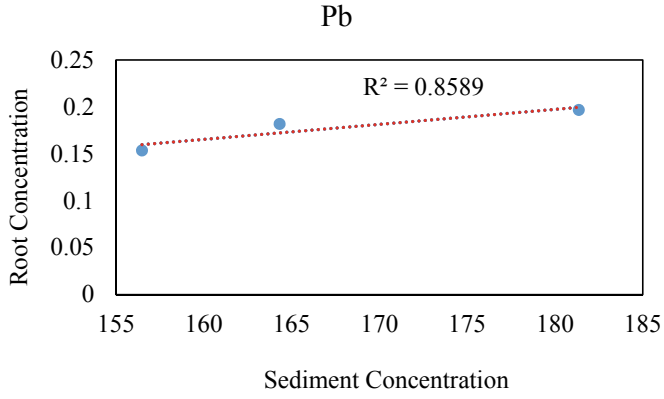

(k)

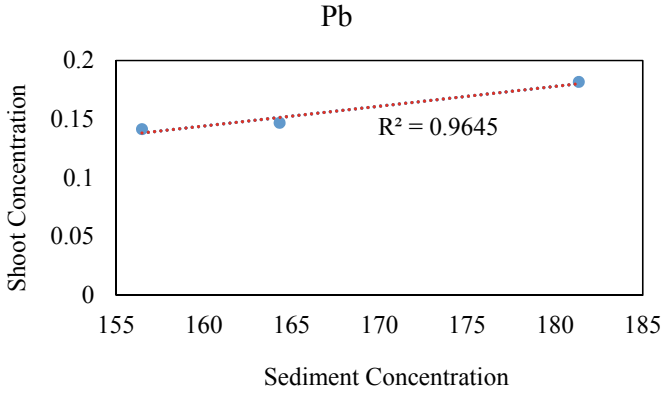

(l)

Fig. 2 (continued)

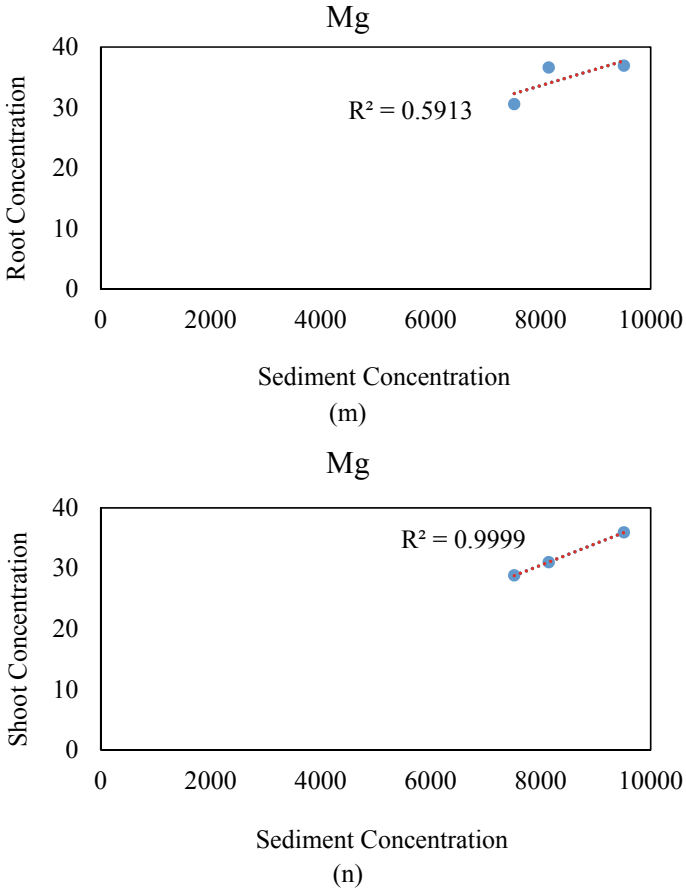

Fig. 2 (continued)

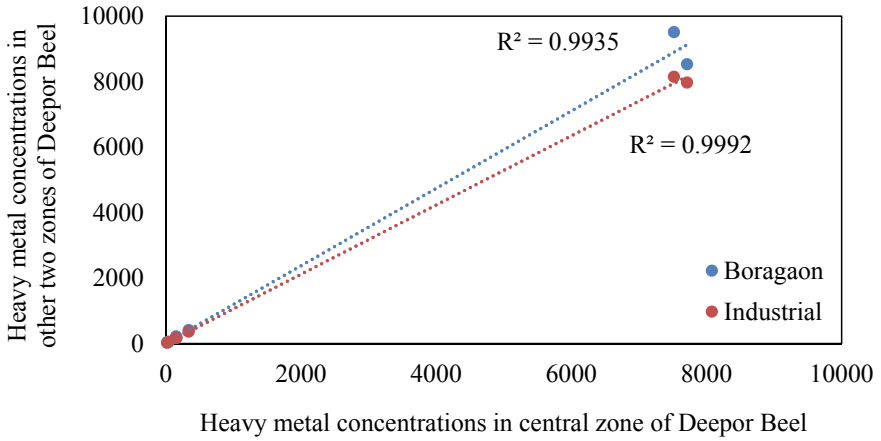

Fig. 3 Correlation between heavy metal concentrations in the sediment column for three different zones of Deepor Beel

samples collected from the Boragaon landfill region of the wetland. This signifies that although the sediment contamination is found to be higher in the landfill region, the metal availability for plants is higher in the industrial as well as the central zone. Furthermore, the transfer of heavy metals from the roots to shoots were observed to be significantly higher for plants in the central zone for Cr, Cd and Fe. On the other hand, Mn, Pb and Mg displayed higher values for plants in the landfill zone. Only Cu showed higher values of TF in the industrial zone. This might be attributed to the presence of smelting industries and brick kilns in the industrial zone, discharging huge amounts of Cu into the wetland, as TF in the plant samples is primarily dependent on metal concentration present in the two zones of the plant, i.e., root and shoot.

4 Conclusion

The present investigation showed the bioindication capacity of water hyacinths in Deepor Beel through their mobility from sediments to roots and from roots to shoots by evaluating the bioconcentration factor (BCF) and translocation factor (TF), respectively. It was observed that the presence of heavy metals in significant quantities does not imply its mobility to the plants, rather, their bioavailability is of primary requirement.

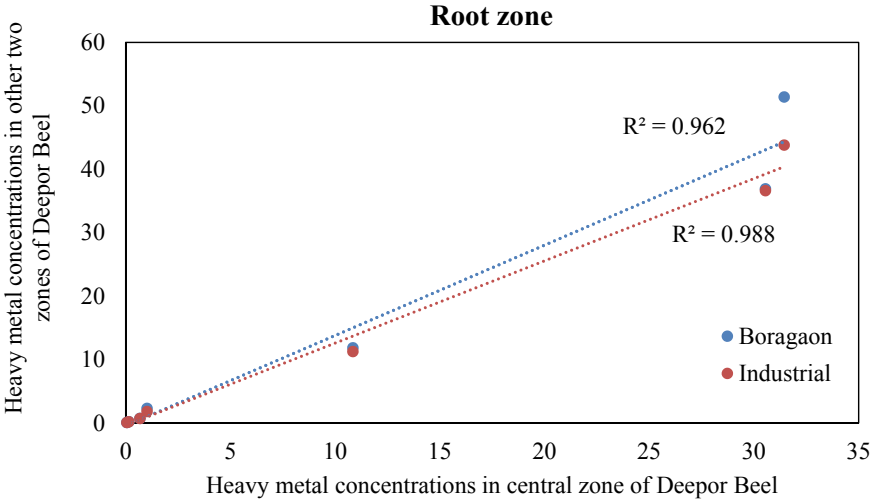

(a)

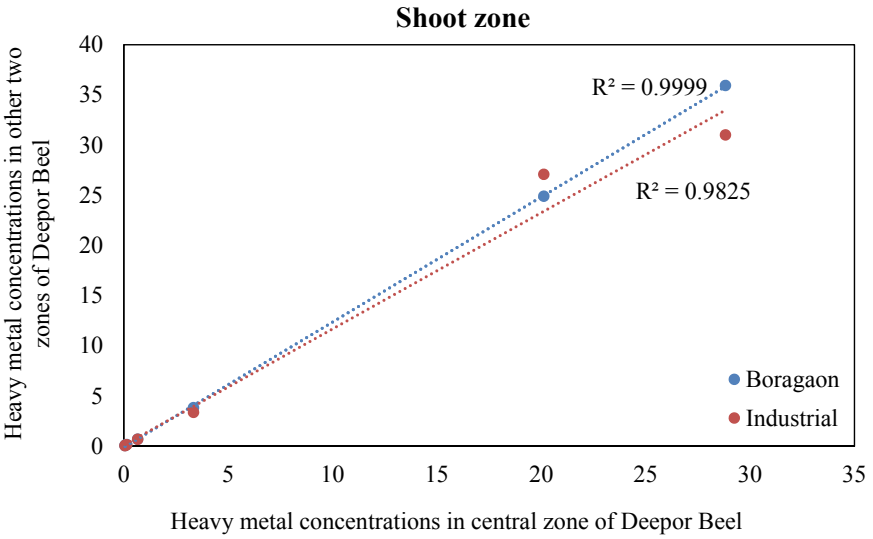

(b)

Fig. 4 Correlation between heavy metal concentrations in *Eichhornia crassipes* for three different zones of Deepor Beel

Table 3 BCF values for *Eichhornia crassipes* in Deepor Beel

Area (Zone)	Cr	Cd	Fe	Mn	Cu	Pb	Mg
Central	0.006656	0.001531	0.004077	0.03206	0.033603	0.00098	0.004063
Boragaon	0.010663	0.001189	0.006024	0.028956	0.024366	0.001084	0.00388
Industrial	0.010409	0.001426	0.005497	0.031186	0.030079	0.001105	0.004495

Table 4 Values of translocation factors of *Eichhornia crassipes* in Deepor Beel

Area (Zone)	Cr	Cd	Fe	Mn	Cu	Pb	Mg
Central	0.073529	0.990795	0.639587	0.307834	0.970803	0.922425	0.943535
Boragaon	0.056522	0.963735	0.484526	0.324895	0.979167	0.924955	0.97372
Industrial	0.055556	0.948882	0.618239	0.3	0.992857	0.808645	0.846805

References

1. Babula P, Adam V, Opatrilova R, Zehnalek J, Havel L, Kizek R (2008) Uncommon heavy metals, metalloids and their plant toxicity: a review. Environ Chem Lett 6:189–213
2. Torres MA, Barros MP, Campos SC, Pinto E, Rajamani S, Sayre RT, Colepicolo P (2008) Biochemical biomarkers in algae and marine pollution: a review. Ecotoxicol Environ Saf 71:1–15
3. Nagajyoti PC, Lee KD, Sreekanth T (2010) Heavy metals, occurrence and toxicity for plants: a review. Environ Chem Lett 8:199–216
4. Tchounwou PB, Yedjou CG, Patlolla AK, Sutton DJ (2012) Heavy metal toxicity and the environment. Molecular, clinical and environmental toxicology, pp 133–164. Springer
5. He ZL, Yang XE, Stoffella PJ (2005) Trace elements in agroecosystems and impacts on the environment. J Trace Elem Med Biol 19:125–140
6. Li J, Lu Y, Yin W, Gan H, Zhang C, Deng X, Lian J (2009) Distribution of heavy metals in agricultural soils near a petrochemical complex in Guangzhou China. Environ Monit Assess 153:365
7. Szyczewski P, Siepak J, Niedzielski P, Sobczyński T (2009) Research on heavy metals in Poland. Pol J Environ Stud 18:755
8. Alloway BJ (2012) Heavy metals in so pp ils: trace metals and metalloids in soils and their bioavailability. Springer Science & Business Media
9. Kabata-Pendias A, Mukherjee AB (2007) Trace elements from soil to human. Springer Science & Business Media
10. Norgate T, Jahanshahi S, Rankin W (2007) Assessing the environmental impact of metal production processes. J Clean Prod 15:838–848
11. Finlayson CM, van der Valk A (2012) Classification and Inventory of the World's Wetlands. Springer Science & Business Media
12. Verhoeven JT, Arheimer B, Yin C, Hefting MM (2006) Regional and global concerns over wetlands and water quality. Trends Ecol Evol 21:96–103
13. Bargagli R (1998) Trace elements in terrestrial plants, Springer
14. Barwick M, Maher W (2003) Biotransference and biomagnification of selenium copper, cadmium, zinc, arsenic and lead in a temperate seagrass ecosystem from Lake Macquarie Estuary, NSW, Australia. Marine Environ Res 56:471–502

15. Roberts DA, Johnston EL, Poore AG (2008) Contamination of marine biogenic habitats and effects upon associated epifauna. Mar Pollut Bull 56:1057–1065
16. Kabata-Pendias A (2011) Trace elements in soils and plants/fourth editions. CRC Taylor and Francis Group, Boca Raton, p 505
17. Jackson L (1998) of metal accumulation in rooted aquatic vascular plants. Sci Total Environ 219:223–231
18. Ralph PJ, Tomasko D, Moore K, Seddon S, Macinnis-Ng CM (2007) Human impacts on seagrasses: eutrophication, sedimentation, and contamination. Sea grasses: biology, ecology and conservation, pp 567–593. Springer
19. Ralph P, Burchett M (1998) Photosynthetic response of Halophila ovalis to heavy metal stress. Environ Pollut 103:91–101
20. Dash S, Borah SS, Kalamdhad AS (2020) Application of positive matrix factorization receptor model and elemental analysis for the assessment of sediment contamination and their source apportionment of Deepor Beel, Assam, India. Ecol Indic 114:106291
21. MoEF (2008) Report on visit to Deepor Beel in Assam: a wetland included under national wetland conservation management programme of the Ministry of Environment and Forests. Govt. of India
22. Dash S, Borah SS, Kalamdhad AS (2020) Study of the limnology of wetlands through a one-dimensional model for assessing the eutrophication levels induced by various pollution sources. Ecol Model 416:108907
23. Dash S, Borah SS, Kalamdhad A (2018) Monitoring and assessment of Deepor Beel water quality using multivariate statistical tools. Water Pract Technol 13:893–908
24. Dash S, Borah SS, Kalamdhad A (2019) A modified indexing approach for assessment of heavy metal contamination in Deepor Beel, India. Ecol Indic 106:105444
25. APHA (2017) Standard methods for the examination of water and wastewater. In: American Public Health Association, American Water Works Association, Water Environment Federation
26. U.E.P. Agency (2007) Framework for metals risk assessment. US Environmental Protection Agency, Office of the Science Advisor: Washington, DC. EPA 120/R-07/001
27. Deng H, Ye Z, Wong MH (2004) Accumulation of lead, zinc, copper and cadmium by 12 wetland plant species thriving in metal-contaminated sites in China. Environ Pollut 132:29–40

Removal of Pb(II) Ion from Aqueous Phase Under Uncontrolled and Controlled pH Conditions by Granular Activated Alumina

Ravindra Jaysing Patil and Mohammad Jawed

Abstract Adsorption is a widely used technique for the removal of heavy metals from water/wastewater. Several published literature has ignored the impact of changes in solution pH during adsorption experiment and consequently the removal of metals by precipitation mechanism. The present work investigates the kinetics and equilibrium of Pb(II) ion removal under uncontrolled and controlled pH conditions using granular activated alumina (GAA). During the kinetic study, Pb(II) ion removal obtained under uncontrolled pH conditions (4.3804 mg/g) was higher compared to the same observed under controlled pH (3.6084 mg/g). Higher Pb(II) metal removal under uncontrolled pH conditions was attributed to precipitation mechanism due to the rise in solution pH during the adsorption process. The lower value for pseudo-second-order kinetic constant 'k_2' [0.0173 (g/mg.min)] and higher value for Freundlich model adsorption capacity parameter 'k' [3.2479 (mg/g)/(mg/L)$^{1/n}$] under uncontrolled pH conditions compared to controlled pH conditions [k_2 = 0.0206, k = 0.8663] has further confirmed higher rate of Pb(II) removal under uncontrolled pH conditions due to rise in solution pH. As the solution pH increased during adsorption, the application of kinetic and adsorption isotherm models to represent the data obtained under uncontrolled pH conditions is not justifiable. Many published studies have only mentioned the initial pH of the solution and never monitored pH during the adsorption process, which eventually wrongly attributed the removal of metal by precipitation mechanism to the uptake by the adsorbent.

Keywords Adsorption · Heavy metal · Lead(II) · Metal precipitation · Metal uptake

R. J. Patil (✉)
Department of Civil Engineering, VP's Kamalnayan Bajaj Institute of Engineering and Technology, Baramati, Pune, Maharashtra 413133, India

M. Jawed
Department of Civil Engineering, Indian Institute of Technology Guwahati, Guwahati, Assam 781039, India
e-mail: jawed@iitg.ac.in

B. Laishram and A. Tawalare (eds.), *Recent Advancements in Civil Engineering*, Lecture Notes in Civil Engineering 172,
https://doi.org/10.1007/978-981-16-4396-5_35

1 Introduction

Most of the heavy metals present in surface water have generally been coming from untreated or treated industrial effluents dealing with metal processing works [1–4]. Similarly, the groundwater may also contain a considerable amount of heavy metals due to underlying geological formation. Simple physical processes like screening, settling, and filtration are inadequate to separate heavy metal ions present at trace levels in water/wastewater. Several methods have been developed and applied to remove heavy metal ions present in water/wastewater at trace levels, which include ion-exchange, membrane processes, electrochemical techniques and biological processes [5]. The methods to remove heavy metals from water/wastewater using precipitation, ion exchange, and membrane processes are expensive or ineffective, especially when the metal concentration is less than 100 ppm [6, 7].

In recent years, the adsorption technique has proven its efficiency in the removal of heavy metals present at trace levels in the water/wastewater. Adsorption is looked upon a better technology due to its simplicity and high efficiency even for a minute amount of heavy metals [8]. The adsorption process is a surface phenomenon by which multi-component fluid (gas or liquid) mixture is attracted to the surface of a solid adsorbent and forms attachments via physical or chemical bonds [1]. A large number of studies have been reported for the adsorption of metals from the aqueous phase on different adsorbents [1–4]. Adsorption kinetics and equilibrium studies of metal removal have been investigated with variation in initial solution pH, agitation/mixing imparted, a dose of adsorbent, initial concentration of adsorbate, temperature, time, etc. Among these parameters, the solution pH impacts the surface characteristics of the adsorbent as well as the ionic speciation of metals. The rate of the surface reactions is the initial solution pH dependent which eventually affects the metal uptake capacity of the adsorbent [9]. During adsorption, the solution pH seldom remains constant. However, scanty studies are available showing/demonstrating changes in the solution pH during an adsorption experiment [10]. It is also well known that pH plays a vital role in the formation of metal hydroxide precipitate, therefore, affecting the availability of metal ions in the solution for the uptake by the adsorbent [11, 12]. Many adsorption studies have been carried out by examining the effect of initial pH on the adsorption of metal ions without mentioning the final solution pH at the end of the experiment [10, 13–15]. If the solution pH increases to favor the formation of metal hydroxide precipitate, the reduction in metal ion concentrations may wrongly be attributed to its removal by adsorption. Therefore, there is a need to monitor the variations in solution pH during adsorption experiments. Also, efforts are needed to compare the metal adsorption results obtained with or without controlling the pH during the adsorption process.

Therefore, present work investigates kinetics and equilibrium of metal removal under uncontrolled and controlled pH conditions from a mono metal ion system. The results of such studies may be used to (a) highlight variations in solution pH with time during adsorption process (b) compare the difference in the amount of metal removal under uncontrolled and controlled pH conditions.

2 Experimental

2.1 Material

In the present study, the commercial grade granular activated alumina (GAA) was procured from M/S Siddhartha Industries, Surat (India) and used as an adsorbent. The Lead [Pb(II)] metal was selected for the investigation of metal removal under uncontrolled and controlled pH conditions.

2.2 Methods

Stock solution of Pb(II) metal was prepared by dissolving required amount of analytical grade lead nitrate [$Pb(NO_3)_2$] in de-mineralized water prepared through RO process (Model: Milli-Q Water, M/S Millipore S.A.S., Molsheim, France). Further, the working solutions of Pb(II) metal were prepared by diluting the stock solution with de-mineralized water. The residual concentration of Pb(II) metal was measured using atomic absorption spectroscopy (Model: 55 B, M/S Spectra AA Varian, Australia).

2.3 Pb(II) Availability with Variation in Solution pH

Experiments were designed to assess the availability of Pb(II) metal in the aqueous phase with variations in solution pH in the range of 5.00–7.00. This pH range was selected based on the desired initial pH of the solution and final pH observed during a few preliminary tests. An adequate volume of Pb(II) ion solution was taken in 150 mL beaker to yield the initial Pb(II) ion concentration of 62.16 mg/L. The beaker containing the solution was mounted on a magnetic stirrer [Make: Eltek, M/S Elektrocraft (India) Pvt. Ltd., Mumbai, India] for mixing and appropriate amounts of acid (1 N, 0.1 N, 0.05 N, 0.01 N HCl) or base (1 N, 0.1 N, 0.05 N, 0.01 N NaOH) were added for adjusting the desired pH with the help of a digital pH meter (Model: µpH System 361, M/S Systronics India Ltd., India). The mixing was continued for approximately 8–10 min. and then the mixture was allowed to stand without any disturbance for 5 min. After that, samples were withdrawn from the top portion and centrifuged at 10,000 rpm (Model: R24, M/S Remi Instruments Ltd., India) for 3 min. and the supernatant liquid was used to estimate the remaining Pb (II) ion concentration in the solution.

2.4 Effect of Contact Time on Pb(II) Ion Concentration Remaining in the Aqueous Phase Under Uncontrolled and Controlled pH Conditions

The effect of contact time on Pb(II) ion concentration remaining in the aqueous phase was investigated with initial Pb(II) ion concentration of 62.16 mg/L. The study was carried out at an initial adjusted/buffered pH value of 5.00 using 0.6 g of GAA. A fixed solution volume of 50 mL was maintained in 9 different specimen tubes of 100 mL capacity. The specimen tubes containing GAA and Pb(II) solution were mounted on an end-over-end rotary shaker (Make: Reico, M/S Reico Equipment and Instrument Pvt. Ltd., Kolkata, India) and mixed at a constant speed of 66 revolutions per minute (rpm) at room temperature. Specimen tubes were taken out from the rotary shaker one-by-one at predetermined time intervals, two phases separated using ordinary filter paper and then solution pH measured. After that, the residual Pb(II) ion concentrations in the liquid portions were estimated. All the experiments were conducted in triplicate, and average values were used for the analysis of the results.

In case of uncontrolled pH conditions, initial pH of the solution was adjusted to a pre-decided value of 5.00 at the beginning of the experiment by using appropriate amounts of either acid (1 N, 0.1 N, 0.01 N HCl) or base (1 N, 0.1 N, 0.01 N NaOH). However, the adjusted initial solution pH was not maintained at the same value during the experiment. Hence, the experiment was termed as carried out under uncontrolled pH conditions. During controlled pH conditions, the initial solution pH was buffered to a pre-decided value of 5.00 by adding 8 mL of acetate buffer {prepared by mixing 680 mL of 0.5 M sodium acetate tri-hydrate with 320 mL of 0.5 M acetic acid [16]. Thereby initial solution pH was maintained at the same value during the experiment. Hence, the experiment was termed as carried out under controlled pH conditions.

2.5 Kinetics of Pb(II) Removal Under Uncontrolled and Controlled pH Conditions

The experimental data obtained in the investigation of effect of contact time on Pb (II) ion concentration remaining in the aqueous phase (as explained in Sect. 2.4) were used to study the kinetics of Pb(II) removal under uncontrolled pH and controlled pH conditions.

2.6 Equilibrium Studies for Pb(II) Removal Under Uncontrolled and Controlled pH Conditions

Equilibrium studies were carried out at an initial adjusted/buffered pH value of 5.00. The experiments were carried out by transferring 50 mL of a Pb(II) ion solution

having an initial concentration of 62.16 mg/L in 9 specimen tubes of 100 mL capacity. Out of 9 specimen tubes, one specimen tube was kept as control while other 8 specimen tubes were added with varying doses of GAA starting with a lower value of 0.2 g and increasing to a higher value of 1.6 g (which worked out as 4 to 32 g GAA/L). The capped specimen tubes containing the mixture were mounted on an end-over-end rotary shaker and mixed at a constant speed of 66 rpm till equilibrium time. The specimen tubes were taken out from the shaker at the end of equilibrium time. The liquid and solid phases were separated immediately using ordinary filter paper, and the final pH was measured. The separated liquid portions were preserved for the estimation of Pb(II) ion concentration. The experiments were conducted in triplicate, and average values were used for the analysis of results.

3 Results and Discussion

3.1 Pb(II) Availability with Variations in Solution pH

The Pb(II) ion availability with variations in solution pH is shown in Fig. 1. The availability of Pb(II) ion in the aqueous phase was approximately 100% up to pH 5.50. The Pb(II) availability reduced to around 72% at pH 6.00, 6% at pH 6.50 and 2% at pH 7.00 (Fig. 1). The availability of Pb(II) in the aqueous phase also decreased rapidly between a pH value of 6.00 and 7.00. Therefore, Pb(II) may be considered 100% available in aqueous phase up to a pH value of 5.50 only.

3.2 Effect of Contact Time on Pb(II) Ion Concentration Remaining in the Aqueous Phase Under Uncontrolled and Controlled pH Conditions

The effect of contact time on Pb(II) ion concentration remaining in the aqueous phase was investigated under uncontrolled and controlled pH conditions, and

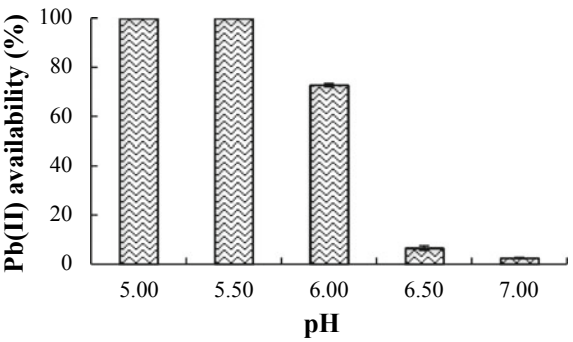

Fig. 1 Availability of Pb(II) ion in aqueous phase with variations in solution pH

results are shown in Fig. 2. During study under uncontrolled pH conditions, the variations in solution pH with time were recorded and presented in Fig. 2a. The solution pH was increased to 5.68 from initially adjusted pH of 5.00 within first 5 min., which further increased to 6.01 at the end of 180 min. of experimentation. Finally, the solution pH was observed as 6.11 toward the end of the experiment. The Pb(II) ion was 100% available in aqueous phase up to solution pH 5.50, and its availability decreased with an increase in solution pH. It indicated that precipitation of Pb(II) ion might have started within the first 5 min. of experimentation. Hence the reduction in Pb(II) ion concentration from the solution under uncontrolled pH conditions might be attributed to combined effects of adsorption and precipitation. Furthermore, in the case of a study carried out under controlled pH conditions (Fig. 2b), the solution pH remained fixed at 5.00 throughout the experiment. Hence, the Pb(II) ion removal under controlled pH conditions might be attributed to adsorption only.

The Pb(II) ion concentration remaining in solution was observed to decrease rapidly in the beginning as could be seen in Fig. 2a, b. The decrease in Pb(II) ion concentration was relatively more in uncontrolled pH conditions compared to

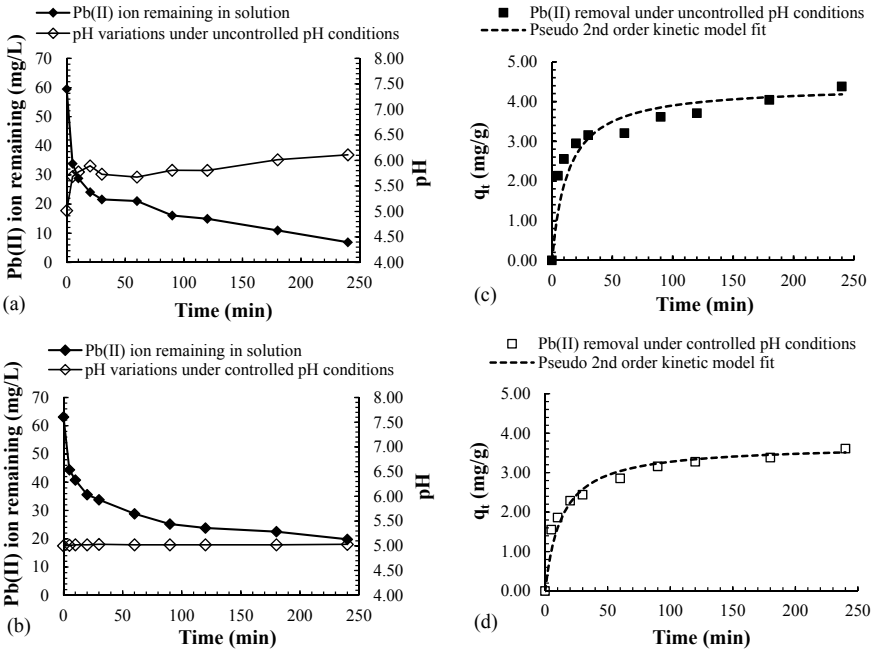

Fig. 2 Variation in solution pH and Pb(II) ion concentration remaining in aqueous phase, **a** under uncontrolled, **b** controlled pH conditions and variations in Pb(II) uptake/removed, **c** under uncontrolled and **d** controlled pH conditions

controlled pH conditions. After a period of initial 20 min., the concentration of Pb (II) ion remaining in solution decreased rather slowly under uncontrolled and controlled pH conditions. By the end of 180 min., the concentration of Pb(II) ion remaining in solution appeared to have reached to a fixed level. At the end of contact period of 240 min., the percentage Pb(II) ion remaining in aqueous phase under uncontrolled and controlled pH conditions were observed as 12% and 31%, respectively. The lower value of the concentration of Pb(II) ion remaining in aqueous phase under uncontrolled pH conditions might be attributed to precipitation of Pb(II) ion due to rise in solution pH along with its migration from the aqueous phase to GAA surface. Whereas, the reduction in Pb(II) ion concentration under controlled pH conditions was most likely due to migration of Pb(II) ion from the aqueous phase to GAA surface.

3.3 *Kinetics of Pb(II) Uptake/removal Under Uncontrolled and Controlled pH Conditions*

The data obtained for Pb(II) ion concentration remaining in the aqueous phase was utilized to investigate the kinetics of Pb(II) uptake/removal under uncontrolled and controlled pH conditions. The amount of Pb(II) metal ion removed from the solution under uncontrolled and controlled pH conditions is estimated using the following equation:

$$q_t = \frac{V(C_o - C_t)}{1000\,m} \tag{1}$$

where q_t is metal uptake/removal (mg/g) at time 't', V is solution volume (mL), C_o is the initial metal concentration (mg/L), C_t is metal concentration remaining in the aqueous phase at time 't' (mg/L) and m is mass of adsorbent (g).

Furthermore, in published studies, the kinetics of metal removal data has been analyzed using pseudo-first-order and pseudo-second-order kinetic models. The pseudo-first-order kinetic model is generally expressed [17] as

$$q_t = q_e(1 - e^{-k_1 t}) \tag{2}$$

whereas the pseudo-second-order kinetic model is derived based on the sorption capacity of the solid phase [18] and its linearized form is expressed as

$$\frac{t}{q_t} = \frac{t}{q_e} + \frac{1}{k_2 q_e^2} \tag{3}$$

where, q_t is metal uptake/removal at time 't' (mg/g), q_e is equilibrium metal uptake/removal (mg/g), k_1 is first-order kinetic constant (1/min), k_2 is second-order kinetic constant (g/mg.min) and t is time (min). The parameters of the pseudo-first-order kinetic model (viz. q_e and k_1) were estimated by the method of least square [5]. Further, the pseudo-second-order kinetic model in its linear form was applied to experimental kinetic data, and the values of k_2 and q_e were determined.

The results of the kinetic study under uncontrolled and controlled pH conditions are presented in Fig. 2. The Pb(II) ion removal under uncontrolled pH conditions appeared to be very fast during the first 20 min (Fig. 2c). This might be due to the quick rise in solution pH around 6.00 (Fig. 2a) within first 5 min., which eventually might have caused removal of Pb(II) ion by precipitation in the beginning and then possibly followed by adsorption. After a period of first 60 min., the Pb(II) removal was observed to be very slow—leading toward equilibrium condition. In the case of a kinetic experiment carried out under controlled pH conditions, the Pb(II) metal removal was observed to be moderately fast up to first 30 min. and became steady after 60 min. of experimentation (Fig. 2d). At the end of 240 min., the Pb(II) ion removal obtained under uncontrolled and controlled pH conditions were 4.3804 mg/g and 3.6084 mg/g, respectively. This revealed that precipitation mechanism had considerable contribution toward the removal of Pb(II) ion from solution along with adsorption mechanism under uncontrolled pH conditions. However, many published studies have only mentioned the initial pH of the solution while carrying out adsorption kinetics studies [10]. These studies have failed to report/monitor pH variations during the adsorption process and might have wrongly attributed the removal of metals by precipitation to the adsorption onto the surface of the adsorbent.

Furthermore, the kinetic data of Pb(II) ion removals under uncontrolled and controlled pH conditions were fitted into pseudo-first- and second-order kinetic models and estimated parameters are presented in Table 1. Higher values of coefficient of determination (R^2) indicated appropriateness of pseudo-second-order kinetic model to describe experimental kinetic data. The lower k_2 value under uncontrolled pH conditions compared to controlled pH conditions has further confirmed a higher rate of Pb(II) removal under uncontrolled pH conditions due to rise in solution pH during the experiment. To our understanding, the estimated kinetic constant under uncontrolled pH conditions was most likely represented the Pb(II) ion removal through precipitation and/or adsorption rather than solely representing the Pb(II) uptake by adsorbent through adsorption. As the constants of pseudo-first- and second-order kinetic models namely k_1 and k_2 represent the rate of uptake of metals onto the surface of the adsorbent, the application of these models to represent the kinetic data obtained under uncontrolled pH conditions is not justifiable.

Table 1 Summary of estimated kinetics and equilibrium isotherm parameters for Pb(II) ion uptake/removal under uncontrolled and controlled pH conditions

Initial conc. (mg/L)	Uncontrolled pH conditions			Controlled pH conditions		
	Parameters	Pseudo-first-order kinetic model	Pseudo-second-order kinetic model	Parameters	Pseudo-first- order kinetic model	Pseudo-second-order kinetic model
Pb (II) = 62.16	$q_{e,exp}$ (mg/g)	4.3804		$q_{e,exp}$ (mg/g)	3.6084	
	q_{em} (mg/g)	3.6071	4.4111	q_{em} (mg/g)	3.1160	3.7051
	k_1 (1/min)	0.1065	–	k_1 (1/min)	0.0735	-
	k_2 (g/mg. min)	–	0.0173	k_2 (g/mg. min)	–	0.0206
	R^2	0.901	0.991	R^2	0.928	0.997
	Parameters	Langmuir isotherm model	Freundlich isotherm model	Parameters	Langmuir isotherm model	Freundlich isotherm model
	q_m (mg/g)	7.8492	–	q_m (mg/g)	5.3191	-
	b (L/mg)	0.5662	–	b (L/mg)	0.0771	-
	k [(mg/g)/(mg/L)$^{1/n}$]	–	3.2479	k [(mg/g)/(mg/L)$^{1/n}$]	–	0.8663
	$1/n$	–	0.2353	$1/n$	–	0.4202
	R^2	0.948	0.956	R^2	0.955	0.979

$q_{e,exp}$ = experimental metal uptake/removal at equilibrium, q_{em} = metal uptake/removal at equilibrium calculated using kinetic models

3.4 Equilibrium Studies for Pb(II) Uptake/removal Under Uncontrolled and Controlled pH Conditions

The adsorption isotherm is the equilibrium relationship between the concentration of the adsorbate in the fluid phase and concentration of the adsorbate on the adsorbent particles at a given temperature. Several mathematical relationships have been developed to describe the equilibrium distribution of adsorbate between the solid and liquid phases and thus aid in the interpretation of adsorption equilibrium data. In the published studies, equilibrium studies data have been frequently analyzed using the most popular isotherm models—Langmuir (Eq. 4) [19] and Freundlich (Eq. 5) [20] isotherm models which are as follows:

$$q_e = \frac{q_m b C_e}{1 + b C_e} \tag{4}$$

$$q_e = k \times C_e^{\frac{1}{n}} \tag{5}$$

where q_e is equilibrium metal uptake/removal (mg/g), C_e is the residual equilibrium concentration of metal (mg/L), q_m (mg/g) and b (L/mg) are Langmuir model adsorption parameters represent maximum adsorption capacity and adsorption affinity, respectively, k and n are Freundlich adsorption parameters representing adsorption capacity and adsorption intensity, respectively.

Equilibrium studies of Pb(II) removal were carried out with a fixed initial concentration of approximately 62.16 mg/L by varying GAA doses in the range of 4–32 g/L. Further, the experimental data were used to estimate equilibrium Pb(II) removal (q_e) under uncontrolled and controlled pH conditions by GAA. The equilibrium studies results are presented in Fig. 3.

The variations in solution pH obtained under uncontrolled and controlled pH conditions are plotted with the residual equilibrium concentration of Pb(II) ion (Fig. 3). During equilibrium study with uncontrolled pH conditions, the solution pH increased with decrease in residual equilibrium Pb(II) concentration (Fig. 3a). This might be due to higher doses of GAA used for obtaining lower values of the equilibrium concentration of Pb(II) ion. Since the solution pH increased beyond 5.50, the removal of Pb(II) ion might be attributed to combined effects of precipitation and adsorption. However, under controlled pH conditions, the equilibrium solution pH was observed in the range of 5.01–5.09 (Fig. 3b). Hence, the removal of Pb(II) ion under controlled pH conditions might be attributed to adsorption only.

The Langmuir and Freundlich isotherm models were applied to equilibrium Pb (II) uptake/removal data and estimated model parameters are presented in Table 1. Higher values of R^2 for the Freundlich adsorption isotherm model indicated its applicability to describe the equilibrium uptake/removal data of Pb(II) ion. The higher value for Freundlich adsorption capacity parameter 'k' under uncontrolled pH conditions compared to controlled pH conditions has further confirmed the

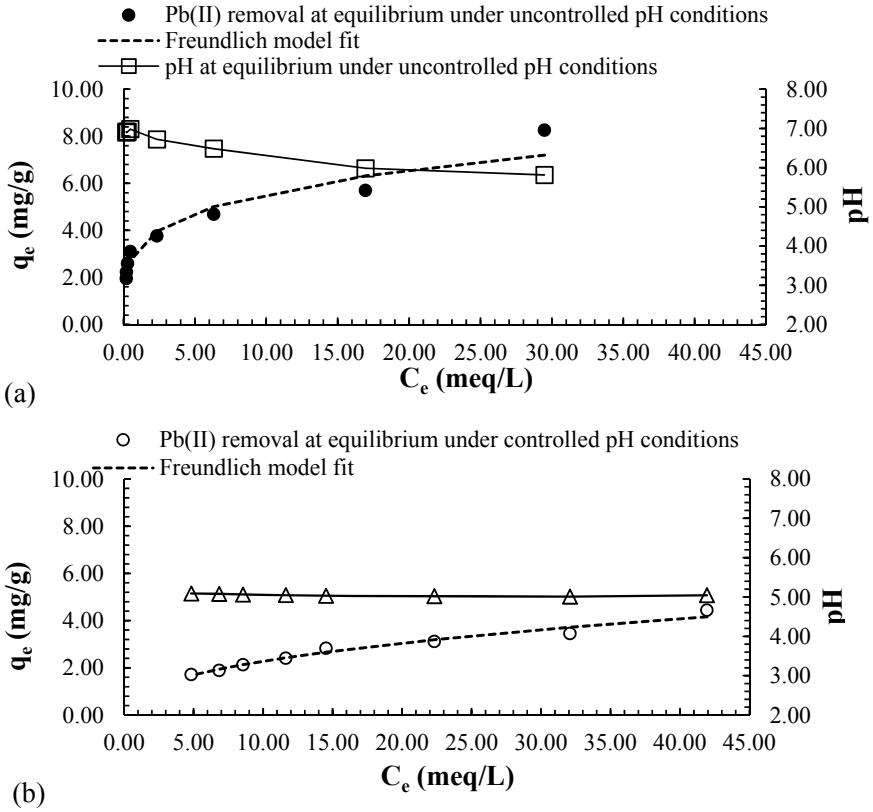

Fig. 3 Variations in Pb(II) uptake/removal and solution pH at equilibrium under, **a** uncontrolled and **b** controlled pH conditions

removal of Pb(II) ions by precipitation along with adsorption under uncontrolled pH conditions.

The Langmuir adsorption isotherm model is based upon two assumptions: (i) the forces of interaction between adsorbed molecules are negligible and (ii) once a molecule occupies a site, no further sorption takes place on the same site [19]. Essentially the Langmuir model is about the surface phenomena of adsorbate adsorption and its parameters q_m and b represent the maximum capacity of the adsorbent to accommodate the adsorbate and free energy of adsorption, respectively. Similarly, the Freundlich isotherm is the earliest known relationship describing non-ideal and reversible adsorption, not restricted to the formation of the monolayer. The development of Freundlich isotherm was based on the assumption that the adsorbent had a heterogeneous surface composed of different classes of adsorption sites, with adsorption on each class of site following the Langmuir isotherm [20]. The Freundlich isotherm parameters k and n indicate relative adsorption capacity and intensity of adsorption, respectively. Therefore, isotherm

parameters q_m and k mainly represent the capacity of the adsorbent to retain the adsorbate onto the surface and do not account for the removal of metals from the solution by precipitation due to rise in solution pH. Hence, the application of these isotherm models to represent the equilibrium isotherm data obtained under uncontrolled pH conditions is not justifiable. However, many published studies have not taken into account the rise in solution pH during equilibrium studies leading to the removal of a part of metal ions by precipitation and eventually attributed metal removal by adsorption onto the surface of the adsorbent. Therefore, the estimated values of the Langmuir and Freundlich isotherm parameters might have given grossly wrong assessment as far as the capacity of the adsorbent was concerned.

4 Conclusions

The present study investigates the kinetics and equilibrium of Pb(II) ion uptake/removal under uncontrolled and controlled pH conditions. The major conclusions are:

1. The lower percentage of Pb(II) ion remaining in aqueous phase under uncontrolled pH conditions (12%) compared to controlled pH (31%) was observed due to precipitation of Pb(II) ion along with its migration from the aqueous phase to GAA surface.
2. Kinetics study revealed higher uptake/removal of Pb(II) ions under uncontrolled pH conditions (4.3804 mg/g) compared to controlled pH (3.6084 mg/g). The lower k_2 value under uncontrolled pH conditions compared to controlled pH conditions has further confirmed higher rate of Pb(II) uptake/removal under uncontrolled pH conditions due to rise in solution pH during the experiment.
3. The higher value for Freundlich adsorption capacity parameter 'k' under uncontrolled pH conditions compared to controlled pH has also confirmed the uptake/removal of Pb(II) ions by precipitation along with adsorption under uncontrolled pH conditions.
4. Many published studies have ignored the amount of metal removed by precipitation mechanism while estimating kinetic as well as adsorption isotherm parameters which eventually lead to the wrong estimation of the capacity of the adsorbent. The application of kinetic and adsorption isotherm models to represent the data obtained under uncontrolled pH conditions is not justifiable due to the removal of metals by precipitation mechanism.

References

1. Foo KY, Hameed BH (2010) Insights into the modeling of adsorption isotherm systems. Chem Eng J 156:2–10
2. Febrianto J, Kosasih AN, Sunarso J, Yi-Hsu J, Indraswati N, Ismadji S (2009) Equilibrium and kinetic studies in adsorption of heavy metals using biosorbent: a summary of recent studies. J Hazard Mater 162:616–645
3. Ayoob S, Gupta AK (2008) Insights into isotherm making in the sorptive removal of fluoride from drinking water. J Hazard Mater 152:976–985
4. Babel S, Kurniawan TA (2003) Low-cost adsorbents for heavy metals uptake from contaminated water: a review. J Hazard Mater 97:219–243
5. Tchobanoglous G, Burton FL, Stensel HD (2003) Wastewater engineering treatment and reuse. Tata McGraw-Hill Publications, New Delhi
6. Miretzky P, Saralegui A, Cirelli AF (2006) Simultaneous heavy metal removal mechanism by dead macrophytes. Chemosphere 62:247–254
7. Schiewer S, Volesky B (1995) Modeling of the proton-metal ion exchange in biosorption. Environ Sci Technol 29:3049–3058
8. Choy KKH, Porter JF, McKay G (2000) Langmuir isotherm models applied to the multi-component sorption of acid dyes from effluent onto activated carbon. J Chem Eng Data 45:575–584
9. Kiran I, Akar T, Tunali S (2005) Biosorption of Pb(II) and Cu(II) from aqueous solutions by pretreated biomass of Neurospora crassa. Process Biochem 40:3550–3558
10. Tien C (2007) Remarks on adsorption manuscripts received and declined: an editorial. Sep Purif Technol 54:277–278
11. Al-Rub AAF, El-Naas MH, Ashour I, Al-Marzouqi M (2006) Biosorption of copper on Chlorella vulgaris from single, binary and ternary metal aqueous solutions. Process Biochem 41:457–464
12. Sheng PX, Ting YP, Chen JP, Hong L (2004) Sorption of lead, copper, cadmium, zinc, and nickel by marine algal biomass: characterization of biosorptive capacity and investigation of mechanisms. J Colloid Interf Sci 275:131–141
13. Bueno BYM, Torem ML, Molina F, de Mesquita LMS (2008) Biosorption of lead(II), chromium(III) and copper(II) by *R. opacus*: equilibrium and kinetic studies. Miner Eng 21:65–75
14. Chen AH, Liu SC, Chen CY, Chen CY (2008) Comparative adsorption of Cu(II), Zn(II), and Pb(II) ions in aqueous solution on the crosslinked chitosan with epichlorohydrin. J Hazard Mater 154:184–191
15. Srivastava VC, Mall ID, Mishra IM (2008) Removal of Cadmium (II) and Zin c(II) metal ions from aqueous solution by rice husk ash. Colloids Surf A Physicochem Eng Aspects 312:172–184
16. Asnin L, Kaczmarski K, Guiochon G (2010) The adsorption of Naproxen enantiomers on the chiral stationary phase Whelk-O1 under reversed-phase conditions: the effect of buffer composition. J Chromatogr A 1217:7055–7064
17. Lagergren S (1898) About the theory of so called adsorption of soluble substances, vol 24, pp 1–39. Kungliga Svenska Vetenskap-Sakademiens, Handlingar
18. Ho Y (2006) Isotherms for the sorption of lead onto peat: comparison of linear and non-linear methods. Polish J Environ Stud 15:81–86
19. Langmuir I (1918) The adsorption of gases on plane surfaces of glass, mica and platinum. J Am Chem Soc 40:1361–1403
20. Freundlich H (1926) Colloid and capillary chemistry. Methuen, London

Assessment of Particulate Exposure in Different Transport Medium at Two Contrasting Land Uses of Bangalore

Smaranika Panda

Abstract In the last few decades, India has witnessed a sharp rise in vehicle population in all the major cities of India. Increase in both public and private transport sectors has augmented the air pollutant concentrations beyond permissible limits. Though the number of studies on vehicular pollution has increased in last few years, however, studies on assessment of personal exposure and health risk assessment in different transport mediums are limited. In Indian cities, the general commute time from home to workplace is quite high (approximately 1.5–4 h to and from home to work place). Bangalore is reported to be one among the top ten metropolitan cities in the world which is considered to be the most congested city resulting in increased commute time by several folds during peak hours. The present study provides an insight to personal exposure and health risk assessment while travelling in various transport medium such as a two wheeler (a Bike), three wheeler (an Auto) and a four wheeler (a Bus) in 2 land use patterns, i.e. commercial and industrial area. Exposure monitoring of PM_5 (particulate matter with aerodynamic diameter less than 5 μm) using personal sampler (EnviroTech APM 801) was carried out considering two road maps in commercial and industrial areas for 35 days (2 samples per day during peak and non-peak hours) while travelling in auto, bus and bike. The total sampling time was 1.5–2 h in different days in each medium with the speed of vehicle maintained identical. Studies on human exposure to vehicular pollution were made under different scenarios with respect to windows (either open or close) in bus and side cover (either open or close) in auto during both peak and non-peak hours. Exposure during weekends was also investigated. In addition, chemical characterizations of PM_5 for 15 elements (Al, Ba, Ca, Cd, Co, Cr, Cu, Fe, K, Mg, Na, Ni, Pb, Sr and Zn) were carried out using inductively coupled plasma optical electron spectroscopy, and cancer risk was assessed for carcinogenic elements.

Keywords PM_5 · Exposure analysis · Industrial · Commercial · Travel medium

S. Panda (✉)
Department of Civil Engineering, CMR Institute of Technology, Bengaluru, Karnataka, India

B. Laishram and A. Tawalare (eds.), *Recent Advancements in Civil Engineering*, Lecture Notes in Civil Engineering 172,
https://doi.org/10.1007/978-981-16-4396-5_36

1 Introduction

The problem of air pollution has assumed serious proportions in some of the major metropolitan cities of India. Recent studies showed an increasing trend in particulate pollution across the country. A total of 37 cities in 2014 from India were recorded in worst 100 cities with elevated PM_{10} contamination [1]. The increased concern of scientific community towards particulate pollution is due to its toxic compositions such as heavy metals, carcinogenic elements, poly aromatic hydrocarbons and black carbon which get emitted from various anthropogenic sources. Among the various sources, vehicular sources were reported to be one among the top contributors to the urban air pollution [2]. In the last few decades, India is witnessing a tremendous increase in vehicular population due to significant improvement in both public and private transport sectors. Further, in urban areas, large no of population are exposed to these elevated particulate concentrations. Short- and long-term exposure to high and low pollutant concentrations can result in various diseases such as asthma, bronchitis, lung- and heart-related disease, allergies and even cancer. The total deaths attributed to air pollution were reported to be more than 1.1 million in India [3]. Alarming increase of particulate pollution in urban areas has resulted in numerous studies based on ambient air quality monitoring at different fixed sites such as traffic intersections and industrial area but studies focusing on personal exposure monitoring due to increased traffic pollution are very limited in India. Past studies have reported metropolitan cities like Delhi, Mumbai, Bangalore, Kolkata, etc. face high congestion throughout the year which increases the exposure period of passengers during every day travel [4, 5]. The increased commute time not only adversely impacts the economy of a country but also had a huge impact on personal exposure of people residing in cities [5, 6]. Studies on assessment of exposure and health risk assessment during travel in different types of transport medium are very important for developing countries as in Indian cities the commute time from the work place to home is quite high and is reported in the range of 1.5–4 h based on the land use and medium of travel. Present study is focused on Bangalore which is the capital of Karnataka. The capital city has seen a vigorous urbanization, industrialization and infrastructural development in a very short time period. Bangalore is one of the biggest IT hubs in India. The industrial and IT job opportunities in the city have attracted people across the country for their livelihood which lead to increase in vehicular population, congestion, unplanned development and expansion of the city, and augmented the pollutant concentrations beyond permissible limits in different regions.

In the present study, an attempt was made to understand the exposure concentration in 3 different travel medium in 2 contrasting land uses. In addition, various scenarios, weekday and weekend variation of exposure were investigated.

2 Methodology

2.1 Study Area Description

Bangalore is one of the metropolitan cities which have become the "silicon valley" of India in a very short span. The rapid multidimensional development of the city has boosted up the growth in various fields such as infrastructure, road network, vehicular population, and small and medium scale industries in and around the city centre. Bangalore metropolitan city spreads over an area of 709 Km^2. Total population of the area is 84.3 lakh based on 2011 Census report which is expected to have reached up to 1.2 crore in 2020, and the annual vehicular growth rate of the city was reported to be 10.6% [7, 8]. Bangalore has a dry and cold climatic condition during most of the time of the year. The average relative humidity of Bangalore during monitoring campaign was observed in the range of 37 ± 5%, and the temperature was in the range of 22 ± 3 °C. Bangalore has 2 major industrial hubs in the southern and northern outskirts of the city namely Jigani Bommasandra industrial area and Peenya industrial area [8]. In the present study, we have considered the Jigani industrial area which is dominated by various metal industries, granite industries, pharmaceutical, chemical manufacturing and research development units, automobile component manufacturing and repair shops, etc. Figure 1 illustrates road map followed at commercial and industrial areas.

2.2 Instrumentation, Sampling and Analysis

PM_5 exposure sampling using personal sampler (Envirotech APM 801) was carried out at 2 different land uses (commercial and industrial area) in different transport micro environment (auto, bus and bike). Also, personal exposure monitoring during

Fig. 1 Road map followed at the **a** commercial and **b** industrial area

different scenarios such as windows (either open or close) in bus and side sheet (either open or close) in auto during both peak and non-peak hours was carried out. Exposure monitoring during weekends was also carried out. A total of 35 samples were collected in auto, bus and bike during peak and non-peak hours with a sampling time of 1.5–2 h during weekdays and weekends. Speeds of vehicles were kept in the range of 10 ± 5 km/hr during peak hours (based on the average speed of bus) and 25 ± 5 km/hr during non-peak hours. PM_5 exposure concentration was quantified by gravimetric principle. Further the filter papers were analysed for 15 elements such as Aluminium (Al), Barium (Ba), Calcium (Ca), Cadmium (Cd), Cobalt (Co), Chromium (Cr), Copper (Cu), Iron (Fe), Potassium (K), Magnesium (Mg), Sodium (Na), Nickel (Ni), Lead (Pb), Strontium (Sr) and Zinc (Zn) using ICP OES (Systronics AST 0231) by following the standard operating procedure provided by United States Environment Protection Agency [9].

2.3 Quantification of Cancer Risk

International agency of research has classified carcinogenic elements into various categories based on potency of carcinogenicity. Among the elements analysed in the present study, Cd, Cr and Ni are established carcinogens and are placed under group 1 category. Pb is a possible carcinogen and placed under group 2B category. Excess cancer risks of Cd, Cr, Ni and Pb were quantified based on their concentration and air inhalation unit risks [10].

2.4 Source Identification Through Enrichment Factor

Enrichment factor (EF) method is one of the source identification methods used to estimate crustal and non-crustal origin of elements. It is a qualitative method. In the present study, aluminium is considered as the reference material assuming its contribution solely from earth's crust [11]. The enrichment factors of elements were quantified by the ratio of air concentration of elements and aluminium to the crustal concentration of the element and aluminium. The crustal concentration of the elements and aluminium was obtained from the literatures [11]. The average concentration in both land uses was considered for quantification of EF. Enrichment factor of 1 denotes crustal origin and suggests both crustal and non-crustal origin when EF reaches 5. EF of more than 5 denotes non-crustal origin and if the value reaches 10 it signifies major contribution from human induced sources.

2.5 Quality Assurance and Control

Filter paper was desiccated 24 h prior to weighing. Filter blanks were collected during every step of monitoring and analysed following the same procedure of samples. Personal sampler was calibrated before starting the monitoring process by the system engineer of EnviroTech. The concentration values provided here are blank corrected.

3 Results and Discussion

3.1 Variation of PM_5 Exposure in Auto, Bus and Bike

The average PM_5 exposure concentration in bus during peak hours (average of morning and evening peaks) with normal condition (window/ side drape open) at the commercial area was 695 $\mu g/m^3$ in bus, 1522 $\mu g/m^3$ in auto and 1387 $\mu g/m^3$ in bike and at industrial area the exposure was 845, 1822 and 1887 $\mu g/m^3$ in bus, auto and bike, respectively. The concentration at morning peak hours (8AM–10AM) was found to be higher than the evening peaks (6PM–8PM) which may be due to the opening of schools, colleges, industries and shops at approximately same time in the morning. However, the staggered closing time during evening resulted in reduction in pollutant concentration during evening peak hours. Buses at both the land uses were observed to have least exposure which could be due to higher sitting height. Comparatively lower exposure height of auto and bike than bus might have resulted in higher exposure in both land uses. Higher exposure concentration of autos could be due to its confined structural design which restricts the dispersion of particulates. Also, re-suspension of road dust could contribute to the exposure levels inside the auto due to lower height of exposure. In both the land uses, the exposure concentration in bike was high. Figure 2 represents the morning and evening exposure concentration in bus, auto and bike. At the industrial site, the exposure concentration was observed highest while travelling in autos and at the commercial area bike travel resulted in highest exposure concentration followed by autos. The exposure concentration in all the three travel mediums and land uses was observed several folds higher than the daily average ambient air quality standard of coarse and fine particulate matter (Daily National Ambient air quality standard for $PM_{2.5}$ = 60 $\mu g/m^3$ and PM_{10} = 80 $\mu g/m^3$) [12].

3.2 Exposure Analysis During Different Window Condition

For buses, PM_5 concentration variation during windows closed condition showed an average weekday reduction of 21% during peak hours. Similarly, for autos, the

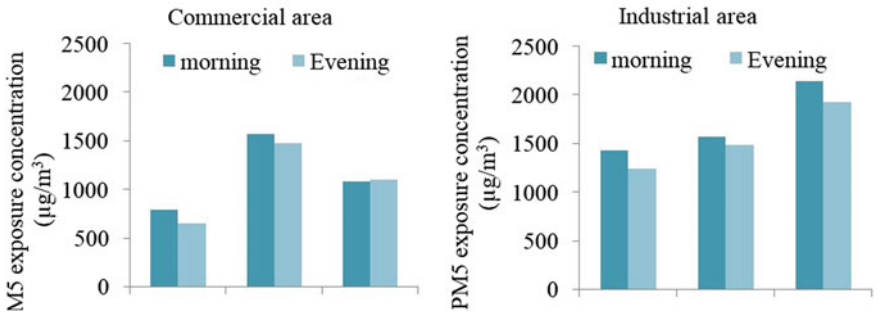

Fig. 2 Average PM5 exposure concentration during morning and evening peak hours at commercial and industrial areas

peak hour reduction with closed side sheets was observed to be 41% (Fig. 3). During non-peak hours, reduction in exposure concentration with respect to peak hours in the buses was 16% during weekdays at the commercial area which could be due to less traffic movement resulting in reduction of vehicular emissions and reduction in upward dispersion of large size road dust particles to the higher sitting height of buses [13–15]. However, in autos, the reduction was comparatively less (9%) probably due to lowering of exposure height of people sitting in autos and results in high exposure of both re-suspension and exhaust particulate emissions. Similar results were also observed at the industrial location with a reduction in exposure concentration by 19% and 12% in buses and autos during non-peak hours of weekdays, respectively, which could be due to significant reduction in frequency of government buses during non-peak hours at the industrial area. During weekend, the vehicular movement and frequency of buses reduce considerably in both commercial and industrial area. Reductions of personal exposure in bike were 44% during weekend compared to weekdays (Fig. 3).

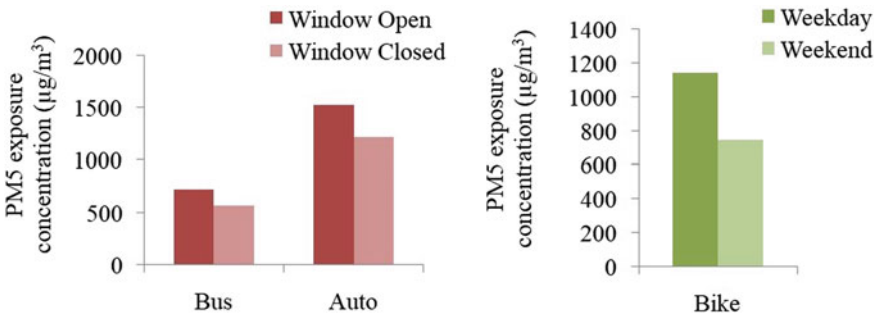

Fig. 3 Variation in exposure concentration in buses and auto during different window operation at commercial area and exposure in bike during weekdays and weekends

3.3 Variation of PM_5 Bound Metal Exposure in Auto, Bus and Bike

Among heavy metals exposure concentration, Ni and Cd exceeded the National Ambient Air Quality Standards (NAAQS). Ni was 1.17, 1.5 and 1.2 times and Cd was 1.24, 2.21 and 2.04 times higher than NAAQS standards (Ni = 20 ng/m^3 and Cd = 5 ng/m^3) in bus, auto and bike, respectively. The elements analysed in the present study could have both natural anthropogenic origins. Past studies reported elements such as Ca, Al, Sr, Fe and Na could have contributed from re-suspension of road dust, construction activities and natural earth crust [10]. Further abrasion action of vehicle tyre and road surface result in emission of Zn and Ba at the vicinity [10]. Elements such as Cr, Fe and Cd could be contributed from the direct vehicle tail pipe [16]. Similarly, at the industrial area metal industries, granite industries, biomedical and chemical industries could contribute to the pollutant concentration in addition to vehicular emissions. At the industrial area, the roads are encroached by small shops and street vendors which reduce the effective road width for traffic movement there by increasing the stagnation of particulate concentration. Figure 4 illustrates the average PM_5 bound abundant and trace elemental concentrations.

3.4 Cancer Risk Assessment of Heavy Metals

The excess cancer risk was highest for bike in all three travel medium followed by auto and bus. Cancer risk due to heavy metals in different transport environment

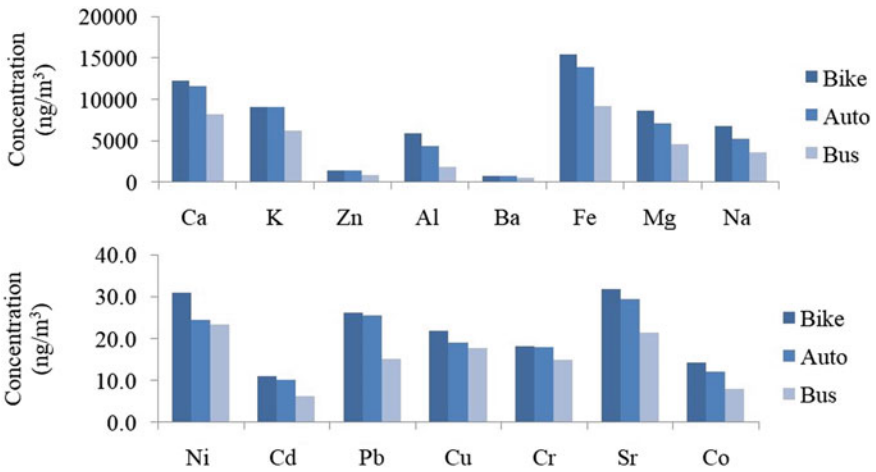

Fig. 4 Abundant and trace metal exposure concentration in Bike, auto and bus (averaged for both commercial and industrial area)

Table 1 Cancer risk due to heavy metals

Pollutant	IUR	Excess cancer risk (10^{-6} population)		
	$(\mu g/m^3)^{-1}$	Bike	Auto	Bus
Cd	1.8×10^{-3}	39.6	18.36	11.16
Cr	1.2×10^{-2}	36.2	36	30
Ni	2.4×10^{-4}	7.3	5.88	5.59
Pb	1.2×10^{-5}	0.31	0.30	0.18

was provided in the Table 1. The average exposure metal concentrations at commercial and industrial area were considered for quantification of cancer risk. Total cancer risk with respect to heavy metals in bike, auto and bus was 64, 61 and 47 per million populations.

3.5 Estimation of Enrichment Factor

In the present study, for auto, Sr was having an EF of close to 1 which denotes its natural crustal origin. K, Ca and Na had EF less than 5 suggesting both non-crustal and crustal origin. Ba, Cd, Co, Cr, Cu, Fe, Mg, Ni, Pb and Zn were observed to be highly enriched which suggests the anthropogenic origin of these elements. Similar results were observed for bike and bus. Past studies have also reported similar results as obtained in the present study [10].

4 Conclusions

PM_5 personal exposure assessment in different transport medium such as auto, bus and bike was carried out in two selected roads of industrial and commercial areas of Bangalore city using personal sampler. The study was carried out to understand the exposure in business as usual and varying operational scenarios. Sampling was taken during peak and non-peak hours of weekdays and weekends. In addition, samples during various vehicular operational scenarios corresponding to window and side drape conditions (open/close) were collected. The exposure monitoring results at the commercial area indicated highest exposure concentration in auto followed by bike and least exposure in bus. Similarly, at the industrial area, the highest exposure was observed in bike followed by auto and bus. Results revealed that closing of windows during peak hours in buses and auto-rickshaw during weekdays can reduce the exposure by 21% and 41%, respectively. At both the commercial and industrial location, morning peak hour showed a higher exposure which could be reduced to a certain extent through a staggered opening pattern of work places. Further, at both the locations, significant reduction in concentration

was observed during weekends due to decreased frequency of government and private vehicles. Particulate bound Ni and Cd concentration at both land uses were observed to be exceeding the NAAQS which demands a detailed source apportionment studies in Bangalore city. Excess cancer risk was estimated to be highest for Cr followed by Cd, Ni and Pb in both land uses and transport mediums.

References

1. WHO (2014) Outdoor air pollution in the world cities world health organization. Geneva, Switzerland
2. Kishore N, Srivastava AK, Nandan H, Pandey CP, Agrawal S, Singh N, Soni VK, Bisht DS, Tiwari S, Srivastava MK (2019) Long-term (2005–2012) measurements of near-surface air pollutants at an urban location in the Indo-Gangetic Basin. J Earth Syst Sci 128(3):55
3. GBD (2018) The global burden of disease 2010 generating evidence and guiding policy institute for health metrics and evaluation, Seattle, USA
4. Chakrabartty A, Gupta S (2014) Traffic congestion in the metropolitan City of Kolkata. J Infrastruct Dev 6(1):43–59
5. Akbar PA, Couture V, Duranton G, Ghani E, Storeygard A (2018) Mobility and congestion in urban India. The World Bank
6. Mashayekh Y, Jaramillo P, Chester M, Hendrickson CT, Weber CL (2011) Costs of automobile air emissions in US metropolitan areas. Transp Res Record 2233(1):120–127
7. Verma A, Rahul T, Dixit M (2015) Sustainability impact assessment of transportation policies —a case study for Bangalore city. Case Stud Trans Policy 3:321–330
8. BDA (2017) Revised master plan for 2031. Bangalore Development Authority. State Government of Karnataka, Bengaluru, India
9. USEPA (1999) Compendium of methods for the determination of inorganic compounds in ambient air, compendium method IO-3.5: determination of metals in ambient particulate matter using inductively coupled plasma/mass spectrometry (ICP/MS), p 349
10. Panda S, Nagendra SS (2018) Chemical and morphological characterization of respirable suspended particulate matter (PM10) and associated heath risk at a critically polluted industrial cluster. Atmos Pollut Res 9(5):791–803
11. Shelley RU, Morton PL, Landing WM (2015) Elemental ratios and enrichment factors in aerosols from the US-GEOTRACES North Atlantic transects. Deep Sea Res Part II: Topical Stud Oceanogr 116:262–272
12. CPCB (2012) National ambient air quality standards central pollution control board, New Delhi
13. Samara C, Voutsa D (2005) Size distribution of airborne particulate matter and associated heavy metals in the roadside environment. Chemosphere 59(8):1197–1206
14. Amato F, Favez O, Pandolfi M, Alastuey A, Querol X, Moukhtar S, Bruge B, Verlhac S, Orza JAG, Bonnaire N, Le Priol T (2016) Traffic induced particle resuspension in Paris: emission factors and source contribution. Atmos Environ 129:114–124
15. Valotto G, Zannoni D, Guerriero P, Rampazzo G, Visin F (2019) Characterization of road dust and resuspended particles close to a busy road of Venice mainland (Italy). Int J Environ Sci Technol 16(11):6513–6526
16. Pant P, Baker SJ, Shukla A, Maikawa C, Pollitt KJG, Harrison RM (2015) The PM10 fraction of road dust in the UK and India: characterization, source profiles and oxidative potential. Sci Total Environ 530:445–452

Adsorption of 2-Picoline on Tea Waste: Studies on Characteristics of Adsorbent and Effects on Various Adsorption Parameters

Upendra R. Darla, Divyanshu Saini, and Dilip H. Lataye

Abstract This paper deals with the adsorption of 2-picoline from aqueous solution to tea waste activated carbon (TWAC). The characteristics and effects of the adsorbent on different parameters of adsorption have been examined. Initial pH (pH_0), adsorbent dose (m), contact time (t), initial concentration (C_0), and temperature (T) are the adsorption parameters tested using a batch adsorption sample. In the present analysis, the adsorbent used comprises approximately 48% fixed carbon and a porous structure revealed from morphological research. Maximum 2-picoline removal was found to be 83% and 56% TWAC for lower (50 mg/L) and higher (500 mg/L) 2-picoline concentrations, respectively, with a dose of 15 g/L 303 K, pH_0 of 6.54, and a contact time of 60 min. Adsorption was found to be very quick, and in the initial 5 min of contact time, about 55% of 2-picoline removal was observed. The adsorption equilibrium analysis was also carried out using the isothermal equations of Langmuir and Freundlich. Compared to Langmuir adsorption isotherm, the adsorption data showed reflecting Freundlich isotherm as well. 16.47 mg/g was found to be the highest monolayer adsorption power. Strong potential for removing contaminants from wastewater has been identified by the activated carbon generated from tea waste.

Keywords Tea waste · Adsorption · Adsorbent · Langmuir and Freundlich · 2-picoline · Adsorbent dose

1 Introduction

2-Picoline (α-picoline) is one of the derivatives of pyridine. 2-picoline is a colorless liquid with a strong sour odor, and it is used to avoid ammonia depletion from fertilizers in several agrochemicals and pharmaceuticals. It is also used as a solvent and a raw material for various chemicals in the manufacturing of different polymers,

U. R. Darla · D. Saini · D. H. Lataye (✉)
Department of Civil Engineering, Visvesvaraya National Institute of Technology, Nagpur, Maharashtra 440010, India

B. Laishram and A. Tawalare (eds.), *Recent Advancements in Civil Engineering*, Lecture Notes in Civil Engineering 172,
https://doi.org/10.1007/978-981-16-4396-5_37

textiles, oils, pesticides, medicines, and dyes. Antituberculosis, respiratory stimulants, local anesthetics, and analgesics function as various pyridine derivatives. It is water-soluble and alcohol-ether miscible. When the 2-picoline is exposed to the blaze, the vapors are a fire and explosion. It emits highly radioactive NO_x gases in an oxidative environment when heated for decomposition. It is harmful when in contact with the skin and eye, absorption, and breathing [1–3].

Wastewaters containing 2-picoline are derived from manufacturing units processing of pyridine and its chemical derivatives. Typical 2-picoline concentration in wastewater produced by multidrug intermediate plant processing of pyridine and its chemical derivatives ranges from 20 to 200 mg/L. The concentration will grow considerably during spill episodes. Odor nuisance causes due to multidrug intermediate plants are a cause of odor nuisance, and this strong odor originates either from sewage lines or from storage facilities [4].

For the treatment of wastewater which contains 2-picoline, different treatment strategies such as adsorption [5] and biodegradation [6] may be employed. Adsorption, given that the adsorption procedure is cost-effective, may be the desired treatment method. Tea waste (TW) is a waste material collected from VNIT campus hostels that are tossed down during use as waste. TW requires no costs, except for its processing and transfer to the point of utility. TW has been used for the removal of various pollutants as an adsorbent, owing to its excellent sorption properties by many researchers [7–14].

The characteristics of the adsorbent and the influence of the initial pH of the solution range from 2 to 12, the adsorbent dosage 2–25 g/L, the contact time 0–360 min, the initial 2-picoline concentration 50–500 mg/L, and the temperature 283–323 K of the 2-picoline adsorption on TW have been studied and presented in the following sections.

2 Materials and Methods

2.1 Adsorbate

In the present analysis, all the chemicals used were analytical reagent grade. Upper India Science Company, Nagpur, India, supplied the adsorbate, 2-picoline (Loba Chemie, CAS-109-06-8, formula = C_6H_7N, molecular mass = 93.13 g/mol and λ_{max} = 262 nm). 1000 mg/L concentration of the 2-picoline stock solution was prepared by taking the right amount of 2-picoline and mixed with double-distilled water (DDW), to achieve the desired test concentrations of 2-picoline obtained by successive dilution of stock solution with DDW.

2.2 Adsorbent

Tea waste was collected from hostels in VNIT, Nagpur, washed several times to extract dirt with DDW, and then kept at 378 K for 48 h for oven drying. 1:0.5 proportions (g:ml) of dried tea waste are combined with orthophosphoric acid [H_3PO_4]. This blender was later heated for 1 h in the muffle furnace at 823 K for carbon preparation. The prepared carbon was washed with DDW again for complete acid removal. The expulsion of acid completely from the prepared activated carbon was washed with DDW. In the hot air oven, the washed activated carbon was dried at 378 K for 2–3 h. The proximate analysis of TWAC was conducted using IS 1350 (I), 1984. Using SEM JEOL JSM-6380A, SEM (scanning electron microscopy) of TWAC before and after adsorption was performed.

2.3 Analytical Measurement

UV–VIS spectrophotometer was used for the reading of the residual 2-picoline concentration at the wavelength (λ_{max} = 262 nm) (model: UV-2450, SHIMADZU, Japan). By plotting 2-picoline concentrations versus absorbance, the calibration graph was prepared. The concentrations of 1–0 mg/L, the 2-picoline solutions were prepared, and the absorbances were noted down and the calibration curve was plotted. To calculate the 2-picoline concentration in an uncertain solution, this calibration graph was used. Solutions were diluted and analyzed for higher 2-picoline concentrations (>10 mg//L). All test were conducted in Erlenmeyer flasks of 250 ml.

2.4 Batch Adsorption Study

An experimental batch analysis was conducted to determine the ability of TWAC for aqueous solution adsorption of 2-picoline. The tests were carried out using a 50 ml 2-picoline solution with known concentration and the quantity of adsorbent taken into 250-ml stoppered Erlenmeyer flasks and shook at 150 RPM in an orbital shaker. 0.1 N NaOH and 0.1 N HCl solutions were used to get the necessary initial pH of the 2-picoline solution. To filter the samples, Grade 1 Whatman filter paper was used. The filtrate analysis was conducted with the UV–VIS spectrophotometer at λ_{max} = 262 nm. The depletion of the 2-picoline solution was examined during the trial. No loss of 2-picoline concentration was detected during the experiments. The adsorbed 2-picoline per unit weight of TWAC and the 2-picoline percent extracted were determined using the following equations:

$$\% \text{ Removal} = \frac{(C_0 - C_e)}{C_0} \times 100 \tag{1}$$

$$q_e = \frac{(C_0 - C_e)V}{m} \tag{2}$$

where

C_0 = initial 2-picoline (mg/L) concentration
C_e = 2-picoline equilibrium concentration (mg/L)
m = quantity of TWAC (g)
q_e = quantity of 2-picoline adsorbed by TWAC (mg/g)
V = 2-picoline solution volume (ml).

3 Result and Discussion

3.1 Adsorbent Characterization

The proximate analysis of TWAC was conducted, and the results having moisture content 9.16%, ash 27.52%, volatile matter 15.13%, and fixed carbon 48.15% were found. There is a fair volume of fixed carbon in the adsorbent TWAC, which increases the absorption potential of the adsorbent. TWAC's BET surface area was estimated to be 342.64 m^2/g.

SEM micrographs analyzed the surface morphology of TWAC. Figure 1a shows the uneven and permeable particles of unloaded TWAC that increase the surface adsorption of 2-picoline. Figure 1b shows the 2-picoline TWAC-loaded SEM

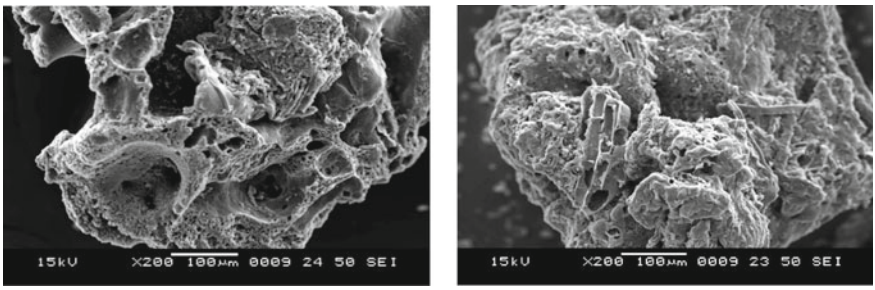

(a) unloaded TWAC (b) TWAC loaded with 2-picoline

Fig. 1 SEM micrographs at 200X magnification, **a** unloaded TWAC, **b** TWAC loaded with 2-picoline

micrograph. It is possible to closely observe the pores filled with 2-picoline molecules, making the surface evener and smoother.

3.2 *Effect of Dose (m) of TWAC*

Adsorption of 2-picoline by TWAC from the aqueous solution was studied using various TWAC doses with an initial 50 mg/L concentration. Figure 2 shows that with the increased dosage of TWAC from 2 to 15 g/L, the percent elimination of 2-picoline was observed to rise steadily (38.4–89.89%). The further increase in the TWAC dosage from 15 to 25 g/L shows a small increment in the adsorption of 2-picoline. With an increase in dose, the 2-picoline adsorption increased due to the existence of a higher number of unoccupied surface spots and a wider surface area. Then again, it decreases with an increase in the dose as a result of site saturation and solid accumulation due to particle–particle interaction [4, 15, 16]. However, there is a marginal improvement in the percentage of reduction after 15 g/L of the TWAC dosage. Thus, the ideal dosage of TWAC is 15 mg/L and upcoming experiments are performed using the same dose.

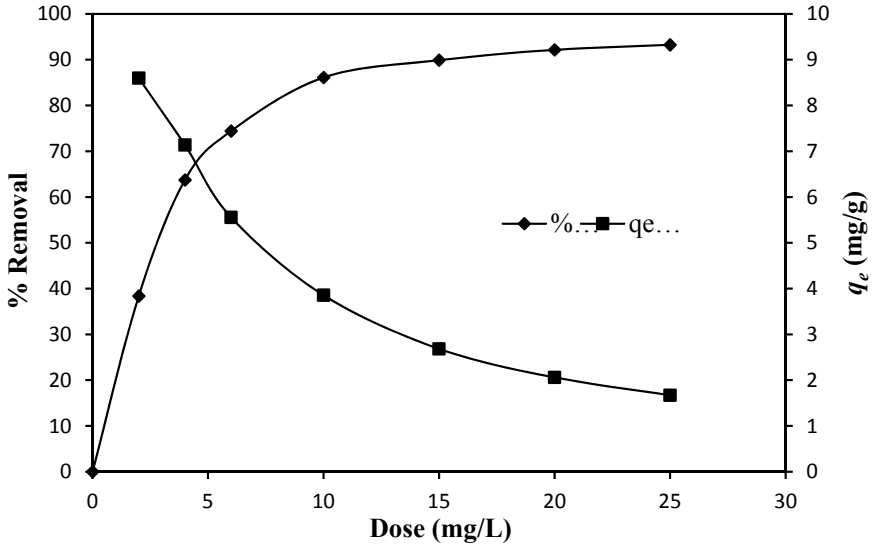

Fig. 2 Effect of TWAC dose on removal of 2-picoline and q_e (initial concentration (C_0) = 50 mg/L, pH = 6.54, time of contact (t) = 60 min, Temperature (T) = 303 K, RPM = 150, volume of sample (V) = 50 ml)

3.3 *Effect of pH_0*

A significant parameter affecting the mechanism of adsorption is the initial pH of the solution. Solution pH_0 influences charge on the adsorbent surface, speciation, and degree of ionization of the solution [17]. The impact of pH_0 on 2-picoline adsorption for C_0 = 50 mg/L with m = 15 g/L was assessed at natural pH and different pH values ranging from 2 to 12 for 1 h contact time at 303 K, and the results are shown in Fig. 3.

It is observed from the pH analysis that more than 83% of the adsorbate is adsorbed at the normal pH after it decreases. The reduction in pH-increasing adsorption is due to ion repulsion.

In the present analysis, the point of zero charge (PZC) has also been tested. The pH at which no charge is borne by the adsorbent surface is known as the point of zero charge. Figure 4 illustrates the surface of TWAC has a PZC of 6.4, and thus, the surface at this pH will behave as neutral. Increasing the pH above 6.4 will make the surface negative and make the surface favorable by reducing the solution pH from 6.4. It is observed that the removal of 2-picoline is greater at pH below PZC.

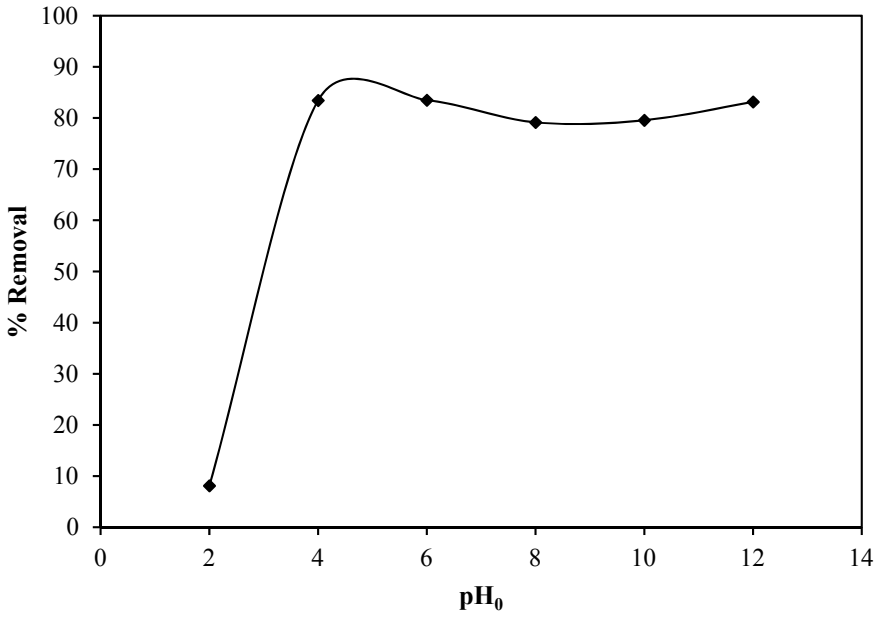

Fig. 3 Effect of initial pH_0 on 2-picoline removal (C_0 = 50 mg/L, V = 50 ml, t = 60 min, RPM = 150, m = 15 mg/L, T = 303 K)

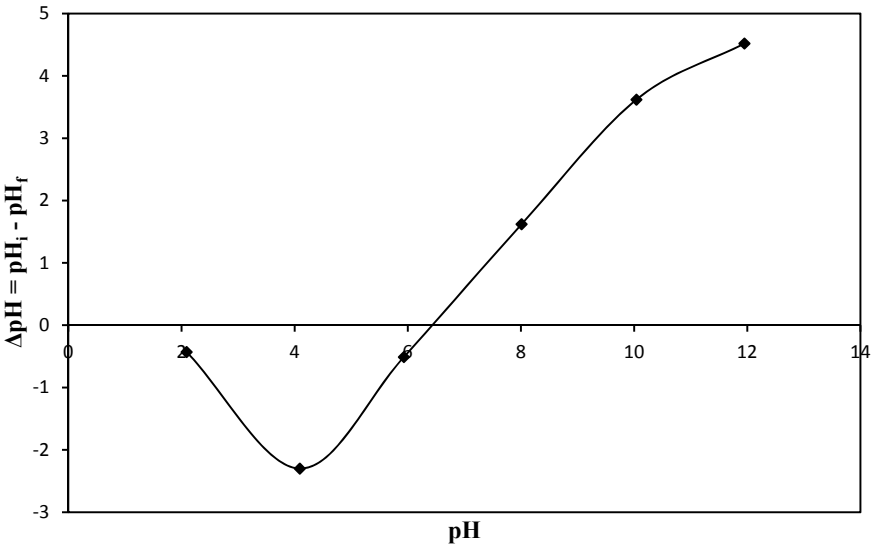

Fig. 4 TWAC point of zero charge in the 0.1 KNO_3 solution

3.4 *Effect of Contact Time (t)*

The purpose of the time analysis is to assess the effect of contact time on the adsorption of 2-picoline and deciding the equilibrium contact time. The effect of contact time studied for C_0 = 50, 100 and 200 mg/L at 303 K and the outcomes are shown in Fig. 5. Due to the presence of more surface sites, 2-picoline removal improves steadily with the contact time initially up to 79% and achieves equilibrium after 60 min. Thus, because of the repulsive force among the 2-picoline on the TWAC surface and that in the solution, certain surface sites remain unoccupied. The research lasted for 360 min, but no substantial improvement in 2-picoline adsorption after 60 min of touch time was found. Therefore, 60 min was known as the touch time of equilibrium. Figure 5 also shows the effect on TWAC of the concentration of 2-picoline on its adsorption.

It is observed that 2-picoline removal decreases at any time with a rising concentration of C_0 (mg/L), but with increasing concentration, the adsorptive potential of q_t (mg/g) increases.

This can be due to the rise in driving force as the solution resistance to 2-picoline molecule adsorption decreases with an increase in the concentration of 2-picoline [18, 19].

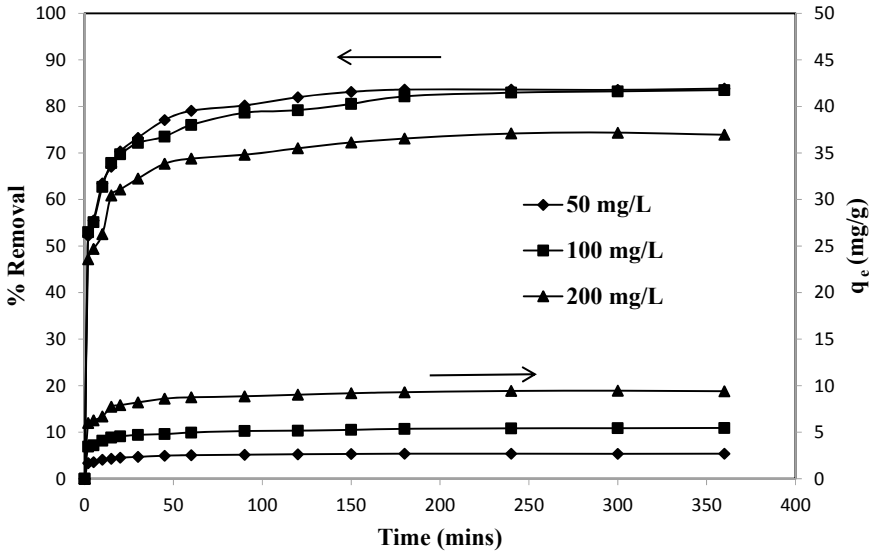

Fig. 5 Contact time effect on 2-picoline removal by TWAC (C_0 = 50 mg/L, 100 mg/L and 200 mg/L, m = 15 g/L, T = 303 K, pH_0 = 6.54, RPM = 150, V = 50 ml)

3.5 *Effect of Initial Concentration (C_0) and Temperature (T)*

The effect of the initial concentration (50 mg/L $\leq$ C_0 $\leq$ 500 mg/L) on the removal and absorption potential of 2-picoline on TWAC along with the temperature (283 K $\leq$ T $\leq$ 323 K) was investigated at a dose of 15 g/L and the contact time of 60 min, and the outcomes are shown in Fig. 6. The outcomes revealed a decline in the removal of 2-picoline with increasing C_0 since TWAC adsorbs a constant volume of 2-picoline at a fixed dose. TWAC adsorptive capacity, i.e., q_e (mg/g), also increases as the C_0 increases as a result of less resistance to 2-picoline mass transfer from the solution. Figure 6 further shows that the adsorption of 2-picoline decreases with the increase in temperature of the solution from 283K to 323K. At high temperature, 2-picoline molecules consist of high kinetic energy which causes very tough to bound on the surface of TWAC.

3.6 *Adsorption Isotherms*

Adsorption equilibrium analysis has been conducted at an equilibrium temperature and time to determine the relationship between 2-picoline adsorbed on TWAC and remaining in solution. By creating a systematic link between equilibrium curves [16], the adsorption mechanism for 2-picoline removal can be optimized.

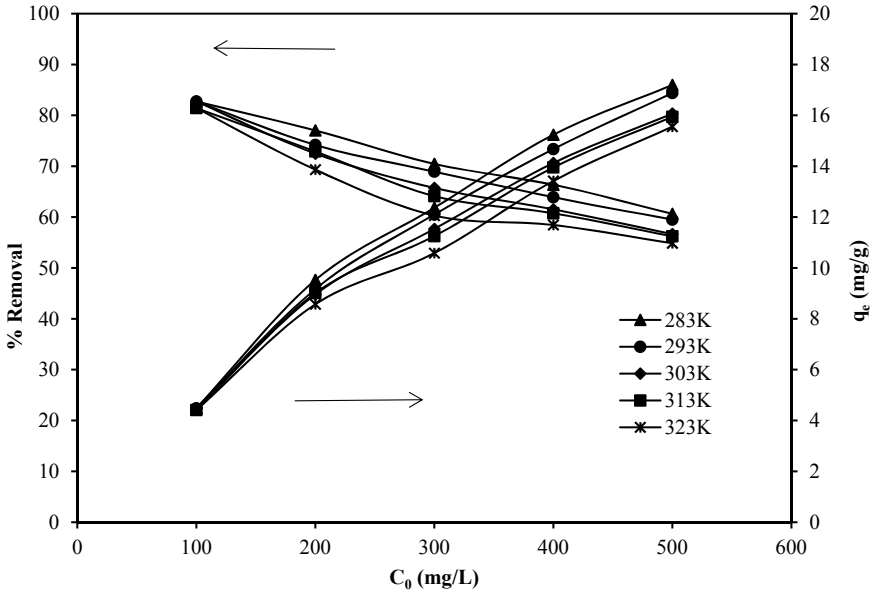

Fig. 6 Concentration and temperature effect on 2-picoline removal and adsorption capacity by TWAC (m = 5 g/L, C_0 = 50–500 mg/L, pH_0 = 6.54, RPM = 150, t = 60 min, V = 50 mL)

Isothermal models such as Langmuir and Freundlich have been researched to resolve equilibrium properties of the phase of adsorption.

The isothermal model of **Langmuir** is given by the equation [20]:

$$\frac{C_e}{q_e} = \frac{C_e}{q_m} + \frac{1}{K_L.q_m} \tag{3}$$

where

C_e = concentration of 2-picoline at equilibrium (mg/L)
K_L = adsorption energy (L/g)
q_e = the sum at equilibrium (mg/g) of 2-picoline adsorbed on TWAC
q_m = maximum capability of adsorption (mg/g) (Fig. 7).

The Langmuir constants were calculated from the above graph as K_L = 0.04 L/g, and the maximal adsorption power was q_m = 16.47 mg/g.

The isothermal model of the **Freundlich** is given by the equation [21]:

$$\ln(q_e) = \frac{1}{n}\ln(C_e) + \ln(K_F) \tag{4}$$

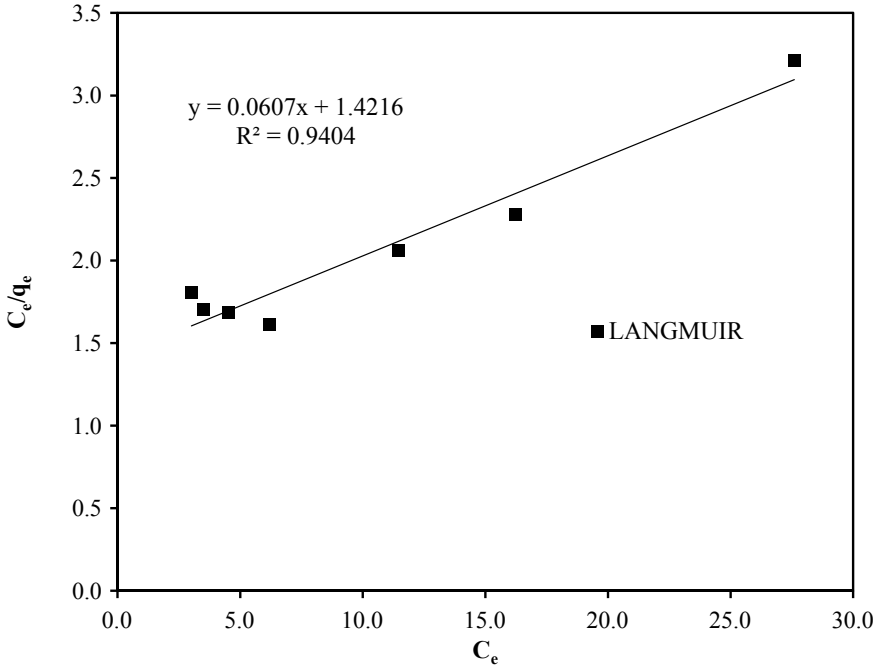

Fig. 7 Langmuir isotherm graph C_e versus C_e/q_e

where

K_F = adsorbent power (L/g)
1/n = adsorption intensity (Fig. 8).

K_F = 0.85 L/g and 1/n = 0.744 were the Freundlich constants obtained from the graph.

4 Conclusions

It can be inferred from the present analysis that tea waste can be used as a cost-effective adsorbent for 2-picoline treatment from the wastewater. Tea waste is an agricultural waste that, if not properly treated, will produce environmental emissions due to its oxidation in the atmosphere. It can then be used as an adsorbent and, by using one waste substance for the disposal of another waste, the world can be preserved. Thus, there is no additional expense for this commodity for tea waste available at the throwaway expense, and therefore, it is very economical relative to activated charcoal. The characteristic analysis of adsorbent showed that TWAC has fixed carbon about 48%, which boosts its effectiveness for the removal of other

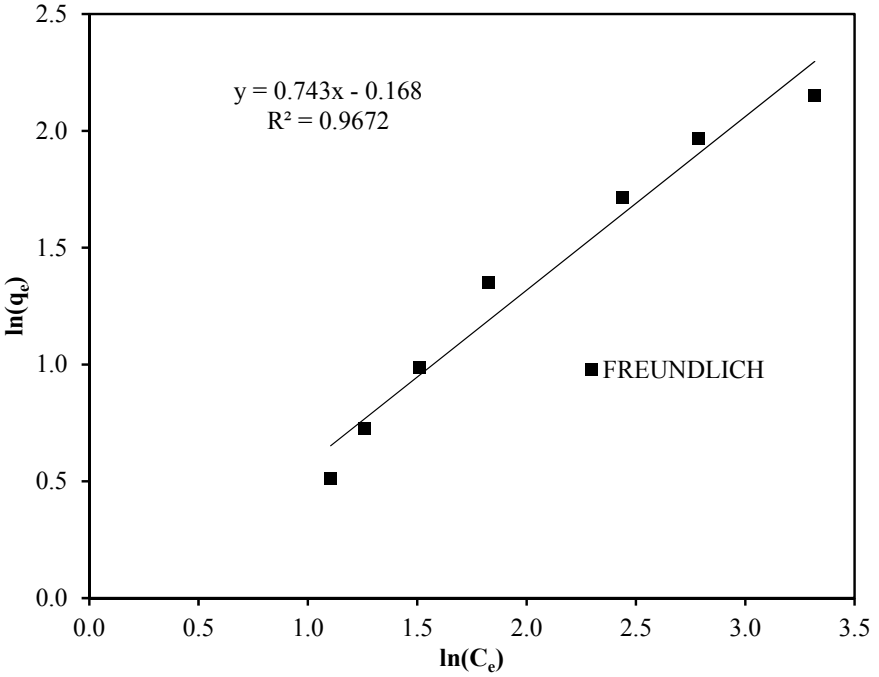

Fig. 8 Freundlich isotherm graph ln C_e versus ln q_e

pollutants from water or wastewater. SEM analysis verified the aqueous solution of 2-picoline adsorption, which revealed that after adsorption there is a change in morphology. The batch adsorption analysis showed that for the concentration of 50 mg/L at 303 K 15 g/L is the optimum dose. For the present analysis, the optimum pH was found to be 6.54. 2-picoline adsorption increases with the solution initial pH increasing. It was found that the equilibrium time for 2-picoline removal was 60 min. For the initial concentration of 50 mg/L and 500 mg/L, the percentage removal and adsorption capacities were 83 percent and 2.64 mg/g and 56% and 16.06 mg/g, respectively. According to the equilibrium analysis, the optimum potential for adsorption is 16.47 mg/g. Compared to the Langmuir equation, the Freundlich isothermal equation was found to describe the adsorption data as well. Therefore, TWAC is cost–cost adsorbent for the removal of 2-picoline and can also be recommended for other hazardous materials as an adsorbent. The effective usage of organic waste has a greater potential for commercial purpose as an adsorbent.

References

1. Yates FS (1984) Pyridine and their benzo derivatives: (vi) applications. In: Katritzky AR, Rees CW (eds) Comprehensive heterocyclic chemistry: the structure, reaction, synthesis and uses of heterocyclic compounds, vol 2, Part 2 A, Chapter 2.09. Pergamon Press, Oxford, pp 511–524
2. Kirk RE, Othmer DF (1968) Pyridine and pyridine derivatives. In: Encyclopedia of chemical technology, 2nd edn, vol 16, pp 780–806
3. Lewis RJ Sr (2004) Sax's dangerous properties of industrial materials, 11th edn. Wiley, Hoboken, New Jersey, p 3106
4. Lataye DH, Mishra IM, Mall ID (2006) Removal of pyridine from aqueous solution by adsorption on bagasse fly ash. Ind Eng Chem Res 45:3934–3943
5. Mohan D, Singh KP, Sinha S, Gosh D (2005) Removal of pyridine derivatives from aqueous solution by activated carbons developed from agricultural waste materials. Carbon 43:680–1693
6. Sims GK, Sommers LE (1985) Degradation of pyridine derivatives in soil. J Environ Qual 14:580–584
7. Abbas MN (2014) Application of used tea leaves for multi functions. Eur Acad Res 2:8660–8690
8. Adachi A, Loku A, Taniyama K, Okano T (2008) Use of tea or coffee lees as adsorbent for removal of benzene from wastewater. J Health Sci 54(4):478–481
9. Ahluwalia SS, Goyal D (2005) Removal of heavy metals by waste tea leaves from aqueous solution. Eng Life Sci 5:158–162
10. Ahmaruzzaman M, Gayatri SL (2010) Activated tea waste as a potential low-cost adsorbent for the removal of p-nitrophenol from wastewater. J Chem Eng Data 55:4614–4623. https://doi.org/10.1021/je100117s
11. Akar E, Altinişik A, Seki Y (2013) Using of activated carbon produced from spent tea leaves for the removal of malachite green from aqueous solution. Ecol Eng 52:19–27. https://doi.org/10.1016/j.ecoleng.2012.12.032
12. Auta M, Hameed BH (2011) Optimized waste tea activated carbon for adsorption of Methylene Blue and Acid Blue 29 dyes using response surface methodology. Chem Eng J 175:233–243. https://doi.org/10.1016/j.cej.2011.09.100
13. Duran C, Ozdes D, Gundogdu A, Imamoglu M, Senturk HB (2011) Tea-industry waste activated carbon, as a novel adsorbent, for separation, preconcentration and speciation of chromium. Anal Chim Acta 688:75–83. https://doi.org/10.1016/j.aca.2010.12.029
14. Lin D, Wu F, Hu Y, Zhang T, Liu C, Hu Q, Hu Y, Xue Z, Han H, Ko TH (2020) Adsorption of dye by waste black tea powder: parameters, kinetic, equilibrium, and thermodynamic studies. J Chem 2020, Article ID 5431046, 13 p. https://doi.org/10.1155/2020/5431046
15. Lataye DH, Mishra IM, Mall ID (2008) Pyridine sorption from aqueous solution by rice husk ash (RHA) and granular activated carbon (GAC): parametric, kinetic, equilibrium and thermodynamic aspects. J Hazard Mater 154:858–870
16. Lataye DH, Mishra IM, Mall ID (2008) Adsorption of 2-picoline onto bagasse fly ash from aqueous solution. Chem Eng J 138:35–46
17. Srivastava VC, Swamy MM, Mall ID, Prasad B, Mishra IM (2006) Adsorptive removal of phenol by bagasse fly ash and activated carbon: equilibrium, kinetics and thermodynamics. Colloids Surf A Physicochem Eng Asp 272:89–104. https://doi.org/10.1016/j.colsurfa.2005.07.016
18. Lataye DH, Mishra IM, Mall ID (2009) Adsorption of α-picoline onto rice husk ash and granular activated carbon from aqueous solution: equilibrium and thermodynamic study. Chem Eng J 147:139–149
19. Lataye DH, Mishra IM, Mall ID (2011) Removal of 4-picoline from aqueous solution by adsorption onto bagasse fly ash and rice husk ash: equilibrium, thermodynamic, and desorption study. J Environ Eng 137:1048–1057

20. Langmuir I (1918) The adsorption of gases on plane surfaces of glass, mica and platinum. J Am Chem Soc 40:1361–1403
21. Freundlich HMF (1906) Over the adsorption in solution. J Phys Chem 57:1100–1107

Evaluation of Groundwater Quality Using Water Quality Index (WQI) in Ambedkar Nagar City, Uttar Pradesh, India

Vijayendra Pratap Dheeraj, Ashwani Kumar Sonkar, and C. S. Singh

Abstract The groundwater is an important natural resource utilized for drinking and many more purposes. The present study is aimed to assess the quality of groundwater using the water quality index (WQI) methods in Ambedkar Nagar district (U.P), India. A total of 10 groundwater samples were collected from ten different areas of Ambedkar Nagar district in November 2018, and samples were analyzed to investigate the suitability of groundwater for domestic purposes. The selection of locations for sampling has been based on a preliminary field survey. Ten groundwater samples were examined for physical and chemical parameters such as pH, electrical conductivity, total dissolved solids, calcium, sodium, magnesium, potassium, bicarbonates, sulfate, nitrate, fluoride, and chloride. The values have been computed and compared with the guideline values for drinking water given by the World Health Organization (WHO). It has been observed that the calculated WQI ranges from 31.2 to 64.3 which represents excellent to good and good to the poor category of groundwater quality of studied areas. The high value of WQI is due to higher concentrations of electrical conductivity (EC), bicarbonate (HCO_3^-), and total dissolved solids (TDS) in the groundwater samples at some of the selected locations. The result shows that the groundwater at few locations required minor treatment before the consumption.

Keywords Physicochemical parameters · Groundwater quality · Water quality index (WQI) · Major ions chemistry

V. P. Dheeraj (✉) · A. K. Sonkar · C. S. Singh
Department of Mining Engineering, Indian Institute of Technology (BHU), Varanasi, India
e-mail: vijayendrapdheeraj.rs.min19@itbhu.ac.in

A. K. Sonkar
e-mail: aksonkar.rs.min14@itbhu.ac.in

C. S. Singh
e-mail: cssingh.min@itbhu.ac.in

B. Laishram and A. Tawalare (eds.), *Recent Advancements in Civil Engineering*, Lecture Notes in Civil Engineering 172,
https://doi.org/10.1007/978-981-16-4396-5_38

1 Introduction

Groundwater is a foremost source of water which fulfills many human, agricultural, and industrial needs, Ahn and Chon [1]. The assessed source of contamination in the groundwater is the anthropogenic source, and the main pollutants present in groundwater are calcium, nitrate, hardness, fluoride, arsenic, etc.; therefore, it is very essential to analyze the groundwater quality along with its quality and quantity for different activity, Singhal et al. [2]. The main source of water supply for different purposes like drinking, agriculture, and industries is groundwater, only in an arid and semi-arid regions in many of the countries of world. The groundwater is used for drinking about 65%, for irrigation and livestock 20%, and about 15% is used for mining and industry, Saeid et al. [3]. According to UNEP and Adimalla [4, 5], about one-third population of the world directly depends on groundwater only for drinking purposes. Especially, in emerging and populated countries like India and China, groundwater plays a crucial role. There are few particular regions for hang on groundwater such as rapid growth of human population, increasing agriculture and commercial sectors, and scarcity of surface water and resulting in exploitation of groundwater for drinking and also for other purposes; therefore, it needed to monitor the groundwater quality and quantity, Adimalla and Li, Singh et al. [6, 7]. Rapid and uncontrolled urbanization, industrialization, and irrigations are being the cause of more quantity of wastewater generation, Mahvi et al. [8]. Therefore, the contamination in the groundwater, quality of water for drinking and irrigation, and occurrence and distribution of geochemical have been widely studied around the world, Narsimha, Khan, Abd El-Aziz, Adimalla, He, and Zhang Li [9–16]**.** A study has been carried out on geochemistry and groundwater in north Jordan; it has been found that the groundwater contamination has been increased due to poor drainage situation, huge agriculture activities, and more sewage system, Abboud [17]. Anthropogenic activities, as well as evaporation, are the main affecting factors to groundwater in the north-western area of Libya, Abd El-Aziz [11]. However, India is the largest user of groundwater in the world. The estimated use of groundwater by India is about 250 billion m^3/year, which is larger than a quarter of total global utilization. It has also been estimated that >60% of groundwater is used in agriculture and 85% of drinking from groundwater; thus, it has been cleared that groundwater is a prime source for rural areas in India, AQUASTAT and Sishodia [18, 19]. However, groundwater's more exploitation is one major problem in many regions of the world. Moreover, India is also one of them. Therefore, it is needed to assess and monitor the groundwater at a certain interval of time where the population is more and industries are at high demand.

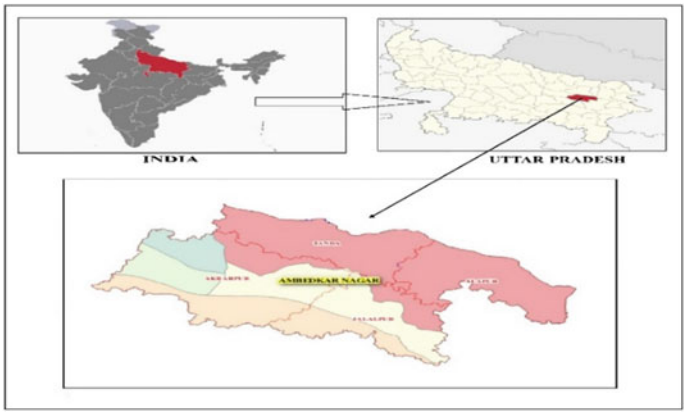

Fig. 1 Study area map of Ambedkar Nagar district

2 Study Area

Ambedkar Nagar district is situated in Faizabad division, Uttar Pradesh, India. It has been established in 1995. Ambedkar Nagar district is situated on the north-eastern part of Uttar Pradesh. Ambedkar Nagar lies between 26° 09' N to 26° 40' N latitudes and 82° 12' E to 83° 05' E longitudes. It bounded on the north-east by Gorakhpur and west by Faizabad. The total Ambedkar Nagar district length from east to west is about 75 km and 42 km north to south width as shown in Fig. 1.

Alluvial soil was found in this area. Ambedkar Nagar forms a part of the central Ganga basin and main river is Sarayu located at the northern boundary of the district. The climates of the region were classified in three seasons, i.e., cold (November–February), hot (March–mid-June), and rainy weather season (mid-June–October). The maximum and minimum temperatures recorded in study areas are 32.15 °C and 8.95 °C https://en.wikipedia.org/wiki/Ambedkar_Nagar_district [20].

3 Materials and Methods

3.1 Sampling Procedure and Laboratory Analysis of Water Samples

The selection of locations is the very initial step, in which a total 10 number of locations were selected after the preliminary survey. The selected sites for analyzes are Railway Station, Akbarpur, REC Engg. College, NTPC Tanda, Baskhari, Shahzadpur, Shiv Baba Temple, Government Medical College, Iltfatganj, MKR Awas, Eklavya Stadium—inside and its exact coordinates in the form of latitudes

and longitudes are also given in Table 1. The map of all selected locations is shown in Fig. 2 which has been taken by satellite view.

The groundwater samples were collected in polyethylene bottles having the 1-L capacity, and it was acidified with nitric acid to a pH below 2. The bottles were marked with the name and date of samples after sampling. The groundwater samples were collected in November 2018 from the ten different selected sampling sites. The following physical and chemical parameters were calculated like TDS, pH, EC, some major cations like Ca^{2+}, Mg^{2+}, Na^{+}, K^{+} and major anions like

Table 1 Details of groundwater samples locations with its coordinates

Sample code	Sampling stations	Latitude (N)	Longitude(E)
GW-1	Railway Station, Akbarpur	26°25′45.21”	82°32′24.02”
GW-2	REC, Ambedkar Nagar Campus	26°27′17.12”	82°33′38.76”
GW-3	NTPC Tanda	26°35′19.5”	82°36′1.08”
GW-4	Baskhari—Kurki Bazar	26°27′9.07”	82°46′52.52”
GW-5	Shahzadpur—Fountain Tiraha	26°24′41.9”	82°32′47.64”
GW-6	Katehari—Shiv Baba Temple	26°27′47.08”	82°29′29.9”
GW-7	Govt.Medical College	26°24′19.92”	82°34′10.77”
GW-8	Iltefatganj—Ghaghra River Bank	26°36′36.25”	82°33′26.14”
GW-9	MKR Awas—Main Road	26°27′39.88”	82°33′28.54”
GW-10	Eklavya Stadium—Inside	26°26′32.21”	82°34′38.36”

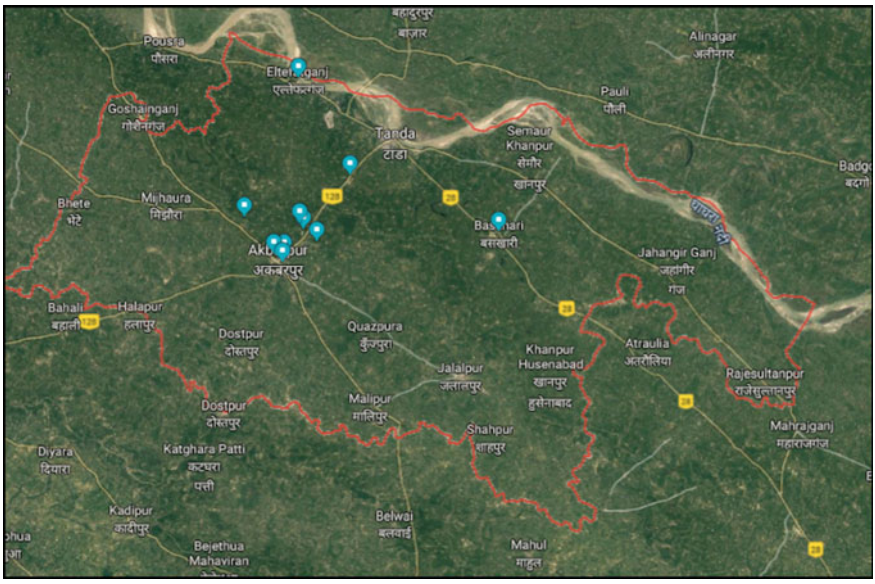

Fig. 2 Map showing the sampling stations

HCO_3^-, SO_4^{2-}, NO_3^-, Cl^-, F^- by the standard procedure to assess the quality of groundwater.

3.2 Estimation of Water Quality Index (WQI)

Water quality index (WQI) means to assess the quality of water at certain time and locations based on some physicochemical parameters. WQI is an effective tool for estimating the overall groundwater quality for drinking purposes only with some physicochemical parameters (like TDS, pH, EC, some major cations like Ca^{2+}, Mg^{2+}, Na^+, K^+, and major anions like HCO_3^-, SO_4^{2-}, NO_3^-, Cl^-, F^-).

Some researchers have done their study on the WQI based on relative methods, Deshmukh, Misaghi, Acharya, and Boufekane [21–24]. As per IS standard [25, 26], it has been recommended for drinking purpose. As per IS standard [25, 26], it has been used for calculating the water quality index (WQI) which includes four important steps.

In the first step, all parameters like TDS, pH, EC, some major cations like Ca^{2+}, Mg^{2+}, Na^+, K^+, and major anions like HCO_3^-, SO_4^{2-}, NO_3^-, Cl^-, F^- have been assigned weight (W_i) from 1 to 5 based on its significance.

In the second step, the relative weight (W_r) of water quality parameter has been calculated as follows:

$$W_r = \frac{W_{ai}}{\sum_{i=1}^{n} W_{ai}}$$

where W_{ai} = definite weight of each parameter W_r = relative weights, Sharma [27], and n = number of parameters considered for the WQI.

In the third step, the quality rating scale (Q_i) has been calculated. It is a ratio of measured concentration to a standard concentration of each parameter as per guideline given by "as per IS standard [25, 26]"; then, result is multiplied by 100 as given below:

$$Q_i = \frac{C_i}{S_i} \times 100$$

where

C_i = measured concentrations of each parameters (mg/l),
Q_i = quality rating scale, and
S_i = standard concentrations of each parameter milligram/liter (mg/l) as per drinking water guideline [25, 26], but Q_i in case of pH has been computed by

$$Q_{\mathrm{i}}\ \mathrm{pH} = [(C_i - V_i)/(S_i - V_i)] \times 100$$

where V_{i} = ideal value for pH = 7.

In the fourth step, the sub-indices (SI) have been computed for deriving the WQI as:

$$\mathrm{SI_i} = W_{\mathrm{r}} \times Q_{\mathrm{i}}$$

WQI value has been calculated by summation of all sub-indices values for each location as given by

$$\mathrm{WQI} = \Sigma \mathrm{SI_i}$$

The computed WQI values were classified according to Ramakrishnaiah and Yadav [28, 29].

4 Results and Discussion

Total 10 number of water samples have been collected from ten different sites. As per sources availability of ground water, the sample of water was collected from hand pump from the decided locations in the month of November during post-monsoon season. For the assessment of ground water suitability for drinking purpose, total twelve physical and chemical parameters like TDS, pH, EC, some major cations like Ca^{2+}, Mg^{2+}, Na^{+}, K^{+}, and major anions like HCO_3^{-}, SO_4^{2-}, NO_3^{-}, Cl^{-}, F^{-} were determined as given in Table 4. It was found that some of the parameters like TDS, EC, and bicarbonate have exceeded their desirable limits as per guideline for drinking water "as per IS standard [25, 26]" shown in Table 5. High EC indicates more chemicals dissolved in water sample, and rest of the parameters like major cations, sodium, potassium, calcium, magnesium and major anions like fluorides, chloride, nitrate, and sulfate have been laid within its desirable limits as per suggested guideline "as per IS standard [25, 26]" shown in Table 5. Electrical conductivity was computed which ranges from 438.4 to 940.6 (μS/cm) with its mean value of 695.86 (μS/cm) as shown in Table 5 in which 100% of water sample have exceeded maximum desirable limits. The suggested guideline value of as per IS standard [25, 26] for EC is 250 (μS/cm). Total dissolved solid (TDS) concentrations have been computed and range from 310.4 to 756.6 (mg/l) with an average value of 513.7 (mg/l) as given in Table 5. About 50% of water samples have been laid within its permissible limits, and rest 50% of water samples exceeded the maximum desirable limits. The high level of TDS in water sample

represents concentrations of chloride, potassium, and sodium ions. pH concentrations range from 7.1 to 8.1 with its mean value of 7.4 as given in Table 5. About 100% of water samples have been laid within its maximum permissible limits as per suggested guideline suggested by "as per IS standard [25, 26]."

4.1 Major Ions Chemistry

The physicochemical parameters of the groundwater samples have been statistically analyzed, and the results are given in Table 4. It was found that the major dominant cation is calcium, while bicarbonate is in the major anion. The mean abundance order of major cations and anions are $Ca^{2+} > Mg^{2+} > Na^{+} > K^{+}$ and $HCO_3^{-} > Cl^{-} > SO_4^{2-} > NO_3^{-}$, respectively. The fluoride (F^{-}) concentration was showing a very less percentage of contribution in major anions; therefore, it has been neglected. The concentration of bicarbonate (HCO_3^{-}) is in the range of 163–320 (mg/l) with its mean value of 224.2 (mg/l) as given in Table 4.

About 60% of water samples lie within its permissible limits, and rest 40% water samples exceed its desirable limits as guidelines suggested by "as per IS standard [25, 26]" shown in Table 5. About 30% of water samples exceeded its maximum desirable limit, and rest 70% of water samples are lying within its maximum desirable limit. The maximum desirable limit of bicarbonate is 200 mg/l as per "as per IS standard [25, 26]." The mean abundance of bicarbonate is 69% in major anions and 48% mean abundance of calcium in major cations. The percentage contributions of individual cations and anions in groundwater samples of the study area in Ambedkar Nagar are shown in Fig. 3. The concentrations of physicochemical parameters in the form of minimum, mean, and maximum values have been presented by box–whisker plots as shown in Fig. 4. In this box–whisker plots, the highest value of bicarbonate ion is 320 mg/l and the lowest value of fluoride is 0.2 mg/l.

Fig. 3 Percentage contribution of major cations and anion

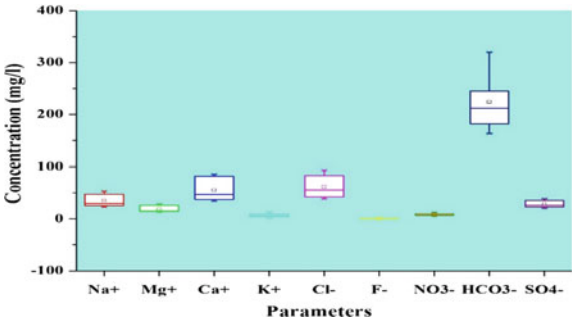

Fig. 4 Box plots of physicochemical parameters

4.2 Water Quality Index (WQI) of the Study Area

It has been observed based on experimental and calculated values of water quality index (WQI) that the calculated water quality index of all selected locations varies from 31.2 to 64.3 with its mean value of 47.6 as shown in Fig. 5. It represents excellent to good water quality according to Ramakrishnaiah [28] but good to poor water quality according to Yadav [29].

The minimum value (31.2) of WQI has been calculated at GW-1 which shows excellent water quality, and maximum WQI value (64.3) at WG-8 has been calculated which shows good water quality according to Ramakrishnaiah [28] as given in Table 2, but according to Yadav [29], it is lying within good to poor water quality category as given in Table 3. Here, it was observed that 60% of water quality found in the category of "excellent," and 40% of water samples showed good water quality which is good for drinking as specified by Ramakrishnaiah [28]. About 60% of water quality found in the category of "good," and the rest of 40% of water samples showed poor water quality and needs some treatment before consumption as per Yadav [29]. The details of the WQI calculation of the mean concentration of groundwater samples have been given in Table 5.

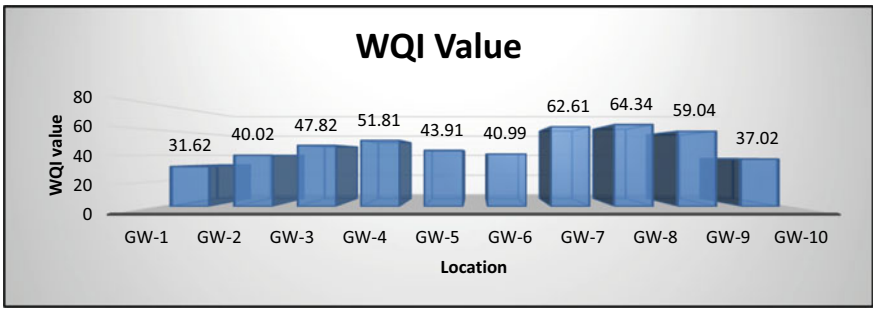

Fig. 5 WQI values variations in November 2018

Table 2 Water quality classification based on WQI value classification as per [28]

SI. No.	WQI value	Water quality	No. of samples	% of sample
1	<50	Excellent	6	60%
2	50–100	Good	4	40%
3	100–200	Poor	Nil	Nil
4	200–300	Very poor	Nil	Nil
5	>300	Unsuitable	Nil	Nil

Table 3 Water quality classification based on WQI value classification as per Yadav [29]

SI. No.	WQI value	Water quality	No. of samples	% of sample
1	0–25	Excellent	Nil	Nil
2	26–50	Good	6	60%
3	51–75	Poor	4	40%
4	76–100	Very poor	Nil	Nil
5	>100	Unsuitable	Nil	Nil

5 Conclusion

It was observed that some of the parameters like electrical conductivity (EC), total dissolved solid (TDS), and bicarbonates (HCO_3^-) are more than their maximum desirable limit in November 2018. It may be attributed many ions present in water samples in the study area. It has also been noticed that a significant decreasing water quality of groundwater through two different classifications. According Ramakrishnaiah [28] classification, groundwater samples belong to excellent to good category of water quality, but according to Yadav [29] classification, the groundwater sample shows good to poor category of water quality. On the basis of calculated WQI values, it is concluded that purification of groundwater of some selected locations is necessary for drinking purposes and domestic uses.

Table 4 Analytical data of groundwater samples and WQI values in November 2018

Sample code	pH	TDS	EC	Na^+	Mg^{2+}	Ca^{2+}	K^+	Cl^-	F^-	NO_3^-	HCO_3^-	SO_4^{2-}	WQI
GW-1	7.1	342.4	438.4	25.3	13.4	37.3	3.7	38.4	0.3	6.8	192	21.3	31.2
GW-2	7.3	431.7	571.3	31.3	15.3	47.4	4.6	55.4	0.3	7.5	223	26.3	39.48
GW-3	7.8	545.6	601.3	27.4	17.1	48.6	8.1	57.4	0.4	8.1	212	27.5	47.82
GW-4	7.5	549.4	801.2	37.3	20.4	51.3	6.1	65.3	0.5	8.2	245	36.2	51.81
GW-5	8.1	347.3	720.4	25.6	13.6	37.4	7.2	42.4	0.4	6.3	182	20.6	43.04
GW-6	7.2	441.3	551.1	29.8	14.7	46.1	4.3	55.4	0.6	7.6	242	25.9	40.59
GW-7	7.7	756.6	590.7	53.4	28.3	85.4	12.2	93.5	0.8	12.6	283	35.5	62.61
GW-8	7.3	731.4	930.3	52.3	27.8	82.3	10.2	87.3	0.6	9.8	320	38.4	64.34
GW-9	7.1	680.4	940.6	47.8	26.3	83.4	9.3	83.3	0.6	9.6	180	32.5	59.04
GW-10	7.2	310.4	812.4	23.4	14.5	34.5	1.9	39.4	0.2	5.3	163.0	23.4	36.4
Min	7.2	310.4	812.4	23.4	14.5	34.5	1.9	39.4	0.2	5.3	163	23.4	36.4
Max	7.1	342.4	438.4	25.3	13.4	37.3	3.7	38.4	0.3	6.8	192	21.3	31.2
AM	7.3	431.7	571.3	31.3	15.3	47.4	4.6	55.4	0.3	7.5	223	26.3	39.48

*All the parameters are expressed in (mg/l) except pH and EC (μS/cm)

**Min—minimum, Max—Maximum, AM—Arithmetic mean

Table 5 Statistical summary of standard values suggested by [25, 26] and calculation of WQI of groundwater

Physicochemical parameters	Mean measured concentration (C_i)	BIS standard (10,500–2012)		Assign weight (W_a)	Standard values (S_i)	Relative weight (W_r)	Ideal values (V_i)	Quality rating scale (Q_i)	Sub-indices (SI_i)
		Maximum desirable	Highest permissible						
pH	7.1	6.5–8.5	7.0–8.5	4	8.5	0.10	7	6.67	0.67
TDS	310.4	500	2000	5	500	0.13	0	62.08	7.76
EC	438.4	250	800	4	500	0.10	0	87.68	8.77
Na +	23.4	50	200	2	200	0.05	0	11.70	0.59
Mg^{2+}	13.4	30	100	1	50	0.03	0	26.80	0.67
Ca^{2+}	34.5	75	200	2	75	0.05	0	46.00	2.30
K^{+}	1.9	15	–	2	200	0.05	0	0.95	0.05
Cl^{-}	38.4	250	1000	3	250	0.08	0	15.36	1.15
F^{-}	0.2	1.0	1.5	5	1.5	0.13	0	13.33	1.67
NO_3^{-}	5.3	45	100	5	45	0.13	0	11.78	1.47
HCO_3^{-}	163	200	600	3	500	0.08	0	32.60	2.45
SO_4^{2-}	20.6	200	400	4	250	0.10	0	8.24	0.82
WQI				40		1.00			28.36 (E&G)

References

1. Ahn HI, Chon HT (1999) Assessment of groundwater contamination using geographic information systems. Environ Geochem Health 21:273–289
2. Singhal DC, Israil M, Sharma VK, Kumar B (2010) Evaluation of groundwater resource and estimation of its potential in Pathri Rao watershed, district Haridwar (Uttrakhand). Curr Sci 98 (2):162–170
3. Saeid S, Chizari M, Sadighi H, Bijani M (2018) Assessment of agricultural groundwater users in Iran: a cultural environmental bias. Hydrogeol J 26(1):285–295. https://doi.org/10.1007/s10040-017-1634-9
4. UNEP (1999) Global environment outlook 2000. Earthscan, UK
5. Adimalla N, Venkatayogi S (2018) Geochemical characterization and evaluation of groundwater suitability for domestic and agricultural utility in semi-arid region of Basara, Telangana State, South India. Appl Water Sci 8, 44. https://doi.org/10.1007/s13201-018-0682-1
6. Adimalla N, Li P (2019) Occurrence, health risks, and geochemical mechanisms of fluoride and nitrate in groundwater of the rock-dominant semi-arid region, Telangana State, India. Human Ecol. Risk Assess 25(1–2):81–103. https://doi.org/10.1080/10807039.2018.1480353
7. Singh K, Hundal HS, Singh D (2011) Geochemistry and assessment of hydrogeochemical processes in groundwater in the southern part of Bathinda district of Punjab, northwest India. Environ Earth Sci 64(7):1823–1833. https://doi.org/10.1007/s12665-011-0989-9
8. Mahvi AH, Nouri J, Babaei AA, Nabizadeh R (2005) Agricultural activities impact on groundwater nitrate pollution. Int J Environ Sci Technol 2(1):1–47
9. Narsimha A, Sudarshan V (2013) Hydrogeochemistry of groundwater in Basara area, Adilabad district, Andhra Pradesh. India J Appl Geochem 15(2):224–237
10. Khan R, Jhariya DC (2017) Groundwater quality assessment for drinking purpose in Raipur city, Chhattisgarh using water quality index and geographic information system. J Geol Soc India 90:69–76. https://doi.org/10.1007/s12594-017-0665-0
11. Abd El-Aziz SH (2017) Evaluation of groundwater quality for drinking and irrigation purposes in the north-western area of Libya (Aligeelat). Environ Earth Sci 76:147. https://doi.org/10.1007/s12665-017-6421-3
12. Adimalla N, Venkatayogi S (2018) Geochemical characterization and valuation of groundwater suitability for domestic and agricultural utility in semi-arid region of Basara, Telangana State, South India. Appl Water Sci 8:44. https://doi.org/10.1007/s13201-018-0682-1
13. He X, Wu J, He S (2018) Hydrochemical characteristics and quality evaluation of groundwater in terms of health risks in Luohe aquifer in Wuqi County of the Chinese Loess Plateau, northwest China. Hum Ecol Risk Assess https://doi.org/10.1080/10807039.2018.1531693
14. He S, Wu J (2018) Hydrogeochemical characteristics, groundwater quality and health risks from hexavalent chromium and nitrate in groundwater of Huanhe Formation in Wuqi County, northwest China. Expo Health. https://doi.org/10.1007/s12403-018-0289-7
15. Zhang Y, Wu J, Xu B (2018) Human health risk assessment of groundwater nitrogen pollution in Jinghui canal irrigation area of the loess region, northwest China. Environ Earth Sci 77(7):273
16. Li P, Wu J, Tian R, He S, He X, Xue C, Zhang K (2018) Geochemistry, hydraulic connectivity and quality appraisal of multilayered groundwater in the Hongdunzi coal Mine, northwest China. Mine Water Environ 37(2):222–237
17. Abboud IA (2018) Geochemistry and quality of groundwater of the Yarmouk basin aquifer, north Jordan. Environ Geochem Health 40(4):1405–1435. https://doi.org/10.1007/s10653-017-0064-x
18. AQUASTAT (2010) Water resources development and management service. Food and agriculture organization of the United Nations, Rome, Italy. Available at: http://www.fao.org/nr/water/aquastat/main/index.stm. Accessed on 27 March 2015

19. Sishodia RP, Shukla S, Graham WD, Wani SP, Garg KK (2016) Bi-decadal groundwater level trends in a semi-arid south indian region: declines, causes and management. J Hydrol: Reg Stud 8:43–58. https://doi.org/10.1016/j.ejrh.2016.09.005
20. https://en.wikipedia.org/wiki/Ambedkar_Nagar_district
21. Deshmukh Keshav K, Sainath P, Aher (2016) Assessment of the impact of municipal solid waste on groundwater quality near the sangamner city using gis approach. Water resources management. https://link.springer.com/article/https://doi.org/10.1007/s11269-016-1299-5
22. Misaghi F, Delgosha F, Razzaghmanesh M, Myers B (2017) Introducing a water quality index for assessing water for irrigation purposes: a case study of the Ghezel Ozan River. Sci Total Environ 589:107–116
23. Acharya SK, Sharma SV (2018) Assessment of groundwater quality by water quality indices for irrigation and drinking in South West Delhi, India. Data Brief 18:2019–2028. https://doi.org/10.1016/j.dib.2018.04.120
24. Boufekane A, Saighi O (2018) Application of groundwater vulnerability overlay and index methods to the Jijel plain (Algeria). Gr Water 56:143–156
25. BIS (2012) Indian standard specification for drinking water (IS 10500: 2012).
26. Bailey JC (1977) Fluorine in granitic rocks and melts—a review. Chem Geol 19(1):1–42
27. Sharma P et al (2013) Changes in water quality index of Ganges River at different locations in Allahabad, sustainability of water quality and ecology
28. Ramakrishnaiah R et al (2009) Assessment of water quality index for the ground water in Tumkur Taluk, Karnataka State, India. E-J Chem 6(2):523–530, ISSN: 0973-4945
29. Yadav AK, Khan P, Sharma SK (2010) Water quality index assessment of groundwater in Todaraisingh Tehsil of Rajasthan State, India—a greener approach. J Chem 7:S428–S432

Performance Evaluation of Electrocoagulation with Hybrid Electrodes in the Decolourisation of Methyl Orange Dye

Anjali Cletus, S. Athira, Anjana G. Ramesh, K. L. Priya, and M. S. Indu

Abstract The study evaluated the influence of electrode characteristics in electrocoagulation (EC) of textile dye wastewater. Methyl orange, an azo dye, has been utilized for the study to represent textile dye. The performance of stainless steel and aluminium electrodes under different electrode configurations was studied keeping other parameters like temperature, interelectrode distance, depth of immersion, current and voltage, volume of the sample and pH as constants. Perforated electrodes of anodes arranged as concentric circles within the cathode were adopted for the study. Under the various configurations of aluminium (Al) and stainless steel (SS) electrodes as anode and cathode, Al-SS-SS-Al showed the maximum colour removal efficiency (CRE) of 98%. But the froth generated and material degradation on using aluminium electrodes have resulted in selecting SS-SS-SS-SS (95% of CRE) as the optimized geometric arrangement which generated comparatively less greasy sludge (by volume) and material consumption. Considering the ease of handling the sludge, efficiency and economy, the combination of stainless steel was identified to be the optimum configuration. The reaction time was optimized to 30 min for maximum CRE. Energy consumption for EC process using perforated stainless steel electrodes under given operating condition was estimated to be 5KWh/m^3. The amount of metal dissolved and deposited with time passage for the same was estimated using theoretical equations as per Faraday's law as 0.107 g of M cm^{-2}.

Keywords Textile dye · Methyl orange · Electrocoagulation · Electrode combination

A. Cletus · S. Athira (✉) · A. G. Ramesh · K. L. Priya · M. S. Indu
TKM College of Engineering, Kollam, Kerala, India

B. Laishram and A. Tawalare (eds.), *Recent Advancements in Civil Engineering*, Lecture Notes in Civil Engineering 172,
https://doi.org/10.1007/978-981-16-4396-5_39

1 Introduction

The wastewater generated from textile industries poses serious environmental problems, as they contain toxic pollutants as well as due to the colour that inhibit aquatic life [1]. Azo dyes are one of the widely used dyes in textile industries. They are organic in nature and are recalcitrant and less biodegradable. About 10–50% of the dyes are released through the effluent and reach aquatic bodies. Due to their toxicity, dyes are categorized as offensive and can cause skin irritation and have carcinogenic effect. Some of the techniques used for colour removal from textile wastewater include adsorption, coagulation–flocculation, oxidation, enzymatic discoloration, microbial degradation, ozonation.

Electrochemical methods are recently being getting attention due to their improved efficiency, ease in operation and better reaction control. Among the electrochemical treatment methods, electrocoagulation is gaining acceptance owing to its simplicity in operation and efficient performance [2]. In this process, the coagulant is generated in situ through electrolytic oxidation of anode material.

The metallic ions released from the anode combine with hydroxide ion released at the cathode to form the coagulant, which agglomerates with the fine impurities present in wastewater to form flocs. These flocs are removed by either by flotation or sedimentation. Thus, the major reactions that take place during the process include electrolytic reactions at the electrode, formation of electron-driven coagulants and adsorption of pollutants onto hydroxyl complexes and removal by sedimentation or floatation. The performance of the electrocoagulation process is influenced by several factors including characteristics of wastewater, operating parameters and electrode characteristics. Most of the studies have focussed on the optimization of operating parameters. The electrode characteristics such as electrode geometry, arrangement of electrodes, electrode material all have a significant role in the treatment efficiency. Thus, the present study investigates the effect of electrode material and combination in the colour removal of methyl orange dye. The influence of aeration and mechanical stirring on the removal efficiency is also studied.

2 Materials and Methods

Batch electrocoagulation studies were carried out for 3 L synthetic dye solution with magnetic stirrer arrangement. Synthetic dye solution of 50 ppm was prepared. NaCl was added to the sample at 1000 mg/L for increasing the conductivity of the sample. Current and voltage of 2A and 15 V were introduced into the solution using DC power supply and were maintained in all the experiments. The electrodes used were perforated ones and arranged in concentric circles kept at an interelectrode distance of 2.5 cm [3].

Stainless steel (SS) and aluminium (Al) were chosen as the electrode materials. Five combinations of electrode arrangement, i.e. AL-SS-SS-AL, SS-SS-SS-SS,

AL-AL-SS-SS, AL-AL-AL-AL, AL-SS-AL-SS, SS-AL-SS-AL, were selected (Fig. 1c). For the optimum combination of electrodes, experiments were performed with perforated electrodes and electrodes made of mesh. A comparative study between linear arrangement and concentric cylindrical arrangement was also carried out. Samples were analysed for pH, EC, CRE before and after the experiments. pH was measured using a pH probe, EC using water quality analyser and CRE measurements were carried out spectrophotometrically after closed reflux digestion. Weight of the electrodes before and after electrocoagulation was noted. The above procedure was done for various combinations of stainless steel and aluminium electrodes. The electrical energy consumed over the entire period of reaction time along with the amount of material degraded with the passage of time was estimated using Eqs. 1 and 2, respectively.

$$\mathrm{Ce} = \frac{U\ x\ i\ x\ t}{V} \tag{1}$$

where Ce is the energy consumption (Wh/m^3), U is the electric potential difference applied in the system (V), i is the electrical current applied (A), t is the application time (h), V is the volume of effluent treated (m^3). The quantity of electrode material dissolved can be obtained from:

$$W = \frac{i\ x\ t\ x\ M}{n\ x\ F} \tag{2}$$

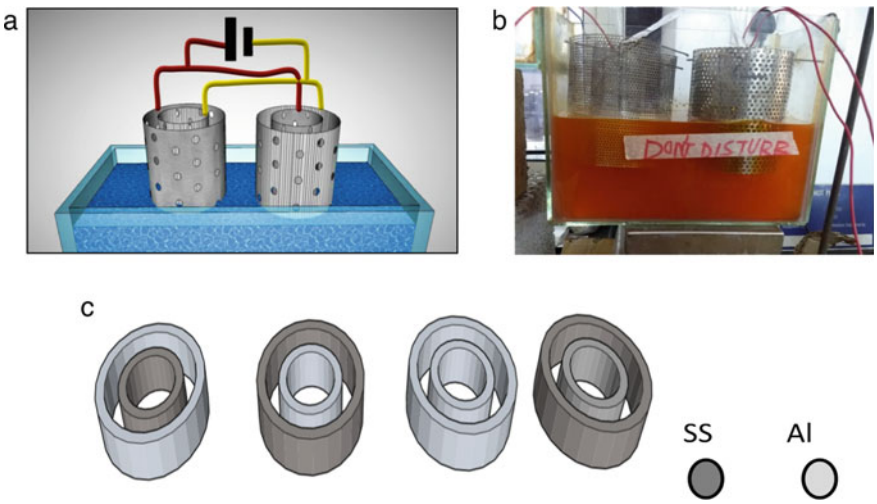

Fig. 1 **a** Experimental set-up of the electrocoagulation reactor, **b** photograph of the experimental set-up, **c** electrode combinations adopted for the study

where W is the quantity of electrode material dissolved (g of M cm^{-2}), i is the current density (A cm^{-2}), t is the time in seconds, M is the relative molar mass of electrode (stainless steel = 54.97 g/mole), n is the number of electrons in oxidation/reduction reaction, and F is the Faraday's constant having a value of 96,500 C mol^{-1}.

3 Results and Discussion

3.1 Effect of Method of Mixing Mechanism

In order to assess the effect of the method of mixing on the performance of the electrocoagulation process, experiments were conducted using magnetic stirrer and diffused aerator with perforated stainless steel electrodes. The magnetic stirrer arrangement obtained a CRE of 95.08%, whereas that of aeration gave a CRE of only 40.72% (Fig. 2). There was a significant increase in efficiency of system in terms of CRE on using magnetic stirrer which was due to better distribution of the hydroxides ions released from the stainless steel electrodes that had a blanketing effect on the impurities present in the synthetic sample in place of the aeration apparatus. The aeration apparatus merely affected the CRE of the solution by aiding the formation of the hydroxide which is an excellent coagulant which formed due to the reaction between the oxygen supplied by the aeration tubes and the oxygen released at the anode.

3.2 Effect of Reaction Time

Batch studies were conducted for stainless steel electrodes for a continuous period of 30 min. Samples were collected at a regular interval of 5, 10, 15 min, etc. up to 30 min and were analysed for colour. Figure 3a represents the samples collected at different intervals of time, and 3b shows the variation of CRE with time. The maximum efficiency of 98.97% was achieved for a voltage of 15 units and for a current intensity of 2 A at 30 min reaction time. EC operated for 23 min of reaction

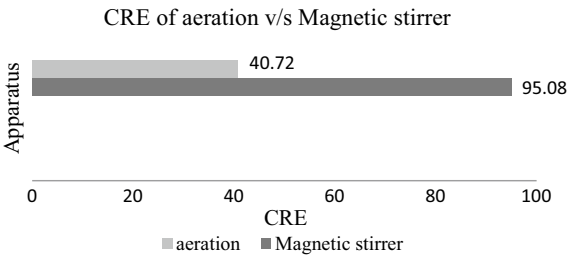

Fig. 2 Comparison of CRE for aeration and mechanical stirring

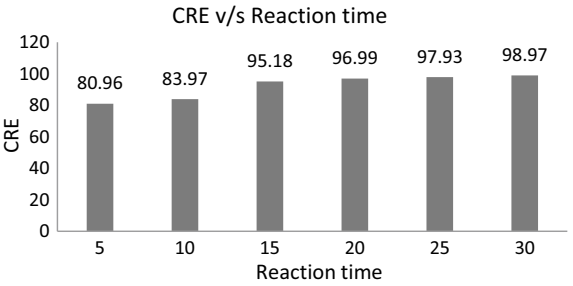

Fig. 3 Variation of CRE with reaction time

time with aluminium electrodes on textile dye wastewater yielded a decolorization efficiency of 97% [4]. Thus, with the passage of time, more of hydroxide ions are produced to enhance the adsorption and coagulation of impurities present in wastewater sample.

3.3 Consumption of Electric Energy

The demand of electricity for EC treatment of dye wastewater was estimated. Results obtained from batch studies conducted by Gaffel et al. [5] with EC on stainless steel (perforated -concentric ring) at 2 A 15 V gave a value of 5 KWh/m^3 at its optimized reaction time of 30 min. Economic analysis of electrocoagulation in terms of energy and electrode consumption along with the cost of operation on electrocoagulation of wastewater from meat industries obtained a result of 14.2 KWh/m^3 for a continuous reaction time of 25 min and 1.08 A [5]. Table 1 shows the values obtained for electricity consumption as the time progresses.

3.4 Metal Consumption

The amount of metal dissolved and deposited with the passage of time using direct supply source was estimated for different time intervals using theoretical equation [6]. Reaction time influences reaction. Basics of Faradays law was used for this. A value of 0.107 g of M cm^{-2} was obtained. The variation of the amount of metal ion dissolved with reaction time is shown in Fig. 4.

Table 1 Electrical energy consumption with reaction time

Reaction time (minutes)	5	10	15	20	25	30
Electrical energy (KWh/m^3)	0.833	1.67	2.5	3.33	4.17	5

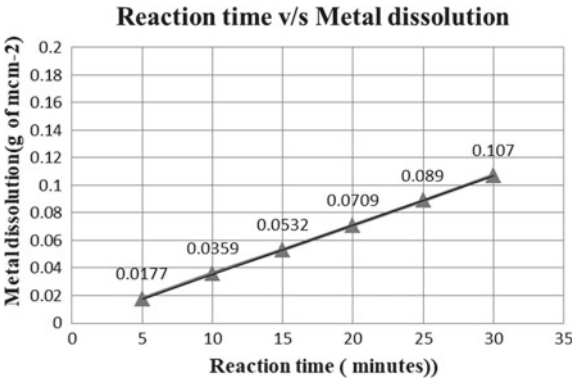

Fig. 4 Variation of metal dissolution with time

3.5 *Selection of Suitable Material Combination*

Different circular concentric arrangements of electrodes were used in the experiment in the order of anode–cathode-anode–cathode in parallel connection. A DC supply of 15 V and electric current of 2 A were used. Six different circular concentric combinations used include Al-SS-SS-Al, SS-SS-SS-SS, Al-Al-SS-SS, Al-Al-Al-Al, Al-SS-Al-SS and SS-Al-SS-Al. The corresponding CRE is shown in Fig. 5. Among which the CRE of Al-SS-SS-Al was obtained to be 98.69%, whereas that of SS-SS-SS-SS was found to be 95.08%. Because of the excessive froth formation on using aluminium electrodes in combination and due to its degradation at a much faster rate than that of stainless steel, it was concluded that perforated stainless steel electrodes in concentric circles can be taken as the optimized geometric arrangement with a combination of SS-SS-SS-SS. Table 2 shows the variation of pH, turbidity and conductivity of solution before and after the process for different electrode arrangements.

The electrochemistry behind the process of electrocoagulation can be demonstrated through the following reactions:

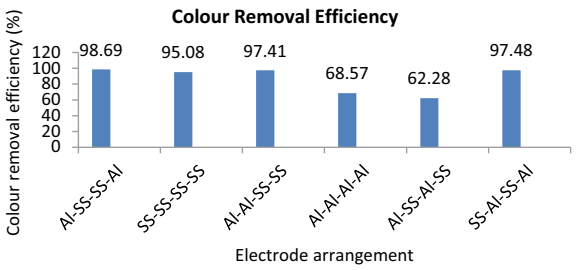

Fig. 5 Colour removal efficiencies of various concentric ring arrangements of electrodes

Table 2 pH, turbidity, conductivity of solution before and after the process for different electrode arrangements

Arrangement		AL-SS-SS-AL	SS-SS-SS-SS	AL-AL-SS-SS	AL-AL-AL-AL	AL-SS-AL-AL	SS-AL-SS-AL
pH	Initial	6.3	6.3	6.3	6.3	6.3	6.3
	Final	9.16	10.43	9.96	8.57	8.73	8.91
Turbidity (NTU)	Initial	26	26	26	26	26	26
	Final	9	13	104	36	43	41
Conductivity (mS)	Initial	2.23	2.23	2.23	2.23	2.23	2.23
	Final	1.91	1.31	2.09	1.96	2.14	2.11

Aluminium as anode

$$Al \rightarrow Al^{3+} + 3e^{-} \tag{3}$$

$$2Al + 3H_2O \rightarrow Al_2O_3 + 6H^{+} + 6e^{-} \tag{4}$$

Aluminium as cathode

$$2H_2O + 2e^{-} \rightarrow H_2 + 2OH^{-} \tag{5}$$

$$O_2 + 2H_2O + 4e^{-} \rightarrow 4OH^{-} \tag{6}$$

In Solution

$$Al^{3+} + 3H_2O \rightarrow Al(OH)_3 + 3H^{+} \tag{7}$$

Stainless Steel as anode

$$Fe \rightarrow Fe^{2+} + 2e^{-} \tag{8}$$

$$Fe \rightarrow Fe^{3+} + 3e^{-} \tag{9}$$

Stainless Steel as cathode

$$2H_2O + 2e^{-} \rightarrow H_2 + 2OH^{-} \tag{10}$$

In Solution

$$Fe^{3+} + 3H_2O \rightarrow Fe(OH)_3 + 3H^{+} \tag{11}$$

When Al is used as both cathode and anode after the reactions (3) and (7), it precipitates aluminium hydroxide which can perform as the coagulant in the reaction. Also, when Al is anode and SS is cathode aluminium hydroxide gets precipitated due to reactions (3), (4), (7) and (10). Whereas when stainless steel is used as both anode and cathode after undergoing reactions (8) and (11) iron hydroxide is formed and when SS is used as anode and Al used as cathode iron hydroxide is formed due to reactions (6), (7), (8), (9) and (11). Though this process has an advantage of better coagulation due to formation of two coagulants, when these electrodes are used in combination because of the excessive froth formation on using aluminium electrodes and due to its degradation at a much faster rate than that of stainless steel it was concluded that perforated stainless steel electrodes in concentric circles can be taken as the optimized material combination.

4 Conclusions

The EC process has gained a considerable interest in the industrial wastewater treatment application because it is compatible to the environment, versatile, efficient in energy use, safe, selective, amendable to automation and cost effective. EC process was carried out for 3 L of 50 ppm methyl orange solution with interelectrode distance of 2.5 cm, depth of immersion of 5.25 cm for an electrolyte concentration of 1 g/L. Perforated electrodes were arranged as concentric circles with anode within the cathode, and mechanical stirring was found to be more efficient for constant mixing of sample than aeration. Among the six different combinations of Al and SS electrodes as anode–cathode-anode–cathode (i.e. Al-SS-SS-Al, SS-SS-SS-SS, Al-Al-SS-SS, Al-Al-Al-Al, Al-SS-Al-SS, SS-Al-SS-Al) under constant operating conditions of 15 V and 2 A current, SS-SS-SS-SS combination was found to be optimum with its considerably high value of CRE efficiency and low volume of sludge produced. The reaction time was optimized to 30 min. Energy consumption for EC process using perforated stainless steel electrodes under given operating condition was estimated to be 5 KWh/m^3. The amount of metal dissolved and deposited with time passage for the same was estimated using theoretical equations as 0.107 g of M cm^{-2}.

References

1. Morsli SM, Merad I, Khebbeb MEH, Soltani N (2015) Potential hazards of a chitin synthesis inhibitor diflubenzuron in the shrimp Penaeus kerathurus: biochemical composition of the hemolymph and muscle during the molt cycle. Adv Environ Biol 9(3):518–525
2. Vidal J, Espinoza C, Contreras N, Salazar R (2017) Elimination of industrial textile dye by electrocoagulation using iron electrodes. J Chil Chem Soc 62(2):3519–3524
3. Thomas J, Kichu V, Premkumar K, Muraleedharan L, Sreeraj S (2018) Studies on the performance evaluation of electrocoagulation process in the degradation of methyl orange dye. B. Tech thesis, TKM College of Engineering, Kollam
4. Khorram AG, Fallah N (2018) Treatment of textile dyeing factory wastewater by electrocoagulation with low sludge settling time: optimization of operating parameters by RSM. J Environ Chem Eng 6(1):635–642
5. Gaffel J, Price N, Prasad P (2018). Evaluation of electrocoagulation as a waste water treatment technology for meat processors. Australian Meat Processor Corporation, 1140-Milestone 1 and 3 combined
6. Sharma G (2011) Electrocoagulation and microfiltration hybrid system for water treatment. Doctoral dissertation

Spatial and Temporal Distribution of Ions in Groundwater of the Dimoria Block of Kamrup Metropolitan District of Assam, India Using Geographic Information System

Priyanka Kotoky, Ajay S. Kalamdhad, and Bimlesh Kumar

Abstract The quality of groundwater in the Dimoria block of the Kamrup Metropolitan district of the state of Assam, India was gauged by determining 5 physicochemical parameters (pH, TDS, turbidity, TH, and TA) and 8 major ions concentrations (Na^+, Ca^{2+}, Mg^{2+}, K^+, F^-, NO_3^-, Cl^- and SO_4^{2-}). The groundwater samples were collected from 10 sampling sites casing the entire study area during 3 seasons (PrM, M, and PoM seasons) during the year 2019–2020. The concentration values obtained were compared with I.S. 10,500:2012 standards. Spatial, as well as temporal deviations in groundwater quality concerning the selected water quality parameters, have been studied using GIS. ArcGIS (v. 10.5) was used to analyze and create spatial variability maps of the selected parameters using IDW spatial interpolation modeling method for generating spatial and temporal distribution maps. Based on the groundwater quality standards, the results revealed that greater parts of the groundwater samples are not apt for consumption rationale. Among the 5 physicochemical parameters, pH, TDS, turbidity, TH, and TA exceeded their respective permissible limits during one or more seasons, the most prominent being pH, turbidity, and TH. Dominant cations found in the study area are Na^+, Ca^{2+} and K^+. Amid the major cations, Na^+ and K^+ played a high-up role. The Mg^{2+} concentrations are relatively very low in contrast to other chief cations. Among the major anions, F^- and NO_3^- played the most Dominant role. The concentrations of Cl^- and SO_4^{2-} are relatively very low in contrast to the other chief anions. The spatial database will thus be obliged for the monitoring and supervision of groundwater contamination in the study area.

Keywords Anions · Cations · Geographic information system · Groundwater quality · Spatial distribution maps

P. Kotoky (✉) · A. S. Kalamdhad · B. Kumar
Department of Civil Engineering, Indian Institute of Technology Guwahati, Guwahati 781039, India
e-mail: kajay@iitg.ac.in

B. Kumar
e-mail: bimk@iitg.ac.in

B. Laishram and A. Tawalare (eds.), *Recent Advancements in Civil Engineering*, Lecture Notes in Civil Engineering 172,
https://doi.org/10.1007/978-981-16-4396-5_40

1 Introduction

Geology, geomorphology, rainfall, and anthropogenic factors are mainly responsible for groundwater occurrence, distribution, and quality, and their interplay gives rise to intricate hydrogeological environments with countless variations in the extent and eminence of groundwater resources. Groundwater is one among the most imperative innate resources. Colossal quanta of groundwater are withdrawn every day for domestic, irrigation, industrial, and commercial use [1]. Also, various natural processes and anthropogenic deeds are incessantly amending the physical, chemical, and organic compositions of groundwater [2, 3]. Therefore, groundwater sources getting contaminated has been a key environmental concern globally due to its direct impact on the environment and health [4, 5]. Thus, long-term conservation, development, and management of this natural resource are critical for preserving and protecting this priceless asset [6]. This includes groundwater quality assessment and mapping that takes into account constant monitoring of the entire groundwater resource, thereby providing unswerving information about the intrinsic possessions of groundwater and its quality [7].

The rise in contamination levels in groundwater has led to abundant monitoring approaches across the world. Spatial and temporal deviations of groundwater quality can be studied using geographic information system (GIS). GIS has come out to be a persuasive computer-based contrivance that detains, amasses, analyzes, supervises, and presents data that is correlated to location; and applying the database for decision making in diverse fields. Precisely, the benefits of using GIS over traditional methods in groundwater monitoring are many as it can serve as a very useful tool for not only groundwater modeling but also for analyzes of decadal variations in the groundwater quality. GIS integration facilitates understanding and monitoring the location-based details of groundwater quality and its contamination and thus, is very useful for deciphering complex planning and management problems related to groundwater. Therefore continuous monitoring provides a complete picture of the spatial as well as the temporal variation of the groundwater quality [5, 8].

The Dimoria block, which is taken up as the study area, despite being a very important block of the Kamrup Metropolitan district of Assam, has been deprived of appropriate measures for seasonal monitoring and management of groundwater quality and use. The dependability on groundwater is more in this block because of the pollution of surface water and the lack of proper and well-maintained water supply networks. During the monsoon season, the surface water becomes unusable for direct use, and during the lean period, water dries up; so the only reliable source for water use comes from groundwater extraction. Adding to it, reliable continuous monitoring of various water quality parameters is not available in this block. Even the topmost government organizations responsible for carrying out groundwater quality analysis take into account only a few parameters and there is an absence of seasonal and continuous monitoring of groundwater. No study or literature is available to cite the detection of the parameters which can be found in high levels in the block causing health and environmental hazards.

According to the reports of Central Ground Water Board and Public Health Engineering Department (Assam), the groundwater of the Dimoria block has been found to be basically contaminated with fluoride, iron, and manganese. The presence of major cations and anions in the groundwater has not been studied extensively and on seasonal basis. Thus, there is a need for exhaustive scientific research with precise monitoring of the groundwater of the block to make certain that the situation of the same does not worsen anymore and at the same time facilitate the authorities in the decision-making process to employ better groundwater utilization, monitoring, and management programs. Therefore, for an effective and sustainable administration of groundwater in the Dimoria block, an understanding of the spatial, as well as temporal changeability of diverse water quality parameters, is required. The purposes of this study are: (1) To assess and endow with an overview of current groundwater quality of the Dimoria block with special reference to 5 physicochemical parameters (pH, TDS, turbidity, TH, and TA) and 8 major ions concentrations (Na^+, Ca^{2+}, Mg^{2+}, K^+, F^-, NO_3^-, Cl^- and SO_4^{2-}); (2) To determine spatial as well as temporal distributions of the selected water quality parameters. This will help both in present groundwater resource planning in the study area as well as provide a baseline for future groundwater quality evolution studies.

2 Materials and Methodologies

2.1 Study Area

Dimoria block of the Kamrup Metropolitan district of the state of Assam, India is taken up as the study area to gauge the groundwater quality. Is located in the Kamrup Metropolitan district which is located between north latitudes 25°43' N and 26°51' N, and between east longitudes 90°36' E and 92°12' E; and has an area of 261.64 km^2. It is bounded on the west by the Guwahati block of the Kamrup Metropolitan district, on the north by the Chandrapur Block of the Kamrup Metropolitan district and Marigaon district, and on the east by the Marigaon district. On the south, lies the state of Meghalaya. As per Assam's administration records, the block has 145 villages and there are a total of 29,840 families in this block. As per Census 2011, Dimoria's population is 143371.

In this block, a major segment of the population takes the benefit of groundwater as a source of drinking water and for other domestic and agricultural purposes. The chief groundwater sources in this block are ring wells (RW), hand tube wells (HTW), hand bore wells (HBW), tara pumps (TP), and deep tube wells (DTW). So, the sampling from these groundwater sources is adequate as the sampling locations have sources that reflect and represent the actual groundwater. Based on reconnaissance survey of the study area, 10 sampling locations were selected based on factors such as accessibility of the sampling location and presence of wells; wells closer to polluting sources like industries, urban wastewater drains, garbage

dumpsites, agricultural lands, etc.; wells suspected for contaminants like fluoride, nitrate, or such contaminants. Thus, the present study is implemented for the appraisal of the water quality parameters in the Dimoria block and also to study whether the groundwater is apposite for domestic rationales without any health hazard or not.

Although the Dimoria block is a very important block of the Kamrup Metropolitan district, as its area is very small covering mostly forests and agricultural areas, thus 10 sampling sites were selected representing the actual groundwater sources. The selected sites were evenly distributed that covered the entire block. For groundwater quality investigation, samples were collected from Amsing, Gomoria Gaon, Lumsum Pathar, Thengabhanga, Murkata, Maloibari, Kamarkuchi, Khetri, Topatali-Umsiang, and Guripathar areas that represent the most populated areas in the block. The information of the sampling locations is specified in Table 1.

2.2 Data Procurement

In the Dimoria block, a total of 10 sampling points were selected to gauge the spatial and temporal variation of groundwater quality. The coordinates of the sampling points were obtained by using GARMIN GPS-60. The importation of the location data to ArcGIS (v. 10.5) was done using WGS_1984_UTM_Zone_46N projection. The map of the Dimoria block demonstrating the sampling locations was delineated using ArcMap (v. 10.5). The Survey of India (SOI) topographic sheet no. ng46 was also utilized to create the final study area map. Using the point feature tool in ArcGIS, the places in the block were digitized. The obtained map and the GPS data build the spatial database. Figure 1 shows the Dimoria block map depicting the sampling sites.

Table 1 Sampling locations of the Dimoria block

Sample no	Pinpoint location	Latitude N in decimal degrees	Longitude E in decimal degrees	Source	Well depth in feet
K1	Lumsum Pathar	26.122466	92.013537	RW	50
K2	Maloibari	26.169411	92.094049	HTW	105
K3	Guripathar	26.138816	92.159106	TP	100
K4	Thengbhanga	26.159509	92.038844	RW	20
K5	Kamarkuchi	26.121182	91.905108	DTW	120
K6	Amsing	26.157043	91.896918	DTW	130
K7	Murkata	26.091313	92.099548	RW	20
K8	Gomoria Gaon	26.143862	91.972853	HTW	20
K9	Khetri	26.126053	92.083430	HTW	70
K10	Topatali-Umsiang	26.102297	92.165109	HBW	90

Seasonal analysis was carried out by sampling in the block for three seasons: pre-monsoon (PrM) season, monsoon (M) season, and post-monsoon (PoM) season during the year 2019–2020. Assortment of the samples, hauling, storage, and investigation were made per APHA guiding principles [9]. The collected groundwater specimens were examined for a totality of 13 water quality parameters, viz. negative logarithm of H^+ ion concentration (pH), total dissolved solids (TDS), turbidity, total hardness (TH), total alkalinity (TA), sodium (Na^+), calcium (Ca^{2+}), magnesium (Mg^{2+}), potassium (K^+), fluoride (F^-), nitrate (NO_3^-), chloride (Cl^-) and sulphate (SO_4^{2-}). The analyzes were executed in triplicates. Table 2 shows the analytical procedures that were used.

2.3 GIS Based Analysis

Spatial Analyst annex of ArcGIS offers a contrivance for scrutinizing and molding spatial data. An array of sample points symbolizing revolution in groundwater variables can be used to envisage the permanence and unpredictability of observed data across a surface in the course of the use of interpolation contrivances. A spatial interpolation technique, a geostatistical interpolation or geospatial analysis method-the Inverse distance weighting (IDW) was utilized to attain the spatio-temporal variations of the water quality parameters.

IDW is a category of deterministic technique for multivariate interpolation with an identified speckled array of points. The allocated values to unidentified points are intended with a weighted average of the values obtainable at the known points. To envisage a value for any unmeasured location, IDW uses the measured values adjoining the prediction location. The calculated values flanking the prediction location have further authority on the envisaged value than those farther away. It offers superior weights to points flanking to the prediction location, and the weights ebb as a function of distance, thus the name inverse distance weighted. Figure 2 shows the methodology used for integrated groundwater quality mapping.

3 Results and Discussion

The levels of the physicochemical entities of the groundwater tasters were statistically examined and the outcomes, for instance maximum, minimum, mean, and standard deviation are furnished in Tables 3 and 4 for the three seasons in the Dimoria block. Table 5 shows the percentage of groundwater samples surpassing the permissible limit in the block.

To establish the spatial allocation outline of the levels of the selected parameters and to differentiate elevated concentration precincts, spatial distribution maps for diverse parameters were engendered through ArcGIS 10.5 software. The spatial and temporal distribution maps were prepared and the concentration levels were

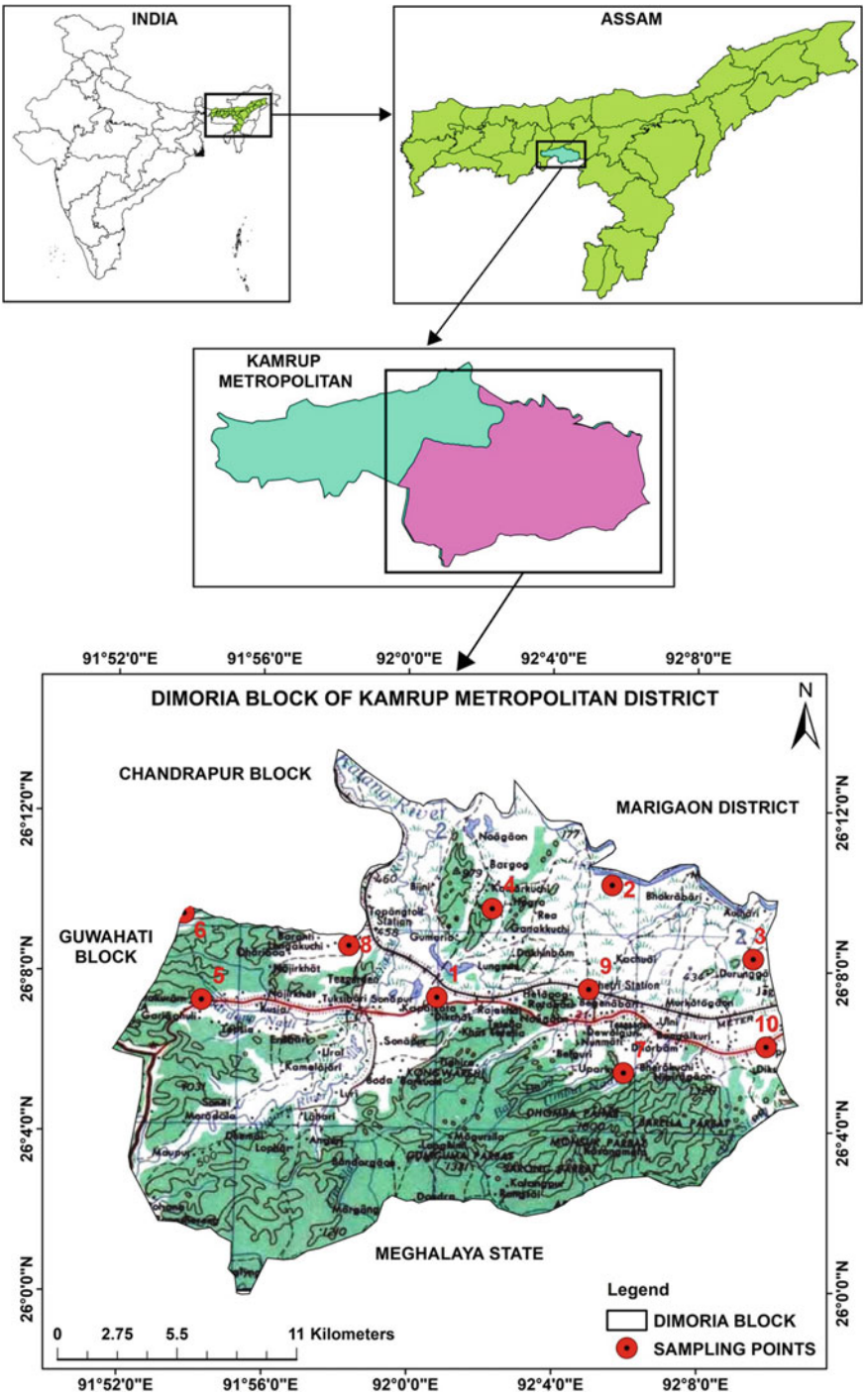

Fig. 1 Study area (Dimoria block) depicting the sites of the sampling points

Table 2 Analytical procedures and instruments used in the investigation

Parameter	Abbreviation	Unit	Instrument used
Negative logarithm of Hydrogen ion concentration	pH		Digital pH meter
Total dissolved solids	TDS	mg/l	Digital EC meter
Turbidity	Tur	NTU	Nephelometric turbidimeter
Total hardness	TH	mg/l as $CaCO_3$	APHA titrimetric method
Total alkalinity	TA	mg/l as $CaCO_3$	
Sodium	Na^+	mg/l	Flame photometer
Calcium	Ca^{2+}	mg/l	
Potassium	K^+	mg/l	
Magnesium	Mg^{2+}	mg/l	Atomic absorption spectroscopy (AAS)
Fluoride	F^-	mg/l	Ion chromatography (IC)
Nitrate	NO_3^-	mg/l	
Chloride	Cl^-	mg/l	
Sulphate	SO_4^{2-}	mg/l	

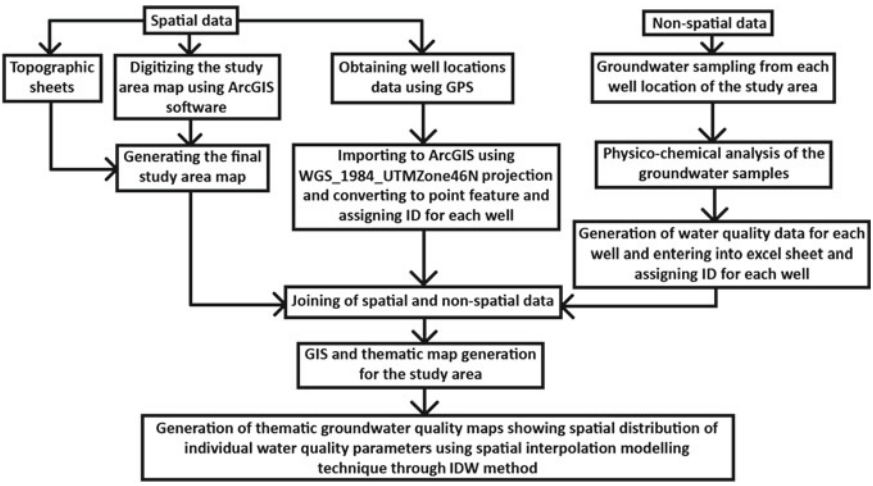

Fig. 2 The methodology used for integrated groundwater quality mapping

categorized according to I.S. 10,500:2012 standards for drinking water. The categorizations made, are for every parameter based upon the permissible limit, maximum permissible limit, and the values surpassing the maximum permissible limit.

Table 3 Statistical parameters for the allocation of the parameters

Parameter	Minimum			Maximum		
	PrM	M	PoM	PrM	M	PoM
pH	5.59	5.59	6.01	6.76	7.66	7.27
TDS	198.40	57.60	327.68	712.96	486.40	821.12
Turbidity	0.35	0.60	0.15	7.12	15.40	12.17
TH	83.00	44.00	60.00	480.00	476.00	390.00
TA	60.00	90.00	60.00	156.00	202.00	178.00
Na^+	13.50	0.90	7.20	149.00	91.00	119.60
Ca^{2+}	11.90	3.90	15.40	91.60	32.90	116.90
Mg^{2+}	4.03	0.21	3.36	24.13	17.73	20.11
K^+	2.10	0.10	1.20	59.20	21.90	39.50
F^-	0.29	0.10	0.44	1.92	1.46	1.69
NO_3^-	5.69	0.26	11.80	70.31	15.57	53.80
Cl^-	18.71	1.42	12.50	44.24	11.20	29.49
SO_4^{2-}	10.26	1.00	6.84	153.00	56.67	102.00

*The unit of all concentrations are in mg/l except for pH and Turbidity. The unit of turbidity is NTU and pH is unitless

Table 4 Statistical parameters for the allocation of the parameters

Parameter	Mean			Standard deviation		
	PrM	M	PoM	PrM	M	PoM
pH	6.06	6.52	6.45	0.37	0.66	0.41
TDS	501.31	210.56	507.46	162.48	131.68	146.00
Turbidity	2.37	4.08	2.36	2.10	4.20	3.52
TH	213.70	168.20	166.80	135.78	134.46	103.15
TA	104.40	144.00	110.40	31.46	43.32	39.44
Na^+	65.51	34.92	49.61	45.96	32.10	38.16
Ca^{2+}	43.01	12.55	46.33	25.16	9.15	36.02
Mg^{2+}	11.10	4.62	9.25	6.00	5.08	5.00
K^+	16.44	2.66	10.05	18.77	6.78	12.83
F^-	0.78	0.55	0.91	0.60	0.51	0.42
NO_3^-	33.73	3.06	21.19	21.72	4.51	12.90
Cl^-	29.06	5.01	19.39	7.10	2.90	4.74
SO_4^{2-}	48.81	12.73	32.54	43.86	17.33	29.24

*The unit of all concentrations are in mg/l except for pH and Turbidity. The unit of turbidity is NTU and pH is unitless

The levels of pH in the groundwater samples range from 5.59 to 6.76, 5.59 to 7.66, and 6.01–7.27 during PrM, M, and PoM seasons correspondingly, which indicates acidic nature. 80%, 60%, and 80% of the samples surpassed the permissible limits of I.S. 10,500:2012 standards during PrM, M, and PoM seasons

Table 5 Percentage of groundwater samples surpassing the permissible limit in the block

Parameter	Permissible limit	Maximum permissible limit	% of samples exceeding the permissible limit		
			PrM	M	PoM
pH	6.5–8.5	6.5–8.5	80	60	80
TDS	500	2000	50	0	60
Turbidity	1	5	60	90	80
TH	200	600	40	30	40
TA	200	600	0	10	0
Na^+	20	40	80	50	70
Ca^{2+}	75	200	20	0	30
Mg^{2+}	30	100	0	0	0
K^+	10	10	60	10	30
F^-	1	1.5	30	20	30
NO_3^-	45	45	40	0	10
Cl^-	250	1000	0	0	0
SO_4^{2-}	200	400	0	0	0

*The unit of all concentrations are in mg/l except for pH and Turbidity. The unit of turbidity is NTU and pH is unitless

correspondingly (Table 5). This decrease in pH values of the groundwater samples may be owing to the increasing levels of various salts and minerals in the groundwater of the block [10]. The spatial, as well as temporal deviations of pH in the Dimoria block, is shown in Fig. 3.

The values of TDS vary from 198.4 to 712.96 mg/l, 57.6 to 486.4 mg/l, and 327.68 to 821.12 mg/l through PrM, M, and PoM seasons correspondingly. 50%, 0%, and 60% of the samples surpassed the permissible limits of I.S. 10,500:2012 standards during PrM, M, and PoM seasons correspondingly (Table 5). Elevated values of TDS during PoM and PrM seasons are owing to the decline of groundwater during non-monsoon seasons (PoM and PrM seasons) and leaching and dissolution of salts from rocks and soil and furthermore by human-induced exploits [11]. The runoff with households' sewage that permeates into the groundwater may also be one of the chief reasons for the augmentation in TDS levels during PoM and PrM seasons. The spatial, as well as temporal distribution of TDS in the Dimoria block, is shown in Fig. 4.

The values of turbidity vary from 0.35 to 7.12 NTU, 0.6 to 15.4 NTU, and 0.15 to 12.17 NTU during PrM, M, and PoM seasons correspondingly. 60%, 90%, and 80% of the samples exceeded the allowable limits of I.S. 10,500:2012 standards during PrM, M, and PoM seasons correspondingly (Table 5). During PrM and PoM seasons, infiltration of precipitation into groundwater is very low compared to the M season. Therefore, there is a low turbid water input to the groundwater during the non-monsoon seasons. The declining trend of turbidity in the PoM and PrM seasons can be attributable to the fact that turbidity in groundwater reduces with the

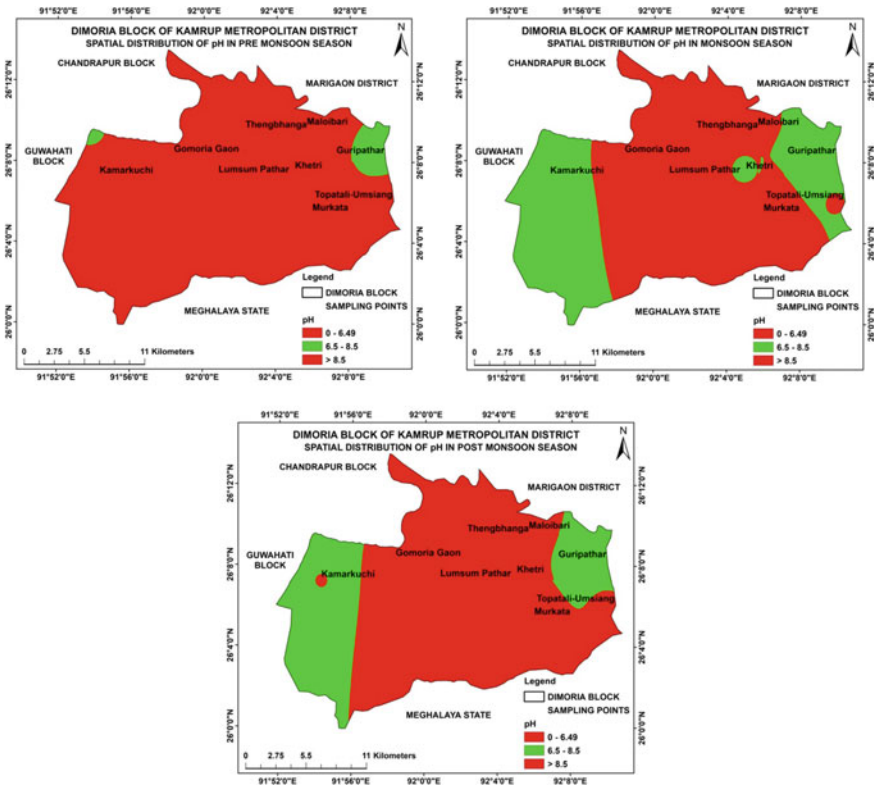

Fig. 3 pH in the PrM, M, and PoM seasons in Dimoria block

augment of deposition time [12]. The spatial, as well as temporal distribution of turbidity in the Dimoria block, is shown in Fig. 5.

The values of TH differ from 83 to 480 mg/l, 44 to 476 mg/l, and 60 to 390 mg/l through PrM, M, and PoM seasons correspondingly. 40%, 30%, and 40% of the samples surpassed the permissible limits of I.S. 10,500:2012 standards during PrM, M, and PoM seasons correspondingly (Table 5). In this study, although, the mean Mg^{2+} concentration of M season samples is found lower than samples of PoM season, the high TH that is found in the M season in contrast to PoM season can be attributed to the fact that the TH in groundwater is primarily due to calcium carbonates and bicarbonates, and secondarily due to magnesium carbonates and bicarbonates; and can consists of other compounds such as calcium sulphate, calcium chloride, magnesium sulphate, and magnesium chloride [13]. Moreover, in the block, the values of Ca^{2+} ions are found to be more, thus the TH levels are also found to be high. The TH-based cataloging of groundwater illustrates that nearly half of the groundwater samples of the Dimoria block plummet in hard water group. The spatial, as well as temporal distribution of TH in the Dimoria block, is shown in Fig. 6.

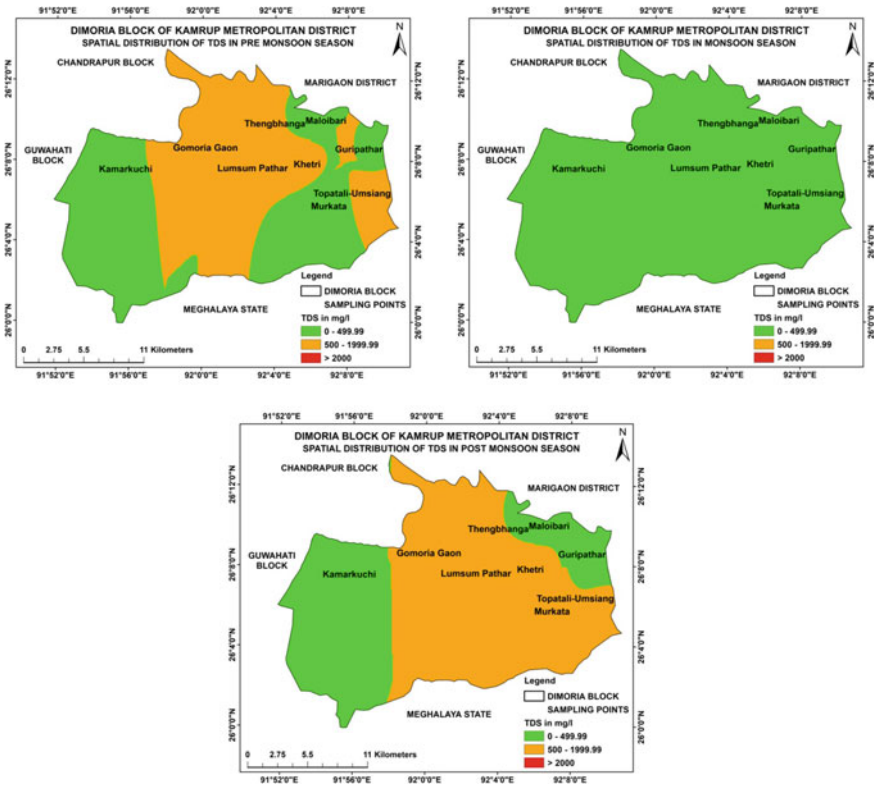

Fig. 4 TDS in the PrM, M, and PoM seasons in Dimoria block

The values of TA differ from 60 to 156 mg/l, 90 to 202 mg/l, and 60 to 178 mg/l during PrM, M, and PoM seasons correspondingly. 0%, 10%, and 0% of the samples exceeded the permitted limits of I.S. 10,500:2012 standards during PrM, M, and PoM seasons correspondingly (Table 5). As the pH values of the groundwater are found to be in acidic range, therefore TA also falls low in level. The spatial and temporal deviations of TA in the Dimoria block are shown in Fig. 7.

The values of Na^+ vary from 13.5 to 149 mg/l, 0.9 to 91 mg/l, and 7.2 to 119.6 mg/l during PrM, M, and PoM seasons correspondingly. 80%, 50%, and 70% of the samples went over the permissible limits of I.S. 10,500:2012 standards during PrM, M, and PoM seasons correspondingly (Table 5). The spatial and temporal disparities of Na^+ in the Dimoria block are shown in Fig. 8.

The values of Ca^{2+} differ from 11.9 to 91.6 mg/l, 3.9 to 32.9 mg/l, and 15.4 to 116.9 mg/l during PrM, M, and PoM seasons correspondingly. 20%, 0%, and 30% of the samples exceeded the acceptable limits of I.S. 10,500:2012 standards during PrM, M, and PoM seasons respectively (Table 5). In view of municipality potential sources like sewage, domestic waste, and industrial wastes that contribute the complex amount of Ca^{2+} ions leading to origin of ionic pollutants. Concentration of

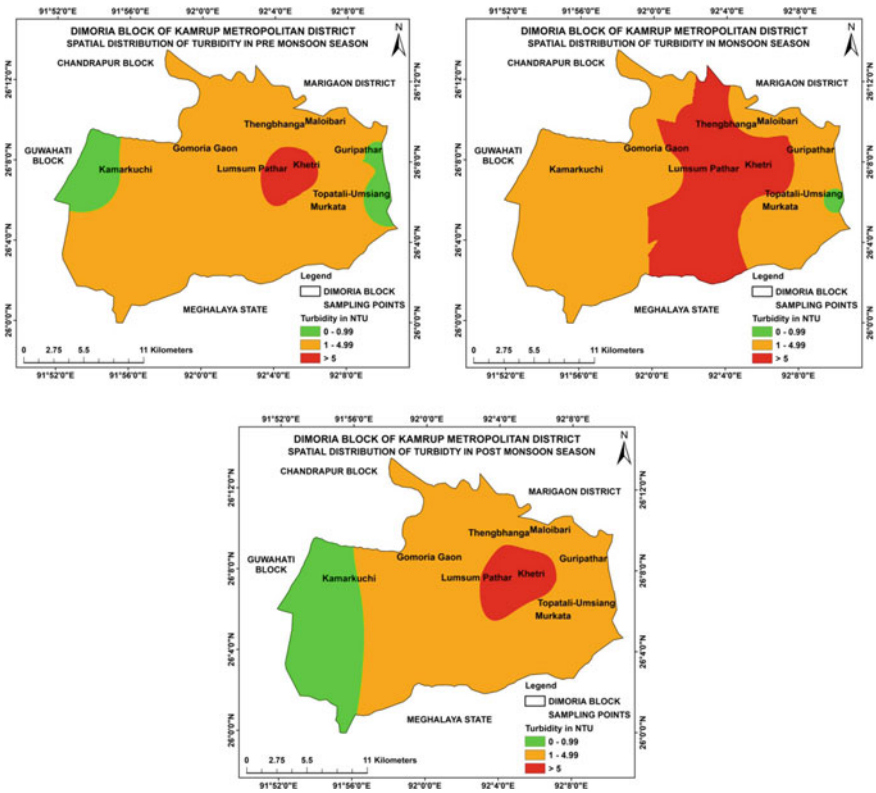

Fig. 5 Turbidity in the PrM, M, and PoM seasons in Dimoria block

Ca^{2+} ions in groundwater might be increasing due to the leaching process [14]. The spatial as well as temporal distribution of Ca^{2+} in the Dimoria block is portrayed in Fig. 9.

The values of Mg^{2+} vary from 4.03 to 24.13 mg/l, 0.21 to 17.73 mg/l, and 3.36 to 20.11 mg/l during PrM, M, and PoM seasons correspondingly. 0% of the samples exceeded the permissible limits of I.S. 10,500:2012 standards during PrM, M, and PoM seasons (Table 5). The major resource of Mg^{2+} in the groundwater of this area is because of Mg^{2+} bearing minerals, ion exchange of minerals from rocks, and also animal, household and industrial squander. The spatial as well as temporal distribution of Mg^{2+} in the Dimoria block is shown in Fig. 10.

The values of K^{+} vary from 2.1 to 59.2 mg/l, 0.1 to 21.9 mg/l, and 1.2 to 39.5 mg/l during PrM, M, and PoM seasons correspondingly. 60%, 10%, and 30% of the samples beat the acceptable limits of I.S. 10,500:2012 standards during PrM, M, and PoM seasons correspondingly (Table 5). K^{+} concentrations at a few sites are bizarrely very soaring, which maybe attributable to salt scrapes existing eugenically

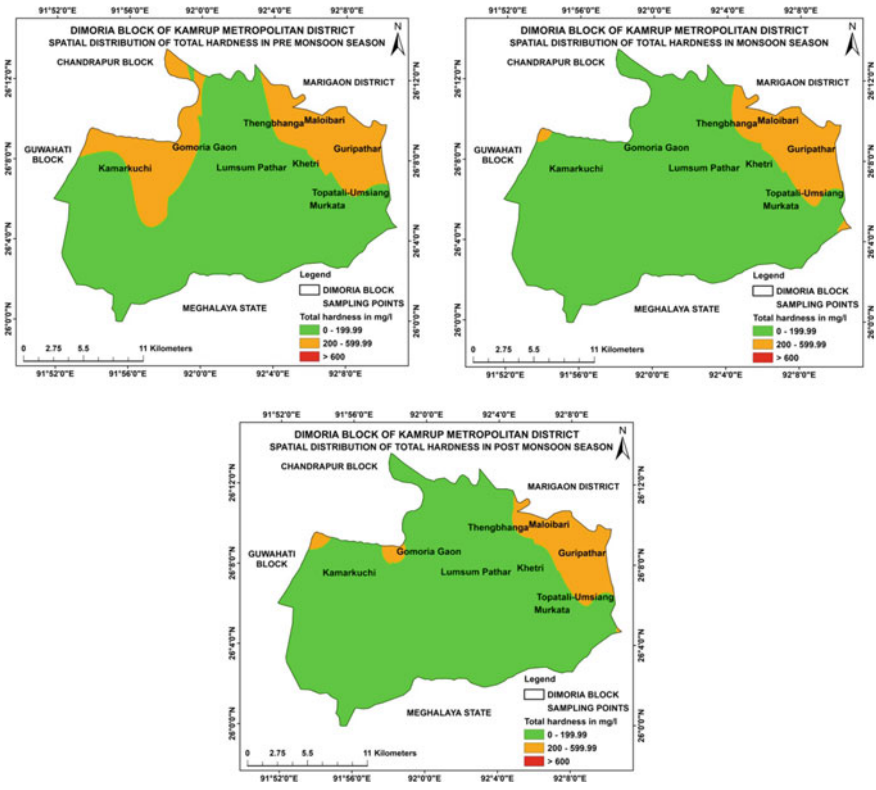

Fig. 6 TH in the PrM, M, and PoM seasons in Dimoria block

and fertilizer percolating/leaching through the sub-surface. The spatial as well as temporal distribution of K^+ in the Dimoria block is shown in Fig. 11.

The values of F^- vary from 0.29 to 1.92 mg/l, 0.1 to 1.46 mg/l, and 0.44 to 1.69 mg/l during PrM, M and PoM seasons correspondingly. 30%, 20%, and 30% of the samples went beyond the acceptable limits of I.S. 10,500:2012 standards during PrM, M, and PoM seasons correspondingly (Table 5). In India, it is recognized that elevated levels of fluoride in groundwater are generally characteristic of geogenic causes: primarily from rocks holding rich fluorine having minerals [15]. The Dimoria block region is occupied by granitic and gneisses rocks and these hold a relatively large quantity of high fluorine minerals [16]. The spatial as well as temporal allocation of F^- in the Dimoria block is shown in Fig. 12.

The values of NO_3^- vary from 5.69 to 70.31 mg/l, 0.26 to 15.57 mg/l, and 11.8 to 53.8 mg/l during PrM, M and PoM seasons correspondingly. 40%, 0%, and 10% of the samples went beyond the permissible limits of I.S. 10,500:2012 standards during PrM, M, and PoM seasons correspondingly (Table 5). Preceding studies on NO_3^- contamination in groundwater, have affirmed that the impending occurrence of NO_3^- and its allocation in groundwater is principally due to the appliance of

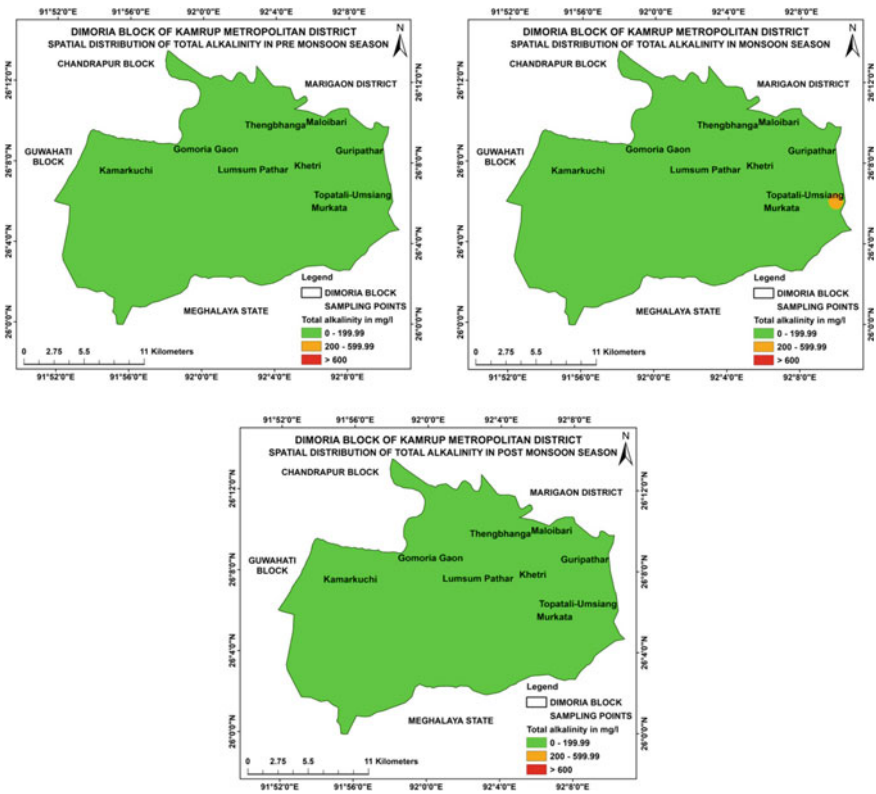

Fig. 7 TA in the PrM, M, and PoM seasons in Dimoria block

inorganic nitrogenous manures as well as fertilizers, cesspit leakage from the septic cisterns, brisk urbanization, industry-laden and community sewage, landfill leachates, and atmospheric desiccated and sodden depositions [17–19]. The presence of NO_3^- maybe from farming areas due to leaching progression from plants' nutrients and NO_3^- fertilizers [20, 21]. The spatial and temporal deviations of NO_3^- in the Dimoria block are shown in Fig. 13.

The values of Cl^- vary from 18.71 to 44.24 mg/l, 1.42 to 11.2 mg/l and 12.5 to 21.49 mg/l during PrM, M and PoM seasons correspondingly. 0% of the samples exceeded the permissible limits of I.S. 10,500:2012 standards during PrM, M, and PoM seasons (Table 5). Even low Cl^- levels in groundwater could be characteristic to leaching from gangrenous cisterns, familial and animal wastes, community sewages, farming, and fertilizers [22–24]. The spatial and temporal distribution of Cl^- in the Dimoria block is shown in Fig. 14.

The values of SO_4^{2-} differ from 10.26 to 153 mg/l, 1 to 56.67 mg/l, and 6.84 to 102 mg/l during PrM, M, and PoM seasons correspondingly. 0% of the samples exceeded the permissible limits of I.S. 10,500:2012 standards during PrM, M, and

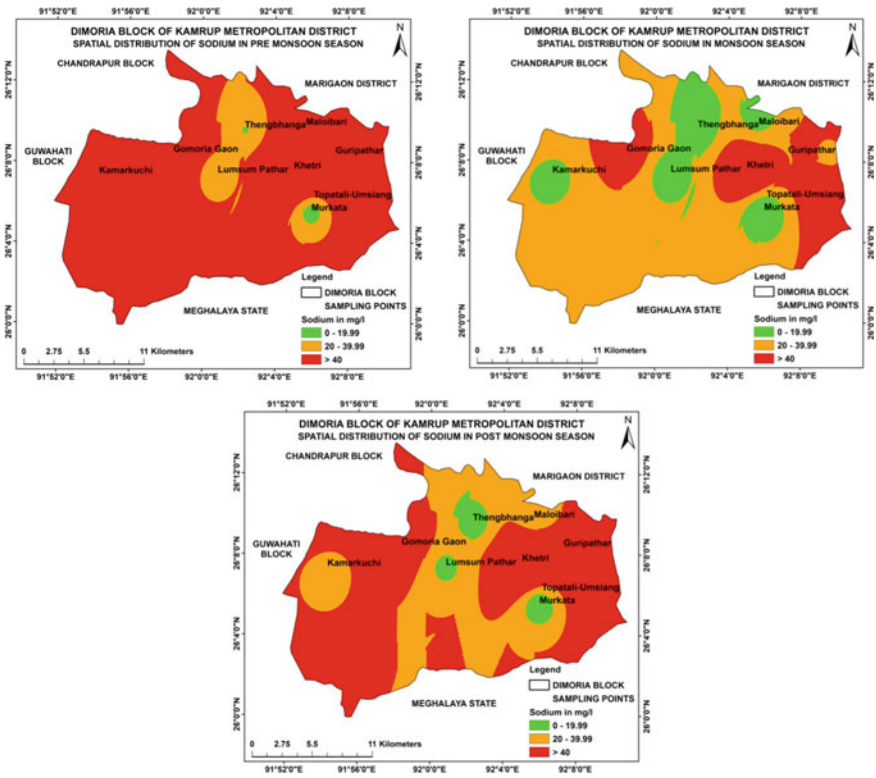

Fig. 8 Na^+ in the PrM, M, and PoM seasons in Dimoria block

PoM seasons (Table 5). The spatial and temporal distribution of SO_4^{2-} in the Dimoria block is shown in Fig. 15.

Based on the water quality standards, the results revealed that bulk of the groundwater samples are not appropriate for consumption rationales in the Dimoria block. In the PrM season, except for TA, Mg^{2+}, Cl^- and SO_4^{2-}, every other parameter surpassed their individual permissible limits. In the M season, except for TDS, Ca^{2+}, Mg^{2+}, NO_3^-, Cl^- and SO_4^{2-}, all other parameters went beyond their respective permissible limits. In the PoM season, except for TA, Mg^{2+}, Cl^- and SO_4^{2-}, every other parameter went above their respective permissible limits.

Among the 5 physicochemical parameters, pH, TDS, turbidity, TH, and TA exceeded their respective permissible limits during one or more seasons, the most prominent being pH, turbidity, and TH. Dominant cations found in the study area are Na^+, Ca^{2+} and K^+. Among the major cations, Na^+ and K^+ played a governing role. The levels of Mg^{2+} are relatively very low in contrast to other major cations. Among the major anions, F^- and NO_3^- played the most Dominant role. The

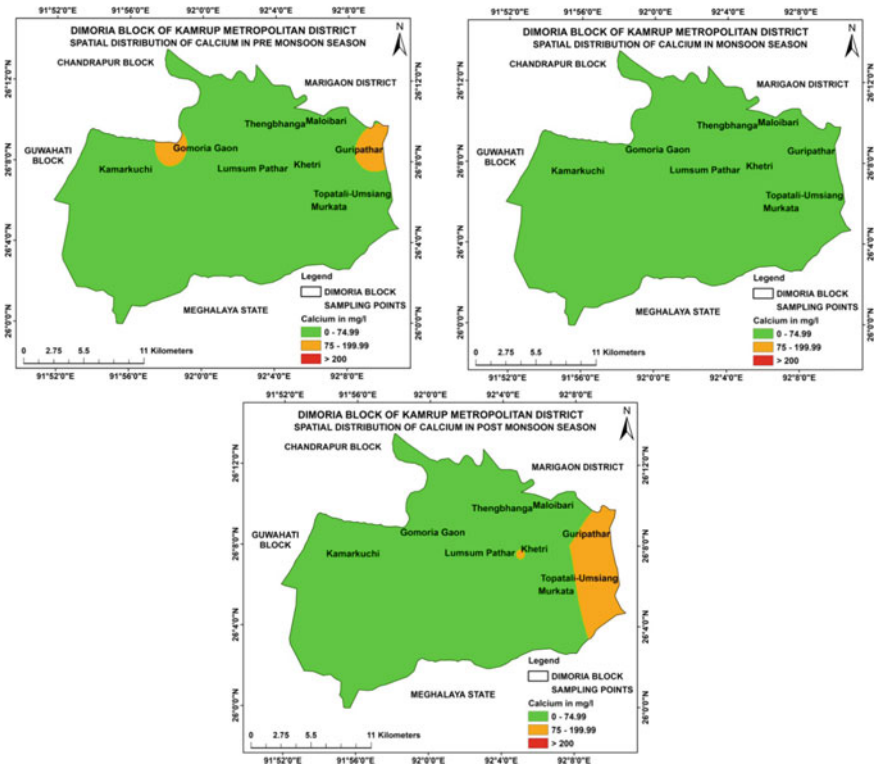

Fig. 9 Ca^{2+} in the PrM, M, and PoM seasons in Dimoria block

concentrations of Cl^{-} and SO_4^{2-} are relatively very low in contrast to other major anions. The levels of the major ions are found to be soaring signifying leaching and human-laden activities preponderate over groundwater dilution.

From the spatio-temporal GIS maps of the Dimoria block, it can be perceived that the groundwater excellence is anticipated to perk up in the M season as compared to the PrM and PoM seasons. This is generally because of the dilution of contaminants during the rainy season.

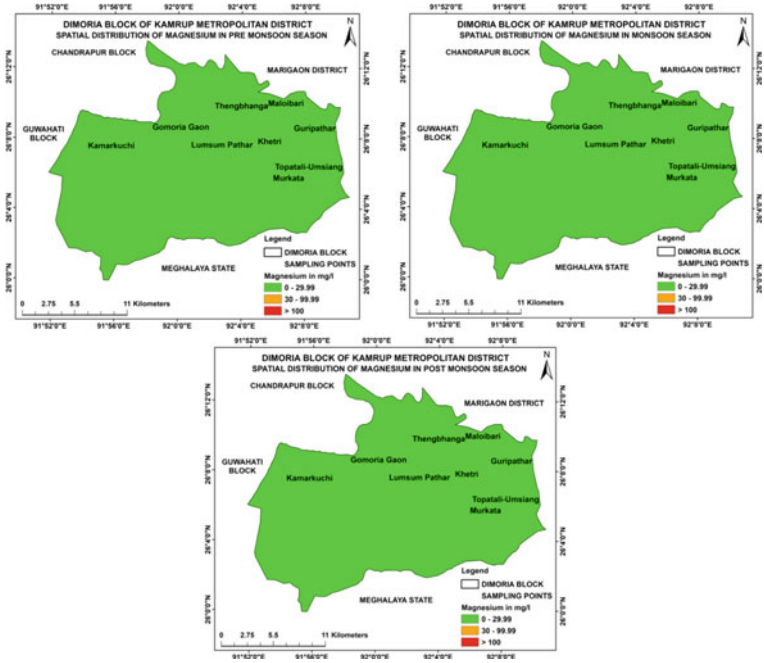

Fig. 10 Mg^{2+} in the PrM, M, and PoM seasons in Dimoria block

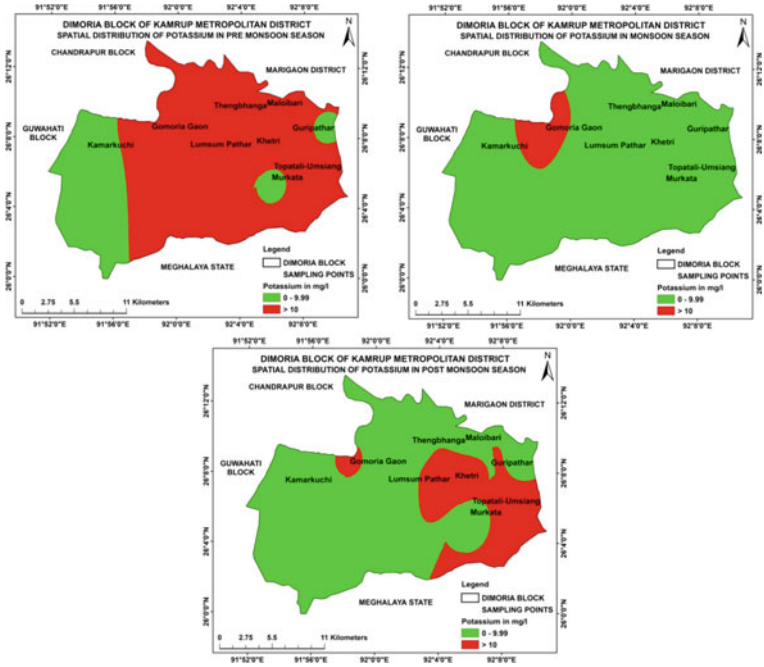

Fig. 11 K^{+} in the PrM, M, and PoM seasons in Dimoria block

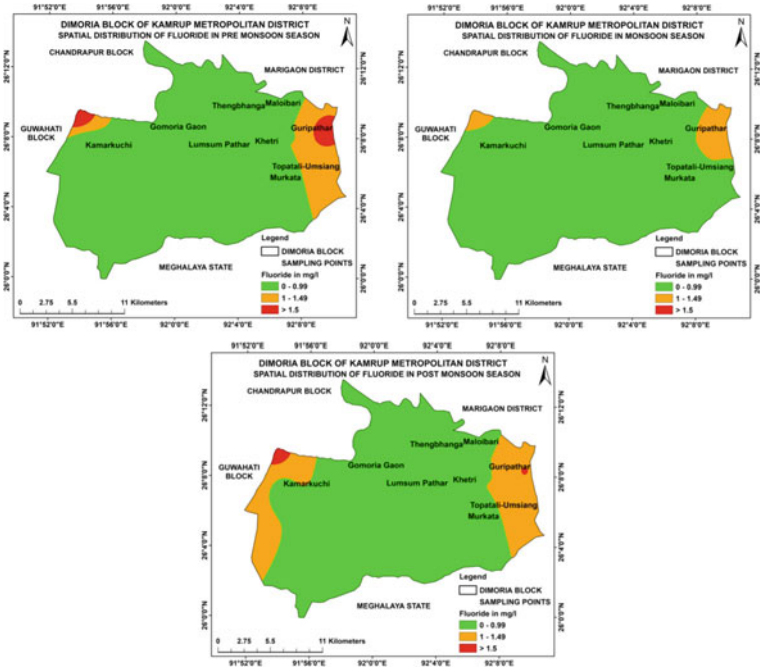

Fig. 12 F^- in the PrM, M, and PoM seasons in Dimoria block

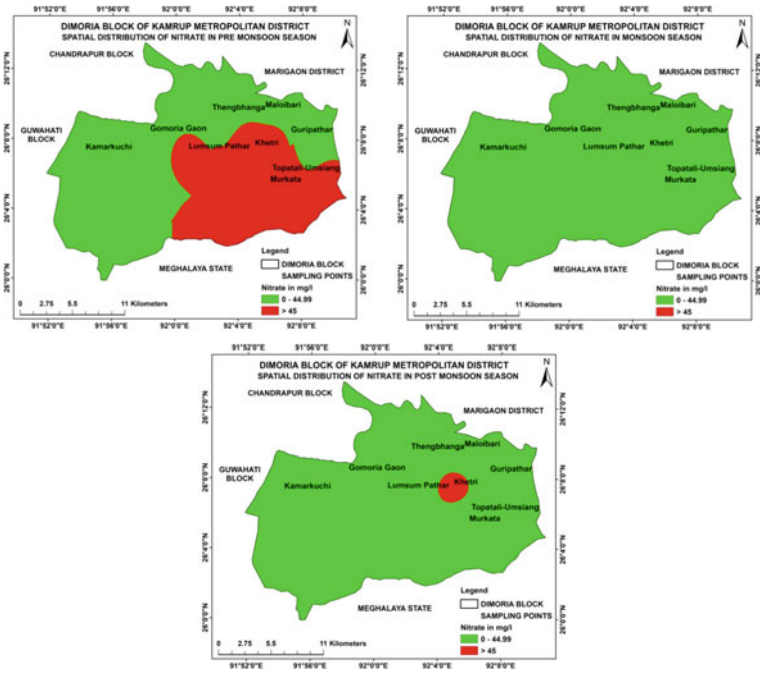

Fig. 13 NO_3^- in the PrM, M, and PoM seasons in Dimoria block

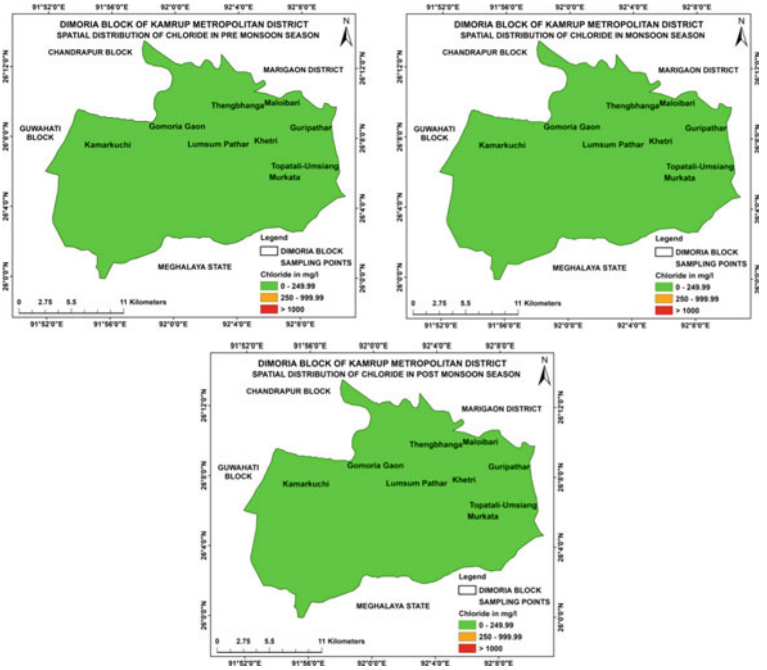

Fig. 14 Cl^- in the PrM, M, and PoM seasons in Dimoria block

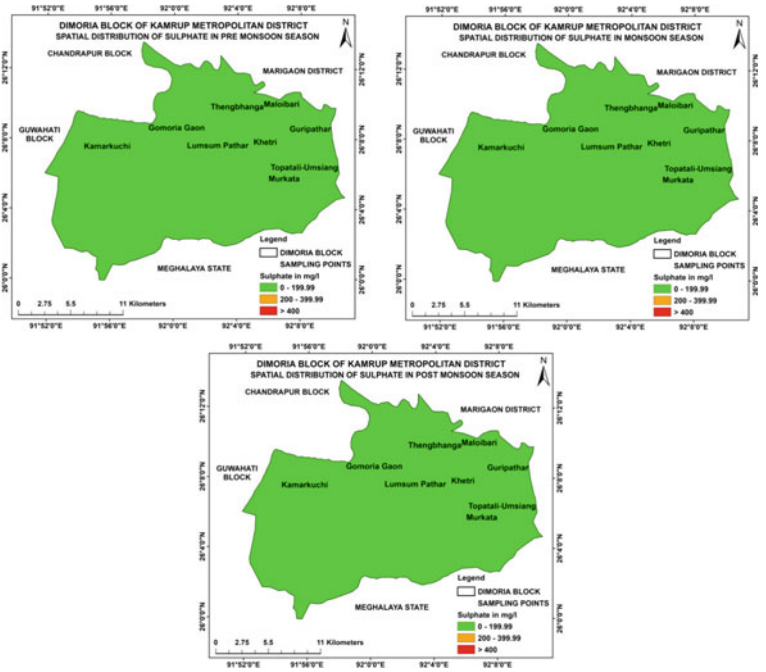

Fig. 15 SO_4^{2-} in the PrM, M, and PoM seasons in Dimoria block

4 Conclusions

The present study exhibits that the employment of GIS techniques could grant constructive information for groundwater quality appraisal. These GIS based techniques have productively established its competence in groundwater quality mapping of the Dimoria block. The spatial variation maps of the groundwater quality in the block signified that the majority of the groundwater samples are not fulfilling the drinking water quality standards prearranged by the I.S. 10,500:2012 standards. Among the 5 physicochemical parameters, pH, TDS, turbidity, TH, and TA exceeded their respective permissible limits during one or more seasons, the most prominent being pH, turbidity, and TH. Dominant cations found in the study area are Na^+, Ca^{2+} and K^+. Amid the major cations, Na^+ and K^+ played a principal role. Among the major anions, F^- and NO_3^- played the most Dominant role. From the spatio-temporal GIS-based maps of the Dimoria block, it can be perceived that the groundwater superiority is anticipated to perk up in the M season in contrast to the PrM and PoM seasons. This is usually because of the dilution of contaminants during the rainy season.

The results acquired bestow the inevitability of addressing the civic, local proprietor, and the administration to be responsive and reactive on the contagion of groundwater existing in the Dimoria block. The administration should make methodical and practicable scheduling for recognizing an effectual groundwater eminence supervision structure and for its accomplishment. In prospect, the groundwater resources will encompass the chief allocation of water delivery schemes, therefore, strategies for the fortification of groundwater excellence are considered utmost necessary. Current condition of groundwater demands the incessant monitoring and obligatory groundwater quality enhancement methodologies accomplishment.

References

1. UNESCO (1995) A global geochemical database for environmental and resource management. In: Earth science, vol 19, UNESCO Publication, Paris
2. Gibbs RJ (1970) Mechanisms controlling world water chemistry. Science 170:1088–1090
3. Butler M, Wallace J, Lowe M (2002) Ground-water quality classification using GIS contouring methods for Cedar Valley, Iron
4. Machiwal D, Jha MK (2015) Identifying sources of groundwater contamination in a hard-rock aquifer system using multivariate statistical analyses and GIS-based geostatistical modeling techniques. J Hydrol Reg Stud 4:80–110
5. Kotoky P, Sarma B, Kotoky ED (2017) Assessment and mapping of fluoride contamination of groundwater of the hatigaon area of Assam, India using geographic information system. Int J Sci Res (IJSR) 6:1692–1698. https://doi.org/10.21275/ART20172734
6. Deshpande RD, Gupta SK (2004) Curr Sci 86(9):1216–1224
7. Hajigholizadeh M, Melesse AM (2017) Assortment and spatiotemporal analysis of surface water quality using cluster and discriminant analyses. Catena 151:247–258

8. Filik Iscen C, Emiroglu Ö, Ilhan S, Arslan N, Yilmaz V, Ahiska S (2008) Application of multivariate statistical techniques in the assessment of surface water quality in Uluabat Lake, Turkey. Environ. Monit Assess 144(1):269–276
9. APHA/AWWA/WEF (2012) Standard methods for the examination of water and wastewater. In: 20th edn, American public health association/American water works association/water environment federation, Washington DC, USA
10. Khwaja M, Anwar AV (2016) Studies on seasonal variation in ground water quality: a statistical approach. J Environ Res Dev 123–131
11. Sharma DA, Rishi MS, Keesari T (2016) Evaluation of groundwater quality and suitability for irrigation and drinking purposes in Southeast Punjab, India using hydrochemical approach. Appl Water Sci 3137–3150
12. Azis A, Yusuf H, Zulfiyah F, Muhammad S (2015) Water turbidity impact on discharge decrease of groundwater recharge in recharge reservoir. Procedia Eng 199–206
13. Pal P (2017) Chemical treatment technology. Ind Water Treat Proc Technol. 21–63
14. Baysal A, Ozbek N, Akman S (2013) Determination of trace metals in waste water and their removal processes. InTech Open, 21–63. https://doi.org/10.5772/52025
15. Mukherjee I, Singh UK (2018) Groundwater fluoride contamination, probable release, and containment mechanisms: a review on Indian context. Environ Geochem Health
16. Kotoky P, Sarma B, Kotoky ED (2017) Fluoride contamination of groundwater of the hatigaon area of Assam, India and the variation of fluoride content levels with the depth of wells. Int J Sci Dev Res (IJSDR) 2(4):509–516. http://www.ijsdr.org/papers/IJSDR1704098.pdf
17. Wei Y, Fan W, Wang W et al (2017) Identification of nitrate pollution sources of groundwater and analysis of potential pollution paths in loess regions: a case study in Tongchuan region, China. Environ Earth Sci 76:423
18. Chen J, Wu H, Qian H, Gao Y (2017) Assessing nitrate and fluoride contaminants in drinking water and their health risk of rural residents living in a semiarid region of northwest China. Expo Health 9(3):183–195
19. Adimalla N, Li P, Qian H (2019) Evaluation of groundwater contamination for fluoride and nitrate in semi-arid region of Nirmal Province, South India: a special emphasis on human health risk assessment (HHRA). Hum Ecol Risk Assess Int J 25(5):1107–1124
20. WHO (1993) Basic epidemiology ISBN 92 4 154446 5
21. WHO (2004) Guidelines for drinking water quality. In: Recommendations, vol 1, p 515, 3rd edn. WHO, Geneva
22. Appelo CAJ, Postma D (1996) Geochemistry, groundwater and pollution. AA Balkema Publ., U.S.A.
23. Narsimha A, Sudarshan V (2013) Hydrogeochemistry of groundwater in Basara area, Adilabad district, Andhra Pradesh, India. J Appl Geochem 15(2):224–237
24. Adimalla N, Venkatayogi S (2018) Geochemical characterization and evaluation of groundwater suitability for domestic and agricultural utility in semi-arid region of Basara, Telangana State, South India. Appl Water Sci 8(1):44

Fuzzy Random Uncertainty-Based Design of Water Distribution Network Using Cross-Entropy Optimization

Prerna Pandey, Shilpa Dongre, and Rajesh Gupta

Abstract Water distribution networks (WDNs) are considered to be one of the prime entities of urban infrastructure, which requires large investment for its construction. Hence, an optimal design of the same is considered appropriate. However, the nonlinear relationship between flow and head loss and availability of the discrete pipe sizes poses difficulty in getting an optimal solution. Also, over the time, uncertainty creeps in due to changes in water demand and values of pipe roughness coefficient which may cause the hydraulic failure of the System. This paper considers the uncertainty in water demand and pipe roughness coefficient which are modelled using fuzzy random variable (FRV) approach. The uncertainty in both the parameters is assumed to be normally distributed with fuzzy mean, and 10% of fuzzy mean as its standard deviation. The cross-entropy (CE) optimization is used for the uncertainty-based design of WDNs. The methodology is illustrated through two example networks from the literature. The computation time and optimal cost both are observed to be less, when compared with other metaheuristic approaches.

Keywords Water distribution networks · Fuzzy-random approach · Uncertainty · Water demand · Cross-entropy

1 Introduction

In the analysis of water distribution networks (WDN), it involves several uncertain parameters such as: (1) Pressure head requirement and future water demand at nodes which is difficult to analyse correctly. (2) Pipe roughness value. (3) Economic and environmental factors, i.e. discount rate and cost of repair of failed components, etc. Precise values of the parameters like future water demand and pipe roughness can be obtained when new. However, due to the ageing process

P. Pandey (✉) · S. Dongre · R. Gupta
Civil Engineering Department, Visvesvaraya National Institute of Technology (VNIT), Nagpur, Maharashtra 440010, India

B. Laishram and A. Tawalare (eds.), *Recent Advancements in Civil Engineering*, Lecture Notes in Civil Engineering 172,
https://doi.org/10.1007/978-981-16-4396-5_41

quantifying these values is difficult and causes some uncertainty. Hence, it is very much necessary to incorporate these uncertainties for a reliable design of WDNs.

In general, there exist two types of uncertainties, i.e. random and fuzzy. The uncertainty of random nature is caused due to natural variability and it is termed as irreducible or aleatoric uncertainty. Similarly, the uncertainty due to lack of knowledge or fuzziness is referred to as reducible or epistemic uncertainty. The major difference between the two approaches is that the prior one is a probabilistic or stochastic approach while the latter is possibilistic approach. The probabilistic approach is mainly statistical in nature and large reliable data are needed to define the probability distribution function (PDF) of any uncertain variable, which is treated as random variable. The approach thus suited best for such uncertain events/processes whose occurrence is uncertain, i.e. whether the event/process can occur or not and is based on binary characterization (either 0 or 1). However, the possibility-based approach considers uncertain parameter as fuzzy parameter and it is based upon possibility approach, thus considers the possibility (between 0 and 1) of occurrence of an event. The uncertainty associated with lack of information is appropriate to handle with fuzzy approach, while the fuzzy random approach holds good for simultaneous representation of randomness and fuzziness for uncertainty analysis. Such uncertain parameters are together known as fuzzy random variables (FRVs).

The probabilistic approach represents the uncertain parameters by means of probability distribution function (PDF) or cumulative distribution function (CDF). From the known PDF of uncertain parameter, PDF for output variable is generated using Monte Carlo simulation (MCS), Latin hypercube sampling (LHS), etc. [1]. This requires evaluations of thousands of alternatives making the process computationally intensive. Reference [2] used chance constrained nonlinear programming to formulate single objective design problem considering nodal demands, required pressures, and roughness coefficients as an uncertain parameter. Reference [3] proposed a robust nondominated sorting genetic algorithm II (RNSGAII), for multi-objective design considering uncertainties in nodal demands and pipe roughness. Reference [4] solved its model by integrating the First-Order-Reliability-Method (FORM) and GRG2 optimization program, hence providing an improved design solution. Reference [5] replaced MCS by integration-based uncertainty quantification technique and solved using modified genetic algorithm (GA).

To study the effect of imprecision and uncertainty in pipe roughness coefficients and nodal demands on system performance, fuzzy sets theory adopted [6]. Reference [7] has shown fuzzy uncertainty modelling to analyse the effect of uncertainty in nodal demands and pipe friction factors on pipe flows in the WDN using impact table approach. Reference [8] used cross-entropy (CE) method for WDN analysis under fuzzy demand. Reference [9] opted Newton–Raphson method with fuzzy demands for WDN analysis; and [10] obtained a reliable solution by transforming a fuzzy constrained optimization model into a deterministic model by taking the relationship between fuzzy demands and fuzzy nodal heads.

For uncertainty-based design of WDN, the uncertain parameters are either treated as random or fuzzy. However, as the water demand is uncertain due to both its random nature and insufficient knowledge about the same, recently some of the studies have considered simultaneous representation of randomness and fuzziness in the consolidated framework [11, 12]. Fuzzy random theory is observed to be one of advanced methods that have been appeared as a valuable tool to deal with probabilistic problems involving fuzzy data [8]. Recently [11] and [12] considered water demand as FRV in multi-objective optimization problem of minimizing the cost and maximizing the reliability, while [11] opted GA and [12] opted CE as optimization tool. The methodology resulted in cost-effective reliable design. The Hazen William coefficient also causes uncertainty due to various reasons such as aging of pipe, clogging, etc.

The aim of this paper is to present the uncertainty-based design of WDN considering through Fuzzy random approach. The uncertainty in both nodal demand and roughness coefficient is considered to be uncertain parameter and a benchmark network of two loop is solved. The cross-entropy technique is used as an optimization approach.

2 Methodology

2.1 Basic Concept of Fuzzy Random Approach

The FRV was first discovered by Kwakernaak [13]. The outcome of the random experiments is considered as fuzzy number instead of the crisp real value. He observed that both fuzzy and random approaches are fundamentally different from each other, as fuzzy is due to lack of data, while random is based upon huge statistical information. The approach holds good for uncertainties which are partially random and partially fuzzy in nature. Hence, a lot of efforts have been made [14] for an individual but simultaneous representation of both the uncertainties is referred to as fuzzy random approach and such variables are termed as fuzzy random variables (FRV) [15].

The concept of FRV is developed by combining the concept of both random and fuzzy approach. The approach can be considered as a mapping from probability space to fuzzy numbers. This can be shown as

$$\xi : \Omega \rightarrow F(\Re) \tag{1}$$

In case of random approach, uncertain parameter x is shown either by probability distribution function (PDF) or cumulative distribution function (CDF). These PDF/CDF can be obtained using various approaches such as MCS, LHS, FOSM, FORM as shown in Fig. 1a, while in case of fuzzy approach any uncertain parameter x is represented by the membership function $\mu(x)$ where its values range between 0 and 1. The most commonly used membership function is triangular one and is mostly

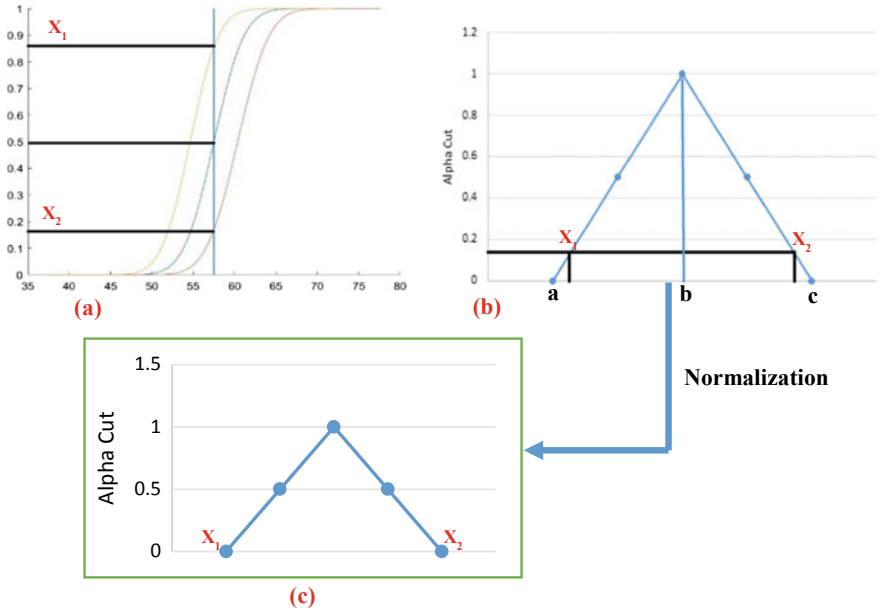

Fig. 1 Layout of fuzzy random representation. **a** CDF of input parameter drawn with the help of MCS. **b** Membership function of uncertain parameter drawn with impact table approach and the improved probability plot is shown in the same. **c** Normalized/new membership function plot considering both randomness and fuzziness

represented by triplet (a, b, c), where [a,c] represents the support and [b] represents the kernel of membership function. The α cut of uncertain parameter is expressed as set containing all values x having membership degree between $\alpha \in [0,1]$ as shown in Fig. 1b.

The approach first uses the probabilistic approach in order to get the improved cumulative probability spread. This new probability is spread is now been projected to fuzzy membership function. After the normalization the output of the dependent parameter is achieved. The layout of same is explained in Fig. 1.

2.2 *Application of the Methodology in Design of WDNs*

The hybrid uncertainty characterization methodology adopted in the paper is significantly different from purely random and purely fuzzy. The two uncertainty characterizations, i.e. fuzziness and randomness, in future water demand and pipe roughness are combined through FRV. As per the literature the uncertainty in both the parameter increases with time due to lack of knowledge about the same. This later causes the uncertainty in the system.

The uncertainty-based design of the network is carried out with the help of cross-entropy (CE) optimization method [12] as shown in Fig. 2. For the design commercial available pipe sizes are considered. Initially the probability is assigned to each candidate size for getting selected for the design. Then the sample size is assigned to set the diameter based on its probability. The EPANET is used for the hydraulic simulation of the WDNs after assigning the mean and standard deviation of the uncertain parameter. Through the simulation, pipe flows and nodal head is calculated which is later compared with minimum required head. If the criteria do not satisfy, the penalty will be applied. Later, the solutions are being arranged in the ascending order and the top 10–20% of the solutions are then being selected. The smoothening parameter is being applied in order to delay the convergence criteria. Lastly the stopping criteria are checked, i.e. whether the probability of selecting the candidate size is either reaching 0 or 1, and then the optimized cost of the network is declared.

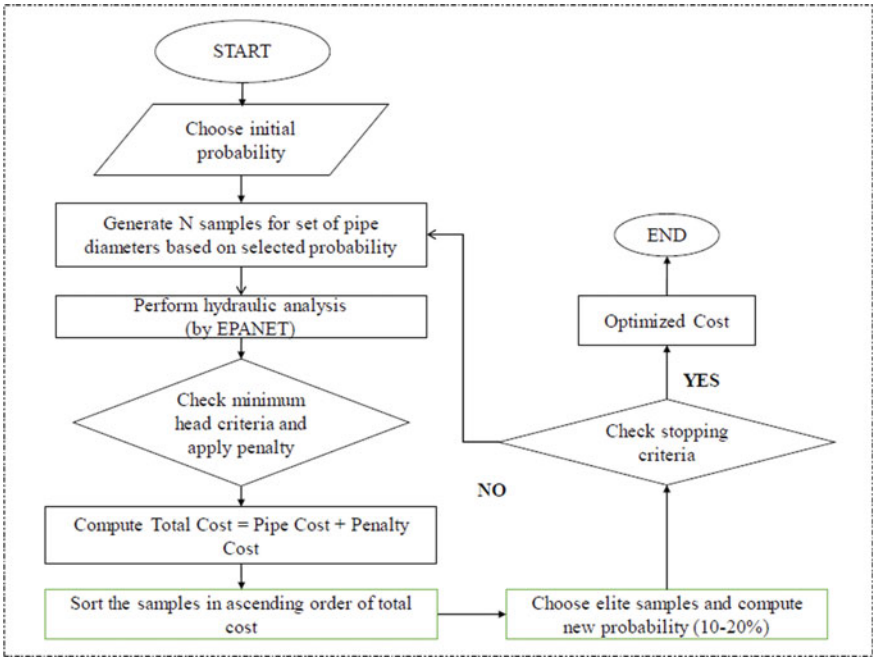

Fig. 2 Flow chart of cross-entropy optimization-based methodology for design of WDNs

2.3 Objective Function

The optimization problem for pipe networks can be formulated by the minimization of the objective function using the penalty function [16].

***Total pipe cost*:**

$$\textbf{Minimize cost},\ S(x) = \sum_{i=1}^{n_p} Cd_i l_i + \sum_{i=1}^{n_n} \text{PN*MAX}(0,\ H_j^{\min} - H_j) \tag{2}$$

***Subject to*:**

$$H_j^{\min} \geq H_j \tag{3}$$

***Conservation of mass*:**

$$\sum_{x \varepsilon j} Q_x^{\min} - q_j^{\min} = 0 \tag{4}$$

$$\sum_{x \varepsilon j} Q_x^{\max} - q_j^{\max} = 0 \tag{5}$$

For all demand node j shown in Eqs. 4 and 5.

Where, n_p is the number of pipe, $C(d)$ is the cost with respect to diameter, l is the length of the pipe, PN is the penalty function, $H_j^{\min}$is the minimum head required by the network, H_j is the head obtained by the hydraulic simulation, Q_x *is* pipe flow, q_j is nodal out flow (as shown in Eqs. 4 and 5).

3 Case Study

3.1 Two-Loop Network

A Two-loop WDN used for the study is opted from Alperovitz and Shamir [17], as shown in Fig. 3. It consists of eight pipes and six demand nodes supplied by a single reservoir at constant head of 210 m. The minimum head requirement at all consumer nodes is 30 m. The roughness coefficient for all the pipes is considered as 130.

The details of the network can be referred from the paper [17]. The uncertainties in roughness coefficient (C_{HW}) and nodal demand (q) are considered as fuzzy random variable. The normal distributions were assumed as 10% of original C_{HW} and q as standard deviation. The original C_{HW} and q value serve as triangular fuzzy number as its kernel of membership function and its support at variation of ±5%. The objective function is as shown in Eq. 1.

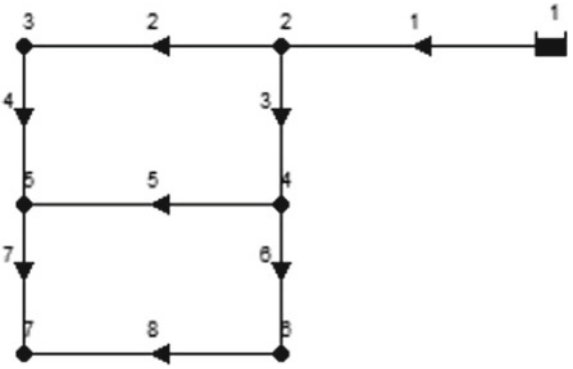

Fig. 3 Layout of two-loop water distribution network

It is considered that each pipe of the network can be constructed from one of 14 pipe diameters, as shown in Table 1. Hence, the problem search space is 1.48×10^9. The network is used by many researchers in the literature for, e.g. [16, 18, 19] and [20] for the optimal design of the network without any uncertainty. The cost of the network reported was 419,000$ after satisfying all the head constraint. The network is designed with fuzzy and fuzzy-random approaches both. For fuzzy 10% uncertainty considered for both the parameters. It is observed that the cross-entropy requires lesser evaluations to obtain the similar results, as shown in Table 3. Hence, the approach is further extended to use for uncertainty-based design. The fuzzy and fuzzy probabilistic-based design of the same networks is carried out and is compared the same (Table 2).

3.2 Hanoi Benchmark Network

Network is single source 34-link, real-life network, first presented by [21], as shown in Fig. 4. The objective of this case study is to test the methodology on a different more complex network. In the network, node one is the source node with HGL of

Table 1 Commercial pipe size and their unit cost for two-loop network

Pipe No	Diameter (in.)	Unit cost ($)	Pipe no	Diameter (in.)	Unit cost ($)
1	1	2	8	12	50
2	2	5	9	14	60
3	3	8	10	16	90
4	4	11	11	18	130
5	6	16	12	20	170
6	8	23	13	22	300
7	10	32	14	24	550

Table 2 Optimal solutions obtained for two-loop WDN considering fuzzy randomness in demand and roughness coefficient and comparing results with fuzzy using cross-entropy

Node no	Required head (m)	Fuzzy obtained head (m)	FRV obtained head (m)	Pipe no	Diameter obtained by fuzzy approach (mm)	Diameter obtained by FRV approach (mm)
1	180	196.4221	205.4209	**1**	16	20
2	190	194.292	201.5143	**2**	16	14
3	185	191.9543	200.8222	**3**	16	16
4	180	189.4915	196.9963	**4**	8	10
5	195	197.8413	196.9139	**5**	16	10
6	190	191.2227	193.9262	**6**	10	6
	210			**7**	12	12
				8	12	10
Deterministic design cost ($)		**419,000**	**COST ($)**		**515,000**	**482,000**

Table 3 Comparison of different evolutionary algorithm on the basis of its number of evaluation required for designing two-loop network

Sr. no	Evolutionary algorithm	No. of evaluations	Cost obtained ($)
1	Genetic algorithm	250,000	419,000
2	Simulated annealing	25,000	419,000
3	Shuffled frog leaping algorithm	11,232	419,000
4	Cross-entropy	7500	419,000

100 m, while nodes 2–32 are demand nodes with minimum HGL requirement of 30 m. The Hazen–Williams coefficient for all the pipes is 130.

The details of the network can be referred from the paper [21]. Both C_{HW} and q are considered as uncertainty where the normal distribution mean is represented by triangular fuzzy numbers which have kernel of original value of uncertain parameters and support of ±5% variation.

It is considered that each pipe of the network can be constructed from one of 6 pipe diameters in mm and their unit cost in rupees per metre length shown in parenthesis is, 304.8 (45.725); 406.4 (70.4); 508 (98.387); 609.6 (129.33); 762 (180.748) and 1016 (278.28). Hence, the problem search space is 2.86×10^{26}. The network is again opted by [16, 19] and many more for the optimal design of the network. Also the uncertainty-based design of the network was done by [10] using GA.

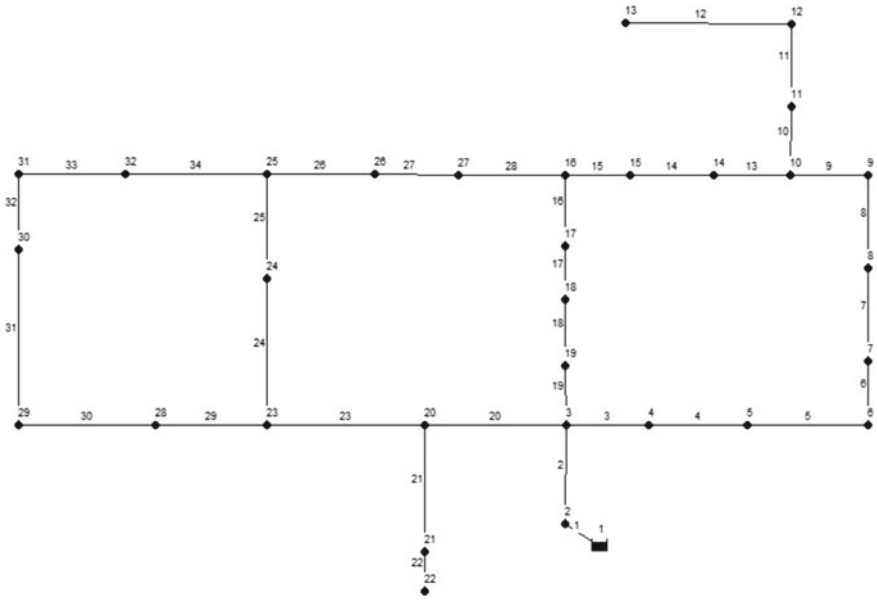

Fig. 4 Layout of Hanoi Benchmark Network

4 Results and Discussion

The methodology is applied to two-loop WDN for uncertainty-based design as explained in above section. To run the CE algorithm, the parameters assumed are as follows: Number of solutions generated, NS = 500, initial probability of selection, P = 1/nd, (nd = no. of nodes), smoothening parameter, α = 0.6, Penalty function, PN = 10^6. The stopping criteria are arrived in 7400 function evaluations. The results are as shown in Table 2. It is observed that the head constraint is satisfied for all the nodes. It is observed that while designing the network it is necessary to consider both the type of uncertainty for much economical and reliable network. The optimal cost obtained for fuzzy-random design of WDN observed is 482,000$.

The solution of fuzzy-randomness design is compared with deterministic and fuzzy-based design as shown in Table 2. The comparison of different evolutionary algorithms is as shown in Table 3. The values other algorithms are obtained from [19].

The methodology is also applied for the Hanoi network to understand the effect of the methodology in large and complex networks. To run the CE algorithm, the predefined parameters adopted are as follows: number of solutions, NS = 1000, initial probability, P = 1/nd; smoothening parameter, α = 0.55; and elite sample = 10. The stopping criteria are achieved at 76,500 function evaluations.

The results obtained by the methodology are as shown in Table 4. The results obtained are compared with deterministic and fuzzy solutions. The deterministic

Table 4 Optimal cost obtained for Hanoi network considering fuzzy randomness in water demand and pipe roughness coefficient using cross-entropy

Pipe no	Diameter (mm)	Pipe no	Diameter (mm)	Pipe no	Diameter (mm)
1	40	**13**	40	**24**	20
2	40	**14**	40	**25**	16
3	40	**15**	40	**26**	16
4	40	**16**	30	**27**	20
5	40	**17**	30	**28**	16
6	30	**18**	16	**29**	30
7	40	**19**	40	**30**	30
8	40	**20**	30	**31**	30
9	40	**21**	24	**32**	30
10	30	**22**	16	**33**	20
11	24	**23**	20	**34**	20
12	30				
Cost (Million $)					**8.141944**

Table 5 Comparison of optimal cost obtained by cross-entropy and genetic algorithm

Sr. no	Methodology (uncertainty; $q = \pm 10\%$, $C_{HW} = \pm 10$)	Cost (million $)
1	Genetic algorithm	9.647
2	Cross-entropy	8.436731

solution of the networks from the CE methodology is observed to be 7.064021 million $. The fuzzy-based results observed after considering q and C_{HW} uncertain parameter ($\pm 10\%$) is 8.436731 million $. Reference [10] also designed the same network considering similar uncertainty using GA, and reported the cost as 9.647 million $. Hence, the results obtained from CE for fuzzy-based design shows much economical solution than that of GA as shown in Table 5. Hence, methodology further applied to fuzzy-randomness design and reported solution as **8.141944 million $** as shown in Table 4**.** Also the head obtained by the methodology is well above the required head, i.e. 30 m. Hence, the methodology is reported to work well in the uncertainty-based design of WDNs.

5 Conclusion

This paper presents uncertainty-based design of WDNs using fuzzy probabilistic approach. The uncertainty in the pipe roughness (C_{HW}) and nodal demand (q) are represented with the help of fuzzy random variable which combines both the uncertainty. The Monte Carlo simulation approach has been used for random

sampling of both C_{HW} and q and the impact table approach is used to define the fuzzy-based uncertainty. To find the optimal solution, a combined simulation–optimization approach is adopted. EPANET is used as hydraulic solver and CE for the optimal design of WDNs.

The methodology is presented using two benchmark Networks. The results obtained are compared with the other evolutionary approach as shown in Tables 3 and 5. The optimal solutions obtained by the current methodology are observed to be cheaper and require less number of evolutions than that of the other approaches. It is also observed that the optimal solution quality is also improved after the combination of the fuzziness and randomness, hence resulting in the more reliable and economic design of WDNs.

References

1. Bao Y, Mays LW (1990) Model for water distribution system reliability. J Hydraul Eng 116 (9):1119–1137
2. Lansey KE, Duan N, Mays LW, Tung YK (1989) Water distribution system design under uncertainties. J Water Resour Plann Manage ASCE 115(5):630–645
3. Kapelan ZS, Savic DA, Walters GA (2005) Multiobjective design of water distribution systems under uncertainty. Water Resour Res 41(11):1–15
4. Xu C, Goulter IC (1999) Reliability-based optimal design of water distribution networks. J Water Resour Plann Manage ASCE 125(6):352–362
5. Babayan A, Kapelan Z, Savic D, Walters G (2005) Least-cost design of water distribution networks. J Water Resour Plann Manage ASCE 131(5):375–382
6. Revelli R, Ridolfi L (2002) Fuzzy approach for analysis of pipe networks. J Hydraul Eng 128 (1):93–101
7. Gupta R, Bhave PR (2007) Fuzzy parameters in pipe network analysis. Civ Eng Environ Syst 24(1):33–54
8. Shibu A, Reddy MJ (2011) Uncertainty analysis of water distribution networks by fuzzy-cross entropy approach. World Acad Sci Eng Technol 59:724–731
9. Spiliotis M, Tsakiris G (2012) Water distribution network analysis under fuzzy demands. Civ Eng Environ Syst 29(2):107–122
10. Dongre SR, Gupta R (2017) Optimal design of water distribution network under hydraulic uncertainties. ASCE-ASME J Risk Uncertainty Eng Sys Part A Civ Eng 3(3):G4017001–1–11
11. Fu G, Kapelan Z (2011) Fuzzy probabilistic design of water distribution networks. Water Resour Res 47(5):1–12
12. Shibu A, Reddy MJ (2014) Optimal design of water distribution networks considering fuzzy randomness of demands using cross entropy optimization. Water Resour Res 28(12):4075–4094
13. Kwakernaak H (1978) Fuzzy random variables-definitions and theorems. Inf Sci 29:1–29
14. Liu YK, Liu B (2003) Fuzzy random variables: a scalar expected value operator. Fuzzy Optim Decis Making 2(2):143–160
15. Pandey P, Dongre S, Gupta R (2020) Probabilistic and fuzzy approaches for uncertainty consideration in water distribution networks—a review. Water Supply 20(1): 13–27
16. Ezzeldin RM, Djebedjian B (2020) Optimal design of water distribution networks using whale optimization algorithm. Urban Water J 17(1):14–22

17. Alperovits E, Shamir U (1977) Design of optimal water distribution systems. Water Resour Res 13(6):885–900
18. El-Ghandour HA, Elbeltagi E (2018) Comparison of five evolutionary algorithms for optimization of water distribution networks. J Comput Civ Eng 32(1)
19. Sedki A, Ouazar D (2012) Hybrid particle swarm optimization and differential evolution for optimal design of water distribution systems. Adv Eng Inform 26(3):582–591
20. Mohan SA, Babu KJ (2010) Optimal water distribution network design with honey-bee mating optimization. J Comput Civ Eng 24(1):117–126
21. Fujiwara O, Khang DB (1990) A two-phase decomposition method for optimal design of looped water distribution networks. Water Resour Res 26(4):539–549

Efficient Division of Water Distribution Network into District Metered Areas: Application to Ramnagar Subzone of Nagpur City

Aniket N. Sharma, Shilpa R. Dongre, and Rajesh Gupta

Abstract Clustering of water distribution networks (WDNs) into hydraulic sectors or district metered areas (DMAs) is a multifaceted problem. It results in effective operation and maintenance by partially isolating some areas of WDNs with selective valves closures, however, may have drawbacks like reduced pressure and resilience in the network. The challenge is to identify a tradeoff between the merits and demerits of DMA formation. This paper therefore presents a simplistic three step methodology to identify the best suited clusters and DMAs configuration with the optimal number of valves and flow meters. The first step involves application of graph theory-based algorithm to identify clusters and subsequently the potential pipes (crossings) in a weighted graph of water network. In the second step, the methodology identifies the optimal combination of potential pipes that need to be kept open or closed without hampering the hydraulic feasibility of network using genetic algorithm (GA). Lastly, the network is evaluated for its performance. The methodology has been applied on a real water distribution network of Ramnagar zone of Nagpur City and results have been discussed.

Keywords District metered areas · Genetic algorithm · Graph theory · Performance indicators

1 Introduction

Rapid Urbanization has led to a tremendous increase in water demand since past few decades which has enhanced the complexity of design of water distribution networks. This causes a problem of poor operational control and leakage management. For a better operational control, the water distribution system can be converted into hydraulic sectors or district metered areas. This in turn gives enormous benefits,

A. N. Sharma (✉) · S. R. Dongre · R. Gupta
Research Scholar, Department of Civil Engineering, Visvesvaraya National Institute of Technology, Nagpur 440010, India

B. Laishram and A. Tawalare (eds.), *Recent Advancements in Civil Engineering*, Lecture Notes in Civil Engineering 172,
https://doi.org/10.1007/978-981-16-4396-5_42

i.e., ease of carrying out water audit, pressure regulation, leakage reduction and water quality control [1].

Converting the water network into systematic zones in terms of operation and maintenance through DMAs involves stepwise procedure. Since last decade innovative approaches have been addressed for network partitioning problem. In general, DMA formation is a two-step problem where first step identifies clusters (zones) of nodes with similar features and second step involves most suitable pipe closure for partial separation of clusters by optimizing objective function(s) without violating the corresponding (hydraulic, economic) constraints followed by implementation of management strategy.

The economic benefits of pressure management on real life district metered areas were analyzed. The optimal solution identified was approximately 2.5 times more beneficial as compared to the existing pressure management scheme [2]. The authors in [3] identified the effects of redesign of water networks into DMAs by evaluating water age, reliability and flow requirements. In [4], a topological clustering method was proposed based on flow direction. A design support methodology was worked out in [5] to identify permanent boundaries and fix up valves and flow meter locations by evaluating hydraulic and statistical performance indicators. The methodology provided satisfactory DMA layout in terms of resilience deviation ranging from 7.25 to 21.49%.

The method proposed in [6] identified optimal entry points at DMA entries for pressure and leakage management, whereas the authors in [7] proposed automatic creation of DMAs with heuristic methodology and compared the results with manually designed DMA layout [3], the results showed nearly similar results of water age and fire flow demand with respect to manually formed DMA configuration. In [8], the authors clubbed graph theoretic algorithm with DMA design criteria of minimum and maximum size and proposed a heuristic method to form DMAs with fixed boundaries. In [9], the existing water network was reconfigured into various zones for pressure and water loss control with various direct and surrogate performance indicators.

Various other approaches have been proposed for automatic and decision support methodologies for DMAs formation [10–13]. In [14], a novel approach of dynamic DMAs formation was proposed where the network is capable to self-adapt its existing boundaries in case of uncertain events like increase in peak demands. Results showed that 82% of the resilience is restored using 94% of the existing infrastructure. Recently, [15] proposed a computationally efficient heuristic methodology for least cost design of DMAs which provided sound and realistic sectorization solutions with same level of operational performance.

Graph theory algorithms (graph partitioning, clustering and communities identification) are generally used in the sectorization problem of water networks where the community identification approaches (*Fast greedy algorithm, Random walk algorithm, Louvain algorithm,* etc.) have been the focus of current research. This is because the complex water networks can be abstracted as a graph for identification of communities which are a group of vertices within which connections are dense but between which the connections are sparse. The former ensures service and

water security (redundancy) considerations while the latter ensures supply of water in each community.

The authors in [16] defined modularity as a performance indicator of network communities. Many researchers have used modularity-based algorithms for DMA formation in water networks [7, 11, 17–19]. Although there is a continuous research in the area, a lot of unexplored areas like defining parameters for suitable pipe weights, main lines identification, DMA formation approaches for single and multi-sourced networks, use of suitable valves and their locations, economic considerations, field application of DMAs formation strategies with consideration of socio-economic factors, etc., still remains untouched.

This study therefore presents a methodology of DMA formation in a most economical way and its application on a real life water network. First, the fast greedy algorithm [20] is used with average nodal pressure as pipe weights so that nodes with near similar pressure can be clustered together. This algorithm optimizes the modularity function in a comprehensive manner; also it reflects the effect of weighted edges in the partitioning. Secondly, the open or closed status of potential boundary pipes is obtained using optimization tool without hampering the hydraulic capability of water network. The objective of the study has been defined based on the cost of implementation of DMA strategy, and lastly, the performance of the partitioned network has been evaluated using energy and statistical indices as performance indicators.

2 Methodology

The methodology used in this paper forms communities with near similar pressure at nodes in each community and gives optimal number of interconnecting pipes which are then evaluated for fixing the DMA boundaries. The flow chart is shown in Fig. 1 and explains the methodology adopted in this paper to form optimal DMA configuration of the network under consideration.

2.1 Mapping the Water Distribution Network as a Graph (Initialization)

Graphs are represented as structures, topologically formed by connecting links (or edges—it is interchangeably used in this paper) and nodes (or vertices). Graph theory is used to study such structures and the topology of water networks coincides with graphs. Thus, the water distribution system has been mapped into an undirected graph $G(V, E)$ [4] where $V = \{v_1, v_2, v_3, \ldots, v_n\}$ represents set of vertices, i.e., demand nodes, tanks, reservoirs; and $E = \{e_1, e_2, e_3, \ldots, e_n\}$ represents set of edges, i.e., pipes, valves and pumps.

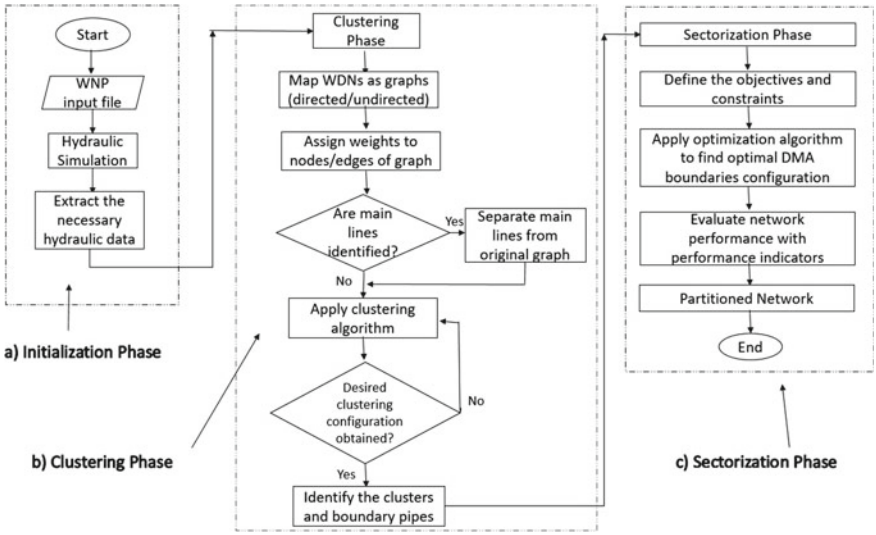

Fig. 1 Flow chart of the proposed methodology

2.2 *Communities Identification (Clustering Phase)*

In this paper, communities in a graph (G) are identified with modularity-based algorithm proposed by [4] because of its capability of fast and reliable decomposition of very large and complex graphs. It states that the edges are densely connected within the communities and they are sparse between the communities. Modularity is used as an indicator of graph division and is defined as the number of edges falling within groups minus the expected number in an equivalent network with edges placed at random. Positive magnitude of modularity indicates the strong presence of a community structure, zero value indicates random distribution of edges and negative value indicates the absence of communities. Mathematically, it can be written as

$$Q = \frac{1}{2m}\sum_{U\omega}\left[A_{U\omega} - \frac{k_U k_\omega}{2m}\right]\delta(C_U, C_\omega) \tag{1}$$

where $A_{U\omega}$ = element of the adjacency matrix of the network ($A_{U\omega} = 1$ if vertices U and ω are connected; otherwise, $A_{U\omega} = 0$); $m = \left(\sum_{U\omega} A_{U\omega}\right)/2$ total number of edges; $k_U = \left(\sum_{\omega} A_{U\omega}\right)$ = degree of vertex U, defined as the number of edges connected to that vertex; $\delta(C_U, C_\omega) = 1$ if $C_U = C_\omega$ (otherwise = 0); C_U and C_ω = two different communities; U and ω = vertices in C_U and C_ω, respectively; and $k_U k_\omega/2m$ = probability of an edge existing between vertices U and ω if connections are randomly made (respecting vertex degrees).

Equation (1) can also be written as

$$Q = \sum \left[e_{ii} - a_i^2 \right] \tag{2}$$

Since this algorithm assues each node as a single community at the initial phase and then merging of communities takes place which increases the modularity, such an approach is called bottom-up approach or agglomerative method. Change in modularity due to merging of communities is given by

$$\Delta Q_{ij} = 2\left(e_{ij} - a_i a_j\right) \tag{3}$$

where e_{ii} is the faction of edges belonging to the same community say 'i'; a_i represents fraction of edges connecting other vertices or communities;e_{ij} are the links connecting the communities 'i' and 'j,' respectively. The initial values of ΔQ_{ij} and a_i are

$$\Delta Q_{ij} = \begin{cases} 1/2m - k_i k_j/(2m)^2, & \text{if } i \text{ and } j \text{ are connected} \\ 0, & \text{otherwise} \end{cases} \tag{4}$$

And

$$a_i = (k_i/2m) \tag{5}$$

The algorithm has been explained with a simple example by considering a small graph having 6 vertices and 10 edges with unit weights assigned to them (different edge weights can be assigned as per the requirements of the problem). Figure 2a–e shows the step by step formation of communities and subsequently the dendogram representation of the procedure (Fig. 2f).

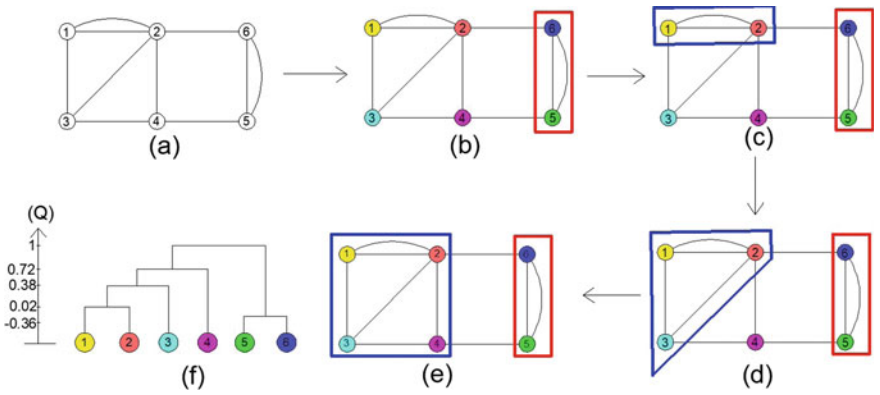

Fig. 2 Application of fast greedy algorithm [4] on a simple graph

Steps involved: Calculations for a single iteration have been explained as follows.

1. Calculate e_{ij} matrix

$$\begin{bmatrix} 0 & 0.2 & 0.1 & 0 & 0 & 0 \\ 0.2 & 0 & 0.1 & 0.1 & 0 & 0.1 \\ 0.1 & 0.1 & 0 & 0.1 & 0 & 0 \\ 0 & 0.1 & 0.1 & 0 & 0.1 & 0 \\ 0 & 0 & 0 & 0.1 & 0 & 0.2 \\ 0 & 0.1 & 0 & 0 & 0.2 & 0 \end{bmatrix}$$

where the elements in e_{ij} matrix (adjacency matrix) indicate the connectivity between adjacent elements divided by the total number of edges.

2. Calculate ΔQ for every possible combination of two vertices using Eq. (3)

$$\Delta Q_{12} = 2(0.2 - 0.3 \times 0.4) = 0.16$$
$$\Delta Q_{13} = 2(0.1 - 0.3 \times 0.3) = 0.02$$
$$\Delta Q_{24} = 2(0.1 - 0.5 \times 0.3) = -0.1$$
$$\Delta Q_{26} = 2(0.1 - 0.5 \times 0.3) = -0.1$$
$$\Delta Q_{23} = 2(0.1 - 0.5 \times 0.3) = -0.1$$
$$\Delta Q_{34} = 2(0.1 - 0.3 \times 0.3) = 0.02$$

3. Merge vertices with maximum value of ΔQ into a single community

From step 2, the highest change in modularity is obtained from ΔQ_{56}, hence vertices 5 and 6 are combined into a single community as shown in Fig. 2b.

4 Calculate modularity (Q) after merging vertices using Eq. (2) and update the dendogram.

$$Q = (-0.3)^2 + (-0.5)^2 + (-0.3)^2 + (-0.3)^2 + \left(0.2 - 0.2^2\right) = -0.36$$

5 Update the e_{ij} matrix post merging for the next iteration and go to step 1

$$\begin{bmatrix} 0 & 0.2 & 0.1 & 0 & 0 \\ 0.2 & 0 & 0.1 & 0.1 & 0.1 \\ 0.1 & 0.1 & 0 & 0.1 & 0 \\ 0 & 0.1 & 0.1 & 0 & 0.1 \\ 0 & 0.1 & 0 & 0.1 & 0.2 \end{bmatrix}$$

Table 1 Modularity change for each iteration and community's identification

Iteration	ΔQ	Communities	Q
1	$\Delta Q_{12} = 0.16$, $\Delta Q_{13} = 0.02$, $\Delta Q_{24} = -0.1$, $\Delta Q_{26} = -0.1$, $\Delta Q_{23} = -0.1$, $\Delta Q_{34} = 0.02$, $\Delta Q_{45} = 0.02$, $\Delta Q_{56} = 0.22$	$C_1 = \{1\}$, $C_2 = \{2\}$, $C_3 = \{3\}$, $C_4 = \{4\}$, $C_{5-6} = \{5,6\}$	−0.36
2	$\Delta Q_{12} = 0.16$, $\Delta Q_{13} = 0.02$, $\Delta Q_{23} = -0.1$, $\Delta Q_{24} = -0.1$, $\Delta Q_{2,5-6} = -0.01$, $\Delta Q_{34} = 0.02$, $\Delta Q_{4,5-6} = 0.02$	$C_{1\text{-}2} = \{1,2\}$, $C_3 = \{3\}$, $C_4 = \{4\}$, $C_{5\text{-}6} = \{5,6\}$	0.02
3	$\Delta Q_{1-2,3} = 0.16$, $\Delta Q_{1-2,4} = 0.04$, $\Delta Q_{1-2,5-6} = 0.04$, $\Delta Q_{34} = 0.02$, $\Delta Q_{4,5-6} = 0.02$	$C_{1\text{-}2\text{-}3} = \{1,2,3\}$, $C_4 = \{4\}$, $C_{5\text{-}6} = \{5,6\}$	0.38
4	$\Delta Q_{1-2-3,4} = 0.22$, $\Delta Q_{1-2-3,5-6} = 0.08$, $\Delta Q_{4,5-6} = 0.08$	$C_{1\text{-}2\text{-}3\text{-}4} = \{1,2,3,4\}$, $C_{5\text{-}6} = \{5,6\}$	0.72

Table 1 shows the calculations of remaining iterations performed in the communities' identification.

A brief idea of identification of communities has been presented in the above steps, in depth explanation of the methods and their application to water distribution network can be found in [7, 11, 20].

Here, the communities have been identified using '*Gephi*' which is a free software program specially used for graph network visualization and analysis. To identify clusters in the graph, suitable data in a compatible file format is given as inputs to '*Gephi.*' The level of decomposition or the number of communities to be formed is controlled by the '*Resolution limit*' function in the software. By default, the value is set to 1.0; higher values form fewer communities and vice versa. This software gives the flexibility to fix the level of decomposition, as it is important in case of water network to find suitable size of clusters or communities and can be achieved based on trial and error by various resolution limits.

2.3 Cost Effective Design of the DMAs (Sectorization Phase)

The optimal DMA design procedure aims at determining the best combination of open/closed status of potential pipes, i.e., status of the interconnecting pipes between two DMAs obtained from clustering phase. This affects the cost of DMA implementation as the fully or partially open pipe leads to an additional cost of flow meter for each open pipe. As we know, changing the pipe status could change the original flow path, resulting in more head loss in the network and subsequently lower operational pressure conditions in the network. This may have good or bad effects on the network depending upon the initial power in the network. For low overall pressure conditions, this is not a desirable option. Thus, the pipe status becomes the decision variables in a cost optimization problem.

The problem of DMA implementation in this study has been expressed as follows:

For a given layout of water network containing links and demand nodes with specified demand patterns, find the Total Cost Function (TCF) for optimal DMAs configuration; subjected to the constraints of node flow continuity, loop head loss and minimum pressure requirements at each demand node.

$$\text{Min(TCF)} = \sum_{l=1}^{N_{\text{iv}}} C_{\text{iv}} + \sum_{k=1}^{N_{\text{fm}}} C_{\text{fm}} \tag{6}$$

$$\text{subject to :} H_{i\,\min} \leq H_i; \quad i = 1, ...n(\text{nodal pressure constraint}) \tag{7}$$

$$\sum_{x\,\text{incident on}\,j} Q_x + q_j = 0; \quad j = 1, ...n(\text{flow continuity constraint}) \tag{8}$$

$$\sum_{x \in y} h_x + \sum E_p = 0; \quad y = 1, \ldots, Y(\text{energy conservation constraint}) \tag{9}$$

In which C_{iv} = unit cost of isolation valve; C_{fm} = unit cost of flow meter; $H_{i\,\min}$ = minimum permissible head at node 'i'; q = nodal demand; n = total number of nodes; x is link in the network; Y represents total number of loops; 'h' = head loss in pipe; E = energy provided by pump.

There are various evolutionary techniques available to handle constrained optimization problems. For this particular study, real coded genetic algorithm (GA) has been used for fixing the pipe status. This is because the real coding does not need coding and decoding of variables, hence reducing the computational complexity.

For handling nonlinear constraints penalty functions can be utilized. The penalty function penalizes the infeasible solution and helps to discard such solutions to achieve convergence toward feasibility. The penalty cost is a function of constraints violations and penalty multiplier; greater the constraint violation, greater is the penalty cost [21]. In this study, the penalty multiplier derived by [21] has been used. As the objective function is not formally defined based on the decision variables, hence, such a relationship is not trivial to formulate. In order to tackle, this problem a hydraulic network solver (EPANET) has been used. Also, the constraints mentioned in Eqs. (8) and (9) are handled through hydraulic network solver and Eq. (7) is considered through a self-organizing penalty factor. Hence, Eq. (6) can be written as:

$$\text{Min(TCF)} = \sum_{l=1}^{N_{\text{iv}}} C_{\text{iv}} + \sum_{k=1}^{N_{\text{fm}}} C_{\text{fm}} + \sum_{j=1}^{n} p \times q_j \times \left\{ \max\left(H_j^{\text{des}} - H_j^{\text{avl}}, 0 \right) \right\} \tag{10}$$

in which p = penalty multiplier; and $\left\{\max\left(H_j^{\text{des}} - H_j^{\text{avl}}, 0\right)\right\}$ = maximum violation of the pressure constraint at node j. Penalty multiplier at a node is calculated based on the capitalized energy cost to pump a unit quantity of water through a unit head and is mathematically expressed as follows:

Capitalized energy cost of pumping is given by

$$C_{\text{e}} = \text{PWF} \times C_{\text{ea}} \tag{11}$$

In which PWF is present worth factor and C_{ea} is annual energy charges

$$\text{PWF} = \frac{(1+i_{\text{r}})^m - 1}{i_{\text{r}}(1+i_{\text{r}})^m} \tag{12}$$

$$C_{\text{ea}} = c_{\text{e}} \times P_{\text{w}} \times t_{\text{p}} \tag{13}$$

$$P_{\text{w}} = \frac{w \times q_j \times h_{\text{p}}}{1000 \times \eta} \tag{14}$$

In which i_{r} = interest rate, expressed as a fraction of one; m = design life of the WDN; c_{e} = cost of the unit energy in monetary units per kWh; P_{w} = pump power (kW); t_{p} = total time of the pump operation in a year (hours); w = specific weight of water (9810 N/m^3); h_{p} = head supplied by the pump (=deficiency in pressure head at node j in meters); and η = overall efficiency (dimensionless).

Therefore, Eq. (11) becomes

$$C_{\text{e}} = \text{PWF} \times c_{\text{e}} \times \frac{w \times q_j \times h_{\text{p}}}{1000 \times \eta} \times t_{\text{p}} \tag{15}$$

And the penalty multiplier p is given by

$$p = \frac{C_{\text{e}}}{q_j \times h_{\text{p}}} \tag{16}$$

Say, if the interest rate i_{r} is 8%; design period (m) = 30 years; per unit pumping cost (c_e) = 4.5 Rs/kWh and efficiency (η) = 0.6 and t_{p} = 24 × 365 (hours), therefore the penalty multiplier (p) = 7.26 × 10^6.

Since the demand driven analysis (DDA) assumes that the nodal demands are always satisfied, it cannot quantify the unsupplied customer demand. Hence, there is a need to analyze the network using pressure dependent analysis (PDA) as it predicts better network performance under deficient conditions considering both demands and pressure requirements simultaneously through node-head-flow relationship (NHFR). The non-iterative use of EPANET suggested in [22] for PDA has been clubbed with the genetic algorithm. Also, the objective function has been slightly modified in terms of penalty multiplier as shown in Eq. (17) [23].

$$\text{Min(TCF)} = \sum_{l=1}^{N_{\text{iv}}} C_{\text{iv}} + \sum_{k=1}^{N_{\text{fm}}} C_{\text{fm}} + \sum_{j=1}^{n} p \times \left(q_j^{\text{des}} - q_j^{\text{avl}}\right) \times \left\{\max\left(H_j^{\text{des}} - H_j^{\text{avl}}, 0\right)\right\} \tag{17}$$

2.4 Performance Evaluation

As the optimal DMA configuration of the given network is obtained, it is necessary to evaluate the reliability of the partitioned network. In this regard, there are many reliability surrogate measures available in the literature where [5] classified the performance indicators into energy indices (resilience index) and statistical indices (mean, minimum, maximum and mean square root of hydraulic heads). This paper uses resilience index introduced by [24] as a performance indicator. It measures the excess power in the system. Since the DMA formation methodology involves closure of pipes, this increases the energy losses in the system. It is the ratio of surplus energy and input energy minus the required energy. Mathematically it is expressed as:

$$f_{\text{RI}} = \frac{\sum_{i=1}^{\text{nn}} q_i\left(h_{a,i} - h_{r,i}\right)}{\sum_{\text{sr}=1}^{\text{nr}} Q_{\text{sr}} H_{\text{sr}} + \sum_{\text{sp}=1}^{\text{np}} \frac{P_{sp}}{\Upsilon} - \sum_{i=1}^{\text{nn}} q_i h_{r,i}} \tag{18}$$

where nn = number of demand nodes; np = number of pumps; nr = number of reservoirs; q_i = demand at node i; $h_{a,i}$ = available head at demand node i; $h_{r,i}$ = required head at demand node i; Q_{sr} = supply at reservoir sr; H_{sr} = head at reservoir sr; P_{sp} = power from pump sp; and Υ = specific weight of water (KN/m^3).

The resilience index is mainly related to hydraulic failure based reliability such as demand variation and fire flow and is not used as mechanical reliability on pipe failure [12]. It is an energy index which is directly proportional to the available power in the water network. Higher resilience index value indicates that the network is more reliable to maintain required nodal heads in abnormal flow conditions. It ranges from 0 to 1 in normal conditions. Similarly, statistical performance indicators like mean (H_{mean}), minimum (H_{min}) and maximum nodal heads (H_{max}) have also been identified in the study to judge the performance of the partitioned network.

3 Case Study

The methodology presented here is implemented on the Ramnagar GSR operational hydraulic zone located in the western part of Nagpur city comprising of residential, institutional and commercial customers. As we know, the maximum hour demand is

Table 2 Main characteristics of Ramnagar GSR operational hydraulic zone

Characteristic	Value
Number of nodes	293
Number of links	377
Number of reservoirs	1
Desired pressure (meters)	8
Average demand (LPS)	139.72
Peak demand (LPS)	208.55

the worst case scenario experienced by a WDN during the daily operations; DMAs should be designed for this condition. The main characteristics of the water network under consideration have been tabulated in Table 2.

As mentioned in the methodology, the hydraulic analysis of the original network was performed in EPANET software and the data of link-nodes connectivity and average nodal pressure of all the demand nodes was extracted. Pressure is an essential parameter to analyze gravity fed and pumped networks since it affects the capability of network to cater the customer demands as well as leakages from pipes.

Use of nodal pressure as an attribute results into a solution of clusters with the least connectivity between two clusters with nearly similar pressure inside the clusters and at the same time, different pressure regimes between contagious clusters. This gives a clear picture of various pressure zones and subsequently reduces the complexity of valves, flow meter and pressure control valves (PCVs) localization problem. Also, it has an added advantage of identifying the most suitable nodes to be used as pressure set points of PCVs for various DMAs.

Equation (19) has been used to assign pressure-based pipe weights [11].

$$W_{ij} = \frac{Pi_{\text{avg}} + Pj_{\text{avg}}}{2} \tag{19}$$

where P_{avg} is the average nodal pressure for nodes 'i' and 'j' respectively.

The weights were assigned to edges (i.e., pipes) of the graph and fast greedy algorithm was applied as explained earlier in this paper. Figure 3 shows the clustering results of five different DMA configurations obtained using the proposed method containing 11–15 clusters.

After identifying the clusters, the next step identified the potential pipes that need to be closed among the set of boundary pipes without hampering the hydraulic capacity of the network using real coded genetic algorithm (available on Kanpur GA Lab, IIT Kanpur http://www.iitk.ac.in/kangal/codes.shtml). Table 3 provides the unit cost of flow meters and valves adopted in this study for various commercial sizes of pipes.

The minimum value of head required to satisfy the customer demand was fixed to 8 m of water column. Hence, any node with value less than the minimum required would lead to unsupplied customer demand. In this study, a minimum

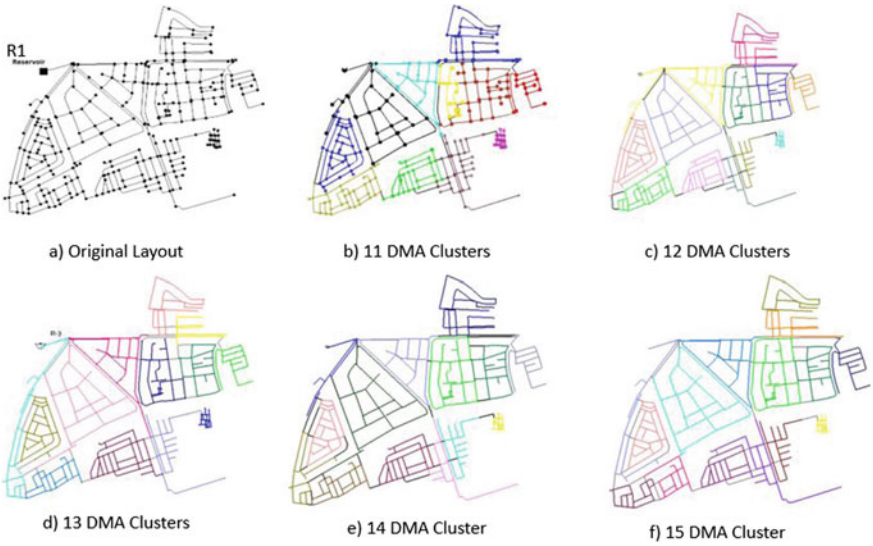

Fig. 3 Results of clustering phase (5 DMAs configurations)

Table 3 Commercial rates of valves and Flow meters

Pipe diameter (mm)	Unit cost of valves (in Rs.)	Unit cost of flow meters (in Rs.)
100	18,831	98,041
150	28,247	1,05,692
200	44,053	1,25,138
225	53,000	1,32,000
250	63,396	1,38,297
300	81,115	1,58,628
350	1,08,154	2,19,362
400	1,80,478	2,49,122
450	2,46,243	2,66,894
500	2,89,697	3,10,486

violation of constraint was allowed, i.e., solution with unsupplied customer demand less than 1% of the total demand was considered in the solution set. Table 4 shows the parameters of genetic algorithm used for optimizing the cost function (Eq. 17). The optimal solutions for each of the DMAs configuration have been evaluated and discussed in the next section.

Table 4 GA parameters used in cost optimization problem

Parameter	Value
Population size	50
Total number of generations	50
Cross over probability	0.8
Mutation probability	0.1
Number of variables	Equal to number of boundary pipes
Lower bound of variable	0
Upper bound of variable	1
Total number of runs performed	1
Unit cost of flow meter (in Rs.)	Refer Table 3
Unit cost of isolation valve (in Rs.)	Refer Table 3
Penalty multiplier (p) (in Rs.)	7.26×10^6

4 Results and Discussion

The main objective of the methodology is to minimize the overall cost of implementation of DMA formation strategy. The obtained network configurations have been evaluated for performance indicators like resilience index; also, the values of minimum, maximum and average nodal heads as well. It is obvious that more number of DMAs will lead to more number of boundary pipes and subsequently a costlier design. The overall operating power in the given network is less, so it becomes necessary to evaluate the network through PDA for unsupplied customer demand.

The results of optimized network configuration obtained for different alternatives have been shown in the following Table 5.

It can be observed from Table 5 that the modularity of the partitioned network configuration for all the alternatives was good (i.e., >0.8). However, the cost of implementation increased as the number of DMAs increased due the fact that number of potential pipes also got increased. The cost of implementation of 13 DMAs and 15 DMAs strategy was nearly similar. The minimum nodal requirements were also violated for these two configurations and which resulted in unsupplied customer demands. The 13 DMAs configuration was the worst out of all alternatives due to higher costs, low availability of nodal heads. The resilience index of this solution was the least (0.3) and the unsupplied customer demand of the solution was relatively higher (0.279).

The 12 DMAs configuration outperformed all other options in all aspects, i.e., at lesser cost of implementation (Rs. 18, 05,943), the network performed relatively better with nodal head requirements being satisfied (>8 MCW) resulting into full demand satisfaction and the resilience index of the network was 0.39 which indicated its ability to sustain uncertainties more efficiently than other configurations.

Table 5 Results of the various DMA configurations

Parameter	Alternative				
	11 DMAs	12 DMAs	13 DMAs	14 DMAs	15 DMAs
Modularity	0.847	0.84	0.837	0.835	0.832
No. of boundary pipes	19	23	31	30	33
No. of isolation valves	10	10	15	15	18
No. of flow meters	9	13	16	15	15
Cost in Rs	1,691,115	1,805,943	2,351,279	2,181,781	2,312,757
Resilience index	0.45	0.39	0.3	0.32	0.39
H_{min} (m)	7.545	8.782	6.466	8.252	6.325
H_{max} (m)	21.51	19.386	17.447	17.592	18.585
H_{mean}(m)	12.53	13.74	12.03	12.4	13.70
Unsupplied customer Demand (LPS)	0.043	–	0.279	–	0.164

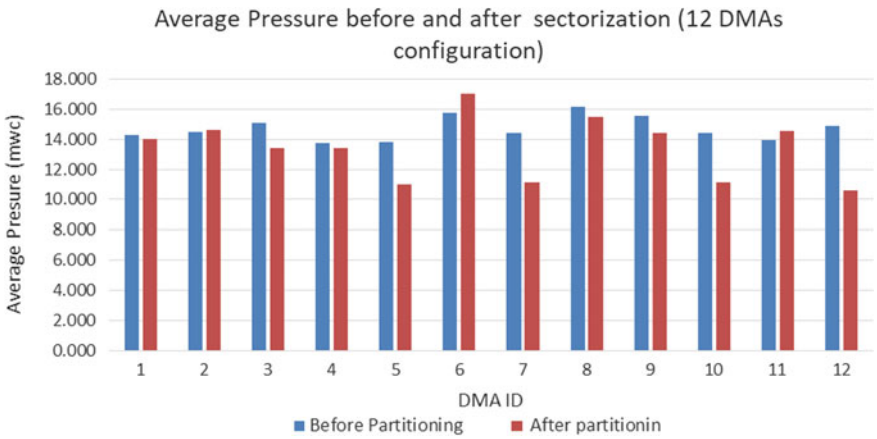

Fig. 4 Average pressure values in each DMA before and after sectorization for 12 DMAs

Figure 4 shows the average pressure values in individual DMAs before and after sectorization for 12 DMAs configuration.

Similarly the 11 DMAs configuration had the least number of potential pipes which resulted into the best solution in terms of cost, but this configuration violates the minimum available nodal head criterion hence resulting into very small unsupplied customer demand. This configuration can also be adopted when the spending capacity of water utilities is less. In fact, this configuration has the best resilience index value among all.

Lastly, the cost of 14 DMAs configuration is relatively higher with respect to 12 DMAs option, when compared to the performance of the two configurations, 12 DMAs configuration gave slightly better performance at lesser cost of implementation of the strategy.

In this study, the performance of individual DMA was evaluated for the best DMA configuration (12 DMAs).It can be seen from Fig. 4 that the average pressure in individual DMA has been reduced due to closure of pipes. Such pipe closure can cause increased water age. The flow inside the pipes takes longer route hence increasing head loss and deteriorating the water quality, water quality has not been covered in this paper.

The next step after identification of DMAs would be to regulate pressures inside them by identifying the most critical nodes inside the DMAs and placing pressure control valves (PCVs) at entry points of DMAs with optimal setting, thus the water network can be monitored at micro level for leakages and pipe burst events. This therefore becomes the extension of the work to apply pressure management scheme to the partitioned network.

Previous studies have reported use of multiple attributes together as pipe weights to identify clusters. There is still a need to explore more on assignment of pipe weights. The pipe weightages changes the configuration of clusters. It is difficult to arrive at generalized equation of pipe weights as it involves both nodal attributes (demand, pressure, elevation) and edge attributes (pipe flow, length of pipe, etc.).

In this study, the sizing criteria of DMAs (500–5000 customers connections per DMA) suggested by IWA guidelines have not been considered. The use of such a criterion is subjective as DMA implementation needs investment. Water utilities with strict budget constraints may not be able to satisfy the sizing criteria. Hence, bigger sized DMAs with manageable configurations can be opted.

Previous studies related to optimal design of DMAs lacked this feature as the penalty multipliers were defined with a fixed value of very high magnitude. The penalty multiplier used in this study quickly converged the solution toward optimum and gave realistic results of cost function. It was also observed that the demand driven analysis depicts higher pressure deficiencies as compared to pressure driven analysis.

Since multiple attributes are evaluated during the whole procedure for evaluating the performance of DMAs configuration, it is necessary to develop a methodology which will deal with many objectives at a time and provide flexibility to select a solution out of a set of solutions.

5 Conclusions

This paper presents a simplistic method for DMA formation based on fast greedy algorithm and cost optimization. The method includes three main steps a) network clustering; b) boundary optimization with genetic algorithm; and c) performance evaluation of partitioned network. The methodology was applied to real water distribution network of Nagpur city. The results indicate that the proposed method can decompose the water network into satisfactory sub-networks and minimum nodal head requirements with minimum cost of implementation can be achieved. The areas of possible future works have been identified and discussed in the paper.

Finally, it is worth noting that with the proposed method, like many other available techniques, good results of DMA configuration can be achieved by carefully applying the method with sound engineering judgment.

References

1. Morrison J, Tooms S, Rogers D (2007) DMA management guidance notes. IWA Publication
2. Awad H, Kapelan Z, Savic DA (2009) Optimal setting of time modulated pressure reducing valves in water distribution networks using genetic algorithms. In: Boxall J, Maksimovic C (eds) Integrating water systems. Taylor & Francis, London, pp 31–37
3. Grayman WM, Murray R, Savic DA (2009) Effects of redesign of water systems for security and water quality factors. In: World environmental and water resources congress 2009, ASCE, Reston
4. Perelman L, Ostfeld A (2011) Topological clustering for water distribution systems analysis. Environ Modell Softw 26(7):969–972
5. Di Nardo A, Di Natale M, Santonastaso GF, Venticinque S (2011) Graph partitioning for automatic sectorization of a water distribution system. In: Proceedings of CCWI 2011, University of Exeter, UK
6. Gomes R, Marques A, Sousa J (2012) Decision support system to divide a large network into suitable district metered areas. Water Sci Technol 65(9):1667–1675
7. Diao K, Zhou Y, Rauch W (2013) Automated creation of district metered area boundaries in water distribution systems. J Water Resour Plann Manage 139(2):184–190
8. Ferrari G, Savic D, Becciu G (2014) Graph-theoretic approach and sound engineering principles for design of districted metered areas. J Water Resour Plann Manage 140(12)
9. Perelman L, Allen M, Preis A, Iqbal M, Whittle A (2015) Flexible reconfiguration of existing urban infrastructure systems. Environ Sci Technol 49:13378–13384
10. Galdiero E (2015) Multi-objective design of district metered areas in water distribution networks. Ph.D thesis, University of Naples Federico II, Italy
11. Zhang Q, Wu Y, Zhao M, Q, J, Huang, Zhao H (2017) Automatic partitioning of water distribution networks using multiscale community detection and multi objective optimization. J Water Resour Plann Manage 143(9)
12. Liu J, Han R (2018) Spectral clustering and multicriteria decision for design of district metered areas. J Water Resour Plann Manage 144(5)
13. Zhang K, Yan H, Zeng H, Xin K, Tao T (2019) A practical multi-objective optimization sectorization method for water distribution network. Sci Total Environ 1401–1402
14. Giudicianni C, Herrera M, di Nardo A, Adeyeye K (2020) Automatic multiscale approach for water networks partitioning into dynamic district metered areas. Water Resour Manag
15. Vasilic Z, Stanic M, Kapelan Z, Prodanovic D, Babic B (2020) Uniformity and heuristics-based DeNSE method for sectorization of water distribution networks. Water Resour Plann Manage 146s(3)
16. Girvan M, Newman MEJ (2002) Community structure in social and biological networks. Proc Natl Acad Sci USA 99(12):7821–7826
17. Giustolisi O, Ridolfi L (2014) A new modularity-based approach to segmentation of water distribution networks. J Hydraul Eng 140(10)
18. Campbell E, Izquierdo J, Montalvo I, Ilaya-Azya A, Perez-Garci R, Tavera M (2016) A flexible methodology to sectorize water supply networks based on social network theory concepts and multi-objective optimization. J Hydroinf 62–76
19. Ciaponi C, Murari E, Todeschini S (2016) Modularity based procedure for partitioning water distribution systems into independent districts. Water Resour Manage 30:2021–2036

20. Clauset A, Newman MEJ, Moore C (2004) Finding community structure in very large networks. Phys Rev E70(6)
21. Kadu MS, Gupta R, Bhave PR (2008) Optimal design of water networks using a modified genetic algorithm with reduction in search space. J Water Resour Plann Manage 134(2)
22. Sayyed MAH, Gupta R, Taniamboh T (2015) Noniterative application of EPANET for pressure dependent modelling of water distribution systems Water Resour Manage 29:3227–3242
23. Sayyed MAH, Gupta R, Taniamboh T (2019) Combined flow and pressure deficit-based penalty in GA for optimal design of water distribution network. J Hydraul Eng (Taylor & Francis). https://doi.org/10.1080/09715010.2019.1604180
24. Todini E (2000) Looped water distribution networks design using a resilience index based heuristic approach. Urban Water 2:115–122

Impact of Lockdown on Ambient Air Quality in Nagpur Due to COVID-19 Pandemic

Divyanshu Saini, Upendra R. Darla, Dilip H. Lataye, Vidyanand M. Motghare, and E. Ravendiran

Abstract The objective of this paper is to study the change in ambient concentration of three of the standard criteria pollutants namely respiratory suspended particulate matters (RSPM or PM_{10}), sulfur dioxide (SO_2) and nitrogen dioxide (NO_2) because of lockdown due to COVID-19 pandemic. It is studied for three locations viz. residential, industrial and commercial in and around the Nagpur city. The data has been collected from January to June 2020, where there was a normal situation from January to March for three months and a complete lockdown from April to June 2020 for three months. The monthly average concentrations of all three pollutants during the normal situation and lockdown period have been compared. It is found that the average concentration of all three pollutants at all the three locations is reduced by about 42–66% due to the lockdown. During the lockdown period the average concentration of SO_2 was reduced to 5 $\mu g/m^3$ from 14 $\mu g/m^3$ in the normal situation. The average concentration of nitrogen dioxide (NO_2) was reduced to 12 $\mu g/m^3$ from 39 $\mu g/m^3$ and the average concentration of RSPM reduced to 72 $\mu g/m^3$ from 133 $\mu g/m^3$ due to lockdown. It is observed that the concentration of all the pollutants during lockdown was below the prescribed CPCB standards. Air quality index (AQI) at all three locations improved from the range of 101–200 in the normal situation to 51–100 in the lockdown period. The quality of ambient air changed from MODERATE to SATISFACTORY. The reduction of pollutants is mainly due to the shutdown of anthropogenic activities in all three locations in and around Nagpur.

Keywords RSPM · PM_{10} · SO_2 · NO_2 · Trends · Air quality index, etc.

D. Saini · U. R. Darla · D. H. Lataye (✉)
Department of Civil Engineering, Visvesvaraya National Institute of Technology, Nagpur, Maharashtra 440010, India

V. M. Motghare · E. Ravendiran
Maharashtra Pollution Control Board, Mumbai, India
e-mail: jdair@mpcb.gov.in

E. Ravendiran
e-mail: ms@mpcb.gov.in

B. Laishram and A. Tawalare (eds.), *Recent Advancements in Civil Engineering*, Lecture Notes in Civil Engineering 172,
https://doi.org/10.1007/978-981-16-4396-5_43

1 Introduction

India is a developing country, where lots of developing activities are taking place. There is a rapid growth of industrialization in each and every city of the country. These increasing developing activities or anthropogenic activities increase the pollution in the atmosphere. Due to these anthropogenic activities, various air pollutants are emitted in the environment due to the burning of fossil fuel viz. carbon monoxide (CO), sulfur dioxide (SO_2), nitrogen dioxide (NO_2) and smaller particles including lead and gasoline additives, in addition to these pollutants the suspended particulate matters are also emitted into the atmosphere.

Vigorous unplanned urbanization, industrialization, the rapid growth of the population due to which the use of automobiles increases in the urban area is some of the major sources of generation of air pollution. The respiratory particles (PM_{10}, $PM_{2.5}$) present in the atmosphere are the main cause of adverse health effects [1]. India consists of 23 major cities in which more than 1 million people reside and many of them are exceed the standard prescribed by the WHO [2]. Vehicles are the main source of pollutants which increase with the number of vehicles and degrade the quality of air in the atmosphere exponentially [3–5]. The major cities in India consist 70% of the total pollution in Delhi, 52% in Mumbai, 30% in Calcutta due to the emission from vehicles [6–8]. In the city serious health effect is due to various total suspended particulate matters, SO_2, NO_2 and lead. At least 500,000 premature deaths and 4–5 million new chronic bronchitis cases are reported each year. On a global scale, the premature deaths due to particulate matter are 4–8%.[9, 10]

Different meteorological conditions like wind speed, temperature, humidity, solar radiation, etc. also affect the quality of air in the atmosphere [11, 12]. Rainfall settles up the pollutants in the atmosphere hence generates less pollution in the monsoon season [13]. Particulate matter also consist the magnetic minerals, these are with typical bulk iron content found to constitute 5–15% of urban atmospheric PM, with iron oxides and hydroxides typically contributing 10–70% of the bulk iron content, primarily mineral found in the particulate matter was magnetite [14].

As we know the whole world is facing the crisis of the novel coronavirus disease (COVID-19) pandemic since November 2019, when the first COVID-19 patient was detected on 1 December 2019 in Wuhan, China. The World Health Organization (WHO) declared the outbreak, a Public Health Emergency of International Concern on 30th January 2020 and a pandemic on 11th March 2020. The first COVID-19 patient was detected in India on 30th January 2020 in Kerala. The first case of COVID-19 in Maharashtra was detected in Pune on 9th March 2020. In Nagpur, the patient was detected on 11th March 2020 and in this way the COVID-19 is spreading day by day all over the world. Since there is no vaccine for the coronavirus, the only way to reduce the effect of coronavirus is the social distancing and to avoid the individual contact and to break the chain, which are only the physical methods for reducing its spread. To break the chain of COVID-19 the lockdown has been applied in all the countries facing the spreading of this virus. The Indian government has implied lockdown from March 25, 2020, which is still

continuing in the country. There were various phases of lockdown; Lockdown 1: from March 25 to April 14, 2020 (21 days), Lockdown 2: April 15 to May 3, 2020 (19 days), Lockdown 3: May 4 to May 17, 2020 (14 days), Lockdown 4: May 18 to May 31, 2020 (14 days) and Lockdown 5/Unlock 1: June 1 to June 30, 2020 (30 days). From 25th March 2020 to May 31, 2020, there was a complete lockdown in the country in a phased manner. From 1st June 2020, the lockdown has been extended with relaxation to few activities or the essential services which are also known as unlock 1. So from January to 25th March, the condition was normal all the anthropogenic activities were going on but from April to June there was a complete lockdown, where all the activities, industries, vehicles and all construction activities were closed completely except a few from 1st June 2020.

In the present work, the effect of lockdown due to COVID-19 pandemic on air quality in Nagpur city has been studied. To study the effect of lockdown on ambient air quality of Nagpur and to compare the effect on concentrations of the pollutants two conditions have been considered; (1) normal condition from January to March 2020 and (2) Lockdown condition from April to June 2020, three months each. For this study, the data of all six months has been collected and monthly average concentrations of SO_2, NO_2 and RSPM has been calculated at residential, industrial and commercial locations in the city. For a comparative study of the reduction in concentration of pollutants, the average of three months in a normal situation and lockdown situation has been compared in presented in the subsequent sections.

2 Materials and Methods

Nagpur is the sub capital of Maharashtra, India situated in the middle of the country. This city is the center point of railways and highways from east to west and north to south. This city is proposed to be one of the smart cities of India. It gives a sudden growth of industrialization and various infrastructures all over the city.

2.1 Monitoring Sites

Three locations (residential, industrial and commercial) in Nagpur city have been selected for the present study. The quality of air is being monitored by Visvesvaraya National Institute of Technology, Nagpur at these three sites under the National Ambient Air Monitoring Programme (NAMP) sponsored by Maharashtra Pollution Control Board, Mumbai, Maharashtra. The first monitoring station is located at the Institute of Engineers (India), North Ambazari Road, Ramdaspeth Nagpur (Station code: 287) indicated as IEI in the residential area. The second monitoring station is located at the office of Executive Engineer, MIDC

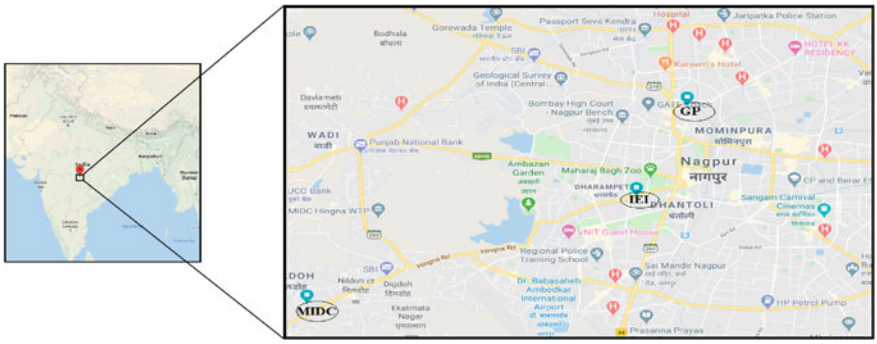

Fig. 1 Location of monitoring sites locations all over the city

Hingna Road Nagpur (Station code: 288) indicated as MIDC in the industrial area and the third monitoring station is located at Government Polytechnic, Mangalwari Bazar, Sadar Nagpur (Station Code: 314) indicated as GP in the commercial area. The satellite view with the location of all the three stations is shown in Fig. 1. At all the three stations, three of the standard pollutants viz, SO_2, NO_2 and respiratory suspended particulate matters (RSPM or PM_{10}) are being monitored twice a week such that a minimum of 104 samples are taken throughout the year. SO_2 and NO_2 are sampled at 4 h interval and RSPM are taken at the interval of 8 h and the daily average concentrations are determined for all the three pollutants. From these concentrations, the average concentration of in month has been determined for all the pollutants at all three locations.

2.2 *Sampling and Analysis of Pollutants*

Respirable dust sampler (RDS), Model: APM 460 manufactured by Envirotech Instruments, New Delhi (India) has been used for sampling of RSPM (PM_{10}), SO_2 and NO_2 at all the monitoring sites. The sampling and analysis of RSPM is done as per IS 5182-23 (2006) [15], the sampling and analysis of SO_2 is done as per IS 5182-2 (2001) [16] and the sampling and analysis or NO_2 is done as per IS 5182-6 (2006) [17]. The details of pollutants, equipment, method, etc. are given in Table 1.

2.3 *Air Quality Index (AQI)*

This index is developed to see the quality of air on the basis of a ratio or number. An air quality index (AQI) is defined as an overall scheme that transforms the weighed values of individual air pollution related parameters (for example,

Table 1 Details of pollutant monitoring

Particular	RSPM	SO_2	NO_2
Equipment	Respirable dust sampler (RDS) APM460	RDS with attached gaseous sampling	RDS with attached gaseous sampling
Media	Glass fiber filter paper	TCM (tetrachloromercurate)	NaOH plus sodium arsenite
Flow rate	1.0–1.3 m^3/min	0.5 L/min	0.5 L/min
Method used	Gravimetric	Spectrophotometer method (west and gaeke method)	Spectrophotometry method (jacobs-hochheiser)
Time frequency	8 h	4 h	4 h
Duration of sampling	Continuously for 24 h, two days in a week	Continuously for 24 h, two days in a week	Continuously for 24 h, two days in a week

Table 2 Categories of air quality Index

AQI	Pollution level	Impact on human health
0–50	GOOD	Minimal impact
51–100	SATISFACTORY	Minor breathing discomfort to sensitive people
101–200	MODERATE	Breathing discomfort to the people with lung, heart disease, children and older adults
201–300	POOR	Breathing discomfort to people on prolonged exposure
301–400	VERY POOR	Respiratory illness to the people on prolonged exposure
>401	SEVERE	Respiratory effects even on healthy people

pollutant concentrations) into a single number or set of numbers. Different category of ambient air quality and their impact on human health based on the AQI is presented in Table 2. The following equation [1] is used for the calculation of AQI:

$$I_p = \left\{ \frac{(I_{HI} - I_{LO})}{(B_{HI} - B_{LO})} \times (C_p - B_{LO}) \right\} + I_{LO} \quad (1)$$

where,

B_{HI} Breakpoint concentration greater or equal to given concentration.
B_{LO} Breakpoint concentration smaller or equal to given concentration.
I_{HI} AQI value corresponding to B_{HI}.
I_{LO} AQI value corresponding to B_{LO}.
C_p Pollutant concentration.

3 Results and Discussion

3.1 Concentration of Pollutants in Residential Location

The station is located at the Institution of Engineers (India) building, on North Ambazari Road, Near Ramdaspeth Nagpur. Figure 2 shows the variation of monthly average concentrations of SO_2, NO_2 and RSPM at this location from January to June 2020. From the figure, it can be seen that the concentration of SO_2 varies from 14 to 6 μg/m^3, the concentration of NO_2 varies from 41 to 12 μg/m^3 and the concentration of RSPM varies from 148 to 76 μg/m^3. The average concentrations of SO_2 in January, February and March are 14, 13 and 10 μg/m^3 respectively, whereas the respective concentrations in April, May and June are 5, 5 and 6 μg/m^3. The average concentration of January–March (during normal situation) is 12 μg/m^3, whereas, it is 5 μg/m^3 for April to June (lockdown /unlock 1 period). It may be noted that the average concentration of SO2 in March is reduced to 10 μg/m^3 may be due to the Janta curfew on 21st March 2020 and the complete lockdown from 25th to 31st March 2020. The average concentration of SO_2 June is 6 μg/m^3, which is may be increased due to the unlock-1 situation, where few of the activities were started.

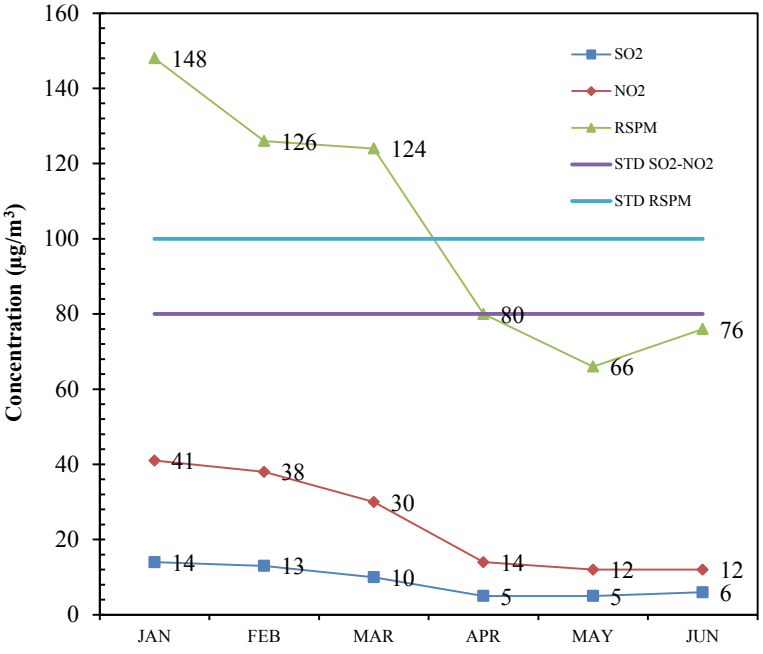

Fig. 2 Concentration of pollutants at a monitoring station located at residential area IEI

The average concentration of NO_2 in January, February and March is 41, 38 and 30 μg/m^3 respectively, whereas the respective concentration in April, May and June is 14, 12 and 12 μg/m^3. The average concentration of January–March (during normal situation) is 36 μg/m^3, whereas, it is 13 μg/m^3 for April to June (lockdown/unlock 1 period). It may be noted that the average concentration of NO_2 in March is reduced to 30 μg/m^3 may be due to the Janta curfew on 21st March 2020 and the complete lockdown from 25th to 31st March 2020.

The average concentrations of RSPM in January, February and March are 148, 126 and 124 μg/m^3 respectively, whereas the respective concentrations in April, May and June are 80, 66 and 76 μg/m^3. The average concentration of January–March (during normal situation) is 133 μg/m^3, whereas, it is 74 μg/m^3 for April to June (lockdown/unlock 1 period). It may be noted that the average concentration of RSPM in March is reduced to 80 μg/m^3 may be due to the Janta curfew on 21st March 2020 and the complete lockdown from 25th to 31st March 2020. The average concentration of RSPM in June is 76 μg/m^3, which is increased as compared to May 2020 due to unlock-1, where few of the activities were started. The percentage reduction of SO_2, NO_2 and RSPM concentration due to lockdown is 57%, 65% and 44% respectively at this station.

3.2 Concentration of Pollutants at Industrial Location

The station is located at the office of Executive Engineer, MIDC, Hingna Raod, Nagpur. Figure 3 shows the variation of monthly average concentrations of SO_2, NO_2 and RSPM at this location from January to June 2020. From the figure, it is observed that the concentration of SO_2 varies from 15 to 5 μg/m^3, the concentration of NO_2 varies from 43 to 15 μg/m^3 and the concentration of RSPM varies from 142 to 73 μg/m^3. The average concentrations of SO_2 in January, February and March are 15, 14 and 12 μg/m^3 respectively, whereas the respective concentrations in April, May and June are 15, 13 and 15 μg/m^3. The average concentration of January–March (during normal situation) is 14 μg/m^3, whereas, it is 6 μg/m^3 for April–June (lockdown/unlock 1 period). It may be noted that the average concentration of SO_2 in March is reduced to 12 μg/m^3 may be due to the Janta curfew on 21st March 2020 and the complete lockdown from 25th to 31st March 2020.

The average concentration of NO_2 in January, February and March is 43, 40 and 34 μg/m^3 respectively, whereas the respective concentration in April, May and June is 15, 13 and 15 μg/m^3. The average concentration of January–March (during normal situation) is 39 μg/m^3, whereas, it is 14 μg/m^3 for April to June (lockdown/unlock 1 period). It may be noted that the average concentration of NO_2 in March is reduced to 34 μg/m^3 may be due to the Janta curfew on 21st March 2020 and the complete lockdown from 25th to 31st March 2020. The average concentration of NO_2 in June is 15 μg/m^3, which may be increased due to the unlock-1 situation, where few of the activities were started.

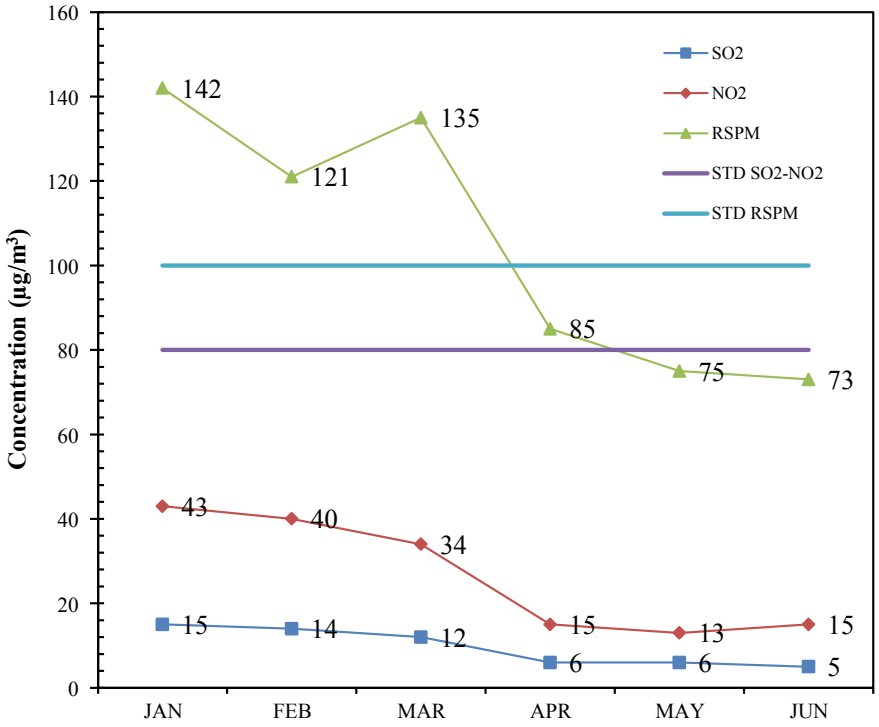

Fig. 3 Concentration of pollutants at a monitoring station located at industrial area MIDC

The average concentrations of RSPM in January, February and March are 142, 121 and 135 µg/m^3 respectively, whereas the respective concentrations in April, May and June are 85, 75 and 73 µg/m^3. The average concentration of January-March (during normal situation) is 133 µg/m^3, whereas, it is 78 µg/m^3 for April to June (lockdown/unlock 1 period). It may be noted that the Janta curfew on 21st March 2020 and the complete lockdown from 25th to 31st March 2020 did not affect the average concentration of RSPM. The average concentration of RSPM in June is 73 µg/m^3. The percentage reduction of SO_2, NO_2 and RSPM concentration due to lockdown is 59%, 63% and 41% respectively at this station.

3.3 Concentration of Pollutants at Commercial Location

The station is located at Government Polytechnic, Mangalwari Bazar, Sadar, Nagpur. Figure 4 shows the variation of monthly average concentrations of SO_2, NO_2 and RSPM at this location from January to June 2020.

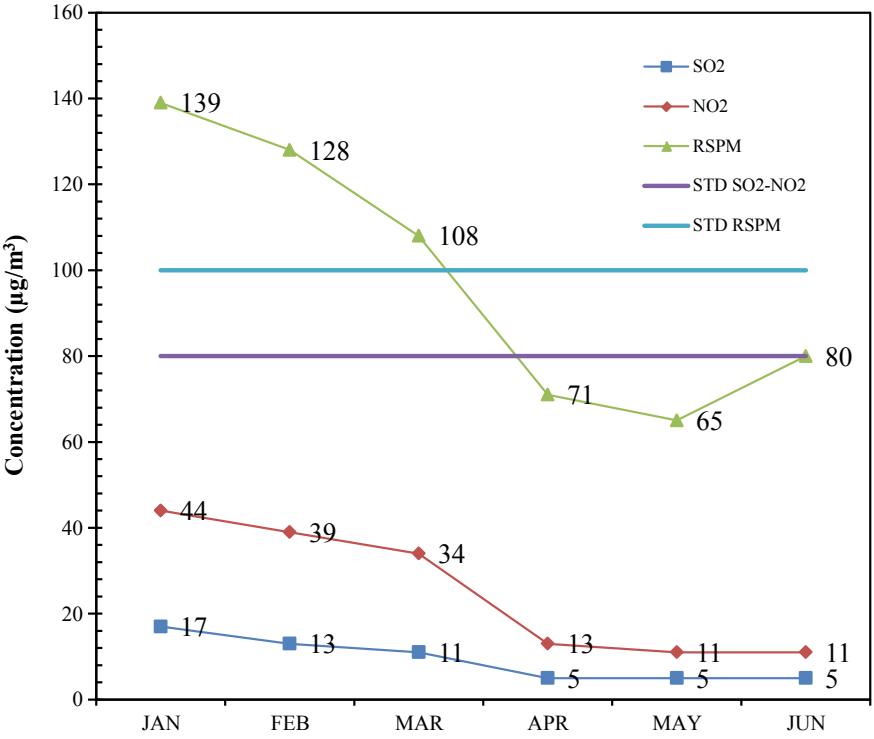

Fig. 4 Concentration of pollutants at a monitoring station located at commercial area Sadar

From the figure, it can be seen that the concentration of SO_2 varies from 17 to 5 µg/m^3, the concentration of NO_2 varies from 44 to 11 µg/m^3 and the concentration of RSPM varies from 139 to 80 µg/m^3. The average concentrations of SO_2 in January, February and March are 17, 13 and 11 µg/m^3 respectively, whereas the respective concentrations in April, May and June are 5, 5 and 5 µg/m^3. The average concentration of January-March (during normal situation) is 14 µg/m^3, whereas, it is 5 µg/m^3 for April to June (lockdown/unlock 1 period). It may be noted that the average concentration of SO_2 in March is reduced to 11 µg/m^3 may be due to the Janta curfew on 21st March 2020 and the complete lockdown from 25th to 31st March, 2020. The average concentration of SO_2 June is 5 µg/m^3, which indicates that the lockdown completely followed even in June 2020.

The average concentration of NO_2 in January, February and March is 44, 39 and 34 µg/m^3 respectively, whereas the respective concentration in April, May and June is 13, 11 and 11 µg/m^3. The average concentration of January-March (during normal situation) is 39 µg/m^3, whereas, it is 12 µg/m^3 for April to June (lockdown/unlock 1 period). It may be noted that the average concentration of NO_2 in March is reduced to 34 µg/m^3 may be due to the Janta curfew on 21st March 2020 and the complete lockdown from 25th to 31st March 2020.

Table 3 Average concentrations (in μg/m^3) of SO_2, NO_2 and RSPM with their standard deviation shown in the bracket at IEI, MIDC and GP

	JANUARY	FEBRUARY	MARCH	APRIL	MAY	JUNE
	IEI					
SO_2	14(±5.86)	13(±5.36)	10(±4.9)	5(±1.37)	5(±1.94)	6(±1.82)
NO_2	41(±13.83)	38(±13.73)	35(±16.25)	14(±5.61)	12(±4.31)	13(±5.56)
RSPM	147(±41.75)	125(±41.9)	124(±43.4)	80(±22.67)	65(±19.63)	77(±24.93)
	MIDC					
SO_2	15(±6.75)	14(±5.95)	12(±6.38)	6(±1.67)	6(±2.01)	5(±1.85)
NO_2	43(±15.21)	40(±13.71)	34(±16.25)	15(±7.39)	13(±4.13)	15(±8.92)
RSPM	142(±40.88)	121(±38.12)	135(±42.28)	85(±16.06)	75(±20.71)	73(±27.37)
	GP					
SO_2	17(±7.2)	13(±5.38)	11(±5.43)	5(±2.12)	5(±1.34)	5(±1.03)
NO_2	44(±14.32)	39(±11.96)	34(±12.2)	13(±4.71)	11(±3.33)	11(±2.23)
RSPM	139(±43.97)	128(±41.62)	108(±37.2)	71(±23.62)	65(±17.4)	80(±21.76)

The average concentrations of RSPM in January, February and March are 139, 128 and 108 μg/m^3 respectively, whereas the respective concentrations in April, May and June are 71, 65 and 80 μg/m^3. The average concentration of January–March (during normal situation) is 125 μg/m^3, whereas, it is 72 μg/m^3 for April to June (lockdown/unlock 1 period). It may be noted that the average concentration of RSPM in March is reduced to 108 μg/m^3 may be due to the Janta curfew on 21st March 2020 and the complete lockdown from 25th to 31st March 2020. The average concentration of RSPM in June is 80 μg/m^3, which is suddenly increased due to unlocking of some activities from 1st June 2020. The percentage reduction of SO_2, NO_2 and RSPM concentration due to lockdown is 63%, 70% and 42% respectively at this station. Table 3 shows the average concentrations of SO_2, NO_2 and RSPM with their standard deviations at all three locations.

3.4 Air Quality Index (AQI)

Air quality index at all three stations has been determined and shown in Table 4 and it is graphically represented in Fig. 5. AQI is calculated for all the three monitoring stations. From Tables 2 and 4 it can be seen that the AQI at all the three stations during the normal period varies from 101 to 200, which indicates that the quality of air at all the three stations was MODERATE during these three months. Whereas, the AQI during the lockdown period, i.e., from April to June 2020 varied from 51 to 100, which indicates the quality of air at all the stations was SATISFACTORY. Means the concentration of air pollutants during the lockdown of April to June 2020 was reduced hence the quality of ambient air at all the three station improved due to the lockdown.

Table 4 AQI values at all three sites

	IEI	MIDC	GP
JAN	132	128	126
FEB	117	114	119
MAR	116	123	105
APR	80	85	71
MAY	66	75	65
JUN	76	73	80

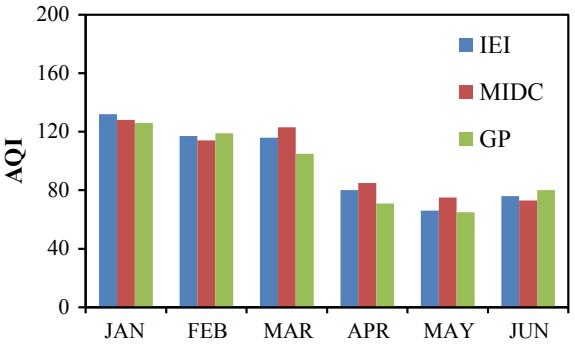

Fig. 5 Monthly air quality indexes at all the stations

4 Conclusion

The Nagpur city is mostly affected by the suspended particulate matters (which is more than the prescribed standard), SO_2 and NO_2 gaseous pollutants due to various anthropogenic activities like transportation vehicles, industries, construction works, etc. Due to the COVID-19 pandemic, the Central and State Governments declared lockdown since March 25, 2020, which is still in existence with some relaxations, which is also known as UNLOCK phase started from 1st June 2020. Due to the lockdown, the anthropogenic activities were stopped and hence the average concentration of pollutants reduced suddenly from March 2020. The concentration of SO_2, NO_2 and RSPM reduced by about 60%, 66% and 42% respectively at all the stations. During the lockdown, i.e., from April to June 2020 the minimum respective monthly average concentration of SO_2, NO_2 and RSPM were found to be 5, 11 and 65 $\mu g/m^3$, whereas the maximum concentrations were 6, 15 and 85 $\mu g/m^3$ at all the stations, which are below the NAAQS. The AQI which varies from 101 to 200 during the normal situation, came down to 51–100, i.e., the quality of air changed from MODERATE to SATISFACTORY. The main cause of the reduction in concentration of the pollutants at all locations is the stopping of anthropogenic activities. Hence, it may be concluded that the lockdown has improved the quality of air in and around Nagpur city and also it gave the background concentrations of the pollutants. Due to the lockdown, there is a recovery of the environment.

Acknowledgments The authors would like to thank the Director VNIT, Nagpur for his support and anchorage, Central Pollution Control Board (CPCB), New Delhi and Maharashtra Pollution Control Board (MPCB), Mumbai for sponsoring the projects under National Air Quality Monitoring Programme (NAMP) and State Air Quality Monitoring Programme (SAMP). Thanks to MPCB Regional Office, Nagpur for providing support. Thanks, Dr. V.A. Mhaisalkar, Professor in Civil Engg. (Rtd.) for his support, Mrs. Rekha Khadse for analyzing the air samples, Rashmi Vishwakarma for providing office assistance and Mr. Krushnakumar B. Bisen and Mr. Shivkumar M. Tembhre for providing help in sampling.

References

1. Guttikunda SK, Goel R (2013) Health impacts of particulate pollution in a megacity-Delhi, India. Environ Dev 6(1):8–20
2. Gulia S, Shiva Nagendra SM, Khare M, Khanna I (2015) Urban air quality management—a review. Atmos Pollut Res 6(2):286–304
3. Pal A, Kulshreshtha K, Ahmad KJ, Yunus M (2000) Changes in leaf surface structures of two avenue tree species caused by auto-exhaust pollution. J Environ Biol 21(1):15–21
4. Patni S, Student PG (2017) Motor vehicle traffic congestion costing in Nagpur City. Int J Civ Eng Technol 8(4):100–106
5. Ristovski ZD et al (2012) Respiratory health effects of diesel particulate matter. Respirology 17(2):201–212
6. Pollution C, Board C, Environment MOF (1974) Environmental laboratories. Environ Sci Technol 8(10):888
7. A World Bank report (2016). The cost of air pollution: Strengthening the economic case for action – A world bank report. http://documents.worldbank.org/curated/en/781521473177013155/The-cost-of-airpollution-strengthening-the-economic-case-for-action
8. CPCB (2016) Air pollution of Delhi: an analysis. ENVIS Cent Control Pollut (Water Air Noise), 1–26
9. Pizzorno J, Crinnion W (2017) Particulate matter is a surprisingly common contributor to disease. Integr Med 16(4):8–12
10. West PW, Gaeke GC (1956) Fixation of sulfur dioxide as disulfitomercurate (II) and subsequent colorimetric estimation. Anal Chem 28(12):1816–1819
11. Kleine Deters J, Zalakeviciute R, Gonzalez M, Rybarczyk Y (2017) Modeling PM2.5 Urban pollution using machine learning and selected meteorological parameters. J Electr Comput Eng 2017:1–14. https://doi.org/10.1155/2017/5106045 (Article ID 5106045)
12. Chan AT (2002) Indoor-outdoor relationships of particulate matter and nitrogen oxides under different outdoor meteorological conditions
13. Ganguly R, Batterman S, Isakov V, Snyder M, Breen M, Brakefield-Caldwell W (2015) Effect of geocoding errors on traffic-related air pollutant exposure and concentration estimates. J Expo Sci Environ Epidemiol 25(5):490–498
14. Muxworthy AR, Matzka J, Petersen N (2001) Comparison of magnetic parameters of urban atmospheric particulate matter with pollution and meteorological data. Atmos Environ 35(26): 4379–4386
15. IS 5182-23 (2006) Methods for measurement for air pollution, part 23: respirable suspended particulate matter (PM 10), cyclonic flow technique. Bureau of Indian Standards, New Delhi, pp 4–12
16. IS 5182-2 (2001) Methods for measurement for air pollution, part 2, sulphar dioxide. Bureau of Indian Standards, New Delhi, pp 4–15
17. IS 5182-6 (2006) Methods for measurement for air pollution, part 6, oxides of nitrogen. Bureau of Indian Standards, New Delhi, pp 4–12

Experimental Assessment of Natural Ventilation as a Mitigation Measure for Indoor Air Pollution Problem

Sangita (Ghatge) Goel and Rajesh Gupta

Abstract Indoor air quality is dependent on numerous factors such as the number of active indoor pollution sources, penetration of outdoor air, building location and the ventilation system in the building. The less ventilated indoor environment leads to dangerous accumulation of PM and hence higher exposure doses to the occupants. Natural and mechanical ventilation plays a major role in diluting the indoor air pollutants. This study aims to quantify the impact of natural ventilation in improving the indoor air quality. The built-up of indoor air pollutants with four indoor air pollution sources was studied in a non-ventilated environment in an indoor air testing unit setup. Air quality was further monitored with the same setup in naturally ventilated environment and the adjacent outdoor. A 31-channel laser spectrometer GRIMM 11 R (MIN-LAS) was used for the continuous real-time measurements of 0.25–32 μm sized PM. The average daily dose to the exposed population was estimated for both the ventilation conditions. It was found that natural ventilation resulted in reducing the indoor PM by 80–90%. The reduction in concentrations ranged from 86 to 90% for PM_{10}, 87–91% for $PM_{2.5,}$ and it was 91–93% for PM_1. The reduction in fine particulates PM_1 was found to be more as compared to the other studied particulates. The quantification of health risk from exposure to $PM_{2.5}$ was carried out by estimating the potential dose to the receptor. The daily dose of 67 mg/kg-day for the 6–11 years age group attributed to PM_{10} was decreased to 7.4 mg/kg-day with the ventilation. Hence, in the regions where outdoor air is not polluted, natural ventilation can be an effective mitigation measure for the indoor air pollution and associated health problem.

CSIR-NEERI/KRC/2020/JULY/APC/2 Date: 29 JULY 2020

S. (Ghatge) Goel (✉)
Environmental Audit and Policy Implementation Division, CSIR-National Environmental Engineering Research Institute, Nehru Marg, Nagpur, Maharashtra 440020, India
e-mail: s_goel@neeri.res.in

R. Gupta
Visvesvaraya National Institute of Technology, Nagpur, Maharashtra, India

B. Laishram and A. Tawalare (eds.), *Recent Advancements in Civil Engineering*, Lecture Notes in Civil Engineering 172,
https://doi.org/10.1007/978-981-16-4396-5_44

Keywords Indoor air pollution · Particulate matter · Natural ventilation · Average daily dose

1 Introduction

Indoor air quality is dependent on numerous factors such as number of active indoor pollution sources, penetration of outdoor air, building location, and the ventilation system in the building. The outdoor air plays an important role in maintaining indoor air quality in the building irrespective of the type of ventilation provided, i.e., mechanical and natural [1]. The optimum level of ventilation varies according to the strength of the air pollution source [2]. The percentage of relative humidity (RH) in indoor air also affects the quality of indoor air [3]. By definition, higher relative humidity means higher moisture content (MC). The presence of moisture in indoor environment is responsible for various problems such as deteriorating of indoor air quality, growth of bacteria, mold/fungi, infestation by insects, numerous health issues for the residents and weakening of the building components [4, 5]. The recommended RH level in indoor environment by "the Environmental Protection Agency (EPA) and the Consumer Product Safety Commission (CPSC)" is 30 and 50% [6]. Therefore, it is very important to maintain the indoor RH at the above recommended optimum range.

The indoor air quality has been identified as one of the basic and primary health risk factors. As a matter of fact, people are very regularly exposed to high concentrations of indoor air pollutants, which leads to huge health related potential doses [7, 8]. The scientific literature involving microenvironments highlighted the areas where high pollutant emitters are usually found, such as residential houses (e.g., cooking) [9], various forms of incense and candle combustion [10], cigarette smoking [11], offices (e.g., printers, copiers) [12] and other workplace environments (e.g., industrial activity) [13], schools [14].

Proper and adequate ventilation provided by means of natural and fresh air from the ambient environment reduces the concentration of pollutants in indoor air and improves indoor air quality [15]. Natural ventilation is not only an essential factor in improving thermal comfort, but it also affects indoor air quality in a very positive way [16]. Approximately 90% of people's time is spent indoors, either in educational institutes or in commercial, residential and industrial buildings [17]. Trompetter et al. [18] highlighted the impact of ventilation on indoor air quality in the study conducted by him to investigate air quality inside and outside of two primary school classrooms in New Zealand. The results indicated that the ventilated classroom had 66% lower PM_{10} concentrations than the unventilated control classroom.

This study aims to quantify the impact of natural ventilation in improving the indoor air quality. The built-up of indoor air pollutants with four indoor air pollution sources was studied in a non-ventilated environment in an indoor air testing unit setup. Air quality was further monitored with the same setup with naturally

ventilated environment. The experiments were carried out in an indoor air testing unit. The monitoring of PM (PM_{10}, $PM_{2.5}$, and PM_1) was carried out for the indoor air pollution sources, viz. incense stick, dhoop, mosquito coil and cigarette. The comparison of these sources with respect to their PM emissions was done by estimating the concentrations per gram of source burnt during each experiment and comparing the data for both the ventilation scenario. The outdoor PM concentrations were also monitored during the ventilation experiments by taking care that no air pollution source was active in the vicinity. Quantification of dilution of indoor air pollutants with the ventilation was carried out. Assessment of health risk for the exposed population was carried out by using the U.S.EPA's inhalation exposure assessor algorithm.

2 Materials and Methods

2.1 Indoor Air Pollution Sources

Four "indoor air pollution sources," viz. incense stick, dhoop, mosquito coil and cigarette, were selected for studying their indoor air pollution potential. The sources comprised of one brand of each source, viz. incense stick (IS); dhoop (DH); cigarette (CG) and mosquito coil (MC), as shown in Fig. 1.

The sources were weighed before start of the experiment and after the finish of each experiment to know the exact quantity of source burnt. The average weight of the source burnt is presented in Table 1. Incense stick, dhoop and cigarette are generally burnt for 5–20 min; however, the mosquito coil is generally burnt for longer duration of 4–6 h. Hence, higher amount of mosquito coil was used for the experiments as compared to the other sources.

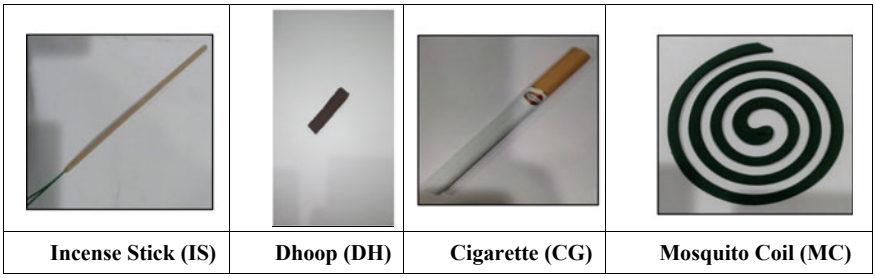

Fig. 1 Indoor air pollution sources

Table 1 Effective weight of source burnt

Source	Effective weight of source burnt (g) (average ± std. dev.)
Incense stick	1.1092 ± 0.07
Dhoop	2.2709 ± 0.02
Cigarette	1.3378 ± 0.01
Mosquito coil	5.1502 ± 0.10

2.2 *Indoor Air Quality Monitoring Setup*

Indoor air quality monitoring experiments were carried out for four hours as per the "US EPA Section 01 81 09, Testing for Indoor Air Quality" [19] per source in an indoor air testing unit (IATU) with size 2.3 × 2.4 × 3.0 m, as shown in Fig. 2. Each source was tested for two scenarios, viz. with and without ventilation, so that a comparison of air quality data could be done and the experiments were repeated thrice. The experiments without ventilation were performed keeping all the openings of the unit completely closed. The experiments with ventilation were performed by keeping the windows of the IATU open, and the wind speed was recorded near the windows. The floor of the IATU was wiped with a wet cloth before the start of each experiment. A ceiling fan was switched on for uniform mixing of air inside the test unit. The source was lighted at the start of each experiment, and the monitoring included the actual source burning phase, smoldering phase and duration after the smoldering phase.

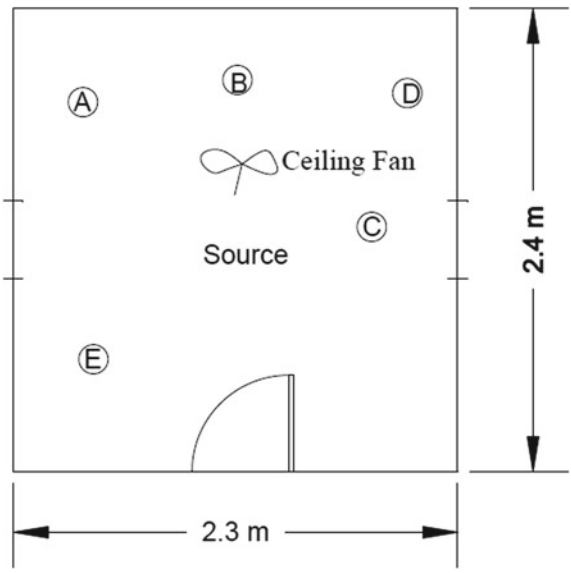

Fig. 2 Indoor air testing unit (IATU). A: BGI PQ200 Air Sampler ($PM_{2.5}$), B: Envirotech Air Sampler (PM_{10}), C: Envirotech Air Sampler ($PM_{2.5}$), D: Envirotech Gaseous Attachment, E: GRIMM 11R (MIN-LAS).

2.3 Sampling and Analysis

A 31-channel GRIMM 11-R Mini Laser Aerosol Spectrometer (MIN-LAS) was used for the continuous real-time measurements of particulate matter (PM_1, $PM_{2.5}$ and PM_{10}) in the range of 0.1 μg/m^3 and 100 mg/m^3. It uses optical particle counter (OPC) which counts up to 20 lakh particles per liter, for particle size distribution ranging between 0.25 and 32 μm.

3 Health Risk Assessment

3.1 Average Daily Dose (ADD)

The indoor air pollution sources are burnt daily in residential premises, and hence, occupants are continuously exposed to these pollutants. The estimation of the health risk is done by using the US EPA's inhalation exposure assessor algorithm and age-specific potential dose/average daily dose (ADD). The ADD is calculated as per Eq. 1 [20]. ADD calculations were performed for both the ventilation conditions.

$$\text{ADD} = \frac{C_{\text{air}} \times \text{InhR} \times \text{ET} \times \text{EF} \times \text{ED}}{(\text{BW} \times \text{AT})} \tag{1}$$

where

ADD = average daily dose, (μg/kg-day), InhR = inhalation rate, C_{air} = concentration of contaminant in air (m^3/h), ET = exposure time (hours/day) = 1 h/day, EF = exposure frequency (days/year) = 365 days/year, ED = exposure duration (years) = 10 years, BW = body weight (kg), AT = averaging time (days).

Inhalation rate was taken from EPA's Exposure Factors Handbook 2011 edition, and the average body weight for Indian children and adults was taken from the Report of the Expert Group of Indian Council Medical Research 2010. The ADD/potential dose values were calculated in μg/kg-day [21–23].

4 Results and Discussions

4.1 PM Concentrations

The mean PM_{10} concentrations for two scenarios of with and without ventilation condition as shown in Fig. 3 in decreasing order were observed for incense stick (IS), dhoop (DH), mosquito coil (MC) and cigarette (CG). Similar trend was observed for $PM_{2.5}$ and PM_1 concentrations for these sources. The trend was similar for both the scenario, viz. with and without ventilation. The outdoor PM

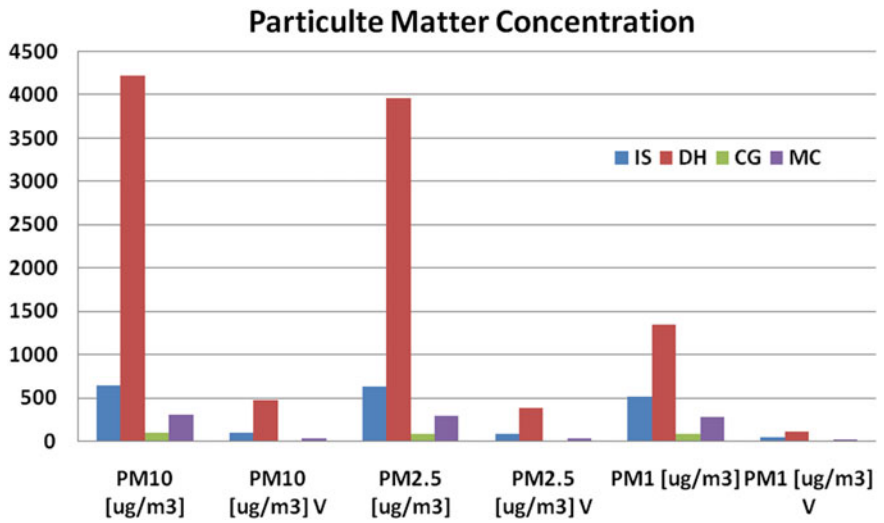

Fig. 3 Particulate matter concentrations for both unventilated and ventilated scenarios

concentrations were also monitored during the ventilation experiments, and it was observed that the average outdoor PM_{10}, $PM_{2.5}$ and PM_1 concentrations were 12, 4 and 2 μg/m^3, respectively. It was observed that during without ventilation scenario, the PM_{10}, $PM_{2.5}$ and PM_1 concentrations from dhoop reached very high values of 4200, 3900 and 1300 μg/m^3, respectively. When natural ventilation was allowed, the PM_{10}, $PM_{2.5}$ and PM_1 concentrations reduced to 460, 380 and 100 μg/m^3, respectively. The reduction in PM_{10} concentrations ranged from 86 to 90%, for $PM_{2.5}$ it was 87 to 91% and for PM_1 91 to 93%. More reduction was observed in the PM_1 concentrations for all the indoor sources as compared to the PM_{10} and $PM_{2.5}$.

The PM concentrations per gram of source burnt were estimated for comparison, and dhoop (DH) recorded the highest PM_{10}, $PM_{2.5}$ and PM_1 concentrations among all the tested sources, followed by incense stick (IS). The sources cigarette (CG) and mosquito coil (MC) resulted in almost similar PM concentrations per gram of burning. It was observed that for DH the PM_{10} concentration per gram of source burnt reduced to 218 μg/m^3 from 1860 μg/m^{3}due to ventilation.

4.2 Health Risk

4.2.1 Average Daily Dose (ADD)

The average daily dose (ADD) was calculated from equation no. 1, and the variation in ADD among all the studied sources and different age groups for both the

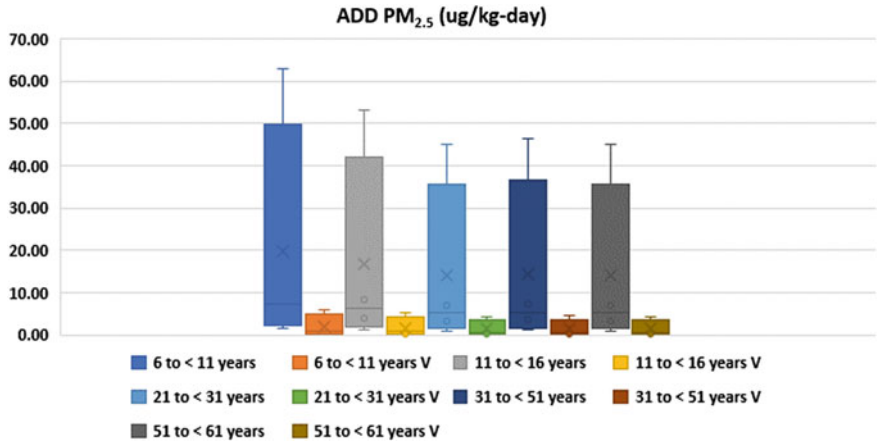

Fig. 4 Box plots of ADD (µg/kg-day) attributed to $PM_{2.5}$ for different age groups for both ventilation scenarios

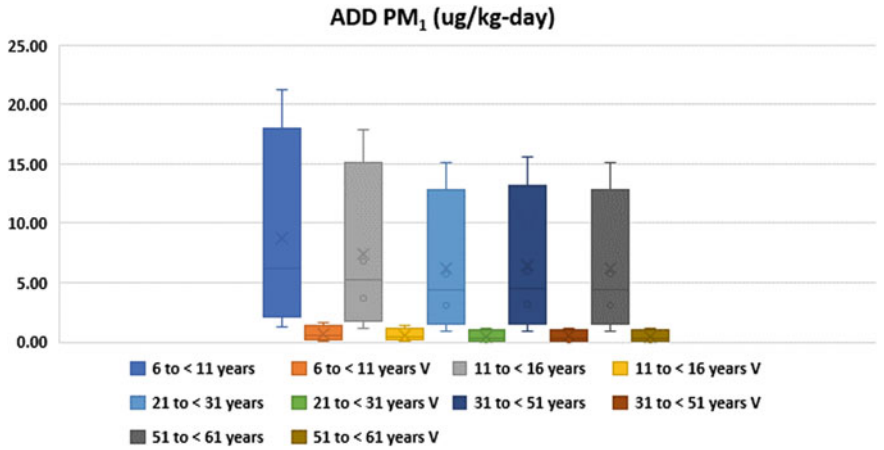

Fig. 5 Box plots of ADD (µg/kg-day) attributed to PM_1 for different age groups for both ventilation scenarios

ventilation scenarios is depicted in Fig. 4 and 5. The ADD of 67 µg/kg-day for the 6–11 years age group attributed to PM_{10} from dhoop (DH) was found be decreased to 7.4 µg/kg-day DH. Similarly, the ADD attributed to $PM_{2.5}$ and PM_1 from DH reduced to 6 and 1.6 µg/kg-day from 63 and 21 µg/kg-day, respectively.

The highest average daily dose (ADD) attributed to particulate matter (PM_{10}, $PM_{2.5}$ and PM_1) was observed to be from DH in all age groups among all the sources, and the lowest was observed for CG. The natural ventilation resulted in reducing the $PM_{2.5}$ and PM_1 ADD values to near negligible for the source CG to the age groups above 21 years.

5 Conclusion

The use of one or more indoor sources like incense sticks, dhoop, mosquito coil, etc., is common in majority of the Indian households. The closed indoor environment leads to dangerous built-up of PM and hence higher exposure doses to the occupants. Hence, natural ventilation in the regions where outdoor air is clean helps in reducing the indoor PM load by 80 to 90%. The reduction in fine particulates PM_1 was found to be more as compared to the other studied particulates. The negligible outdoor PM concentrations observed in this study assisted the outdoor air to dilute the indoor PM significantly. Remarkable reduction in the ADD was also observed for the naturally ventilated indoor environment, thereby reducing the inhalation-related health risk. In regions where outdoor air pollution is high, exhaust fan can serve the purpose of lowering indoor air pollutant levels. The religious rituals should be performed in well-ventilated environment, and use of exhaust fan may be employed. This study is conducted with an objective to know the contaminant concentration with different types of indoor air pollution sources individually, and their reduction with respect to natural ventilation. There could be multiple sources at a time, or in a series. A model is necessary to determine buildup of contaminant concentration over period of time, such as 24 h or more, with such series of sources. The results of this study can be used in developing an indoor air quality prediction model.

Acknowledgements The authors are grateful for the support provided by Dr. Rakesh Kumar, Director, CSIR-National Environmental Engineering Research Institute (NEERI), Nagpur, and Dr. K. V. George, Head, Air Pollution Control Division, CSIR-National Environmental Engineering Research Institute (NEERI), Nagpur.

References

1. Kukadia V, Palmer J (1998) The effect of external atmospheric pollution on indoor air quality: a pilot study. Energy Build 27:223–230
2. Parent D, Stricker S, Fugler D (1998) Optimum ventilation and air flow control in buildings. Energy Build 27:239–245
3. Woloszyn M, Kalamees T, Abadie MO, Steeman M, Kalagasidis AS (2009) The effect of combining a relative-humidity-sensitive ventilation system with the moisturebuffering capacity of materials on indoor climate and energy efficiency of buildings. Build Environ 44:515–524
4. Morse R, Acker D (2006) Indoor air quality and mold prevention of the building envelope, whole building design guide (WBDG)
5. Aglan H (2003) Predictive model for CO_2 generation and decay in building envelopes. J Appl Phys 93(2)
6. Wendt R, Aglan H, Livengood S, Khan M, Ibrahim E (2004) Indoor air quality of an energy-efficient, healthy house with mechanically induced fresh air. ASHRAE Trans 110 (2):77–84
7. Buonanno G, Giovinco G, Morawska L, Stabile L (2015) Lung cancer risk of airborne particles for Italian population. Environ Res 142:443–451

8. Trassierra CV, Stabile L, Cardellini F, Morawska L, Buonanno G (2016) Effect of indoor-generated airborne particles on radon progeny dynamics. J Hazard Mater 314:155–163
9. See SW, Balasubramanian R (2006) Physical characteristics of ultrafine particles emitted from different gas cooking methods. Aerosol Air Qual Res 6:82–92
10. Stabile L, Fuoco FC, Buonanno G (2012) Characteristics of particles and black carbon emitted by combustion of incenses, candles and anti-mosquito products. Build Environ 56:184–191
11. Fuoco F, Stabile L, Buonanno G, Scungio M, Manigrasso M, Frattolillo A (2017) Tracheobronchial and alveolar particle surface area doses in smokers. Atmosphere 8:19
12. Scungio M, Vitanza T, Stabile L, Buonanno G, Morawska L (2017) Characterization of particle emission from laser printers. Sci Total Environ 586:623–630
13. Buonanno G, Morawska L, Stabile L (2011) Exposure to welding particles in automotive plants. J Aerosol Sci 42:295–304
14. Stabile L, Dell'Isola M, Frattolillo A, Massimo A, Russi A (2016) Effect of natural ventilation and manual airing on indoor air quality in naturally ventilated Italian classrooms. Build Environ 98:180–189
15. Turanjanin V, Vučićević B, Jovanović M, Mirkov N, Lazović I (2014) Indoor CO_2 measurements in Serbian schools and ventilation rate calculation. Energy 77:290–296
16. Heracleous C, Michael A (2019) Experimental assessment of the impact of natural ventilation on indoor air quality and thermal comfort conditions of educational buildings in the Eastern Mediterranean region during the heating period. J Build Eng 26:100917
17. European Environmental Agency (2013) Indoor air quality. European Environmental Agency, Denmark
18. Trompetter WJ, Boulic M, Ancelet T, Garcia-Ramirez JC, Davy PK, Wang Y, Phipps R (2018) The effect of ventilation on air particulate matter in school classrooms. J Build Eng 18:164–171
19. US EPA Section 01 81 09 (2007) Testing for indoor air quality
20. US EPA Guidelines for exposure assessment, EPA/600/Z-92/001. Risk Assessment Forum, Washington, DC
21. US Environmental Protection Agency (USEPA). Exposure factors handbook, http://www.epa.gov/ncea/efh/pdfs/efh-complete.pdf
22. Report of the Expert Group of Indian Council Medical Research (2010) Nutrient requirements and recommended dietary allowances for Indians, http://icmr.nic.in/final/rda-2010.pdf
23. Goel S, Patidar R, Baxi K, Thakur RS (2017) Investigation of particulate matter performances in relation to chalk selection in classroom environment. Indoor Built Environ 26(1):119–131

Impact of Different Mode of Electrode Connection on Performance of Hybrid Electrocoagulation Unit Treating Greywater

Khalid Ansari and Avinash N. Shrikhande

Abstract Increasing freshwater stress due to rapid rise in population has led to a renewed interest in developing low-cost and efficient treatment technologies for greywater which could be recycled and reused. A hybrid process of electrocoagulation is look upon as a cost-effective treatment technology to treat greywater, and further research is being carried out in this direction. The present study envisages studying the impact of modifying the electrode connections on performance of the hybrid unit. Examinations are done on the versatility of hybrid combination of electrode (Al–Fe–Al–Fe) and (Fe–Al–Fe–Al) performing at anode and cathode in different mode configuration of electrocoagulation process followed by filtration beds in batch mode. The study reveals about 90% of COD removal at 12 V of 60 min working period of which cathode and anode isolated at 30 mm for Al–Fe with specific energy 1.75 kWh/m^3 causing operational cost of 14.56 INR.

Keywords Greywater · Electrocoagulation · Hybrid electrode · Electrolysis time · Electrode configuration

1 Introduction

Water is considered as the most important essential and remarkable substance that exists on the earth both qualitatively and quantitatively [1]. But it is overused and wasted which ultimately is of no use as it may contain undesirable substances during its flow and gets contaminated. Many times, it is observed that people use improper way for disposal of dirty and filthy water which leads to insanitation [2]. With the rise of civilization, urbanisation, and population expansion, freshwater demand grew, necessitating the developmentof more wastewater treatment options [3]. It has been observed in last few years that excess use of water resulted in water scarcity, which has given scientists and researchers a specific goal for introducing

K. Ansari (✉) · A. N. Shrikhande
Department of Civil Engineering, Kavikulguru Institute of Technology and Science, Ramtek, India

B. Laishram and A. Tawalare (eds.), *Recent Advancements in Civil Engineering*, Lecture Notes in Civil Engineering 172,
https://doi.org/10.1007/978-981-16-4396-5_45

effective, economical and eco-friendly technology for wastewater treatment for reuse and recycle of wastewater generated from domestic and industrial areas [4]. Wastewater (WW) is water of no use at a point where it loses its initial properties and becomes undesirable for further use. Depending on water characteristics, wastewater is a combined form of greywater and blackwater. Greywater (GW) is untreated wastewater collected separately from sewage flow that generated from kitchens, bathrooms, floor washes and laundry areas [5, 6]. Greywater is generally comprised of 70% of total consumed water, 30% of organic matter and (9–20) % of nutrients which is expected to be less than blackwater which is comprised of major part of organic matter [7]. Greywater possesses higher quality characteristics and standards than blackwater due to its low level pollution and higher capability for reuse [8]. In many countries like India, greywater along with blackwater is treated in single treatment unit which ultimately increases load on that treatment unit for which scientists and researchers have conducted various researches and studies using different technologies for greywater treatment individually [6, 8]. There have been many biological, chemical and physiochemical technology came forward for treatment of greywater independently. Biological technologies like rotating biological contractors (RBC), sequencing batch reactor (SBR), constructed wetlands, up-flow anaerobic sludge blankets (UASB) [9], with some innovative technologies like membrane bioreactors and reed beds gave good and effective results in removing objectionable from high-strength greywater [8, 10, 11]. Many chemical treatments like coagulation, ion exchange and granular activated carbon investigated which gave effective results in removal of organics and pathogens from the greywater but failed to meet reuse and recycle criteria for high loadings [10]. In recent years, many technologies have been investigated and studied for greywater treatment of which physiochemical treatment like electrocoagulation gave effective and economic results in removal of turbidity, TSS, organics and surfactants from greywater compared to that of biological and chemical treatments due to its large required area and retention time [12–14]. Therefore, many researchers focus on electrocoagulation (EC) which is a simple affordable and efficient method used for wastewater treatment. This electrochemical treatment got great attention for wastewater treatment due to its high effectiveness, low maintenance and lesser need for labour. The EC process mechanism run through three steps that is electrode oxidation at sacrificial anode, gas bubble formation like hydrogen bubble at cathode and flocs formation. Because of coagulation, forming a sludge blanket which is removed by the filtration process enhances alternative methodologies to break pollutants for easy removal from different variety of waste water [9, 13]. Greywater has been treated using electrocoagulation proved to be an effective alternative for removal of objectionable organics [3, 4, 11, 15] by very few authors, and there is no published research based on hybrid electrocoagulation and filtration process. The prime objectives of this research are study the impact of electrode connection on the performance of hybrid process of electrocoagulation process followed by sand bed filtration. The hybrid electrode of (Al–Fe) with different electrode arrangement such as monopolar parallel (MP-P), and series (MP-S) are used and the observation is made on the overall treatment efficiency of the hybrid reactor.

2 Materials and Methods

2.1 Greywater Influents Samples

Influents GW samples were collected from ten different families with 1–5 members, following the sampling protocol [3, 16], located in Nagpur City, India. Especially, samples taken from bathtub/shower, hand basin, kitchen sinks and laundry were combined and composite in plastic container. The influents characteristics of samples are shown in Table.1.

2.2 Experimental Set-up

The experimental set-up consists of laboratory scale where influents is passed through electrocoagulation reactors followed by sand bed filter and activated carbon adsorption process in batch mode as shown in Fig. 1a, b. The EC reactors cell [24 cm (H) × 20 cm (L) × 10 cm (W)], having volume of 5 L, made from acrylic material, with thickness as 0.4 cm, performed with electrode materials of aluminium and iron sheets with dimensions 18.5 cm (H) × 5 cm (W) × 0.02 (thickness) cm each, having surface area of 92.5 cm^2. In order to take out floating material, an additional tank of same dimensions was attached on either side of reactors. The electrode space between the anode and cathode was maintained at 2 cm to customise the energy loss and placed vertically. The configuration of electrode is arranged in Monopolar parallel (MP-P) and Monopolar series (MP-S) in each run with direct current (DC) power supply (model RPS 3005) performing a range of with operating condition shown in Fig. 1a. The tests were conducted with 4.5 L (each run), and greywater was gently stirred at 150 rpm with four plate placed vertically immersed with surface region of 82.5 cm^2. A DC power supply is used to provide applied voltage at 6 and 12 V for 60 min. Scum (colloidal particles)

Table 1 Greywater characteristics feed as influents to EC process, no: 15 samples, SD: standard deviation

Parameters	Min	Max	Average	SD
pH	5.6	8.5	7.5	1.3
Turbidity (NTU)	26	78	46	10.8
TDS (mg/l)	180	680	295	135
TSS (mg/l)	19	170	78	52
COD (mg/l)	130	550	278	196
Chloride (mg/l)	10.2	45	24.5	9.3
Sulphate (mg/l)	26	68	30	12.5
Ammonium nitrogen (mg/l)	1.7	6.6	3.4	2.3
Orthophosphorus (mg/l)	1.51	7.8	4.5	3.2

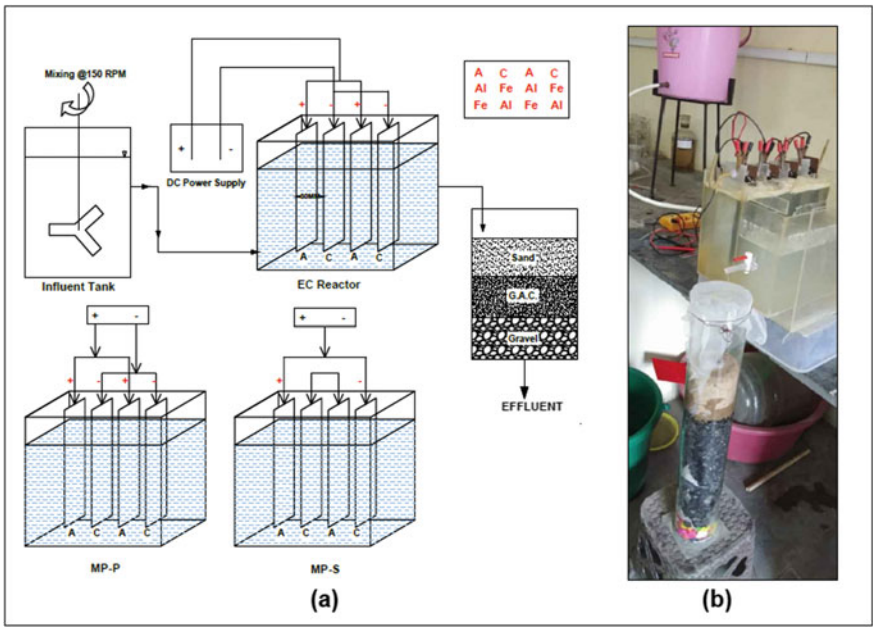

Fig. 1 **a** Laboratory-scale experimental flow diagram with **b** real image of electrocoagulation and filtration process

generated during process was removed by floatation and sedimentation mechanism, achieved by gas bubbles developed at cathode [4, 5]. The effluent from EC reactor is passed in filtration beds by 1 cm orifice opening at 12 cm (*H*) of EC reactors as shown in Fig. 1b. After each run, electrodes were dipped to 2 N HCL solution of removing organic pollutants.

2.3 Preparation of Filter Bed

The lab-scale sand filter bed is made up of acrylic materials, having dimension 60 cm (height) with 10 cm (diameter) having an orifice opening of 1.5 cm at centre of bottom. Prior to experiments, the sand and coconut shell-activated carbon was properly washed and dried at 105 °C, which then, sieved and range to finer sand of effective size (0.2–0.6) mm at top followed by granular coconut shell-activated carbon with gravel support of effective size (4.75 mm) as shown in Fig. 1b. The experiments were conducted with ambient room temperature and final effluents are continuously monitored at time interval, i.e. of 15, 30 and 60 min operating time. At the end of each run, EC reactors and filter were backwashed.

2.4 Analytical Studies

Influents and effluents characteristic were sampled and analysed with aim to focus on physiochemical greywater treatment facility followed by floatation with sand filtration process. All feed samples were examined with different water quality parameter [3, 10]such as chemical oxygen demand (COD), according to cuvette tests with Hach Spectrophotometer (Hach, DR 2000), total suspended solids (TSS), and total dissolved solids (TDS), pH, turbidity, chloride and sulphate according to prescribed Standard Methods [17].

3 Result and Discussion

The efficiency of removal of pollutants from greywater at different voltage with filtration depends on operational parameters such a pH of greywater, electrolysis operating time, electrode type and arrangement of distances between electrodes, etc. which promotes the effectives of EC followed by filtration process under specific condition and system. The removal efficiency of greywater characteristic was applied by following equation [18]

$$\left\{\mathrm{Re}(\%) = \left[100 * \left(1 - \left(\frac{X_i}{X_f}\right)\right]\right\}. \quad (1)$$

3.1 Effects of Different Electrode Pairs

The tests performed used four aluminium and iron electrodes each arranged in Al–Fe–Al–Fe and Fe–Al–Fe–Al mode in MP-P and MP-S as shown in Fig. 1a. The investigation reveals that hybrid electrode pairs of Al and Fe in EC reactor performs because of electrochemical reactions taking place at anode and cathode as shown in Table 2, which results in higher removal efficiency than Al and Fe electrodes utilized individually, because of higher oxidation potential type of material placed at anode [15, 19]. The results indicate that different electrode combinations, e.g. Al–Fe–Al–Fe, result in the highest COD removal of 95% withan applied voltage of 12 V after a 60-minute time interval followed by filtration in MP-P condition, and that more coagulantsare produced, but for Fe–Al–Fe–Al–Al at the same configuration, the COD removal decreases to 85% as shown in Fig. 2a. From the equation, it is clear that Al and Fe ions from the anode are gradually hydrolyzed, while the solution from the cathode becomes alkaline over time owing to the production of $Al(OH)^n$ or $Fe(OH)^n$ and resulting in the generation of hydrogen bubbles. Henceforth, mix of two different electrodes (Al–Fe) provides higher removal efficiency in MP-P condition. However, in MP-S electrode configuration, the sacrificial

Table 2 Equation at anode and cathode reactions for Al or Fe electrodes [9, 20]

Aluminium electrode	
Anode	$Al \rightarrow Al^{3+}_{(aq)} + 3e^{-}$
In the solution	$Al^{3+}_{(aq)} + 3H_2O \rightarrow Al\ (OH)^{3+} 3H^{+}_{(aq)}$
Cathode	$nAl\ (OH)^{3} \rightarrow Al_n(OH)_{3n}$
Iron electrode	
Anode	$4Fe_{(s)} \rightarrow 4Fe^{2+}_{(aq)} + 8e^{-}$ $Fe_{(s)} \rightarrow Fe^{2+}_{(aq)} + 2e^{-}$
In the solution	$Fe^{2+}_{(aq)} + 2OH^{-}_{(aq)} \rightarrow Fe(OH)^{2}_{(s)}$
Cathode	$2H_2O_{(l)} + 2e^{-} \rightarrow H_{2(g)} + 2OH_{(aq)}$

electrodes are internally connected with each other which require higher effort of current potential, and this makes the electrochemical reaction between Al and Fe weak and results decline in removal efficiency of GW treatment.

3.2 *Effect of Applied Voltages and Operating Time Along with Filtration Mechanism*

In EC process, applied voltages play important phenomena on removal efficiency of greywater organics, suspended and colloidal parameters with respect to operating time as they control the reaction rate inside the EC reactor [21]. It was observed that COD, NO_3–N and TSS were also reduced to 12.8 mg/l from 276 mg/l, 0.78 from 3.6 mg/l and 10 mg/l from 82 mg/l, respectively, obtained at 12 V for 60 min in hybrid system of Al–Fe–Al–Fe in MP-P connection, ultimately showing greater performance, as compared to Fe–Al–Fe–Al in MP-P, and it is due to higher dissolution of Fe^{2+} ions with experimental condition which affect the growth of flocs. As seen in Fig. 2b, the impacts of additional pollutants such as sulphate, chloride, and turbidity were reduced to acceptable levels at 12 V settings for MP-P and somewhat less in MP-S due to a decrease in H_2 production, which results in emulsion dissolution and aggregation. Increment in voltages hike shows increment in inorganic removal efficiency which is based on the fact that condition of driving force in anodic reaction allows kaolinite suspension to more destabilise the particles' size, maintaining to settle down effectively [4] and thus, the results reflect an increase in energy consumption with respect to operational time. However, after certain value of voltage, dissolution of anode electrode stopped so is floc formation and also removal efficiency decreased with respect to operating time, as shown in Fig. 1 [12, 22].

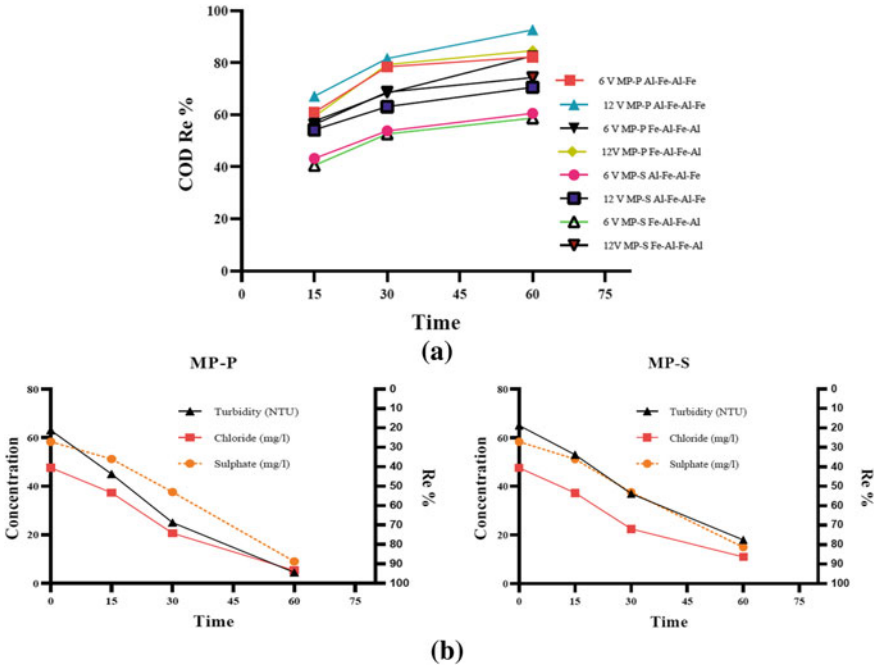

Fig. 2 **a** Effect of applied voltages and operating time for COD removal during EC and filtration process. **b** Degree of sulphate, chlorides, turbidity removal at 12 V Al–Fe–Al–Fe MP-P and MP-S mode

3.3 Effect of Electrode Material and Electrode Gap

The EC reactor is constituted with Al and Fe electrodes which play a key role due to its consistency and easily accessibility. Researchers mainly focus on same type of electrode materials and found quite good results, but if electrode material is different, then more destabilizing of colloidal particle is possible. Henceforth, in present study, Al–Fe–Al–Fe as anode and cathode electrodes have a pronounced influence over other configuration of Fe–Al–Fe–Al because at anode, Fe ions are weak to produce $Fe(OH)_2$ which result in weak coagulants due to lower charge of ions to break colloidal particle, and hence, Fe–Al–Fe–Al combination gives slightly less result. Effect of electrode gap is again one of the important parameters in EC process. The finding shows that when inter-electrode distances are increased, (i) ohmic loss in concern of both anode and cathode [23] over varying voltages and (ii) resistance to mass exchange increases which decreases the development of charge transfer and electrode oxidation [23], and hence, MP-S combination of various voltage connection were insufficient to provide enough removal efficiency. Therefore, inter electrode distance is kept at an appropriate lower side to 30 mm as to diminish energy consumption and raise removal efficiency [8].

3.4 *Effect of Electrode Mode*

The productivity of EC process is strongly linked to electrode configuration as shown in Fig. 1a where the electrodes are arranged in Monopolar parallel (MP-P) and series (MP-S) [4]. From studies, it is investigated that four different electrodes are connected parallel to each electrode possessing current which increased resistance in every electrodes. On another hand, in Monopolar series configuration, current is passed through two outermost electrodes and inner two electrodes are connected without connection which reduces the consumption pattern at anode and current passivation occur at cathode. Therefore, it was found that Al–Fe–Al–Fe/Fe–Al–Fe–Al Monopolar-parallel mode (MP-P) of connection gave best results than (MP-S) mode of same connections because of electrode configuration of polarity had no such effects on sacrificial electrode consumption.

3.5 *Effect of pH*

EC process is confined with pH which is directly related to efficiency of greywater [1, 6, 24]. From performed experiments, it was observed from Figs. 2a, and 3a, b that when Fe–Al, i.e. (12 V MP-P and 6 V MP-S), used as sacrificial electrode, i.e. inner electrode placed at anode and cathode, it gave better results at lower pH values and Al–Fe, i.e. (12 V MP-P and 12 V MP-S), as sacrificial anode stood still in giving good removal efficiencies even at higher pH values. According to the observations, the best conditions for COD removal were when the pH range was (7.3–7.5), which progressively increased and decreased with the initial at a given time and condition of electrode materials and configuration, owing to hydrolysis and oxidation of electrodes $(OH)_{4^-}$ occurring at the anode and cathode. Also, it was observed that greywater at low, neutral or slightly alkaline pH gave favourable good removal efficiency and decreased the same when pH increased towards highly alkalinity.

4 Operating Cost Estimation

For practical execution of EC process on real basis, it is important to be economical and the major factor responsible for maintaining the same is cost of operation [5]. Operational rate (OPc) of ECF process includes electrical energy used, cost of electrode consumption and maintenance cost for disposal of sludge on landfill, filtration media and other fixed charges which is expected to be INR 2.1 kg/m^3. Operating cost mainly is evaluated by adding cost for electrical energy and electrode material with maintenance cost and their equations are given below [4, 5, 7].

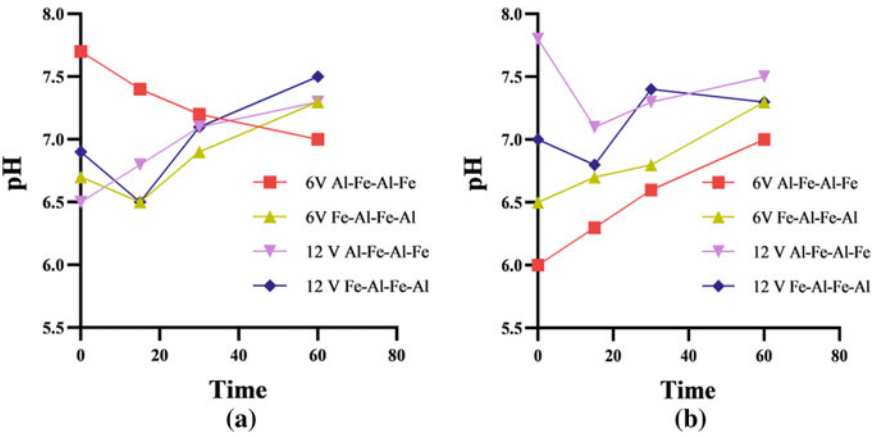

Fig. 3 **a** Effect of pH trends during MP-P and **b** MP-S mode connection

Table 3 Operation cost for EC and filtration process for different combination

EC+ Filtration	Mode	U (V)	CD (A)	C_{energy} KWh/m^3	$C_{electode}$		C_{Main} (INR) kg/m^3	OPc in INR/m^3
					kg Al/m^3	kg Fe/m^3		
Al-Fe-Al-Fe	MP-P	6	0.3	0.375	0.008	0.018	2.1	3.85
Al-Fe-Al-Fe		12	0.7	1.75	0.020	0.042	2.1	14.56
Fe-Al-Fe-Al		6	0.4	0.50	0.011	0.024	2.1	5.11
Fe-Al-Fe-Al		12	0.8	2.00	0.023	0.048	2.1	19.93
Al-Fe-Al-Fe	MP-S	6	0.45	0.562	0.013	0.027	2.1	5.88
Al-Fe-Al-Fe		12	0.85	2.125	0.024	0.051	2.1	17.64
Fe-Al-Fe-Al		6	0.5	0.625	0.014	0.030	2.1	6.44
Fe-Al-Fe-Al		12	0.9	2.250	0.026	0.054	2.1	22.17

$$\text{OPc} = \text{Cost}_{\text{Energy}} + \text{Cost}_{\text{Electrode}} + \text{Cost}_{\text{Maintenance}} \quad (2)$$

$$\text{Cost of energy, Cost}_{\text{Energy}}\left(\text{kWh/m}^3\right) = \{(U * i * t_o)/V\} \quad (3)$$

$$\text{Cost of Electrode, Cost}_{\text{Electrode}}\left(\text{kg/m}^3\right) = \{(i * t_o * M_w\}/(z * F * V)\} \quad (4)$$

where U = cell voltages (V); i = current (Amp); to = operating time (h); V = wetted volume of reactor (m^3); M_w = molecular wt. of Fe/Al (g/mol); z = amount of electrons involved in the EC process (2 for Fe and 3 for Al); F = faradays constant (96,485 C/mol); CD = current density (A).

For calculation of operational cost (Table 3), electrical consumption unit price was taken as INR 6.7/unit of kWh for the Nagpur area, and price of electrode material were INR 30/kg and INR 130/kg for iron and aluminium, respectively. On

Table 4 Cooperative study EC process

Greywater treatment	CD/V	EC	EM	Energy req	Re %	OP_{Cost} INR/m^3	Ref
Electrocoagulation and disinfection	135 V	BP-S	Al–Al	0.08 kWh/m^3	60% (COD)	18.90	[15]
					65%(turbidity)		
Electrocoagulation	10 V	MP-P	Al–Al–Al–Al	0.03 kWh/m^3	70% (COD)	12.60	[3]
					85% (turbidity)		
Electrocoagulation and 0.45 (micro-m) millipore membrane	1 mA/cm^2	MP-P	Al–Fe–Fe–Al	9.45 kWh/m^3	96% (COD)	ND*	[4]
					65% ($SO4^{2-}$)		
					71% (Cl^-)		
					92%(turbidity)		
Electrocoagulation and filtration unit	12 V	MP-P	Al–Fe–Al–Fe	1.75 kWh/m^3	95% (COD)	14.56	[PS]
					89% ($SO4^{2-}$)		
					92% (Cl^-)		
					95% (turbidity)		

*ND** not detected, *EC* electrode configuration, *CD* current density, *V* voltage, *EM* electrode material, *PS* present study, *BP-S* bipolar series, *MP-P* monopolar parallel, *INR* Indian rupees

total, during EC process 0.139 kg/m^3 and 0.294 kg/$m^3$of Al and Fe electrode, respectively, were consumed. Based on the comparative studies shown in Table 4, it is found that electrocoagulation process depends on many treatment conditions for estimation of operational cost such as current density, volume of treated effluents, electrode material and connection, EC reactors and type of power supply.

5 Conclusion

In this study, the electrocoagulation process along with filtration strategy was led to dissect the achievability of greywater evacuation with aluminium and iron cathodes in different combination. The outcomes showed that blends of four aluminium–iron anodes orchestrated in MP-P and MP-S association mode are sufficiently proficient to give great evacuation efficiencies of almost acquiring 90% removal efficiency. At outcome of pH, 7.3 show that hybrid electrode for both combinations reflect great strength in removal efficiency with increase in applied voltage to working time. Economical figure of operating cost at 12 V, the combination of Al–Fe–Al–Fe in MP-P required less electrical energy than Fe–Al–Fe–Al of 1.75 kWh/m^3 and 2.0 kWh/m^3, respectively, which results in higher COD current efficiencies. As a result, under optimum condition operating cost for greywater treatment by EC with filtration process using 4 Al–Fe electrodes in MP-P was found out to be INR 14.56/$m^3$and INR 17.64/m^3 for Al–Fe in MP-S combination. The supplementary step of filtration proves to reduce significantly the organic matter. The modification suggested on electrode combination provides enhanced performance of the hybrid reactor.

References

1. Moussa DT, El-Naas MH, Nasser M, Al-Marri MJ (2016) A comprehensive review of electrocoagulation for water treatment: potentials and challenges. J Environ Manage xxx:1–18
2. Abdel-Shafy HI, El-Khateeb MA, Shehata M (2014) Greywater treatment using different designs of sand filters. Desalination Water Treatment 5237–5242
3. Vakil KA, Sharma MK, Bhatia A, Kazmi AA, Sarkar S (2014) Characterization of greywater in an Indian middle-class household and investigation of physicochemical treatment using electrocoagulation. Sep Purif Technol
4. Sibel B, Turkay O (2016) Domestic greywater treatment by electrocoagulation using hybrid electrode combinations. J Water Process Engg 56–66
5. Kobya M, Akyol A, Demirbas E, Oncel MS (2013) Removal of arsenic from drinking water by batch and continuous electrocoagulation processes using hybrid Al–Fe plate. Wiley Online Library
6. Ghaitidak DM, Yadav KD (2013) Characteristics and treatment of greywater—a review. Environ Sci Pollut Res 20(5):2795–2809
7. Demirci Y, Pekel LC, Alpbaz M (2015) Investigation of different electrode connections in electrocoagulation of textile wastewater treatment. Int J Electrochem Sci
8. Li F, Wichmann K, Otterpohl R (2009) Review of the technological approaches for grey water treatment and reuses. Sci Total Environ 3439–3449
9. Umran TU, Savas Koparal A, Oğütveren UB (2009) Hybrid processes for the treatment of cattle-slaughter house wastewater using aluminum and iron electrodes. J Hazard Mater 164(2–3):580–586. https://doi.org/10.1016/j.jhazmat.2008.08.045. Epub2008 Aug 22. PMID: 18819748
10. Khalid B, Al-Shannag M, Alrousana D, Al-Kofahic S, Al-Qodahd Z, Rasool Al-Kilania M (2017) Impact of soluble COD on grey water treatment by electrocoagulation technique. Desalination Water Treatment
11. Ansari K, Shrikhande AN (2019) Feasibility of greywater treatment by electrocoagulation process: a review. Int J Emerg Technol 10(1):92–99
12. Mollah MA, Robert S, Parga JR, Cocke DL (2001) Electrocoagulation (EC)—science and applications. J Hazard Mater 84:29–41
13. Kobya M, Gengec E, Demirbas E (2016) Operating parameters and costs assessments of a real dye house wastewater effluent treated by a continuous electrocoagulation process. Chem Eng Proc 101:87–100
14. Katal R, Pahlavanzadeh V (2011) Influence of different combinations of aluminum and iron electrode on electrocoagulation efficiency: application to the treatment of paper mill wastewater. Desalination 265:199–205
15. Lin C-J, Lo S-L, Kuo C-Y, Wu C-H (2005) Pilot-scale electrocoagulation with bipolar aluminum electrodes for on-site domestic greywater reuse. J Environ Eng
16. Lakshmi PM, Sivashanmugam P (2013) Treatment of oil tanning effluent by electrocoagulation: influence of ultrasound and hybrid electrode on COD removal. Sep Purif Technol 378–384
17. Standard methods for examination of water and wastewater, 21st edn. (2005). American Public Health Association (APHA), Washington DC
18. Aouni A, Fersi C, Ali MBS, Dhahbi M (2009) Treatment of textile wastewater by a hybrid electrocoagulation/nanofiltration process. J Hazard Mater
19. Padmaja K, Cherukuri J, Anji Reddy M (2020) A comparative study of the efficiency of chemical coagulation and electrocoagulation methods in the treatment of pharmaceutical effluent. J Water Process Eng
20. Daghrir R, Drogui P, Jean F, Blais Guy M (2012) Hybrid process combining electrocoagulation and electro-oxidation processes for the treatment of restaurant wastewaters. J Environ Eng

21. Ingle NW, Gujare Sr (2019) Iron and aluminium as electrode material in removal of COD and colour from textile industry wastewater—a comprehensive study. J Indian Water Works Assoc
22. Asaithambi P, Sajjadi B, Raman A, Aziz A (2016) Performance evaluation of hybrid electrocoagulation process parameters for the treatment of distillery industrial effluent. J Process Saf Environ Protection
23. Khaled B, Wided B, Béchir H, Elimame E, Mouna L, Zied T (2019) Investigation of electrocoagulation reactor design parameters effect on the removal of cadmium from synthetic and phosphate industrial wastewater. Arab J Chem
24. Sivakumar M, Emamjomeh MM (2009) Review of pollutants removed by electrocoagulation and electrocoagulation/flotation processes. J Environ Manag

Numerical Simulation of Drive-Drill-Drive Techniques for Open-Ended Pile Installations

Joaquin Goycoolea Castillo, Sparsha Nagula, Christoph Schallück, and Jürgen Grabe

Abstract Pile penetration refusal in difficult soils has been a subject of concern. In recent past, the Drive-Drill-Drive technique has been deployed to facilitate the penetration of open-ended piles after refusal. In this technique, the soil inside the pile is drilled using regular drilling tools that once the pile reaches a refusal state. The drilled material is then pulled out of the pile. The reduced internal friction then facilitates the further penetration of the pile. The removal of the drilled soil also causes stress state changes both within and outside the pile. The work plans to study the changes in the stress state of the soil outside the pile due to the drilling and removal of soil. The work studies the effect of this installation process on end bearing resistance and vertical bearing capacity of the open-ended pile. Numerical FE model using a hypoplastic soil constitutive model was developed to simulate the installation process. The results were compared to results obtained from commercial software GRLWEAP. Unlike, observations made on field, the final end bearing resistance of the pile as per the simulation results was found to be around 65% of the value estimated by the GRLWEAP without any soil removal. Four driving variations with different driving depths and diameters were studied.

Keywords Pile refusal · Drive-Drill-Drive · Zipper technique · Hypoplastic model · ABAQUS/explicit · Offshore wind

J. G. Castillo · S. Nagula (✉) · J. Grabe
Institute of Geotechnical Engineering and Construction Management, Hamburg University of Technology, 21079 Hamburg, Germany
e-mail: sparsha.nagula@tuhh.de

J. Grabe
e-mail: grabe@tuhh.de

C. Schallück
Van Oord Offshore Wind Germany GmbH, 20097 Hamburg, Germany
e-mail: christoph.schallueck@vanoord.com

B. Laishram and A. Tawalare (eds.), *Recent Advancements in Civil Engineering*, Lecture Notes in Civil Engineering 172,
https://doi.org/10.1007/978-981-16-4396-5_46

1 Introduction

Many wind offshore farms have been constructed in the recent years in Europe. The most common foundations for wind turbines are monopiles (MP), which generally are installed using the hammer technique. Pile penetration refusal is the term used when the hammer is not able to drive the pile further. It has become common for wind turbines to be installed in difficult soils for wind offshore industry as best locations in terms of water depth and soil conditions, in the North and Baltic seas are already taken. For this reason, new places with not so favorable conditions for the wind turbine installations are being explored. The pile refusal risk must be acknowledged during the planning phase of the project. If an unplanned refusal occurs at the execution stages, it may lead to huge time delay and increase the overall cost of the project.

This paper tried to study the Drive-Drill-Drive method of pile installation. The method involves drilling and removal of soil inside the pile when it reaches refusal depth, in order to reduce the soil resistance to driving (SRD). This removal of soil and reduction of resistance to driving enables the penetration of the pile to target depth. A numerical simulation of this process was executed using the commercial finite element method (FEM) code ABAQUS. A pile was simulated as wished in place at 5-m-depth and was displacement driven to a refusal depth of 15 m, following that the soil inside the pile was removed, and the pile was further driven for 2 m. The SRD reductions were compared with results obtained from one-dimensional wave program GRLWEAP. The effect of different drill diameters and depths on SRD was studied.

2 Theoretical Framework

Monopiles for the offshore wind industry are often driven via hydraulic hammers. Pile driving by hammering follows the principle that the pile overcomes the SRD until it reaches its target depth. This is achieved by inputting energy at the pile top via impact. Currently, majority of the suitable locations in terms of water depths and soil conditions to construct wind turbines are already taken. On the contrary, the size and capacity of wind turbines are growing [1], leading to an increase in demand for larger diameters monopoles, as large as 12 m. In this context, one of the proposed solutions is the drilling procedure. It consists of drilling and removing the soil inside the monopile in order to reduce the inner shaft friction and make pile driving easier till the target depth. Figure 1 describes a schematic representation of Drive-Drill-Drive technique.

Various numerical methods have been used till date for simulating pile penetration. Starting from the cavity expansion solutions well explained by Cudmani [2] and Yu [3], followed by the Strain Path method, contact models [4, 5], advanced FE formulations as Arbitrary Lagrangian Eulerian (ALE) and Coupled Eulerian

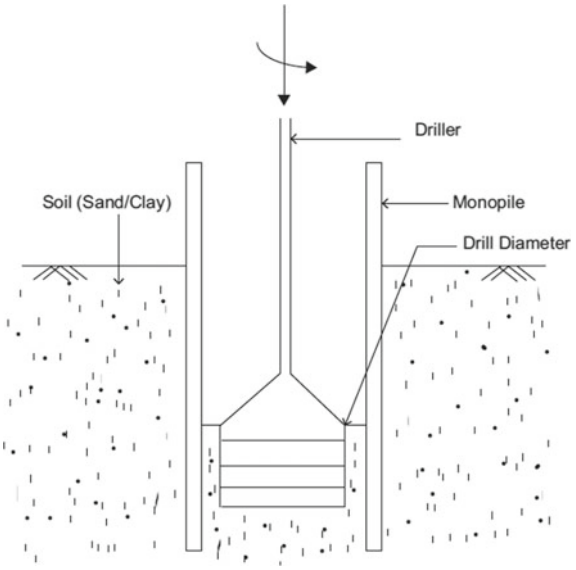

Fig. 1 Schematic representation of the Drive-Drill-Drive technique

Lagrangian (CEL) techniques. The Drive-Drill-Drive technique has not been modeled till date, and hence, this work focusses on the numerical simulation of the method in order to gain better insight of the same.

3 Numerical Methodology

In this work, the pile penetration was simulated following the zipper technique. This method involves modeling of a rigid tube with a thickness of 1 mm along the wall of the pile. The 1-mm-tube was in frictionless contact with the surrounding soil. During pile penetration, the pile slid over the tube, and the soil was separated from the tube. In this way, contact between the penetrating pile and the surrounding soil was established.

The numerical model was developed using commercial software ABAQUS 6.14. Making use of symmetry, the model was simplified to a two-dimensional axisymmetric model using the center vertical axis of the pile as symmetry axis. The soil model was 25 m in radial direction and 45 m in depth. The soil is fixed on the horizontal direction at the right and left side, meanwhile it is fixed in both directions at the bottom. The pile can only move vertically. The BC's are as shown in Fig. 2. The pile was wished in place at a 5-m-depth. It had a diameter of 10 m, 0.10-m-wall thickness and a length of 30 m. The pile tip was modeled with a 75° inclination. This was necessary for the zipper technique to function properly so as to let the pile separate the soil elements from the rigid 1-mm-tube. Tangential contact between the soil and the pile was defined as penalty contact with the

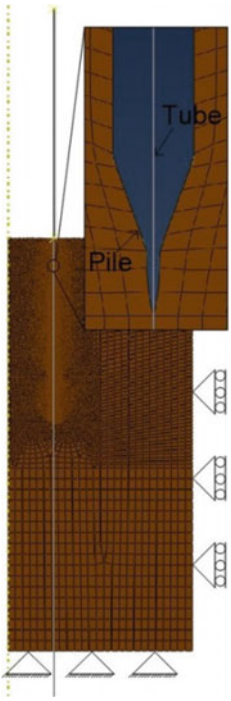

Fig. 2 Axis symmetric model for pile penetration

Coulomb's friction law. Normal contact was defined as per hard pressure over-closure allowing separation after contact.

The soil was modeled using the hypoplastic model first proposed by Von Wolffersdorff in 1996 with the extension for intergranular strain from Niemus and Herle [6]. This constitutive model combines hypoplasticity principles with traditional critical state soil mechanics. It is capable of reproducing nonlinear soil behavior, incorporates the influence of barotropy and pyknotropy as well as captures soil behavior at small strains. The hypoplastic soil parameters of well know Kalsruher sand are shown in Table 1.

Where:

ρ density.
Φ_c critical friction angle.
h_s granular stiffness.
ν poisson coeficient.
e_{d0} void ratio at maximum compaction.
e_{c0} critical void ratio.
α pycnotropy exponent.
β pycnotropy exponent.
m_T increase factor at 90º change in direction.
m_R increase factor at 180º change in direction.

Table 1 Karlsruher sand hypoplastic model properties

Parameter	ρ	Φ_c	–	h_s	ν	e_{d0}	e_{c0}	α	β
Value	1.1	30	0	5800	0.28	0.53	0.84	0.13	1
Unit	[kN/m^3]	[°]	[–]	[MPa]	[–]	[–]	[–]	[–]	[–]

Parameter	m_T	m_R	R_{max}	β_R	χ	d_{50}	e_0
Value	2	5	0.0001	0.5	6	0	0.7
Unit	[–]	[–]	[–]	[–]	[–]	[–]	[–]

R_{max} maximum intergranular strain.
β_R exponent.
χ exponent.
d_{50} mean grain diameter.
e_0 initial void ratio.

In order simulate the Drive-Drill-Drive process, it was necessary to correctly recreate the drill procedure. For this purpose, the elements inside the pile wall were to be removed after drilling of the soil. This was not possible in the ABAQUS/Explicit module, and for this reason, the model results once that the pile reached refusal depth was exported to ABAUQUS/Implicit. The soil elements which were supposed to be drilled, and removed were deleted from the numerical model, and the updated model was once again imported back to ABAQUS/Explicit. This was followed by further driving of the pile into the soil by 2 m. The simulation steps are shown in Fig. 3. The driving procedure is calculated in two steps. The gravity or K_0 step followed by penetration step. The pile was simulated as a rigid body and was displacement driven into the soil with a penetration rate of 0.02 m/s.

Numerical simulation was carried out for different drill diameters and depths. This was done in order to study the effect of quantity of soil removed on SRD and on the final vertical end bearing resistance.

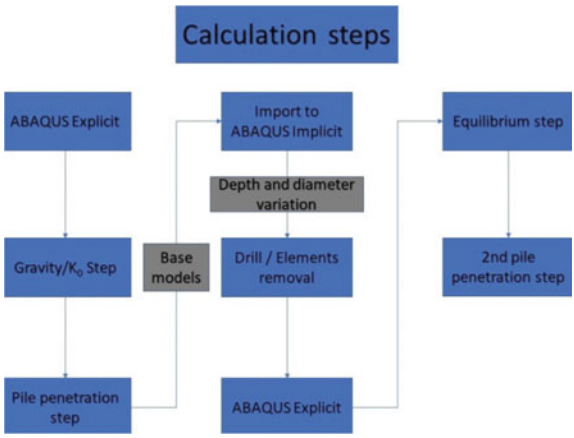

Fig. 3 Simulation steps

4 Results

4.1 Comparison with GRLWEAP

The SRD results from the FEM simulation were compared with a driveability simulation executed using GRLWEAP program. GRLWEAP is a one-dimensional wave equation analysis program that simulates the pile response to pile driving. The simulation in GRLWEAP was carried out with a pile similar to the one simulated in ABAQUS. Single soil layer with a cone penetration tip resistance value of 15 and 30 MPa at top and bottom of soil layer, respectively, was considered. The method uses Cone Penetration Test (CPT) values-based framework proposed by Alm and Hamre [7]. The variation of SRD with time and depth as obtained from ABAQUS and GRLWEAP software before drilling of soil is simulate, are described in Fig. 4. An instant rise in SRD to 20 MN can be observed in both figures (blue curve). The SRD reaches a peak value of 80 MN at the end of the installation. In Fig. 4 (right) four curves are shown, three of them correspond to the driveability analysis using the Alm and Hamre method for three different scenarios called upper bound, best estimate and lower bound. The upper and lower bounds are the best estimate scenario multiplied by a factor of 1.25 and 0.75, respectively. During first few meters of pile penetration, the SRD calculated by ABAQUS model was found to be below the lower bound estimated by GRLWEAP. This was due to the fact that penetration in ABAQUS was initiated at 5-m-depth whereas in GRLWEAP analysis, the penetration was initiated at soil surface. After five meter of pile penetration (10 m depth in the graph), the ABAQUS curve begins to approach the GRLWEAP best estimate calculation culminating in near perfect match when the pile is at a depth of 12 m.

Following the first virgin pile installation to a depth of 15 m, the model was exported to ABAQUS Implicit as described before, and soil elements were removed to simulate different drill diameters and depths. A total of four different drill

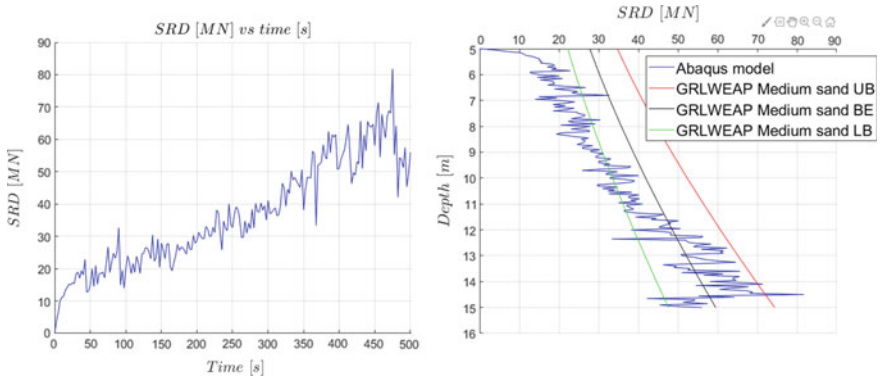

Fig. 4 Development of SRD with time (left) and depth (right)

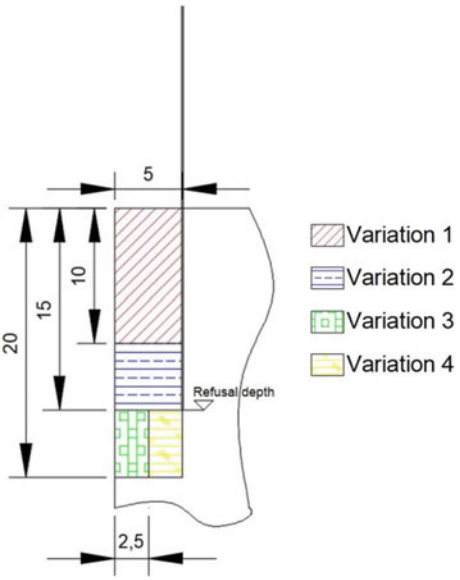

Fig. 5 Drill depth and diameter variations

variations were calculated as described in Fig. 5. Variation 2 (Var2) includes removal of the soil as per previous Variation 1 with additional removal depth. The same holds good for variations Var3 and Var4. In Var1, the soil elements inside the pile up to 5 m above refusal depth were removed with a drill radius of 5 m. Var2 consisted of removal of soil up to refusal depth with the same drill radius as Var1. Var 3 corresponded to drilling of soil up to 5 m below refusal depth with a drill radius of 2.5 m and finally Var4 with drill depth of 5 m below refusal depth and a drill radius of 5 m.

4.2 Drill Variations Results

Figure 6 describes the SRD development between refusal and target depth as obtained from ABAQUS simulations for various variations. Each figure also depicts the SRD calculated as per GRLWEAP till refusal depth (red curve) without any soil removal. For this reason, the GRLWEAP end bearing resistance is the same for all variations. The four variations were executed using the same base model. The progressive soil removal with each variation, leads to a logical SRD reduction further leading to reduction in end bearing resistance.

In Variation1, it can be observed that beyond 25 MN SRD the blue curve has approximately a linear growth. Meanwhile for other three variations, almost no increase in SRD was observed. A marginal difference in SRD at target depth was observed across variations.

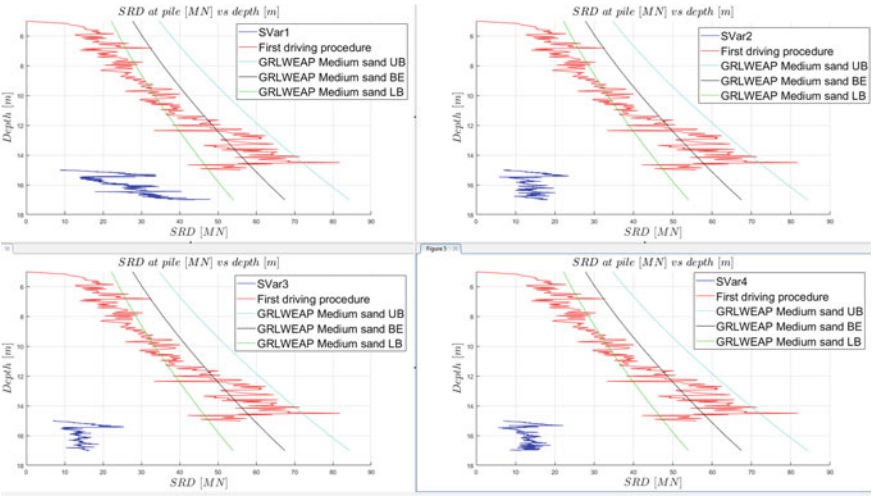

Fig. 6 Development of SRD with depth for different scenarios

The SRD and vertical end bearing resistance of the pile values are shown in Table 2. The end bearing resistance is calculated as the SRD at target depth. The end bearing resistance decreased with each progressing variation. The highest percentage of vertical end bearing resistance compared to the GRLWEAP prediction at target depth, was 65.10% as achieved by Variation1. This indicates at a serious capacity reduction caused due by drilling, nevertheless the short driving path of 2 m after refusal depth must be kept in mind. The pile was driven to only two meters after drilling. This fact prevents the pile from reaching a higher end bearing resistance, considering the linear SRD increase in Variation1. The other variations have a considerable lesser vertical end bearing capacity, but a trend can be acknowledged: the more soil removed by drilling, the less end bearing resistance the pile tends to reach.

Figure 7 compares the variation of reduction in SRD after soil removal and end bearing resistance at target depth with drilled soil quantity. The SRD capacity after the drilling procedure and before the second driving starts, meaning at refusal depth

Table 2 SRD and end bearing resistance for various scenarios

Results/case	Variation 1	Variation 2	Variation 3	Variation 4
End bearing resistance [MN]	43.90	17.96	16.52	11.13
SRD [MN]	10.29	8.65	7.55	6.97
End bearing resistance as per GRLWEAP [MN]	67.4	67.4	67.4	67.4
End bearing resistance % of GRLWEAP prediction	65.10	26.64	24.50	16.51

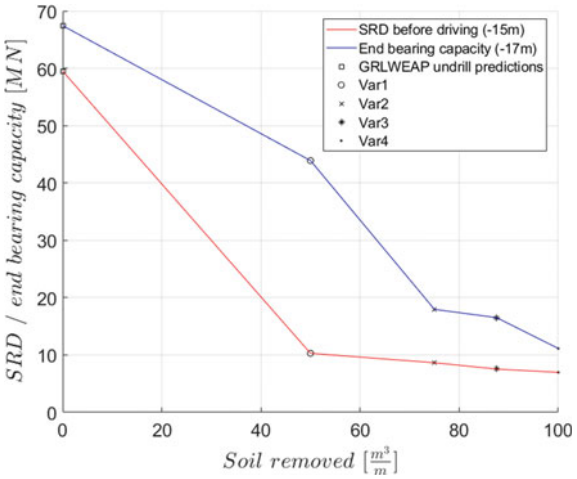

Fig. 7 Reduction in SRD and end bearing resistance with removed soil

(15 m), is represented by the red line. A considerable SRD reduction is observed for Variation1. Following Variation1, nearly a linear reduction in SRD was observed with increasing removed soil quantity. The blue line in Fig. 7 depicts the vertical end bearing capacity when the pile reached target depth (−17 m). A major reduction in resistance was observed between Variation 1 and 2, while variation along 2 through 4 was not abrupt. It must be observed that Variation 2, 3 and 4 involve minimum drilling till refusal depth whereas for Variation1 drilling depth is less than refusal depth. This could probably explain the sudden drop in magnitudes between Variation 1 and 2. All variations present a drastic resistance reduction compared to the GRLWEAP predictions without soil removal.

5 Conclusions

The effects of the Drive-Drill-Drive technique on the SRD and end bearing resistance were studied using numerical simulation. The absence of similar studies in this specific topic, makes this work a first attempt to develop a better understanding of the method. A FE model using the ABAQUS program with the zipper technique was developed to simulate the pile driving process. Parametric study was carried on involving different drill diameters and depths. The SRD simulation results were found to compare well with GRLWEAP calculations. Drilling of soil was found to bring in the desirable reduction in SRD to make further driving easier beyond refusal depth. This was achieved for all drill depths and diameter. A reduction in end bearing resistance was also observed with increase in amount of soil removed. Further pile driving after soil removal observed a linear increase in end bearing resistance when drilling depth was less than refusal depth. This observation should be further studied in order to arrive at an optimized drilling depth and penetration

depth beyond refusal where pile would reach required end bearing resistance. The effectiveness of drilling in Drive-Drill-Drive method to overcome pile refusal was confirmed. The quantity of soil removed must be designed carefully so as to ensure no drastic reduction in end bearing resistance of the pile.

The pile was driven only two meters after drilling due to numerical limitations, whereas in field it would be driven to further depths. Validation of the numerical model is out of the scope of this work, and therefore, the results have not been validated against field measurements, this is planned on future works.

References

1. Wind Europe (2019) Offshore wind in Europe key trends and statistics 2018. Report, Wind Europe
2. Cudmani R (2001) Statische, alternierende und dynamische Penetration in nichtbindigen Boden (Static, alternating, and dynamic penetration in noncohesive soils). PhD dissertation, University of Karlsruhe, Kalsruhe, Germany
3. Yu H-S (2010) Cavity expansion methods in geomechanics. Springer, The Netherlands
4. Mahutka KP, König F, Grabe J (2006) Numerical modelling of pile jacking, driving and vibratory driving. In: Triantafyllidis T (ed) Proceedings of international conference on numerical simulation of construction processes in geotechnical engineering for urban environment (NSC06), Bochum. Balkema, Rotterdam, pp 235–246
5. Henke S (2009) Influence of pile installation on adjacent structures. Int J Numer Anal Meth Geomech 34(11):1191–1210
6. Von Wolffersdorff PA (1996) A hypoplastic relation for granular materials with a predefined limit state surface. Mech Cohesive-friction Mater: Int J Experiments Modell Comput Mater Struct 1(3):251–271
7. Alm T, Hamre L (2001) Soil model for pile driveability predictions based on CPT interpretations. In: International conference on soil mechanics and geotechnical engineering, pp 1297–1302

Effect of Anthropogenic and Natural Activities on a Rock Slope Failure Using Rate, State, Temperature and Pore Pressure Friction

Nitish Sinha, Arun K. Singh, and Avinash D. Vasudeo

Abstract In this article, we study numerically the effect of anthropogenic and natural activities such as vehicular motion, blasting, rainfall, seismic activities etc. on time of failure of a rock slope using the rate, state, temperature and pore pressure friction (RSTPF) model proposed by Sinha et al. [6]. The initial creep velocity, gravitational stress and pore pressure are varied to investigate their effects on time of failure of the rock slope. It is observed that time of failure decreases with an increase in creep velocity, gravitational stress and pore pressure. The mechanism for these observations is also elucidated.

Keywords Time of failure of a rock slope · Anthropogenic and natural activities · Rate · state · temperature and pore pressure friction (RSTPF) model

1 Introduction

Rock slope failures and landslides are often encountered in hilly regions due to human activities and natural phenomena in form of vehicular motion, blasting in mines, tunnelling and road cutting, heavy rainfall, earthquake and volcanic activities [1, 2]. A typical rock slope failure occurs due to imbalance of the gravitational stress over frictional resistance [2–6]. This results in propagation of shear crack along the weak interface of the rock slope and followed by the sliding [7, 8]. Despite extensive experimental and theoretical investigations behind the causes of failure of rock slopes, there are still varieties of issues which are not yet fully understood in the literature [2, 4–6, 9]. For example, it is not yet known in literature

N. Sinha
Department of Mechanical Engineering, G. H. Raisoni Institute of Business Management, Jalgaon 425002, India

A. K. Singh (✉)
Department of Mechanical Engineering, VNIT Nagpur, Nagpur 440010, India

A. D. Vasudeo
Department of Civil Engineering, VNIT Nagpur, Nagpur 440010, India

B. Laishram and A. Tawalare (eds.), *Recent Advancements in Civil Engineering*, Lecture Notes in Civil Engineering 172,
https://doi.org/10.1007/978-981-16-4396-5_47

what factors cause the creep failure of a rock mass. More significantly, it is also not reported in literature the mechanism behind creep to catastrophic failure of the rock slope. Nevertheless, majority of studies have been carried out using static stress analysis such as limit equilibrium analysis of the rock slopes [1]. The present study, in contrast, enables to predict dynamic failure process of a rock slope.

In recent decades, the rate and state friction (RSF) model is widely used for predicting the time of failure along the sliding interface [3–6, 10]. The RSF laws are more valid for predicting the early stages of nucleation of the rock failure in which the slope creeps gradually [5, 6, 10]. Failure of a rock slope, on the other hand, occurs mainly due to the loss of frictional strength of the weak interface or joint [4–6, 10]. Frictional strength is often defined as the minimum force required to initiate the sliding of the rock mass [6, 9]. Chau [3] used the RSF laws to study the dynamic stability of a planar rock mass on an inclined plane. Helmstetter et al. [10] have also used the RSF laws for investigating the failure of the Vaiont and La Clapière slopes. Singh et al. [4] used the slightly modified approach of the Helmstetter et al. [10] for predicting the factor of safety of a planar rock slope in dynamic conditions. They have established theoretically that a rock slope fails without giving warning once its inertial force becomes important [4]. The present study concerning the failure of a rock slope is useful for nucleation or early stage of the slope failure during which the role of inertia is negligible. Later, they have also extended the RSF approach to model the creep failure of the rock interface by considering temperature of the sliding interface as well as its surroundings [5].

There are rock slope failures wherein temperature and pore pressure at the sliding surface also become important [5, 8, 9, 11–15]. This has further motivated researchers to modify the original RSF law which is known as the rate, state, temperature and pore pressure friction (RSTPF) model [6, 16, 17]. This modified frictional model has been studied in detail in view of both earthquake instability and failure of the rock slopes [6]. It has been established that thermal pressurization reduces the effective normal stress of the sliding surface due to increase in pore pressure [14, 16, 17]. However, hydraulic diffusivity and dilatancy of the fluid result in decrease of the pore pressure, thus increase in the frictional stability [6, 16–19]. Despite the recent applications of the RSTPF model, the effect of change in initial creep velocity, frictional stress and pore pressure at sliding interface using this particular friction model is not yet reported in literature. As these changes encounter due to human and natural activities such as vehicular movement, mine blasting, rainfall, earthquakes etc.

2 The Rate, State, Temperature and Pore Pressure Friction (RSTPF) Model

The present friction model is based on the assumption that magnitude of gravitational stress is constant and is equal to the frictional resistance along the sliding surface [5, 6, 10]. It is also assumed that the heat conduction and fluid advection are

perpendicular to the slip interface where the slip velocity and shear stress are allowed to vary with time [14]. The weak sliding interface fails due to the thermally activated creep in which the creep velocity increases gradually before it surges [14]. Chester [12] has introduced that frictional shear stress τ of rock surfaces depends on normal stress σ_n, pore pressure p_s, sliding velocity v, state variable θ and temperature T_s of the sliding surface as.

$$\tau = (\sigma_n - p_s)\left[\mu_* + a\ln(v/v_*) + b\ln(\theta v_*/d_c) + \frac{(Q_a a - Q_b b)}{R}\left(\frac{1}{T_s} - \frac{1}{T_*}\right)\right] \quad (1)$$

where μ_*,v_* and T_* represent reference coefficient of friction, velocity and temperature, respectively. Where a and b are the constitutive constants related to the sliding rock surfaces and their magnitudes are less than 1% of μ_* [20]. Further constants Q_a and Q_b are Arrhenius activation energies corresponding to a and b, while R is universal gas constant [11, 12]. Moreover, d_c is characteristic slip distance over which evolution of micro contacts occurs in step velocity experiments [20, 21]. At the same time, d_c is a scale-dependent property varying in range of micron to millimetre depending on size of the rock mass [20]. Segall and Rice [17] have proposed an idea for analysing earthquake process along a fault by assuming that shear heating of the highly damaged thin layer with thickness occurs at the sliding interface. The thin layer is surrounded by a less damaged rock mass having small thickness and thermal conductivity. In the present study, we have extended the aforementioned idea for analysing failure of a rock slope along the weak interface as depicted in Fig. 1. The thickness of the highly damage zone (slip zone) h is surrounded on both sides by comparatively less damage zone thickness h_w with permeability of the rock surface are κ_c and κ_w, respectively. Further, rate of heat conduction q_h and heat advection q_f transfer perpendicular to the creeping zone from slip surface. The temperature and pressure P_s, T_s and P_∞, T_∞ of the slip surface and surrounding, respectively [15].

The heat conduction takes place to the perpendicular to the sliding interface and its surrounding temperature T_∞. The governing equation proposed by Singh and Singh [5] as follows:

$$\rho_{total} c_v \frac{dT_s}{dt} = \tau\frac{v}{h} - \frac{2}{hh_w}K_T(T_s - T_\infty) \quad (2)$$

where ρ_{Total} and c_v are density and specific heat of the damaged layer. Further upon neglecting the thin layer h at the sliding interface, Eq. (2) takes the form as following

$$2\rho_{total} c_v \frac{dT_s}{dt} = \frac{\tau v}{h_w} - \frac{2k_T}{h_w^2}(T_s - T_\infty) \quad (3)$$

Shear heating may cause increase in temperature of pore water along the sliding interface and this is known as thermal pressurization [17, 22]. Segall and Rice [16,

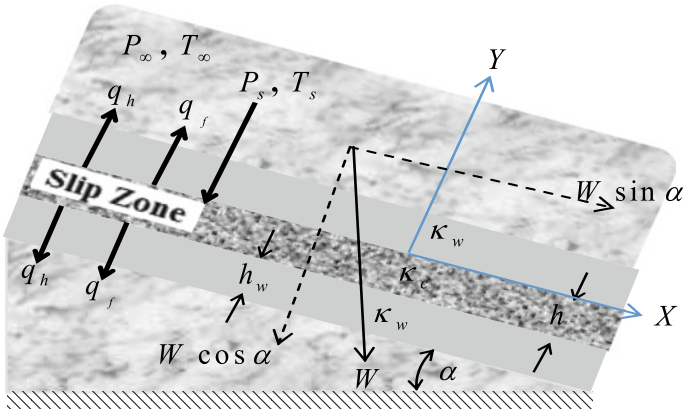

Fig. 1 A schematic diagram of the creeping zone of a rock slope with the slope angle α. Moreover, transportation of heat and pore fluid occurs in the direction perpendicular to the sliding interface

17] have used the following relation concerning thermal pressurization p_s in terms of coefficient of thermal pressurization Λ, pore plasticity ϕ_{plastic} and hydraulic diffusivity c_w as

$$\frac{\mathrm{d}p_s}{\mathrm{d}T} = \Lambda \frac{\mathrm{d}T_s}{\mathrm{d}T} + \frac{\dot{\phi}_{\text{plastic}}}{\beta_c} - \frac{2c_w}{hh_w}(p_s - p_\infty) \tag{4}$$

where p_∞ is fluid pressure surrounding the sliding interface, $\phi_{\text{plastic}} = \phi_0 - \varepsilon \ln(v_* \theta / d_c)$ with ϕ_0 reference porosity and ε is dilatancy factor. This is because of the fact that the creep failure of a rock slope with inclination α from horizontal occurs due to a component of gravitation force [4]. The modified governing differential equation of the system is given for a rigid mass on an inclined surface as following:

$$\left.\begin{aligned}
\frac{\mathrm{d}\phi}{\mathrm{d}T} &= \frac{\psi_g}{(\hat{\sigma}_n - \hat{p}_s)^2}\left\{\Lambda'\left[c_1 \mathrm{e}^{\phi}\psi_g - c_2(\hat{T}_s - \hat{T}_\infty)\right] - \varepsilon' \mathrm{e}^{\phi} + \varepsilon' \mathrm{e}^{\left[\hat{\mu}_* + \phi + c(\hat{T}_s^{-1} - 1) - \psi_g/(\hat{\sigma}_n - \hat{p}_s)\right]\beta^{-1}} - c_h(\hat{p}_s - \hat{p}_\infty)\right\} \\
&\quad + c\hat{T}_s^2\left[c_1 \mathrm{e}^{\phi}\psi_g - c_2(\hat{T}_s - \hat{T}_\infty)\right] + \beta \mathrm{e}^{\phi} - \beta \mathrm{e}^{\left[\hat{\mu}_* + \phi + c(\hat{T}_s^{-1} - 1) - \psi_g/(\hat{\sigma}_n - \hat{p}_s)\right]\beta^{-1}} \\
\frac{\mathrm{d}\hat{T}_s}{\mathrm{d}T} &= \left[c_1 \mathrm{e}^{\phi}\psi_g - c_2(\hat{T}_s - \hat{T}_\infty)\right] \\
\frac{\mathrm{d}\hat{p}_s}{\mathrm{d}T} &= \left\{\Lambda'\left[c_1 \mathrm{e}^{\phi}\psi_g - c_2(\hat{T}_s - \hat{T}_\infty)\right] - \varepsilon' \mathrm{e}^{\phi} + \varepsilon' \mathrm{e}^{\left[\hat{\mu}_* + \phi + c(\hat{T}_s^{-1} - 1) - \psi_g/(\hat{\sigma}_n - \hat{p}_s)\right]\beta^{-1}} - c_h(\hat{p}_s - \hat{p}_\infty)\right\}
\end{aligned}\right\} \tag{5}$$

where the modified dimensionless terms are $\psi_g = \mathrm{Tan}(\alpha)/a, \hat{\sigma}_n = \rho g h \cos(\alpha)/a$ and other terms are the same as defined in Eq. (5). The dimensionless terms in Eq. (5) are $\psi = \tau/ap_*, \hat{\sigma}_n = \sigma_n/p_*$, $\hat{p}_s = p_s/p_*$, $\hat{p}_\infty = p_\infty/p_*$, $\hat{\mu}_* = \mu_*/a$, $T = tv_*/d_c$, $\hat{v}_0 = v_0/v_*$, $\phi = \ln(v/v_*)$, $\beta = b/a$, $q = Q_b/Q_a$, $c = Q_a(1 - \beta q)/RT_*$,

$\hat{T}_s = T_s/T_*$, $\hat{\theta} = \ln(\theta v_*/d_c)$, $\hat{T}_\infty = T_\infty/T_*$, $k = Kd_c/a$, $v_0 = v_0/v_*$. The dimensionless terms $c_1 = ap_*d_c/2\rho_{total}c_v h_w T_*$ and $c_2 = k_T d_c/\rho c_v v_* h_w^2$ in Eq. (5) signify shear heating and heat conduction effect. Similarly, the other dimensionless terms $\Lambda' = \Lambda T_*/p_*$, $\hat{\varepsilon} = \varepsilon/\beta_c p_*$, $c_h = 2c_w L/v_* h_w^2$ are coefficient of thermal pressurization, dilatancy factor and hydraulic diffusivity, respectively [6]. The above system of governing differential equations is valid under the quasistatic conditions in which until inertia of the sliding mass becomes negligible. Moreover, the role of thin shear zone is neglected since this factor may not be critical in contrast to earthquake fault zone [5]. We have solved Eq. (5) numerically for creep velocity and corresponding change in pore pressure and effective frictional resistance along the sliding interface using the solver *ode23s* of MATLAB®. In addition, unlike earlier numerical simulations in which frictional and thermal properties of the rock slope are varied to investigate their effects on time of failure of the rock slope [5, 6]. In the present investigation the effect of perturbation in initial creep velocity, gravitational stress and pore pressure on time of failure of the rock slope is studied. Frictional and other material properties are considered in the range as reported in the literature. For instance, $(\rho_{total}c_v) = 2.7\,\text{MPa}\,^\circ\text{C}^{-1}$ [13], $(k_T)_{Rock} = 2.4$ Wm $^\circ\text{C}^{-1}$ (Slip and Fujita 1997), compressibility of the pore fluid $\beta_c = 10^{-6}\,\text{Pa}^{-1}$ [14] and coefficient of thermal pressurization $\Lambda = 0.5$ MPa $^\circ\text{C}^{-1}$, viscosity of the fluid $v = 10^{-4}$ Pa s, dilatancy factor $\varepsilon = 10^{-4}$, permeability of the fault core or joint of the rock $\kappa = 10^{-20}$ m^2 [17]. The following mechanical and physical properties of the rock were used in numerical simulation $\psi_g = 55$, $\hat{\mu}_* = 50, d_c = 10^{-2}$ m, $v_* = 10^{-6}\,\text{ms}^{-1}$, $h_w = 0.1$m, $T_\infty = 390$ K, $T_{sint} = 300$K, $p_\infty = 1.3$ MPa, $p_{sint} = 1.0$ MPa, $\beta = 1.2$ and a fixed normal stress $\sigma_n = 1$ MPa.

3 Results and Discussion

3.1 *Effect of Initial Creep Velocity on Time of Failure of the Rock Slope*

First, an initial creep velocity v_{0c} at the sliding interface is varied in the numerical simulations. In field condition, this situation arises due to vehicular motion and tectonic actives nearby the rock slope. Figure 2a demonstrates the effect of velocity perturbation on time of failure of the rock slope. However, the rock interface creeps before it reaches to a critical velocity. Time of failure t_f of the rock slope is defined as the time at which creep velocity changes suddenly [5]. It is evident that t_f decreases with increase in v_{0c}. The corresponding change in temperature and pore pressure at sliding interface is also presented in Fig. 2b. The reason for the present observations is attributed to the frictional shear heating even though magnitude of frictional stress is constant [17, 22]. But due to the increase in creep velocity, the rate of heat generation also increases. This, in turn, causes increase in the pore

pressure at the sliding interface. This results in decrease of effective normal stress and corresponding frictional stress at slip interface also [17, 22]. Thus, this particular study explains the observation that increase in the creep velocity results in decrease in t_f of a rock slope as Fig. 2a. However, no significant change in temperature at slip interface was seen.

3.2 *Effect of Change in Gravitational Stress on Time of Failure of the Rock Slope*

In this particular numerical simulation, the magnitude of gravitational stress is increased while the normal stress remains constant. In practical situations, the magnitude of constant gravitational stress may change because of rainfall, blasting, road cutting activities and seismic effect. Figure 3a presents the effect of change in gravitational effect on t_f of the rock slope and corresponding change in pore pressure at sliding interface in Fig. 3b. It is observed that t_f decreases with increase in the gravitational stress. In this case, pore pressure increases substantially, but the shear resistance and time of failure t_f decrease. In this case also, there is no change in temperature at the sliding interface.

3.3 *Effect of Change in Initial Pore Pressure Time of Failure of the Rock Slope*

The effect of change in initial pore pressure $p_{\sin t}$ is also investigated on t_f. This real-life scenario may arise due to heavy rainfall. Figure 4a, b shows that t_f of the rock slope decreases with increase in initial pore pressure. The reason for this observation is attributed to the decrease in shear resistance at the sliding interface.

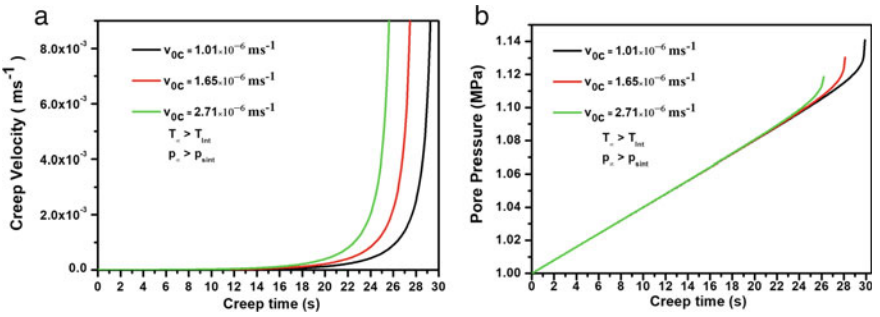

Fig. 2 Effect of initial creep velocity perturbation on creep velocity and pore pressure at the slip interface of the rock slope

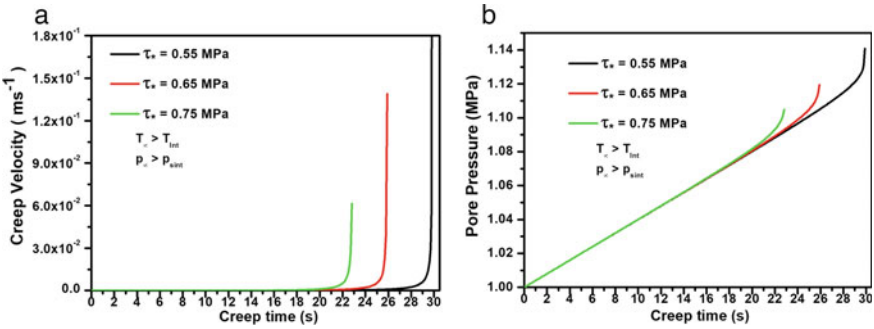

Fig. 3 Effect of initial gravitational stress on creep velocity and pore pressure

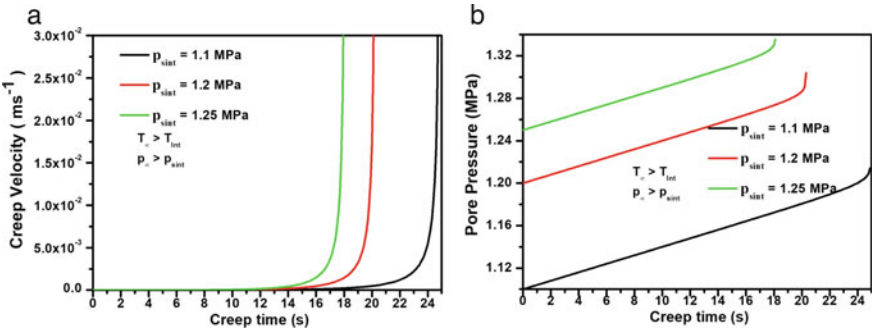

Fig. 4 Effect of initial pore pressure at the slip interface on creep velocity and pore pressure

An interesting conclusion from the above numerical simulations that t_f is almost the same range as 12–30 s due to change in initial creep velocity, gravitational stress and pore pressure. However, the rate of change in creep velocity is more ($\sim$cm/s) in perturbation of the initial gravitational stress than the perturbation in initial creep velocity and pore pressure ($\sim$mm/s). However, the change in t_f is considerable, that is, in range of 15–120 s due to perturbation of initial interface temperature owing to the slow rate of change in creep velocity ($\sim$μm/s).

Finally, it would be interesting to repeat the above study in the presence of inertia to understand the role of temperature and pore pressure in post-failure conditions. Nonetheless, it would also be interesting to validate the present results with practical rock slope failures.

4 Conclusions

The present study investigates numerically the effect of perturbation in initial creep velocity, frictional resistance as well as pore pressure at the sliding interface. It is observed that time of failure of the rock slope decreases with increase in creep velocity, gravitational stress and pore pressure.

Acknowledgements This work is supported by NRDMS-DST (order No. NRDMS//02/43/016 (G)) Government of India.

References

1. Willie DC, Mah CW (2004) Rock slope engineering, 4rd edn. Spon Press
2. Handwerger AL, Rempel AW, Skarbek RM, Roering JJ, Hilley EG (2016) Rate-weakening friction characterizes both slow sliding and catastrophic failure of landslides. Proc Nat Acad Sci 113(37):10281–10286
3. Chau KT (1995) Landslides modeled as bifurcations of creeping slopes with nonlinear friction law. Int J Solids Struct 32(23):3451–3464
4. Singh AK, Kainthola A, Singh TN (2012) Prediction of factor of safety of a slope with an advanced friction model. Int J Rock Mech Min Sci 1997(55):164–167
5. Singh AK, Singh TN (2016) Stability of the rate, state and temperature friction model and its applications. Geophys J Int 205:636–647
6. Sinha N, Singh AK, Singh TN (2019) Dynamic stability of the rate, state, temperature, and pore pressure friction model at a rock interface. Pure Appl Geophys 176(11):4969–4982
7. Eberhardt E, Stead D, Coggan JS (2004) Numerical analysis of initiation and progressive failure in natural rock slopes-the 1991 Randa rockslide. Int J Rock Mech Min Sci 41:69–87
8. Faillettaz J, Sornette D, Funk M (2010) Gravity-driven instabilities: Interplay between state- and velocity-dependent frictional sliding and stress corrosion damage cracking. J Geophys Res 115:B03409. https://doi.org/10.1029/2009JB006512
9. Goren L, Aharonov E (2007) Long runout landslides: the role of frictional heating and hydraulic diffusivity. Geophys Res Lett 34:L07301. https://doi.org/10.1029/2006GL028895
10. Helmstetter A, Sornette D, Grassol J-R, Andersen JV, Gluzman S, Pisarenko V (2004) Slider-block friction model for landslides: application to vaiont and la clapière landslides. J Geophys Res 109:B202409
11. Chester FM, Higgs NG (1992) Multimechanism friction constitutive model for ultrafine quartz gouge at hypocentral conditions. J Geophys Res 97(B2):1859–1870
12. Chester FM (1994) Effects of temperature on friction: constitutive equations and experiments with quartz gauge. J Geophys Res 99(B4):7247–7261
13. Lachenbruch AH (1980) Frictional heating, fluid pressure, and the resistance to fault motion. J Geophys Res 85:6097–6112
14. Lorenzo SD, Loddo M (2010) Effect of frictional heating and thermal advection on pre-seismic sliding: a numerical simulation using a rate-, state- and temperature-dependent friction law. J Geodyn 49:1–13
15. Veveakis E, Vardoulakis I, Di TG (2007) Thermoporomechanics of creeping landslides: the 1963 Vaiont slide, Northern Italy. J Geophys Res 112:F03026
16. Segall P, Rice JR (1995) Dilatancy, compaction and slip instability of a fluid-infiltrated fault. J Geophys Res 100(B11):22155–22171
17. Segall P, Rice JR (2006) Does shear heating of pore fluid contribute to earthquake nucleation? J Geophys Res 111:B09316. https://doi.org/10.1029/2005JB004129

18. Davis RO, Smith NR, Salt G (1990) Pore fluid frictional heating and stability of creeping landslides. Int J Numer Anal Meth Geomech 14:427–443
19. Mase CW, Smith L (1987) Effects of frictional heating on the thermal, hydrologic, and mechanical response of a fault. J Geophys Res 92:6249–6272
20. Ruina AL (1983) Slip instability and state variable friction law. J Geophys Res 88 (B12):10359–10370
21. Marone C (1998) Laboratory derived friction laws and their application to seismic faulting. Ann Rev Earth Planet Sci 26:643–696
22. Rice JR (2006) Heating and weakening of faults during earthquake slip. J Geophys Res 111: B05311. https://doi.org/10.1029/2005JB004006

Investigation on Behaviour of Open-Ended Driven Piles in Different Cohesionless Soils Using Image-Based Measurements

G. Sreelakshmi and M. N. Asha

Abstract Driven piles are the most common types of deep foundation elements installed using impact or vibration hammers to a desired depth of resistance. Hollow driven piles are always preferred since it is suitable for all ground conditions and can be installed at a faster rate with minimal ground disturbances. This paper discusses the prospective of using Geo-PIV image-based technique to investigate the pile soil interaction behaviour in different soil deposits. The plane strain experimental studies are carried out in a steel tank of dimensions 600 mm × 200 mm in plan and 450 mm depth. Half-section hollow aluminium piles modelled using wood's scaling law are used in the experiments. Three different infill mediums such as cohesionless sand, quarry dust and crushed stones at different densities are used, and impact load has been applied to drive the piles. The deformation behaviour at interface region is captured using a high-resolution digital camera that is later analysed through Geo-PIV software. From strain contours obtained through image analysis, it is observed that for piles driven in crushed stones, shear flow of grains around piles is highest, whereas it is lowest for piles driven in sand deposits.

Keywords Cohesionless infills · Engineering strain · Geo-PIV · Shear flow

1 Introduction

During the last 200 years, there has been a large-scale development of infrastructural facilities. Nevertheless, increasing land scarcity and population growth in urban areas forced city to expand in vertical direction in most of the world cities.

G. Sreelakshmi
Department of Civil Engineering (VTU RRC), CMR Institute of Technology, Bengaluru, India
e-mail: sreelakshmi.g@cmrit.ac.in

M. N. Asha (✉)
Department of Civil Engineering, CMR Institute of Technology, Bengaluru, India
e-mail: asha.n@cmrit.ac.in

B. Laishram and A. Tawalare (eds.), *Recent Advancements in Civil Engineering*, Lecture Notes in Civil Engineering 172,
https://doi.org/10.1007/978-981-16-4396-5_48

So, pile foundations are economical foundations for these structures. Among the different types of pile foundations, open-ended driven piles are preferred as efficient deep foundation system as they have reliable source of load transferring mechanism with shorter construction period, reduced vibrations, and lesser costs for large-scale piling projects. Open-ended driven hollow piles being slender in section also offer lesser driving resistance and develop soil plug that increases skin friction capacity of piles. Due to complex nature of pile soil interaction, a detailed investigation needs to be carried out to assess the possible behaviour of driven piles. So, the following section summarises literatures related to open-ended piles for different infills, installation and loading stages.

2 Literature Review

The behaviour of driven piles in different types of cohesion less soil has always been a matter of research. Effect of soil parameters, pile properties, and various methods of hollow pile have been studied by many researchers [1–4]. But these research works were not able to offer detailed understanding of the soil behaviour during and after pile installation. Recent years have seen several advancements in the field of X-ray CT scanner, stereo-photogrammetric techniques, digital image correlation techniques (DIC), etc. From this particle image velocimetry (PIV) emerged as a versatile tool which is used to measure strain conditions in model studies carried out in different fields of Civil Engineering. Originally developed by [5], Geo-PIV is a MATLAB-based module which is developed on the principles of particle image velocimetry (PIV) which operates by tracking the texture (i.e. the spatial variation of brightness) within an image of soil through a series of images. Reference [6] adopted PIV technique to investigate the behaviour of movement of soil around jacked pile and concluded that there is a reduction in infill volume at pile tip. Reference [7] carried experimental studies using a half-caisson model to observe the soil deformation due to suction in layered sand-silt soil and concluded that upward deformation of the silt layer occurred due to volumetric expansion. Reference [8] studied the movement of clay during pile installation using PIV technique and concluded that this technique can be used to evaluate the impact of disturbance due to pile installation on surrounding structures. Reference [9] presented results of cone penetration tests in a half-circular chamber with three silica sands of different gradation and stated that crushing occurred below and around the cone tip for all test conditions. Reference [10] investigated the behaviour of hollow and solid piles of different length to diameter ratio under axial compressive loading and concluded that surface heave developed is more in the case of hollow piles than solid piles due to lesser mass density. Reference [11] investigated the effect of pile location on the stabilized slope and analysed failure behaviour along upslope/downslope. From the literature, it can be concluded that physical modelling has established its wider scope in diverse geotechnical situations

and image analysis emerged as an efficient tool to capture sub-soil deformations. Based on this, the following objectives have been established for the present paper:

- Develop a laboratory experimental model to investigate pile soil interaction under impact loading
- Study the deformation patterns in soil surrounding the driven piles and at the pile–soil interface using the principles of particle image velocimetry
- Investigate the influence of type of infill on the strain contours developed around the pile.

3 Methodology

Methodology adopted for the present paper can be sequenced as follows:

- Characterization of different materials (infill and pile model)
- Use of scaling laws for modelling pile and chamber
- Modelling of hammer energy for impact loading (impact energy corresponding to SPT)
- Plane strain analysis to study the interaction between pile and soil using Geo-PIV software
- Analyse, interpret, and compare the plugging behaviour of piles driven in different cohesionless medium.

4 Experimental Work

This section describes about materials used, dimensions of model pile and test tank, details of experimental set-up and test procedure adopted for the present study.

4.1 Materials Used

Generally, piles are driven through heterogenous deposits. To simulate field conditions in the present study, three different types of cohesionless soil, i.e., sand, quarry dust and crushed stone, are selected for embedding the piles. The materials selected are locally available and are deposited by pluviation method to achieve uniform density. Three different heights of fall had been used in the present study, viz., 5, 10 and 15 cm. Figure 1 shows the pluviation curves for three infill materials. The initial characterization for the materials is also carried out through laboratory experiments, and physical properties of the infill are listed in Table 1.

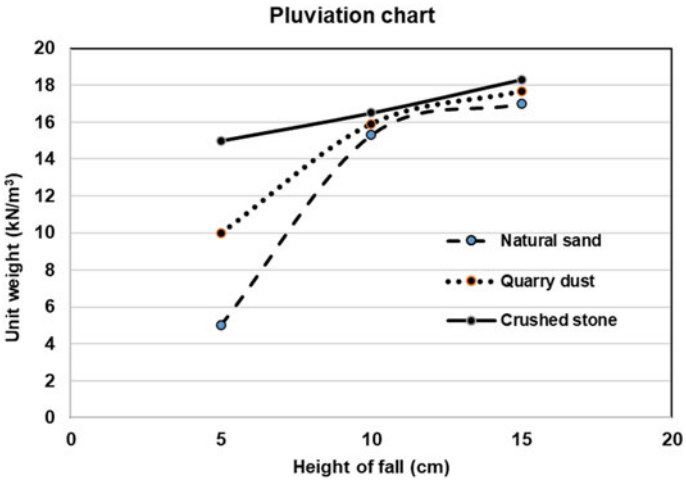

Fig. 1 Pluviation curves for natural sand, quarry dust and crushed stone

Table 1 Physical properties of infill materials

Property	Natural sand	Quarry dust	Crushed stone
Coefficient of uniformity C_u	0.96	10.83	3.6
Coefficient of curvature C_c	0.66	1.02	1.74
Specific gravity G_s Soil classification	2.67	2.78	2.2
Unit weight of soil (kN/m^3), (15 cm), peak friction angle without and with plate	16.5, 43.60°, 18.50°	18.3, 33.10°, 19.05°	15.2, 50.10°, 36.50°

4.2 Model Pile

For modelling pile–soil interaction [12] and to maintain similitude between prototype and model, flexural rigidity has to be scaled [5, 13]. For scaling, the '*n*' factor used in the present study is 10 and accordingly aluminium hollow pipe section with outer diameter 32 mm and inner diameter 31.5 mm (length to diameter ratios of 10) is selected as the model pile with a length scaling factor of 1/10^5. This is used to simulate the prototype pile of 250-mm-diameter solid section made of reinforced concrete with a compressive strength of 20 MPa. Hollow pile of half-section with scaled markings at 1 cm spacing is used for the study. Figure 2 shows the model pile section.

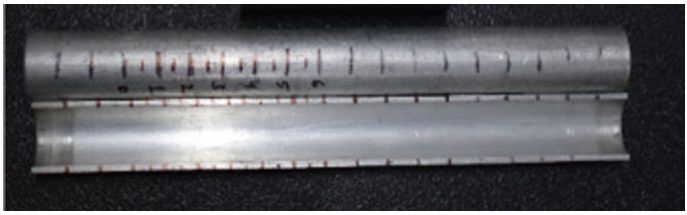

Fig. 2 Hollow pile section

4.3 Test Tank

The dimensions of the tank are selected such that the boundary effects are avoided while testing the model pile under impact loads. Taking zone of influence as 3–8 times the pile diameter [7], steel tank dimensions are fixed as 600 mm × 200 mm in plan and 450 mm depth [14]. To replicate plain strain conditions, vertical partitions are arranged and a window of perspex material with grid markings is placed on the longer face to capture deformation during pile driving.

4.4 Test Setup and Loading Arrangement

To drive the pile by impact load, hammer has been used whose energy corresponds to that of standard penetration test hammer. The modelled hammer has a mass of 760 gm falling from a height of 100 mm for driving the hollow piles, and videos of soil deformations of surrounding the soil are captured with the help of high-resolution digital camera till the end of 45 mm. The image grabber software is adopted to convert videos to compatible image format for a specified number of frames per seconds. This image source forms an input source for GeoPIV software which becomes as input source to Geo-PIV software. Generally, Geo-PIV follows four types of image analysis, viz. control point analysis, leapfrog analysis, Eulerian, and Eulerian velocity mode analysis. In the present work, coupled control and leap frog method of analysis is adopted wherein displacements are evaluated with reference to an initial image while in leapfrog analysis, correlation coefficients are fixed for images sets and if calculated coefficients of images do not match with set values, initial reference image is updated as last image from sequences of images. Geo-PIV later works by determining the difference in variation of spatial brightness between images. Bicubic interpolation method is used to estimate variation in displacement in a patch region in terms of pixel which is converted to X and Y natural coordinate system expressed in millimeter units. Figure 3 shows the working principle of Geo-PIV software.

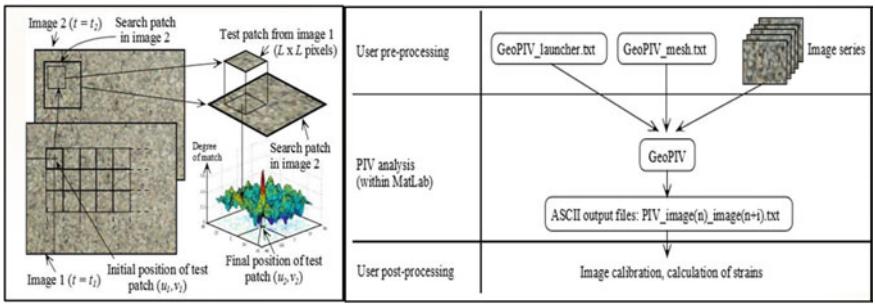

Fig. 3 Working principle of Geo-PIV software

Fig. 4 Test set-up

A total of 24 tests were conducted with sand, quarry dust and crushed stones at two different densities. Figure 4 shows test set-up, and Fig. 5 also shows the still images of pile as well as the different infill as seen through the Perspex window.

5 Results and Discussions

5.1 Variation of Engineering Strain (Shear Strain) for Natural Sand, Quarry Dust and Crushed Stone (2.36 mm – 4.75 mm) for Pluviation Height Fall of 15 cm

To obtain a proper visualization of the engineering strains, a colour scale range strip from blue (minimum value) to red (maximum value) is selected. The strain contours illustrate the formation of shear bands around the penetration zone of the pile

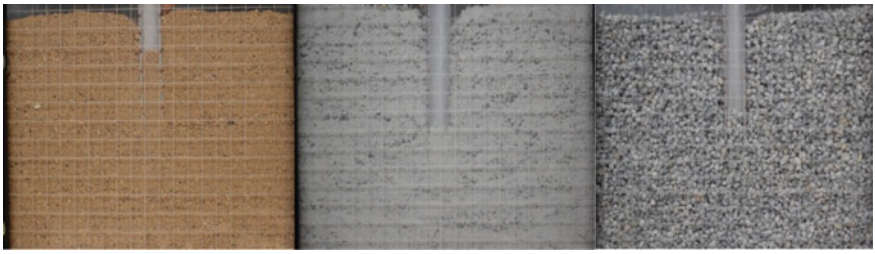

Fig. 5 Still images of grid marked Perspex sheet with infill and pile in background for sand, quarry dust and crushed stone

(Fig. 6). In all cases, depth of pile penetration is maintained the same. It is observed that with increase in density there is a restriction of soil lateral movement which pushes the soil upwards, generating higher penetration resistance and lesser strain zone development in all conditions. But it is also evident that highest strain value is observed when crushed stone is the infill material (approximately in the order of 350% along depth direction). The crushed stone being nonplastic in nature offers least resistance to driving at pile interface. In the case of quarry dust with high density state (18.3 kN/m^3) lowest strain value in the order of 60% has been observed due to cohesive nature imparted by quarry dust particles. Also, zone of influence of strain contours is least in the case of sandy soils (16.5 kN/m^3) than with other infill material since sandy soil offers greater resistance to driving due to denser packing nature.

The shear strain contours are highest for crushed stone and least for sand. The interfacial friction angle along grain size analysis plays a crucial role as far as the strain contours are considered. For crushed stone, though the friction angle is high, the infill is not well graded. Hence, interlocking between the stone grains is poor and hence results in higher shear strains. Quarry dust corresponds to a well graded infill, but the presence of fines reduces its interfacial friction and hence results in higher strains in comparison with sand. This infers that the grain size analysis along with interfacial friction influences the deformation profile around pile–infill interface.

Reference [15] stated that increase in frictional angle affects the formation of influence zone and near pile penetrating zones, strain contours are confined to region of 1.5–2.5 outer diameter of pile in sandy soil. In all the cases, it is found that in all types of infill conditions, shear strains contours developed around the hollow pile shaft in sandy soil is nearer to distance of 2.5 times the outer diameter that agrees with the literature [15]. Furthermore, the behaviour of infill materials is very crucial as it affects the scaling parameters during physical modelling of driven pile interaction problems. According to [16], the strains developed in the fill are dependent upon crushing of infill and for driven piles, the crushing happens within the pile shaft also. In fact, crushed stone has a higher capacity to crush when compared to all other infills used in the experiment and that is captured in this study.

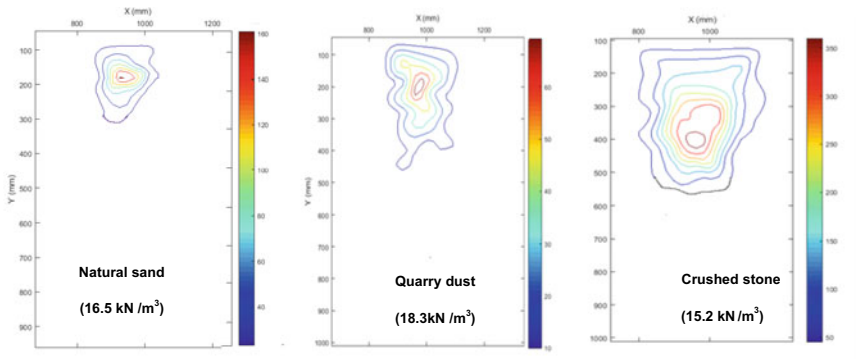

Fig. 6 Engineering shear strain in sand, quarry dust and crushed stone at densities of 16.5, 18.3 and 15.2 kN/m^3

Experimental studies for investigating soil-pile interaction (full scale or prototype modelling) involve high level of instrumentation (Strain gauges, load cells, data analyser and data acquisition system, etc.). Current approach involves prototype modelling by application of Wood's law followed by image analysis wherein interface behaviour can be precisely captured and analysed. This avoids complicated experimentation process and the methodology also permits assessment of movement of soil particles in and around the pile which is impossible otherwise.

6 Conclusions

- GeoPIV has emerged as suitable tool of image analysis in capturing the deformation behaviour of infill while driving an open-ended pile.
- Through strain contours obtained from image analysis, it is observed that with different types of cohesionless soils, there is variation in magnitudes of engineering shear strain contours with increase in density causing lesser displacement of soil around pile soil interface.

7 Scope of Future Study

The study indicates that the shear deformation around pile is dependent upon the grain size as well as interfacial friction of the infill. However, the studies carried out are model tests and are scaled to a laboratory scale. Large-scale model tests enable a better understanding of the crushing phenomenon also which can be considered as a

limitation of the present study and can be studied in the future. In the present study, clayey infills at different water content have not been considered which can be added as a scope for future research. Numerical modelling of driving conditions and comparing the results to model and field measurements can also be considered for future study.

References

1. Paikowsky SG, Whitman RV, Baligh MM (1989) A new look at the phenomenon of offshore pile plugging. Mar Georesour Geotechnol 8(3):213–230
2. Paikowsky SG, Whitman RV (1990) The effects of plugging on pile performance and design. Can Geotech J 27(4):429–440
3. Paik K, Salgado R (2003) Determination of bearing capacity of open-ended piles in sand. J Geotech Geoenviron Eng 129(1):46–57
4. Madhusudan Reddy K, Ayothiraman R (2015) Experimental studies on behavior of single pile under combined uplift and lateral loading. J Geotech Geoenviron Eng 141(7):04015030
5. Stanier SA, Blaber J, Take WA, White DJ (2016) Improved image-based deformation measurement for geotechnical applications. Can Geotech J 53(5):727–739
6. White DJ, Bolton MD (2002) Observing friction fatigue on a jacked pile. Centrifuge and constitutive modelling: two extremes, pp 347–354
7. White DJ (2002) An investigation into the behaviour of pressed-in piles. Doctoral dissertation, University of Cambridge
8. Ni QCCI, Hird CC, Guymer I (2010) Physical modelling of pile penetration in clay using transparent soil and particle image velocimetry. Géotechnique 60(2):121–132
9. Arshad MI, Tehrani FS, Prezzi M, Salgado R (2014) Experimental study of cone penetration in silica sand using digital image correlation. Géotechnique 64(7):551–569
10. Sreelakshmi G, Asha MN, Viswanath D (2018) Investigations on Pile-Soil Interaction Using Image Analysis. PanAm Unsaturated Soils 2017:466–475
11. Lei G, Wu W (2020) Centrifuge study on the effect of pile bending stiffness on the slope stabilised by piles. Int J Phys Modell Geotech 20(4):212–223
12. Wood DM, Crewe A, Taylor C (2002) Shaking table testing of geotechnical models. Int J Phys Modell Geotech 2(1):01–13
13. Reddy RC, Rao GT (2012) Study of soil interaction in a model building frame with plinth beam supported by pile group. Int J Adv Struct Eng 4(1):11
14. Parkin AK, Lunne T (1982) Boundary effects in the laboratory calibration of a cone penetrometer for sand. Norwegian Geotechnical Institute Publication, 138
15. Yang J (2006) Influence zone for end bearing of piles in sand. J Geotech Geoenviron Eng 132 (9):1229–1237
16. Lobo-Guerrero S, Vallejo LE (2007) Influence of pile shape and pile interaction on the crushable behavior of granular materials around driven piles: DEM analyses. Granular Matter 9(3–4):241

Investigation of Gabion Wall Failures and Recommendations

Ganesh Chikute and Ishwar Sonar

Abstract Gabion retaining walls are very much popular in present era, due to its simplicity in construction, high speed of construction, flexible in nature, release of water pressure due to voids in stones of Gabion wall and eco-friendly nature. Though Gabion wall is famous, there are some failures are also observed in Gabion walls. Till date, very less literature works are available on failures of Gabion walls. Failure analysis is a very important tool to identify causes of failures, which is useful in possible modifications in Gabion wall not only to avoid Gabion wall failure, but also avoid loss of human life and cost. This paper represents field investigation of eleven existing Gabion wall sites from Pune district, India. Different types of failures, along with reasons of failures of Gabion walls, are reported in this paper. Remedies to avoid such failures are also suggested to modify Gabion wall. Author[1] is doing research on modification of Gabion of wall is also explained.

Keywords Field investigation · Failures · Gabion wall · Modification

1 Introduction

In the Gabion wall as shown in Fig. 1, to form a shape of retaining wall, stones are filled in the mesh boxes which are prepared with a zinc and/or PVC-coated wires of varying diameters from 2.2 mm to 3.4 mm which are tied together forming a modern kind of retaining wall. The box sizes are in multiples of 0.5 m and the opening mesh sizes are of 60 × 80 mm, 80 × 100 mm and 100 × 120 mm [1]. The steel wire Gabion boxes and mattresses are factory-fabricated boxes manufactured using mechanically woven double twisted hexagonal-shaped wire meshes. Mechanically woven double twisted wire meshes are non-ravelling, manufactured by twisting continuous pairs of wires through three one-half turns (commonly

G. Chikute (✉) · I. Sonar
Government College of Engineering Pune (COEP), Pune, Maharashtra, India
e-mail: ips.civil@coep.ac.in

B. Laishram and A. Tawalare (eds.), *Recent Advancements in Civil Engineering*, Lecture Notes in Civil Engineering 172,
https://doi.org/10.1007/978-981-16-4396-5_49

called double twisted) to form hexagonal-shaped mesh openings which are then interconnected to adjacent wires to form hexagonal meshes. The edges of the mesh are toughened with a thicker wire called the selvedge/edge wire. Details of Gabion wall are given in IS 16014-2012 [2] and ASTM A975-2016 [3]. MoRTH means Ministry of Road Transport and Highway. It is explained in reference [4].

A wide range of Gabion wall applications are already reported by number of researchers including energy dissipation Gabion-stepped weir [5], Gabion-stepped weirs [6], stream bank stabilization [7], landfill embankment for dumping site [8], acoustic performance [9], flood protection work [10], Gabion mattress for canal erosion prevention, earth retaining structure, [11].

The reported case histories and the studies on the field performance have highlighted the failures of advanced retaining walls like MSE, geo-textile walls, etc., due to its poor performance, defects, failures [12–18]. Kenneth et al. has reported the need for strict quality control during construction to avoid financial and human loss through a case study of structural failure during construction and stressed [19]. Limited literature is available which reports the failure of Gabion wall. Edward et al. reported the use of poor quality of backfill soil and flood situation is responsible for instability of Gabion wall through the geotechnical investigation.

In the present investigation, to know the current status of existing Gabion walls and modifications required in further similar constructions, a rigour field

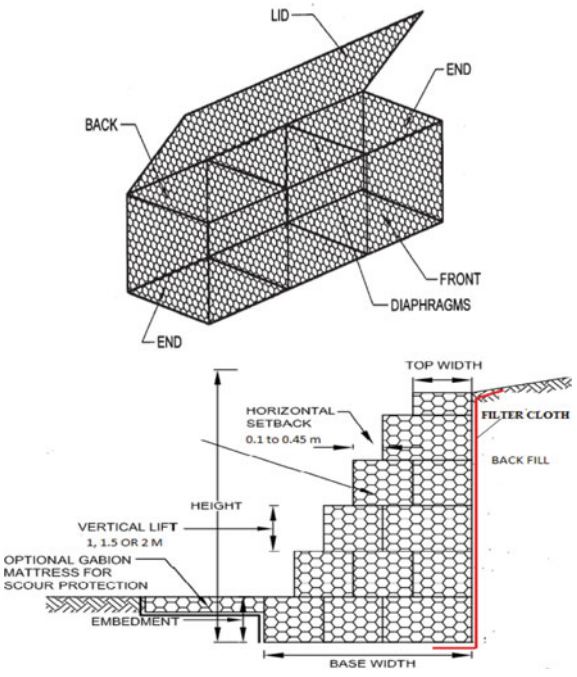

Fig. 1 Gabion box and Gabion wall cross section

Table 1 Investigation site list and its details

Site no	Address	Wall height (m)	Wall base width (m)	Location
1	Reliance petrol pump compound wall, Mumbai-Pune expressway	8	7	Earth fill
2	Side of Bhugaon Lake	4	4	Earth fill
3	Lavasa city Ghat-1, Lavasa	3	3	Hill slope
4	Lavasa city Ghat-2, Lavasa	2	2	Hill slope
5	Lavasa city Ghat-3, Lavasa	4	4	Hill slope
6	Temghar Dam Ghat, Lavasa road	3	3	Hill slope
7	Mutha Village, Lavasa road	3	3	Hill slope
8	Dr. B. R. Ambedkar Bridge Sangvi, PCMC	8	7	River side
9	Old Bridge at Narsinha School, Sagnvi, Pune	7	7	River side
10	Dolphin school Madhuban Sagnvi, Pune	7	7	River side
11	Someshwarwadi, Pune	3	3	River side

investigation is carried out. It is observed that number of Gabion walls is on the verge of failure and many of them are reporting deviation in its performance. The data obtained are from the part of Deccan Traps having a huge igneous province has average mountainous topography with average rainfall from Pune district. The field investigation is reported with a view to showcase the cause of failure of Gabion walls and to find remedial measures to avoid further such causes.

The observations related to various failures cases of Gabion walls reported in this paper will provide a basis for further detailed case study and possible modifications in the Gabion walls.

Eleven sites from the locality were selected and inspected to identify present performance. The study reports the defects and failures with probable reasons for their occurrence based on data obtained during investigation. The failures may be avoided for such type of walls for which the suggestions are also mentioned at the end.

2 Field Investigation

List of sites considered for investigation [20] is given in Table 1.

In field investigation of these 11 existing sites, following defects are observed, which are classified as cracks in backfill, erosion of soft stone, erosion of foundation soil, corrosion of mesh and bulging of the wall. Percentage-wise failures are shown in Fig. 2 and Table 2. Some of actual photographs are also shown in Fig. 3.

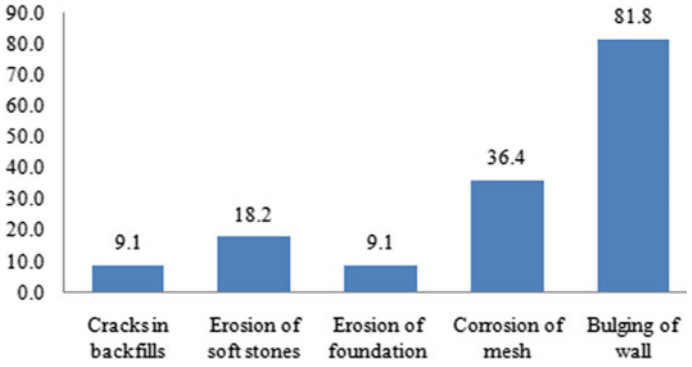

Fig. 2 Percentage- different type of failures

Table 2 Failure summary of all sites

Defects / Site no	Cracks in backfills	Erosion of soft stones	Erosion of foundation soil	Corrosion of mesh	Bulging of wall
1					*
2	*				*
3			*		
4					*
5		*			
6					*
7					*
8				*	*
9				*	*
10				*	*
11		*		*	*
Total	1	2	1	4	9
% Failure	**9.1**	**18.2**	**9.1**	**36.4**	**81.8**

2.1 Design Verification

Cross sections of wall used at above existing sites are verified by using software GEO5 [21]. Various checks like overturning, sliding and base pressure check are evaluated for above walls by using GEO5 software. The results of design verifications are summarized in Table 3.

Table 3 contains details of all required stability checks for the retaining wall. As per Table 3 values, all stabilitychecks of walls are well within the range (hence says Satisfy).

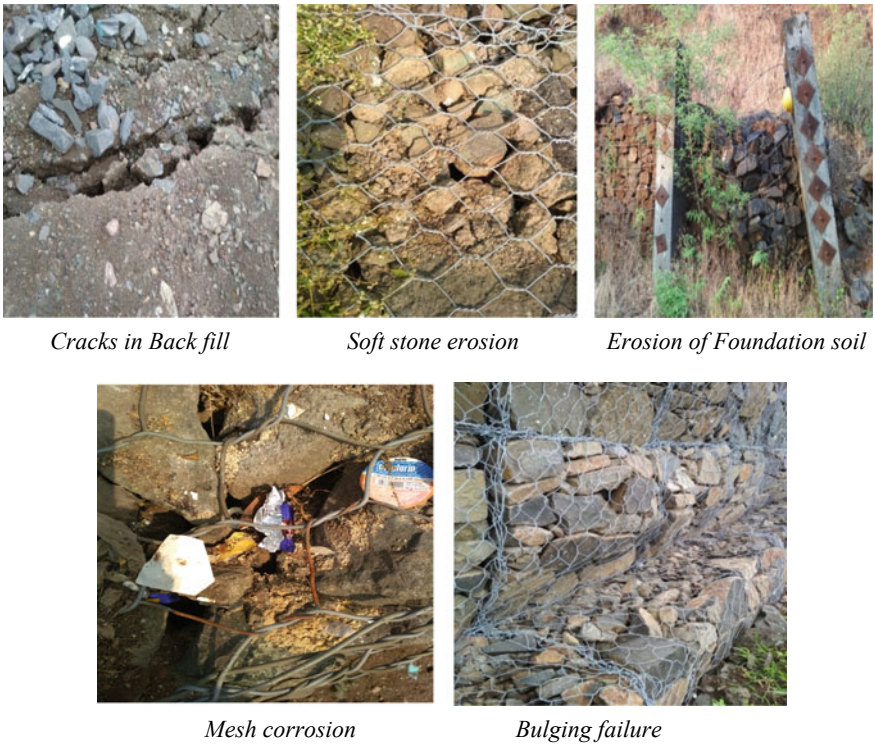

Fig. 3 Actual site photographs of different type of failure

Though there is no any design issue with these existing Gabion walls, still there failures are observed. These failures are mainly due to improper stone used, improper workmanship, improper construction procedure, etc. Reasons of failure and effects [20] of sites are summarized in Table 4.

2.2 Failure Reasons and Effects

2.3 Modification Recommended to Avoid Above Failures Are as Follows

2.3.1 Cracks in Backfill

Expansion on wetting means, black cotton soil expand on wetting (absorption of water) and contraction (shrinkage) on drying means drying (Evaporation of absorbed water). This will reduce the effect of adjustment of backfill pressure on the wall.

Table 3 Design checks verification of existing Gabion sites

Site no	Base width (m)	Height (m)	Overturning check		Sliding check		Base pressure check	
			Value (kNm)	FOS	Value (kN)	FOS	Value (Kn/m^2)	FOS
1	7	8	3514 > 486	7.24 > 1.5 OK	571 > 185	3.09 > 1.5 OK	305 > 202	1.52 > 1.5 OK
2	4	4	547 > 49.7	11.01 > 1.5 OK	178 > 36.1	4.92 > 1.5 OK	150 > 92.6	1.62 > 1.5 OK
3	3	3	224.6 > 19	11.8 > 1.5 OK	105.4 > 18.6	5.66 > 1.5 OK	150 > 69.4	2.16 > 1.5 OK
4	2	2	65.2 > 5.2	12.5 > 1.5 OK	52.4 > 7.8	6.7 > 1.5 OK	100 > 46.8	2.14 > 1.5 OK
5	4	4	54.9 > 5.0	11.05 > 1.5 OK	179 > 36.1	4.94 > 1.5 OK	150 > 93	1.60 > 1.5 OK
6	3	3	153 > 19	8.07 > 1.5 OK	85.9 > 18.6	4.61 > 1.5 OK	150 > 74.46	2.01 > 1.5 OK
7	3	3	154 > 19	8.10 > 1.5 OK	86.2 > 18.6	4.63 > 1.5 OK	130 > 75	1.73 > 1.5 OK
8	7	8	3028 > 477	6.35 > 1.5 OK	528 > 183	2.88 > 1.5 OK	305 > 202	1.5 = 1.5 OK
9	7	7	3059 > 322	9.5 > 1.5 OK	509 > 193	3.66 > 1.5 OK	250 > 166	1.51 > 1.5 OK
10	7	7	2242 > 312	7.18 > 1.5 OK	433 > 136	3.19 > 1.5 OK	250 > 165	2.50 > 1.5 OK
11	3	3	152 > 21	8.14 > 1.5 OK	88.1 > 19.6	4.73 > 1.5 OK	130 > 78	1.80 > 1.5 OK

Table 4 Failure reasons and effects

Failure type	% failure	Possible reasons	Effects
Cracks in backfill	9.1	Type of backfill	Expansion and contraction of soil on the wetting–drying process especially of back cotton soil, causes cracks in backfill as well as alteration of earth pressure on the wall
		Rainfall and drainage	Improper rain water drainage arrangement leads to cracks in backfill
		Improper backfilling	Filling of improper backfill material without proper layer and compaction
Erosion of stone	18.2	Soft/weathering prone stone	Soft stone crushed easily due to applied load and weathering effect, leads to bulging
Erosion of foundation soil	9.1	Heavy rainfall and no protection to the foundation	If location of wall is in mountainous and heavy rainfall area or even near a flowing stream, constructed without foundation protecting blanket, soil will be washed out from under foundation leading to the collapse of the wall
		Foundation depth	If proper foundation depth is not provided especially wall is located in rainfall and mountainous area or near flowing stream, there is more possibility of wall collapse
Corrosion	36.4	Sharp edges of a stone	Sharp edges of stone may cut Gabion mesh wire. Weathering action and presence of water corrode such cut mesh wire leads to the breaking of wires. Splitting of stones from such opening may cause a collapse of the wall
		Placing direction of the stone	Sharp edge of the stone may cut the mesh wire, if it is not kept parallel to mesh wire
Bulging	81.8	Improper Packing	This happens due to the use of single size stones and poor workmanship leads to more voids
		Irregular shape of the stone	Bulging may be caused due to more voids leading to rearrangement of stones On the outer side of the Gabion box, if the inclined faced stones are used, it gets slipped under loading causing bulging
		Size of stone	If smaller size stones may bulge more than stones with all size
		Soft stone	Uniform strong stones may not available. If such soft stones are used at middle or bottom wall, leads to bulging

Backfill should be placed in layers and well compacted. Appropriate drainage planning for percolated water in backfill should be done.

2.3.2 Erosion of Soft Stone

Strength and weathering action tests should be carried out on the stones which are to be used as filler in Gabion. Pre-tested block made from recycled concrete [22] will be better alternative to non-uniform and soft stones used in Gabion.

2.3.3 Erosion of Foundation Soil

Wall should have proper foundation depth. A concrete blocks/stone blanket on the toe side should be provided to avoid soil erosion from foundation generally during heavy rainfall and mountainous region.

2.3.4 Corrosion of Wire

Proper placing of stones cutting wires and succession corrosion of Gabion mesh get reduced. Selection of Proper Gabion mesh as per mentioned in IS CODE 16014, rather than just available in the market and its type should be selected from design requirement. Using pre-tested concrete blocks, the possibility of cutting wires and succession corrosion of Gabion mesh get reduced. Stress concentration will be reduced on wire mesh.

2.3.5 Bulging of Wall

Void in stones used in Gabion box should be minimum, for that, all in size stones should be used rather than use of single size stone, which minimizes the voids and increases the self-weight of Gabion, leads to the possible reduction in wall cross section and control bulging of wall. Concrete block may be used to replace the stone. Concrete blocks produced from construction demolition waste [22] may prove effective and eco-friendly.

3 Other Observations

Gabion wall is gravity type of retaining wall. It resists lateral backfill load by its self-weight and hence cross section area required for Gabion wall is much higher, i.e. it is 3–5 times than other type of retaining wall, such space may not be available at site.

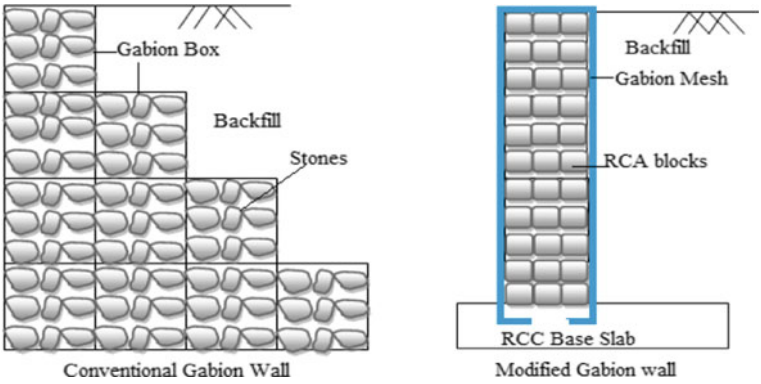

Fig. 4 Conventional and modified Gabion wall

Steel mesh used in Gabion wall has high tensile strength 550 MPa [23]. Such high tensile mesh is just used for holding stones in proper position. Very small tensile strength of Gabion mesh is utilized in conventional Gabion wall system, hence if designing of Gabion wall changes from gravity to cantilever, it utilizes the at most tensile capacity and reduced the cross section of wall also, which results in much more economical Gabion structure. Author is doing research on modification of Gabion, which is shown in Fig. 4.

Modified Gabion wall has 45% less cross section area than conventional Gabion wall. Maximum deflection is observed in modified Gabion wall of 5.24 mm and maximum tensile stress in wire mesh of about 60 MPa against its capacity of 550 Mpa. Above observed results show that modification in Gabion wall reduces the required cross section of wall and makes it more stable and more economical also.

4 Conclusions

Observed failures of Gabion wall from site investigation are, budging, corrosion, erosion of filled stone, backfill crack and foundation erosion. Bulging (82%) and corrosion (36%) are failures observed at most of the sites. In most cases, it is observed that the improper stones and improper stone filling in Gabion box result in failure. Cross section adopted at these sites passes all required design checks, meaning that there is no any issue of design with failure of these walls. These failures are mainly due to improper stone used, improper workmanship and improper construction procedure.

Alternative materials like concrete block on place of irregular, improper-shaped stone are one of the solutions to most of above failures. Material like recycled blocks will prove to be cost-effective and eco-friendly solution alternatives. Use of

proper backfill material, in layer with compaction will avoid cracks in backfill and alteration of earth pressure on wall. Making Gabion wall partial cantilever will reduce the required cross section area of Gabion wall, and ultimately, cost effectiveness with proper stability will be achieved.

Acknowledgements I express my sincere thanks to my Ph.D. Guide Dr. Ishwar Sonar, Ass. Professor, Government College of Engineering Pune, for his continuous support and motivation.

References

1. Product data sheet of Metal Gabion of Garware-Wall Ropes Ltd. Geosynthetics Division
2. IS 16014-2012-Indian standard code 'IS 16014-2012-Indian standard code, Mechanically woven, double-twisted, hexagonal wire mesh gabions, revet mattresses and rock fall netting (galvanized steel wire or galvanized steel wire with pvc coating) specification
3. ASTM A975-2016 American Standard, Specification for double twisted hexagonal mesh Gabions
4. MoRTH 5TH revision 3100-Ministry of Road Transport and Highways (MoRTH), 3100, Specifications for road and bridge works, 5th revision, IRC, 2013 New Delhi
5. Wüthrich D, Chanson H (2014) Hydraulics, air entrainment, and energy dissipation on a gabion stepped weir. J Hydraul Eng 140(9):04014046
6. Chinnarasri C, Donjadee S, Israngkura U (2008) Hydraulic characteristics of gabion-stepped weirs. J Hydraul Eng 134(8):1147–1152
7. Brunet G, Shuey R (2005) Stream bank stabilization with vegetated gabion. Intervale Country Club Golf Course Manchester, New Hampshire
8. Vashi JM, Desai RMD, Desai AK, Solanki CH (2011) Gabion GRS wall for raising solid waste dump site at Surat- case study. In: Proceedings of Indian geotechnical conference, Kochi paper no.Q-217. Indian Geotechnical Society
9. Koussa F, Defrance J, Jean P, Blanc-Benon P (2012) Acoustic performance of gabions noise barriers: numerical and experimental approaches. Appl Acous 74:189–197
10. Jayswal AR, Malekwala FS, Rautela C (2014) Flood protection work by Terramesh wall. Int J Sci Res Dev 2(01):2321–2613
11. Toprak B, Sevim O, Kalkan I (2016) Gabion walls & their use. Int J Adv Mech Civ Eng 3(4)
12. Wu JY, Chou NN (2013) Forensic studies of geosynthetic reinforced structure failures. J Perform Constr Facil ASCE 27(5):604–613
13. Leonards GA, Frost JD, Bray JD (1994) Collapse of geogrid-reinforced retaining structure. J Perform Constr Facil ASCE 8(4):274–292
14. Feng SJ, Lu SF (2016) Failure of a retaining structure in a metro station excavation in Nanchang City China. J Perform Constr Facil ASCE 30(4)
15. Benjamim CVS, Bueno BS, Zornberg JG (2007) Field monitoring evaluation of geotextile-reinforced soil-retaining walls. Geosynth Int 14(2):100–118. https://doi.org/10.1680/gein.2007.14.2.100
16. Portelinha FHM, Bueno BS, Zornberg JG (2012) Performance of geotextile reinforced soil wall in unsaturated poorly draining backfill soil conditions. In: 5th European geosynthetics congress, Valencia 5, pp 455–465. http://www.eurogeo5.org/
17. Portelinha FHM, de Souza Bueno B, Zornberg JG, Pimentel V (2012) Field performance of steep walls of nonwoven and woven geotextiles reinforcing poorly draining soils. In: Second pan American geosynthetics conference, Lima, Peru, pp 136–144
18. Huang CC, Luo WM (2010) Behavior of cantilever and geosynthetic-reinforced walls on deformable foundations. Geotext Geomembr 28:448–459

19. Carper KL (1987) Structural failures during construction. J Perform Constr Facil ASCE 1(3): 132–144
20. Chikute G, Sonar I (2019) Failures of Gabion Walls. Int J Innov Technol Explor Eng (IJITEE) 8(11):2278–3075
21. GEO5 software
22. Chikute GC, Sonar IP (2018) Techno-economical analysis of recycled masonry block for eco-friendly and economical construction. In: ASCE India conference 2017, IIT Delhi, India
23. IS Code 280-Indian standard code, CODE 280-2006, Steel wire for general engineering purposes

Determination of Resilient Modulus of Layered Bio-stabilized Soil

V. Divya and M. N. Asha

Abstract Expansive soils exhibit high swelling and shrinkage characteristics due to which they are unsuitable for many Civil Engineering applications. Many conventional methods of stabilization have been practiced on such problematic soils by researchers in the past. Lately, bio-stabilization is a technique which is gaining importance in the field of ground improvement due to sustainability and its eco-friendly nature. In the design and construction of any infrastructure, the load application is considered to have significant impact only within the zone bounded by isobar. In the present work, it is proposed to quantify the zone of influence of enzyme blended black cotton soil with respect to wheel load application on pavements. Laboratory tests were performed on oven dried black cotton soil for the determination of its index and engineering properties. CBR (California Bearing Ratio) value is commonly used for the design of pavements in Indian conditions wherein enzyme blended soil is prepared in three lifts. The mechanical behavior of enzyme blended expansive soil of different thickness was studied through the evaluation of its resilient modulus on the basis of bearing ratio values. It is also proposed to suggest an optimum thickness of enzyme blended soil, which would be effective in withstanding the applied wheel load, thereby enhancing economic pavement constructions. In order to have a comparative study and effective assessment, the experiments were conducted for varying dosages and curing periods. It was observed from the experimental studies that enzyme treatment is effective in improving modulus of bio-stabilized black cotton soil. Further, a reduction in pavement thickness was also observed as a result of enzyme treatment and curing effect.

Keywords Black cotton soil · Terrazyme · Resilient modulus · CBR value

V. Divya (✉)
Department of Civil Engineering (VTU RRC), CMR Institute of Technology, Bengaluru, India
e-mail: divya.v@cmrit.ac.in

M. N. Asha
Department of Civil Engineering, CMR Institute of Technology, Bengaluru, India
e-mail: asha.n@cmrit.ac.in

B. Laishram and A. Tawalare (eds.), *Recent Advancements in Civil Engineering*, Lecture Notes in Civil Engineering 172,
https://doi.org/10.1007/978-981-16-4396-5_50

1 Introduction

Black cotton soils are found across the world in many countries such as India, Africa, France, Australia and so on. In India, the black cotton (BC) soil is spread over large regions of the Deccan Plateau such as Gujarat, Maharashtra, Karnataka and Madhya Pradesh. Although these soil deposits respond well to irrigation, the infrastructures constructed on BC soil have been subjected to damages, failures and repair or maintenance works. Hence, such problematic soil deposits are sidestepped in most of the engineering projects. The major shortfall of these soils from engineering aspect is that they exhibit high swelling and compressibility characteristics. This weakness exists in black cotton soils due to the change in basic mineralogical composition viz., presence of montmorillonite clay. As a result of this short coming, the soil loses its bearing capacity when it comes in contact with moisture. The prevailing abnormal characteristics of BC soil make it very difficult to be a good foundation material. Hence, special treatment methods need to be adopted to render the problematic soil feasible for engineering projects.

Reference [1] conducted experimental studies to improve the geotechnical properties of black cotton soil using waste materials such as river sand, fly ash and marble dust. They concluded that due to stabilization BC soil is converted mix of higher strength properties and thereby contributes to substantial reduction in the construction cost. Hence, it can be successfully applied to various construction fields. An improvement in mechanical properties such as compaction parameters and California Bearing Ratio (CBR) of BC soil using slag and glass fibers was studied by [2]. They observed that CBR value increases with increasing length of glass fibers. Reference [3] explored the change in characteristics of BC soil using cement waste dust and lime as stabilizing agents. They reported substantial increase in plasticity index and unconfined compressive strength (UCS) of cement dust-treated BC soil when compared with the effect of lime. Reference [4] carried out a literature survey to understand the potential of using solid waste material for improving the characteristics of weak soil. They inferred from their investigation that admixtures such as rice husk ash (RHA), cement or lime are effective in improving the swelling behavior of expansive soils. The influence of curing conditions on strength parameters of lime-treated expansive soil was evaluated by [5]. Their results revealed that UCS increased with different magnitude for all the curing environments considered for the stabilized soil. Reference [6] investigated the variation in engineering properties of expansive soil treated with Ground Granulated Blast Furnace Slag (GGBS) and summarized that results were substantially pronounced at an optimum percentage of GGBS beyond which the changes were relatively less.

Stabilization using environment friendly agents such as bio-enzymes have also been explored by few researchers in recent years. Reference [7] studied the effect of swelling properties of BC soil on treatment with Terrazyme. Their studies revealed that a reduction in swelling characteristics was observed in enzyme treated soil as a result of change in structure from flocculated state to a dispersed state on dry side of

optimum. Reference [8] explored the effect of curing periods on bio-modified lateritic and BC soil. Based on their results, it was comprehended that Terrazyme was relatively more effective in improving the mechanical properties of BC soil when compared with laterite soil especially at lower enzyme dosages.

In the present work, the potential of improving the strength parameters of enzyme modified BC soil is explored. Presently, the BC soil is treated with bio-enzyme in three lifts and the variation in strength characteristics in terms of resilient modulus is evaluated and results compared. Based on the results, the suitability of layered bio-stabilization for subgrade construction is evaluated for pavements built on BC soil. The current work may also project sustainable and cost-effective solution for flexible pavement construction on weaker soils.

2 Materials and Methodology

2.1 Methodology

The black cotton soil is collected from field, pulverized and laboratory tests are conducted for its physical and engineering characterization. The enzyme dosages to be used in the study and the curing periods to be taken is fixed based on literature [9]. The BC soil is prepared in three lifts and enzyme treatment is simultaneously carried out on each of the lifts. The variation in CBR values of layered enzyme treatment is studied and results are compared. The suitability of layered bio-stabilization on BC soil is predicted based on resilient modulus and hence an optimum thickness of bio-stabilized soil is suggested for application in the field.

2.2 Material Characterization

The BC soil used in the current study was obtained from Chitra Durga district of Karnataka state. The soil was gray to black in color and possessed a specific gravity of 2.63. The plasticity index was found to be 33% and was hence classified as CH as per [10]. The natural BC soil attained maximum dry density of 1.5 g/cc at an optimum moisture content of 16.25%. The significant strength parameters of unconfined compressive strength and CBR values were found to be 151.14 kPa and 4.6%, respectively.

The enzyme used in this study, Terrazyme, was obtained from a commercial vendor. The enzyme was in liquid state and had specific gravity same as that of water. It possessed a smell of molasses and had a non-toxic behavior. The pH value of Terrazyme was of the order of 4.3–4.6. The enzyme dosages taken for the current study were 100 and 200 ml/m^3, respectively. The dosages were obtained by volume proportioning and was subjected to a curing period of 7 and 28 days. Figure 1 represents the variation in moisture density relationship for Terrazyme blended soil.

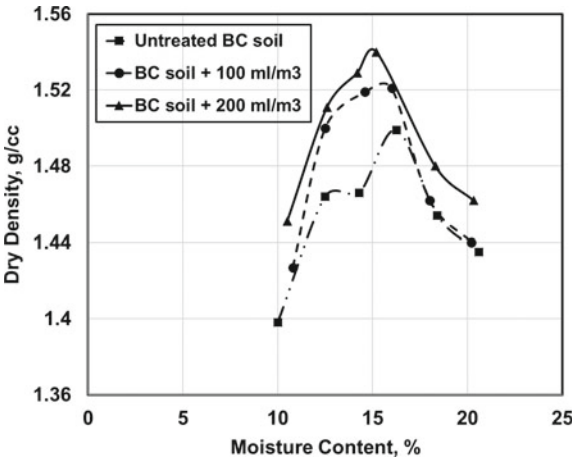

Fig. 1 Moisture–density relationship for treated and untreated BC soil

3 Laboratory Studies

The experimental studies performed in the present work are explained in the following session. The effect of bio-stabilization on BC soil prepared in different thicknesses are compared with respect to the bearing ratio values.

3.1 Effect of Layer Thickness on Bearing Ratio

The conventional method of flexible pavement design depends largely on bearing ratio value as per [11]. The California Bearing Ratio (CBR) indicates the subgrade strength of stabilized or unstabilized pavement. The variations in CBR as a result of bio-stabilization on layered BC soil has been interpreted in this session. The three different test conditions taken for the determination of CBR in this work, as indicated in Fig. 2, are as follows:

(a) Untreated BC soil divided into three lifts (of 50 mm thickness) with the enzyme dosage blended to the top most layer.
(b) Terrazyme was treated to the top two layers of soil (100 mm thickness).
(c) The entire BC soil was treated uniformly with enzyme (150 mm thickness).

The bearing ratio test was conducted on all the above three conditions after subjecting to curing periods of 7 and 28 days.

Figure 3 represents the variation in CBR as a result of layered treatment of bio-enzyme in BC soil. It can be interpreted from the results that increasing dosage and curing period plays a significant role in bio-stabilization process. Apart from these two parameters, the effect of depth of stabilized soil was also studied. It was observed that with respect to untreated soil, the maximum percentage improvement

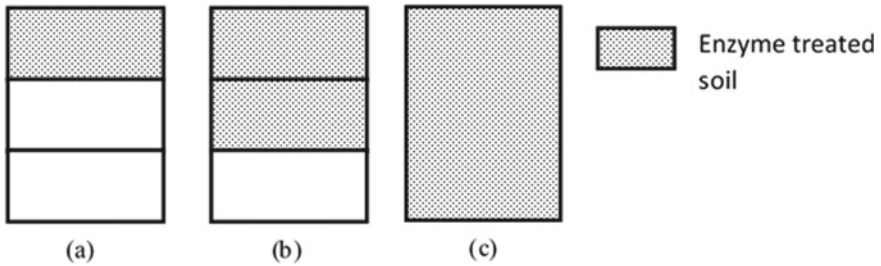

Fig. 2 Pictorial representation of BC soil treated with enzyme in **a** one, **b** two and **c** three layers

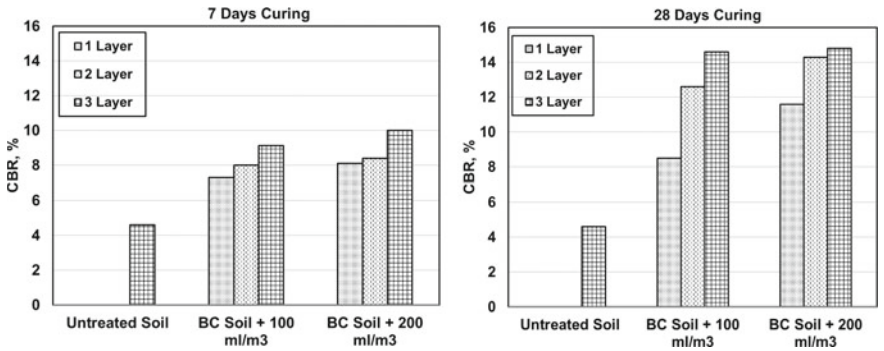

Fig. 3 Variation in CBR with curing period

in CBR is observed for a stabilized mix of 150 mm thickness (Fig. 2c) and the percentage improvement even gets doubled on 28 days curing period. The percentage increase in CBR for 100-mm-thick stabilized soil (Fig. 2b) and 150-mm-thick stabilized soil (Fig. 2c) thickness was marginal as observed in Fig. 3 (28 days Curing). This infers that for construction of any pavement, it is not necessary to mix the entire formation depth with the enzyme, instead 2/3 of the depth only needs to be stabilized. However, the result needs to be verified for different types of soil.

3.2 Variation in Resilient Modulus

The resilient modulus is a fundamental input parameter used in the conventional design of pavements. It indicates the elastic behavior of unbound pavement materials under the action of wheel loads. In this study, resilient modulus (M_R) of subgrade BC soil is determined from the co-relation [11] as:

$$M_R = 17.6 * \mathrm{CBR}^{0.64} \text{for CBR} > 5\%$$

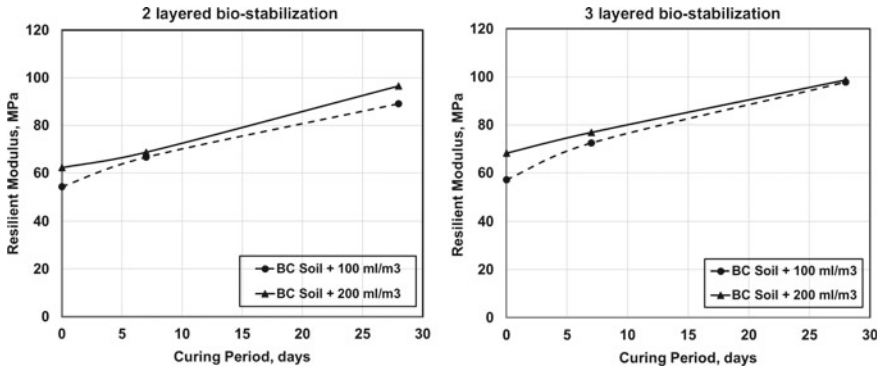

Fig. 4 Variation in resilient modulus for layered bio-stabilization with curing period

Figure 4 represents the variation in resilient modulus for two layered and three-layered treatment of BC soil with Terrazyme. The resilient modulus for the natural BC soil was obtained as 46.54 MPa. On comparison it was observed that the increase in resilient modulus for conditions (b) and (c) as presented in Fig. 2 with respect to plain BC soil was in the order of 43–65% on 7 days and up to 112% on 28 days curing period. The differential in percentage variation of resilient modulus between conditions (b) and (c) was 3% on 7 days and up to 9% on 28 days curing period. It can be summarized that the disparity in percentage difference for both the cases are nearly the same and hence two-layered stabilized soil (Fig. 2b) can be taken as the optimum thickness of Terrazyme blended soil for practical applications. The results also emphasize economic benefits in pavement construction as the depth of the soil to be treated reduces substantially.

3.3 Determination of Pavement Thickness

As per [11] the thickness of pavement has been determined based on the CBR value of the treated and untreated BC soil. The pavement is assumed to be a three-layer elastic structure having bituminous surfacing, granular base and subbase and subgrade. The traffic conditions assumed in the analysis are 10, 30 and 50 msa, respectively, and curing period taken is 28 days. As BC soil with two layered bio-stabilization has been identified as the optimum thickness, the overall pavement thickness has been calculated for the same condition.

Figure 5 represents the overall pavement thickness estimated for optimum layer of subgrade on 28 days of curing period. It was observed that thickness of pavement required for sustaining wheel load decreases in the range of 21–23% with enzyme treatment. It is evident from Fig. 5 that after the initial stage of Terrazyme application, the increase in dosage does not cause pronounced changes in pavement thickness required. Also, it is noteworthy that with rising design traffic the increase

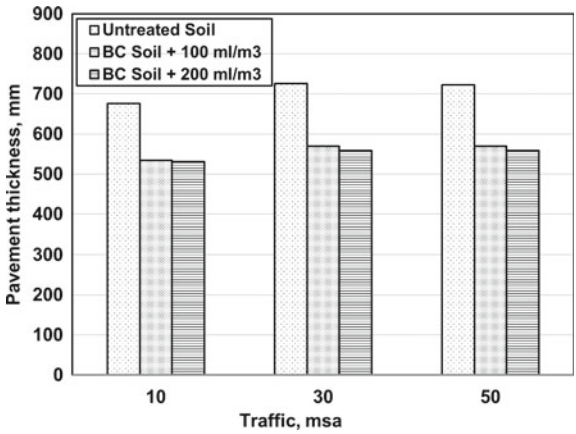

Fig. 5 Pavement thickness for optimum layer on 28 days curing period

in pavement thickness needed is relatively less. Hence, it is summarized that bio-stabilization of the optimum soil layer thickness ensures effective and economic construction of flexible pavements.

4 Mechanism of Terrazyme Stabilization

Terrazyme is a non-toxic liquid derived from sugar molasses, and it is a sustainable and natural material. The enzyme is an organic surfactant that changes clay from being hydrophilic to hydrophobic. Black cotton soil comprises of Montmorillonite mineral and has a high affinity for water due to the presence of negative charge on its surface. On addition of Terrazyme, stronger cations are supplied and it decreases clay's affinity for water. The reaction between the Terrazyme and the BC soil helps in lubricating the soil and improves the bonding between the soil particles. Hence, soil particles move to a denser packing. The chemical bonds so developed increase the stability of clay thereby increasing its bearing capacity.

5 Conclusions

Based on the experimental results, the following conclusions have been arrived at:

1. Bio-stabilization significantly improves the bearing ratio of black cotton soil with increasing dosage of enzyme as well as curing period.
2. Bearing ratio increases with the thickness of stabilized soil, curing period and enzyme dosage, and the maximum percentage increase is around 200%.
3. Black cotton soil blended with Terrazyme in two layers was obtained as the optimum thickness which can sustain the pavement wheel loads. The resilient

modulus was obtained as 96.5 MPa on 28 days curing time for the optimum layered bio-stabilized soil.

4. The percentage reduction in pavement thickness was found to be of the order of 21–23% for all the design traffic considered. Hence, bio-stabilization of optimum thickness of BC soil can successfully be applied for effective and economic pavement construction.

References

1. Gupta C, Sharma RK (2016) Black cotton soil modification by the application of waste materials. Period Polytech Civ Eng 60:479–490
2. Kulkarni VR, Patil GK (2014) Experimental study of stabilization of B.C. soil by using slag and glass fibers. J Civ Eng Environ Technol Print 1:2349–8404
3. Oza JB, Gundaliya PJ (2013) Study of black cotton soil characteristics with cement waste dust and lime. Proc Eng 51:110–118
4. Dahale PP, Nagarnaik PB, Gajbhiye AR (2012) Utilization of solid waste for soil stabilization: A review. Electron J Geotech Eng 17:2443–2461
5. Elkady TY (2016) The effect of curing conditions on the unconfined compression strength of lime-treated expansive soils. Road Mater. Pavement Des 17:52–69
6. Boulanger RW, Khosravifar A (2012) Design of extended pile shafts for liquefaction effects. In: GeoCongress 2012 state of the art and practice in geotechnical engineering, pp 1690–1699
7. Naagesh S, Gangadhara S (2010) Swelling properties of bio-enzyme treated expansive soil. Int J Eng Stud 2:155–159
8. Viswanath D, Asha MN (2020) Experimental investigations on bio-modified soil geotechnical special publication. In Geo-congress 2020: foundations, soil improvement, and erosion. American Society of Civil Engineers, Reston, VA, pp 641–648
9. Shankar AUR, Rai HK, Mithanthaya RI (2009) Bio-Enzyme stabilised laterite soil as a highway material. J Indian Roads Congr 553:143–151
10. IS 1498:1970 (2016) Classification and identification of soils for general engineering purposes
11. IRC-37 (2001) Guidelines for the design of flexible pavements. 37

Development of a Plastic-Coated Natural Fibre Reinforcement for Geotechnical Applications

K. S. V. Durga Prasad and Anjan Patel

Abstract Different kinds of geosynthetic elements as well as natural fibres are being used for various applications in geotechnical and transportation engineering. However, natural fibres are biodegradable and happen to be less durable. On the other hand, the synthetic materials are costly and not eco-friendly. Keeping this in view, the present study is undertaken to develop and find out the feasibility of a plastic-coated natural fibre reinforcement (here named as Semi-Geosynthetic Material) for various applications in civil and construction industries. Jute and coir were used as the natural fibres and polyethylene as the coated material. The composite material was developed in-house for research purpose and tested for its strength properties. Feasibility studies were carried out for using this material to improve the engineering properties of some locally available soil, and the results are presented.

Keywords Coir · Jute · Geosynthetics · CBR

1 Introduction

There are various ground improvement techniques available and some of which are based on soil reinforcement viz., soil anchoring, soil nailing, micro-piling, stone columns, etc. In addition to this, natural fibres and geosynthetic (defined as a product manufactured from polymeric material used with soil, rock, earth, or other geotechnical engineering-related material as an integral part of a man-made project, structure, or system) material are being widely used in construction industry since last few decades [1–4]. The advantage of using geosynthetics materials is that it can be used for all types of soil/ground conditions. Moreover, the geosynthetics materials are easy to handle in the field; it requires less time to install and can be placed in any orientation as per the engineering requirement and as suitable to

K. S. V. Durga Prasad (✉) · A. Patel
Department of Civil Engineering, Visvesvaraya National Institute of Technology, Nagpur 440010, India

B. Laishram and A. Tawalare (eds.), *Recent Advancements in Civil Engineering*, Lecture Notes in Civil Engineering 172,
https://doi.org/10.1007/978-981-16-4396-5_51

ground conditions [5–8]. As such, the major classified geosynthetics materials include geogrids, geotextiles, geomembranes, geonets and geocomposites, which are extensively being used for subgrade soil reinforcement, separating layers, erosion control, slope stabilization and for drainage purpose [8]. However, it cannot be denied that the geosynthetics materials are costly, not eco-friendly and beyond the reach of many in remote areas even as today. On the other hand, various natural fibres such as jute, coir, flax, hemp and sisal have much potential for soil reinforcement, which are largely available in different parts of the world, are biodegradable and hence not a threat to the environment [4]. Out of these various natural fibres, the coir and jute fibres are considered as of superior qualities due to its unique physical mechanical, chemical, hydraulic and biological properties [9]. Natural geogrids and geotextile materials are easily manufactured in large scale and with low cost from jute and coir these days but its use for soil reinforcement is still questionable as it decompose in soil in presence of moisture by the microorganism and has comparatively less mechanical strength.

Considering these advantages and disadvantages of both the natural and synthetic fibres, some of the researchers [10, 11] have worked in the direction of natural fibre-reinforced composite as those of synthetic composites. In the same line, a new philosophy of using natural fibres coated with synthetic material to develop a geogrid-like product (named here as Semi-Geosynthetic material) has been demonstrated in this paper. Geogrid is basically a geosynthetic formed by a regular network of integrally connected elements with suitable apertures sizes to allow interlocking with surrounding soil, rock, earth, and other surrounding materials to primarily function as reinforcement. The geogrid-like product in this study was developed in-house for a small-scale demonstration and just for research purpose. Subsequently, tensile strength tests were conducted on these materials to know its rib (the continuous elements of a geogrid which are either in the machine or cross-machine direction as manufactured) and junction strength (the point where geogrid ribs are interconnected to provide structure and dimensional stability) and then the California Bearing Ratio (CBR) tests were done to check its potential to improve the soil properties. On the basis of the test results, it is confirmed that these semi-geosynthetic materials have large potential to be used for various applications in civil and construction industries. Most importantly, these materials are eco-friendly, cost effective, durable and sufficient mechanical strength and thus overcoming the limitations of both natural and synthetics fibres.

2 Materials and Methods

In present study, polyethylene was used as the coating material covering inside it the natural fibres, i.e. coir or jute. In order to give a coating of polyethylene over the ropes made of jute and coir, a simple equipment was fabricated in the workshop as shown in Fig. 1.

Fig. 1 Equipments fabricated for developing the semi-geosynthetic material

Initially, the 'T' shaped tube was filled with polyethylene granules. Then, it was heated up to the working temperature (about 110 °C for polyethylene) using an oven, after which a coir or jute rope was gradually drawn through the tube from one end to the other. Simultaneously, pressure was also applied from the backside using a handle as shown in the figure. The semi-geosynthetic material as obtained after coating is depicted in Fig. 2a. Once the coating process is over, the semi-geosynthetic ropes were placed and woven like a grid pattern by joining the junctions with molten polyethylene as adhesive as shown in Fig. 2b.

Physical properties of the semi-geosynthetic grid viz., aperture shape, aperture size (Machine Direction × Cross -Machine Direction), aperture open area percentage, rib spacing, rib width and rib length were kept as per the synthetic geogrids available in the market. Rib depth was kept on slightly higher side (3.05–3.5 mm in case of jute and 7–7.5 mm for coir), in order to ease the fabrication. Also, for the same reason, rib shape was made circular as compared to square or rectangular of

Fig. 2 Development of semi-geosynthetics material

Table 1 Physical properties of jute and coir semi-geosynthetic grid

Property	Semi-geosynthetic grid (Jute)	Semi-geosynthetic grid (Coir)
Aperture shape	Square	Square
Aperture size (MD × CMD) (mm)	40 × 40	50 × 50
Aperture open area (%)	53	91
Rib spacing (mm)	40	50
Rib depth (mm)	3.05–3.5	7–7.5
Rib length (mm)	40	50
Rib shape (cross-section)	Circular	Circular

most of the synthetic geogrid available in market. Various physical properties of the semi-geosynthetic grid made up jute and coir are summarized in Table 1.

The cost of geogrids varies from about Rs. 100 to 200 per m^2 in the market depending upon the product and manufacturing process. On the other hand, cost of natural fibres like coir is about Rs. 20 to 40 per kg. Further considering the fact that giving a coating of polyethylene will be much easier and cheaper than manufacturing the geogrids, the semi-geosynthetic grids are supposed to be economical if production is done at large scale.

3 Experimental Investigations

The semi-geosynthetic grid was tested for its various mechanical properties viz., single rib, multi-rib and wide width tensile strength (as per ASTM D6637 [12]) and for its junction strength and efficiency (as per ASTM D7737 [13]). All these tests were conducted at the Geosynthetics Engineering Laboratory, IIT Madras using the standard equipments as shown in Fig. 3.

In order to check its utilization prospects for improving weak soils, soaked CBR tests were conducted in the laboratory as per ASTM D1883-16 [14] by placing layers of the semi-geosynthetic grid in a compacted soil at different depth in the CBR mould (i.e. 0.33H, 0.66H and both at 0.33H and 0.66H, where H is the height of the mould) as shown in Fig. 4. The same tests were repeated with placing the geogrid layers without coating, i.e. made of coir and jute fibre only.

The soil used in the present study was characterized for its various geotechnical properties as included in Table 2.

Fig. 3 Determination of tensile strength and junction strength

Fig. 4 Placing of semi-geosynthetic geogrid layers in CBR mould

Table 2 Soil properties

Soil properties	Value
Liquid Limit (LL) %	42
Plastic Limit (PL) %	25
Shrinkage Limit (SL) %	13
Optimum Moisture Content (OMC) %	16
Maximum Dry Density (MDD) g/cc	1.82
Specific gravity	2.6
Fine content (%)	33

4 Results and Discussion

The results as obtained from the tensile strength tests (ref Fig. 5) are summarized in Table 3. It was found that the results are higher than that can be obtained with natural fibre only.

The load–deformation curves as obtained from the soaked CBR test are presented in Fig. 6. The CBR value at 2.5 mm penetration was generally higher and was adopted as the CBR value of the sample. However, for the cases when higher CBR value was obtained at 5.0 mm penetration, the CBR test was repeated to verify the result. If CBR value at 5.0 mm penetration was higher in the repeat test also, this higher value was adopted as the CBR value of the soil sample. The CBR

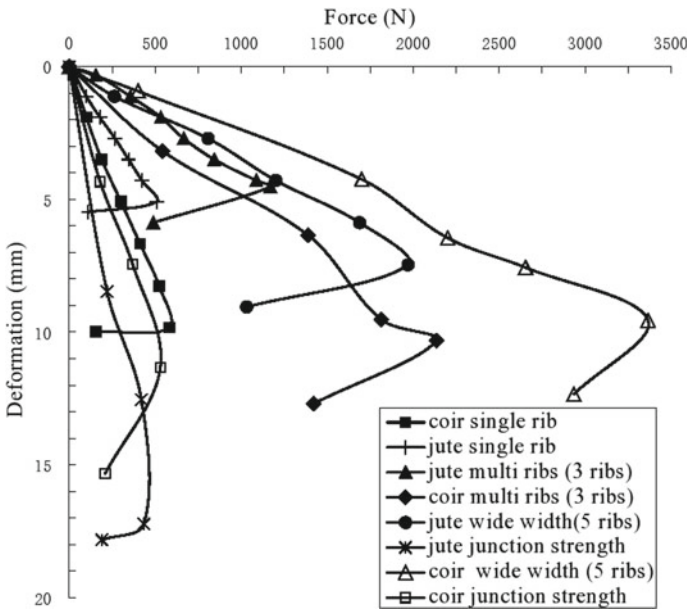

Fig. 5 Load-deformation curves from the tensile and junction strength test

Table 3 Mechanical strength properties of the jute and coir semi-geosynthetic grid

Property	Semi-geosynthetic grid (Jute)	Semi-geosynthetic grid (Coir)
Tensile load single rib (kN/rib)	0.50	0.59
Tensile load multi-rib (kN/3 ribs)	1.25	2.2
Wide width tensile load (kN/5 rib)	1.97	3.32
Junction strength (kN) per rib	0.43	0.52

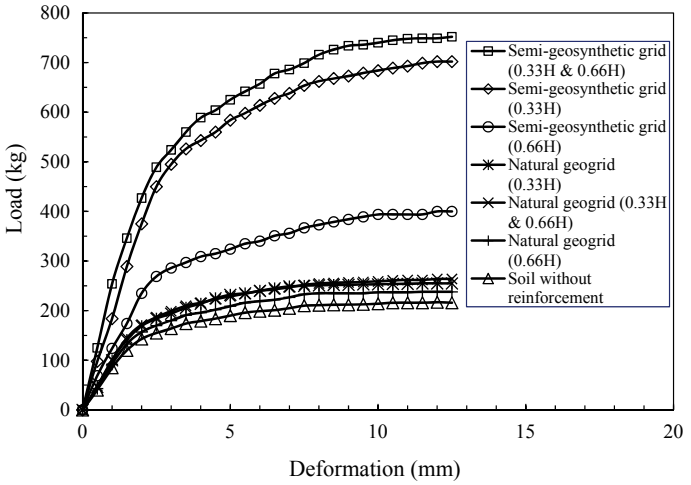

Fig. 6 Load-deformation curves as obtained from CBR tests

Table 4 CBR value with semi-geosynthetics grid

Reinforcement type	CBR value (%)
Soil only	11.31
Soil + Natural geogrid (@0.33*H* depth)	13.43
Soil + Natural geogrid (@0.66*H* depth)	12.4
Soil + Natural geogrid (@0.33*H* and 0.66*H* depth)	13.64
Soil + Semi-geosynthetic grid (@0.33*H* depth)	32.5
Soil + Semi-geosynthetic grid (@0.66*H* depth)	19.63
Soil + Semi-geosynthetic grid (@0.33*H* and 0.66*H* depth)	35.69

values, so calculated, are summarized in Table 4. It can be observed from the table that when the soil is reinforced with natural geogrid (i.e. made of jute without a coating of polyethylene), the CBR value is improved very marginally (i.e. 11.31 to 12.4, 13.43 and 13.64 depending upon the position of geogrid in the mould and the nos. of geogrid layers). On the other hand, when the geogrid is made of

polyethylene coated jute fibre, the CBR value is improved almost by 2–3 times (i.e. 11.31 to 32.5, 19.63, and 35.69, depending upon the depth and nos of geogrid layer). It can be stated that the position of the geogrid in the sample is an important factor governing its CBR value. This is evident from the results that when the geogrid is placed at a depth of 0.66 times the sample height (H), there is no significant improvement in CBR value as compared to when it is placed at a depth of 0.33H.

5 Conclusions

The semi-geosynthetic grids as presented in this paper are eco-friendly, cost effective, durable and have sufficient mechanical strength and thus overcoming the limitations of both natural and synthetics fibres. Mechanical properties of these semi-geosynthetic grids were found to be much superior than the natural fibre-made grids, and the CBR value of soil can be improved to 2–3 folds by using these materials. In addition, these products are more stable due to the polyethylene coating. Moreover, production of these semi-geosynthetic grids in large scale is assumed to be economical as compared to the available geosynthetics products.

The results presented in this paper are soil and material specific, and the work is carried out in laboratory scale for research purpose as such. It is suggested to conduct these studies in industrial scale to further explore the possibility of using such materials in the field.

Acknowledgements The authors are very much thankful to Prof. K. Rajagopal for allowing Mr. K. S. V. Durga Prasad to conduct the tensile strength tests at the Geosynthetics Engineering Laboratory, Indian Institute of Technology, Madras, during his MTech project work in 2016.

References

1. Kaniraj SR, Gayatri V (2003) Geotechnical behaviour of fly Ash mixed with randomly oriented fiber inclusions. Geotext Geomembr 21:123–149
2. Babu GLS, Vasudevan AK (2008) Strength and stiffness response of coir fiber-reinforced tropical soil. J Mater Civ Eng 20(9):571–577
3. Hejazi SM, Sheikhzadeh M, Abtahi SM, Zadhoush A (2012) A simple review of soil reinforcement by using natural and synthetic fibers. Constr Build Mater 30:100–116
4. John NJ, Patel A (2015) Utilization prospects of coir fibre and coir pith for improvement of black cotton soils. Indian J Geosyn Ground Improvements 4(2):9–17
5. Lawson CR (1995) Subgrade stabilisation with geotextiles. Geosynth Int 2(4):741–763
6. Basu G, Roy AN, Bhattacharyya SK, Ghosh SK (2009) Construction of unpaved rural road using jute–synthetic blended woven geotextile-A case study. Geotext Geomembr 27(6): 506–512
7. Estabragh AR, Bordbar AT, Javari AA (2011) Mechanical behavior of a clay soil reinforced with Nylon fibers. Geotech Geol Eng 29:899–908
8. Koerner RM (2012) Designing with geosynthetics vol. 1. Xlibris Corporation

9. Harish S, Michael DP, Bensely A, Lal DM, Rajadurai A (2009) Mechanical property evaluation of natural fiber coir composite. Mater Charact 60:44–49
10. Torres FG, Cubillas ML (2005) Study of the interfacial properties of natural fiber reinforced polyethylene. Polym Testing 24:694–698
11. Sen T, Reddy HN (2011) Application of sisal, bamboo, coir and jute natural composites in structural upgradation. Int J Innov Manage Technol 2(3):186–191
12. ASTM D6637/D6637M-15. Standard test method for determining tensile properties of geogrids by the single or multi-rib tensile method. 100 Barr Harbor Drive, West Conshohocken, USA
13. ASTM D7737/D7737M-15. Standard test method for individual geogrid junction strength. 100 Barr Harbor Drive, West Conshohocken, USA
14. ASTM D1883-16. Standard test method for california bearing ratio (CBR) of laboratory-compacted soils. 100 Barr Harbor Drive, West Conshohocken, USA

An Experimental Study of Unreinforced and Reinforced Soil Slope Under Static Loading

Vishal S. Ghutke, Simran Sheikh, and Anirban Mandal

Abstract In this experimental study, the effect of non-reinforced and nailed reinforced slopes with soil under a gradually increasing vertically applied load is carried out. The soil slopes are constructed in a tank at an angle of 45° and 60° to the horizontal. These soil slopes models are reinforced by inserting nails horizontally. The effect of the soil slopes is observed with different soil nail patterns. Nails are inserted in square, diamond, and staggered shape. Slope stability is observed to increase significantly by providing nails to the soil slopes. The nails installed in a zigzag way also give more stability.

Keywords Gradually increasing load · Soil slope models · Reinforced soil slope · Soil nail pattern

1 Introduction

The stability of a slope is always discussed in terms of vulnerability to failure and is an area of great concern to civil engineers. The slope stability as the resistance of a sloping surface, the wall of an open pit or a cut, to failure due to sliding or collapse. Any soil surface that is at an angle to the horizontal is called an uncontrolled slope and can be of natural or artificial origin. Since the soil surface is not horizontal, there is always the tangential component of gravity that tends to move the materials that form the slope downward. If the tangential component of gravity is more and the internal shear strength of the soil is quite low, slope failure can occur.

Soil nailing is a ground improvement technique used as a corrective measure for the treatment of unstable natural or man-made slopes. With this method of ground improvement technique, a relatively thin reinforcing element is guided into the

V. S. Ghutke (✉) · A. Mandal
Civil Engineering Department, VNIT, Nagpur, India

S. Sheikh
Civil Engineering Department, PCE, Nagpur, India

B. Laishram and A. Tawalare (eds.), *Recent Advancements in Civil Engineering*, Lecture Notes in Civil Engineering 172,
https://doi.org/10.1007/978-981-16-4396-5_52

slope of the terrain. The reinforcing elements, generally used in this technique, are generally made of HYSD steel bars or hollow steel pipes, depending on the needs.

In recent years, ground improvement by soil nailing has been used to improve the stability of steep slopes. In this, large numbers of steel bars (called soil nails) are required, to reinforce the soil slope in the field. Many researchers use soil nails as reinforcement to improve slope stability. Researchers used model testing programs and numerical modeling methods to obtain the most critical surface at failure and the value of factor of safety of a reinforced slope, cut, or retaining wall. The effect of load on a soil reinforced slope with nail stiffness, orientation, nail length, nail diameter, nail slope is analyzed. The influence of slope inclination and angle of frictional resistance on the reinforced soil slope is also studied.

Surender Singh [1] studied the behavior of nailed soil slope under different surcharge load. The soil slopes are reinforced with hollow aluminum pipes with different inclinations and different patterns. Rawat and Gupta [2] have also used aluminum hollow pipes with different inclinations to study the slope stability by soil nailing. Rawat and Gupta [3] used screwed soil nails for two different slope inclination of soil model. They observed higher factor of safety for screw nailed slopes. Manna [4] studied the effect of different slope inclinations on stability of slopes. Suganya [5] and Rawat [6] used the soil nails to increase the stability of slopes. Effect of geotextiles and geogrids on soil slope models are studied by Inanc Onur et al. [7]. In this study, an attempt has also been made to study the effect of soil nail pattern on stability of slope. The soil slope with two different inclination is reinforced with mild steel nail with different patterns. The results found in this present study are similar to the study done by other researchers in the similar work.

2 Materials

2.1 Model Box

The size of the prototype box is fixed as per the test space available in the universal testing machine. A box of internal dimension 630 mm × 380 mm × 500 mm is fabricated. The three sides of a box are fabricated by using mild steel, and the front side is formed with perspex sheet of 8 mm thickness through which the failure surfaces are observed.

2.2 Slope Material

The slope material sand, collected from Kolar River, Koradi, Dist. Nagpur, is used for preparation of slopes. The characteristics of the slope material are shown in Table 1.

Table 1 Characteristics of slope material

Characteristic	Result
Slope material	Sand
Particle size distribution	Well graded sand
Moisture content	21.19 [%]
Specific gravity	2.94
Relative density	0.92
Field density	15.79 [KN/m^3]
Cohesion (c)	28 [KN/m^2]
Angle of friction	31°

2.3 Nails

Solid nails of mild steel with 10 mm diameter and 150 mm long are used as a reinforcing material (Fig. 1).

2.4 Strain Gauges

Strain gauges of a gauge length of 3 mm with a resistance of 350 ± 0.3 Ω are used to determine the deformation created in the mild steel bars at the time of loading.

2.5 Digital Multimeter

Digital multimeter is an apparatus which is used for measurement of resistance change at the time of loading. The strain created in the nails at the time of loading is calculated from the value of resistance change shown by multimeter.

Fig. 1 Solid nail

2.6 *Universal Testing Machine*

The universal testing machine (UTM) of 400 kN loading capacity is used to impose gradually increasing vertical load to the top of the slope.

3 Construction of Unreinforced and Reinforced Soil Slopes

The soil slopes are constructed by well-graded sand with an inclination of 45° and 60° to the horizontal. A base layer with a thickness of 100 mm is provided through out at the base of model box. A soil layer of 50 mm is placed on top of the base layer by light compaction. This process is continued until a full height of 450 mm is reached. A thin layer of red dye (gulal) is used between the layers to identify slope failure (Figs. 2 and 3).

A width of 200 mm at the top and 630 mm at the bottom along the longitudinal direction of the model box is kept for all the model slops. The soil is compacted so that the density of 10.79 kN/m^3 is developed. Total 9 mild steel solid nails of 150 mm of length are used to reinforce the soil slope. The strain gauges are soldered with wires and glued to the nails. The nails are inserted at square, diamond, and staggered shape. A 100 mm of horizontal and vertical distance between the adjacent nails was maintained.

4 Testing Procedure

The soil slope model is prepared at slope inclination 45° and 60° in a model box. The complete assembly is then kept on the universal testing machine. A bearing plate measuring 200 mm × 190 mm × 10 mm is kept on the top of the slope to

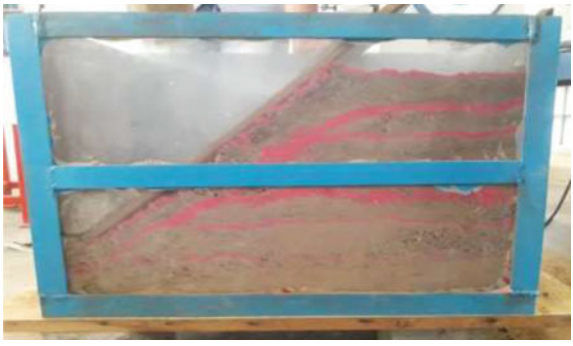

Fig. 2 Complete soil slope model

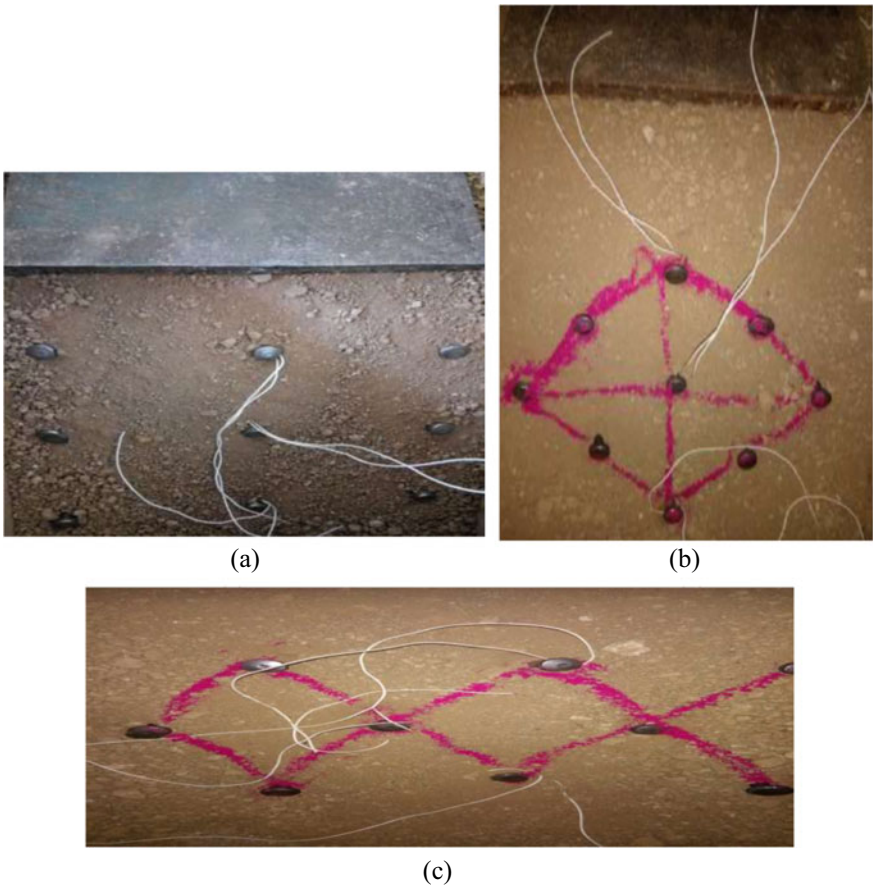

Fig. 3 Nail pattern **a** square, **b** diamond, and **c** staggered

distribute the load evenly. A load is gradually imposed on bearing plate through UTM at a rate of 20 N/s. The deformation of the top of the slope with the gradually increased loading is observed from the computer attached to the UTM. The soil slopes are then reinforced by solid nails at square, diamond, and staggered form. A strain gauge is attached to the nail to measure the strain created at the time of loading. The load is then gradually applied on the top of the slope through bearing plate. The strain in nails in unstrained and strained state is noted. After measuring the resistances in the strain gauges, the following equation is used to find the strain as indicated (Fig. 4).

$$\varepsilon = \Delta R_g / \left(R_g \text{x G.F.}\right) \tag{1}$$

Fig. 4 Soil slope model mounted on UTM

where,

ε strain.
G.F. gauge factor of 2.11.
R_g resistance by strain gauge in unstrained state, and
ΔR_g change in resistance from unstrained to strained state.

After calculating strain, stress–strain curves are constructed for top, middle, and bottom nails for both the slopes inclined at 45° and 60°.

5 Test Results

As per the methodology as discussed above, unreinforced and reinforced slopes were prepared which were subjected to gradually increasing load by using UTM. The failure pattern of each soil slope was observed and studied. Load versus

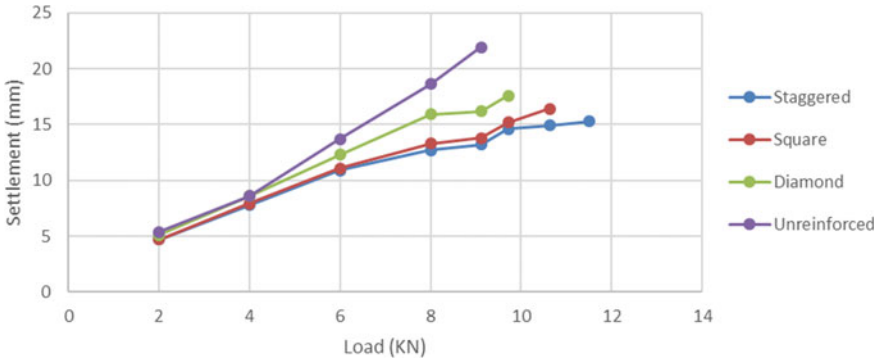

Fig. 5 Load settlement curve for various nail forms of 45° slope model

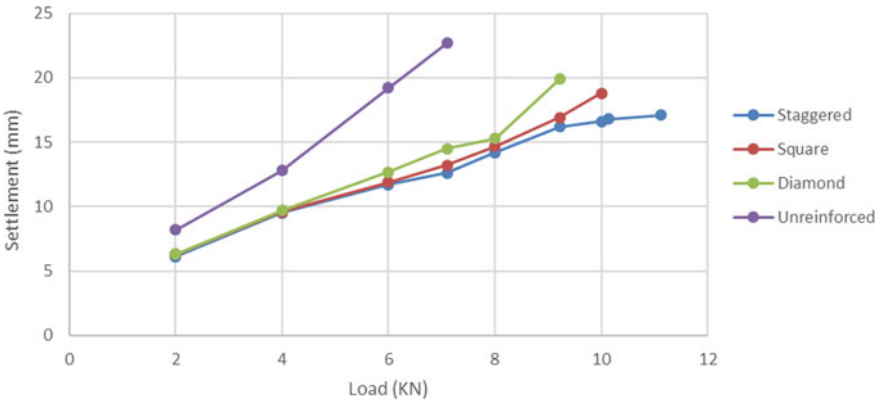

Fig. 6 Load settlement curve for various nail forms of 60° slope model

settlement curves were formed for both unreinforced and reinforced soil slope models at 45° and 60° slope inclination (Figs. 5 and 6).

From Table 2, it is observed that maximum load is sustained by nails installed at staggered form. It is also observed that slope models installed with nails at staggered form shows less settlement. The percentage increase in load bearing capacity by soil slope when slope inclination is 45° with respect to 60° is found as 28.73%. The percentage increase in load bearing capacity by 45° soil slope when nails are placed in staggered form is observed as 25.82%. The percentage increase in load bearing capacity by 60° soil slope when nails are placed in staggered form is found equal to 56.61%. The percentage reduction in final settlement when slope inclination is 45° with respect to 60° is 3.52%. Percentage decrement in ultimate settlement when nails are arranged in staggered form for 45° slope is 30.13%. Percentage decrement in ultimate settlement when nails are placed in staggered form for 60° slope is 24.66%.

Table 2 Observation for load at failure load and corresponding settlement for various nail forms with different inclinations of slope

Slope angle	Nail form	Load at failure (KN)	Ultimate settlement (mm)
45°	Unreinforced	9.14	21.9
	Square	10.63	16.4
	Diamond	9.72	17.1
	Staggered	11.50	15.3
60°	Unreinforced	7.10	21.9
	Square	10.14	18.5
	Diamond	9.22	19.9
	Staggered	11.12	17.1

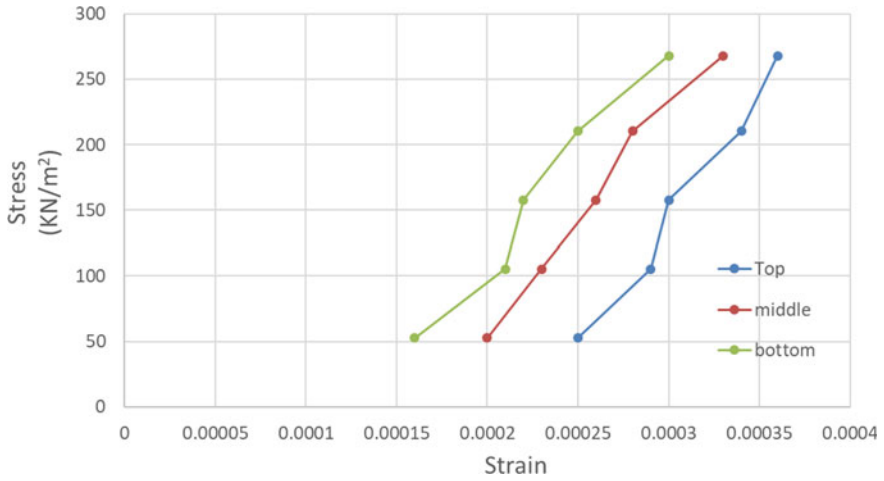

Fig. 7 Variation in strains in different positions of nails for 45° square form

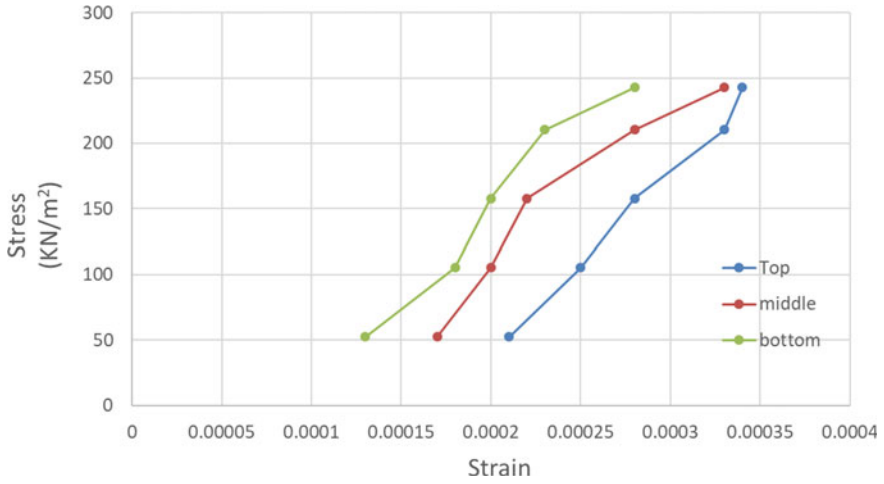

Fig. 8 Variation in strains in different positions of nails for 45° diamond form

From Figs. 7, 8, 9, 10, 11 and 12, it is observed that the top nail is subjected to more strain followed by middle and bottom nail for the entire ceases slope model.

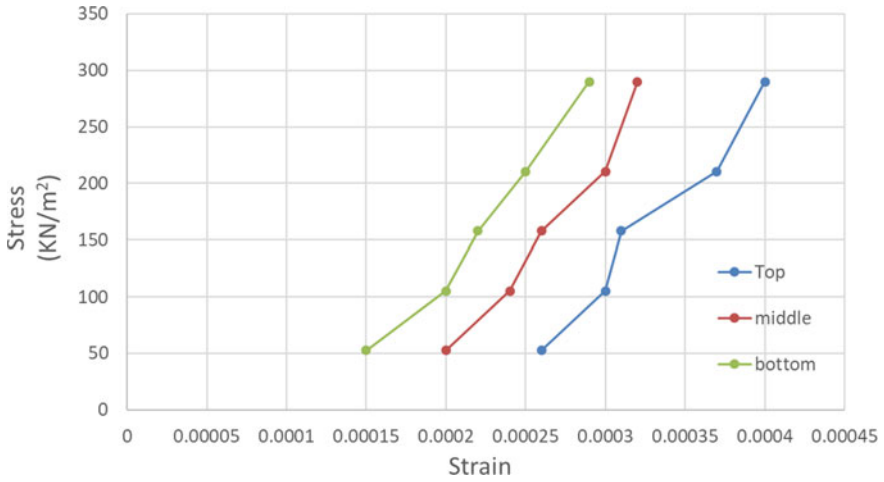

Fig. 9 Variation in strains in different positions of nails for 45° staggered form

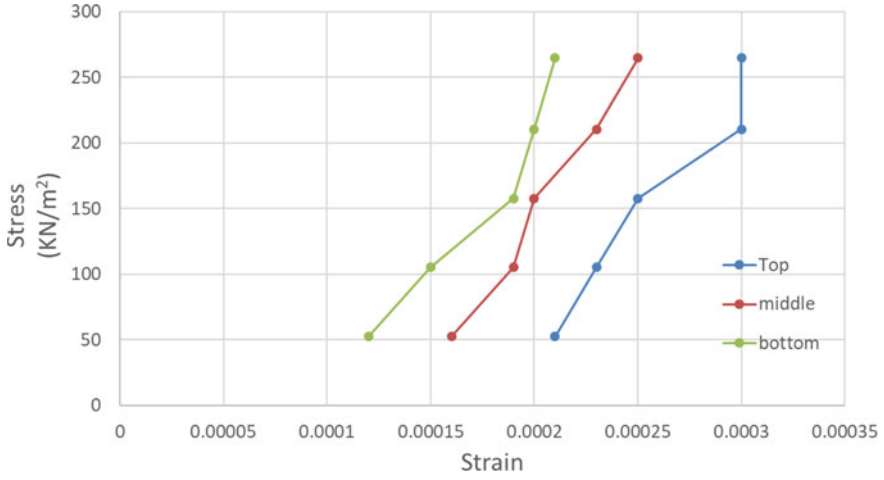

Fig. 10 Variation in strains in different positions of nails for 60° square form

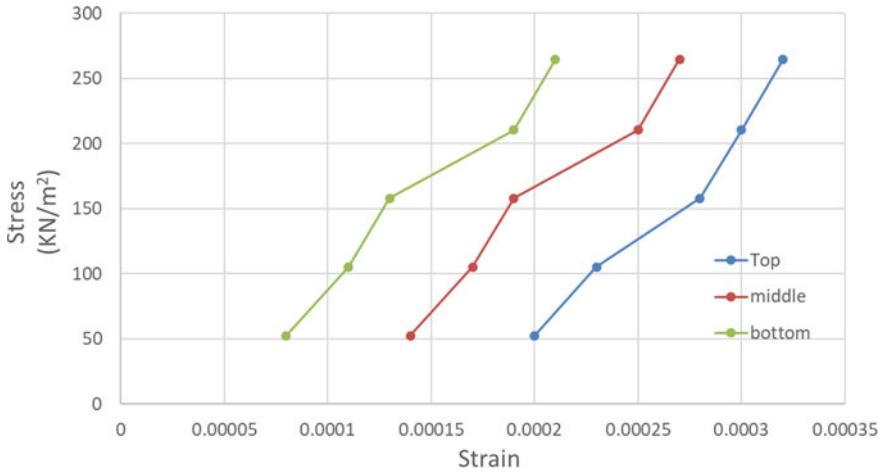

Fig. 11 Variation in strains in different positions of nails for 60° diamond form

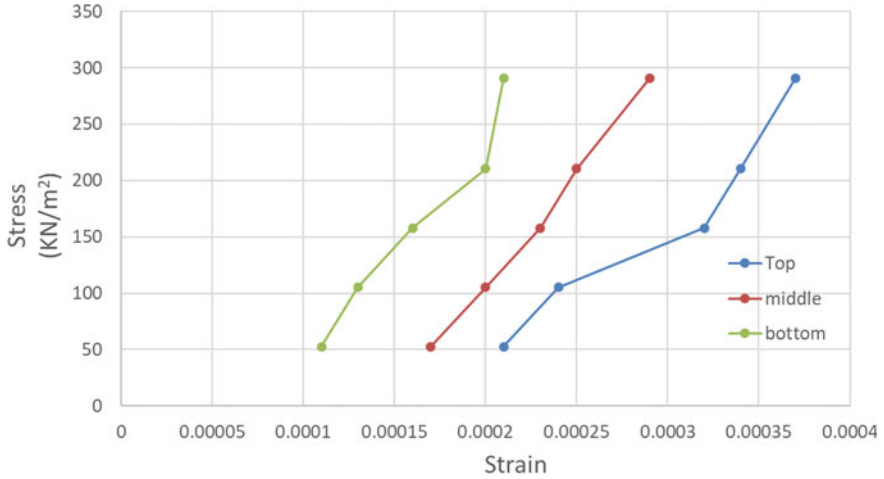

Fig. 12 Variation in strains in different positions of nails for 60° staggered form

6 Conclusions

It is found that the highest load is taken by the slope with 45° slope angle compared to 60° slope angle.

It can be concluded that reinforcement in soil slopes is subjected to an increase in the load bearing capacity and a significant decrease in the ultimate settlement of the slope.

It has been observed from the above study that solid nails placed in staggered form offered more stability followed by square nail form and diamond nail form.

From the deformation of nails in model testing, it can be deduced that highest load is taken by the solid nails placed at the top of the slope models.

From the above study, it is suggested to provide a slope at an angle of 45° with staggered nail form.

References

1. Singh S (2017) Soil nailing for stability of slopes. Electr J Geotech Eng (22.10):4235–4248
2. Rawat S, Gupta AK (2016) An experimental and analytical study of slope stability by soil nailing. Electr J Geotech Eng (21.17):5577–5597
3. Rawat S, Gupta AK (2017) Testing and modelling of screw nailed soil slopes. Indian Geotech J. https://doi.org/10.1007/s40098-017-0229-7
4. Manna B, Rawat S, Zodinpuii R, Sharma KG (2014) Effect of surcharge load on stability of slopes—testing and analysis. Electr J Geotech Eng
5. Suganya S, Sathees Kumar M (2018) Software analysis and model study of soil nailed wall. Int J Modern Trends Eng Res 5(03)
6. Rawat S, Zodinpuii R, Manna B, Sharma KG (2014) Investigation on failure mechanism of nailed soil slopes under surcharge loading:testing and analysis. Int J Geomech Geoeng
7. Inanc Onur M, Tuncan M, Evirgen B, Ozdemir B, Tuncan A (2016) Behavior of soil reinforcements in slopes. In: International conference on transportation geotechnics

EPS-Based Lightweight Geomaterial—A Review

Anupam Pande and Amit Padade

Abstract Expanded polystyrene beads-based geomaterial is a completely new concept of low-density construction material. This material is usually made by blending EPS beads with soil and water in the presence of a binding agent such as cement. Studies have also been carried out to replace soil by other industrial by-products such as fly ash, bottom ash stone dust, etc. to produce a new geomaterial. These elements play a very important role in characterizing various geotechnical properties of geomaterial. Geomaterial made using this technique is not only easy in manufacturing but it can also occupy any volume. This lightweight material can be modified accordingly to achieve the target strength. These properties have resulted in having numerous applications in the field of civil engineering. The composite material has been widely used in forming embankment, backfilling bridge abutments, retaining structures and conduit trenches. Less density and good compressive strength of the geomaterial have helped in reducing vertical stresses on soil, decreasing earth pressure and minimizing settlement problems. A thorough attempt has been made to study the unit weight and strength properties on EPS beads-based material by reviewing the prominently available literature. Several case histories have also been discussed in this manuscript.

Keywords Expanded polystyrene (EPS) beads · Lightweight soil · Geomaterial

1 Introduction

Japan in the late 1980s conceived the idea of lightweight expanded polystyrene (EPS)-based composite soil. Reference [1] blended EPS beads and shreds in the sand in the presence of cement and water to make a lightweight composite soil. This knowledge was used to fill the pipeline trench with a length of 359.3 m with 100 m^3 of lightweight geomaterial [1, 2]. Since then, this concept was used widely

A. Pande (✉) · A. Padade
Department of Civil Engineering, Visvesvaraya National Institute of Technology, Nagpur, Maharashtra, India

B. Laishram and A. Tawalare (eds.), *Recent Advancements in Civil Engineering*, Lecture Notes in Civil Engineering 172,
https://doi.org/10.1007/978-981-16-4396-5_53

for various engineering works to reduce the overburden pressures. EPS foam has a variety of applications not only in the field of packaging but also in the field of construction. On the other hand, a substantial quantity of EPS waste is generated and its disposal becomes problematic.

The European Union has limited the discarding of EPS foam into landfills by prioritizing recycling of such wastes [3–5]. Maharashtra Government has also raised concerns about the usage and disposal of plastic and polystyrene products. In their notification, they have imposed a complete ban on such products [6]. Including expanded polystyrene in geomaterial not only helps in making a low-density stable construction material but also helps in resolving the disposal complications of EPS. Apart from having low density, EPS has significant compressive strength and also acts as a good insulator. These properties have enhanced the multipurpose functioning of EPS as a building material. EPS geofoam has effectively condensed extreme settlement complications over soft ground [7]. Though its applications are versatile, it has certain limitations. EPS products have weak buoyancy endurance and are sensitive to heat and petroleum products [8]. Moreover, these products do not fit in irregular volumes. Thus, blending EPS beads with soil and other material can be used in filing irregular areas and underground cavities.

EPS composite soils have drawn attention from many researchers. Quite a few articles are available in the literature describing the manufacturing process, properties and importance of such combined materials. But there are fewer texts that give a consolidated analysis of behaviour and applications of EPS-based geomaterial. An effort has been taken in this manuscript to highlight the significant work done in this matter. Researchers have called the mixture by various names such as ‘lightweight soil’, ‘Expanded polystyrene geomaterial’, ‘EPS composite soil’, etc. In this article, we will commonly refer to EPS-based material as ‘geomaterial’.

2 Components of EPS Composite Geomaterial

The lightweight geomaterial comprises of soil, EPS beads and water. Both coarse-grained and fine-grained soil can be used in the manufacturing process. Separate studies are available to compute the behaviour of EPS beads in various clays and sands from different locations. The polystyrene resins are steamed under controlled pressure. The expanded beads are spherical in shape and are about 35–40 times larger in the volume of the resin. These beads can be formed in the density range of 13–22 kg/m^3 depending on the requirement. Cement has been widely used in improving the strength of soils since long [9, 10]. Many researchers have used cement as a binding material for keeping all the constituents of geomaterial together. Other pozzolanic materials such as lime and fly ash can also be used for binding purposes. Water is added to make a homogenous mixture and to initiate the hydration process. The quantity of water added is to be fixed depending on the properties of the base material.

3 Engineering Properties of Geomaterial

Various engineering properties of EPS beads-based lightweight geomaterial have been studied. These properties include unit weight, strength parameters, permeability and water absorbability, deformation and creep properties of geomaterial. Several investigations are done to analyse various parameters governing these properties. This manuscript gives a brief analysis of unit weight and compressive strength properties of EPS-based geomaterial and various factors affecting them.

3.1 Unit Weight

Unit weight is an important parameter of the lightweight geomaterial [2, 11, 12]. EPS content is the dominant factor governing the unit weight of any such material. Liu et al. [4] studied the effect of EPS to soft silty clay ratio on the unit weight of geomaterial at different cement contents. It can be seen from Fig. 1 that there was a linear decrease in density with an increase in EPS content. The density of geomaterial also decreased with an increase in water content.

Padade and Mandal [12] blended EPS beads of the density of 20 kg/m^3 with class F fly ash in the presence of cement and water content. As in the case of [4], it was observed that with an increase in EPS content, the density decreased linearly. From Fig. 2, it can be concluded that the cement content had a very marginal effect on the density of geomaterial. The same results were observed by [2, 13].

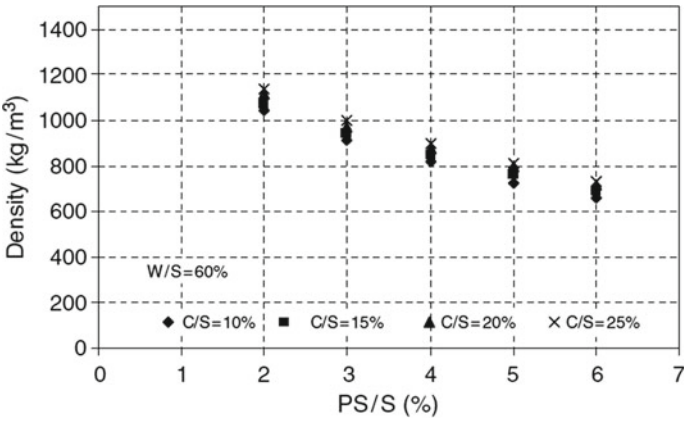

Fig. 1 Effect of EPS to sand ratio on unit weight of geomaterial for various cement to soft silty clay proportions [4]

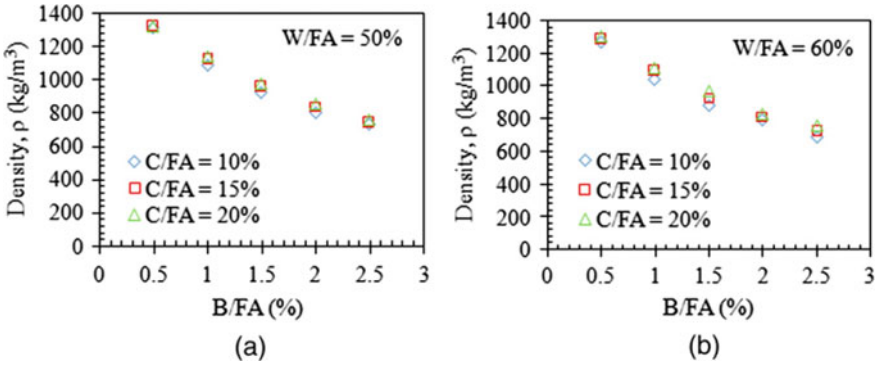

Fig. 2 Effect of EPS to fly ash ratio content on the density of geomaterial for different cement to fly ash ratios at different water contents [12]

Lal and Nawkhare [11] combined EPS beads with bottom ash and cement by reinforcing the product by plastic strips of the different aspect ratios of 5 and 10. It was observed that for both aspect ratios, the density decreased linearly with an increase in EPS and plastic content to bottom ash ratio. Also, for a particular EPS content, the density decreased with a decrease in plastic content (Fig. 3).

Marjive et al. [14] studied the effect of varying EPS densities on the unit weight of stone dust-based geomaterial. EPS beads of densities 16 and 22 kg/m^3 were used in the study. The density of geomaterial decreased gradually when EPS beads with higher density were used, whereas on the other hand, it can be seen from Fig. 4 that there was a sharp decrease in the density value of geomaterial with EPS beads of lower density. As found in previous studies, the density of geomaterial decreased with an increase in EPS content.

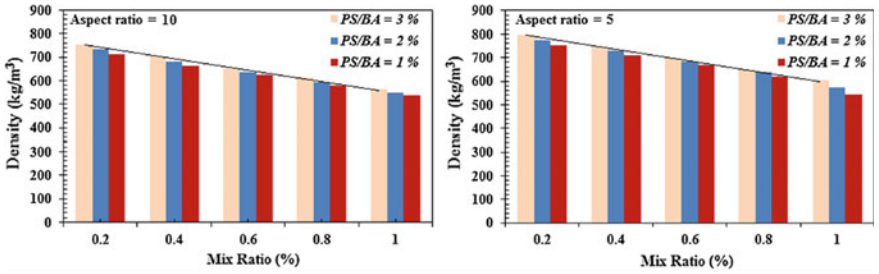

Fig. 3 Effect of EPS mix ratio on the density of plastic strip reinforced bottom ash-based geomaterial for various aspect ratios of plastic strips [11]

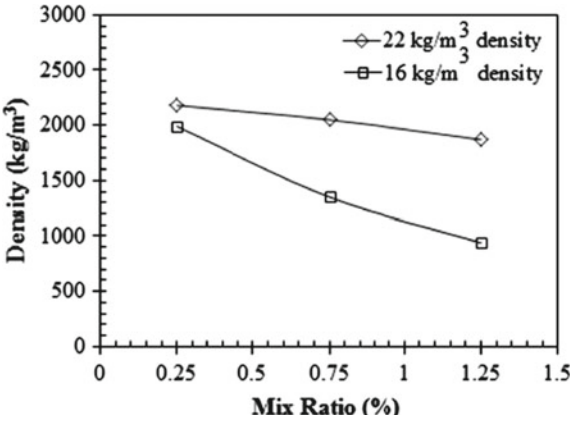

Fig. 4 Effect of density of EPS beads on density of geomaterial [15]

3.2 Strength of Geomaterial

The influence of water pressure on the compressive strength of geomaterial for submerged applications was studied by [16]. This material was created using sand, cement, water and EPS shreds. It was observed that there was a linear decrease in compressive strength with an increase in water pressure. This decrease in strength may be due to damage in the inner structure of geomaterial.

Yoonz et al. [17] determined the compressive strength of geomaterial made from dredged mud and EPS beads through both triaxial and unconfined compression tests. It was observed that the ultimate compressive strength in both triaxial and unconfined tests decreases rapidly as EPS content is increased from 1 to 2% (Fig. 5).

Later, with an increase in EPS content from 2 to 3%, the decrease in compressive strength was gradual. The geomaterial is significantly applicable in reducing earth pressure acting on the retaining structures.

To verify the effect of applied pressure for the curing period, [17] performed triaxial compression tests with different curing pressure. He concluded that the ultimate compressive strength of geomaterial decreased until the curing pressure was 200 kPa, and it increased with pressure above 200 kPa. Reference [4] conducted unconfined compressive tests on geomaterial made up of different cement and EPS ratios and constant water content. From Fig. 6, it is observed that for a particular EPS content, an increase in cement content increased the compressive strength, whereas for particular cement content, an increase in EPS content decreases the compressive strength. It was also seen that an increase in EPS and water content decreased the compressive strength in general. The 28 days compressive strength of geomaterial in various combinations of EPS, cement and water was in the range of 100–150 kPa.

Shear strength properties of EPS beads–sand mixture were studied by [18]. It was observed that the density and strength of geomaterial undergo a marginal change when volumetric content is considered, but they change significantly when gravimetric content is considered. In the study, EPS content was taken by volume,

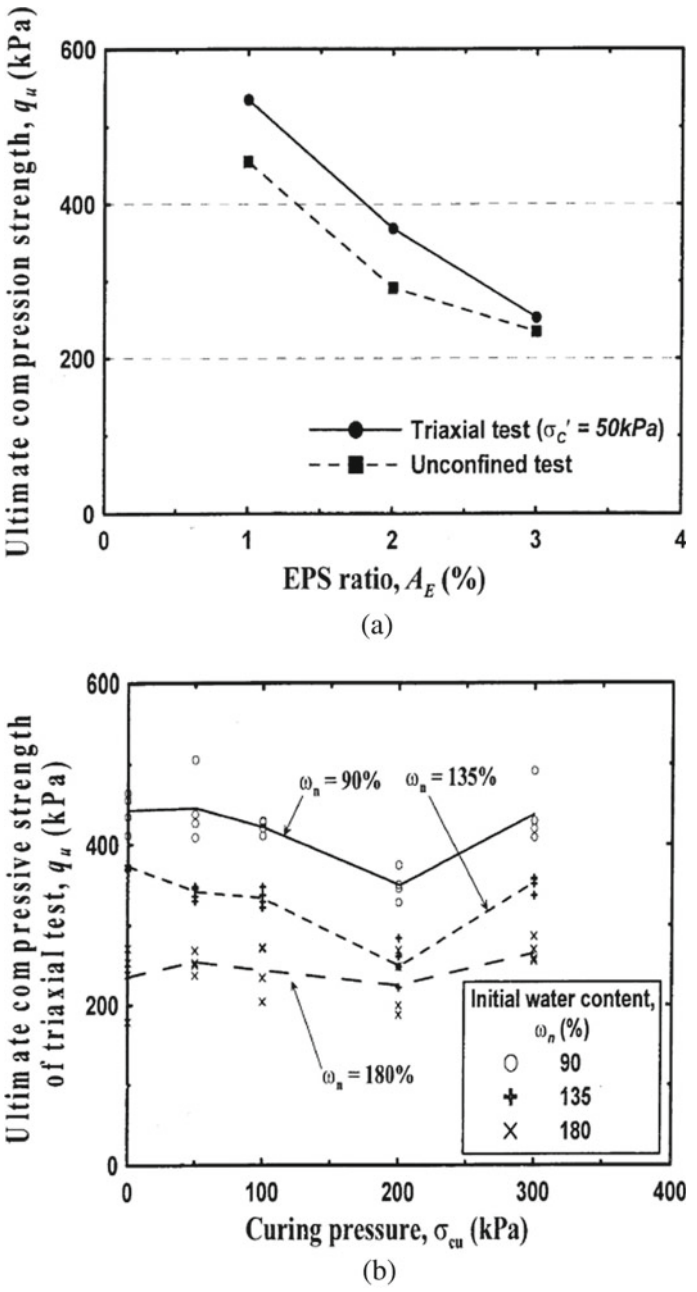

Fig. 5 **a** Effect of EPS ratio on the ultimate compressive strength of geomaterial from triaxial (σ_c' = 50 kPa) and unconfined tests [17] **b** Effect of curing pressure on the ultimate compressive strength of geomaterial from triaxial test for various initial water contents of dredged mud [17]

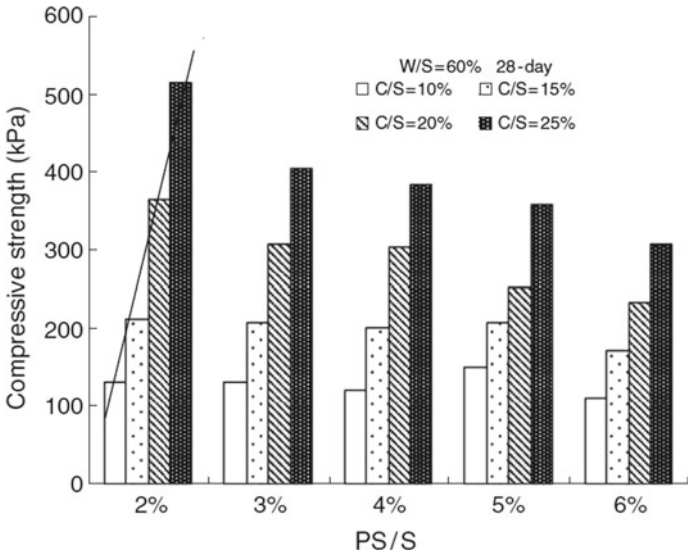

Fig. 6 Effect of EPS to sand ratio and cement to sand ratio on 28 days compressive strength of EPS geomaterial at 60% water to sand content [4]

Fig. 7 Effect of volumetric content of EPS beads on shear strength parameters of geomaterial [18]

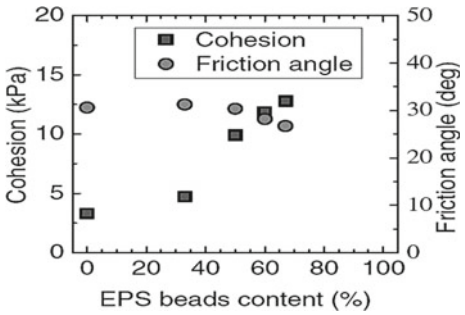

whereas water content was taken by weight. From Fig. 7, it can be seen that the cohesion of geomaterial increased, whereas the internal friction angle decreased with an increase in EPS content. According to [18], the increase in cohesion may be caused by embedding of sand grains into EPS beads, and a decrease in internal friction angle may be caused by easy sliding of EPS beads.

To check the behaviour of sand–EPS-based geomaterial, [19] performed direct shear and triaxial compression tests at various normal and confining stress. It was commonly seen that there was a substantial decrease in density and shear strength with an increase in EPS content. The shear strength also decreased with a decrease in normal stress and confining pressure. From Fig. 8, it can be seen that when EPS content increases from 0 to 0.5%, there is a sudden fall in shear strength. At low EPS content, EPS particles are surrounded by sand and the sand particles slide over EPS bead thereby reducing shear strength.

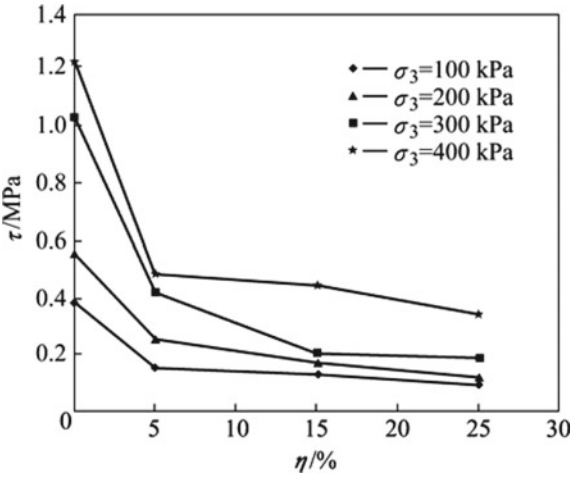

Fig. 8 Effect of EPS content on shear strength of sand–EPS beads geomaterial at various confining stresses [19]

Deng and Xiao [20] that EPS plays a significant role in the stress–strain behaviour of EPS–sand specimens. Figure 9 represents K_f lines for pure sand and EPS–sand geomaterial. It was seen that geomaterial prepared at relatively high EPS content showed a piecewise two-segment linear K_f line and a substantial cohesion intercept stress coordinate s, t where $s = (\sigma 1 + \sigma 3)/2$ and $t = (\sigma 1 - \sigma 3)/2$.

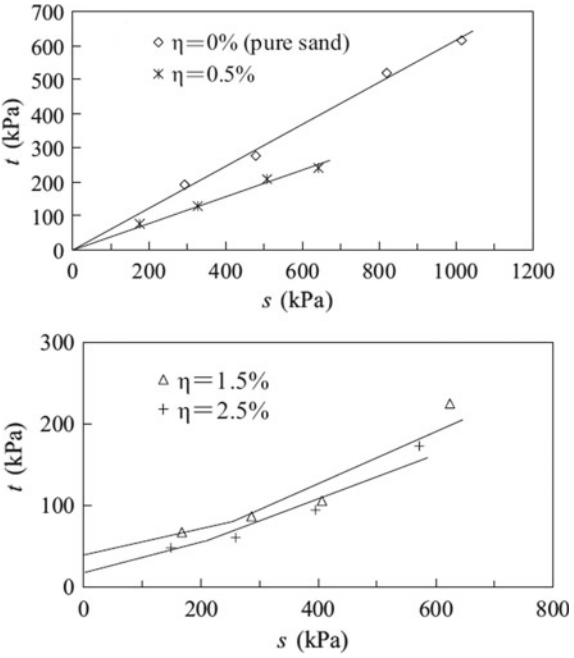

Fig. 9 K_f lines for pure sand and EPS-sand mixture (η = 0.5%, 1.5%, 2.5%) [20]

Edinclier and Ozer [21] studied the effect of EPS beads gradation of geomaterial made up of EPS beads–sand mixtures. As seen in Table 1, EPS beads of three different unit weights (0.14, 0.19, 0.3 kN/m^3) were mixed with sand at different content.

The study has proved that the deviator stress of geomaterial is the function of EPS volumetric content as well as gradation. EPS–sand geomaterial behaved like that of loose sand under low confining pressure and showed strain hardening behaviour under high confining pressure. It was suggested that the smaller sized EPS beads resulted in producing higher stiffness in the lightweight geomaterial. From Fig. 10, it can be concluded that the peak deviator stress of EPS beads–sand-based geomaterial is much less than that of sand. Also, geomaterial in which EPS beads of high density was used showed higher deviator stress.

Table 1 Physical properties of raw materials used by Edincliler and Ozer for making sand-EPS geomaterial [21]

Material	Specific gravity (Gs)	Dry unit weight (kN/m^3)	Effective size D_{10} (mm)	Uniformity coefficient Cu	Coefficient of curvature Cc
Sand	2.65	14.2 (Min) 16.4 (Max)	0.2	2.7	1.2
EPS-1	0.02	0.14	2.2	1.6	1.0
EPS-2	0.03	0.19	2.0	1.6	1.0
EPS-3	0.05	0.30	1.2	2.2	0.8

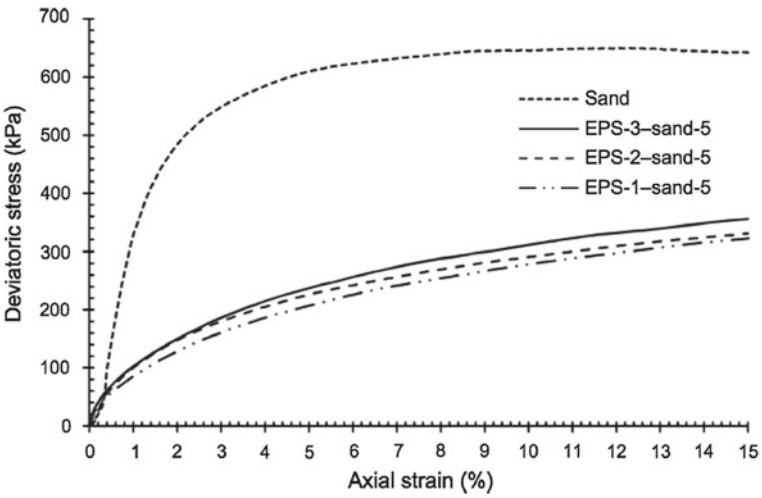

Fig. 10 Stress–strain behaviour of sand and various EPS–sand mixes at volumetric content of 5% under 200 kPa cell pressure [21]

The applicability of the EPS beads–sand mixture was investigated by [22] in five EPS/sand combinations by conducting large-scale oedometer tests. It was observed that with an increase in EPS content, there was a decrease in the internal angle of friction and permeability. However, the volume compressibility and earth pressure at rest increased with an increase in EPS content.

Padade and Mandal [12] studied the mechanical behaviour of EPS-based geomaterial using fly ash and cement. When compared with other geomaterials such as geofoam blocks, EPS-soil mixes, this material required less cement content, and it also reduces environmental problems such as disposal of fly ash. Using the same concept, [13] mixed EPS beads with fly ash and sand to make a lightweight geomaterial. Reference [2] blended EPS beads with bottom ash in the presence of cement. Later, [11] made use of plastic strips to enforce the geomaterial made up of bottom ash and cement. Table 2 compares the density and compressive strengths of various geomaterial made using industrial waste, EPS beads and cement. Figure 11a demonstrates effect of EPS content in fly ash on 28th day compressive strength of geomaterial for various cement ratios. Figure 11b illustrates effect of EPS beads on compressive strength of bottom ash at various cement contents. Figure 11c depicts the result of inclusion of EPS beads and plastic strip on compressive strength of bottom ash.

4 Applications and Case Studies

EPS-based lightweight material was first used as fill material in the late 1980s for a 359.3 m long underground pipeline. A total volume of 100 m^3 geomaterial of unit weight 11.25 kN/m^3 was used. The post-construction settlement of the ground surface was around 15 mm [1]. 2600 m^3 of geomaterial made up of EPS shreds and waste soil was used as a backfilling material for a retaining wall in 1990 [16]. A total volume of 800 m^3 of EPS geomaterial was used to fill cavities to reduce the differential settlements in residential buildings in Japan [23]. From 1988 to 1994, EPS-based geomaterial has been widely used in filling underground pipelines,

Table 2 Density and compressive strength of EPS based geomaterial

Sr. no	Author (year)	Materials	Density (kg/m^3)	Compressive strength (kPa)
1	Padade and Mandal [12]	Fly ash, cement, EPS beads, water	1320–725	243–3290
2	Golait and Patode [13]	Sand, fly ash, cement, EPS beads, water	900–1970	65–1685
3	Lal and Badwaik [2]	Bottom ash, cement, EPS beads, water	360–650	150.41–686.94
4	Lal and Nawkhare [11]	Bottom ash, cement, plastic strips, EPS beads, water	500–800	38–257

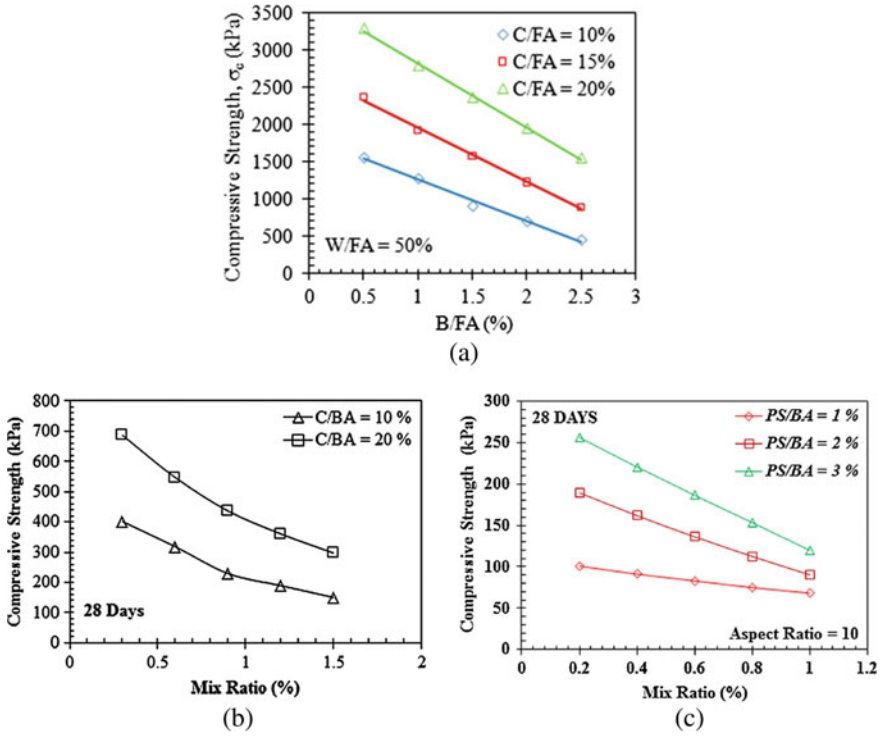

Fig. 11 **a** Effect of EPS to fly ash ratio on 28 days compressive strength of geomaterial at 50% water content and various cement ratios [12]. **b** Effect of EPS to bottom ash ratio on 28 days compressive strength of geomaterial at 30% water content at various cement ratios [2]. **c** Effect of EPS to bottom ash ratio on 28 days compressive strength of geomaterial at 10% cement and various plastic strip contents of aspect ratio 10 [11].

trench walls, retaining walls, highway embankments, river embankments and bridge abutments in 17 engineering cases in Japan with a total construction volume of 19,490 m^3 [16].

In the year 2000, a total volume of 6,000 m^3 had been used for river embankments and 195,000 m^3 of geomaterial in ports and airports [24]. China started using lightweight geomaterials in the early 2000s. The Zhangzhou-Shaoan Expressway Project in Fujian had an embankment of stabilized geomaterial [25]. A slop was stabilized in Xinanjiang Power Plant in Zhejiang China, by using 200 m^3 of EPS-based soil [26]. Later in 2005, EPS-based geomaterial was used for embankment construction on very soft ground in the Yong-Yu Express Project in Zhejiang, China [27].

References

1. Yamada S, Nagasaka Y, Nishida N, Shiroi A (1989) Light soil mixture with small pieces of expanded polystyrol and sand. Soil Mech Found Eng 37:25–30
2. Ram Rathan Lal B, Badwaik VN (2016) Experimental studies on bottom ash and expanded polystyrene beads-based geomaterial. J Hazardous Toxic Radioact Waste 20:1–8. https://doi.org/10.1061/(ASCE)HZ.2153-5515.0000305
3. Gao H, Liu J, Liu H (2011) Geotechnical properties of EPS composite soil. Int J Geotech Eng 5:69–77. https://doi.org/10.3328/IJGE.2011.05.01.69-77
4. Liu HL, Deng A, Chu J (2006) Effect of different mixing ratios of polystyrene pre-puff beads and cement on the mechanical behaviour of lightweight fill. Geotext Geomembranes 24:331–338. https://doi.org/10.1016/j.geotexmem.05.002
5. Montreal protocol on substances that deplete the ozone layer (2003)
6. Séé É (2018) Marashtra plastic and thermocol ban notification. 1:1–24
7. Arellano D, Aaboe R, Stark TD (2001) Comparison of existing EPS-block geofoam creep models with field measurements by senior engineer and Department of Civil and Environmental Engineering. Paper submitted to EPS geofoam 2001 3rd International Conference, pp 1–10
8. Negussey D, Jahanandish M (1993) Comparison of some engineering properties of expanded polystyrene with those of soils (with discussion and closure). Transp Res Rec
9. Mitchell JK (1981) Soil improvement-state of the art report. In: Proceedings of 11th international conference on SMFE, pp 509–565
10. Porbaha A, Shibuya S, Kishida T (2000) State of the art in deep mixing technology. Part III: geomaterial characterization. Proc Inst Civ Eng Improv 4:91–110
11. Ram Rathan Lal B, Nawkhare SS (2016) Experimental study on plastic strips and EPS beads reinforced bottom ash based material. Int J Geosynth Gr Eng 2:1–12. https://doi.org/10.1007/s40891-016-0066-2
12. Padade AH, Mandal JN (2014) Expanded polystyrene-based geomaterial with fly ash. Int J Geomech 14:1–7. https://doi.org/10.1061/(ASCE)GM.1943-5622.0000390
13. Goliat YS, Patode AS (2015) Indian geotechnical conference. In: 50th Indian geotechnical conference
14. Marjive et al (2016) An experimental study on stone dust and EPS beads based material. https://doi.org/doi/10.1061/9780784480151.004
15. Marjive VR, Badwaik VN, Ram Rathan Lal B (2016) Experimental studies on controlled low strength material using stone dust and EPS beads. Int J Eng Technol 8:265–268. https://doi.org/10.7763/ijet.v8.896
16. Nagasaka Y, Yamada J, Teji F (1994) The lightweight mixture soil mixed with EPS beads and construction soil. Soil Mech Found Eng 42:25–30
17. Yoonz G, Jeon S, Kim B, Kim B (2004) Mechanical characteristics of light-weighted soils using dredged materials. Marine Georesour Geotechnol 37–41. https://doi.org/10.1080/10641190490467747
18. Wei Z, Mingdong L, Chunlei Z, Gan Z (2008) Density and strength properties of sand-expanded polystyrene beads mixture. Geotech Spec Publ 36–43. https://doi.org/10.1061/40972(311)5
19. Deng A, Xiao Y (2008) Shear behavior of sand-expanded polystyrene beads lightweight fills. 4:175–179. https://doi.org/10.1007/s11771-008-0454-4
20. Deng, Xiao (2010) Measuring and modeling proportion-dependent stress-strain behavior of EPS-sand mixture, https://doi.org/10.1061/(ASCE)GM.1943-5622.0000062
21. Edinçliler A, Özer AT (2014) Effects of EPS bead inclusions on stress-strain behaviour of sand. Geosynth Int 21:89–102. https://doi.org/10.1680/gein.14.00001

22. Jamshidi Chenari R, Karimpour Fard M, Pourghaffar Maghfarati S, Pishgar F, Lemos MacHado S (2016) An investigation on the geotechnical properties of sand-EPS mixture using large oedometer apparatus. Constr Build Mater 113:773–782. https://doi.org/10.1016/j.conbuildmat.03.083
23. Miki H, Senda S, Nishida K (1992) The construction case of reinforced EPS composite soil. In: Proceedings of the 47th annual symposium of civil engineering, pp 1080–1081
24. Illuri HK (2007) Development of soil-EPS mixes for geotechnical applications
25. Ma S-D (2001) The properties of stabilized light soil (SLS) with expanded polystyrene. ROCK SOIL Mech 22:245–248
26. Zhu W (2004) Highway embankment filled with lightweight soil in Xinanjiang Power Plant. Eng Rep
27. Yang S (2007) Embankment filled with man made lightweight soil

Laboratory Investigation on Dynamic Small-Strain Shear Modulus of Fly Ash Stabilized Expansive Soil

Ritesh Ingale and V. Srinivasan

Abstract The shrink–swell property exhibited by expansive/collapsible soils is mainly due to the presence of certain clay minerals. This leads to sudden change in strength and stiffness of soil underneath the foundation and ultimately causes the premature failure of a structure. An experimental probe was carried out to study the swelling and stiffness characteristics of black cotton soil by inclusion of class F fly ash. The percentage of fly ash was varied between 2 to 20%. A set of bender element test was conducted to study the dynamic properties of fly ash stabilized soils for different curing periods. It has been found that the curing period does not influence the small-strain modulus of fly ash stabilized specimens significantly. However, the small-strain stiffness of soil is intensified with increasing fly ash content. Moreover, the free swell index decreases with increasing fly ash content in BC soil.

Keywords Shear wave · Bender element · Clayey soil · Stiffness

1 Introduction

Black cotton (BC) soils are the clays which exhibit shrink–swell viz-a-viz cracking characteristics, etc., strongly linked to its soil–water characteristics curve [1]. The problems associated with the soils located in central India with semiarid climatic region are well known to the geotechnical engineers. One of the method for controlling the volume change parameter is the inclusion of some admixtures which is most effective and commonly used technique. On the other hand, increasing energy

R. Ingale
Department of Civil Engineering, National Institute of Technology Srinagar, Srinagar, Jammu & Kashmir, India

V. Srinivasan (✉)
Department of Civil Engineering, Visvesvaraya National Institute of Technology, Nagpur, Maharashtra State, India
e-mail: srinivasanv@civ.vnit.ac.in

B. Laishram and A. Tawalare (eds.), *Recent Advancements in Civil Engineering*, Lecture Notes in Civil Engineering 172,
https://doi.org/10.1007/978-981-16-4396-5_54

demand resulted in the production of fly ash as a by-product from the coal-dependent power plants. Fly ash is an alkaline material composed of non-crystalline silicate, iron oxides, and aluminum and also some microcrystalline materials along with free lime and unburnt carbon, etc. [2]. Disposal of such material requires highly skilled workers and large area of land which creates serious environmental concerns.

India is a one of the largest fly ash producing country with 73 billion tons of coal reserve. Out of which 50% fly ash is being used by cement producing industries. Despite that, large amount of fly ash still remains unused. Studies have been done so far to improve the swelling characteristics of expansive soils using lime, geo-polymer, rice husk ash, stone dust, fly ash, etc., based on unconfined compression test, compaction test, and CBR test, respectively, before in-situ application [3]. However, very few studies have been undertaken to study the dynamic properties of fly ash treated expansive soils. Small-strain stiffness of geo-materials based on shear wave velocity measurement is more sensitive to the moisture content. Dynamic properties of soils are very much important in the design of pavement structures, buildings, and dams subjected to seismic loading [4].

The objective of this article is to study the small-strain stiffness characteristics of expansive soils using laboratory bender element. Series of bender element tests were performed by inclusion of class F fly ash in soil from 2 to 20%. The soil specimens were compacted at maximum dry density corresponding to optimum moisture content. Similarly, swelling potential at different fly ash contents were studied and compared with small-strain stiffness parameters.

2 Experimental Investigations

2.1 Materials

The soil tested for this investigation were sampled from Vidarbha region of India. Table 1 shows the physio-mechanical properties of expansive soil. The soil classified according to AASHTO and the Unified Soil Classification System (USCS) is A-7-6 and CH, respectively. Further, the soil sample was examined for its compaction characteristics [5, 6] to obtain the maximum dry density corresponding to its optimum moisture content. The standard Proctor test was conducted by replacing the soil with different fly ash percentage as 2, 4, and 8 up to 20%. The compaction curve for all the cases is presented in Fig. 1. The composition of fly ash varies from place to place due to the quality of coal and operational characteristics of industry. The fly ash collected from Sipat Thermal Power Plant, India, was used in this study. The fly ash was characterized and classified as Class F [5].

Table 2 shows the physiochemical properties of fly ash obtained from the chemical composition using X-ray fluorescence (XRF) test. The cylindrical soil specimens having aspect ratio as 2 were prepared using cylindrical mold of size 50 mm diameter and 100 mm length. All the soil specimens were prepared at optimum moisture content corresponding to its known dry density using results of

Table 1 Physio-mechanical parameters of expansive soil

Properties	Value
Specific gravity	2.66
Maximum dry density (kN/m^3)	15.7
Liquid limit (%)	69
Plastic limit (%)	35
OMC (%)	21.4
D_{50} (mm)	0.051
FSI (%)	90

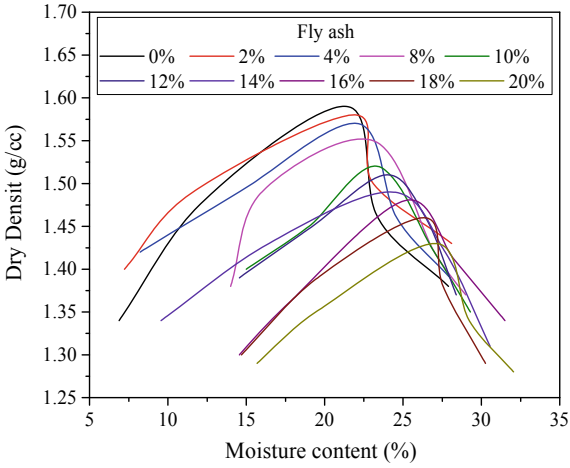

Fig. 1 Compaction characteristics of soil specimen at different fly ash content

Table 2 Physiochemical properties of class F fly ash

Properties	Values
Specific gravity	2.09
Specific surface area	368.6 m^2/kg
Particle size range	37–420 μm
Median particle size	152.4 μm
SiO_2	50.36
Al_2O_3	24.69
Fe_2O_3	7.45
CaO	7.59
K_2O	0.79
MgO	1.26
Na_2O	0.06
TiO_2	1.45
SO_3	0.09
P_2O_5	0.54
Loss on ignition	5.09

compaction curve, and fly ash was added to the soil in varying percentage by weight from 2 to 20% to perform bender element test.

2.2 Experimental Test Setup

The test setup consists of a transmitter and a receiver bender element to transmit and to capture the electromechanical shear wave through the soil specimen [7]. Figure 2 depicts the schematic of experimental setup adopted for the present study. The transmitter element is excited using single-cycle sinusoidal transverse motion using frequency pulse generator, and the response of the transmitter is recorded at the receiver bender element located at another end of specimen using a data acquisition system, and data is further processed through the computer. The wave travel time is then calculated by knowing the tip–tip distance between transmitter and receiver [8, 9].

3 Results

Received waveforms were interpreted by adopting the most popular time domain method as peak to peak of received and transmitted signals as shown in Fig. 3. The shear wave velocity and the small-strain shear modulus can be measured as

$$V_s = L_{tt}/\Delta t \tag{1}$$

$$V_s = \sqrt{G_{max}/\rho} \tag{2}$$

where V_s is the shear wave velocity, L_{tt} is the tip-to-tip length between transmitter and receiver, Δt is the time required to travel the waveform from transmitter to

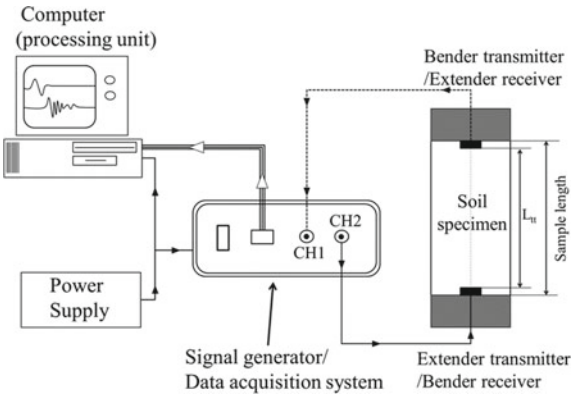

Fig. 2 Schematic of experimental setup

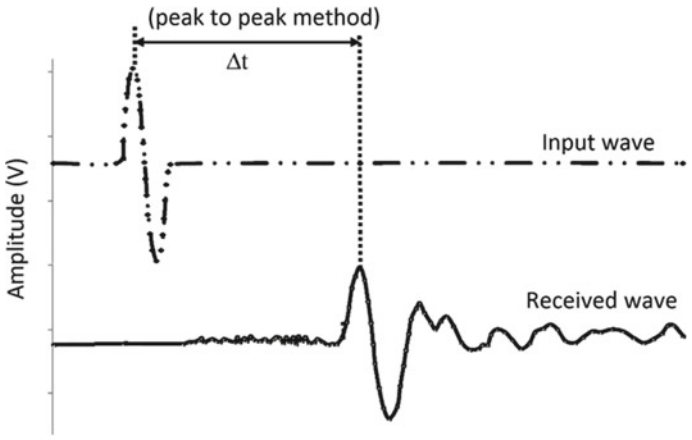

Fig. 3 Interpretation technique for transmitted and received waveforms

receiver, and ρ is the density of the soil specimen, respectively [10–13]. The shear wave velocity using bender element test is determined in untreated and treated soil specimens using Eq. 1, and the small-strain shear modulus is determined using Eq. 2.

3.1 Effect of Fly Ash Percentage on Free Swell Index (FSI)

Figure 4 shows the effect of addition of fly ash on the swelling characteristics of black cotton soil. Increase in the fly ash percentage results in the decreased free swell index. It is noteworthy to mention here that the replacement of 20% fly ash can reduces the free swelling index of black cotton soil by 20% from the initial value of 90%. This may be attributed toward the inhibition of the reactive swelling minerals in clay in the presence of fly ash mineral.

This indicates the drastic change in the performance of fly ash treated soil. The similar behavior was observed in previous studies, which implies the usefulness of the replacement of expansive soil with soil waste material such as fly ash [1, 9].

3.2 Effect of Fly Ash Addition on Small-Strain Shear Modulus of Soil

Figure 5 establishes the relation between small-strain shear modulus of black cotton soil with addition of different fly ash fractions at different curing periods. However, no such effect was observed for the curing time. Table 3 represents the percentage

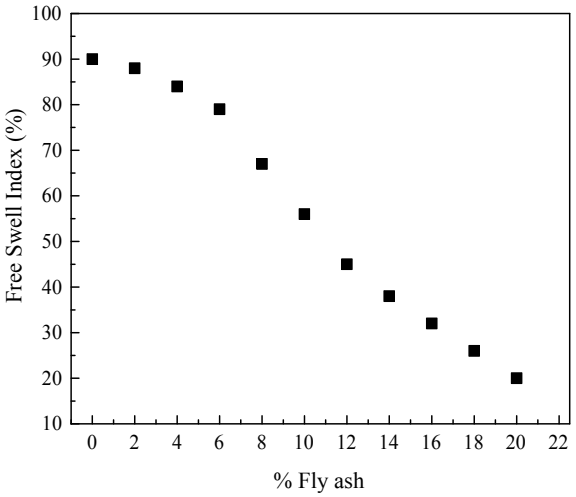

Fig. 4 Effect of fly ash inclusion on free swell index of soil

deviation in shear modulus value at different fly ash content and curing time. Curing period of three days period indicates very less increase in the modulus as 0.5 to 1%. On the other hand, 7 days curing period expresses increment from 2 to 4%. However, 28 days curing improves the modulus value up to 8% which is very less effective.

Figure 6 establishes the relation between free swell index and small-strain shear modulus for black cotton soil with different fly ash percentage and different curing periods. The reduction in FSI results in higher shear modulus, whereas increase in the fly ash content leads to the enhanced modulus which is inherent due to the presence of pozzolonic and cementitious minerals in fly ash [3]. However, the inclusion of fly ash rises the water consumption which makes this method uneconomical which must be considered while applying to field.

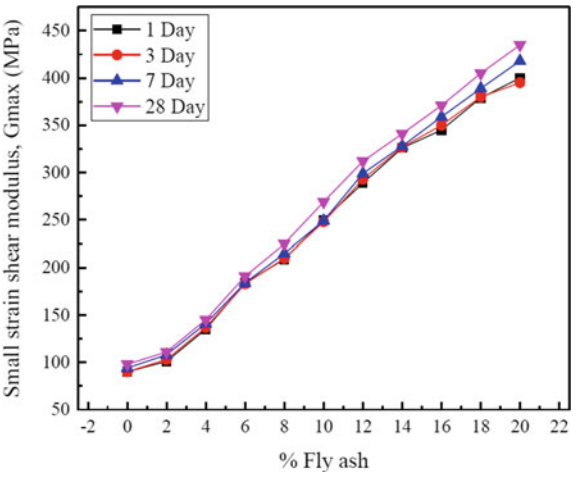

Fig. 5 Small-strain shear modulus variation with fly ash inclusion at different curing periods

Table 3 Percentage deviation in modulus value at different fly ash content and curing time

% fly ash	Shear modulus, G_{max} (MPa)		% deviation	Shear modulus, G_{max} (MPa)	% deviation	Shear modulus, G_{max} (MPa)	% deviation
	1 day	3 days		7 days		28 days	
0	90	90	0.00	92	2.22	97	7.77
2	101	103	1.98	105	3.96	111	9.90
4	135	137	1.48	141	4.44	145	7.41
6	184	183	−0.54	192	4.35	191	3.80
8	209	210	0.48	219	4.78	225	7.66
10	250	248	−0.80	259	3.60	269	7.60
12	289	293	1.38	299	3.46	312	7.96
14	326	327	0.31	336	3.07	341	4.60
16	345	350	1.45	359	4.06	371	7.54
18	379	380	0.26	389	2.64	405	6.86
20	400	395	−1.25	418	4.50	435	8.75

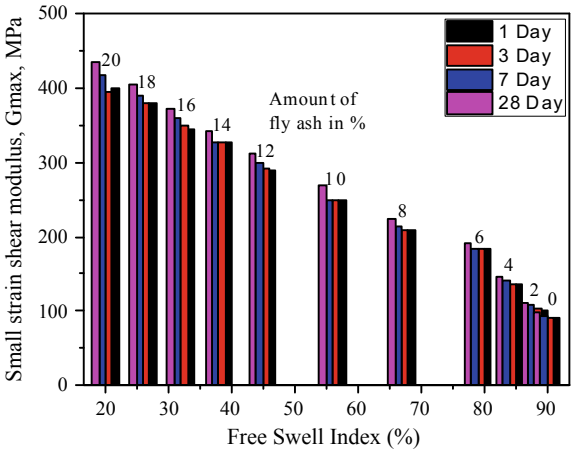

Fig. 6 Combined effect of swelling characteristics of fly ash treated soil on small-strain shear modulus with curing period

4 Conclusion

The present study is conducted to investigate the dynamic properties of fly ash treated black cotton soil. A significant portion of black cotton soil was replaced with fly ash and characterized in the laboratory for different index properties including proctor compaction. All the samples were conditioned using free swell index test. Further, the bender element tests were performed on soil specimens treated with different fly ash content. The outcome from the present study enables to understand the behavior of the soil to the shear stress at small-strain range. Some of the concluding remarks from the present analysis are as follows:

- The inclusion of fly ash from 0 to 20% in black cotton soil decreases the free swell index from 90 to 20%.
- The small-strain shear modulus reduction was observed with reduction in fly ash content in BC soil.
- The curing period does not spring up the stiffness of fly ash treated soil significantly.
- The method is quite useful and effective; however, the amount of moisture content required also increases with increased fly ash content, which must be considered during in-situ field practices.

Acknowledgements The authors would like to express their gratitude to Prof. Anjan Patel of VNIT Nagpur for providing encouragement and technical support.

References

1. Phani Kumar BR, Sharma RS (2003) Effect of fly ash on engineering properties of expansive soils. J Geotech Geoenv Eng 130(7):764–767. https://doi.org/10.1061/(ASCE)1090-0241(2004)130:7(764)
2. Correa-Silva M, Araújo N, Cristelo N, Miranda T, Gomes AT, Coelho J (2018) Improvement of a clayey soil with alkali activated low-calcium fly ash for transport infrastructures applications. Road Mater Pavement Des 1–15. https://doi.org/10.1080/14680629.2018.1473286
3. Kim B, Prezzi M, Salgado R (2005) Geotechnical properties of fly and bottom ash mixtures for use in highway embankments. J Geotech Geoenv Eng 131:914–924. https://doi.org/10.1061/(ASCE)1090-0241(2005)131:7(914)
4. Gokhan I, Nazli Y, Takaaki K (2003) Experimental investigation of dynamic response of compacted clayey soils. Geotech Test J 26:1–17. https://doi.org/10.1520/GTJ11328J
5. ASTM C618-03 (2003) Standard specification for coal fly ash and raw or calcined natural Pozzolan for use in concrete. ASTM International, West Conshohocken, PA
6. ASTM D698-12e2 (2012) Standard test methods for laboratory compaction characteristics of soil using standard effort (12 400 ft-lbf/ft3 (600 kN-m/m3)). ASTM International, West Conshohocken, PA
7. Patel A, Mehta A, Ingale R, Bhanarkar K (2018) Modeling of permeability in stratified sands using a wave-propagation method. Int J Geomech 18(5)
8. Ingale R, Patel A, Mandal A (2017) Performance analysis of piezoceramic elements in soil: a review. Sensors Actuators A Phys 262:46–63. https://doi.org/10.1016/j.sna.2017.05.025
9. Patel A, Ingale R, Bhanarkar KB, Mandal A (2018) Poisson's ratio of layered soils at different confining stresses using bender/extender elements. Soil Mech Found Eng 1–7
10. Lin B, Cerato AB, Megan A, Madden M (2013) Effect of fly ash on the characteristics of expansive soils in Sudan effect of fly ash on the characteristics of expansive soils in Sudan. Environ Eng Geosci XIX:85–94
11. Patel A, Ingale R, Mandal A (2020) Measurement of wave velocities in compacted clay using bender/extender and accelerometer: an experimental and numerical approach. Measurement 157:107676. https://doi.org/10.1016/j.measurement.2020.107676
12. Patel A, Singh D, Singh K (2010) Performance analysis of piezo-ceramic elements in soils. Geotech Geol Eng 28(5):681–694
13. Patel A, Bartake P, Singh D (2009) An empirical relationship for determining shear wave velocity in granular materials accounting for grain morphology. Geotech Test J 32(1):1–10

Macroscopic Analysis of Traffic Flow Behaviour on Multilane Highways Under Heterogeneous Traffic Conditions

Kanchumurty Anusha, Poojari Yugendar, and S. Moses Santhakumar

Abstract Traffic flow behaviour is a complex phenomenon and needs better understanding and concepts for its analysis. The highways in India normally operate under mixed traffic conditions, and the driving behaviour varies from one place to another. Macroscopic models which are quite suitable for describing the behaviour of entire stream and further accepted worldwide for estimation of capacity. The present study demonstrates the dynamic nature of PCU factors on two-way two-lane highways under highly heterogeneous traffic composition. Dynamic PCU's were estimated based on speed and size of vehicle type in the traffic stream with respect to a standard passenger car. The PCU values obtained in this study were compared with the existing static PCU's to get an overview of how the PCU varies when dynamics is involved. The present study also analyses the macroscopic traffic flow behaviour such as capacity and speed flow modelling on multilane highways. The VISSIM model parameters those were sensitive to capacity are calibrated based on the traffic composition observed in field by taking measure of effectiveness as traffic volume, speed and capacity. Validation of model was also performed by the same methodology with the help of VISSIM model on four-lane divided highways.

Keywords Capacity · Traffic flow · Microscopic simulation · VISSIM

K. Anusha · S. M. Santhakumar
Transportation Division, Department of Civil Engineering, National Institute of Technology Tiruchirappalli, Tiruchirappalli, Tamil Nadu 620015, India
e-mail: moses@nitt.edu

P. Yugendar (✉)
Department of Civil Engineering, Chaitanya Bharathi Institute of Technology, Gandipet, Hyderabad, Telangana 500075, India
e-mail: pyugendar_civil@cbit.ac.in

B. Laishram and A. Tawalare (eds.), *Recent Advancements in Civil Engineering*, Lecture Notes in Civil Engineering 172,
https://doi.org/10.1007/978-981-16-4396-5_55

1 Introduction

Traffic flow behaviour on multilane highways is a complex phenomenon and needs better conceptual and logical way of understanding and analysis. There are three main approaches to analyse the traffic flow behaviour. First is microscopic approach that considers the response of each individual vehicle in a disaggregate manner. The individual driver—vehicle combination was examined. Second is the mesoscopic approach which provides the medium detail and description of traffic flow. Third is the macroscopic approach which provides the medium detail and description of traffic flow. Third is the macroscopic approach that at the traffic flow behaviour in aggregate sense and also provides details of overall operational efficiency of the system. A number of parameters are also associated with traffic flow analysis approaches, and those are interrelated with one another to develop traffic flow models. Traffic flow models describe the motion of a traffic stream with the mathematical formulation. Traffic flow behavioural analysis describes theoretical relationships between the various traffic variables that define the characteristics of traffic streams. The variable describes the operational performance of roadway in terms of flow (Q), density (K) and speed (V) and defines the level of service experienced by drivers. The variables are basically related to each by the equation given below.

$$Q = K \times V \tag{1}$$

Multilane highways were defined as carriage ways with two or more lanes dedicated to one-way traffic with or without any physical separation between the opposite traffic streams. Unlike freeways and expressways, multilane highways do not have controlled access points. Therefore, the traffic flow on these highways was not as efficient as on freeways and expressways. Multilane highway traffic was frequently interrupted by the movement of traffic from facilities adjacent to these highways. These corridors were mainly provided to cater the need of high-density traffic moving between the centres of significant activities like commercial, industrial, trading, etc.

Traffic comprised of motorized and non-motorised vehicles of different size moves along the roadway without following lane discipline is termed as mixed traffic. In Indian roads, various vehicles share the same space of the road without segregation. In the absence of physical segregation, diversified mix of vehicles moves simultaneously with close interaction. The vehicular interactions generate a complex traffic phenomenon which in the absence of lane discipline adversely affects the capacity, stream speed and the level of service of the traffic facility along with the safe movement of vehicles. Designing of a facility was required to ensure smooth, safe and economic operations of traffic and understanding of traffic flow characteristics. Macroscopic traffic flow analysis includes the study of traffic flow behaviour from global perspective. Macroscopic traffic flow behaviour observed in developed countries under fairly homogeneous traffic conditions which were

formed as a basis for developing fundamental traffic flow models. In heterogeneous traffic, validity of these models is completely limited with respect to traffic and roadway conditions. On Indian roads, vehicles do not follow lane discipline and make their own virtual lanes instead of demarcated physical lanes. The macroscopic stream behaviour was affected by lateral and longitudinal movement of vehicles which was ignored in conventional models. Field data always limited in describing behaviour of traffic flow stream in generalized manner as far as mixed traffic is concerned.

Traffic simulation was found to be a powerful tool to overcome such problems. Microscopic simulation was best method which includes complete details about the individual vehicles types having greater impact on traffic flow operation. Hence, simulation model was used in the present study to generate traffic flow data that helps to analyse the mixed traffic condition.

2 Review of Literature

Various studies have been conducted around the world on traffic flow behaviour; this section provides a brief review of the studies conducted.

Schofield [15] investigated traffic behaviour in terms of speed, flow and capacity on a three-lane carriage way. The plots of speed–flow relationships showed wide band of speeds for any given level of flow and its width increased as the traffic level increased above 2000 vph. The observed phenomenon was defined by proportions of heavy vehicles, weather conditions, light conditions and traffic congestion. Vaziri [16] studied speed and traffic flow data of six-lane and eight-lane basic freeway sections in Iran. Six models, namely Greenshields, Greenberg, Underwood, Drake, Pipe and Munjal and Drew, were evaluated for the observed traffic data. As no significant difference was observed in the sum of square of errors of all the calibrated models, Greenshields model of speed density was selected due to its simplicity. After the calibration of model coefficients, equations were suggested for the observed data. The transportation manuals of developed countries are non-reliable for application in many developing countries like Iran. Minh et al. [14] developed speed–flow relationship for motorcycles on four-lane divided roads in Hanoi, Vietnam. MCU (motorcycle unit) was developed for each vehicle category to study the parameters of heterogeneous traffic. The speed–volume relationship for four locations (1 and 2 locations were on four-lane divided highways with raised median and 3 and 4 are on two-lane streets) were analysed. *F*-test and *t*-test were used to compare the speed variances of two locations. Maximum speed, minimum speed and mean speed values showed a reduction of 10 kmph at sections 3 and 4 with respect to sections 1 and 2. Frequency distribution of motorcycle speed corresponded to normal function at 5% level of significance. Chandra and Kumar [7] compared the five different methods of PCU estimation in mixed traffic condition and calculated PCU for six different vehicle types and revealed the demerits of each method in heterogeneous condition. Arasan and Koshy [2] analysed traffic data on

mid-block sections in Chennai city as a part of a microscopic simulation study to evaluate the level of service enjoyed by various vehicle categories in heterogeneous traffic conditions. One-way traffic on two-lane roads was simulated with different traffic volumes.

Velmurugan et al. [17] studied the changes in operating speed characteristics on various rural highways, based on the outcomes of Road User Cost Study (RUCS)-1982, 1992 and 2001. The comparison of results showed statistically significant increase in speeds of all vehicle categories on roads of different widths between 1982 and 2001 and also between 1982 and 1992. Basic desired speed (BDS) on four-lane divided highways with paved shoulders were similar to that on two-lane bi-directional roads with paved shoulders and representing insignificant impact of the geographical factors on BDS. Free speed of new technology cars was observed to be 21 to 28% higher than that of old ones for both two- and four-lane highways. Chandra and Kumar [9] studied the effect of road width on PCU values on two-lane highway on different sections. Average dimension and projected rectangular area are calculated for nine different vehicle categories at ten different sections. Arasan and Dhivya [1] proposed a new concept named area occupancy to describe the traffic density to overcome the limitations of occupancy for mixed traffic conditions. This concept was applied to mixed traffic conditions, and a relationship was developed between area occupancy and traffic stream speed and found to be logical indicating the appropriateness. Mallikarjuna et al. [12] collected microscopic data such as lateral distribution of vehicles, lateral gaps and longitudinal gaps using video image processing technique on a 10 m wide road and found that the lateral distribution of vehicles is influenced by traffic composition and traffic volume and also found that the difference in lateral positioning is influencing longitudinal gaps along with speeds and vehicle type.

Arasan and Arkatkar [3] analysed that traffic volume and roadway width were influencing the PCU values estimated from simulation. Traffic simulation model HETEROSIM was used to analyse the vehicular interactions at microscopic level of detail by simulating a heterogeneous traffic flow. Field data related to free speed, acceleration and lateral clearance between the vehicles, etc., were collected and analysed to input in simulation model. Calibration and validation of the simulation model were performed to study the effect of road width on PCU value. The PCU values estimated at different v/c ratios were increased significantly with increase in the width of the roadway. Chitturi and Benekohal [10] described a procedure for calibration of VISSIM for the freeways to obtain the desired capacity and queue length. The calibration procedure has been developed for freeway work zones application. The speed limit of 55 mph was fixed for free-flowing vehicles in work zones on interstate highways in Illinois. The range of capacity was evaluated with different CC0 and CC1 parameters. It was observed that the range of capacity tends to decrease as the value of CC1 is increasing. At CC1 values below 0.8 s, the variance in the capacity was ordered with magnitude more than the variance when the CC1 value is above 0.8 s. The parameter of CC1 below 0.8 s in VISSIM was not recommended.

In India, very few studies are available on for heterogeneous traffic conditions. However, these studies were also based on speed data of one or two sections which does not provide generalized speed behaviour of vehicular traffic on multilane highways. Fundamental traffic flow diagram is found to be most appropriate method for the determination of capacity, and it required sufficient amount of traffic flow data collected from the field. Many studies demonstrated that speed–flow curve was a better representation of traffic flow behaviour. The traffic flow simulation models and its application into modelling traffic flow operations have been gigantic from last few decades. Many researchers estimated PCU values using several parameters such as speed, delay, density, head way and queue discharge flow. But, all these studies are mainly related to the estimation of PCU for heavy vehicles under homogeneous traffic, and hence, these methods cannot be applied for mixed traffic. Thus, researchers introduced new parameters along with those used in homogeneous conditions for estimating PCU values of different types of vehicles in mixed traffic conditions analysis. Based on the literature review conducted in the study, it is evident that microscopic simulation tool VISSIM possesses better capabilities and features for modelling heterogeneous traffic flow operations other commercially available simulation packages. It allows to experiment with the required geometric and traffic conditions. Many authors have demonstrated different ways of calibrating the driver behaviour parameters of simulation model VISSIM. Therefore, VISSIM has been used to analyse the macroscopic traffic flow behaviour like capacity under mixed traffic conditions.

3 Field Data Collection

Field data was collected on two sections with bitumen concrete pavement on national highway. Locations of highways where data was collected exist on plain terrain with straight alignment, access control in both the directions of travel and are away from any influence of bus stop, parking, pedestrians or other side frictions. Both the sections were four-lane divided highway with 7.0 m (two lanes of each 3.5 m width) carriage way width and 1.5 m paved shoulder. First section was located near Head Post Office (NH210), Tiruchirappalli district, Tamilnadu. The second section was located near Mannarpuram, Trichy–Madurai highway (NH45), Tiruchirappalli district, Tamilnadu. Both the sections differ from the type of access control. Section-1 was partially access controlled, whereas section 2 was full control of access. A snap shot of section I (Head Post Office) and section 2 (Mannarpuram) is shown in Fig. 1.

Traffic survey was conducted on both the sections to record the operations of vehicular traffic flow under clear weather conditions. Traffic volume count and speed data were collected using video graphic technique. A camera mounted on tripod was set to record the traffic flow data for about four hours from 09:00 AM to 01:00 PM on both section 1 and section 2. A trap length of 60 m was selected for

Fig. 1 Section 1 and section 2

collecting spot speeds of vehicles. Two thick white lines were marked across the road width for one direction using a self-adhesive cloth tape about 60 m apart to act as reference lines for the trap length.

4 Data Extraction

Traffic survey was conducted on both the sections to record the operations of vehicular traffic flow under clear weather conditions. Traffic volume count and speed data was collected using video graphic technique. The collected data from field were extracted with the aid of traffic data extractor software. Speed of individual type of vehicles was measured by noting down the time taken by a vehicle to cross the longitudinal trap length using a stop watch of 0.01 s accuracy. Classified traffic volume counts and speed data were obtained at every five-minute interval from recorded film. Traffic data extractor software developed by the IIT Bombay was employed for the purpose to obtain speed and volume data. The vehicles present in the traffic stream were classified into the following six vehicle types such as car (4W), motorized two wheelers (2W), low commercial vehicle (LCV), motorized three wheelers (3W), heavy vehicle (HV) and bus (B). The physical sizes of the different types of vehicles were given in Table 1.

Vehicle counting and speed extraction were done using the traffic data extractor software from the recorded film as shown in Fig. 2. Speeds were also measured manually by taking a sample of data observed directly during field survey, and the

Table 1 Vehicle type, dimension and their projected areas

Vehicle type	Notation	Width (m)	Length (m)	Projected area (m^2)
Motorized two wheeler	2W	0.7	1.9	1.4
Car/jeep	4W	1.6	3.9	6.3
Light commercial vehicle	LCV	1.9	6.8	12.9
Heavy vehicle	HCV	2.4	9.5	22.6
Motorized three wheeler	3W	1.4	3.2	4.5

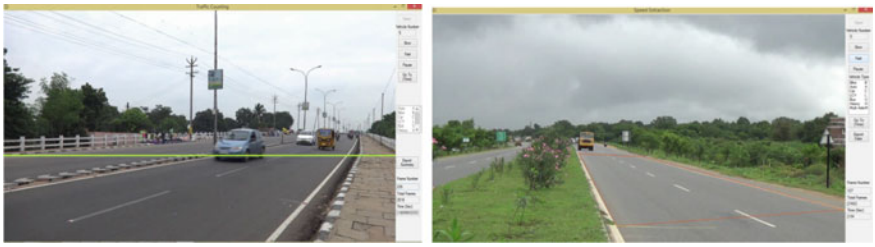

Fig. 2 Vehicle counting and speed using traffic data extractor software

error of the software was observed which was very less. Hence, data obtained from the software was used for the study. Four calibration points were given which are used as reference lines for speed extraction.

5 Results and Analysis

The results of field data analysis carried out and the study are presented in this section. Figure 3 shows the composition of different vehicle types on section 1 (Head Post Office) and section 2 (Mannarpuram). It can also be observed that there was higher two-wheeler proportions on section 1 and higher proportion of cars on section 2. Two-wheeler proportions were about 50% on section 1, whereas on section 2 the proportion is about 27%. High proportions of heavy vehicles were observed on section 2. Three-wheeler proportions were less on both the sections. Figure 4 shows the comparison of speeds on two sections. It can be observed that speeds on section 1 are less than speeds on section 2.

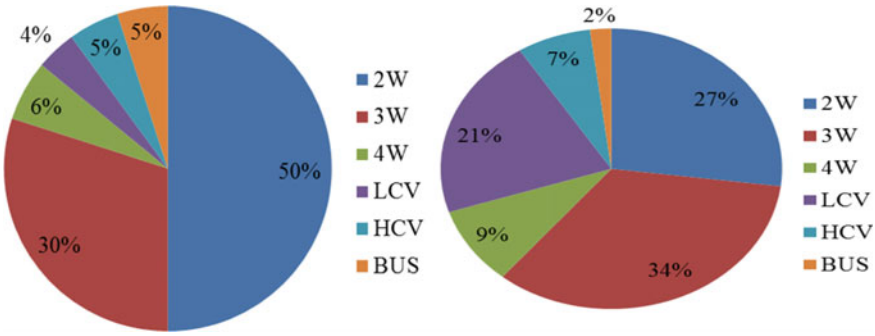

Fig. 3 Vehicular composition on sections 1 and 2

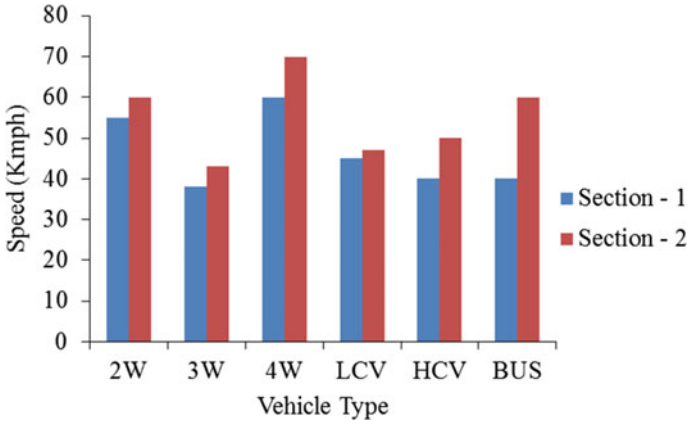

Fig. 4 Comparison of speeds on section 1 and section 2

6 Estimation of PCU Factors

The results of field data analysis carried out and the study are presented in this section. Figure 3 shows that the composition of different traffic volume obtained under mixed traffic conditions was required to convert into uniform passenger car units (PCU). The PCUs were estimated based on speed and area ratio of subject vehicle. The equation used to estimate the PCU of subject vehicle is given Eq. (2).

$$\mathrm{PCU}_i = \frac{\frac{V_C}{V_i}}{\frac{A_C}{A_i}} \tag{2}$$

where PCU_i is the passenger car value of the *i*th type of vehicle, speed ratio of car to the *i*th vehicle, area of the car to the *i*th vehicle, V_c is the speed of small car in kmph, V_i is the speed of *i*th vehicle type in kmph, A_c is the projected area of the small car and A_i is the projected area of the *i*th vehicle type.

In the above equation, speed ratio is a ratio of average speed of vehicle type which is a dynamic quantity and depends up on composition of traffic, whereas area ratio is static in nature which depends up on type of vehicle mixed in composition. The area ratios of vehicle type were estimated based on the dimensions of each category of vehicle. Projected areas of all vehicles considered in the present study are given in Table 1. The average PCU values of each vehicle types calculated at section 1 are presented in Fig. 5.

The PCU values estimated for vehicle types 4W, HV, B, 2W, 3W and LCV were analysed to see its variation along with traffic volume and speeds.

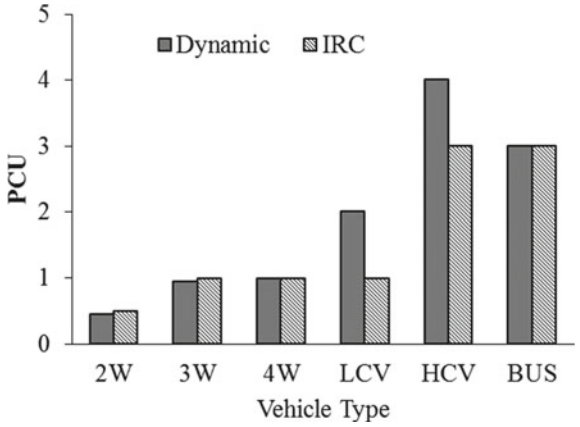

Fig. 5 PCU values at section 1

7 Estimation of Capacity

The estimated PCU factors of each vehicle type were multiplied to their respective volumes, and total volume in PCU/hr was measured. Once the total traffic volume converted to PCU, stream speed was obtained at corresponding volume at the same interval. Weighted average mean stream speeds were estimated by using Eq. (3) at five minute interval.

$$\text{Stream Speed} = \frac{\sum \text{Speed of individual vehicle} \times \text{volume of that vehicle category}}{\text{total traffic volume in five minute interval}} \tag{3}$$

Speed and volume relationship was established to determine the capacity of section 1 which is near Head Post office (NH 210). It was observed that field data did not reach maximum volume and an incomplete shape of speed flow curve was obtained. Therefore, complete shape of curve was drawn using theoretical fundamental relation between speed–flow and density. Speed–flow relation in section 1 was shown in Fig. 6. From figure, the capacity of four-lane section with 1.5 m paved shoulders was determined as 5000 PCU/hr/dir on section 1.

8 Simulation

VISSIM is a microscopic traffic simulation developed based traffic behaviour. It is used to analyse the public transportation functions and operations. This simulation consider vehicle and driver units as single units. It was developed by using car following model and rule-based algorithm. Free driving, approaching, following and breaking are four driving modes. Multiple simulations of six runs were carried

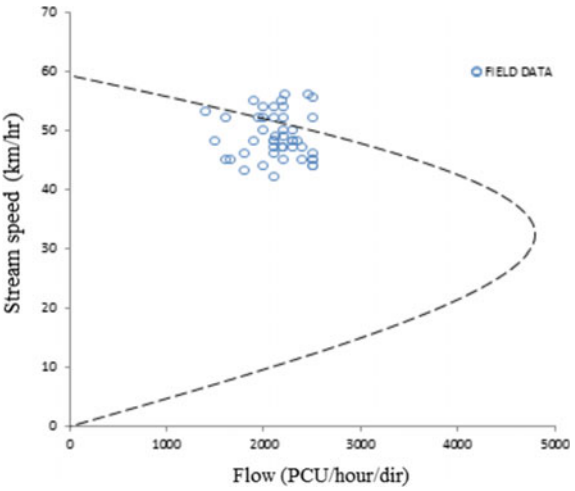

Fig. 6 Speed–flow curve on section 1

out, and average travel time for each section and delay for each vehicle category were calculated. Simulations with and without proper speed change lanes were analysed and compared. The simulation was run for a period of one hour (peak hour). From the simulation results, it can be observed that average speed obtained using VISSIM is 57 kmph and average speed of vehicles, i.e. stream speed from field data is 55 kmph. Hence, it was observed that the average speeds estimated using VISSIM were little bit more but the error was very less. It can be considered and can be used for calibration and validation of model.

9 Conclusions

Field data was collected by video graphic method using cameras. The camera was installed at high rise building to avoid occlusions. Vehicles were classified into seven categories as 2W, 3M, 4W, LCV, HCV and bus. The speed–flow data was extracted from video and density was measured by using Eq. (1). The speeds were observed more on section 2 compared to section 1 because of absence of congestion. The dynamic PCU values were calculated for each vehicle type by using Eq. (2). Mixed traffic volume obtained from field was converted into uniformed traffic flow using estimated values of PCUs. Speed–flow curve was established with field data, and capacity of four-lane divided section was determined. Dynamic PCU values and IRC PCU values were compared. The values are observed more in the case of dynamic method as compared to IRC method. The study uses microscopic simulation model VISSIM to generate speed flow data for analysis of macroscopic behaviour. The speeds estimated using field data and speeds obtained using VISSIM were compared, and the error was observed minimum.

References

1. Arasan VT, Dhivya G (2010) Methodology for determination of concentration of heterogeneous traffic. J Transp Syst Eng 10(4):118–125
2. Arasan VT, Koshy R (2005) Methodology for modeling highly heterogeneous traffic flow. J Transp Eng 131(7):544–551
3. Arasan VT, Arkatkar SS (2008) Simulating passenger car unit for vehicles in heterogeneous traffic. Traffic Eng Control 49(11):436–440
4. Ashutosh A, Velmurugan S, Madhu E (2013) Methodological framework towards roadway capacity estimation for Indian multi-lane highways. Proc Soc Behav Sci 104:477–486
5. Brilon W, Ponzlet M (1996) Variability of speed-flow relationships on German autobahns. Transportation Research Record, Transportation Research Board, National Research Council, Washington DC, vol 1555, p 91
6. Chandra S (2003) Estimation of capacity of urban roads. J Ind Road Cong 150:98–120
7. Chandra S, Kumar P (1996) Effect of shoulder condition on highway capacity. In: Proceedings of the international seminar on civil engineering practices in twenty first century, Roorkee, India, pp 512–519
8. Chandra S, Kumar U (2002) Effect of lane width on capacity under mixed traffic conditions in India. J Transp Eng 129:155–160
9. Chandra S, Kumar U (2003) Effect of lane width on capacity under mixed traffic conditions in India. J Transp Eng ASCE 129:155–160
10. Chitturi MV, Benekohal RF (2008) Calibration of VISSIM for freeway. In: Proceedings of 87th TRB annual meeting, transportation research board, National Research Council, Washington D.C.
11. Greenshields BD (1934) A study of traffic capacity. Proc Highw Res Board 14:448–477
12. Mallikarjuna C, Ramachandra RK, Naga VSK (2010) Analysis of microscopic data under heterogeneous traffic conditions. J Transp Syst Eng 25(3):262–268
13. Menneni S, Sun C, Vortisch P (2008) Micro simulation calibration using speed-flow relationships. Transp Res Record J Transp Res Board 2088(1):1–9
14. Minh CC, Sano K, Matsumoto S (2005) The speed, flow and headway analyses of motorcycle traffic. J Eastern Asia Soc Transp Stud 6:1496
15. Schofield M (1986) Speed, flow and capacity on the M6 motorway. Traffic Eng Control 27 (10):509
16. Vaziri M (1995) Traffic flow characteristics for Iranian freeways. In: Proceedings, international conference on new horizons in roads and road transport (ICORT-95), December 11–14, Indian Institute of Technology, Roorkee, India, pp 1398–1403
17. Velmurugan S, Errampalli M, Reddy TS (2002) Changing operating speeds on rural highways. In: Proceedings of the emerging trends in road transport (RORTRAN), vol II, IIT, Kharagpur, India, pp 5.29–5.40

Solving Fuzzy Shortest Path Problem with Decision Maker's Perspective

Vishnu Pratap Singh, Kirti Sharma, and Udit Jain

Abstract The shortest path problem is a very well-known optimization problem where the purpose is to find a path originating from the source node and terminating at vertex node in such a way that the sum of edge weights of constituent edges is minimum. This paper presents shortest path problem in an imprecise environment, edge weights being represented by Interval Type 2 Triangular fuzzy number. This paper introduces fuzzy preference ordering between any two Interval type 2 triangular fuzzy numbers and uses that to choose a path according to varying degrees of optimism and pessimism of decision maker. A numerical example has also been solved to present the effectiveness of the method presented and explains how the path changes as the degree of optimism and pessimism varies.

Keywords Shortest path problem · Interval type 2 triangular fuzzy number · Network · Decision maker

1 Introduction

In a well-connected network, the basic problem of finding a path which is shortest between any two desired nodes [1] finds its application in various real life problems. Mathematically, this problem is termed as shortest path problem [1] and there are various algorithms developed by researchers like Bellman, Dijkstra's, etc. [2, 3]

V. P. Singh (✉) · K. Sharma
Department of Mathematics, Visvesvaraya National Institute of Technology Nagpur, Nagpur, India
e-mail: vpsingh@mth.vnit.ac.in

U. Jain
Department of Civil Engineering, Visvesvaraya National Institute of Technology Nagpur, Nagpur, India
e-mail: uditjain@civ.vnit.ac.in

B. Laishram and A. Tawalare (eds.), *Recent Advancements in Civil Engineering*, Lecture Notes in Civil Engineering 172,
https://doi.org/10.1007/978-981-16-4396-5_57

which solves the problem efficiently and effectively in deterministic environment. Real life applications of shortest path problem involve various phenomenons such as randomness and uncertainty, which makes the problem a bit more realistic and hence tough to solve. Uncertainty in such problems is least avoidable [4] and while taking decisions in uncertain environment, the risk taking nature of decision maker (DM) affects the decision a lot. An optimistic decision maker is the one who can take risk in the form of uncertainty but a pessimistic decision maker always tries to avoid uncertainty, thus, may take a decision which is not optimal, but associated uncertainty is lesser as compared to the optimal solution.

In this work, a fuzzy shortest path problem [5] has been considered where edge lengths have been represented by using Interval Type 2 Triangular Fuzzy numbers (IT2TFNs). A shortest path is obtained first by modifying one of the famous algorithms as given by [6] and then the perspective of decision maker is applied on that decision and it has been observed that the perspective of DM has a high influence on the final decision he/she should take about the shortest path to be followed. For example, in case of higher uncertainty, a pessimistic decision maker might like to change his/her decision because of his/her risk adverse nature, whereas an optimistic decision maker may take risk and may not change their decision.

In the literature, various researchers have discussed fuzzy shortest path problem (FSPP) and suggested methods like [2, 7, 8] to solve the FSPP. The task which separates FSPP from SPP is the comparison of two fuzzy numbers. Ordered relation like less than $<$, greater than $>$ are clearly defined in the literature of real numbers but such a comparison method does not exist for fuzzy numbers. Various researchers have introduced their own comparison measures for comparing two fuzzy numbers. Chein and Hsieh [9] proposed a comparison method based on PGMIR expression. A method based on centroid of fuzzy numbers has been proposed by [10]. Calculating similarity between any two uncertain numbers is also a big task and has been solved by many researchers. Sengupta and Pal discussed about the comparison of interval numbers in [11] and discussed how the decisions of DM change as the degree of their optimism and pessimism varies [12]. In that work, the profits or costs were given in the form of intervals. Inspired by [13–16], in this work, a similar acceptability index has been generated which compares the degree of acceptability of a particular IT2TFN with respect to another IT2TFN when the perspective of DM changes.

This paper is structured in the following way: In Sect. 2, a brief discussion on the basic concepts of the fuzzy set theory is given; Sect. 3 presents the newly formulated value judgement index for the comparison of IT2TFNs and its relation with decision maker. Section 4 presents the description, mathematical model of the problem and the algorithm used in this paper to solve the FSPP. A numerical example has been presented in Sect. 5 and the last section presents the concluding remarks.

2 Preliminaries and Concepts

2.1 Fuzzy Set [17]

Definition 1. If X is a universal set and x is a particular element of X, then a fuzzy set $\tilde{A}$ on X is defined as a collection of ordered pairs.

$$\tilde{A} = \left\{ \left(x, \mu_{\tilde{A}}(x) \right) : x \in X \right\} \tag{1}$$

where

$$\mu_{\tilde{A}}(x) : X \to [0, 1]. \tag{2}$$

is known as membership function and represents the degree of membership of $x \in X$ in the fuzzy set $\tilde{A}$.

2.2 Fuzzy Number [18]

Definition 2. A fuzzy set $\tilde{A}$ on $\mathbb{R}$ qualifies for a fuzzy number if given all three properties are satisfied:

1. Fuzzy set must be normal, i.e. $\exists\, x$ such that sup $\mu_{\tilde{A}}(x) = 1$, where sup stands for supremum.
2. The support of the fuzzy set, i.e. set of all the elements with non-zero degree of membership must be bounded.
3. α level set, i.e. set of all the elements with membership degree greater than α, must be closed interval for $\alpha \in [0, 1]$.

2.3 Triangular Fuzzy Number [18]

Definition 3. A fuzzy number is said to be a triangular fuzzy number if the graph of its membership function is triangular. The membership function of a triangular fuzzy number is denoted by Eq. (3).

$$\mu_{\tilde{A}}(x) = \begin{cases} 0 & \text{if } x < a \\ \frac{x-a}{b-a} & \text{if } a < x < b \\ \frac{c-x}{c-b} & \text{if } b < x < c \\ 0 & \text{if } x > c \end{cases}. \tag{3}$$

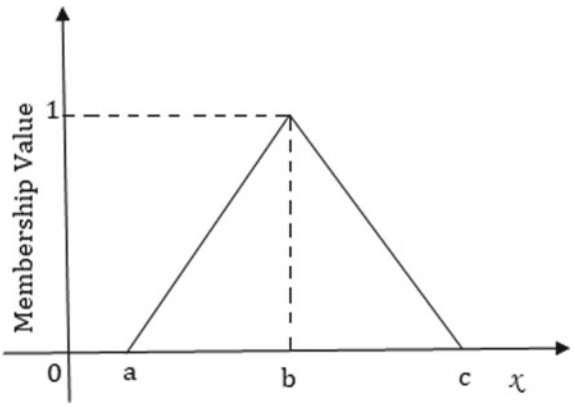

Fig. 1 Triangular fuzzy number (a, b, c)

This triangular fuzzy number is denoted by (a, b, c). The graph of the membership function of a triangular fuzzy number is given by Fig. 1.

2.4 Interval Type 2 Triangular Fuzzy Number [19]

Definition 4. An Interval Type 2 Triangular fuzzy number (IT2TFN), $\tilde{\tilde{A}}$ is defined on the interval $[\overline{a}, \overline{c}]$, its lower membership function, takes the value equal to $\underline{h} \in [0, 1]$ at $\underline{b}$ and $\overline{h} \in [0, 1]$ at $\overline{b}$, respectively, where $\overline{a} \leq \underline{a} \leq \underline{b} = \overline{b} \leq \underline{c} \leq \overline{c}$.

Thus, IT2TFN, $\tilde{\tilde{A}}$ is notated as $\tilde{\tilde{A}} = (\underline{A}, \overline{A}) = ((\underline{a}, \underline{b}, \underline{c}), (\overline{a}, \overline{b}, \overline{c}))$. A graphical interpretation of IT2TFN, $\tilde{\tilde{A}}$ is shown in Fig. 2.

2.5 Arithmetic Operations on IT2TFNS

If $\tilde{\tilde{A}} = ((\underline{a}, \underline{b}, \underline{c}), (\overline{a}, \overline{b}, \overline{c}))$ and $\tilde{\tilde{B}} = ((\underline{p}, \underline{q}, \underline{r}), (\overline{p}, \overline{q}, \overline{r}))$ are two IT2TFNs, then

1. Addition:

$$\tilde{\tilde{A}} \oplus \tilde{\tilde{B}} = ((\underline{a} + \underline{p}, \underline{b} + \underline{q}, \underline{c} + \underline{r}), (\overline{a} + \overline{p}, \overline{b} + \overline{q}, \overline{c} + \overline{r})). \tag{4}$$

2. Subtraction:

$$\tilde{\tilde{A}} - \tilde{\tilde{B}} = ((\underline{a} - \underline{r}, \underline{b} - \underline{q}, \underline{c} - \underline{p}), (\overline{a} - \overline{r}, \overline{b} - \overline{q}, \overline{c} - \overline{p})). \tag{5}$$

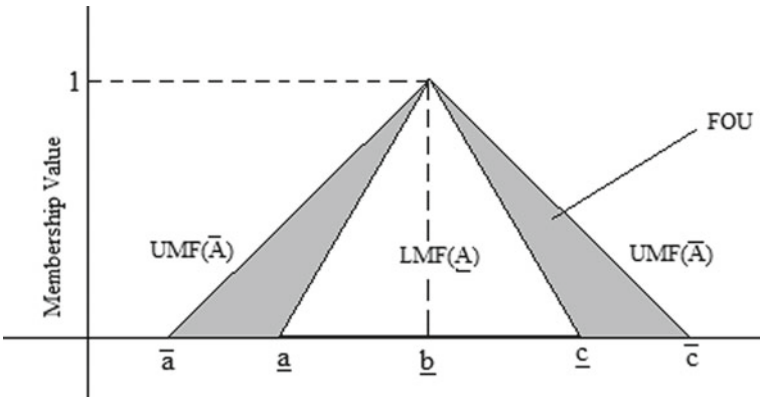

Fig. 2 A type 2 triangular fuzzy number

3. Scalar Multiplication:

$$k \otimes \tilde{\tilde{A}} = \begin{cases} ((k\underline{a}, k\underline{b}, k\underline{c}), (k\overline{a}, k\overline{b}, k\overline{c})) & \text{if } k \geq 0 \\ ((k\underline{c}, k\underline{b}, k\underline{a}), (k\overline{c}, k\overline{b}, k\overline{a})) & \text{if } k < 0 \end{cases}. \tag{6}$$

2.6 *Parametric Graded Mean Integration Representation [19]*

Let $L(x)$ and $R(x)$ be the left and right functions of a fuzzy number $\tilde{A}$, then the GMIR representation of $\tilde{A}$ is given by Eq. (7)

$$P(\tilde{A}) = \frac{\int_0^h \frac{h}{2}(L^{-1}(x) + R^{-1}(x))\mathrm{d}x}{\int_0^h x \, \mathrm{d}x}. \tag{7}$$

where $0 < h \leq 1$ is height of $\tilde{A}$. For the IT2TFN $\tilde{\tilde{A}} = (\underline{A}, \overline{A}) = ((\underline{a}, \underline{b}, \underline{c}), (\overline{a}, \overline{b}, \overline{c}))$, the PGMIR expression is

$$P(\tilde{\tilde{A}}) = \frac{1}{12}(\underline{a} + \underline{c} + \overline{a} + \overline{c}) + \frac{1}{3}(\overline{b} + \underline{b}). \tag{8}$$

2.7 Distance and Similarity Measure Between Two IT2TFNs

An IT2TFN can be defuzzified by using its PGMIR expression. The distance between any two IT2TFNs can be defined as the absolute difference in the value of their PGMIR expression. So, if $\tilde{\tilde{A}}$ and $\tilde{\tilde{B}}$ are given two IT2TFNs, then the distance between them is given by

$$D(\tilde{\tilde{A}}, \tilde{\tilde{B}}) = \left| P_{\tilde{\tilde{A}}} - P_{\tilde{\tilde{B}}} \right|. \tag{9}$$

Various researchers have worked upon finding the formula for similarity measure, and a very common intuition for similarity measure is regarding the inverse of the distance measure between two IT2TFNs.

3 The Value Judgement Index for Comparison of Two IT2TFNs

In deterministic environment, quantities are given in crisp form, thus making it easier to compare such quantities and as a result, making the task of decision maker easier, but if representation of quantities involves uncertainty in them, then various researchers have introduced various methods for comparison of these uncertain numbers, and such kind of uncertainty also affects the decision of DM. There are various traits of decision maker, the DM may be risk averting in nature or may be risk taking in nature. In an environment, where decisions are taken by DMs on certain basis, DMs are basically classified into 2 categories, namely pessimistic and optimistic. The risk averting DM is known as pessimistic, whereas risk taking DM is known as optimistic. Uncertainty of real world can be handled by using fuzzy set theory and this section comprises of the effect of uncertainty on the decision of DM.

Definition 5. The proposition $\tilde{\tilde{A}} < \tilde{\tilde{B}}$ is accepted only when PGMIR expression of $\tilde{\tilde{A}}$ is less than the PGMIR expression of $\tilde{\tilde{B}}$.

Let $\mathscr{F}$ be the set of all IT2TFNs on $\mathbb{R}$ then a value judgement index $A(\tilde{\tilde{A}} < \tilde{\tilde{B}})$ representing degree of acceptability of IT2TFN $\tilde{\tilde{A}}$ to be lesser than $\tilde{\tilde{B}}$ is defined by Eq.

$$\mathrm{A}(\tilde{\tilde{A}} < \tilde{\tilde{B}}) = \frac{P_{\tilde{\tilde{A}}} - P_{\tilde{\tilde{B}}}}{U(\tilde{\tilde{B}}) + U(\tilde{\tilde{A}})}. \tag{10}$$

where $U(\tilde{\tilde{B}}) + U(\tilde{\tilde{A}}) \neq 0$.

In Eq. (10), $P_{\tilde{\tilde{A}}}$ and $U(\tilde{\tilde{A}})$ represents the PGMIR expression and uncertainty of IT2TFN $\tilde{\tilde{A}}$, respectively.

Remark: If $\tilde{\tilde{A}} = (\underline{A}, \overline{A}) = ((\underline{a}, \underline{b}, \underline{c}), (\overline{a}, \overline{b}, \overline{c}))$, then $U(\tilde{\tilde{A}}) = \overline{c} - \underline{b}$.

If $A(\tilde{\tilde{A}} < \tilde{\tilde{B}}) = 0$ then the premise $\tilde{\tilde{A}} < \tilde{\tilde{B}}$ is accepted. If $0 < A(\tilde{\tilde{A}} < \tilde{\tilde{B}}) < 1$ then the premise is accepted with varying degree of satisfaction and when $A(\tilde{\tilde{A}} < \tilde{\tilde{B}}) > 1$, then the premise $\tilde{\tilde{A}} < \tilde{\tilde{B}}$ is accepted.

3.1 Preference Ordering According to Pessimistic DM's Perspective

Some assumptions which are used for shortest path problem according to a pessimistic decision maker's point of view are given below:

1. Minimum distance is provided more preference as compared to maximum distance.
2. For a pessimistic decision maker, less uncertainty is given higher preference.
3. If less distance is associated with more uncertainty, a decision -maker undergoes a trade-off between the two.
4. For a pessimistic decision maker, uncertainty is given more weight.

If $A(\tilde{\tilde{A}} < \tilde{\tilde{B}})$ is created for two IT2TFNs $\tilde{\tilde{A}}$ and $\tilde{\tilde{B}}$, then.

(a) $(\tilde{\tilde{A}}, \tilde{\tilde{B}}) \in S_1$ if $A(\tilde{\tilde{A}} < \tilde{\tilde{B}}) \geq 0$ and $U(\tilde{\tilde{A}}) < U(\tilde{\tilde{B}})$.

(b) $(\tilde{\tilde{A}}, \tilde{\tilde{B}}) \in S_2$ if $A(\tilde{\tilde{A}} < \tilde{\tilde{B}}) > 0$ and $U(\tilde{\tilde{A}}) > U(\tilde{\tilde{B}})$.

For FSPP, if $(\tilde{\tilde{A}}, \tilde{\tilde{B}}) \in S_1$, $\tilde{\tilde{A}}$ is always the best choice and this conclusion can be simply made on assumption 1 and 2, unless both are same. But, as in the manner above, some conclusions can't be made for $(\tilde{\tilde{A}}, \tilde{\tilde{B}}) \in S_2$ according to a pessimistic DM's perspective.

Depending upon situation, one of IT2TFN may be strictly preferred over another, or there may be a fuzzy preference ordering between two IT2TFNs.

For any pair $(\tilde{\tilde{A}}, \tilde{\tilde{B}}) \in S_2$, if $A(\tilde{\tilde{A}} < \tilde{\tilde{B}}) > 1$ then for the shortest path problem, $\tilde{\tilde{A}}$ is strictly preferred to $\tilde{\tilde{B}}$ If $A(\tilde{\tilde{A}} < \tilde{\tilde{B}}) = 0$ then $\tilde{\tilde{B}}$ is strictly preferred to $\tilde{\tilde{A}}$ since it has lesser uncertainty than $\tilde{\tilde{A}}$, and a pessimistic decision maker prefers lesser uncertainty. If $A(\tilde{\tilde{A}} < \tilde{\tilde{B}}) \in [0, 1]$, then there exists a fuzzy set $\tilde{A}'$ entailing the degree of rejection of $\tilde{\tilde{A}}$ while comparing $\tilde{\tilde{A}}$ and $\tilde{\tilde{B}}$.

The membership function of $\tilde{A}'$ is defined as

$$\mu_{\tilde{A}'} = \begin{cases} 1 & \text{if } P(\tilde{\tilde{A}}) = P(\tilde{\tilde{B}}) \\ \max\left\{0, \frac{P(\tilde{\tilde{B}}) - U(\tilde{\tilde{B}}) + U(\tilde{\tilde{A}}) - P(\tilde{\tilde{B}})}{P(\tilde{\tilde{B}}) - U(\tilde{\tilde{B}}) + U(\tilde{\tilde{A}}) - P(\tilde{\tilde{A}})}\right\} & \text{if } P(\tilde{\tilde{B}}) \geq P(\tilde{\tilde{A}}) \geq P(\tilde{\tilde{B}}) - U(\tilde{\tilde{B}}) + U(\tilde{\tilde{A}}) \cdot \\ 0 & \text{otherwise} \end{cases} \tag{11}$$

3.2 Effect of Decision Maker on the Degree of Rejection

For a pessimistic decision maker, the degree of rejection may vary as the degree of pessimism varies

$$\pi_{\tilde{A}'} = (\mu_{\tilde{A}'})^{1/M}. \tag{12}$$

Equation (12) gives the degree of rejection of $\tilde{\tilde{A}}$ as the degree of pessimism, M varies.

For an optimistic decision maker, the degree of rejection may vary as the degree of optimism varies

$$\pi_{\tilde{A}'} = (\mu_{\tilde{A}'})^{M}. \tag{13}$$

Equation (13) gives the degree of rejection of $\tilde{\tilde{A}}$ as the degree of optimism, M varies.

4 Methodology

4.1 Problem Description

We are given a connected network where s is the source node and d is the destination node. In the given problem, the arc lengths are given by IT2TFNs and the objective is to find a shortest path from shortest node to destination node. The graph under consideration is a directed graph and there may be various paths which starts from source vertex and terminate at destination vertex. The weights on various edges may represent various physical quantities like time required to traverse the edge, the distance of the edge or the cost required to traverse the edge. In real world situations, if the quantity represented by edge weight is the time taken to traverse the edge, then time may not be always crisp. It may depend upon various factors like number of stoppages on that certain edge, amount of traffic on the link or the

varying speed of the vehicle on that edge, and such factors are responsible for the addition of impreciseness in the problem and such factors bridge the gap between real life problem and their respective mathematical version. Though this imprecise nature of the problem can be handled by using fuzzy set theory and there are numerous areas where imprecise problems are being solved by using fuzzy set theory. This section describes the FSPP and a mathematical model for FSPP has been formulated and an algorithm for finding FSPL and FSP corresponding to a given network has been presented.

4.2 Mathematical Model

The mathematical model of the problem described can be given by:

Objective: Minimize: $\sum \tilde{\tilde{c}}_{ij}.x_{ij}$.

Where x_{ij} is an indicator function.

$$x_{ij} = \begin{cases} 1 & \text{if edge } ij \text{ is included in path} \\ 0 & \text{otherwise} \end{cases}. \tag{14}$$

Subject to:

$$\sum_j x_{ij} - \sum_i x_{ji} = \begin{cases} 1 & \text{if } i \text{ is source node} \\ -1 & \text{if } j \text{ is destination node} \\ 0 & \text{otherwise} \end{cases}. \tag{15}$$

4.3 Algorithm for Fuzzy Shortest Path

First, we find the set of paths which starts from source vertex and ends at destination vertex. Assume that there are k such paths in the network whose lengths are given by $\tilde{\tilde{L}}_i$, $i = 1, 2, \ldots, k$, then the algorithm to find the fuzzy shortest path is given by:

Step 1: Sort all the lengths according to their PGMIR expressions and form a list $Q = \{\tilde{\tilde{Q}}_1, \tilde{\tilde{Q}}_2, \ldots, \tilde{\tilde{Q}}_k\}$ where $\tilde{\tilde{Q}}_i = ((\underline{a}_i, \underline{b}_i, \underline{c}_i), (\overline{a}_i, \overline{b}_i, \overline{c}_i))$ for $i = 1, 2, \ldots, k$.
Step 2: Set $\tilde{\tilde{Q}}_1$ as the minimum length, represented by $\tilde{\tilde{L}}_{\min}$.
Step 3: Let $i = 2$.
Step 4: Calculate

$$\underline{b} = \overline{b} = \begin{cases} \underline{b} & \underline{b} \le \underline{a}_i \\ \frac{\underline{b}*\underline{b}_i - \underline{a}*\underline{a}_i}{\underline{b} + \underline{b}_i - (\underline{a}*\underline{a}_i)} & \underline{b} > \underline{a}_i \end{cases}.$$

$$\underline{a} = \min(\underline{a}, \underline{a}_i). \quad \overline{a} = \max(\overline{a}, \overline{a}_i).$$
$$\underline{c} = \min(\underline{c}, \underline{b}_i). \quad \overline{c} = \min(\overline{c}, \overline{b}_i).$$

Step 5: Set $\tilde{\tilde{L}}_{\min} = ((\underline{a}, \underline{b}, \underline{c}), (\overline{a}, \overline{b}, \overline{c}))$.
Step 6: Set $i = i + 1$.
Step 7: Repeat steps 4 to 6 until $i = k + 1$.
Step 8: Find the similarity degree between $\tilde{\tilde{L}}_{\min}$ and $\tilde{\tilde{L}}_i$ for all $i = 1, 2, \ldots, k$.
Step 9: The path with the highest similarity degree will be chosen as the shortest path.

5 Numerical Example

A classical network with IT2TFNs as edge weights representing the time required to traverse the edge is shown in Fig. 3. The objective is to find a shortest path from node 1 to node 6 in this network.

Here, a directed graph has been given where 1 is the source and 6 is the sink node. This example has been taken from Okada and Soper [20] and has been further modified from trapezoidal fuzzy numbers to IT2TFNs. There are various paths between our desired nodes but as a decision maker looking for optimum path, we want the path with least travel time. Moving forward according to algorithm, first we find all the paths between the desired nodes and then arrange all of them in increasing order according to their PGMIR values. The corresponding list is represented by Q and whose members according to their order are given by:

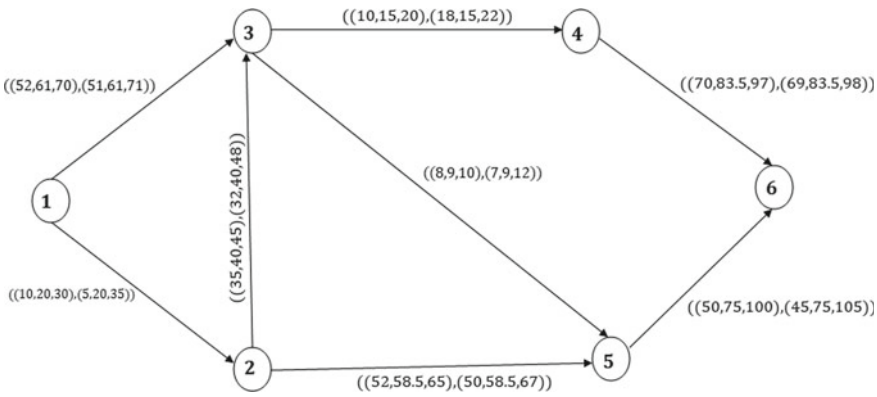

Fig. 3 Network

$\tilde{\tilde{Q}}_1 = ((103, 144, 185), (89, 144, 193))$ $\tilde{\tilde{Q}}_2 = ((110, 1455, 180), (103, 145, 187))$
$\tilde{\tilde{Q}}_3 = ((112, 153.5, 195), (100, 153.5, 207))$ $\tilde{\tilde{Q}}_4 = ((125, 158.5, 187), (114, 158.5, 203))$
$\tilde{\tilde{Q}}_5 = ((132, 159.5, 185), (128, 159.5, 191))$

Now, we set the first element of this list as shortest path length, i.e. we set $\tilde{\tilde{L}}_{\min} = ((103, 144, 185), (89, 144, 193))$. Moving forward, until all the paths have been operated upon, we keep on changing the value of minimum length as stated in the algorithm given above, and calculating the minimum length which has been observed here to be $((103, 120.80, 145), (89, 120.80, 145))$. Thereafter, we calculate the degree of similarity of minimum length which has been obtained by the procedure above with all the elements of set Q and it has been obtained as:

$s(\tilde{\tilde{L}}_{\min}, \tilde{\tilde{Q}}_1) = 0.0429$ $s(\tilde{\tilde{L}}_{\min}, \tilde{\tilde{Q}}_2) = 0.0411$
$s(\tilde{\tilde{L}}_{\min}, \tilde{\tilde{Q}}_3) = 0.0304$ $s(\tilde{\tilde{L}}_{\min}, \tilde{\tilde{Q}}_4) = 0.026$
$s(\tilde{\tilde{L}}_{\min}, \tilde{\tilde{Q}}_5) = 0.0205$

Since the degree of similarity is highest with $\tilde{\tilde{Q}}_1$, hence the shortest path is given by $1 \rightarrow 2 \rightarrow 3 \rightarrow 5 \rightarrow 6$ with corresponding length $((103, 144, 185), (89, 144, 193))$. In the example given above, the path $\tilde{\tilde{Q}}_2$ also has approximately the same degree of similarity as that of $\tilde{\tilde{Q}}_1$ Now, we see the effect of uncertainty on the degree of rejection of $\tilde{\tilde{Q}}_1$ according to varying degrees of optimism and pessimism of decision maker.

Consider $\tilde{\tilde{A}} = \tilde{\tilde{Q}}_1 = ((103, 144, 185), (89, 144, 193)$ and $\tilde{\tilde{B}} = \tilde{\tilde{Q}}_2 = ((110, 1455, 180), (103, 145, 187))$. The degree of rejection of $\tilde{\tilde{A}}$ is 0.928. According to a pessimistic decision maker, as the degree of pessimism, M, increases from 1 to 2, 2 to 4 and then 4 to 8, the degree of rejection of $\tilde{\tilde{A}}$ changes from 0.928 to 0.963, 0.963 to 0.9814 and then from 0.9814 to 0.9907, respectively. It can be concluded that even if $P(\tilde{\tilde{A}}) < P(\tilde{\tilde{B}})$, i.e. 144 < 145, even then a pessimistic decision maker gives some weight to the uncertainty associated with the path length and since more uncertainty is associated with $\tilde{\tilde{A}}$, so the degree of rejection of that path increases as the level of pessimism increases.

According to an optimistic decision maker, as the degree of optimism, M, increases from 1 to 2, 2 to 4 and then 4 to 8, the degree of rejection of $\tilde{\tilde{A}}$ changes from 0.928 to 0.861, 0.861 to 0.7416 and then from 0.7416 to 0.5500, respectively. It can be concluded that as the level of optimism increases, degree of rejection of $\tilde{\tilde{A}}$ decreases. So, acceptability of $\tilde{\tilde{A}}$ increases. From this, it can be inferred than an optimistic decision maker is willing to take risk in the form of uncertainty.

According to a moderate decision maker, the degree of rejection of shortest path is 0.928. So, there are high chances that a moderate DM will reject this path. With

this example, it can be understood in a very clear fashion that as the degree of risk taking or risk averting varies, the decision changes, thus making the DM happier with their own choices.

6 Conclusion

This paper extended the SPP to FSPP with IT2TFNs as edge weights. Two key issues are addressed in this work. One is to determine the fuzzy shortest path and its corresponding path length and another is to find the effect of uncertainty of path length on the decision of DM. The varying degrees of optimism or pessimism may suggest the decision maker to take a risk or to avoid a risk as per their choice. In this work, an example has also been provided which discusses the degree of rejection of a certain path if level of optimism or pessimism varies. The results may be useful to find shortest path in a network, considering decision maker's perspective.

References

1. Rosen KH, Krithivasan K (2012) Discrete mathematics and its applications: with combinatorics and graph theory. Tata McGraw-Hill Education
2. Broumi S, Talea M, Bakali A, Smarandache F, Nagarajan D, Lathamaheswari M, Parimala M (2019) Shortest path problem in fuzzy, intuitionistic fuzzy and neutrosophic environment: an overview. Complex Intell Syst 5(4):371–378
3. Dijkstra EW (1959) A note on two problems in connexion with graphs. Numer Math 1 (1):269–271
4. Klein CM (1991) Fuzzy shortest paths. Fuzzy Sets Syst 39(1):27–41
5. Lin KC, Chern MS (1993) The fuzzy shortest path problem and its most vital arcs. Fuzzy Sets Syst 58(3):343–353
6. Chuang TN, Kung JY (2005) The fuzzy shortest path length and the corresponding shortest path in a network. Comput Oper Res 32(6):1409–1428
7. Dey A, Pradhan R, Pal A, Pal T (2018) A genetic algorithm for solving fuzzy shortest path problems with interval type-2 fuzzy arc lengths. Malays J Comput Sci 31(4):255–270
8. Gil MA, López-Díaz M, Ralescu DA (2006) Overview on the development of fuzzy random variables. Fuzzy Sets Syst 157(19):2546–2557
9. Chen SH, Wang CC (2006) Fuzzy distance of trapezoidal fuzzy numbers. In: 9th joint international conference on information sciences (JCIS-06). Atlantis Press
10. Chakraborty C, Chakraborty D (2006) A theoretical development on a fuzzy distance measure for fuzzy numbers. Math Comput Model 43(3–4):254–261
11. Sengupta A, Pal TK (2009) On comparing interval numbers: a study on existing ideas. Fuzzy preference ordering of interval numbers in decision problems. Springer, Berlin, pp 25–37
12. Sengupta A, Pal TK (2006) Solving the shortest path problem with interval arcs. Fuzzy Optim Decis Making 5(1):71–89
13. Singh VP, Sharma K (2020) Capacitated Vehicle Routing Problem with Interval Type-2 Fuzzy Demands. Advances in Mechanical Engineering. Springer, Singapore, pp 83–89
14. Singh VP, Chakraborty D (2017) Solving bi-level programming problem with fuzzy random variable coefficients. J Intell Fuzzy Syst 32(1):521–528

15. Singh VP, Chakraborty D (2019). Bi-level optimization based on fuzzy if-then rule. Croatian Oper Res Rev 315–328
16. Singh VP, Chakraborty D (2019) Solving Knapsack problem with fuzzy random variable coefficients. International conference on innovation in modern science and technology. Springer, Cham, pp 1037–1048
17. Zimmerman HJ (1996) Fuzzy set theory and its applications
18. Klir G, Yuan B (1995) Fuzzy sets and fuzzy logic, vol 4. Prentice hall, New Jersey
19. Chiao KP (2016) Ranking interval type 2 fuzzy sets using parametric graded mean integration representation. In: 2016 international conference on machine learning and cybernetics (ICMLC), vol 2, IEEE, pp 606–611
20. Okada S, Soper T (2000) A shortest path problem on a network with fuzzy arc lengths. Fuzzy Sets Syst 109(1):129–140

Split Tensile Behavior of HCFA Based SCC Including CBA and RCA

Pawan Kumar, Navdeep Singh, and Amit Kumar

Abstract The current exploration focuses on tensile strength behavior of high content fly ash (HCFA)-based self-consolidating concrete (SCC) prepared with coal bottom ash (CBA) and recycled concrete aggregates (RCAs) as substitution of natural fine aggregates (NFAs) and natural coarse aggregates (NCAs), respectively. Split tensile behavior was performed according to Indian Standard (IS 5816 1999). The results prove that the mechanical (split tensile) conduct of HCFA-SCC mixes gets reduced with the enhancement of RCA together with constant amount of CBA. With the full substitution of conventional aggregates with non-conventional aggregates, a maximum decrement of 21% was experienced in HCFA-SCC combinations. In general, the split tensile behavior has attained minimum reduction for HCFA-SCC mixes up to $\leq 25\%$ substitution levels of RCA with a constant amount of CBA (10%) compared to the control HCFA-SCC mix.

Keywords Coal bottom ash · High content fly ash · Recycled concrete aggregates · Self-consolidating concrete

1 Introduction

The groundwork for concrete success is not just that it is inexpensive but also sufficient supremacy and serviceability [1, 2]. Self-consolidating concrete (SCC) is a highly flow able concrete which can disperse and fill the formwork without mechanical vibration [3, 4]. In the recent past, SCC has been the most substantial

P. Kumar · N. Singh (✉)
Department of Civil Engineering, Dr B R Ambedkar National Institute of Technology Jalandhar, Jalandhar, India
e-mail: navdeeps@nitj.ac.in

A. Kumar
Department of Civil Engineering, Malaviya National Institute of Technology Jaipur, Jaipur, India
e-mail: amitkumar.ce@mnit.ac.in

B. Laishram and A. Tawalare (eds.), *Recent Advancements in Civil Engineering*, Lecture Notes in Civil Engineering 172,
https://doi.org/10.1007/978-981-16-4396-5_58

advancement in concrete technology having a major influence on concrete placement and on building processes in particular. The concrete made with $\geq 30\%$ of fly ash (FA) by weight is normally considered as high content fly ash (HCFA)-based concrete. As HCFA-SCC has already gained considerable appreciation worldwide due to higher paybacks in the context of sustainability, cost-effectiveness, and durability with other long-term behavior features, while on the other hand, use of FA in PC-Portland cement lowers/sinks the generation of CO_2 (about 5% globally) [5, 6].

The academicians are now concentrating on the usage of unwanted products produced from construction and demolition wastes (C&D wastes) and industrial wastes [Coal bottom ash (CBA) and fly ash (FA)] rather than utilizing the available natural assets. Recycled concrete aggregates (RCAs) are obtained from left over concretes from C&D wastes and are commonly regarded as non-conventional aggregates.

Regardless of having poor structural conduct, the utilization of RCA as substitute of natural coarse aggregates (NCAs) in SCC has been outshined from the previous some of the years [7–12]. The required nominal size can be attained by proper gradation of waste crushed concrete. Although having relatively lower density and higher water absorption compared to NCA, it is still possible to make concretes with suitable/reasonable conduct by adopting proper mixing and proportioning of its constituents [13, 14]. Further, it has been witnessed from the past/previous studies that SCC containing RCA results in significant drop in strength [15–23].

2 Research Significance

Many studies have been conducted in which mechanical behavior of SCC made with either HCFA/RCA/CBA has been assessed as mentioned in earlier section. As already described in the previous section, that there is almost no information available on the split tensile behavior of SCC made with the combination of entirely waste products, i.e. HCFA, CBA, and RCA. In addition to this, it is planned to recommend the most appropriate combination of constituents in relation to substitution level of FA, CBA, and RCA for best performance toward split tensile behavior of SCC. The mechanical test has been conducted on two (2) various groups of SCC mixes having different substitution levels of NCA with RCA. Fly ash has been varied in both the groups (Group-I and Group-II), while CBA has been used in fixed proportion as partial alteration of PC and NFA, respectively.

3 Materials

3.1 Portland Cement

Portland cement (43 grade) has been used during the whole experimental program. The chemical composition of PC of grade 43 confirms Indian Standard: IS 269.The chemical and physical characteristics of the PC are given in Tables 1 and 2.

3.2 Fly Ash

Class F-FA has been used as a substitute of PC in all SCC mixes throughout the entire investigation. The concrete made with FA levels more than equal to 30% are considered to be HCFA based mixes. The chemical composition of FA (Class F) confirms IS: 1727 (1967) and ASTM C-618 (1991). The physical characteristics and chemical composition of FA are presented in Table 3.

3.3 Natural Fine Aggregates

Natural river-based sand was used having particle size ≤ 4.75 mm. The NFA was acquired from Pathankot quarry, Punjab (India). The NFA used in the entire SCC mixes were stored under normal environmental conditions. The physical characters are presented in Table 4.

3.4 Coal Bottom Ash

Coal bottom ash was acquired from Thermal Power Plant (in Ropar), Punjab, India. Table 5 showcases the chemical composition of CBA.

Table 1 Chemical composition of PC

Parameters	Test value (%)	Recommended value (%)
Total loss of ignition	1.2	5 (max)
Total sulfur content	1.3	2.5 (max)
Total alkali	0.49	0.6 (max)
Magnesia	2.6	6 (max)
Calcium oxide	61.3	
Aluminum oxide	6.80	
Silica	20.1	

Table 2 Physical characteristics of PC

Characteristics	Units	Observation	Allowable range (IS-8112-1989)
Fineness	cm^2/gm	2340	2250 (min)
Normal consistency	%	34	30–35
Specific gravity	–	3.15	3.10–3.15
Soundness	Mm	3	10 (max)

Table 3 Physical and chemical properties of FA

Composition	Weight (%)
SiO_2	56.50
Al_2O_3	17.70
Fe_2O_3	11
CaO	3.20
Specific gravity	2.38
Loss of ignition	1.20

Table 4 Physical characteristics of NFA

Characteristics	Corresponding value
Fineness modulus (FM)	3.969
Water absorption (%)	1.25
Specific gravity	2.75

Table 5 Chemical composition of CBA

Compound	Weight (%)
MgO	1.19
SiO_2	57.76
Al_2O_3	21.58
Fe_2O_3	8.56
K_2O	1.08
Na_2O	0.14
SO_3	0.02

3.5 Natural Coarse Aggregates

In all SCC mixes, the maximum size of 10 mm was used throughout the experimental program. Table 6 presents the physical characteristics of NCA.

Table 6 Physical characteristics of NCA

Physical characteristics	Corresponding value
Aggregate impact value (%)	16.35
Water absorption (%)	0.68
Specific gravity (g/cm^3)	2.68
Aggregate crushing value (%)	15.80

Table 7 Physical properties of RCA

Physical characteristics	Corresponding value
Water absorption (%)	5.65
Specific gravity (g/cm^3)	2.44
Aggregate impact value (%)	30.51
Fineness modulus (FM)	6.88
Aggregate crushing value (%)	25.8

3.6 Water

Water having pH value varying from 6.5 to 8.5 was used during casting and curing of SCC mixes. The water used for SCC mixes was complied with relevant Indian Standards.

3.7 Recycled Concrete Aggregates

The physical nature of RCA influences the workability of concrete mixes. The gradation of RCA has been kept identical to NCA during the entire experimental program. The physical characters are displayed in Table 7.

4 Mix Details and Proportion

Total ten (10) number of HCFA-SCC mixes comprising different substitutions of RCA were prepared as presented in Tables 8 and 9. These mixes were further divided into two different/separate groups (Group-I and Group-II). Group-I mixes contain constant amount of CBA (10%) as substitution of NFA and 40% of FA as substitution of PC. Further, NCA substitutions with RCA were kept at 25, 50, 75, and 100% for both the groups (Group-I and Group-II).

While Group-II mixes consisting 50% of FA as substitution of PC and fixed quantity of CBA (10%) as substitution of NFA, all the aforesaid HCFA-SCC mixes were prepared complying with EFNARC guidelines [24]. No bleeding was observed in any of the HCFA-SCC mixes. The dosage of SP was found to be in

Table 8 Detailed proportions of Group-I HCFA-SCC combinations

Mix designation	W/B	Water	SP	FA	PC	CBA	NFA	RCA	NCA
		(kg per m^3)							
1. ChFB-R0 (Control)	0.45	277	1.05	185.8	369	62	738	0	652
2. ChFB-R25	0.45	277	1.26	185.8	369	62	738	150.5	489
3. ChFB-R50	0.45	277	1.57	185.8	369	62	738	301	326
4. ChFB-R75	0.45	277	1.89	185.8	369	62	738	451.5	163
5. ChFB-R100	0.45	277	2.1	185.8	369	62	738	602	0

Table 9 Detailed proportions of Group-II HCFA-SCC combinations

Mix designation	W/B	Water	SP	FA	PC	CBA	NFA	RCA	NCA
		(kg per m^3)							
1. CHFB-R0 (Control)	0.45	277	2.1	232	307.5	62	738	0	652
2. CHFB-R25	0.45	277	2.41	232	307.5	62	738	150.5	489
3. CHFB-R50	0.45	277	2.62	232	307.5	62	738	301	326
4. CHFB-R75	0.45	277	3.04	232	307.5	62	738	451.5	163
5. CHFB-R100	0.45	277	3.36	232	307.5	62	738	602	0

range of 0.5–2% by weight of PC for various HCFA-SCC mixes. Tables 8 and 9 present the detailed proportions of both the groups (Group-I and Group-II) having various HCFA-SCC combinations prepared with CBA and RCA, respectively. The per cubic meter capacity of all the aforesaid HCFA-SCC mixes has been determined by 'Equivalent volume method' approach.

5 Specimen Details and Test Setup

Fresh properties of SCC mixes were evaluated using the slump flow, J-ring, L-box, and V-funnel tests. J-ring test was done to find out the passing ability of HCFA-SCC. Generally, a difference less than 25 mm indicates good passing ability, whereas difference greater than 50 mm indicates the poor passing ability. Further, V-funnel tests were performed to evaluate the flow-ability of HCFA-SCC. Figure 1 represents the workability tests performed on HCFA-SCC.

Cubes measuring 100 mm × 100 mm × 100 mm were used to quantify and measure mechanical behavior (split tensile strength). All the molds (cubes) were cleaned, brushed, and oiled well prior to casting. The molds were filled in two layers. The specimens were marked with their respective designations after four/five hours of casting and were allowed to set in the molds for 24 h. The strength of all the HCFA-SCC mixes has been estimated at 7, 28, 56, and 90 days of curing.

Fig. 1 Workability tests performed on HCFA-SCC

Fig. 2 Split tensile strength test setup

Split tensile strength test was completed according to (IS 5816 1999). Figure 1 presents the setup for the split tensile strength test. As shown in Fig. 2, cube specimen was positioned in Universal Testing Machine (UTM-2000 KN), and further load was applied without shock and increased constantly at a level of 1.2–2.4 N/mm^2 till the failure. The maximum load applied for each specimen was recorded. Further average value of three (3) specimens was measured as the splitting tensile strength of SCC mix.

6 Results and Discussion

Generally, the workability of all HCFA-SCC combinations prepared with varying content of RCA and fixed amount of CBA has deteriorated in comparison with control SCC combination. The worst performance in aspect of workability has been identified for SCC combinations containing 75% of RCA instead of NCA, whereas the comparable performance has been noticed for combinations containing up to 25% of RCA in place of NCA when compared to control SCC combination. The similar reduction in the workability has been found for the SCC combinations prepared with RCA [14]. The physical nature of RCA and CBA holding rough and porous surfaces resulted in decrease of workability of HCFA-SCC mixes [1, 3, 4]. Table 10 represents the workability results of all the HCFA-SCC combinations (both Group-I and Group-II).

The split tensile strength of all HCFA-SCC mixes was assessed to analyze the role of RCA. In general, with the improving content of RCA (>75%), the strength was decreased. Figures 3 and 4 represent the split tensile strength development for Group-I (having 60% PC) and Group-II (having 50% PC) HCFA-SCC combinations with 0%, 25%, 50%, 75%, and 100% substitution of NCA with RCA at curing ages of 7 days to 90 days, respectively.

The strength of HCFA-SCC combinations comprising up to 50% of RCA (ChFB-R25 and ChFB-R50) was noted to be reduced at all ages (curing ages) when related to the reference HCFA-SCC combination ChFB-R0. For HCFA-SCC combination ChFB-R25 the decrement up to 10% was noticed when related to reference HCFA-SCC combination ChFB-R0 after 90 days of curing. Similarly, the strength of SCC combination ChFB-R50 was observed to be lessened by up to 16%, whereas strength of HCFA-SCC combination ChFB-R75 and ChFB-R100

Table 10 Workability results of HCFA-SCC combinations (both Group-I and Group-II)

Mix no.	Mix notation	Slump		V-funnel (s)	L-box (h2/h1)	Conforming to EFNARC guidelines
		T500 (s)	*D* (mm)			
M1	ChFB-R0 (control)	2.3	735	6.3	0.98	Yes
M2	ChFB-R25	2.6	710	6.7	0.96	Yes
M3	ChFB-R50	2.9	690	7.1	0.92	Yes
M4	ChFB-R75	3.5	655	9.0	0.86	Yes
M5	ChFB-R100	3.1	670	7.4	0.88	Yes
M6	CHFB-R0 (control)	2.5	740	6.6	0.97	Yes
M7	CHFB-R25	2.8	720	6.9	0.95	Yes
M8	CHFB-R50	3.2	705	7.6	0.92	Yes
M9	CHFB-R75	4.0	665	9.7	0.87	Yes
M10	CHFB-R100	3.6	685	8.4	0.88	Yes

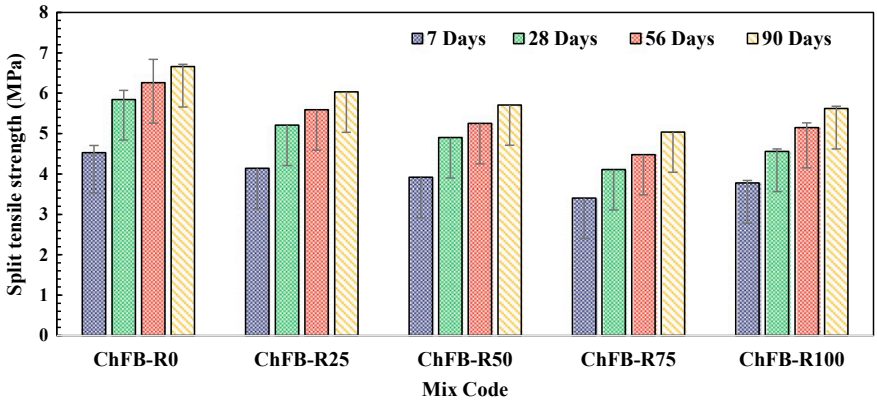

Fig. 3 Split tensile strength test results of Group-I HCFA-SCC combinations

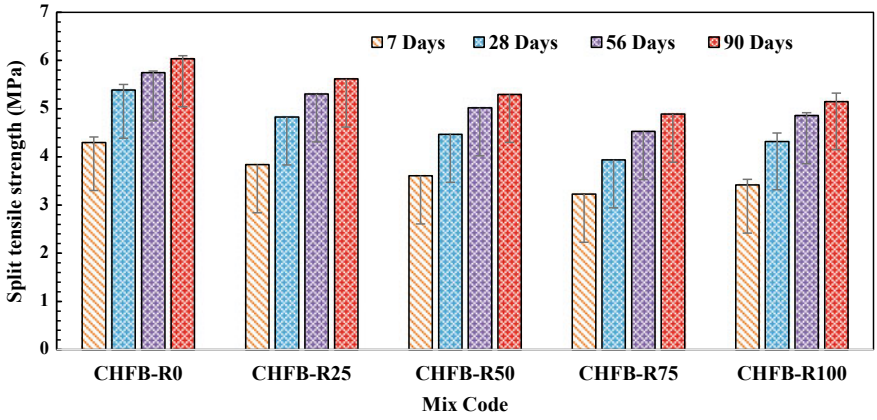

Fig. 4 Split tensile strength test results of Group-II HCFA-SCC combinations

has been decreased up to 29% and 21% when related to reference HCFA-SCC combination after 90 days of curing, respectively.

The strength of HCFA-SCC mixes comprising up to 50% of RCA (CHFB-R25 and CHFB-R50) was again noticed to be lessened at all ages (curing ages) when related to reference HCFA-SCC combination CHFB-R0. For HCFA-SCC mix CHFB-R25, the reduction up to 10% has been experienced when related to reference HCFA-SCC mix CHFB-R0 after 90 days of curing. Similarly, the strength of SCC mix CHFB-R50 was identified to be dropped maximum by 17% while strength of HCFA-SCC combinations CHFB-R75 and CHFB-R100 was further lessened maximum by 26% and 20% when related to the reference HCFA-SCC combination after 90 days of curing, respectively.

Normally, the mechanical behavior (Split tensile strength) is affected by aggregate's characteristics. The existence of the permeable layer of residual mortar on RCA (typical RCA) unfavorably disturbs the strength of concrete. Besides, the strength of concrete generally depends on the cement matrix, strength of the aggregates, and interfacial transition zone (ITZ) between the aggregates and the matrix. Hence, for the similar reasons, HCFA-SCC mixes made with constant amount of CBA and varying amount of RCA resulted in lower strength [15–23, 25].

Additionally, the physical properties of CBA also decrease the quality/worth of the paste, further resulting in decrement of strength. The availability of pores in form of RCA, overcame the pore refining action and efficiency of CBA at initial and later ages, successively endorsing the development/advancement of cracks thus declining the strength [7, 26–28].

7 Conclusions

The workability of all (both groups) HCFA-SCC combinations prepared with different levels of RCA and constant amount of CBA has declined when related to control SCC combination. The split tensile strength of all HCFA-SCC combinations (both Group-I and Group-II) prepared containing varying content of RCA and fixed amount of CBA has deteriorated when related to control SCC combination. The strength of all the SCC mixes decreases with the enhancement in the content of RCA. The worst conduct in aspect of mechanical behavior has been identified for HCFA-SCC combination containing 75% of RCA, whereas the comparable conduct has been noticed for HCFA-SCC combination having 25% of RCA when related to control SCC mix. The maximum deviation of 29% in behavior has been found for SCC combination having 75% of RCA in Group-I. The similar findings were observed in case of Group-II, and maximum drop of 26% was observed for the same mix. Further, it has been concluded from the results that incorporation of RCA up to 25% imparts minimum effect on the mechanical behavior of SCC after satisfying all conditions in accordance to EFNARC.

Acknowledgements The authors would like to acknowledge Council of Scientific and Industrial Research (CSIR), New Delhi for financially supporting the entire experimental investigation (Project No-22(0812)/19/EMR-II). The authors also appreciate the support and encouragement provided by the staff of Dr B R Ambedkar National Institute of Technology, Jalandhar, India.

References

1. Behera M, Bhattacharyya SK, Minocha AK, Deoliya R, Maiti S (2014) Recycled aggregate from C&D waste & its use in concrete—a breakthrough towards sustainability in construction sector: a review. Constr Build Mater 68:501–516

2. Singh N, Singh SP (2016) Reviewing the carbonation resistance of concrete. J Mater Eng Struct 3:35–57
3. Singh N, Kumar P, Goyal P (2019) Reviewing the behaviour of high-volume fly ash based self-compacting concrete. J Build Eng 26:100882
4. Singh N, Singh SP (2018) Carbonation resistance of self-compacting recycled aggregate concretes with silica fume. J Sustain Cem Based Mater 7:214–238
5. Bouzoubaâ N, Lachemi M (2001) Self-compacting concrete incorporating high volumes of class F fly ash: preliminary results. Cem Concr Res 31:413–420
6. Şahmaran M, Christianto HA, Yaman IÖ The effect of chemical admixtures and mineral additives on the properties of self-compacting mortars. Cem Concr Compos 28:432–440
7. Singh N, Singh SP (2016) Carbonation resistance and microstructural analysis of low and high-volume fly ash self compacting concrete containing recycled concrete aggregates. Constr Build Mater 127:828–842
8. Kurda R, de Brito J, Silvestre JD (2017) Combined influence of recycled concrete aggregates and high contents of fly ash on concrete properties. Constr Build Mater 157:554–572
9. Kurda R, de Brito J, Silvestre JD (2017) Influence of recycled aggregates and high contents of fly ash on concrete fresh properties. Cement Concr Compos 84:198–213
10. Khodair Y, Luqman (2017) Self-compacting concrete using recycled asphalt pavement and recycled concrete aggregate. J Build Eng 12:282–287
11. Kurda R, de Brito J, Silvestre JD (2017) Water absorption and electrical resistivity of concrete with recycled concrete aggregates and fly ash.Cem Concr Compos 95:169–182
12. Khodair Y, Bommareddy B (2017) Self-consolidating concrete using recycled concrete aggregate and high volume of fly ash and slag. Constr Build Mater 153:307–316
13. Ponikiewski T, Gołaszewski J (2014) The influence of high-calcium fly ash on the properties of fresh and hardened self-compacting concrete and high-performance self compacting concrete. J Clean Prod 72:212–221
14. Singh N, Singh SP (2016) Carbonation and electrical resistance of self-compacting Concrete made with recycled concrete aggregates and metakaolin. Constr Build Mater 121:400–409
15. Nassar RUD, Soroushian P (2012) Strength and durability of recycled aggregate concrete containing milled glass as partial replacement for cement. Constr Build Mater 29:368–377
16. Thomas C, Setién J, Polanco JA, Alaejos P, De Sánchez JM (2013) Durability of recycled aggregate concrete. Constr Build Mater 40:1054–1065
17. Xiao J, Li W, Sun Z, Lange DA, Shah SP (2013) Properties of interfacial transition zones in recycled aggregate concrete tested by nanoindentation. Cement Concr Compos 37:276–292
18. Mirjana MGB, Vlastimir R (2014) Properties of the recycled aggregate concrete. Appl Mech Mater 2:239–249
19. Yehia S, Helal K, Abusharkh A, Zaher A, Istaitiyeh H (2015) Strength and Durability Evaluation of Recycled Aggregate Concrete. Int J Concr Struct Mater 9:219–239
20. Etxeberria M, Vázquez E, Marí A, Barra M (2007) Influence of amount of recycled coarse aggregates and production process on properties of recycled aggregate. Concr Cem Concr Res 37:735–742
21. Otsuki N, Miyazato S, Yodsudjai W (2003) Influence of recycled aggregate on interfacial transition zone, strength chloride penetration and carbonation of concrete. J Mater Civ Eng 15:443–451
22. Salem Rohi M, Edwin BG (1998) Role of chemical and mineral admixtures on the physical properties and frost-resistance of recycled aggregate concrete. ACI Mater J 95:558–563
23. Pin K, Ashraf W, Cao Y (2018) Properties of recycled concrete aggregate and their influence in new concrete production. Resour Conserv Recycl 133:30–49
24. EFNARC 2002 Specification and guidelines for self-compacting concrete Rep from EFNARC 44 32
25. Singh N, Arya MMS (2019) Utilization of coal bottom ash in recycled concrete aggregates based self-compacting concrete blended with metakaolin. Resour Conserv Recycl 144:240–251

26. Over I, States U (1996) Investigation of lignite-based bottom ash for structural concrete by Nader Ghafoorit Member ASCE and Jeffrey Bucholc 2 Associate Member ASCE. J Mater Civil Eng 128–137
27. Singh M, Siddique R (2014) Strength properties and micro-structural properties of concrete containing coal bottom ash as partial replacement of fine aggregate. Constr Build Mater 50:246–256
28. Singh N, Shehnazdeep BA (2020) Reviewing the role of coal bottom ash as an alternative of cement. Constr Build Mater 233:117276

Economic Strategies to Alleviate Traffic Congestion: Evidences from an Indian City

C. P. Muneera and Krishnamurthy Karuppanagounder

Abstract This paper seeks a straightforward question: Is the infrastructure improvement or demand management strategy is a better solution to traffic congestion problem to the region's economy? This research focussed on the economic evaluation of congestion relief measures under heterogeneous traffic condition. A comprehensive methodology is developed and estimated the congestion cost annually for urban links in the Indian city. Road widening and private vehicles that are prominent in India such as two wheeler and car shift to public bus are considered separately as the relief measures. The percentage reductions of congestion cost with the relief measures and normal congestion state are compared. The result shows that the percentage reduction of congestion cost due to road widening is 55.55%, two wheeler shifts to bus is 94.99% and car to bus is 94.92%. Benefit cost analysis is conducted to find the optimal solution for congestion problem. The b/c ratio for road widening is 1.1, shift of car to bus is 2.5 and mode shift of two wheeler to bus is 2.9. The analysis revealed that the demand management strategy is a better solution compared to road widening for the Indian city.

Keywords Traffic congestion cost · Value of travel time · Mode shift · Road widening · Heterogeneous traffic

C. P. Muneera (✉)
Department of Civil Engineering, MES College of Engineering Kuttippuram, Kuttippuram, Kerala 67958, India

K. Karuppanagounder
Department of Civil Engineering, National Institute of Technology Calicut, Calicut, Kerala 673601, India
e-mail: kk@nitc.ac.in

B. Laishram and A. Tawalare (eds.), *Recent Advancements in Civil Engineering*, Lecture Notes in Civil Engineering 172,
https://doi.org/10.1007/978-981-16-4396-5_59

1 Introduction

Growing economy in any country may witness a rise in demand for transport infrastructure and services, may deteriorate the performances of an existing transport sector. Therefore, the transport sector has to keep pace with rising demand by providing proper solution with viable financial inflow. Traffic congestion, a negative impact to the transportation system, causes an abrupt change in the vehicle operating cost, road user cost, fuel consumption cost and emission cost resulting in the tremendous economic loss to the transport sector. Various policy measures such as road widening, road pricing [1] taxes, subsidies for vehicles [2] infrastructure planning and investments, travel demand shift policies [3] and optimization of fuel economy [4], etc. have to be implemented under the banner of supply side and demand side strategy was implemented globally to reduce congestion at the roadway.

Perusal of literature reveals that the congestion mitigation strategies are divided into two broad categories including supply side and demand side strategies [5]. Supply side strategies are meant for to reduce traffic congestion by expanding the existing infrastructure and providing new capacity for transportation system. The highway expansion and widening of roadway often support the economic growth of the country by reducing congestion cost. But, research found that the improving capacity of roadway provides only short run congestion relief measures because expansion and construction of highway produce generated and induced traffic which may subsequently reach the capacity [6]. Demand side framework deals with mitigation of traffic congestion by reducing the demand of vehicles in the transportation system [7]. To reduce traffic congestion for any city, both infrastructure and demand side economic strategy have to be considered to propose optimal congestion relief measures.

Even though several mitigation measures are available for congestion problem to provide an optimal congestion relief measures to the locality, the economic evaluation of possible congestion relief measures has to be conducted. Therefore, this study focuses on the economic evaluation of traffic congestion relief measures to provide optimal solution to the congestion problem that prevails in Indian city. The two important mitigation measures for urban link such as infrastructure improvements and mode shift to public transport based are considered for this study. This study mainly concentrates on whether demand side strategy or infrastructure improvements provides better solution to India's region economy.

2 Congestion Cost Quantification

The congestion causes while waiting time of road users to ease the queue thus by missing important activities and also late arrival in the destination. Hence, delay is reflected as the major predominant reason for traffic congestion and causes

economic losses for the road users. Research from the past revealed that traffic volume, delay, value of travel time and occupancy are the major influencing parameters for delay cost quantification [8–11].

The road traffic in developing countries is characterized by a mix of different vehicle, and heterogeneity refers to mix of different vehicle such as two wheeler, bus, car, etc. participating in the traffic operation as chaotic and does not follow strict lane discipline. Due to the complexity in the traffic operation and different mix of vehicles in the roadway made to incorporate the mix of vehicles in the congestion cost estimation. The link delay cost estimation formula is shown in Eq. 1.

$$C_{\text{het}} = \sum_{m=1}^{k} \text{delay} * v_m * o_m * \text{vot}_m \tag{1}$$

where c_{het} is the congestion cost at link under heterogeneous traffic condition, delay is the average delay per vehicle, v is volume of the vehicle, vot is the value of travel time, o is the passenger occupancy of the vehicles, m is the vehicle type.

3 Methodology

The proposed methodology for this study is depicted in Fig. 1. The methodology comprises of quantification of traffic congestion, economic evaluation of traffic congestion, economic evaluation of congestion relief measures and congestion relief measure proposal.

4 Study Area

The study area for data collection was selected from Ernakulum, located on the south-western India at a latitude of 9°59′0″ N and a longitude of 76°17′0″ E and it is in the central part of Kerala. Six dual carriageway links in Ernakulam, which prevail traffic delay, were selected through a pilot survey. Geometric data, classified traffic volume count, travel time data and occupancy of vehicles for each urban links formed the database for this study. In dual Carraigeway due to the to and fro motion of the vehicle, the traffic parameters such as delay and traffic volume varies in both the direction. So, the vehicle moves in the direction towards the Central Business District area is taken as the direction '*a*' and the opposite direction is taken as direction '*b*' for the analysis.

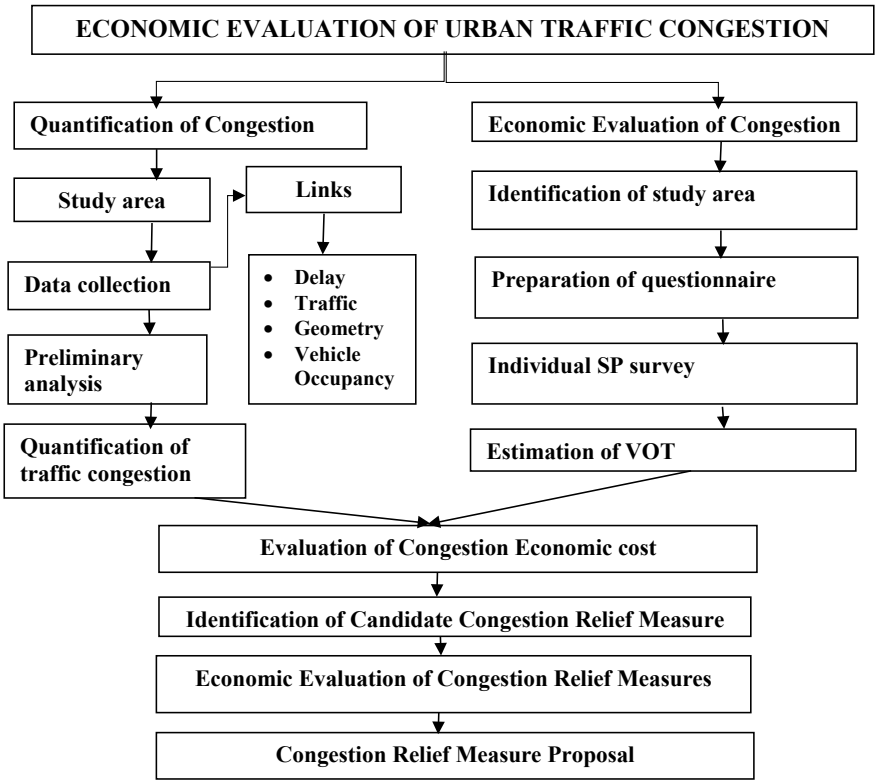

Fig. 1 Proposed methodology

5 Data Collection and Analysis

5.1 Computation of Traffic Volume

Traffic volume data were collected using videographic survey. Data were collected from 7:30 AM to 6:0 PM and collected data was converted into digital form and data base created for traffic volume. The traffic composition of vehicle in the study stretches is shown in Table 1.

From the analysis, it is clearly observed that the percentage of two wheeler is high which constitutes a maximum of 61% of the entire traffic. The traffic composition of car is a maximum of 51% of the total traffic. The percentage of auto and bus constitute 16–17% of total traffic. This indicates that the influence of private vehicle ownership is very high in the study stretches. The minimum and maximum traffic flows of each stretch are depicted in Fig. 2.

Table 1 Traffic composition of the study stretches

Sl no.	Road name	TW (%)	Auto (%)	Car (%)	Bus (%)	LCV (%)	MCV (%)	HCV (%)	Cycle (%)
1	Link 1a	49	16	22	5	6	1	1	0
	Link 1b	50	15	22	7	5	1	0	0
2	Link 2a	46	16	24	8	4	1	0	0
	Link 2b	50	15	24	7	3	0	1	0
3	Link 3a	19	12	51	7	8	2	1	0
	Link 3b	12	13	50	9	8	6	2	0
4	Link 4a	61	13	20	4	2	0	0	0
	Link 4b	54	12	22	8	3	1	0	0
5	Link 5a	42	7	31	17	3	0	0	0
	Link 5b	46	11	26	15	2	0	0	0
6	Link 6a	48	10	31	6	3	1	1	0
	Link 6b	49	7	33	7	3	1	0	0
	Average	44	12	30	8	4	1	1	0
	Maximum	61	16	51	17	8	6	2	0

Note: two wheeler (*TW*), light commercial vehicle (*LCV*), medium commercial vehicles (*MCV*)

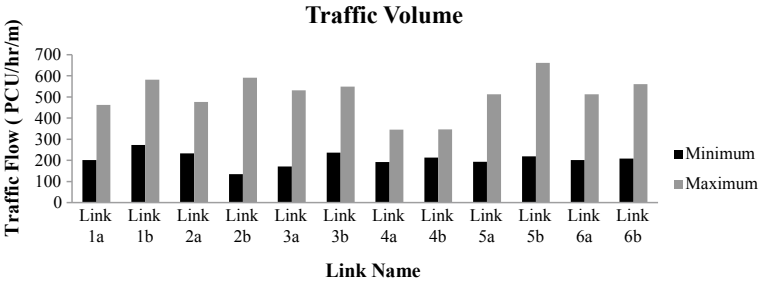

Fig. 2 Traffic volume for the study stretches

5.2 Estimation of Delay

Travel time data were collected using videographic survey. The licence plate matching technique was used to measure the travel time for the link. Free flow travel times for vehicles at urban links were also collected when the traffic volume was very less, and delay was estimated.

Model was developed for delay to predict the effect of roadway and traffic parameters on congestion. Correlation analysis was done with explanatory variables and from the correlation analysis, it is seen that traffic volume, length of dual carriageway section and carriageway width are the significant variables that affect delay. A prediction model for delay is developed with the significant variables and shown in Table 2. From the field observed data, delay data were segregated for

Table 2 Delay model for urban link

Index	Model	R^2	Standard error			RMSE (s)	
			Coef of flow	Coef of length	Coef of CW	CD	VD
Delay	$\text{Delay} = e^{0.010v} + 0.578\,\text{length} - 11.40\,\text{Carraigeway width}$	0.801	0.010	0.045	1.526	85	82

CD calibration data set and *VD* validation data set

5 min intervals along the links and the average delay is observed. From the data set available from the links, nearly two-third data was used for the model prediction and the remaining data were used for model validation. Of the different models tried with nonlinear regression model, and the best relation was selected as the final model.

Statistical parameters for evaluating delay model for dual carriageway are given in Table 5. Considering R^2 value from the table; nonlinear model provides fairly good prediction. The RMSE value, which provides better result, and hence, the calibrated model is validated. This model predicts traffic volume has an exponential increasing trend with delay, length shows an increasing trend and while carriageway width shows decreasing trend with delay at dual carriageway. Additionally, this model is used for the estimation of congestion cost under widening process.

5.3 Computation of Passenger Occupancy

Passenger occupancy of the vehicle is done by manual observations. For data collection, enumerators are positioned on the sites and noted down the person occupied on it for different mode of vehicles. From the analysis, it is observed that the average passenger occupancy of car, two wheeler, auto rickshaw and bus for Ernakulam city is found to be 1.56, 1.38, 1.51 and 50.43, respectively.

5.4 Computation of Value of Travel Time

Value of travel time was estimated using a questionnaire survey, which includes household information, personal information and travel details. A total of 2773 data were used for the value of travel time quantification. Preliminary analysis of data was conducted to find the socio-economic characteristics and trip characteristics of respondents. The value of travel time is calculated as the ratio of the parameters for travel time over the travel cost on the utility equation [12]. Models were developed based on multi nominal logistics (MNL) regression to find the value of travel time for different modes and the parameter estimates for the model is presented in Table 3.

The Pseudo R^2 (ρ^2) values of the model lie between 0.2 and 0.4. This represents acceptable model fit. Alkaline information criteria (AIC) values of the model are low, which also indicates best model. From the model developed, value of travel time for car, bus, auto and two wheeler estimated as 270 Rs/h, 51 Rs/h, 204 Rs/h and 240 Rs/h, respectively, and that is used for delay cost estimation.

Table 3 Parameter estimates of value of travel time for Ernakulam city

Variables	Car		Bus		Auto rickshaw		Two wheeler	
	A	B	A	B	A	B	A	B
Travel time	−0.0994	−14.312	−0.689	9.154	−0.160	−5.104	−0.112	−6.140
Travel cost	−0.022	−8.482	−0.809	−8.956	−0.047	−5.311	−0.028	−3.656
Gender	0.184	1.25	0.300	1.90	0.064	1.99	0.272	2.75
Age	0.317	1.67	0.117	1.563	−0.709	−1.113	0.248	1.407
Marital status	0.003	1.24	0.017	2.078	−0.014	−5.12	0.013	1.809
Education	0.066	1.89	0.027	2.56	0.223	1.898	0.105	1.56
Employment	0.034	2.78	0.029	2.90	0.191	1.71	0.03	1.97
Personal income	0.227	2.851	−0.167	−2.51	−0.527	−1.843	0.03	2.97
VOT (Rs/h)	270		51		204		240	
pseudo R^2			0.287					
Akaline Information Criteria (AIC)			−1767.26					
Log−likelihood of estimated model			1.29					

Where *A* is the coefficient and *B* is the *t*-statistics

6 Cost Estimation

The total delay cost is made up of different components such as traffic volume, delay, vehicle occupancy and value of travel time for different modes. Based on the hourly volume and delay data, congestion cost estimation was done using Eq. 1 for each study stretches. Figure 3 shows the hourly congestion cost at Link 1. Furthermore, congestion cost is estimated annually for study sites and presented in Table 4.

The congestion cost in each link is estimated in terms of crores of rupees, indicating that the congestion cost is high on these links because of a greater number of vehicles having delay on these roads. Therefore, relief measures have to be proposed to alleviate congestion, and the corresponding economic strategy has to be quantified.

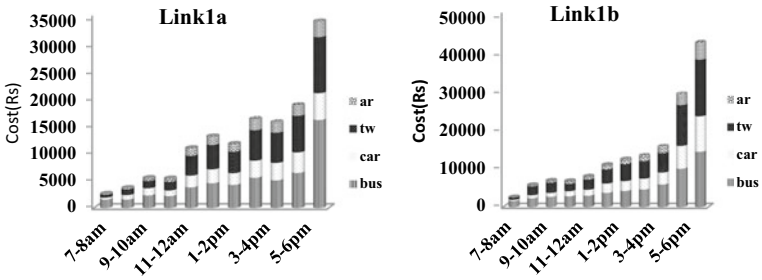

Fig. 3 Congestion cost for each study sites

Table 4 Total delay cost for dual carriageway

Road name	Delay cost per annum (Rs)
Link 1a	43,871,324
Link 1b	49,670,122
Link 2a	52,266,773
Link 2b	21,656,972
Link 3a	95,938,216
Link 3b	306,538,665
Link 4a	13,566,561
Link 4b	69,698,846
Link 5a	113,591,774
Link 5b	75,660,496
Link 6a	135,211,868
Link 6b	194,330,941

7 Relief Measure Proposal

The supply side, widening of roadway and demand side mode shifting from private vehicles to public transport bus is considered for this study. To conduct the mode shift as congestion relief measure as from private vehicles to public vehicles, two scenarios were created. Firstly, reduce the two wheeler mode share in unit percentage and the same shifted to bus (Scenario 1). Second scenario was created in such a way that decreases the car mode share in unit percentages and transfer to bus (Scenario 2). To compare economic strategies for different relief measures, unit widening is considered and changes in the congestion cost are quantified. The percentage reduction in the congestion cost due to road widening scenario I scenario II is shown in Table 5.

From the analysis, it is observed that the percentage reduction of congestion cost due to widening of road is 55.55, due to two wheelers shifting is 94.99 and car shifting is 94.92. The percentage reduction of congestion cost is observed more on two wheeler compared to car. Hence, as based on economic evaluation, Indian scenario suggest the mode shift of two wheeler to bus is more economical compared to car to bus for congestion relief measure.

8 Benefit-Cost Analysis

The cost benefit analysis aims to identify the optimal solution to traffic congestion and to quantify the cost associated with the project implementation. Approximate cost required to implement congestion cost reduction measures in road widening, mode shift from two wheeler to bus and mode shift from car to bus, is found to be 3Cr, 5,545,000 Rs and 5,100,000 Rs, respectively. With the introduction of relief

Table 5 Percentage reduction in the congestion cost due to mode shift scenario I

Road name	Road widening process		Scenario I		Scenario II	
	Percentage reduction	Average percentage reduction	Percentage reduction	Average percentage reduction	Percentage reduction	Average percentage reduction
Link 1a	44.3	55.55	95.91	94.99	95.83	94.92
Link 1b	92.2		95.93		95.86	
Link 2a	73.1		95.71		95.65	
Link 2b	72.2		95.63		95.55	
Link 3a	70.1		95.96		95.92	
Link 3b	91.1		96.32		96.26	
Link 4a	42.8		94.82		94.75	
Link 4b	12.0		96.24		96.16	
Link 5a	92.4		96.31		96.26	
Link 5b	61.0		95.65		95.60	
Link 6a	5.8		97.43		97.40	
Link 6b	9.6		83.99		83.84	

Table 6 Benefit-cost analysis

	Widening of road	Shift from TW to bus	Shift form car to bus
Benefit (Rs)	31,669,446	16,000,679	12,926,017
Cost (Rs)	30,000,000	5,545,000	5,100,000
Benefit/cost ratio	1.1	2.9	2.5

measures in terms of supply side and demand side strategies and with the do-or nothing case, the benefit cost associated with each relief measure is estimated and presented in Table 6.

The benefit cost ratio is greater than 1 which means the project is feasible for all the congestion relief measures. This study reveals that all the supply side and demand side strategy is feasible for congestion problem in the Indian city. The benefit cost ratio is high which is 2.9 for the relief measure of shift of two wheeler to bus. Hence, this study recommends a demand measure, a mode shift of two wheeler to bus as an optimal economic solution for traffic congestion problems for Ernakulam City.

9 Conclusion

This study addresses a problem, whether the infrastructure improvements or demand management strategy is a better solution for traffic congestion problem to region's economy. A comprehensive methodology is developed to address this

problem for a city which prevails heterogeneous traffic condition. Widening of road as infrastructure improvements and mode shift as demand measure for traffic congestion problem for Ernakulam city in Indian is considered for this study.

This study quantifies the traffic congestion cost for urban incorporating operational, traffic flow and passengers' characteristics. Nonlinear regression delay model is developed and validated for delay to predict the effect of roadway and traffic parameters on congestion. Value of travel time for different vehicle types is estimated using multi nominal logit model (MNL) and it was found that the value of travel time for car, bus, auto and two wheeler estimated as 270 Rs/h, 51 Rs/h, 204 Rs/h and 240 Rs/h, respectively. The factors were aggregated and annual congestion cost for six dual carriageway urban link were estimated.

The economic evaluation of congestion relief measures such as widening of road and mode shift from private to public vehicles is conducted. It was found that the percentage congestion reduction cost is more on mode shift process compared to widening process. The cost benefit analysis was done for the proposed congestion relief measures. The b/c ratio for widening of road is 1.1 and mode shift of two wheeler to bus is 2.9 and that of car to bus is 2.5. Hence, this study processes mode shift of two wheeler to bus having high b/c ratio is proposed an optimal economic strategy for congestion problem in the Indian city. The study reveals that the demand side strategy is more economical compared to widening of road for the Indian city. Economic strategic congestion evaluation to the urban roadway importantly provides transport planners and policy makers to provide cost-effective solution to traffic congestion problem.

Acknowledgements The authors sincerely thank the support received from the Centre for Transportation Research, Department of Civil Engineering, National Institute of Technology Calicut, a Centre of Excellence setup under FAST Scheme of MHRD, Govt. of India.

References

1. Palma A, Lindsey R (2011) Traffic congestion pricing methodologies and technologies. Transp Res Part C Emerg Technol 19:1377–1399
2. Basso LJ, Guevara CA, Gschwender A, Fuster M (2011) Congestion pricing, transit subsidies and dedicated bus lanes: efficient and practical solutions to congestion. Transp Policy 18:676–684
3. Currie G, Sarvi M (2010) Evaluating the congestion relief impacts of public transport in monetary terms. J Public Transp 13:1–24
4. Stevanovic A, Stevanovic J, Zhang K, Batterman S (2009) Optimizing traffic control to reduce fuel consumption and vehicular emissions: integrated approach with VISSIM, CMEM, and VISGAOST. Transp Res Rec J Transp Res Board 2108:105–113
5. Downs A (2004) Still stuck in traffic: coping with peak-hour traffic congestion. Brooking Institution Press
6. Litman T (2013) Smart congestion relief. Victoria Transp Policy Inst P12–5310:3–40
7. OECD Transport Research Centre (2007) Managing traffic congestion. European Conference of Ministers of Transport

8. Jayasooriya SA, Bandara YM (2017) Measuring the economic costs of traffic congestion. Moratuwa engineering research conference MERCon, pp 141–146
9. Errampalli M, Velmurugan S (2015) Effect of congestion on fuel cost and travel time cost on multi-lane highways in India. Int J Traffic Transp Eng 5:458–472
10. Ali MS, Adnan M, Noman SM, Baqueri SF (2014) Estimation of traffic congestion cost-a case study of a major arterial in Karachi. Proc Eng 77:37–44
11. The Cost of Urban Congestion in Canada (2013) Transp Canada Environ Aff, vol 53 pp 1689–1699
12. Hensher DA (2001) Measurement of the valuation of travel time savings. J Transp Econ Policy 35:71–98

Performance of Geogrid Reinforced Asphalt Layers—A Review

B. A. V. Ram Kumar and Harishbabu Jallu

Abstract The implementation of geogrids in soils and flexible pavements has been studied since the early 1980s. However, recent studies reported that the geogrids enhancing pavement performance by increasing their structural capacity and reducing distress potential. Geogrids have incurred tremendous benefits over traditional methods by improving the overall performance of a flexible pavement system by enhancing their mechanical properties. Besides, the more energy is required for the fracture damage and crack initiation for the geogrid reinforced pavements. The tensile strains are reduced significantly due to the stiffness modulus and interlocking properties of the geogrids. The main aim of this paper is to explore the efficacy of geosynthetic interlayers as reinforcement in asphalt layers. In addition to that, the existence of the geogrids sandwiched between the bituminous layers subjected to interfacial shear properties was summarized. Therefore, the flexural fatigue properties, interfacial shear characteristics, and mechanical properties of geogrids embedded with asphalt layers were reviewed in this paper. Further, the effect of reflective cracking, vertical deformation, and service life of flexible pavements was presented.

Keywords Asphalt · Geogrids · Geosynthetics · Reflective cracking

1 Introduction

The flexible pavements are considered as most economical over rigid pavements and are commonly used all over the world. However, because of environmental conditions and massive traffic volumes, flexible pavements may undergo pavement distresses. To avoid structural failure situations and improve the design life of flexible pavements, reinforcement is vital with different materials. The reinforcement acts as additional support, and which eventually increases in the structural

B. A. V. Ram Kumar (✉) · H. Jallu
Department of Civil Engineering, GMRIT, Rajam, Andhra Pradesh, India
e-mail: ramkumar.bav@gmrit.edu.in

B. Laishram and A. Tawalare (eds.), *Recent Advancements in Civil Engineering*, Lecture Notes in Civil Engineering 172,
https://doi.org/10.1007/978-981-16-4396-5_60

capacity of the pavement. Instability in any of the pavement layers will result in pavement distress; therefore, Proper care should be taken while constructing each layer. The distress experienced by the pavement can be mainly due to environmental distress and structural distress. Among all distresses, Fatigue and Rutting failures are the major causes in flexible pavements. Fatigue cracking, Rutting, and Pothole formation are the significant failures that occur in flexible pavements mostly due to failure of wearing or binder course.

2 Geosynthetic Interlayers

The utilization of geosynthetic materials in flexible pavements has become acceptable in recent years due to their high stiffness, durability, and ability to absorbing stresses by reinforcing the pavement systems (Fig. 1). Geosynthetics are made by polymeric material, and it is observed as a major component in a system or any earth structures to attain engineering objectives. The prefix "geo" indicates whose performance has to do with soil, rock, and earth. According to Dr. Robert M. Koerner geosynthetics are characterized into eight different types, i.e., geogrids, geotextiles, geonets, geomembranes, geosynthetic clay liners, geocells, geofoam, and geocomposites. Figure 2 shows various types of geosynthetic interlayers, i.e., Glass grid composite (GGC), Polyester grid (PE), Polypropylene grid (PP), and Geo jute mat (GJ).

Application of geosynthetics in pavement layers is not a new concept, but in the recent times, there are various case studies with related publications that have been attempted to explore the advantageous and importance subjected to the construction and maintenance of flexible pavements [1]. In addition to that, the inclusion of geosynthetic materials in road structures may support in respect of separation, reinforcement, stress relief function, and acts as a moisture barrier. The previous studies reveal that geogrids perform better as a reinforcing element, because of their interlocking properties and tensile modulus characteristics. Geogrids have gained tremendous advantages over traditional methods. In the current situations, interlayer

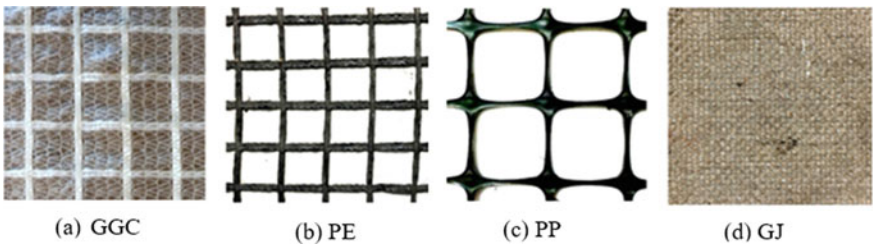

Fig. 1 Various types of geosynthetics (Obtained from Kumar and Saride 2018)

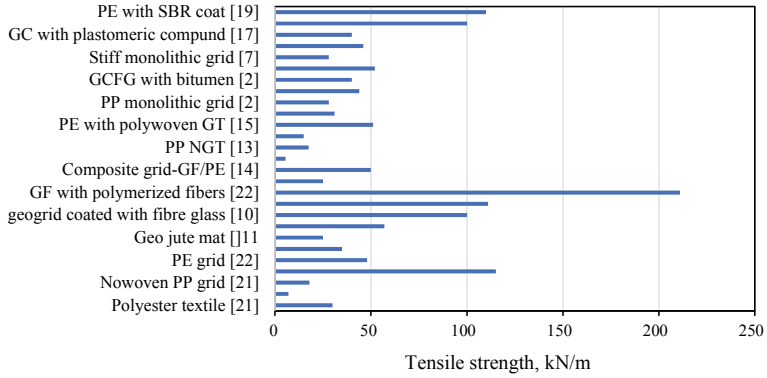

Fig. 2 Tensile strength characteristics of various geosynthetics used in literature

systems with geogrid have received significant attention as feasible solutions to intensify flexible pavement performance [2].

3 Geogrids

Geogrids are a distorted or non-distorted netlike polymeric material used as an essential part of human-made projects related to soil, rock, earth foundations, or any other geological engineering purposes. It has adequately high strength, high tensile modulus, and low-creep-sensitive polymers having apertures ranging from 10 to 100 mm in size or more. Generally, the geogrids are consisting of different opening shape patterns, i.e., squares, rectangles, elongated ellipse shape, squares with rounded corners, etc. Geogrids can be of the uniaxial grid, biaxial grid, or triaxial grids manufactured by extrusion processes, i.e., integrally joined or bi-directionally oriented meshes.

4 Geogrid Reinforced Asphalt Layers

Flexible pavements are the most used road structures in several countries, achieving a low cost of construction and maintenance operations when compared to other pavements. The higher traffic volumes and repeated vehicular traffic at frequent intervals of time can cause fatigue failure in flexible pavements. This distress is proposed as one of the most fundamental challenges in bituminous pavements. During repetitive action through vehicular loads, they were ensuring the formation of microcracks and exhaustive breakdown of pavement structure [3]. Geogrids are feasible to improve fatigue life and control the reflecting cracking that appears on the surface of an asphalt pavement. There are several researchers have been studied

on the geogrid application in asphalt layers since the 1980s [4], which results, lower the thickness and greater the durability of pavement that triggers to development of fatigue life. In addition to that, which acts as a reinforcement that improves the tensile modulus characteristics and interlayers shear properties of bituminous layers, these inherent properties of geogrids can mobilize at high strain levels over traffic loading. Predominantly geogrids were used to renovate the cracked pavements, but recently, these are popular in reinforcing the new asphalt pavements by restricting the fatigue crack propagation [4].

5 Literature Review

5.1 Nithin et al. [5]

This study illustrates the development of cracks, and their pattern in the asphalt concrete beam sample was investigated through a single-edge notched beam (SENB) test. Additionally, flexural and fracture properties of reinforced and control sections were evaluated. From the results of this study, it was concluded that the reinforcement effect did not exhibit much development in crack initiation, but it delays the propagation of crack growth at a specific temperature. The displacement in the time of crack propagation was observed as 0.5 mm is the constant value with a maximum variation. In the case of reinforced section (except for geotextile) at 10 °C, it was observed that the required applied force was reduced from 5 to 60% to initiate the crack in a beam sample in contrast to the control section.

5.2 Kumar and Saride [6]

Has performed their studies on double-layered asphalt specimens having a new bituminous layer compacted on the old pavement layer with several geogrids as interlayer reinforcement. Among all the interlayers, glass grid composite (GGC) was performed better than the others, such as the cracking resistance with energy dissipation was noticed as high as 2150 J/m^2, i.e., 2.8 times more than the reference sample. In addition to that, the tensile stiffness index of 33 kN/mm was recorded as the highest when compared with remaining geogrids.

5.3 Kumar and Saride [7]

Have carried another study using digital image correlation (DIC) analysis on three different geogrids for understanding the efficacy of geogrid reinforcement concerning the flexural fatigue performance of asphalt layers. Findings from the whole

research are illustrating that the fatigue performance of bituminous concrete beams was enhanced by nearly 39, 12, and 1.7 times for polyester geogrid, polypropylene geogrid, and geo jute mat, respectively. Further, the tensile strains are reduced to 70% for the polyester grid and increasing approximately 40 times against the polypropylene grid and geo jute mat. It was also noticed from the unreinforced section is the strains developed at the crack tip about 4.75% as the maximum at 335 cycles, and in the case of the polyester grid, it is 1.42% at 13,116 loading cycles.

5.4 *Loana et al. [5]*

Has focused on the flexural fatigue characteristics of glass fiber reinforced tri-layered beams by conducting four point bending tests. Results from the fatigue curves of both reinforced and unreinforced beams represent that the geogrid improves the fatigue life around 62% at 10 °C temperature with a frequency of 25 Hz. In addition to that, the tensile strain was increased by 10.52%, and the slope of the fatigue curve improved by 11.55%.

5.5 *Zofka et al. [8]*

Have experimented on three different asphalt beam combinations, including glass and carbon geogrids underneath the beam sample. Both the grids were placed in the tension zone and providing adequate asphalt concrete thickness on either side of the geogrid, i.e., approximately 30 mm from the lower part of the beam. From the cyclic four point bending tests, it was observed that the carbon geogrid reinforced section takes more number of loading cycles than the unreinforced one and the crack propagation was significantly decreased due to reinforcement action. In addition to that, the deflection was decreased to 51% and 31% because of the glass grid and carbon grid, respectively, and multiple times more energy is needed to spread the crack through the carbon grid reinforced section when compared to the unreinforced one.

5.6 *Canestrari et al. [9]*

Have carried a study on evaluating the bending resistance and interfacial shear resistance of geogrid reinforced bituminous layers. Three interface conditions are considered in this study, including no interlayer condition, carbon fiber geogrid (CF), and fiber-reinforced polymer geogrid (FP) interface types. The interlayer shear resistance and flexural resistance were improved in the case of CF geogrid.

5.7 Norambuena-Contreras and Gonzalez-Torre [10]

In this study, eight geosynthetics of two groups were examined through a dynamic test to analyze the mechanical, morphological, and thermal properties. Geosynthetics in the first group are manufactured using carbon or glass fibers, and the second group is composed of polymeric materials. Further, the effect on interlayers due to cyclic loads, installation procedures were evaluated, and the contribution to restrain the cracking was estimated. Conclusions from this study were reported that the geosynthetics having appreciable tensile properties, there is no need to show a high contribution to restraining the propagation of a crack in pavements. The cyclic load test results that the loss of mechanical properties of interlayers after completion of the test.

5.8 Emiliano et al. [11]

The whole study consists of a twofold target to approving the optimization procedure of designated geocomposites and evaluating the reflective cracking resistance of flexible pavement systems strengthened with such materials. The reflective cracking resistance of geogrid reinforced bituminous layers was investigated through the wheel tracking testing apparatus. Results from the research were indicated that the utilization of geocomposites prompts to de-bonding effect. Besides, the geocomposites arranged with an elastomeric bituminous layer strengthened with a fiberglass grid of 12.5 mm aperture size can be intended as the more suitable composite for flexible pavement reinforcement.

5.9 Lubinda et al. [12]

Has studied on eight different geosynthetics combined with hot mix asphalt samples to understand their cracking resistance and flexural behavior of test samples. As a means to evaluate its feasibility in pavement systems, the overlay tester was accommodated with a monotonic tensile loading condition. The results from the experimental study were reported that a noticeable development in the crack resistance and flexural performance with the inclusion of geosynthetic interlayers. When compared with the unreinforced section, there was about 40% increment was observed reinforced sections. The improvement concerning to the flexural properties in geosynthetics is established in descending order from the interlayer G1 to G8.

5.10 Fereidoon et al. [13]

This study focuses on the rate of crack growth, several load cycles before failure, and the effect of thickness on the geosynthetic reinforced asphalt overlays was studied. From the findings of this research, it was observed that the utilization of geotextiles and geocomposites were enhanced the bending resistance and can reduce the crack propagation. Samples having lower thickness embedded with geosynthetics could decreasing the reflective cracking drastically. In addition to that, geosynthetics having higher modulus gives more favorable results in thick overlays when compared with thinner layers, and it took more number of loading cycles.

5.11 Ferrotti et al. [14]

In this study, an experimental investigation was conducted to check the influence of tack coat application and their effect on the mechanical behavior, performance of fiberglass geogrid in the asphalt pavements. It was performed in two separate stages, in the first stage, the impact of various asphalt binders for their adhesion properties was studied. During the second stage, an extensive testing program was executed. Findings from the whole research reported that the effect of asphalt binder has a significant impact on the geogrid performance.

5.12 Millien et al. [15]

Has performed experimental research on assessing the mechanical performance of asphalt layers concerning fatigue cracking and thermal cracking with the help of tensile bending testing. The glass fiber grid acts as a metallic reinforcement, which delays the fatigue cracking in pavements due to repeated loading action. Thermal traction and bending nature occurred in the beam samples were reduced with a carbon fiber grid. The thickness of the beam was reduced to 20% with the conventional test samples.

5.13 Ferrotti et al. [16]

Has performed various laboratory studies for analyzing the performance of geogrid reinforced flexible pavements. Therefore, the research was initiated with four point bending experiments and ancona shear testing research and analysis (ASTRA) test using fiberglass geogrid to obtain the overall resistance performance of two-layered

asphalt samples. The results from the testing program were showed that the geogrid reinforced specimens contribute to increasing the service life of about 1.2–1.8 times higher than the reference samples. In the case of repeated loading cycles, it was observed that the reference samples were lost their stiffness quickly, demonstrating that the geogrid contribution leads when the bituminous concrete reaches the cracking.

5.14 Zamora-Barraza et al. [17]

Was made a comparison of three different geogrids for determining the fatigue life and vertical deformation of the asphalt beams. Results concluded that the polyester grid (G1) sustained 6. 4 kN/m, polyester grid with polyvinyl chloride (G2) withstands 11.8 kN/m, and geogrid with glass fiber threads (G3) takes 64 kN/m for 1.2% of vertical deformation. All the geogrids irrespective of their composition shows better performance than the reference sample. In addition to that, G3 has illustrates better results with 50% more repeated loading cycles than G2 and three times higher than the grid G1.

5.15 Virgili et al. [1]

This research focuses on the effectiveness of geosynthetic reinforced asphalt concrete beams on flexural properties for the repeated loading cycles. As well as this study correlated the double-layered systems of untreated and tack coat treated beam samples and to comprehend the flexion behavior of the asphalt samples more readily. Since the results of improvement ratio (IR) and vertical displacements (VD), the geomembrane (GM) combination permits to improve the service life keeping less vertical displacement values. Which represents the GM goes about as a pressure-retaining framework and enables to disperse load equitably. On the other hand, glass fiber geogrid (GG) and polyester geogrid (PG) show acceptable IR values yet besides, high VD values. High shape function values of 4.3 for untreated series and 4.4 for emulsified series are accomplished at the fast increment of fractures in permanent deformation.

6 Observations and Analysis

See Fig. 3 and Table 1.

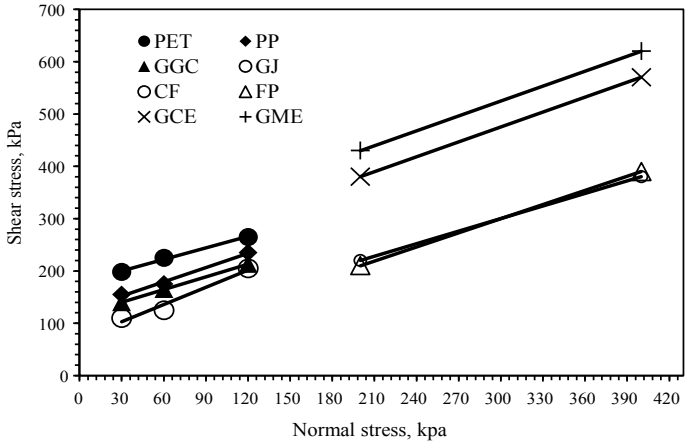

PET,PP,GGC,GJ (Kumar, V. V., & Saride, S. 2017); CF,FP (Canestrari et al. 2015); GCE,GME (Ferrotti et al. 2011)

Fig. 3 Interfacial properties of various geosynthetics of various geosynthetics used in literature

7 Conclusions

The conclusions drawn from an extensive literature review were described in the following section.

- Geogrids are the most effective stress relief barriers among all the geosynthetic interlayers due to their higher stiffness property of grid mesh, and interlocking effect. It contributes to increasing the durability of overlaying asphalt layers by restricting the structural deformations and thermal cracking.
- Geosynthetics acts as a crack impeding interlayer system due to their high stiffness by restricting the reflective cracking significantly. Further, the maintenance and rehabilitation of pavement systems were controlled with the protection of hot mix asphalt layers.
- The more fracture energy for initiating the crack from bottom to top due to repeated loading action was taken when compared to the unreinforced sections by introducing geosynthetics at the interface of asphalt concrete layers.
- The inclusion of geogrids in asphalt overlays reduced the overall thickness of the flexible pavement and delayed the speed of crack propagation by diverting into the interface grid system.
- Geogrids improved the fatigue life of an asphalt pavement system by taking a higher number of loads with less vertical deformation. This phenomenon leads to increasing the service life of the flexible pavement.

Table 1 Properties of different geosynthetics from various studies

Geosynthetic name	Aperture size (mm^2)	Source	Test conditions	Location of the grid	Specimen size ($l \times b \times h$ mm^3)	Binder type
Glass fiber grid	17 × 14	Zofka et al. [8]	13 ± 1 °C; 1 Hz	30 mm from the bottom layer	400 × 200 × 100	Quartzite sand
Carbon fiber grid	19 × 19					
Paving mat having fiber glass strands	–	Wargo et al. [18]	15 °C, 20 °C, 23 °C, 25 °C; 5 Hz and 10 Hz	Mid length of the specimen	400 × 64 × 100	SS-1; CRS-2; High polymer modified tack coat
Paving mat combination of FG and PE fibers	–					
FG grid with polymer-modified coating	25 × 25					
PE combined with NGT	–	Zamora-Barraza et al. [17]	15 °C	Eeach bonding section of the 3 layers	305 × 305 × 150	ECR-3 emulsion
PE grid	NA					
GF grid	NA					
GT	NA					
Biaxial PE grid	18 × 18	Kumar and Saride [6]	20 °C, 30 °C, 40 °C	Mid depth of the sample	400 × 300 × 90	PG 60-70
Biaxial PP grid	40 × 40					
GJ	NA					
GGC	NA					
Fiber glass grid	25 × 25	Lee et al. (2000)	21 ± 1 °C; 5 Hz	Interface zone of the both layers	380 × 63 × 100	PG 64-28
FP grid with thermosetting epoxy resin	33 × 33	Ferrotti et al. [16]	20 °C, 1 Hz	Mid depth of the specimen	305 × 90 × 75	Conventional cationic emulsion and SBC modified emulsion

(continued)

Table 1 (continued)

Geosynthetic name	Aperture size (mm^2)	Source	Test conditions	Location of the grid	Specimen size ($l \times b \times h$ mm^3)	Binder type
Glass fiber grid	40 × 40	Loana et al. [5]	5 °C, 10 Hz	Each interface zone of 3 layers	630 × 100 × 150	Residual bitumen
PE with light unwoven fabric	40 × 40	Zamora-Barraza et al. [17]	20 °C, 10 Hz	Mid depth of the sample	305 × 305 × 100	ECR-3 emulsion
PE with PVC	35 × 35					
PE with pressure sensitive glue	12.5 × 12.5					
Glass fiber geogrid	20 × 20	Millien et al. [15]	5 °C, 1 Hz	Interface zone	560 × 110 × 95	Residual bitumen
Carbon fiber geogrid	33 × 33					
Jute woven GT	–	Nithin et al. [5]	10 °C, 20 °C, 30 °C	30 mm from the bottom	400 × 100 × 100	VG 30
Coir GT	–					
Synthetic GT	–					
Polyethylene terephthalate NGT	–	Fereidoon et al. [13]	20 °C, 10 Hz	Overlay thickness of 50,75,100 mm	380 × 150 × 150	PG 64-22
Geocomposite of PP and glass fibers	–					
Polypropylene NGT	–	Canestrari et al. [9]	2 °C, 10 Hz	Interface zone	410 × 260 × 100	C69 B3 emulsion (EN 13,808)
NGT Reinforced with glass fiber	40 × 40					
PE bonded with PP NGT	40 × 40					
PP stiff monolithic geogrid	40 × 40					
GF with PE NGT	65 × 65					

(continued)

Table 1 (continued)

Geosynthetic name	Aperture size (mm^2)	Source	Test conditions	Location of the grid	Specimen size ($l \times b \times h$ mm^3)	Binder type
PP punched sheet drawn	28 × 33	Ling and Liu [2]	20 °C, 2 Hz	Bottom of the asphalt layer	60 mm thick bituminous layer	NA
Glass fiber geogrid	33 × 33	Canestrari et al. [9]	5 Hz	30 mm from the bottom layer	240 × 90 × 75	SBC polymer modified tack coat
Carbon fiber geogrid	20 × 20					
Fiber glass grid coated with thermo epoxy resin	33 × 33	Ferrotti et al. [14]	20 °C, 1 Hz	30 mm from the bottom layer	305 × 305 × 75	Cationic bitumen emulsion

Note: *CF* carbon fiber geogrid; *CRS* cationic rapid setting; *GC* geocomposites; *GCE* geogrid with conventional emulsion; *GME* geogrid with modified emulsion, *GM* geomembrane; *FG* fiber glass geogrid; *GF* glass fiber geogrid; *GGC* glass grid composite; *GJ* geo jute mat; *GT* geotextile; *NA* not addressed, *NGT* nonwoven geotextile; *PE* polyester geogrid; *PET* polyester grid coated with polymeric modified binder; *PG* performance grade; *PP* polypropylene geogrid; *PVC* polyvinyl chloride; *PV* polyvinyl; *SS* slow setting

Table 2 Summary of the geosynthetic reinforced asphalt overlays

Source	Topic of the study	Type of the reinforcement	Tests performed	Major findings
Nithin et al. [5]	Find out a proper methodology for SENB tests and flexural, fracture properties of reinforced asphalt layers at various temperatures	1. Jute woven geotextile 2. Coir geotextile 3. Synthetic geotextile	– Three point bending test – Leutner shear test	– Fracture energy was increased about 2–14 times
Kumar and Saride [6]	Examined the crack resistance potential of geosynthetic reinforced asphalt overlays by digital image correlation	1. GGC 2. Polyester grid 3. Polypropylene grid 4. Geo jute mat	– Direct tensile strength test	– All test samples show good cracking resistance at 20 °C
Kumar and Saride [7]	Flexural fatigue characteristics of geosynthetic reinforced asphalt beams were studied	1. Polyester grid (PE) 2. Polypropylene grid (PP) 3. Geo jute mat (GJ)	Four point bending test under cyclic loading condition	– The induced tensile strains were noted as 1.42% in the case of PE than the control section of 4.75%
Loana et al. [5]	Investigated the fatigue behavior of geogrid reinforced bituminous concrete	Glass fiber grid	– Three point bending test – Four point bending test	The fatigue life was increased by 62% with glass fiber geogrid at 10 °C
Zofka et al. [8]	Characterized and evaluated the advantages of using geogrids in bituminous layers	– Glass fiber grid (GG) – Carbon fiber grid (CG)	– Three point bending test – Four point bending test	CG performs better than the GG with respect to the repeated loading cycles
Canestrari et al. [9]	A laboratory and field studies were carried out to examine the reflective cracking potential of geocomposite reinforced asphalt pavements	– Plastomeric geocomposites (PG) – Elastomeric geocomposites (EG) – Fiber glass grids (FG)	– Ancona Shear Testing Research and Analysis (ASTRA) tests – Simulative reflective cracking (SRC) tests	– PG leads to lessen the interface shear resistance than the EG and FG with higher mesh size

(continued)

Table 2 (continued)

Source	Topic of the study	Type of the reinforcement	Tests performed	Major findings
Lubinda et al. [12]	Fracture performance and cracking resistance of geosynthetic established asphalt layers was studied	Fiber glass grids composed by polyester, polypropylene	Overlay Tester	– The fiber glass grid composed of polyester exhibits surpassing statistical fracture performance than the grids with polypropylene
Fereidoon et al. [13]	The impact of the overlay thickness and geosynthetic modulus on load cycles for generating the crack and its growth rate was examined	Geotextiles and geocomposites blended with polyethylene and polypropylene	Repeated cyclic loading tests with hydraulic Universal testing machine	– Geosynthetics with greater modulus was more effective in the thicker layers, and it was highly influenced the rate of crack growth, vertical displacement in the asphalt overlays
Ferrotti et al. [14]	Geogrid reinforced asphalt layers with several mesh sizes were studied by applying different surface coatings on the grid surface	Fiberglass geogrid	– Pneumatic adhesion tensile test – ASTRA test – Four point bending test	– Geogrid with thermosetting epoxy resin coating was commenced the highest pull of bond strength
Millien et al. [15]	The mechanical performance of the geogrid reinforced two-layered asphalt layer was examined	– Carbon fiber geogrid – Glass fiber geogrid	– Tensile bending test	– Glass fiber geogrid was most efficient with respect to time performance
Ferrotti et al. [16]	Fatigue behavior and interfacial shear characteristics of geogrid reinforced bituminous layers were investigated	Fiber glass geogrid	– Four point bending test – ASTRA test	– Interfacial shear characteristics were improved with modified emulsion
Zamora-Barraza et al. [17]	Examined the adherence properties of geosynthetic reinforced asphalt layers	– Geotextile – Glass fiber geogrid	Adherence test with cyclic loading	– Geotextiles are less sensitive to the asphalt binder content having low shear resistance
Virgili et al. [1]	The impact of geosynthetic reinforcement on flexural characteristics and resistance to cyclic loading is studied	– Glass fiber geogrid (GF) – Polyester geogrid (PG) – Geomembrane (GM)	Four point bending test	– GM is having low vertical deflections which contribute to more service life

(continued)

Table 2 (continued)

Source	Topic of the study	Type of the reinforcement	Tests performed	Major findings
Hartman and Gilchrist [19]	Fatigue crack development in two-layered asphalt beams is assessed through digital image captured configuration	– No interlayer	Four point bending fatigue tests	– Crack development in Linear elastic fracture mechanics model was evaluated
Ling and Liu [2]	The effectiveness of geosynthetic reinforced bituminous pavement system is evaluated under different loading configurations	– Polypropylene geogrid – Polyester geogrid	– Monotonic loading test – Cyclic loading test	– Restraining effect concerning beam stiffness is increased in the region of the loading area

- Geogrids usage in pavement has enhanced the pavement performance by strengthening structural capacity, decreasing distress potential, and arresting aggregate material from moving laterally under applied wheel loading.
- Geosynthetic materials helped in reducing the depth of rut in terms of lesser permanent deformation in the surface of the asphalt concrete layer when compared to unreinforced pavements (Table 2).

References

1. Virgili A, Canestrari F, Grilli A, Santagata FA (2009) Repeated load test on bituminous systems reinforced by geosynthetics. Geotext Geomembr 27(3):187–195. https://doi.org/10.1016/j.geotexmem.2008.11.004
2. Ling HI, Liu Z (2001) Performance of geosynthetic-reinforced asphalt pavements. J Geotech Geoenviron Eng 127(2):177–184. https://doi.org/10.1061/(ASCE)1090-0241(2001)127:2(177)
3. Di Benedetto H, D La Roche C, Baaj H, Pronk A, Lundström R (2004) Fatigue of bituminous mixtures. Mater Struct 37(3):202–216.2 https://doi.org/10.1007/BF02481620
4. Brown SF, Thom NH, Sanders PJ (2001) A study of grid reinforced asphalt to combat reflection cracking. J Assoc Asphalt Paving 70:543–569
5. Sudarsanan N, Arulrajah A, Karpurapu R, Amrithalingam V (2020) Fatigue performance of geosynthetic-reinforcedasphalt concrete beams. J Mater Civil Eng 32(8):04020206. https://doi.org/10.1061/(ASCE)MT.1943-5533.000326
6. Kumar VV, Sarid S (2018) Evaluation of cracking resistance potential of geosynthetic reinforced asphalt overlays using the direct tensile strength test. Constr Build Mater 162:37–47. https://doi.org/10.1016/j.conbuildmat.2017.11.158
7. Kumar V, Saride S (2017) Evaluation of interface shear properties of Asphalt layers reinforced with geosynthetic interlayers. Indian geotechnical conference GeoNEst.
8. Zofka A, Maliszewski M, Maliszewska D (2017) Glass and carbon geogrid reinforcement of asphalt mixtures. Road Mater Pavement Design 18(sup1):471–490. https://doi.org/10.1080/14680629.2016.1266775
9. Canestrari F, Belogi L, Ferrotti G, Graziani A (2015) Shear and flexural characterization of grid-reinforced asphalt pavements and relation with field distress evolution. Mater Struct 48 (4):959–975. https://doi.org/10.1617/s11527-013-0207-1
10. Norambuena-Contreras J, Gonzalez-Torre I (2015) Influence of geosynthetic type on retarding cracking in asphalt pavements. Constr Build Mater 78:421–429. https://doi.org/10.1016/j.conbuildmat.2014.12.034
11. Pasquini E, Pasetto M, Canestrari F (2015) Geocomposites against reflective cracking in asphaltpavements: laboratory simulation of a field application. Road Mater Pavement Des 16 (4):815–835. https://doi.org/10.1080/14680629.2015.1044558
12. Walubita LF, Faruk AN, Zhang J, Hu X (2015) Characterizing the cracking and fracture properties of geosynthetic interlayer reinforced HMA samples using the Overlay Tester (OT). Constr Build Mater 93:695–702, ISSN 0950-0618. https://doi.org/10.1016/j.conbuildmat.2015.06.028. (https://www.sciencedirect.com/science/article/pii/S0950061815007102)
13. Moghadas Nejad F, Noory A, Toolabi S, Fallah S (2015) Effect of using geosynthetics on reflectivecrack prevention. Int J Pavement Eng 16(6):477–487. https://doi.org/10.1080/10298436.2014.943128
14. Ferrotti G, Canestrari F, Pasquini E, Virgili A (2012) Experimental evaluation of the influence of the surface coating on fiberglass geogrid performance in asphalt pavements. Geotext Geomembr 34:11–18. https://doi.org/10.1016/j.geotexmem.2012.02.011

15. Millien A, Dragomir ML, Wendling L, Petit C, Iliescu M (2012) Geogrid interlayer performance in pavements: tensile-bending test for crack propagation. In: 7th RILEM international conference on cracking in pavements, pp 1209–1218. Springer, Dordrecht. https://doi.org/10.1007/978-94-007-4566-7_115
16. Ferrotti G, Canestrari F, Virgili A, Grilli A (2011) A strategic laboratory approach for the performance investigation of geogrids in flexible pavements. Constr Build Mater 25(5):2343–2348. https://doi.org/10.1016/j.conbuildmat.2010.11.032
17. Zamora-Barraza D, Calzada-Pérez MA, Castro-Fresno D, Vega-Zamanillo A (2011) Evaluation of anti-reflective cracking systems using geosynthetics in the interlayer zone. GeotextGeomembr 29(2):130–136. https://doi.org/10.1016/j.geotexmem.2010.10.005
18. Wargo A, Safavizadeh SA, Kim YR (2017) Comparing the performance of the fiberglass grid with composite interlayer systems in asphalt concrete. Transp Res Record 2631(1):123–132. https://doi.org/10.3141/2631-14
19. Anton H, Gilchrist M (2004) Evaluating four-point bend fatigue of asphalt mix using image analysis.J Mater Civil Eng 16:60–68. https://doi.org/10.1061/(ASCE)0899-1561(2004)16:1(60)
20. Gonzalez-Torre I, Calzada-Perez MA, Vega-Zamanillo A, Castro-Fresno D (2015) Experimental study of the behavior of different geosynthetics as anti-reflective cracking systems using a combined-load fatigue test. GeotextGeomembr 43(4):345–350. https://doi.org/10.1016/j.geotexmem.2015.04.001
21. Kumar V, Saride S (2017) Use of digital image correlation for the evaluation of flexural fatigue behavior of asphalt beams with geosynthetic interlayers. Transp Res Record 2631(1):55–64. https://doi.org/10.3141/2631-06
22. Sudarsanan N, Karpurapu R, Amirthalingam V (2019) Investigations on fracture characteristics of geosynthetic reinforced asphalt concrete beams using single edge notch beam tests. Geotext Geomembr 47(5):642–652. https://doi.org/10.1016/j.geotexmem.2019.103461
23. Arsenie IM, Chazallon C, Duchez JL, Mouhoubi S (2017) Modelling of the fatigue damage of a geogrid-reinforcedasphalt concrete. Road Mater Pavement Desig 18(1):250–262

Study on Travel Time Characteristics of Hubli-Dharwad Bus Rapid Transit System in Comparison with Heterogeneous Traffic Lane

Shivaraj Halyal, Raviraj H. Mulangi, M. M. Harsha, and Himanshu Laddha

Abstract Bus Rapid Transit System, which is also known as BRTS, is a very effective transit system in terms of travel time reduction. It has advantages compared to conventional road-based public transport like dedicated lane and pre-board fare collections. In the current study, performance-based travel time characteristics like travel time and travel speeds are evaluated by conducting the speed and delay survey for the BRT buses and private vehicles separately. The survey was performed by moving the car observation method to find out travel time and respective delays that are currently hampering the operations. Speed and delay survey for BRT buses was performed through the manual observation by travelling in the bus. Based upon the study, it has been found that there is a positive side effect of a dedicated corridor on the operation of BRTS buses, as obtained trial running speed values are almost very near to measured free-flow speed values on the selected study corridors. Meanwhile, it has been observed that the BRTS bus operation has faced many delays due to bus bunching, dwell time at the stations and delays at the intersections but delays occurring at the stations have contributed major proportion in the total delay.

Keywords Station delay · Travel time · Speed · Public transit

1 Introduction

From the last couple of years, there has been a rise in mobility in metro cities of India because of economic activity and an increase in average income and with Delhi leading [1]. Also, India's population in major metro cities increased by 1.9 times during the period 1981 to 2001, the number of vehicles multiplied by over

S. Halyal (✉) · R. H. Mulangi · M. M. Harsha · H. Laddha
Department of Civil Engineering, NITK Surathkal, Surathkal, Karnataka 575025, India
e-mail: shivaraj.halyal@kletech.ac.in

R. H. Mulangi
e-mail: ravirajmh@nitk.edu.in

B. Laishram and A. Tawalare (eds.), *Recent Advancements in Civil Engineering*, Lecture Notes in Civil Engineering 172,
https://doi.org/10.1007/978-981-16-4396-5_61

7.75 times during a similar period [2] and for the same time duration, the increased rate of growth of personal vehicle is around 9.9% [3]. These give challenges to the prevailing transport sector and available infrastructures. The reason for these increases in a private vehicle is especially economic activities and deteriorated public transport. For many years' comforts and Travel time never been a parameter to choose public transport unlike fare prices but from a previous couple of years, people choose comfort and time of travel over fare prices. As an answer to those problems concept of Bus rapid transit system (BRTS) adopted in India. As per the Institute for Transportation and Development Policy, "Bus rapid transit is a high-quality bus-based transit system that delivers fast, comfortable, and cost-effective services at metro-level capacities". Currently, in the world, 172 cities have a BRT system with 3,38,65,329 average passengers per day on around 5163 km of BRT corridors [4]. In India, 23 BRT systems are sanctioned, out of that in 14 cities BRT, the system is operational and others are within the planning phase. Rainbow BRTS (Pune and Pimpri-Chinchwad) is the first BRTS that started in India on Dec. 2006. Some of the features of BRTS are well-designed routes, fast and low-end routes, early fare collection and fare verification, secure and comfortable closed stations, detailed route maps, landmarks, and real-time data details, and automotive automotive technology to manage traffic. BRTS system performance can be tested from parameters such as travel time, Identity and image, safety and security and power. All of these parameters are affected by BRTS signals. All these parameters are affected by the characteristics of BRTS. The idea behind the introduction of the BRT programme in the country is to prioritize street buses, some of which are stuck in traffic jams due to congestion so that a large number of people can be transported to the city faster. As BRT system is implemented based on the travel time reduction concept and to validate a preliminary study is needed. So in the current study, performance-based operational characteristics like travel time and travel speeds are evaluated by conducting the speed and delay study for the BRT buses and private vehicles separately.

2 Literature Review

Detailed revisions are made with BRT bus travel time signs on a dedicated road and mixed traffic route. The study focussed on travel time and the number of delays that occur on BRT buses compared to the normal flow of traffic. Basically, studies involving a variety of travel-related factors and how they should be measured were studied. Macababbad and Regidor [5] tried to address the questions regarding suitable and practible methodology which can be necessary to collect effective travel time and delay data of road corridor. Also, authors were interested in suitable method for analysis and presentation. This study shows effective methodology using tool to analysis speed and delay data. Authors collected data with probe vehicle method and GPS unit. The use of GPS in this study helps to the design of the test vehicle system with some extend. Authors found that the use of GPS devices alone allows

processing post data received from a survey run while the test vehicle system was designed Real-time updates and traffic information collection. In order to develop an investigative vehicle system, other important IT requirements such as a centralized communication system should be put in place. Chepuri et al. [6] examined the traffic flow characteristics of the BRTS road in Surat city. Travel time is calculated using the app box, GPS devices, which provide real-time speed every 0.1 s. As a result, it was found that on many roads, the V/C ratio was very low and in many areas, high and therefore it was suggested to balance the shift from certain traffic from high to low. Kathuria et al. [7] conducted a study on BRTS performance using GPS data for two routes in Ahmadabad. Performance appraisals were conducted based on both objectives, namely transport performance and traffic law. Performance-based performance assessments use indicators such as percentile time travel, coefficient of variation (COV) of travel time, average travel speed and distribution of travel time, while transportation law uses indicators such as schedule adherence and head familiarity. As a result, it was found that the change in the LOS network from 2013 to 2016 was based on the average travel time per km and COV per travel time. A left-hand shift in the collection plan has been found, suggesting that the full network performance improvement for 2016 compared to 2013. Godabarthi et al. [8] tried to find out the optimum V/C ratio to evaluate the capacity of MT lanes and BRT lane for Delhi and Ahmedabad. To generate large data set, they used VISSIM software along with that he performed Traffic volume survey and speed-delay survey (Probe vehicle method) in both of the cities. Roadway capacity was also estimated to understand the performance of the BRTS for MT lanes and bus lanes.They found that a 0.688 V-C ratio is the optimal flow value for BRT corridors. This implies that up to 0.688, both the MT lane users and bus lane users will enjoy reasonable travel speeds and smaller delays. If the V-C ratio is exceeded on either BRT lane or MT lane(s), then the BRT system becomes untenable for the MT lane and BRT users, creating traffic congestion. Sharma et al. [9] attempted to obtain the result that dedicated bus routes end at the correct distance before the stop lane at busy intersections indicating distance, and bus routes were made available to all motorists at intersections in Delhi. Performance tests are performed on the average queue length, maximum queue length, and the time delay for each vehicle, and various gas emissions from vehicles. It was found that the availability of bus routes on other motorbikes at the right distance significantly reduced queue length, average delay time per vehicle and emission output of each vehicle, while there was an increase in traffic flow and average speed of all vehicles on the network. In addition, the average vehicle speed in the network was increased by about 23%.

3 Methodology and Data Collection

Performance evaluation of BRTS mostly incorporates the travel time and delays occur to BRT buses. So, identification of factors that affect the travel time and delay is important to improve the BRT system. Mainly travel time depends on the

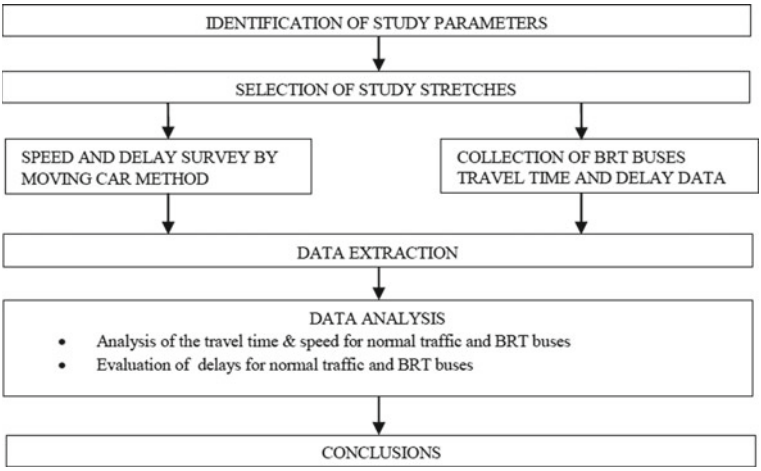

Fig. 1 Flow chart of the methodology

passenger service time, delays and running time, but all these parameters have many sub-factors that affect the travel speed of BRTS. Analysis of the travel time of normal traffic and BRT buses will help us to identify the factors which affect the BRT bus delay and also will helpful for the improvement of the system. Figure 1 shows the systematic flow chart of the methodology for this study.

3.1 Study Area

Hubli and Dharwad city combined called twin cities of Karnataka in India. In 1962, Hubli and Dharwad were combined and recognized as twin cities with the formation of the Hubli-Dharwad Municipal Corporation, which is also known as HDMC. The population (According to the 2011 census) of HDMC is approximately 10 lakh and covers an area of 202 km^2 where the developed area is approximately 72.78 km^2 including 45 villages and a large number of extensions spread on all sides. Both cities are separated by 22 km and are connected by a state highway (PB road), a national highway (NH4) and the Mumbai Bangalore railway line.

3.2 Data Collection

Speed and delay survey was conducted on the route of Hubli-Dharwad for the mixed traffic and BRTS routes. In HDBRTS dedicated corridor are on the three different ROW, which is 35, 44 and 35 m again. On 44 m ROW, there are very

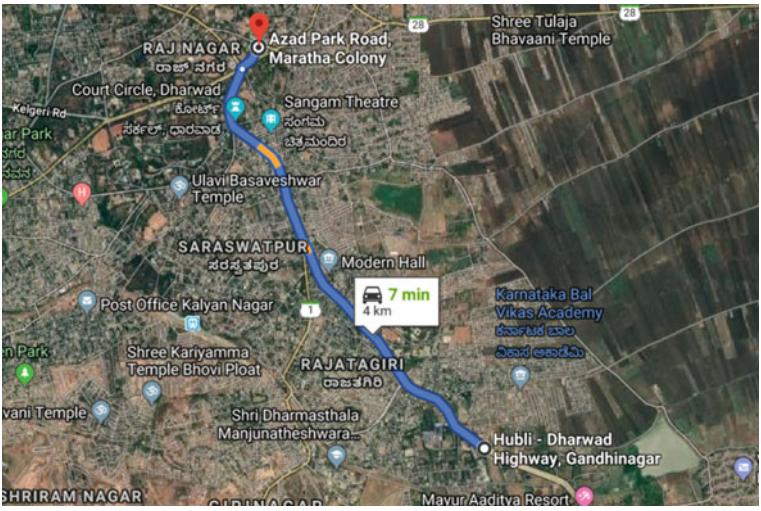

Fig. 2 Study Stretch from Lakhamanahalli BRT station to Dharwad BRTS Terminal. *Source* Google Map

chances for congestion so speed and delay study was performed on the 35 m ROW and mixed traffic lane with moving car observation method on 4.0 km long fully dedicated stretch from Lakhmanahalli BRT (LH BS) stop to Dharwad BRTS Terminal (DWD T). The study stretch is shown in Fig. 2.

The study was performed two typical weekdays (Tuesday and Wednesday) and one weekend day (Sunday) in 2 sessions.

1. Morning Session: 8AM–2:30PM
2. Evening Session: 3:30PM–8:00PM

For this study, total six enumerators were used. Out of these six enumerators, four enumerators were used for the moving car observation method in one car along with the driver, and the other two enumerators were used for collecting data of BRT bus travel time and delay. The survey was performed in such a way that the starting time of the journey for car and BRT buses were nearly the same. The duty of each enumerator is described as following.

Enumerator 1: This person is responsible for collecting data of journey time and the various delay occurs for moving car mainly intersection delay.

Enumerator 2: This person is responsible for collecting data of overtaken and overtaking vehicles to the moving car.

Enumerator 3&4: The number of the opposite vehicles is more so it is difficult to count all opposite vehicles by one enumerator, so this work was divided between both the enumerators. One enumerator counted two-wheelers, autos and trucks the same way another enumerator counted cars/jeep, tempo/LCV and buses.

Enumerators 5&6: Enumerators 5 and 6 are responsible for collecting data on journey time and amount of delay occurring because of the intersection, station stop, bus bunching and other types of delays concerning BRT buses along with their respective location.

Besides, four runs of moving cars were performed at midnight to collect the data of free-flow speed and related travel time. The average free-flow speed for Lakhamanahalli bus stop (LH BS) to Dharwad BRTS (DWD T) terminal is found to be 54.14 kmph. The same free-flow speed taken for BRT buses also as at midnight there is no much difference in the speed of BRTS and a moving car. The motive behind this free-flow study is to know about the increase in travel time because of congestion.

4 Methodology and Data Collection

4.1 Selection of Passenger Car Unit (PCU) Values for Different Vehicles

The PCU value of different vehicle categories doesn't remain constant under all situations because PUC/PCE is a function of physical dimensions and speed of the respective class of vehicles. For urban situations, the speed difference in different vehicle classes is generally low so it mainly dominated in physical dimensions of vehicles. As per IRC 106-1990, PCU values in urban areas depend on the percentage composition of vehicles in the urban traffic stream, and related values of PCU shown in Table 1.

Figure 3 shows the proportion of different class of vehicle for LH BS to DWD T and vice versa. It was found that out of total traffic two-wheeler has the highest proportion that is 53%. Also, it was found that car/jeep remains on 29% of the total traffic. Therefore, it means two-wheelers and car/jeep have more than 10%

Table 1 Recommended PCU factor for various types of vehicles on the urban road (IRC 106-1990)

Vehicle type	Percentage composition of vehicle type in the traffic stream	
	Less than 5%	10% and above
Two-wheelers (motorcycle or scooter, etc.)	0.5	0.75
Three wheeler (auto-rickshaw)	1.2	2.0
Passenger car	1.0	1.0
Light commercial vehicle	1.4	2.0
Truck or bus	2.2	3.7
Cycle	0.4	0.5
Cycle rickshaw	1.5	2.0

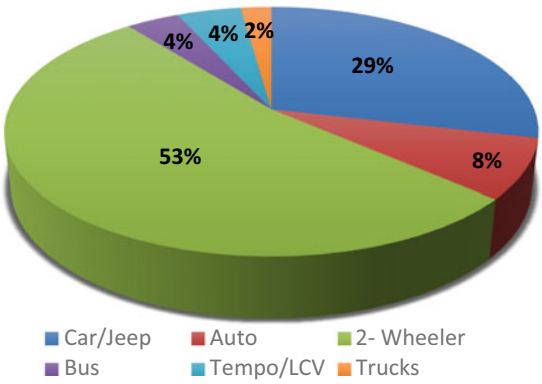

Fig. 3 The proportion of different class of vehicle in the traffic stream

Table 2 Adopted PCU values for a different class of vehicle in this study

Vehicle	Car/jeep	Auto	2-wheeler	Bus	Tempo/LCV	Trucks
PCU value	1.0	1.2	0.75	2.2	1.4	2.2

proportion of total traffic so adopted PCU values for a different class of vehicle is shown in Table 2.

4.2 Calculation of Journey Speed for Moving Car

To calculate journey speed for the car from the moving car observation method journey time is necessary to evaluate. To find out journey time, Eqs. 1 and 2 are used that are derived from the theory of moving car observation method. The volume (q_w) in the LH BS to DWD T direction can be obtained from the expression given in Eq. 1.

$$q_w = \frac{m_a + m_o - m_p}{t_a + t_w} \tag{1}$$

The average travel time in the LH BS to DWD T direction is obtained from the expression given in Eq. 2.

$$t_w(\text{avg}) = t_w - \frac{m_o - m_p}{q_w} \tag{2}$$

where,

m_a Number of vehicles travelling in the opposite lane while the test car is travelling DWD T to LH BS

m_o Number of vehicles that overtake the test car while it is travelling LH BS to DWD T
m_p Number of vehicles that the test car passes while it is travelling LH BS to DWD T
t_a Time which takes to travel DWD T to LH BS
t_w Time in minutes it takes to travel LH BS to DWD T (journey time)

Journey speed is the distance divided by total journey time which includes all delays due to traffic. Running speed is the distance divided by running time, i.e., total journey time minus delays. For BRT, Buses' total delay which is comprised of mainly three types of delays which are intersection delay (Signal delay), station Delay (dwell time), bus-bunching delays. At midnight, there was no difference in the travel time of BRTS buses and moving cars because of less traffic on their respective routes hence the free-flow speed of the BRTS bus is considered as same as the free-flow speed of moving cars.

5 Results and Discussion

This section comprises the comparison of various parameters concerning a journey starting time of moving car and BRT buses are described. After analysis summarized results for average journey time, average journey speed, average running speed and free-flow speed are described in Table 3.

5.1 Journey Speed, Running Speed and Free-Flow Speed of Moving Car

The comparison of average journey speed, average running speed and average free-flow speed for moving car concerning a journey starting time is shown in Fig. 4. The average free-flow speed is taken as 54.14 kmph. Average journey speed

Table 3 Summarized result of analysis

Parameters	Time	BRT buses	Moving car
Average journey time (Min.)	Peak hour	11.79	9.32
	Off-peak hour	11.01	8.94
Average journey speed (kmph)	Peak hour	20.65	25.99
	Off-peak hour	22.05	27.28
Average running speed (kmph)	Peak hour	39.5	32.37
	Off-peak hour	33.75	32.29
Free-flow speed (kmph)	–	54.14	54.14

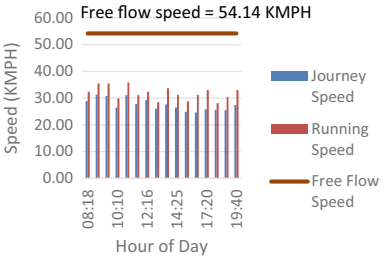

Fig. 4 Comparison of various speeds with respect to a journey starting time of moving car

is nearly around 27 kmph and average running speed is nearly around 33 kmph. It is observed that the difference between journey speed and running speed is less but the difference with respect to free-flow speed is more, which indicates less amount of stop delay and more congestion delay. Also, less variation of speeds found in the case of moving car for peak hour and off-peak hour.

5.2 *Journey Speed, Running Speed and Free-Flow Speed of BRT Buses*

The comparison of average journey speed, average running speed and average free-flow speed for BRT buses with respect to a journey starting time is shown in Fig. 5. From the figure, it is seen that average journey speed for the BRT Bus is nearly 22 kmph and for the same average running speed is around 37 kmph, which indicates more stop delay which includes signal delay, station delay and bus-bunching delay. Also, there is less difference between running speed and free-flow speed at peak hours which indicates the effectiveness of a dedicated corridor for BRT buses.

5.3 *Travel Time of BRT Buses and Moving Car*

The travel time comparison of the BRT bus and the Moving car is shown in Fig. 6. From the figure, the gap between the travel time of BRT Bus and the moving car is

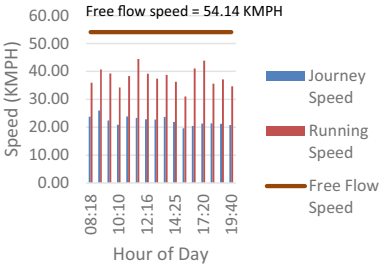

Fig. 5 Comparison of various speeds with respect to a journey starting time of BRTS buses

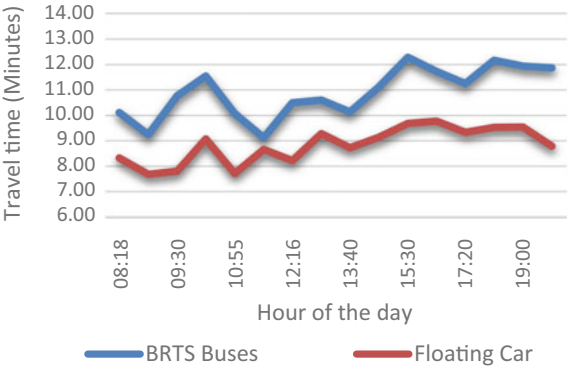

Fig. 6 Variation in travel time with respect to the journey start time of the day

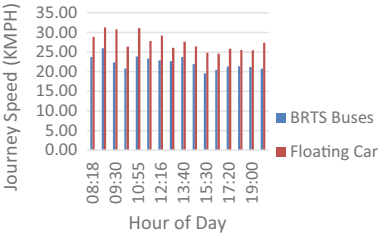

Fig. 7 Variation in the of the journey with respect to journey start time

visible with BRT bus travel time is more. At off-peak hour moving car and BRT buses are taking nearly the same time to reach their destination. At peak hours, this gap is more as compared to an off-peak hour, which indicates BRT buses taking a long time to reach their destination compared to the moving car. This might be because of the additional delays that occur to BRT buses which include bus bunching and station delay.

5.4 Journey Speed of BRT Bus and Moving Car

It has been found that in all the cases, BRT buses have lesser journey speed as compared to moving car, and many trips it is the same. The reason behind this mainly because of BRTS buses facing more amount of delays at the stations and intersection delays. Figure 7 shows the variations in the journey speeds of the BRT buses and moving car over the hour of the day for survey location. During peak hours, the speed difference between BRT Buses and moving car was found to be more as compared to off-peak hours.

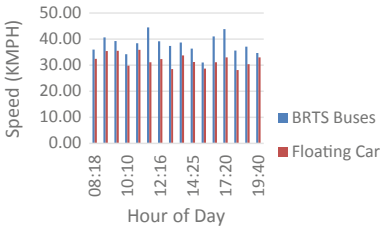

Fig. 8 Variation in running speed with respect to journey start time

5.5 Running Speed of BRT Bus and Moving Car

For most of the trips, BRT buses have more running speed as it has an advantage of the dedicated corridor but for non-dedicated lanes, it shows the same running speed as a moving car. Figure 8 shows the comparison of the running speed of the BRT buses and moving car over the hour of the day. From this figure, it can be observed that BRT buses have more running speed because of dedicated lanes. Also for peak hours, running speed differences between BRT buses and the moving car is more compared to an off-peak hour. This is clearly because of the off-peak hour moving car faced fewer delays.

6 Conclusions

In this study, the speed and delay survey for the BRT buses and private vehicles analysed with the moving car observation method for 4 km study stretch in the city of Dharwad. The performance of HDBRTS in terms of travel time was evaluated in the present study. The positive effect of the dedicated corridor on the BRTS bus operation is found, as running speed is very near to free-flow speed. Congestion during peak hours is one of the reasons for the reduction in journey speed and running speed of both vehicles, i.e., moving car and BRTS buses. In addition to that speed and travel characteristics of BRTS, and mixed traffic lanes were found to be almost the same. The reason behind this, operation of BRTS is exclusively is on the dedicated corridor and traffic volume is less on the MT lane. Station delay, i.e., dwell time is found to be an 80% share in the total delay caused to BRT buses. This delay should be minimized for increasing the journey speed of BRT buses. It is also observed that bus bunching at many stations, varying dwell time, more passenger demand, all these factors may lead to a reduction in bus station capacity. As most of the intersections are very nearby bus stations and there is no signal priority for BRT buses that is one of the causes for speed as well as the capacity problems of bus stations.

References

1. CSIR-2012 Evaluation of bus rapid transit performance from final report Ambedkar Nagar to Mool chand, Delhi
2. Ministry of Urban Development (2007) National urban transport policy. Retrieved 25 May 2010, from http://www.urbanindia.nic.in/policies/Transportpolicy.pdf
3. Darshini M, Rutul J, Abhijit D (2013) Low-carbon mobility in India and the challenges of social inclusion: bus rapid transit (BRT) case studies in India, UNEP. ISBN: 978-87-92706-77-5
4. The Global BRT Data, from http://brtdata.org/
5. Macababbad RJRM, Regidor JRF (2011) A study on travel time and delay survey and traffic data analysis and visualization methodology. In: Proceedings of the 9th international conference the Eastern Asia society for transportation studies, vol 8, pp 318
6. Chepuri A, Kulakarni R, Bains MS, Arkatkar S, Joshi G (2015) Evaluation of BRTS corridor in India using microscopic simulation: a case study in Surat City. In: Proceedings of the Eastern Asia society for transportation studies, vol 10
7. Kathuria A, Parida M, Sekhar CR (2017) Route performance evaluation of a closed bus rapid transit system using GPS data. Curr Sci 112(8):1642–1652
8. Godabarthi GR, Chalumuri RS, Velmurugan S (2014) Measuring the performance of bus rapid transit corridors based on volume by the capacity ratio. J Transp Eng 140(10):04014049
9. Sharma HK, Swami M, Swami BL (2012) Optimizing performance of at-grade intersection with bus rapid transit corridor and heterogeneous traffic. Int J Transp Sci Technol 1(2):131–145
10. IRC 106-1990 Guidelines for capacity of urban roads in Plain Area, New Delhi

Reuse of Crushed Concrete in Granular Sub-Base in Pavements

A. Sai Krishna, Sudhara, and Sita Rami Reddy

Abstract Construction and demolishing waste (CDW) is being generated in large quantity due to increasing in construction, maintenance activities, demolishing and infrastructure development projects. The CDW consists of reclaimed asphalt pavement, recycled concrete aggregates and crushed bricks. Recycled concrete aggregate and crushed bricks waste are obtained from the demolishing of an existing building, concrete pavement, kerb and block pavements. The generated concrete aggregate waste is not frequently used as recycling material in the construction of a base layer of pavement instead they are used for land fillings without proper recyling. This land fillings are causing pollution of groundwater due to leaching from waste material. The main objective of this study is to investigate the reuse of concrete aggregate in the construction of granular sub-base layer of pavement. The concrete aggregate from construction and demolition waste is crushed into smaller sizes and mixed with natural aggregate in different proportions. In this study, Granular Sub-Base (GSB) grading VI of MoRTH (MoRTH in Specifications for road works and bridges. Ministry of Road Transport and Highways, New Delhi, India 2013) specification was considered. Moisture-density relationship and California Bearing Ratio (CBR) value were evaluated on the prepared aggregates mixes. These tests are carried on the mixes prepared by varying the percentage of recycled concrete aggregates and the results were compared with the test results on the natural aggregate mix. Based on the results obtained from the moisture-density relationship and CBR, it is ascertained that the recycled concrete aggregates have the potential to be used in the construction of pavements GSB layer in normal and in low volume roads.

Keywords CBR · CDW · Granular sub-base

A. S. Krishna · Sudhara · S. R. Reddy (✉)
Civil Engineering Department, Visvesvaraya National Institute of Technology, Nagpur, India

B. Laishram and A. Tawalare (eds.), *Recent Advancements in Civil Engineering*, Lecture Notes in Civil Engineering 172,
https://doi.org/10.1007/978-981-16-4396-5_62

1 Introduction

Construction and Demolition waste is generated in large amounts in medium and large-sized cities in India. In India, the CDW was estimated as 24 million tonnes in the year 2010. The wide production of CDW and its illegal deposition are serious problems in India. The management of this material is becoming a major concern for town planners. Researchers have identified that CDW has a great potential to be reused as aggregate in road construction [1–4]. The typical composition of CDW produced in India is shown in Fig. 1. The aggregate from recycled construction and demolition waste is an attractive alternative material for the bases and sub-bases due to its high resistance, non-expansive behaviour and it also reduces the demand of the natural aggregate. However, the quality of the recycled materials varies considerably and is quiet difficult to control; some proper guidelines on the production and application of these aggregates are needed. So far many studies have been done to determine the properties of CDW aggregate. Nataatmadja and Tan [5] evaluated the resilient modulus of four recycle CDW aggregates. Resilient modulus was observed to increase with an increase in the compressive strength of the source concrete. The study concluded that the resilient modulus of recycled CDW was comparable, if not better, than that of typical virgin road aggregates. Arulrajah et al. [1] studied the physical property and shear strength of the recycled CDW aggregates with typical quarry material by conducting gradation, Los angeles abrasion test, unconfined compression strength (USC), California bearing test (CBR), direct shear test (DST), modified compaction test and static triaxial test. Based on the test results, author ascertained that CDW materials have the potential to be used in sub-base/base course application. Gomez-Meijide et al. [2] studied the binder-aggregate adhesion property and resistance to permanent deformation of the CDW aggregate. The author concluded that the bitumen mixture with both sort of aggregate shows very similar deformation at the end of the tests, but in those mixtures made with CDW aggregate, the deformation developed more slowly, which indirectly indicates the tertiary stage and the consequent material failure of the material will be reached after greater number of loading cycles. And the binder—aggregate affinity shows same for both the natural and CDW aggregates. This study, focus on evaluating the strength of the CDW aggregate as base/sub-base course by conducting CBR experiment and comparing the results of CDW aggregate with that of natural aggregate.

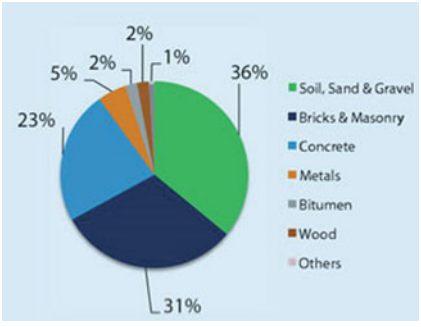

Fig. 1 Typical composition of CDW in India [6]

2 Material and Methodology

In this study, the materials used are natural crushed stone aggregates and the crushed concrete waste from the laboratory of M25 grade cubes. The aggregate properties are presented in Table 1. Granular Sub-Base (GSB) grading VI of MoRTH [7] specification is considered, which is shown in Fig. 2.

The tests performed were optimum moisture content (OMC) and California bearing ratio (CBR), these tests are conducted on five different mixes by varying the percentage of replacement of Natural Aggregate (NA) with the crushed Recycled Concrete Aggregate (RCA) are mentioned in Table 2. The sequence of RCA preparation is show in Fig. 3.

Modified compaction is used for the preparation of samples for CBR and OMC test, the soil is compacted in five layers, each layer being given 55 blows by dropping 4.89 kg rammer from height of 45 cm following the specification of IS:2720 Part VIII [11].

Table 1 Natural aggregate property

S. No	Property	Values	MoRTH [7] specification	Test methods
1	Aggregate crushing (%)	13.2	Max 30	IS:2386 Part IV [8]
2	Los Angeles abrasion (%)	12.4	Max 30	IS:2386 Part IV [8]
3	Aggregate impact (%)	9.4	Max 24	IS:2386 Part IV [8]
4	Water absorption (%)	0.55	Max 2.0	IS:2386 Part III [9]
5	Combined flakiness and elongation index (%)	32	Max 35	IS:2386 Part I [10]

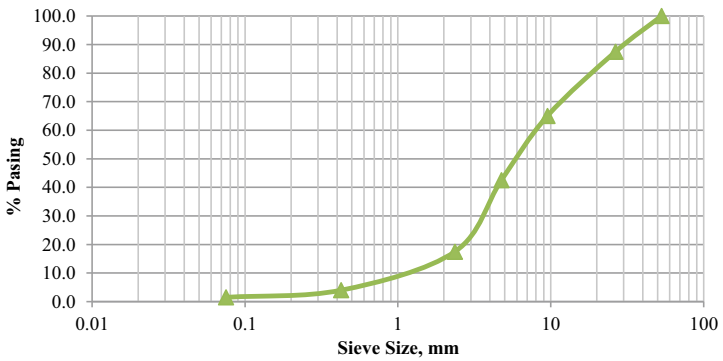

Fig. 2 Aggregate gradation of GSB VI [7]

Table 2 Summary of different mixes investigated

Mix	Natural aggregate (NA) in %	Recycled concrete aggregate (RCA) in %
NA100 + RCA0	100	0
NA95 + RCA5	95	5
NA90 + RCA10	90	10
NA85 + RCA15	85	15
NA80 + RCA20	80	20

Fig. 3 RCA preparation: **a** laboratory tested concrete beams, **b** crushing concrete beam and **c** crushed concrete beam

3 Test Procedure

3.1 Optimum Moisture Content (OMC)

Optimum moisture content for granular sub-base mix prepared with different replacement of natural aggregate with different percentage of RCA was estimated as per IS:2720 part VIII [11] procedure.

3.2 California Bearing Ratio (CBR)

CBR test was conducted on the granular sub base mix specimen prepared with different percentage of RCA material at optimum moisture content and maximum dry density. The test was conducted 4 days soaked specimens. The test was conducted by following IS: 2720 part XVI [12] procedure.

3.2.1 Preparation and Testing of Samples

At first sample material is collected and sieved through various sieves for obtaining the various sizes of the aggregates according to the gradation. The sample is prepared in a tray according to the gradation mentioned in Fig. 2 and kept in the oven

for around 24 h at a temperature of 110 °C for the removal of water in the material. The oven-dried sample is now kept outside for cooling and tests are performed on the sample. The RCA material used in mix is obtained from laboratory waste concrete cubes of M25 grade. The cubes are crushed into pieces and sieved through different IS sieves for obtaining different sizes of the gradation. Five different mixes were prepared by varying the proportions of NA and RCA. The modified compaction was performed on these prepared mixes. The graph between the water content and dry density is obtained and OMC is reported. The CBR test was also done on all the fives mixes prepared at their respectives OMC.

4 Test Results

Five different mixes are evaluated for the suitability of mix as pavement sub-base material. This mix consists of completely natural aggregates prepared by sieving through standard IS sieves as per grade VI of granular sub-base [7].

The graph is plotted for all the mixes against OMC is shown in Fig. 4, the OMC increases with increase in percentage of RCA in the mix, but Maximum Dry Density (MDD) decreases with the increase in the percentage of RCA in the mix as shown in Fig. 5. The increase in OMC and decrease in MDD with increase in percentage of RCA in mix is due to the high water absorption and low particle density of RCA [13]. Water absorption and density property of RCA depend on the residual adhered mortar on aggregate. The density of RCA is less than natural aggregate because adhered mortar is less dense that the aggregate and high water absorption is due to the high porosity of adhered mortar which allows the RCA to hold more water than natural aggregate [14].

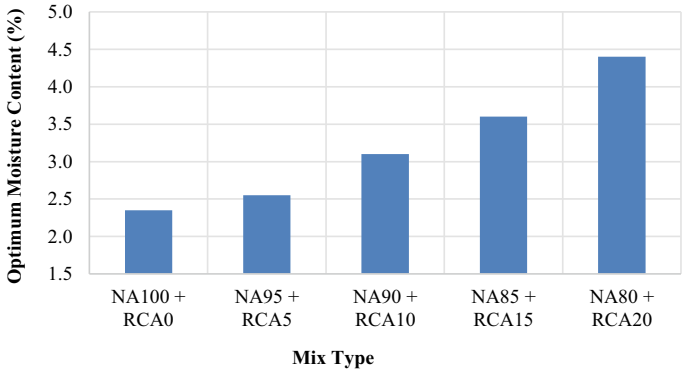

Fig. 4 OMC for different mixes

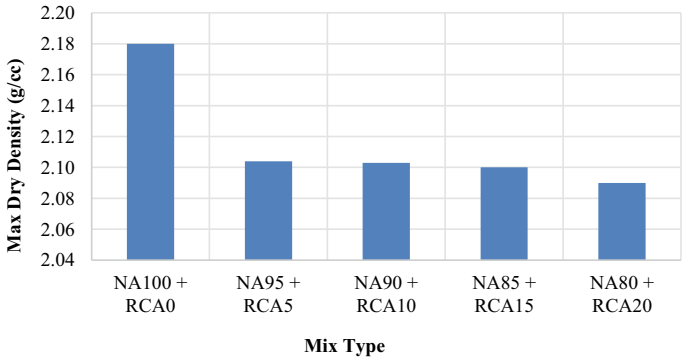

Fig. 5 Max dry density for different mixes

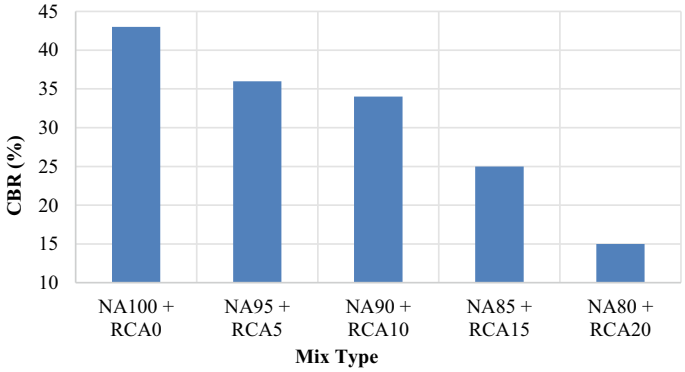

Fig. 6 CBR for different mixes

The percentage of CBR decreases with the increase in percentage of RCA in the mix as shown in Fig. 6. The strength of RCA depends on the source concrete strength; if the strength of concrete is high then the strength of the RCA will be high. In this study, we have used concrete strength of M25, which shows the softer strength due to attached mortar on the RCA.

In Fig. 7, it is shown that the percentage change of mix CBR goes on increases with increase in percentage of RCA in the mix. The mix with 15% and 20% RCA has higher percentage of reduction in mix CBR, which suggests using the RCA up to 10% in the mix.

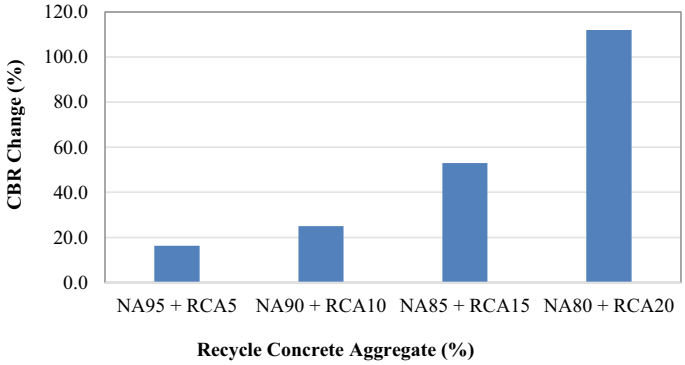

Fig. 7 Percentage change in CBR with RCA

5 Conclusion

The study evaluated the granular sub base material properties of the samples which were prepared using the RCA as a replace of the natural aggregates and also evaluated the effect of RCA on mix properties such as OMC, MDD and CBR values. The results show that CBR of crushed waste was slightly less to that of natural aggregate i.e. RCA presented a fairly decrease in its CBR. However, Mix NA95 + RCA5 and Mix NA90 + RCA10 can be used for high volume roads because the CBR values are greater than 30% and Mix NA85 + RCA15 can be used for lower volume roads as CBR value is less than 30% and greater than 20%. But the Mix NA80 + RCA20 cannot be used for pavement as CBR value is less than 20%.

References

1. Arulrajah A, Disfani MM, Horpibusuk S, Suksiripattanapong C, Prongmanee N (2014) Physical properties and shear strength response of recycled constructiin and demolition materials in unbound pavement base/sbbase application. Constr Biuld Mater 58:245–257
2. Gomez-Meijide B, Perez I (2016) Binder-aggregate adhesion and resistance to permanent deformation of bitumen-emulsion-stabilized materials made with construction and demolition waste aggregates. J Cleaner Prod 129:125–133
3. Evangelista L, de Brito J (2007) Mechanical behaviour of concrete made with fine recycled aggregate. Cement Concr Compos 29:397–401
4. Khatib JM (2005) Properties of concrete incorporating fine recycled aggregate. Cement Concr Compos 35:763–769
5. Nataatmadja A, Tan YL (2001) Resilient response of recycled concrete road aggregate. J Transp Eng 127(5):450–453
6. TIFAC (2001) Utilization of waste from constructin industry, technology information. Forecasting and Assessment Council, TIFAC, New Delhi
7. MoRTH (2013) Specifications for road works and bridges. Ministry of Road Transport and Highways, 5th edn, New Delhi, India

8. IS 2386, Part 4 (1963), Reaffirmed (2007), Indian standard methods of test for aggregates for concrete, mechanical properties. The Bureau of Indian Standards, New Delhi
9. IS 2386, Part 3 (1963), Reaffirmed (2002), Indian standard methods of test for aggregates for concrete, specific gravity, density, voids, absorption and bulking. The Bureau of Indian Standards, New Delhi
10. IS 2386, Part 1 (1963), Reaffirmed (2007), Indian standard methods of test for aggregates for concrete, particle size and shape. The Bureau of Indian standards, New Delhi
11. IS 2720, Part 8 (1983) Reaffirmed (1995), Indian standard methods of test for soils, determination of water content-dry density relation using heavy compaction, 2nd revision. The Bureau of Indian Standards, New Delhi, India
12. IS 2720, Part 16 (1983), Reaffirmed (1995), Indian standard methods of test for soils, determination of CBR. The Bureau of Indian Standards, New Delhi, India
13. Behiry AEAE (2013) Utilization of cement treated recycled concrete aggregates as base or subbase layer In Egypt. Ain Shams Eng J 4:661–673
14. McNeil K, Kang THK (2013) Recycled concrete aggregates: a review. Int J Concr Struct Mater 7:61–69

Industrial Waste Utilization in Road Construction: A Review

S. S. Patil and Dilip D. Sarode

Abstract As industrialization is growing all over the world, industrial waste generated is also increasing with it. Disposal of the same is a greater concern in many countries. However, utilization of these waste materials for value-added applications will not only help to have sustainable development but also address the disposal problem. In this study, the properties and performance of fly ash, bottom ash and plastic waste in the construction of various types of roads are highlighted. Based on this review, it can be concluded that fly ash and plastic waste can be utilized in different types of road construction to get better results and for sustainable development. However, some waste such as bottom ash requires pre-treatment before using it as a replacement of aggregate or used in the flexible pavement or used for subgrade improvement. There is a need to study the properties of bottom ash to enable its use to develop value-added applications.

Keywords Fly ash · Bottom ash · Plastic waste · Industrial waste

1 Introduction

An increase in industrialization increases the need for more power, steel and other materials per capita. So, a large quantity of waste like fly ash (FA), bottom ash (BA), plastic waste [1], blast furnace slag [2] continuously generated throughout the world [3]. As per government report 2017–2018, in India only, fly ash generated every year is more than 196.44 million tons and its utilization is about 63% [4], which is very low even though many rules and regulations are enforced by the Government. A huge amount of unutilized fly ash is dumped on landfilling sites which covers considerable cultivable land or used for other activities. The bottom

S. S. Patil (✉)
Institute of Chemical Technology, Mumbai, India

D. D. Sarode
Department of General Engineering, Institute of Chemical Technology, Mumbai, India
e-mail: dd.sarode@ictmumbai.edu.in

B. Laishram and A. Tawalare (eds.), *Recent Advancements in Civil Engineering*, Lecture Notes in Civil Engineering 172,
https://doi.org/10.1007/978-981-16-4396-5_63

ash generated is about 20% that of the fly ash generated. However, utilization of bottom ash is very low as compared to the utilization of fly ash which shows the availability of a high volume of unutilized bottom ash [5]. The same scenario can be observed for plastic waste, particularly thermoset plastics all over the world. All these waste materials will create an environmental problem if not dealt with properly care.

A large quantity of natural materials is being used every year for the construction of roads. In different types of roads like rigid, flexible, Water Bound Macadam (WBM), Wet Mix Macadam (WMM) pavements lot of natural materials like sand, aggregate, soil, rocks are used abundantly. If this practice is continued, it is not a good sign for sustainable development [6]. As connectivity to every part of the country plays an important role in its development, it is one of the major factors which will improve trading, industrial growth and agricultural output of the country [7]. Out of the total road network, 80% of road networks in India consists of rural roads. Road network construction depends mainly on the cost-benefit ratio and population density in different areas of the country. Thus, low population density areas need to be connected with a road type having fewer construction costs. Owing to this fact, construction or maintenance work of road networks has not been properly done, particularly in rural areas. The literature review reveals that the problem of a large quantity of waste generated in various industrial processes is unutilized, which is locally available for the construction of the road in rural areas. Low-cost construction of rural roads for low population density areas can be done using waste materials like fly ash, bottom ash, slag, plastic waste available from nearby industries. Fly ash can be used as filler, binder, and stabilizer [8] in the subgrade, sub-base and base course of road pavements. Incorporation of fly ash/slag shows better results in California Bearing Ratio (CBR), unconfined compression strength, axial deformation, tensile cracking and bonding of materials [9]. Many studies have shown that fly ash used with different materials in different layers of pavement gives better results in the form of improved the life and performance of the road. Different combinations like fly ash and plastic waste, fly ash and lime, fly ash and bagasse ash, fly ash and bottom ash can be used as a secondary material which not only reduces demand for natural materials but also reduces construction cost and addresses the environmental issue of waste disposal. There is variation in the optimal composition of fly ash used; the variation depends upon the combining material. Similarly, bottom ash can be used in different layers of road construction economically. Plastic waste utilized in asphalt road gives better results. Hence, now Government of India has also decided to build 1 lakh kilometer length of roads containing plastic waste. A combination of plastic with fly ash in flexible pavement shows the better binding property, stability, stiffness, density and extra resistance to water. These types of roads are very suitable for changing climatic conditions like in India.

2 Literature

2.1 Fly Ash

Fly ash and coal wash are used to improve sub-base and subgrade performance in road construction. After some initial testing program, it is concluded that 7% of fly ash is considered as an optimum percentage. Maximum dry density (MDD) increases with an increase in fly ash content up to 10%. After that, MDD decreases. When 10% of fly ash used void ratio decreases from 0.35 to 0.26. It proves that fly ash is acting as a void filler. Coal wash and fly ash with 7–13% can give higher compacted density. Maximum axial stress decreases with an increase in water content. CBR increases from 72 to 125% when fly ash content was 7%, CBR was 66% at fly ash content 10% and it was 58% when fly ash content is increased to 13%. Only in the sample with 7% fly ash content, the CBR complies with the requirement of sub-base and base course material. Collapse potential decreases by 70% when 7% of fly ash was added. Permeability decreases with an increase in fly ash content due to a reduction in voids [10]. Fly ash is non-plastic material when blended with soil, reduces liquid and plastic limit. The addition of fly ash as filler with soil reduces maximum dry density (MDD) and increases optimum moisture content (OMC), which results in increased resistance to compaction [11].

Similarly, Fly ash and bagasse ash effect on clayey soil of medium compressibility were studied. For this, separate samples were prepared to fly ash and clay, bagasse ash and clay with varying percentage of fly ash (FA) and bagasse ash. To study the performance of these, different test like CBR, Unconfined Compression Test (UCS), SEM analysis were conducted [12].

In samples from soil and fly ash, it was observed that maximum CBR value was found at 25% fly ash content. An appreciable improvement of CBR value with curing time was observed and hence prolong relative humidity curing is suggested. UCS value increases with an increase in FA content, and this rate of improvement was rapid up to 15% FA content, after which it becomes slow up to 25%. The highest value was found at 30% FA. To understand the role of fly ash in moisture, using SEM, morphological properties of (soil + FA) mix were studied. As expected, Calcium Silicate Hydrate (C–S–H) gel was observed. Also, a better degree of agglomeration of FA and soil particles was also distinctly noticed for 25% fly ash content [12].

In samples from soil and bagasse ash, it was observed that CBR increases with an increase in bagasse ash content, significant CBR increase was observed up to 15% bagasse ash. The maximum CBR was observed at the incorporation of 25% BA. There is an increase in CBR value as relative humidity and curing time increases. SEM images demonstrated that bagasse fibers were uniformly distributed among the mass [12].

To improve the performance of fly ash, poor graded fine sand reinforcement is suggested [13]. In this paper, fly ash of class F having low compressibility, poor graded fine sand and polypropylene fibers as reinforcement were used. OMC and

MDD were determined; results show that OMC and MDD decrease with an increase in fiber content; this is due to the fact that fibers are lighter than fly ash. UCS at failure was enhanced with an increase in fiber content. It is due to skin friction between fiber and FA. The variation of UCS with fiber percentage is linear. However, it is nonlinear with aspect ratio. It is observed that the CBR value of fly ash, fly ash + 25% soil and fly ash + 15% soil was less than that required for rural roads. Hence, reinforcement is a must. There was an increase in CBR value with an increase in fiber content of up to 3%. Fiber reinforcement results in a reduction in permanent strain. That means fiber reinforcement reduces the rutting formation in the pavement. To confirm laboratory CBR test results, field CBR was conducted [13]. Results found are as shown in Table 1.

As per IRC 2002 [14], CBR should be a minimum of 15%.

Fly Ash as filler in Hot Rolled Asphalt pavements, the poor performance of bitumen mixture is due to poor mixing and compaction. When the temperature falls to 120 °C during the transportation of mix, it becomes unworkable. The optimum percentage of coarse aggregate + (limestone + fly ash) filler + sand was 34% + 10% + 56%, respectively. Different tests were carried out, and it was found that fly ash as a filler in hot rolled asphalt has higher workability than conventional hot rolled asphalt. That means, at 110–85 °C, the hot-rolled asphalt can be mixed and compacted. There is a huge saving in energy. Hence, we can classify this as low energy material [15]. But when along with fly ash, cement is used in rolled asphalt, results show that cement and/or fly ash was better to improve the strength and to strip resistance of the asphalt mixture. Mechanical properties indicate that the use of 1.5% cement + 1.5% fly ash gives better resilient modulus (Mr) of the mix at both low as well as high temperatures. The results show that the mix of 1.5% cement and 1.5% fly ash gives the best rutting resistance [16].

Reclaimed asphalt pavement means reclaimed aggregate from the older pavement with fly ash as a stabilizer. The construction of 200-mm-thick pavement for design traffic of 150 million standard axles (MSA), the aggregate required is 13,000–15,000 MT per km for two-lane road [17]. Hence, as sustainable construction material reclaimed asphalt pavement material as aggregate and cold recycled lime fly ash as the stabilizer can be used in road construction. Cold recycling technology can be used in the pavement base and sub-base course. It consists of 18–25% lime fly ash of aggregate weight. The ratio of lime: FA is 1:4 to 1:2. As this material generates C–S–H and aluminate hydrate in gel condition, it is widely accepted as a cost-effective paving material [18].

Table 1 CBR values for soil with FA and fibers

Sr. No	Material	CBR value
1	FA	9.1%
2	FA + 25% soil	14.6%
3	FA + 0.2% fiber	16.6%
4	FA + 0.2% fiber + 25% soil	34.4%

Some researchers used fly ash as a mineral admixture in roller compacted concrete with natural and manufactured sand (M-sand). Three combinations were made—(A) FA and river sand (B) FA and M-sand (C) FA and river and M-sand. In each combination, cement is replaced by fly ash in varying percentages. The compressive strength and dynamic modulus of elasticity were decreased with an increase in fly ash content. The compressive strength and UPV values are lower in the mix having M-sand 100% due to the fact, M-sand produces a harsh mix if not properly designed. The mix having 50% river sand 50% M-sand shows higher strength because of density increases due to proper packing of aggregate in a mix. At 7 and 28 days, mix A and B at the replacement of 50% and 60% of cement produces doubtful results. Hence, M-sand can be considered as a partial replacement [19].

Above different studies shows that, fly ash can be utilized up to 30% to get better results in CBR and UCS in sub-base and subgrade layer of pavement. Fly ash with coal wash gives higher compacted density at sub-base layer. To improve CBR of clayey soil, bagasse ash with fly ash were successfully used. Fly ash with polypropylene fibers results in increase in UCR and CBR values. To address problems like poor mixing, compaction and temperature fall during the transportation of hot rolled asphalt, fly ash with limestone were successfully used. Also, it was proved that reclaimed asphalt pavement material as aggregate and cold recycled lime fly ash in base and sub-base layer of pavement accepted as cost-effective paving material.

2.2 Plastic Waste

Fly ash as a filler and plastic waste as coating material can be used in bituminous concrete. The study was conducted to explore this idea. To prepare samples, aggregates were heated at 135 °C then bitumen 5–6% by weight of mix was added. The marshal compactor moulds were filled by giving 75 blows; after 24 h, specimens were demoulded and kept at 60 °C for 40 min in a water bath. Results shows, use of 0.76% plastic and 3% fly ash improves the volumetric properties of bituminous concrete. Also, it is observed that plastic will increase the melting point of bitumen [20].

High-density polyethylene (HDPE) waste strips from plastic waste can be used as reinforcement in flexible pavements. The research was done to study this material combined with fly ash improves CBR and to reduce pavement thickness. In the study, HDPE 0.40 mm thickness and 12 mm length having aspect ratios 1, 2 and 3 were used. The samples prepared with varying strip contents as 0.25, 0.5, 1, 2, 4%. Fly ash with and without reinforcement compacted in CBR mould 152 mm diameter and 178 mm height at OMC and MDD in three layers by giving 56 blows to each layer. CBR test was carried out as per IS 2720 Part 16. Test results show that the CBR value for unreinforced fly ash at 2.5 mm and penetration were found to be 2.33 and 3.11%. These values of CBR increased to 3.65 and 4.38%,

respectively, when 0.25% strip contents were added in the mixture. When 2% of strip content was used, the CBR value increased to 10.95 and 13.87%, these increase in CBR value observed up to 4% increase in strip content. That means reinforcement, along with fly ash, results in an increase in CBR. It is concluded that the total thickness of pavement can be reduced if HDPE waste strips are used as reinforcement in the subgrade. Thickness can be reduced up to 70% depending on service life and designer's requirement [21].

The study was done in Ghana in 2017, but along with HDPE, polypropylene (PP) fibers were used in bitumen concrete. In this study, modified bitumen preparation was done by using a melting blending technique. To prepare the samples, bitumen was heated and the polymer was slowly added at 160–170 °C; PP and HDPE percentage ranges between 0.5 and 3 by weight of the blend and then mixing were done for thirty minutes to one hour. On this prepared samples, penetration test, softening point and viscosity test were conducted. Results show that a decrease in penetration value was observed for modified bitumen because of the use of high molecular weight polymer. Polyethylene at temperature 160 °C melts and absorbs some oil and releases low molecular weight fraction into bitumen, which increases viscosity. HDPE shows a rapid increase in softening point as compared to PP. Polymer modified bitumen with an increase in softening point should have better performance in terms of rutting fatigue and temperature susceptibility. Polymer-modified bitumen with PP offers better rutting resistance [22]. A similar kind of study was done to investigate the benefits of the bituminous concrete mixture with the incorporation of fly ash and plastic. The study shows the plastic waste melting temperature is 123–124 °C, but its decomposition temperature is 399 °C which means at 399 °C, plastic will change its chemical property. Therefore, anyone can use plastic up to 200 °C.

It was observed that rutting values are in between 3.29 and 3.91 for binder and fly ash and plastic composites. Higher resistance to rutting was observed when in bituminous concrete fly ash and plastic was used. Results of creep modulus were high and at the same time, permanent deformation was also high, but the percentage of creep recovery was high in the composite sample with fly ash and plastic. Finally, it is concluded that fly ash and a plastic waste composite of bituminous concrete reduces rutting, improves creep modulus, creep recovery, resilient modulus and indirect tensile strength [23]. Utilization of waste plastic reduces the need for bitumen by 10%, increases strength and avoids the use of an anti-stripping agent. Also, it solves the problem of plastic waste disposal in an eco-friendly way [24].

From above literature studies, it is observed that, plastic waste and fly ash used as coating material in bituminous concrete improves volumetric properties of bituminous concrete. HDPE reinforcement along with fly ash can be useful to reduce thickness of flexible pavement.

2.3 Bottom Ash (BA)

An attempt was made to evaluate the applicability of BA mixed with aggregate in a binder layer of the surface course. At first, fly ash utilized in asphalt concrete was in 1930 and the first large-scale use was Hungry Horse Dam in 1949. A recent study shows that BA will not degrade properties when used as a replacement of fine aggregate in the asphalt mix. Bottom ash contains pyrites, porous particles, which are not ideal for wearing courses. Hence, it is advisable to use it in intermediate courses. BA (15%) as part of fine sand does not modify mechanical properties. Marshall stability increased when BA quantum increased from 15 to 20%, and it is almost constant when the percentage of BA was increased from 20 to 25%. Experimental work shows that bottom ash improves stability and reduces wearing resistance. Hence, BA cannot be used in wearing courses. When the leaching test was carried out on samples, none have released the number of substances exceeding limits. Unquestionably BA can be used in asphalt mix without risk of release of dangerous substances into the environment [25]. Due to these some drawbacks, thermal analysis and thermogravimetric analyses of bottom ash were done. It was found that 60.88% carbon in BA having particle size 2–5 mm and BA having a particle size less than 2 mm contains 40.6% carbon. Carbon content affects the compression strength of concrete if BA is used as a replacement for sand as it is. Hence, some pre-treatment is required for BA before it is used in road pavements. So, the floating sinking method is used and shows good results. The carbon content in pre-treated BA reduced up to 30%. Results show that BA from NICOLA Tesla Plant cannot be utilized for road construction without pre-treatment. Treated BA could be used as fine aggregate in the mix for road construction because the compression strength meets the required values in JUS U.E9.024 standards for sub-base in road construction [26]. Untreated BA as a component in the mixture for road construction affects the applicability, but pre-treated BA (low carbon %) can be used for road construction in a sub-base layer. DTA/TGA results show that unburnt carbon in BA did not hinder the reaction of Portland cement and fly ash with water [27]. Physiochemical and geotechnical characterization is done for BA. From that, it is understood BA should be treated to improve its mechanical properties [28]. BA treated with lime and calcarenite sand improves compressive strength, dry and wet CBR and dry density of the mix. The use of 4% lime in mix significantly improves dry density and CBR properties, the calcarenite sand 25% results in max density. Finally, the use of treated BA with 4% lime and 25% calcarenite sand is recommended as material for roads in a rural area [29].

Another attempt was made for stabilizing expansive soil (Clay) by using biomass bottom ash (BBA) [29]. Biomass means any organic non- fossil material burnt as fuel. BBA contains porous particles with rough surface textures. The chemical composition of BBA consists of Si, Ca and K and the amount of Mg, Fe, Al, Na and Ti were less than 5%. X-ray diffraction analysis shows that the representative phase was quartz. In the study, different percentage 0, 15, 50, 100% of BBA was added to expansive soil. Expansive clayey soil and BBA improves soil bearing capacity.

If compared with only expansive clayey soil, the value increased by 98%. Before this study, many authors stated that CBR decreases while using Rise husk ash, palm oil fuel ash, bagasse ash. The addition of BBA increases the bearing capacity of clayey soil and reduces the free swelling by 99%. So, it was clear that BBA reduces the expansion of clayey soils to the same extent as that of lime treatment [29].

The effects of BA as fine aggregate on normally vibrated concrete (NVC) and self-compacting concrete (SCC) were studied by researchers [30]. The different test conducted on concrete shows that BA used in NVC and SCC satisfied workability criteria. Compressive strength has been reduced with a higher content of BA. The use of cement admixtures proved beneficial to improve compressive strength at 28 days. SCC gives better strength than NVC on account of fine aggregate replacement by BA. Tensile strength decreases when 30% replacement of fine aggregate with BA is done in SCC. The abrasion resistance of NVC made using BA has been improved, whereas, for SCC, it is decreased. Carbonation depth has been decreased when BA was up to 10%. The replacement by BA beyond 20% has increased carbonation depth [30].

The study was done on ash from the solid waste incinerator in the concrete road and asphalt concrete road. Results show that as stabilized bottom ash content increases in cement bound mix, bulk density, workability and mechanical properties decreased. As stabilized bottom ash exceeds 10%, the asphalt concrete mixture lost mechanical performance. This loss is due to stabilized bottom ash fragility [31].

A various attempts shows that due to pyrites and porous particles, bottom ash should not be utilize in wearing coat of pavement. So use of bottom ash in intermediate course is advisable. Bottom ash contains high carbon percentage so it is weak in bonding so pre-treatment of bottom ash or use of combinatory material having bonding properties was proposed by different authors.

3 Conclusions

1. Fly ash utilized in the soil will improve the mechanical properties of the soil mixture. This makes it suitable for base and sub-base courses on the road. Fly ash utilized in soil act as a void filler and as moisture content goes on increasing up to a certain limit due to the composition of fly ash, hydro silica gel formation was observed. Due to these facts, maximum dry density, CBR, optimum moisture content, unconfined compression test was increased. Different combinations of fly ash were also studied by many researchers, which prove its suitability in rigid and flexible pavement construction as a sustainable material.
2. Fly ash along with limestone as a filler in hot-rolled asphalt has higher workability than conventional hot-rolled asphalt mix. It results in energy saving.
3. From various studies, it is also clear that fly ash utilized in the rigid pavement to improve concrete properties possess some cement-like properties and having less percentage of carbon. But when local fly ash (Kokan Region, Maharashtra)

we will utilize, it is very important to study the chemical composition of the fly ash to decide the technique of utilization in the rigid pavement.
4. Fly ash, when utilized in bitumen it acts as a filler in bitumen mix, but the best results were seen when it is used with plastic waste in flexible pavement.
5. Plastic waste used with fly ash in hot bitumen asphalt will improve many properties of hot mix asphalt and also solve the problem of plastic disposal. Polyethylene plastic used in the mix increase the viscosity of bitumen and bitumen aggregate bond strength, which will improve stripping resistance.
6. An attempt is required to explore the use of coal bottom ash in different layers of pavement with reliable guidelines so that percentage of coal bottom ash use will increase in India.
7. Considerable potential is there in the development of material for the construction of low-cost roads with low traffic density for a rural area with different industrial waste materials so as to satisfy the standards laid down by different authorities.

References

1. Moharir RV, Kumar S (2019) Challenges associated with plastic waste disposal and allied microbial routes for its effective degradation: a comprehensive review. J Clean Prod 208:65–76
2. Ogea, M, Ozkana D, Celikb MB, Goka MS, Karaoglanlic AC (2019) An overview of utilization of blast furnace and steelmaking slag in various applications. Mater Today 11:516–525
3. Senapati MR (2011) Fly ash from thermal power plants—waste management and overview. Curr Sci 100(12)
4. Surabhi (2017) Fly ash in India: generation vis-à-vis utilization and global perspective. Int J Appl Chem 13:29–52
5. Haque ME (2013) Indian fly-ash: production and consumption scenario. Int J Waste Resour 3910:22–25
6. Kumar S, Patil CB (2006) Estimation of resource savings due to fly ash utilization in road construction. Resour Conserv Recycl 48:125–140
7. Aggarwal S (2018) Do rural roads create pathways out of poverty? Evidence from India. J Dev Econ 133:375–395
8. Anil KumarSharman and P.V.Sivapullaiah 2016 Ground granulated blast furnace slag amended fly ash as an expansive soil stabilizer. Soils Found 56(2):205–212
9. Fly Ash utilization in road construction 2015 *Fly Ash resources centre, Odisha* (FARC)
10. Dong Wang, Miriam Tawk, Buddhima Indraratna, Ana Heitor, Cholachat Rujikiatkamjorn 2019 A Mixture of Coal Wash and Fly Ash as a Pavement Substructure Material. *Transportation Geotechnic* vol 21
11. Athanasopoulou A, Kollaros G (2015) Fly ash exploited in pavement layers in environmentally friendly ways. Toxicol Environ Chem 97(1):43–50
12. Anupam AK, Kumar P, Ransinchung GD, Shah YU (2017) Study on performance and efficacy of industrial waste materials in road construction: fly ash and bagasse ash. In: International conference on highway pavements and airfield technology, Philadelphia (Pennsylvania)

13. Kumar P, Singh SP (2008) Fibre-reinforced fly ash subbases in rural roads. *ASCE* 134 (4):171–180
14. Indian Road Congress special publication 20–2002 Rural roads manual
15. Zoorob SE, Cabrera JG (1997) Design and construction of a road pavement using fly ash in hot rolled asphalt. Waste Mater Constr Putting Theory Pract Stud Environ Sci 71:149–165
16. Likitlersuang S, Chompoorat T (2016) Laboratory investigation of the performances of cement and fly ash modified asphalt concrete mixtures. Int J Pavement Res Technol 9:337–344
17. Saride S, Someshwar Rao DT, M, Prasad SC, Dayakar Babu JR (2014) Evaluation of fly ash treated reclaimed asphalt pavement for design of sustainable pavement bases-an Indian. ASCE Geo-Congress, Atlanta (Georgia)
18. Li Q, Wang Z, Li Y, Shang J (2018) Cold recycling of lime-fly ash stabilized macadam mixtures as pavement bases and sub bases. Constr Build Mater 169:306–314
19. Krishna Rao S, Sravana P, Chandrasekhara Rao T (2016) Experimental studies in ultrasonic pulse velocity of roller compacted concrete pavement containing fly ash and M-sand. Int J Pavement Res Technol 9:289–301
20. Shedame PP, Nikhil HP (2014) Experimental study of bituminous concrete containing plastic waste material. IOSR J Mech Civil Eng 11:37–45
21. Choudhary AK, Roy N, Sinha AK (2014) Utilization of fly ash with plastic wastes as construction materials in flexible pavement. In: Proceedings of national conference GEPSID, Ludhiana
22. Appiaha JK, Berko-Boatenga VN, Tagbor TA (2017) Use of waste plastic materials for road construction in Ghana. Case Stud Constr Mater 6:1
23. Rongali U, Singh G, Chourasiya A, Dr. Jain PK (2013) Laboratory investigation on use of fly ash plastic waste composite in bituminous concrete mixtures. Procedia Soc Behav Sci 104:89
24. Kalpana MRS, Surendar D (2018) Utilization of waste plastic in bituminous roads—a review. Int J Pure Appl Math 119(17)
25. Colonna P, Berloco N, Ranieri V, Shuler ST (2012) Application of bottom ash for pavement binder course. Procedia Soc Behav Sci 53:962
26. Marinkovic S, Trifunovic P, Tokalic R, Matijasevic S, Kostic-Pulek A (2009) DTA/TGA studies of bottom ash from the nikola tesla power plant from serbia for the purpose of its utilization in road construction. In: 36th Int Conf SSCHE
27. Trifunovica PD, Marinkovica SR, Tokalica RD, Matijasevic SD (2010) The effect of the content of unburned carbon in bottom ash on its applicability for road construction. Thermochim Acta 498:1
28. El Moudni El Alami S, Moussaoui R (2019) Lime treatment of coal bottom ash for use in road pavements: application to El Jadida Zone in Morocco. Article Mater (2674) 12(17)
29. Cabrera M, Rosales J, Ayuso J, Estaire J, Agrela F (2018) Feasibility of using olive biomass bottom ash in the sub-bases of roads and rural paths. Constr Build Mater 181
30. Singh N, Mithulraj M, Arya S (2018) Influence of coal bottom ash as fine aggregates replacement on various properties of concretes: a review. Resour Conserv Recycl 138:257–271
31. Toraldo E, Saponaro S, Careghini A, Mariani E (2013) Use of stabilized bottom ash for bound layers of road pavements. J Environ Manage 121:117

Characterization of Shredded Waste Plastic on Warm Stone Mastic Asphalt

Khalida Muntasher and Shivaraj Halyal

Abstract The heavy traffic on the national highways demand for durable bituminous mixtures for long run. To serve this purpose, the Stone Mastic Asphalt (SMA) can be used, which is a gap-graded mixture with high binder content. In this study, the stone mastic asphalt was prepared using viscosity grade (VG) 30 binder and stabilized with shredded waste plastic (SWP) by varying percentage of plastic by the weight of total mix (0–1% with an increment of 0.2%) to prevent drain down characteristic of the binder. The experimental study was carried out to assess the Warm SMA stabilized with shredded plastic waste and subjected to performance tests including Marshall mix design, Indirect tensile strength by IDT setup to evaluate the performance of Warm SMA. It was observed that optimum bitumen content for the desired WSMA mix with SWP is 6.1%, for the optimum dosage of shredded waste plastic as 0.8% of the total mix. The lowered mixing and compaction temperature were determined for Warm SMA and Tensile strength ratio (TSR) was determined for the chosen temperature. However, unit cost of shredded waste plastic is lesser than that of cellulose fibers. Hence, the designed WSMA mix with shredded waste plastic is cost effective as well as eco-friendly.

Keywords Stone mastic asphalt (SMA) · Shredded waste plastic (SWP) · Drain down

K. Muntasher (✉) · S. Halyal
School of Civil and Environmental Engineering, K L E Technological University, Hubli, India
e-mail: khalida@kletech.ac.in

S. Halyal
e-mail: shivaraj.halyal@kletech.ac.in

B. Laishram and A. Tawalare (eds.), *Recent Advancements in Civil Engineering*, Lecture Notes in Civil Engineering 172,
https://doi.org/10.1007/978-981-16-4396-5_64

1 Introduction

1.1 General

The increase in traffic has increased demand for good quality pavements, which is challenge for pavement engineers to construct sustainable pavements. Municipal solid waste and plastics are of great concern. Where Disposal and reuse of plastic is the need of the hour. Plastic waste generated from domestic and industry can be used for the construction of pavements as they soften during heating and do not produce any toxic gases while heating.

1.2 Stone Mastic Asphalt

Stone mastic asphalt is a hot mix asphalt developed in 1960s in Germany. It is a gap graded bituminous mixture contains high coarse aggregate fractions and filler with high binder content, and prepared at high temperature. SMA is a rut resistance and durable, preferred for high traffic roads [1]. The philosophy of SMA is that the coarse aggregate skeleton stone portion provides a stone-on-stone contact to prevent rutting and provide skid resistance [2]. The presence of high binder content results in drain down of the material from the mixture during different stages such as mixing transporting, laying and compacting at high temperatures. Therefore, in order to control drain down, it is suggested to use stabilizing additives [3].

The Plastic Coated Aggregate (PCA) performs better when used in the construction of flexible pavements and have shown higher Marshall stability value and load bearing capacity of pavement was increased by 100% [4]. In order to improve the properties of asphalt mixture and reduce the negative impact of the waste materials on nature and the environment, an experimental research on the application of waste plastic bottles (Polyethylene Terephthalate (PET)) was used as a stabilizing additive in SMA. Wheel tracking, moisture susceptibility, resilient modulus and drain down tests were carried out on the mixtures and results show that the addition of waste PET into the mixture has a significant positive effect on the properties of SMA which could improve the mixture's resistance against permanent deformation (rutting), increase the stiffness of the mix, provide lower binder drain down and promotion of reuse and recycling of waste materials in a more environmentally and economical way [5]. The benefit of adding shredded waste plastic in SMA is that around 10% of plastic content in the mix increases stability about 64%, split tensile strength by 18% and compressive strength by 75% [6].

SMA has higher coarse aggregate content with stone-on-stone contact structure, modified asphalt and fibers. The coarse fractions in the mix enable SMA with high degree of compaction temperature or more compaction effect to obtain enough level of compaction during construction. Since the compaction ensures resistance to rutting and durability [7]. Warm Mix Asphalt (WMA) is an additive which provides

better working environment by lowering production and construction temperature of the mix, also lowers carbon emission, improves workability and life of pavement structure. The compaction temperature can be reduced by 30–40 °C when using Sasobit or Evotherm DAT and results in decrease moisture resistance ability and low temperature cracking resistance ability of SMA [8].

SMA is a good rut resistant and highly durable wearing course for flexible pavement, it requires high mixing and compacting temperature which increases its cost. Also, the bitumen tends to drain down due to high binder content. In the current study, the authors would like to investigate the performance of Warm SMA stabilized with optimum shredded waste plastic making it cost effective, energy efficient and eco-friendly mix.

2 Objectives of the Present Study

The present study is aimed to prepare Warm SMA with stabilizing additive. To study the effect of shredded waste plastic and Warm SMA on strength properties of SMA, Mixes were prepared with Marshall method, using VG 30 bitumen and Zycotherm as warm mix additive to reduce the mixture temperature. Shredded waste plastic was used as stabilizing additive to control drain down of the mixture.

3 Methodology

In this investigation, the Warm SMA was stabilized with shredded waste plastic. The methodology involves laboratory investigation, which is as shown in Fig. 1.

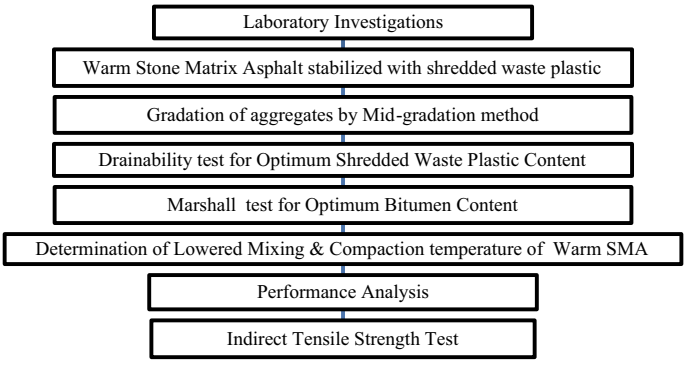

Fig. 1 Methodology

4 Materials Used

4.1 Physical Properties of Aggregates

Crushed stones of Basalt were used for coarse aggregate and fine aggregate [9]. In order to reduce test errors, all aggregates were sieved into single-size particles as per IRC: SP-79:2008 [10]. The cement was used as a filler. The obtained values for the various physical properties of aggregate are shown in Table 1. The aggregate gradation was adopted from Ministry of Road Transport and Highways (MoRTH). The nominal aggregate size used was 13 mm. Three particle sizes of coarse aggregate (19–13.2 mm, 13.2–9.5 mm and 9.5–4.75 mm) and five particle sizes of fine aggregate (4.75–2.36 mm, 2.36–1.18 mm, 1.18–0.6 mm, 0.6–0.3 mm and 0.3–0.075 mm) were chosen [11].

4.2 Physical Properties of Bitumen

In this study, VG 30 bitumen was used to prepare the mixture. The values obtained for fundamental properties of bitumen are shown in Table 2.

Table 1 Physical properties of aggregate

Property	Test	Obtained value	Standard requirement
Strength	Impact value	11.1%	<18%
Particle shape	Combined flakiness and elongation index	29%	<30%
Hardness	Los Angeles abrasion value	19.7%	<25%
Specific gravity	Specific gravity	2.96	2.5–3.0
Water absorption	Water absorption	0.70%	<2.0%

Table 2 Physical properties of bitumen

Property	Virgin bitumen	Bitumen + zycotherm	IRC SP 79 requirement
Penetration	62	44	60/70
Ductility	>100 cm	>100 cm	40 cm (min)
Softening point	51 °C	52 °C	47 °C (min)
Specific gravity	1.02	1.00	0.99–1.02
Viscosity	27 s	29 s	30 s
Flash and fire point	240 °C 260 °C	250 °C 270 °C	220 °C (min) 240 °C (min)

4.3 Stabilizing Additive

The processed garbage in the form of shredded waste plastic (SWP) was used as a modifier in Warm SMA supplied by K. K. Waste Plastics, Bangalore, India.

4.4 Warm Mix Additive

The Samples of Warm SMA are prepared with Zycotherm as warm mix additive by adopting a dosage of 0.1% by total weight of binder.

5 Experimental Investigation

5.1 Drain Down

Drain-down of the loose WSMA with SWP was conducted according to ASTM D6390 [12] and thereafter, the optimum shredded waste plastic was determined for the prepared mix. The drain-down test was conducted to determine the efficiency of the Shredded Waste Plastic as a stabilizer used to prevent the drain-down of the binder and mineral filler. The initial bitumen content of the mixture for the adopted gradation was minimum of 6% as per IRC: SP-79:2008 [10]. Shredded waste plastic (SWP) was added by varying percentage of plastic by the weight of total mix (0–1% with an increment of 0.2%). The mass of loose WSMA with varying percentage of SWP sample and the initial mass of the pan is determined. The loose SMA sample is then transferred and placed into the wire basket without consolidating or disturbing it. The basket is placed on the pan and the assembly is placed in the oven at a prescribed temperature of 175 °C for 1 h. After the sample has been kept in the oven for 1 h, the basket and the pan are removed and the final mass of the pan is determined and recorded. The drainability was calculated using Eq. (1)

$$\text{Draindown } \% = \frac{E - A}{D} \times 100 \tag{1}$$

where

A—Mass of initial pan (g).
E—Mass of final pan (g).
D—Mass of initial total sample (g).

The results of drainability test conducted for optimizing the shredded waste plastic content are as shown in Table 3. The results show that there is decrease in

Table 3 Drain down test results

Stabilizer content (%)	0	0.4	0.6	0.8	1.0
Drain-down (%)	2.5	0.73	0.08	0	0

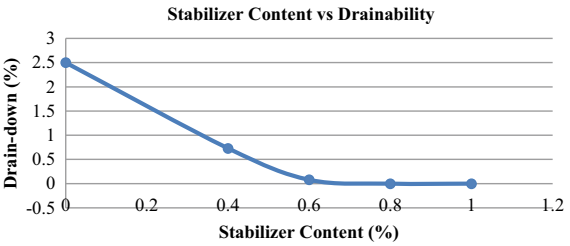

Fig. 2 Variation of drain-down of bitumen with increase in stabilizer content

drain-down with increase in shredded waste plastic content [13] as shown in Fig. 2. It can be concluded that the optimum shredded waste plastic content is 0.8% by total weight of the mix, since the observed drain-down at this dosage of shredded waste plastic is 0% which is less than 0.3%.

5.2 SMA Mix Design

The combined grading of the coarse aggregate, fine aggregate and mineral filler of the WSMA mixture was designed using IRC: SP-79 (2008) by adopting mid-gradation method. WSMA mixture samples were prepared using Marshall method and three samples were prepared for each bitumen content. The Marshall placed in water bath and specimen while testing is shown in Figs. 3 and 4, respectively. The mix design consists of determination of maximum theoretical specific gravity (G_{mm}), voids in coarse aggregates in dry rodded condition (VCA_{DRC}), the value of VCA_{DRC} should be more than VCA_{MIX} which ensures stone to stone contact and was calculated using Eqs. (2) and (3) [14],

$$VCA_{DRC} = \frac{G_{CA} \cdot \gamma_w - \gamma_S}{G_{CA} \cdot \gamma_w} * 100 \tag{2}$$

$$VCA_{MIX} = 100 - \left(\frac{G_{mb}}{G_{CA}}\right) * P_{CA} \tag{3}$$

where

G_{CA} = Bulk specific gravity of coarse aggregate fraction.
G_{mb} = The bulk specific gravity of compacted mixture.
γ_w = Unit weight of water (998 kg/m^3).
γ_S = The unit weight of coarse aggregate fraction in dry rodded condition.

Fig. 3 Marshall samples placed in water bath

Fig. 4 Testing of Marshall samples

Dry mixing method was adopted to add SWP to the aggregate. The aggregates were heated and required amount of SWP was added uniformly and mixed at a temperature of 150°–160 °C, as the melting temperature reported by manufacturer for SWP is 160 °C. After the sufficient coating of SWP around the aggregate surface, the heated warm-mix binder was then poured onto the mixture and performed mixing to obtain uniform mixture. Table 4 shows the Volumetric Properties obtained from a designed WSMA mix with SWP for the Optimum bitumen content. The obtained optimum bitumen content for the desired WSMA mix with 0.8% SWP was 6.1%. The mixing and compaction temperature as per IRC: SP-79:2008 are 160° and 150 °C, respectively.

5.3 Determination of Lowered Mixing and Compaction Temperature

The purpose of this experiment is to determine the lowered mixing and compaction temperature by using the Zycotherm as a Warm Mix Additive in the Warm SMA mixture. Two Marshall samples for each of the below combination of mixing and compaction temperatures were prepared as shown in Table 5. Marshall Mix Design

Table 4 Volumetric properties of warm SMA with 0.8% SWP

Sl. No.	Mix design parameters	Obtained properties for warm SMA with SWP at 0.8% drainability	IRC SP 79:2008 requirements
1	Optimum bitumen content	6.1%	5.8 min
2	% Air voids	4.0%	4.0%
3	VMA %	19.93	17 min
4	VFB %	76.04%	–
5	VCA_{DRC}	41.46	–
6	VCA_{MIX}	38.63	Less than VCA_{DRC}

Table 5 Stability values for various combinations of mixing and compaction temperature

Sl. No.	Mixing temperature (°C)	Compaction temperature (°C)	Height of sample (mm)	Max. proving ring reading (div.)	Stability value (kg)	
					Measured	Corrected
1	140	120	64.0	165	937.50	928.13
		110	63.0	150	852.27	863.85
2	130	110	63.5	160	909.09	909.09
		100	65.1	155	880.68	845.45
3	120	100	65.3	110	625.00	597.50
		90	65.0	105	596.59	574.52

was carried out for all the prepared samples. Stability, flow and volumetric properties were determined for all the combinations. The combinations, satisfying the stability and flow requirements as per IRC: SP-79:2008 [10], are chosen. Performance analysis for the satisfactory combinations was carried out to arrive at the combination which gives the highest tensile strength ratio. It was observed from the results that the two combinations of mixing and compaction temperature, viz., 140–120 °C and 130–110 °C, reported high stability value [15] and was adopted in order to carry out the performance analysis using IDT setup. It is analyzed that an average value of mixing and compaction temperature was reduced by 35 °C and 25 °C respectively.

5.4 Indirect Tensile Strength (ITS)

The purpose of ITS test is used to determine tensile strength of mix by applying load on the diametrical plane of cylindrical specimen. The Indirect Tensile Strength ratio is determined in accordance to AASHTO T283 [16] which helps to assess the

Table 6 Tensile strength ratios of the unconditioned and conditioned samples

Sl. No.	Mixing temperature (°C)	Compaction temperature (°C)	Indirect tensile strength 'ITS'		Tensile strength ratio 'TSR' (%)
			Unconditioned sample 'ITS_d' (kPa)	Conditioned sample 'ITS_c' (kPa)	
1	140	120	644.63	567.57	88.05
2	130	110	615.96	527.39	85.62

resistance to moisture. The two sets of specimens were prepared at OBC and 0.8% SWP with Warm mix additive and subjected to conditioned and unconditioned test prior to loading. One set sample unconditioned was tested after keeping in water bath maintained at 25 °C for 2 h. The second set of samples was induced with accelerated weathering in laboratory by subjecting samples to freeze and thaw cycle. The moisture conditioning involved a freeze–thaw cycling, in which the saturated specimen with 70–80% degree of saturation was covered tightly with a plastic wrap and placed in a freezer bag containing 10 ml water. The sealed freezer bag containing specimen was then placed in a freezer at about −18 °C for a minimum of 16 h. After removing from the freezer, the specimen was placed into a 60 °C water bath for 24 h. Prior to loading, the conditioned specimen was moved to water bath maintained at 25 ± 0.5 °C for about 2 h to bring the specimen to the testing temperature.

Table 6 shows the TSR values for unconditioned and conditioned specimens. Each combination of mixing and compaction temperature satisfies the TSR value which is greater than 85% and this indicates that the designed WSMA mixture with 0.8% of SWP has good resistance against moisture. It is reported that the TSR value for the combination of mixing and compaction temperature 140°–120 °C resulted is higher, as compared to a combination of 130°–110 °C. Therefore, it is concluded that the Warm SMA prepared with 0.1% Zycotherm and 0.8% SWP shows good resistance to moisture damage.

6 Conclusions

The optimum bitumen content for the desired WSMA mix with 0.8% SWP (Optimum dosage of SWP from drainability test) is 6.1%. This OBC value is sufficient to properly coat the aggregate particles and to provide the required durability and workability. The shredded waste plastic stiffens the matrix, thereby reducing the drainage of the mixture at high temperatures during various stages of preparation. However, Drainability test so conducted, the results show that Optimum dosage of Shredded Waste Plastic was 0.8% by total weight of the mixture as draindown value is 0%. The volumetric properties were determined for the mix, and it was found that the VCA_{DRC} was more than VCA_{MIX} which enables

stone-on-stone contact. Zycotherm was found to be effective in lowering the mixing and compaction temperature of SMA for the combination of 140–120 °C and 130–110 °C with high stability values and TSR of the Warm SMA stabilised with 0.8% SWP was observed to be greater than 85% which indicates that it is resistance against moisture damage. Hence, the designed WSMA mix with 0.8% SWP is cost effective as well as eco-friendly.

References

1. Brown ER, Haddock JE (1997) A method to ensure stone-on-stone contact in stone matric asphalt paving mixtures, vol 1583, no 1. National Center for Asphalt Technology, Auburn University, AL, pp 11–18
2. Talati A, Talati V (2014) Study of stone matrix asphalt for the flexible pavement. Int J Eng Dev Res 2(1). ISSN: 2321-9939
3. Sarang G, Lekha BM, Krishna G, Ravi Shankar AU (2016) Comparison of Stone matrix asphalt mixtures with polymer-modified bitumen and shredded waste plastics. Road Mater Pav Des 17(4):933–945
4. Vasudevan R, Saravanavel S, Rajasekaran S, Thirunakkarasu D (2006) Utilization of waste plastics in construction of flexible pavement. Indian Highways 34(7):5–20
5. Ahmadinia E, Zargar M, Karim MR, Abdelaziz M, Ahmadinia E (2012) Performance evaluation of utilization of waste polyethylene terephthalate (PET) in stone mastic asphalt. Constr Build Mater 36:984–989
6. Beena KS, Bindu CS (2010) Waste plastic as a stabilizing additive in Stone mastic asphalt. Int J Eng Technol 2(6):379–387
7. Kok BV, Akpolat M (2015) Effects of using Sasobit and SBS on the engineering properties of bitumen and stone mastic asphalt. J Mater Civil Eng 27(10):04015006
8. Du SW, Li SS (2011) Laboratory evaluation of warm stone matrix asphalt mixture. Adv Mater Res 243–249:4178–4181
9. Cao W, Liu S, Feng Z (2013) Comparison of performance of stone matrix asphalt mixtures using basalt and limestone aggregates. Constr Build Mater 41:474–479
10. IRC SP 79-2008. Tentative specifications for stone matrix asphalt. Special Publication of Indian Roads Congress (IRC), New Delhi
11. Kandhal PS (2007) Specifications for stone matrix asphalt (SMA). Indian Highways 35 (2):37–48
12. ASTM D6390-11 (2011) Standard test method for determination of draindown characteristics in uncompacted asphalt mixtures. In: Annual book of ASTM standards. ASTM International, West Conshohocken, PA
13. Yadykina V, Tobolenko S, Trautvain A, Zhukova A (2015) The influence of stabilizing additives on physical and mechanical properties of stone mastic asphalt concrete. Procedia Eng 117:381–386
14. Sarang G, Lekha BM, Ravi Shankar AU (2014) Stone matrix asphalt using aggregates modified with waste plastics. Pavement Mater Struct Perform 9–18. ISBN: 9780784413418
15. Ravi Shankar AU, Koushik K, Sarang G (2013) Performance studies on bituminous concrete mixes using waste plastics. Highway Res J 6(1):1–11
16. ASTM T283 (2014) Standard method of test for resistance of compacted asphalt mixtures to moisture-induced damage. In: Annual book of ASTM standards. ASTM International, West, Conshohocken, PA

Comparative Study Between Proposed Rigid Pavement and Flexible Perpetual Pavement for Western Alignment of Pune Ring Road

Saurabh Kulkarni and Mahadeo Ranadive

Abstract Pune is the second-largest city in terms of population in Maharashtra. It is also an industrial, cultural, and socioeconomic hub of Maharashtra. The traffic around Pune city has been increasing at high rate, thus necessitating increase of width of the existing roads. Besides, traffic originating outside Pune and destined outside Pune is passing through Pune City resulting in traffic congestion inside the city limits. Pune Ring Road is a proposed circumferential outer road for Pune metropolitan region to overcome this situation. The project road is proposed to be a six-lane rigid pavement having design life of 30 years as per provisions of Ministry of Road Transport and Highways (MoRT&H) Expressway Guidelines. This study aims to suggest an alternative of choosing perpetual pavement over proposed rigid pavement. There were no official standard provisions for the design of perpetual pavement in India until the year 2012. However, with the publication of the guidelines by the Indian Roads Congress (IRC37:2012), the design to satisfy 50 year design periods can be adopted with mechanistic pavement design methodology. A comparative study was carried out between four combinations of flexible pavement mentioned in IRC guidelines with perpetual pavement design criteria and proposed rigid pavement on the grounds of sustainability, life cycle cost assessment (LCCA), and carbon dioxide (CO_2) emissions. The perpetual pavements were designed by using mechanistic-empirical design software IITPAVE. It is observed that the perpetual flexible pavement becomes a better choice considering the factors like expected design life, economy, and environment.

Keywords Perpetual pavement · Mechanistic methodology · Life cycle cost assessment · Carbon footprint

S. Kulkarni (✉) · M. Ranadive
Department of Civil Engineering, College of Engineering Pune, Pune, India

B. Laishram and A. Tawalare (eds.), *Recent Advancements in Civil Engineering*, Lecture Notes in Civil Engineering 172,
https://doi.org/10.1007/978-981-16-4396-5_65

1 Introduction

The Maharashtra State Road Development Corporation (MSRDC) has decided to take up the development of an outer ring road for Pune in order to provide unobstructed passage to outer traffic which will in turn help in decongesting the internal city traffic. MSRDC has divided the proposed ring road into two different alignments, i.e., eastern and western. MSRDC has also published Pre-Feasibility Report (PFR) [1] for each alignment. In this paper, data on western alignment is used for analysis and design purpose. Western alignment starts from Khed Shivapur on NH-4 and culminating at Urse on Mumbai–Pune Expressway via Malkhed and Ghotavade Phata. The proposed road width is 22.5 m. The proposed rigid pavement as shown in Fig. 1 is consisting of 320 mm thick pavement quality concrete (PQC) resting over 150 mm thick dry lean concrete (DLC). Below DLC layer, a 200 mm thick granular sub-base (GSB) is proposed to be provided throughout the road width to tackle heavy monsoons. As per guidelines, 500 mm thick subgrade is also recommended.

1.1 Objectives and Scope

The specific objectives of this study are to,

- Design perpetual pavement structure using the design philosophy of IRC 37:2012.
- Perform LCCA comparison between proposed rigid pavement and four different combinations of perpetual pavement.
- Determine and compare total CO_2 emissions caused by proposed rigid and different combinations of perpetual pavement.
- Identify the best-suited option among four combinations of perpetual pavements.

2 Alternative Perpetual Flexible Pavement Design

A perpetual pavement is a long-lasting pavement designed to last for about 50 years. It does not undergo major structural rehabilitation or reconstruction and needs only periodic surface renewal in response to distresses confined to the top of the pavement [2]. The mechanistic-empirical approach is generally observed for analysis and

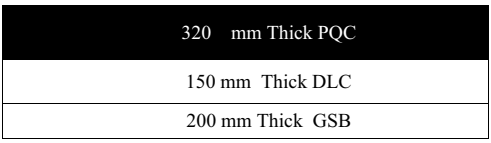

Fig. 1 Proposed rigid pavement layers

design of perpetual pavements. Various limiting values of strain for different layers of pavement are considered while designing or analyzing the performance of perpetual pavements. As a perpetual pavement structure is subjected to only non-structural deteriorations, only a periodic surface renewal involving a repair strategy of shave and pave of the surface layer is generally required. The growing traffic in India is imparting substantial distress on its roads in the form of structural as well as surface rutting and fatigue cracking leading to increased maintenance cost and material consumption. Conventional pavements need structural rehabilitation and reconstruction after their design life has been reached and engages numerous traffic closures and rerouting of traffic in addition to the cost of pavement reconstruction [3]. Perpetual pavements come handy in these circumstances as no significant structural rehabilitation is required for 50 years [4]. The critical characteristic of perpetual pavements lies in the fact that it is never replaced entirely and removed. The fact that only the surface layer is renewed with the base structure staying in place, there is a substantial reduction of construction materials [3].

2.1 Design Criteria for Perpetual Pavement

The tensile strain acting in the horizontal direction at the bottom of asphalt layer and the compressive strain acting in the vertical direction at the top of subgrade are considered as the critical strains in any pavement structure. The general principle of perpetual pavement design is to keep these strains in some particular limits, and many researchers have adopted a maximum limit of 70 microstrains (μs) and 200 microstrains (μs) for horizontal tensile strain and vertical compressive strain, respectively [5]. Indian Roads Congress has also proposed the strain values of 70 μs and 200 μs, respectively, for the fatigue and rutting endurance limit. The Endurance Limit (EL) is a level of strain below which there is no cumulative damage over an infinite number of cycles. A bituminous layer experiencing strain levels less than EL should not fail due to fatigue. Similarly, if compressive strain acting in the vertical direction at the top of subgrade is less than the EL, it should not fail due to rutting.

2.2 Traffic Data

As per IRC-37-2012, the cumulative number of standard axles (MSA) to be carried during the design life is given by following equation with values provided in IRC code.

$$N = \frac{365 \times [(1+r)^n - 1] \times A \times D \times F}{r} \quad (1)$$

where N = Cumulative number of standard axles in terms of million standard axle (MSA), r = Growth rate according to IRC is considered as 5%, n = Design life is considered as 30 years, A = Commercial vehicle per day in the year of completion of construction; D = Lane distribution factor (0.60), and F = Vehicle damage factor (4.5).

From the data about design traffic from Pre-Feasibility and Summary Report of Pune Ring Road, approximately 6780 commercial vehicles per day are expected to be served in this project after completion. Hence, pavement is designed for 444 MSA.

2.3 Design of Four Combinations of Perpetual Pavement

The soils of the region are the weathering products of basalt and have various shades from gray to black, red, and pink color. The California bearing ratio (CBR) of the subgrade soil for the design of the proposed pavement was determined as per IS: 2720 Part-16. The design CBR as per PMRDA summary report was found out to be 10%.

In IRC 37:2012, five different combinations have been considered for which pavement composition has been suggested in the form of design charts presented in Plates 1 to 24. The five combinations proposed are.

- Bituminous surface course with granular base and sub-base (I)
- Bituminous surface course with cement-treated base (CTB), cement-treated sub-base, (CTSB) and granular crack relief layer (CRL) (II)
- Bituminous surface course with CTSB, CTB, and with stress-absorbing membrane interlayer (SAMI) at the interface of base and the bituminous layer (III)
- Bituminous surface course with GSB, CTB, and CRL (IV)
- Bituminous surface course with CTSB and reclaimed asphalt pavement (RAP) (V)

Combination V, which represents use of RAP, is not considered in the evaluation as these options are constrained with the availability of adequate quantity of RAP and data regarding availability of RAP for this project was not at hand.

As per IS SP53:2010, SAMI may consist of elastomeric modified binder (complying with MoRT&H clause 521) like styrene-butadiene rubber (SBR) applied at the rate of minimum 1 kg/m^2. For the pavement analysis, the SAMI layer is not considered as a structural layer [2]. As per the IRC guidelines, viscosity grade 40 (VG 40) bitumen shall be used for surface course and for the DBM, and it shall have a minimum viscosity of 3600 Poise at 60 °C temperature to

Table 1 Properties considered for structural layers as per IRC guidelines

Material type	Elastic/resilient modulus (MPa)	Poisson's ratio
Bituminous layer with VG40	3000	0.35
Cement-treated base	5000	0.25
Crack relief layer	450	0.35
Cement-treated sub-base	600	0.25
Unbound granular layers	$0.2(h^*)^{0.45} M_{R\ Subgrade}$	0.35
Subgrade	$17.6 \times (CBR)^{0.64} = 76.82$	0.35

*Thickness of sub-base layer in mm

safeguard against rutting. The modulus and poisons ratios of different pavement layers as mentioned in Table 1 are considered for analysis here.

The design of pavement was carried out by trial and error with IITPAVE till endurance limit of the strain values closest to 70 μ and 200 μ, respectively, for the fatigue and rutting endurance limit is obtained, which are then used to calculate the values of maximum allowable MSA as given in Table 4 for rutting and fatigue failure using following Eqs. (2) and (3).

$$N_f = 0.711 \times 10^{-4} \times \left(\frac{1}{\varepsilon_t}\right)^{3.89} \times \left(\frac{1}{M_r}\right)^{0.854} \tag{2}$$

$$N_r = 1.41 \times 10^{-8} \times \left(\frac{1}{\varepsilon_v}\right)^{4.5337} \tag{3}$$

where N_f is the cumulative number of repetitions for fatigue failure, N_r is the cumulative number of repetitions for rutting failure, ε_t is the tangential strain, ε_v is the vertical strain, and M_r is the resilient modulus for bituminous layer. From Eqs. (2) and (3), maximum allowable horizontal tensile strain at the bottom of the bottom bituminous layer is 88.57 μs, and maximum allowable vertical strain in subgrade is 229.61 μs for the estimated design traffic.

The proposed pavement combinations were designed using guidelines given in IRC 37:2012. In this study, minimum thickness permissible for sub-base, base, CRL, and for BC is considered for all the trial sections and remaining pavement layers are kept as variable ones for perpetual pavement design. It was adopted for providing sufficient stiffness in the upper pavement layers as per the concept of perpetual pavements. Combinations with CTSB and CTB were checked against fatigue cracking as per the guidelines in IRC 37.

After trying number of iterations with IITPAVE software, the design satisfying endurance limit criteria was chosen for analysis as given in Table 2. For inputs to the IITPAVE software, a single-axle dual-wheel assembly was considered for the analysis. The standard axle load considered was 80 kN. The contact radius was assumed as 15.5 cm with a tire pressure of 0.56 MPa.

Table 2 Thickness of pavement layers for different trial combinations and corresponding pavement responses from IITPAVE

Trial combination	Sub-base	Base	CRL / SAMI	DBM	BC	Total (mm)	ε_t (μs)	ε_v (μs)
I	200 (GSB)	150 (WMM)	–	290	50	690	67.95	140.6
II	200 (CTSB)	100 (CTB)	100 (CRL)	170	50	620	69.73	169.5
III	200 (CTSB)	100 (CTB)	SAMI	140	50	490	13.70	194.08
IV	200 (GSB)	100 (CTB)	100 (CRL)	180	50	630	69.87	150.8

Table 3 Expected service life comparison of perpetual pavement using Eqs. (2) and (3)

Trial combination	N_f (msa)	Expected service period 'n' (in years) considering N_f	N_r (msa)	Expected service period 'n' (in years) considering N_r
		Top layer		Bottom layer
I	1245.24	47.84	4102.97	70.84
II	1126.07	45.98	1758.05	54.32
III	631,867.93	173.43	951.49	42.93
IV	1117.32	45.84	2986.77	64.57

Expected service period (n) is calculated from Eq. (1) using corresponding MSA values

From Table 3, it can be said that perpetual design provides better service period for far larger amount of traffic than rigid pavement designed for 30 years. This demonstrates the basic premise of designing a perpetual pavement of placing asphalt on a stable foundation which results in relocating the distresses that originate at the bottom of the pavement to the upper layers. The top layer acts as a protective barrier, since the distresses are confined to the wearing course. Even though some of the expected service periods given in Table 3 are less than 50 years, the strain values are within the permissible limit for perpetual design concept. Significance of EL is that such a limit would provide a thickness limit for the pavement and increasing the thickness beyond this limiting thickness would provide no increased structural resistance to fatigue and rutting damage, and hence, it helps to avoid extra expenditure.

3 Construction Cost Calculation

The cost comparison for a 1 KM stretch for proposed rigid pavement and for a perpetual pavement was done using the standard rates in Indian Rupees as per the state government's public works department schedule of rates for year 2019–20 as given in Table 4 (Table 5).

Table 4 Schedule of rates [6]

Type of pavement	Material	Specification clause	Rate (INR)	Unit
Proposed rigid pavement	PQC	MoRT&H 602	6929	Cubic meter
	DLC	IRC:SP-49 and MoRT&H 601	2970	Cubic meter
	Sub-base	IS:383, MoRT&H 601	1598	Cubic meter
Proposed flexible perpetual pavement	BC	MoRT&H 509	7272	Cubic meter
	DBM	MoRT&H 507	6742	Cubic meter
	SAMI	MoRT&H 517	110	Square meter
	CRL	MoRT&H 401	1657	Cubic meter
	CTSB	MoRT&H 404	1827	Cubic meter
	CTB	MoRT&H 404	1902	Cubic meter
	WMM	MoRT&H 406	1657	Cubic meter
	GSB	MoRT&H 401	1598	Cubic meter

Table 5 Cost comparison for 22.5 m wide road

Pavement design	Proposed rigid road	Perpetual pavement design combination			
		I	II	III	IV
Total cost (Millions)	67.10	64.95	50.19	44.39	50.68

4 Life Cycle Cost Analysis

Life cycle cost is considered to include the initial or direct cost of construction, cost of rehabilitation/reconstruction, and cost of potential maintenance regime. In the present study, LCCA is carried out for 50 years for comparing the overall cost associated with construction of one-kilometer length of perpetual pavements with the proposed rigid pavement using net present value (NPV) method. The steps involved in the LCCA methodology were:

1. Estimate the initial construction cost.
2. Develop a maintenance plan and determine maintenance cost.
3. Determine life cycle costs using the NPV method.

Here, in this paper, the long-term economic viability of pavements types using the NPV method of analysis has been studied. The discount rate is the interest rate by which future costs will be converted to present value and has been adopted as 10%, and an inflation rate of 5% was adopted.

The design period for the perpetual pavement is 50 years. Hence, to provide a parallel platform for comparison, LCCA is carried out for total life of 50 years in case of rigid pavement as well as perpetual pavement as given in Tables 6, 7, 8, 9, and 10.

According to the MORT&H specifications [7], a layer of 25 mm BC is to be provided once every five years in case of flexible pavements. As per IRC guidelines

Table 6 Year-wise maintenance schedule and economics of proposed rigid pavement (service period 30 years)

Year (n)	Maintenance for proposed rigid pavements	Current cost per KM for a 22.5 m wide road (Millions)	Inflation @5.0% per annum (Millions)	NPV (Millions)
10th	Overlay of 25 mm overlay slab	3.90	6.35	2.45
20th	Overlay of 25 mm overlay slab	3.90	10.34	1.53
Reconstruction and major repair work in 30th year as given in Table 8				
40th	Overlay of 25 mm overlay slab	3.90	27.44	0.61
50th	Overlay of 25 mm overlay slab	3.90	44.72	0.38
Total				4.95

Table 7 Year-wise maintenance schedule and economics for perpetual pavements

Year (n)	Maintenance for proposed perpetual pavements	Current cost per KM for a 22.5 m wide road (Millions)	Inflation @5.0% per annum (Millions)	NPV (Millions)
5th	Overlay of 25 mm BC	4.09	5.22	3.24
10th	Overlay of 25 mm BC	4.09	6.66	2.57
15th	Overlay of 25 mm BC	4.09	8.50	2.04
20th	Overlay of 25 mm BC	4.09	10.85	1.61
25th	Overlay of 25 mm BC	4.09	13.85	1.28
30th	Overlay of 25 mm BC	4.09	17.68	1.01
35th	Overlay of 25 mm BC	4.09	22.56	0.80
40th	Overlay of 25 mm BC	4.09	28.79	0.64
45th	Overlay of 25 mm BC	4.09	36.75	0.50
Reconstruction and major repair work in 50th year as per concept of perpetual pavement				
Total				13.69

Table 8 Economics of pavement reconstruction (after 30 years) for proposed rigid pavement

Pavement type	Initial construction cost (Millions)	Inflation @5.0% per annum (Millions)	NPV (Millions)
Rigid pavement	67.10	290.00	16.62

for rigid pavement, a thin overlay is laid over the existing slab after preparing the existing surface by etching or scarifying by milling machines and coating it with cement mortar. Such an overlay acts monolithically with the existing slab and requires the minimum thickness of 25 mm. As the proposed rigid pavement was designed 30 years, they need to be reconstructed after the 30th year of pavement service.

Table 9 Economics of pavement reconstruction (after 50 years) for proposed perpetual pavement

Perpetual pavement design combination	Initial construction cost	Inflation @5.0% per annum (Millions)	NPV (Millions)
I	64.95	744.80	6.34
II	50.19	575.54	4.90
III	44.39	509.03	4.34
IV	50.68	581.17	4.95

Table 10 Life cycle cost analysis for perpetual and conventional pavements with respect to NPV for period of 50 years

Pavement type	Initial construction	Net present value (in Millions INR) per km			
		Maintenance (overlay)[a]	Major maintenance/ reconstruction[b]	Total	Saving in case of perpetual pavement (%)
Proposed rigid	67.10	4.95	16.62	88.67	–
Perpetual pavement design combination					
I	64.95	13.69	6.34	84.98	4.16
II	50.19	13.69	4.90	68.78	22.43
III	44.39	13.69	4.34	62.42	29.60
IV	50.68	13.69	4.95	69.32	21.82

[a]From Tables 6 and 7
[b]From Tables 8 and 9

Based on these parameters, year-wise maintenance schedule and economics of laying overlay for conventional pavements are reported in Tables 8 and 9.

The LCCA has been worked out in Table 10 where it can be seen that perpetual pavements have lesser life cycle costs than rigid pavements due to reduced maintenance costs in comparison. It can be observed from Tables 3 and 10 that combination III has the least thickness and least life cycle cost among all the combinations of flexible pavement analyzed.

5 Environmental Aspect with Respect to Emission of CO_2

Embodied carbon means all the CO_2 emitted in producing materials. It is estimated from the energy used to extract, transport, and manufacture raw materials as well as deconstructing and disposing of it at the end of its lifetime. After literature review on the subject, the calculations for embodied CO_2 done by University of Bath [8] and by Auroville Earth Institute (AEI) [9] were adopted. A generalized proportioning of bitumen, cement, coarse aggregates, and fine aggregates for different layers of the pavement are listed in Table 12 which are based on the MoRT&H specifications, IRC SP:49 [10], IRC SP:53 [11], and IRC SP:89 [12] (Table 11).

The sample calculation for the embodied CO_2 released during laying of the DBM layer, prepared as per the mix proportioning stated in Table 13, has been discussed in the following section.

Embodied CO_2 for 1 m^3 of pavement layer (kg) = Volume of layer 1 m^3 × Density of the layer × [(Bitumen by mass × Embodied CO_2 of bitumen) + (coarse aggregates by mass × Embodied CO_2 of coarse aggregate) + (fine aggregates by mass % × Embodied CO_2 of fine aggregates)] (Table 14).

Embodied CO_2 for 1 m^3 of DBM layer (kg) = 79.90.

Table 11 Embodied CO_2 of materials [8, 9]

Material	Embodied CO_2 (kg/kg material)
Bitumen	0.48
Coarse aggregate	0.0216
Fine aggregate	0.002
Cement	0.83

Table 12 Generalized properties of different layers of rigid and flexible pavements

Properties of the mix	Pavement layers								
	PQC	DLC	BC	DBM	WMM	GSB	CTB	CTSB	CRL
Density (kg/m^3)	2500	2400	2400	2300	2300	2300	2300	2300	2300
Bitumen by mass (%)	–	–	5.5	4.5	–	–	–	–	–
Cement by mass (%)	8	8	–	–	–	–	2	2	–
Aggregates by mass (%)	92	92	94.5	95.5	100	100	98	98	100
Coarse fraction of total aggregates (%)	60	65	55	60	70	80	65	80	70
Fine fraction of total aggregates (%)	40	35	45	40	30	20	35	20	30

Table 13 Embodied CO_2 for pavement layers

Pavement layer	BC	DBM	WMM/ CRL	GSB	CTB	CTSB	PQC	DLC
Embodied CO_2 for 1/ m^3 (kg)	92.34	79.90	36.15	40.66	71.40	78.03	197.65	191.90

Table 14 Total CO_2 emission for proposed rigid and perpetual pavement combinations

Type of pavement	Proposed rigid road	Perpetual pavement design combination			
		I	II	III	IV
Total embodied CO_2 (ton)	2253.71	930.20	1002.62	929.45	852.43

In case of combination III, embodied CO_2 value for SBR is considered as 2.76 kg/kg [13].

So, embodied CO_2 for SAMI layer per KM is = 2.76 × 22.5 × 1000 = 62.10 tons.

6 Conclusions

Present study shows that perpetual pavement is clearly a better choice considering factors like longevity, material consumption, life cycle cost, and carbon footprint. The study led us to conclude that bituminous surface course with CTSB, CTB, and SAMI, i.e., combination III, is the most cost-friendly option in addition to have least design thickness among various combinations discussed. This also shows that strong base and sub-base layers with higher modulus can provide cost-effective and strong pavement structure. Further, investigation about CO_2 emissions of all the pavements demonstrate that rigid pavements contribute much more to carbon footprint than flexible pavements. Comparison of embodied CO_2 among perpetual pavement combinations indicate that bituminous surface course with GSB, CTB, and CRL, i.e., combination IV, is the most eco-friendly option even though it is costlier by almost 10 percent than the option III. India is still a developing country and signatory of Kyoto Protocol, ergo there can be a dilemma in choosing between least costly and most eco-friendly option. Overall it can be said that perpetual pavements should be advocated for construction of highways in India.

References

1. Pre-feasibility Report of Pune Ring Road, September 2016
2. Indian Road Congress (IRC 37) Guidelines for design of flexible pavement, July 2012
3. National Asphalt Pavement Association (APA) (2002) Design, construction, and maintenance of open-graded asphalt friction courses. Asphalt Institute, National Asphalt Pavement Association
4. Mahadeo S, Ranadive S, Kulkarni S (2016) Perpetual pavement for rural roads: a concept. In: A national conference on fifteen years of Pmgsy, Transportation Engineering Group, Civil Engineering Department, Indian Institute of Technology Roorkee, India, p 23, 6–7 Aug 2016
5. Walubita LF, Scullion T (2010) Texas perpetual pavements—new design guidelines. Report No: 0–4822-P6, Texas Department of Transportation and the Federal Highway Administration
6. Government of Maharashtra, PWD Schedule of Rates (2019–20)
7. Ministry of Road Transport and Highways Government of India (2013) Specification for road and bridge works
8. Hammond G, Jones C (2008) Inventory of carbon & energy: ICE. Bath: sustainable energy research team, Department of Mechanical Engineering, University of Bath, U.K.
9. Maini S, Thautam V (2009) Embodied energy of various materials and technologies, Auroville Earth Institute (AEI), Tamil Nadu, India

10. Indian Road Congress (IRC SP:49) Guidelines for the use of dry lean concrete as sub-base for rigid pavement (First Revision)
11. Indian Road Congress (IRC SP:53) Guidelines on use of modified bitumen in road construction (Second Revision)
12. Indian Road Congress (IRC SP:89) Guidelines for soil and granular material stabilization using cement lime and fly ash
13. www.plasticfantasticlibrary.com/library/plastic/121/styrene_butadiene_rubber.html

Urban Compatible Roads and Traffic Calming

Jan Riel

Abstract The effects of climate change on the one hand and several fatalities of cyclists and pedestrians in urban traffic on the other hand highlight more than ever the need of a mobility transformation. This article focuses on the re-design of urban roads and on the usage of speed humps to make cycling and walking safer and more attractive. A key factor in this context is the speed of car-traffic. It has to be reduced significantly to increase safety and feel good of unmotorized road users. When (re) building roads, designing them according to the shared space principle can have a high benefit. On existing roads, however, the correct use of suitable speed bumps can lead to a significant reduction in speeds. When constructing new roads, designing them according to the shared space principle can have a high benefit. On existing roads, however, the correct use of suitable speed bumps can lead to a significant reduction in speeds.

Keywords Traffic calming · Participation · Speed humps · Shared space · Climate adaptation

1 Introduction

In cities, numerous activities take place in public space. The three essential functions of roads (connection, access and stay) compete for the limited public space. While in the 1960s to 1980s, roads were mainly adapted to the needs of motor vehicle traffic, and this development has been increasingly questioned since the 1990s. While a more pedestrian- and cyclist-friendly re-design of urban roads is already taking place for several years, the effects of climate change now additionally require a redesign of public space in the sense of climate-adaptation.

The climate-adaptation of roads (e.g., through greening and unsealing) is usually accompanied by an increase in the quality of stay, which in turn benefits walking

J. Riel (✉)
Karlsruhe University of Applied Sciences, Moltkestraße 30, 76133 Karlsruhe, Germany
e-mail: jan.riel@hs-karlsruhe.de

B. Laishram and A. Tawalare (eds.), *Recent Advancements in Civil Engineering*, Lecture Notes in Civil Engineering 172,
https://doi.org/10.1007/978-981-16-4396-5_66

and cycling. A key factor in this context are low speeds in car-traffic. This article describes Korean and German experiences in achieving a "city-compatible" speed level in the sense of a sustainable redesign on urban space.

2 Redesign of Urban Roads

2.1 Territories, Safety, Speed

As motorists, we assume that the driving lane is our territory which is separated from other traffic modes by a curb. Accordingly, we feel safe in our territory, and we pay less attention to, e.g., pedestrians on the other side of the curb and we therefore can drive faster. This has two consequences:

(1) Pedestrians and cyclists feel uncomfortable. Possibly this is a reason not to walk or use the bicycle which would counteract the goal of a climate-friendly mobility-turnaround.
(2) In case of an accident, there are significantly higher consequences: The fatality risk of a pedestrian's collision with a car is 42% at a car-speed of 50 km/h. At a speed of 30 km/h, the fatality risk is reduced to 6% [1] (see Fig. 1, left). In addition, as speed increases, the driver's field of vision increasingly focuses on the area directly in the direction of travel. Movements in the lateral area are perceived much less quickly [2] (see Fig. 1, right).

Therefore, the reduction of car speeds can be seen as an important key for the urban-compatible redesign of urban roads.

2.2 Example 1: From Separation to Shared Space

The following example describes the redesign of a narrow main road in a Karlsruhe residential district. The road was originally built according to the separation

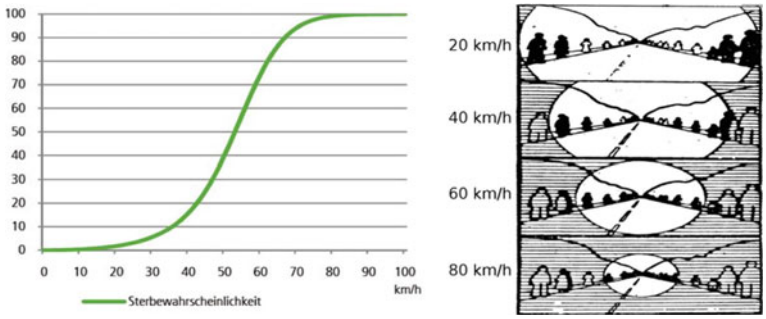

Fig. 1 Fatality risk of pedestrian in case of collision with car (left), visibility field in dependency of speed (right)

principle with sidewalks and carriageway separated by curbs. The roadway was designed for the encounter of two buses, but the sidewalks were partly so narrow that pedestrians could not use them (Fig. 2, left). The goal was to improve the situation for pedestrians and decrease the car traffic speed.

After a long discussion process with the residents, the separation principle was abolished and the street was converted into a shared-space scheme instead. Two asphalt "stipes" (width 1.40 m) in the middle of the road were intended to make car drivers mainly use the middle part of the road. The rest of the space was paved and, therefore, looked more like pedestrian space (Fig. 2, right). Anyway, the paved area has to be used by cars and pedestrians commonly in case of two vehicles encounter. This constellation is not known in German traffic law. We, therefore, evaluated the effects of the redesign on traffic safety and traffic flow with a video-based survey. As a result, it turned out that:

- The motor vehicle traffic is oriented towards the asphalt strips in the middle of the roadway and thus keeps a bigger distance from the buildings (see Fig. 3).
- The v_{85} reduced from 39 to 30 km/h. This is assumed to be a result of the visually narrowed lane (without a clear demarcation to the side area).
- The (enlarged) side areas are used by pedestrians over their entire width, the number of pedestrians has increased by 70% compared to the time before the conversion.

The example shows that the redesign of a road can result in a more urban-friendly traffic flow.

2.3 Example 2: Road Design More Important Than Signs

In a similar case, we redesigned a Karlsruhe residential road (speed limit 30 km/h) with high parking pressure. Here, not only the sidewalks were so narrow for the encounter of two pedestrians, but also the driving lane was too narrow.

Fig. 2 Steinkreuzstraße before (left) and after (right) redesign

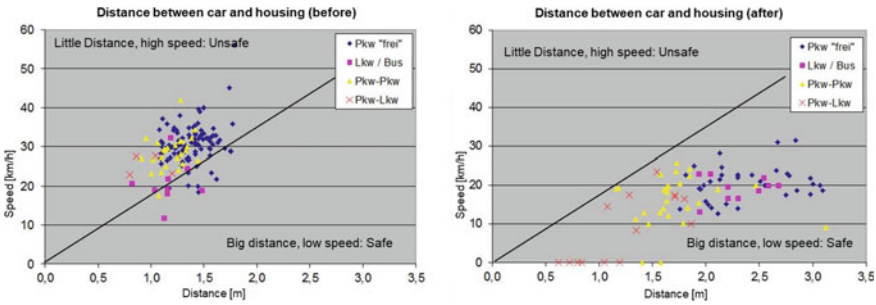

Fig. 3 Distances (housing/car traffic) and car speeds before and after redesign of the road

Fig. 4 Redesigned road in phase 1 (left) and survey results (right)

In the redesign, the narrow pavements were abandoned and parking was moved directly to the houses. So, in the middle of the road, a shared-space area was created which is wide enough for the encounter of two cars (Fig. 4, left). In a series of three configurations, different sign-postings were tested to meet the needs of the residents. In each phase, passersby were asked how safe they felt on the street (Fig. 4, right):

(1) Speed limit 20 km/h
(2) Traffic-calmed area
(3) Traffic-calmed area and one-way road (to additionally reduce traffic volume).

Perception of Pedestrians

The speed limit of 20 km/h leads to uncertainty regarding the use of the remaining space between parking and buildings: Pedestrians did not know whether this area was a sidewalk or not and weather the shared-space area was car "territory" or not. Therefore, in Phase 1 (speed limit only) the majority of the pedestrians felt unsafe. After changing the sign posting to a "traffic-calmed area" in phases 2 and 3, pedestrians felt significantly safer than before.

Speed

The car traffic speeds were monitored in all phases using a side-radar device. In contrast to the pedestrian's changing perception of traffic safety, there were no differences in the car speeds. Although the traffic-calmed area is accompanied by a speed limit of 7 km/h, the v_{85} remained constantly at about 28 km/h.

The example shows that the design of a road can have a bigger influence on the car traffic speed than the presence of signs. In contrast, pedestrians seem to be significantly influenced by the signs.

3 Speed Humps

3.1 Types of Humps

Generally, two types of speed humps can be distinguished on the basis of the hump's crossing length. Internationally, uniform terms for the two types are not defined, so in this article, the distinction is made between "short" and "long" humps on the basis of the crossing length:

Short Speed Humps

In Germany, short speed humps have a crossing length of 40–50 cm and a height of approximately 5–10 cm (see Fig. 5). Particularly at speeds above 20–30 km/h, these humps cause a hard impact on the car's suspension. For this reason, car drivers brake hard before the hump and accelerate rapidly shortly after the hump. Thus, the traffic calming effect of humps is partly compensated. For cyclists in particular, short speed bumps can be uncomfortable or even dangerous due to their rapid inclination.

Long Speed Humps

Long speed humps are usually a construction part of the road and have (nationally varying) crossing lengths of 2–5 m and heights of 10 cm. The following Fig. 6 shows the dimensions of long humps in Germany and Korea. Since the ramp inclination of

Fig. 5 Examples for short speed humps in Germany

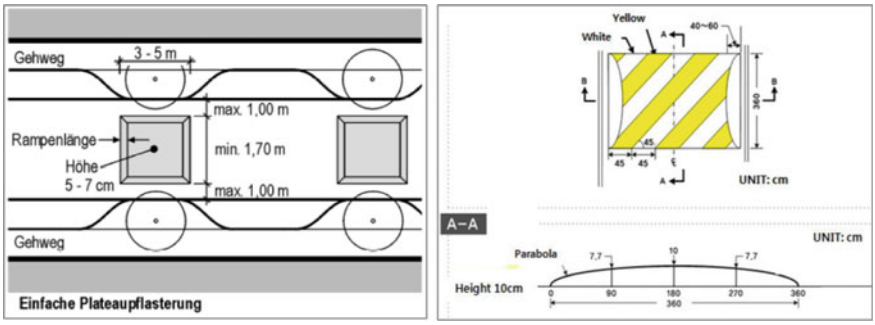

Fig. 6 Dimensions of long humps in Germany [3] (left) and Korea [4] (right)

long humps is significantly lower than that of short humps (Germany) or even rounded (Korea), braking or acceleration is less intensive before and after the humps.

The car speed on a long hump is obviously higher than on a short hump. However, it is not proven whether this has any influence on the level of safety of the different hump types. Additional analysis of accident data should be done here. Nevertheless, long humps also lead to lower car speeds. Considering the smoother braking and accelerating and the less critical impact on cyclists due to the smoother ramp inclination, this article focuses on this type of humps.

The next two chapters describe experiences from Germany and Korea about two questions:

(1) What speed reduction can be reached with (long) humps and
(2) What is the optimum distance between humps to avoid acceleration of cars between the humps?

3.2 Experience of Korea

In Korea, long humps for speed absorption are widely used and can be found in almost every street with adjoining residential use. Kim et al. studied numerous sections of roads with long humps in Korea. The researchers also came to the conclusion that a single hump produces only a locally limited effect of speed damping: After the hump, the drivers accelerate the car back to their desired speed.

However, if the drivers recognize that other humps follow behind the first hump, the car is not accelerated significantly (Fig. 7).

Kim et al. call a sequence of several thresholds “continuous humps.” The researchers studied the influence of the distance between the humps on the level of speed reduction using 26 road sections equipped with humps at intervals of 23–90 m.

As a result, the researchers concluded that the optimal distance for achieving a consistently low speed level of 30 km/h is 20 m. At distances of 30–40 m, the

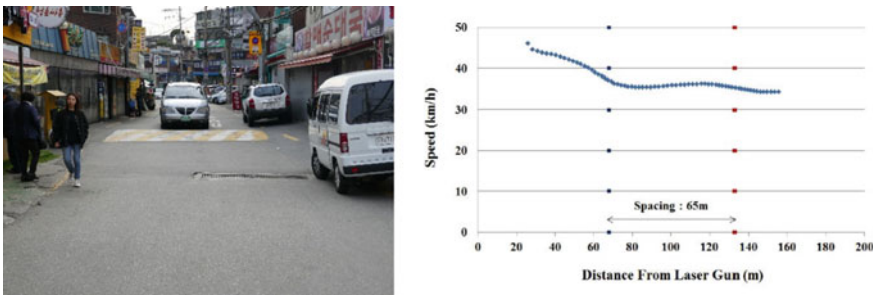

Fig. 7 Speed hump in Korea (left), and speed profile between continuous humps (right) [4]

speed level increases only slightly. Finally, a distance of 70 m between the humps is defined as the maximum, since from this distance on the braking deceleration before the second hump is again as high as before the first hump. The positive effect of the hump sequence then no longer occurs (Fig. 8).

3.3 Experience in Germany

3.3.1 General Use of Humps

In Germany, humps for speed reduction are generally only rarely used. If humps are used after all, these are mainly short humps. This is astonishing insofar as they do not have an official road traffic certification, and their use is therefore legally uncertain. In the past, road maintenance authorities have also been held liable for damage caused to cars when driving over humps—even if the vehicles were proven to have been driving too fast.

Long humps are used even less frequently in Germany than short speed humps. This is again astonishing, since long humps are anchored in the German guidelines and therefore there is legal certainty for their use. The regulations not only describe

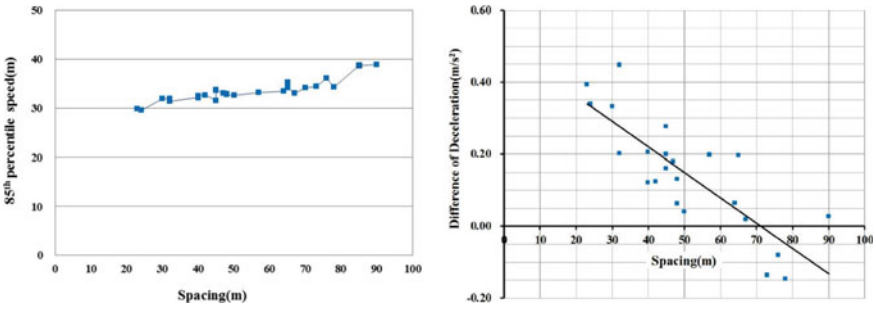

Fig. 8 Relationship between interval and $v85$ (left) and deceleration (right) [4]

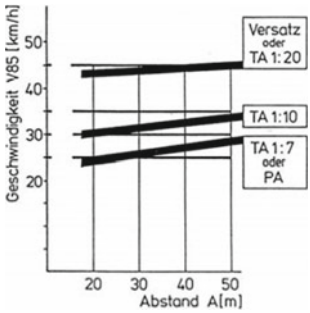

Fig. 9 Recommended distance long between speed humps in German guidelines right [3]

the geometry (see Fig. 9) but also give recommendations on the distances between the humps to achieve a certain v_{85}.

3.3.2 Karlsruhe Living Lab with Long Humps

Background

During the participation process of an urban redevelopment program it turned out that pedestrians felt uncomfortable in some of the quarter's roads, especially because of cars driving too fast. Goal of the living lab was to find out if a series of temporary long humps can contribute to the pedestrian's well-being, so that—in case of a successful test—a proper re-design of the road can be planned.

Test Tracks

Altogether, two test tracks were installed. Layout and results were very similar, so in this article, only one of them is described in detail. The overall length of the test track was about 335 m, and the distances between the humps were 40–80 m (Fig. 11). Thus, the distances were at or over the upper end of the Korean and German recommendations (Fig. 10).

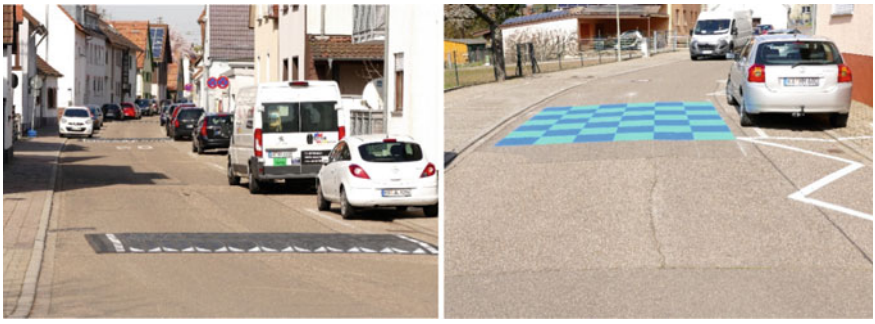

Fig. 10 Installation of humps and paintings in test tracks

Evaluation Part 1: Speed Measurements

For the speed measurement, side radar devices (Type Sierzega SR4) were used at the six positions on the test track (see Fig. 11, left) and the v_{85} was determined. Two devices were available, so the devices had to be mounted over three days at two positions each.

The result of the speed measurement is shown in Fig. 11 (right). Before the test, the v_{85} was in a range of 28–35 km/h. Thus, the speed level was already relatively low anyway. However, during the test phase with humps, the v_{85} was measured with 21–24 km/h. So, a continuous speed reduction of approximately 30% over the test track turned out (Fig. 11, right).

Evaluation Part 2: Digital Participation in Living Labs

Public participation is a widespread practice in Germany since decades. In the classic approach, the inhabitants of a redevelopment area, for example, are informed about upcoming information and participation events via direct mail, the Internet or print media. These events usually take place on weekdays in the late afternoon or early evening. Experience shows, however, that such events are often attended by only a few residents, most of whom have already reached retirement age. The feedback of this person group therefore is not representative.

In the living-lab project "GO Karlsruhe" [5], we tried to get in touch with the (other) residents, too, using digital media and new feedback instruments. For this purpose, among others, "interactive posters" were developed. On these, a single question or statement like "Here I feel comfortable as a pedestrian" was written. The passersby could then vote for the statement by pushing one of four buttons on a

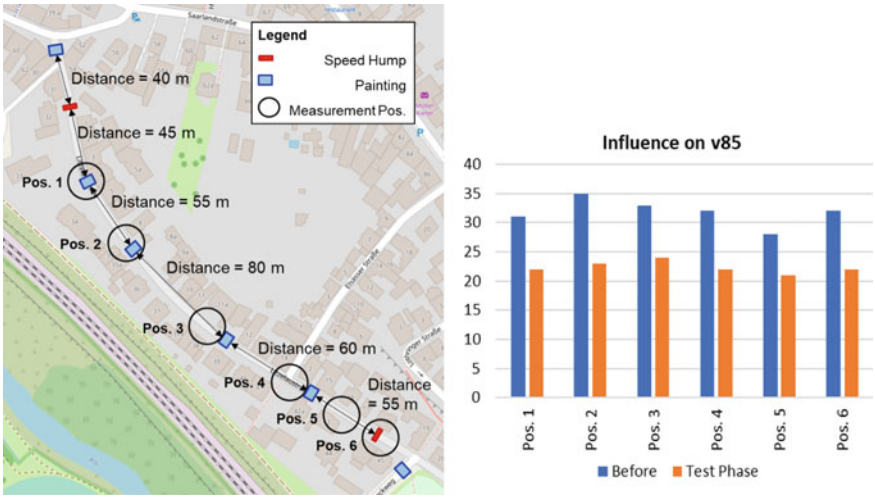

Fig. 11 Test field arrangement in Karlsruhe (left) and *v*85 before and after installation of humps (right)

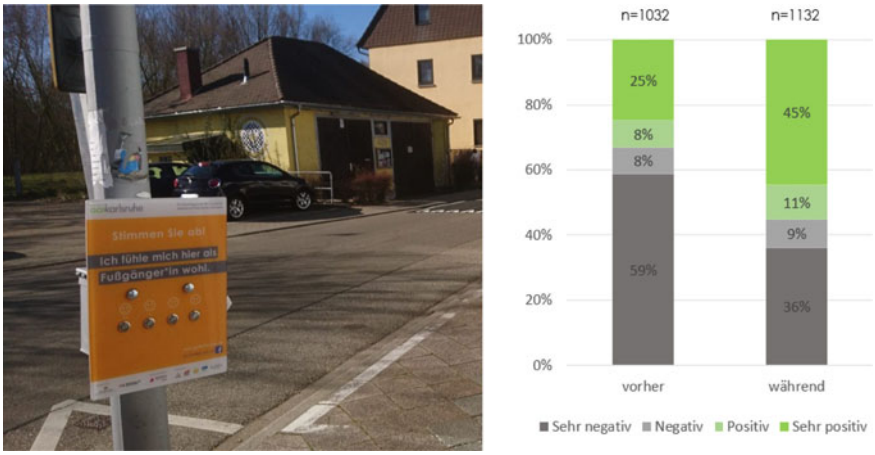

Fig. 12 Feedback by new participation formats

scale from "very negative" to "very positive" (Fig. 12, left). Misuse (e.g., by repeatedly pressing a button) could be prevented by filtering out presses that occurred too quickly in succession.

Results and Inferences

The results of the living-lab (together with the Korean experiences) show, that long humps lead to a significant reduction of car speeds. Obviously, this should result in a reduced number and severity of road accidents. Anyway, there is the need for further research to extend the data-base, also with regard to the question to what extent the effects of painting and humps differ.

Korean and German examinations confirmed that in longer sections without installations (in Karlsruhe 80 m between positions 2 and 3), the highest speeds were measured in the course of the test track. Thus, in remodeling of roads the distance between long humps should be well below 80 m.

The result of the new digital participation method using "feedback posters" was clearly in favor of traffic calming (see Fig. 12, right): Without the humps, 2/3 of the passersby assessed the situation as negative, and with the humps, the ratio was almost the opposite and 56% assessed the situation positive. It can be assumed that such a different awareness of public space will contribute to the acceptance of walking and cycling.

4 Conclusion

Low speeds of motor vehicle traffic are an essential key in making the use of public spaces attractive for pedestrians and cyclists. There are many ways of slowing down traffic. Pure restrictions in the form of signs, controls and penalties are not a good solution, especially when the road space invites speeding. An urban-compatible redesign of road space can also make a major contribution and offers the additional potential to improve the quality of stay and integrate measures for climate adaptation (greening). However, remodeling is expensive and cannot be implemented across the whole area within a few years. However, significant effects of speed reduction can also be achieved with retrofitting elements such as long humps (made of recycled material). These are relatively inexpensive and also contribute to greater road safety and the well-being of pedestrians.

Additional offers for feedback from residents or users of public space are an important supplement to scientific accompanying evaluations. It is correct and important to describe the effects of engineering measures (humps) with measurements (speed) according to engineering scientific methods. But it is at least as important to know the opinion of the users, too. Only measures that are accepted by the users will help to achieve sustainable restructuring of the transport system.

References

1. Ewert U, Scaramuzza G, Niemann S, Walter E (2010) Der Faktor Geschwindigkeit im motorisierten Straßenverkehr bfu Sicherheitsdossier 06, Bern
2. Bockelmann W (1982) Auge—Brille—Verkehr München
3. Forschungsgesellschaft für Straßen- und Verkehrswesen (FGSV) (2006) Richtlinien zur Anlage von Stadtstraßen (RASt)
4. Kim YS, Yeo I, Baek J-G, Choi J-W (2013) The optimal spacing of speed humps in traffic calming areas. Int J Highway Eng 15(3):151–157
5. Karlsruhe university of applied sciences: living lab “GO Karlsruhe”. https://www.gokarlsruhe.de/

Development of Free-Flow Criteria for Divided Rural Highway: A Case Study

Rahul Tanwar, Naynish Pandey, and Subhadip Biswas

Abstract Various highway capacity manuals and research articles recommended different headway-based free-flow criteria of a traffic stream. These criteria are used to identify a free-flowing vehicle. Since vehicles belonged to different categories possess different dynamic characteristics, free-flow criteria of these vehicles may not be the same. However, none of the criteria recommended in different manuals acknowledged this vehicle category-wise variation. Further, behavioral changes in vehicular movements are yet to observe across lanes. On this background, the present study examines whether free-flow criteria should be vehicle-specific. If yes, then the present study further aims to develop free-flow criteria for different vehicle categories separately in context of divided rural highway. Also, the study emphasizes the lane-wise variation of free-flow condition. Traffic data which includes classified traffic volume, speed and time headway were collected using videography at a mid-block segment of NH-58 in the district of Uttar Pradesh, India. Data required for the study were extracted by playing the video files on a computer screen. The study revealed that a headway corresponding to 0.75% increase in speed can be considered as critical headway. Unique relationship between 'percent increase in speed' and headway was developed for each vehicle category. Based on these relationships, this paper finally forwards vehicle-specific free-flow criteria for divided rural highway. The outcome of this research will be helpful to find free-flow speed of different vehicle categories separately under mixed traffic conditions.

Keywords Free-flow speed · Categorical analysis · National highway · Headway · Mixed traffic

R. Tanwar · N. Pandey · S. Biswas (✉)
Department of Civil Engineering, N.I.T. Hamirpur, Hamirpur, Himachal Pradesh, India

B. Laishram and A. Tawalare (eds.), *Recent Advancements in Civil Engineering*, Lecture Notes in Civil Engineering 172,
https://doi.org/10.1007/978-981-16-4396-5_67

1 Introduction

Fundamental traffic flow parameters describe the nature or attribute of traffic flow and help in analyzing the behavior and the variation in traffic movements. Time headway is the fundamental microscopic parameter in traffic flow and is defined as the time gap between two successive vehicles while passing through a given point. Due to nonuniform arrival of vehicles, headway is not expected to be constant, rather it is observed varying substantially on a rural highway. Since free-flow criteria on a road segment are usually based on headway, the study of distributions of prevailing headways is prerequisite to develop the free-flow criteria of a roadway segment. Moreover, in analyzing traffic movements on a multilane roadway, distributions of headway should be considered lane-wise. In addition, the mixed nature of traffic in Indian conditions adds further complexity to headway analysis. Vehicles with different static and dynamic characteristics do not respond similarly to a particular traffic condition. For example, being small-sized and highly maneuverable, motorized two-wheelers and three-wheelers can move through a small lateral gap resulting in insignificant reduction in speed at higher traffic volume. Conversely, due to limited opportunity of accepting preceding lateral gap, speed of heavy vehicles reduces substantially with increase in traffic volume. Also, larger vehicles like trucks are expected to have higher braking distance as compared to small-sized vehicles like motorized two-wheelers and three-wheelers. Hence, it is quite obvious that different categories of vehicles behave differently in spite of having the same frontal headway. Due to this, category of the subject vehicle plays a crucial role in determining the relationship between headway and speed.

2 Literature Review

A good volume of research was conducted estimating free-flow speed (FFS) of traffic stream. Salim [1] forwarded Kalman filter-based nonlinear equations to estimate free-flow speed. However, the approach is suitable when there is less volume of traffic. Ye et al. [2] analyzed the influences of few factors such as, proportion of truck, land use, speed limit, road category, number of lanes, etc., on FFS. Authors further revealed that FFS at night and daytime are different. Similarly, De Luca et al. [3] added pavement conditions and intensity of side obstacles to this list of influencing factors of FFS. Weather conditions may also have a significant impact on FFS. Ji and Shao [4] examined the influence of rainstorm and revealed that FFS decreases by 40% when intensity of rainfall increases by 2.2 mm/min. Another study [5] reported that reduction in FFS as 0.2, 3.4 and 0.8% at shoulder lane and 0.3, 0.4 and 1.5% at median lane corresponding to slight, moderate and heavy snow fall. Further, it is to be mentioned that headway-based criterion is the most popular approach for estimating free-flow speed. Vogel [6] revealed that a vehicle can be considered as free flowing if it has a headway of more than 6 s with

respect to its preceding vehicle. US Highway Capacity Manual [7] recommended that a vehicle can be defined as free flowing if its frontal and back headway are more than 8 s and 5 s, respectively. Criteria of free-flow condition may vary depending upon the context specifically driving culture and road configuration. Few investigations were performed to estimate FFS in context of Indian traffic condition. Recent capacity manual of India, Indo-HCM [8] considered a headway of minimum 8 s as the basis of free-flow condition irrespective of vehicle category. Hence, question arises whether the free-flow criteria should be the same for all vehicles specifically for Indian heterogeneous traffic conditions. Although few studies [9, 10] realized these variations and estimated FFS for individual vehicle category, none of these study came out with categorical free-flow criteria. On this background, the present study aims at developing individual free-flow criteria for each vehicle category for accurate estimation of FFS.

3 Data Collection

The present study adopted videography as primary tool to collect headway, traffic speed and volume data at a mid-block segment of four lane-divided rural highway in Meerut, Uttar Pradesh, India. Width of each lane was 3.5 m making the carriageway 7 m wide in one direction. The segment was straight without gradient and there was no busstop, walkways or on-street parking in the vicinity of the location as may be seen in Fig. 1.

A trap length of 60 m was chosen at the mid-block segment. A video recorder was placed on the rooftop of a building in such a manner so that the traffic movements within the segment could be captured uninterruptedly. Videography was conducted for ten hours (7 a.m. to 5 p.m.) on a weekday in normal weather

Fig. 1 Location selected for data collection

conditions. Then, video files were taken to the laboratory and played on a computer screen to extract the required data. The time of entry and exit into the trap length was noted with an accuracy of 0.01 s for each vehicle. Headway of a vehicle was measured as the difference of entry times of the preceding vehicle and the subject vehicle. Similarly, the speed of a vehicle was measured based on the time taken by the vehicle to reach the exit line from the entry line. A total of 3169 and 2354 vehicles were observed at edge at median lane, respectively. All vehicles were classified into six categories: small car (SC), big car (BC), heavy vehicle (HV), motorized three-wheeler (3W), motorized two-wheeler (2W) and bicycle (BY). Big cars are SUVs having an engine capacity of over 1400 cc and rest of vehicles in passenger car category are taken as small cars. Buses, trucks and light commercial vehicles (LCV) are taken in the category of heavy vehicles. Statistical details of headway and speed data are given in Tables 1 and 2, respectively.

4 Analysis and Results

4.1 Relationship Between Speed and Headway

Extracted data provide the information of headway and speed along with the category of the subject vehicle. The present study initially merged all data irrespective of vehicle category and attempted to find out the relationship between speed and headway as given in Table 3.

Since collected traffic data covered only uncongested condition, speed of the subject vehicle was observed increasing with the increase in headway with its preceding vehicle. If average speeds of two consecutive headways h_1 and h_2 are v_1 and v_2, respectively, then percentage increase in speed (Δv) corresponding to headway $h_2$was determined using Eq. 1.

Table 1 Statistical details of extracted headway data

Vehicle category	Headway at edge lane			Headway at median lane		
	No. of observation	Mean (s)	Standard deviation (s)	No. of observation	Mean (s)	Standard deviation (s)
SC	260	6.01	5.09	986	7.10	5.80
BC	166	6.03	5.73	803	6.56	5.44
HV	64	5.92	4.41	477	8.32	5.62
3W	242	6.24	5.13	–	–	–
2W	2233	6.01	5.23	88	6.55	4.94
BY	204	5.32	4.89	–	–	–

Table 2 Statistical details of extracted speed data

Vehicle category	Speed at edge lane			Speed at median lane		
	No. of observation	Mean (km/h)	Standard deviation (km/h)	No. of observation	Mean (km/h)	Standard deviation (km/h)
SC	260	76.31	23.74	986	83.83	23.78
BC	166	82.18	24.77	803	89.09	25.03
HV	64	56.99	22.02	477	64.78	19.34
3W	242	46.54	12.47	–	–	–
2W	2233	54.07	17.14	88	72.32	23.62
BY	204	19.85	5.60	–	–	–

Table 3 Variation in speed with the change of headway

Serial	Headway interval (s)	Mean headway (s)	Average speed (km/h)	Percentage increase in speed, Δv (%)
1	1.5–2.5	2.0	55.11	–
2	2.5–3.5	3.0	61.70	11.96
3	3.5–4.5	4.0	64.44	4.44
4	4.5–5.5	5.0	65.97	2.37
5	5.5–6.5	6.0	66.96	1.50
6	6.5–7.5	7.0	67.63	1.00
7	7.5–8.5	**8.0**	68.14	**0.75**
8	8.5–9.5	9.0	68.52	0.56
9	9.5–10.5	10.0	68.83	0.45
10	10.5–11.5	11.0	69.07	0.35

$$\Delta v(h_2) = \left(\frac{v_2 - v_1}{v_1}\right) \times 100\% \tag{1}$$

where $h_2 = h_1 + 1$.

Percentage increase in speed (km/h) for different headways is given in Table 3, and the relationship between headway and Δv is shown in Fig. 2.

As may be seen in Fig. 2, it is quite prominent that percent increase in speed reduces with the increase in headway. Since Indo-HCM recommends a headway of 8 s as the basis of free-flow condition, Δv of 0.75% was noted as per Table 3.

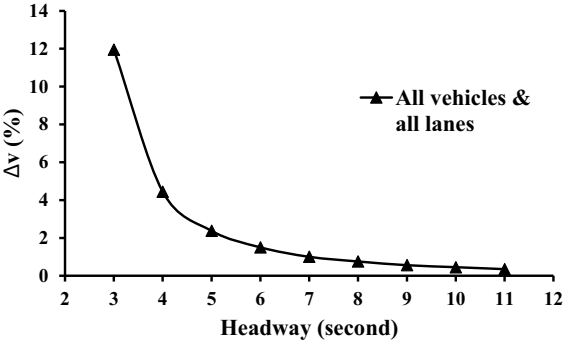

Fig. 2 Relationship between headway and speed for all vehicles and lanes

4.2 Categorical Analysis

In the next phase of analysis, speed and headway data were segregated based on the category of the subject vehicle. Further, the lane which is being accessed by the subject vehicle was also taken into consideration. For a particular direction of a four-lane divided road, there are two lanes. The lane adjacent to the shoulder is referred to as 'edge lane' and the lane adjacent to the median is referred to as 'median lane.' Table 4 provides 'percentage increase in speed' corresponding to different headways observed for each vehicle category at edge lane.

Similarly, speed and headway data were monitored at median lane. Three-wheelers and bicycles were found significantly less at median lane and therefore, these two vehicle categories were not considered for the analysis for median lane. Table 5 provides 'percentage increase in speed' corresponding to different headways observed for each vehicle category at median lane.

Table 4 Details of percent increase in speed with respect to headway at edge lane

Serial	Headway interval (s)	Mean headway (s)	Δv (%)					
			SC#	BC#	HV#	3W#	2W#	BY#
1	1.5–2.5	2.0	16.84	52.85	46.78	17.95	9.81	6.61
2	2.5–3.5	3.0	3.56	5.66	6.74	3.66	2.67	2.93
3	3.5–4.5	4.0	1.62	2.33	2.64	1.65	1.26	1.38
4	4.5–5.5	5.0	0.95	1.28	1.43	0.94	0.74	0.80
5	5.5–6.5	6.0	0.60	0.82	0.91	0.61	0.48	0.52
6	6.5–7.5	7.0	0.43	0.57	0.62	0.43	0.35	0.37
7	7.5–8.5	8.0	0.31	0.42	0.46	0.32	0.25	0.27
8	8.5–9.5	9.0	0.24	0.32	0.35	0.24	0.20	0.21
9	9.5–10.5	10.0	0.19	0.25	0.27	0.20	0.16	0.17
10	10.5–11.5	11.0	0.16	0.20	0.22	0.16	0.13	0.14

#*SC* Small car; *BC* Big car; *HV* Heavy vehicle; *3W* Three-wheeler; *2W* Two-wheeler; *BY* Bicycle

Table 5 Details of percent increase in speed with respect to headway at median lane

Serial	Headway interval (s)	Mean headway (s)	Δv (%)			
			SC	BC	HV	2W
1	1.5–2.5	2.0	–	–	–	6.31
2	2.5–3.5	3.0	10.57	–	–	1.95
3	3.5–4.5	4.0	8.33	19.28	–	0.96
4	4.5–5.5	5.0	3.37	5.76	30.73	0.57
5	5.5–6.5	6.0	1.91	2.85	6.55	0.38
6	6.5–7.5	7.0	1.25	1.75	3.26	0.27
7	7.5–8.5	8.0	0.89	1.20	2.03	0.20
8	8.5–9.5	9.0	0.66	0.89	1.41	0.16
9	9.5–10.5	10.0	0.52	0.67	1.05	0.12
10	10.5–11.5	11.0	0.41	0.53	0.80	0.10
11	11.5–12.5	12.0	0.34	0.43	0.64	0.08

Tables 4 and 5 indicate that the adverse relationship between headway and 'percent increase in speed' exists for each category of vehicle also similar to the trend observed in aggregated analysis (Fig. 2). However, Δv holds higher value at median lane corresponding to the same headway for all vehicles except two-wheeler. To examine the relationship between mean headway and Δv, data given in Tables 4 and 5 were plotted in Fig. 3. Although the trend of the curve is similar for each vehicle category, there are considerable deviations from each other depending upon the category of subject vehicle.

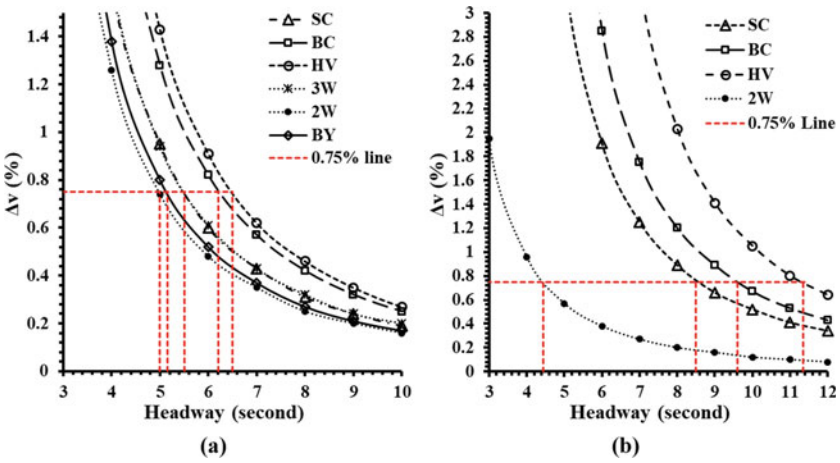

Fig. 3 Relationship between headway and speed for individual vehicle category at **a** edge lane and **b** median lane

Table 6 Proposed free-flow criteria in terms of critical headway for individual category of vehicle

Vehicle category	SC	BC	HV	3W	2W	BY
Lane	Critical headway (s)					
Edge lane	5.5	6.0	6.5	5.5	5.0	5.0
Median lane	8.5	9.5	11.5	–	4.5	–

Hence, headway corresponding to 0.75% of 'percentage increase in speed' was recorded for each vehicle category separately at edge and median lane as given in Table 6. These values of headway hold significance. Because, beyond these values, average speed of the subject vehicle does not increase significantly. Therefore, these headways can be referred as critical headways and considered as the basis of free-flow condition for different vehicle categories.

As may be noticed, critical headways for majority of vehicles (small car, big car and heavy vehicles) are lower at the edge lane as compared to the median lane. It is owing to the fact that vehicles at the edge lane expect frequent interactions with slow-moving vehicles like bicycles and three-wheelers. Hence, drivers do not tend to increase their speed further at edge lane to ensure safety. As a result, saturation in increasing speed comes at lower headway at the edge lane in comparison with the median lane.

5 Conclusions

The present study developed a new free-flow criterion which captures the behaviour of individual vehicle category and thus proves to be more compatible with Indian mixed traffic condition. Major findings of this study are presented below.

- 'Percentage increase in speed' reduces gradually as headway of the subject vehicle to its preceding vehicle increases. A headway of 8 s which is considered as the critical headway for free-flow condition in Indo-HCM (2017), corresponds to 0.75% increase in speed if category-wise segregation is not done.
- Categorical analysis showed considerable deviations among vehicle categories in determining the relationship between headway and speed. This indicates the need of considering vehicle categories separately in order to develop free-flow criteria.
- Larger-sized vehicles have higher critical headways. For example, heavy vehicles like truck, which require more stopping sight distance, start moving at free-flow speed at higher headway as compared to other vehicles. Conversely, two-wheelers being highly maneuverable and small in size, have low critical headway.
- Free-flow criteria also vary depending upon the lane at which the subject vehicle is moving. For safety reasons, free-flow condition reaches at much lower headway on the edge lane as compared to the median lane.

- It is to be acknowledged that traffic data were collected in the present study in limited duration at daytime. Capturing traffic movements during nighttime was beyond the scope of the study. Hence, that aspect can be addressed in the future studies and the difference between FFS obtained at day and night time can be examined. Also, similar methodology can be adopted to develop free-flow criteria for other roadway facilities like undivided rural highways, urban roads, etc. Influence of geometric factors and weather conditions on FFS can be taken up in future studies in the context of Indian mixed traffic.

References

1. Salim A (2010) Estimation of average space headway under heterogeneous traffic conditions. Int J Recent Trends Eng Technol 3(5):6–10
2. Ye Q, Tarko A, Sinha K (2001) Model of Free-Flow Speed for Indiana Arterial Roads. Transp Res Rec 1776(01):189–193
3. De Luca M, Lamberti R, Dell'Acqua G (2012) Freeway free flow speed: a case study in Italy. Procedia Soc Behav Sci 54:628–636
4. Ji X, Shao C (2019) Modeling and analyzing free-flow speed of environment traffic flow in rainstorm based on geomagnetic detector data. Ekoloji 28(107):4223–4230
5. Yasanthi RGN, Mehran B (2020) Modeling free-flow speed variations under adverse road-weather conditions: case of cold region highways. Case Stud Transp Policy 8(1):22–30
6. Vogel K (2002) What characterizes a free vehicle in an urban area? Transp Res Part F Traffic Psychol Behav 5(1):15–29
7. Transportation Research Board (2010) Highway capacity manual. Washington D.C
8. CSIR—Central Road Research Institute (2017) Indian highway capacity manual (Indo-HCM). New Delhi, India
9. Balakrishnan S, Sivanandan R (2015) Influence of lane and vehicles subclass on free-flow speeds for urban roads in heterogeneous traffic. Transp Res Procedia 10:166–175
10. Biswas S, Singh B, Saha A (2016) Assessment of level-of-service on urban arterials: a case study in Kolkata metropolis. Int J Traffic Transp Eng 6(3):303–312

Use of Lime as Filler in Cold Mix Asphalt

Shobhit Jain, Bhupendra Singh, and Nikhil Saboo

Abstract Considerable advantages could be attained if cold bituminous emulsion mixes (CBEM's) show superior engineering properties than hot mix asphalt (HMA). Particularly, cold mix asphalt (CMA) does not require any heating at the time of manufacturing and laying process. This reduces emission of harmful greenhouse gases considerably and makes it economical also. Despite of these advantages, CMA has limited utilisation in the field because of issues such as poor performance, lower moisture resistance. So, the present paper focuses on improving the performance of CMA with filler replacement. Lime is used as filler in this study to improve the mechanical properties of CMA. Stone dust was replaced with lime in the proportion of 1, 2, 3% dry weight of aggregate in mixture. Marshall stability retained stability and indirect tensile strength were performed. Results obtained from these tests were compared, and lime was found to be improving CMA properties considerably.

Keywords Cold mix asphalt · Filler · Lime

1 Introduction

Cold mix asphalt (CMA) is defined as a mixture of aggregate, filler and binding material, manufactured at ambient temperature. Emulsion, cutback or foamed bitumen is used as binding material in CMA. CMA carries several economic and environmental advantages over conventional hot mix asphalt (HMA). Despite these advantages, the use of CMA is largely limited to minor construction and repairing works like surface dressing, surface treatment, slurry surfacing, reinstatement works

S. Jain · B. Singh (✉)
NIT Patna, Patna, Bihar 800005, India
e-mail: bhupendra@iitj.ac.in

N. Saboo
IIT (BHU) Varanasi, Varanasi, Uttar Pradesh, India
e-mail: nikhilsaboo.civ@iitbhu.ac.in

B. Laishram and A. Tawalare (eds.), *Recent Advancements in Civil Engineering*, Lecture Notes in Civil Engineering 172,
https://doi.org/10.1007/978-981-16-4396-5_68

on low traffic roads, etc. This is due to the fact that CMA has some critical disadvantages like lower strength, higher porosity and greater moisture susceptibility [1–4].

Over the past decade, many researchers have used different methods to eliminate the disadvantages of CMA. Some researchers have used modifiers to improve the performance of the CMA and found it effective [5–8]. Some researchers have used different fillers for the purpose [6, 9–12]. Lime is one filler material which has been used extensively in conventional HMA and WMA [13–15] and found to be very effective in improving various properties of the bituminous mix. Few researchers have also taken up the studies to incorporate lime as a filler material. These studies have concluded that lime improves the moisture resistance and stability of the CMA [16] but the literature at large lacks the studies which have extensively examined the effect of lime (as filler) on the properties of CMA. So, the present paper examines the usage of lime as filler in CMA.

The central effort of the present study is the use of lime as a filler material in CMA to solve the drawbacks associated with CMA, i.e. low strength, high air voids and high moisture susceptibility. In this study, the traditional stone dust filler was replaced by lime with different percentages ranging from, 20, 40 and 60% of filler weight, i.e. 1, 2 and 3% of total dry weight of aggregate. The improvement in mechanical properties was determined using the Marshall test and indirect tensile strength test (in conditioned and unconditioned state).

2 Material

Aggregates having nominal size of 20 mm and 10 mm are used in the present work. The physical properties of aggregates are presented in Table1. The emulsion used in this study was cationic emulsion medium setting (CMS). Cationic, medium setting bituminous emulsion (CMS) is used as it does not break immediately after coming in contact with aggregate but breaks during mixing. The emulsion had 64.5% bitumen and 35% water which translates to a residual bitumen content of 65.4%. The properties of emulsion are given in Table 2. In this study, quick lime and stone dust are used as fillers. The chemical composition and properties of lime are shown in Table 3. Emulsion, aggregates and filler materials were collected locally.

This study is conducted on dense graded bituminous concrete (BC). Aggregate gradation has been adopted as given in MoRTH [17]. All the mixes in the study were prepared at ambient temperature. The gradation is presented in Fig. 1.

Table 1 Properties of aggregate

Properties	Coarse aggregate	Fine aggregate	Code
Water absorption	0.35%	0.4%	BIS test method: IS-2386, part III
Specific gravity	2.77	2.74	
Aggregate impact value	8.15	4.57	BIS test method: IS-2386, part IV
Aggregate crushing value	17.26	20.3	
Los Angeles abrasion value	14.40	24.5	
Flakiness index	19.5		
Elongation index	22.4		

Table 2 Properties of emulsion

Properties	CMS emulsion	Code
Specific gravity	1.01	BIS test method: IS-1202
Residual asphalt content (%)	64.5	BIS test method: IS-8887
Residual ductility at 27 °C/cm, Min	75	BIS test method: IS-1208
Viscosity by say bolt (Furol) 50 °C (sec)	120	ASTM test method: D88
Residual penetration, 25 °C	90	BIS test method: IS-1203

Table 3 Properties of quick lime

Physical properties	
Specific gravity	3.20
Fineness	5020 (m^2/kg)
PH	12.66
Chemical composition	
Calcium oxide (Cao)	91.25
Silicon dioxide (Sio_2)	1.97
Aluminium oxide (Al_2O_3)	0.32
Iron oxide (Fe_2O_3)	0.36
Magnesium oxide (Mgo)	1.29
Sulphur trioxide (So_3)	0.27
Sodium oxide (Na_2O)	<0.02
Phosphorus pentoxide (P_2O_5)	0.01
Potassium oxide (K_2O)	0.06
Titanium dioxide (Tio_2)	0.02
Strontium oxide (Sro)	0.097
Manganese oxide (Mno)	0.012
Loss in ignition	4.32

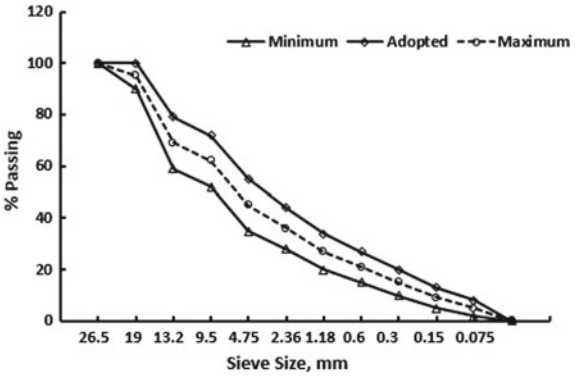

Fig. 1 Aggregate gradation

3 Experimental Plan

To provide a better understanding of experimental plan which has been followed in the present paper, experimental flowchart of the study is given in Fig. 2.

3.1 Marshall Mix Design

Mix design procedure of CMS is different from HMA mix design. There are additional parameters which are needed to be calculated for CMA. The calculation procedures of these parameters are described as below:

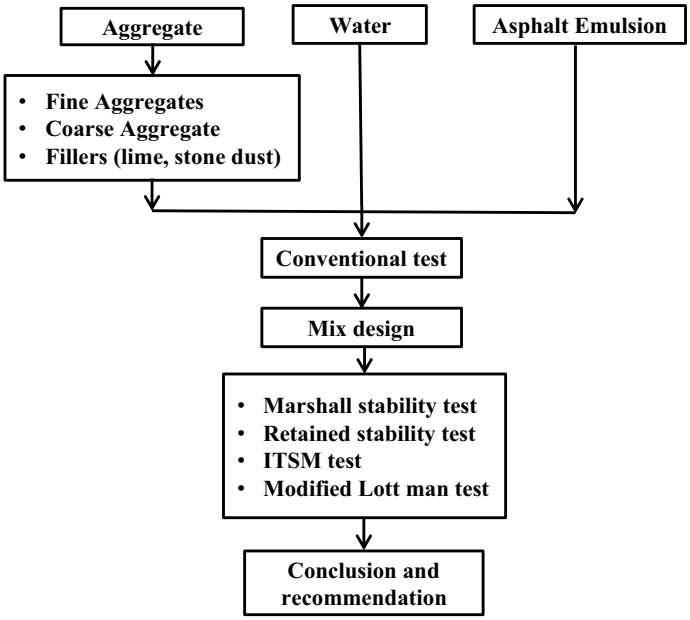

Fig. 2 Experimental flowchart of the study

Step 1 Initial residual bitumen content (IRBC) and initial emulsion content (IEC) are calculated by using Eqs. (1) and (2), respectively, given by Asphalt Institute's MS-14 (2007) [18]. These equations have been given

$$\text{IRBC} = (0.05A + 0.1B + 0.5C) \times 0.7 \tag{1}$$

$$\text{IEC} = \frac{\text{IRBC}}{Y(\%)} \tag{2}$$

where Y is the asphalt content of the emulsion, A is the % of aggregate retained on 2.36 mm sieve, B is the % of aggregate passing through 2.36 mm and retained on 0.075 mm sieve, and C is the % of aggregate passing through 0.075 mm sieve.

Step 2 Optimum prewetting water content (OPWC) is calculated using maximum dry density test. Water content at which maximum density is achieved called OPWC.

Step 3 Optimum total liquid content (OTLC) is calculated by using Eq. (3). This parameter is calculated using dry Marshall stability test.

$$\begin{aligned}\text{OTLC} = {} & (\text{PWC at maximum dry density}) \\ & + (\text{Liquid cotent of Initial emulsion content})\end{aligned} \tag{3}$$

Step 4 Optimum residual bitumen content (ORBC) is calculated using soaked Marshall stability test. Marshall samples are prepared at different residual bitumen contents (RBC). Then, these samples are tested and different parameters like stability, dry density, air void and flow value are optimised to obtain ORBC. The primary parameter to obtain ORBC is Marshall stability. Its value should be maximum, and all other parameters should fulfil the compulsory criteria given by MoRTH [17].

3.2 *Retained Stability Test*

After finding ORBC value, six samples in which three samples of dry stability and three samples of soaked stability were prepared. These samples were prepared at ORBC only keeping OTLC constant. The ratio of soaked stability to dry stability is retained stability. The retained stability is calculated by Eq. (4) [19].

$$\text{Retained Stability} = \frac{\text{Soaked stability}}{\text{Dry stability}} \times 100 \tag{4}$$

3.3 Indirect Tensile Strength (ITS) Test

ITS test is used to find the water sensitivity of the CMA as specified by AASHTO T283. The AASHTO T283 procedure is more suitable for HMA as an exposure at 60 °C for 24 h may be too harsh for CMA. To overcome this problem, the conditioning temperature of the samples was reduced to 25 °C, and curing time was extended to 48 h. Two repeats were run for each of the dry and conditioned samples. ITS of the asphalt mix samples is calculated by using Eq. (5), and tensile strength ratio (TSR) is calculated with help of Eq. (6) [20]. From Eq. (6), it can be seen that TSR is the ratio of tensile strength of unconditioned and conditioned asphalt mixture sample. So, TSR represents the moisture susceptibility of asphalt mixture. Higher TSR value indicates greater moisture resistance.

$$S_t = \frac{2000P}{td} \tag{5}$$

where S_t is tensile strength of the mix in kPa, P is maximum load applied on the sample in N, t is thickness of sample in mm, d is diameter of sample in mm.

$$TSR = \frac{S_{tm}}{S_{td}} \tag{6}$$

where TSR is tensile strength ratio, S_{tm} is tensile strength of conditioned asphalt mix samples in kPa, S_{td} is average tensile strength of dry asphalt mix samples in kPa.

4 Results and Discussion

As discussed in Sect. 3.1, the usual method for estimating ORBC is based on a principle of using the IRBC. In the present study, first IRBC was calculated with the help of formula given in Eq. (1) and it was found to be 6%. After IRBC, IEC was calculated by the formula given in Eq. (2) which was 9.3%. Following IEC, OPWC was determined based on maximum dry density approach (Fig. 3a). OPWC was further validated by checking the Marshall stability value, and it was found to be fulfilling the criteria (Fig. 3b). OPWC was 3%. OPWC calculation graphs are shown in Fig. 3. Then, OTLC was determined using Eq. (3), which was found to be 6.21% and finally based on Marshall test results, and ORBC was calculated. These parameters are presented in Table 4.

ORBC value of CMA samples was found to be 4.66%, and Marshall stability value was 6.34 KN. For Bituminous Concrete HMA, MoRTH [17] suggests a minimum stability value of 9KN. This again highlights the lower strength of HMA which makes it unsuitable to be used in important road construction. To deal with the problem, stone dust filler was replaced with lime. Lime is added in mix with 1, 2

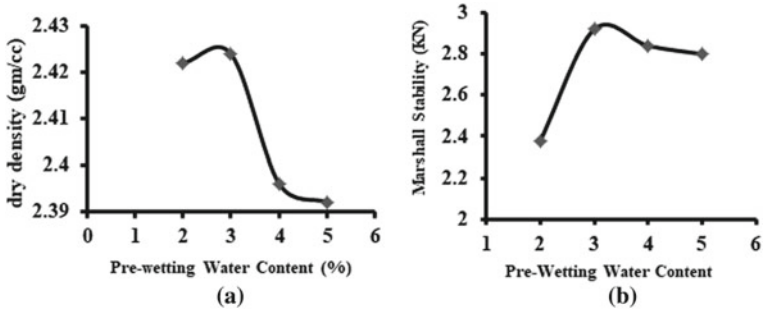

Fig. 3 Determination of OPWC

Table 4 CMA design parameters

Parameter	Value (%)
IRBC	6
IEC	9.3
OPWC	3
OTLC	6.21
ORBC	4.66

and 3% of dry aggregate mass. In the present study, mixes with 0, 1, 2 and 3% lime are denoted with abbreviation CMA, CMA-1L, CMA-2L and CMA-3L.

From the observation of Marshall test results, it was found that ORBC values decreased with increasing lime percentage. ORBC value of CMA, CMA-1L, CMA-2L and CMA-3L was 4.66%, 4.63%, 4.58% and 4.5%, respectively (Fig. 4a). This decreasing ORBC content may be credited to hydration process of lime. Lime reacts with water present in CMA and undergoes hydration. During the hydration process, lime particles absorb water molecules which increases their overall volume [21]. This increased volume occupies more voids in mineral aggregates (VMA) which reduces the volume of voids available to be filled with binder. This can further be validated with decreasing VFB values with increasing lime content as presented in Fig. 4d. Addition of 3% lime reduced the ORBC to lower than 4.52%. 4.52% asphalt content (ORBC) is equal to 7% emulsion content which is against the recommendations given by MoRTH [17]. MoRTH [17] suggests 7% as the lowest emulsion content for CMAs.

Air voids were found to be increasing with increasing lime content (Fig. 4b). Air voids values of CMA, CMA-1L, CMA-2L and CMA-3L were 7.16%, 7.31%, 7.43% and 7.81%, respectively. Increased air void may be the result of hydration of lime. As discussed above, hydration process increases the volume of lime. This increased volume contains smaller voids. Due to their smaller size, bitumen does not fill these voids, so at one hand, these decrease ORBC by occupying VMA and, on the other hands, increase overall air void content of the mix. This can further be

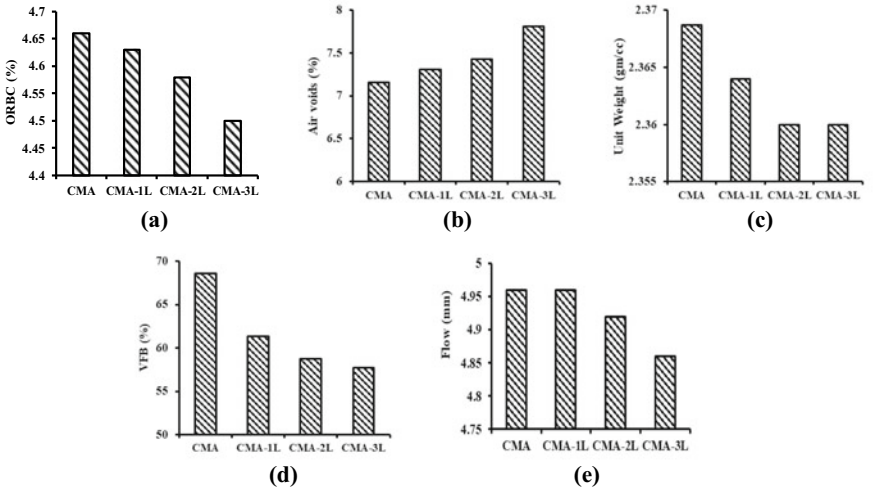

Fig. 4 Marshall test results of CMA with 0, 1, 2 and 3% Lime

seen with the decreasing unit weight of the mixes with the increasing lime content (Fig. 4c).

Flow value of the mixes was found to be decreasing with increasing as shown in Fig. 4e. At lower asphalt content, the difference in flow value was lower. This difference increased with increasing asphalt content.

Observing the stability values in Fig. 5a, it can be seen that addition of lime improved the stability value of CMA. CMA had a stability vale of 7.28 kN which is lower than the stability requirement given by MoRTH [17] for HMA. CMA-1L, CMA-2L and CMA-3L stability values were 12.04, 12.37 and 12.73, respectively. These values are greater than 9 kN (stability requirement given by MoRTH [17]) which makes it suitable to be used for the construction of structural pavement layers. The increase in stability value is the result of hydration of lime. Lime has good amount of CaO, which has very high affinity for water. It instantaneously reacts with water and undergoes slaking leading to formation of hydration lime. This improves the bonding between binder and aggregates which results in improved strength to the mix.

In order to access the moisture susceptibility of the mix, retained stability of the mix samples was calculated. Retained stability value of the mixtures is presented in Fig. 5(b). Like most of the previous parameters, lime improved the moisture susceptibility of CMA. Retained stability values kept on improving with the increment of lime content. CMA-3L was found to have highest retained stability value.

From the above results, it can be seen that increasing lime content keep on improving the properties of CMA but 3% addition of the lime reduced emulsion content lower than 7% which is not desirable according to MoRTH [17] guidelines. So, based on this 2%, lime content is chosen as optimum lime content for the further study.

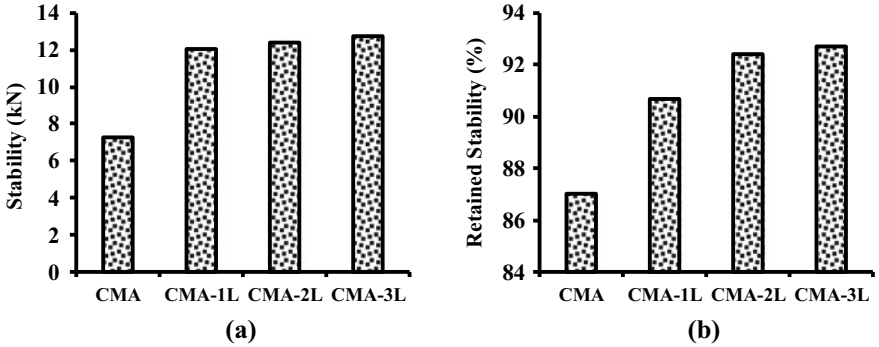

Fig. 5 Stability and retained stability of CMA with 0%, 1%, 2% and 3% lime

Table 5 ITS and TSR value of asphalt mixtures

Mixture	Conditioning	ITS (kPa)	TSR (%)
CMA	Wet Dry	321.33 518.27	0.62
CMA-2L	Wet Dry	811.08 891.8	0.97

The indirect tensile strength (ITS) test is used to examine the tensile properties of the asphalt mixture. ITS values can further be associated with cracking resistance of the pavement. Mixture having higher ITS values is known to have higher cracking resistance. In the present study, 12 ITS samples were prepared, six each CMA and CMA-2L. Out of these six samples were tested in unconditioned state and six were tested after conditioning. After testing these samples, ITS and TSR values were obtained. These values are presented in Table 5. From the test results, it can be observed that lime improved both ITS and TSR values which signifies better cracking and moisture resistance. CMA was found to have TSR value 0.62 which is less than 0.7. TSR value less than 0.7 generally implies a pavement that will be susceptible to moisture-induced damage. TSR value for CMA-2L was 0.97. TSR value greater than 0.8 designates good performance of the pavement in terms of moisture susceptibility.

5 Conclusion

The present paper explored the effect of lime as a filler material on the properties of CMA. From the experimental results, analysis and conclusion following conclusions have been drawn:

- Lime was found to effective in improving the properties of CMA. Due to the hydration process of the lime, all the important parameters such as Marshall

stability, retained stability, indirect tensile strength and tensile strength ratio improved with increase in lime content.

- Mix with 3% lime was found to have highest values among other mixes, but at 3% lime content, emulsion content of CMA came down below 7% which is not recommended. So, based on this 2%, lime content was found to be optimum lime content for the mix.
- With 2% lime Marshall stability, retained stability, ITS and TSR value improved by 80%, 6.2%, 72.11% and 56.45%, respectively, which according to MoRTH [17] guidelines are comparable to HMA.

Based on the present study, CMA with lime showed the promise to be used for the construction of structural pavement layers. But in order to give more confidence to constructors and practitioners (for field implementation), more work should be carried out, including more gradation, emulsion and aggregate type.

References

1. Jain S, Singh B (2021) Cold mix asphalt: an overview. J Clean Prod 124378. https://doi.org/10.1016/j.jclepro.2020.124378
2. Needham D (1996) Developments in bitumen emulsion mixtures for road (PhD Thesis University of Nottingham)
3. Thanaya IEA, Zoorob SE, Forth JP (2009) A laboratory study on cold-mix, cold-lay emulsion mixtures. Mater Sci 162(1):47–55
4. OrucSCelik F, Akpinar MV (2007) Effect of cement on emulsified asphalt mixture. J Mater Eng Perform 16:578–583
5. Asi I, Assaad A (2005) Effect of Jordanian oil shale fly ash on asphalt mixes. J Mater Civil Eng (ASCE) 17(5):553–559
6. Al-Busaltan S, Al-Nageim H, Atherton W, Sharples G (2012) Mechanical properties of upgrading cold-mix asphalt using waste material. J Mater Civil Eng (ASCE) 24(12):1484–1491
7. Benedito De S, Da Silva WR, De Lima DC, Minete E (2003) Engineering properties of fibre reinforced cold asphalt mixes. J Environ Eng (ASCE) 129(10):952–955
8. Chavez-Valencia LE, Alonso E, Manzano A, Pérez J, Contreras ME, Signoret C (2007) Improving the compressive strength of cold-mix asphalt using asphalt emulsion modified by polyvinyl acetate. Constr Build Mater 21(3):583–589
9. James AD, Needham D, Brown PSF (1996) The benefits of using Ordinary Portland Cement in solvent free dense graded bituminous emulsion mixtures. In: Proceedings of international symposium on asphalt technology (Washington)
10. Brown SF, Needham D (2000) A study of cement modified bitumen emulsion mixtures. In: Proceedings of association of asphalt paving technology vol 69, pp 1–22
11. Thanaya INA (2007) Evaluating and Improving the Performance of Cold Asphalt Emulsion Mixes. Civil Eng Dimension 9(2):64–69
12. Saadoon T, Garcia A, Gómez-Meijide B (2017) Dynamic of water evaporation in cold asphalt mixtures. Mater Des 134:196–206
13. Sebaaly PE, Bazi G, Hitti E, Weitzel D (2003) Effectiveness of lime in hot-mix asphalt pavements. Transp Res Rec 1832(1):34–41
14. Mohammad LN, Abadie C, Gokmen R, Puppala AJ (2000) Mechanistic evaluation of hydrated lime in hot-mix asphalt mixtures. Transp Res Rec 1723(1):22–36

15. Kok BV, Yilmaz M (2009) The effects of using lime and styrene–butadiene–styrene on moisture sensitivity resistance of hot mix asphalt. Constr Build Mater 23(5):1999–2006
16. Dash SS, Panda M (2018) Influence of mix parameters on design of cold bituminous mix. Constr Build Mater 191:376–385
17. MoRTH (2013) Specifications for road and bridge works Fifth Revision (Ministry of Road Transport and Highways New Delhi)
18. Asphalt Institute Manual Series No.14 (MS-14) (1997) Asphalt cold mix manual (Third Edition), Lexington, KY 40512–4052 USA
19. STP 204–22 (1993) Standard test section: standard test section procedures manual for retained marshall stability. Saskatchewan Ministry of Highways and Infrastructure, Canada
20. AASHTO T 283 (2014) Standard method of test for resistance of compacted asphalt mixtures to moisture-induced damage. AASHTO Provisional Standards: Washington, DC, USA
21. Wang GC (2016) Usability criteria for slag use as a granular material. In: The utilization of slag in civil infrastructure construction, pp 185–199

Experimental and Numerical Studies on FRC for Use in Dowel-Jointed Rigid Pavements

Priya Grace Itti Eipe, Anitha Joseph, and Reebu Zachariah Koshy

Abstract High initial investment acts as a deterrent in the large-scale adoption of rigid pavements in India. Usage of fibre-reinforced concrete, FRC, can help improve the performance characteristics of rigid pavements, thereby leading to reduced sections, bringing down the cost of construction. In this paper, a comparison study between the strength and durability parameters of FRC specimens when steel, glass, polypropylene, nylon, polyester and coir fibres are added at specified percentages was conducted. The optimum dosage for each fibre was obtained. The maximum load carried as well as the corresponding deflection at the dowel joint, for the various FRC pavement specimens made of optimum fibre dosage, was then obtained. A numerical nonlinear static analysis was then conducted using the finite element software ANSYS, and the experimental results were validated. Results show that with the addition of fibre there is an increase in the compressive, flexural and split tensile strength as well as an improvement in impact resistance, abrasion resistance and resistance to crack formation. Synthetic fibres can be seen to give good economical results, whereas a natural fibre like coir can be used to a reasonably good extent if available in abundance.

Keywords Rigid pavement · FRC · Fibre · Dowel joint · ANSYS

1 Introduction

Surface transport infrastructure is essential for the economic and socio-economic development of a country at a regional, national, as well as international level. The main element of surface transport is the solid pavement. Pavements can be either flexible pavements or rigid pavements. The increasing demand to adopt a sus-

P. G. I. Eipe (✉)
Department of Civil Engineering, Mahaguru Institute of Technology, Mavelikkara, Kerala, India

A. Joseph · R. Z. Koshy
Department of Civil Engineering, Saintgits College of Engineering, Kottayam, Kerala, India

B. Laishram and A. Tawalare (eds.), *Recent Advancements in Civil Engineering*, Lecture Notes in Civil Engineering 172,
https://doi.org/10.1007/978-981-16-4396-5_69

tainable construction solution has led to a preference for rigid or concrete pavements. Advantages of concrete pavements are its good strength and durability properties leading to long service life and also the minimum maintenance required. Disadvantages of concrete pavements are its high initial cost and deterioration that may occur due to its brittleness and also the expensive rehabilitation techniques that may be required. For the large-scale adoption of concrete pavements, good structural capacity and satisfactory long-term performance are to be ensured. This can be achieved by the use of proper design procedures. Another option would be the adoption of fibre-reinforced concrete (FRC), which is defined as a composite material consisting of concrete reinforced with discrete randomly but uniformly dispersed short length fibres. Proper design of pavement joints also plays a major role since pavement performance depends to a large extent on the performance of its joints. Advantages of using FRC are the improved strength properties, improved long-term pavement properties as well as an economical pavement design. Types of fibres used for FRC can be metallic fibres such as steel, synthetic fibres such as acrylic, aramid, carbon, nylon, polyester, polyethylene, or polypropylene, hybrid fibres such as steel/synthetic fibre blends and natural fibres such as coir and jute. Metallic fibres have the best strength properties, whereas synthetic fibres are chemically stable, light, impermeable and have reduced plastic shrinkage, increased toughness (post-cracking), etc. Natural fibres can be used wherever available in abundance. Adoption of a suitable design methodology using an economic and improved material such as FRC, with a special focus on the satisfactory performance of joints, can lead to a viable solution in this area.

1.1 Experimental Analysis

Belletti et al. [1] conducted an experimental and numerical study on the fracture behaviour of fibre-reinforced concrete slabs on grade for industrial pavements, and the comparison between experimental and numerical results showed a good agreement. Elsaigh et al. [2] conducted investigations to evaluate the use of SFRC for road pavements and compared its performance with plain concrete under traffic loading. Sorelli et al. [3] carried out extensive experimental investigations to study the structural behaviour of slabs on ground made of SFRC and showed improved bearing capacity and ductility of SFRC slabs on ground. Cominoli et al. [4] conducted experiments to determine the behaviour of construction joints in steel FRC pavements and improved joint performance was recorded against plain concrete pavements.

1.2 Numerical Analysis

Westergaard [5] conducted an analysis of a concrete slab, a raft unit, on a subgrade, which forms the basis of almost all rigid pavement design methods, but is only available for three single-wheel load positions, namely interior, edge and corner loading. This requirement restricts the use of Westergaard's analysis, as does the requirement that the concrete slab must be of infinite or semi-infinite dimensions in the horizontal direction. Belletti et al. [6] arrived at an effective NLFE method for the analysis up to failure of slabs on grade. Belletti et al. [7] conducted a numerical study on the fracture behaviour of fibre-reinforced concrete slabs on grade for industrial pavements, and the comparison between experimental and numerical results was validated. Maitra et al. [8] conducted a finite element model analysis of a dowel-jointed concrete pavement to study the effects of different parameters on load transfer efficiency of a joint and arrived at relationships useful for the estimation of relative load shared by individual dowel bars. Joseph et al. [9] conducted a nonlinear static analysis of rigid plain cement concrete pavements using the finite element software ANSYS and established a close similarity between the values of the numerical analysis and Westergaard's method. Elsaigh et al. [10, 11] conducted research aimed at providing a modeling approach that can be used to model the behaviour of SFRC concrete and SFRC ground slabs. The calculated results compared well with the experimental observations. Koshy et al. [12] conducted a nonlinear static analysis to evaluate the performance and efficiency of PCC pavements and steel FRC pavements with contraction joints and showed that there is significant improvement in the ultimate load-carrying capacity and joint efficiency for the SFRC slabs. Mackiewicz [13] analysed the distribution of stresses around dowel bars using the finite element method (FEM) and arrived at empirical equations and relationships.

2 Experimental Studies

The experimental study included the determination of properties of the fresh and hardened FRC concrete made up of the different fibres at different dosages. Also tests were conducted on slab specimens to study the load deflection parameters when PCC as well as FRC with different fibres is used.

2.1 Materials

The various materials used for the specimens are given below.

2.1.1 Cement

Ordinary Portland cement of 53 grade conforming to IS 12269 was used. The properties of cement are given in Table 1.

2.1.2 Aggregates

Crushed stone sand was used as fine aggregate, and crushed granite stone was used as coarse aggregate. The physical properties of coarse aggregates are given in Table 2 and that of fine aggregates are given in Table 3.

2.1.3 Water

Potable water was used as mixing water.

Table 1 Properties of cement

Property	Value
Fineness of cement	6%
Specific gravity of cement	3.13
Consistency of standard cement paste	30.75%
Initial setting time	92 min
Final setting time	267 min
Third day compressive strength	28 (N/mm^2)
Seventh day compressive strength	32 (N/mm^2)

Table 2 Physical properties of coarse aggregate

Property	Value
Specific gravity	2.65
Void ratio	0.771
Bulk density (Kg/m3)	1.57
Porosity	0.435

Table 3 Physical properties of fine aggregate

Property	Value
Specific gravity	2.6
Sand type	Medium
Grade	Zone II

2.1.4 Fibres

The fibres used for the study were steel fibres, glass fibres, synthetic fibres such as polypropylene, nylon and polyester fibres and also a natural fibre, coir. The fibre contents used are 0, 0.25, 0.50, 0.75, 1 and 1.25%. The physical properties of the different fibres provided by the manufacturer are given in Table 4.

2.1.5 Plasticizer

The super-plasticizer Cementone Conflo was used to improve the workability of the concrete mix. The various particulars of Cementone Conflo are given in Table 5.

2.2 Mix Design

The concrete mix was designed to obtain a suitable mix proportion for M25 grade concrete. M25 grade concrete was adopted since on addition of fibres, the fibre-reinforced concrete exhibited properties of grade M30 and above concrete, which is the minimum required grade for concrete pavements. Specifications according to IRC 44–2008 were followed for the mix design. The concrete mix proportion of 1:2.16:3.75 with a water/cement ratio of 0.45 was adopted.

Table 4 Fibre properties

Property	Steel	Glass	Coir	Polypropylene	Nylon	Polyester
Filament type	Mono	Mono	Mono	Mono	Mono	Mono
Diameter (mm)	0.5	0.5	0.48	0.44	0.030	0.036
Aspect ratio	60	100	104	113.6	633.33	333.33
Sp. gravity	7.80	2.54	1.15	0.91	1.14	1.4
Water absorption (%)	33.33	85	210	30.21	66.66	44.72
Density (kg/m^3)	7850	2550	2057	763	657	1380

Table 5 Particulars of Cementone Conflo

Particulars	Details
Physical form	Liquid
Colour	Black
Specific gravity	1.09
Dosage	0.3–0.4% by weight of cement
Chloride content	Nil

2.3 Specimens

Cube, cylindrical, disc and beam specimens were cast for the various laboratory tests. Also, the pavement slab and joint were simulated in the laboratory by casting a pair of slabs having length of 1 m, width 0.5 m and thickness 0.17 m each with optimum fibre dosage for each type of fibre. A gap of 2.5 cm was kept between the slabs. The slabs were joined by a mild steel dowel bar of 25 mm diameter and 50 cm length. The dowel bar was placed at the mid-depth of the slabs and the middle of the slab width with equal lengths of 23.75 cm in both the slabs. The dowel bar was embedded in one slab and allowed to form a bond with the concrete, whereas in the other slab the dowel bar was coated with bitumen and kept in a sleeve of length 26.25 cm so as to allow the dowel to expand or contract freely. A thickness of 170 mm was adopted instead of the minimum 200 mm for the slab since a scaled down version of the concrete pavement was used in the laboratory. The details of the various specimens cast and their numbers are given in Table 6.

2.4 Laboratory Tests

Various laboratory tests were conducted on standard specimens as well as slab specimens.

2.4.1 Tests on Standard Specimens

Tests for workability such as the slump test and compaction test, strength tests such as the tests for compressive strength, split tensile strength, flexural strength, and modulus of elasticity and also tests for durability such as the impact strength test, carbonation test, sulphate resistance test and bulk diffusion test were conducted on standard specimens.

Table 6 Details of concrete specimens

Specimen	Size (mm)	Numbers
Cube	150 × 150 × 150	300
Cube	100 × 100 × 100	96
Cylinder	150 × 300	120
Cylinder	100 × 200	96
Beam	500 × 100 × 100	96
Beam	900 × 120 × 150	30
Cylindrical Disc	150 × 50	24
Slab specimen	1000 × 500 × 170	8

2.4.2 Tests on Slab Specimens

Tests were conducted on the slab specimens to determine the joint capacity as well as deflection occurring at the joints. As per IRC 15, the modulus of subgrade reaction is 8 kg/cm^3 for the particular soil subgrade chosen for the design of rigid pavement. To simulate this subgrade on which the slab specimen is to be placed while testing in the laboratory, concrete blocks of size 300 × 200 × 150 were loaded in compression, and the average stiffness of the single block was found to be 3.85 kN/mm. These concrete blocks were then laid to form a bed, and the obtained stiffness of the simulated subgrade was then seen to be 8 kg/cm^3 as required. The dowel-jointed concrete slab specimen placed on top of the simulated subgrade was then placed on a hydraulic loading frame set-up of capacity 100 tonnes. LVDTs were attached to the slab at required points. A single-point hydraulic load was then applied at the location of the dowel joint on the slab in which the dowel is bonded with concrete. The deflections were measured at the loaded points on the slab with the help of the LVDTs attached. The loading frame set-up is shown in Fig. 1.

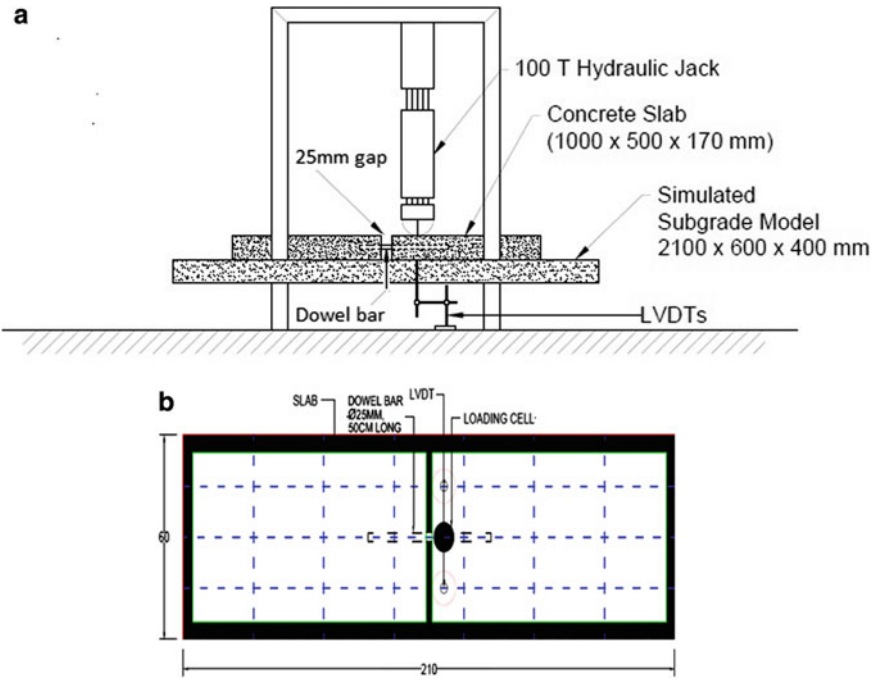

Fig. 1 **a** Elevation of testing set-up of slab specimen. **b** Plan of testing set-up of slab specimen

3 Numerical Analysis

A nonlinear analysis was conducted using the FEM software ANSYS. The various steps carried out are given below.

3.1 Modeling

The rigid pavement set-up was modeled in the software using appropriate elements. The slab was modeled using element SOLID185, whereas the soil subgrade was modeled using element COMBIN14. Dowel bars were modeled using BEAM188. The movable part of the dowel placed in the sleeve is represented by defining the contact element CONTA178 between the surface of the embedded dowel and the concrete slab.

3.2 Real Constants

Real constants such as section property for BEAM188 as well as normal stiffness for contact element CONTA178 were given. A spring constant was assigned for element COMBIN14 to represent the subgrade modulus.

3.3 Material Properties

The appropriate material properties for concrete and dowel bars such as the subgrade spring constant, elastic modulus, Poisson's ratio, yield stress, and tangent modulus were given.

3.4 Meshing

3D meshing was done in the slab portion. Dowel bars were modeled as line geometry, and hence, a line mesh was used.

3.5 Boundary Conditions

The base of the soil subgrade element was constrained for all degrees of freedom.

3.6 Loading

A point load was applied as was done in the experimental set-up at the dowel joint of the slab.

3.7 Analysis

A nonlinear analysis was carried out.

4 Results

The experimental and numerical test results are presented here. The various test results have been compared with the values of conventional concrete. Also a comparison study is done for the results when different dosages of fibre for different types of fibre are used and the optimum dosage for each fibre is obtained.

4.1 Experimental Analysis Results

The results of the workability tests, strength tests and durability tests conducted on fresh and hardened concrete are given below. The optimum percentage of each fibre is determined as the percentage of fibre, which gives the highest values for the various strength tests such as compressive strength test, flexural strength test and split tensile strength test. It can be seen that for each fibre all strength values peak at the same percentage of fibre. Nylon and glass fibres have an optimum percentage of 0.25%, polyester and coir have an optimum percentage of 0.5%, whereas steel fibres have an optimum percentage of 1%. The various durability tests such as the impact strength test, carbonation depth, chloride ion penetration and sulphate exposure tests have been conducted on specimens of FRC of optimum fibre dosage.

FRC slab specimens are also of optimum fibre dosage. Two specimens each of the different fibres are tested, and the average deflections are taken.

4.1.1 Slump Test

Results for slump tests conducted on fresh concrete are given in Fig. 2.

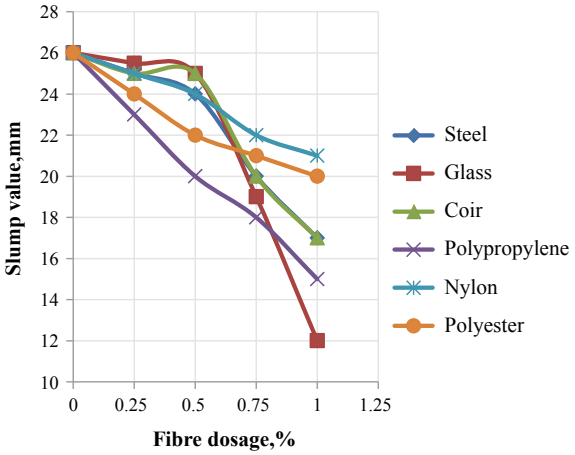

Fig. 2 Slump values for different fibres

4.1.2 Compaction Test

Results for compaction tests conducted on fresh concrete are given in Fig. 3.

4.1.3 Compressive Strength

Results for compressive strength tests conducted on concrete in Fig. 4.

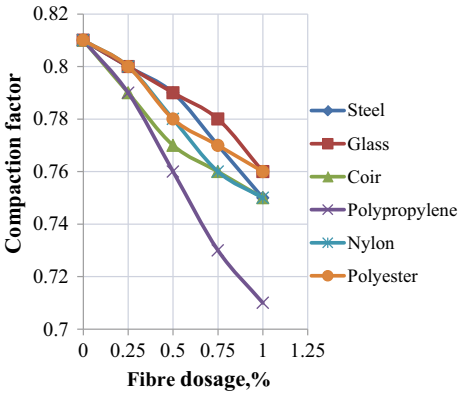

Fig. 3 Compaction factor values for different fibres

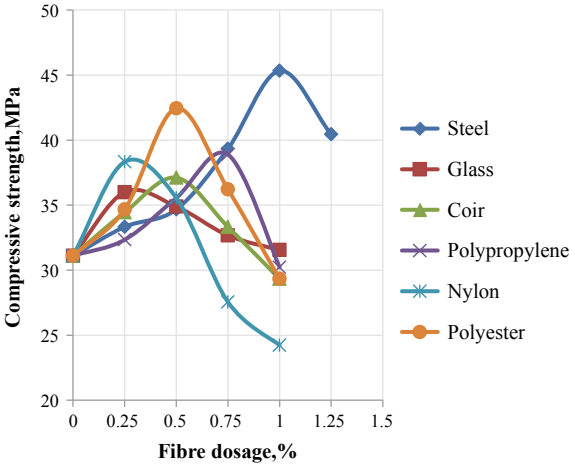

Fig. 4 Compression strength values

4.1.4 Flexural Strength

Results for flexural strength tests conducted on concrete specimens are given in Fig. 5.

4.1.5 Split Tensile Strength

Results for split tensile strength tests conducted on concrete specimens are given in Fig. 6.

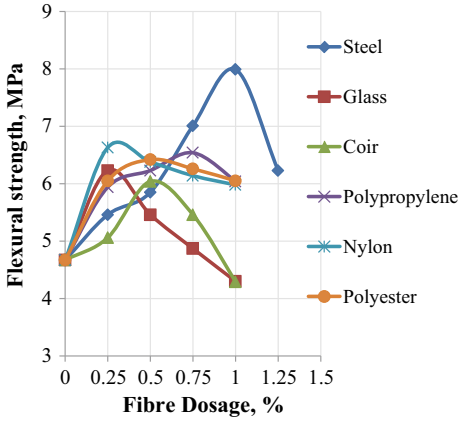

Fig. 5 Flexural strength values

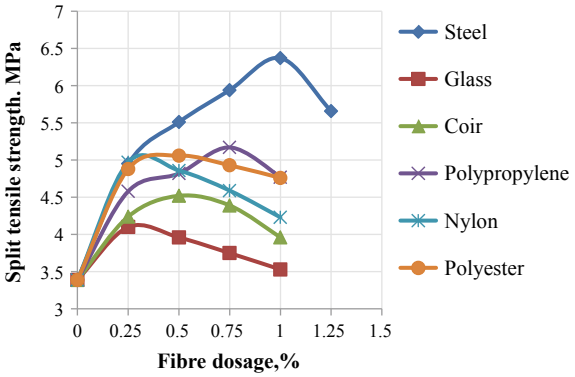

Fig. 6 Split tensile strength values

4.1.6 Modulus of Elasticity

Results for modulus of elasticity conducted on concrete specimens are given in Fig. 7.

4.1.7 Impact Strength

Results for impact strength tests conducted on concrete specimens are given in Fig. 8.

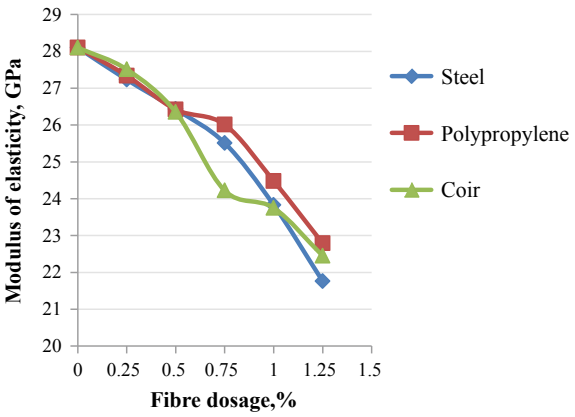

Fig. 7 Modulus of elasticity values

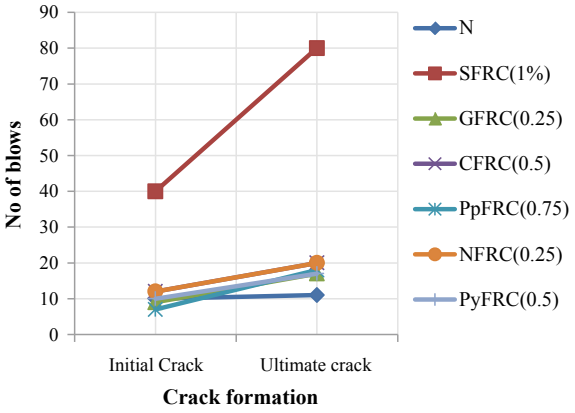

Fig. 8 Impact strength values

4.1.8 Carbonation Depth

Results for carbonation depth tests conducted on concrete specimens are given in Fig. 9.

4.1.9 Chloride Ion Penetration

Results for chloride ion tests conducted on concrete specimens are given in Fig. 10.

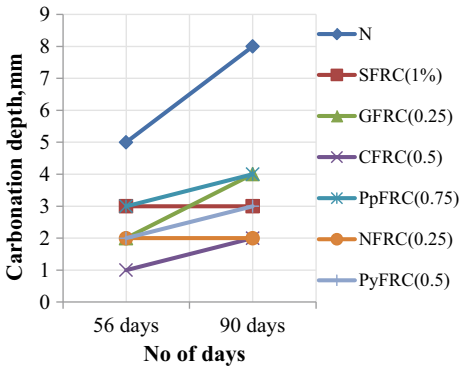

Fig. 9 Carbonation depth values

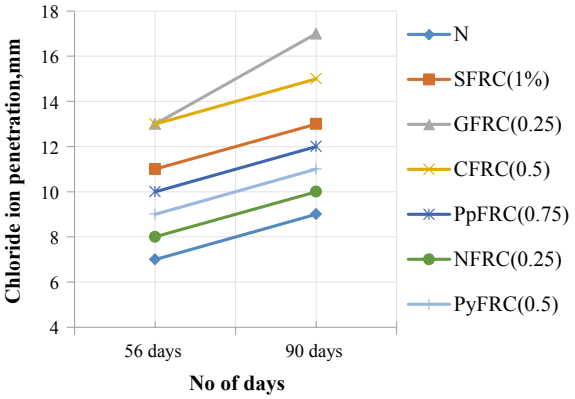

Fig. 10 Chloride ion penetration depth for different fibres

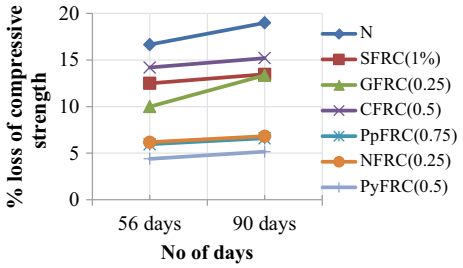

Fig. 11 Loss of compressive strength for different fibres

4.1.10 Sulphate Exposure

Results for sulphate exposure tests conducted on concrete specimens are given in Fig. 11.

4.1.11 Slab Test Results

The computer-generated load–deflection curves obtained from the slab tests give the ultimate loads and the corresponding deflections which are given in Table 7 and Fig. 12. The loading frame with specimen is shown in Fig. 13.

Table 7 Average deflections for slab specimens

Specimen	Ultimate load (kN)	Deflection 1 (mm)	Deflection 2 (mm)	Avg. deflection (mm)
Control	61.03	18.11	14.01	16.06
Steel	179.5	28.36	31.16	29.76
Polypropylene	128.1	16.22	21.28	18.75
Coir	149.37	20.75	16.35	18.55

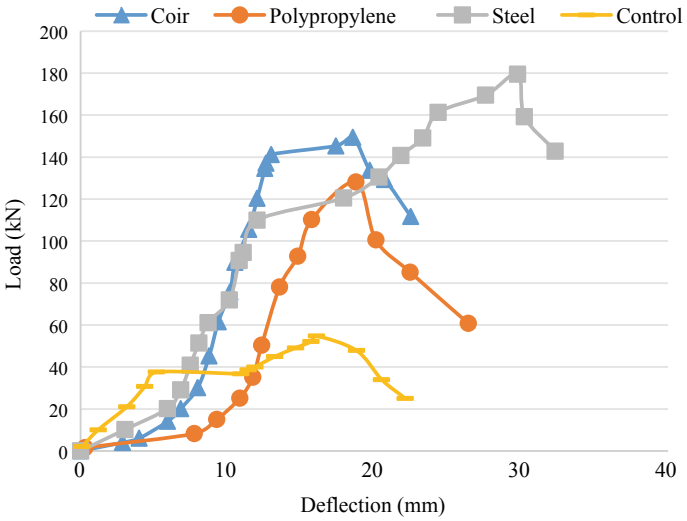

Fig. 12 Load–deflection curve for slab specimens

Fig. 13 Loading frame set-up with specimen

4.2 Numerical Analysis Results

The obtained results of the numerical analysis are given below.

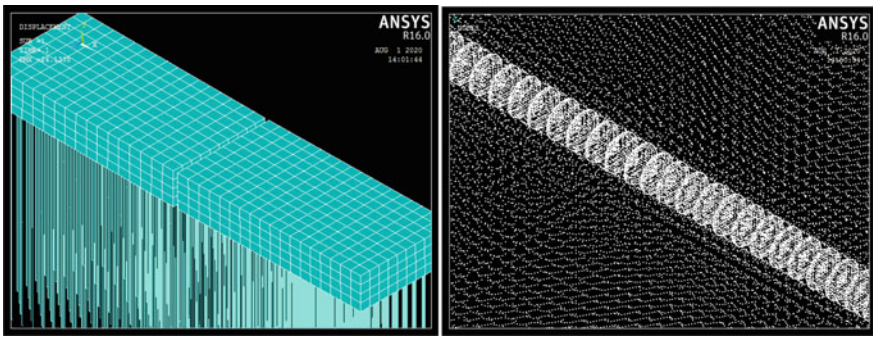

Fig. 14 Plots of ANSYS

4.2.1 Deflections

The maximum deflection value at the point of loading at the dowel joint node is 24.1338 mm for the steel fibre-reinforced concrete specimen, which was modeled based on the specimen cast in the laboratory. The result can be seen to closely match the results of the experimental loading test conducted on the slab specimen (Fig. 14).

4.2.2 Discussions

The workability test results for slump as well as compaction factor show that there is a reduction in the workability of concrete once fibres are added. This can be attributed to the loss of mobility of aggregates due to the presence of the fibres. However, the test results for compressive strength, flexural strength and split tensile strength indicate an increase in the strength values on addition of fibres until the optimum percentage of that particular fibre is reached beyond which the values start decreasing. The durability test results show that the impact strength of concrete increases, the carbonation depth reduces, and the loss of strength due to sulphate attack reduces on addition of fibres. However, the chloride ion penetration is seen to increase on fibre addition, which may be due to the interfacial zones between the fibres and cement paste that act as additional connected routes for chloride transport in concrete. The modulus of elasticity in compression of concrete shows a decrease in value on addition of fibres. This can be because the strain in compression of concrete generally increases with increase in fibre volumetric ratio.

The tests conducted on slab specimens help in simulating the field pavement in the laboratory. From the results, it can be seen that the maximum load that the slab can carry increases with the addition of fibre. Correspondingly, it can withstand a higher deflection also. Steel fibres are seen to give the best results.

5 Conclusions

The use of FRC results in improved strength and durability properties in rigid pavements. The durability parameters in particular show a marked improvement on using FRC. Steel fibres give the best strength properties, whereas synthetic fibres give the best durability properties. Natural fibres are best used when available in abundance. The numerical analysis conducted can be used for simulating different pavement field conditions since results for the given slab specimen are closely matching the experimental results. FRC pavements can therefore be seen to provide a solution to the various problems faced by using conventional concrete pavements.

References

1. Belletti B, Cerioni R, Meda A, Plizzari GA (2004) Experimental and numerical analyses of FRC slabs on grade. In: Proceedings of FRAMCOS5 Conference (Vail Colorado), pp 973–980
2. Elsaigh WA, Kearsley EP, Robberts JM (2005) Steel fibre reinforced concrete for road pavement applications. In: Proceedings of the 24th South African transport corporation ISBN No. 1-920-01712-7
3. Sorelli LG, Meda A, Plizzari G (2006) Steel fiber concrete slabs on ground: a structural matter. ACI Struct J 103-S58(Jul/Aug 2006):551–558
4. Cominoli L, Meda A, Plizzari GA (2008) Experimental behaviour of construction joints in FRC pavements (Pavement Cracking Mechanisms, Modeling, Detection, Testing and Case Histories). In: Proceedings of 6th RILEM international conference on cracking in pavements USA, pp 761–771
5. Westergaard HM (1926) Stresses in concrete pavements computed by theoretical analysis. Public Roads 7(2):25–35
6. Belletti B, Bernardi P, Meda A, Plizzari G (2004) A NLFM method for the prediction of slabs on grade behaviour. In: Digital Repository, Convegno IGF XVII Bologna
7. Belletti B, Cerioni R, Meda A, Plizzari G (2008) Design aspects on steel fiber-reinforced concrete pavements. J Mater Civil Eng © ASCE 20/9:599
8. Maitra S, Reddy K, Ramachandra L (2009) Load transfer characteristics of dowel bar system in jointed concrete pavement. J Transp Eng 135(11):813–821
9. Joseph A, Koshy RZ, Nair SS (2011) Numerical modeling of rigid pavements using finite element method. In Proceedings of international conference on advances in materials and techniques for infrastructure development NIT Calicut T031
10. Elsaigh WA, Robberts JM, Kearsley EP (2011) Modeling the behavior of steel-fiber reinforced concrete ground slabs. I: development of material model. J Transp Eng © ASCE 137(12):882–889
11. Elsaigh WA, Robberts JM, Kearsley EP (2011) Modeling the behavior of steel-fiber reinforced concrete ground slabs. II: development of slab model. J Transp Eng © ASCE 137(12):889–896
12. Koshy RZ, Joseph A, Nair SS (2013) Steel fibre reinforced concrete pavement slabs with contraction joints. In: Proceedings of international conference on advances in civil, structural and environmental engineering—Zurich, pp 130–133. ISBN 978-981-07-7965-8
13. Mackiewicz P (2015) Finite-element analysis of stress concentration around dowel bars in jointed plain concrete pavement. J Transp Eng 141(6):06015001 (1–8)

Spatial Statistical Analysis of Traffic Accidents Using GIS and Python for Optimum Resource Allocation

Lakshmi Srikanth, Sneha Srikanth, and Ishwarya Srikanth

Abstract This paper deals with traffic accident analysis using Geographic Information System (GIS) and Python for identifying traffic accident hotspots as well as for determining the primary parameters affecting the severity of the accidents. The methodology is demonstrated for traffic accidents in the Des Moines city, Polk county of Iowa State, USA. Crash locations are geo-coded using Geographic Information System (GIS). The Kernel density estimation method is applied to locate the crash hotspots. Five hotspots are identified for accidents that result in injury as well as for those resulting only in property damage. Subsequently, feature selection is performed using Python to identify the parameters primarily affecting the severity of the accidents. The top three features relevant to the severity level are determined using chi-square statistic. It is found that the top three features affecting the severity level of accidents are—the type of intersection/interchange at the location of accident, surface condition at the time of accident and the object with which the vehicle collided during the accident. The methodology and results from this study could be utilized for decisions on incorporating traffic safety measures with optimum resource allocation.

Keywords Traffic accident hotspots · GIS · KDE · Python · Feature selection

L. Srikanth (✉)
CMR Institute of Technology, Bengaluru, India

S. Srikanth
Indian Institute of Technology Madras, Chennai, India

I. Srikanth
Florida Atlantic University, Boca Raton, USA
e-mail: isrikanth2016@fau.edu

B. Laishram and A. Tawalare (eds.), *Recent Advancements in Civil Engineering*, Lecture Notes in Civil Engineering 172,
https://doi.org/10.1007/978-981-16-4396-5_70

1 Introduction

Traffic accidents cause loss of human life and damage to the property globally. The first step involved in road traffic and safety management is the identification of accident hotspots. Efficiency of locating hotspots depends on precise data collection and appropriateness of data analysis. Hotspots, also known as black spots, are hazardous road locations that satisfy certain criteria that varies from country to country [1]. For example, in Denmark, a site is known as hotspot if 4 accidents are recorded within a span of 5 years. The duration, used in identifying hotspots, varies between 1 and 5 years. The accuracy of hotspot identification diminishes marginally for a period of more than 3 years [2]. There are different geostatistical methods that are applied to identify hotspots. Some of the popular methods are (i) K-mean clustering algorithm [3], (ii) k-nearest neighbour method [4], (iii) Moran's *I*, (iv) Getis-Ord G [5], (v) Kernel density estimation (KDE) [6, 7] and (vi) kriging [8]. Among all *KDE* is the widely used method in locating accident hotspots as this method visually represents density of accidents [9].

In addition to identifying hotspots, understanding the factors affecting the severity level of accidents will aid traffic management authorities to devise strategies for road safety while achieving optimum resource allocation. Different feature selection methods are available based on the type of data. They can be broadly classified as supervised and unsupervised. Supervised methods are further divided into filter, wrapper and intrinsic methods. Filter feature selection methods involve calculating a statistical measure to evaluate the relevance of the feature to the target variable (in this case, severity level) and using this value to filter/select it [10]. The choice of statistical measure depends on the variable data types. Since the target variable and the features are categorical in nature, chi-squared test is utilized. The objective of this research is to identify crash hotspots and parameters primarily affecting severity of accidents to aid traffic authorities to take preventive measures.

2 Methodology

2.1 Study Area and Traffic Accident Data

The study area considered for this research is Des Moines city, Polk County, Iowa State in the USA. Traffic accident data were collected for a period of 5 years from 2008 to 2012 based on publicly available data [11].

The data set consists of 24,660 entries, including information on the location of accidents, day and time of occurrence, surface condition, severity of accident, etc. The distribution of severity level across the accident records is—17,536 involving only property damage, 7068 resulting in injuries and 56 fatalities.

2.2 Kernel Density Estimation

Kernel density estimation (KDE) is a nonparametric method that uses density estimation technique to detect hotspots in 2D Euclidean space [12]. KDE is a widely used and well-established technique in traffic accident analysis owing to its lucidity, simple execution and visually appealing outputs. The entire study area is divided into number of cells. *KDE* is evaluated by placing a symmetrical surface over centre of each cell and then measuring the distance from the centre to the accident locations based on a mathematical function (Eq. 1) and summing the value of all the surfaces for that reference location (Fig. 1).

The mathematical formulation of KDE is defined as follows [13]

$$\widehat{\lambda_\tau}(s) = \sum_{i=1}^{n} \frac{1}{\tau^2} k\left(\frac{s - s_i}{\tau}\right) \tag{1}$$

where $\widehat{\lambda_\tau}(s)$ is density estimate at a point s, n is the number of crashes, s_i is the location of ith crash, τ is the bandwidth, also known as search radius, and $k(\ )$ is kernel function which is a function of the distance and the bandwidth.

Various authors have proposed different kernel functions including quartic, triangular, Gaussian, etc., in traffic accident analysis. The choice of cell size and bandwidth have a greater effect than selection of a particular kernel function [14]. Quartic kernel function is adopted in this research. After trying out various combinations of cell size and bandwidth, the values of 100 m and 500 m are chosen for cell size and bandwidth, respectively, for optimum level of clarity in visualization of KDE. Figures 2 and 3 illustrate the KDE values for injury and property damage accidents. Since a number of fatality cases are very less, KDE is performed for only injuries and property damage only accidents.

From Figs 2a, b, it is noticed that the hotspots are of similar distribution, with both KDEs having 5 primary locations. However, the ranking of the locations differs. Table 1 shows the ranking of major hotspots in the study area for injury type accident and property damage only accident.

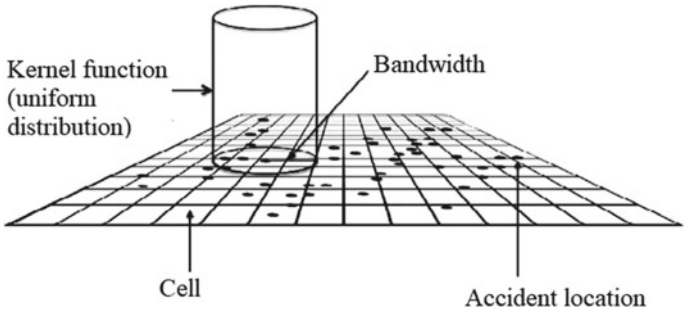

Fig. 1 Pictorial representation of kernel density estimation [9]

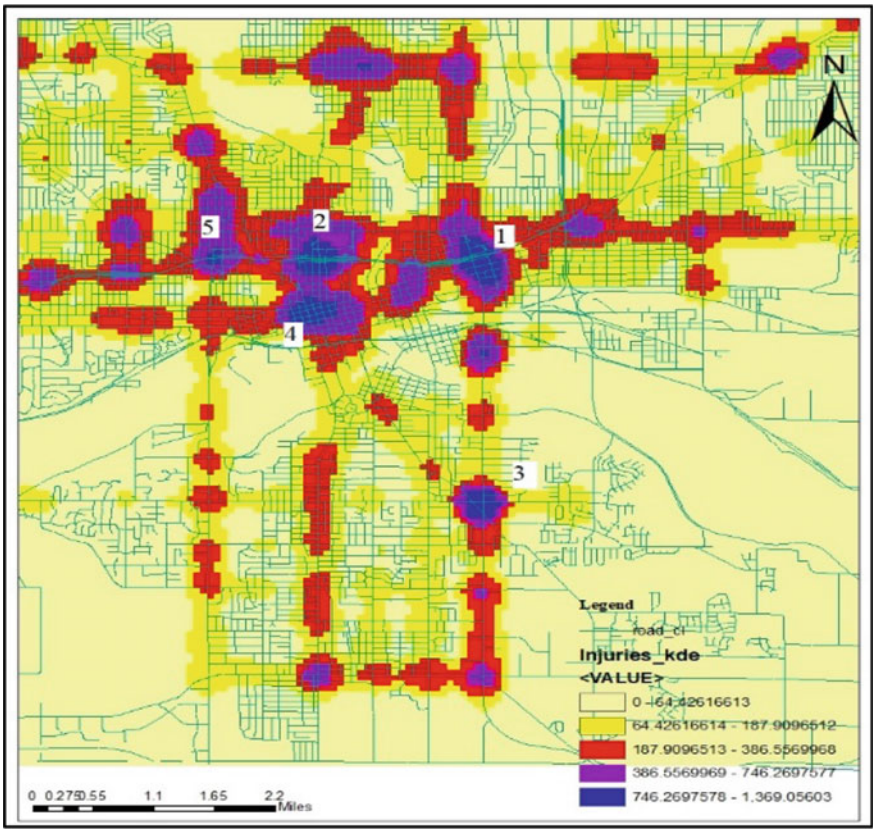

Fig. 2 KDE of accidents with level of severity "injury"

2.3 Feature Selection Using Python

The aim of this section is to find the features that primarily affect the severity level of the accident. It is pointed out that the focus here is not on the frequency of accidents but rather on the severity level. The outcome of an accident, i.e. its severity level, is classified into four categories—property damage only, possible/unknown injury, minor injury, major injury and fatal. In the previous section, since KDE is a nonparametric technique, no data cleaning was required, all the records were considered. For ease of visualization, possible/unknown, minor and major

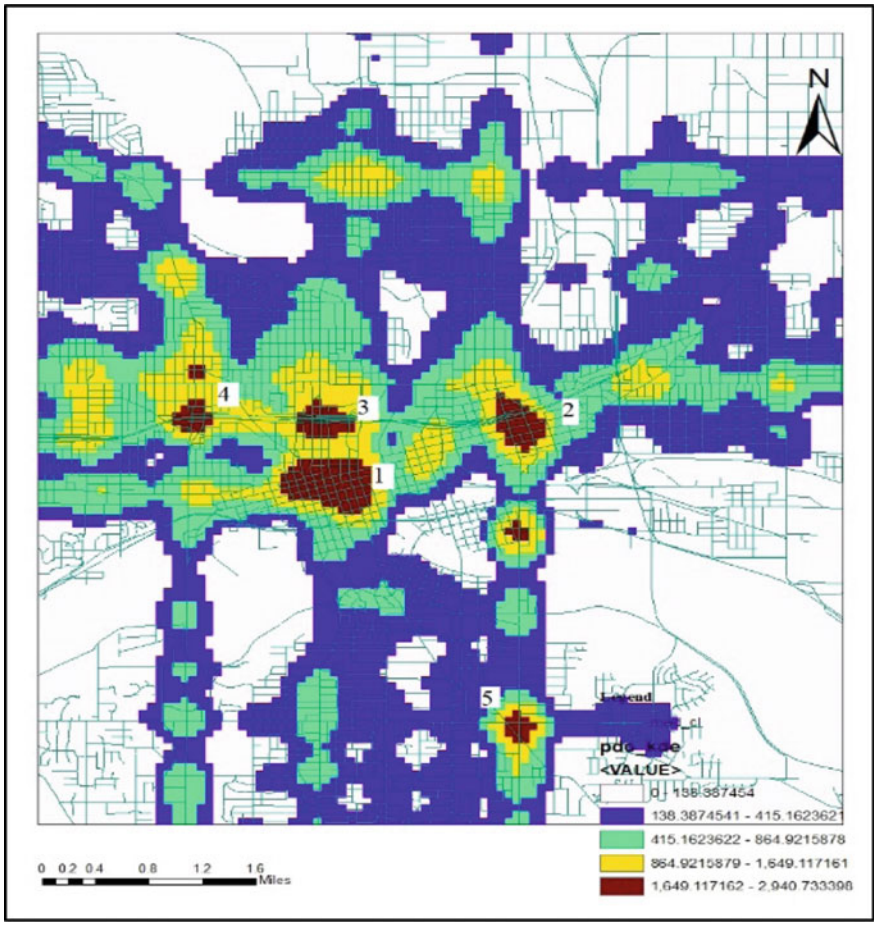

Fig. 3 KDE of accidents with level of severity "property damage only"

injuries were combined into a single category "injury". On the other hand, it is necessary to have a clean, balanced data to perform feature selection (Table 2).

The severity level of the accidents is recorded in the CSEV column of the data [11]. Therefore, the work in this section can be summarized as determining which input features are most relevant to the target variable CSEV. Python is utilized to perform data analysis since it is open source and offers an extensive set of libraries dedicated to data science.

Thirteen input features are taken into account and are briefly described as follows:

Table 1 Major hotspots in the study area

Hot spot rank# Injury type accidents	Hot spot rank# Property damage only	Location	Latitude (in degrees)	Longitude (in degrees)
1	2	235 and Lyon Street	−93.5779	41.5949
2	3	US highway 69, Maple Street	−93.6260	41.5963
3	5	US highway 69 and E 14th street	−93.5971	41.5546
4	1	Grand Avenue, 8th street	−93.6278	44.5876
5	4	I 235 and Martin Luther King Jr	−93.6440	41.5960

Table 2 Distribution of CSEV column of the unbalanced data after cleaning

CSEV (Severity level)	No. of records
Property damage only	16,262
Possible/unknown	4202
Minor injury	2071
Major injury	489
Fatal	54

- YEAR—the year of the accident.
- MONTH—the month of the accident.
- WEEKDAY—the day of the week when the accident occurred.
- COL_WITH—the object with which the accident occurred. Eg.: Collision with a pole, collision with a moving vehicle or a non-collision event such as a jackknife accident.
- LOC_ROAD—the location on the road where the accident occurred. Eg.: On the roadway, median or shoulder.
- COL_DIR—the direction at which the collision between vehicles occurred (broadside, head-on, sideswipe, etc.).
- DRUGALC—states if the driver had consumed drug or alcohol and if so, was it within the statutory limit or not.
- HOURS—the hour at which the accident occurred.
- LIGHT—lighting condition at the time of the accident. Eg.: Daylight, dawn or dark with roadway lighting, etc.
- SURFACE—surface condition—dry/wet/snow/slush, etc.
- WEATHER—the weather condition when the accident took place (Clear, cloudy, fog, hail, etc.).
- RDTYP—mentions the type of intersection, road interchange or non-intersection spot where the accident happened.
- PAVED—whether the road was paved or unpaved.

First, the data is cleaned, null and similar inapplicable values are removed. String values are encoded with OrdinalEncoder class in ScikitLearn library. This class encodes categorical features as an integer array. Following this, it is observed from the table that the data are highly imbalanced, with only 0.23% of the accidents being fatal. With that being the case, performing feature selection and subsequently using that to create a prediction model would prove to be inaccurate. In the previous section, the density of the accidents was under consideration. So, the data were not balanced and fatal accident records were ignored due to their negligible density levels. However here, we are concerned with the relationship between the features and severity and not the accident density itself. So, fatal accident records should be considered and data balancing is carried out.

One way to balance the data would be to oversample the minority class. The simplest approach involves duplicating records which have a fatal severity level. However, this does not give any new information to the model. In lieu of that, data augmentation of the minority class is implemented, i.e. new examples of the minority class are synthesized using the existing data. The most widely used method to carry this out is Synthetic Minority Oversampling Technique (SMOTE) [15].

SMOTE works by first selecting a particular example "a" in the minority class. It then finds its k nearest neighbours in the feature space. One of these neighbours "b" is randomly selected. Finally, the synthetic example is generated by connecting a line between a and b in the feature space and calculating convex combination of the two chosen instances a and b [16]. Instead of directly performing SMOTE, it is observed that performing under sampling first to reduce the number of instances in majority class gives better performance [15]. The imbalanced-learn python library provides the Random Under Sampler Class and SMOTE class. The data are ultimately balanced after tuning the various parameters (F).

In the next step, the strength of relationship between the features and the target variable is calculated. Since all the features are categorical in nature, chi-square test is performed. This involves testing a hypothesis about two variables. The null hypothesis here is that there is no association between the two variables. It is ascertained whether the relationship between two variables is substantial enough to discard random chance or sampling error. However, chi-square does not provide any information regarding the direction of the relationship, and additional statistical analysis is required to draw further inferences. In addition to the chi-square statistic, p-value of the tests are also evaluated to test for statistical significance.

The features are then shortlisted based on p-values, considering only those with p-value less than 5%. As seen from the bar chart shown in Fig. 4, six out of the thirteen input features are eliminated in this manner. Out of the remaining seven features, RDTYP, SURFACE and COL_WITH are most relevant to CSEV, followed by HOURS, LIGHT, COL_DIR and DRUGALC.

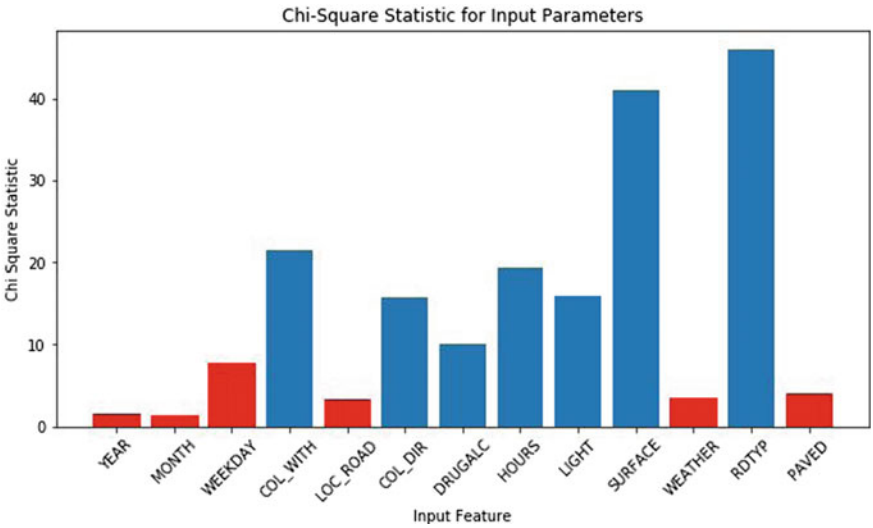

Fig. 4 Chi-square statistic for input parameters (red- p-value >5%, blue- p-value $\leq 5\%$)

3 Conclusion

This study presents traffic accident hotspot analysis using KDE and feature selection for identifying the accident hotspots and the parameters affecting the severity level of the accidents. Based on the KDE performed on the study area, five hotpots are detected which should be given utmost priority while implementing road safety measures.

The top three features affecting the severity level of accidents are—the type of intersection/interchange at the location of accident, surface condition at the time of accident and the object with which the vehicle collided during the accident. This offers an insight into how safety measures can be implemented to maximize the reduction in severity level of accidents. Using the results from both KDE and feature selection, optimum resource allocation can be achieved to lower the extent of accidents, particularly at hotspots. For example, in this case study, surface conditions have a greater effect on seriousness of accident than lighting conditions. Hence, any accident prevention plan can give more emphasis on improving the former than the latter. It is to be noted here that these results pertain to the geographical area under consideration and need not apply to other areas. However, the methodology presented in the paper can be applied to different cities, counties, etc. to derive their corresponding results.

With the selected features and balanced data, a classification model, such as an artificial neural network, can be built to perform predictions on severity level of accidents given the values of these input features [17, 18]. Feature selection reduces the number of inputs to the model and therefore reduces its computational cost, and

in some cases, improves its performance. The model can then be utilized to show not only what parameters affect the severity level, but also how they affect it. These results will be discussed in subsequent papers by the authors.

References

1. Elvik R (2008) A survey of operational definitions of hazardous road locations in some European countries. Accid Anal Prev 40(6):1830–1835
2. Cheng W, Washington SP (2005) Experimental evaluation of hotspot identification methods. Accid Anal Prev 37(5):870–881
3. Levine N, Kim KE, Nitz LH (1995) Spatial analysis of Honolulu motor vehicle crashes: I. Spatial patterns. Accid Anal Prev 27(5):663–674
4. Levine N (2009) A motor vehicle safety planning support system: the Houston experience. In: Planning support systems best practice and new methods. Springer, Dordrecht, pp 93–111
5. Prasannakumar V, Vijith H, Charutha R, Geetha N (2011) Spatio-temporal clustering of road accidents: GIS based analysis and assessment. Procedia Soc Behav Sci 21:317–325
6. Khan G, Qin X, Noyce DA (2008) Spatial analysis of weather crash patterns. J Transp Eng 134(5):191–202
7. Erdogan S, Ilçi V, Soysal OM, Kormaz A (2015) A model suggestion for the determination of the traffic accident hotspots on the turkish highway road network: A pilot study. Boletim de Ciências Geodésicas 21(1):169–188
8. Thakali L, Kwon TJ, Fu L (2015) Identification of crash hotspots using kernel density estimation and kriging methods: a comparison. Journal of Modern Transportation 23(2): 93–106
9. Srikanth L, Srikanth I (2020) A case study on kernel density estimation and hotspot analysis methods in traffic safety management. In: 2020 international conference on COMmunication Systems & NETworkS (COMSNETS). IEEE, pp 99–104
10. Kuhn M, Johnson K (2013) Applied predictive modeling, vol 26. Springer, New York
11. https://catalog.data.gov/dataset?tags=crash&res_format=CSV
12. Silverman BW (1986) Density estimation for statistics and data analysis, vol 26. CRC press
13. Hart T, Zandbergen P (2014) Kernel density estimation and hotspot mapping. Policing. Int J Police Strateg Manag 305–323
14. Xie Z, Yan J (2008) Kernel density estimation of traffic accidents in a network space. Comput Environ Urban Syst 32(5):396–406
15. Chawla NV, Bowyer KW, Hall LO, Kegelmeyer WP (2002) SMOTE: synthetic minority over-sampling technique. J Artif Intell Res 16:321–357
16. He H, Ma Y (eds) (2013) Imbalanced learning: foundations, algorithms, and applications. John Wiley & Sons
17. Alkheder S, Taamneh M, Taamneh S (2017) Severity prediction of traffic accident using an artificial neural network. J Forecast 36(1):100–108
18. Rezaie Moghaddam F, Afandizadeh S, Ziyadi M (2011) Prediction of accident severity using artificial neural networks. Int J Civil Eng 9(1):41–48

3-D Geomodelling for Dam Site Characterization

D. S. Aswar and P. B. Ullagaddi

Abstract The geological exploration along with scientific data analysis is required for site characterization. The diverse data integration and use of geostatistical modelling along with cognitive knowledge can prove to be a useful tool for better site characterization and consequent success of the dam project. The paper discusses statistical geological modelling for dam foundation substratum using geomodeller software Rockworks and geophysical data modelling using Surfer and IPI2Win. The geoparameters such as lithology, core recovery, RQD, fracture zones and percolation were modelled over the selected project area. The modelling of supplementary geophysical resistivity (vertical electrical sounding—VES) data was carried to check the subsurface geoelectric parameters beyond the existing bore log depth. The modelling gives a spatial representation of geological and geophysical data, for the conceptualization of geological formations at the dam site. The basics of modelling methodology, data evaluation, selection of modelling algorithm, modelling validity and the engineering implications of generated 3-D model for dam site characterization are discussed. The application and effectivity of geomodelling were checked through a case study of energy dissipation assembly (EDA) failure of Bhama Askhed dam, Pune, India. The portion of the tail channel immediate to the EDA is also analysed for tail channel erosion problem. The critical locations in foundation substratum are identified considering the spatial distribution of geoparameters. The findings of the study are in agreement with the bore logging interpretation results and further improve the conventional geological understanding. Recommendations for selected project are made based on geomodelling analysis outcomes. The study emphasizes the need to support the conventional geological understanding with geomodelling and spatial data analysis for better geological site characterization of the dam project. The engineering geological

D. S. Aswar (✉)
Department of Civil Engineering, Sinhgad College of Engineering, Pune, India
e-mail: dsaswar.scoe@sinhgad.edu

P. B. Ullagaddi
Department of Civil Engineering, S.G.G.S. Institute of Engineering and Technology, Nanded, India

B. Laishram and A. Tawalare (eds.), *Recent Advancements in Civil Engineering*, Lecture Notes in Civil Engineering 172,
https://doi.org/10.1007/978-981-16-4396-5_71

model can provide a reliable mean of identifying, project-specific, critical geological issues and decisions making for dam foundation.

Keywords Bore log data · Vertical electrical resistivity data · Geostatistical interpolation · Geomodelling · Site characterization · Rockworks · Surfer · IPI2Win

1 Introduction

The degree of accuracy in predicting, evaluating and interpreting the quality of substratum is a key for successful project completion. As per the Commission of International Association for Engineering Geology and Environment (IAEG), the engineering geological model is the indispensable tool, for engineering quality control, and provides a reliable mean of identifying project-specific critical geological issues. The three-dimensional (3-D) geomodel enables conceptualizing geological formations and processes over the geographic areas. The 3-D geomodel can portray subsurface, showing formation depths, thicknesses and material properties within a 3-D volumetric space [1]. It gives more reliable geological representation, compared to the conventional paper-based 2-D approach, thus ensuring enhanced geospatial understanding of site subsurface geology and better decision making.

2 Literature Review

Several examples of geomodelling application in the field of mining and petroleum industries are quoted in the literature. The georeferenced geological, geotechnical and geophysical data can be used for developing 3-D attributed geomodels, for project site characterization.

The 3-D modelling can be used to effectively identify, visualize and analyse subsurface geological conditions for engineering structures [1–9]. 3-D conceptual block models of geoparameters can be built, using spatial database and GIS environment. The modelling can be performed based on two different approaches, namely knowledge-based "Bulk Attribution Approach" [1, 10–14] and the algorithm-based "Geostatistical Approach" [3, 4, 13, 15–17]. Algorithm-based geostatistical modelling is preferred over knowledge-based bulk attribution modelling for high density, evenly spaced data. The field observed geoparameters can be evaluated and compared with the modelling predicted values [11, 12, 15, 17, 18].

Geophysical investigations such as electrical resistivity survey can be conducted to delineate the extent and distribution of subsurface geological formations. [19–23]. The resistivity data can be interpreted to determine the geoelectric parameters and to form resistivity cross sections [19, 20, 22, 24, 25]. The 3-D

representation of geophysical data is more complete and with the realistic ability of display and data query [2, 26–30]. The results of geophysical testing are comparable, with the conventional field and laboratory testing. Geophysical profiles can assist in the planning the intrusive investigations and assessment for the need of treatment measures [19, 23].

3 Methodology—Modelling Process

Geomodelling was carried out for dam site characterization and dam foundation evaluation. The site evaluation results were used to check alignment sections, characterized by specific geological or geotechnical scenarios. Also, the existing location of spillway section was analysed for foundation suitability. Based on the geomodelling analysis, grouting treatment need and its extents are recommended. Conceptual workflow for geomodelling consists of following sequential steps,

(i) Data evaluation, standardization, integration and re-interpretation.
(ii) Data organization, through geodatabase formation.
(iii) Geomodelling through geostatistical interpolation.
(iv) Geomodelling validation, by statistical and optical correlations.
(v) Data extraction for thematic models, for spatial analysis and interpretation.
(vi) Thematic models analysis for the project foundation decisions and comparison with adopted measures based on conventional understanding.

The georeferenced borehole data of geoparameters, namely core recovery, RQD, lithology, permeability and joints/fracture data from 88 boreholes with the total length of 1748.81 m, were used for modelling. Software environment used for data processing and modelling consists of QGIS for spatial data georeferencing and Rockworks software as Geomodeller. Also, IPI2Win and Surfer software was used for electrical resistivity data processing.

Modelling extend of 1500 × 800 m is selected to cover the project area of interest, along the dam alignment including the portion of the tail channel for erosion analysis. Geomodels without base filter were constructed, thus extending uniform continuous properties from the deepest borehole as per the conventional geological understanding. Thematic maps (profiles/sections/fences/surface maps) were developed from 3-D attribute models. Figure 1 shows the details of dam alignment, borehole, VES and resistivity profile locations for the study area.

The modelling of supplementary geophysical VES data was carried to check the subsurface geoelectric parameters beyond the bore log depth, thus complementing existing geological data. The subsurface geoelectric parameters (resistivity distribution, layers thickness and depth to bedrock) were obtained to check the occurrence and extend of weaker formations. VES survey consists of four geoelectric traverses (Profile-I to Profile-IV) with a total 25 VES stations (VES-1 to VES-25)

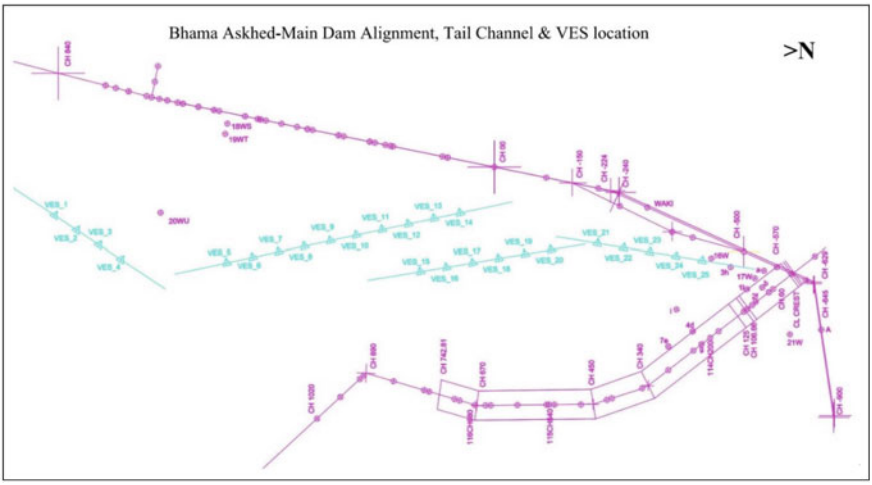

Fig. 1 The boreholes and VES locations for the study area

and collective profile length of 1450 m, conducted with Wenner configuration. VES data were interpreted through qualitative analysis with sounding curves, apparent resistivity pseudo-sections, iso-apparent resistivity maps and also by quantitative methods using resistivity inversion (IR) by IPI2WIN by Bobachev [31] and inverse slope method (ISM) by Ramanujachary [32]. However, the discussion of qualitative interpretation, IR and ISM is not elaborated and only result interpretation is expressed.

4 Case Study

The Bhama Askhed Irrigation Project (18°15'N, 73°43'E) is situated on the river Bhama, a right-bank tributary of river Bhima (Krishna Basin), at village Waki, Taluka–Khed District—Pune, Maharashtra (India). The project consists of 51.125 m high and 1425 m long earthen dam with gross storage capacity at FRL of 230.47 MCM and 55.5 m long ogee side spillway. Geologically, the tail channel is located on the untreated flow of, fractured, closely jointed Chlorophaeitic Porphyritic Basalt (CHLO.POR.B.), prone to disintegration on exposure to the atmosphere. It is underlain by soft, erodible, Hydrothermally Altered Volcanic Breccia (H.T.A.V.B.) with a Red Tachylytic Basalt (R.T.B.) which is having serve erosion potential.

During 2005, heavy seepage accompanied with the dynamic spillway discharge forces uplifted and displaced thirteen concrete panels (7 × 11 × 0.30 m each) of flip bucket type, energy dissipating assembly (EDA). The structural failure of the EDA portion has occurred due to excessive seepage and associated uplift pressure

[37]. The EDA failure highlights the inadequacy of geological data integration, interpretation and assessment of foundation treatment measures. Geomodelling was attempted to address these concerned effectively.

5 Geomodelling

The data standardization consists of normalization of the data heterogeneity in the terms of descriptions and reinterpretations of available data to produce consistent dataset. Data characteristics such as consistency, variation and its directionality trends were analysed for the selection of appropriate modelling algorithm. Data evaluation over the project site shows variograms anisotropy values closer to "1"; thus, the geoparameters are less directional, i.e. anisotropic. The small sill values were showing low variability between the data points, and also, higher range values indicate greater similarity over larger distances. The right abutment (with the direction heading towards upstream) data show high standard deviation (SD), for geoparameters. Besides, the values of coefficient of variation are also high compared to overall project data, with a higher variability at spillway, EDA and tail channel.

Standardized and validated data from all the stages of geological exploration were used for geodatabase generation within the geomodeller environment. The conventional data were first converted to Microsoft Excel format, following IS4078 [33], IS5313 [34], IS4464 [35], and later modified to specific database format in Microsoft Access. Geomodelling was performed with various combinations of stage-wise data (Models M-I, M-II, M-III) and consolidated data (Model M-IV), with different resolutions, viz. X, Y and Z spacing in metres (Case-I $5 \times 5 \times 1$, Case-II $10 \times 10 \times 1$, Case-III $10 \times 10 \times 1.5$). These modelling combinations were tried with literature recommended algorithms for checking the effect of data quantity on modelling (root mean square error—RMSE) and for selection of modelling algorithm producing the optimal model. The limited data only from a specific stage of geological exploration giving the model with least RMSE value may not reflect the entire geological setup of the site. Hence, for geological characterization of the entire project site, the consolidated data from various stages of investigation have to be used for the comprehensive modelling [3, 12, 14, 17, 27]. Hence, the final geomodels were created with comprehensive integrated data from all the investigation stages.

The selection of appropriate modelling resolution ensures that the data are properly represented in the model and not averaged out. Based on the thumb rule for selection of optimal model resolution, *X*- and *Y*-spacings are set to half the average distance between the boreholes. The *Z*-spacing relates to the downhole sampling intervals. The models were tried with *x*/*y*/*z* node spacing density of 5/5/1, 10/10/1 and 10/10/1.5 to find out the optimum resolution and the best-suited interpolation algorithm for optimum modelling efficiency. The proper voxel size is the one with the minimum SD and RMSE values. Models were compared, based on

least RMSE values to ensure the precision of the resulting model. For dam site borehole data, half of the average distance between the boreholes along the dam alignment is 11.30 m. Hence, the *X*- and *Y*-spacing was finalized to 10 m after optimization trials and the *Z* interval was selected as 1.5 m based on core logging sample and Lugeon test intervals. The chosen units for model dimension in *XY* (horizontal) units are in UTM meters and *Z* (vertical) is in meters. Projection is UTM (Universal Transverse Mercator), Datum = WGS-84 1984, and Zone = 43 N.

For lithology modelling with both closest point (CP) and lithoblending algorithm (LB), the RMSE values gradually coincide together with increasing data quantity. However, CP is the algorithm that produces a solid model with abrupt changes between nodes (material boundary) rendering them unrealistic in appearance. The LB algorithm minimizes the abruptness with randomized blending and interpolated outliers giving the realistic geological modelling. Hence, LB algorithm based on geological characteristics was preferred for final lithology modelling, with slight compromise in RMSE values compared to CP.

Variogram analysis indicated anisotropic characteristics of the geoparameters. Hence, inverse distance isotropic solid modelling (IDWA) algorithm was selected, over inverse distance isotropic solid modelling (IDWI) for modelling geoparameters. The method gives the additional advantage of reducing localized highs around the boreholes. Thus, selected modelling algorithms are horizontal lithoblending—for lithology modelling, and inverse distance anisotropic—for core recovery, RQD and permeability data modelling.

6 Validation of Geomodels

6.1 Statistical Correlation

Models were validated by checking the concordance between statistical parameters of field data and the model-predicted (modelled) data. Statistical correlation carried out consists of,

(i) Comparison of statistical parameters for observed field data and modelled data (the results shows low SDs values).
(ii) Check for solid model residuals, i.e. the difference between observed field data and computed values from the interpolated model (shows low SDs and very few anomalies).
(iii) Correlation scatterplot between observed and predicted parameters (high correlation).

Table 1 Summary of correlation between the modelled data and reserved borehole

Borehole	Statistical parameter	Lithology	Recovery%	RQD%	Percolation
DH-105	Correlation coefficient	0.33	0.9	0.94	0.75
	RMSE	5.76968	7.60024	6.47013	0.09107
DH-108	Correlation coefficient	0.4	0.9	0.85	0.44
	RMSE	5.01947	8.54643	12.06086	0.07693
DH-I (3)	Correlation coefficient	0.76	0.96	0.8	0.97
	RMSE	3.75002	5.66147	13.15297	0.3597
DH-TL (14)	Correlation coefficient	1	0.94	0.94	0.86
	RMSE	–	8.92977	8.73976	1.20572
Average correlation coefficients		0.63	0.925	0.883	0.755

(iv) Comparison of statistical parameters for observed and predicted data values of randomly selected reserved boreholes not included in modelling. The results give low RMSE values and high correlation coefficients as shown in Table 1.
(v) Correlation of reserved boreholes data with model-predicted data (shows low SDs).
(vi) Check for RMSE as a measure of model performance (shows low RMSE).

Correlation coefficient greater than +0.70 indicates a strong linear relationship between observed and modelled data. The results (Table 1) show average correlation coefficients between the modelled data and reserved boreholes are recovery = 93%, RQD = 88%, percolation = 76% and lithology = 63%.

In geosciences, RMSE is the standard statistical unit, for accuracy assessment of spatial analysis and the measure of model performance. The low RMSE values indicate high model accuracy. However, it is a relative measure; thus, there is no absolute good or bad threshold. Mere efforts to get the model with the least RMSE values will not result in proper site characterization. The core logging is the most reliable direct method used for geological exploration. This method reflects the complexity of natural geological formations in the form of outlier values. The normalization of this geoparametric data of multiple measurements between either the same minima and maxima or the user-specified range may not respect the natural variability of geological formations. Hence, the modelling efforts considering the field verified outlier values were preferred though it is giving slightly higher RMSE values. Apart from RMSE, the RSR (RMSE to the observation standard deviation ratio) and NSE (Nash–Sutcliffe efficiency) is also recommended for standardizing model performance Singh J. et al. [36]. Table 2 shows that for all the geoparameters, RSR is close to 0.5 and also NSE is between 0 and 1; hence, applied geomodelling indicates good model simulation.

Table 2 RSR and NSE statistical measures for generated geomodels

Parameter	Std. deviation	RMSE	RSR	NSE
Lithology	4.8272	3.24771	0.67	0.55
Recovery%	24.0395	13.5920	0.57	0.68
RQD% residual	31.6080	15.37537	0.49	0.76
Percolation	3.7368	2.23979	0.60	0.64

6.2 Optical Correlation

The optical correlation is a qualitative method to evaluate the validity of geomodelling by visual verification. Cross sections from 3-D geomodels were compared with actual borehole logs to visually correlate between them. The modelled parametric values show the correlation in the form of similar properties and low- or high-value trends with the original data between selected boreholes. The model confirms the expected geology and "honours" the project data. Besides, for optical validation, the geomodel cross section was compared with generated conventional "Expert Cross section". The generated hole-to-hole RQD% cross sections (spillway) compare well with the corresponding model cross section. The differences are mainly due to the effect of data from the several nearest adjoining boreholes, participated in modelling. The reasonable match of extracted data with the reserved field-core data shows the ability of the model to generate the missing spatial data for non-data/limited data through geostatistical interpolation techniques with reliability and accuracy.

7 Geophysical Investigations

The qualitative and quantitative analysis of resistivity data shows that most of the project site is underlain by fresh basement rocks at comparatively shallow depth. For the left abutment, resistivity increases with depth, indicating less heterogeneity and consistent geological formation. However, more resistivity anomalies were observed towards the right abutment (spillway) section. The qualitative resistivity analysis reveals the occurrence of low-resistivity (35Ωm), low-density, weathered formation (possibly of R.T.B.) at depth of 40–45 m, towards the spillway end. This weak rock may lead to potential seepage problems. These VES results are also consistent with known geology and nuclear logging test findings [37].

The VES interpretation results were correlated with the nearest, deepest core log to establish the correlation between the resistivity and lithological formations. For ISM, layer thickness and resistivity correlate fairly with nearest core log lithology (i.e. ground truth) compared to the IR method. IR method fails to identify the deep laying low resistivity layers. Also, ISM is more suitable for identifying deeply located, low resistivity formations [32]. Hence, it is adopted for geoelectric analysis. Result of

Table 3 Correlation of VES-25(ISM) with DH-112-S/CH -599 m

Borehole DH-112-S/CH-599			Geoelectric interpretation VES-25(ISM)				
Formation	Tk. (m)	Depth up to (m)	No. of layers	Tk. (m)	Depth up to (m)	ρ (Ω m)	Formation
O.B	2.20	2.20	1	3.5	3.5	12.83	Highly weathered formation
CHLO.C. POR.B.W.P. P	35.05	37.25	2	12.25	15.75	110	Jointed formation
			3	26.75	42.5	54	Vesicular, fractured, jointed
			4	3.25	45.75	34	Slightly weathered
			5	12.25	58	48	Vesicular, fractured, jointed

O.B.—Overburden,
CHLO.C.POR.B.W.P.P.—Chlorophaeitic Compact Porphyritic Basalt with Plagioclase phenocrysts

ISM analysis identified high resistivity, high layer thickness towards left abutment, whereas there is low-density formation at depth 42–46 m towards the spillway section as shown in Table 3.

Figures 2 and 3 represent the iso-resistivity maps showing resistivity distribution and the thickness isopach map showing corresponding individual layer thickness variation for each layer. The last layer of isopach map indicates hard massive basaltic bedrock.

8 Geomodelling Analysis for of Specific Geotechnical Domain

The entire dam length was divided chainage-wise (CH) into three portions for analysis purpose as left abutment (CH. +340 m to +795 m), the middle portion (CH. +340 m to −145 m) and right abutment (CH. −145 to −630 m) with spillway. Each of these portions along with failure affected EDA portion including approach, spillway and the tail channel section was analysed for geological suitability and grouting requirements. Chainage-wise positions of geologically critical areas for specific geoparametric values, their elevations and the zone thickness were identified along these sections by taking the cross sections of the generated 3-D block geomodels. Thus, the geomodelling analysis was carried out to locate conditions of unfavourable lithology, low recovery, low RQD%, high percolation and existence of fracture zones, with respect to adopted foundation and grouting levels. Also, the generated filtered and Boolean geomodels were investigated for the variation of specific geoparameters which affects the project foundation decisions. The upper

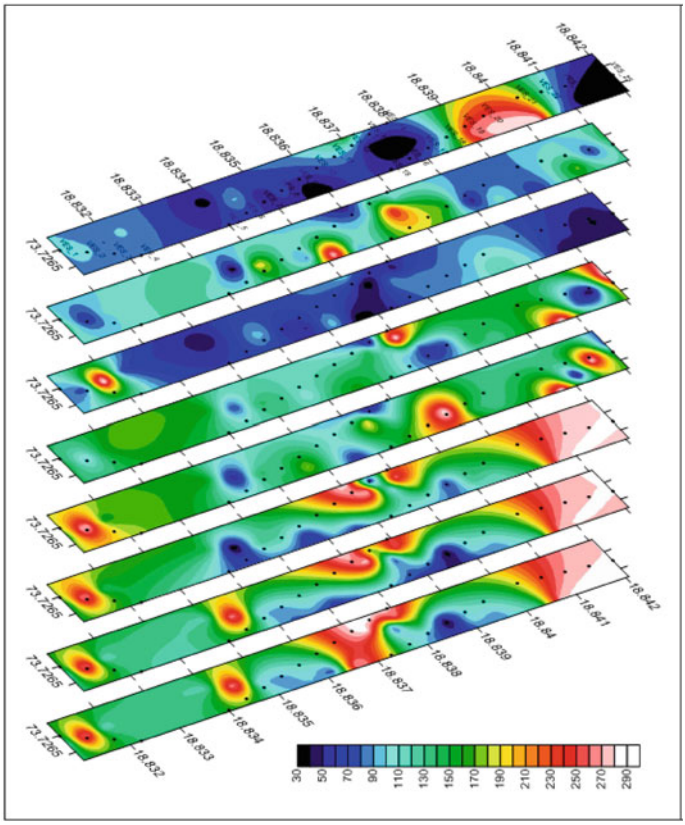

Fig. 2 Stacked layer absolute resistivity contour map (ISM)

dotted lines (blue) indicate the adopted grouting levels, whereas lower dotted lines (white/red) mark the suggested grouting levels based on geomodel analysis. The three alternative spillway locations initially suggested by designers were also analysed and compared based on geological suitability. However, the representation and discussion here are mostly kept limited to failure analysis of the spillway section.

8.1 Recovery and RQD% Variation Along Right Abutment

There is low (65–75%) recovery zone at EDA failure portion, chainage TL +65 to TL +100 m at the grouting level (640 m) as evidence from cross section of recovery% model along right abutment and along tail channel. Low average RQD% (26.77%) at approach channel shows the existence of poor quality fractured and jointed rock as observed in Figs. 4 and 5.

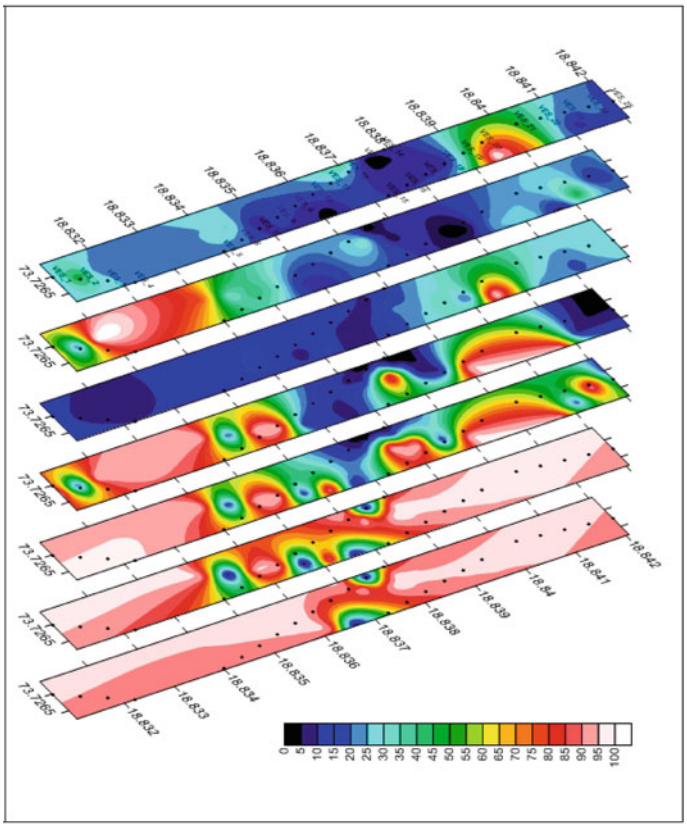

Fig. 3 Stacked layer thickness contour map (ISM)

For both spillway and approach channel, recovery and RQD% values show inconsistent variation over the depth. These values are decreasing with depth, indicating fractured and jointed formation there. The average percentage variation between recovery and RQD for the right abutment, left abutments and the middle portion is 3.87%, and this percentage variation is 63.08% for approach channel which is quite high showing the fractured state of rock there.

8.2 Modelling Fracture Zones and Percolation Using Boolean Models

The closely jointed fractured zones, with high fracture intensity (>5 joints/m run), were modelled for checking the discontinuities over the study area. Cross section of fracture zone 3-D model and Boolean model for tail channel shows the occurrence

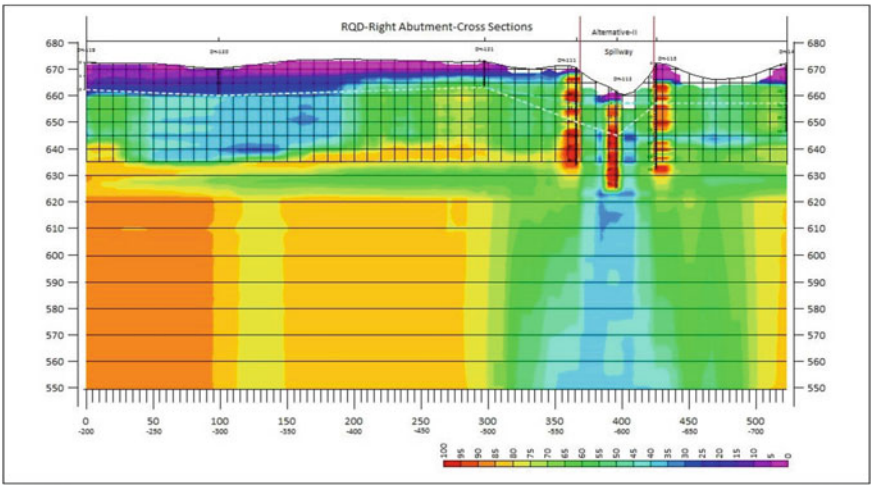

Fig. 4 Cross section of RQD% model along right abutment

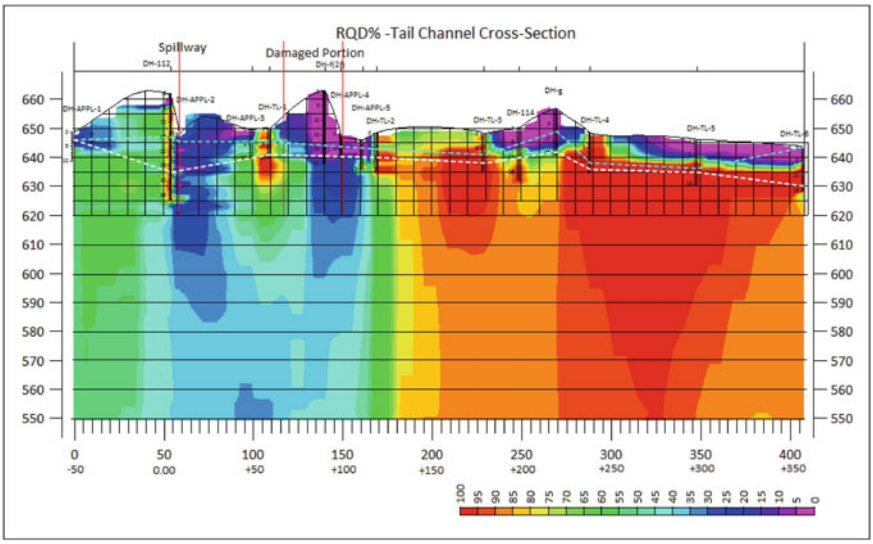

Fig. 5 Cross section of RQD% model along tail channel

of fracture zone with high fracture intensity at spillway location, RL 630 m below the selected grouting (RL 635 m).

The tail channel section at damaged EDA portion is marked with the existence of the fracture zone at RL 640 m (tail channel chainage—TL +90 m) (Fig. 6). The selected local grouting level (RL640m) is insufficient considering the fracture zones close to the spillway location.

To prevent the foundation erosion, the limiting Lugeon values of 3 Lu (Lugeon) are recommended for deciding the necessity of grouting by IS 6066: 1994/2004 [38]. The percolation values at approach and tail channel are higher than 10Lu, indicating excessive seepage through the substratum. Percolation data show numerous occurrences of no pressure or 100% water loss in the percolation test. Variation Lugeon values with RQD % were also analysed for the approach channel and spillway section.

The solid models were converted to a Boolean (true/false) model for the nodes grade values falling within a specified limiting range and selected conditions in Table 4.

In rock masses, the hydraulic conductivity depends on the aperture opening, spacing and infilling characteristics of its discontinuities [39]. To count for these parameters, Recovery_RQD_Percolation and Fracture Zone_ Percolation Boolean model was analysed to identify the critical areas as shown in Table 4.

The majority (69.7%) of the Lugeon values in approach and tailrace channel (EDA) between (tail channel) chainage −50 m and +112 m across the spillway section was found to be higher than 10 Lu indicating excessive leakage through the rock foundations thus open fractures which need to be grouted. The average percolation for approach channel was above 9 Lu and for a tail channel about 3.67 Lu. Figure 7 shows the Boolean model cross section along the tail channel with percolation >3 Lu. The entire approach sections and tail channel section (including EDA discharge section) immediate to spillway need proper grouting to check the seepage and uplift pressure. The Boolean percolation model with permeability >3 Lu evidences the occurrence of high permeability zone at the spillway and EDA

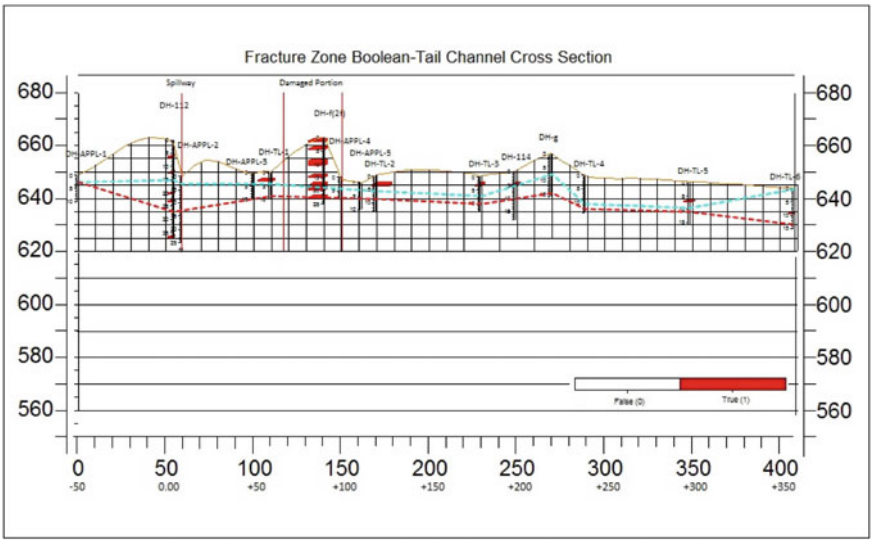

Fig. 6 Cross section of fracture zones Boolean model along tail channel section

Table 4 Schematic representation of mathematical operation for Boolean models

1	(Recovery_boolean.mod) * (RQD _boolean.mod) = Recovery _RQD_boolean.mod (Remark-resulting model with Recovery and RQD both lesser than 50%)
2	(Recovery_RQD_boolean.mod) * (Percolation boolean.mod) = Recovery_RQD_Percolation_boolean.mod (Remark-model of Recovery and RQD both lesser than 50% and Percolation greater than 3 Lu)
3	(Fracture Zone.mod) * (Percolation_boolean.mod (Lu > 3)) = Fracture Zone_Percolation_zone_boolean.mod (Remark-resulting model with Overlapping fracture zones and percolation (>3 Lu) areas
4	(Fracture Zone_ Percolation_zone_boolean.mod) * (RQD__boolean.mod (RQD% < 50)) = Fractured_water loss zone_boolean.mod (Remark-model with Fracture zones with both Recovery and RQD lesser than 50% and Percolation greater than 3 Lu)

portion between the chainage −550 m and −670 m along the spillway alignment. The high permeability zone extends up to RL 550 m, which is well below the selected grouting zone (RL 645 m). At tail chainage, TL +20 m high permeability zone occurs at around RL 633 m, which is below the selected local grouting depth of RL 635 m as observed in Fig. 7.

8.3 Analysis for Unfavourable Lithology

The occurrence of problematic rock masses at the site was investigated using geomodel filtered for unfavourable litho-types. Conventional 2-D geological understanding applies data in the specific section, whereas the 3-D geostatistical interpolation has added advantage of several references from adjoining boreholes (control points). Unfavourable lithology cross section along right abutment shows unfavourable lithology along right abutment specifically at spillway section. Spatially V.B.B.T.B. with an average thickness of 1 m to 3 m extends over the approach channel approximately 3 m (RL 643 m) below the executed grouting level (640 m). The rock exists at considerable shallow depth, and it should be grouted (reconsideration of grouting depth) as shown in Fig. 8.

9 Recommendation for Grouting

The potential weak zones which need to be considered in foundation decision making are identified considering the spatial extent of unfavourable conditions, for lithology (Table 5), recovery, RQD, fractured zone and associated permeability collectively (Table 6).

Based on the analysis, the average and the specific grouting depths are recommended. The specified area between chainage −570 m and −620 m is part of

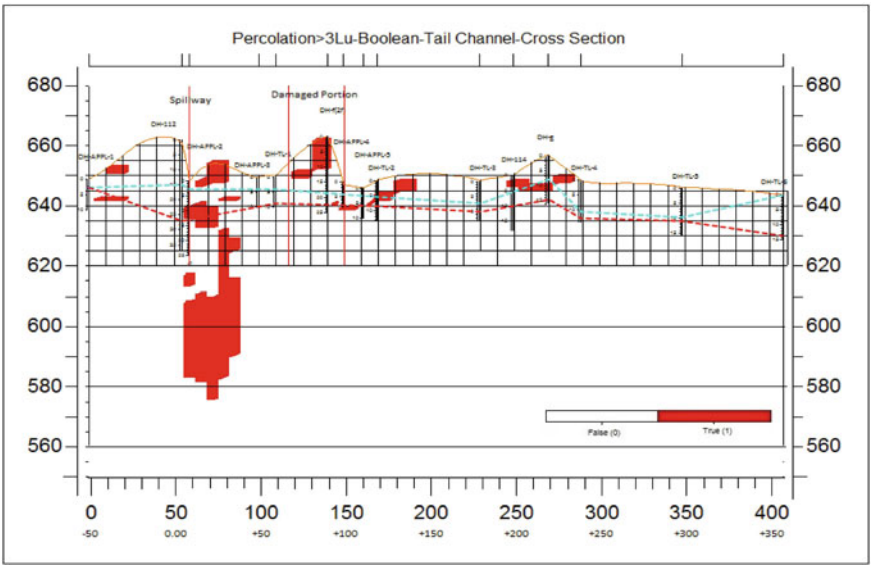

Fig. 7 Percolation Boolean model >3 Lu cross section along tail channel

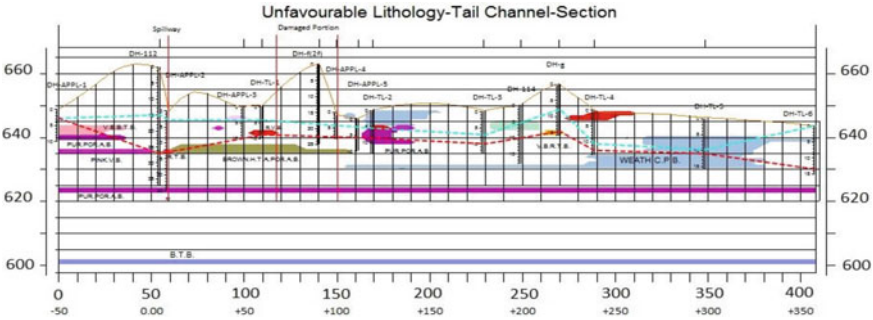

Fig. 8 Unfavourable lithology cross section along tail channel

spillway portion and is marked with problematic lithology (Table 5) and unfavourable values of geoparameters (Table 6). The area is having low recovery (55–70%), RQD (35–45%) and percolation (>3Lu). It is also marked with two critical fracture zones below the executed grouting zone, rendering it unsuitable for spillway construction.

The distribution of geoparameters and lithology should be considered collectively for grouting decision. Depth of grouting recommended considering unfavourable conditions of all the geoparameters together gives a greater depth of grouting than executed (Fig. 9). However, the isolated deep laying unfavourable conditions existing well below the foundation level may be ignored safely, based on

Table 5 Unfavourable lithology at right abutment and recommended grouting levels

Lithology	Location	Location chainage (m)		RL (m)		Selected grouting elevation (up to)	Recommended grouting elevation (RL.)
		From	To	From (Top)	To (Bottom)		
B. Hydrothermally Altered Porphyritic Amygdaloidal Basalt	−500 to −700 Right abutment	−360	−590	638	635	635	620 m (+15)
Pink Volcanic Breccia		−590	−700	636	635		
Volcanic Breccia with Black Tachylytic Basalt	−50 to +100 Tail channel	−50	+15	644	641	635	620 m (+15)
Pink Volcanic Breccia		−50	00	637.5	635		
B. Hydrothermally Altered Porphyritic Amygdaloidal Basalt		00	+110	638	635		
Weathered Compact Porphyritic Basalt	100–400 Tail channel	100	+350	635	630	635	625 m (+10)

the judgement of actual site geological conditions. Due to lack of grouting details, the efficiency of executed grouting could not be investigated. The further seepage at the spillway section through the identified weaker zones cannot be ruled out. It is recommended to be grouted to the specified locations and depths.

Representation and discussion for the paper are mostly kept limited to failure analysis of the spillway section. However, considering the similar geomodel analysis along the entire dam alignment including left abutment and a middle portion indicates Alternative Spillway-I location with reasonable grouting need and geologically more feasible compared to other alternatives.

Table 6 Variation of geoparameters along the right abutment

Location	Geoparameter	Values	Chainage (m)	Elevation (m)	Grouting RL (m)		Remark (Spillway)
					selected	proposed	
Right abutment (−200 to −720 m)	Recovery	55–70%	−220 to −380	635	660	635	–
		65–77%	−490 to −550	650	662	650	–
		55–70%	−600 to −700	645	655	645	Spillway
		55–70%	TL0 to TL50	620	637	620	EDA
	RQD	35–45%	−570 to −625	620	640	620	–
		35–45%	−625 to −720	635			–
	Fracture (Fract.)	Fract. zone	−595	625			Spillway
		Fract. zone	−570	648	640	645	Spillway
	Percolation	2.5–3.5 Lu	−560 to −710	600	640	620	–
EDA portion (TL 0 to +125 m)	Recovery	65–75%	0 to +50	610	640	610	–
	RQD	25–35%	0 to +50	610	640	610	–
		25–35%	+80 to +120	620	640	620	–
	Fracture	Fract. zone	+90	620			–
	Percolation	>4–8Lu	0 to +10	625	640	625	–

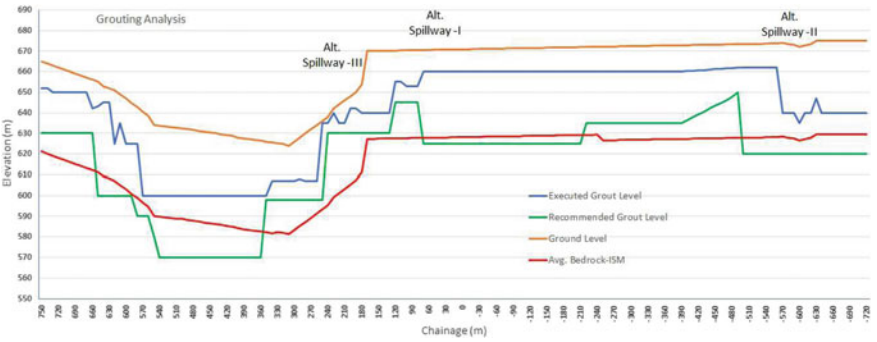

Fig. 9 Grouting depth analysis

10 Tail Channel Erosion

The EDA end portion and patchy outcrop exposed in tailrace channel are witnessing gradual removal by erosion. The degree of erosion of this artificially excavated tail channel at Bhama Askhed was checked by comparing designed tail channel RLs with the profile survey RLs carried out by the author. The profile survey was carried over the 351 m length of the tail channel, ahead of EDA portion in 2015 for mapping tail channel erosion. The 2015 RLs are compared with the

Table 7 Quantity of tail channel erosion

Net volume of erosion	Yr. 2000–06	Yr. 2006–15	Yr. 2000–2015
	9866.44 (m^3)	3340.28 (m^3)	12,885.79 (m^3)

design/executed RLs-1997 and RLs-2005 (EDA failure) to check the tail channel erosion due to the existence of weak rocks. Volumetric calculations based on the prepared grid models (Surfer) quantified the amount of erosion. Table 7 shows the estimated volume of tail channel erosion over time.

The result of grid models of tail channel has confirmed the erosion gradually progressing towards spillway section around EDA area. The tail channel erosion needs to control; else it will expedite the weathering and consequent seepage through exposed Tachylytic formation. The presence of dolerite dyke across the spillway in the tail channel may further aggravate the seepage and the uplift problem in the stilling basin. It required to be sealed by blanketing to avoid further erosion. The reliable performance of relief holes in EDA portion, against the chocking of filter with passing fines, needs to be assured for effectively relieving the uplift.

11 Conclusion

Intensive analysis of generated geomodels gives the following conclusions,

1. 3-D geomodelling allows integrated representation of the geological substratum, marked with the geoparametric variations. This site characterization through geomodelling helps in the identification of potential situations for engineering applications.
2. The geomodels, attributed with geoparameters, clearly marked the unsuitable areas for careful consideration for foundation conditions of dam and location of key structures.
3. The alignment analysis shows that adopted Alternative Spillway-II location is geologically unsuitable and needs further grouting, whereas the entire middle portion of Alternative-I is mostly favourable, with few exceptions at Alternative Spillway-III.
4. The appropriate geostatistical interpolation methods can extend the investigation data over the project extends. This inferred that the modelling results could be suitably extended to non-data or limited data areas with suitable checks. Geomodelling has potential to reveal anomalous zones, for planning further site investigation.
5. Though geomodels are both geology and project-specific, its applications highlight the engineering implications for dam foundation stratum characterization, evaluation, treatment measures and tail channel erosion. It can provide a reliable mean of identifying project-specific, geological issues and decisions making for dam foundation.

The site characterization using geomodelling can address predesign issues for new project, troubleshooting for existing projects with foundation issues and even for failure analysis conditions. The study also emphasizes need to support the conventional geological understanding with geomodelling for better characterization of the dam site.

12 Future Scope

Engineering Implications of Geomodelling can open the new era for site characterization, project foundation decisions and control. The 3-D geomodel representing complete site characterization can be used for various domains of advance research. The generated geomodel may be used to improve the calibration of other, numerical, hydro-geological flow models and for overall substratum structural stability analysis. High-performance foundation decision support system may be created combining the 3-D visualization, with decision analysis and artificial intelligence applications. The other geophysical data such as seismic profiles, gravity or magnetic data may be used as geometric constraints for developing a probabilistic 3-D geomodels.

References

1. Aldiss DT et al (2012) Benefits of a 3D geological model for major tunnelling works:example from Farringdon, London, UK. J Eng Geol Hydrogeol (Geological Survey of London) 45:405–414
2. Abdollahisharif J (2018) Using geostatistical simulation to determine optimal grout injection pressure in dam foundation based on geomechanical characteristics. Bull Eng Geol Environ (Springer-Verlag GmbH Germany, part of Springer Nature)
3. MacCormack KE (2005) Viewing the subsurface in three dimensions: initial results of modelling the Quaternary sedimentary infill of the Dundas Valley. Hamilton, Ontario Geosphere 1(1):23–31. https://doi.org/10.1130/GES00007.1
4. Marache A et al (2009) Geotechnical modelling at the city scale using statistical and geostatistical tools: the Pessac case. Eng Geol (Sciencedirect) 107:67–76
5. Royse KR (2008) 3D modelling and visualisation of digital geoscientific data as an aid to land-use planning in the urban environment: examples from the Thames Gateway and their limitations. In: 2nd international GSI3D conference (British Geological Survey), UK
6. Royse KR et al (2009) Property attribution of 3D geological models in the Thames Gateway, ways of visualising geoscientific information. Bull Eng Geol Environ (Springer) 1–16
7. Scott GA (1997) Foundation studies for theodore roosevelt dam. Int J Rock Mech Min Sci (Elsevier) 34(3–4). ISSN 0148-9062
8. Wakeley LD, Kelley JR (2007) Geologic conceptual model of Mosul Dam. U.S. Army Engineer Research and Development Center
9. Wakeley LD, Kelley JR (2007) Hydrogeology and 3-D visualization of dam foundations and abutments. U.S. Army Engineer Research and Development Center
10. Turrini C et al (2014) Present-day 3D structural model of the Po Valley basin, Northern Italy. Mar Pet Geol (Elsevier) 56:266–289

11. Elkadi AS et al (2002) 3D-GSIS geotechnical modelling of tunnel intersection in soft ground: Second Heinenoord Tunnel, Netherlands. Tunn Technol (Sciencedirect) 17:363–369
12. Olivier K et al (2009) 3D geological modelling from boreholes, cross-sections and geological maps, over natural gas storages in mines. Comput Geosci (Elsevier) 35:70–82
13. Kessler H et al (2008) Unlocking the potential of digital 3D geological subsurface models for geotechnical engineers. In: 2nd International GSI3D Conference (BGS) Keyworth, UK, September
14. Wycisk P et al (2009) High-resolution 3D spatial modelling of complex geological structures for an environmental risk assessment of abundant mining and industrial mega sites. Comput Geosci (Elsevier) 35:165–182
15. Ahmed AA (2007) Using lithologic modeling techniques for aquifer characterization and groundwater flow modeling of Sohag Area, Egypt. GRMENA II:355–382
16. Akiska S et al (2013) Three-dimensional subsurface modelling of mineralization: a case study from the Handeresi (Turkey) Pb-Zn-Cu deposit. J Earth Sci (Springer) 22:574–587
17. Sweetkind DS (2010) Three-dimensional geologic modelling of the Santa Rosa Plain, California. Geosphere (Geological Society of America) 6(3):237–274
18. MacCormack KE et al (2016) Using a multiple variogram approach to improve the accuracy of subsurface geological models. Can J EarthSci 1–16
19. Bairu A et al (2013) Application of vertical electrical sounding and horizontal profiling methods to decipher the subsurface stratification in River Segen Dam Site, Tigray, Northern Ethiopia. J Environ Earth Sci 3(10). ISSN 2224-3216 (Paper) ISSN 2225-0948 (Online) (IISTE)
20. Azi BJ et al (2016) Use of the electrical resistivity method in the investigation of the axis of a small Earth Dam, Angware Area, Jos Plateau, Northcentral Nigeria. Int J Curr Res 6 (05):6905–6910
21. Berhane G (2010) Geological, geophysical and engineering geological investigation of leaky Micro-dam in Northern Ethiopia. Agric Eng Int (the CIGRE journal) XII (Manuscript No. 1346)
22. Ahmed MM et al. (2012) Application of vertical electrical sounding to delineate and evaluate the hydrological conditions in Baiji—Tikrit Basin (geosp.net)
23. Di Q, Wang M (2010) Determining areas of leakage in the Da Ye Dam using multi-electrode resistivity. Bull EngGeol Environ (Springer) 69:105–109
24. Jatau BS et al (2013) The use of vertical electrical sounding (VES) for subsurface geophysical investigation around Bomo Area, Kaduna State, Nigeria. IOSR J Eng 3. https://doi.org/10.9790/3021-03141015.
25. Oluwakemi Olanike Adeoye (2011) Geoelectric investigation of Owuruwuru Dam site, Ikere Ekiti, South-western Nigeria. J Geol Min 3(12):325–340
26. Fallara F et al (2006) 3-D integrated geological modeling in the Abitibi Subprovince (Québec, Canada): techniques and applications. Explor Min Geol (GeoScienceWorld) 15(1–2):pp 27–43. https://doi.org/10.2113/gsemg.15.1-2.27
27. Gallerini G et al (2009) 3-D modelling using geognostic data: The case of the low valley of Foglia River (Italy). Comput Geosci (Elsevier) 35:146–164
28. Jones RR et al (2009) Integration of regional to outcrop digital data: 3D visualisation of multi-scale geological models. Comput Geosci (Elsevier) 35:4–18
29. Hubbard JL (2009) Use of electrical resistivity and multichannel analysis of surface wave geophysical tomography in geotechnical site characterization of Dam, Arlington
30. Marley M et al (2007) The geotectonics and geotechnics of traveston crossing dam foundation. Proc NZSOLDANCOLD Queenstown, NZ 33(1):1–9
31. Bobachev C (2002*)* IPI2Win" A windows software for an automatic interpretation of resistivity sounding data. Ph. D, Moscow State University, Moscow, Russia, p 320
32. Ramanujachary KR (2012) A monograph on geophysical techniques for groundwater exploration with special reference to resistivity techniques. Integrated geo instruments & Services Pvt. Ltd, Hyderabad. (Professional Book Publisher) ISBN 978-81-909728-2-6

33. IS:4078: 1980 (R2004) Indian standard code of practice for indexing and storage of cores (BIS).
34. IS:5313–1980 Indian standard code of guide for core drilling observations, BIS
35. IS:4464 1985 (R2004) Indian standard code of practice for the presentation of drilling information and core description in foundation Investigation, Bureau of Indian Standards
36. Singh J et al (2004) Hydrologic modelling of the Iroquois River watershed using HSPF and SWAT. ISWS. CR. Champaign, Ill.: Illinois State Water Survey
37. Kamble RK (2011) Mapping seepage in the tailrace channel, Bhama-Askhed dam: a case study. Bull Eng Geol Environ (Springer) 70:643–649
38. IS 6066: 1994 (2004) Pressure grouting of rock foundations in. River valley projects R2 (BIS)
39. Goodman RE (2013) Some safety issues for dams on rock foundations. The Manuel Rocha Centennial lecture—at LNEC, Lisbon

Comparison of Morphometric Parameters for Jonk Watershed Derived from Integrated Tool Developed in ArcGIS and QGIS Platform

Vinit Lambey, Indrajeet Sahu, and A. D. Prasad

Abstract In the present study, an automatic integrated tool has been developed for morphometric parameters using a proprietary software, Aeronautical Reconnaissance Coverage Geographical Information System (ArcGIS) developed by Environmental Systems Research Institute (ESRI) and an open-source software, Quantum Geographical Information System (QGIS). Seven morphometric parameters have been evaluated that are drainage density (DD), Compound Topographic Index (CTI), stream order, form factor, elongation ratio, circulatory ratio and Lemniscate's ratio. All parameters have been computed and compared between developed tool in ArcGIS, QGIS and a reference study. Fifteen randomly chosen points have been considered based on different elevation zones of watershed namely high elevation (HP) zone, moderate elevation (MP) zone and low elevation (LP) zone. Obtained results from both the tools show a variation in values of 2° in the slope. The average difference in slope obtained from ArcGIS tool and QGIS tool at high elevation zone is 5.32%, at moderate elevation zone is 2.72%, and at low elevation zone is 5.47%. The change in total stream length is found to be 2.56%. The average difference in drainage densities at high elevation zone is 33.79%, at moderate elevation zone is 25.86% and at low elevation zone is 16.69%. The average difference in CTI values obtained at high elevation zone is 11.61%, at moderate elevation zone is 14.75% and at low elevation zone is 13.87%. The percentage difference in elongation ratio is 14.80%, for circulatory ratio is 6.5%, for form factor is 17% and Lemniscate ratio is 0.74%, respectively. Results were compared with the reference study done on the same watershed, and it was found that for stream order, ArcGIS and QGIS tools match with the reference study. For drainage density, form factor and elongation ratio, ArcGIS tool produces better results and for circulatory ratio, QGIS tool is producing better results when compared with reference study. Although there are discrepancy in the obtained results, this method generates a reliable database of morphometric parameters and is very useful in the field of hydrology and watershed analysis.

Keywords Morphometric parameters · ArcGIS · QGIS · Reliable database

V. Lambey (✉) · I. Sahu · A. D. Prasad
Civil Engineering Department, National Institute of Technology, Raipur, India

B. Laishram and A. Tawalare (eds.), *Recent Advancements in Civil Engineering*, Lecture Notes in Civil Engineering 172,
https://doi.org/10.1007/978-981-16-4396-5_72

1 Introduction

Drainage basin evaluation is a significant source for any hydrological research as it offers data concerning the quantitative interpretation of the drainage system which is an essential stage in the characterisation of the basin [1]. Measurements of spatial characteristics, areal dimensions, channel network gradient and supporting drainage basin ground slopes are subject to morphometric analysis [2]. Morphometric analysis refers to comparatively simple methods of defining and comparing basin properties [3, 4]. For any hydrological study such as groundwater assessment and management and environmental assessment, morphometric analysis is significant [5, 6]. It is also useful in the prioritisation of the watersheds and management of natural resources [7].

Advanced technologies such as remote sensing (RS) coupled with geoinformatics has been verified to be an effective method for water resource management and water drainage planning [8–10]. Geoinformatics techniques are also used to analyse morphometric management of watershed-scale hydrological response. Such an evaluation is critical in the planning and management of the basins [4, 11–14]. Many researchers have carried out work in this field using open-source GIS tool with the integration of remote sensing [15, 16]. The main work has been done by [17] by developing a GIS-based automated tool for morphometry analysis of basin. It directly provides the stream network and other morphometric parameters on a single click. Based on this study, Ref. [4] performed the morphometric analysis on the Narmada basin.

Geoinformatics plays a significant role in study of morphometry in designing and development of hydraulic structures. Using traditional methods such as field observation and topographical maps, the identification of drainage networks in a basin can be achieved alternatively by advanced methods such as remote sensing and extraction from digital elevation models [18–21]. However, it requires step-by-step method without any flaw to carry out the evaluation. Various sources are available for deriving the morphometric parameters. The available tools make the processing tedious job which involves various sources. It gives strain to system and also increases chances of human error. To overcome this task, an integrated tool has been developed in ArcGIS and QGIS environment to identify the drainage networks with the help of digital elevation model (DEM) which is an input parameter for basin demarcation and additional supportive data for morphometric analysis.

The principal aim of this study is to develop an automated tool for deriving morphometric parameters using both proprietary and open-source GIS software. The developed tool has been tested over the Jonk river sub-basin, and the model-based data were found to be accurate for further morphometric investigation. Results from both the software have been compared to know which one gives the best parameter results. The morphometric parameters are extracted for Jonk river sub-basin. For describing drainage basin processes, the measured outputs are represented as maps and analysed using GIS with numerical formulas. The results

obtained by studying the drainage basin provide data for a better assimilation of the hydrological properties of the watershed region and are also very important in interpreting the influence of morphometry on hydrology. As per the literature review done for this study, there is no tool developed in the QGIS environment for the morphometric analysis. In this study, evaluation of some extra morphometric parameters using developed tool has also been added which is not available in the previous studies.

2 Study Area and Methodology

2.1 Study Area

The Jonk watershed is selected as study area which lies between geographic latitude 20° 28′ and 21° 44′ N and longitudes 82° 20′ and 83° 00′ E. The Jonk River arises from Nuapada in Orissa at an altitude of 700 m from MSL. It joins with Mahanadi at Seorinarayan in Chhattisgarh which is situated at upstream of Hirakud Dam and has 3424 km^2 of drainage area. Hot summer dominates the climatic condition of the area except during the south-western monsoon. During the monsoon, the watershed receives about 90% of the rainfall that is effective from mid-June to the end of September. The maximum and minimum temperature is 43 °C and 10 °C, respectively. The drainage area has the gneiss rock formation. The sub-basin consists of multiple thicknesses of sedimentary formation. Figure 1 shows the location map of study area.

2.2 Methodology

The morphometric study of the Jonk basin is accomplished using integrated tool developed in ArcGIS and QGIS environment. The main remotely sensed data used in the study is digital elevation model (DEM). Calculation of parameters like slope, Compound Topographic Index, drainage density and stream order generation has been done using integrated tool. The methodology is given in Fig. 2.

For comparison of developed tool in ArcGIS and QGIS, different points have been considered based on different elevation zones of watershed. The DEM of Jonk watershed has the lowest and highest value of 217 m and 867 m, respectively. Here, the elevation zone is mainly divided into three major parts, i.e. low elevation zone (217–342 m), moderate elevation zone (342–520 m) and high elevation zone (520–867 m). The classification is done in the GIS software and method of classification is based on natural breaks method available in GIS software. In total, 15 points have been considered on the study area, i.e. 5 points each for each elevation zone. Points at high elevation zone are abbreviated as HP. Similarly, for moderate

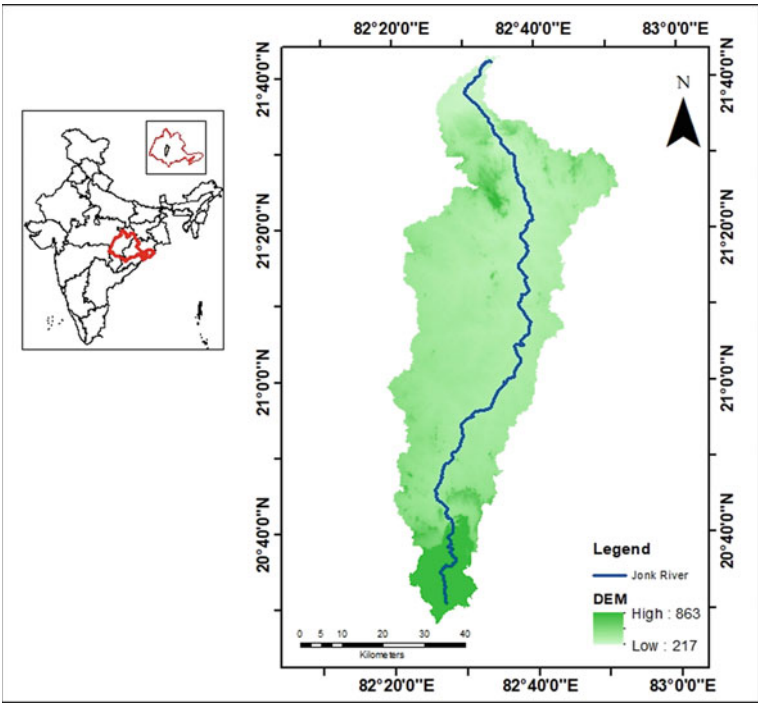

Fig. 1 Study area

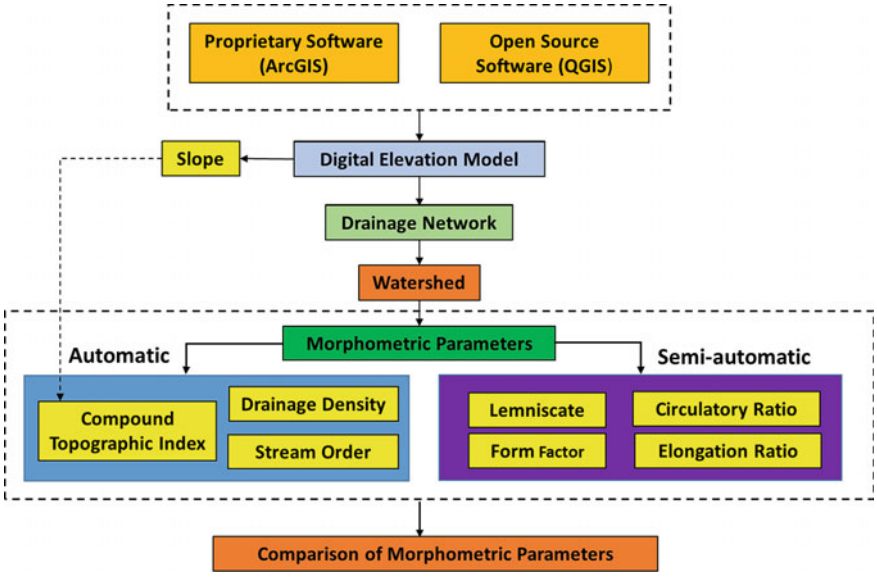

Fig. 2 Methodology

elevation and low elevation zone, points are abbreviated as MP and LP, respectively. Out of five points of high elevation zone considered as HP1 to HP5, two points (HP and HP5) are considered on the boundary of high elevation zone and moderate elevation zone, while the remaining three points (HP2, HP3, HP4) are considered inside the high elevation zone. In case of moderate elevation zone, three points are considered inside the mentioned zone (MP1, MP2, MP5) while one point (MP4) is considered on the boundary of moderate elevation zone and low elevation zone, and the remaining one point (MP3) is considered on the boundary of watershed. For low elevation zone, four points (LP1, LP2, LP3 and LP5) are considered inside the low elevation zone while 1 point (LP4) is considered on the watershed boundary. The location points on the DEM of watershed is shown in Fig. 3.

2.3 Integrated Tools

A GIS-based tool has been developed on the basis of methodology adopted by [17]. The model input parameters which are user defined are DEM, watershed outlet shape file and number of cells to define stream. Also, the location path for the resultant output parameters has to be given by the user.

Projected DEM is the first and the primary input to the model. Fill tool is used to process the DEM which eliminates the gaps that have occurred during process of DEM formation. The processed DEM is the input to the flow direction tool. This tool measures the direction of water flowing out of the pixel. It follows the eight direction (D8) rule which was coined by [21]. The output of flow direction acts as an input to flow accumulation tool. By applying the condition of number of cells required for stream development, streams have been developed and segmented. This output data is input to stream order tool which follows Strahler's method. The resultant data obtained from this process is converted to polylines (vector file). Line density tool is applied to the resultant stream network shapefile to create drainage density raster. Field geometry option in the attribute table has been used to calculate stream length of each stream order. Figure 4a, b shows the graphical user interface (GUI) for the developed model in ArcGIS and QGIS, respectively.

3 Results and Discussions

The morphometric parameters derived from automated tool developed in both ArcGIS and QGIS environment for Jonk watershed have been studied and compared are discussed below. Although slope is not a morphometric parameter, it has been discussed here due to the change in its values obtained from developed tool.

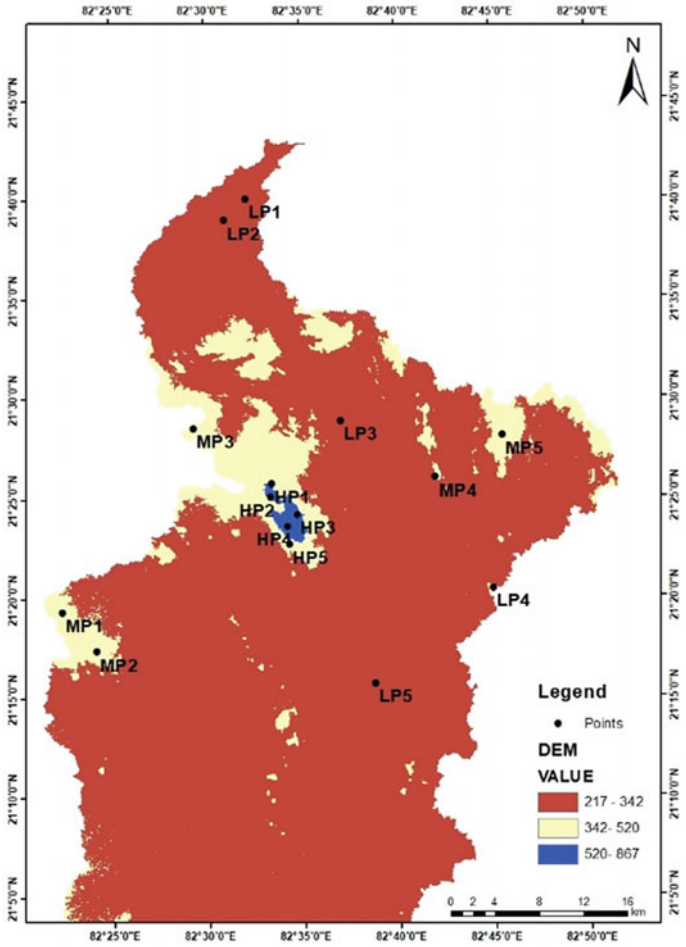

Fig. 3 Location of points considered for comparison of parameter values obtained from ArcGIS and QGIS tool

Figure 4a, b shows the maps of slope, drainage density and Compound Topographic Index (CTI) obtained from ArcGIS and QGIS developed model, respectively.

3.1 Slope

Slope shows the rate of change of elevation. Areas having steeper slope (>30°) are less susceptible to water storage area, while areas having gentle slope (<12°) are having more water storage area. The slope value varies from 0° to 58° as obtained

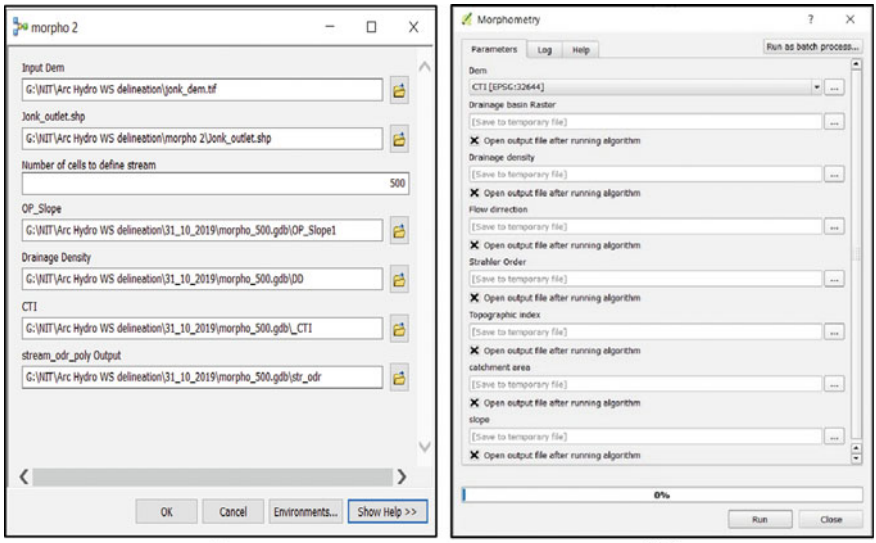

Fig. 4 GUI for morphometry model developed in **a** ArcGIS, **b** QGIS

from automated tool developed in ArcGIS while it varies from 0° to 56° in QGIS developed tool. At plain area, the slope value obtained is 0° in both the tools, but for the hilly areas, the slope difference of 2° has been observed. Figure 5a shows the slope map obtained from ArcGIS tool and Fig. 5b shows the slope map obtained from QGIS tool. The values of slope at considered 15 points are shown in Table 1. The average difference in slope values obtained from ArcGIS tool and QGIS tool at high elevation zone is 5.32%, at moderate elevation zone is 2.38% and at low elevation zone is 5.47%.

3.2 Drainage Density (DD)

As per Reference [22], drainage density is the length of the stream in the basin or watershed area per unit area. It is defined as the ratio of the total length of the stream segment of all order in a basin to the basin area exhibited in km/km^2 and is expressed as shown in Eq. (1). There are five classes of drainage density with the following value ranges (km/km^2), i.e. very coarse (<2), coarse (2–4), moderate (4–6), fine (6–8), and very fine (>8) [23]. The drainage density shows that how closed are the streams spaced from each other.

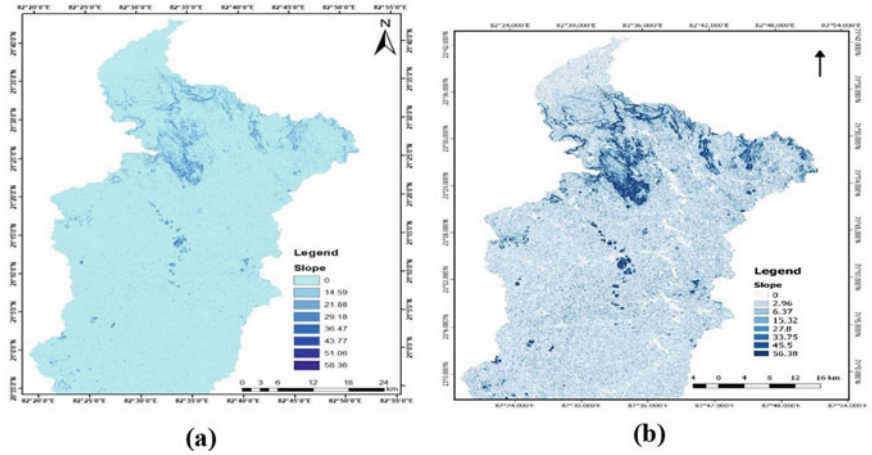

Fig. 5 Slope map obtained from **a** ArcGIS tool, **b** QGIS tool

Table 1 Comparison of slope

Location	ArcGIS	QGIS	% difference
HP1	9.37	8.79	10.76
HP2	25.94	25.46	1.86
HP3	31.45	30.98	1.50
HP4	2.89	2.55	12.5
HP5	18.29	18.29	0
Average	17.58	17.21	5.32
MP1	13.72	13.34	2.80
MP2	24.73	23.99	3.03
MP3	27.21	26.65	2.07
MP4	14.22	13.82	2.85
MP5	32.06	31.69	1.16
Average	22.38	21.89	2.38
LP1	6.78	6.48	4.52
LP2	20.03	20.03	0
LP3	5.21	4.29	19.36
LP4	15.32	15.09	1.51
LP5	25.89	25.38	1.98
Average	14.64	14.25	5.47

$$D_d = \frac{L_s}{A} \quad (1)$$

where L_s is the total length of stream and A is the area of watershed in km^2.

The drainage density value obtained from ArcGIS tool ranges from 0.71 to 2.28 which falls under range (<2 and 2–4) represents the coarse and very coarse class, while value obtained from QGIS tool varies from 0.44 to 1.81 and comes under range (<2) represents very coarse class. The percentage variation in the value obtained at considered points from both the tools is shown in Table 2. The average difference in drainage density values obtained from ArcGIS tool and QGIS tool at high elevation zone is 33.79%, at moderate elevation zone is 25.86% and at low elevation zone is 16.69%. This variation is due to the change in watershed area and stream length obtained from ArcGIS and QGIS tool. Figure 6a, b shows the drainage density obtained from ArcGIS tool and QGIS tool, respectively.

3.3 Stream Order

Stream order means the level of branching within a river system. Stream ordering is the fundamental step of river basin study. Reference [22] initially promoted the stream ordering systems, but [24] anticipated this ordering system with some

Table 2 Comparison of drainage density

Location	ArcGIS	QGIS	% difference
HP1	0.86	0.61	34.01
HP2	0.76	0.54	33.84
HP3	0.72	0.49	38.01
HP4	0.87	0.63	32.00
HP5	0.78	0.57	31.11
Average	0.79	0.56	33.79
MP1	0.86	0.61	34.01
MP2	0.78	0.57	31.11
MP3	0.98	0.86	13.04
MP4	0.96	0.83	14.52
MP5	0.71	0.49	36.66
Average	0.85	0.67	25.86
LP1	1.34	1.23	8.56
LP2	1.63	1.57	3.75
LP3	2.00	1.86	7.25
LP4	0.76	0.54	33.84
LP5	0.88	0.65	30.06
Average	1.32	1.17	16.69

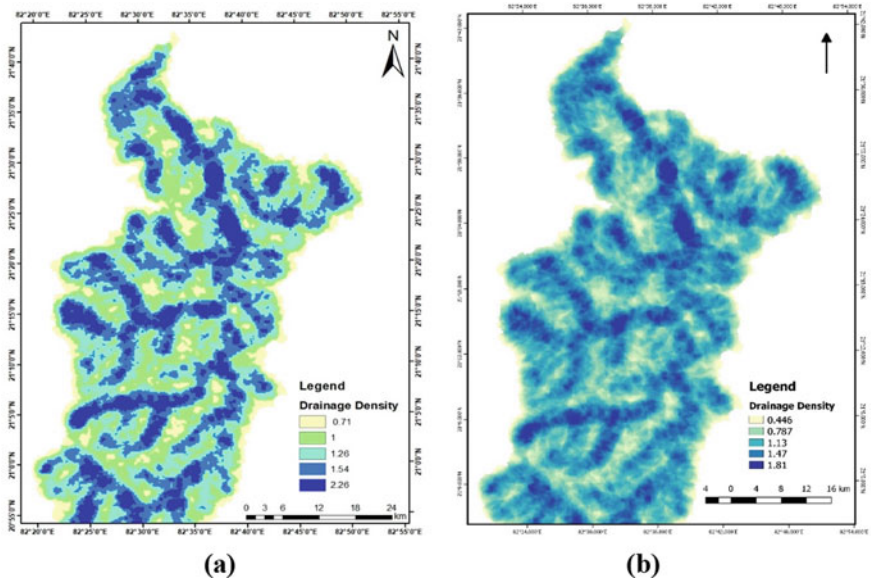

Fig. 6 Drainage density obtained from **a** ArcGIS tool, **b** QGIS tool

modifications. The stream order number details are useful when connecting to the size of its contributing basin and based on a hierarchical ranking of streams [25]. In both the tools, i.e. in ArcGIS and QGIS, stream order is found using Strahler method, and it has been observed that the Jonk watershed has 6th order of stream. It has been obtained by providing threshold value of minimum cells to define a stream as 500. Stream length of all orders has also been compared, and it was found that the stream length obtained from ArcGIS tool is more than values obtained from QGIS tool as shown in Table 3. Figure 7a depicts the stream order obtained from

Table 3 Comparison of stream length of different orders

Stream order	Stream length (km)		% difference
	ArcGIS	QGIS	
1st	2029	2053	(−)1.17
2nd	1091	1024	6.33
3rd	479	432	10.31
4th	214	236	(−)9.77
5th	102	89	13.61
6th	126	106	17.24
Total	4044	3942	2.56

Note Negative sign in some values is due to the following formula used for calculation of percentage difference

percentage = $\left(\frac{|ArcGIS-QGIS|}{\frac{ArcGIS+QGIS}{2}}\right) * 100$. Where some values obtained from ArcGIS tool are less than QGIS tool

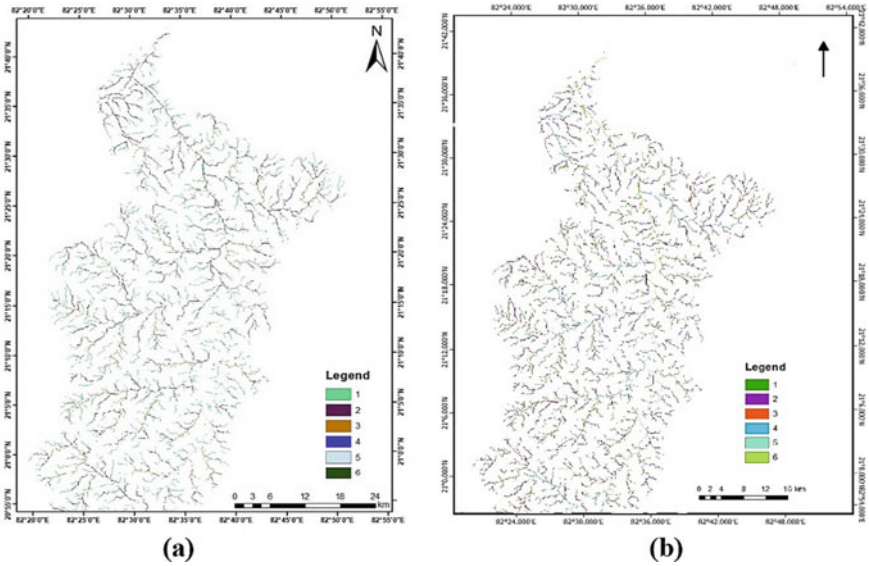

Fig. 7 Stream order obtained from **a** ArcGIS tool, **b** QGIS tool

ArcGIS tool, and Fig. 7b depicts the stream order obtained from QGIS tool. The change in total stream length is found to be 2.56%.

3.4 Compound Topographic Index (CTI)

Compound Topographic Index is widely used to measure hydrological procedures. It describes the tendency of terrain to accumulate water. The Compound Topographic Index (CTI) is also referred to as the Topographic Moisture Index. It is defined as a ratio of the slope to the catchment area.

$$\mathrm{CTI} = l\left(\frac{A}{\tan\beta}\right) \tag{2}$$

where A is the area of watershed and β is the slope angle.

The CTI value obtained from ArcGIS tool ranges from 4.4 to 16.39, while value obtained from QGIS tool varies from 3.25 to 11.10. The percentage variation in the value obtained at considered points from both the tools is shown in Table 4. The average difference in CTI values obtained from ArcGIS tool and QGIS tool at high elevation zone is 11.61%, at moderate elevation zone is 14.75% and at low elevation zone is 13.87%. The variation in the values obtained is due to the change in values of slope and area obtained from ArcGIS and QGIS tool. Figure 8a shows the

Table 4 Comparison of CTI

Location	ArcGIS	QGIS	% difference
HP1	6.96	6.15	12.35
HP2	7.78	6.96	11.12
HP3	7.66	6.79	12.04
HP4	6.74	5.98	11.94
HP5	8.13	7.31	10.62
Average	7.45	6.63	11.61
MP1	7.19	6.07	16.89
MP2	7.90	7.01	11.93
MP3	5.23	4.44	16.33
MP4	5.48	4.65	16.38
MP5	7.63	6.75	12.23
Average	6.68	5.78	14.75
LP1	4.74	3.99	17.18
LP2	4.86	4.10	16.96
LP3	5.40	4.54	17.30
LP4	8.04	7.37	8.69
LP5	8.73	7.96	9.22
Average	6.35	5.59	13.87

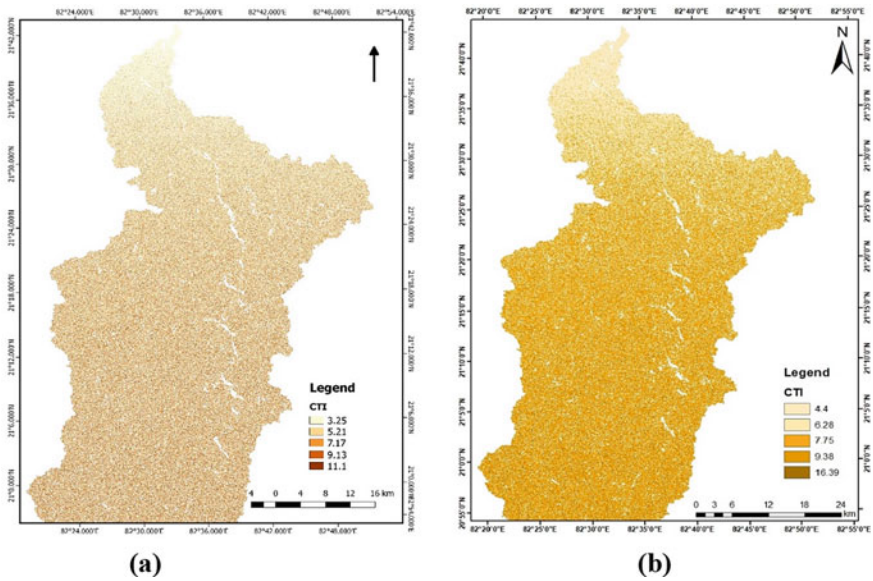

Fig. 8 CTI obtained from **a** ArcGIS tool, **b** QGIS tool

Compound Topographic Index obtained from ArcGIS tool, and Fig. 8b shows the Compound Topographic Index obtained from QGIS tool.

3.5 Elongation Ratio

Reference [26] defined the elongation ratio as the diameter ratio between a circle of the same area as the basin and the total length of the basin. This proportion covers a wide range of climatic and geological forms from 0.6 to 1.0. Reference [24] classified the different watershed slopes using the different Elongation Ratio Index as circular (0.9–0.10), oval (0.8–0.9), less elongated (0.7–0.8) and elongated (<0.5). It is computed as,

$$R_e = \left(\frac{2}{L_b}\right) * \sqrt{\frac{A}{\Pi}} \tag{3}$$

where L_b is the length of basin in km, A is the area of watershed km^2.

The computed value from integrated model is found to be 0.486 from ArcGIS tool and 0.419 from QGIS tool which shows steep slope, high relief and elongated. The percentage difference in values obtained from ArcGIS and QGIS tool is 14.80% as given in Table 5.

3.6 Circulatory Ratio

As per References [1] and [27], circulatory ratio is the ratio of watershed area to the area of a circle having the circumference equal to perimeter of watershed. Reference [27] defined the circulatory ratio basin ranging from 0.40 to 0.50, suggesting highly elongated and highly pervious homogeneous geological materials. The ratio is calculated as,

$$R_c = 12.57 * \left(\frac{A}{P^2}\right) \tag{4}$$

where A is the area of watershed km^2, P is the perimeter of the watershed in km.

The circulatory ratio of the Jonk basin is 0.088 from ArcGIS tool and 0.094 from QGIS tool which designates that the watershed is elongated in shape and is highly permeable. Table 6 shows the percentage difference in values obtained from ArcGIS and QGIS tool.

Table 5 Comparison of elongation ratio

Parameter	ArcGIS	QGIS	% difference
Elongation ratio	0.486	0.419	14.80

Table 6 Comparison of Circulatory ratio

Parameter	ArcGIS	QGIS	% difference
Circulatory ratio	0.088	0.094	(−) 6.5

Note Negative sign in some values is due to the following formula used for calculation of percentage difference percentage = $\left(\frac{|ArcGIS-QGIS|}{\frac{ArcGIS+QGIS}{2}}\right) * 100$. Where some values obtained from ArcGIS tool are less than QGIS tool

3.7 Form Factor

Form factor is defined as the ratio of basin area to square of the basin length. The smaller the form factor value, the more elongated will be the watershed. Form factor of Jonk watershed as obtained from ArcGIS and QGIS is 0.0185 and 0.0156, respectively. The percentage difference in values obtained from ArcGIS and QGIS tool is 17% as given in Table 7. This value indicates the high elongated shape of the watershed. Equation (5) shows the formula for estimating form factor.

$$F_{\mathrm{f}} = \frac{A}{L_{\mathrm{b}}^2} \tag{5}$$

3.8 Lemniscate's (k) Ratio

Lemniscate's value computes the slope of the basin as stated by [28]. A basin is circular when $k = 1$, and becomes more elongate as k increases. Equation (6) shows the formula for Lemniscate. In present study, Jonk watershed is found to be more elongated as the value obtained from integrated tool is 1.346 for ArcGIS and 1.336 for QGIS. Table 8 depicts the percentage difference in values obtained from ArcGIS and QGIS tool.

$$k = \frac{L_{\mathrm{b}}^2}{4A} \tag{6}$$

Table 7 Comparison of form factor

Parameter	ArcGIS	QGIS	% difference
Form factor	0.0185	0.0156	17.00

Table 8 Comparison of Lemniscate's ratio

Parameter	ArcGIS	QGIS	% difference
Lemniscate's ratio	1.346	1.336	0.74

Table 9 Comparison of obtained parameters with the reference study

Parameters	Value or range obtained from		Value or range obtained from reference study [29]	% difference		Remarks
	ArcGIS tool	QGIS tool		Between ArcGIS tool and reference study	Between QGIS tool and reference study	
Stream order	6	6	6	0	0	The stream order found from developed tool of ArcGIS and QGIS matches with the stream order of reference study
Drainage density	0.71–2.18	0.44–1.81	0.728–0.859	(−)1.39–87.78	(−) 48.27–72.18	The values obtained from the ArcGIS tool is giving nearby values when compared with reference study
Elongation ratio	0.486	0.419	0.446–0.865	8.58–(−) 56.10	(−)6.24–(−)69.47	Compared with reference study, the ArcGIS tool gives nearby values
Circulatory ratio	0.088	0.094	0.101–0.230	(−) 13.75–(−)89.30	(−)7.17–(−)83.95	QGIS tool gives nearby values when compared with reference study
Form factor	0.0185	0.0156	0.156–0.587	(−) 157.59–(−) 187.77	(−) 163.63–(−) 189.64	ArcGIS tool gives nearby values when compared with reference study

Note Current study has been done on the whole watershed as one unit but in the reference study, the watershed has been divided into nine sub watershed

For validation purpose, the parameters values obtained from the present study has been compared with the study done by [29] on the same watershed. The comparison of the parameters is shown in Table 9.

4 Conclusion

Automatic extraction of morphometric parameters derived from developed integrated tool using ArcGIS and QGIS has demonstrated its efficiency for sub-basin analysis, although there is a minor difference in the values obtained from the both

the tools. Seven morphometric parameters have been evaluated that are drainage density (DD), Compound Topographic Index (CTI), stream order, form factor, elongation ratio, circulatory ratio and Lemniscate's ratio. All parameters have been computed and compared between developed tool in ArcGIS, QGIS and a reference study. Fifteen randomly chosen points have been considered based on different elevation zone of watershed namely high elevation (HP) zone, moderate elevation (MP) zone and low elevation (LP) zone. Obtained results from both the tools shows a variation in values of 2° in the slope. The average difference in slope obtained from ArcGIS tool and QGIS tool at high elevation zone is 5.32%, at moderate elevation zone is 2.72% and at low elevation zone is 5.47%. The change in total stream length is found to be 2.56%. The average difference in drainage density at high elevation zone is 33.79%, at moderate elevation zone is 25.86 % and at low elevation zone is 16.69%. The average difference in CTI values obtained at high elevation zone is 11.61%, at moderate elevation zone is 14.75% and at low elevation zone is 13.87%. The percentage difference in elongation ratio is 14.80%, for circulatory ratio is 6.5%. For form factor is 17% and Lemniscate ratio is 0.74%, respectively. Results were compared with the reference study done on the same watershed and it was found that for stream order, ArcGIS and QGIS tools matches with the reference study. For drainage density, form factor and elongation ratio, ArcGIS tool produces better results and for circulatory ratio, QGIS tool is producing better results when compared with reference study.

References

1. Strahler AN (1964) Part II. Quantitative geomorphology of drainage basins and channel networks. Handbook of applied hydrology. McGraw-Hill, New York, pp 4–39
2. Nautiyal MD (1994) Morphometric analysis of a drainage basin using aerial photographs: a case study of Khairkuli basin, district Dehradun, UP. J Indian Soc Remote Sens 22(4):251–261
3. Rai PK, Mohan K, Mishra S, Ahmad A, Mishra VN (2017) A GIS-based approach in drainage morphometric analysis of Kanhar River Basin, India. Appl Water Sci 7(1):217–232
4. Rai PK, Mishra VN, Mohan K (2017) A study of morphometric evaluation of the Son basin, India using geospatial approach. Remote Sens Appl Soc Environ 7:9–20
5. Magesh NS, Jitheshlal KV, Chandrasekar N, Jini KV (2013) Geographical information system-based morphometric analysis of Bharathapuzha river basin, Kerala, India. Appl Water Sci 3(2):467–477
6. Prakash K, Rawat D, Singh S, Chaubey K, Kanhaiya S, Mohanty T (2019) Morphometric analysis using SRTM and GIS in synergy with depiction: a case study of the Karmanasa River basin, North Central India. Appl Water Sci 9(1):13
7. Jasmin I, Mallikarjuna P (2013) Morphometric analysis of Araniar river basin using remote sensing and geographical information system in the assessment of groundwater potential. Arab J Geosci 6(10):3683–3692
8. Javed A, Khanday MY, Ahmed R (2009) Prioritization of sub-watersheds based on morphometric and land use analysis using remote sensing and GIS techniques. J Indian Soc Remote Sens 37(2):261

9. Pankaj A, Kumar P (2009) GIS-based morphometric analysis of five major sub-watersheds of Song River, Dehradun District, Uttarakhand with special reference to landslide incidences. J Indian Soc Remote Sens 37(1):157–166
10. Samal DR, Gedam SS, Nagarajan R (2015) GIS based drainage morphometry and its influence on hydrology in parts of Western Ghats region, Maharashtra, India. Geocarto Int 30 (7):755–778
11. Thomas J, Prasannakumar V (2015) Comparison of basin morphometry derived from topographic maps, ASTER and SRTM DEMs: an example from Kerala, India. Geocarto Int 30(3):346–364
12. Das S, Pardeshi SD (2018) Morphometric analysis of Vaitarna and Ulhas river basins, Maharashtra, India: using geospatial techniques. Appl Water Sci 8(6):158
13. Kadam AK, Jaweed TH, Kale SS, Umrikar BN, Sankhua RN (2019) Identification of erosion-prone areas using modified morphometric prioritization method and sediment production rate: a remote sensing and GIS approach. Geomat Nat Haz Risk 10(1):986–1006
14. Parupalli S, Padma-Kumari K, Ganapuram S (2019) Assessment and planning for integrated river basin management using remote sensing, SWAT model and morphometric analysis (case study: Kaddam river basin, India). Geocarto Int 34(12):1332–1362
15. Chandra V, Gidde MR (2019) Morphometric analysis of Balitra watershed using QGIS platform. Int J Recent Technol Eng 8(2)
16. Bera A, Mukhopadhyay BP, Das D (2018) Morphometric analysis of Adula River Basin in Maharashtra, India using GIS and remote sensing techniques. Geo-spatial data in natural resources, pp 13–35
17. Magesh NS, Ch N (2012) A GIS based automated extraction tool for the analysis of basin morphometry. Bonfring Int J Ind Eng Manag Sci 2(Special Issue Special Issue on Geospatial Technology Development in Natural Resource and Disaster Management):32–35
18. Verstappen HT (1983) Applied geomorphology: geomorphological surveys for environmental development (No. 551.4 VER)
19. Maidment DR, Morehouse S (2002) Arc Hydro: GIS for water resources. ESRI, Inc
20. Magesh NS, Chandrasekar N, Soundranayagam JP (2011) Morphometric evaluation of Papanasam and Manimuthar watersheds, parts of Western Ghats, Tirunelveli district, Tamil Nadu, India: a GIS approach. Environ Earth Sci 64(2):373–381
21. Fairfield J, Leymarie P (1991) Drainage networks from grid digital elevation models. Water Resour Res 27(5):709–717
22. Horton RE (1945) Erosional development of streams and their drainage basins; hydrophysical approach to quantitative morphology. Geol Soc Am Bull 56(3):275–370
23. Sukristiyanti S, Maria R, Lestiana H (2018) February. Watershed-based morphometric analysis: a review. In: IOP conference series: earth and environmental science, vol 118, pp 12–28. IOP Publishing
24. Strahler AN (1952) Hypsometric (area-altitude) analysis of erosional topography. Geol Soc Am Bull 63(11):1117–1142
25. Singh P, Thakur JK, Singh UC (2013) Morphometric analysis of Morar River Basin, Madhya Pradesh, India, using remote sensing and GIS techniques. Environ Earth Sci 68(7):1967–1977
26. Schumm SA (1956) Evolution of drainage systems and slopes in badlands at Perth Amboy, New Jersey. Geol Soc Am Bull 67(5):597–646
27. Miller VC (1953) Quantitative geomorphic study of drainage basin characteristics in the Clinch Mountain area, Virginia and Tennessee. Technical report (Columbia University. Department of Geology); no. 3
28. Chorley RJ, Malm DE, Pogorzelski HA (1957) A new standard for estimating drainage basin shape. Am J Sci 255(2):138–141
29. Gunjan P, Mishra SK, Lohani AK, Chandniha SK (2020) The study of morphological characteristics for best management practices over the Rampur watershed of Mahanadi River Basin using prioritization. J Indian Soc Remote Sens 48(1):35–45

Generation of Thematic Layers for Flood Hazard Zonation Along the Banks of Koyna River Near Patan

Gaurav Sanjay Ghare, Purushottam Kashinath Deshpande, and Abhijeet Arun Bhondwe

Abstract Floods are the most frequent and devastating natural hazards. Floods tend to cause large-scale loss of human life and extensive damage to property. Flood hazard mapping is a critical component of effective land use planning in flood-prone areas. This allows the development of charts and maps that help recognize areas of risk and offer priority to mitigation and response efforts. The objective of this study is to generate a flood hazard zonation map for part of Koyna River along Patan town, Dist. Satara, Maharashtra, India. High-resolution remote sensing images from Google Earth imagery and IRS–1D satellites are combined with hydraulic analysis of ASTER DEM to derive layers in ILWIS software developed by ITC, Netherlands. These layers were used to identify the flood-susceptible area of the study area. The flood hazard map developed can be further used for vulnerability and mitigation studies.

Keywords Geographic information system GIS · Aster DEM · Google Earth imagery · ILWIS · Flood hazard mapping

1 Introduction

Floods are one of the most destructive of natural disasters. In addition to the loss of precious human and animal life, floods lead to devastation of crops, dwellings and public services. Flooding can occur as a result of heavy precipitation, combined

G. S. Ghare
Gajanan Housing Society (East), Vidyanagar, Karad, Satara, Maharashtra, India

P. K. Deshpande
Department of Civil Engineering, Walchand College of Engineering, Vishrambag, Sangli, Maharashtra, India
e-mail: purushottam.deshpande@walchandsangli.ac.in

A. A. Bhondwe (✉)
Department of Civil Engineering, Government College of Engineering, Karad, Satara, Maharashtra, India

B. Laishram and A. Tawalare (eds.), *Recent Advancements in Civil Engineering*, Lecture Notes in Civil Engineering 172,
https://doi.org/10.1007/978-981-16-4396-5_73

with inadequate channel capacity, or as a result of obstruction in the river bed. Extreme floods occur almost every year in one or more regions of India.

It has been experienced that the best way of flood management is a combination of various measures. First, preventive measures and, subsequently, necessary damage mitigation measures must be taken together through a combination of structural and non-structural measures.

The remote sensing satellites are capable of providing coverage of very large areas at regular interval and with quick turnaround time. We have extensive, synoptic and multi-temporal coverage of wide areas in real-time and at regular intervals. This has made them important for the continuous monitoring of flood-related atmospheric and surface parameters. Geographic information is contained in a geographical information system (GIS) database that can be queried and graphically represented for analysis. Through overlaying or intersecting various geographical layers, flood-prone areas can be identified and targeted for mitigation and implementation of flood-prone management practices [1].

Flood maps are used for many purposes. The primary flood maps are used to assess flood insurance costs, construction guidelines and flood preparedness for those at risk. Government authorities use them to establish zoning, land use and construction standards; flood warning, evacuation and emergency response planning; and to anticipate and respond to floods. Maps do not prevent floods from occurring, but they are an essential tool in avoiding or minimizing the damage to property and loss of life caused by floods, and for communicating flood risk.

In the creation of quality flood hazard data, high-quality topographic information is essential. From Advanced Spaceborne Thermal Emission and Reflection Radiometer (ASTER), commonly known as the Global Digital Elevation Model (GDEM), the degree tile of the GDEM was obtained. It was developed jointly by the Ministry of Economy, Trade, and Industry (METI) of Japan and the National Aeronautics and Space Administration (NASA) of the United States of America. This elevation dataset has multiple uses, and associated costs are avoided since this data are available freely on internet [2].

2 Study Area Location

Koyna River is a fifth-order perennial stream basin which is about 119 km in length. The basin is developed in the uppermost reaches of the drainage system of Krishna river, in Satara district of Maharashtra and is included within the survey of India topographic sheet number 47G/11 on the scale of 1 Inch: 1 Mile. The study area is lying between the latitudes 73° 53′ 1.23″ E, 73° 54′ 40.32″ E and the longitudes 17° 23′ 00.2″ N, 17° 21′ 49.5″ N. Koyna River receives its water from the catchment of Koyna Dam built at Deshmukhwadi, Tal.-Patan, Dist.-Satara and its tributaries Kera, Morna and Wang. Also from the Sahyadri ranges, on both sides of Koyna River drains an area of about 891 km^2. The area under study experiences

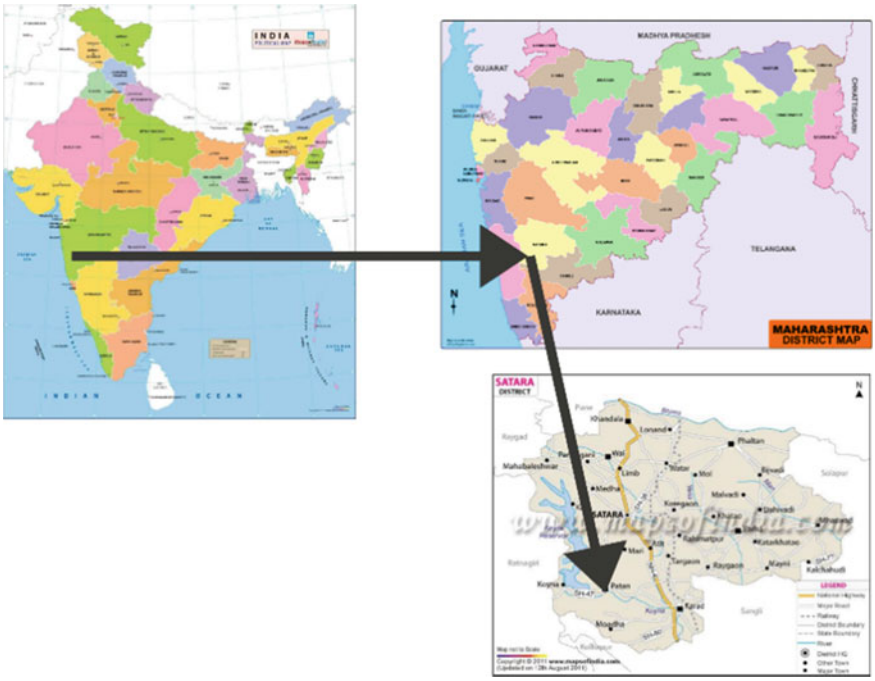

Fig. 1 Location of study area

semiarid to sub-humid climate. During the period from June to October it receives heavy rainfall, the annual rainfall being in excess of 2000 mm in Patan Tehsil. The summer is dry with maximum temperature reading from 38 to 40 °C [3] (Fig. 1).

3 Objectives

The objective of this study is to generate a flood hazard zonation map for part of Koyna River along Patan town, Dist. Satara, Maharashtra, India. The present study deals with the observation, analysis and interpretations of remote sensing data, ASTER DEM, IRS–1D panchromatic (PAN) data, Google Earth imagery and various GIS layer outputs derived from it. Flood hazard zonation map has been generated in GIS environment. High-resolution colour composite from Google Earth imagery data has also been imported and geo-referenced. The observations at the site made during the ground truth finding field visit were correlated with the GIS data layers. The interpretative outcome can be brainstormed and remedial measures based on them may further be designed.

4 Methodology

4.1 Standard FCC of Study Area

The high-resolution satellite data of the study area, near Patan, were collected from Google Earth satellite imagery. Google Earth imagery has good discrimination capacity for different land cover types or individual objects. This data were imported in ILWIS software via geo-gateway. The further generated raster maps were glued, and standard colour composite was made by assigning red, green and blue bands to final raster map. For further analysis, this high-resolution map was geo-referenced, and new coordinate system was generated.

4.2 Base Map

Land surface reference information describing streams, roads, buildings, settlements, agricultural land and administrative boundaries was digitized. These vector layers with high-resolution satellite data of a study area make a base map that shows the background context for mapping the flood hazard zone.

4.3 Interpolated Flood Level Map

Digital elevation model and IRS–1D PAN data procured from NRSC Hyderabad were used for the analysis. The mid-section of the stream was taken as datum and digitized with the value "zero" in value domain. Perpendiculars were drawn to the datum level. The text of available DEM was enabled to get reduced level at any point. By adding 5 m to the datum, 5 m level segment was created in value domain. Similarly, 10 and 15 m levels were extracted.

These vector layers were added on DEM of the study area, and contour interpolation operation was done at 0.1 m precision [4]. This led to the development of flood inundation map.

Geo-coded and geo-referenced high-resolution satellite data were overlaid on flood discharge model. The flood level value in metres for which a point on the ground shall be inundated can be displayed with a single click at the corresponding point on the imagery.

4.4 Flood Hazard Zonation Map (in Terms of Flood Levels in Metres)

Flood level map was analysed for settlement vulnerability. The area above the 1.9 m level where structures go under inundation is considered to be vulnerable and the rest as non-vulnerable. The area above 1.9 m is divided into three zones according to risk to structures. Finally, the slicing operation was done to generate the flood hazard zonation map layer.

This map can be easily used for the zonation of flood level. Here, in the present study, the flood inundation model has been sliced into three flood hazard zones. These layers along the interpretative aspect of the satellite data can be used for the assessment of the degree of hazard and vulnerability condition along both the banks of Koyna River [5].

5 Interpretation and Analysis of GIS Layers

5.1 Standard FCC of High-Resolution Map of Study Area

Here, we can see the stretch of study area—Patan Town. This map is a result of putting red, green, blue band images together in one colour composite. This map can give a better visual impression of the reality on the ground, than by displaying one band at a time. The spatial resolution of data is 0.125 m. It serves as a base map for different map generations. A colour composite was created to serve as a background image during sampling and subsequent image classification and for visual interpretation purposes, a printed colour composite may be useful as a field map, but you can also use a colour composite as a background image during on-screen digitizing [6] (Fig. 2).

5.2 IRS–1D PAN Data

IRS–1D panchromatic data were used to extract a sub-map around Koyna River at Patan. The 5.6 m single band data were stretched so as to highlight the water bodies, agriculture and forest, hilly area, plateau and drainage with 8-bit radiometric resolution. It has been observed that Koyna River, flowing east to west is confluences by Kera River from North near Patan and Morna River from South. A particular stretch ending near Kera confluence has been selected for mapping the flood mapping. The main stretch of Koyna, bound by high reliefs of Deccan trap hills, was digitized to develop mainstream vector. The moderately dark tone agriculture and the settlement patterns of Patan are seen on the image. The brighter tone of the hill slopes indicates barren land and lateritic plagues. The darker tones near the Koyna and Morna-Gureghar water bodies indicate dense forest of Western Ghats (Fig. 3).

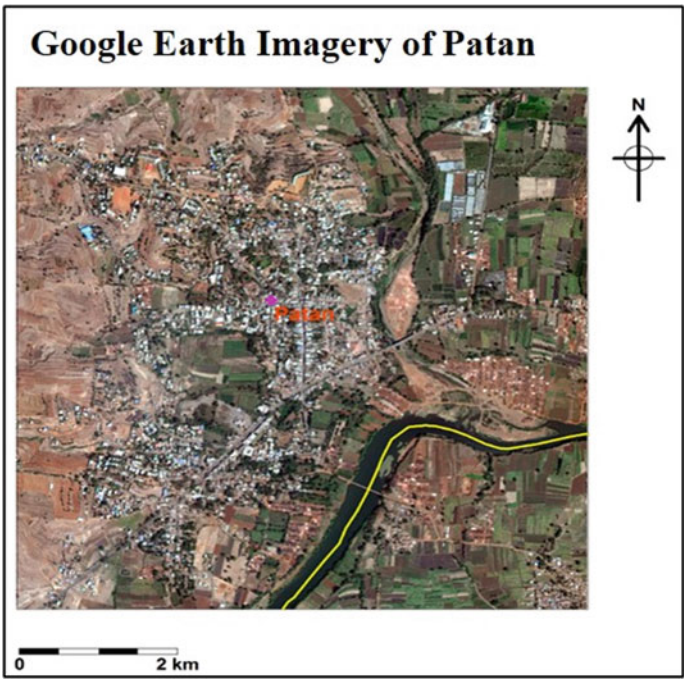

Fig. 2 Google Earth imagery of Patan

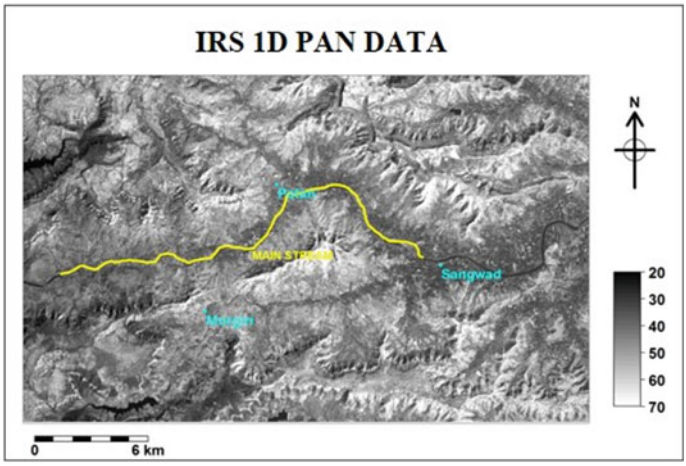

Fig. 3 IRS–1D PAN data

5.3 Digital Elevation Model

The ASTER DEM (Product of METI and NASA) was used for terrain analysis. This DEM has been prepared after the analysis of 30 m resolution stereo data. This DEM is a regular grid of elevation. Each node of the grid shows an altitude value. The resolution of the grid corresponds to the distance between neighbour nodes.

The spatial resolution of DEM used is 30 m with the vertical accuracy of 1 m. It can be observed from the DEM that Koyna River flows almost in a straight slope in the selected stretch. Both the banks are marked by gradually increasing altitudes towards the plateau at the elevation of about 1200 m for the study. This DEM was found to be very useful for extracting the flood levels to different Reduced Levels. Here, the DEM is superimposed in white by the mainstream segment (Fig. 4).

5.4 Digitized Flood Level Segment Map

Here, we assumed the mainstream as a datum level. The reduced levels of 5, 10, and 15 m were extracted and digitized with respect to the datum level. This map gives the scenario of the flood in terms of flood levels (Fig. 5) [7].

5.5 Interpolated Flood Levels Map

The flood level segments were interpolated to derive the flood level map. It has been observed that very large area is inundated near Patan for the lower flood level. Upon analysing this particular sheet, the Patan sub-map was selected and extracted for further research on flood hazard zonation, vulnerability assessment and

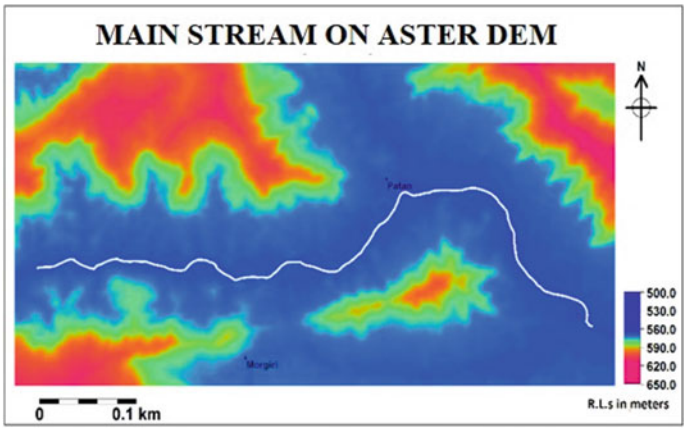

Fig. 4 ASTER DEM (Product of METI and NASA)

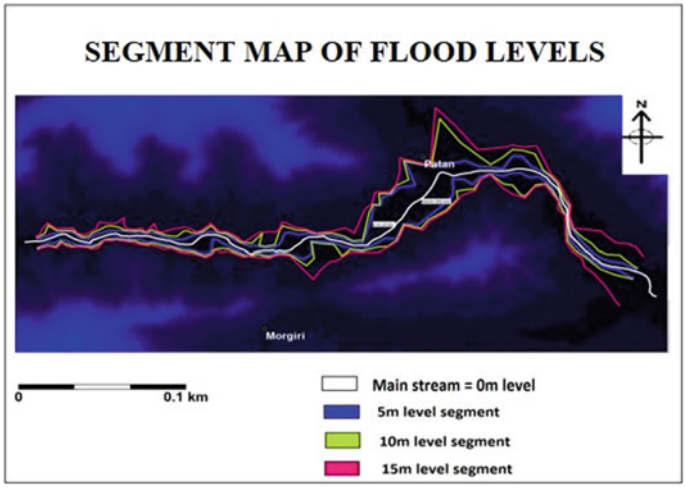

Fig. 5 Segment map of digitized flood levels

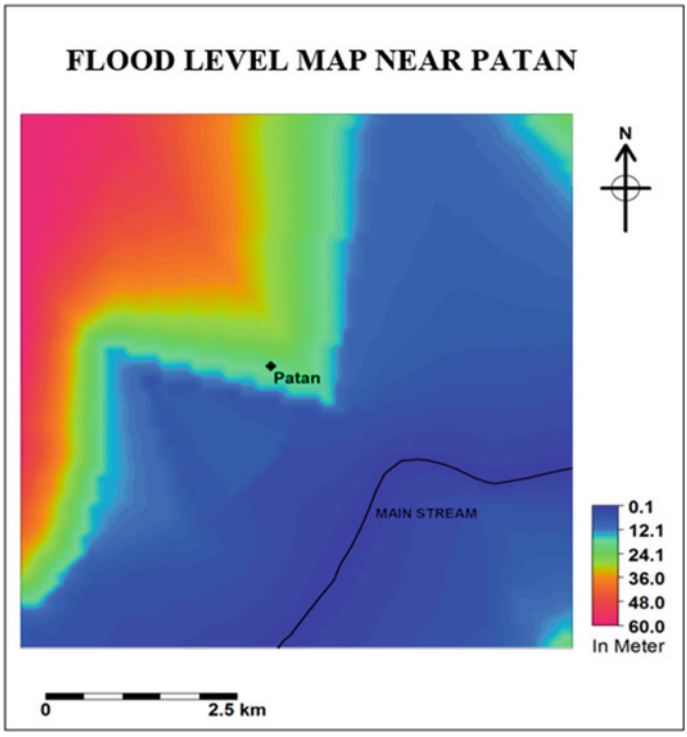

Fig. 6 Interpolated flood level map near Patan

preventative civil engineering measures. The sub-map was studied along with the high-resolution colour composite of Google Earth imagery data (Fig. 6).

5.6 *Flood Hazard Zonation Map (in Terms of Flood Levels)*

This map is the final result of the integration of different layers generated in ILWIS software. It includes 5 zones for flood hazard zonation mapping. High-resolution map of study area, Patan, is added for vulnerability analysis. First two zones are

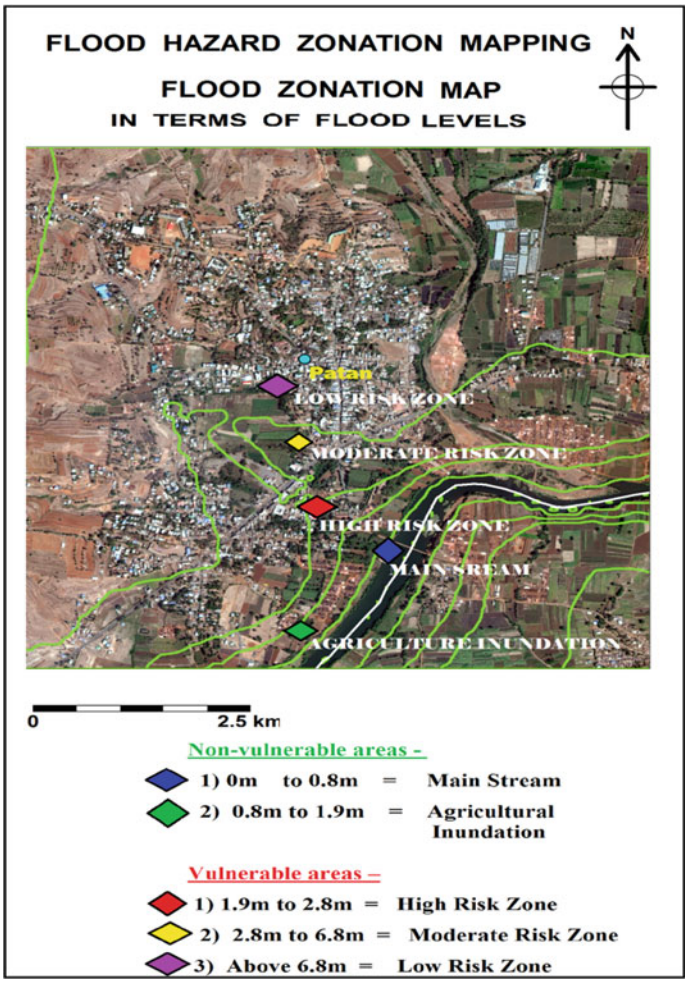

Fig. 7 Flood hazard zonation map in terms of flood level

Table 1 Area under flood hazard zones

Flood levels (m)	Settlement vulnerability	Zones	Area (km^2)
0–0.8	No	Main stream flow	2.55
0.8–1.9	No	Agricultural inundation	3.34
1.9–2.8	Yes	High risk zone	3.02
2.8–6.8	Yes	Moderate risk zone	12.14
Above 6.8	Yes	Low risk zone	33.3

non-vulnerable. Here, we can see 0–0.8 m region from the mainstream comes under areas of the stream zone. It indicates agricultural land that undergoes flooding. Remaining 3 zones are vulnerable as the flooding in those areas would impact the settlement. Flood water extends for various elevations in those three areas (Fig. 7 and Table 1).

6 Conclusions

ASTER DEM, IRS–1D PAN data and moreover the well processed high-resolution Google Earth imagery available for the common man with its impactful user interface have improvised the domain of data users. Remote sensing and GIS techniques have emerged as a powerful tool for addressing diverse facets of flood control in flood hazard prevention, notification, preparedness and relief control. They have a greater role to play as an improvement over the existing methodologies. In this study, attempts are made to illustrate the use of RS and GIS techniques in the flood hazard assessment. Using these techniques, the flood zone mapping of the Koyna River Basin has been carried out.

The primary purpose of making flood maps is to make them accessible to the public, which would help raise awareness. In this study, efforts were made for floodplain zoning for the settlements in Koyna river basin near Patan through the remote sensing data interpretation, and GIS database was generated after vector digitization and raster analysis.

With the help of remote sensing data, the study area has been divided into three flood risk zones, i.e. low, middle and high level. Based on the above study, it is found that about 3.02 km^2 area comes under high-risk zone, whereas 12.14 and 33.3 km^2 area comes under moderate and low-risk zone, respectively.

It is observed that ASTER DEM is an effective tool for many applications and can be used in planning for flood disaster management and mitigation. This work is an attempt to corelate the output from ASTER DEM with the flood hazard-related data generated from IRS–1D PAN data and high-resolution Google Earth imagery data.

References

1. Kumar A (2005) Application of GIS in flood hazard management: an alternative plan for the floods of North Indian Plain. Map India, New Delhi
2. Yamaguchi Y, Kahle A, Tsu H, Kawakami T, Pniel M (1998) The advanced spaceborne thermal emission and reflection radiometer (ASTER). IEEE Trans Geosci Remote Sens 36 (4):1062–1071. https://doi.org/10.1109/36.700991
3. Water Resources Department (2018) Integrated state water plan for Maharashtra. Government of Maharashtra
4. Khanna RK, Agrawal CK, Kumar P (2006) Remote sensing and GIS applications in flood management. In: Indian disaster management congress, National Institute of Disaster Management, New Delhi, India
5. Shinde VM, Deshpande PK, Kumthekar MB (2013) Application of ASTER DEM in watershed management as flood zonation mapping in Koyna River of the Western Ghats. Int J Sci Eng Res 4(5)
6. Cees van Westen, Jamshid Farifteh (2001) ILWIS 3.0 academic user's guide
7. Sathe B, Khire M, Sankhua R (2011) Integrated remote sensing and GIS for flood hazard mapping in Upper Krishna River Basin (India). Int J Sci Technol

Flood Hazard Mitigative Protection Measures Along the Banks of Koyna River Near Patan Based on Spatial Data

Gaurav Sanjay Ghare, Purushottam Kashinath Deshpande, and Abhijeet Arun Bhondwe

Abstract Study of flood hazard mapping along the Koyna river bank near Patan (Dist. Satara, Maharashtra, India) was done in ILWIS environment. Tools of RS and GIS were used to produce flood hazard map depicting inundation areas at different flood levels. The present study uses these maps of flood hazard zones along with vulnerability aspect. Also, the problems associated with flood, in study area, have been studied. Effort has been made to propose the most suitable remedial measures after analyzing several measures. These measures may protect the river banks and reduce damages to the structures and agricultural land over a considerable period of time.

Keywords Remote sensing (RS) · Geographic information system (GIS)

1 Introduction

The river Koyna is considered as the lifeline of Maharashtra. On the other hand, there is also a possibility of flash flooding caused by a number of factors along its banks. The problems of bank erosion and water contamination are also severe in the Koyna river basin.

River flood mapping is the process of determining inundation extents and depth by comparing river water levels with ground surface elevation. The flood hazard zonation map was prepared by using RS and GIS technologies along Koyna river

G. S. Ghare (✉)
Gajanan Housing Society (East), Vidyanagar, Karad, Satara, Maharashtra, India

P. K. Deshpande
Department of Civil Engineering, Walchand College of Engineering, Vishrambag, Sangli, Maharashtra, India
e-mail: purushottam.deshpande@walchandsangli.ac.in

A. A. Bhondwe
Department of Civil Engineering, Government College of Engineering, Karad, Satara, Maharashtra, India

B. Laishram and A. Tawalare (eds.), *Recent Advancements in Civil Engineering*, Lecture Notes in Civil Engineering 172,
https://doi.org/10.1007/978-981-16-4396-5_74

bank, near Patan town. This map was carefully examined, and the study area was explored at the ground level. This study was used to propose the different remedial measures.

We adopted two ways to manage these floods, first, non-structural measures such as flood hazard mapping, channel improvement and structural measures like construction of flood protective structures along the banks of the river. The most critical task of the public authorities in the wake of a natural disaster is to provide the victims with the essential necessities. Once first responders have satisfied the basic needs of the survivors, then it is the responsibility of civil engineers to restore public confidence in the engineering profession. As the public sees successfully designed structures preventing flood and protecting cities, people will regain faith in infrastructure and the entire civil engineering sector.

2 Flood Hazard Map

The extent of the flooding is measured in terms of depth of water. For this purpose, the reduced level at the mid-section of the mainstream is considered as zero meter flood level, as the Koyna River flows in nearly flat slope. Contours were interpolated in accordance with this at 5, 10, 15 and 100 m flood levels. The resultant DEM was sliced at 0.8, 1.9, 2.8, and 6.8 m to generate flood hazard map as shown in Fig. 1.

3 Vulnerability Aspect

A vulnerability assessment is the process of identifying, quantifying, and prioritizing the vulnerabilities in a system. Vulnerability function for the different element at risk is formulated based on flood water level shown in flood level map. Each land use class has been treated separately. In this study, we have considered the flood vulnerability assessment only for structures and population. Different risk zones are as shown in Table 1.

4 Study Area Location

The Koyna River is a fifth-order perennial stream basin which is about 119 km in length. The basin is developed in the uppermost reaches of the drainage system of Krishna River, in Satara district of Maharashtra. It is included within the survey of India topographic sheet number 47G/11 on the scale of 1 Inch: 1 Mile. The study area is lying between the latitudes 73° 53′ 1.23″ E, 73° 54′ 40.32″ E and the longitudes 17° 23′ 00.2″ N, 17° 21′ 49.5″ N. The Koyna River receives its water

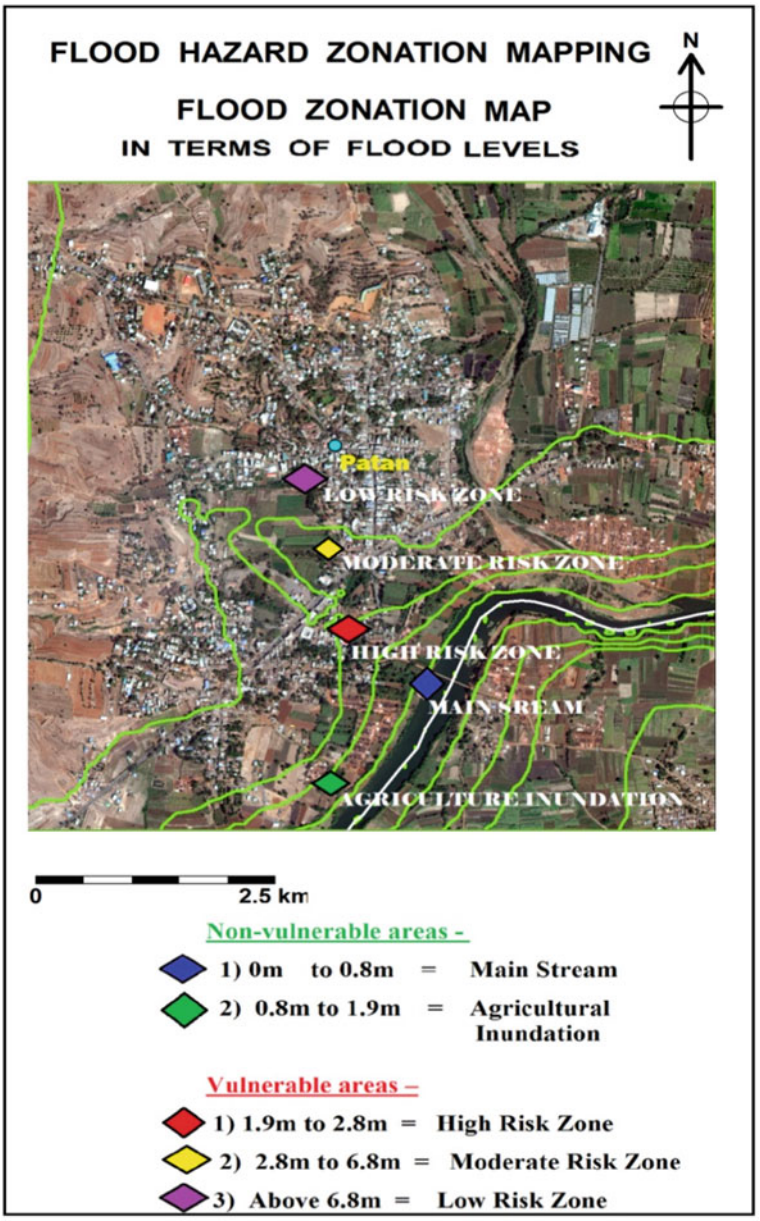

Fig. 1 Layout of flood hazard zonation map

Table 1 Analysis of flood hazard zones

Sr. No.	Flood hazard zones	No. of structures	Percentage of structure	Population*	Area (km^2)
1	High risk zone	61	4.7	400	3.02
2	Moderate risk zone	436	33.62	2810	12.14
3	Low-risk zone	800	61.68	5160	33.3

*Ref: Census 2011 for population data of Satara district

from the catchment of Koyna Dam built at Deshmukhwadi, Tal.-Patan, Dist.-Satara and its tributaries Kera, Morna and Wang. It also receives water from the Sahyadri ranges on both side of Koyna River and drains an area of about 891 (km^2). The area under study experiences a subtropical monsoon type of climate. During the period from June to October it receives heavy rainfall, the annual rainfall being in excess of 2000 mm in Patan Tehsil. The summer is dry with maximum temperature reading of 38–40 °C [1] (Fig. 2).

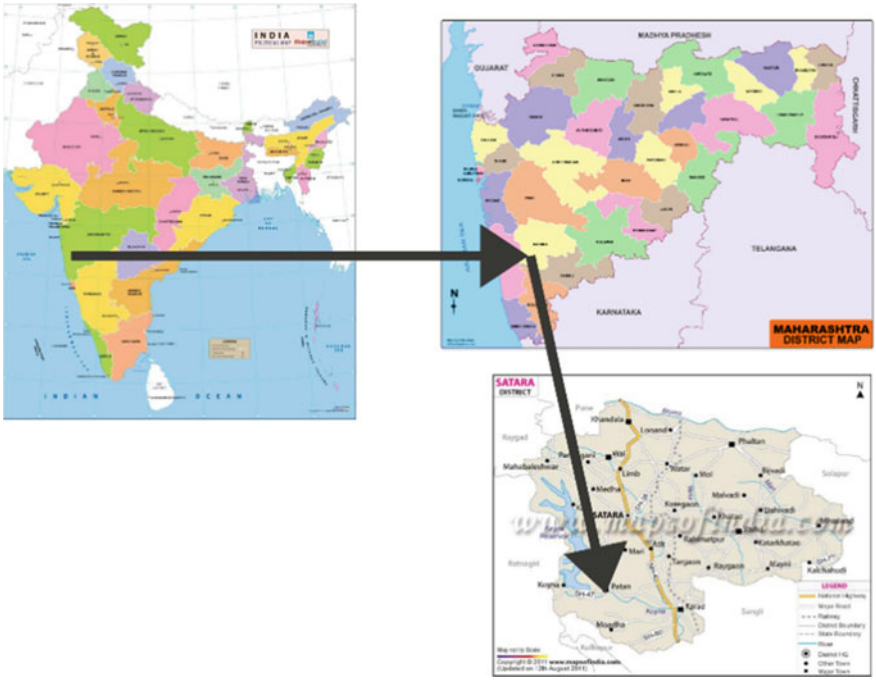

Fig. 2 Location of study area

5 Reason of Flood in Koyna River Basin

The Koyna River flows for about 75–80 km to the south from Mahabaleshwar to Koynanagar. This particular North–South stretch lying high above the Western Ghats is directly exposed to monsoon and fed by numerous high yielding tributaries. Hence, there is often a very rapid accumulation of water in the Koyna reservoir in heavy rains, which enforces the enormous discharge from the dam. While Koyna River's flood carrying capacity is very high, the dam discharge of over 90,000 cusecs is responsible for spilling out of the stream, causing the flooding along both banks of river.

6 Problems Due to Flood in Koyna River Basin

6.1 Erosion of Riverbanks

The Koyna River as a high magnitude alluvial river has sediment erosion–deposition problems associated with it. The Koyna River is distinguished by its extremely large flow, enormous sediment load, and constant changes in channel morphology, rapid degradation of the beds and recession and erosion of bank lines. The lateral changes in channels cause severe erosion along banks, resulting in a substantial loss of good fertile land every year. Bank oscillation also causes its tributaries to shift outflows bringing newer areas underwater. Hundreds of hectares of farmland continuously suffer from severe erosion in the Koyna basin [2].

6.2 Probability of Flash Flood

A flash flood is generally defined as a rapid onset flood of short duration with a relatively high peak discharge. During 2011 floods, 1.28 lakh cusecs of water were released from Koynanagar dam in to the Koyna River stream. Again during 2019 floods in Western Maharashtra, Koynanagar dam outflow was increased from around 20,000 cusecs to 1.25 lakh cusecs within a span of two days.

7 Mitigative Recommendations

From analyzing flood hazard map and problems associated with the flood in the study region, we conclude that there is need to construct civil engineering structures to protect the river banks and peoples nearby. Such small steps in the future can have major positive results. Such steps for mitigation are:

1. Construction of counterfort retaining wall
2. Construction of gabion wall
3. Precautions for buildings in flood prone areas
4. Kera river dredging operation.

7.1 Counterfort Retaining Wall

7.1.1 Need of Counterfort Wall

A retaining wall is one of the most prominent types of structures that preserve soil. The primary function of the retaining wall is to hold the soil or other material in or close to the vertical position. This is commonly used in a range of situations such as road engineering, railway engineering, bridge engineering, port and harbour engineering, irrigation engineering, land restoration, marine engineering and so on. If the height of the soil to be maintained exceeds 5 m, the bending moment of the stem, heel and toe slabs becomes very high, resulting in a broad thickness of the structural components and being uneconomical. Therefore, the retaining wall form of the counterfort is designed for greater heights.

7.1.2 Structural Design

As shown in Fig. 4, counterfort retaining walls are similar to cantilever walls except they have thin vertical concrete webs at regular intervals along the backside of the wall. These webs are known as counterforts. These can be precast or formed on site. Counterfort retaining walls are more economical than cantilever walls for heights about 6 m. The counterforts tie the base slab and wall stem together and they act as tension bracing which strengthens the connection between wall and base slab. The counterforts help to reduce bending moment and shear forces induced by soil pressure on the retaining wall. Moreover, it also serves to increase the self-weight of the retaining wall which adds stability to the retaining wall [3].

7.1.3 Proposed Location of Counterfort Wall

Patan is located on left bank of Koyna River. There is the confluence of River Koyna and River Kera. Due of the discharge of more than 1.1 lakh cusecs, the water enters up to the bus stand in Patan City, as the land has almost levelled slope. The counterfort retaining wall of sufficient stability of 2300 m is proposed on the left bank of the Patan Bridge to stop water from spreading in the town and to resist soil erosion (Figs. 3 and 4).

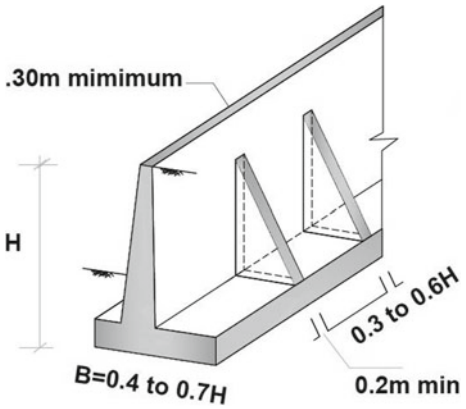

Fig. 3 Criteria for design of counterfort retaining wall

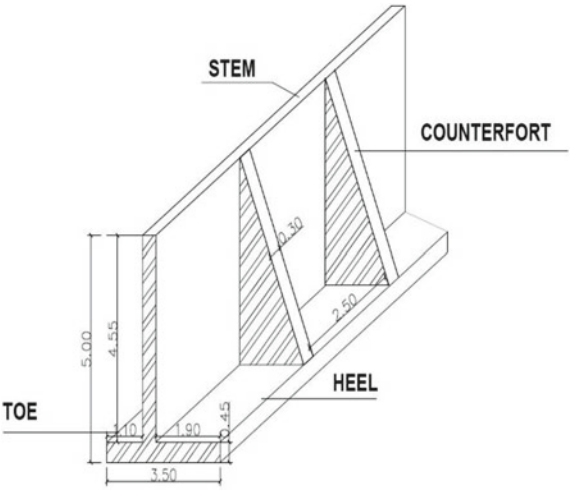

Fig. 4 Proposed design of counterfort retaining wall

7.2 Gabion Wall

7.2.1 Need of Gabion Wall

Gabions are engineered retaining structures designed as mass gravity walls to hold back earth or other solid materials without overturning, sliding or foundation failure. Gabions can be used in various applications. These are an important tool for combating erosion and stabilizing and repairing embankments, as well as restricting water flow. Gabions have long been proven construction method for maintaining structures worldwide, offering solutions that are economically and environmentally acceptable. Gabion structures function as perforated barriers which enable water to gradually pass through them. It is a beneficial advantage in that the hydrostatic pressure rarely builds up behind or under the system and prevents the gabion

mechanism from collapse. Gabion structures are considered to be permanent. In the early stages after completion, silting takes place between stone fill that encourages vegetation and contributes to the permanence of the structure. In view of the environmentally friendly nature of gabion construction compared to concrete, gabions are becoming more popular in river bank engineering works that require a natural-looking environment with growing vegetation and a potential for ecological life [7].

7.2.2 Structural Design

The gabions are steel wire cages that vary in size and are designed to abate the destructive forces of erosion. Gabions are uniquely woven by twisting each pair of wires one and one-half turns continuously providing the inherent strength and flexibility required. Gabion cages are normally designed to contain quarry run or river run stones available at the site of erection. Cages are stacked to construct structures of great durability and flexibility. The formed structure is capable of carrying stress in biaxial tension. Gabion cages are not merely containers of stone since each unit is securely connected to each adjacent cage during construction. The wire mesh is monolithic through the structure in three dimensions, from top to bottom, end to end, and from outer face to inner face. It is, therefore, apparent that the wire reinforces the stone filling in tension [4].

7.2.3 Location of Gabion Wall

The southern bank of the Koyna River near Patan is a vertical cliff, as can be seen in Picture 1. This has been under erosion for many years and a large cutting can be seen along the canal. In order to conserve the fertile agricultural land and contain the flow of the river inside the channel, we propose a Gabion wall of about 1500 m along the southern bank of the river Koyna, as shown in Fig. 5. The height of the planned wall will be 4 m. This wall would also avoid the meandering impact that is noticeable on the ground. Figure 6 demonstrates a standard model for a wall 4 m long. Reno Mattress is recommended to be used against local scouring at the toe of the gabion wall.

7.3 Protections for Buildings in Flood Prone Areas

The damage resistance of existing houses to low intensity inundation, say low risk zone and medium risk zone, can be achieved by making the lower portions of walls water proof up to the estimated level of saturation by inundation through application of water-proof mud plaster or pointing or plastering as appropriate. It will help a good deal if the adjacent area of floor inside the house and the ground outside could also be made water proof up to a width of about 900 mm.

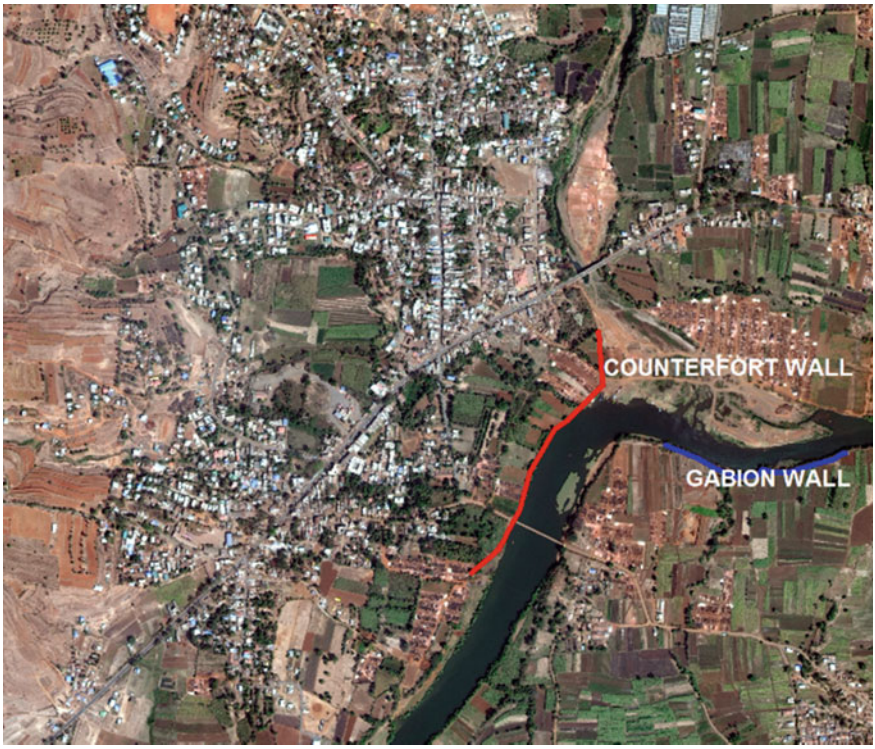

Fig. 5 Location of counterfort retaining wall and Gabion wall on Koyna River

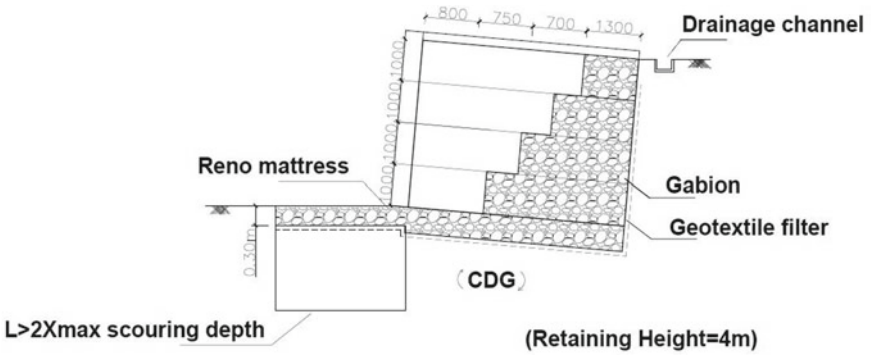

Fig. 6 Typical Layout of Gabion Wall

New buildings may be constructed on raised ground with apron around. Stilts or columns with wall-free space at ground level permitting free access to water whether inundation or flowing, will be safer in flood prone areas, provided that

Picture 1 Erosive bank on southern side of river

columns are circular, strong, and their foundation taken down to below the deepest scour level.

The following provisions should to be incorporated in the building bye-laws of Patan Municipality for buildings in flood prone areas:

(a) Plinth levels of all buildings should be 0.6 m above the drainage/flood submersion levels under the mean annual flood.
(b) All the buildings should preferably be two or more storeys.
(c) In single storey buildings, a stairway must be provided to the roofs which could be used as temporary shelter for which roof should be made of flat type.
(d) The roof levels of the single storey buildings and the first floor level in double-storey buildings should be kept above 100-year flood levels [5].

7.4 Kera River Dredging

7.4.1 Need of Dredging

Significant rainfall-induced drainage problems arise at the mouth of the Kera River. The intensity of the flow of water in the Koyna River is very high after discharge from the Koyna Dam. As a result, the water flowing through the Kera River at Patan is blocked, and large areas along its bank run under water. Drainage blocking is mainly due to heavy short-lived rainfall coupled with high levels of flow in the

Koyna River, preventing the rapid flow of water from the Kera River into the Koyna River. They are also induced by sedimentation, encroachment on the flood plains by Brick kilns, growth of water hyacinth and algae at the mouth of the Kera River, which obstructs natural flow.

7.4.2 The River Dredging Operation

The term 'dredging' covers a range of activities from the removal of material from the bed and sides of river channels through to the wholesale straightening (canalization) and/or deepening of watercourses. Dredging works can be undertaken to drain land for agriculture and to improve flood protection. The rivers carry runoff and silt from the catchment area to the estuaries, so as soon as the dredging is complete, the material begins to re-accumulate. In turn, the river would have to adapt to a more natural shape in terms of cross sections, gradients and meanders, with potentially significant unintended effects, including bank collapse and erosion. As a result, dredged channels require long-term maintenance. Dredging of a reach (length of channel) results in an increase in the cross-sectional area (and hence its volume), as well as a reduction in the roughness of the channel. If dragging is used to straighten and funnel the water, the effect is to decrease its length and thereby raise the gradient of the canal. Such effects can increase the efficiency of the channel in moving water (increasing the conveyance). Dredging would also lead to a reduction in water levels and thus to a reduction in the frequency of flash flooding in the local region.

7.4.3 Advantages of Kera River Dredging

The stream of the Kera River needs to be deepened by dredging the large amount of silt which is accumulated each year. This will increase the river's capacity to carry flow. The water must flow smoothly into the river Koyna preventing backflow resulting in the regular flooding of region on the river's west side. Therefore, flood situations along its bank can be avoided without any high costs.

8 Conclusion

High rainfall, the sudden release of huge river discharge from Koyna dam and the confluence of Kera–Koyna Rivers are causes of flooding in the study region. Maps depicting flood hazard areas are the basis of sound floodplain management policies at the local, levels. Adequate, accurate, and current maps are essential for the proper floodplain management.

The vulnerability studies show that about 497 structures in Patan come under high and medium-risk flood prone areas. The total population affected is about 8370 out of which 3210 people live in high and medium flood risk zones.

To protect the flood invasion in the settlement, the counterfort retaining wall of 5 m height and 2300 m length is suggested along the northern bank of Koyna River near Patan. Also, to protect the southern bank from high hydrostatic pressure generated from Kera river siltation, Gabion wall is suggested. It will also protect the agricultural land from erosion.

Preventive measures must be undertaken to protect existing buildings against inundation. Provisions need to be incorporated in the building bye-laws of Patan Municipality for buildings in the flood prone area. Drainage congestion problem at the confluence of Koyna and Kera River can be resolved by regular dredging operation of Kera River.

A small investment in implementing suggested measures can result in huge savings in flood-related disaster assistance in the future.

References

1. Water Resources Department (2018) Integrated state water plan for Maharashtra. Government of Maharashtra
2. Naik P, Awasthi A (2003) Groundwater resources assessment of the Koyna River Basin, India. Hydrogeol J 11:582–594. https://doi.org/10.1007/s10040-003-0273-5)
3. Patil SS, Bagban AAR (2015) Analysis and design of stepped cantilever retaining wall. Int J Eng Res Technol (IJERT) 4(2)
4. Lal KC (2006) Report No. RD 1045 Geotechnical Design of Gabion Wall. Mainland North Division Drainage Services Department
5. BMTPC (2010) Guidelines improving flood resistance of housing. Ministry of Housing & Urban Poverty Alleviation, Government of India, New Delhi
6. Coto EB (2002) Flood hazard, vulnerability and risk assessment in the city of Turrialba, Costa Rica. International Institute for Geo-information Science and Earth Observation, Enschede, The Netherlands
7. Shinde SR, Chaudhari PS (2014) Evaluation of non-structural and structural flood management measures. Int J Innov Res Adv Eng (IJIRAE) 1(2):83–87

Optimization of the Location of Check Valve to Minimize the Water Hammer Effects in a Pipeline

P. D. Jiwane, A. D. Vasudeo, and A. K. Singh

Abstract Water hammer occurs when the pressure waves are created due to sudden closure of a valve or failure of a pump and continue to move back and forth in the pipeline. This could damage the entire pipe system. The present study describes the simulation of these pressure waves in a pipeline using Bentley Hammer V8i software to model the water pipeline and also to analyse the water hammer effect. In this study, check valve (CV) has been used for the prevention of the surge to the pump. The present numerical simulations establish the location of the valve in the pipeline is to be placed near the pump so as to minimize the effects of the water hammer on the pump.

Keywords Water hammer · Check valve · Transient analysis · Bentley Hammer · Optimization · Optimum location

1 Introduction

When the water flowing through a pipeline is forced to stop abruptly due to sudden closure of a valve or failure of a pump, it results in creation of pressure waves. This is known as water hammer effect [1]. Water hammer is caused by a fast shift in flow velocity in the pipelines. This is due to sudden opening or closing of the valve, pump starting or stopping, device mechanical failure, quick change in demand situation, etc. It could lead to a violent shift in the pressure head to propagate in the pipeline in the form of a rapid pressure wave that may result in serious damage [1].

Whenever failure of the power occurs, the running pump stops working. As a result, a forward motion of the water in the pipeline come to standstill after that reversal of the flow takes place. This process continues until the whole energy of the water gets dissipates due to wall friction of the pipeline. In order to avoid the damage of the pipeline, a valve in the downstream of the pipeline is installed, and this is generally done using a check valve (CV) and is assumed that it is open when

P. D. Jiwane (✉) · A. D. Vasudeo · A. K. Singh
Visvesvaraya National Institute of Technology, Nagpur 440010, India

B. Laishram and A. Tawalare (eds.), *Recent Advancements in Civil Engineering*, Lecture Notes in Civil Engineering 172,
https://doi.org/10.1007/978-981-16-4396-5_75

the water is flowing through it and closes immediately as soon as the flow is reduced to zero, and hence, it acts as zero velocity valve (ZVV) [2]. The main function of a ZVV is to break the energy of returning water column by stopping it just when the water column begins to reverse. The principle behind the design of ZVV is to arrest the forward moving water column at zero movement, i.e. when its velocity is zero and before any return velocity is established. With the sudden stoppage of the pump, forward velocity of the water column goes on decreasing due to friction and gravity. The disc comes to the fully closed position when forward velocity approaches zero magnitude. The water column on the upstream side of the valve is thus prevented from acquiring a reversed velocity and taking part in creating surge pressure [2].

2 Water Hammer Equations

The transient analysis is done with the help of the water hammer equations which are widely used for application in simulating softwares. For unsteady pipe flow, the one-dimensional differential equations of motion and continuity are implemented. There is also a presentation of the modified equation of motion [3].

The fundamental governing equations under the assumptions are described by continuity and momentum equations [3]. The one-dimensional conservation of mass equation also known as continuity equation for slightly compressible fluids in cylindrical tube on any slope is expressed as

$$\frac{\partial H}{\partial t} + \frac{a^2}{g}\frac{\partial V}{\partial x} = 0 \tag{1}$$

with independent variables are x = distance and t = time. Other parameters are H = piezometric head, V = flow velocity, a = wave speed, and g = gravitational acceleration [5].

Brunone et al. (1991) [4] had studied unsteady friction model which assumes the term of friction consisting in two parts, namely a quasi-steady contribution and an unsteady contribution. The later contribution is linked to the instantaneous acceleration $\partial V = \partial t$ and the instantaneous convective acceleration $\partial V = \partial x$ [4].

$$F = \frac{f}{D}\frac{V|V|}{2g} + \frac{k_2}{g}\left(\frac{\partial V}{\partial t} - a\frac{\partial V}{\partial x}\right) \tag{2}$$

where F = total head loss due to steady and unsteady friction, f = Darcy—Weisbach friction factor, D = diameter of pipe, V = average velocity of flow, g = acceleration due to gravity, and k_2 = constant coefficient for the unsteady friction model [5].

Insertion of Eq. (2) into the momentum equation as mentioned by Chaudhry (1979) expresses the fundamental equation of motion as in Eq. 3.

$$g\frac{\partial H}{\partial x}+\frac{\partial V}{\partial t}+\frac{f}{D}\frac{V|V|}{2}+k_2\left(\frac{\partial V}{\partial t}-a\frac{\partial V}{\partial x}\right)=0 \tag{3}$$

3 Modelling of Check Valve

Figure 1 shows a sketch of a typical swing check valve which is frequently used in a pipeline not permitting the reverse flow. This sort of check valve closes and valve slam is prevented in case of reverse flow. Water hammer can generate overpressure on the valve opening [5]. Although a single check valve cannot be a safe way to prevent backflow, it is an important component of backflow prevention assembly [5]. A check valve is designed to allow water to pass in only one desirable direction [5]. In this study, a check valve is used as zero velocity valve (ZVV).

The movement of the valve disc relies on the valve disc, the disc mass and the angular speed of the valve. The torques acting on the check valve disc consist of the submerged weight of the disc assembly, the torque due to the friction of the valve shaft, any internal torque induced by a spring or counter weight, and the torque due to the stream around the valve disc. The torque of weight and the internal torque are functions of the angular position of the disc [6].

The dynamic behaviour of a check valve can be described by the moment-of-momentum equation of the check disc. The moment-of-momentum equation can be written as

$$T_w+T_e+T_f+T_h=I\frac{\mathrm{d}^2\theta}{\mathrm{d}t^2} \tag{4}$$

where T_w = torque due to weight of the rotating disc, T_h = torque due to hydrodynamic pressure, T_e = external torque applied to the disc, T_f = torque due to friction, I = moment of inertia, and θ = disc angle [6].

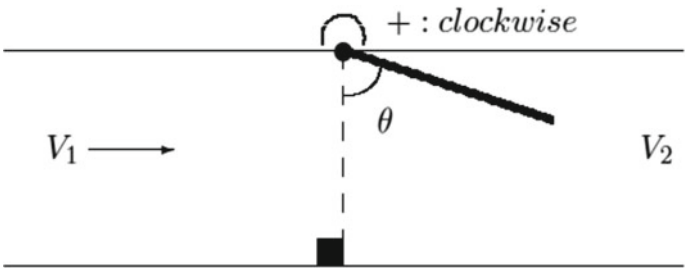

Fig. 1 A schematic sketch of the check valve in a pipeline [6]

All the torques in Eq. 4 are determined as mentioned by Kim (2012) which are later on substituted in Eq. 4 to give the final equation for the valve as

$$I\frac{\mathrm{d}^2\theta}{\mathrm{d}t^2} = W_s r_c \sin\theta + s\theta + \frac{\gamma \bar{r} A v Q|Q|}{2g(CdAo)^2} \tag{5}$$

where W_s = submerged weight of the disc assembly, r_c = length from the hinge to the mass centre of the disc assembly, s = torsional spring stiffness, $\bar{r}$ = distance from the hinge to the point of application of the average pressure change across the valve, Av = disc area over which ΔH acts, γ = unit weight of water, C_d = flow coefficient, A_o = the open area through which the flow passes, g = acceleration due to gravity, and Q = flow rate in the disc [5].

4 Methodology

In this study, the numerical expressions as mentioned in Eqs. (1), (3) and (5) are used for simulating the transient analysis in the pipeline for different conditions using Bentley Hammer V8i. This is a commercial package and a very powerful tool for simulating hydraulic transients in pipelines and networks. It is an advanced numerical simulator of hydraulic transient phenomenon in water [7].

In this study, check valve is used as a ZVV, which could be justified on the basis that the check valve's time of closure could be changed manually as required. Water hammer effect is studied in the inclined pipeline. Under a power failure situation when the pump stops operating, the flow is reversed. This reversal of the flow produces high pressure waves that move towards the pump and can harm the entire system of the pump and pipeline. The effect of water hammer is investigated with and without check valve in water pipeline.

Table 1 presents the elevation for all the elements in the pipeline with distance between the two elements 300 m. This data are required in Bentley Hammer for the simulation of water hammer effects. Geometry is drawn in Bentley Hammer using data given in Table 1, and the parameters as given below are considered in the study to compute the transients in the pipeline. The transient analysis is studied in two cases, i.e. effects of water hammer with and without check valve and to minimize them using a valve by changing its position throughout the pipeline. The parameter used for the study are: Speed of pump = 2900 RPM, inertia of pump = 34.569 Kgm^2, length of pipe = 2400 m, diameter of pipe = 1200 mm, steady flow rate = 206L/s, wave velocity = 1120 m/s, pump efficiency = 85%, pump power = 1224.4 KW, time for study = 120 s, and the pipe material is steel [3].

In Table 1, R-1 and R-2 denote reservoir, PMP-1 signifies pump station 1, and J-1, J-2, … J-7 define the junctions.

Table 1 Elevations for the elements in the pipeline system [3]

Elements	R-1	J-1	PMP-1	J-2	J-3	J-4	J-5	J-6	J-7	R-2
Elevation	383	380	363	363	453	543	633	723	813	903

5 Result and Analysis

5.1 Case 1: Effect of Water Hammer Without Check Valve in the Pipeline

In this study, effect of water hammer on the pipeline is analysed in the absence of any safety device such as a check valve. The length of pipe is 2400 m shown in Fig. 2. It is seen that the pipeline is horizontal till J-2 and after that its elevation rises till the reservoir R-2.

Figure 2 shows R-1 and R-2 denote reservoir, PMP-1 signifies pump station 1, J-1, J-2, … J-7 define the junctions, and P-1, P-2, … P-9 is pipe length between two junctions.

In order to identify the initial condition for the surge assessment, the steady-state calculation was first performed for the pipeline scheme. Figure 3 displays the steady-state case hydraulic grade line.

Simulation of the water hammer in pipeline in view of the given data using Bentley Hammer software. This gives the results as the variation of the pressure with respect to distance and time.

Figure 4 shows the variation of pressure with distance for a 2400 m pipeline. It is seen that maximum and minimum pressures are 5500 and 5000 kPa at a section right after the pump and pump outlet junction. Thus, the amplitude of the pressure is 500 kPa.

Figure 5 is the result concerning variation of pressure with time. It is observed that fluctuation of pressure at a most critical location, i.e. at the outlet of pump for the study time of 120 s. Noting that in the absence of the check valve, fluctuation of the water pressure results in direct force on the pump body.

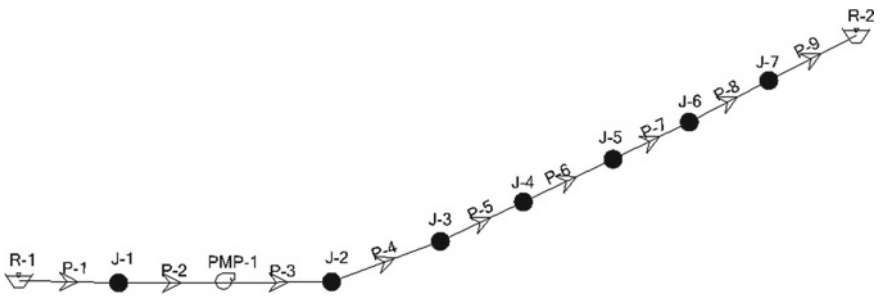

Fig. 2 Geometry of pipeline for the given data without check valve

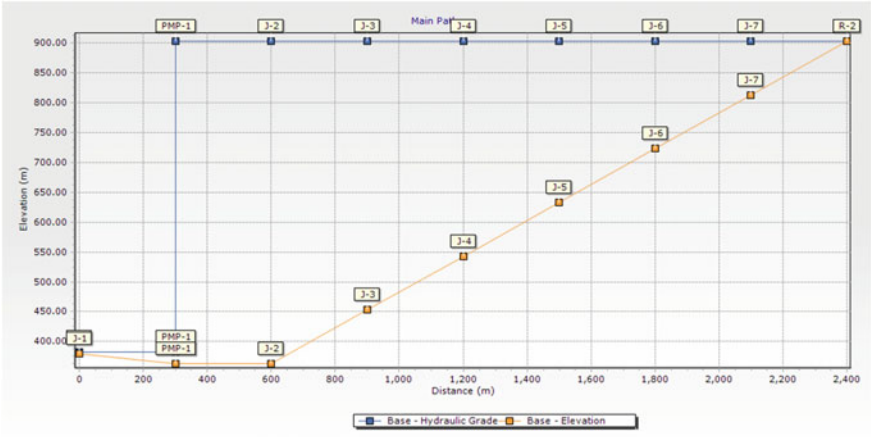

Fig. 3 Hydraulic grade line in the absence of a check valve

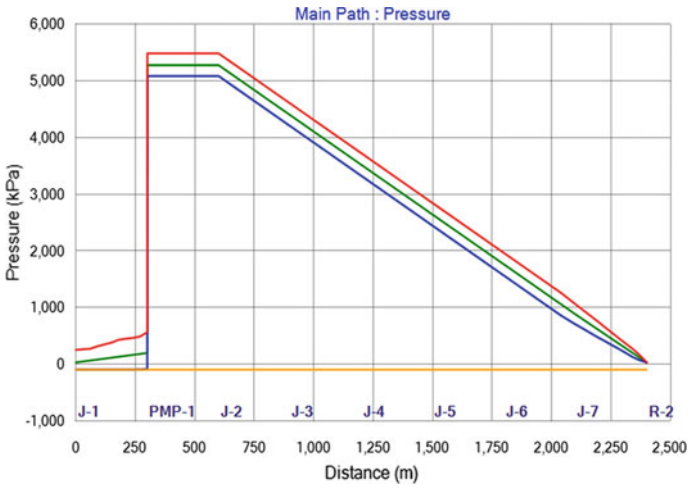

Fig. 4 Variation of pressure versus distance in the absence of check valve

5.2 *Case 2: Effect of Water Hammer with Check Valve in the Pipeline*

For the analysis of this condition, check valve CV-1 is added in the pipeline, and the model is created in the presence of check valve.

Figure 6 shows a pipeline having a check valve at the junction nearest to the pump outlet, and CV-1 denotes the check valve (other legends as per Fig. 2). For example, the check valve is inserted at a random location.

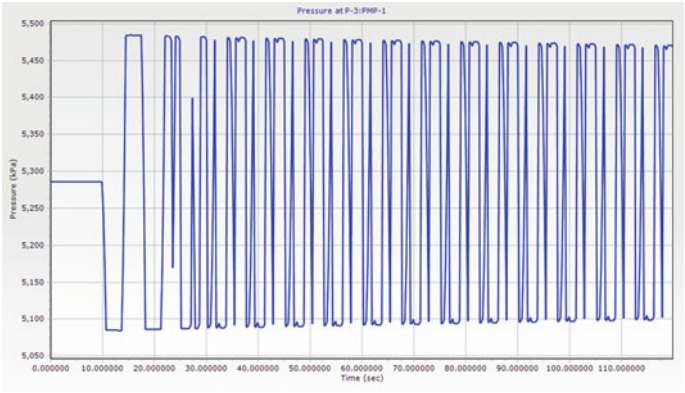

Fig. 5 Variation of pressure versus time in the absence of check valve

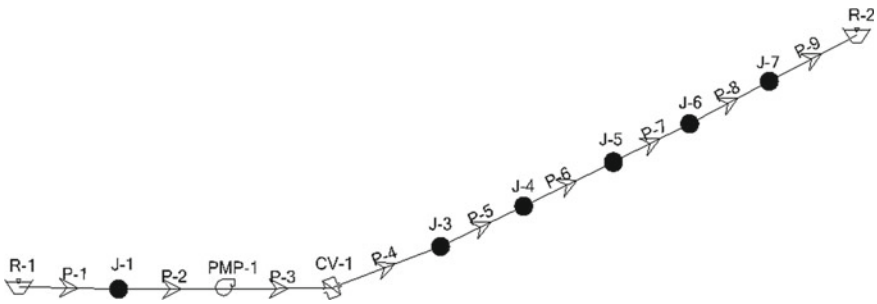

Fig. 6 Geometry of pipeline for the given data with check valve

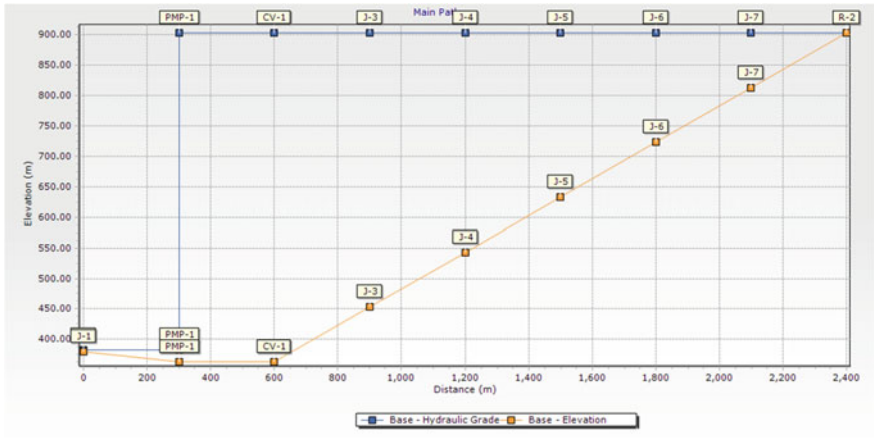

Fig. 7 Hydraulic grade line in the presence of check valve

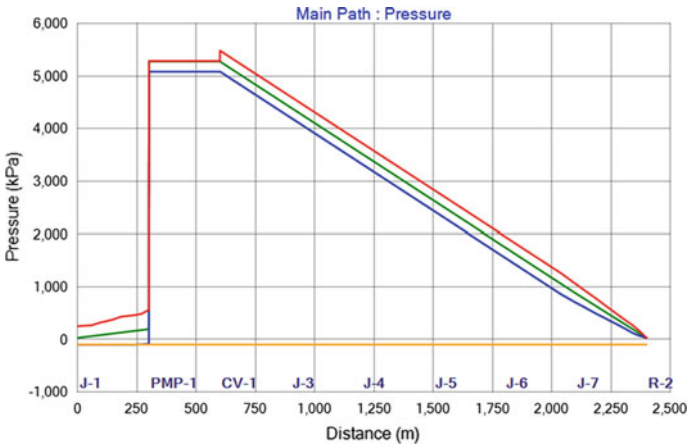

Fig. 8 Variation of pressure versus distance in the presence of check valve

In order to identify the initial condition for the surge assessment, the steady-state calculation was first performed for the pipeline scheme. Figure 7 displays the steady-state case hydraulic grade line.

Simulating the given data in Bentley Hammer software gives the following results as the variation of the pressure with respect to distance and time.

Figure 8 illustrates the pressure variation with distance when check valve is used. Here, pressure variation has reduced on upstream side of check valve after closing of check valve. However, at the same time, there increase in pressure on the downstream of check valve due to the impact of water with check valve.

Figure 9 shows the variation of pressure with time when check valve closes at a particular time at upstream side of the check valve between pump outlet and check valve.

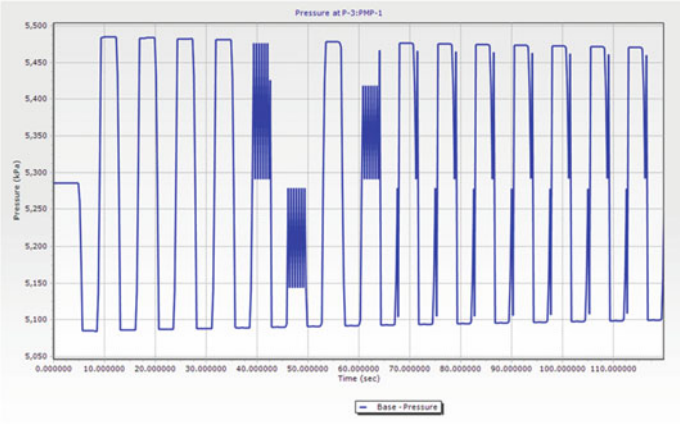

Fig. 9 Variation of pressure versus time in the presence check valve

5.3 *Optimum Location of the Valve in Water Pipeline*

Aiming to find out the optimum location of the check valve-based ZVV, valve closure time (Tvc) is kept constant throughout the length of the pipe and the location of the check valve is changed in the upward direction at different junctions of the pipeline and the attention is to focus on studying the effect of pressure fluctuations.

Following are the results concerning the pressure versus distance and pressure versus time at the outlet of the pump for a constant Tvc of 8 s of the check valve and varying the position of the check valve.

From Figs. 10a, 11a, 12a, 13a, 14a and 15a, it is observed that pressure variation has been remarkably reduced on the upstream side of wherever the check valve is placed.

Pressure versus time plots as mentioned in Figs. 10b, 11b, 12b, 13b, 14b and 15b show that fluctuation of water pressure is varying as the location of the check valve is changed. It is observed that as the check valve is moved to the upper junctions, the variation in water pressure becomes more erratic.

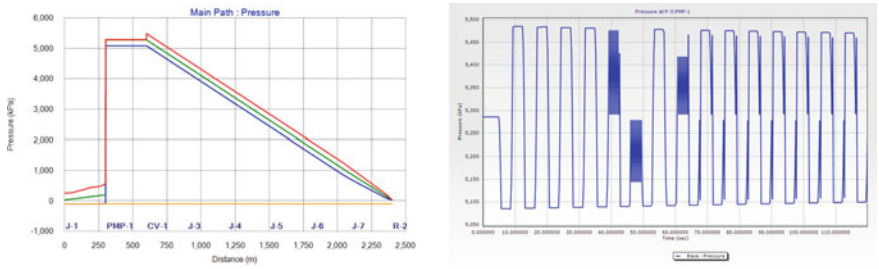

Fig. 10 **a** Variation of pressure versus distance plot when CV is at J-2. **b** Variation of pressure versus time plot when CV is at J-2

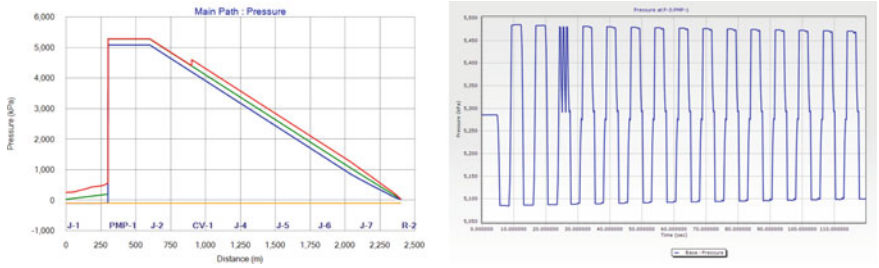

Fig. 11 **a** Variation of pressure versus distance plot when CV is at J-3. **b** Variation of pressure versus time plot when CV is at J-3

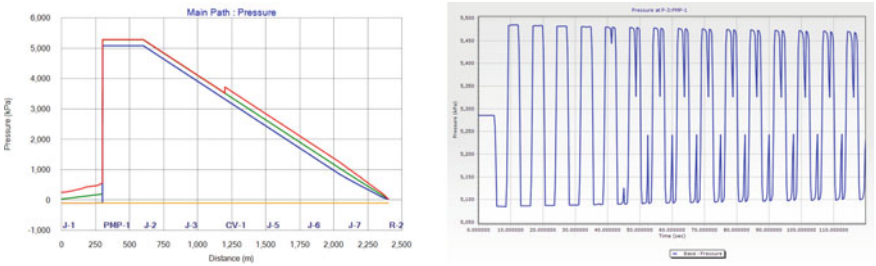

Fig. 12 **a** Variation of pressure versus distance plot when CV is at J-4. **b** Variation of pressure versus time plot when CV is at J-4

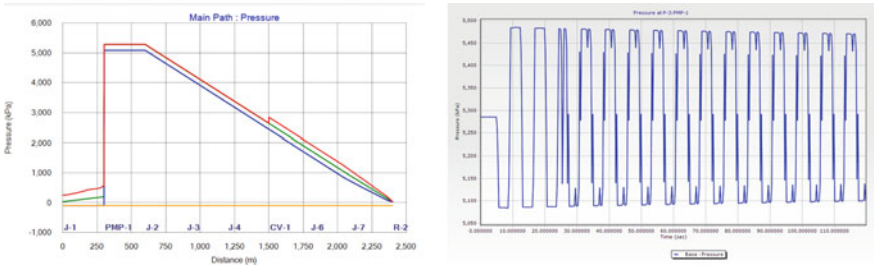

Fig. 13 **a** Variation of pressure versus distance plot when CV is at J-5 **b** Variation of pressure versus time plot when CV is at J-5

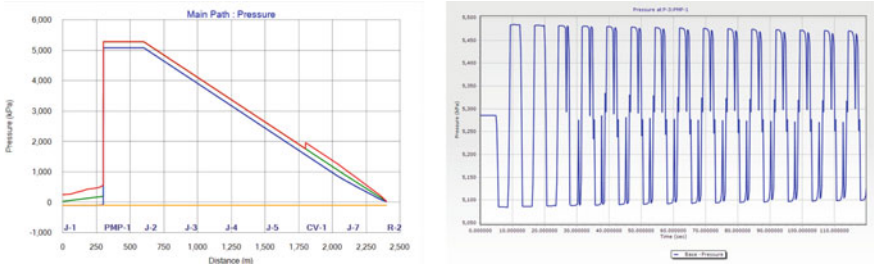

Fig. 14 **a** Variation of pressure versus disatance plot when CV is at J-6. **b** Variation of pressure versus time plot when CV is at J-6

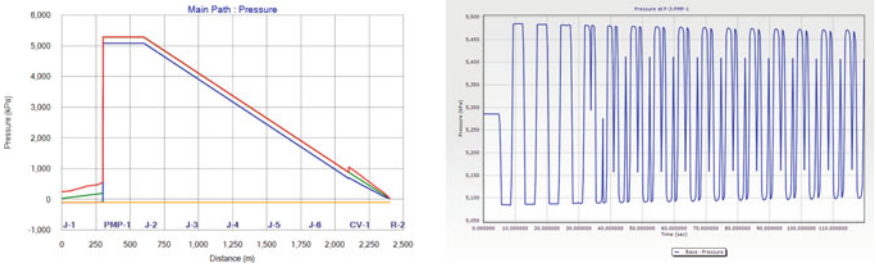

Fig. 15 **a** Variation of pressure versus disatance plot when CV is at J-7 **b** Variation of pressure versus time plot when CV is at J-7

By studying the pressure versus time plot in Figs. 10b, 11b, 12b, 13b, 14b and 15b, it is observed that when the check valve is located at Junction J-3, the pressure fluctuation is least as compared to the other plots.

Thus, from the above discussions, it is concluded that J-3 is the optimum location for the valve in the pipeline.

6 Conclusion

The present numerical simulations of the water hammer in a pipe line indicate that effect of the water hammer on the pump is quite considerable as compared to in the absence of the CV. This results in quite high fluctuation of water pressure in the pipeline. However, the pressure fluctuation approaches to the steady state and also reduces significantly in the presence of the CV. Further, for a fixed time of closure of the CV, length of the pipeline, fluctuation of water pressure is almost constant near the valve. But as the CV is placed at the upper junctions (J-4, J-5, J-6 etc.), fluctuation of the water pressure near the pump outlet increases and also becomes erratic. So, effort should be made to place the CV near to the pump in downstream direction.

References

1. Afshar MH, Rohani M (2008) Water hammer simulation by implicit method of characteristic. Int J Press Vessels Pip 85(12):851–859
2. Bentley Communities Forum— https://communities.bentley.com/products/hydraulicshydrology/f/haestad-hydraulics-and-hydrology-forum/109282/zero-velocity-valve-in-hammer
3. Chaudhry MH (1979) Applied hydraulic transients. Van Nostrand Reinhold, New York
4. Brunone B, Golia UM, Greco M (1991) Modelling of fast transients by numerical methods. InProc Int Conf on Hydr Transients with Water Column Separation, 273–280
5. Kim HJ (2012) Numerical and experimental study on Dynamics of unsteady pipe flow involving backflow prevention assemblies
6. Tran PD (2014) Pressure transients caused by tilting-disk check-valve closure. J Hydraul Eng 141(3):04014081
7. Bentley HAMMER CONNECT Edition Help - https://docs.bentley.com/LiveContent/web/Bentley%20HAMMER%20SS6-v1/en/GUID-448D36A5-3AA9-44C2-B205-40D6473FF386.html

Reduction in Live Storage Capacity of a Reservoir Due to Sedimentation Using Satellite Imageries

Tulshidas Jibhakate and Ashwini Mirajkar

Abstract Sedimentation is one of the main factors that reduce the gross storage capacity of a reservoir over the period of time. Live storage capacity can be estimated with the help of satellite imageries. Remote sensing technique gives a synoptic view of a reservoir to estimate sedimentation in live storage zone. In this study, LANDSAT 8 satellite imageries are used to find out the loss of live storage capacity and rate of siltation of a Mula reservoir, Maharashtra, India, for the years 2014 and 2018, respectively. The percentage loss of live storage for the years 2014 and 2018 is 5.15 and 5.5, respectively. Rate of siltation for both the study years is same, i.e. around 310 m^3/km^2/year, which is good under prevailing conditions of Indian reservoirs. The Mula reservoir has not much significant sedimentation issue.

Keywords Sedimentation · Satellite imageries · LANDSAT 8 · Mula reservoir · Live storage capacity · Elevation capacity curve

1 Introduction

When water flows into the river, it carries silt/sand/clay particles with it. As the flow takes place with high velocity, it scours the bed of river. When water gets obstructed with some artificial hydraulic structures such as weir, barrage or dam, sediment particles get deposited. Mostly, we concern the sedimentation in reservoirs because huge storage of the same reduces the capacity of a reservoir. Sedimentation means deposition of sediment particles due to obstruction in the flow of river. Maximum deposition is occurred at the site of a reservoir. Usually, India gets 40–45 days of rainfall in a year. Rainfall in India is uncertain, i.e. it may occur at some places heavily and at some places drought condition occurs. There is a need to store the water up to the next monsoon season for the different demand purposes

T. Jibhakate · A. Mirajkar (✉)
Civil Engineering Department, Visvesvaraya National Institute of Technology, Nagpur, Maharashtra, India

B. Laishram and A. Tawalare (eds.), *Recent Advancements in Civil Engineering*, Lecture Notes in Civil Engineering 172,
https://doi.org/10.1007/978-981-16-4396-5_76

such as irrigation, domestic water supply, electricity generation and industrial water supply and for biotic life [1].

Sedimentation takes place in both live storage zone and dead storage zone. It is necessary to find out the percentage of sediment deposition and rate of sedimentation after particular time of interval considering impounding year as a reference. Loss of storage capacity should be calculated and compared with the originally designed data to estimate the sediment deposition in a reservoir [2].

Rather than going for new construction of dams, it is better to handle the sedimentation issues to restore the storage capacity of the reservoir to fulfil the various demands and avoid flood situation. Effective planning of water in a reservoir is one of the important factors to cater to the water shortage problem. Therefore, huge amount of water needs to be stored in a reservoir to fulfil the required demand. If sedimentation takes place at higher rate, then definitely it will reduce the designed life of reservoir [2].

In earlier days, hydrographic survey was used for sediment deposition studies which were time-consuming and less accurate compared with remote sensing technique [3, 4].

The present study deals with the sediment assessment of Mula reservoir, Maharashtra, India, using satellite remote sensing technique over the past 42 and 46 years using LANDSAT 8 satellite data, as it is one of the major and important projects within the upper Godavari basin water resources complex system.

2 Study Area

Mula dam is an earth fill and gravity dam on the Mula River near Rahuri in Ahmednagar district in the state of Maharashtra, India, forming a reservoir on its upstream. Index map of the study area is presented in Fig. 1. The latitude and the longitude of a reservoir are 19° 19′ 46″ N and 74° 31′ 46″ E, respectively. Year of impoundment of a reservoir is 1972, minimum drawdown level (m) = 534.01, full reservoir level (m) = 552.30, dead storage capacity (MCM—million cubic metre) = 129.55, live storage capacity (MCM) = 609.39, area at F.R.L. = 53.6 km^2 and catchment area = 2275.86 km^2 (source: https://www.india-wris.nrsc.gov.in/).

3 Data Used

The LANDSAT 8 satellite orbits the Earth in a sun-synchronous, near-polar orbit, at an altitude of 705 km (438 mi), inclined at 98.2° and circles the Earth every 99 min. The satellite has a 16-day repeat cycle with an equatorial crossing time: 10:00 a.m. ± 15 min. Different bands of the LANDSAT 8 are shown in Table 1.

Satellite imageries were downloaded from USGS earth explorer website for the years 2013, 2014, 2017 and 2018 by considering the minimum drawdown level and

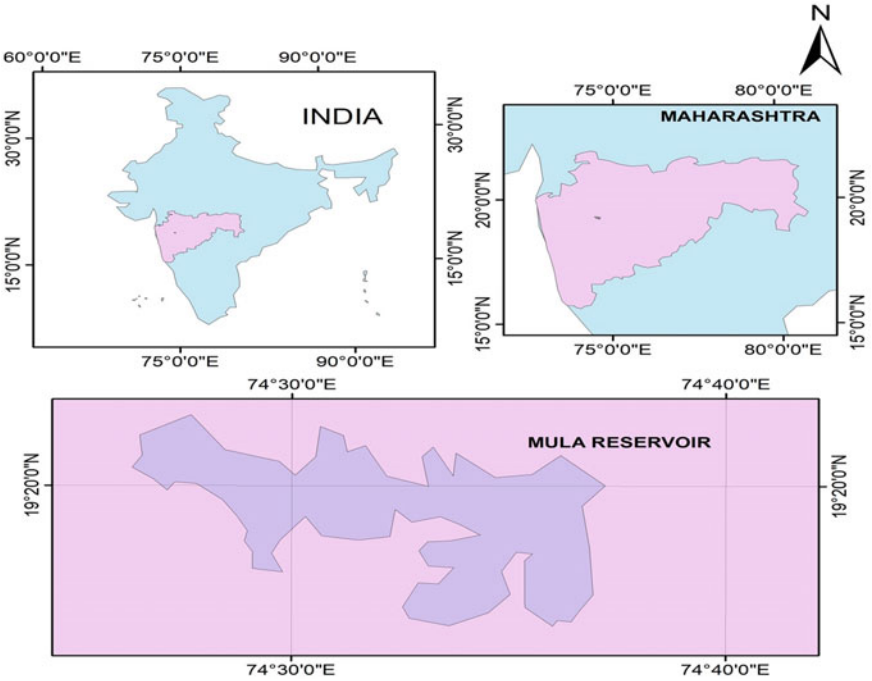

Fig. 1 Index map of Mula reservoir, Maharashtra (India). *Source* ArcGIS software

Table 1 All bands of LANDSAT 8 OLI and TIRS with their wavelength and resolution. *Source* https://www.usgs.gov/

LANDSAT 8 operational land imager (OLI) and thermal infrared sensor (TIRS)	Bands	Wavelength (μm)	Resolution (m)
	Band 1—Coastal Aerosol	0.43–0.45	30
	Band 2—Blue	0.45–0.51	30
	Band 3—Green Red	0.53–0.59	30
	Band 4—Red	0.64–0.67	30
	Band 5—Near Infrared (NIR)	0.85–0.88	30
	Band 6—Shortwave Infrared (SWIR) 1	1.57–1.65	30
	Band 7—Shortwave Infrared (SWIR) 2	2.11–2.29	30
	Band 8—Panchromatic	0.50–0.68	15
	Band 9—Cirrus	1.36–1.38	30
	Band 10—Thermal Infrared (TIRS) 1	10.60–11.29	100
	Band 11—Thermal Infrared (TIRS) 2	11.50–12.51	100

full reservoir level. Satellite imageries are freely available. Reservoir elevation data were downloaded from IWRIS website for the same year mentioned above.

4 Methodology

To estimate the storage capacity of any reservoir using satellite remote sensing technique, field data and satellite imageries are required.

Reservoir elevations were procured for the same date of downloaded satellite imageries. Elevation capacity curve at the time of first impounding of reservoir was also obtained from National Institute of Hydrology Website. Reservoir elevations were downloaded from IWRIS site which provides data for water resources engineering and management. Cloud-free satellite images were downloaded from USGS earth explorer website (LANDSAT 8). NDWI used for extracting the water spread area. Trapezoidal formula was used to estimate the volume/capacity of reservoir. Figure 2 shows the flowchart of sediment assessment technique using satellite imageries in ArcGIS software.

Sedimentation reduces the water spread area of a reservoir at various elevations, and ultimately, it reduces the live and dead storage capacity of the reservoir. Satellite imageries (Cloud-free images) are used for calculating water spread area at different elevations. Live storage zone is zone considered in between minimum drawdown level (M.D.D.L) and full reservoir level (F.R.L).

Normalized difference water index (NDWI) is used to find out water pixels which give water spread area, and then, by multiplying elevation between two reservoir levels, storage capacity for that height interval is obtained. NDWI formula is mentioned in the following. NIR represents near-infrared band.

$$\text{NDWI} = \frac{(\text{Greenband} - \text{NIRband})}{(\text{Greenband} + \text{NIRband})}.$$

Figure 3 shows the Raster calculator tool window in ArcGIS software, and the stepwise chart is shown in the following.

Figure 4 shows clip tool process window in ArcGIS software. Area of interest (AOI) can be extracted from the satellite image. Stepwise chart for Clip tool is shown in the following.

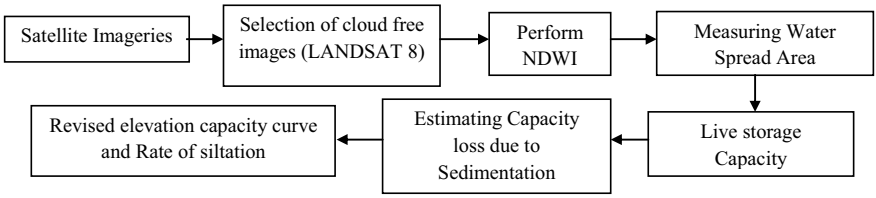

Fig. 2 Flowchart of sediment assessment technique using satellite imageries in ArcGIS software

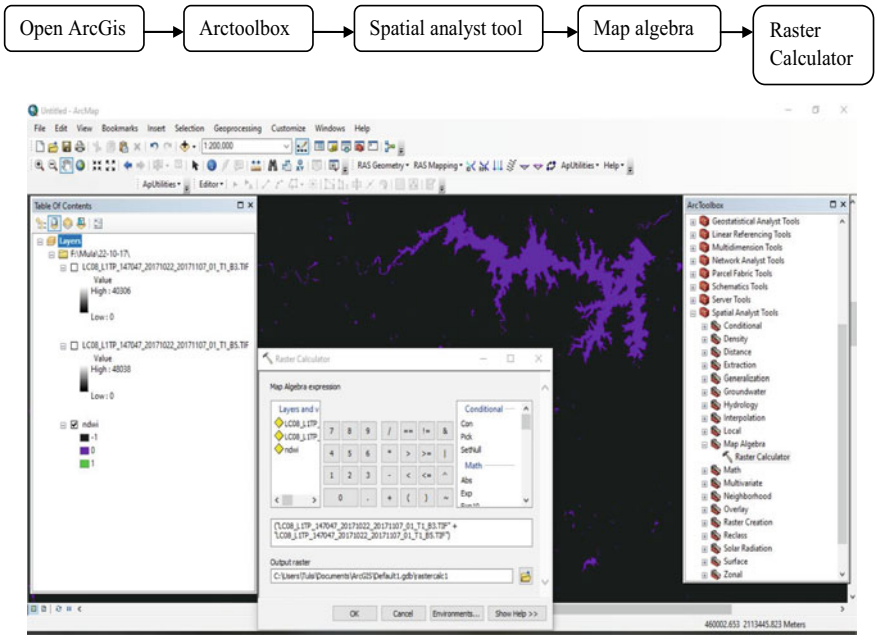

Fig. 3 Raster calculator tool in ArcGIS software

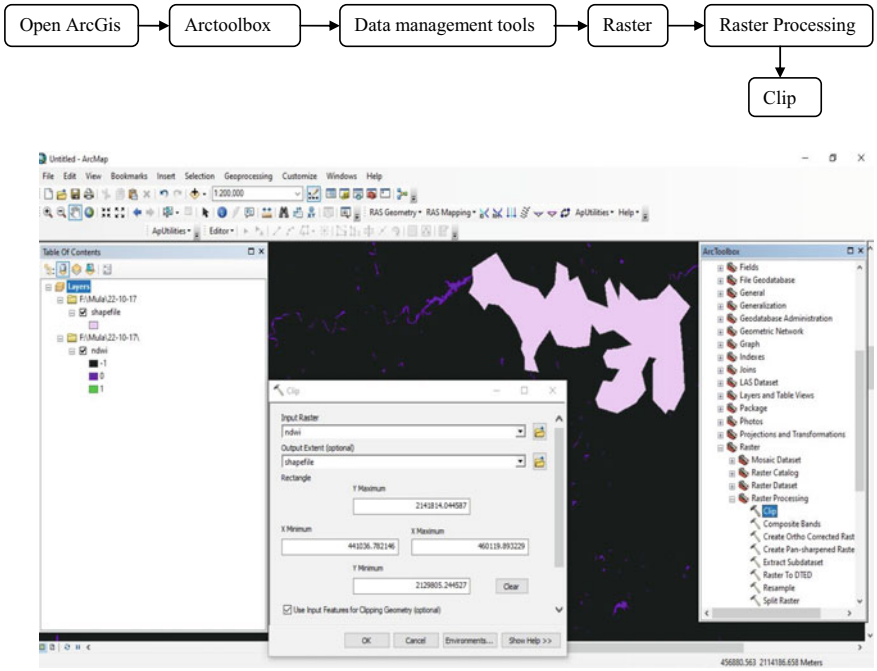

Fig. 4 Clip tool process in ArcGIS software

NDWI values range from −1 to 1. NDWI is most appropriate for water body mapping. It uses green and near-infrared bands of remote sensing. Generally, NDWI values greater than zero represent water spread area. NDWI is sensitive to built-up areas and often results in over-estimated water bodies. This technique was introduced by Mcfeeters (1996).

$$\text{Water spread area} = \text{No. of water pixels} * \text{pixel size}.$$

$$\text{Pixel size} = 30\ \text{m} * 30\ \text{m}\ (\text{LANDSAT 8 Spatial resolution}).$$

Capacity of reservoir between two successive RL or water levels is calculated using trapezoidal formula given as follows:

$$V = \frac{h}{3}\left[A1 + A2 + \sqrt{A1 * A2}\right]$$

where $A1$ is the water spread area at RL 1, $A2$ is the water spread area at RL 2 and h is the difference between RL or height interval [5].

5 Results and Discussion

After finding out the number of water pixels using Raster calculator (i.e. NDWI) and by multiplying it with spatial resolution size, water spread area can be obtained. By using trapezoidal formula, capacity of reservoir can be found out. Table 2 shows the observed and calculated data using pixel numbers.

Figure 5 shows the graph of original trend at the time of first impoundment—1972 and revised trend of elevation capacity curve for the year 2014.

Calculations:

$$\text{Cumulative revised live storage capacity} = 544.747\ \text{Mm}^3$$

$$\text{Designed original live storage capacity} = 574.36\ \text{Mm}^3$$

$$\text{Loss of live storage capacity} = (574.36 - 544.747/574.36) * 100 = 5.15\%$$

$$\text{Rate of siltation} = \frac{\text{Cumulative loss in live storage capacity}}{\text{Catchment area} * \text{year of last survey}} = \frac{29.613}{2275.86 * 42} = 0.3098\ \text{m}^3/\text{km}^2/\text{year}$$

Revised live storage capacity of Mula reservoir between near F.R.L. at R.L. 551.8 m and near MDDL at R.L. 535.02 m is estimated to be 544.747 Mm^3 for the year 2014 as against designed capacity of 574.36 Mm^3 with loss of 29.613 Mm^3 in 42 years.

Table 2 Observed data and findings

Date	Elevation (m)	Pixel no.	Spatial resolution (m)	Revised area (Mm^2)	Revised live capacity (Mm^3)	Cumulative revised live capacity (Mm^3)
24/06/2014	535.02	17,732	30	15.9588	–	–
08/06/2014	535.70	18,582		16.7238	11.111	11.111
23/05/2014	538.42	24,000		21.6000	51.979	63.090
07/05/2014	541.62	32,094		28.8846	80.493	143.583
21/04/2014	544.05	37,764		33.9876	76.306	219.889
15/01/2014	548.63	48,494		43.6446	177.317	397.206
14/12/2013	549.97	51,461		46.3149	60.264	457.470
28/09/2014	551.80	54,537		49.0833	87.277	544.747

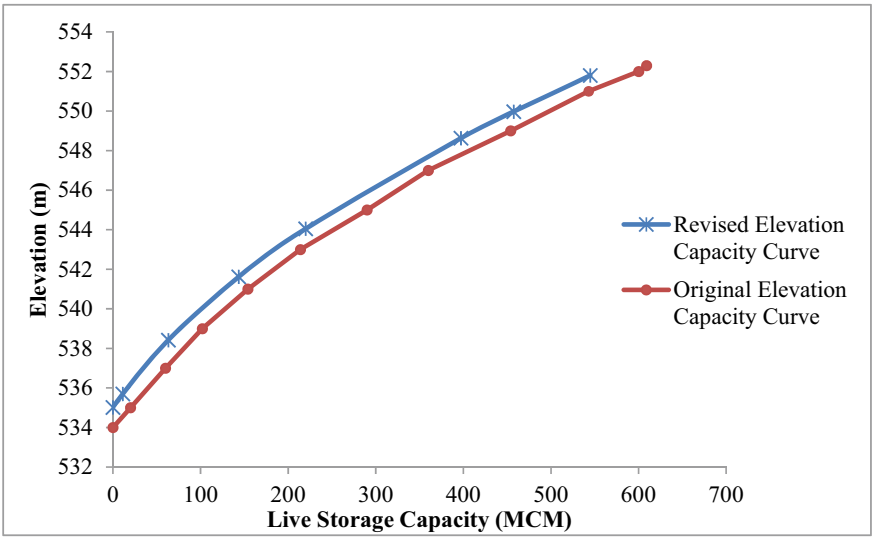

Fig. 5 Elevation capacity curve of live storage capacity for Mula reservoir (2014)

Table 3 Observed data and findings

Date	Elevation (m)	Pixel no.	Spatial resolution (m)	Revised area (Mm^2)	Revised live capacity (Mm^3)	Cumulative revised live capacity (Mm^3)
31/05/2017	534.95	17,575	30	15.8175	–	–
15/05/2017	538.35	20,840		18.7560	58.704	58.704
18/05/2018	539.57	24,066		21.6594	24.632	83.336
02/05/2018	542.14	32,771		29.4939	65.473	148.809
16/04/2018	543.06	35,734		32.1606	28.352	177.161
31/03/2018	544.89	40,178		36.1602	62.478	239.639
27/02/2018	548.67	48,513		43.6617	150.641	390.280
22/10/2017	552.29	53,860		48.4740	166.689	556.969

Rate of siltation in live storage zone is estimated to be 310 m^3/km^2/year.

Table 3 shows observed and calculated data using pixel numbers.

Figure 6 shows the graph of original trend at the time of first impoundment—1972 and revised trend of elevation capacity curve for the year 2018.

Calculations:

$$\text{Cumulative revised live storage capacity} = 556.969\ \text{Mm}^3$$

$$\text{Designed original live storage capacity} = 589.36\ \text{Mm}^3$$

$$\text{Loss of live storage capacity} = (589.36 - 556.969/589.36) * 100 = 5.5\%$$

$$\text{Rate of siltation} = \frac{\text{Cumulative loss in live storage capacity}}{\text{Catchment area} * \text{year of last survey}} = \frac{32.391}{2275.86 * 46} = 0.309\ \text{Th.m}^3/\text{km}^2/\text{year}$$

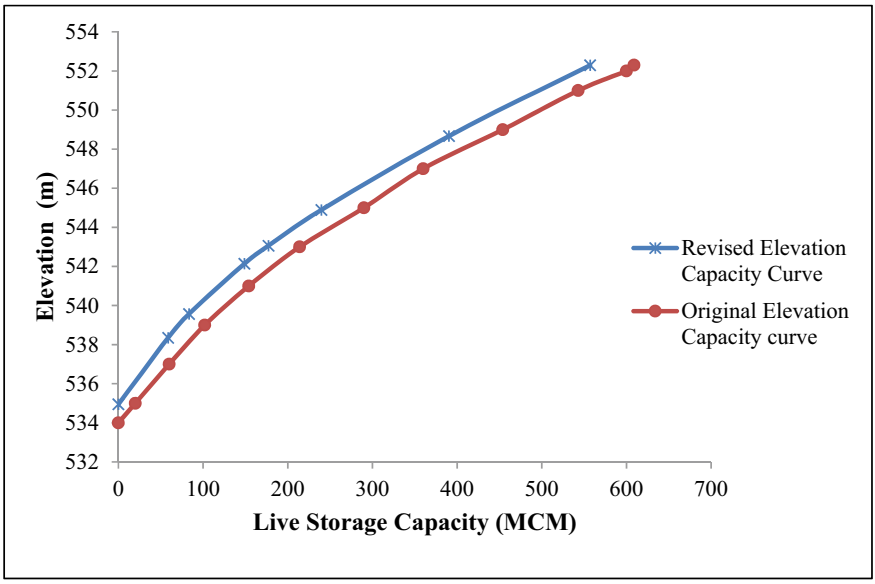

Fig. 6 Elevation capacity curve of live storage capacity for Mula reservoir (2018)

Revised live storage capacity of Mula reservoir between near F.R.L. at R.L. 552.29 m and near MDDL at R.L. 534.95 m is estimated to be 556.969 Mm^3 for the year 2018 as against designed capacity of 589.36 Mm^3 with loss of 32.391 Mm^3 in 46 years.

Rate of siltation in live storage zone is estimated to be 309 m^3/km^2/year.

Water spread area is calculated using Raster calculator tool process in ArcGIS software, which is shown in the following figures. Thus, Figs. 7 and 8 show water spread area on 31/05/2017 (near M.D.D.L) and 22/10/2017 (near F.R.L.), respectively.

Fig. 7 Water spread area on 31/05/2017 (near M.D.D.L)

Fig. 8 Water spread area on 22/10/2017 (near F.R.L.)

6 Conclusion

Sediment deposition in the reservoir gradually reduces the storage capacity of reservoir. Runoff coming from whole catchment area is accumulated in the reservoir which carries sediment particles with it. Accumulation of sediment particles over long period of time reduces the designed life of reservoir. There is not much variation in the percentage loss of live storage capacity of Mula reservoir. Rate of siltation for both the study years is same. The percentage loss of live storage for the years 2014 and 2018 is 5.15 and 5.5, respectively. Rate of siltation for both study years is found to be same, i.e. around 310 m^3/km^2/year, which is good under prevailing conditions of Indian reservoirs as per CWC study in 2001 [6]. Mula reservoir has not much significant sedimentation issue.

Acknowledgements The authors are thankful to Science and Engineering Research Board (SERB-ECR/2016/001409) affiliated to the Department of Science and Technology (DST), New Delhi, for providing necessary funds for the present study.

References

1. Jibhakate TM, Mirajkar AB (2019) Reservoir sedimentation-estimation and remedial measures. J Indian Water Works Assoc 4:295–301
2. MERI Nashik Report (2012) Reservoir capacity evaluation and sedimentation assessment in Pench (Kamathi Khairi) Reservoir District Nagpur by Satellite Remote Sensing Technique
3. Deshmukh DN, Roman UC, Jatwa S (2007) Assessment of sedimentation in Jayakwadi reservoir using satellite imageries—a case study Hydro2007 book
4. Jain SK, Singh P (2002) Assessment of sedimentation in Bhakra Reservoir using Remote sensed data. Hydrol Sci J 47(2):203–212
5. Khadtare MY, Jedhe SH (2017) Sediment assessment of UJJANI Reservoir in Maharashtra by using remote sensing technique. Int Res J Eng Technol 4(8):1255–1258
6. CWC Report Capacity Survey of Jayakwadi reservoir by RITES-Rail India Technical and Economic Service January 2001. https://www.india-wris.nrsc.gov.in/. https://www.earthexplorer.usgs.gov/

Application of Remote Sensing and GIS for Tidal Power Potential Assessment

Vishvesh Hanumantrao Kodihal, Harsha Satish Maheshwari, Prathamesh Avinash More, and Purushottam Kashinath Deshpande

Abstract Tidal power is an alternative of one of the pioneer approaches for sustainable development. This type of energy generation has been developed very little, but in support of less research and tough job in finding locations, favourable to establish tidal power plants. The methodology, used in the present work, can be harnessed for any of the future tidal power plants having small scale but local sustainable domain in terms of energy. By briefing the status of tidal energy worldwide as well as in India and learning the model used for estimating the power potential, an attempt has been made on the potential assessment carried out at specific location of Talasheel creek of Gad river (District Sindhudurg, Maharashtra, India) and reassessment of the energy potential in terms of scientific evaluation and strategic planning by the study of tidal stream generator and types of stream generator and proposing the suitable turbine for required site by analysing their specifications, measuring the actual hydrodynamic parameters have been incorporated in present study. Depth and velocity along cross section was found, and correlating them with satellite image data and obtaining the profile of cross section of creek by terrain view as well as by mathematical model using Lagrange Nth degree polynomial interpolation, has been attempted. It is observed that the correlation between the power rating of stream turbines can be performed thereby power generation potential for local zones can be estimated as a fraction of total energy requirement in future, incorporating influence of population rise and withholding the number of turbines to be accommodated. The geological and topographical constraints have also been considered. Further, it is concluded that the similar geoinformatic approach can be extended for different creeks/estuaries along the Indian coast for estimation as well as assessment of tidal power generation potential in an easy manner.

Keywords Tidal power generation · Satellite imagery · Hydrodynamic parameter · Energy requirement · Creek · Sustainable source · Forecast · Turbine

V. H. Kodihal (✉) · H. S. Maheshwari · P. A. More · P. K. Deshpande
Department of Civil Engineering, Walchand College of Engineering, Sangli, Maharashtra 416415, India
e-mail: purushottam.deshpande@walchandsangli.ac.in

B. Laishram and A. Tawalare (eds.), *Recent Advancements in Civil Engineering*, Lecture Notes in Civil Engineering 172,
https://doi.org/10.1007/978-981-16-4396-5_77

1 Introduction

GIS and RS are being used in every sector these days. It is possible to obtain geomorphological properties of any region from any place around the world. Not just this, but processing of the data and its projection to form an illusion of future have taken a trend.

Working in such a dynamic technique needs dynamic attention. Selection of project which would be remarkable in this Indian Phenomenon that is tidal power development. Using RS and GIS is the main objective, and it is possible to workout suitable sites for the tidal power plant with the remote sensing data.

1.1 Objectives

1.1.1. To find locations using RS and GIS for tidal power plant establishment which will further lead to development of the coastal region in terms of sustainability in power and ecotourism.
1.1.2. To acquire geomorphological data about selected locations from different working satellites as well as on site observations and processing data for power plant pattern design.
1.1.3. To theoretically estimate the number of turbines required for effective power generation of selected zone/area.

1.2 Scope of Project

Tidal power generation is considered in clean energy development as it does not lead any harm to the nature. Tides are renewable source of energy so its utilisation would not hamper an account of resources available in nature; therefore, it stands as sustainable source of energy [1].

Power availability leads to development in terms of business, industry and productivity. Tidal power will provide an opportunity to rely on self-efficiency of the region in terms of electricity which enhances the economy of the region. Scope of the project is to find and study the suitable locations using remote sensing data and estimate theoretically about the turbine requirement and power generation.

2 Literature Review

2.1 La-Rance Tidal Power Station, France

OES Environmental Metadata—La Rance Tidal Barage. The Rance river estuary was picked because of its huge tidal range, with the site really flaunting the most noteworthy range in the country with a depth of 8-m among low and high tide. In the spring and neap range, this figure can jump to as high as 13.5-m. During the initial two years of development, two dams were worked to obstruct the Rance, guaranteeing the estuary was totally depleted and empowering the supply's foundation over the site. Altogether, development took five years with an underlying structure cost of $100M. While it took around 20 years to pay for itself, the task has now recouped the whole of its expenses through investment funds produced using its life—and the tidal energy produced costs less than nuclear or solar power. Since its development, the plant has generated roughly 27,600 GWh of power, proportionate to around £3.3B at the present costs [2].

2.2 Gulf of Kutch, Gujarat, India

Tidal power potential assessment along the Gulf of Kutch, Gujarat, India.

Satheesh Kumar Jeyaraj Indian Institute of Technology Bombay, Revathi, B VIT University.

The main objective of this study was to estimate the tidal power potential along the Gulf of Kutch and to identify the potential tidal power extraction locations. A regional depth-averaged hydrodynamic model has been used to estimate the spatial and temporal distributions of tidal energy in the Gulf of Kutch. The Gulf is characterised by strong current with averaged velocities exceeding 2 m/s. The model is simulated with global tidal constituents, and the results are successfully calibrated and validated with earlier field measured literature based data. The estimation of currents and tidal levels obtained from the numerical model are in good agreement with that of field data all over the gulf. The estimation of annual power and energy output are calculated, considering spatial and temporal variations in flow velocities and in power density both across and along the gulf [3].

2.3 Tidal Power Potential in India

Study on Tidal and Waves Energy in India: Survey on the Potential and Proposition of a Roadmap.

AgenceFrançaise De Développement (Afd) and Indian Renewable Energy Development Agency Limited (Ireda).

This case study is based on one of the earliest works done by Ministry of New and Renewable Energy (MNRE). The study indicated an estimated potential of about 8000 MW with 7000 MW in the Gulf of Kambhat, 1200 MW in the Gulf of Kutch in Gujarat and about 100 MW in the Gangetic delta in Sunderbans in West Bengal. Since the potential assessment depends largely on the technology and methodology to be used, these figures could be updated continuously based on the proposed technology and methodology. This case study presents the fact that three regions in India provide the largest concentration of energies. These are namely Khambat, Kutch and Sundarbans regions because of their large tidal ranges. However, it brings out the fact that when flow velocities are enhanced at the openings on the coastline, it is possible to release reasonably good amount of energy in terms of KE. Hence, for regions with low tidal range, the obvious choice will be to modify the flow pattern of the tidal flooding and ebbing so that reasonably good currents are generated [4–6].

3 Overview and Methodology

Tidal power plants around the world have been located in deep sea zones. Finding out the site which will be easy in terms of its maintenances and construction has been point of interest; this term of condition for the site of plant led to the conclusion that site can be any confluence of creek with the open sea.

1. Initially, an appropriate location was scrutinised with the help of Google Earth at the reconnaissance level. Further, the longitudinal as well as cross-sectional profile of the selected creek was assessed using digital elevation model and bathymetric data by sub-setting the required area. This data was verified against practical morphological data.
2. The depth and the velocity obtained during practical site inspection is used in order to compute the energy generation per turbine, which is one of methodologies used for evaluating tidal power potential of water bodies in the literatures which have been reviewed.
3. The fraction of energy that can be furbished through tidal turbines is estimated by calculating both energy projection (using energy unit per dwelling) and the energy generated by turbines (finding grid pattern and optimum number of turbines).

4 Location of the Proposed Tidal Power Project

Site to be creek cleared a point that it can be found in south-east or south-west part of the country. In consideration of Google Earth imagery, the team worked and located slopes of the creeks in the region of Kokan, Maharashtra. After a delicate comparison a creek of Gad river (Talashil Creek) above the Malvan, Maharashtra,

Fig. 1 Talasheel Creek, Malvan, Maharashtra India (Google Earth) [7]

India, seemed to be location of interest with earth coordinates (Lat, Long): (16° 05′ 15″, 73° 27′ 43″), at mouth 271 m wide (Fig. 1).

5 Satellite Data and Processing (ILWIS 3.3 Academic)

1. USGS EARTH EXPLORER- Landsat 8 (30 m) [8] (Fig. 2).

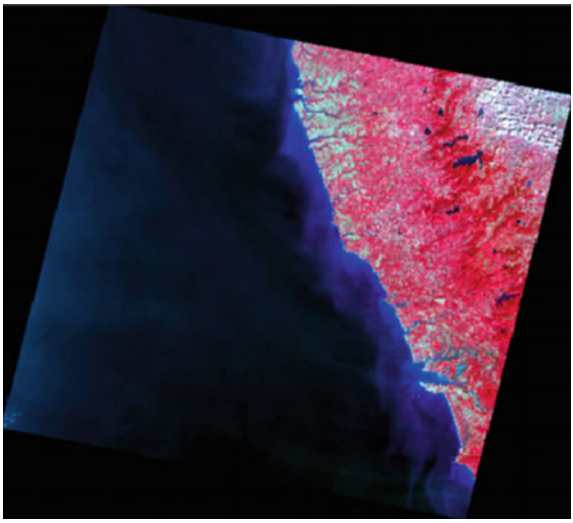

Fig. 2 Landsat 8 standard FCC

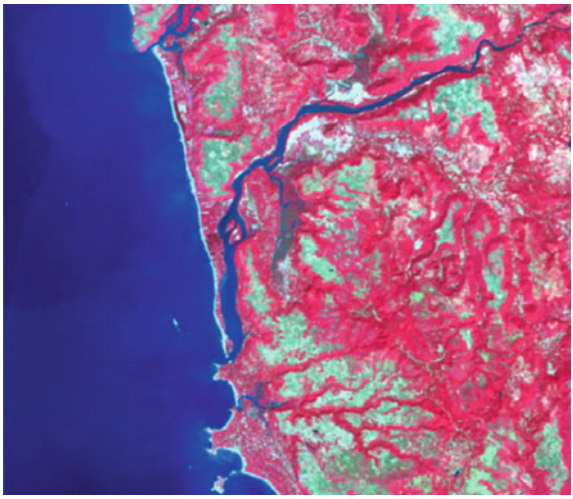

Fig. 3 FCC of the western zone having selected site

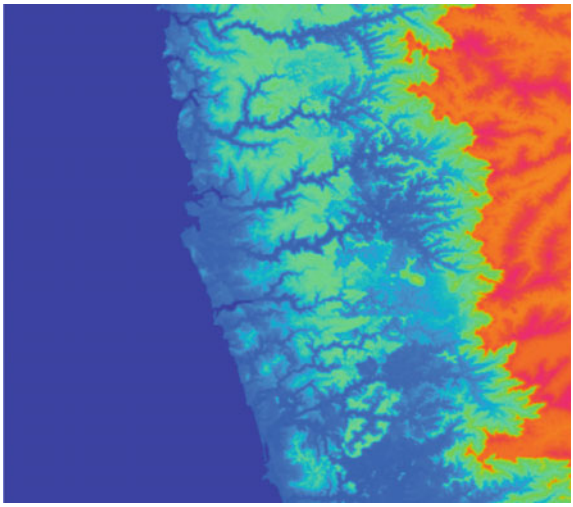

Fig. 4 Processed DEM (Using ILWIS Academic) [13]

2. ResourceSAT 1 LISS-III (23.5 m) [9].
3. DEMCartosat-1 [10–12] Resolution-30 m Smallest Tile Size (Fig. 4).

Resolution of the data acquired for assessment is not sufficiently high. Hence, further base computation was opted.

Fig. 5 Stretch at mouth of the creek (Google Earth) [7]

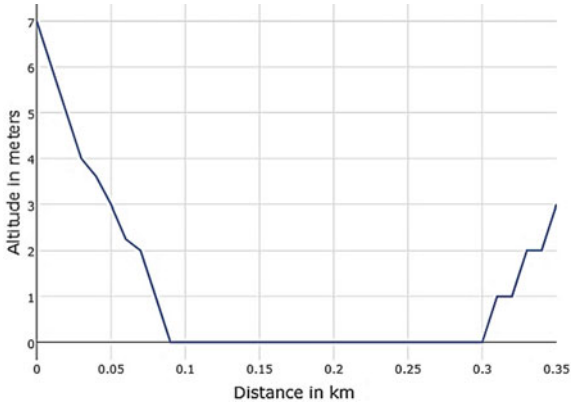

Fig. 6 Graph of elevation versus distance

6 Computation of Base Profile

Estimating the base of the cross section of the river: Initially the base was plotted using Terrain **Profile Plotter** (3D terrain view) from Bhuvan 3D, provided by NRSC/ISRO Bhuvan. This profile is plotted for a distance of 300–350 m. Snap distance used for the plotting was **1 m** which was the finest/least snapping distance available on Bhuvan.

As the above graph (Fig. 6) does not reflect the similar morphology of creek, on-site data was obtained by practically visiting and measuring the depth at different points (Fig. 5).

Following is the data set collected (Table 1).

Further in order to get the base profile (Fig. 7), polynomial tracing using Langrange Interpolation was used;

Table 1 Data set Collected

X (distance from one end) [m]	Y (depth available) [m]
0	0
100	8.65
214	6.2
300	0

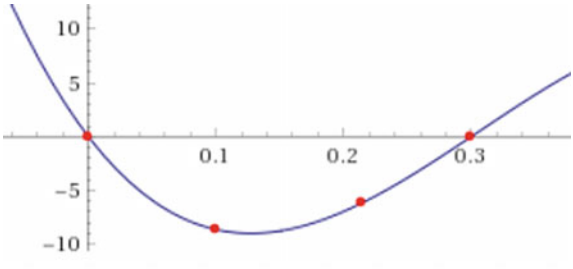

Fig. 7 Curve of depth versus base

Langrange Polynomial:

*N*th degree polynomial approximation formula to the function $f(x)$, which is known at discrete points x_i, $i = 0, 1, 2...$ *N*th.

$$f[x_0, x_1, ...x_n, x] = 0$$

$$f(x) = \frac{(x-x_2)(x-x_3)\ldots(x-x_n)}{(x_1-x_2)(x_1-x_3)\ldots(x_1-x_n)}y_1 + \frac{(x-x_1)(x-x_3)\ldots(x-x_n)}{(x_2-x_1)(x_2-x_3)\ldots(x_2-x_n)}y_2 + \cdots + \frac{(x-x_1)(x-x_2)\ldots(x-x_n-1)}{(x_n-x_1)(x_n-x_2)\ldots(x_n-x_n-1)}y_n \quad (1)$$

Hence the polynomial obtained:

$$f(x) \rightarrow -853.743x^3 + 767.997x^2 - 154.912x \quad (2)$$

Depth is in metres and the distance is in kilometres (Fig. 7)

7 Power Requirement Estimated for year, 2050

7.1 Population Projection

Power required is calculated using the method of population projection for 2050 assuming five people per house.

Following is the data according to 2011 Census Survey; population of Malvan is equal to **18,648**.

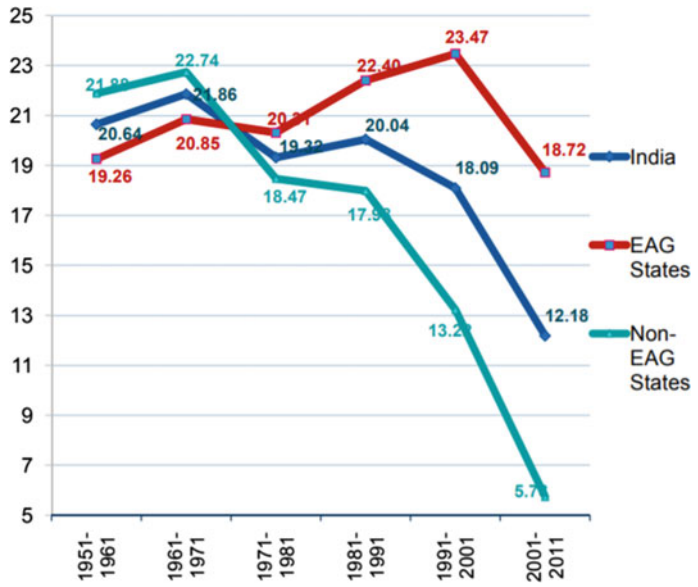

Fig. 8 Population projection

The rate of growth of population (in percentage) versus end of decade for rural/suburban areas of the country are shown in the graph (Fig. 8).

As Malvan falls under Non-EAG states of India the average decade growth rate is equivalent to 5.7% but assuming the growth rate of rural states in **6%**.

Assumed growth in population (r) = **6%/decade**.

Hence, from the year 2011 till the end of year 2050, as the town is in rural area and growth pattern is using arithmetic progression for population forecasting.

$$\begin{aligned} \text{Total population} &= P + nC \\ &= 18,648 + (4 \times 0.06 \times 18,648) \\ &= 23,123 \\ &= 23,500 \end{aligned} \tag{3}$$

Number of household units in Malvan at the end of 2050 = 23,500/5 = **4700 units**.

7.2 Calculation of Energy Requirements

Energy calculation has been done for domestic (residential) purposes only; the data required for the energy unit division is taken from prayaspune.org in cooperation

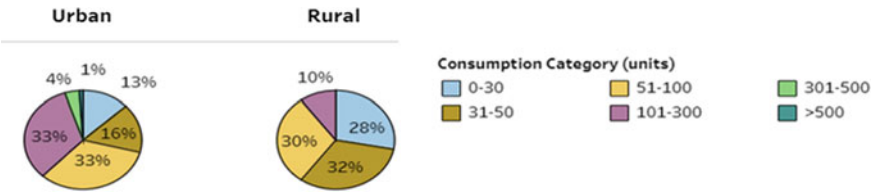

Fig. 9 Power consumption

Table 2 Calculation of energy (Data interpreted from Fig. 9 of Power Consumption)

Sr. no	Consumption category [units]	Average consumption [units]	Percentage	No of households w. r.t percentage	Consumption [kWh]
1	0–30	15	28	1316	19,740
2	31–50	40	32	1504	60,160
3	51–100	75	30	1410	105,750
4	101–300	200	10	470	94,000
5	301–500	400	0	0	0

with Centre for Policy Research and all the data is captured by Central Electricity Authority, India [14].

As Malvan comes under rural category, specific electricity requirement can be calculated as follows, dividing the 4700 household units according to the given pie chart (Fig. 9, Table 2).

Total energy consumption in units is equal to **279,650 kWh**.

As the above computed energy is on monthly basis, converting it on hourly basis at the end of 2050:

$$\frac{279650}{24 \times 30} = \mathbf{388.41\,kWh}$$

7.3 Energy Generated Using Turbine

Depending on the profile of the cross sectional base of the creek and also the utilisation of the boundaries,

1. It is beneficial to the left part of the creek for turbine installation as the right boundary mostly consists of the commercial values and is also the boundary which connects the city.

Fig. 10 Dock at the creek

Fig. 11 Longitudinal stretch at the mouth of creek

2. The profile obtained on the leftmost boundary is steeper as compared to the right boundary (Fig. 6) which provides higher depth as required by the turbines at shorter distance ensuring high velocity of streams.
3. Considering the neck region in order to avail maximum velocity at the confluence of sea and creek.
4. Even though from the imagery creeks looks shallow on the right border, it has enough depth for the movement of the boats (Fig. 10).

Therefore Stretch selected:

1. Along longitudinal equal to 400 m approximately (ensuring the zone of confluence) (Fig. 11)
2. Along cross section equal to 100 m approximately (ensuring the mobility of boats).

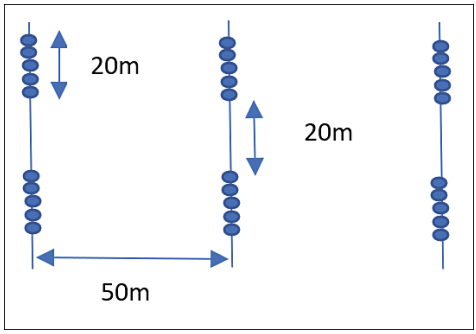

Fig. 12 Grid system for the turbine

Hence, following the grid connection system (Fig. 12).

This method is thought from the solar power generation grid system.

Along cross section, connecting five turbines in series and allowing space of 20 m between two series connection to avoid grid failure and feasibility for maintenance.

Along the cross section each, parallel line is placed at distance of 50 m to ensure normalisation of the flow past the preceding turbines (Fig. 12).

Length of one turbine is equal to 3.2 m (taking as 3.5 m); hence, length of five turbines is equal to 17.5 m. Hence, 20 m as an overall requirement.

7.3.1 Total no of Turbines that Can Be Placed According to the Design Adopted:

Along Cross section:

$5 \times 3(\text{stretch}) = 15$ turbines

Along length section: $400/50 = 8$

Therefore total no. of turbines $= 8 \times 15 = 120$

Type of turbine used is Monofloat turbine:

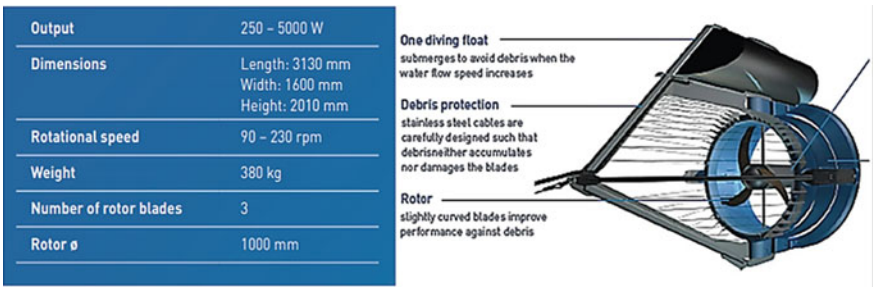

Fig. 13 Monofloat turbine [4]

7.3.2 Power Generated by Single Turbine

As described above, the power generation of monofloat turbine depends on the velocity of the water (Fig. 13).

1. Velocity of water was measured on the site at the water surface,
2. Data was collected on 3rd–4th day after the occurrence of **New Moon Day** which ensures that available tidal range and velocity would pertain larger values than following:

During the **low tide,** velocity was found to be 1.62 m/s, method used was float method as the maximum velocity is at distance of 0.05d–0.15d below the surface; hence, an increase in 5% can be seen.

Also, applying a kinetic correction factor of 1.1 as the flow is considered as turbulent.

Therefore, **low tide flow velocity = 1.871 m/s**.

During the **high tide** in the evening, the velocity at the confluence reached as high as 2.1 m/s after applying the required corrections.

Therefore, **high tide velocity = 2.4 m/s**.

Considering average flow velocity for the determination power generation.

Average Velocity:

$$\frac{2.4 + 1.871}{2} = \mathbf{2.1355\,m/s}.$$

From graph (Fig. 14):

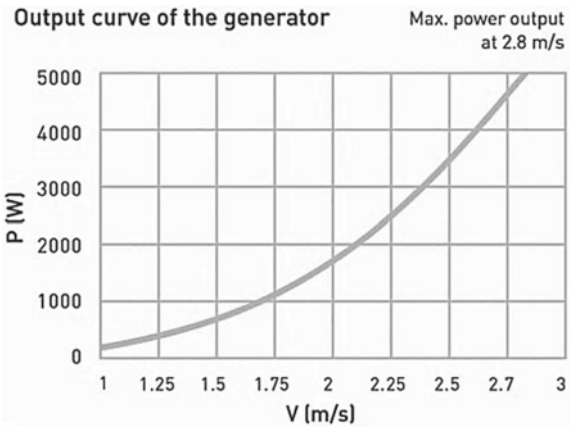

Fig. 14 Plot of $P[W]$ versus V[m/s] [12]

$P(W)$ for Velocity equal to 2.13 m/s ranges between 2.1 and 2.3 kW.

Assuming on the lower side i.e. 2.1 kW.

Hence, energy generation per hour is equal to 2.1 kWh.

Total energy generated by 120 turbines:

$=120 \times 2.1 =$ **252 kWh**.

Providing 20 turbines for standby purpose or to cater transmission losses, thereby available number of turbines is equal to 100 turbines.

Energy generated by 100 turbines:

$=100 \times 2.1 =$ **210 kWh**.

Calculation of fraction of electrical energy requirement that can be provided by turbines is as follows:

Considering Full Potential:

$$\text{Fraction of Electrical Energy provided at the end of 2050} = \frac{\text{Electrical Energy generated by Turbine}}{\text{Total Energy Demand}} \times 100 = \frac{252\,\text{kWh}}{388.41\,\text{kWh}} \times 100 = 64.87\%$$

Considering 20 Turbine to overcome Transmission loss:

Transmission loss = 20% of production

$$\text{Fraction of Electrical Energy provided at the end of 2050} = \frac{\text{Electrical Energy generated by Turbine}}{\text{Total Energy Demand}} \times 100 = \frac{210\,\text{kWh}}{388.41\,\text{kWh}} \times 100 = 54.06\%$$

Added Benefit—Due to global warming further increase in water level will ensure higher energy rates as the capacity of single turbine is about 5000 W whereas only 2100 W energy is being considered in design, which can be achieved by changing the shaft level of the turbines.

8 Conclusion

Tidal power being renewable source of energy leads the sustainable development, which is growing need of this era since gadget life is growing with every second turn of time. The results of study of Talasheel Creek near Malwan, India, show that even after considering 20 turbines on standby a fraction of about 54.06%, total electrical energy requirement of Malvan at the end of year 2050 can be provided by harnessing tidal power energy which also promotes towards the sustainability and cuts the usage of coal based energy generation. Hence, with the use of remote sensing and GIS data, the properties such as tidal velocity, depth and stretch of

different creeks can be obtained and similar methodology can be applied to obtain the tidal energy potential of various similar places and profitable extraction of energy can be estimated and planned.

References

1. Salequzzaman M (2002) Prospects and sustainability of green power: case study of tidal power. 10th international conference of the greening of industry network. Göteborg, Sweden, pp 23–26
2. La Rance Tidal Power Plant. http://www.reuk.co.uk/la-rance-tidal-power-plant.html
3. Satheesh-Kumar J, Balaji R (2016) Tidal power potential assessment along the Gulf of Kutch, Gujarat, India. In: Proceedings of the Asian wave and tidal energy conference (AWTEC)
4. Murali K, Sundar V (2017) Reassessment of tidal energy potential in India and a decision-making tool for tidal energy technology selection. Int J Ocean Clim Syst 8(2):85–97
5. AgenceFrançaise De Développement (AFD) & Indian Renewable Energy Development Agency Limited (IREDA) (2014) Study on Tidal & Waves Energy in India: Survey on the Potential & Proposition of a Roadmap Final Report.
6. www.toppr.com/bytes/tidal-energy-in-india/amp/s
7. Google Earth, https://earth.google.com/, 1 (2019)
8. https://landsat.gsfc.nasa.gov/landsat-data-continuity-mission/
9. https://en.m.wikipedia.org/wiki/Resourcesat-1
10. www.isro.gov.in/Spacecraft/cartosat-1
11. https://data.gov.in/resources/cartosat-1dem-version-1
12. https://en.m.wikipedia.org/wiki/Cartosat-1
13. https://bhuvan-app1.nrsc.gov.in/globe/3d.php
14. Prayas Energy Group: www.prayaspune.org/peg/trends-in-india-s-residential-electricity-consumption
15. Etemadi A, Emami Y, AsefAfshar O, Emdadi A (2011) Electricity generation by the tidal barrages. In: ICSGCE 2011 Chengdu, China, Energy Procedia 12, pp 928–935

Rainfall Trend Anomalies Over Wainganga Basin, Central India

Saranya C. Nair and Ashwini B. Mirajkar

Abstract Trend analysis has been carried out to account for the flood studies of the Wainganga basin, Central India, for a period of 1913–2013. Gridded rainfall data of 0.25° × 0.25° resolution collected from India Meteorological Department (IMD) is used for the analysis. Three different approaches namely the Mann–Kendall method, Spearman's rho test (with 0.05 significance level), and Innovative trend method have been used for detecting the rainfall trend of the study area. ArcGIS 10.2 software was used for generating the choropleth map of rainfall variability. Results are pointing to the fact that there is a decreasing trend in rainfall across the basin; however, the trend is gradually increasing for extreme events of rainfall. The augmented number of extreme events is causing a knockdown to the agricultural economy of the area.

Keywords Mann–Kendall · Trend analysis · Flood

1 Introduction

India, being an agrarian country, solely depends on its water resources to sustain the livelihood and economy. The major management issue our nation is handling is that it has to attend 16% of world population with 4% of world's water resources [4]. In addition to this, there is disarray in the climatic behavior with erratic rainfall and unpredictable drought/flood episodes [16]. The only solution to address the situation is to conduct a thorough study of the existing hydrologic parameters and appositely integrating existing resources and demands [6]. Hence, water resources planning and management with proper account of the hydrological parameters is the

S. C. Nair
Water Resource Engineering VNIT, Research Scholar, Nagpur 440010, India
e-mail: saranyanair@students.vnit.ac.in

A. B. Mirajkar (✉)
Department of Civil Engineering VNIT, Nagpur 440010, India
e-mail: abmirajkar@civ.vnit.ac

B. Laishram and A. Tawalare (eds.), *Recent Advancements in Civil Engineering*, Lecture Notes in Civil Engineering 172,
https://doi.org/10.1007/978-981-16-4396-5_78

need of the hour. But the present scenario with unpredictable flood–drought events and erratic monsoon pattern is making the situation worst for planners. Before proposing any water resources strategy, it is important to check the future rainfall scope of the region [1]. Time series analysis is a statistical application to scientifically identify the trend behavior in the future with the help of past data [2, 10, 11]. The research was carried out to contribute the flood management studies of Wainganga basin situated in Vidarbha region of Maharashtra, India. Wainganga basin with an average annual rainfall of 1500 mm is under the threat of flooding with floods having intensity of 1600–1900 mm occurring in every 5–6 year [14]. Before proposing a flood mitigation strategy to the study area, it is important to ascertain the changes in rainfall pattern and to foresee the trend following. The main purpose of time series analysis is to collect past data, analyze it precisely and to draw generalizations which describe the inherent trend [5]. Trend analysis is testing the tendency of values in a series to ascertain the behavior or pattern for a parameter of interest. The nonparametric Mann–Kendal trend statistics is widely used to investigate the future scenario of rainfall [7, 9, 13, 21]. Taxak in 2014 studied the rainfall trend of Wainganga basin with 0.5 × 0.5 resolution data, covering 18 grids and found out that the rainfall trend is decreasing [19]. In the present study, the data at 0.25 × 0.25 resolution, covering 100 grids is analyzed. The monthly maximum and annual maximum rainfall trend analysis was carried out to reveal how the basin is still under the threat of flooding even if the overall rainfall trend is decreasing.

2 Study Area

The geographic location of Wainganga basin extends from 19°30′N to 22°30′N latitude and 79°00′E to 80°30′E longitude. It is one of the largest subbasins of the Godavari River with the highest forest cover in the state of Maharashtra. Wainganga River originates from the southern slopes of the Satpura range of Madhya Pradesh and joins the Wardha River after completing a course of around 580 km. After Wardha, it finally reaches Pranhita (229 km) and ultimately combines with the Godavari River. Most part of the basin is made up of igneous rocks formed from volcanic eruptions, geologically termed as “Deccan Trap.” The basin is characterized predominantly by black regular loamy soil along with clayey loams.

The climatology of the study area can be outlined as three dominant seasons via summer, monsoon, and winter, following the order March–May, June–October, and November–February, respectively. Temperature hits up to 47 °C during summer and minimum temperature during winter varies from 7 to 13 °C. The southwest monsoon owes a major part of the rainfall of the basin. Wainganga basin lies in the medium rainfall zone of 900–1600 mm [8]. It is observed that the basin experiences a contrasting climatic behavior against the whole state of Maharashtra [3]. The rainfall rate is progressively increasing devising flood as a major problem of the area. The location map of study area is given in Fig. 1.

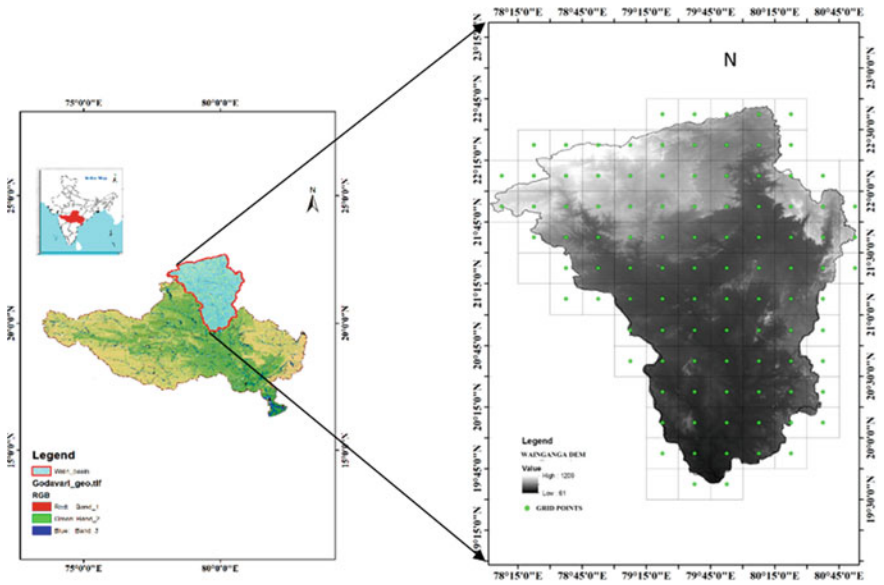

Fig. 1 Location map of Wainganga Basin, India

3 Data and Methodology

The data required for the analysis was procured from India Meteorological Department, Pune (IMD). Daily gridded rainfall data having 0.25 × 0.25 spatial resolution from 1913 to 2013 (101 years) was extracted, sorted, and analyzed. Before taking the data for trend analysis, the given data was checked for preliminary analysis like computing mean, standard deviation, and checking outliers. Homogeneity analysis was carried out to the data series as a prerequisite to check whether the data belongs to the same statistical population. Trend analysis was carried out using two different approaches, nonparametric method, and graphical method to incorporate as many possible hypotheses, changes in distribution, and changes in average. Nonparametric tests were used so that the skewness of the data series can be sidestepped. Mann–Kendall test (MK) and Sen's slope estimator were the nonparametric tests conducted and innovative method of trend analysis by [20] was the graphical method adopted.

3.1 Mann–Kendall Test

Mann–Kendall test is one of the most popular nonparametric tests used by researchers all over the world for detecting the trend of different climatic variables [15, 17].

3.2 Sen's Slope Estimator

Sen's slope method is a nonparametric method in which trend prediction is carried out by slope calculation and is given in Eq. (1).

$$S_i = \frac{a_j - a_k}{j - k}, \text{ for } i = 1, 2 \ldots N \tag{1}$$

where a_j and a_k are the values at respective times of j and k. If there is only a single data point for the given time period, then $N = \frac{n(n-1)}{2}$ and for multiple data points, $N < \frac{n(n-1)}{2}$, n is the total number of observations.

3.3 Spearman's Rho Test

Spearman's rho test is a nonparametric test which is similar to the Mann–Kendall test, but the correlation of data is carried out with respect to time [12].

3.4 Innovative Trend Analysis

Innovative method of trend analysis proposed by Şen [18] is simple as well as a powerful tool for detecting the trend. The concept behind the method is to arrange the series along the 1:1 line of the Cartesian plane and examine the scatter to get an idea about the trend [18]. Based on the clustering of data points in the graph, analysis can be carried out. According to Sen, the plotted points will cluster on the 1:1 line; if the series is devoid of trend and for increasing or decreasing trend, the points will be seen above or below the 1:1 line.

4 Result and Discussions

Rainfall variability pattern along with trend analysis was carried out for the Wainganga basin. The 100-year rainfall data was divided into three sets, with the first two sets having 30 years each and 40 years in last set and rainfall variability map was generated and given in Fig. 2. Rainfall variability map depicts the degree to which rainfall varies with time.

Grid-wise observation shows that during 1914–1943, maximum rainfall of 1500–1700 mm was observed in Gondia and Balaghat districts, which reduced to 1300–1400 mm in 1974–2013, and it was observed that during 1914–2013, there occurs a temporal variation of around 100 mm decrease in annual rainfall for each grid.

4.1 Trend Observed for Monthly Rainfall Series

The daily rainfall data were converted into monthly data for a period of 101 years (1913–2013). The trend for each month was carried out separately. There were no missing values or outliers in the series. The homogeneity test results inferred that the test statistics are from the same population without any inhomogeneity. The trend analysis outcome for monthly and annual series is given in Table 1. The null hypothesis H_0 was taken as "There is no trend in the series" and alternate hypothesis H_a was "There is a monotonic trend." The probability of hypotheses was also estimated for 95% confidence interval and 5% significance level. Sen's slope estimator helps to ascertain the increasing and decreasing propensity of the data.

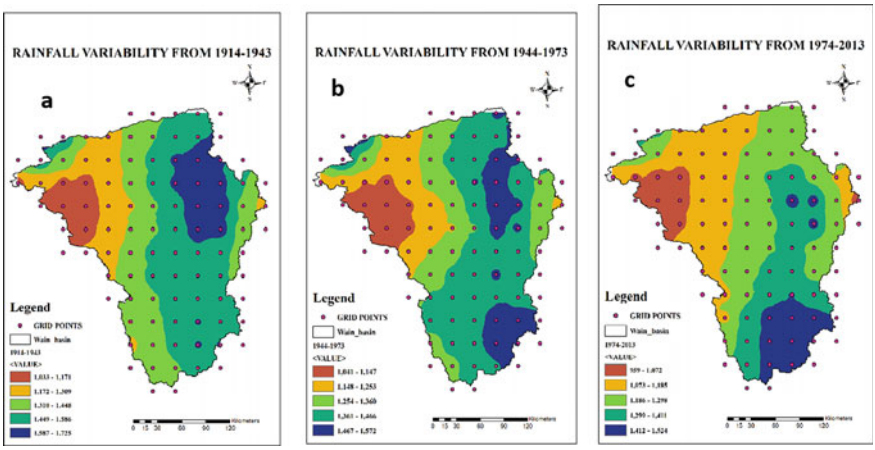

Fig. 2 Rainfall variability pattern over 100 years (**a** from 1914–1944, **b** from 1944–1973 and **c** 1974–2013)

Table 1 Trend analysis test results for monthly rainfall series

Period	Mann Kendall Z	M K trend (95% Confidence interval)	Probability of accepting the null hypothesis (%)	Sen's slope	Spearman's rho coefficient
January	−0.12	No Trend	90.89	9.65×10^{-5}	−0.022
February	−2.09	Decreasing trend	3.80	−0.074	−0.213
March	−1.65	Decreasing trend	13.15	−0.036	−0.155
April	−2.06	Decreasing trend	4.51	−0.043	−0.189
May	−1.36	Decreasing trend	21.89	−0.027	−0.129
June	−1.02	Decreasing trend	35.23	−0.303	−0.089
July	−2.11	Decreasing trend	3.44	−0.083	−0.221
August	+0.14	Increasing trend	99.9	4.65×10^{-5}	0.007
September	−1.59	Decreasing trend	14	−0.486	−0.143
October	−0.68	Decreasing trend	54.36	−0.079	−0.053
November	−0.49	Decreasing trend	73.78	-2.824×10^{-5}	−0.035
December	−1.03	Decreasing trend	33.71	-9.35×10^{-5}	−0.102
Annual	−2.85	Decreasing trend	0.44	−2.481	−1.00

Apart from the month of January, all other months are experiencing a decreasing trend, in which the month of august alone indicating an increasing trend with a probability of 99.9%. The possibility of the existence of a trend for January is rejected with a 90.89% probability. All other months including the annual rainfall series show a decreasing trend.

4.2 Trend Observed for Maximum Rainfall Series

For each month, the maximum rainfall entry from daily rainfall data was noted and grouped. The preliminary analysis shows that the data is homogenous and devoid of outliers. The test results are illustrated in Table 2.

Table 2 Trend analysis test results for maximum monthly series

Period	Mann Kendall Z value	M K trend (95% Confidence interval)	Probability of accepting H_0(%)	Sen's slope	Spearman's rho coefficient
January	+0.40	Increasing trend	65.33	+0.016	+0.029
February	–1.55	Decreasing trend	14.31	−0.081	−0.141
March	–0.68	Decreasing trend	56.91	−0.029	−0.058
April	–1.38	Decreasing trend	19.47	−0.053	−0.117
May	–0.52	Decreasing trend	64.29	−0.019	−0.043
June	+0.28	Increasing trend	73.36	+0.054	+0.036
July	–0.77	Decreasing trend	52.62	−0.109	−0.062
August	+0.85	Increasing trend	39.32	+0.177	+0.087
September	−0.56	Decreasing trend	67.91	−0.073	−0.33
October	−0.68	Decreasing trend	53.78	−0.067	−0.052
November	−0.43	Decreasing trend	78.48	−0.004	−0.020
December	−0.70	Decreasing trend	49.82	−0.004	−0.074
Annual	+2.01	Increasing trend	3.83	+0.409	+0.206

For maximum monthly analysis, the predominant trend observed is a decreasing trend. Only the months of January, June, and August are showing an increasing trend. However, there is no momentous trend observed in November month. It is observed that all three methods discussed in Table 2 are showing the same result.

4.3 Innovative Method of Trend Analysis

The rainfall values are divided into two halves and arranged in ascending order. The first half is aligned on the abscissa and the second half on the ordinate. After plotting, a 1:1 line is drawn along which divides the plot area into two triangles. Here, the analysis can be made on the basis of clustering of points. The points are classified as low points, medium points, and high points as given in Fig. 3. The low/high points are more in the upper triangle indicates the increasing trend and low/high points are more in lower triangle indicates the decreasing trend.

From Fig. 4, the monthly rainfall graph of June shows that there is the presence of low, medium, and higher points, but the points tend to cluster over the 1:1 line indicating the absence of trend, whereas for July, all the points are present in the 1914–1963 duration showing a decreasing trend. Coming to August, maximum points tend to fall on the line showing there is no significant trend. September and October show that there is no rainfall value present in 1963–2013 duration which shows monotonic decreasing trend and gives a warning that there is a chance for droughts and floods in future. For annual series also, there is a monotonic decrease in trend as all the points are present in the lower triangle.

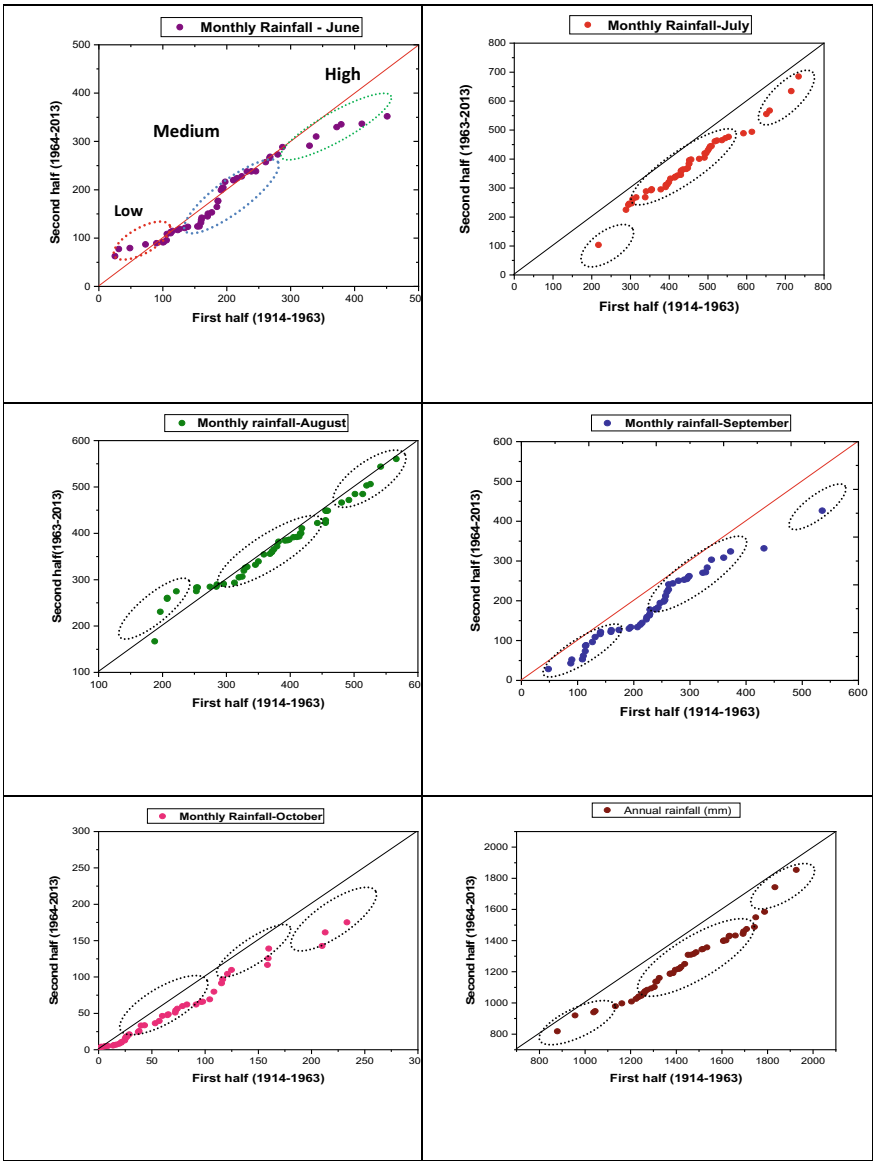

Fig. 3 Innovative trend graph for monthly and annual rainfall

The monthly maximum rainfall graph of June and September shows that most of the points tend toward the 1:1 line indicating the absence of a trend. For July, the points are present on either side of the 1:1 line, with low values more on the lower triangle indicating a non-monotonically decreasing trend. Similarly, for October, low and high points are present in the 1914–1963 duration signifying decreasing

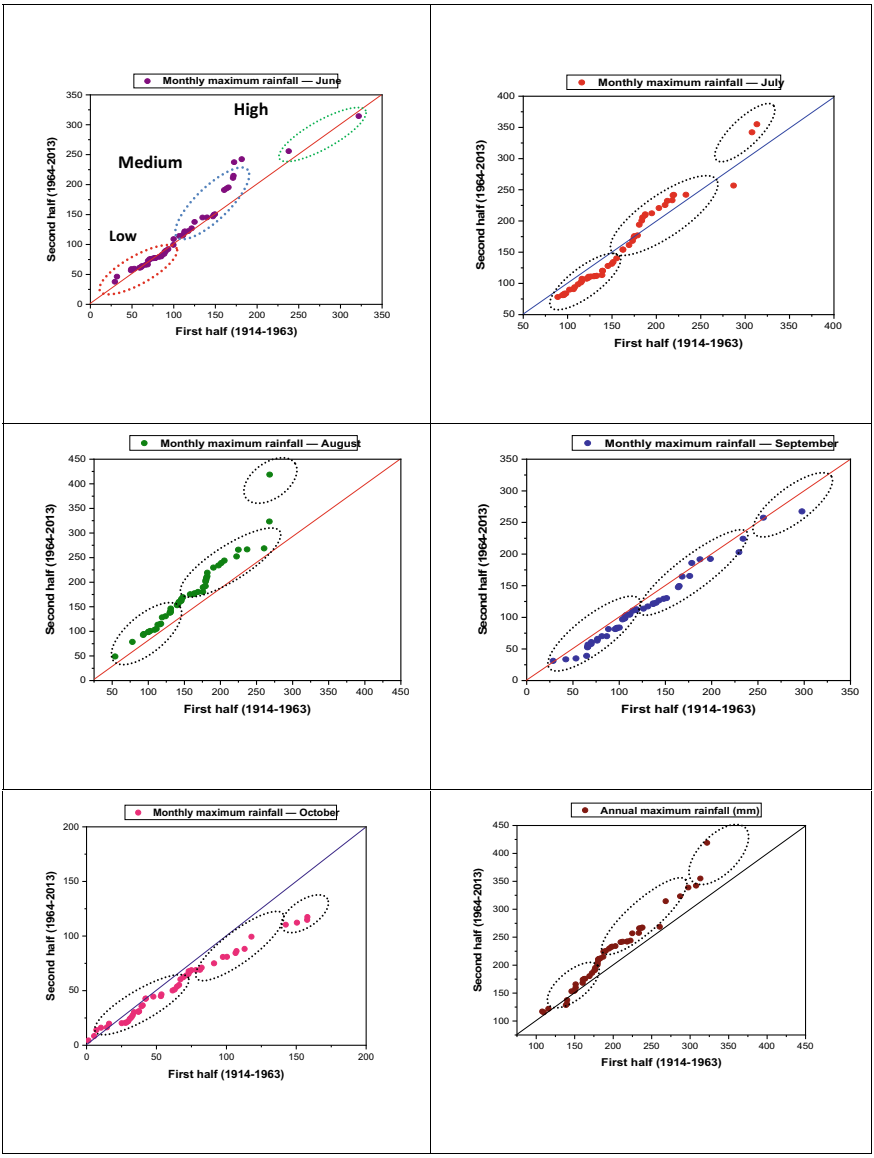

Fig. 4 Innovative trend graph for monthly and annual maximum rainfall

trend in rainfall. The maximum monthly rainfall values of August and the annual maximum rainfall values are clustered in the upper triangle confirming the presence of monotonically increasing rainfall trends.

4.4 Rainfall Data and Flood Frequency Analysis

- The annual rainfall from 1913 to 2013 was procured from IMD, Pune and the return period was calculated using Gumbel's distribution (Table 3). It was observed that rainfall of around 1500 mm magnitude is repeated in every 5 years, which makes the basin flood-prone. Rainfall of more than 1200 mm is occurring in every 2 years creating a runoff depth of 360 mm.

The recurrence interval shown in Table 3 indicates that rainfall of severity more than 1500 mm is expected every 5 years, resulting in a similar runoff pattern. Hence, it is important to seek proper management measures for this floodwater from getting wasted.

5 Conclusions

With the data of 101 years of rainfall for the Wainganga basin, the following conclusions can be drawn.

The monthly rainfall pattern of the basin shows a decreasing trend except for the month of August, which is monsoon month and the monthly maximum rainfall (extreme event) pattern shows an increasing trend with a maximum rainfall of 418 mm and return period 102 years.

The annual rainfall trend is observed to be decreasing with a variation of 1500–1900 mm occurring every 5–6 years. Annual maximum values of the rainfall indicate that there is an increasing trend in rainfall peaks, showing more intense rainfall over a shorter period. These peaks significantly contribute to the projects constructed on the Wainganga River. The flood mitigation measures should progress considering that the intensity of rainfall is trending upwards which indicates a higher probability of flash floods, which is more hazardous. The catastrophic events of floods have an impact on the life of farmers there with the maximum number of farmer suicides are reported. With this study, the future yield can be estimated for the long-term planning of the projects within the basin area.

Table 3 Rainfall frequency analysis for 101 years

Return period (Year)	Frequency factor (K_T)	Expected flood (X_T)	Rainfall (mm)
2	–0.164	53.554	1285.296
5	0.719	62.38102	1497.144
10	1.305	68.23904	1637.737
50	2.592	81.10469	1946.513
100	3.137	86.55285	2077.268

Acknowledgements The authors wish to express their sincere gratitude tothe India Meteorological Department (IMD) for providing rainfall data.

References

1. Ahmad I, Tang D, Wang T, Wang M, Wagan B (2015) Precipitation trends over time using Mann-Kendall and Spearman's rho tests in Swat River Basin, Pakistan. Adv Meteorol. Retrieved fromhttps://doi.org/10.1155/2015/431860
2. Bera S (2017) Trend analysis of rainfall in Ganga Basin, India during 1901–2000. Am J Clim Chang 6:116–131. https://doi.org/10.4236/ajcc.2017.61007
3. Bhagat RS, Bisen DK (2016) Flood study of Wainganga River in Maharashtra using GIS and remote sensing techniques. Int J Sci Res 5(4):2013–2016
4. Cronin AA, Prakash A, Priya S, Coates S (2014) Water in India: situation and prospects. Water Policy 16(3):425–441
5. Ghosh S, Luniya V, Gupta A (2009) Trend analysis of Indian summer monsoon rainfall at different spatial scales. Atmos Sci Lett 10(4):285–290
6. Gleick PH (2000) A look at twenty-first century water resources development. Water Int 25 (1):127–138
7. Gocic M, Trajkovic S (2013) Analysis of changes in meteorological variables using Mann-Kendall and Sen's slope estimator statistical tests in Serbia. Global Planet Change 100:172–182
8. Gosain AK, Khosa MJA (2012) Impact of water resources projects—a case study of Wainganga
9. Hamed KH (2008) Trend detection in hydrologic data: the Mann-Kendall trend test under the scaling hypothesis. J Hydrol 349(3–4):350–363
10. Machiwal D, Jha MK (2006) Time series analysis of hydrologic data for water resources planning and management: a review. J Hydrol Hydromech 54(3):237–257
11. Marques R, Santos CAG, Moreira M, Valeriano C, Isabella CLS (2015) Rainfall and river flow trends using Mann–Kendall and Sen's slope estimator statistical tests in the Cobres River basin. Nat Hazards 1205–1221. https://doi.org/10.1007/s11069-015-1644-7
12. Miller WP, Piechota TC (2008) Regional analysis of trend and step changes observed in hydroclimatic variables around the Colorado River Basin. J Hydrometeorol 9(5):1020–1034. https://doi.org/10.1175/2008JHM988.1
13. Mondal A, Kundu S, Mukhopadhyay A (2012) Rainfall trend analysis by Mann–Kendall test: a case study of north-eastern part of Cuttack district, Orissa. Int J Geol Earth Environ Sci 2 (1):70–78
14. Patel S, Hardaha MK, Seetpal MK, Madankar KK (2016) Multiple linear regression model for stream flow estimation of Wainganga River. Am J Water Sci Eng 2(1):1–5
15. Rahman A, Begum M (2013) Application of non-parametric test for trend detection of rainfall in the largest Island of Bangladesh. ARPN J Earth Sci 2(2):40–44
16. Rangwala I, Miller JR (2012) Climate change in mountains: a review of elevation-dependent warming and its possible causes. Clim Change 114(3–4):527–547
17. Sang YF, Wang Z, Liu C, Gong T (2013) Temporal-spatial climate variability in the headwater drainage basins of the Yangtze river and yellow river, China. J Clim 26(14):5061–5071. https://doi.org/10.1175/JCLI-D-12-00523.1
18. Şen Z (2012) Innovative trend analysis methodology. J Hydrol Eng 17(9):1042–1046. https://doi.org/10.1061/(ASCE)HE.1943-5584.0000556
19. Taxak AK, Murumkar AR, Arya DS (2014) Long term spatial and temporal rainfall trends and homogeneity analysis in Wainganga basin, Central India. Weather Clim Extremes 4:50–61. https://doi.org/10.1016/j.wace.2014.04.005

20. Timbadiya PV, Mirajkar AB, Patel PL, Porey PD (2013) Identification of trend and probability distribution for time series of annual peak flow in Tapi Basin, India. ISH J Hydraul Eng (July):37–41. https://doi.org/10.1080/09715010.2012.739354
21. Yue S, Wang C (2004) The Mann-Kendall test modified by effective sample size to detect trend in serially correlated hydrological series. Water Resour Manag 18(3):201–218

Steady and Unsteady Hydrodynamic Simulation of Pili River as a Potential Flood Warning System Using HEC-RAS

Siddhant Dash, Ritesh Vijay, and Rajesh Gupta

Abstract In the present study, one-dimensional hydrodynamic simulation of the Pili River (Study Area) for the steady flow was carried out using ArcGIS and HEC-RAS considering floods of 5, 10, 25, 50 and 100 years return period under existing and modified river geometry. The results were transferred to Google Earth for the delineation of flood lines. Furthermore, one and two-dimensional unsteady-state simulations were carried out for floods of 25, 50 and 100 years return period using RAS Mapper, which provided a 2D visualization of the unsteady flow on Digital Elevation Model (DEM) and Google Earth. Validation of the model output results was carried out for the average dry weather flow, the depths of which were obtained from 14 different locations along the entire stretch of the study area. The validation results indicated the model having a correlation factor of 0.6447 with the actual on-site data obtained. Hence, the model was used to provide reliable information regarding the amount of submergence during an event of a flood. The flood lines obtained through the model will further help in providing a potential warning for floods and will also act as a guiding measure for the implementation of river training works such as dredging, slope stabilization and construction of levees for future riverbed planning and development activities along the river stretch.

Keywords Flood · HEC-RAS · Hydrodynamic Simulation · Riverbed Planning

S. Dash (✉)
Department of Civil Engineering, Indian Institute of Technology Guwahati, Guwahati, Assam 781039, India

R. Vijay
Mumbai Zonal Centre, Mumbai Zonal Centre/Centre of Strategic Urban Management, NEERI, Nagpur, Maharashtra 440020, India

R. Gupta
Department of Civil Engineering, Visvesvaraya National Institute of Technology, Nagpur, Maharashtra 440010, India

B. Laishram and A. Tawalare (eds.), *Recent Advancements in Civil Engineering*, Lecture Notes in Civil Engineering 172,
https://doi.org/10.1007/978-981-16-4396-5_79

1 Introduction

Urbanization associated with economic growth, particularly in developing countries, has become an inevitable fact of progress in the past half-century [1]. With more than 50% of the world's population now residing in urban areas, the hazards of environmental degradation and changes are increasing rapidly [2]. One of the significant natural calamities which the world is facing in this twenty-first century is floods. In the recent past, human activities have emerged as one of the primary causes of floods [3]. The increasing human activities along the floodplains of the river along with heavy rainfalls as a result of the climate change effect have given rise to significant risks of flooding during the storms in the monsoon. It has impacted the humans and development on a large scale with a loss of lives and economy of the country [4]. India has witnessed severe flooding events in the last decade. Floods of Mumbai (2005), Uttarakhand (2013, 2016), Kashmir (2014), Chennai (2015), and Gujarat (2017) have proved the adverse effects it has on living beings and the economy of the states [5]. With the rise in such events and noticing the common cause, the government and local bodies have started giving importance to flood management [6]. With the rapid advancement in computational technology and research in numerical techniques, various one and two-dimensional (1D, 2D) hydrodynamic models based on hydraulic routing have been developed, calibrated, validated and successfully applied for flood forecasting and inundation mapping [7–10]. One of the main reasons for the floods in cities in India is the low carrying capacity of the rivers due to silting and sedimentation, inadequate drainage systems, encroachments and improper flood management plans [11–17]. In order to reduce the impacts of floods, several flood management practices are required, which in turn require space–time variation of flood flow in one as well as two dimensions [18]. Hydrodynamic models that reproduce the hydraulic behavior of river channels have proved to be practical tools in floodplain management. The one-dimensional flood modeling has become more comfortable with the advent of computers and a good number of research works have come up in the past two decades on river flood modeling [18–25]. Nagpur has seen rapid development in the past decade. With this, the activities taking place along the banks of the rivers are increasing. Large amounts of residential and commercial settlements have come up along the Pili River, thereby increasing the flooding problem. It becomes necessary to know the maximum possible extent of the flood arising during the worst storms for preventing the plausible future damage to property and lives. Therefore, an in-depth study of the flood and water quality is required for the river stretch so as to rejuvenate the river back to its original condition. In the present study, the hydrodynamic simulation of the Pili River in the city of Nagpur, Maharashtra, India, has been carried out for steady and unsteady flow for storms of 5, 10, 25, 50 and 100 years return periods respectively with existing and modified riverbed geometry.

2 Materials and Methods

The methodology of the present study has been described in three sections, representing the steady-state flow using the flood frequency analysis, the unsteady-state flow in one and two dimensions and the model conceptualization and simulation.

2.1 Study Area

Nagpur is located in the exact center of the Indian peninsula and at a mean altitude of 310 m above the mean sea level, with an area of 217.56 sq km [26] and a population of 2.549 million [27]. The average rainfall is 1242 mm. Water supply to Nagpur city is about 700 MLD and sewage generation is around 550 MLD. There are several natural and artificial lakes in the city. The city is divided into three zones: north zone, central zone and south zone, based on the drainage pattern of the three rivers, namely Pili, Nag and Pora, respectively flowing through the city. The Pili River is approximately 18 km long, originates from Gorewada Lake in the northwest part of the city and flows from west to east in the northern part of Nagpur. It confluences with the Nag river and finally merges into the Kanhan river. Figure 1 represents the base map and the catchment of the Pili River. Ten major drains (Drain 1–Drain 10) are entering the river at 2.1, 2.4, 4.4, 7.1, 12.3, 13.6, 15, 17.5, 17.6 and 17.9 km chainage, respectively, which contribute additional stormwater into the river stream. Eleven sub-watersheds, one due to Gorewada Catchment and ten of the drains entering the river, are delineated using Carto DEM for the present study area (Fig. 1).

2.2 Steady-State Condition

The 1D steady-state simulation includes determining the peak flows for floods of different return periods, thereby acting as an input for the model. The peak flows have been determined by the flood frequency analysis, as described below.

Flood frequency analysis was used for the determination of maximum rainfall intensities. The peak flow was calculated using the rational method [28]. The available data acquired from the Regional Climate Center (RA II region), India Meteorological Department (IMD), Pune includes 24 h Rainfall data basis from 1969–2000 for Nagpur city (based on the published data by Nagpur Municipal Corporation). The maximum daily rainfall recorded for each of the years is tabulated from the available data and the hourly maximum rainfall is evaluated based on the Indian Meteorological Department (IMD) reduction formula. From the evaluated maximum hourly rainfall data, the mean and standard deviation are evaluated.

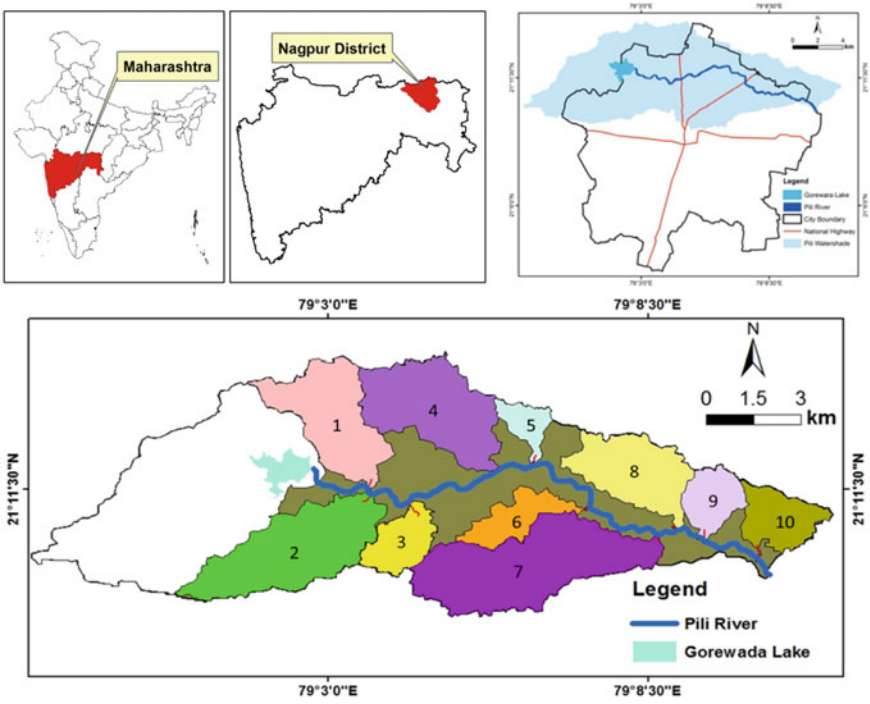

Fig. 1 Study area with details of Pili River and adjoining drains

The hourly precipitation depth analysis is carried out for various return periods using the probability distribution function. Maximum precipitate depths are converted into hourly intensities and tabulated. A graph is plotted using the values of hourly intensities and duration for different return periods in MS Excel.

As per Intensity–Duration–Frequency (IDF) generalized formula.

$$i = \frac{a}{d^n} \tag{1}$$

$$a = c * T^m \tag{2}$$

where,

i—Intensity in mm/hr.

T—Return period in Years.

c, m, n are regional coefficients.

d—Duration in Hours.

The values of the regional coefficients 'c', 'm' and 'n' was thus obtained as 34.32, 0.2 and 0.67 respectively and are substituted in the equation to obtain the generalized equation for Nagpur City. The intensities for various return periods and durations are evaluated (Fig. 2). The watershed characteristics were delineated

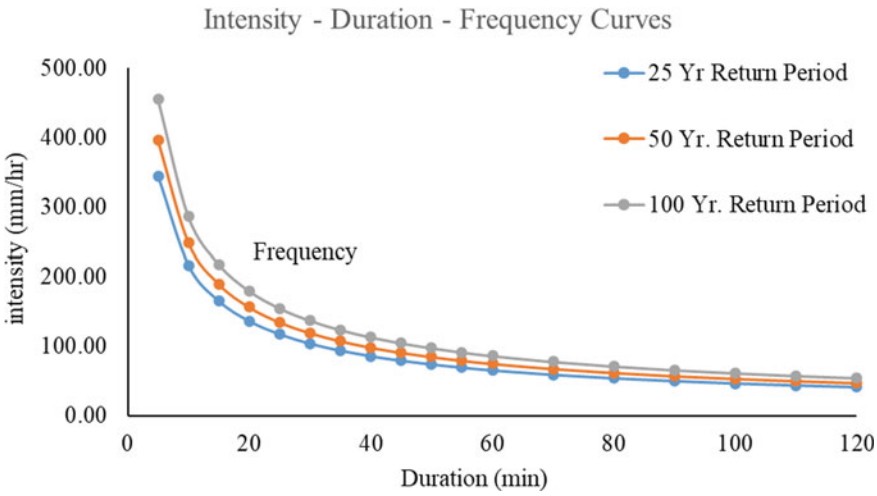

Fig. 2 Intensity–frequency–duration curves by Gumbel's extreme value (Type 1) distribution

using CartoDEM and with the help of ArcGIS (v. 10.2), the area contributing to the proposed drain was calculated in hectares based on topography. The composite coefficient of runoff 'C value' was calculated as 0.7 considering different land uses contributing to a single catchment.

For calculation of flood flow, the rational method was used as per the following equation:

$$Q = 10CiA \tag{3}$$

where,

C = Coefficient of runoff.

A = Area of catchment (Gorewada lake).

i = Intensity of rainfall for t_c.

Based on the equation, storm flows were calculated, considering 60 min. The intensities of the required duration were estimated as 47.3, 54.4, 65.3, 74.9 and 86.0 mm/hr for once in 5, 10, 25, 50 and 100 years return period, respectively.

2.3 *Unsteady-State Flow Condition*

The unsteady-state flow was calculated for both one and two dimensions. 1D unsteady-state simulation was performed by providing the flow hydrographs as input to the model (Fig. 3), whereas the 2D simulation was performed based on the grids of size 40 m × 40 m formed by selecting the flow area in the RAS Mapper (Fig. 4). Figure 3 represents the flow hydrographs for the river as well as the ten

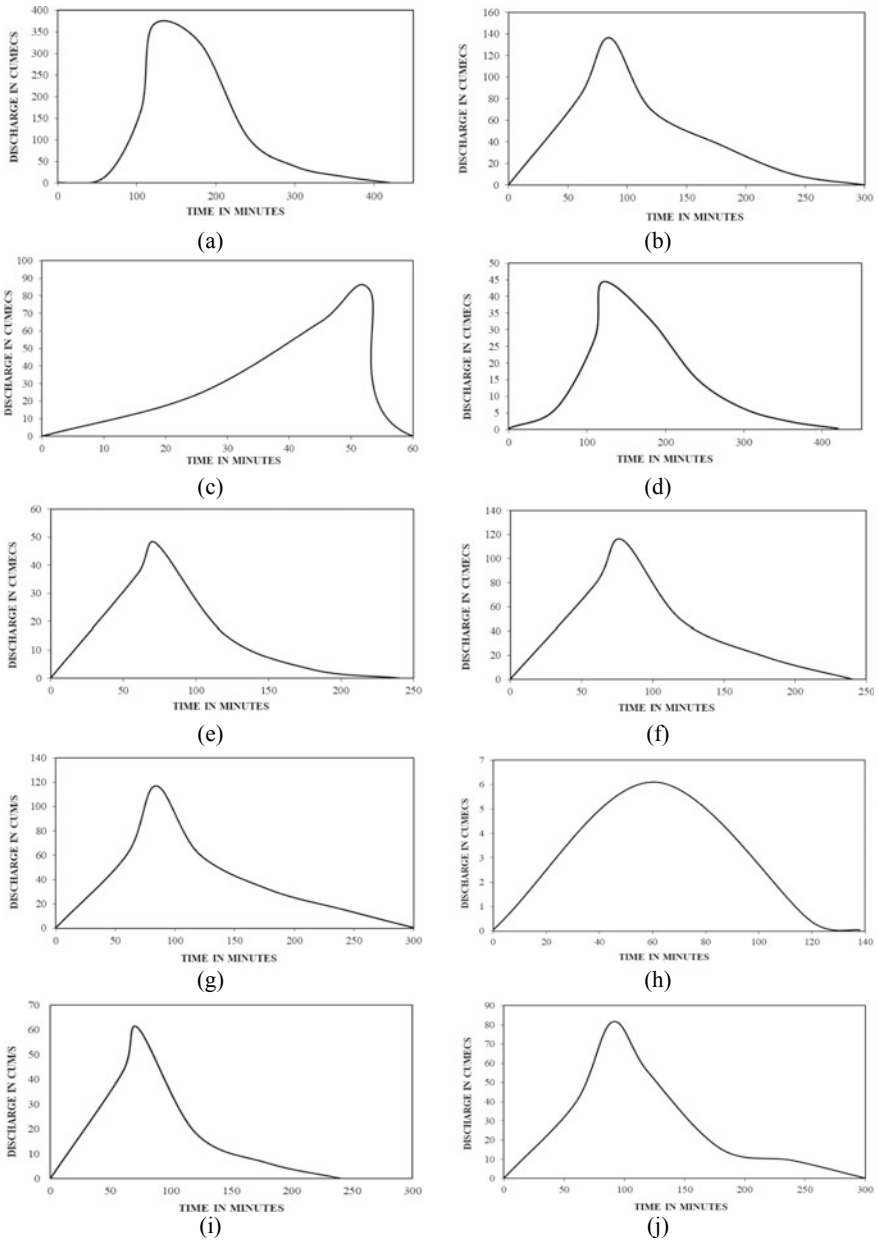

Fig. 3 Flow hydrographs for **a** Gorewada Lake, **b** Drain 1, **c** Drain 2, **d** Drain 3, **e** Drain 4 **f** Drain 5 g Drain 6 h Drain 7 **i** Drain 8 **j** Drain 9 k Drain 10 considered for unsteady-state simulation

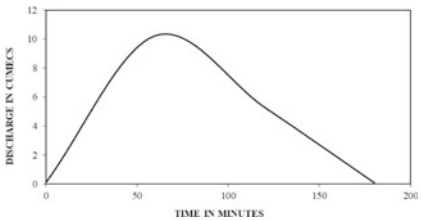

(k)

Gorewada Lake: 365.06
Drains 1-10: 136.47, 83.95, 44.47, 48.13, 115.86, 116.88, 6.11, 61.01, 81.48, 10.24, respectively
All discharges are in cumecs.

Fig. 3 (continued)

drains joining it for 25 years return period. Similar hydrographs are also generated for floods of 50 and 100 years return period for unsteady-state simulation [Flood Estimation report for the Lower Godavari Subzone—3(f) (Revised)]. To obtain the design flood of the required return period, the effective rainfall for design storm duration was applied to the unit hydrograph of a catchment. Procedure adopted for computing the design flood peak and the design flood hydrograph for T year return period by SUG approach includes the following steps:

- Step 1: Synthetic Unit Hydrograph
- Step 2: Design Storm Duration
- Step 3: Design Storm Rainfall
- Step 4: Design Flood Peak
- Step 5: Design of Flood Hydrographs.

The following relationships (Table 1) helped developing flood hydrographs for the 2-D unsteady-state simulation.

Based on the above procedure the Design Flood Hydrographs for the river as well as the drains were derived for floods of 25, 50 and 100 years return periods.

The flow area was selected from the Triangular Irregular Network (TIN) of the watershed and various grids were created based on which the flow calculations for the unsteady-condition were simulated, as the 2D representation of the unsteady-state condition is based on the finite-difference analysis (Fig. 4).

2.4 Model Conceptualization and Simulation

The model was conceptualized in HEC-RAS (5.0.1) by using the data obtained from the above processes as an input. The river length and its cross-sections were used as an input in geometric data. The base flow of the river and peak flood flows of corresponding sub-watersheds pertaining to different return periods were given as input for steady-flow data. The flow profiles for 5, 10, 25, 50 and 100 years' storms were created and the model was simulated for steady-state conditions considering the sub-critical flow regime.

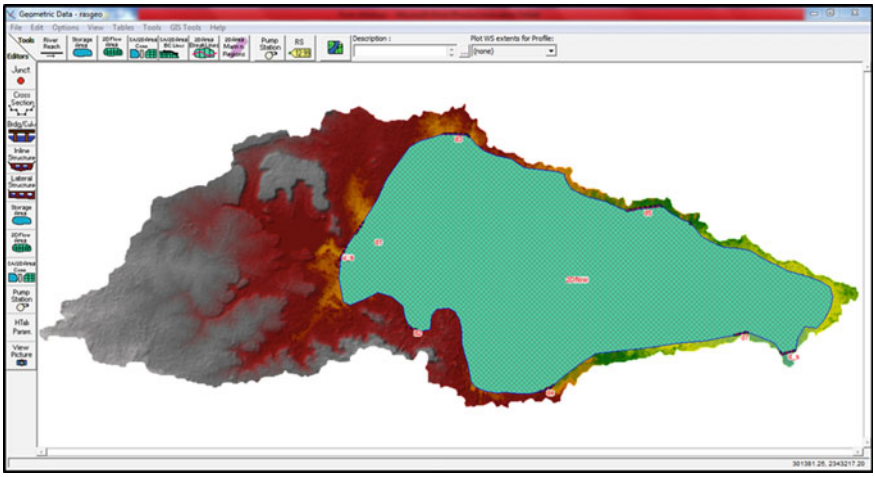

Fig. 4 Grid representation (40 × 40 m) 2D for unsteady-state simulation

Table 1 Derived relations between physiographic and unit hydrograph parameters

Sl. No	Relationship
1	$t_p = 0.348 \left(L * \frac{L_c}{\sqrt{S}}\right)$
2	$q_p = 1.842\, t_p^{-0.804}$
3	$W_{50} = 2.353 \left(q_p^{-1.005}\right)$
4	$W_{75} = 1.351\, q_p^{-0.992}$
5	$WR_{50} = 0.936\, q_p^{-1.047}$
6	$WR_{75} = 0.579\, q_p^{-1.004}$
7	$T_B = 4.589\, t_p^{0.894}$
8	$T_m = t_p + t_r/2$
9	$Q_p = q_p + A$

The length of the river was obtained by digitizing the river on Google Earth. This also gave the river a schematic plot for further input in the model. The river cross-sections were obtained from the field survey. The reduced levels for every 10 m along the width of the river were taken up to 80 m on left- and right-hand sides from the center of the river.

Similarly, for the 1D unsteady simulation, the flow hydrographs were given as input to the model instead of the peak flows, as in the case of the steady-state simulation. For the 2D unsteady-state simulation, the same hydrographs were given as input to the points of the confluence of the drains and the river in the TIN, which was obtained from the DEM of the study area. For both 1D and 2D simulations,

normal depth was assumed. This makes the river flow under normal (uniform flow) conditions at the downstream boundary. This also lets the model provide an energy slope, after which the RAS will automatically back-calculate the depth employing Manning's equation.

Empirical Manning's equation (Eq. 4) was employed, determining the channel roughness coefficient and establishing a relationship between the river discharge, geometry, hydraulic resistance and frictional energy loss. Equations (5) and (6) determined the head loss due to energy losses and the water surface from the energy equation, respectively.

$$Q = kS_f^{\frac{1}{2}} \tag{4}$$

$$h_e = LS_f + C\left\{\frac{\alpha_1 v_1^2 + \alpha_2 v_2^2}{2g}\right\} \tag{5}$$

$$H = Z + \gamma + \frac{\alpha v^2}{2g} \tag{6}$$

where Q = flow rate; K = conveyance of the channel; S_f = energy slope; g = acceleration due to gravity; h_e = energy head loss; C = expansion or contraction coefficient; α_1 and α_2 = velocity weighting coefficients; v_1 and v_2 = average velocities; H = water surface level above a specified datum; Z = bed elevation; y = depth of flow; α = kinetic energy correlation coefficient; and v = average velocity.

The HEC-RAS model for the Pili River was calibrated by determining a single value of Manning's coefficient "n". To check the reliability of the calibrated model, the water levels for different river flows were considered at various stretches of the river. The root mean squared (RMS) value (Eq. 7) predicted the Manning's coefficient appropriate for the model.

$$\text{RMS} = \sqrt{\frac{\sum_{i=1}^{n}\{Y_{\text{isim}} - Y_{\text{iobs}}\}^2}{N}} \tag{7}$$

n = 0.015 was found to have the most reliable as the RMS value was observed to be the minimum for the value of Manning's coefficient.

For the modification of the riverbed, the river bed was dredged for 0.5 m depth from the invert level to reduce the flooding effect. The steady-state hydrodynamic simulation was rerun and the difference between water levels at cross-sections due to 5 years, 10 years, 25 years, 50 years and 100 years storm for the existing and modified condition was observed. Also, levees were provided at appropriate locations to check the flooding of river water at several points in the stretch and the water surface profiles at all the cross-sections were observed.

The results of the simulation were then transferred to the GIS Platform. The width of submergence at each cross-section was noted and was plotted in ArcGIS

(v. 10.2). The joining of these points provided flood lines along the river stretch. Similarly, the same procedure was repeated for the modified sections of the river and the provision of levees.

3 Results and Discussion

This section deals with the output of the simulation of flood scenarios carried out with the help of HEC-RAS. It deals with the analysis of flood for 1D Steady and Unsteady flow as well as 2D Unsteady flow. The one-dimensional steady flow takes into consideration the peak flood flows of return periods, one in 5, 10, 25, 50 and 100 years and computes the water surface elevations at the cross-sections along the river stretch. Similarly, the 1D unsteady flow simulation takes into account the variation of the flow concerning time for the flood of a particular return period. The 2D unsteady-state simulation provides a more realistic picture of a flood in the catchment. Although it is well known that the processes occurring in the natural system are hardly one-dimensional, the one-dimensional analysis acts as a precursor for further two- and three-dimensional analyzes. In the present study, a two-dimensional unsteady flow model has also been considered for flood simulation.

3.1 1-D Steady-State Flow

The steady-state simulation for floods of different return periods include:

- Water Surface profile (Cross-sectional).
- Water Surface (Longitudinal) Profiles.
- Flood Lines.

The flood lines were delineated in Google Earth and Digital Elevation Model (DEM) to visualize the submergence during a flood of a particular return period based on the output of the water surface profiles for various cross-sections.

3.1.1 Water Surface Profiles

The water surface elevations at various cross-sections are simulated for floods of different return periods. The normal output of the model provides the water surface profiles without any provision of levees [Fig. 5a]. Nevertheless, this gives an unrealistic picture as the water levels are shown to be present in the depressions outside the river banks without the banks getting overflown. Hence the provision for levees has also been considered to provide a more rational picture of the water

surface profiles [Fig. 5b]. It can also be seen that the water tends to overflow the river banks for the floods of 10, 25, 50 and 100 years return periods. Hence, the existing cross-sections of the river are not sufficient to accommodate the floods of even 10 years return period and need immediate attention towards riverbed planning and development. Figure 5c shows the water surface elevations for the

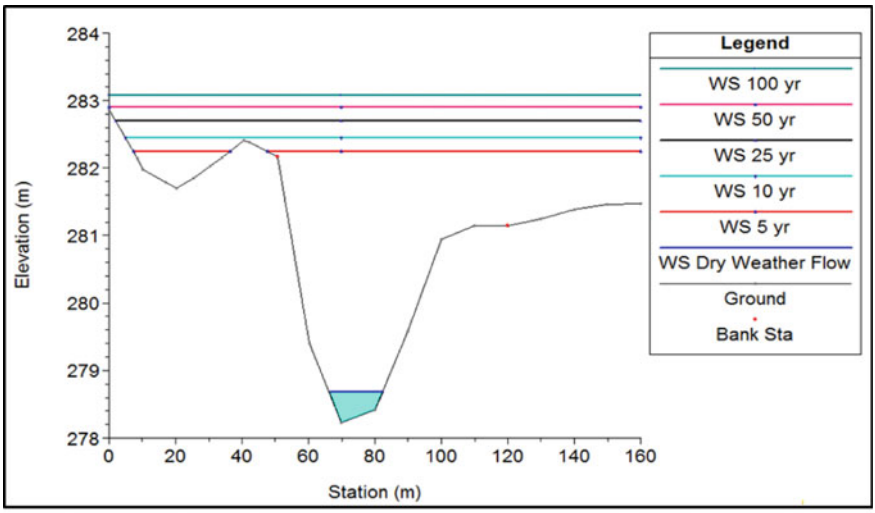

(a) Existing River Geometry without provision of Levees

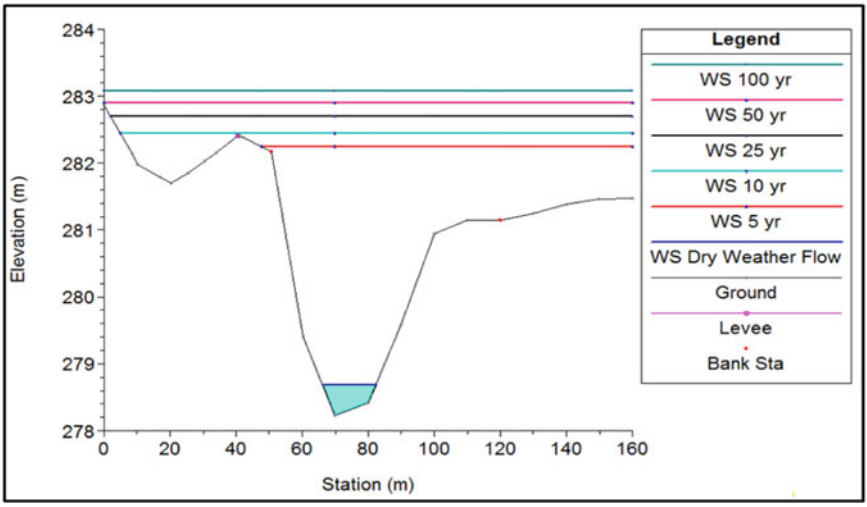

(b) Existing River Geometry with the Provision of Levees

Fig. 5 Water Surface Profiles for floods of different return periods at River Station (RS) 1350

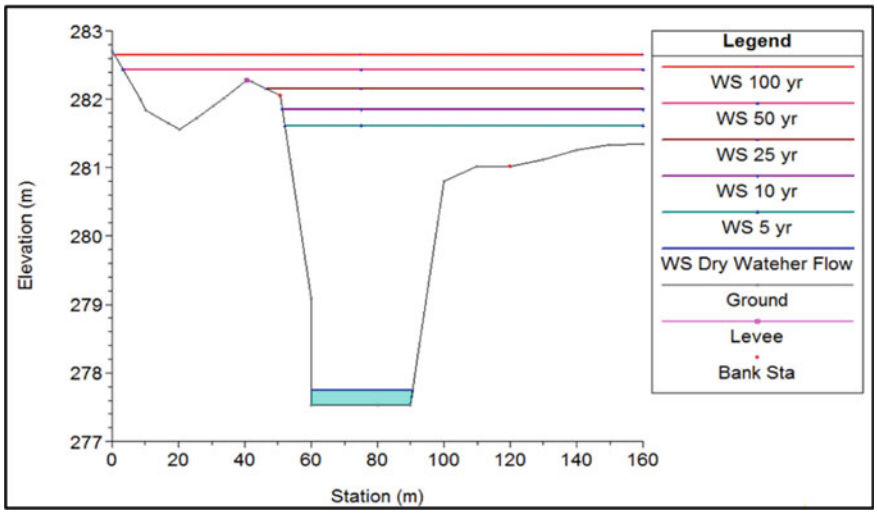

(c) Modified River Geometry with the provision of levees

Fig. 5 (continued)

particular cross-section after the river bed has been developed using dredging as an option for increasing the river channels' capacity. It can be seen that the water surface elevations tend to come down significantly to accommodate floods up to 25 years, thereby reducing the chances of flooding to a great extent.

3.1.2 Longitudinal Profiles

The longitudinal profiles were obtained after the simulation for base flow (dry weather flow) and once in 5, 10, 25, 50 and 100 years return period flows for existing cross-sections of the river. Figure 6a, b describe the water surface profiles for existing and modified riverbed geometry. The difference in the water surface profile can be observed in the insets considering river dredging. A drop of 0.3–0.6 m in the water surface profile is observed due to modification in the riverbed considering all the cross-sections along the river stretch.

3.1.3 Flood Lines

The simulation results of the water surface profile for once in 25, 50 and 100 years were used to delineate the flood lines along the river using flood points. The flood points are those that match the ground elevation with the flood water surface elevation of that particular storm. The flood points were marked on the Google Earth based on the results obtained from the simulation before and after dredging of

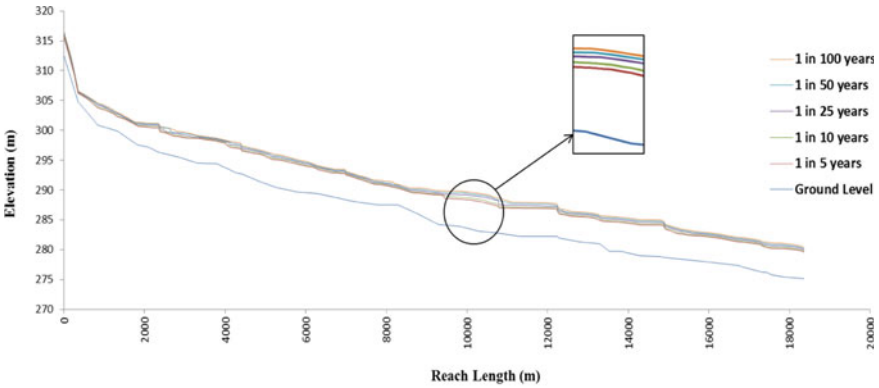

(a) Existing River Geometry

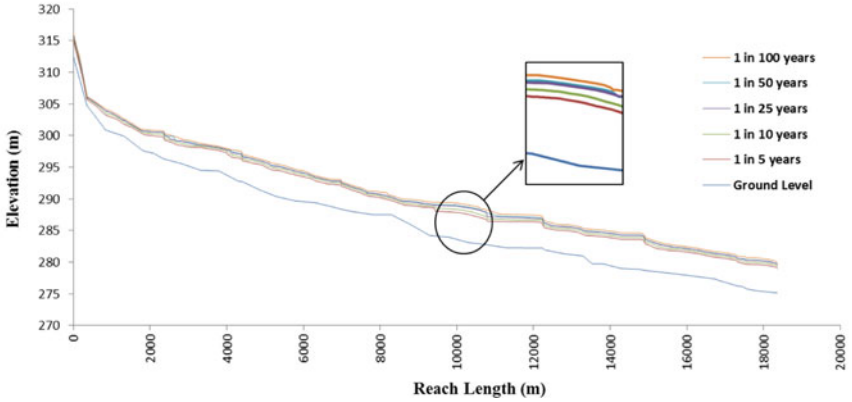

(b) Modified River Geometry

Fig. 6 Longitudinal Profiles of the river

the sections. These flood points were joined along the length of the study area due to 25, 50 and 100 years return period storms for existing and modified river geometry, as shown in Fig. 7a, b, c respectively. A significant difference in the flood lines can be seen at some points along the stretch of the river due to modifications in the river bed geometry.

3.2 1-D Unsteady-State Flow

The outputs for the unsteady-state simulation provide.

- Water Surface Profiles (Cross-Sectional).
- Longitudinal Profiles.

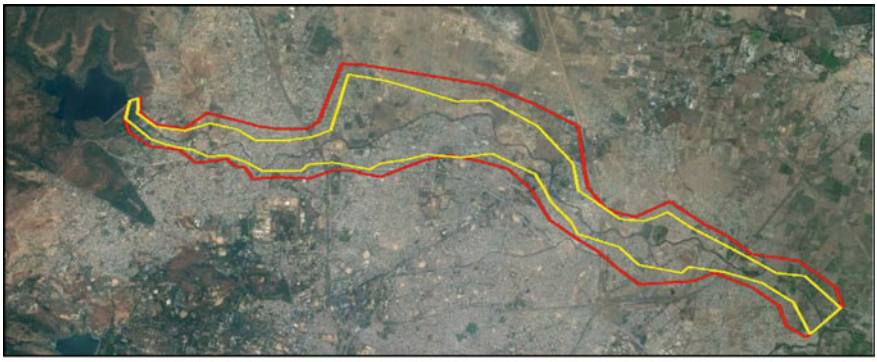

(a) Once in 25 Years

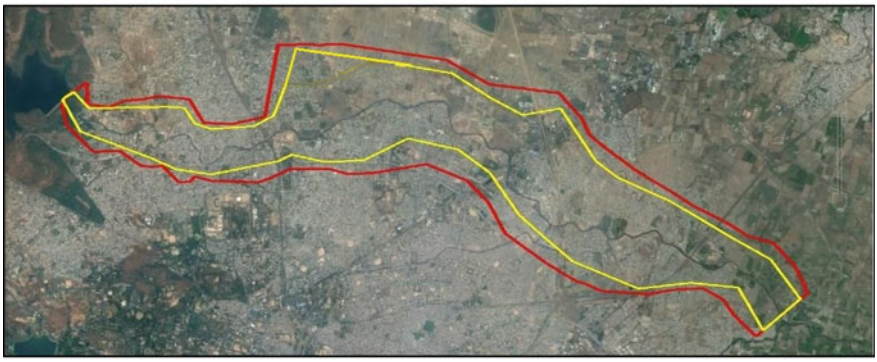

(b) Once in 50 Years

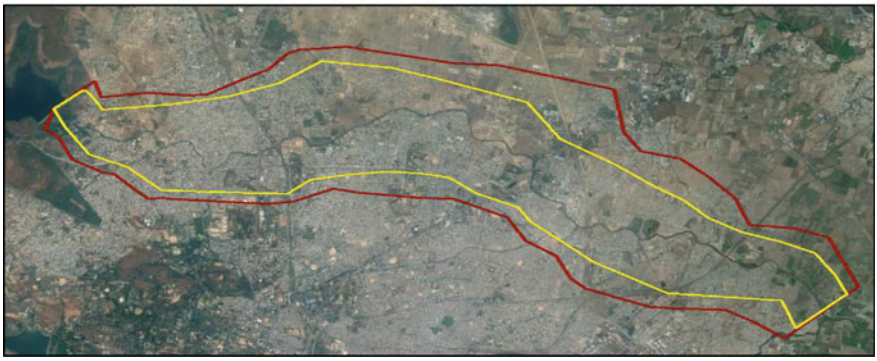

(c) Once in 100 Years

Fig. 7 Delineation of flood lines under existing and modified river geometry on Google Earth for floods of different return periods. Yellow line indicates the modified river geometry and the red line for the existing river geometry

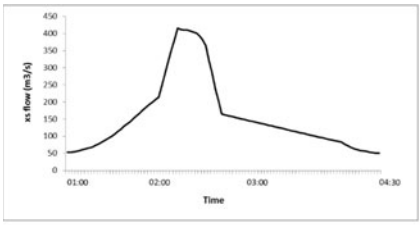

(i) Flow Variation (Flow Hydrograph)

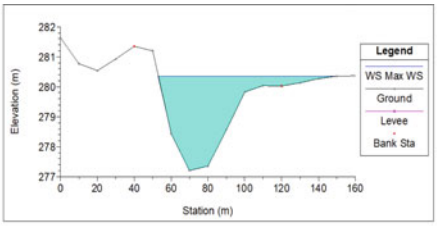

(ii) Maximum Water Surface Elevation

(a) Once in 25 years

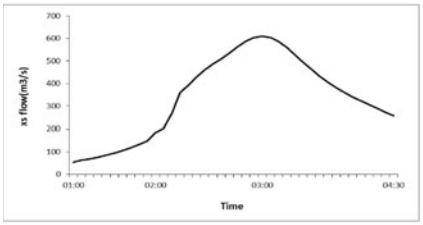

(i) Flow Variation (Flow Hydrograph)

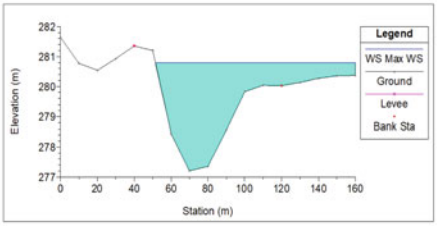

(ii) Maximum Water Surface Elevation

(b) Once in 50 years

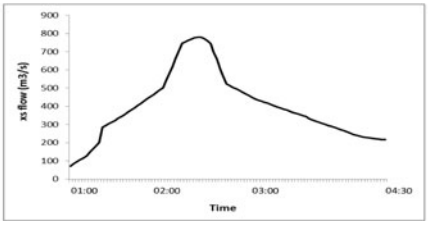

(i) Flow Variation (Flow Hydrograph)

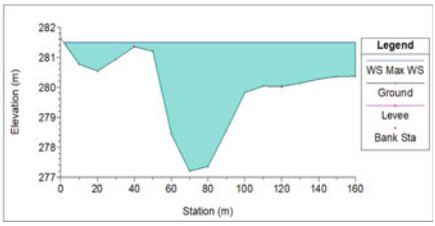

(ii) Maximum Water Surface Elevation

(c) Once in 100 years

Fig. 8 Maximum Water Surface Elevation for RS 980 under flood hydrograph

- Stage and Flood Hydrographs.
- Unsteady Flow Time-Series Plot.

3.2.1 Water Surface Profiles

The variation of the water surface elevation has been represented in Fig. 8, which shows a time-series variation of the water surface elevations for the RS 980. Figure 8a (i) represents the variation of flow in the RS 980 for 25 years return period and based on the flow variation curve obtained, the variation of the water surface elevations was computed. Figure 8a (ii) shows the maximum water surface elevation for that particular cross-section. Similarly, the unsteady-state simulation

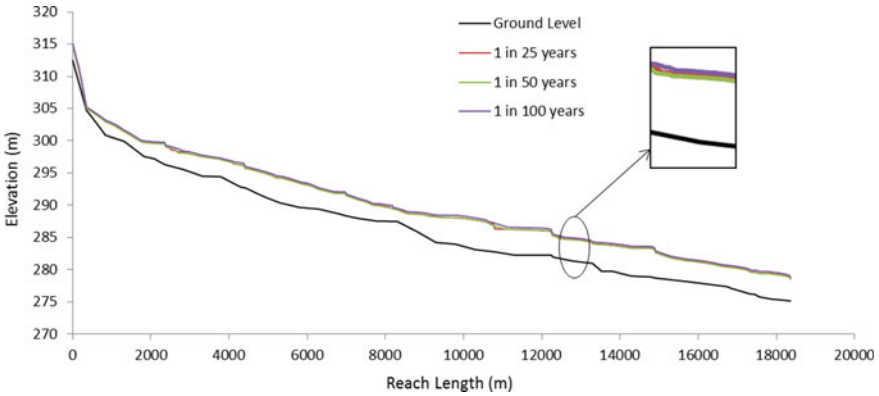

Fig. 9 Longitudinal profile of the river (Existing river geometry)

has been performed for the flood of the return period of 50 and 100 years and the maximum water surface elevation have been represented and can be compared to that of the elevation obtained in the peak of the steady-state condition, which can be seen to be providing a very close resemblance [Fig. 8b, c].

3.2.2 Longitudinal Profiles

The longitudinal profiles were obtained after the simulation for floods with 25, 50 and 100 years return periods for the existing geometry of the river. Figure 9 describes the water surface profiles for the existing riverbed geometry.

3.2.3 Stage and Flow Hydrographs

One of the outputs of the unsteady-state simulation is the Stage and Flow hydrographs, which give a plot between Stage and Flow versus the simulation time. This provides information about the total flow and the variation of the water levels for the entire simulation period, helping to correlate the water surface elevation with the flow at a particular River Station. Figure 10 shows the stage versus flow hydrographs for RS 18360 and RS 0, respectively.

3.3 2-D Unsteady-State Flow

The 2D unsteady-state simulation provided the flood inundation mapping in a two-dimensional representative way. The problems of preparing flood inundation maps manually on Google Earth in case of the steady-state simulation are overcome

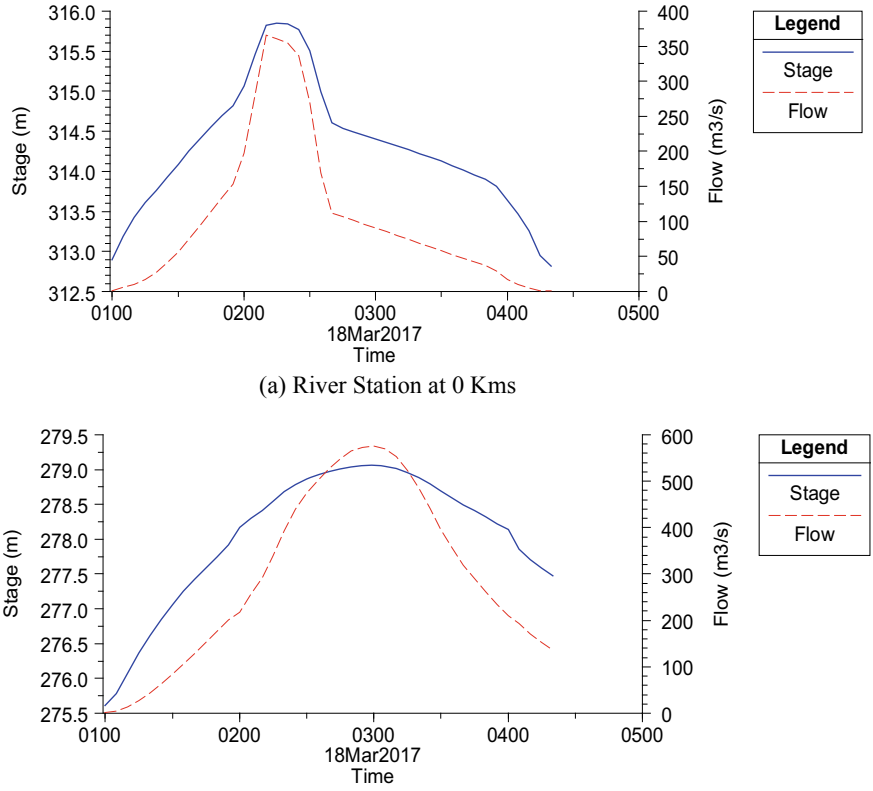

(a) River Station at 0 Kms

(b) River Station at 18.36 Kms

Fig. 10 Stage and flow hydrographs

in this case and the flood inundation maps are prepared by the model itself in the DEM and on Google Earth and provide a more realistic view of the flood conditions. Figure 11 represents the flood inundation maps for the unsteady-state condition at different times. Figure 11a depicts the initial condition of the watershed before the simulation. As the flow from the river and the drains enter during a particular flood, water starts overflowing from the cross-sections and starts to inundate the nearby areas. Figure 11b, c and d represent the flood inundation map created by the model for the peak flow for 25, 50 and 100 years return period, respectively, which gives maximum inundation of the watershed. Some parts of the areas of the catchment remain flooded even after the storm recedes. These are the low-lying areas or the depressions where the water remains stagnant for some time before getting removed.

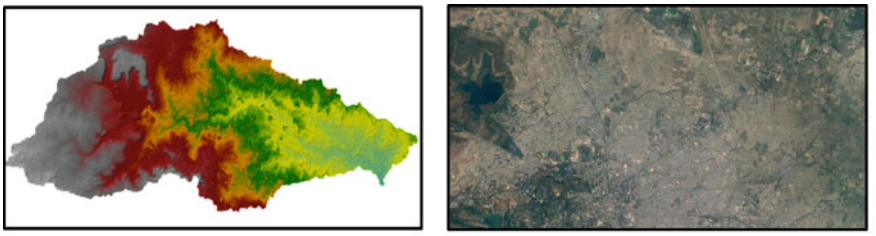

(a) Initial Condition before start of the simulation

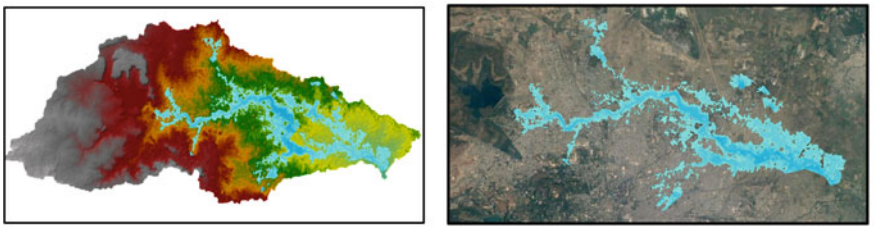

(b) Peak for 25 years return period

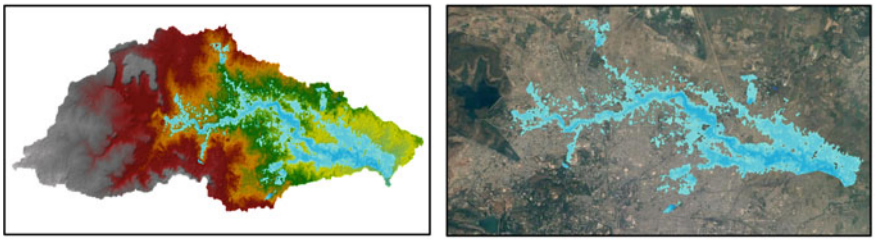

(b) Peak for 50 years return period

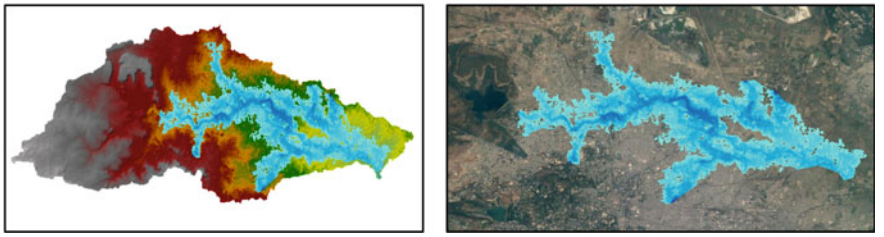

(b) Peak for 100 years return period

Fig. 11 Representation of flood inundation maps on DEM and Google Earth

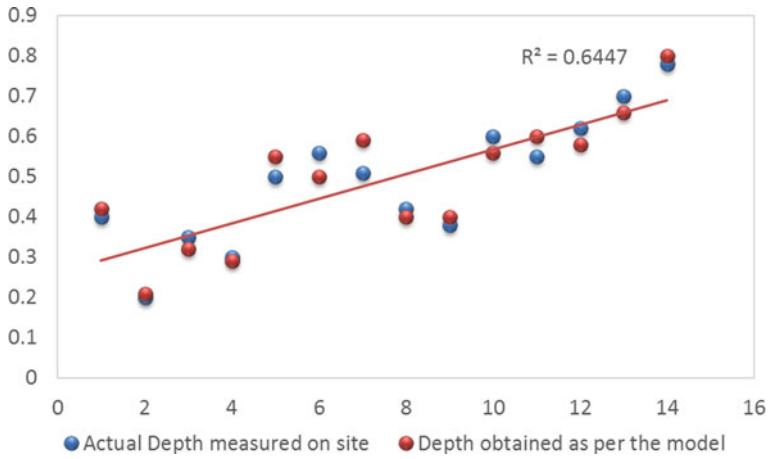

Fig. 12 Comparison between the on-site and model output water surface profiles

3.4 Validation of the Simulated Results

Figure 12 shows the validation of the results obtained from the model to the actual water depths measured on-site. Fourteen sampling points along the entire river stretch were selected for the validation of the results with the modeled output values and the results indicate that the water surface profile for the average dry weather flow obtained from the model correlated with the actual on-site data by about 64.47%. Hence, the predicted water levels for the floods of different return periods from the model may be assumed to be valid to an acceptable magnitude.

4 Conclusion

The study was conducted for both steady and unsteady flood flow simulation and an attempt was made to compute the water level and discharge profile for normal and flood conditions along with the existing and modified river geometry. The profile was also computed for depressed portions beyond the elevated main channel. This is observed as an inappropriate representation of the water surface profile along the cross-section. To overcome this problem, levee points were assigned to the existing cross-sections as a result of which it was observed that computation of water surface profile was checked beyond the levee points. There was a significant decrease in the water surface elevation due to the modified cross-section and as a result, flooding was checked up to a great extent. The water surface elevations were transferred on Google earth and flood lines were delineated for the extent of submergence under different storms. The extent of flooding was also determined from the two-dimensional visualization of the unsteady flow simulation carried out for a

flood of a 25-year return period on DEM and Google Earth. The results obtained were compared with the 25-year return period storm for steady-state condition, which was found to provide a close resemblance with that of the unsteady-state condition. This will help determine the land use under submergence and river training works by considering dredging, slope stabilization and construction of levees for future planning and construction activities along the river. It has been observed that various residential areas such as Ayappa Nagar, Lumbini Nagar, Siddharth Nagar, Shiivkrupa Nagar which are located near the river stretch are susceptible to be affected by the flood of 25 years return period and areas such as Anant Nagar, Adarsh Colony, Mansarovar Colony, Chopde Town, Chaitanya Nagar and Bharat Nagar, which are located relatively far away from the river stretch would be prone to submergence by the flood of 100 years return period. Based on the simulation results and flood lines, various activities may be planned for riverbed development. This study also helps in delineating an emergency plan during the flood and area under submergence. It would also prove to be a proactive rather than a reactive tool for such a flood condition.

Acknowledgments The authors are acknowledged to the Director VNIT Nagpur and Director CSIR-NEERI for their continuous support and infrastructural facility to carry out this research study. The authors are also thankful to the anonymous reviewers for their valuable suggestions in improving the quality of the manuscript substantially.

References

1. Bertinelli L, Black D (2004) Urbanization and growth. J Urban Econ 56:80–96
2. Alam MJ, Alam M, Rahman M, Khan S, Munna G (2006) Unplanned urbanization: assessment through calculation of environmental degradation index. Int J Environ Sci Technol 3:119–130
3. Shah AA (2015) Assessing the influence of watershed characteristics on the flood vulnerability of Jhelum Basin in Kashmir Himalaya by Gowhar et al. Nat Hazards 77:2139–2143
4. Gupta K (2020) Challenges in developing urban flood resilience in India. Phil Trans R Soc A 378:20190211
5. Ray K, Pandey P, Pandey C, Dimri A, Kishore K (2019) On the recent floods in India. Curr Sci 117
6. Plate EJ (2002) Flood risk and flood management. J Hydrol 267:2–11
7. Vijay R, Sargoankar A, Gupta A (2007) Hydrodynamic simulation of river Yamuna for riverbed assessment: a case study of Delhi region. Environ Monit Assess 130:381–387
8. Rangari V, Gonugunta R, Umamahesh N, Patel A, Bhatt C (2018) 1d-2d modeling of urban floods and risk map generation for the part of hyderabad city. In: International Archives of the Photogrammetry, Remote Sensing & Spatial Information Sciences.
9. Rangari VA, Sridhar V, Umamahesh N, Patel AK (2019) Floodplain mapping and management of urban catchment using HEC-RAS: a case study of Hyderabad City. J Inst Eng (India) Ser A 100:49–63
10. Rangari VA, Umamahesh N, Bhatt C (2019) Assessment of inundation risk in urban floods using HEC RAS 2D. Model Earth Syst Environ 5:1839–1851

11. Lavanya AK (2012) Urban flood management—a case study of Chennai City. Archit Res 2:115–121
12. Singh AK, Sharma AK (2009) GIS and a remote sensing-based approach for urban flood-plain mapping for the Tapi catchment, India. IAHS Publ 331:389
13. Mohapatra P, Singh R (2003) Flood management in India. In: Flood problem and management in South Asia. Springer, pp 131–143
14. Chigurupati R (2008) Urban growth, loss of water bodies and flooding in Indian cities: the case of Hyderabad. In: Water and urban development paradigms: towards an integration of engineering, design and management approaches, pp 121–125
15. Jameson S, Baud I (2016) Varieties of knowledge for assembling an urban flood management governance configuration in Chennai, India. Habitat Int 54:112–123
16. Suriya S, Mudgal B, Nelliyat P (2012) Flood damage assessment of an urban area in Chennai, India, part I: methodoogy. Nat Hazards 62:149–167
17. Gupta AK, Nair SS (2010) Flood risk and context of land-uses: Chennai city case. J Geogr Reg Plan 3:365
18. Pramanik N, Panda RK, Sen D (2010) One dimensional hydrodynamic modeling of river flow using DEM extracted river cross-sections. Water Resour Manage 24:835–852
19. Maksym T, Jeffries MO (2000) A one-dimensional percolation model of flooding and snow ice formation on Antarctic sea ice. J Geophys Res Oceans 105:26313–26331
20. Beffa C, Connell RJ (2001) Two-dimensional flood plain flow. I: model description. J Hydrol Eng 6:397–405
21. Wong M, Parker G (2006) One-dimensional modeling of bed evolution in a gravel bed river subject to a cycled flood hydrograph. J Geophys Res Earth Surf 111
22. Lhomme J, Bouvier C, Mignot E, Paquier A (2006) One-dimensional GIS-based model compared with a two-dimensional model in urban floods simulation. Water Sci Technol 54:83–91
23. Cook AC (2008) Comparison of one-dimensional HEC-RAS with two-dimensional FESWMS model in flood inundation mapping. Graduate School, Purdue University, West Lafayette
24. Dhungel S, Barber ME, Mahler RL (2019) Comparison of one-and two-dimensional flood modeling in urban environments. Int J Sustain Dev Plan 14:356–366
25. Catella M, Bechi G, Paris E, Rosier B, Schleiss A (2019) One-dimensional numerical scheme to model bed evolution in presence of a side overflow. In: River, Coastal and Estuarine Morphodynamics: RCEM 2007, Two Volume Set, CRC Press, pp 1130–1137
26. Saratkar AN (2020) Smart city project a study of Nagpur municipal corporation. Sanshodhan 9:91–97
27. Chandramouli C (2011) R. General, Census of India 2011, Provisional Population Totals. Government of India, New Delhi, pp 409–413
28. Subramanya K (2013) Engineering Hydrology, 4e, Tata McGraw-Hill Education

Performance Evaluation of Groundwater Recharge Infrastructure in Junewani Watershed, Nagpur, Maharashtra Using Spatial Approach

Y. B. Katpatal, Digambar S. Londhe, M. S. Mukesh, and Priyesh Biroju

Abstract The water resources management requires a holistic approach including surface as well as the groundwater resources, especially in the areas where there are hard crystalline rocks as aquifers. Recent advancements and capabilities of remote sensing and geographical information system (GIS) techniques have opened opportunities of field-level mapping and creation of database for irrigation projects. In order to do the assessment, the application of remote sensing and GIS in watershed mapping and detailed performance evaluation of Junewani watershed was attempted in the present study. The command area of Junewani watershed in Nagpur district of Maharashtra, India was mapped for irrigation and crop acreage using IRS P6 LISS-III remote sensing data. The performance of Junewani watershed was evaluated using NDVI (normalized difference vegetation index) data and groundwater data collected in the field studies. NDVI of the watershed is computed by using LISS III remote sensing data. However, data at micro-level were not available completely where groundwater levels in desired frequency, soil characteristics, data on porosity and permeability etc., hence the groundwater modelling has been attempted only to scientifically visualize the watershed.

Keywords Junewani watershed · NDVI · Groundwater · GIS and remote sensing

1 Introduction

Agriculture sector is the largest employer in Indian economy contributing a share of 16% in the country's gross domestic product as per the estimations in the year 2017–2018 [1]. Government of India has made many attempts to utilize the maximum possible irrigation potential for accelerated food production to meet the

Y. B. Katpatal (✉) · D. S. Londhe · M. S. Mukesh · P. Biroju
Department of Civil Engineering, VNIT, Nagpur, Maharashtra, India
e-mail: digambarlondhe@students.vnit.ac.in

B. Laishram and A. Tawalare (eds.), *Recent Advancements in Civil Engineering*, Lecture Notes in Civil Engineering 172,
https://doi.org/10.1007/978-981-16-4396-5_80

essential requirements of the ever-growing population [2]. Water scarcity will affect irrigation and water supply in agriculture. The FAO forecasts 14% growth in irrigation withdrawals from 1995 to 2025 whereas the IWMI gets a 17% growth in withdrawals for irrigation. But food production from irrigated lands during the same period must grow by at least 40% to meet the needs of a 33% increase in population and to satisfy trends for improved nutrition [3].

Many authors have analysed groundwater system performance for irrigation purpose and have proposed indicators for evaluation [4–11]. Most of the work done in performance evaluation irrigation project has been focused on the internal processes of irrigation systems. Many internal process indicators relate performance assessment to management skills and targets such as time, duration, flow rates of water, irrigated area and cropping patterns. The main purpose of performance evaluation is to contribute irrigation system managers for improvement in water supply to users and farmers. Some of the performance indicators are external. These indicators are used to study the relationship between input and output to the system. These indicators assist policy makers and managers to make long term and strategic decisions and researchers to study and analyse comparative differences between irrigation systems. Nowadays, remote sensing and GIS techniques along with traditional ground data collection sites helps in collecting the information over an entire area. Combined with ground information, remote sensing and GIS techniques can be an effective tool to evaluate the performance of micro-watershed and to obtain spatio-temporal information [12]. Also many case studies on assessment of irrigation performance by using remote sensing have been carried out [12–14].

The water resources management requires a holistic approach including surface as well as the groundwater resources, especially in the areas where there are hard crystalline rocks as aquifers. The hard-crystalline rocks have to be addressed in a different manner for water resources management as they pose a different morphological feature as well as basin characteristics. The study area presents traps topography. Basaltic rocks generate very fine black cotton soil and hence allow very less infiltration. Hence, at many places wherever the surface morphology is conducive, surface water resource management is advocated. But, since the surface irrigation has covered only around 30% of the agricultural area for irrigation, most of the farmers still depend on the groundwater resources. Hence, there are efforts for groundwater recharge in the hard-crystalline terrains with basalt. Government of India has given appropriate stress on groundwater recharge which requires proper analysis of the terrain and the aquifer characteristics. Many state governments have also joined these efforts but still the focus on groundwater recharge is still demanding many more efforts with participation and awareness of people.

The present study hence has been aimed at understanding the efforts of the government and non-government bodies to take up the groundwater recharge activities at many places. It is known that the basic unit for development of surface as well as groundwater resources is a watershed. Watershed is further divided into sub-classes based on the size as well as the order of the drainage.

2 Study Area

The study area is Junewani watershed at geographical coordinates 78.90° E and 21.03° N in Hingna Tehsil, Nagpur district, Maharashtra. It is southern to Nagpur city and covers an area of 886.852 ha. Location map of the Junewani watershed is shown in Fig. 1. The topographic elevation varies from 294 to 415 m. The whole watershed has an elevation difference of 121 m. The top soil layer in the watershed is of black cotton soil up to a depth of 1.5 m. Lithology in the study area shows that extensively vesicular basalt in various weathering levels.

In the present study, Junewani watershed in Hingna Taluka of Nagpur District has been selected. This watershed has been selected only because many efforts have been taken by government of Maharashtra and also by other Non-Governmental organizations for groundwater recharge in this watershed. Many recharge structures (Fig. 2) have been constructed in this watershed on many streams of different order and also silt removal activities have also been taken across many streams.

3 Methodology

The methodology consists of collecting all the required data for the study, carrying out all the necessary correction and processing of the collected data to get the desired output and then finally modelling using ModelMuse to understand the groundwater flow regime and also, the performance of the GW recharge structures. For the orderly completion of the present study, the overall methodology has been divided into following basic steps: (i) selection of study area, (ii) relevant data

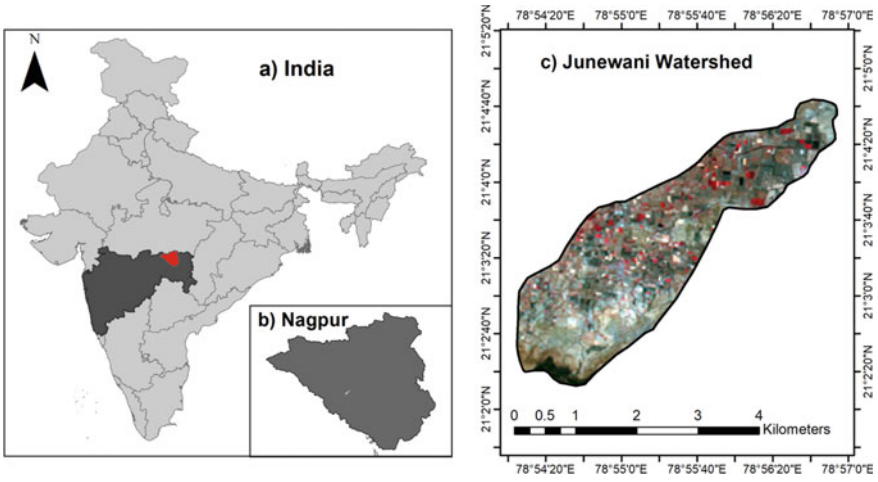

Fig. 1 Location map of Junewani watershed

Fig. 2 Water harvesting structures in Junewani watershed

collection, (iii) generating and modifying the available data for modelling, (iv) creating the model with the data and run the model, (v) validation of result.

3.1 Data Generation

The basic information on parameters related to groundwater occurrence and the seasonal availability of groundwater was collected by arranging field visits to the watershed. Many farmers in the watershed were interviewed for getting the correct information. This information was collected to know the groundwater status and the crop yields before the groundwater recharge structures were constructed and after it. This information was collected by designing formats with appropriate questions in simple language. The government of Maharashtra is monitoring the status of groundwater but it cannot get the information continuously at micro-level. Hence, it was observed that there are no observation wells in the watershed monitored by the state department.

The sites selected for desilting and the construction of the recharge structures have also been discussed for their scientific suitability and whether they have improved the groundwater availability in the watershed and also the yields have been increased. In the end, the groundwater modelling was attempted to observe the groundwater dynamics in the watershed. But it was observed that since all the groundwater parameters are not being observed in the watershed continuously, the groundwater modelling can generate information only suitable for academic interests which is not filling all the gaps regarding change in the groundwater dynamics in the region. This means that, the study generate inference in the beginning only that micro-level data collection must be done if groundwater management has to be converted into sustainable format.

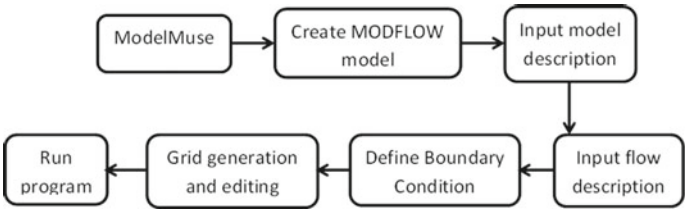

Fig. 3 Steps involved in modelling the groundwater in ModelMuse

3.2 Modelling Steps

The study has utilized ModelMuse for modelling the ground information. Figure 3 shows the systematic steps involved in the modelling. Before the use of the modelling tool, the prerequisite tools needed for analysis using Model program location. The type of modelling method that needs to be considered for analysis need to select at the first stage and need to input parameters to this modelling method.

3.3 Model Validation

The model results obtained after modelling by considered boundary condition were checked for field condition reality. To compare and interpret the results obtained the time series analysis has been carried. Time series analysis was carried out for the study area to monitor the Land Cover changes and change in the agricultural practices by considering NDVI index. For conducting the time series analysis, the LISS-3 image of the region for pre- and post-monsoon condition is considered to understand the variation in groundwater with respect to change in monsoon over a time span. The satellite image dated 28-Jan-2014 (pre-monsoon) and 25-Sep-2014 (post-monsoon) were considered which were before the construction to improve groundwater recharge. And image of 6-Apr-2017 (pre-monsoon) and 08-Nov-2017 (post-monsoon) were considered to measure the changes. The time series is carried for before and after the deepening of natural water streams, which were constructed to improve groundwater recharge.

3.3.1 NDVI Map Generation

Normalized difference vegetation index (NDVI) is an index to measure the extent of vegetation in the region. NDVI is quantifies vegetation by measuring the difference between near infrared and red light (Eq. 1). The value of NDVI ranges from −1 to 1. The value close to one indicates high vegetation.

$$\text{NDVI} = \frac{\text{NIR} - \text{Red}}{\text{NIR} + \text{Red}} \quad (1)$$

4 Results

The water resources management requires a holistic approach including surface as well as the groundwater resources, especially in the areas where there are hard crystalline rocks as aquifers. Hence, at many places wherever the surface morphology is conducive, surface water resource management is advocated. The variation of surface profile along the line was the groundwater modelling was considered is shown in Fig. 4.

4.1 Groundwater Modelling

However, data at micro-level were not available completely where groundwater levels in desired frequency, soil characteristics, data on porosity and permeability etc., hence the groundwater modelling has been attempted to scientifically visualize the watershed only. The figure shows the watershed region obtained from ModeMuse after considering the boundary condign and Fig. 5 shows the

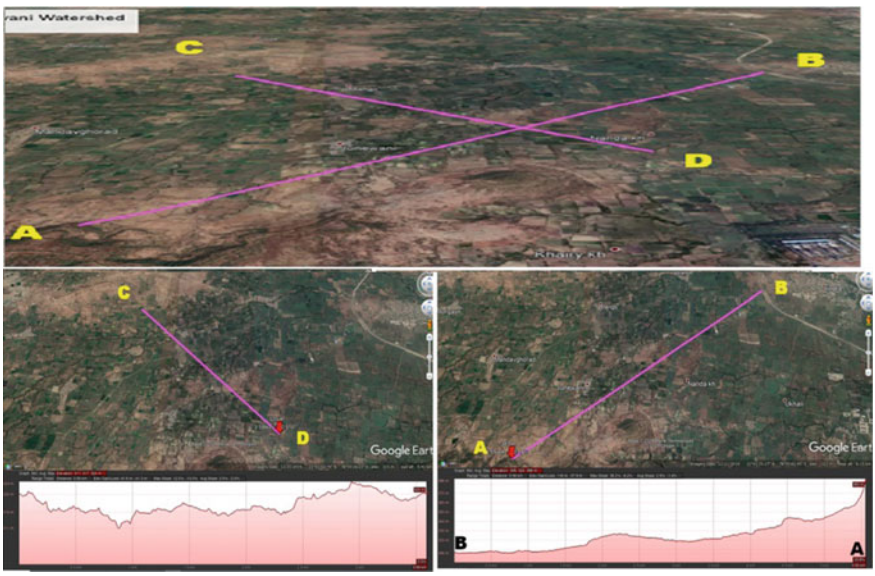

Fig. 4 Surface variation along two modelling lines over Google earth image

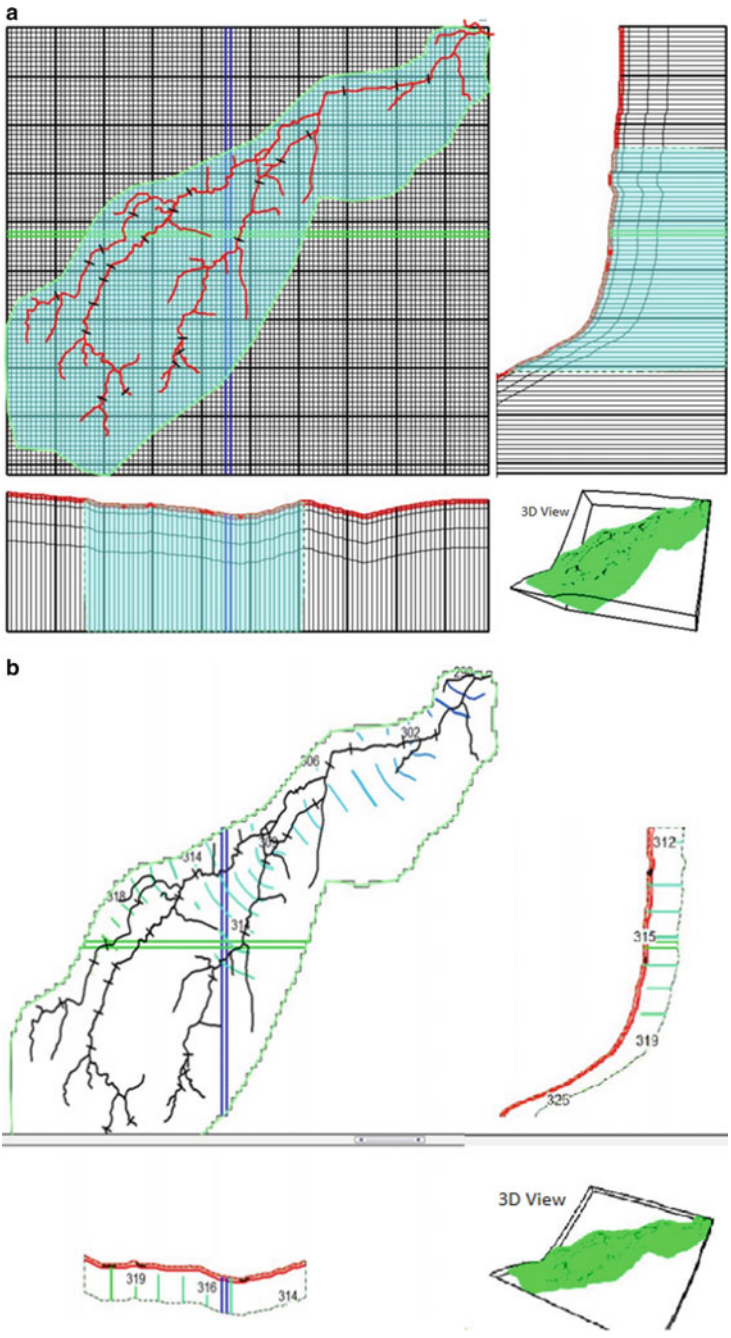

Fig. 5 **a** Groundwater model grids derived to enter the hydrological parameters pertaining to each grid. **b** Groundwater profiles along two section lines in the watershed

groundwater level long the line AB and CD. Form the modelling results, the change in groundwater level in the watershed can was observed.

4.2 Time Series Analysis

The biggest advantage of the remotely sensed data is its synoptic availability as time series data which enables observation of the water resources parameters in a continuous mode. The changes observed here utilize the pre-monsoon and the post-monsoon images of the area during the period 2002–2020. The changes in agriculture observed could also be statistically given through NDVI analysis. The changes in agriculture also bear the impact of the change in the rainfall in the study area on annual basis. But, the main objective of the comparative analysis is to see changes before the recharge structures were constructed and after they were constructed. The construction of the structures for groundwater recharge was taken up in 2014–15 and it was complete in the year 2015. The study also includes sites where desilting was taken up to 2–3 m. Some sites where desilting was done have been shown in Fig. 2. Figure 6 shows the LISS-3 image of the watershed region for

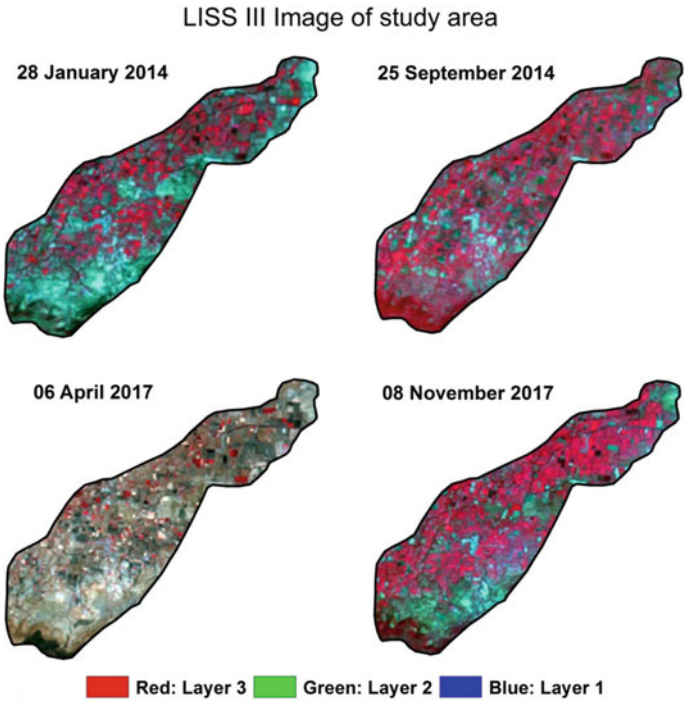

Fig. 6 Satellite images of pre-monsoon and post-monsoon for the year 2014 and 2017

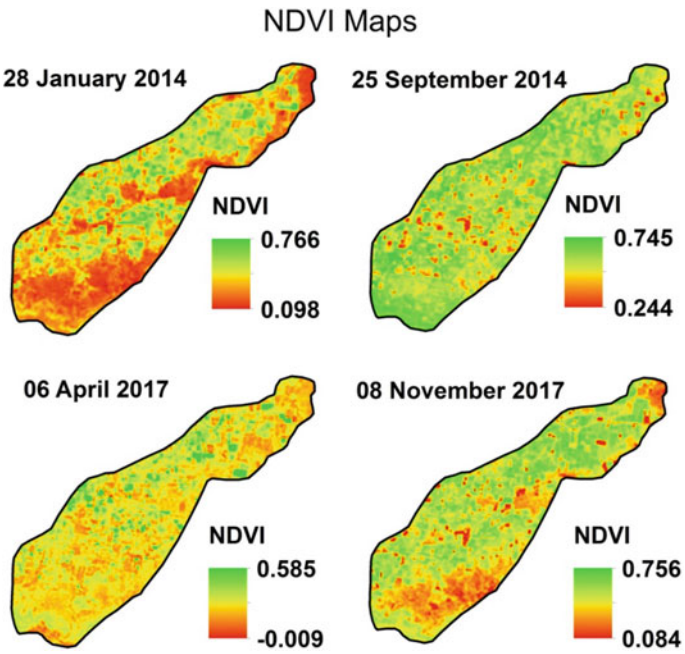

Fig. 7 NDVI maps of pre-monsoon and post-monsoon for the year 2014 and 2017

two different time span with pre- and post-monsoon condition. The variation in NDVI has been shown in Fig. 7. The change in NDVI value for the post-monsoon condition reveals that there is some improvement in the vegetation in the region. This increase in results may be due to increased availability of water in the region.

4.3 The Overall Groundwater Dynamics and Proposed Recharge

The study depicts the overall groundwater dynamics in the watershed which has been used along with the field observations to suggest the recharge mechanism in the watershed. The overall groundwater dynamics may be understood with the help of Fig. 8 which shows arrows with different colours suggesting location of the groundwater recharge structures and operations.

The groundwater flow is from west to east and the surface runoff follows the slope in the area. The locations have been shown where a particular type of groundwater recharge mechanism has been suggested based on the observations and analysis of the present study. The areas where white coloured arrows have been

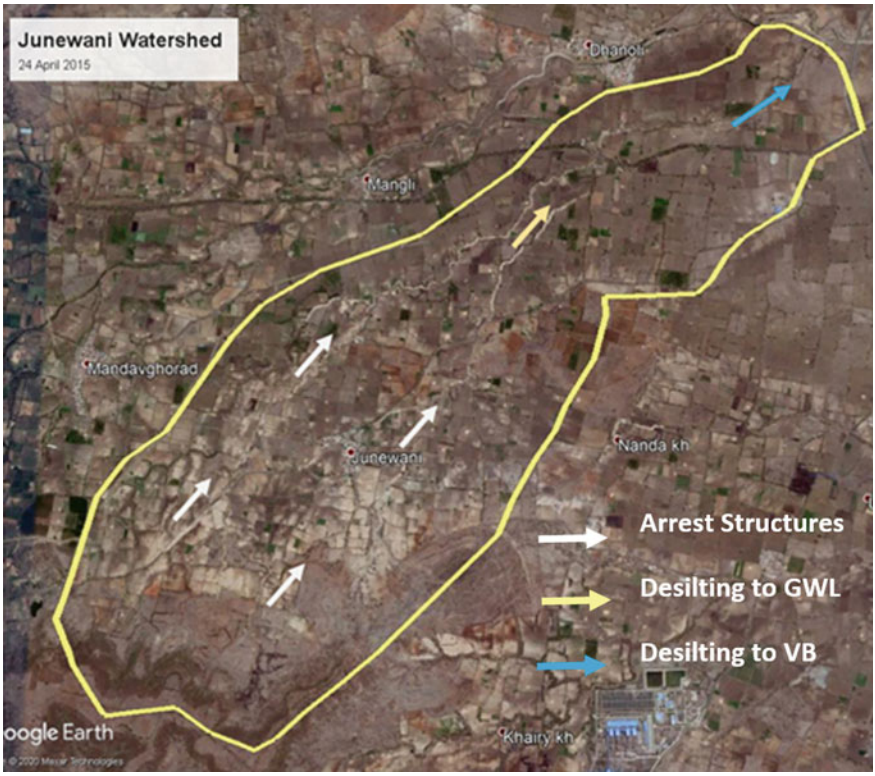

Fig. 8 Overall groundwater dynamics in the watershed and locations of recharge mechanisms to be adopted

shown in Fig. 8, rainwater harvesting in the form of arrest structures on the drainages and streams should be taken. Areas with yellow-coloured arrow have potential for desilting only up to the maximum groundwater levels observed in the post-monsoon season. The areas where blue-coloured arrow has been shown desilting may be done only when vesicular basalt is present as outcrops underlain by compact basalt.

The study found that deeper groundwater recharge should be adopted in the watershed as Gondwana formations are present below the Deccan basalts which must be recharged while Deccan basalts must be recharged through surface recharge techniques [15]. Only surface techniques will not be fully effective in this and hence recharge through wells must be adopted in the bed of the streams where recharge shafts can be constructed.

5 Conclusions

Groundwater, although the overall quantity is negligible compared to other water bodies, and is one of the major resources for fresh water. It is because of this reason understanding and management of groundwater is necessary. In present study, attempts were made to understand the mechanisms of groundwater flow through modelling of watershed characteristics. From time series analysis, it is observed that there are some changes in the drainage pattern but the crop pattern remained same throughout the time span. Also, the interaction with farmers confirmed the same.

The farms which are present in downstream and near to the stream have seen a little rise in groundwater level interestingly the opposite can be said to the upstream farms where the water level gone down after the recharge structures were erected. It has been observed that desilting has effect on first order streams and on higher order streams it is better to go for deeper groundwater recharge mechanisms. Hence, recharge through wells can be adopted at the bed of the streams where recharge shafts are connected. Overall, the recharge mechanisms are to be arranged for proper groundwater recharge but the suitability of the said mechanisms is to be identified and adopted as per the requirement. It also benefits a lot to include the farmers into the feedback loop so that the stakeholder can express his views and help in further effectively develop and manage the groundwater.

References

1. Bisht DS, Sridhar V, Mishra A, Chatterjee C, Raghuwanshi NS (2018) Drought characterization over India under projected climate scenario. Int J Climatol 39(4):1889–1911
2. Prasad VH, Chakraborti AK, Nayak TR (1996) Irrigation command area inventory and assessment of water requirement using IRS-1B satellite data. J Indian Soc Remote Sens 24 (2):85–96
3. Bos MG, Burton MA, Molden DJ (2005) Irrigation and drainage performance assessment: practical guidelines. CABI Publishing, Trowbridge, US, p 155
4. Bos MG, Murray-Rust DH, Merrey DJ, Johnson HG, Snellen WB (1994) Methodologies for assessing performance of irrigation and drainage management. Irrig Drain Syst 7:231–261
5. Menenti M, Visser TNM, Morabito JA, Draovandi A (1989) Appraisal of irrigation performance with satellite data and georeferenced information. In: Rydzewsky JR, Ward K (eds) Irrigation theory and practice. Pentech Press, London, pp 785–801
6. Ray SS, Dadhwal VK, Navalgund RR (2002) Performance evaluation of an rrigation command area using remote sensing: a case study of Mahi command, Gujarat, India. Agric Water Manag 56(2):81–91
7. Sener M, Yuksel AN, Konukcu F (2007) Evaluation of hayrabolu irrigation scheme in Turkey using comparative performance indicators. J Tekirdag Agric Fac 4(1):43–54
8. Bumbudsanpharoke W, Prajamwong S (2015) Performance assessment for irrigation water management: case study of the great Chao Phraya irrigation scheme. Irrig Drain 64:205–214
9. Katpatal YB, Pophare AM, Lamsoge BR (2014) A groundwater flow model for overexploited basaltic aquifer and Bazada formation in India. Environ Earth Sci 72(11):4413–4425

10. Katpatal YB, Dube YA (2010) Comparative overlay analysis through analytical hierarchical process to delineate groundwater potential zones using satellite data. Int J Earth Sci Eng 3(5):638–653
11. Bhusari V, Katpatal YB, Kundal P (2016) An innovative artificial recharge system to enhance groundwater storage in basaltic terrain: example from Maharashtra, India. Hydrogeol J 24 (5):1273–1286
12. Bastiaanssen WGM, Thiruvengadachari S, Sakthivadivel R, Molden DJ (1999) Satellite remote sensing for estimating productivities of land and water. Int J Water Resour Dev 15(1–2):181–196
13. Vidal A, Perrier A (1990) Irrigation monitoring by following the water balance from NOAA-AVHRR thermal infrared data. IEEE Trans Geosci Remote Sens 28:949–954
14. Roerink GJ, Bastiaanssen WGM, Chambouleyron J, Menenti M (1997) Relating crop water consumption to irrigation water supply by remote sensing. Water Resour Manag 11(6):445–465
15. Bhusari V, Katpatal YB, Kundal P (2017) Performance evaluation of a reverse-gradient artificial recharge system in basalt aquifers of Maharashtra, India. Hydrogeol J 25(3):689–706

Assessment of Interbasin Water Transfer Using Geoinformatics Approach: A Case Study of Shivnath Basin, India

Chandan Kumar Singh, Divesh Lanjewar, Ishtiyaq Ahmad, and Y. B. Katpatal

Abstract Irregular precipitation and inadequate water infrastructure have caused severe droughts and floods in various parts of the basin worldwide. The plausible solution is to allocate water from an area of surplus water to an adjacent area, with insufficient water, this development is called interbasin water transfer. There are solutions for transferring water within a basin, the most common being open canals and pipes, but there are very few explanations to know the feasibility of transfer. The purpose of this study is to investigate the feasibility of water transfer within a basin. The Tandula and Ravishankar reservoirs of the Shivnath Basin of central India were the study sites. Change detection analysis was used to assess the feasibility of water transfer with inputs as normalized differential vegetation index and reservoir discharge. We have conducted a questionnaire survey to verify our findings and the farmer's feedback on water-related issues in the basin. Our finding shows that the Tandula reservoir faces water scarcity issues during the pre-monsoon season and may face socio-economic losses in the near future. The method described in the study can shape the decision-making process of Interbasin water transfer easier and opt for a better solution.

Keywords Drought · Flood · Water transfer · Irrigation

C. K. Singh (✉) · D. Lanjewar · I. Ahmad
Department of Civil Engineering, National Institute of Technology Raipur, GE road, Raipur, (C.G.) 492010, Maharashtra, India
e-mail: csingh6@ucmerced.edu

I. Ahmad
e-mail: iahmad.ce@nitrr.ac.in

Y. B. Katpatal
Department of Civil Engineering, VNIT Nagpur, S.A. Road, Nagpur 440010, Maharashtra, India

B. Laishram and A. Tawalare (eds.), *Recent Advancements in Civil Engineering*, Lecture Notes in Civil Engineering 172,
https://doi.org/10.1007/978-981-16-4396-5_81

1 Introduction

Water supply and demand for freshwater are disproportionate in space and time. In addition, irregular precipitation patterns and lack of water infrastructure make the situation more challenging. The total availability of water in a basin remains constant while the need for water for domestic, industrial and agricultural purposes increases as the population increase [1]. Transferring water from surplus to deficit basin have large impacts on both areas with regards to political, technical, economic and social aspects [2]. Uneven water distribution in a basin and lack of water management practices may result in severe water shortage in some areas instead of having surplus water in other parts of the same region [3]. An Interbasin water transfer (IWT) management approach is needed when water demand exceeds supply, to ensure sustainable water supply. Sustainable water supply in deficit areas is of the highest importance to safeguard water, food and socio-economic status. Persistent drought-like conditions also prompt decision makers to build water transfer infrastructure [4]. The feasibility assessment of water transfer projects is of extreme importance during planning before actual construction and operation. This involves deciding an approach to estimate net water transfer benefits that should be reasonable for both the destination basin and the area of origin.

Extensive research has been conducted to evaluate the impact of IWT projects worldwide. Several approaches were reported in the past dealing with assessing IWT projects. Water balance, hydraulic and data-driven models are widely adopted [5]. Soil water and assessment tool (SWAT) has been used to understand the hydrological changes in Umiam Watershed in Meghalaya, India [6]. The SWAT model is coupled with the chloride mass balance (CMB) method to model streamflow for basin receiving interbasin groundwater flow [7]. Essenfelder [8] used a hydrological model to simulate the basin's rainfall-runoff process, while machine learning algorithms are used to simulate the decision-making process of the IWT. Data-driven studies have been used to assess the feasibility of the ‘Ken-Betwa project’, India using the entropy method combined with the strengths, weaknesses, opportunities and threats (SWOT) model [9]. Xi [10] has developed a data-driven approach to estimate water supply and risk evaluation with consideration of rainfall forecast information. Integrated optimization framework with the water evaluation and planning system (WEAP) model to reduce the reservoir capacity of water transfer infrastructures and maximize the reliability of water supply for destined agricultural areas in the Bashar-to-Zohreh IWT project [10]. The Water Supply Sustainability Index model was used to analyze changes in climate and related hydrology, as well as developed water demand for each county in the united states [11]. Geospatial approaches, such as the analytical network process, were used to decide on water transfer projects characterized by complex, multiple and conflict management objectives [12].

From the literature reviewed, it is apparent that to date methods focus more on water transfer projects of large-scale basins with high temporal frequency or continuous data of seasonality. Additionally, these approaches are not well-suited in assessing the feasibility of IWT for small scale and short distance water transfer projects. It is not suitable for studies in a basin with sparse climate and hydrological network data. Hence, in this study, we focus on a geospatial-based approach to use remotely sensed data, field and statistical information for evaluating small scale and short distance (less than 100 km) IWT projects.

To evaluate the feasibility of IWT, this study aims to answer the following questions (1) How geospatial-based approach combines with field data to assess the feasibility of water transfer of planned/proposed project? (2) How does crop season in the basin affect irrigation water requirements? (3) What is the efficacy of water transfer considering water availability, crop water demand and socio-economic aspects? To answer the above questions, we used a geospatial-based approach to combine remotely sensed data and field information in agriculture regions of the Shivnath Basin, India. This research presents a case study of Tandula and Ravi Shankar reservoir of the Shivnath basin located in central India. Change detection analysis was carried out to assess the short and long-term feasibility of water transfer with major input as Normalized Difference Vegetation Index (NDVI), daily reservoir outflow and questionnaire survey data.

2 Materials and Methods

2.1 Study Area

The Shivnath basin receives 1150 mm of average precipitation annually. The climate in the region comes under humid and dry conditions, with average temperatures of 30 and 45 °C in summer and 0 and 25 °C during winter. The Tandula reservoir project is an irrigation project constructed on the Tandula River, a tributary of Shivnath and a sub-tributary of the Mahanadi river.

It is located near village Lohara in Balod tehsil of Durg district of Chhattisgarh, India and the coordinates are 21° 29′ 33.62″ N, 81° 53′ 10.77″ E. The cultivable command area (CCA) of the project is 2463.62 km^2 and the area to be irrigated by canal, command area (CA) is 853.44 km^2. The Ravi Shankar Sagar reservoir is also known as Gangrel located in Dhamtari district of Chhattisgarh, India and coordinates are 20° 37′ 36″ N, 81° 33′ 36″ E. The CCA of the project is 3010 km^2 and net irrigable area or CA is 2903.1 km^2. The main crop in both areas is paddy and Khesari. The command area of Tandula and Ravi Shankar Sagar reservoir is shown in Fig. 1.

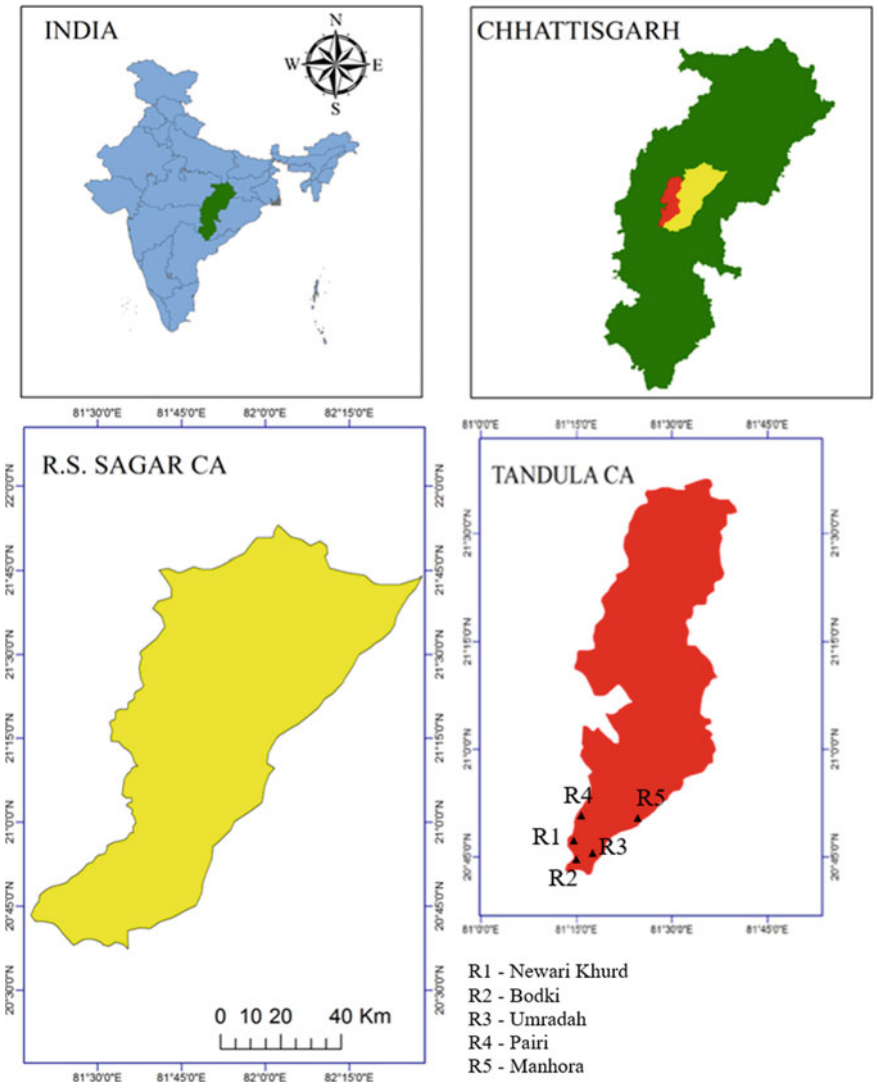

Fig. 1 Study area: Ravi Shankar Sagar/Gangrel and Tandula reservoir of the Shivnath basin, Chhattisgarh, India. CA: Command Area, R is the identification number given to the respondent in a questionnaire survey

2.2 Data Source

Data used for this research are: (1) moderate-resolution imaging spectroradiometer (MODIS) normalized difference vegetation index (NDVI) data of study sites were downloaded from MODIS web [13]. The spatial and temporal resolution of the data

was 250 m and 8 days, respectively; (2) Landcover of study sites were derived using high resolution LISS IV satellite imagery [14]; (3) Crop water depth requirement in different seasons in a year received from national food security mission, the government of India [15]; (4) Hydrological data, i.e., reservoir data received from state data processing center of hydrometeorology, Raipur, India. (5) Questionnaire surveys were performed to know the socio-economic aspects of the farmers.

2.3 Geospatial Method

A case study has been presented in the Shivnath Basin which illustrates the feasibility of transfer of water from Ravi Shankar Sagar reservoir to Tandula reservoir. The shortage of water for irrigation in the Tandula reservoir has led to the need for water import from the adjacent Ravi Shankar Sagar reservoir. This method was designed to assess the feasibility of water transfer at the planning level. The approach described in this section estimates the net water transfer benefits that should be equitable for both the Ravi Shankar Sagar reservoir and Tandula reservoir. The overall method used in the present study is shown in Fig. 2.

The geospatial approach is the process of collecting, manipulating and explicitly presenting satellite imagery from the historical data of a geographic model [16]. In this study, ArcGIS tool was used to perform geographic information systems and remote sensing analysis to study vegetation during different cropping seasons. Land cover data were used to demarcate the irrigated region in both Gangrel and Tandula command areas and further NDVI analysis. Land cover data were used to demarcate the irrigated area in both Gangrel and Tandula command areas and further NDVI analysis was performed. Remotely sensed MODIS NDVI data were used to map the vegetation in the rabi (February) and kharif (October) crops in the years 2002, 2012 and 2018. Change detection analysis was used to identify spatial variations of crops in the Rabi and Kharif seasons and their linkage with crop water requirements. The NDVI range obtained for the year 2018 was subtracted from the NDVI values from the years 2012 and 2002 for the months of February and October and the resulting differences show regions with increased and decreased crops for the respective months. Areas of barren rock, sand, or no crop features typically have NDVI values of 0.2 or less, so the lower NDVI range, i.e., less than 0.2, was neglected.

2.4 Statistical Approach and Questionnaire Survey

For all crops in a basin, the crop water requirement (million cubic meters) is determined as follows (Table 1).

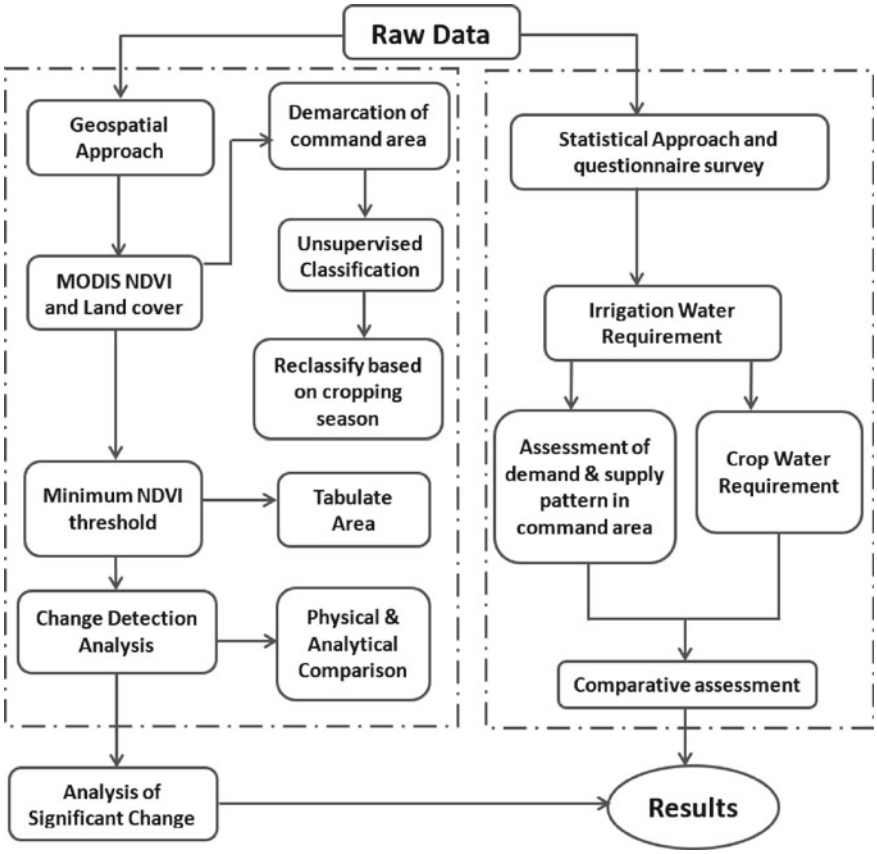

Fig. 2 Flowchart of the study showing the overall method

$$\text{Crop water requirement} = \text{irrigated area}\left(\text{km}^2\right) \times \text{water requirement}(\text{m}) \quad (1)$$

Water availability in both Gangrel and Tandula reservoirs was estimated using the water balance equation as follows:

$$\text{Inflow} - \text{Outflow} - \text{Losses} = \text{Storage} \quad (2)$$

Telephone survey was carried out to collect data on Tandula reservoir. The goal of the survey was to collect data for agriculture and the socio-economic status of

Table 1 Crop wise area distribution and water requirement

S. no.	Type of crop	Water requirement (cm)
1	Kharif (October)	120
2	Rabi (February)	60

farmers. Five random villages around Tandula reservoir have been selected in this survey (Fig. 2). To collect a representative sample, we decided to approach the sarpanch, the democratically elected head of each village. A sarpanch represents about 1000 people in a village. As the head of a village, the sarpanch is aware of the problem at the ground level. We have used English and Hindi language (vernacular) to make the questions simple and clearly target the population. The three sections of the survey were agricultural, economic and social, with five questions in each section (Appendix 1). The length of the survey was kept short to avoid dropping the question. The survey was based on telephonic conversations and took an average of one hour per respondent. The analysis results of the survey are discussed in a later section.

3 Results

3.1 Change Detection Analysis

Change detection analysis was performed to detect changes in agricultural patterns in different cropping seasons. The main purpose was to demarcate the agricultural region which directly depends on the outflow of the reservoir. Area irrigated by the canal using Gangrel and Tandula reservoir was demarcated to detect the changes in the command area. The NDVI map of the study area was prepared for the years 2002, 2012 and 2018 of February and October (Fig. 3). Paddy crop, which is the main crop, is grown during February and October and hence change in vegetation is related to consumptive water use in the command area.

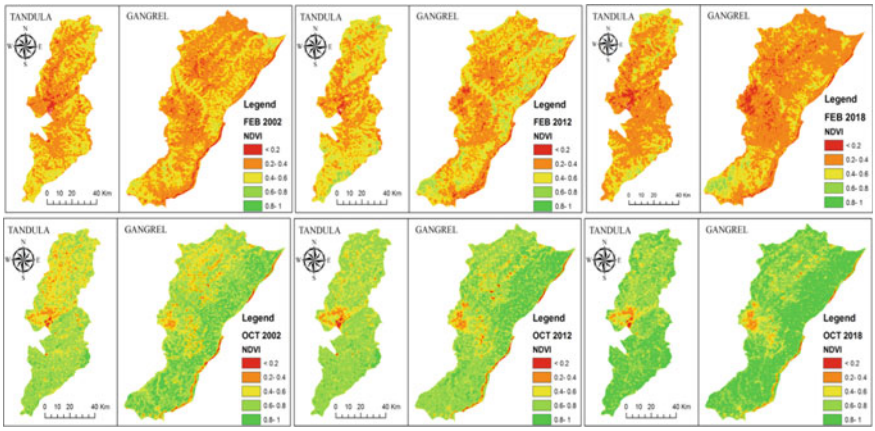

Fig. 3 Normalized difference vegetation index (NDVI) map of Tandula and Ravi Shankar Sagar reservoir

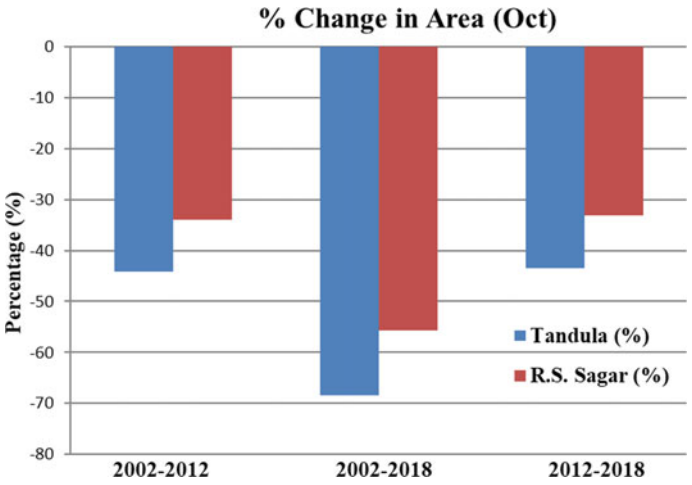

Fig. 4 Percentage change in command area for Tandula and R.S. Sagar reservoir in February month

Change detection analysis revealed that there was both decreased and increased trend in crop covers in the command area of both the reservoirs. The agricultural area of Tandula reservoir has shown a declining trend on a long-term and short-term basis. The percentage change of agricultural region in Ravi Shankar Sagar Reservoir is 55%, 31% and 56% in 2002–2012, 2002–2018 and 2012–2018, respectively (Fig. 4). In February, the agricultural region shows a rising trend on both short and long-term basis (Fig. 5). Similarly, Tandula agricultural area shows a declining and rising trend on both long-term basis and short-term basis. The percentage change of transformation of agriculture region in Ravi Shankar Sagar Reservoir is 44%, 68% and 43% in 2002–2012, 2002–2018 and 2012–2018 respectively, which is greater than a change in the agricultural command area compare to Tandula reservoir. In February month, the agricultural region shows a declining trend on both short and long-term basis (Fig. 5). These changes in the agricultural sector are attributed to the availability of water for irrigation and the lack of water infrastructure.

3.2 Water Availability and Demand

Water availability in both Gangrel and Tandula reservoirs was estimated using the water balance approach. The monthly minimum and maximum amount of water storage in R.S. Sagar and Tandula Reservoir have been shown in Figs. 6 and 7. The availability of water was estimated after deducting all demands (except irrigation) and losses in the R.S. Sagar reservoir and Tandula reservoir. The need for crop

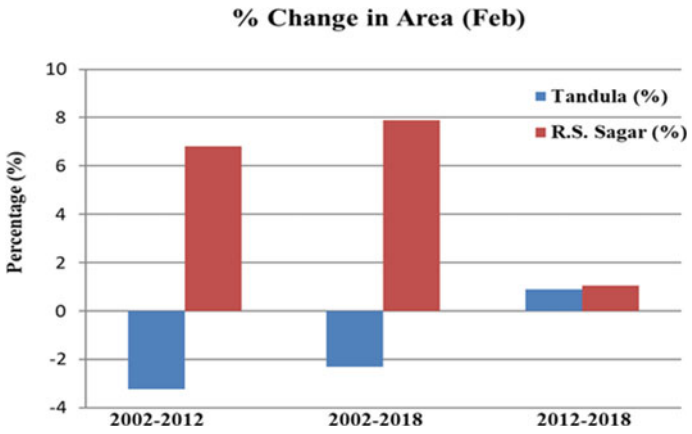

Fig. 5 Percentage change in command area for Tandula and R.S. Sagar reservoir in October month

water in the command area for agricultural use was estimated as the product of the irrigated area and the water required for a crop from its sowing period to the harvesting period (Table 2). The amount of water required for irrigation is shown in Table 2, for all crop seasons in a year. A comparative analysis of the demand and supply of water from Tandula and R.S. Sagar reservoir shows that the water is insufficient in September–October and October–November to meet the demand for paddy crops (Table 2; Figs. 6 and 7). This state of water scarcity begins with the developed interbasin water transfer structure.

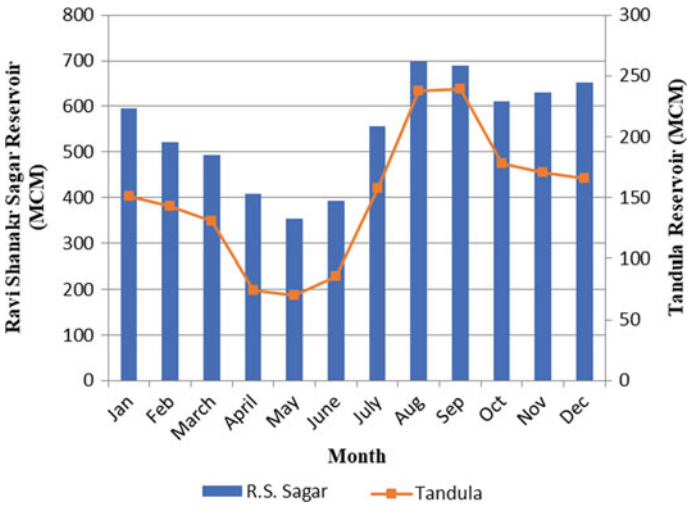

Fig. 6 Water availability in Ravi Shankar Sagar reservoir and Tandula Reservoir

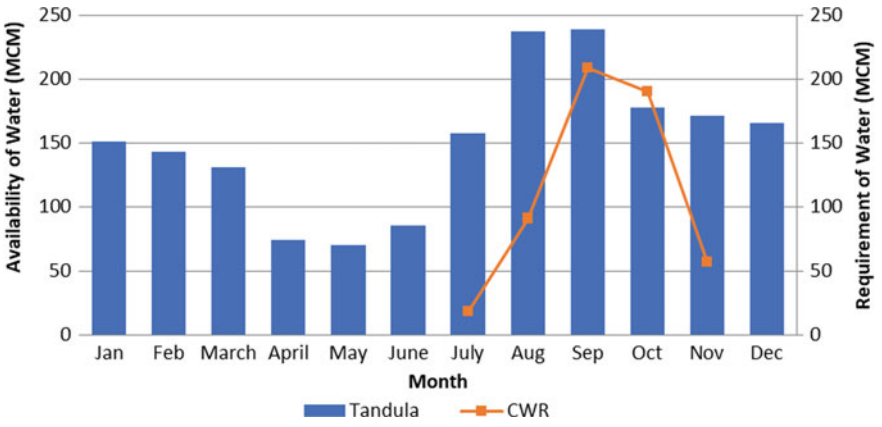

Fig. 7 Crop water requirement (CWR) and availability of water in Tandula reservoir

Table 2 Crop water requirement in a year [17]

S. no.	Type of crop	% area	Area (km^2)	Water requirement (cm)	Water requirement in total area (MCM)
1	Kharif	44.190	455.157	120	1.2 * 455.157 = 546.188
2	Rabi	5.30	54.59	60	0.6 * 54.59 = 32.754
3	Zaid	0.180	1.854	30	0.3 * 1.854 = 0.38625
4	Double/ Triple	50.33	518.933	120	1.2 * 518.933 = 622.678

3.3 Socio-Economic Aspects Based on Questionnaire Survey

Telephone survey was carried out to collect data on Tandula reservoir. The goal of the survey was to collect data for agriculture and the socio-economic status of farmers. Five random villages around Tandula reservoir have been selected in this survey (Fig. 2). All respondents have a canal in their village, but very few of them can use water for irrigation. The reasons behind inadequate water were poor maintenance of the canal, less access to ditches, tail end water problem, water theft, etc. Reacting to water availability issues, farmers responded that water is not available during peak summer and if available from an adjacent source, they are ready to grow more crops (Fig. 8). In economic aspects, we found that farmers' income is based solely on crop yield and livestock. All respondents agree that crop failure due to lack of water availability is one of the main reasons for less income the loss of income (Fig. 9).

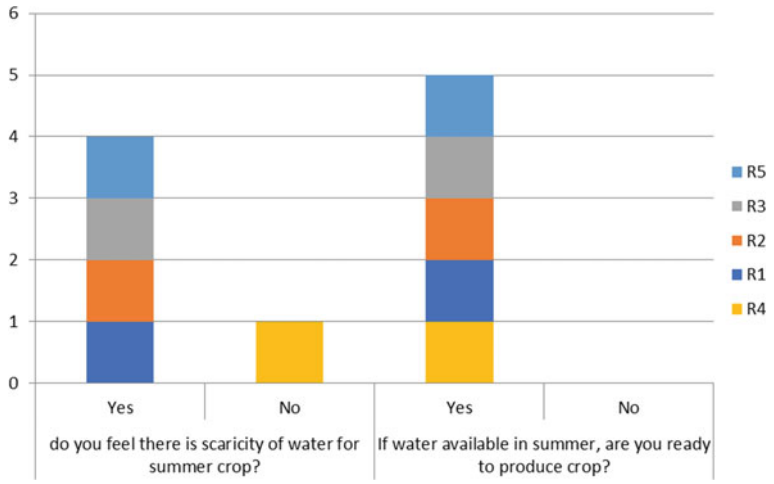

Fig. 8 Water scarcity and availability (each yes and no was given equal point)

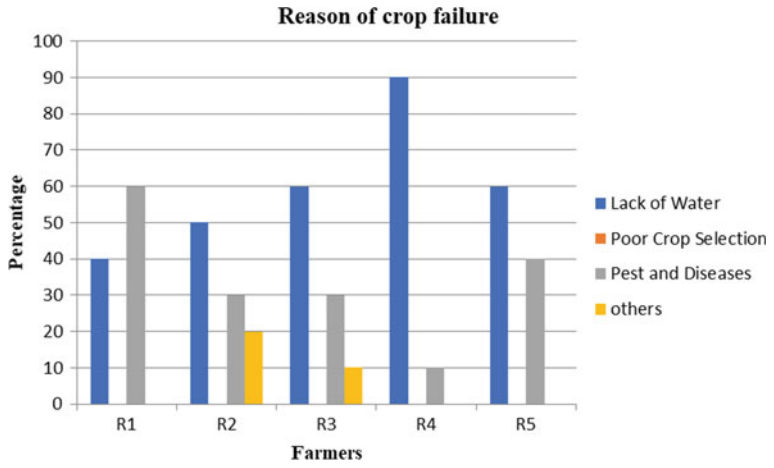

Fig. 9 Reason of crop failure based on questionnaire survey

4 Conclusions

This study evaluates the feasibility of IWT based on water availability, crop water requirements and socio-economic aspects using a geospatial approach. The change detection analysis and reservoir outflow data estimate the demand and supply of water during the growing season in the command area of Gangrel and Tandula reservoir. The study shows that the Tandula reservoir cannot withstand the problem of water scarcity in the long run (more than 10 years). However, the Ravi Shankar

reservoir shows surplus water in the pre-monsoon season. It has been observed that the water transfer project from Ravi Shankar Sagar reservoir to Tandula reservoir is feasible from a technical and economic point of view. The questionnaire survey supports our finding that Tandula needs water during the growing season. Farmers also believe that connecting the canal between the Ravi Shankar Sagar reservoir and Tandula reservoir will solve water shortage issues and improve socio-economic status. This study, therefore, suggests that it is possible to construct a water structure between Gangrel and Tandula. The method described in the study is simple and utilizes existing field and available remote sensing data, which has been found useful in the decision-making and planning process in the design of water transfer infrastructure and in analyzing water transfer within the basin.

Appendix 1 (Questionnaire Survey)

Agricultural Impact:

11. What Kind of Crop Do You Produce?
12. What is the Source of Irrigation?
13. Do You Feel Water Shortage for Summer Crops?
14. If Water Transfer Increases the Amount of Water, Will You Plant Another Crop?
15. Which Method of Irrigation Do You Use in the Field?

Economic Impact:

16. What is Your Annual Income?
17. What is the Reason Behind Loss of Income?
18. Is Water Supply the Reason for Low Income?
19. What Was the Annual Income in a Normal and Dry year?
20. Were You Able to Pay off the Loan During the Normal year/drought year?

Social Impact:

21. What Are the Sources of Income Other Than Agriculture?
22. How Many Livestock Do You Own? or Average Livestock Per Household?
23. What is the Availability of Agricultural Labor Today?
24. Does the Water Supply Enough for Drinking?
25. Is There a Risk to Food Supply During Drought Period?

References

1. Gupta N, Pilesjö P, Maathuis B (2010) Use of geoinformatics for inter-basin water transfer assessment. Water Res 37(5):623–637. https://doi.org/10.1134/S0097807810050039
2. Rezapour Tabari MM, Yazdi A (May 2014) Conjunctive use of surface and groundwater with inter-basin transfer approach: case study Piranshahr. Water Resour Manag 28(7):1887–1906. https://doi.org/10.1007/s11269-014-0578-2

3. Dahasahasra SV, Katpatal YB, Mahajan MM (2003) National river-linking. J Indian Water Works Assoc 35(4):12
4. Gurung P (2015) Inter-basin water transfer: is this a solution for water scarcity? https://doi.org/10.13140/RG.2.1.3592.5607
5. Tien Bui D, Talebpoor D, Ghanavati E, Al-Ansari N, Khezri S, Chapi K, Amini A, Pham B (January 2020) Effects of inter-basin water transfer on water flow condition of destination basin. Sustainability 12:1–20. https://doi.org/10.3390/su12010338
6. Marak JDK, Sarma AK, Bhattacharjya RK (October 2020). Assessing the impacts of interbasin water transfer reservoir on streamflow. J Hydrol Eng 25(10):05020034. https://doi.org/10.1061/(ASCE)HE.1943-5584.0001984
7. Senent-Aparicio J, Alcalá FJ, Liu S, Jimeno-Sáez P (March 2020) Coupling SWAT model and CMB method for modeling of high-permeability bedrock basins receiving interbasin groundwater flow. Water 12(3):657. https://doi.org/10.3390/w12030657
8. Essenfelder AH, Giupponi C (September 2020) A coupled hydrologic-machine learning modelling framework to support hydrologic modelling in river basins under Interbasin Water Transfer regimes. Environ Model Softw 131:104779. https://doi.org/10.1016/j.envsoft.2020.104779
9. Srinivas R, Pratap Singh A, Jain V, Sharma P (July 2020) Development of an advanced entropy-based decision support system to assess the feasibility of linking of rivers in a sustainable manner. Int J River Basin Manag 1–24. https://doi.org/10.1080/15715124.2020.1790579
10. Jamshid Mousavi S, Anzab NR, Asl-Rousta B, Kim JH (September 2017) Multi-objective optimization-simulation for reliability-based inter-basin water allocation. Water Resour Manage 31(11):3445–3464. https://doi.org/10.1007/s11269-017-1678-6
11. Dickson KE, Dzombak DA (2017) Inventory of interbasin transfers in the United States. JAWRA J Am Water Resour Assoc 53(5):1121–1132. https://doi.org/10.1111/1752-1688.12561
12. Toosi SLR, Samani JMV (May 2012) Evaluating water transfer projects using analytic network process (ANP). Water Resour Manag 26(7):1999–2014. https://doi.org/10.1007/s11269-012-9995-2
13. MODIS Web. Retrieved December 4, 2018 from https://modis.gsfc.nasa.gov/
14. Bhuvan (2018) Thematic data dissemination. Free GIS Data. OGC Services. Clip and Ship. Retrieved December 2, 2018 from https://bhuvan-app1.nrsc.gov.in/thematic/thematic/index.php
15. Crop Calender. Retrieved November 3, 2018 from https://nfsm.gov.in/nfmis/rpt/calenderreport.aspx
16. Thakur JK, Singh SK, Ramanathan AL, Bala Krishna Prasad M, Gossel W (eds) (2011) Geospatial techniques for managing environmental resources. Springer, Netherlands. https://doi.org/10.1007/978-94-007-1858-6
17. Thakur NK, Khalkho D, Katre P, Tonde J (March 2018) Development of optimal crop plan for IGKV, farm Raipur, Chhattisgarh. J Pharmacognosy Phytochem 7(2):172–176

Application of Modified Penman Method for Assessment of Crop Water Requirement in Venna Basin, Maharashtra India

Sarang V. Paranjpe, Y. B. Katpatal, and M. S. Kadu

Abstract Availability of water resources in a watershed or a basin has always compelled the hydrologists across the globe to think and devise various methods to arrive at the correct estimate of the same. Although the exact estimation of this precious resource is not possible, its availability and proper use helps greatly in the management of water resources in a basin. The amount of water required for the crops to grow healthy and achieve maximum yield is called as the crop water requirement. This is the amount of water required over and above the requirement met with the rainfall by a crop to grow healthy. Correct estimation of the available water and its management with proper use over the basin would result in maximum crop yield and meeting the needs of other stake holders like the drinking water, industrial use, etc. Present study aims to estimate the crop water requirement for various crops in Venna river basin, Maharashtra. Food and Agriculture Organization (1984) Modified Penman method is a globally accepted method for crop water requirement estimation which gives the most accurate results.

Keywords Evapotranspiration · Crop water requirement · Irrigation · GIS

1 Introduction

With the rise in the population across the globe, availability of water and food has always been the worry point for the hydrologists and the administrators. With the increasing population, the use of water increased and it calls for the effective and proper estimation and management of the available water resources in the basin. Supply of water in required quantity at required time is necessary for the crops to grow healthy and produce maximum yield. The estimation of the crop water

S. V. Paranjpe (✉) · M. S. Kadu
Department of Civil Engineering, RCOEM, Nagpur 440013, India
e-mail: kadums@rknec.edu

Y. B. Katpatal
Department of Civil Engineering, VNIT Nagpur, S.A. Road, Nagpur 440010, India

B. Laishram and A. Tawalare (eds.), *Recent Advancements in Civil Engineering*, Lecture Notes in Civil Engineering 172,
https://doi.org/10.1007/978-981-16-4396-5_82

requirement is a vital parameter in overall management of the water resources in the river basin [1]. The correct and assured supply of water for crops ensures the better yield and good quality produce. Food and Agricultural Organization FAO (1984) United States has defined crop water requirement as "the depth of water needed to meet the water loss through evapotranspiration of a crop, being disease free, growing in large fields under non restricting conditions and achieving full production under given growing environment."

2 Materials and Methods

2.1 Study Area

The present study was carried for Venna river basin in Vidarbha, Maharashtra, India. The study area lies between 21° 00′ 00″ N and 23° 01′ 00″ N latitude and 78° 18′ 00″ E and 79° 06′ 15″ E longitude. The total area of the basin is 5674.57 km^2 which is spread in Wardha, Nagpur and Chandrapur districts of Vidarbha, Maharashtra, India (Fig. 1). Out of the total area, Wardha district contributes 3278.96 km^2, Nagpur 2120.99 km^2 whereas Chandrapur district contributes a small area of 274.63 km^2. River Venna originates at village Khairi in Katol tehsil of Nagpur district and after flowing a distance of 163 km, and meets Wardha river at village Dindora in Warora tehsil of Chandrapur district. Average annual monsoon rainfall over the basin ranges from 900 to 1100 mm. Most of the area within the basin is underlain with basaltic formation, whereas small areas have alluvium, limestone and sandstone.

2.2 Input Data

The study period for this study was from year 2000 to 2015. Information about tehsil wise crop area sown, its yield and productivity, etc., was collected from the Agriculture Department, Govt. of Maharashtra. This data was collected for Kharif as well as Rabi season. It was observed that Wheat and Gram are the major Rabi crops, whereas Soybean and Cotton are major Kharif crops in the basin. This input was used for the calculations of crop water requirement for various crops. Similarly the information about the daily rainfall data and the crop coefficients were also taken from Agriculture department Govt. of Maharashtra. The input about the fortnightly evapotranspiration was collected from Water Resources Department, Govt. of Maharashtra.

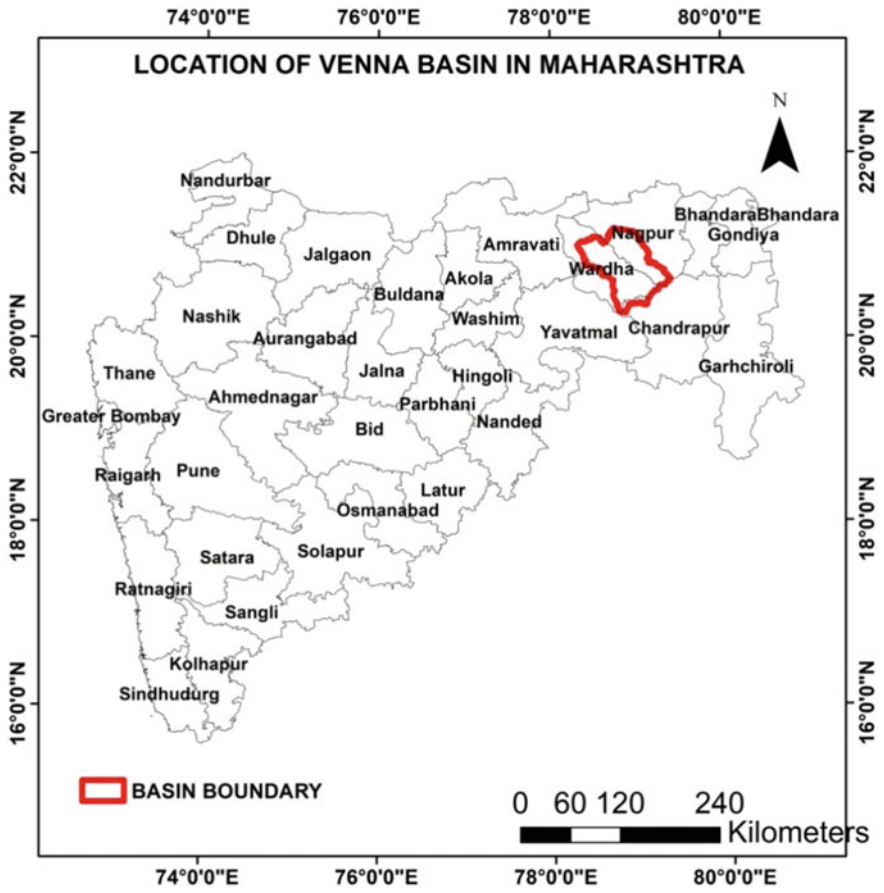

Fig. 1 Location map of Venna basin in Maharashtra

2.3 Material and Methods

Crop water requirement can be defined as the water required for the healthy growth of the crops. The required amount of water is defined as the amount of water needed to meet the loss of water through evapotranspiration. While calculating the crop water requirement of various crops in a basin, the water requirement to be met by the surface irrigation needs to be considered. For surface irrigation through canals, the availability of surface runoff within a basin needs to be assessed. SCS-CN method has proved to be effective in giving the realistic results about the surface runoff estimation [2]. Although the surface water irrigation system bears many losses due to evaporation, theft, leakages, etc., the same is not taken into account in the present study. Groundwater has been a reliable source of irrigation. However its availability varies spatially as the lithology varies. The availability of ground water

resource needs to be assessed and monitored and various tools in GIS environment have proved to be very effective in this [3]. As per the Food and Agricultural Organization FAO (1984), the crop water requirement is 'the depth of water needed to meet the water loss through evapotranspiration of a crop, being disease free, growing in large fields under non restricting conditions and achieving full production under given growing environment'.

Evapotranspiration (ET) is the process by which water is released into the air by the transpiration from plant surfaces and by evaporation from the soil. Evapotranspiration is the total movement of water vapor into the atmosphere from land which supports plant life. It includes transpiration from the plants, evaporation from soil and evaporation from any open water that may be present in ponds following irrigation or heavy rainfall. It is expressed in terms of depth of water (millimeters), and the rate of evapotranspiration in millimeters per hour. Evapotranspiration is caused by an energy gradient difference between water in plants and soil and water in the atmosphere. It is influenced by climatic factors, such as sunshine, temperature, humidity and wind speed. Out of the total evapotranspiration, evaporation account for about 10% and plant transpiration for the remaining 90% [4]. Hence the crop water requirement includes all losses like:

(a) Transpiration loss through leaves (T)
(b) Evaporation loss through soil surface in cropped area (E)
(c) Amount of water used by plants (WP) for its metabolism.

Evapotranspiration is one of the major components of the hydrologic cycle and affects crop water demand. Therefore, its quantification is necessary for proper irrigation planning. The term evapotranspiration refers to combination of two processes, namely, evaporation and transpiration Evaporation is a process by which water is lost in the form of vapor from natural surfaces, such as free water surface, bare soil, from live or dead vegetation. Transpiration is a process by which water is lost in the form of vapor through plant leaves. Therefore evapotranspiration is a combined loss of water from the soil (evaporation) and plant (transpiration) surfaces to the atmosphere through vaporization of liquid water, and is expressed in depth per unit time (for example mm/day). Potential evapotranspiration is defined as "the rate of evapotranspiration from an extensive surface of 8–15 cm tall, green grass cover of uniform height, actively growing, completely shading the ground and not short of water" [5]. As the definition suggests that the PET is for a grass reference ETo. The concept of reference ET is being used to avoid ambiguities associated in the definition of PET [6, 7]. There are many methods of estimation of crop water requirement but Penman–Monteith equation for calculation of PET is recommended as the standard equation by the Food and Agriculture Organization (FAO). The results obtained from various methods of estimation of evapotranspiration have been analyzed and compared with the results obtained from Modified Penman method [8]. Results obtained from the temperature based and the radiation-based methods of estimating evapotranspiration have been compared with Penman method and it was found that the radiation-based methods are more suitable [9].

FAO-24 Modified Penman (1977) Method.

$$\text{PET} = [WRn + (1 - w)f(u)(ea - ed)c] \quad (1)$$

where

PET = potential evapotranspiration (mm/day).

W = Temperature related weighing factor.

Rn = Net radiation (mm/day).

$f(u)$ = wind related function.

$(ea - ed)$ = difference between saturation vapor pressure (SVP) at mean air temperature and mean actual vapor pressure of air (mb).

c = correction factor.

There are two cropping seasons in India, namely, Kharif and Rabi.

(a) Kharif: The crops in the Kharif season are sown at the beginning of the South-West monsoon and harvested at the end of the monsoon period. Sowing starts mostly in the month of May till July depending on the rainfall whereas the harvesting season is between September to October. The major Kharif crops include Soybean, Cotton, Rice, Bajra, Maize, Groundnut, Sugarcane, Jowar, etc.

(b) Rabi: The Rabi season generally starts from the month of October to December every year. The crops in this period need relatively cool climate during the period of growth but warm climate during the germination of their seed and maturation. Harvesting time lies between February to April. The major crops cultivated include Wheat, Gram, Barley, Linseed, Mustard, Masoor, Potatoes, etc.

3 Result and Discussion

Ten major crops which are grown in Venna Basin were selected for this study and the crop water requirement for these crops was calculated. The selected crops include Soybean, Groundnut, KharifJowar, Tur/Mung/Udid, Sugarcane, Cotton, Kharif Paddy, Maize, Wheat and Gram. It is observed that Soybean and Cotton are the major crops in Kharif season whereas Wheat and Gram are the major crops in Rabi season in Venna Basin. The crops selected for the study purpose include 8 major crops of the Kharif season and 2 major crops from Rabi season. During the analysis of the crop sown area, it was noticed that the sown area of other minor crops varies between 5 and 8% excluding the area of Soybean and Cotton in Kharif and Wheat and Gram is Rabi. The crop water requirement for these ten crops was computed by FAO-24 Modified Penman method. Tehsil wise crop water requirement for various crops was computed for a period from year 2000 to 2015. The details of the crop area sown for 14 tehsils over which Venna basin is spread was collected from the concerned Agriculture Department, Govt. of Maharashtra. A sample crop sown area for the year 2001–02 for 14 tehsils of the basin is given below (Table 1).

Table 1 Crop sown area for various crops in Venna Basin for year 2001–2002

2001–02 (area in ha) Tahsil	KJ	T/M/U	GN	SB	C	SG	KP	M	W	G
ARVI	6150	8157	75	14,250	22,875	0	15	0	1110	1115
KARANJA	4350	5620	1540	19,550	11,510	0	40	0	2075	2810
WARDHA	8372	14,523	9	11,153	18,472	0	94	0	1987	2750
SELOO	4215	6135	0	11,135	21,865	0	0	0	3410	1980
HINGANGHAT	7415	11,965	10	14,680	22,120	0	50	0	4800	4860
SAMUDRAPUR	3010	10,395	0	29,010	25,250	0	45	0	4210	5155
NAGPUR	3200	3894	10	11,444	12,554	240	27	0	3808	2878
HINGNA	6750	4998	10	5563	18,250	50	15	0	1298	718
KATOL	12,950	9775	4900	14,225	10,800	0	35	0	1658	3850
KALMESHWAR	9530	6670	1200	7730	13,500	116	0	0	2980	1420
UMRER	134	3655	0	29,115	7620	219	1910	0	6286	5546
BHIWAPUR	0	2040	0	21,810	1425	0	3070	0	5058	1900
WARORA	1680	6100	0	18,000	24,000	500	3310	0	7500	5870
CHIMUR	0	4920	0	25,000	1200	0	17,700	0	5030	2730
Total in ha	67,756	98,847	7754	232,665	211,441	1125	26,311	0	51,210	43,582

KJ—KharifJowar, T/M/U—Tur/Mung/Udid, GN—Ground Nut, SB—Soya Bean, C—Cotton, SG—Sugar-Cane, KP—Kh.Paddy, M—Maize, W—Wheat, G—Gram

FAO-24 Modified Penman method uses average rainfall for a fortnight, hence, the daily rainfall data was averaged at every fortnight for all the months of the year from 2000 to 2015. Table 2 presents the same.

Fortnightly evapotranspiration values for the basin area were collected from Water Resources Department, Govt. of Maharashtra as given in Table 3 and the mean fortnightly consumptive use is computed and shown in Table 4. Researchers [10] prepared a computer model for computing crop water requirement and concluded that the results were comparable with the traditional methods.

Annual crop water requirement for each crop is computed for the year 2000–2015 using the spatial and digital data. Reference [11] explained that estimation of evapotranspiration by remote sensing yield very good results. Table 5 gives the tehsil wise annual crop water requirement for the selected major crops in Venna Basin for a study period of 2000–2015.

The crop water requirement is minimum at 9.7 Mm^3 for Chimur tehsil while it is maximum at 314.0 Mm^3 for Samudrapur tehsil. The requirement is for the portion of tehsil inside the Venna river basin area. The crop water requirement is the demand of water for irrigation over and above the water received by crops from rainfall. Hence, for the study period from 2000 to 15, it is observed that in the Samudrapur tehsil, the monsoon and the available resources are insufficient and hence water requirement from the external source is high followed by Seloo and Hingna tehsils.

The tehsil wise crop water requirement is generated in Geographical Information System (GIS) environment in spatial form in Fig. 2. It shows that the major tehsils like Hingna, Seloo, Umrer and Hinganghat have crop water requirement in the range of 98–234 Mm^3 and Samudrapur has crop water requirement of more than 234 Mm^3. Since watershed is a basic unit in any hydrological study, watershed wise crop water requirement was also generated from this analysis for the basin and is presented in Fig. 3. It may be observed that watersheds WRWBD5, WRWBD7, WRW3, WRW7, WRWI and WRW1 have lower crop water requirement whereas watersheds WRW6 has highest crop water requirement. There are watersheds with medium crop water requirement which are WRW2 and WRWP1.

4 Conclusions

For achieving the best possible use of the water resources in the basin and to get the maximum crop yield, required amount of water has to be supplied to the crops at right time. Estimation of the crop water requirement in a basin depends on various parameters like rainfall, type of crop etc. However evapotranspiration is also an important governing factor in a hydrological cycle. The assessment of the crop water requirement depends upon the precise assessment of the evapotranspiration. Modified Penman method has proved to be a reliable method for assessing the evapotranspiration which gives results very close to the actual figures. Assessment of evapotranspiration and ultimately the crop water requirement is essential for

Table 2 Average fortnightly rainfall* in mm for year 2000–2015 over Venna Basin

AVG RF 2000–2015	AR		KJ		WR		SL		HN	
Fortnight	I	II	I	II	I	II	I	II	I	II
Jan	1.07	1.67	2.66	2.81	3.10	5.20	2.08	2.88	2.51	7.83
Feb	1.40	2.00	1.19	1.78	2.06	2.29	1.54	2.60	2.08	2.54
March	9.60	1.97	8.21	2.02	7.06	5.17	8.02	3.62	6.18	3.53
April	3.00	1.63	0.06	0.25	3.07	1.98	2.21	1.06	1.40	1.80
May	4.43	6.36	3.35	4.99	4.71	3.77	4.26	9.28	3.57	4.19
June	87.46	109.32	46.76	113.54	53.80	119.81	54.20	133.19	64.73	137.40
July	118.90	167.05	108.37	160.48	121.36	152.85	118.08	171.65	126.41	171.93
August	130.21	114.61	117.31	106.29	129.21	120.97	114.50	135.25	144.79	138.20
September	106.70	44.74	105.45	50.65	112.79	45.46	114.16	58.52	109.60	52.29
October	35.21	11.84	37.49	12.53	34.19	16.49	36.61	15.77	45.30	9.56
November	6.57	5.82	8.31	9.00	6.71	4.61	7.94	5.61	9.44	1.68
December	2.09	1.96	2.65	3.13	4.53	3.58	3.70	2.63	2.16	1.64

*Shown as example for Tehsil namely AR—Arvi, KJ—Karanja, WR—Wardha, SL—Seloo, HN—Hinganghat. Also prepared for SM—Samudrapur, NG—Nagpur, HI—Hingna, KT—Katol, KL—Kalmeshwar, UM—Umrer, BH—Bhiwapur, WA—Warora, Ch—Chimur

Table 3 Fortnightly evapotranspiration for Venna Basin

SN	Fortnight	ET_O (mm)	SN	Fortnight	ET_O (mm)
1	JAN I	73.08	13	JULY I	72.14
2	JAN II	86.26	14	JULY II	64.56
3	FEB I	89.81	15	AUG I	59.85
4	FEB II	80.90	16	AUG II	69.56
5	MARCH I	95.74	17	SEPT I	65.31
6	MARCH II	107.92	18	SEPT II	77.98
7	APRIL I	103.71	19	OCT I	87.02
8	APRIL II	105.95	20	OCT II	95.28
9	MAY I	122.43	21	NOV I	84.36
10	MAY II	147.36	22	NOV II	78.32
11	JUNE I	123.51	23	DEC I	73.77
12	JUNE II	85.56	24	DEC II	78.67

Table 4 Mean fortnightly consumptive use, mm (ET crop)

Fortnightly mean rainfall (mm)	Mean fortnightly consumptive use (mm) (ET crop)									
	12.5	25	37.5	50	62.5	75	87.5	100	112.5	125
	Mean fortnightly effective rainfall (mm)									
6.25	3.80	4.00	4.40	4.50	4.60	5.00	5.30	5.60	5.90	6.25
12.50	7.50	8.10	8.80	9.00	9.30	9.90	10.30	11.00	12.30	12.50
18.75	11.00	12.00	13.10	13.80	14.10	14.60	15.50	16.50	18.50	18.75
25.00	12.50	16.10	17.30	17.90	18.40	19.50	20.30	21.90	23.50	25.00
31.25		19.90	21.30	22.30	23.00	24.30	25.30	26.90	28.00	31.25
37.50		23.10	24.90	26.40	27.50	28.80	30.10	31.90	33.80	36.90
43.75		25.00	28.40	30.10	31.90	33.00	34.90	36.90	38.90	42.30
50.00			31.90	33.90	36.00	37.10	39.40	41.50	43.90	47.50
56.25			35.30	37.50	40.10	41.30	43.00	46.40	49.00	52.50
62.50			37.50	40.80	43.90	45.30	47.90	51.00	54.00	57.50
68.75				44.40	47.60	49.40	52.00	55.50	59.00	63.00
75.00				47.00	51.00	53.00	56.00	60.00	63.50	68.00
81.25				50.00	54.50	56.50	60.00	64.00	67.50	72.50
87.50					57.50	60.00	63.50	67.50	71.50	77.00
93.75					60.50	63.00	67.00	71.00	75.50	80.50
100.00					62.50	66.50	70.00	74.00	79.00	84.00
112.50						72.00	71.50	88.00	85.50	91.00
125.00						75.00	80.00	85.00	91.50	97.00
137.50							87.50	90.50	97.00	102.50
150.00								95.50	101.50	107.50

(continued)

Table 4 (continued)

Fortnightly mean rainfall (mm)	Mean fortnightly consumptive use (mm) (ET crop)									
	12.5	25	37.5	50	62.5	75	87.5	100	112.5	125
	Mean fortnightly effective rainfall (mm)									
162.50								99.00	106.50	112.00
175.00								100.00	110.00	116.00
187.50									112.50	120.00
200.00										123.00
212.50										125.00
225.00	12.50	25.00	37.50	50.00	62.50	75.00	87.50	100.00	112.50	125.00

Table 5 Tehsil wise Annual crop water requirement for Venna basin

Year/Tehsil	AR	KJ	WR	SL	HN	SM	NG	HI	KA	KL	UM	BH	WA	CH	ANNUAL CWR (MM^3)
2001–02	89.6	57.3	80.0	215.8	155.1	305.9	87.5	134.4	35.8	20.1	145.6	52.8	88.1	9.3	1477.2
2002–03	79.4	50.7	78.6	194.9	137.5	280.6	75.1	141.2	35.9	19.4	129.7	43.6	60.8	8.4	1335.9
2003–04	78.7	51.3	82.3	195.7	137.8	274.5	81.2	163.1	39.8	21.0	161.2	52.1	78.3	9.8	1426.8
2004–05	77.0	43.7	66.3	193.4	125.8	224.9	71.6	256.2	35.3	18.9	131.6	50.9	63.0	9.4	1368.1
2005–06	80.9	51.5	78.4	215.4	146.9	244.4	80.5	151.8	40.4	21.4	156.4	60.4	68.2	8.4	1405.0
2006–07	86.6	52.6	80.2	214.8	144.5	264.8	78.3	158.9	44.1	22.1	144.8	55.4	75.6	9.2	1431.9
2007–08	87.2	55.8	81.6	222.1	156.6	266.3	74.8	156.6	43.0	22.5	134.3	41.1	72.8	10.3	1425.0
2008–09	78.4	43.8	83.8	190.8	129.6	240.6	59.4	145.3	41.4	19.7	127.8	49.0	93.0	9.2	1311.7
2009–10	89.6	54.5	93.2	254.7	165.7	345.6	65.9	174.8	49.7	22.5	196.6	96.9	66.5	8.2	1684.4
2010–11	98.5	64.8	103.1	257.2	207.1	442.6	80.7	188.3	53.2	25.8	195.0	104.5	114	9.6	1944.9
2011–12	107.3	54.9	106.1	232.2	180.2	364.3	64.7	195.7	46.4	21.1	155.1	101.5	95.7	9.3	1734.5
2012–13	105.3	58.0	144.2	255.0	223.8	379.9	65.2	188.5	53.8	25.1	181.7	109.1	97.9	10.5	1897.9
2013–14	104.9	60.8	145.3	267.4	224.8	387.4	72.8	197.1	57.2	25.3	183.7	111.4	95.6	12.2	1945.7
2014–15	112.5	65.0	126.3	279.4	211.9	331.6	76.4	186.6	61.8	29.2	163.7	78.7	85.0	10.2	1818.4
2015–16	109.6	67.7	125.6	298.5	213.7	369.7	76.4	171.1	64.1	27.3	173.5	72.9	85.4	12.2	1867.9
A. CWR	92.4	55.5	98.3	232.5	170.7	314.9	74.0	174.0	46.8	22.8	158.7	72.0	82.7	9.7	

AR—Arvi, KJ—Karanja, WR—Wardha, SL—Seloo, HN—Hinganghat, SM—Samudrapur, NG—Nagpur, HI—Hingna, KT—Katol, KL—Kalmeshwar, UM—Umrer, BH—Bhiwapur, WA—Warora, Ch—Chimur, A. CWR—Average Crop Water Requirement

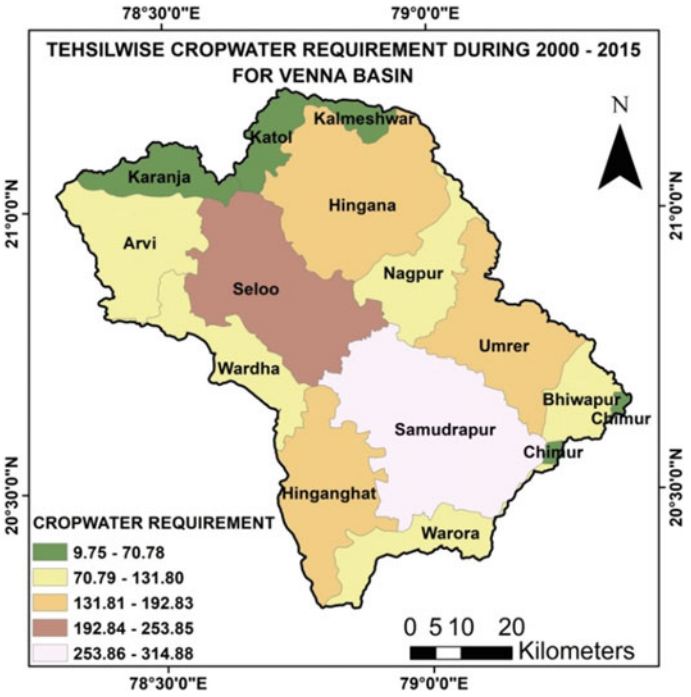

Fig. 2 Tehsil wise average crop water requirement of Venna basin for year 2000–2015

assessing the water to be supplied to crops by irrigation. The water cycle for the crops in a basin can be better managed with the correct assessment of the crop water requirement. Moreover, the cropping pattern can be suitably modified based on the availability of the water resources in the river basin. In Indian weather conditions, rainfall during monsoon is very widely spread over time and space. In such a scenario, accurate estimation of the availability of surface water resources, cropping pattern and the crop water requirement is very essential for better management of the basin and achieving the maximum yield within the available resources.

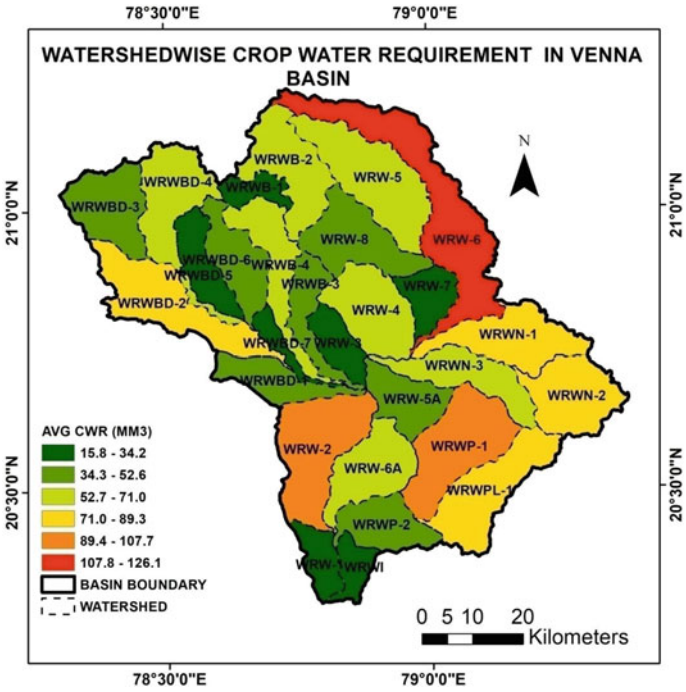

Fig. 3 Watershed wise average crop water requirement of Venna basin for year 2000–2015

References

1. Paranjpe SV, Katpatal YB, Kadu MS (2018) Crop water requirement estimation using remote sensing data and GIS in Venna Basin, Maharashtra, India. In: 2018 AGU fall meeting, 10–14 December 2018, Walter E Washington Convention Center, 801 Mt. Vernon Place, NW, Washington DC, USA
2. Paranjpe SV, Katpatal YB, Kadu MS (2014) Validation of SCS CN method for runoff estimation with field observed regression analysis results in Venna Basin, Central India. 2014, AGU fall meeting, 15–19 December 2014, in San Francisco, California, USA
3. Paranjpe SV, Katpatal YB, Kadu MS (2017) Suitability of spatial interpolation techniques in varying aquifer systems of a Basaltic terrain for monitoring groundwater availability. In: 2017 AGU fall meeting, 11–15 December, 2017, New Orleans, Louisiana, USA
4. Phociades A (2001) Handbook on pressurized irrigation techniques. F.A.O, Rome
5. Doorenboss J, Pruitt WO (1977) Guidelines for predicting crop water requirements. Irrigation and drainage, paper No 24, 2nd edn. Food and Agriculture Organization, Rome, pp 156
6. Jensen ME (ed) (1974) Consumptive use of water and irrigation water requirements. Rep. Tech. Com. OnIrrig. Water requirements, Irrig. and Drain. Div., ASCE, pp 227
7. Perrier A (1982) Land surface processes: vegetation. In: Eagleson PS (ed) Land surface processes in atmospheric general circulation models. Cambridge Univ. Press, Cambridge, Mass, pp 395–448
8. Kulkarni AK, Masuti R, Limaye VS (2015) Comparative study of evaluation of evapotranspiration methods and calculation of crop water requirements at Chaskaman command area in Pune region, India. Int J Res Eng Technol 4(03):323–326

9. Tukimat NNA, Harun S, Shahid S (2012) Comparison of different methods in estimating potential evapotranspiration at Muda Irrigation Scheme of Malaysia. J Agric Rural Dev Tropics Subtropic 113(1):77–85
10. Ali OO (2013) A computer program for calculating crop water requirements, greener. J Agric Sci 3(2):150–163
11. Hafeez M, Khan S (2003) Remote sensing application for estimation of irrigation, water consumption in Liuyuankou irrigation system in China. In: Proceedings of 3rd international workshop, NHRI symposium 17, NASA, Maryland, USA

Development of IBWT-Based Common Drainage Broker Canal Network Towards Integrated Floodplain Management Across East-Flowing Rivers Region of India

B. T. Gurusamy, S. P. Godbole, and A. D. Vasudeo

Abstract The design of a building involves collection, transmission and distribution of loads. Any insufficient distribution of loads may cause for failure of foundation. Because of the deposited soil profile in the delta regions, the natural rivers suffer from insufficient distribution of the collected water in order to drive into the ocean and causing for flood damages across the highly populated natural delta regions. This article focuses on the investigation of potential possibilities and technical feasibilities for the development of inter-basin water transfer (IBWT)-based common drainage broker (CDB) canal network towards integrated floodplain management across east-flowing rivers region of India. The draining capacity of the natural concentrated delta systems of the rivers is decreasing with respect to time because of the deposited soil and corresponding decrease in bed slope. This situation converts the delta regions as flood-prone region. Because all the east coast delta regions are highly populated, an attempt has been made to share the drainage burden of the natural rivers including Krishna, Godavari and Mahanadi using the strategy of artificial delta systems with steep lined bed slope and distributed across the high bed slope regions along entire east coast of India and driven by an interface called CDB canal network having controlled lateral outlets and passing through an alignment along a contour line in between 50 and 90 m elevation approximately. These CDB canals bypass the flood water to protect flood-prone natural delta regions. Typical design of CDB canal network by accommodating various links of the National River Linking Projects of India including Chunar–Sone Link from the north and Pennar–Cauvery Link to the south has been presented. The benefits and limitations of such artificial distributed delta system based on CDB canal network have also been explored.

B. T. Gurusamy (✉) · A. D. Vasudeo
Department of Civil Engineering VNIT, Nagpur, India

S. P. Godbole
Dr. Ambedkar Institute of Management Studies, Nagpur, India

B. Laishram and A. Tawalare (eds.), *Recent Advancements in Civil Engineering*, Lecture Notes in Civil Engineering 172,
https://doi.org/10.1007/978-981-16-4396-5_83

Keywords Integrated floodplain management · Inter-basin water transfer · Common drainage broker · Artificial distributed delta system · East-flowing rivers region of India

1 Introduction

The transmission of flux generated from the source and moving towards the destination through the channel is controlled by the flux handling capacities of these three components of the transmission system such as source, channel and destination. The lowest value of the capacities of these three components decides the system capacity. One of the managerial strategy to minimize the input resources is to balance these three capacities. The presence of any bottleneck along the channel will bring down the carrying capacity of the channel. The flux can be anything that flows [1]. Assuming the flux as the water flowing in the river, in order to accommodate the water flow well within the channel/river width, the carrying capacity of the river needs to be increased or to be adjusted and thereby to create a balance along the length of the river. This can be achieved by increasing the capacity of the channel or by creating an additional bypass for the excess flux flow. When the demand for road reaches closer to the carrying capacity of the road, extreme traffic congestion gets created [2]. Accordingly, when the inflow discharge reaches the capacity of the river, the flood gets created causing for the submergence on the banks of river. The excess traffic can be diverted or bypassed through other route in order to avoid the entry into the traffic congestion region. The existence of flood-prone areas in the delta regions of east flow rivers like Ganga, Mahanadi, Brahmani, Godavari and Krishna has been presented by [3] as shown in Fig. 1.

A set of structural and non-structural measures to reduce the impact of flood has also been presented by Das et al. [3]. According to National Water Policy, both structural and non-structural measures of handling flood have been recommended to reduce the loss due to flood. The structural measure includes the diversion of flood water [4]. In this paper, attempt has been made to investigate the possibility and technical feasibility of diverting the partial flood water through the system of canal networks designed in collaboration with the National River Linking Projects (NRLP) of India designed by NWDA [5] based on the provisions given in the National Perspective Plan framed by Ministry of Water Resources [6]. Such canal networks common for all the east flow river regions can share the drainage burden of the east-flowing rivers in their natural concentrated delta regions in order to bring down the impact of flood mainly in the delta regions.

Fig. 1 Flood-prone zones of India [3]

2 Materials and Methods

Even though the modern trend is to use grid-based analysis of Water balance parameters as explained by many literatures including Bell [7], the recommendation of National Water Policy developed by MoWR [4] is to use basin / sub-basin as a unit towards the planning, development and management of Water Resources. Accordingly, the basin-wise delineation of India by Soil and Land Use Survey of India (SLUSI) in the form of regions, basins, sub-basins, catchments, etc. has been used for this study. The delineation of east flow river regions of India along with various basins accommodated in the east flow river region shown in Fig. 2 has been considered as the study area for the analysis of floodplain management.

From the knowledge of hydraulics, the well-known Manning's formula is being used to determine or to design the carrying capacity of the channel. According to Manning's formula the flow width, flow depth, longitudinal bed slope and the characteristics of river bed materials are the four parameters deciding the channel capacity. The longitudinal bed slope is decided by the natural terrain of the land and we have little control over the bed slope. The Manning's channel discharge equation is given as $Q = (A * (R_h^{2/3} S_f^{1/2})/n)$ is valid for SI units where S_f is the bed

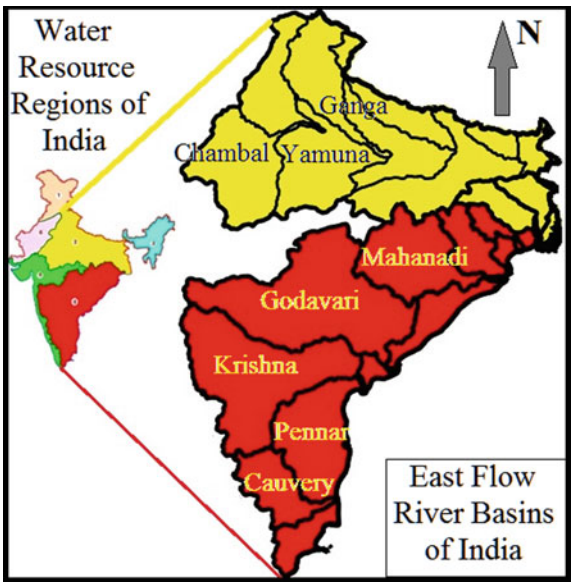

Fig. 2 Delineation of east flow river basins of India [8]

slope, $R_h = (A/P)$ is the hydraulic mean radius in m, A is the flow area in m^2 and P is the wetted perimeter in m [9]. The values of Manning's roughness coefficients (n) for various open channel surfaces as recommended by Chow [10] have been used in the Manning's formula for the determination of discharge carrying capacity of the canals [10]. Based on the provisions in the National Perspective Plan of India framed by August, 1980 [6], NWDA had prepared a set of feasibility studies reports of the Peninsular Components which includes hydrological data about the inter-basin water transfer (IBWT) links [11]. These hydrological data including the alignment of the IBWT canals have been used for this analysis. A broker has been defined to act as an intermediate agency or as an interface between the buyer and the seller in order to enhance the transaction between them. Because this common canal network can act as interface between the east-flowing rivers and the artificially developed distributed delta system to drive the flood water in to the ocean, in order to enhance the drainage capacity of the basins in the east flow rivers region, it has been named as common drainage broker canal network [12].

According to Global Water Partnership Technical Advisory Committee [13], integrated water resources management (IWRM) involves coordinated development and management of water, land and other related resourced in order to maximize the economic and social welfare and thereby to achieve the Sustainable Development Goals (SDGs) [13]. The importance of partnership and social participatory approach for the successful implementation of IWRM strategy has been presented by UNESCO [14]. Based on World Meteorological Organization [15], the integrated floodplain management (IFM) is an integral part of IWRM. IFM involves the integration of water resources management, land use management, hazard management and coastal zone management. A set of strategies such as (1) reducing

flooding, (2) reducing susceptibility to damage, (3) mitigating the impacts of flooding and (4) preserving the natural resources of floodplain have been listed by WMO (2009) along with explanations of various structural and non-structural measures towards integrated implementation of such strategies [15]. Central Water Commission of India has well adopted such strategies in the development of guidelines and reports presenting the implementation of such strategies [16, 17]. One of the structural measures to implement the strategy of reducing flooding is high flow diversion or flood bypass along with dams and reservoirs. The development of IBWT-based CDB canal network involves the implementation of the strategy of reducing flooding in collaboration with other strategies of integrated floodplain management.

3 Results and Discussion

The digital elevation model (DEM) data obtained from Shuttle Radar Topography Mission (SHTM) and provided by the United States Geological Survey (USGS)-based HydroSHEDS Technical Documentation System is graphically presented in Fig. 3 for east flow rivers region of India. The existence of the concentrated delta system for the east flow rivers such as Mahanadi, Godavari, Krishna and Cauvery can be interpreted from Fig. 3. The white colour thin line represents the basin boundary of east flow rivers from Mahanadi to Cauvery.

The longitudinal bed level profiles obtained from DEM of all east flow rivers of India from Ganga to Cauvery for the last 100 m elevation above mean sea level are presented in Fig. 4. The existence of relatively very low bed slope in the delta regions of Ganga and Godavari with respect to that of Pennar and Vamsadhara delta regions can be interpreted from Fig. 4. The bed slope of all east flow rivers in the

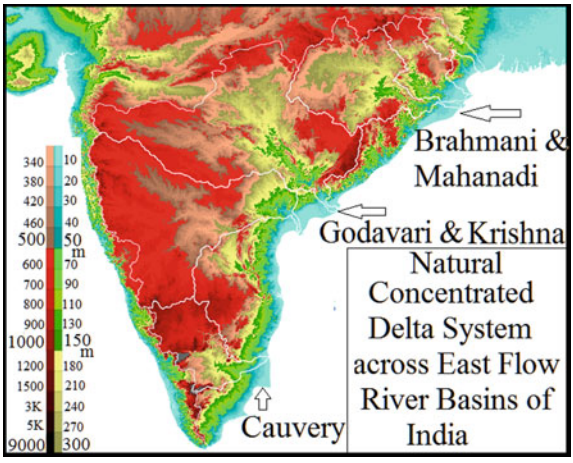

Fig. 3 DEM data showing natural concentrated delta system across east-flowing river basins of India [18]

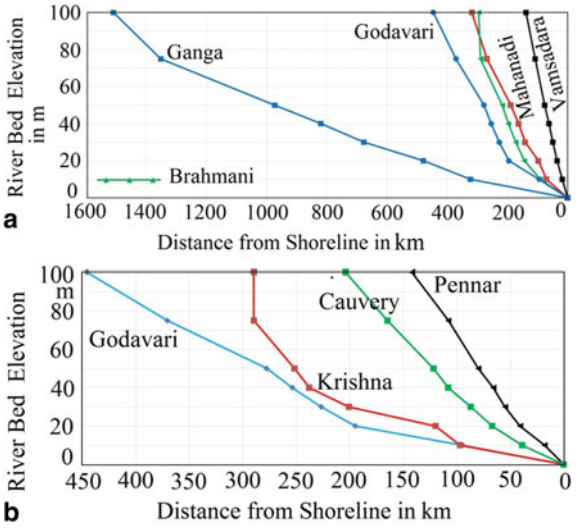

Fig. 4 Comparison of bed level profile across delta region. **a** Ganga to Godavari and **b** Godavari to Cauvery [18]

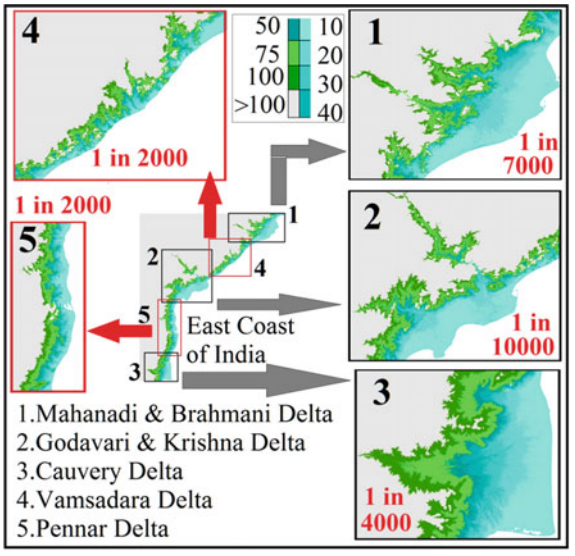

Fig. 5 Comparison of average bed slopes below 10 m elevation across east flown rivers delta regions of India [18]

delta regions of last 10 m elevation above mean sea level is compared as shown in Fig. 5.

The bed slope of Pennar and Vamsadhara delta region of the east coast is relatively higher than that of concentrated delta regions of Godavari, Krishna and Mahanadi. The existence of unfavourable dislocation of high peak flood discharge present over low delta bed slope and vice versa is presented and compared for both the cases of Ganga to Godavari section and Godavari to Cauvery section of east

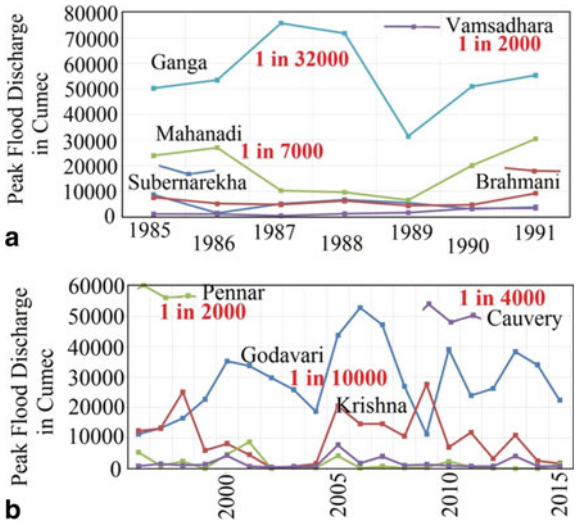

Fig. 6 Unfavourable dislocation of high peak flood discharge present over low delta bed slope and vice versa. **a** Delta North of Godavari and **b** Delta South of Godavari [19, 20]

flow rivers region of India as shown in Fig. 6. The bed slope of Ganga Delta is about 1 in 32,000 and that of Vamsadhara region between deltas of Godavari and Mahanadi is 1 in 2000. According to Manning's formula when bed slope increases from 1 in 32,000 to 1 in 2000, the flow carrying capacity increases by four times. As reported by Chow [10], the Manning's roughness coefficient for the concrete channel surface is $n = 0.012$ and that for natural straight stream channel surface is $n = 0.030$. Accordingly, for the same flow cross section area and bed slope, the canal discharge with concrete channel surface is estimated to be 2.5 times higher than that of natural stream discharge. Hence, it can be interpreted that if the flood water from Ganga is diverted to Vamsadhara delta region using concrete canals, for the same flow cross section, the delta draining capacity or in other words the capacity to drive the flood water into the ocean can be increased by 10 times.

Based on the National Perspective Plan of India, Peninsular Components of various IBWT canals of NRLP of India have been designed by National Water Development Agency and the corresponding feasibility reports have been published. Some of the salient features of such IBWT links present in the Godavari to Cauvery section of east flow rivers regions are presented as shown in Table 1. The location and elevation profiles of IBWT links present from Ganga to Cauvery section of east flow rivers region are shown in Fig. 7. The proposed diversion of water from water surplus region to deficit region as in Table 1 has been supported and justified by CWC and NWDA using the data shown in Figs. 8 and 9.

Based on the observed peak flood discharge at the terminal sites for both the Ganga and Godavari Basins as shown in Fig. 6, the flood discharge is in the magnitude of more than 50,000 Cumec. For the longitudinal bed slope of 1 in 20,000 adopted by NWDA for IBWT-based NRLP canal links designed for the purpose water supply to satisfy the agricultural and domestic water demand, the

Table 1 Salient features of IBWT links designed by NWDA from Godavari to Cauvery section of east flow river regions of India [11]

#	Link	Source reservoir			Destination reservoir			Canal system			Annual Transfer MCM	Remarks
		GSC MCM	LSC MCM	FRL (m)	GSC MCM	LSC MCM	FRL (m)	Length (km)	Slope lowest	Capacity Cumec		
1	Godavari (Icchampally)–Krishna (Nagarjuna Sagar)	10,374	4285	113	11,560	5733	180	300	1 in 20,000	1090	16,426	By lift (107 m)
2	Godavari (Icchampally)–Krishna (Pulichintala)				1296	1026	53.3	312	1 in 20,000	304	4370	Gravity
3	Godavari (Polavaram)–Krishna (Vijayawada)	5511	2130	45.7	85	75	24	174	1 in 20,000	405	5325	Gravity
4	Krishna (Almatti)–Pennar (Kalvapalli)	3440	3105	520	83	73	475	587	1 in 20,000	230	1980	Gravity
5	Krishna (Srisailam)–Pennar (Somasila)	8723	7078	270	2208	1994	101	204	1 in 20,000	163	2310	Natural stream
6	Krishna (Nagarjuna Sagar)–Pennar (Somasila)	11,560	5733	180	2208	1994	101	393	1 in 20,000	488	12,146	Gravity
7	Pennar (Somasila)–Cauvery (Grand Anicut)	2208	1994	101	80	70	59.2	529	1 in 20,000	603	8565	Gravity

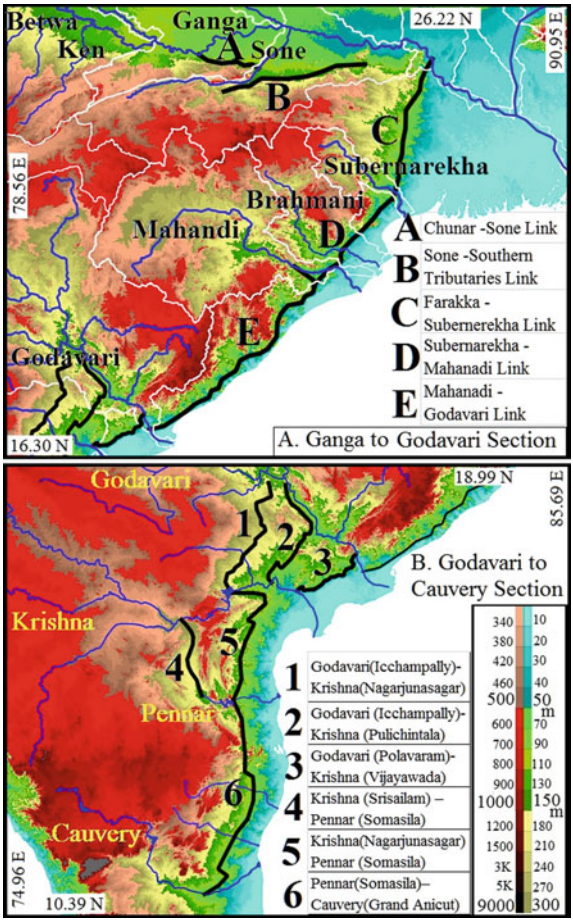

Fig. 7 Location and elevation profiles of NRLP canals across east flow delta regions designed by NWDA: **a** Ganga to Godavari section. **b** Godavari to Cauvery section [11]

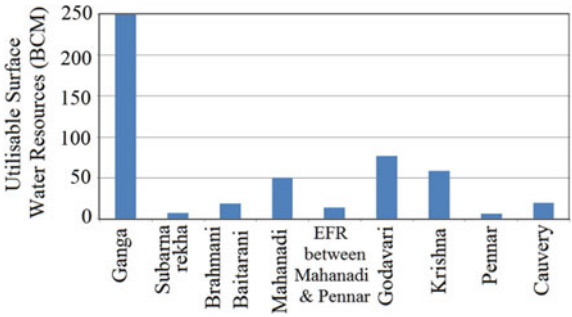

Fig. 8 Utilizable surface water resources across the basins of east flow rivers regions of India [21]

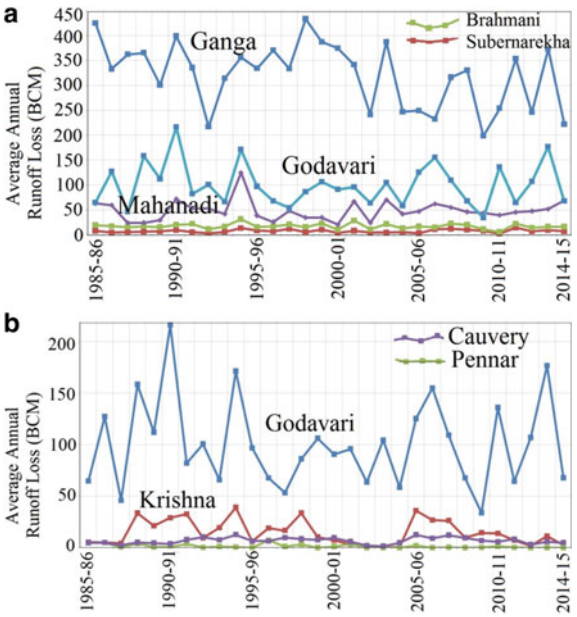

Fig. 9 Observed Average annual runoff loss data motivating the diversion of water from north to south. **a** Ganga to Godavari section and **b** Godavari to Cauvery section [22]

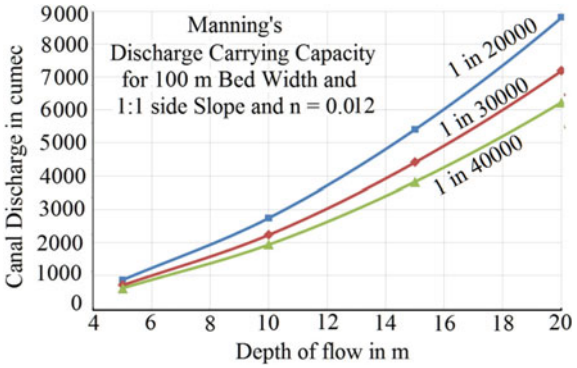

Fig. 10 Manning's flow carrying capacity of canal [9, 10]

design discharge capacities of IBWT links are well below 1000 Cumec using limited width and depth of flow as shown in Table 1. Assuming the possibility of development of a concrete-lined canal with bed width 100 m with longitudinal bed slope 1 in 20,000, the discharge carrying capacity as a function of flow depth based on the Manning's formula is graphically presented in Fig. 10.

When the magnitude of the well-developed high capacity Narmada Canal is less than 1200 Cumec [23], by suitably designing and deciding the values of Bed width and flow depth of canal considering the practical constraints in the implementation process, high flood discharge diversion magnitude can be made to be in between 1000 and 10,000 Cumec. Anyhow IBWT-based NRLP of India includes the

development of live storage capacity (LSC) of more than 4000MCM at Icchampally site and more than 2000 MCM at Polavaram Site. A peak flood can be attenuated by 10,000 Cumec for duration of 1 day using a LSC of about 1000 MCM. Most of the Godavari Peak Flood discharge observed is having duration less than 2 days. Hence, the live storage capacities of IBWT-based Polavaram and Icchampally Projects can be effectively utilized and operated in collaboration with flood forecasting and flood warning systems of CWC, in order to attenuate the peak flood magnitude by more than 20,000 Cumec. The possible enhancement of the discharge carrying capacities of the diversion canals can further increase the flood handling capacities of the system. When the Godavari Flood water diverted to Krishna, to bring down the impact of flood across the concentrated delta regions of Godavari and Krishna Rivers, by proper operation and design of Krishna–Pennar links, the Krishna Flood Water if any can be diverted to Pennar from where the diverted flood discharge can again be diverted towards Cauvery or can be drained to the Bay of Bengal through Pennar River or by a set of lateral outlets developed along the Nagarjuna Sagar–Pennar Links with enhanced carrying capacity of canal designed in such a way that the discharge carrying capacity of canal is balanced with canal inflow and canal outflow capacity. Anyhow such management of flood discharge diversion strategy is likely to demand for the development of standardized procedure and operation manual for the coordinated and synchronized operations of all the reservoirs located in the Godavari, Krishna and Pennar Basins along with the Coordination of all the State Government Officials involved to implement the standardized procedure.

On seeing the A part of Fig. 7, regarding the location and elevation profiles IBWT links designed by NWDA and present in the Ganga to Godavari section of east flow rivers region of India, anybody may get motivated to extend the Link A (Chunar–Sone link) through Link B up to Link C in order to get a common series links connecting A, B, C, D and E so that Ganga Water diverted from Chunar or Sone will get transferred to Godavari through Vamsadhara delta region of high bed slope. Such canal extension may run at a level in between 90 and 40 m and may demand for deep cutting or tunnels at some locations near south east tributaries of Ganga Basin. Any such diversion more than 1000 Cumec from Chunar of Ganga or from Indrapuri Barrage or from Sone Dam across Sone River draining Sone Sub-basin of Ganga Basin can reduce the flood impact across the State Bihar, while the diversion from Sone Dam does not demand for any Lift, Chunar–Sone Link design needs to be enhanced to avoid lift [24].

4 Conclusions

Water has the tendency to flow through a line of steepest flow path and thereby creating a line called as valley line representing the river. When the water is diverted using a canal, the average bed slope of canal is likely to be lesser than that of the valley line. Hence, the residence time of canal flow water is higher than that

of river flow water. It can be proved that when the residence time increases the magnitude of peak flood will get reduced. Hence, any water transfer structure in the name of inter-micro-watershed water transfer or inter-catchment water transfer or inter-sub-basin water transfer or inter-basin water transfer, it will bring down the peak flood level as well as it will increase the utility and usability of river water. Because all water transfer structures are getting developed in collaboration with water storage structures, the further increase in residence time has the potential to reduce the peak flood level. In a generalized way, any catchment or sub-basin can be developed to have three tier system of drainage where the lower tier represents the natural river. The upper tier of the drainage system to be developed represents the high level contour canal in the upper stages of the river followed by the ridge canal developed in the lower stages of the river. The middle tier of canal-based drainage system represents the low level contour canal running along a level in between the upper tier and the valley line. Such an enhanced IBWT canal-based 3-tier drainage system as a preventive measure of floodplain management strategy developed from micro-watershed level to basin level in collaboration with a set distributed artificial recharge structures has a potential to increase the residence time of runoff water and thereby to reduce the peak flood discharge level.

A structural measures designed and developed to reduce the impact of 100-year flood may not be enough to withstand the impact of 1000-year flood. A 1000-year flood does not have a meaning that it will occur only one time for every 1000 years. Even for a 1000 year flood, there is a probability of occurrence in the next 10 or 20 years. Hence, the non-structural measures such as control of floodplain development using proper regulations and policies along with the development of risk sharing strategy using flood insurance program can bring down the vulnerability and magnitude of flood damage. Hence, in all dynamic scenario of floodplain management programme, the coordinated development of structural and non-structural measures need to be encouraged.

The IBWT canals network designed and developed at basin level for the east flow river regions with the extended purpose of high flood diversion along with original purpose of diversion of water from surplus region to deficit region can be managed by a separate Private or Government Agency called as common drainage broker (CDB) in order to develop and manage the project economically beneficial. The developed canals can be made to be operated in different modes such as (1) high flood diversion mode, (2) water supply and irrigation canal mode, (3) storage reservoir mode, (4) inland waterways mode in collaboration with ongoing Buckingham canal-based Inland National Waterway No 4 [25] and (5) enhanced AR facilities mode so that the agency/broker can maximize the profit.

Acknowledgements The research facilities that have been provided by the administration of VNIT, Nagpur, the water resources data that have been published by USGS, UN and Government of India through its organizations such as CWC, CGWB, NWDA, IMD, NRSC and WRIS along with the financial supports provided by MHRD and Various Services such as Web, Google Earth, Wikipedia & Search Engines available through internet communications, are acknowledged.

References

1. Weekley E (1967). An etymological dictionary of modern English. Courier Dover Publications, p 581. ISBN 0-486-21873-2
2. Treiber et.al (2012) Traffic flow dynamics: data, models and simulation. Springer Science & Business Media. ISBN 978-3-642-32459-8
3. Das SK, Gupta K, Varma HK (2007) Flood and drought management through water resources development in India. WMO Bull 56(3):179–188. https://public.wmo.int/en/bulletin/flood-and-drought-management-through-water-resources-development-india
4. MoWR (2012) National water policy, ministry of water resources. Government of India
5. NWDA (2018) Annual report 2017–18. National Water Development Agency, Ministry of Water Resources, River Development and Ganga Rejuvenation, Government of India, New Delhi. http://nwda.gov.in/content/innerpage/Annual-Report.php
6. MoWR (1980) National perspective for water resources development. Ministry of Water Resources, Government of India
7. Bell VA, Moore RJ (1998) A grid-based distributed flood forecasting model for use with weather radar data: part 1. Formulation. Hydrol Earth Syst Sci Discuss Eur Geosci Union 2(2/3):265–281
8. SLUSI (1990) Digital watershed Atlas of India, Soil and Land Use Survey of India, Government of India. http://slusi.dacnet.nic.in/dwainew.html
9. Manning R (1891) On the flow of water in open channels and pipes. Trans Inst Civil Eng Ireland 20:161–207
10. Chow VT (1959) Open-channel hydraulics. McGraw-Hill, New York
11. NWDA (2010) Feasibility Studies Reports for the Peninsular Components of NRLP of India. National Water Development Agency, Ministry of Water Resources, Government of India. http://nwda.gov.in/content/innerpage/feasibility-studies.php
12. Spiro RL et al (2003) Management of a sales force. McGraw-Hill/Irwin
13. GWPTAC (2000) Integrated water resources management. Global Water Partnership Technical Advisory Committee, Technical Background Paper No. 4, Stockholm, GWP. https://www.gwp.org/globalassets/global/toolbox/publications/background-papers/04-integrated-water-resources-management-2000-english.pdf
14. UNESCO (2003) Integrated water resources management on a basin level: a training manual: a training material. http://unesdoc.unesco.org/images/0013/001319/131933e.pdf
15. WMO (2009) Integrated flood management. Associated Programme on Flood Management (APFM) and World Meteorological Organization, WMO-No. 1047 ISBN 978-92-63-11047-3. https://library.wmo.int/?lvl=notice_display&id=108#.XzQhLfMzbZ4
16. CWC (2018) Comprehensive flood management in India. Central Water Commission. http://www.cwc.gov.in/sites/default/files/comprehensive-flood-management-india-2018.pdf
17. CWC (2012) Hand book for flood protection/anti erosion & river training works. Central Water Commission, Ministry of Water Resources, Government of India, New Delhi. http://www.cwc.gov.in/sites/default/files/Handbook-05-Jun-12_0.pdf
18. Lehner B, Verdin K, Jarvis A (2006) HydroSHEDS technical documentation. World Wildlife Fund US, Washington, DC. http://hydrosheds.cr.usgs.gov
19. CWC (2018) Discharge year book 2017–2018. Godavari Basin, Krishna Basin, Mahanadi Basin, Central Water Commission, India
20. GRDC (2020) The Global Runoff Data Centre, 56068 Koblenz, Germany. https://portal.grdc.bafg.de/
21. CWC (2013) Water and related statistics-2013. Central Water Commission, Ministry of Water Resources, India. http://www.cwc.gov.in/sites/default/files/water-and-related-statistics-2013.pdf
22. CWC (2019) Reassessment of water availability in india using space inputs. Volume I and II, Basin Planning & Management Organization, Central Water Commission, India

23. Yadav SM, Chauhan KA (2011) Case study of Narmada main canal based drinking water supply project: issues and challenges. WIT Trans Ecol Environ 167. ISSN 1743–3541 (on-line) https://doi.org/10.2495/ST110331
24. NRSC & CWC (2014) Ganga basin report version 2.0. National Remote Sensing Centre & Central Water Commission, Government of India, Ministry of Water Resources, India
25. IWAT (2010) DPR for development of navigation in Kakinada -Pondicherry Canal Along with River Godavari & Krishna (National Waterway-4). Inland Waterways Authority of India

Integrated Use of Remote Sensing and GIS Techniques for the Assessment of Groundwater Potential Zone Using Multi-influencing Factors in Kulhan Watershed, Chhattisgarh, India

Tanushri Jaiswal, Suvendu K. Sahu, N. P. Praveen, T. Ramkumar, Kamalesh Chandra Mondal, and D. C. Jhariya

Abstract Groundwater is one of the major naturally occurring resources that is considered the most crucial water supply source for various purposes throughout the world. Here, the study is being conducted in the Kulhan watershed, a sub-watershed of Kharun River. It has a total geographical area of about 949.69 km^2, which lies entirely in the District of Raipur, Chhattisgarh. The area's groundwater potential is delineated using RS and GIS techniques, which has been of great use to get the desired output. As per the result obtained from the present work, the whole study area has been categorized into five groundwater potential zones, such as low (16.29%), medium (41.35%), and medium to high (11.59%), high (28.16%) and very high (2.61%). The generated groundwater potential zone map was validated with the existing borehole yield data. It is found that about 77% of the output matches the actual wells yield data, which shows the adopted method's capability. This study can be utilized for the proper development and management of available groundwater resources.

Keywords Groundwater · Groundwater potential zone · Remote sensing · GIS

1 Introduction

With the rise in the population globally, water and food availability have always been groundwater resource that is considered to be among the essential resources present on the Earth. Overall, about 80% of the drinking water is fulfilled by the

T. Jaiswal (✉) · S. K. Sahu · K. C. Mondal · D. C. Jhariya (✉)
Department of Applied Geology, National Institute of Technology, Raipur, India
e-mail: dcjhariya.geo@nitrr.ac.in

N. P. Praveen · T. Ramkumar
Department of Earth Sciences, Annamalai University, Chidambaram, India

B. Laishram and A. Tawalare (eds.), *Recent Advancements in Civil Engineering*, Lecture Notes in Civil Engineering 172,
https://doi.org/10.1007/978-981-16-4396-5_84

groundwater resources natural [1]; hence, it is a leading source of drinking, agricultural, and other industrial and residential uses.

Groundwater is the primary source for various purposes like drinking, irrigation, and industrial use throughout the world; therefore, groundwater study is gaining much more importance. Many researchers are working on different groundwater perspectives as per requirement. Some of them are working on groundwater's physical and chemical properties to study the water quality, while some are working on the water-level fluctuation by calculating the groundwater level's difference in temporal data. Many of them are working on groundwater potential zoning using remote sensing and GIS techniques.

Groundwater potential zone mapping has become more comfortable with the inputs from remote sensing (RS) and geographical information system (GIS) techniques [1]. Here, the present work is done to find out the groundwater potential zones by introducing the RS and GIS techniques in it. The occurrence of groundwater in any geological formation and its use is dependent primarily on its porosity. The area with a higher steep slope will have a high run-off rate, whereas the area with depressed topography will have increased infiltration [2]. Groundwater potential zone map for the Kulhan watershed was prepared after preparation of thematic layers and weighted sum calculation [3–5].

2 Study Area

Kulhan watershed, the part of Kharun Basin, is selected as the study area for the present study with its extent lying between 21° 04′ 12″ to 21° 34′ 48″ N latitude and 81° 27′ 00″ to 82° 09′ 36″ E longitude, which covers mainly the central part of Raipur District with total geographic area of 949.69 km^2 covers Survey of India (SOI) Toposheet No. 64G/10, 64G/11, 64G/12, 64G/14, 64G/15 and 64G/16. The study area covers four blocks from the entire district: Abhanpur, Arang, Raipur and Tilda. The location map for the study area is shown in Fig. 1. Based on LULC classification, the whole watershed was mainly classified into 6 types out of which cultivation constitutes maximum coverage of 68.29%, open land covers 18.64% of the total area, settlement and road networks, 9.33% is the total area covered by water bodies which cover about 2.81% of the area, while vegetation is about 0.93%. As per the CGWB report map, the watershed soil type comprises three kinds: Ultisole Laterite and, Vertisol Medium Black, and Vertisol Deep Black. The area receives an annual rainfall of about 1245 mm and has majorly flat and gently undulating features with the maximum slope lying in between 3 and 5%, while the highest slope is approximately 13.56%.

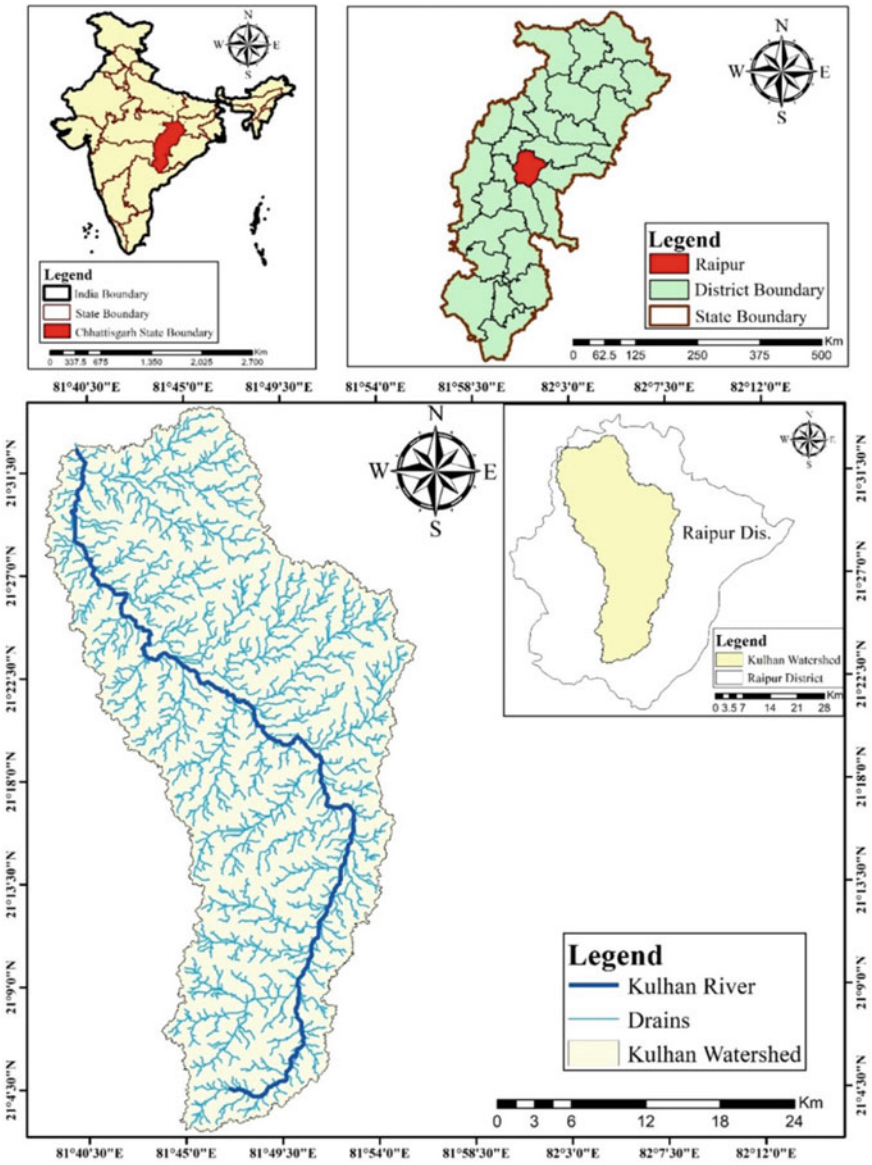

Fig. 1 Location of study area

3 Material and Method

SRTM (DEM) data were downloaded from the NRSC site, an open-source data for developing the Slope and Drainage Density maps, and Sentinel 2B with a resolution of 15 m is used for the classification of LULC. Also, the other data like geology and geomorphology as well as the Soil data, CGWB reports, and even data provided by the GSI and CGWB, have been used. Lineaments were created using the WMS layer from Bhuvan, and for rainfall, IMD data have been used, while groundwater-level data were downloaded from IWRIS. A list of all data used is given in Table1.

All the thematic layers were prepared, and further analysis and processing of the data was done by using the basic GIS and Image processing software (ArcGIS and ERDAS Imagine). The workflow for the present study is shown in Fig. 2.

4 Objectives

The aim of conducting the present study was to find the groundwater potential zone of the Kulhan watershed using remote sensing and GIS techniques. The main objectives covered in this study are:

(a) Preparation of all the thematic layers for Kulhan watershed.
(b) Reclassification of all the prepared layer based on their influence on groundwater potential.

Table 1 Data used

S. no.	Data used	Data description	Source
1	Sentinel 2A	Tile No: L1C_T44QNJ_A014273_20180317T050912	https://earthexplorer.usgs.gov/
2	SRTM 1 arc-second Global	Tile No: n20_e081_1arc_v3	https://earthexplorer.usgs.gov/
3	Geology	District resource map—Raipur District	Geological survey of India
4	Geomorphology	District resource map—Raipur District	Geological survey of India
5	Groundwater level	Block-wise data for year 2017 and 2018	India-WRIS and CGWB
6	Lineament	WMS layer	http://bhuvan-noeda.nrsc.gov.in/gis/thematic/index.php
7	Rainfall	Average annual rainfall	India meteorological Department
8	Soil	Distribution of soil in the Chhattisgarh	Ground water year book of Chhattisgarh 2016–17

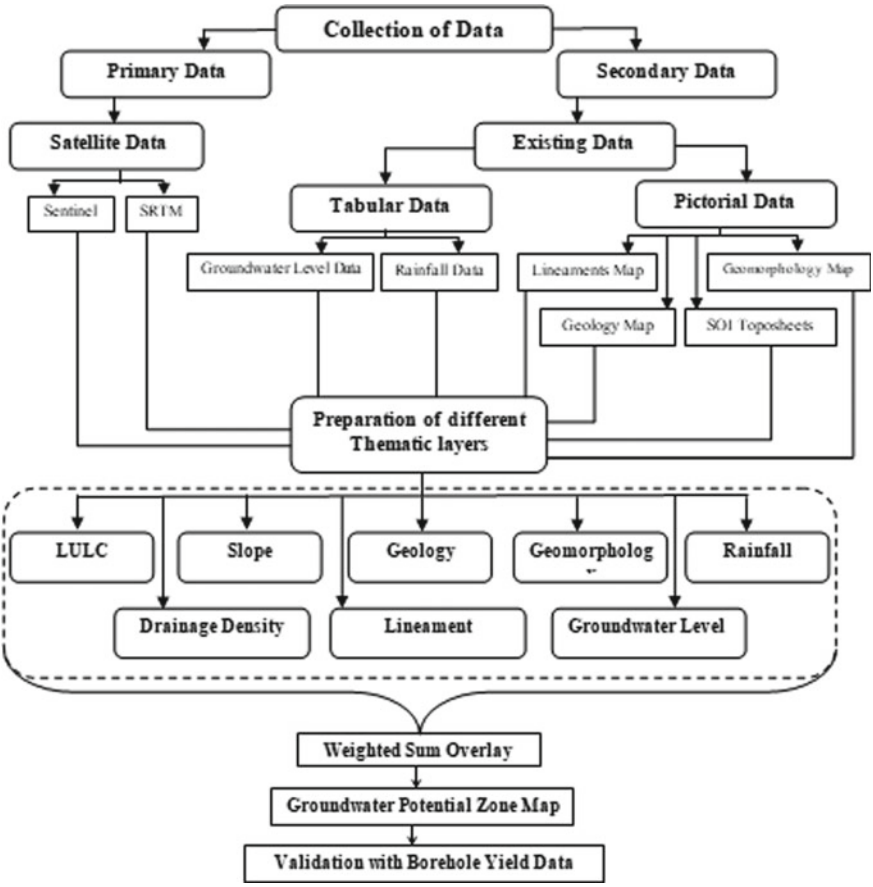

Fig. 2 Workflow for the present study

(c) Identification of the groundwater potential zone by integrating all the reclassified thematic layers in the GIS environment.
(d) Validation of the data using borehole yield data of the area.

5 Methodology

The systematic methodology was adopted in this study, and the workflow is shown in Fig. 2.

5.1 Drainage Density

Drainage density can be defined as the total length of all the rivers and the streams that are coming under a drainage basin divided by the total area of the drainage basin. Drainage density is one of the essential factors playing a significant role in identifying groundwater potential zone. For the present study, the stream data have been created using SRTM-DEM, which have been downloaded from (https://earthexplorer.usgs.gov/) after which the watershed and drainage have been delineated using the IDW tool of spatial analyst tool in ARC MAP [6] and the drainage density has been calculated using line density tool in ArcGIS. The drainage density is then defined into five classes: very low, low, medium, high, and very high (see Fig. 3), which is then reclassified by assigning more weights to lower drainage density and less to the region with higher drainage density [7].

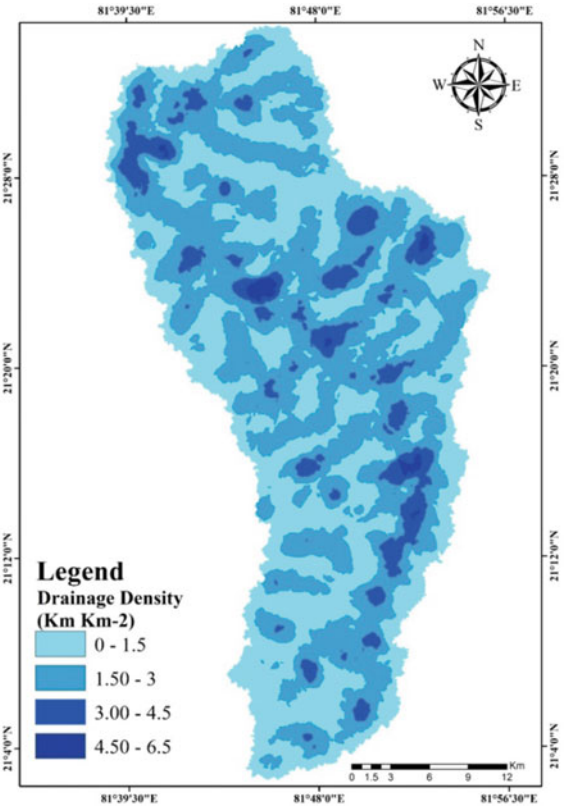

Fig. 3 Drainage density for Kulhan watershed

5.2 Geology

The geology of any region plays an essential role in the occurrence of groundwater and its distribution [7]. Here, in the present study the geology is classified into 3 types (Fig. 4) as per the data provided by the Geological Survey of India, where about 641.67 km^2 is covered with Stromatolitic limestone and Dolomite with argillaceous rock, 304.79 km^2 is Stromatolitic limestone and Dolomite with arenaceous rock, while only 3.07 km^2 is Shale with intercalations of limestone and intraformational Conglomerate described in Table 2. The weights have been assigned to the classified geology type as per their influence on the groundwater.

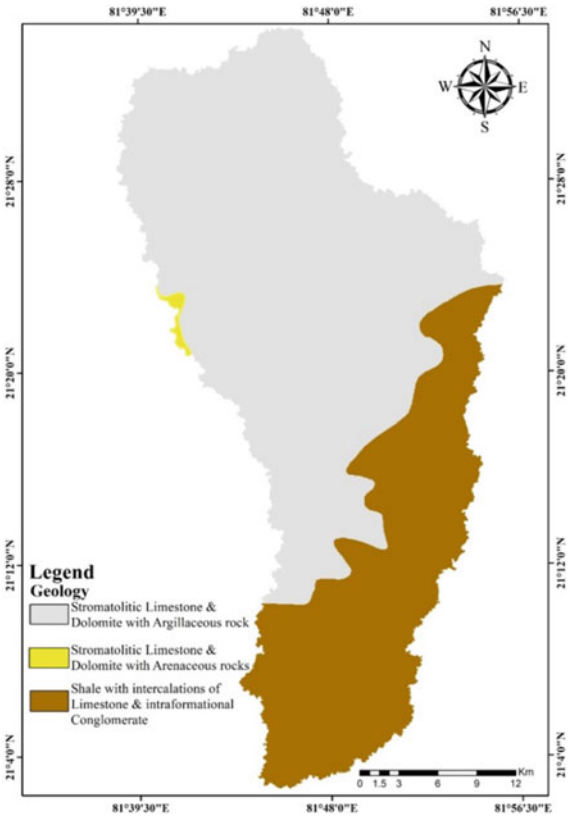

Fig. 4 Geology of the Kulhan watershed

Table 2 Area covered by different geology type in Kulhan watershed

S. no.	Geology type	Area covered (km^2)	% coverage
1	Stromatolitic limestone and Dolomite with argillaceous rock	641.67	67.57
2	Stromatolitic limestone and Dolomite with arenaceous rock	3.07	0.32
3	Shale with intercalations of limestone and intraformational Conglomerate	304.79	32.09

5.3 Geomorphology

Geomorphology can be defined as the study of the Earth's structure, which includes various landforms. The geomorphology of any area depends upon its formation. Therefore, it has a significant influence on groundwater potential. The Kulhan watershed has only one type of geomorphology, which is structural plain on the Proterozoic rock. As per its characteristics, it is reclassified by assigning four as its weightage value based on its influence on groundwater potential (Fig. 5).

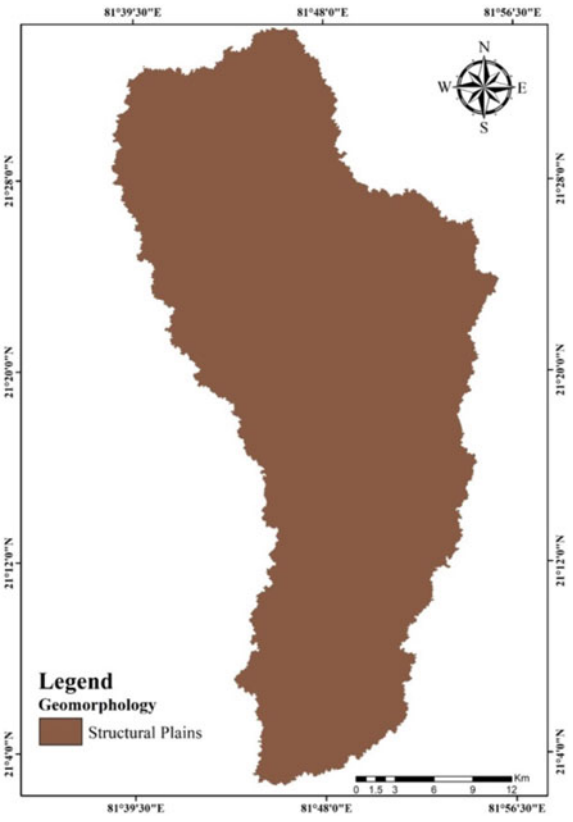

Fig. 5 Geomorphology of the Kulhan watershed

5.4 Groundwater Depth

Groundwater level for the study area has been downloaded from India-WRIS and CGWB-Raipur (http://india-wris.nrsc.gov.in/) for different locations throughout the study area, and from these collected data groundwater depth map was prepared using a method of interpolation in spatial analyst tool in ArcMap. Groundwater depth for the study area ranged between 1.5 and 13.5 mbgl. The areas with water level below 6.5 were categorized under the areas with a moderate and deep water level. In contrast, areas with water level above 6.5 were categorized under shallow and very shallow shown in Fig. 6.

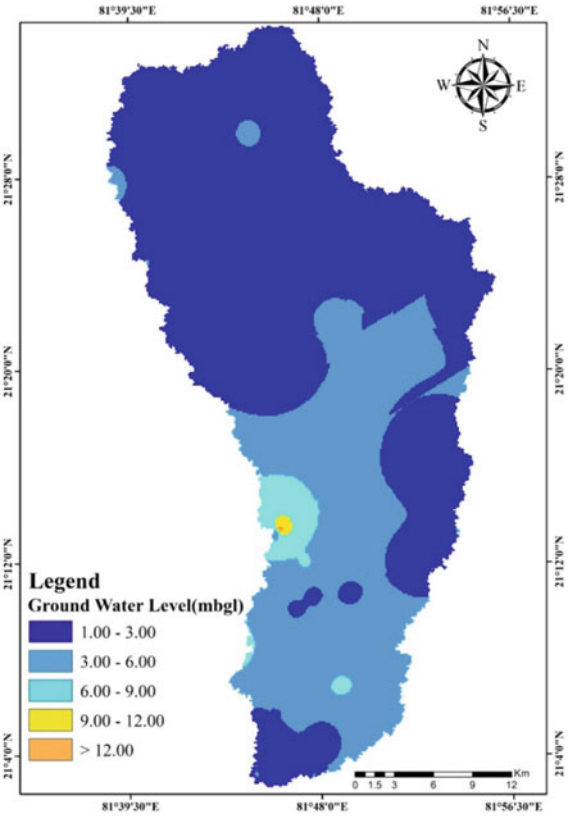

Fig. 6 Groundwater level of the Kulhan watershed

5.5 *Land Use and Land Cover (LULC)*

Land use/land cover study is among the essential factors which give an extent of groundwater requirements and its utilization. It is also a vital indicator for selecting sites for the process of artificial groundwater recharge [8, 9]. Sentinel 2A (10 m) data are used in this study for the LULC classification. To attain much of accuracy, the classification is done using the visual interpretation method and the basis of this, the LULC is majorly classified into six classes which are: cultivation, open land, waterbodies, vegetation, settlement and road network, and based on this map, is created shown in Fig. 7. The LULC is reclassified based on their water-holding and run-off capacity by assigning them the values between 1 and 5 (Table 3).

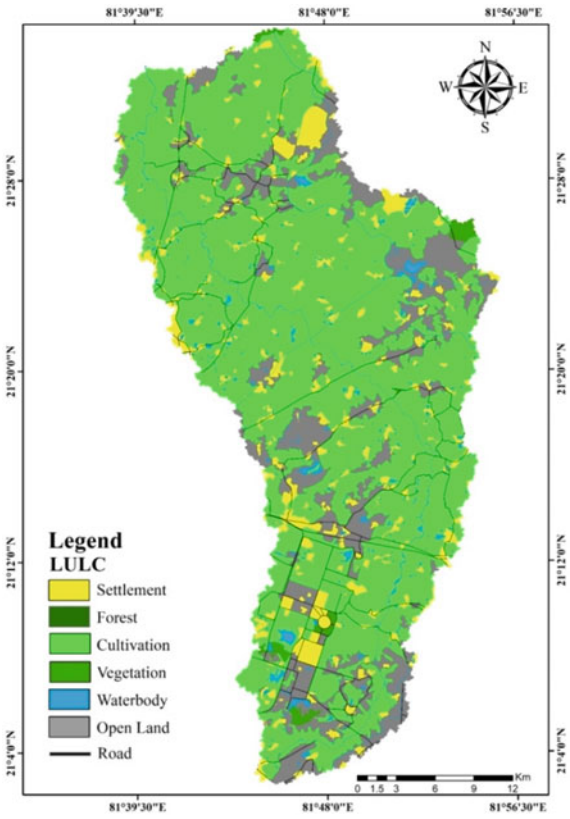

Fig. 7 Land use/land cover classification of the Kulhan watershed

Table 3 Area covered by different fields in LULC classification

S. no.	Feature name	Area covered (km^2)	% coverage
1	Waterbody	26.65	2.81
2	Cultivation	648.56	68.29
3	Vegetation	8.84	0.93
4	Open land	177.03	18.64
5	Settlement and road network	88.60	9.33
	Total basin area	949.69	100.00

5.6 Lineament

Lineament is the linear feature of a landscape with its expression on the geological structure under which it lies; the example of such elements is a fault. Lineaments are typically represented as the discontinuity of the Earth's surface. Many different geological features are responsible for the formation of lineaments; these are faults and fractures, etc. Based on the WMS layer taken from the Bhuvan portal, a lineament map was made for the area shown in Fig. 8.

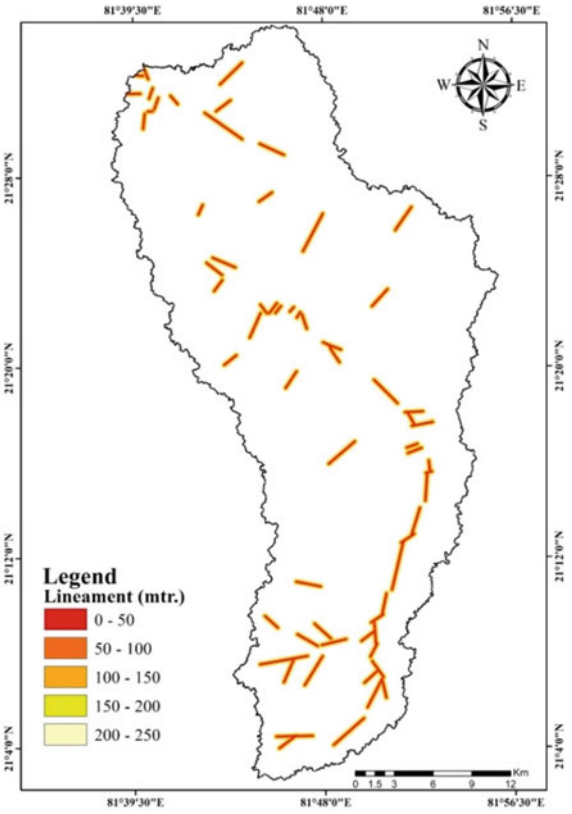

Fig. 8 Lineament of the Kulhan watershed

5.7 Rainfall

The primary source of groundwater replenishment is rainfall, but it is not the same for different places. It varies depending upon the difference in environmental conditions; moreover, this rainfall varies with a particular area's environmental conditions, but it also differs temporally. Groundwater has its dependency on rains as the possibility of occurrence is higher in the regions with a high amount of rainfall. In contrast, areas with lower rainfall may have the chance of low groundwater availability.

For the present work, the mean annual rainfall value of rain gauge stations of stations in Raipur district is then interpolated using the IDW method to find the amount of rainfall distribution in the study area. After interpolating, the spatial distribution for the rainfall map has been prepared by classifying the area into five zones based on the interval of 1 mm, after that reclassification is done, assigning suitable weightage for each class (Fig. 9).

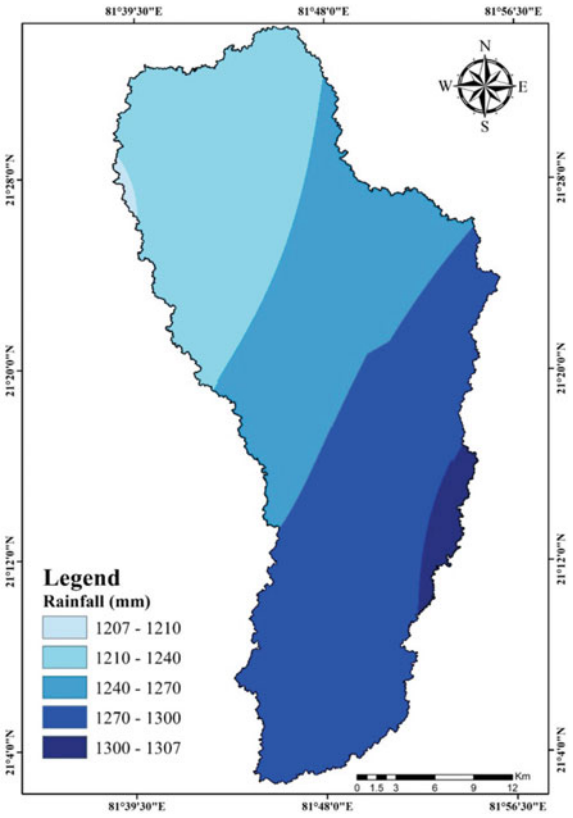

Fig. 9 Rainfall distribution of the Kulhan watershed

5.8 Slope

Slope determines the hydrological characteristics of a catchment. If the lower slope angle is there, there will be lower hydraulic gradients, resulting in a high infiltration rate and low run-off. In contrast, places with higher slope angles will have low infiltration rates due to the increased surface run-off speed. This water-holding capacity depends on the slope, resulting in an increased or decreased groundwater recharge rate. For the present study, the slope has been calculated in percent rise using SRTM-DEM (1 Arc Second) data from which slope has been classified into five classes, which is shown in Fig. 10 and then as per the percent of inclination slope weightage has been assigned to them, i.e., high weightage is given to the area with a lower slope. In comparison, the higher slope is entrusted with the low weightage value.

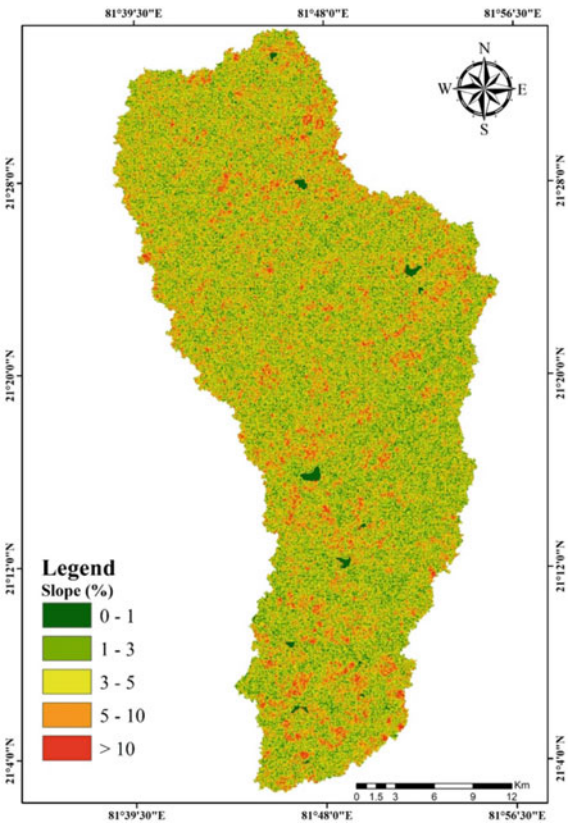

Fig. 10 Slope map of the Kulhan watershed in 2017

5.9 Soil

Soil is one of the most important factors on which the amount of groundwater depends, as different soil group have some specific properties which differ from the other and rate of percolation depends on these properties; hence, by studying these factors we can find out the water holding and infiltration rate of the particular soil. As the groundwater movement and the infiltration depend on the soil's porosity and permeability, to determine the amount of groundwater at any place, it is essential to study soil characteristics for that place.

The base data for the soil classification of the present study have been obtained from CGWB Report. As per the soil classification, the study area has been classified into three types: Ultisole Laterite, Vertisol Deep Black and Vertisol Medium Black (see Fig. 11). As the infiltration rate differs in some aspects for all the three soil types, hence weightage has been assigned to each class (Table 4).

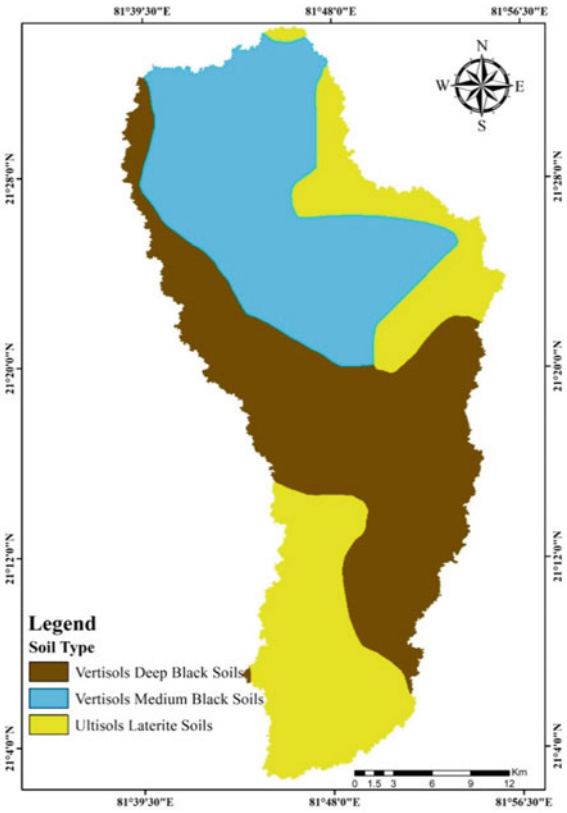

Fig. 11 Soil type of the Kulhan watershed

Table 4 Area covered by different soil type in Kulhan watershed

S. no.	Soil type	Area covered (km^2)	% coverage
1	Vertisols medium black soils	313.87	33.05
2	Vertisols deep black soils	360.52	37.96
3	Ultisole laterite soils	275.14	28.97

5.10 Weighted Overlay

The weighted sum is used by several other researchers notably (is calculated for different thematic layers that provide an ability to weight multi-layers as the input by assigning them weights to get an integrated analysis based on the inputs) [7, 10–14]. Here, the weighted sum method was applied to all the thematic layers for the present study after assigning separate weightage separately to each feature type within a particular thematic layer (Table 5).

5.11 Classification of Groundwater Potential Zones

Groundwater potential zone map was made after applying the weights of different thematic layers based on their role in groundwater potential zone mapping. The potential groundwater map was classified into five classes which are: very high, high, medium, low, and very low. Based on the assessment of the groundwater potential map was generated (Fig. 12). It may be observed that the distribution is more or less a reflection of the rainfall, drainage density, lineament, slope and soil patterns, and the geomorphic and geological features.

5.12 Validation with Borehole Yield Data

Discharge data from the bore wells from 9 different locations throughout the watershed, which is shown in, were taken to validate the groundwater potential zones, Fig. 13, which were analyzed using remote sensing and GIS techniques (given in Table 6). The borehole yield data used for the validation obtained from the CGWB report were classified into three categories. The area with the yield value <3 lps has a low yield, the area between 3 and 6 lps has a medium, while areas with borehole yield value >6 will have a high yield.

As per the validated output, approximately 77% is attained in analyzing the groundwater potential zone; as out of 9 bore well data, 7 were found to be matching with the predicted result which means the derived output is (7/9) * 100 = 77.7% accurate, which suggest that the methodology adapted for the groundwater potential zones was correct and accurate and, hence, can be used for future studies.

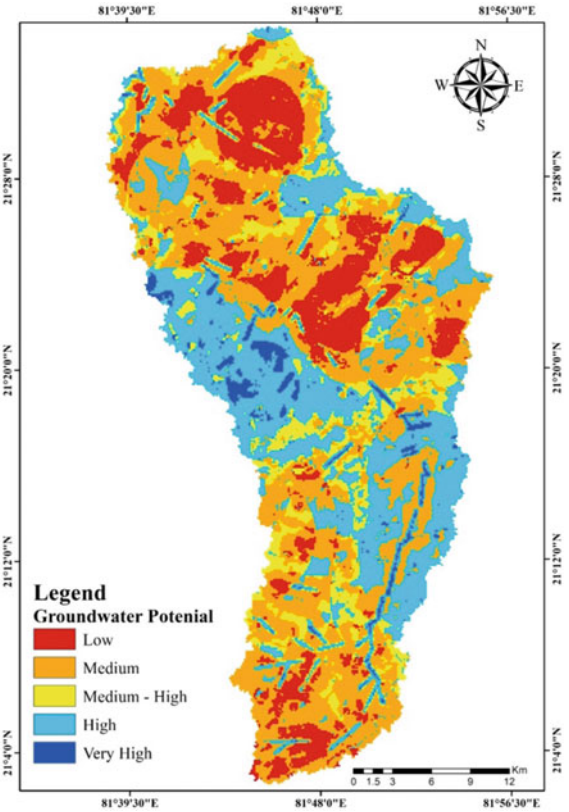

Fig. 12 Groundwater potential of the Kulhan watershed

6 Results and Discussion

The use of GIS and remote sensing in integration has proven to be an advantageous method that saves time and effort and gives an effective and efficient output for the determination of groundwater potential zone. This study was performed under the GIS platform by preparing 9 different thematic layers: LULC, geology, geomorphology, lineament, drainage density, soil, rainfall and groundwater-level data using the primary or secondary data from different data sources. Based on these thematic layers, groundwater potential zones for the Kulhan Watershed were delineated.

As per the result obtained from the present work, the study area has been categorized into five groundwater potential zones, such as low (16.29%), medium (41.35%), and medium to high (11.59%), high (28.16%), and very high (2.61%). The groundwater potential zone map generated using the above methodology was validated with the borehole yield data. It is found that 77% of the output matches the actual wells yield data, which shows the adopted method's capability.

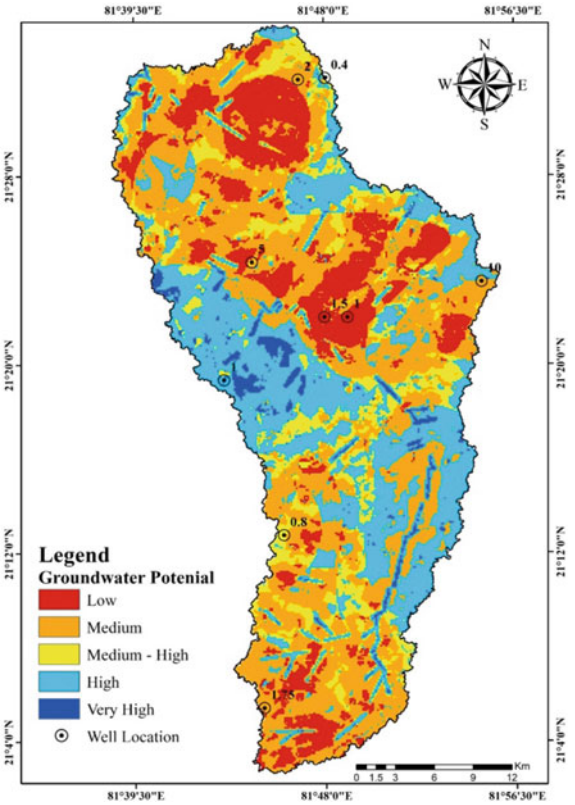

Fig. 13 Groundwater potential zone validation with borehole yield data of the Kulhan watershed

Table 5 Different classes and their relative weightage

Sl no.	Category	Weights assigned	Classification	Rank
1	Geology	9	Stromatolitic limestone and Dolomite with arenaceous rock	4
			Stromatolitic limestone and Dolomite with argillaceous rock	3
			Shale with intercalations of limestone and intraformational Conglomerate	2
2	Land use land cover	7	Cultivation	3
			Open land	2
			Road network	1
			Settlement	1

(continued)

Table 5 (continued)

Sl no.	Category	Weights assigned	Classification	Rank
			Vegetation	4
			Waterbody	5
3	Drainage density	4	Very low	6
			Low	5
			Medium	4
			High	3
			Very high	1
4	Lineament	6	0–50	5
			50–100	4
			100–150	3
			150–200	2
			200–250	1
5	Geomorphology	8	Structural plain on Proterozoic Rock	4
6	Rainfall (mm)	9	<1210	4
			1220–1240	4
			1240–1270	5
			1270–1300	5
			>1300	5
7	Slope (%)	3	0–1	5
			1–3	4
			3–5	3
			5–10	2
			>10	1
8	Groundwater depth	5	1–3	5
			3–6	4
			6–9	3
			9–12	2
			>12	1
9	Soil types	8	Ultisole laterite	3
			Vertisol medium black	2
			Vertisol deep black	1

Table 6 Validation of groundwater potential zones with borehole yield data

S. no.	Borehole yield data	Description of Borehole data	Expected yield description	Validation results
1	2.00	Low	Low	Agree
2	0.40	Low	Low	Agree
3	5.00	Medium	Medium	Agree
4	1.00	Low	High	Disagree
5	1.50	Low	Low	Agree
6	1.00	Low	Low	Agree
7	10.0	High	Low	Disagree
8	0.80	Low	Low	Agree
9	1.75	Low	Low	Agree

7 Conclusion

The present study reflected that remote sensing and GIS techniques are a powerful tool for assessing groundwater potential zones and that reliable outputs can be achieved by using it. Therefore it can be well used in the area with the low potential zone to introduce artificial groundwater recharge practice. In this way, the present study can be beneficial for the sustained management of groundwater resources. The result also illustrates that the approach outlined has merits and can be successfully used elsewhere with appropriate modifications.

References

1. Chaudhary BS, Kumar S (2018) Identification of groundwater potential zones using remote sensing and GIS of K-J watershed, India. J Geol Soc India 91:717–721
2. Bagyaraj M, Ramkumar T, Venkatramanan S, Gurugnanam P (2013) Application of remote sensing and gis analysis for identifying groundwater potential zone in parts of Kodaikanal Taluk, South India. Frontiers Earth Sci 7(1): 65–75
3. Ganapuram S, Kumar GTV, Krishna IVM, Kahya E, Demirel MC (2009) Mapping of groundwater potential zones in the Musi basin using remote sensing data and GIS. Adv Eng Softw 40:506–518
4. Hutti B, Nijagunappa R (2011) Identification of groundwater potential zone using geoinformatics in Ghataprabha basin, North Karnataka, India. Int J Geomatics Geosci 2(1)
5. Suganthi1 S, Elango L, Subramanian SK (2013) Groundwater potential zonation by Remote Sensing and GIS techniques and its relation to the Groundwater level in the Coastal part of the Arani and Koratalai River Basin, Southern India. Earth Sci Res SJ 17(2):87–95
6. Al-Manmi DAM, Rauf LF (2016) Groundwater potential mapping using remote sensing and GIS-based, in Halabja City, Kurdistan, Iraq. Arab J Geosci 9:357
7. Jhariya DC, Kumar T, Gobinath M, Diwan P, Kishore N (2016) Assessment of groundwater potential zone using remote sensing, GIS and Multi Criteria Decision Analysis Techniques. J Geol Soc India 88:481–492

8. Kumar GRS, Shankar K (2014) Assessment of groundwater potential zones using GIS. Frontiers Geosci (FG)
9. Zeinolabedinia M, Esmaeilyb A (2015) Groundwater potential assessment using geographic information systems and AHP method (Case Study: Baft City, Kerman, Iran). In: International conference on sensors & models in remote sensing & photogrammetry, vol XL-1/W5
10. Ramu MB, Vinay M (2014) Identification of groundwater potential zones using GIS and remote sensing techniques: a case study of Mysore taluk—Karnataka. Int J Geomatics Geosci 5(3)
11. Waikar ML, Nilawar AP (2014) Identification of groundwater potential zone using remote sensing and GIS technique. Int J Innov Res Sci Eng Technol 3(5)
12. Kumar P, Herath S, Avtar R, Kazuhiko T (2016) Mapping of groundwater potential zones in Killinochi area, Sri Lanka, using GIS and remote sensing techniques. Sustain Water Resour Manag 2:419–430
13. Bhusari V, Katpatal YB, Kundal P (2016) An innovative artificial recharge system to enhance groundwater storage in basaltic terrain: example from Maharashtra, India. Hydrogeol J 24 (5):1273–1286
14. Katpatal YB, Dube YA (2010) Comparative overlay analysis through analytical hierarchical process to delineate groundwater potential zones using satellite data. Int J Earth Sci Eng 3 (5):638–653

Finite Element Analysis of Punching Shear in RC Column to Footing Connection Considering the Material Parameters

Tsenat Befkadu, Pandurang B. Khawal, and Shashi Shekhar Singh

Abstract In the reinforced concrete column to footing connection design, the region around the column is exposed to punching shear failure. This is an undesirable failure since it results in a brittle failure and it governs the strength of the footing in column to footing connection. The shear stresses that act around the perimeter of the column tend to punch through the footing and develop a failure surface in the form of a truncated cone or pyramid shape.

In this research, a nonlinear finite element modelling and analysis of the punching shear capacity of the reinforced concrete column to footing connection is conducted. The modelling of the reinforced concrete footing is based on existing literature on the experimental investigation to support the finite element analysis output. The modelling is conducted by using the ABAQUS software. The material used in modelling is modelled considering the nonlinear effects, for concrete material behaviour defined based on the concrete damage plasticity model and reinforced steel model as an elastic–perfectly plastic material. The validity of finite element analysis has been verified through comparison with available experimental data from other researchers. Four different reinforced concrete columns to footing connections have been model numerically. A systematic parametric study of the material parameters compressive strength and flexural reinforcement ratio is carried out in this research to identify the effects of the material parameters on punching shear strength of footing in column to footing connection.

Keywords Column–footing connection · Punching shear · Reinforced concrete · Material parameters · Finite element analysis

T. Befkadu (✉) · S. S. Singh
Department of Civil Engineering, Madda Walabu University, Bale Robe, Ethiopia

P. B. Khawal
Dr. Babasaheb Ambedkar, Marathwada University, Aurangabad, India

B. Laishram and A. Tawalare (eds.), *Recent Advancements in Civil Engineering*, Lecture Notes in Civil Engineering 172,
https://doi.org/10.1007/978-981-16-4396-5_85

1 Introduction

Reinforced concrete footings are structural elements that transmit loads from a structure to the supporting soil. For the structural design of flat slab and footings, punching shear is considered as one of the most critical parameters. This punching shear failure is normally a brittle-type failure of structural concrete which occurs when shear stress around a column to footing connection exceeds the shear capacity of the footing pad. The punching shear behaviour of footing pad in column connection has been investigated by some researchers in the laboratory in past. The tests indicate that the punching shear behaviour of footings differs from flat slabs due to more compact dimensions and soil–structure interaction (ACI Committee 31, 8 (2008) [1]). Hallgren and Kinnunen (1998) [2] carried out experimental research on punching shear in column to footing connection considering shear reinforcement, from the result they conclude that concrete strength had a strong influence on the punching shear strength, Ratio of flexural reinforcement only slightly influences the punching shear strength and type of anchorage did not influence the punching shear strength. Punching shear failure is a diagonal crack type it occurs some d-distance from the face of the column, this distance differs in the different code of provision (EBCS—2 M of W & U D 1997 [3]).

The punching shear capacity of footing pad is affected by some parameters in this study consider compressive strength of concrete and flexural reinforcement ratio. These parameters are main effect to increase or decrease the capacity of footing pad in punching shear and also the parameters are incorporated in the analysis. This finite element analysis is done by using ABAQUS software. The numerical modelling of footing considers such parameter and applies concentrated load anthill to reach ultimate capacity of footing pad, the result of this study to validate from other laboratory test results [4]. During modelling time used the same material property, cross-section and applied load, from previous researcher experimental work, this help to validate modelling results of punching shear capacity, cracking pattern, concrete damage in tension and compression to experimental results.

2 Finite Element Modelling of Column to Footing Connection

In reinforced concrete footing in column connection modelling, to define each element in the part in solid and truss, this element type used in modelling is 2D truss element and 3D solid element type which are used to define geometry. 2D elements that are long and slender have two nodes and can be oriented anywhere in 3D space. These element types are transmitting force axially. In this study, the internal reinforcement is modelled using 2D truss element, the steel for the finite element models is assumed as an elastic–perfectly plastic material and identical in

tension and compression, and the other one is 3D elements. It have eight-node soiled element and is defined by isotropic material property. In this study, 3D solid element has been used in modelling of concrete and soil structures, generally leading to the most realistic results and accuracy in the modelling.

The concrete footing modelled nonlinear analysis and using 8-node solid elements system, the behaviour of this material is not a straightforward task because concrete is a quasi-brittle material and has different behaviour in compression and tension. The mechanical behaviour of concrete is nonlinear in both tension and compression. In compression, the stress–strain curve for concrete is linearly elastic up to 30% of the maximum 40 compressive stress fc′ above this point, the stress increases gradually up to the maximum compressive strength after it reaches the maximum compressive strength σcu, the curve descends into a softening region, and eventually crushing failure occurs at an ultimate strain εcu. In tension, the stress–strain curve for concrete is approximately linearly elastic up to the maximum tensile strength. After this point, the concrete cracks and the strength decrease gradually to zero according to this put in to the software to model concrete in both tension and compression.

Rebar is typically used with metal plasticity models to describe the behaviour of the rebar material. The steel reinforcement is modelled as a one-dimensional element; only a one-dimensional stress–strain relation for steel is required. The stress–strain relation in compression is assumed to be the same as the one in tension. The material coefficients of steel are used in ABAQUS linear elastic material model modulus of elasticity $E = 210$ GPa, Poisson's ratio of $V = 0.3$ and density of $p = 7850$ kg/m^3.

Modelling of interaction between concrete and steel reinforcement material used contact interaction; the steel is embedded within concrete. This arrangement when in use acts as a single material with the steel providing adequate tensile capacity to concrete, which has high compression capacity. However, the interaction between the concrete mass and the steel reinforcement is not very simple, when subjected to various loading conditions. Also the footing contact to soil used surface to surfaces contact, where the normal and tangential behaviour must be specified in ABAQUS/CAE. For the normal behaviour, it was decided to use a hard contact together with the penalty constraint enforcement method; also the surface in contact was allowed to separate. Regarding the tangential behaviour, the penalty algorithm was chosen as the constraint enforcement method.

3 Application of Loads and Boundary Conditions

In numerical modelling, vertical load has been gradually increased to develop crack and crack growth; finally, failure occurs. In this thesis, finite element models of footing subjected to applied concentrated load on the column and the boundary conditions have been applied on bottom of soil. A 25-mm-thick steel plate is used in modelling. It added at the column support the concentrated load that acts in

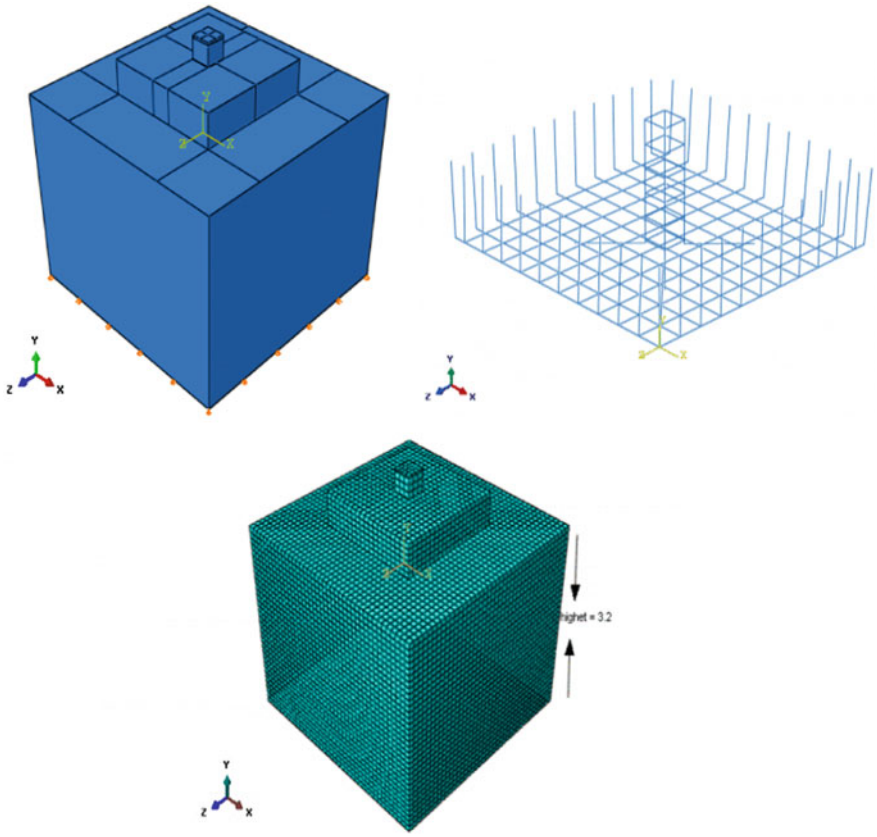

Fig. 1 Typical finite element model of concrete footing in reinforcement detail and mesh

column; the main purpose of plate is to distribute and transfer the stress to the different element of column to footing connection structure. The load is applied to a steel plate and transferred to column and footing (Fig. 1).

4 Description of Column to Footing Connection Used in FE Modelling

To carry out finite element analysis in order to predict the behaviour of structure, it is essential to verify the developed modelling against some well-established experimental results to ensure that the developed model gives the actual response closely. Four RC footings in column connection are selected from the recognized journals for modelling, analyses and their validation with the experimental results.

Table 1 Detail of simulation of footing in column connection in ABAQUS

Experimental test	*D* (m)	*C* (m)	*A* (m^2)	*fc* (MPa)	a/d
Footing-1	0.39	0.2	1.2	19	1.28
Footing-2	0.39	0.2	1.4	20.9	1.53
Footing-3	0.25	0.2	1.2	20.9	2
Footing-4	0.25	0.2	1.2	38.1	2

D = Effective depth of footing
C = Square column side length
A = Area of square footing
fc = Cylindrical characteristic compressive strength of concrete
a = Distance from face of the column to end of footing

These four footings tested by Hegger and Ricker (2009) [4] are numerically modelled by using finite element method (Table 1).

5 Validation of Finite Element Analysis Result

Comparing the numerical modelling result with experimental test study for column to footing connection, with the start of a small loading process both concrete and steel behave in a linear and elastic manner so that no cracking or yielding is observed. When the first crack arises which corresponds to the cracking load, small loss of stiffness is observed. This crack is a tangential crack type; it starts near the column circumference and extends radially in footing as the load increases present in (Fig. 2). The first tangential crack is stress-free crack; the behaviour of the footing changes and resistance is mobilized. This shear behaviour is characterized

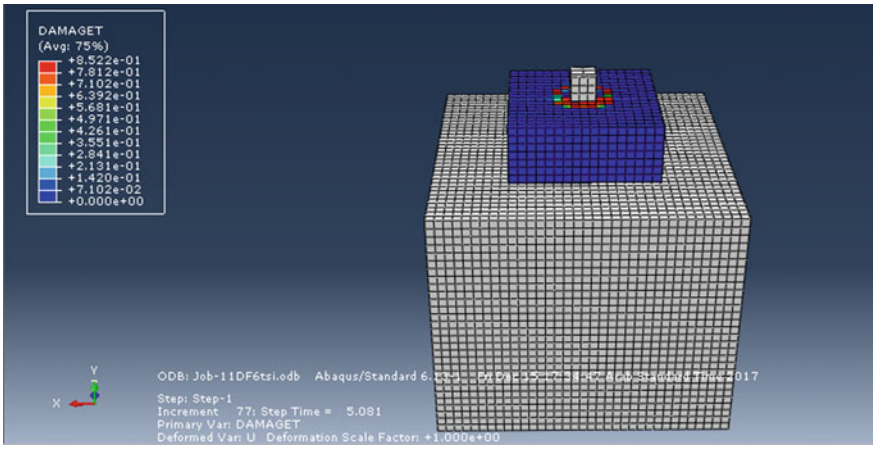

Fig. 2 Tension damage of concrete footing-1

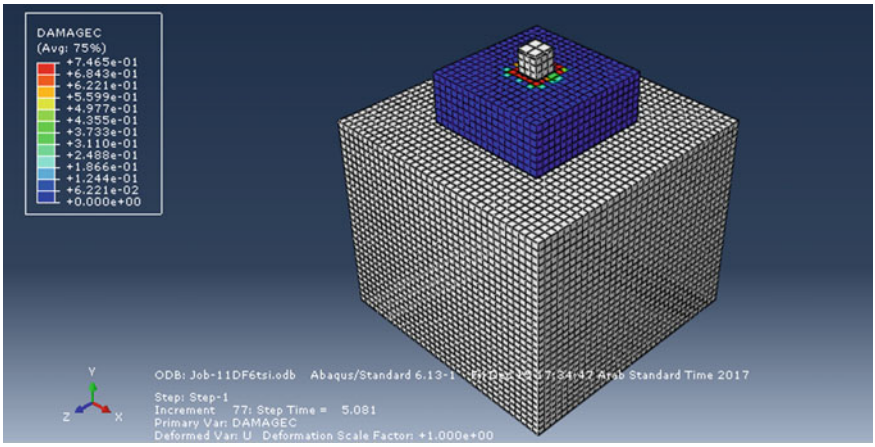

Fig. 3 Compression damage of concrete footing-1

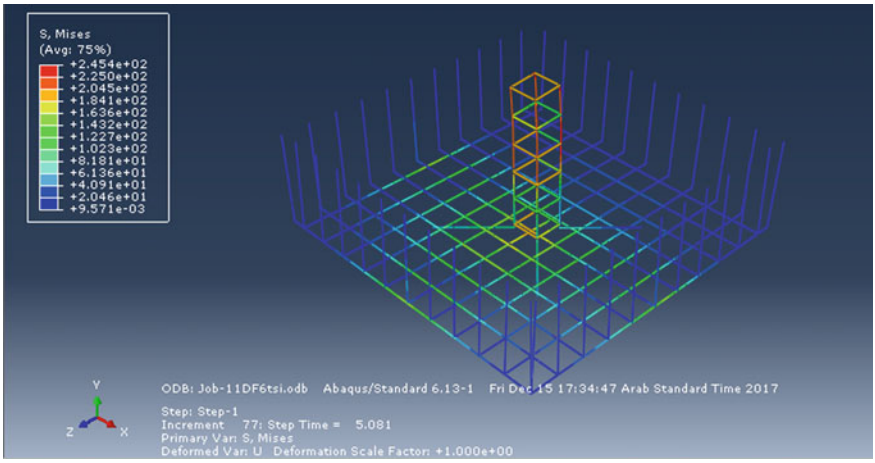

Fig. 4 Steel yield stress of footing-1

by inclined cracks across the footing cross section. Tension damage and concrete compressive values of footing-1 are shown in (Figs. 2 and 3), numerical modelling result of compressive damage value of 7.4% in increment of 77 and concrete tension damaged value of 8.5% in increment of 77 at ultimate capacity of 2871 kN. Footing-1 steel yield stress results shown in Fig. 4.

All footings specified in table are modelled numerically by using ABAQUS 6.13 software. During these analyses, it is observed that with the increase in vertical loads, footing tends to punch around the column perimeter and it forms a truncated pyramid shape. In these analysis, it is also observed that the general behaviour of

Table 2 Summarized results of finite element analysis and experimental test

Experimental test	*D* (m)	*C* (m)	*A* (m^2)	*fc* (MPa)	*a/d*	*Vc* (kN) (experimental test)	*Vc* (FEM) kN
Footing-1	0.39	0.2	1.2	19	1.28	2836	2871
Footing-2	0.39	0.2	1.4	20.9	1.53	2569	2595
Footing-3	0.25	0.2	1.2	20.9	2	1203	1336
Footing-4	0.25	0.2	1.2	38.1	2	1638	1783

the finite element model like cracking pattern and tensile or compressive damage of concrete due to applied load, development of stresses and the load–displacement graph represented a good agreement with experimental study results.

It is observed that for table footing-1, footing-2, footing-3 and footing-4, the punching loads obtained in numerically (2871, 2595, 1336 and 1783 kN) and experimental failure loads are (2836, 2569, 1203 and 1638 kN), respectively, which is 1.2, 1.01, 11.05 and 8.85% higher than experimental failure loads. However, the cracking pattern and failure phenomenon of finite element model is in good agreement with the experimental result. It has been noticed that the finite element analysis is slightly stiffer than the actual footing because in finite element full bond between concrete and reinforcement is assumed no slip occurs, but in actual case footing slip occurs. Shown below are result of finite element analysis and comparison to test study result.

The predicted ultimate capacity of footing by the simulation and the test is presented in Table 2, and load versus displacement curves are shown in Figs. 5 and 6. The results in general show good agreement in finite element analysis with the test study result. Finite element result on footing-1 is show in Fig. 5; the critical point of 2871 kN ultimate capacity of footing occurs in displacement of 6.68 mm

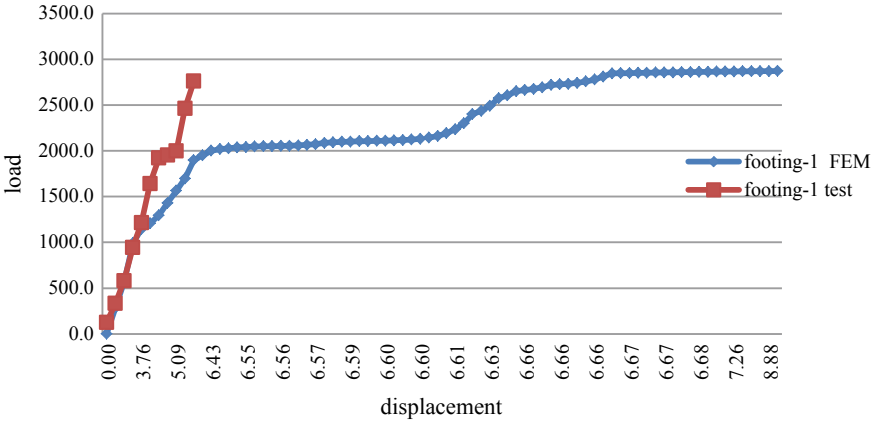

Fig. 5 Load–displacement response for footing-1

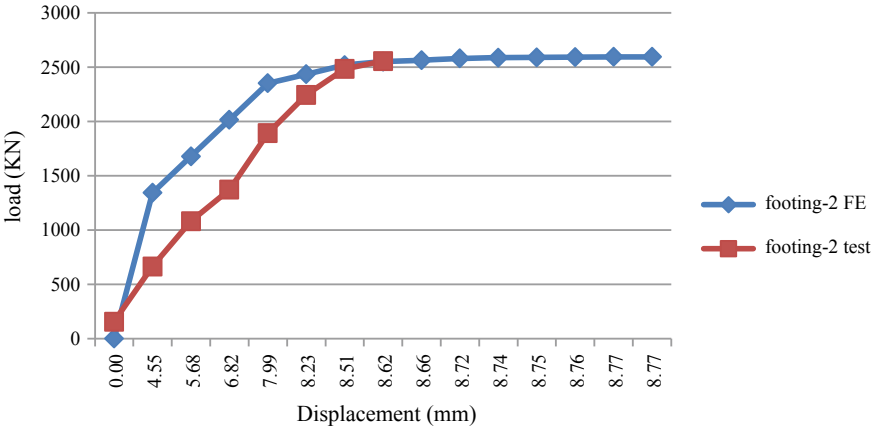

Fig. 6 Load–displacement responses for footing-2

and increment of 77 at 37,622 nodal points. In Fig. 6, curve result of footing-2 shows that critical point of 2595 kN ultimate load occurs in displacement of 8.75 mm and increment of 77 at 10,198 nodal point.

6 Influence of Material Property in Punching Shear

Material parameters mainly studies in these sections are concrete compressive strength and flexural reinforcement ratio. For this parametric study by fixing material constant to show the effect of this material, consider footing cross section 1.2 m × 1.2 m with 0.4 m effective depth and column cross section of 0.2 m × 0.2 m.

6.1 Concrete Compressive Strength

Concrete strengths used in this finite element analysis are 20, 25 and 30 MPa with fixing span to depth ratio of 1.25 m. From the figure, it shows that the slope of load–displacement curve gradually increases with increase in concrete compressive strength. Variation of the ultimate loads to get for these column footings with varying concrete compressive strength is graphically present; the ultimate loads are numerically to get 11.60%, 13.62% and 16.37% with concrete compressive strength of 20 MPa, 25 MPa and 30 MPa, respectively shown in Fig. 7. Hence, it may be concluded that concrete compressive strength has significant effect on increasing the ultimate load capacity for particular reinforcement ratio.

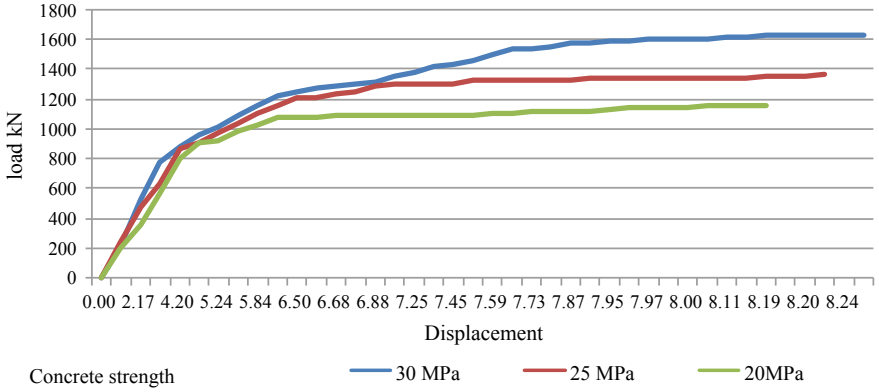

Fig. 7 Load–displacement response varying concrete strength

6.2 *Flexural Reinforcement Ratio*

The variation of ultimate load with respect to change in the compressive strength and percentage of flexural reinforcement ratio is illustrated. In reinforced concrete footing, the percentage of flexural reinforcements is higher; it failed in punching shear. However, ultimate load capacity is increased significantly by increasing the percentage of flexural reinforcement. Figure 8 also shows the influence of flexural reinforcement ratio on ultimate load capacity for varying concrete compressive strength. From Fig. 8, it is clear that with increase in the percentage of

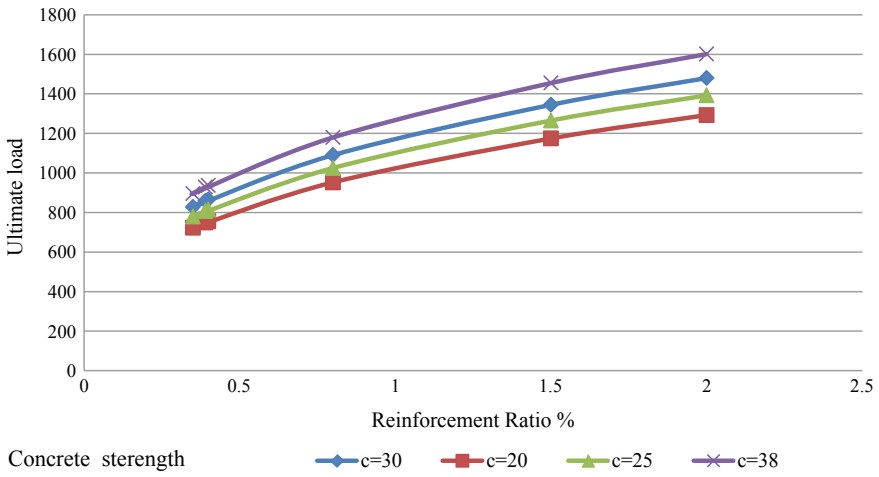

Fig. 8 Ultimate loads–reinforcement ratio response varying reinforcement ratio for different compressive strength of concrete

reinforcement ratio, the value of the punching load is increased. The rate of increase in ultimate loads is 12.92%, 13.92%, 14.79% and 16%, for concrete compressive strength 20 MPa, 25 MPa, 30 MPa and 38 MPa, respectively, under reinforcement ratio from 0.4 to 2%. It is seen that the percentage of reinforcement ratio increases; the ultimate capacity of footing also increases.

7 Conclusions

- Finite element analyses of footing punching shear capacity and stress distribution have good agreement with the test data. Footing punching loads obtained in numerically (2871, 2595, 1336 and 1783 kN) and experimental failure loads are (2836, 2569, 1203 and 1638 kN), respectively, which is 1.2, 1.01, 11.05 and 8.85% higher than experimental failure loads.
- Concert compressive strength has its own effect on punching shear capacity of column to footing connection; the ultimate loads are numerically to get 11.60%, 13.62% and 16.37% with concrete compressive strength of 20 MPa, 25 MPa and 30 MPa, respectively. These results show that concrete compressive strength has significant effect on increasing the ultimate load capacity for particular reinforcement ratio.
- Flexural reinforcement ratio is an important effect in punching shear, used 0.4, 0.8 and 2% of flexural reinforcement in concrete compressive strength of 25 MPa; the ultimate capacity of 814, 1025 and 1392 MPa is obtained. With concrete compressive strength of 30 MPa, the ultimate capacity obtained is 865, 1090 and 1479 MPa. This shows ultimate load increased with increase in concrete compressive strength and flexural reinforcement ratio.

References

1. ACI Committee 31, 8 (2008) Building code requirements for reinforced concrete (Farmington Hills American Concrete Institute MI), pp 430
2. Hallgren and Kinnunen (1998) Punching shear tests on column footings. Nordic Concr Res 21 (1 N 1 Oslo):1–12
3. EBCS—2 M of W & U D (1997) Structural use of concrete Addis Ababa Ethiopia
4. Hegger and Ricker (2009) Experimental investigations on punching behaviour of reinforced concrete footings. ACI Struct J 106(5):706–716

Effect of Tapered Flattened End Tubes of Various Thicknesses and Angles on Axial Compression Loading

Pravin Patil and I. P. Sonar

Abstract Hollow circular section is the strongest section in axial compression loading due to higher moment of inertia, but connecting hollow circular section is problematic and flattened tapered end tube is the solution. Fe250 grade of steel is used for hollow circular section and tapered flattened end tube. The allowable stress of hollow circular section for various thicknesses is evaluated as per IS800-2007 in SAP2000. The performance of tapered flattened end tube of various thicknesses has been studied in ANSYS software. The incremental load on tapered flattened has been applied up to the allowable stress and compute the maximum compression design load (Capacity) of each thickness as per theories of failure. The performance of tapered flattened angle of various thicknesses was compared.

Keywords Tapered flattened angle tube · Allowable compressive stress · Loading on tapered flattened end tube · Maximum compression design load

1 Introduction

Hollow circular tube is tapered flattened at the end for single bolted connection as shown in Fig. 1. From literature review, this paper introduces a space truss system newly developed as an attempt to reduce the cost of space trusses without a compromise in their behavior or ease of construction [1]. This paper presents two new approximate analysis methods suitable for the dynamic analysis of space trusses [2]. The paper introduces a space truss system newly developed as an attempt to reduce the cost of space trusses without a compromise in their behavior or ease of construction [3]. In this paper, efficient neural networks are analyzed for the design of double layer grid. Square diagonal on diagonal with span varying 26.5–75 m is considered [4]. The results show a 68% increase for local collapse and a 17%

P. Patil (✉) · I. P. Sonar
Civil Engineering Department, Government College of Engineering (Coep) Pune, Pune, Maharashtra, India
e-mail: ips.civil@coep.ac.in

B. Laishram and A. Tawalare (eds.), *Recent Advancements in Civil Engineering*, Lecture Notes in Civil Engineering 172,
https://doi.org/10.1007/978-981-16-4396-5_86

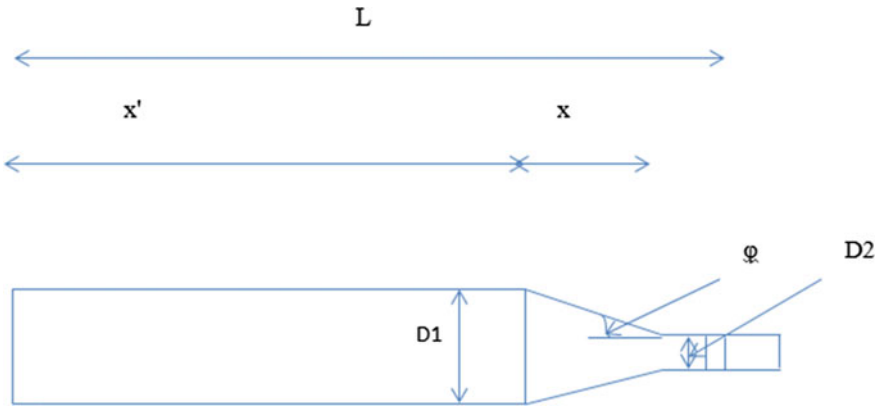

Fig. 1 Detailing of tapered flattened end tube

increase for global collapse in the truss load carrying capacity. Global and local collapses are, respectively, associated with the ultimate limit state and serviceability limit state [5, 6]. Based on these experiments, the structural behavior, up to collapse, of simple eccentric and reinforced eccentric nodes was discussed. A study of structural reinforcements is created to improve the structural load carrying capacity and minimize deflections [7]. The geometric details of tapered flattened end are given in Table 1 and Fig. 1. Flattened end tube has the maximum stresses at the end when load is applied so increase thickness at the end to reduce the stresses which is known as tapered flattened end tube. Now in tapered flattened end tube, the interested area should be angle of tapered flattened end tube. In this study, we have changed angle of tapered flattened end tube and analyzed the stress calculation on ANSYS software. This model was created on Catia software and imported into workbench. As the angle changes, x values should vary as shown in Table 1. The angles of tapered flattened end tube are 5°,10°,15°, 20°,30°, 45° and 50°.

Table 1 Detailing of tapered flattened end tube

Thickness (mm)	Tapered angle (°)	External diameter (D1) (cm)	Thickness at tapered end (D2) (cm)	*x*' (cm)	*x* (cm)	*L* (cm)
1/2/3	5	5	1	40.14	22.86	63
	10	5	1	51.66	11.34	63
	15	5	1	55.54	7.46	63
	20	5	1	57.51	5.49	63
	30	5	1	59.54	3.46	63
	45	5	1	61	2	63
	50	5	1	61.328	1.678	

2 Analysis of Hollow Circular Tube in SAP 2000

Analysis of hollow circular tube of 50 mm outer diameter and 2 mm thickness is done in SAP 2000 software for calculating the allowable stress in simple hollow circular tube. Steel with yield strength 250 MPa (Fe250) is assigned to the tube. The tube is loaded to incremental load up to maximum design load (capacity) for given section of tube in SAP2000 as per IS 800-2007, and the bottom end was fixed (Fig. 2).

Allowable compression stress is calculated as below.

Allowable compression stress at elastic limit in simple compression (σc) = 140.255 MPa.

3 Loading on Tapered Flattened End Tube in ANSYS

The load is applied in the bolt fixed in the vertical downward direction in the incremental order of 2 kN for varying flattening angles 5°, 10°, 15°, 20°, 30°, 45° and 50°. The behavior of tapered flattened angle tube for incremental load is studied. Principal and shear stresses are observed for incremental load (Fig. 3).

4 Analysis and Design (Capacity) of Tapered Flattened End Tube as Per Shear Stress Theory

For compression loading (Fig. 4 and Table 2).

For failure material

$$1/2\,(\sigma 1 - \sigma 3) \geq 1/2\sigma * c$$

or

$$(\sigma 1 - \sigma 3) \geq \sigma * c$$

Equation given below is used for design purpose as per shear stress theory (Table 3)

$$1/2(\sigma 1 - \sigma 3) = 1/2\sigma c$$

$\sigma c =$ Allowable simple compressive stress

$$\sigma c = 140.255\,\text{MPa}$$

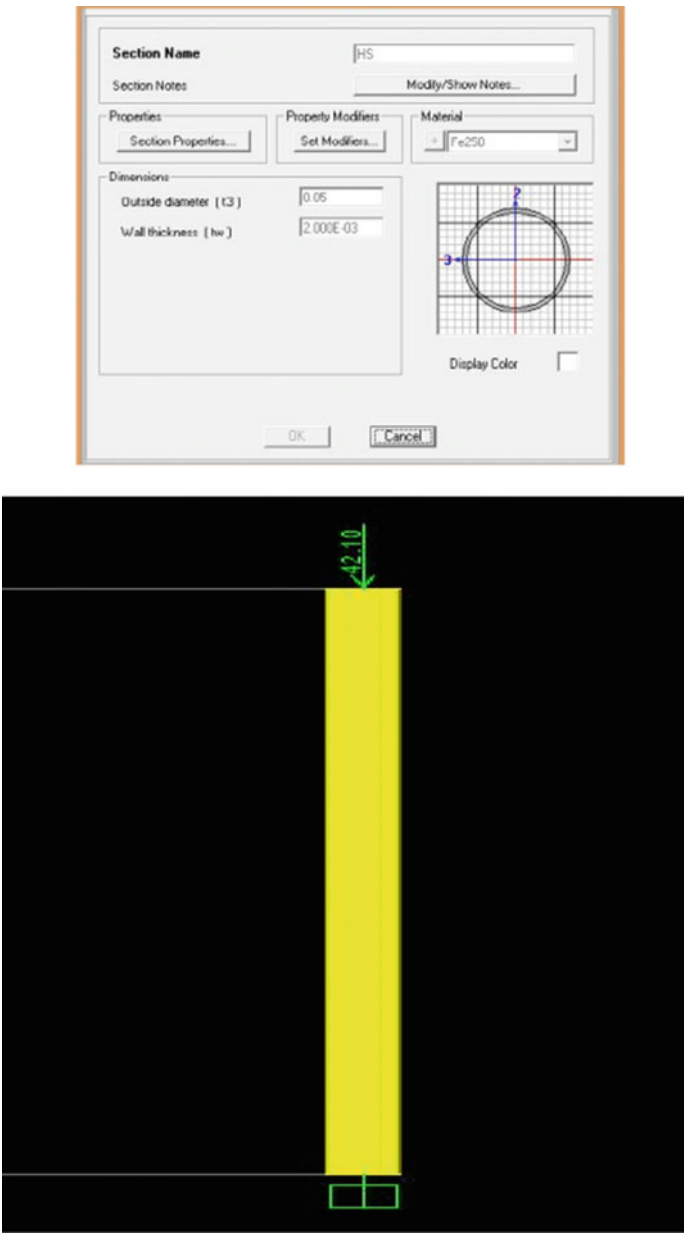

Fig. 2 SAP2000 model

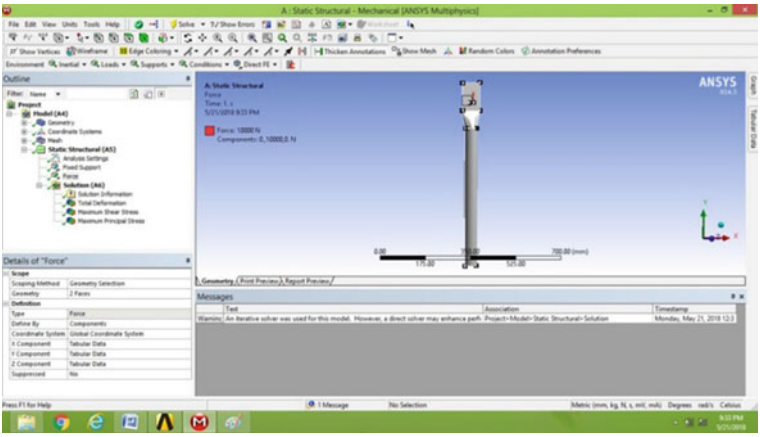

Fig. 3 Incremental load on tapered flattened end tube at bolted joint

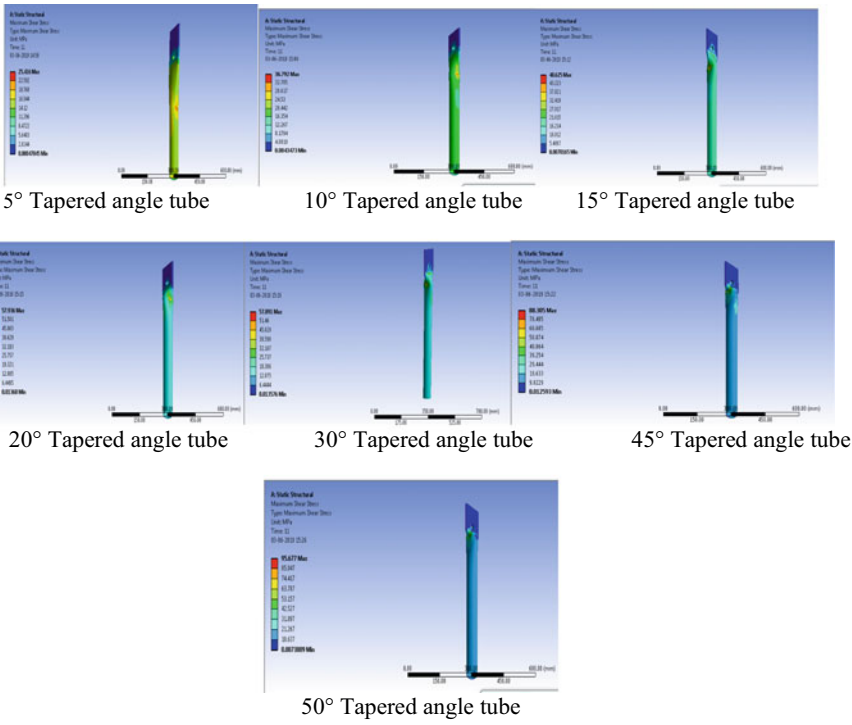

Fig. 4 Maximum shear stress of tapered flattened end tube

Table 2 Maximum shear stress of tapered flattened end tube

Thickness (mm)	Angle (°)	Maximum shear stress in MPa									
		5 kN	10 kN	15 kN	20 kN	2 kN	30 kN	35 kN	40 kN	45 kN	50 kN
1	5	28.78	52.77	76.76	100.7	124	148.7	172.7	196.7	220.6	244.6
	10	36.49	66.90	97.31	127.7	158	188.5	218.9	249.3	279.7	310.2
	15	48.79	89.45	130.1	170.7	211	252.1	292.7	333.4	374.0	414.7
	20	65.05	119.2	173.4	227.7	281	336.1	390.3	444.5	498.7	552.9
	30	117.8	216.0	314.2	412.4	510	608.8	706.9	805.1	903.3	1001
	45	194.2	356.0	517.9	679.7	841.6	1003	1165	1327	1489	1650
	50	230.3	422.3	614.3	806.3	998.2	1190	1382	1574	1766	1958
2	5	10.86	21.72	32.59	43.45	54.31	65.18	76.04	86.91	97.77	108.6
	10	16.68	33.36	50.04	66.72	83.40	100.0	116.7	133.4	150.1	166.8
	15	24.95	49.9	74.85	99.80	124.7	149.7	174.6	199.6	224.5	249.5
	20	30.23	60.46	90.70	120.9	151.1	181.4	211.6	241.8	272.1	302.3
	30	43.52	87.04	130.5	174.0	217.6	261.1	304.6	348.1	391.7	435.2
	45	74.87	149.7	224.6	299.5	374.3	449.2	524.1	599.0	673.9	748.78
	50	125.5	251	376.4	501.9	627.4	752.9	878.4	1004	1129	1255
3	5	14.69	26.94	39.19	51.43	63.68	75.93	88.17	100.4	112.6	124.9
	10	14.13	25.91	37.69	49.47	61.25	73.02	84.80	96.58	108.3	120.1
	15	15.95	29.24	42.54	55.84	69.13	82.43	95.72	109.0	122.3	135.6
	20	20.91	38.34	55.77	73.2	90.62	108.0	125.4	142.9	160.3	177.7
	30	29.20	53.54	77.88	102.2	126.5	150.9	175.2	199.5	223.9	248.2
	45	53.30	97.72	142.1	186.5	230.9	275.41	319.84	364.26	408.68	453.1
	50	74.261	136.15	198.03	259.91	321.8	383.68	445.57	507.45	569.34	631.22

Table 3 Maximum design compression load of tapered flattened end tube

Thickness (mm)	Tapered flattened end tube (°)	Maximum compression design load for tapered flattened end tube (capacity) (kN)	Maximum compression design load (capacity) for simple Hollow circular section tube (kN)	Maximum compression design load (capacity) in percentage of hollow circular section (capacity)
1	5	13.8	21.6	63.88
	10	10.7		49.53
	15	7.6		35.18
	20	5.5		25.46
	30	2.7		12.5
	45	1.3		6.01
	50	0.8		3.70
2	5	23	41.1	55.96
	10	21		51.01
	15	14.05		34.08
	20	11.59		28.19
	30	8.05		19.58
	45	4		9.73
	50	2.5		6.08
3	5	27.1	61.7	43.92
	10	28.5		46.19
	15	25.1		40.68
	20	18.96		30.72
	30	13.2		21.39
	45	6.8		11.02
	50	4.67		7.47

5 Analysis and Design of Tapered Flattened End Tube as Per Principal Stress Theory

For compression loading.

As per maximum principal stress theory, the failure will take place if (Fig. 5 and Table 4)

$$|\sigma 3| \geq \sigma * c \text{ in simple compression}$$

Design criteria for maximum principal stress theory (Table 5)

$$\text{Hence } \sigma 3 = \sigma c$$

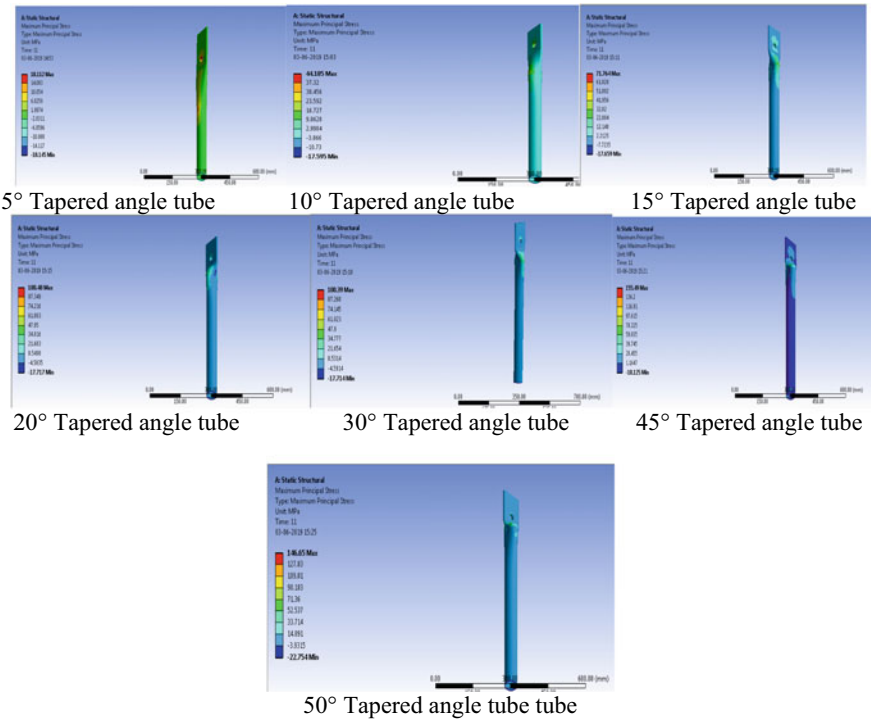

Fig. 5 Maximum principal stress of tapered flattened end tube

6 Results and Discussion

1. It is observed from Fig. 6 that 1 mm model will experience less design load if angle exceeds 15° and maximum compression design load for angle 5°. The 2 mm model will experience maximum design load at angle 10°, and 3 mm model will experience maximum design load when angle exceeds 10°. Hence, for maximum design compression loading 3 mm thickness between 15° and 50° models can be preferred (Fig. 6).
2. It is observed from Fig. 7 capacity maximum compression load for 1 mm is in angle 5° to 20°, and for 3 mm is in angle 45° and 50°. For 2 mm model, capacity is found to be least at angle 20° and 30°.

In 1 mm thickness least design load is in 50°, and the effectiveness in reducing maximum compression design load is in the order of 5°, 10°, 15°, 20°, 30° and 45° as shown in Fig. 7.

Table 4 Maximum principal stress for all tapered end tube model

Thickness (mm)	Angle (°)	Maximum principal stress in MPa									
		5 kN	10 kN	15 kN	20 kN	25 kN	30 kN	35 kN	40 kN	45 kN	50 kN
1	5	41.089	75.33	109.5	143.8	178.0	246.5	280.7	280.7	315.0	349.2
	10	39.911	73.17	106.4	139.6	172.9	206.2	239.4	272.7	305.9	339.2
	15	66.409	121.7	177.0	232.4	287.7	343.1	398.4	453.8	509.1	564.4
	20	88.141	161.5	235.0	308.4	381.9	455.3	528.8	602.3	675.7	749.2
	30	141.3	259.0	376.8	494.5	612.3	730.0	847.8	965.5	1083	1201
	45	210.47	385.8	561.2	736.6	912.0	1087	1262	1438	1613	1789
	50	247.04	452.9	658.7	864.6	1070	1276	1482	1688	1894	2099
2	5	31.264	54.32	84.45	121.3	155.3	220.2	240.3	250.1	290.8	320.1
	10	28.46	56.92	85.38	113.8	142.3	170.7	199.2	227.6	256.1	284.6
	15	33.777	67.55	101.3	135.1	168.8	202.6	236.4	270.2	303.9	337.7
	20	47.264	94.52	141.7	189.0	236.3	283.5	330.8	378.1	425.3	472.6
	30	78.958	157.9	236.8	315.8	394.7	473.7	552.7	631.6	710.6	789.5
	45	121	242.0	363.0	484.0	605.0	726.0	847.0	968.0	1089	1210
	50	138.91	277.8	416.7	555.6	694.5	833.4	972.3	1111	1250	1389
3	5	30.14	55.25	80.37	105.4	130.6	155.7	180.8	205.9	231.0	256.1
	10	27.156	49.78	72.41	95.04	117.6	140.3	162.9	185.5	208.2	230.8
	15	30.405	55.74	81.07	106.4	131.7	157.0	182.4	207.7	233.1	258.4
	20	36.557	67.02	97.48	127.9	158.4	188.8	219.3	249.8	280.2	310.7
	30	56.447	103.4	150.5	197.5	244.6	291.6	338.6	385.7	432.7	479.8
	45	64.678	118.5	172.4	226.3	280.2	334.1	388.0	441.9	495.8	549.7
	50	87.175	159.8	232.4	305.1	377.7	450.4	523.0	595.7	668.3	740.9

Table 5 Maximum design load of tapered flattened end tube

Thickness (mm)	Tapered flattened end tube (°)	Maximum design load (capacity) for tapered flattened end tube (kN)	Maximum design load (capacity) for simple tube (kN)	Maximum design load (capacity) in percentage of hollow circular section (capacity)
1	5	19.8	21.6	91.66
	10	19.5		90.277
	15	11.6		53.70
	20	8.55		39.58
	30	4.97		23
	45	3		13.88
	50	2.32		10.74
2	5	22	41.1	53.52
	10	24.640		59.95
	15	20.76		50.51
	20	9.889		24.06
	30	8.90		21.65
	45	5.79		14.08
	50	5.048		12.28
3	5	26.9	61.7	43.59
	10	29.9		48.46
	15	26.7		43.27
	20	21.94		35.59
	30	13.8		22.36
	45	11.95		19.36
	50	8.6		13.93

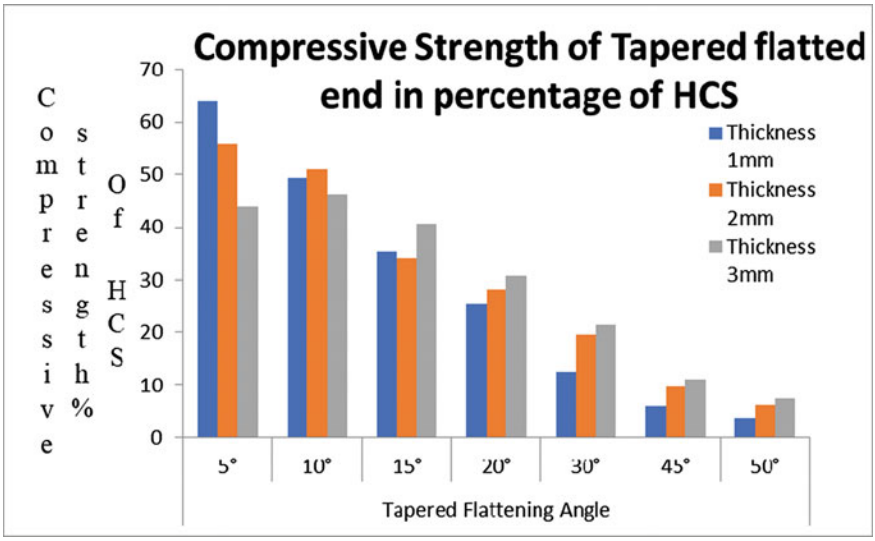

Fig. 6 Compressive strength versus tapered angle as per shear stress theory

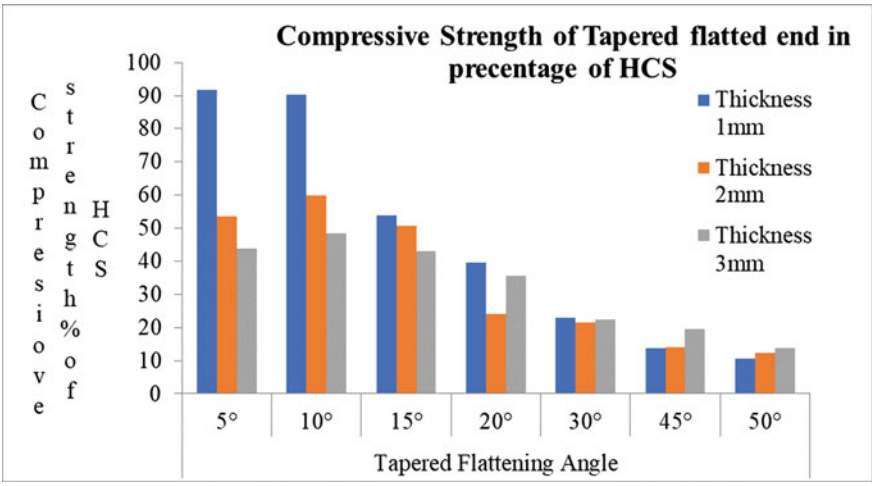

Fig. 7 Compressive strength versus tapered flatted angle as per principal stress theory

7 Conclusion

For lesser thickness (less than 2 mm), suggested tapered angle is 5°–20°. As thickness of tube increases (3 mm), it is observed that efficiency tapered flattened end tube increases for tapered flattening angle 30°–50°.

References

1. El-Sheikh A (1996) Development of a new space truss system. J Constr Steel Res 37
2. El-Sheikh A (2000a) Approximate dynamic analysis of space trusses. J Eng Struct 22
3. El-Sheikh A (2000b) New space truss system from concept to implementation. J Eng Struct 22
4. Kaveh A, Servati H (2001) Design of Double layer grid using back propagation neural networks. J Comput Struct 79
5. de Freitas CAS, Bezerra LM, Araujo RM, Araújo GM (2013) Experimental and numerical Investigation of the space-truss with reinforce of the stamped connection. J Exp Trusses Roofs Connections ICSDEC 2012 ASCE
6. Bezerra LM, de Freitas CAS, Matias WT, Nagato Y (2009) Increasing load capacity of steel space trusses with end- flattened connections. J Constr Steel Res 65
7. de Andradea SAL, Vellascob PCGS (2005) Tubular space trusses with simple and reinforced end-flattened nodes-an overview and experiments. J Constr Steel Res 61

Performance Assessment of Coupled Dam-Foundation System for Recorded Seismic Excitations

Aniket R. Tidke and Shrabony Adhikary

Abstract The aim of the present work is to investigate the seismic performance of coupled dam-foundation system using finite element analysis. For this purpose, different damage indicators and damage variables are adopted. Seismic analysis of dam-foundation system is performed for a combination of horizontal and vertical components of ground motion records which are selected using the Conditional Mean Spectrum method. The Concrete Damaged Plasticity model is used to simulate material non-linearity in the dam; however, the foundation is considered to be linear. One-way plane strain infinite elements are provided to the far end of the foundation domain to allow seismic wave propagation away from the foundation. Non-linear time-history analysis is performed considering nine number of recorded ground motions. The amount of post-seismic tensile crack failure in the dam is illustrated using multi-variable damage indicators in which damage dissipation energy, crack length and maximum drift takes into consideration as a damage variables. Further, crest displacement, dissipation energy and accumulated failure in the dam are correlated with different ground motion parameters. The results show that the ground motion with low-frequency contents and long duration has a considerable effect on the displacement response of the dam; however, the high amplitude ground motions significantly influence the tensile failure and dissipation energy in the dam.

Keywords Koyna dam-foundation system · Conditional mean spectrum approach · Concrete damaged plasticity model · Damage indices · Ground motion parameters

A. R. Tidke (✉) · S. Adhikary
Department of Civil Engineering, Visvesvaraya National Institute of Technology, Nagpur 440010, India

B. Laishram and A. Tawalare (eds.), *Recent Advancements in Civil Engineering*, Lecture Notes in Civil Engineering 172,
https://doi.org/10.1007/978-981-16-4396-5_87

1 Introduction

Gravity dams serve a strong purpose, like water storage, flood control, irrigation, power generation, etc. In India, many dams are constructed in recent years, as their demands have been increasing rapidly. However, the large number of gravity dams is situated in the seismic zone IV and V according to Indian seismic code IS 1893 (part 1)—2016 [1]. Earthquakes are very uncertain and cause a severe level of damages in the superstructures. Therefore, seismic analysis and design of dams are very important to examine for engineers and researchers. The 6.5 magnitude Koynanagar earthquake devastated the Koyna gravity dam and cracks were observed on both faces of the dam [2]. Since then, the Koyna dam is considered a benchmark problem to study the seismic analysis of gravity dams. Many existing dams throughout the world were subjected to high-intensity earthquakes, out of which Koyna (India), Kasho (Japan), Uh (Japan), Takou (Japan), Rapel (Chile), Techi (Taiwan), Hsinfenkiang (China), Sefid Rud (Iran) dams were shown minor damages [2]. Meanwhile, the seismic performance of the concrete dams needs to be assessed.

Numerical investigation is a good tool for engineers and researchers worldwide to evaluate the seismic performance of large-scale problems. For years, seismic damage assessment using different damage indicators has been widely adopted for numerical study. However, the selection of damage indices (DIs) and various damage variables are required for the quantitative metric failure assessment. Damages indices can be classified as local, global, single variable, multivariable, cumulative, non-cumulative, etc. [3]. Local DIs show damages in an element or member or limited part; however global DIs depict the damages in the entire system. Single or multi damage variables can be used for the evaluation of DIs; however, multi-variable DIs give a more comprehensive indicator of damage extent. The cumulative and non-cumulative DIs show damage extent during transient analysis and end state, respectively. Banon and Veneziano [4] proposed displacement based, cumulative damage indices which take into account maximum rotations in cycle and yield value. Park and Ang [5] introduced multi-variable damage indices which take maximum deformation, ultimate deformation, yield strength and dissipated energy as a damage variable. Wang and Shah [6] introduced force-based, cumulative damage indices. The deformation-based, non-cumulative, local damage indices were proposed [7]. Cosenza and Manfredi [8] used non-recoverable dissipated hysteretic energy and hysteretic energy capacity of the structure obtained from pushover analysis for the evaluation of damage indices. Bending moments and axial forces were considered for the evaluation of damage indices [9]. Zhang and Wang [10] proposed local and global damage indices based on the crack length and dissipated energy. Alembagheri and Ghaemian [11] introduced damage indices based on maximum deformation and dissipated energy. Hariri-Ardebili and Saouma [3] proposed multi-variable damage indices based on crack length, dissipated energy and maximum drift. Damage indices for the Pine flat dam, Koyna dam and Folsom dam was evaluated based on the cumulative inelastic

area demand capacity ratio (CIA-DCR) response curve [12]. Ansari and Agarwal [13] evaluated damage indices on the basis of factor of safety against sliding.

In the present research, non-linear time-history analysis of the Koyna dam-foundation system is performed by applying nine number of ground motions. Ground motions are selected according to the Conditional Mean Spectrum method. To depict the tensile crack failure in the dam, the concrete damaged plasticity model is used. Performance assessment of coupled dam-foundation system is done using multi-variable damage indices, failure profile of dam, and different damage variables. Further, ground motion amplitude, frequency contents and duration parameters are studied.

2 Numerical Simulation of Dam-Foundation System

A 103 m Koyna concrete gravity dam is taken for numerical investigation. The coupled Koyna dam-foundation system is modeled in a commercially available Finite Element Method (FEM) software, Abaqus. Finite element model of coupled Koyna dam-foundation system is shown in Fig. 1. For the numerical investigation, the damping, inertia and flexibility properties are assigned to the dam as well as the foundation. The concrete damaged plasticity (CDP) model is used to capture the cracks in the dam; however, the foundation is considered linear elastic. A Koyna concrete gravity dam is assumed to be resting on 350 × 140 m foundation block. A 2-dimensional dam and foundation are modeled using 4-node plane strain quadrilateral reduced integration elements. At the dam-foundation interface, the dam and foundation surface are assumed to be tied with each other for rigid surface constraints. A base of the foundation is assumed to be fixed and earthquake time-histories are applied as an input motion to the base of the foundation. However, for the time-history analysis, the horizontal and vertical components of the ground motions are applied simultaneously. A one-way plane strain infinite element has been used to simulate wave absorption on the far end of the foundation domain. The infinite elements are mathematically extended to infinity to show an unbounded domain of foundation.

2.1 Material Properties of Dam and Foundation

Initially, before the dynamic analysis, frequency analysis of the coupled dam-foundation system is carried out. Based on the frequency analysis using the Lanczos iteration method, the natural frequency of the first three modes is 2.7942 Hz, 4.1098 Hz and 6.7391 Hz, respectively. Khosravi et al. [14] reported the first mode natural frequency of the dam-foundation system as 2.930 Hz; however, in the present study, the calculated first mode natural frequency shows 4.63% deviation from the earlier presented first mode natural frequency. Figure 2

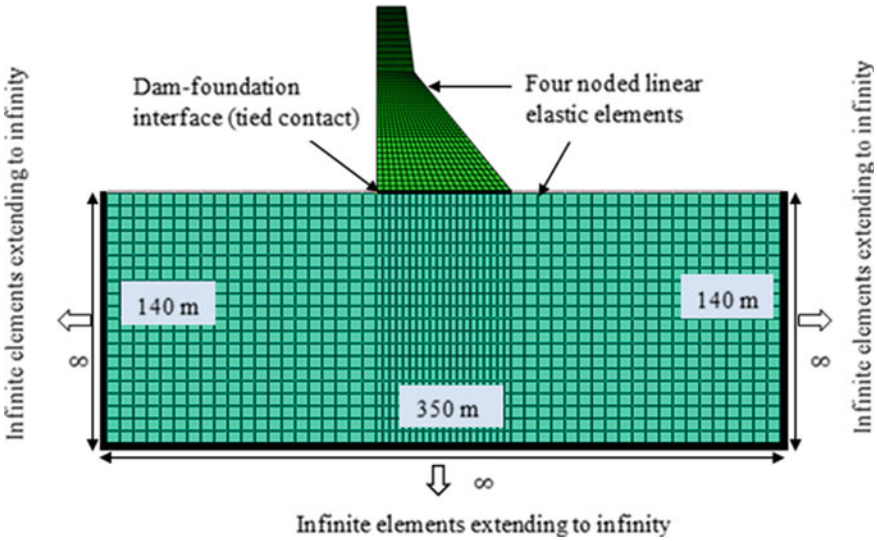

Fig. 1 Representation of finite element modeling of coupled dam-foundation system

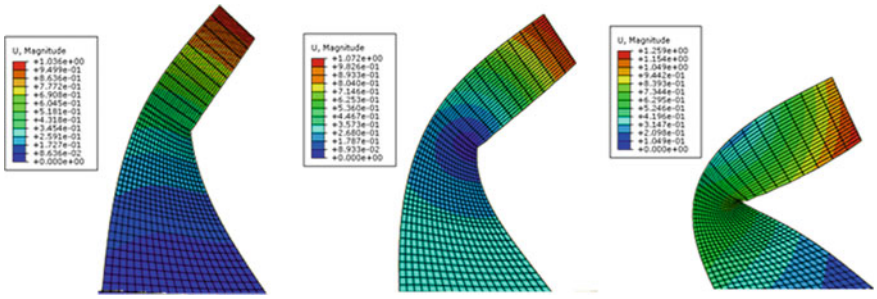

Fig. 2 Modal shapes and natural frequency of dam

shows the mode shapes and associated natural frequency of the dam. It is observed that the first two modes show translation behavior; however, the third mode shape shows translation plus rotational behavior. Meanwhile, for the evaluation of Rayleigh damping coefficients, first two modes natural frequency is considered. Using Eqs. 1 and 2, the Rayleigh damping coefficients (α and β) are evaluated as 1.04456 sec^{-1} and 0.0023064 sec respectively and assigned to the dam and the foundation.

$$\alpha = \xi \frac{2\omega_i \omega_j}{\omega_i + \omega_j} \tag{1}$$

Table 1 Linear material properties of dam, reservoir and foundation

Sr. no.	Parameters	Dam	Foundation
1	Elastic modulus (E) (MPa)	31,027	62,054
2	Poisson's ratio (μ)	0.2	0.33
3	Mass density (ρ) (kg/m^3)	2643	3300

Table 2 Non-linear material properties of the CDP model

Dilation angle (ψ_c)	Compressive initial yield stress (σ_{co}) (MPa)	Compressive ultimate stress (σ_{cu}) (MPa)	Tensile failure stress (σ_{to}) (MPa)	Flow potential eccentricity (e)	Ratio of the initial equibiaxial to the uniaxial compressive yield stress
36.31°	13	24.1	2.9	0.1	1.16

$$\beta = \xi \frac{2}{\omega_i + \omega_j} \tag{2}$$

where α and β are the mass proportional and stiffness proportional damping coefficients respectively, ζ is damping ratio (5% damping ratio is considered), ω_i and ω_j are the natural frequencies of the system in 1st and 2nd modes of vibration. Table 1 shows the linear material properties of the dam and foundation. In the present work, the FEM modeling of dam-foundation system and the associated material properties of dam and foundation is adopted from the study presented by Sarkar et al. [15].

Further, Table 2 shows the material properties of the concrete damaged plasticity (CDP) model for the dam. In CDP model, the stress–strain curve of tensile and compressive behavior of concrete is incorporated. Furthermore, the concrete tension damage curves are also used in which scalar damage variable d_t shows 0 at undamaged state and 1 at fully damaged state of concrete.

3 Ground Motions Selection

For the ground motion selection, the conditional mean spectrum (CMS) approach is used. Baker [16] proposed the CMS approach in which the mean spectrum can be adopted as a target spectrum for ground motion selection. The procedure for spectrum calculation is presented earlier [17]. Jayaram et al. [18] presented the algorithm for the ground motion selection in which the ground motions are matched with target spectrum mean and variance. Later, the algorithm proposed by Jayaram

Table 3 Selected ground motions using conditional mean spectrum approach

Seismic event	Year	Station	(M)	Distance to fault (km)	Vs_{30} (m/s)	PGA (g)	PGA (g)	Duration (s)
						H	V	
Koyna	1967	Koyna dam	6.3	13	800	0.41	0.28	10
Parkfield	1966	Temblor-Pre	6.19	15.96	527.92	0.28	0.14	30.39
Coyote Lake	1979	Gilroy Array #	5.74	3.11	663.31	0.26	0.16	26.83
New Zealand-02	1987	Matahina Dam	6.6	16.09	551.3	0.25	0.14	24.6
Kocaeli, Turkey	1999	Izmit	7.51	7.21	811	0.23	0.15	29.99
Irpinia, Italy-01	1980	Brienza	6.9	22.56	561.04	0.22	0.21	34.98
Northridge-01	1994	LA – Chalon Rd	6.69	20.45	740.05	0.22	0.16	31
Santa Barbara	1978	Cachuma Dam Toe	5.92	27.42	465.51	0.21	0.08	13.18
Northern Calif-07	1975	Cape Mendocino	5.2	34.73	567.78	0.21	0.04	29.14

et al. [18] was improved [19]. The mean spectrum is generated using the MATLAB code developed by Baker [16].

The first mode period is considered as a period of interest. For dam-foundation system, the first modal natural frequency is 2.7942 Hz, so the fundamental period of the system is calculated as 0.35788 s. The other important parameters such as magnitude, mean distance, fault type, average shear wave velocity to a 30 m depth (Vs_{30}) for Koyna (1967) earthquake are considered. The nine horizontal and vertical component of ground motions are selected from the PEER ground motion database [20] and these ground motions are shown in Table 3. All the selected ground motions have variable amplitudes, frequency contents and duration (Table 3).

4 Seismic Performance Evaluation

4.1 Seismic Damage Indicators

Failure analysis of a structure under seismic excitation is inherently nonlinear [3]. Seismic failure analysis of a multipurpose structure like a dam using various damage indicators has been a common practice. However, the selection of appropriate damage variables for the evaluation of damage indices (DIs) is a noteworthy step. Damage indices (DIs) show the amount of failure in the structure. Based on the past failure studies presented on dams, it can be said that most of the Dis is either dissipation energy or deformation based. For the evaluation of seismic damages in the dam, two multi-variable DIs proposed by Zhang and Wang [10], Hariri-Ardebili and Saouma [3] have been adopted. Former DIs take into account the crack length and dissipation energy as a damage variable; while, latter DIs consider crack length,

dissipation energy and maximum drift as a damage variables. Both DIs indicates the failure at local and at the global level.

Figure 3 shows the failure profile of the Koyna dam subjected to the H + V components of all selected ground motions. Dam shows cracks mainly at neck and heel region; however, amount of tensile damage is observed for Koyna time-histories followed by Parkfield, Northern Calif, etc. No damage is seen for New Zealand and Santa Barbara. From the past studies, it is revealed that the damage at the upstream face of the dam may be mostly due to the hydrodynamic pressure effect. However, in the present study, the effect of the reservoir is not considered. Though, the dam shows tensile damage at the upstream face due to the Parkfield earthquake. However, the damage profile of the Koyna dam as a result of Koyna (H + V) time-histories are nearly matched with the damage profile of the dam reported by Sarkar et al. [15].

Figure 4 shows the critical paths for the tensile crack in the dam. Dam neck and heel observe as critical regions in the dam were cracks in the neck initiate from the downstream side; however, cracks in the heel initiate from the upstream side of the dam, and propagate towards the other end. Local damage index (DI_{Li}) at particular

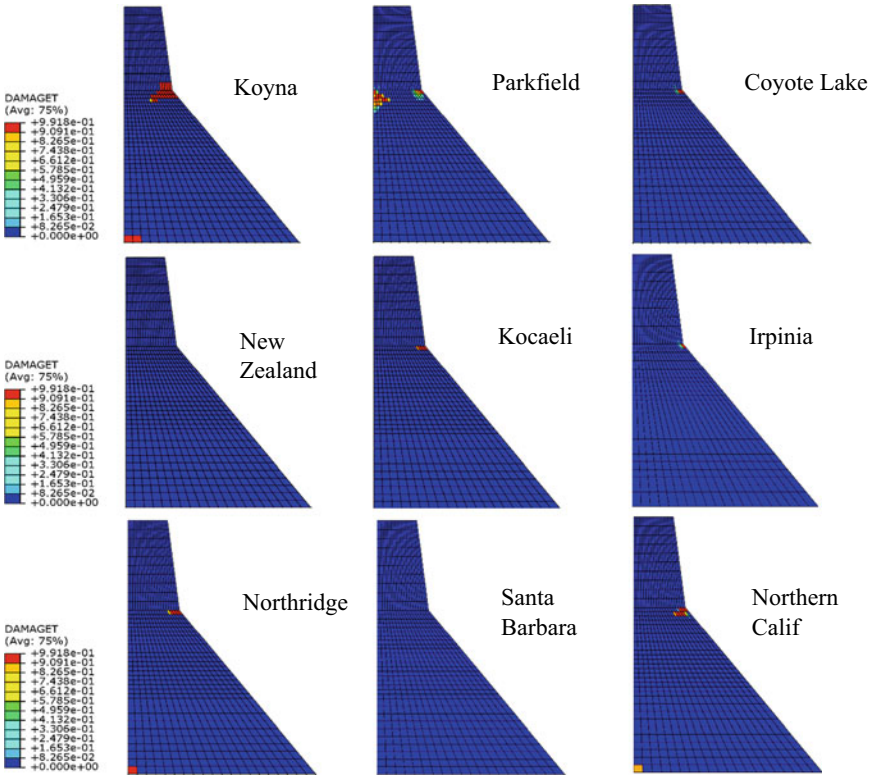

Fig. 3 Failure profile of the gravity dam subjected to the seismic excitation

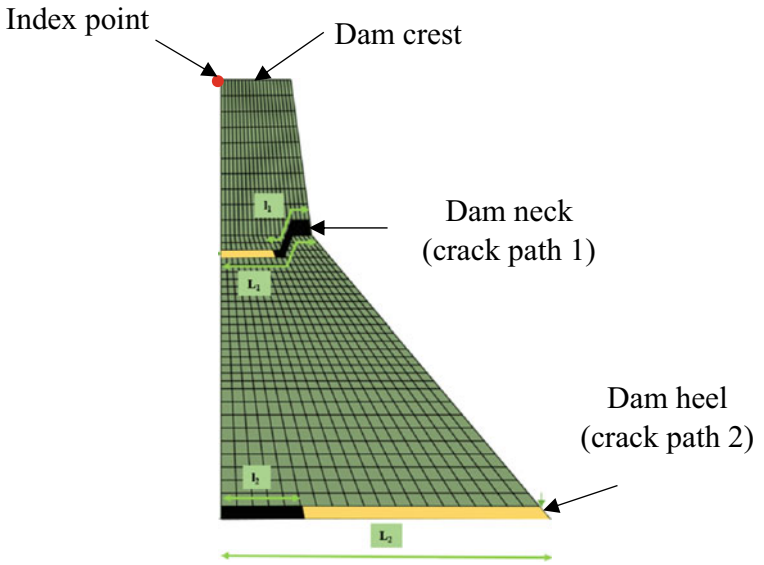

Fig. 4 Critical paths for failure in the dam

path and global damage index (DI_G) at the entire dam can be evaluated using Eqs. (3) and (4) [10].

$$DI_{Li} = \frac{l_i}{L_i} \tag{3}$$

$$DI_G = \frac{\sum_{i=1}^{n} DI_{Li} \times E_i}{\sum_{i=1}^{n} E_i} \tag{4}$$

Further, a cumulative multi-variable DIs proposed by Hariri-Ardebili and Saouma [3] are evaluated for the accumulated damage in the dam. This DIs take into account the crack length L^C, dissipation energy E_H and maximum drift $u_{\max}$ (Eq. 5).

$$DI = f\left(L^C,\ E_H,\ u_{\max}\right) \tag{5}$$

Firstly, a micro DI (DI_i^j) for each critical path (dam neck and heel) is evaluated which is defined as the ratio of the cracked path over the total crack path. Further, a meta DI ($\overline{DI}^j$) for each critical path is evaluated. The meta DI ($\overline{DI}^j$) at each critical path can be defined by combining the micro DI and dissipation energy. Equations (6) and (7) can be used for the evaluation of micro and meta DI.

$$DI_i^j = \beta_\Delta \times \frac{L_i^C}{L_i^T} \tag{6}$$

$$\overline{DI}^j = \sum_{i=1}^{n} DI_i^j \times \Delta_i^j \tag{7}$$

where i and j refer to crack path 1 and 2 respectively, L_i^C and L_i^T are the cracked length and total length, respectively, β_Δ is the controlling coefficient which is computed based on the index point displacement. The index point in the dam is assumed at the crest level (Fig. 4). For the evaluation of β_Δ, the drift ratio needs to be evaluated. The drift ratio is defined as the ratio of maximum displacement to the height of the dam. In the present study, the maximum displacement at index point and total height of the dam from the base to the index point are taken for the calculation of the drift ratio. Finally, macro *DI* for the entire dam-foundation coupled system is evaluated using Eq. (8).

$$\overline{\overline{DI}} = \sum_{j=A}^{m} \overline{DI}^j \tag{8}$$

Meanwhile, for the evaluation of the above-mentioned DIs, crest displacement and dissipation energy response are required. As shown in Fig. 5, crest displacement and dissipation energy response between considered ground motions are compared. The dissipation energy response shows a similar response to the failure profile of the dam. The peak crest displacement (Fig. 5a) is observed for Parkfield followed by Northern Calif, Koyna, etc.; however, peak dissipation energy (Fig. 5b) is observed for Koyna followed by Parkfield, Northern Calif, etc. It is observed that Koyna causes more structural failure, which is responsible for high dissipation energy (15 kN-m) in the dam.

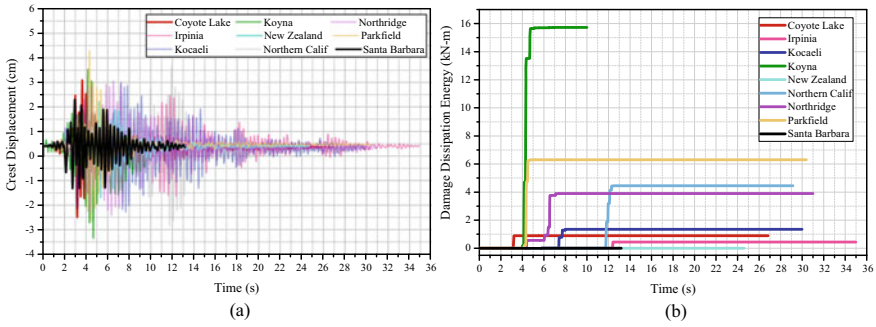

Fig. 5 Comparison of seismic responses in between all ground motions: **a** Crest displacement. **b** Dissipation energy

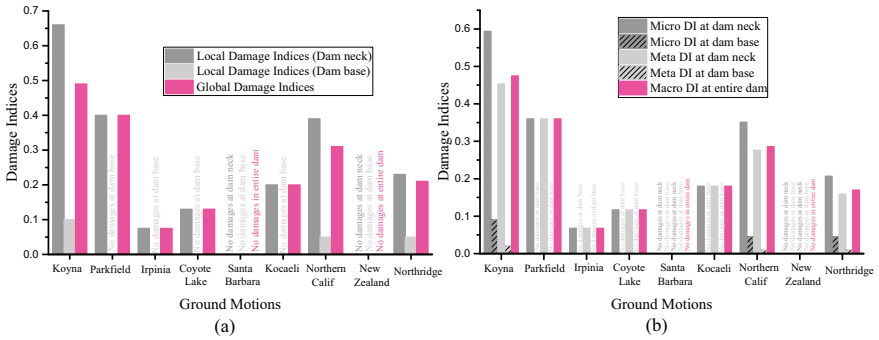

Fig. 6 Damage indices for the coupled dam-foundation system

Post-seismic structural failure in the forms of damage indices is shown in Fig. 6. Damage indices show failure at the local and global levels (Fig. 6a); while, Fig. 6b shows micro and meta DI at different paths and macro DI at the global level. Peak DI observes for Koyna time-histories followed by Parkfield, Northern Calif, etc. Both the DIs show nearly similar values; however, micro, meta and macro DIs consider all cracking patterns at a particular path; moreover; consideration of crest displacement response in its evaluation is advantageous over the other DIs.

4.2 Investigation of Input Ground Motions Using Different Parameters

Failure analysis of brittle material like mass concrete under dynamic loading depends on both intensity of loading and duration of the shaking [21]. Different ground motion characteristics and their effect on the structural response was studied [22–27]. Based on the obtained results, it is found that Koyna, Parkfield and Northern Calif trigger greater structural response and failure than other considered ground motions. Different ground motion parameters viz. PGA, total duration, bracketed duration, v_{max}/a_{max} ratio, arias intensity is considered. An attempt has been made to correlate the seismic response obtained in the previous section with the ground motion characteristics.

It was observed that Koyna (H + V) ground motion, followed by Parkfield, northern calif, etc. causes moderate failure in the dam and affects damage indices, displacement and dissipation energy response very severely. Therefore, in this current section, different ground motion parameters for Koyna (H), Parkfield (H) and Northern Calif (H) have been investigated to identify which ground motion characteristics viz. Amplitude, frequency contents and duration, are predominant for the increased seismic response. Figure 7 shows the comparison of different ground motion parameters for Koyna, Parkfield and Northern Calif ground motions.

Figure 7a shows the comparison between input time-histories between selected horizontal components of ground motions. The PGA of Koyna (0.41 g) is higher than Parkfield and Northern Calif. It is observed from Fig. 5b that tensile cracks initiate at 3.9 s, 4.2 s and 11.7 s for Koyna, Parkfield and Northern Calif, respectively which can be observed from Fig. 7a. Ground motion PGA better represents amplitude characteristics significantly [28]. It can be said that a higher dissipation energy response for Koyna may be as a result of its high peak ground acceleration.

The long duration of strong ground motion can have a strong influence on seismic damage as it can produce enough load reversals to cause substantial damage [28]. The comparison of absolute acceleration between selected ground motions is shown in Fig. 7b. Additionally, total and bracketed duration are shown. The bracketed duration is defined as the time between the first and last exceedance of a threshold acceleration [29]. The total duration of Parkfield (30.39 s) is higher; while, bracketed duration of Northern Calif (17.81 s) is higher than other considered ground motions. It is observed that the durational characteristics are predominant for the higher displacement response of Parkfield and Northern Calif.

Fourier spectra show frequency content of ground motion very clearly; while, v_{max}/a_{max} can be considered as a strong frequency content parameter [28]. Figure 7c shows the comparison between Fourier spectra of considered ground motions; also, v_{max}/a_{max} values are shown. Fourier amplitude spectra show peak value of Fourier amplitude for Koyna than other considered ground motions. The

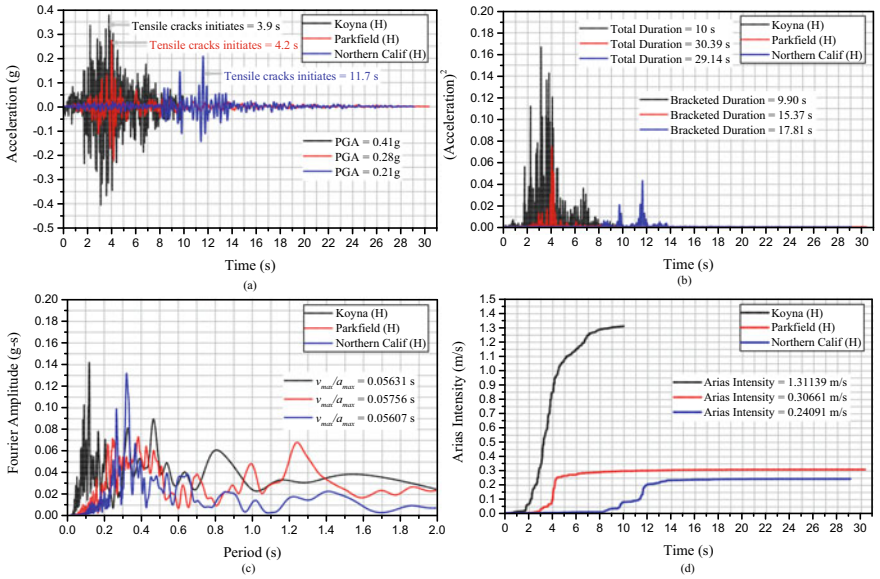

Fig. 7 Comparison of different ground motion parameters for Koyna, Parkfield and Northern Calif ground motions: **a** Acceleration time-history. **b** Absolute acceleration. **c** Fourier amplitude spectra. **d** Arias intensity

v_{max}/a_{max} for Koyna, Parkfield and Northern Calif are 0.05631 s, 0.05756 s and 0.05607 s, respectively. However, from v_{max}/a_{max} values, it is found that Northern Calif has higher frequency contents followed by Koyna and Parkfield. It is revealed that low-frequency content ground motions are significantly influencing the seismic response than high-frequency contents ground motions.

Figure 7d shows the comparison between arias intensity of the considered ground motions. Arias intensity shows amplitude, frequency contents and durational characteristics significantly [28]. The arias intensity of Koyna (1.31139 m/s) is greater than other considered ground motions. However, the effect of ground motion amplitude on the structural response can be better represented using the arias intensity parameter.

5 Conclusions

Seismic performance evaluation was done for coupled Koyna dam-foundation system using numerical investigation. Seismic analysis of Koyna dam was performed for nine ground motion records including Koyna ground motions and the results were presented in terms of tensile damage profile of dam, damage indicators and damage variables. Displacement and dissipation energy responses were observed and compared for the selected ground motions. Also, failure investigation is carried out using multi-variable damage indices which take into account the crack length, dissipation energy and maximum drift as the damage variables.

It is observed that the Koyna ground motion causes high structural failure and dissipation energy; however, Parkfield triggers peak crest displacement response. It shows the cumulative effect of amplitude, frequency contents and duration on the seismic response of a gravity dam. It is concluded that the damage indicator which considers dissipation energy and crest displacement for its evaluation better represents the failure states of the dam. It is also concluded that long-durational and low-frequency contents ground motions affect the displacement response of the dam; while high amplitude ground motions trigger more seismic failure and ultimately increase the dissipation energy in the dam. Arias intensity can be observed as a better amplitude parameter and it has a good correlation with the tensile failure and dissipation energy in the dam.

References

1. IS 1893 (Part 1) (2016) Criteria for earthquake resistant design of structures: general provisions and buildings. Bur. Indian Stand. Delhi
2. Nuss LK, Matsumoto N, Hansen KD (2012) Shaken, but not stirred—earthquake performance of concrete dams. United States Soc. Dams
3. Hariri-Ardebili MA, Saouma V (2015) Quantitative failure metric for gravity dams. Earthq Eng Struct Dyn 44:461–480. https://doi.org/10.1002/eqe.2481

4. Banon H, Veneziano D (1982) Seismic safety of reinforced concrete members and structures. Earthq Eng Struct Dyn 10:179–193. https://doi.org/10.1002/eqe.4290100202
5. Park YJ, Ang AHS (1985) Mechanistic seismic damage model for reinforced concrete. J. Struct. Eng. (United States) 111:722–739. https://doi.org/10.1061/(ASCE)0733-9445(1985)111:4(722)
6. Wang M-L, Shah SP (1987) Reinforced concrete hysteresis model based on the damage concept. Earthq Eng Struct Dyn 15:993–1003. https://doi.org/10.1002/eqe.4290150806
7. Powell GH, Allahabadi R (1988) Seismic damage prediction by deterministic methods: concepts and procedures. Earthq Eng Struct Dyn 16:719–734. https://doi.org/10.1002/eqe.4290160507
8. Cosenza E, Manfredi G (2000) Damage indices and damage measures. Prog Struct Eng Mater 2:50–59. https://doi.org/10.1002/(sici)1528-2716(200001/03)2:1%3c50::aid-pse7%3e3.3.co;2-j
9. Kamaris GS, Hatzigeorgiou GD, Beskos DE (2013) A new damage index for plane steel frames exhibiting strength and stiffness degradation under seismic motion. Eng Struct 46:727–736. https://doi.org/10.1016/j.engstruct.2012.07.037
10. Zhang S, Wang G (2013) Effects of near-fault and far-fault ground motions on nonlinear dynamic response and seismic damage of concrete gravity dams. Soil Dyn Earthq Eng 53:217–229. https://doi.org/10.1016/j.soildyn.2013.07.014
11. Alembagheri M, Ghaemian M (2013) Seismic assessment of concrete gravity dams using capacity estimation and damage indexes. Earthq Eng Struct Dyn 42:123–144. https://doi.org/10.1002/eqe.2196
12. Alembagheri M (2016) Earthquake damage estimation of concrete gravity dams using linear analysis and empirical failure criteria. Soil Dyn Earthq Eng 90:327–339. https://doi.org/10.1016/j.soildyn.2016.09.005
13. Ansari MI, Agarwal P (2016) Categorization of damage index of concrete gravity dam for the health monitoring after earthquake. J Earthq Eng 20:1222–1238. https://doi.org/10.1080/13632469.2016.1138167
14. Khosravi S, Salajegheh J, Heydari MM (2012) Simulating of each concrete gravity dam with any geometric shape including dam-water-foundation rock interaction using APDL. World Appl Sci J 17:354–363
15. Sarkar R, Paul D, Stempniewski L (2007) Influence of reservoir and foundation on the Nonlinear dynamic response of concrete gravity dams. J Earthq Technol 44(2)
16. Baker JW (2011) Conditional mean spectrum: tool for ground-motion selection. J Struct Eng 137:322–331. https://doi.org/10.1061/(ASCE)ST.1943-541X.0000215
17. Baker JW, Cornell CA (2006) Spectral shape, epsilon and record selection. Earthq Eng Struct Dyn 35:1077–1095. https://doi.org/10.1002/eqe.571
18. Jayaram N, Lin T, Eeri M, Baker JW (2010) a computationally efficient ground—motion selection algorithm for matching a target response spectrum mean and variance. Earthq Spectra 27:1–25. https://doi.org/10.1193/1.3608002
19. Baker JW, Lee C (2018) An improved algorithm for selecting ground motions to match a conditional spectrum. J Earthq Eng 22:708–723. https://doi.org/10.1080/13632469.2016.1264334
20. Peer Strong Motion Database (2000). http://peer.berkeley.edu/smcat
21. Zhang S, Wang G, Pang B, Du C (2013) The effects of strong motion duration on the dynamic response and accumulated damage of concrete gravity dams. Soil Dyn Earthq Eng 45:112–124. https://doi.org/10.1016/j.soildyn.2012.11.011
22. Wang G, Wang Y, Lu W, Yan P, Zhou W, Chen M (2016) A general definition of integrated strong motion duration and its effect on seismic demands of concrete gravity dams. Eng Struct 125:481–493. https://doi.org/10.1016/j.engstruct.2016.07.033
23. Wang G, Zhang S, Zhou C, Lu W (2015) Correlation between strong motion durations and damage measures of concrete gravity dams. Soil Dyn Earthq Eng 69:148–162. https://doi.org/10.1016/j.soildyn.2014.11.001

24. Wang C, Hao H, Zhang S, Wang G (2018) Influence of ground motion duration on responses of concrete gravity dams. J Earthq Eng 00:1–25. https://doi.org/10.1080/13632469.2018.1453422
25. Trifunac MD, Brady AG (1975) On the correlation of seismic intensity scales with the peaks of recorded strong ground motion. Bull Seismol Soc Am 65:139–162. https://doi.org/10.1193/1.1586022
26. Murphy JR, O'Brien LJ (1977) The correlation of peak ground acceleration amplitude with seismic intensity and other physical parameters. Bull Seismol Soc Am 67:877–915
27. Rathje EM, Faraj F, Russell S, Bray JD (2004) Empirical relationships for frequency content parameters of earthquake ground motions. Earthq Spectra 20:119–144. https://doi.org/10.1193/1.1643356
28. Kramer S (1996) Geotechnical earthquake engineering. Pearson Education, Inc.
29. Bolt BA (1969) Duration of strong motion. In: Proc. 4th world conf. earthq. eng., Santiago, Chile, pp 1304–1315

Development of Computer-Aided Educational Tool for Multi-Degree-Of-Freedom System

Suryakant K. Mahajan and Ranjan S. Sonparote

Abstract A computer-aided self-learning tool entitled CALMDOF is presented here. The concept of juxtaposition in a comparative visualization strategy is implemented in designing the user interface of the proposed tool. The main objective during the development was to help and enhance the understanding of the multi-degree-of-freedom system under vibration. This tool can be useful in blended teaching/learning of the multi-degree-of-freedom system in the course of the structural dynamic for undergraduate and postgraduate students.

Keywords Juxtaposition · Visualization · Pedagogy · Computer-aided learning · Multi-degree-of-freedom system

1 Introduction

The civil engineering curriculum comprises the structural dynamics course which acts as a base to understand earthquake engineering. Hence, conceptual understanding and envisioning the vibration response of structures leads to an improved understanding of earthquake engineering. The traditional chalk and talk format of the teaching of this course can place a substantial strain on the learner as this course needs them to imagine concepts and problem-solving skills.

Visualization allows the human mind to convey intricate spatial concepts that improve learner's observations and conclusions [1]. Hence, many academic disciplines have combined information visualization with education very effectively [2]. Computer-aided simulation, animations and interactive training have a significant share in civil engineering courses [3]. Considerable enhancement was seen in the learning of structural mechanics by implementing a finite element based computer simulation tool with interactive visualization and simulation [4, 5]. Rafiq and

S. K. Mahajan (✉) · R. S. Sonparote
Department of Applied Mechanics, Visvesvaraya National Institute of Technology, Nagpur, India
e-mail: rssonparote@apm.vnit.ac.in

B. Laishram and A. Tawalare (eds.), *Recent Advancements in Civil Engineering*, Lecture Notes in Civil Engineering 172,
https://doi.org/10.1007/978-981-16-4396-5_88

Easterbrook [6] attempted to enhance the understanding of structural behavior by implementing computer-assisted learning with a problem-based learning approach. The engineering dynamics course was supplemented by computer simulation and animation (CSA) suite [7, 8].

The implementation of computer-aided learning tools for structural dynamics was started by Paultre et al. [9] in the early days, by developing the tools for dynamic structural analysis problems. The study of linear and nonlinear behavior of structures in structural dynamics is simplified by ENGLTHA [10] and NONLIN [11] software. The structural dynamics course mainly includes the study of a single-degree-of-freedom (SDOF) system and multi-degree-of-freedom (MDOF) system. Maghrabi and Abbasy [12] developed an educational software tool to study the response of SDOF and MDOF systems. Sonparote and Mahajan [13] focused on the simplification of physical structure to its equivalent analytical model of the SDOF system using a computer-aided learning (CAL) tool.

The development of virtual laboratories in structural dynamics was started by Gao et al. [14] and Sim et al. [15] followed by the web-based virtual laboratories for the structural dynamics and earthquake engineering, due to easy accessibility of the internet [16, 17]. The MATLAB based educational tools were developed to study linear structural dynamics [18] and the seismic design of reinforced concrete buildings [19].

The study of the literature on the development of CAL tools related to structural dynamics course shows the primary focus on the visualization or animation of a single illustration at a time. Here, to perform a parametric study, the learner needs to vary a particular parameter and perceive the visual and numerical outcomes one after another. In such cases, learning through the comparative study of two successive visible results mostly depends on the remembrance of the learner [20], causing significant strain on the learner.

Commonly, it is seen that the humans instantly compare the two objects visually, placed side by side. This aids them in finding the similarities and the differences between these two objects. Earlier, the visualization has focused on the development of tools to examine distinct objects. Still, for the past few years, its emphasis is to design the system to compare the two objects using comparative visualization [20]. There are three types of comparative visualization strategies, namely: (1) juxtaposition, (2) superposition and (3) explicit encoding. These strategies are later investigated by Tominsky et al. [21] and suggested likely key methods for visual comparison as side by side interaction, shine-through interaction and folding interaction.

The juxtaposition comparative visualization strategy simplifies the comparison by placing the two objects next to the other or side by side. The juxtaposition visualization pedagogy can play an essential role in CAL tool development based on visual cognition for engineering courses. This can be implemented in structural dynamics by keeping the analysis outcomes (visual and numerical) of two vibrating systems side by side, as shown in Fig. 1. Here, the visual result can include the animation of systems vibration.

(a) placing images next to each other (b) placing oscillators next to each other

Fig. 1 Implementation of Juxtaposition [20]

Taking this idea forward, Mahajan and Sonparote [22] developed an educational tool called CALSIDOF, a computer-assisted learning tool based on juxtaposition comparative visualization pedagogy to aid the learning of the SDOF system. The CALSIDOF [22] was successfully implemented in the learning of structural dynamics course in the postgraduate program in structural engineering at the Applied Mechanics Department of Visvesvaraya National Institute of Technology, Nagpur, India. The students' feedback and the positives in the learning during this implementation, lead to the motivation to develop another educational tool to support the learning of the MDOF system, named CALMDOF (Computer-Assisted Learning of Multi-Degree-of-Freedom System).

The primary focus during the development of the CALMDOF tool is to implement juxtaposition comparative visualization pedagogy to study the response of the MDOF system under vibration. The learning objectives were set before the development of the CALMDOF, as given below.

1. To classify the variance between
   a) Free and forced vibrations.
   b) Undamped and damped vibrations
2. To compare the effect of structural parameters like lumped mass, structural stiffness and damping on the vibration response of the structure.
3. To predict and visualize the effect of external forcing functions like harmonic, periodic and arbitrary loading at different mass levels.
4. To distinguish the vibration response due to harmonic, periodic and arbitrary forcing functions.
5. To solve and evaluate the solutions of numerical exercises.

2 Software Description

Java [23] is used to develop the CALMDOF tool, due to its large third party open-source libraries for scientific calculations and graphics capabilities. It is also an object-oriented, platform-independent and open-source programming language.

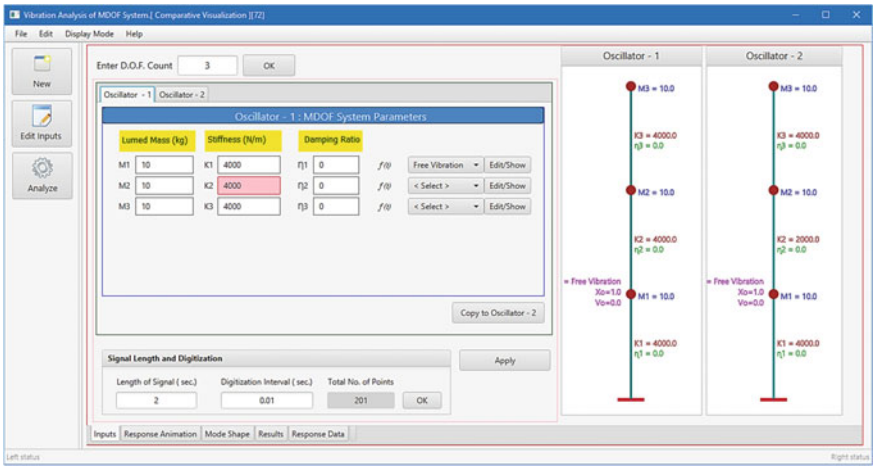

Fig. 2 Screenshot of the main window of CALMDOF showing Inputs tab

CALMDOF has a user-friendly intuitive graphical user interface (GUI). The juxtaposition strategy of comparative visualization is the primary basis for GUI design. This tool allows the user to enter the DOF count in the range of 2–6 only to display the legible graphics of the MDOF system and its animation. The main application window displays the three buttons, named New, Edit Inputs and Analyze. The New button opens the Inputs tab to enter new input parameters of the MDOF system. The Edit Inputs button facilitates the editing of existing input parameters and the Analyze button runs the analysis of the given MDOF system as shown in Fig. 2.

To start inputs, the user needs to specify the degree-of-freedom count in the Enter D.O.F. Count textbox and click on the OK button. This action will open the two tabs entitled Oscillator-1 and Oscillator-2, to enter the input parameters. These tabs include the text boxes to enter mass, stiffness, damping and forcing function drop-down-lists as per the DOF count, as shown in Fig. 2. The user needs to enter all the input data for Oscillator-1 in these textboxes. All the Oscillator-1 inputs can be copied to the Oscillator-2 tab by clicking the Copy to Oscillator-2 button or otherwise can be supplied manually.

The Forcing Function drop-down-list includes (1) Free Vibration, (2) Harmonic/Periodic Force, (3) and Arbitrary Force. The free and forced vibration parameters will be supplied through the Wave Generator dialog. The Wave Generator facilitates the inputs for free and forced vibration conditions on the respective mass level of the MDOF system as shown in Fig. 3.

The user interface of the Wave Generator is self-explanatory and user-friendly. The harmonic loading comprises cosine and sine wave presets, whereas, the non-harmonic cyclic loading comprises triangular and square wave presets. The generation of loading wave data is automatic, after supplying the force amplitude, time period and wave duration for the user-selected wave preset. The user can also

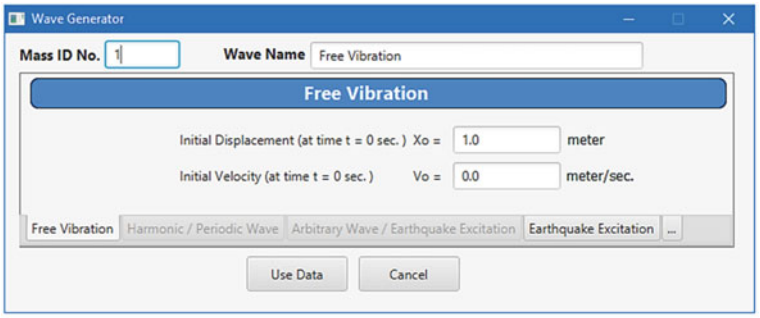

(a)Free vibration parameters input

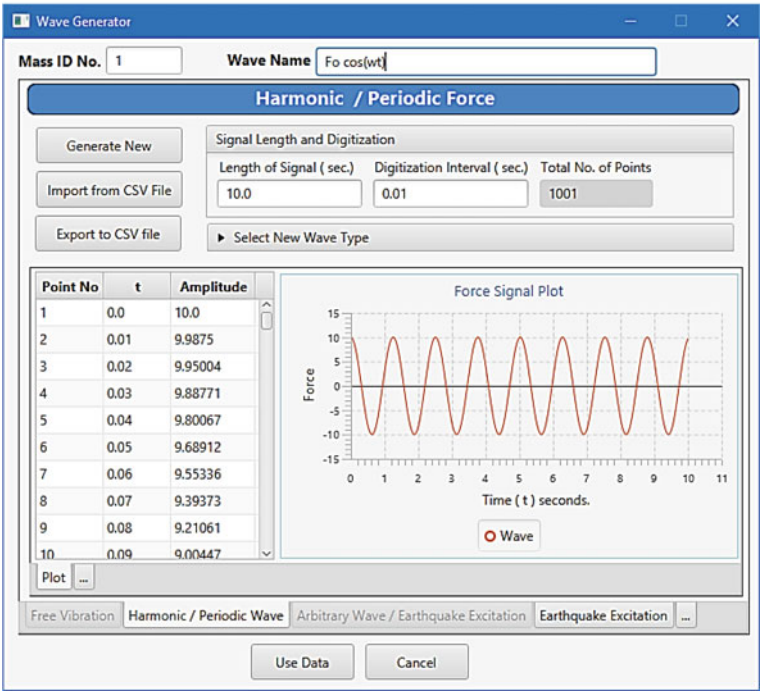

(b)Forced vibration parameters input

Fig. 3 Screenshot of Wave Generator dialog

create customized forcing data directly by entering the loading time history in the given table or by importing it in the prescribed format from another source. Users can see the generated loading wave in graphical format. The arbitrary loading and impulse time history can either imported or can be entered manually in tabular format. This generated wave loading is applied as a forcing function on the respective lumped mass level of the MDOF system. The user needs to supply

comparing parameter values separately in Oscillator-1 or Oscillator-2 tab to perform the comparative study.

The Analyze button performs the linear analysis of both the MDOF systems. The vibration response of the MDOF system is determined based on the solution of the basic equation of motion shown in Eq. 1.

$$[m]\{\ddot{u}\} + [c]\{\dot{u}\} + [k]\{u\} = \{f\} \tag{1}$$

where, $[m]$, $[c]$ and $[k]$ are mass matrix, viscous damping matrix and stiffness matrix, respectively and $\{\ddot{u}\}$, $\{\dot{u}\}$, $\{u\}$ and $\{f\}$are acceleration vector, velocity vector, displacement vector and force vector, respectively. The real-time animations of both oscillator's vibrations are displayed side by side as per the juxtaposition comparative visualization, as shown in Fig. 4. The displacement response plots for 'Oscillator-1' and 'Oscillator-2' at the same mass levels are superimposed and plotted adjacent to the respective mass levels.

The animation of vibration of oscillators and plotting of displacement response is simultaneous. The mode shapes are displayed in the Mode Shape tab. The user can play and stop the animation of the oscillator's vibration and the animation of mode shapes by clicking on the Play and Stop buttons, respectively. The analysis results, including input parameters and intermediate calculated values, are displayed side by side in the Result tab. The displacement time history values for both the oscillators are also displayed side by side in tabular format in the Response Data tab. The solution accuracy of CALMDOF was verified by resolving the solved numerical examples given in Rao [24] and Chopra [25], using CALMDOF.

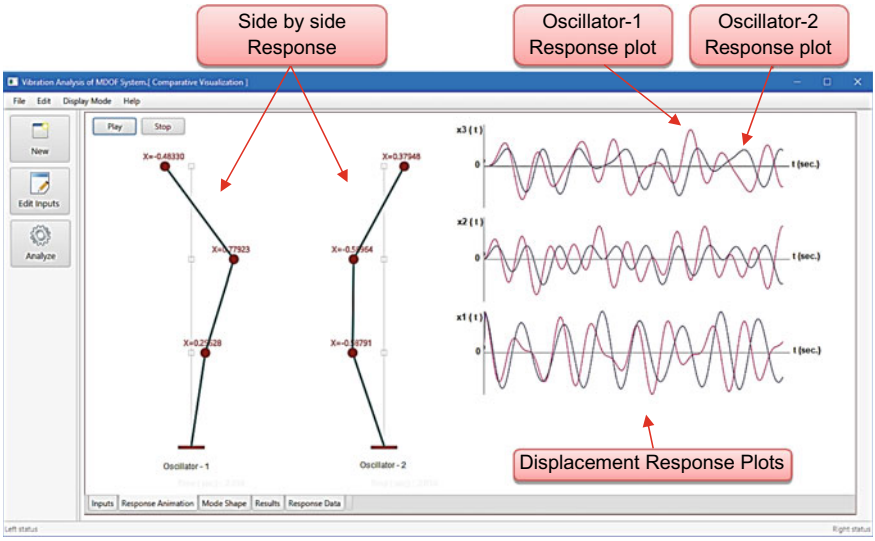

Fig. 4 Screenshot of Response Animation tab showing response animation and plot

3 Illustration of CALMDOF Tool

The CALMDOF offers flexibility in the modeling of the MODF system for the following parameters.

1. *Number of DOF*: The user can model the MDOF system from 2-DOF to 6-DOF.
2. *Stiffness and mass*: The user can provide variable values of stiffness and mass for every spring and lumped mass level, respectively.
3. *Initial displacement and initial velocity*: The user can provide variable values of initial displacement and initial velocity at every lumped mass.
4. *External force*: The user can assign specific external forces like a harmonic, periodic and arbitrary force to every lumped mass.

The "What if" studies can be performed by judicially selecting the parameters and recognizes its influence on the behavior of the MDOF system. The two illustrations of these parametric studies are briefly discussed in the following section.

3.1 Illustrative Example 1

Objective: To understand the effect of change in stiffness on displacement response.

Example Statement: An undamped free vibration of 3-DOF system is assumed from Rao [24] Example 6.21, having mass $m_1 = m_2 = m_3 = 10$ kg, stiffness $k_1 = k_2 = k_3 = 4000$ N/m, initial conditions at time $t = 0$ s., $u_1(0) = 1.0$ m, $u_2(0) = u_3(0) = 0$ and $v_1(0) = v_2(0) = v_3(0) = 0$. This undamped 3-DOF system is compared with another similar system except for stiffness $k_2 = 2000$ N/m.

CALMDOF Execution Procedure: The step-wise procedure to start the analysis and comparative study of the above 3-DOF systems is given below.

1. Click the New button and supply Enter DOF count equal to 3.
2. Enter all the input parameters like lumped mass, stiffness, damping and initial conditions in the respective text boxes of the Oscillator-1 tab (representing $k_2 = 4000$ N/m).
3. In the Oscillator-2 tab (representing $k_2 = 2000$ N/m), supply comparing parameter k_2 equal to 2000 and other inputs the same as to Oscillator-1.
4. Select Forcing Function as 'Free Vibration' for mass m_1 and click Edit/Show button to open the Wave Generator dialog. Supply Xo = 1 and Vo = 0 and click Use Data button (see Fig. 3a).
5. Click Analyze to perform the analysis.
6. After analysis, the vibration animation of Oscillator-1 and Oscillator-2 will be displayed side by side in the Response Animation tab, as shown in Fig. 5.
7. The displacement response plots at the respective mass levels are also displayed adjacent to it.

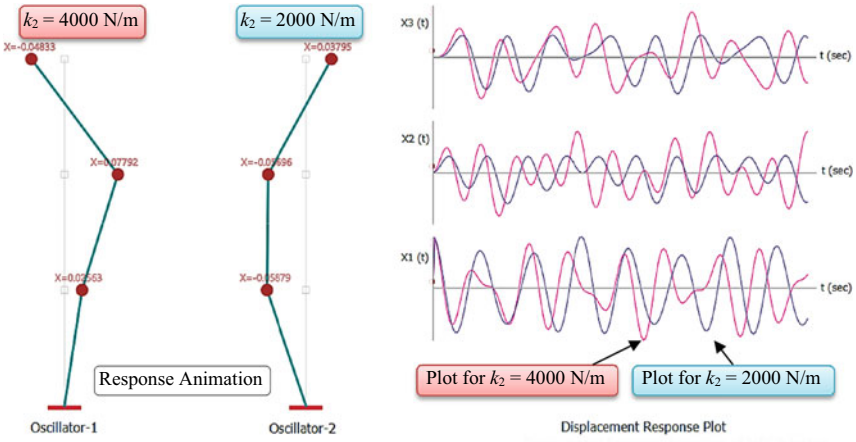

Fig. 5 Displacement response animation and plot for Example-1

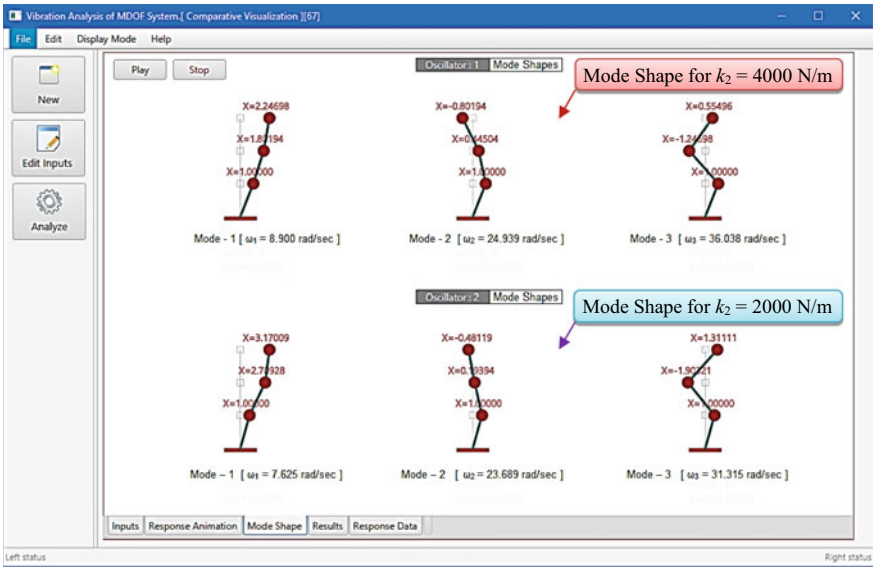

Fig. 6 Screenshot of the mode shape tab for Example-1

8. The mode shapes along with natural frequencies of Oscillator-1 and Oscillator-2 will be displayed in Mode Shapes tab as shown in Fig. 6.

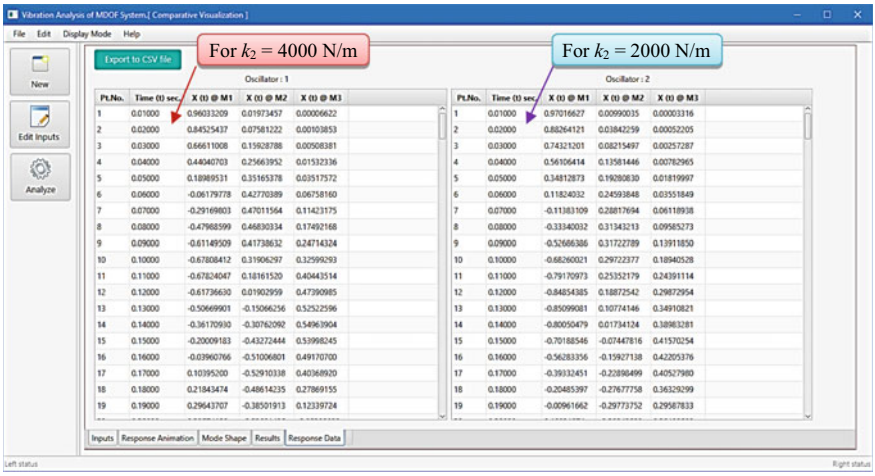

Fig. 7 Screenshot of response data tab for Example 1

9. The displacement responses for both oscillators are displaced in tabular format in the Response Data tab (see Fig. 7). At the same time, the intermediate calculated values are displayed in the textual report format under the Results tab.

Here, the side by side vibration animation and displacement response plots of oscillator-1 (representing $k_2 = 4000$ N/m) and oscillator-2 (representing $k_2 = 2000$ N/m) can benefit the students to effectually recognize the effect of change in stiffness on the response of the 3-DOF system through comparative visualization.

3.2 *Illustrative Example 2*

Objective: To understand the effect of change in the position of application of external harmonic force.

Example Statement: To understand the outcome of change in harmonic force application position, the 3-DOF system stated in Illustrative Example 1 is assumed, excluding the initial conditions. The initial conditions assumed in this example are $u_1(0) = u_2(0) = u_3(0) = 0$ and $v_1(0) = v_2(0) = v_3(0) = 0$. The total displacement response of this 3-DOF system desires to find for harmonic force, $f(t) = F_0 \cos(\omega t)$, where, $F_0 = 10$ N and $\omega = 5$ rad/s. under the following conditions.

(a) f (t) applied at mass level m_1.
(b) f (t) applied at mass level m_2.

CALMDOF Execution Procedure: The step-wise procedure to start the analysis and comparative study of the above 3-DOF systems is given below.

1. Enter the input parameters m_1, m_2, m_3, k_1, k_2 and k_3 in the respective text boxes of Oscillator-1 tab (representing $f(t)$ applied at mass level m_1).
2. Copy this input data to the Oscillator-2 tab (representing $f(t)$ applied at mass level m_2) by clicking Copy to the Oscillator-2 button.
3. Select Harmonic/Periodic force option from the respective mass level's '$f(t)$' list-box.
4. Generate the harmonic forcing wave for given amplitude and frequency by using the Wave Generator at m_1 level (see Fig. 3b) and m_2 level for Oscillator-1 and Oscillator-2, respectively.
5. Perform analysis by clicking the Analyze button.
6. The vibration animation of Oscillator-1 and Oscillator-2 will be displayed side by side along with the displacement response plot at all the mass levels, as shown in Fig. 8.

Here, the vibration animation (in juxtaposition) and displacement response plots (in superposition) of oscillator-1 and oscillator-2 can help the students to distinguish the effect of harmonic force at m_1 and m_2 on the response of the 3-DOF system through comparative visualization.

3.3 Illustrative Example 3

Objective: To understand the effect of change in the type of external non-harmonic periodic force.

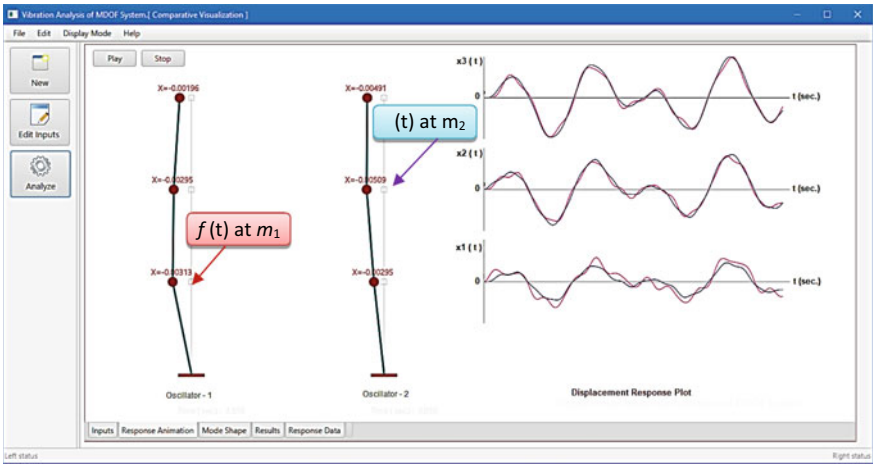

Fig. 8 Screenshot of response animation tab for Example 2

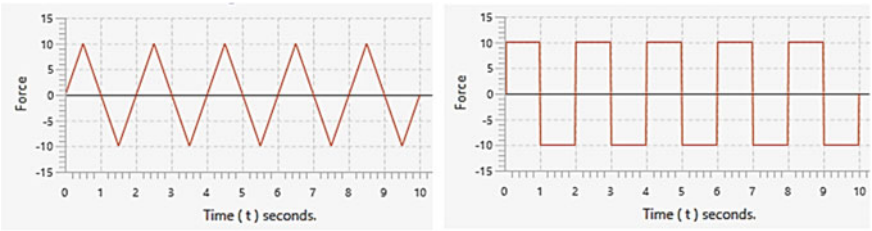

(a) Saw tooth wave forcing function (b) Square wave forcing function

Fig. 9 Non-harmonic periodic forcing function for Example 3

Example Statement: To understand the outcome of change in the type of non-harmonic periodic force wave, the 3-DOF system stated in Illustrative Example 1 is assumed, excluding the initial conditions. The initial conditions assumed in this example are $u_1(0) = u_2(0) = u_3(0) = 0$ and $v_1(0) = v_2(0) = v_3(0) = 0$. The total displacement response of this 3-DOF system desires to find for non-harmonic periodic force under the following conditions.

(a)Saw tooth wave f (t) with F_0 = 10 N, T = 2 s applied at mass level m_3 (see Fig. 9a).

(b)Square wave f (t) with F_0 = 10 N, T = 2 s applied at mass level m_3 (see Fig. 9b).

CALMDOF Execution Procedure: The step-wise procedure to start the analysis and comparative study of the above 3-DOF systems is given below.

1. Enter the input parameters m_1, m_2, m_3, k_1, k_2 and k_3 in the respective text boxes of Oscillator-1 tab. Select Harmonic/Periodic force option from the mass level m_3 '$f(t)$' list-box. Using Wave Generator, apply saw tooth wave periodic force with F_0 = 10 N, T = 2 s.
2. Like step 1, enter the mass and stiffness inputs in Oscillator-2 tab. Using Wave Generator, apply square wave periodic wave at mass level m_3.
3. Perform analysis by clicking the Analyze button.
4. The vibration animation of Oscillator-1 and Oscillator-2 will be displayed side by side along with the displacement response plot at all the mass levels, as shown in Fig. 10.

Here, the vibration animation and displacement response plots of oscillator-1 and oscillator-2 can aid the students to differentiate the effect of sawtooth wave periodic force and square wave periodic force of the same amplitude and time through comparative visualization.

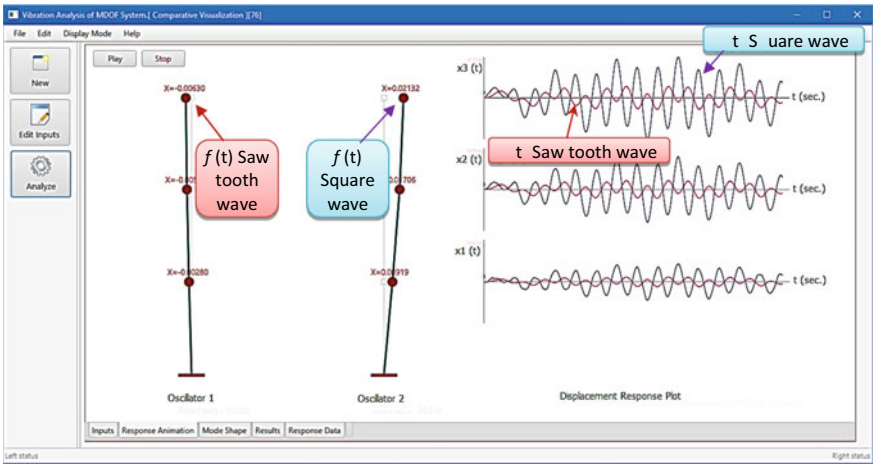

Fig. 10 Screenshot of response animation tab for Example 3

4 Conclusions

The main intention during the development of the CALMDOF tool was to help the student in conceptual learning through "What if" studies. The literature studied disclosed that visualization is playing an important role in designing the computer-assisted educational tool. Hence, the user interface of the CALMDOF tool is designed using a juxtaposition visualization strategy, which can be beneficial for the "What if" studies. The developed tool can be useful in enhancing the conceptual learning of a multi-degree-of-freedom-system in a blended teaching/learning environment. This may also help the students to increase their interest in learning the subject.

References

1. Birt J, Nelson J, Hovorka D (2015) Towards a pedagogy of comparative visualization in 3D design disciplines. In: Paper presented at Australasian Society for Computers in Learning and Tertiary Education ASCILITE 2015 conference, Perth, Australia, 29 Nov–2 Dec 2015
2. Hoffler TN (2010) Spatial ability: its influence on learning with visualizations—a meta-analytic review. Educ Psychol Rev 22:245–269
3. Philpot TA, Hall RH (2006) Animated instructional software for mechanics of materials: implementation and assessment. Comput Appl Eng Educ 14(1):31–43
4. Lee JY, Ahn SY (2014) Finite element implementation for computer-aided education of structural mechanics: frame analysis. Comput Appl Eng Educ 22(3):387–409
5. Lee JY, Ryu HR, Park YT (2014) Finite element implementation for computer-aided education of structural mechanics: Mohr's circle and its practical use. Comput Appl Eng Educ 22(3):494–508

6. Rafiq MY, Easterbrook DJ (2005) Using the computer to develop a better understanding in teaching structural engineering behavior to undergraduates. J Comput Civil Eng 19(1):34–44
7. Jacquot RG, Smith DA, Whitman DL (1995) A software package to enhance the teaching of engineering dynamics. Comput Appl Eng Educ 3:21–28
8. Fang N (2012) Using computer simulation and animation to improve student learning of engineering dynamics. Procedia Soc Behav Sci 56:504–512
9. Paultre P, Leger P, Proulx J (1991) Computer-aided education in structural dynamics. J Comput Civil Eng 5(4):374–390
10. Clarke RP (2011) ENGLTHA: An educational tool for earthquake nonlinear and general linear dynamics. Comput Appl Eng Educ 19(1):97–106
11. Charney FA, Barngrover B (2004) NONLIN: software for earthquake engineering education. Paper presented at Structures Congress; Tennessee, USA, 22–26 May 2004
12. Maghrabi MN, Abbasy AA (2014) Educational computer program for simulating behaviour of structures under dynamic loads. In: Paper presented at 2014 Zone 1 conference of the American Society for Engineering Education, Connecticut, USA, 3–5 Apr 2014
13. Sonparote RS, Mahajan SK (2018) An educational tool to improve structural dynamics through idealization of physical structure to analytical model. Comput Appl Eng Educ 26 (5):1270–1278
14. Gao Y, Yang G, Spencer BF Jr, Lee GC (2005) Java-powered virtual laboratories for earthquake engineering education. Comput Appl Eng Educ 13(3):200–212
15. Sim SH, Spencer BF Jr, Lee GC (2009) Virtual laboratory for experimental structural dynamics. Comput Appl Eng Educ 17(1):80–88
16. Munipala A, Pasupuleti VDK, Ramancharla PK (2012) Structural dynamics virtual laboratory: a learning toolkit for young engineers and practicing professionals. In: Paper presented at 15th World conference on earthquake Engineering, Lisbon, Portugal
17. Christos GP, George DM (2016) A Web-based educational software for structural dynamics. Comput Appl Eng Educ 24(4):599–614
18. Brownjohn JMW, Pavic A (2008) NDOF: A MATLAB GUI for teaching and simulating structural dynamics. In: Paper presented at: 26th international modal analysis conference (IMAC XXVI); 2008. Orlando, Florida, USA
19. Katsanos EI, Taskari ON, Sextos AG (2014) A Matlab-based educational tool for the seismic design of flexibly supported RC buildings. Comput Appl Eng Educ 22(3):442–451
20. Gleicher M, Albers D, Walker R, Jusufi I, Hansen CD, Roberts JC (2011) Visual comparison for information visualization. Inf Vis 10(4):289–309
21. Tominski C, Forsell C, Johansson J (2012) Interaction support for visual comparison inspired by natural behavior. IEEE T Vis Comput Gr 18(12):2719–2728
22. Mahajan SK, Sonparote RS (2018) Implementation of comparative visualization pedagogy for structural dynamics. Comput Appl Eng Educ 26(5):1894–1902
23. Schildt H (2017) Java: the complete reference. McGraw Hill Education, New Delhi
24. Rao SS (2010) Mechanical vibrations. Prentice Hall, Upper Saddle River, NJ
25. Chopra AK (2012) Dynamics of structures-theory and applications to earthquake engineering. Prentice Hall Inc., Upper Saddle River, NJ

Effect of Material Models on Dynamic Behavior of Reinforced Concrete Slabs Exposed to Blast Loading

Manmohan Dass Goel, Shivani Verma, Sandeep Panchal, and Nikhil Sirdesai

Abstract Numerical simulations for structures using advanced material models have become more systematic and reliable in recent times. This is more important for loadings resulting from explosion as it is extremely difficult to carry out real-scale field tests. Considering all the hardware capabilities of modern computers, the computation time for the analysis of structures under the blast load can be reduced significantly. In the present study, an effort is made to perform the numerical simulation of reinforced concrete slab under blast load to determine the dynamic response of reinforced concrete slab considering four different material models. The analysis is carried out with the focus on the study of the effectiveness of mesh size and material model on central point displacement. Finally, recommendations are suggested about the use of the available material models on the behavior of concrete under such extreme loadings.

Keywords Blast loading · ConWep · FE analysis · ABAQUS/Explicit® · Concrete damage plasticity · Cap plasticity · Drucker–Prager model

M. D. Goel (✉)
Department of Applied Mechanics, Visvesvaraya National Institute of Technology (VNIT), Nagpur, Maharashtra 440 010, India
e-mail: mdgoel@apm.vnit.ac.in

S. Verma · S. Panchal · N. Sirdesai
Department of Mining Engineering, Visvesvaraya National Institute of Technology (VNIT), Nagpur, Maharashtra 440 010, India
e-mail: sandeeppanchal@mng.vnit.ac.in

N. Sirdesai
e-mail: nikhilsirdesai@mng.vnit.ac.in

B. Laishram and A. Tawalare (eds.), *Recent Advancements in Civil Engineering*, Lecture Notes in Civil Engineering 172,
https://doi.org/10.1007/978-981-16-4396-5_89

1 Introduction

Blast/explosions have become very frequent in the recent time, and this field of research has become very important for proper analysis and design of structures in order to safeguard the lives. Blast not only results in the loss of property and life but also leads to long-term effects over the economy of a country. While studying the impact of blast on the structures, it becomes very important to see how different material behaves when exposed to the blast loading. Since concrete is among the major construction material in the structures, it becomes essential to study about the behavior of concrete under such loading conditions. It is a well-known fact that performing experimental test to analyze the effect of blast loading is quite expensive in terms of capital and time. Thus, many experimental tests cannot be performed to investigate concrete behavior when it comes to the parametric study to understand the concrete behavior. The reason is attributed to the fact that even the small change in any parameter would cost a lot of money to perform the test again. Due to this major disadvantage of experimental analysis, the need of numerical simulation and modeling got raised. Numerical modeling of any problem can be performed with meager resources as compared to the experimental tests, and it takes lower overall time to get the results of any problem. There exist several softwares which can perform the dynamic analysis, for example, ABAQUS®, LS-DYNA®, AutoDyn®, etc., for structures under blast loading.

In this study, ABAQUS/Explicit® [1] is used to analyze the effect of blast loading on a concrete slab using four different material models of concrete. Many researchers had effectively investigated the failure of various RC elements subjected to the blast by carrying out experimental tests, and most of these are covered in book by Bangash and Bangash and Karauthammer [2, 3]. In the past, several researchers used different material model in their analysis, but a quantitative comparison is still missing particularly under blast loading [4–7]. Moreover, in most of these studies, CDP material model is used to model the concrete. However, there exist many other material models for modeling the concrete behavior and these need to be explored for arriving comparable and acceptable solutions with minimum input parameters. Thus, the current study explains the numerical model technique and evaluates the response of RC slab with various available material models when exposed to the blast loading. Herein, to gain the better knowledge of the behavior of concrete structure, the finite element (FE) analysis is carried out using ABAQUS/Explicit® [1] by employing various nonlinear material models of concrete.

2 Three-Dimensional Finite Element (FE) Modeling and Model Geometry

2.1 FE Modeling of Reinforced Concrete (RC) Slab

The FE models of RC slab of size 1 m × 1 m × 0.12 m is developed with the help of 3-D part option available in ABAQUS/Explicit® using brick element with eight nodes having hourglass control, reduced integration and distortion control, i.e., C3D8R elements available in ABAQUS/Explicit® element library [1]. The reinforcement of concrete slab is modeled using beam elements, i.e., B31, and is embedded in RC slab to act as a one unit. Appropriate bonding between reinforcement bars and concrete is secured by using constraints with embedded region selection accessible in ABAQUS/Explicit® with reinforcement as embedded region and slab as host region.

2.2 Slab Geometry

The geometry and mesh details of slab are shown in Fig. 1a, b, respectively. The details of the reinforcement in the concrete slab and the location of the blast explosion are shown in Fig. 2a, b, respectively.

3 Material Model and Properties

Behavior of concrete under such extreme loading depends on many parameters. It is important to mention that in order to use any material model effectively in FE investigation, input of many parameters for that particular material model is required and it demands the need for detailed investigation of such parameters

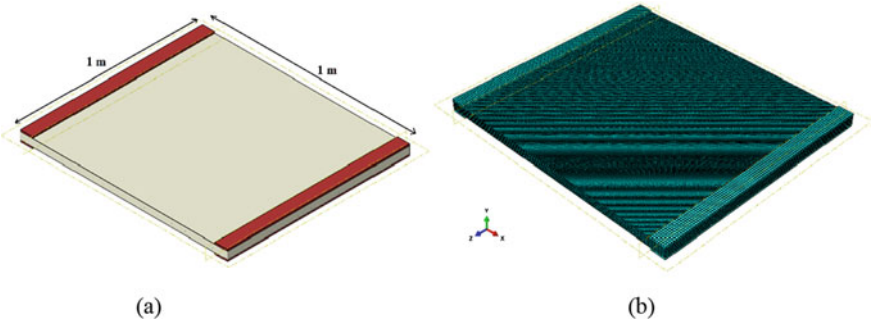

Fig. 1 **a** Geometry of the slab and **b** typical mesh details of the slab

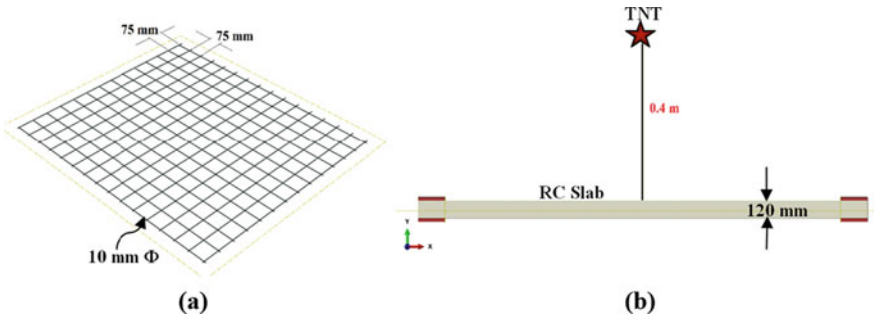

Fig. 2 **a** Reinforcement details of the slab and **b** location of the blast

under identical test conditions. This is almost impossible to be carried out by one group of researchers. But many researchers did carry out studies in marginally different circumstances and hence, these parameters can be used with some marginal level of variation. Considering this limitation, the available data for all the considered material models, with marginal variation within these, are used to show the effectiveness of such investigation.

3.1 FE Modeling of Reinforced Concrete (RC) Slab

3.1.1 Drucker–Prager (D–P) Material Model

This material model is one of most commonly material model used for modeling soil and concrete. Figure 3 shows behavior of this model, and it is expressed by Eq. 1.

$$f_{DP} = \sqrt{J_{2D}} - \alpha I_1 - k \tag{1}$$

where $\sqrt{J_{2D}}$ represents the second invariant of deviatoric tensor and α and k are material constant. In the present study for D–P material model, values of angle of friction = 30°, flow stress ratio = 1 and dilation angle = 20° are used. The plastic behavior of concrete is taken from the study carried out by Mokhatar and Abdullah [4].

3.1.2 Cap Plasticity Material Model

In this model, the elliptic strain-hardening cap model is used to define plastic volumetric change in the material. Behavior of this model is defined as,

$$f_{PC} = (I_1 - l)^2 + R^2 J_{2D} - (x - l)^2 \tag{2}$$

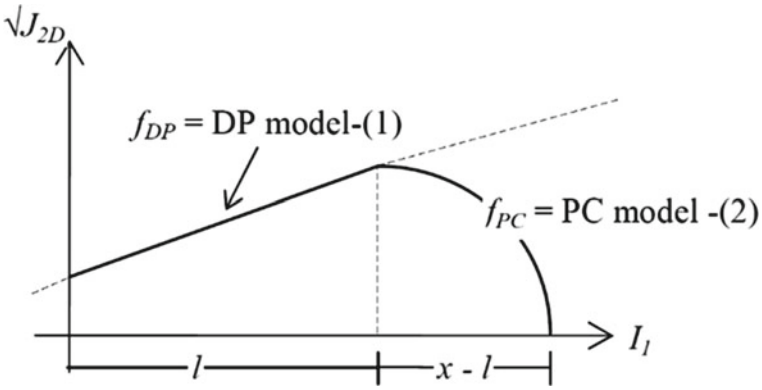

Fig. 3 Drucker–Prager material model

Here, l represents initial cap yield surface and R is ratio of major to minor axis of elliptic cap, which is a function of l. For defining this material, values of material cohesion = 4.71 MPa, angle of friction = 51°, cap eccentricity parameter, $R = 0.65$, initial cap yield surface position parameter = 0.0011, flow stress ratio = 1 and strain rate effect factor = 1.5 are used [4].

3.1.3 Simplified Concrete Damage Plasticity Model

In concrete damage plasticity models, plastic hardening strain in compression $\tilde{\varepsilon}_c^{pl}$ played an important role in finding the relation between compressive strength and the damage parameters of concrete as follows:

$$\sigma_c = (1 - d_c)E_0\left(\varepsilon_c - \tilde{\varepsilon}_c^{pl}\right) \tag{3}$$

The present study has used Kent and Park [8] parabolic constitutive model for unconfined concrete, which is expressed by the following equation

$$\sigma_c = \sigma_{cu}\left[2\left(\frac{\varepsilon_c}{\varepsilon_c'}\right) - \left(\frac{\varepsilon_c}{\varepsilon_c'}\right)^2\right] \tag{4}$$

where σ_c and ε_c are nominal compressive stress and strain, respectively. Further, σ_c and ε_c' are ultimate compressive strength and unconfined cylinder specimen strain, respectively. In concrete damage plasticity models, plastic hardening strain in tension $\tilde{\varepsilon}_t^{pl}$ is derived as follows:

$$\sigma_t = (1 - d_t)E_0\left(\varepsilon_t - \tilde{\varepsilon}_t^{pl}\right) \tag{5}$$

In this paper, 1% of tensile strength is considered during the analysis regardless of the reasonable condition to prevent numerical instability. Properties of material used in this analysis are adapted from the Hafezolghorani et al. [9].

3.1.4 Concrete Damage Plasticity (CDP) Model

In this study, CDP model is used to predict the blast behavior of RC slabs. In this model, the essential parameters are suitably studied so as to simulate the reliable response of structural system. The function of this model is expressed in Eqs. (6) and (7).

$$f_{CDP} = \omega \left(\sqrt{3J_{2D}} + \alpha I_1 + \beta(\sigma_{\max}) - \gamma - (\sigma_{\max}) \right) \tag{6}$$

with

$$\omega = \frac{1}{1-\alpha} \tag{7}$$

where β and γ represent dimensionless constants. Essential parameters used in this model for both tension and compression are adapted from Mokhatar and Abdullah [3].

3.2 Material Properties for Reinforcement Bars

In current nonlinear simulation, high-strength rebars having high yield strength of 500 MPa have been used as the reinforcement for the concrete slab for the present analysis. It has Young's modulus of 200 GPa and density of 7850 kg/m^3 with a Poisson's ratio of 0.33 [4].

4 Results and Discussion

In the present study, comparison of material models available in ABAQUS/Explicit® to model the concrete behavior is performed for RC slab under blast loading. Concrete is modeled as three-dimensional solid deformable element, whereas reinforcement is modeled as wire element. The basic FE model of slab is taken from the study proposed by Wang et al. [5]. They carried out experimental evaluation of the RC slab of size 1 m × 1 m × 0.12 m. Based on their experiments, displacement value at the mid-point of the RC slab was found to be 35 mm for 0.46 kg of TNT. Thus, in this numerical study, we used the same size and TNT

location for comparison of the four different material models available for modeling the concrete behavior under such extreme loadings and the results of their filed tests will be used for comparison of results obtained using various material models.

A reinforced concrete slab has been exposed to the blast loading in the current study. Mesh effectiveness study has been also performed to see the impact of mesh density on the results. An individual analysis for all the models considered in the present study has been carried out in terms of mesh size. For mesh study, element sizes of 15 units, 10 units and 5 units are considered. The displacement–time history for TNT explosion of 0.46 kg for DP, CP, SCDP and CDP material models for three different mesh densities is shown in Fig. 4. It can be seen from this figure that D–P model is showing least displacement for all the mesh density considered in this study, whereas in CDP material model, peak displacement is close to the field results of Wang et al. [5] for a mesh density of 5 units. Further, in SCDP model, results are higher and lower than the field results of Wang et al. [5] for mesh density of 5 and 10 units. Among all the models considered, close agreement is with the CDP model for 5 units of mesh density. Thus, it is very important to consider a suitable material model and its effective mesh density. Based on mesh density, CDP model performs better in this study.

The displacement–time history of the slab under consideration for different concrete models for different mesh sizes is shown in Fig. 5. In this study, mesh

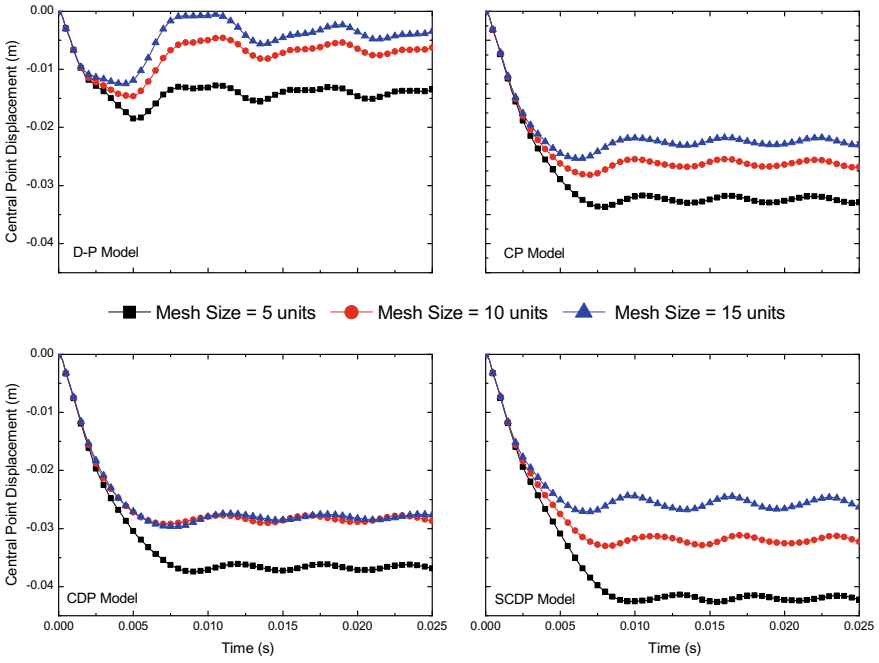

Fig. 4 Variation of displacement with time for **a** D–P, **b** CP model, **c** CDP and **d** SCDP material models

element size of 15 units, 10 units and 5 units is considered. It can be seen from Fig. 5 that D–P material model was least realistic among other concrete models considered in this study. It can also be seen that concrete modeled with DP model also indicates larger vibrations after the peak displacement. CP model indicates displacement values close to the experimental results reported by Wang et al. [4]. Further, SCDP model with reducing element size up to 5 units overestimates the displacement values. In CDP model, the rate to increase in the displacement values with reduction of element size was intermediate between the CP and SCDP model. As it can be seen from Fig. 5 that the results of CDP model were similar to CP and SCDP model when the mesh sizes were 15 units and 10 units, it can be concluded that the reducing mesh size up to 10 units from 15 units will not be sufficient enough to seen get the converged results. It can further be seen that with element

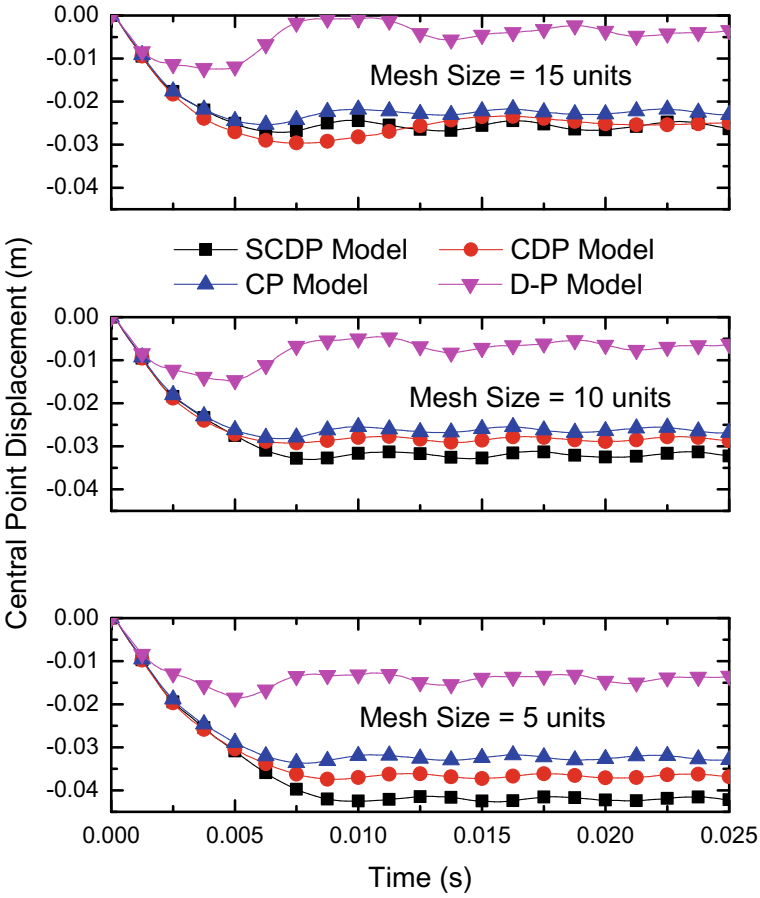

Fig. 5 Variation of displacement with time for **a** D–P, **b** CP model, **c** CDP and **d** SCDP material models for mesh size of 15, 10 and 5 units

Table 1 Peak displacement for different concrete models and corresponding mesh size

Concrete model	Experimental results of Wang et al. [4] (mm)	Element size		
		15 units (mm)	10 units (mm)	5 units (mm)
DP	35	12.46	14.73	18.53
CP		25.34	28.20	33.70
CDP		29.64	29.26	37.43
SCDP		27.10	33.03	

size of 5 units the CDP model gives quite realistic results among all other models in comparison with experimental results of Wang et al. [5]. The peak displacement value at the mid-point of the slab for all the models considered in this study is shown in Table 1. From the results, it has been seen that when the mesh size is reduced, the results of all models considered approach the experimental value.

5 Conclusions

In this study, reinforced concrete behavior for four different concrete models has been studied considering the effect of mesh and the following conclusions are drawn from the study:

1. CDP model gives the most realistic results among the other concrete model. SCDP and CP models can also be used to predict the behavior of the concrete under blast loading as these two models also provide considerable results. However, DP model cannot be used for blast loading prediction as the results were very unrealistic.
2. As the element size decreases, the accuracy of the results also increases. In the current study, it is concluded that concrete having 5 units element size gives the most realistic results.

References

1. ABAQUS/Explicit® (2018) User's manual. Dassault Systemes Simulia Corporation, France
2. Bangash MYH, Bangash T (2005) Explosion-resistant buildings: design, analysis, and case studies. Springer Science & Business Media
3. Krauthammer T (2008) Modern protective structures. CRC Press
4. Mokhatar SN, Abdullah R (2012) Computational analysis of reinforced concrete slabs subjected to impact loads. Int J Integr Eng 4(2):70–76
5. Wang W, Zhang D, Lu F, Wang S, Tang F (2013) Experimental study and numerical simulation of the damage mode of a square reinforced concrete slab under close-in explosion. Eng Fail Anal 27:41–51

6. Li J, Wu C, Hao H, Su Y, Liu Z (2016) Blast resistance of concrete slab reinforced with high performance fibre material. J Struct Integrity Maintenance 1(2):51–59
7. Yao S, Zhang D, Chen X, Lu F, Wang W (2016) Experimental and numerical study on the dynamic response of RC slabs under blast loading. Eng Fail Anal 66:120–129
8. Kent DC, Park R (1971) Flexural members with confined concrete. J Struct Div 97(7):1969–1990
9. Hafezolghorani M, Hejazi F, Vaghei R, Jaafar M, Bin S, Karimzade K (2017) Simplified damage plasticity model for concrete. J Int Assoc Bridge Struct Eng 27(1):68–78

Structural Health Monitoring Using Multifractal Cross-correlation Analysis

Ayisha Anwar and S. Adarsh

Abstract Structures undergo deterioration of strength after construction due to loading and environmental impacts. Structural health monitoring (SHM) is of paramount importance to ensure the safe functioning of structures, especially after natural disasters. The introduction of smart structures increased the potential of structural health monitoring (SHM) process. This study proposes a novel multifractal cross-correlation analysis (MFCCA)-based framework for SHM. Damage diagnosis was carried out by measuring the acceleration responses from a four-storey analytical structure, developed in SAP2000. The study determined the damage location through MFCCA method by cross-correlating the responses from various floors with that of the ground floor. A damage index (DI) is propounded to investigate the potential of MFCCA approach of health monitoring through proper quantification of the damage location estimates. The damage index had quantified the MFCCA results, which reinforced the reliability of this new health monitoring technique. It is evident from the results that the MFCCA approach of damage location has effectively detected damage, even with the interference of noise into the signals.

Keywords Multifractal · Damage · Cross-correlation · Structural health monitoring

1 Introduction

Structural health monitoring (SHM) provides information about the health status of the structure, which can be impacted by the loading in the structure, deterioration, and environmental aspects. The knowledge about the condition of the structure further evaluates the need of retrofitting, which helps in effective utilization of resources. SHM becomes more pronounced especially after catastrophic events,

A. Anwar (✉) · S. Adarsh
Department of Civil Engineering, TKM College of Engineering, Kollam, India
e-mail: adarsh1982@tkmce.ac.in

B. Laishram and A. Tawalare (eds.), *Recent Advancements in Civil Engineering*, Lecture Notes in Civil Engineering 172,
https://doi.org/10.1007/978-981-16-4396-5_90

such as earthquakes, floods, cyclones, etc., to ensure the safety and the utility of building thereafter. SHM mainly focuses on damage detection, determination of damage severity, and estimation of life of building under the present health condition. Vibration-based SHM techniques had made a new milestone in the field of health monitoring, which can assess the global condition of the structure effectively [1]. These techniques involve determination of dynamic properties such as natural frequency mode shape and modal damping [2–4]. Recent developments in vibration-based SHM includes the use of multiscale entropy [1], detrended fluctuation analysis (DFA), detrended cross-correlation analysis (DCCA) [5], multifractal detrended cross-correlation analysis (MFDXA) [6, 7], and multi-task sparse Bayesian learning [8].

Mandelbrot described *fractal* as "a rough or fragmented geometric shape that can be split into parts, each of which is a reduced-size copy of the whole" [9]. Later on, fractal analysis was found to be an effective tool in signal processing due to its ability to interpret complex, irregular, and natural phenomenon [10]. Multifractal analysis of time series has gained considerable attention among the researchers of the fields such as biomedicine [11], finance [12], and geophysics [10]. Peng et al. [11] proposed DFA demonstrating its usefulness on heartbeat time series. Kandelhardt et al. [10] propounded the multifractal extension of DFA called multifractal detrended fluctuation analysis (MF-DFA). Many other algorithms were also defined to explain the cross-correlations between time series such as DCCA [13] and multifractal cross-correlation analysis (MFCCA) [14]. MFCCA is superior to other methods as it accounts proper sign for co-variance [14]. Its potential to describe the complex and irregular phenomena leads to wider applicability and its enormous unexplored potential in the field of structural engineering is to be attended by the research community. Lin and Fajri [5] explored the potentiality of DCCA for evaluating damage in the structure. The objectives of this study are: (i) to present MFCCA based framework for location of the unhealthy section of the structure under vibration measurement; (ii) to check the efficacy of MFCCA based SHM procedure under the effect of noise.

2 Methodology

The first step of the MFCCA-based evaluation of SHM approach is developing a numerical or experimental model. The structure is excited and the responses of different floors are recorded under different damage conditions. Subsequently, MFCCA is applied to find the damage location by cross-correlating the signals of ground floor with that of other floors. The efficacy of this can be quantified in terms of damage index (DI). The complete procedure provided in Fig. 1. The details of MFCCA algorithm are provided in the following section.

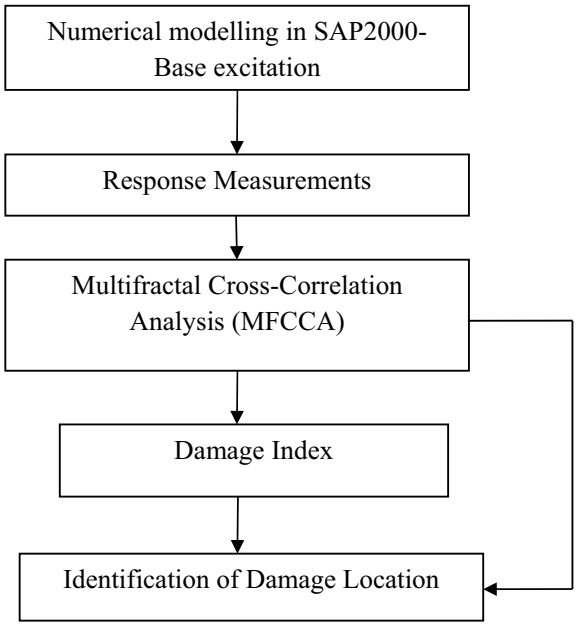

Fig. 1 Flowchart of proposed method of structural health monitoring

2.1 Algorithm of MFCCA

Unlike the other existing multifractal cross-correlation analysis, MFCCA proposed by Oswiecimka et al. [12], accounts for proper incorporation of the sign of the cross-covariance. The procedure for MFCCA is described below:

1. For the time series $x(i)$ and $y(i)$ having equal length N. The time series are converted to random walk by subtracting their respective mean values (Eqs. 1 and 2).

$$x(i) = \sum_{k=1}^{i} [x_k - x_{mean}] \tag{1}$$

$$y(i) = \sum_{k=1}^{i} [y_k - y_{mean}] \tag{2}$$

where, i= 1, 2, 3, …, N.

2. Both the profiles are divided into N_s non-overlapping segments, where N_s = int (N/s) and stands s for scale. N may not be always a multiple of s, so the procedure is done for total of 2 N_s segments.

3. The local trend for each divided segment is found out using least square fitting and is eliminated to determine the covariance as per Eq. 3:

$$F_{xy}^2 = \frac{1}{s}\sum_{i=1}^{s}\left\{x[(v-1)s+i] - x_{v(i)}^m\right\} * \left\{x[(v-1)s+i] - y_v^m(i)\right\}. \quad (3)$$

where $v = N_s + 1, \ldots, 2N_s$; $x_v{}^m(i)$ and $y_v{}^m(i)$ are the local trends in segment v. Repeat the procedure for various scales s and q values.

4. The MFCCA fluctuation function is found out as per Eq. 4.

$$F_{\mathrm{MFCCA}}(s) = \left[\frac{1}{2N_s}\sum_{i-1}^{2N_s}\mathrm{sign}(F_{xy}^2(v,s))\left|F_{xy}^2(v,s)\right|\right]^{\frac{1}{2}}. \quad (4)$$

The log–log plot of detrended covariance versus scale derived through MFCCA was utilized to identify the damage location of the steel structure.

2.2 Damage Index (DI)

To strengthen the efficacy of estimation of damage location through MFCCA a damage index is introduced. It provides quantification of MFCCA results of damage location. The area between the MFCCA fluctuation function plots is taken as the measure for calculating the damage index. The MFCCA results of undamaged condition serve as the reference. The area between the curves of adjacent floors for undamaged case for a structure with N floors is given by Eq. 5.

$$UD = \{UD_1, UD_2, UD_3, \ldots, UD_N\} \quad (5)$$

where UD_1 represent the behavior of the first floor under undamaged condition and is obtained by subtracting the logarithmic value of detrended covariance of first floor from that of ground floor (previous floor) for different scales. Similarly, the area between the adjacent curves for damaged case for a structure with N floors is given by Eq. 6.

$$D = \{D_1, D_2, D_3, \ldots, D_N\} \quad (6)$$

where D_1 represent the behaviour of the first floor under damaged condition.

The damage index of each floor was obtained by summation of difference between the values of undamaged case UD_i and damaged case D_1 for various scales, where i varies from 1 to N.

3 Model Structure and Numerical Modelling

The time history analysis was performed in the four-storey structure in order to obtain the structural response of each storey for 40 s under different damage cases. The structural response captured from SAP2000 was imported to MATLAB for evaluation of damage through MFCCA and damage index.

3.1 Numerical Modelling

A single-bay, four-storey steel structure was developed in SAP2000 software with height 1.06 m, length 1.32 m, and width 0.92 m for a storey. The columns and the beams were designed as steel plates measuring 75 × 50 mm^2 and 70 × 100 mm^2, respectively [15]. Two L-shaped steel bracings of 65 × 65 × 6 mm size are provided in each storey. A 500 k- load was added additionally in each floor. The structure was excited with a time history function of El-Centro Earthquake.

The damage was introduced in the structure by means of removal of bracings and results in stiffness reduction. The different damage cases considered in this study are tabulated in Table 1. The undamaged case depicted in Fig. 2a, serve as the reference pattern for the analysis. For the case of first floor damage (1F), it means that the damage is created in the structure by removing the two bracings in the first floor only. For introducing damage in first and second floor (12F), all the bracings in the first and second floors are removed simultaneous.

4 Results and Discussion

4.1 Identification of Damage Location

The detrended covariance derived through MFCCA was utilized to spot the damage location of the steel structure. The scale adopted for the implementation of MFCCA

Table 1 Damage groups and locations

Sl. No.	Severity of damage	Representation of damage
1	Undamaged	UD
2	One floor	1F 2F 3F
3	Two floors	12F 23F
4	Three floors	123F
5	All floors	AD

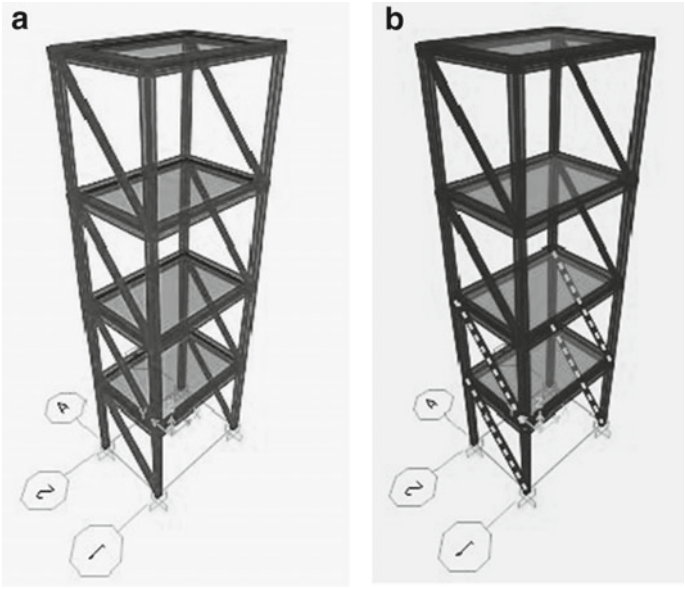

Fig. 2 Damage patterns **a** Undamaged case. **b** Damage on first floor and second floor (12F)

ranges from 16 to 512. The cross-correlation strategy in MFCCA is implemented by cross-crossing ground floor signal with that of other floors. Hence, a total of five MFCCA curves (G-G, G-1F, G-2F, G-3F, and G-4F) are developed from the four-storey structure. The cross-correlation G-G is obtained by cross-crossing of signals between ground and ground. Similarly, G-1F, G-2F, G-3F, and G-4F correlation curves are curves developed by cross-crossing the ground signal with the signals from first, second, third and fourth floors, respectively. For the study, eight damage cases are considered. The result of damage location of healthy or undamaged case is set as reference.

The existence of damage of a floor is depicted with the separation from the curves of top floors and adherence to the bottom floors (Fig. 3). The log–log plot of detrended covariance versus scale, as shown in Fig. 3a, depicts that all the cross-correlation curves almost coincides for undamaged case (reference). The damage diagnosis of first floor represented in Fig. 3b shows that G-G curves has dropped, making an increase in area between G-G and G-1F curves when compared to the undamaged case. The other curves remain close to one another. In the case of damage occurred in the first floor and second floor (12F) of the structure shown in Fig. 3f, the curves G-G and G-1F are significantly away from the other curves. Therefore, these trends indicated that the damage is located in the first and second floors (12F). When the damage is made on all floors, all curves showed increased departures from curves of adjoining floors and hence owing to an increase in area between curves. It is depicted in Fig. 3k. Hence, all the damage cases were perfectly located with MFCCA.

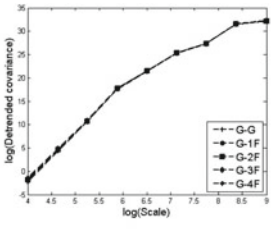

(a) Undamaged case (UD)

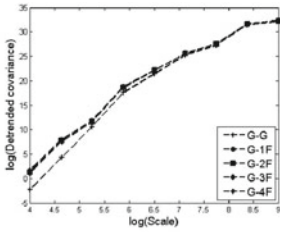

(b) Damage on first floor (1F)

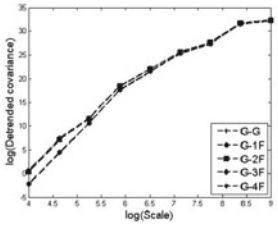

(c) Damage on second floor (2F)

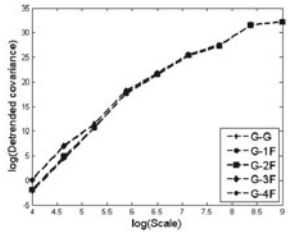

(d) Damage on third floor (3F)

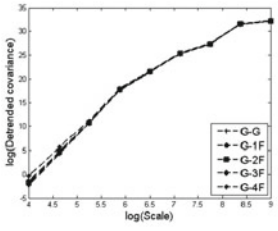

(e) Damage on fourth floor (4F)

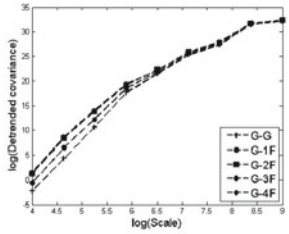

(f) Damage on first and second floor (12F)

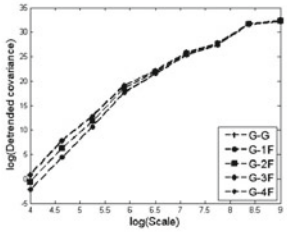

(g) Damage on second and third floors (23F)

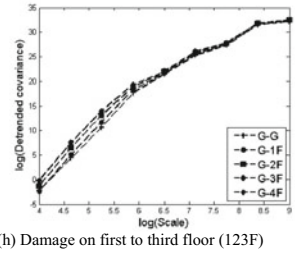

(h) Damage on first to third floor (123F)

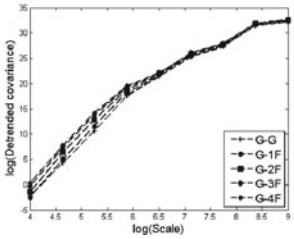

(k) Damage on all floors (AD)

Fig. 3 Log–log plot of detrended covariance versus scale for different damage cases

4.2 Computation of Damage Index

The damage index helps to quantity the results of damage location. The area between the adjacent MFCCA fluctuation function curves of all healthy and damaged cases are calculated for different scales. Positive DI values indicate the absence of damage as it shows the area between detrended covariance curves of damaged structure does not show significant variation compared to the healthy structure. The presence of damage is demarcated by a negative DI.

The DI value is illustrated for four damage cases as shown in Fig. 4a–d. Damage index is negative in Fig. 4a implies the presence of damage in first floor (1F). For damage on second and third floors, negative damage is shown by second and third floors alone (Fig. 4b). The damage in all floors shows negative damage indices for all the floors as illustrated in Fig. 4d. The damage indices all the ten damage cases are represented in Fig. 4. Hence, damage index based on MFCCA can be approved as an effective method for quantifying the damage location.

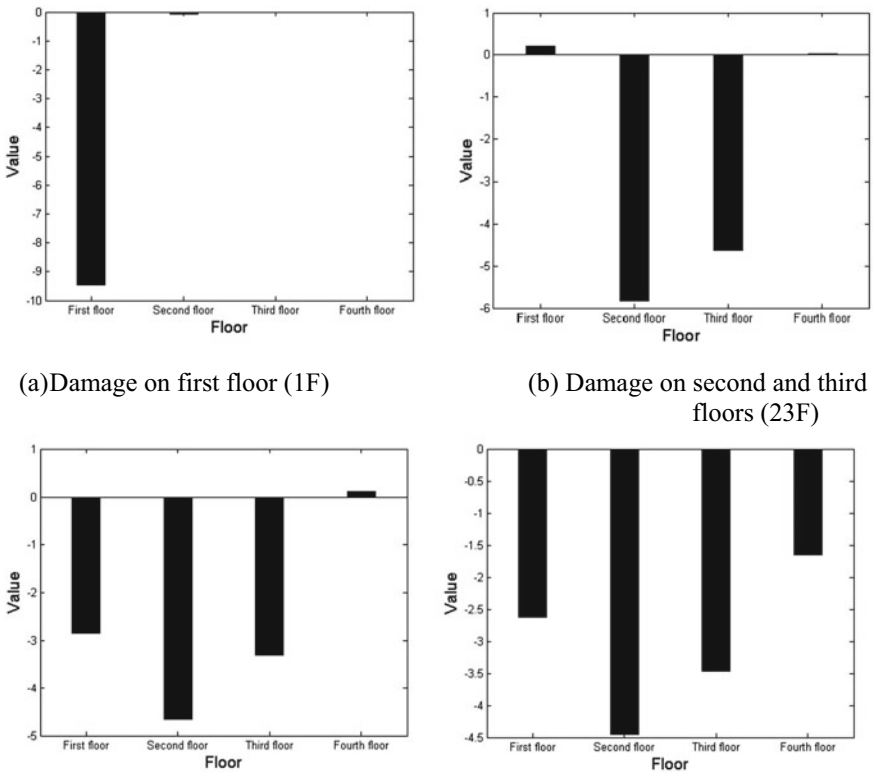

(a)Damage on first floor (1F)

(b) Damage on second and third floors (23F)

(c) Damage on first to third floor (123F)

(d) Damage on all floors (AD)

Fig. 4 Damage indices for different damage cases

4.3 *Effect of Noise on Damage Location*

Intrusion of noise into the signals is very common during experimental sessions and it may further influence the accuracy of the results. To check the efficacy of the proposed MFCCA method of damage location due the intrusion of noise, the noise was added to the captured responses of each storey with different signal-to-noise ratios (SNRs). The SNRs considered in this study are 60, 50, and 40 dB. The damage indices of different floors under the external noise effect are represented in Fig. 5. A negative DI observed in the first floor (Fig. 5a), implying the damage is

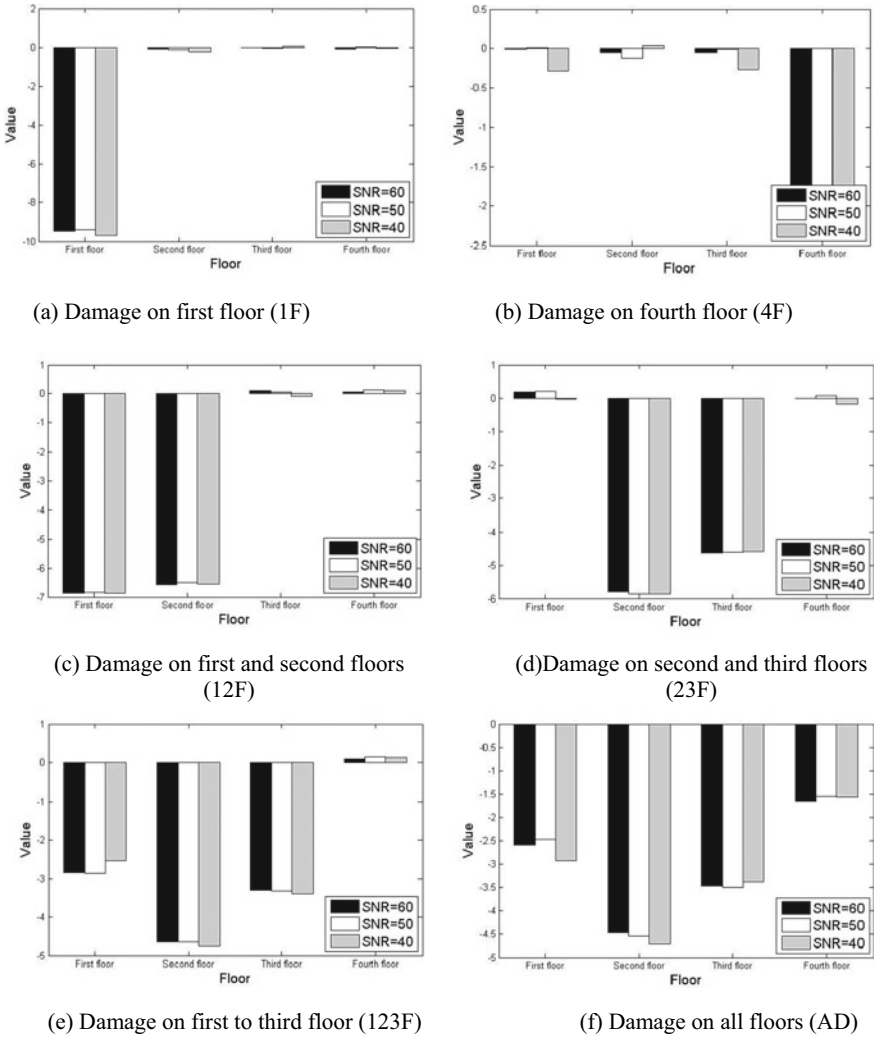

(a) Damage on first floor (1F)

(b) Damage on fourth floor (4F)

(c) Damage on first and second floors (12F)

(d)Damage on second and third floors (23F)

(e) Damage on first to third floor (123F)

(f) Damage on all floors (AD)

Fig. 5 Damage indices for different damage cases under the influence of noise

on the first floor. Figure 5b indicates the error in results due to the intrusion of noise as negative index is shown by first, second, and third floors, in case of damage on fourth floor (4F). But, the negative index of fourth floor is much larger compared to the other floors. This pronounces the accuracy of damage index, even in the presence of noise.

5 Conclusion and Future Scope

A structural health monitoring system based on multifractal cross-correlation analysis (MFCCA) is proposed in this study. The detrended covariance from MFCCA method was utilized to locate the damage. The results reveal that the damage cases were effectively determined through MFCCA. The quantification of MFCCA based damage detection was confirmed through the computation of a damage index. Further, the efficiency of the proposed method was checked under interference of noise in the signals. The accuracy of the results has been depleted slightly due to the intrusion of noise.

The proposed method is to be validated for structures with different configurations and the damage need to be analyzed with signals having different characteristics, to ensure its credibility. As intrusion of noise had slightly affected the accuracy of the proposed SHM, an empirical mode decomposition (EMD) based approach in combination with the multifractal analysis can bring better results in identifying damage location due to the intrusion of noise in the signals. The proposed method should be applied for different types of damage simulation to find whether the proposed SHM can detect incipient and moderate damages.

References

1. Lin TK, Liang JC (2015) Application of multi-scale (cross-) sample entropy for structural health monitoring. Smart Mater Struct 24:1–18
2. He K, Zhu WD (2011) Structural damage detection using changes in natural frequencies: theory and applications. J Phys: Conf Ser 305:1–10
3. Radzienski M, Krawczuk M (2009) Experimental verification and comparison of mode shape-based damage detection methods. J Phys: Conf Ser 181:1–9
4. Pandey AK, Biswas M, Samman M (1991) Damage detection from changes in curvature mode shapes. J Sound Vib 145:321–332
5. Lin TK, Fajri H (2017) Damage detection of structures with detrended fluctuation and detrended cross-correlation analyses. Smart Mater Struct 26:1–19
6. Lin TK, Chien YH (2016) Development of a structural health monitoring system based multifractal detrended cross-correlation analysis. In: The 2016 structures congress (Structures) Jeju Island Korea Auguste 28–September 1, 2016 pp 1–15
7. Lin TK, Chien YH (2017) A structural health monitoring system based on multifractal detrended cross-correlation analysis. Struct Eng Mech 63:751–760

8. Huang Y, Li H, Wu S, Yang Y (2018) Fractal dimension based damage identification incorporating multi-task sparse Bayesian learning. Smart Mater Struct 27:1–18
9. Mandelbrot BB (1982) The fractal geometry of nature. WH freeman, New York
10. Kantelhardt JW, Koscielny-Bunde E, Koscielny-Bunde Rego H, Havlin S, Bunde A (2001) Detecting long-range correlations with detrended fluctuation analysis Physica A 295(3–4):441–454
11. Peng CK, Havlin S, Stanley HE, Goldberger L (1995) Quantification of scaling exponents and crossover phenomena in non-stationary heart beat time series. Chaos 5:82–87
12. Drozdz S, Minati L, Oswiecimka P, Stanuszek M, Watorek M (2019) Signatures of the crypto-currency market decoupling from the forex future internet 11(154):1–18
13. Podobnik B, Stanley HE (2008) Detrended cross-correlation analysis: a new method for analyzing two nonstationary time series. Phys Rev Lett 100:084102
14. Oswieecimka P, Drozdz S, Forczek M, Jadach S, Kwapien J (2014) Detrended cross-correlation analysis consistently extended to multifractality. Phys Rev E 89:023305
15. Lin TK, Lainez AG (2018) Entropy-based structural health monitoring System for damage detection in multi-bay three-dimensional structures. Entropy 20:3–26